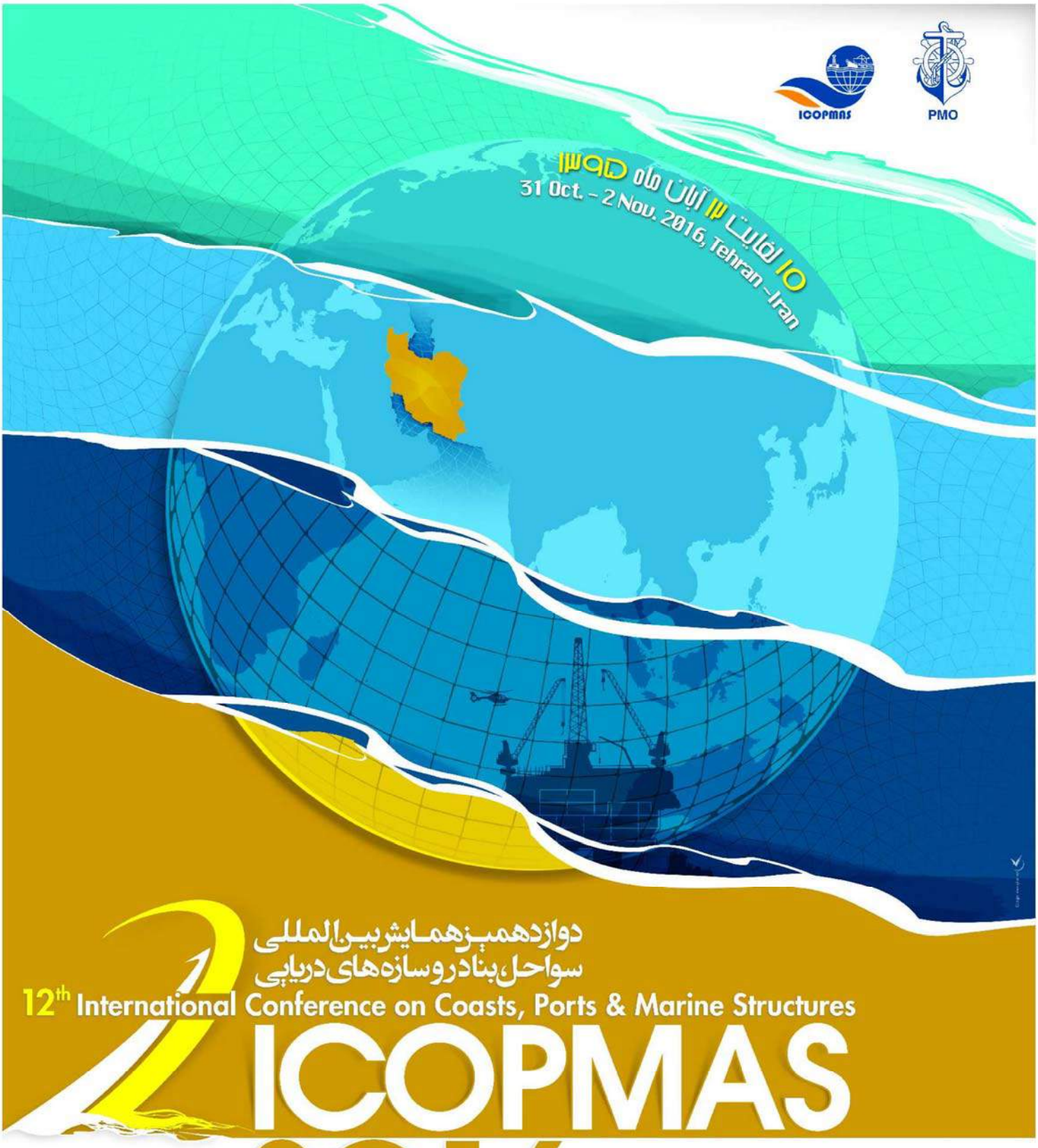

دوازدهمین همایش بین‌المللی سواحل، بنادر و سازه‌های دریایی

12th International Conference on Coasts, Ports & Marine Structures

ICOPMAS 2016

http://icopmas.pmo.ir

پایان اردیبهشت ماه، آخرین مهلت ارسال مقالات

ICOPMAS Secretariat, 6th Floor, Ports & Maritime Organization (PMO)
Shahidi St., Shahid Haghani Highway, Vanak Sq., Tehran, Iran
Tel: +9821 84932866-8 Fax: +9821 84932279

تهران، میدان ونک، بزرگراه شهید حقانی، بعد از چهار راه جهان کودک
خیابان شهیدی، سازمان بنادر و دریانوردی، طبقه ششم
دبیرخانه دایمی همایش، تلفن: ۸-۸۴۹۳۲۸۶۶ نمابر: ۸۴۹۳۲۲۷۹

Introduction

Ports and Maritime Organization of Iran is going to hold 12th International Conference on Coasts, Ports and Marine Structures (ICOPMAS 2016) in it's the Twenty-Sixth holding anniversary in cooperation with International Maritime Associations and organizations, domestic and foreign universities, contractors and consulting engineers. The Conference emphasizes on invigorating technical and specialized cooperation among all countries, especially coastal neighboring countries.

History of conference

On 27th may 1990, the first International Conference on Ports & Marine Structures was held in Tehran University. After sequential success of this biennial event, the Eleventh International Conference on Coasts, Ports and Marine Structures (ICOPMAS 2014) was held at Olympic hotel-Tehran on Nov 24-26, 2014.

Objectives

ICOPMAS, as one of the most important scientific events in Iran and in the Persian Gulf Region, affords an appropriate ground to exchange the latest scientific innovations and technical-executive achievements.

In addition, this conference leads to accurate use of new methods in marine industry for innovative management systems, strategic and economical technology and to promote future cooperation among employers, investors and consultant engineers.

IMPORTANT DATES

Procedure	Deadline
Registration	Oct 12, 2016
Article Evaluation Process & Result Announcement	Jun 21 – Aug 22, 2016
Conference	Oct 31 – Nov 2, 2016

Language

The official languages of the conference are English and Farsi.

Venue

Olympic Hotel, Tehran, Iran

Oct 31 – Nov 2, 2016

Tel: (+9821) 44739300 I Fax: (+9821) 44739191

info@olympichotel.ir I www.olympichotel.ir

Keynote Speakers

Prof. Michael J. Risk

- McMaster University - Canada
- **Subject:** Integrated Aquaculture for Iran: Avoiding Pitfalls while Preparing for the Future

Prof. Charitha Pattiaratchi

- The University of Western Australia – Australia
- **Subject:** Application of Oceanographic Drift Modeling

Prof. Jun Sasaki

- University of Tokyo - Japan
- **Subject:** Strategies and Policies towards Environmental and Fisheries Restoration in Tokyo Bay

Prof. Robert Kirby

- Ravensrodd Consultants Ltd.
- **Subject:** Twin Related Aspects of Engineered Mud Suspensions for the NW European and Iranian Port Industry

Prof. Magnus Larson

- Lund University, Sweden
- **Subject:** Ship-Generated Waves and the Effects on Bed and Bank Erosion

Prof. Jacqueline Michel

- Research Planning, Inc., USA
- Subject: A Comprehensive Approach to Oil Spill Preparedness – Planning, Response and Assessment

Prof. Lawrence P. Sanford

- University of Maryland Center for Environmental Science – USA
- **Subject:** Physical-Biological Interactions in Muddy Nearshore Environments

Prof. Han Ligteringen

- Delft University of Technology and UNESCO IHE, Netherland
- **Subject:** Port Development in the 21st Century

Prof. Dano Roelvink

- UNESCO-IHE – Netherland
- **Subject:** Predicting Coastal Impacts at a Range of ScalesThemes

Hydrodynamic and Sediment

- Waves and Currents
- Tropical Storms and Tsunami
- Sediment Transport, Erosion and Geomorphology
- Metocean Measurements and Analysis
- Marine Renewable Energy

Port and Coastal Management

- Integrated Coastal Zone Management (ICZM)
- Crisis Management of Marine Hazards
- GIS and Remote Sensing
- Port's Technologies and Management
- Marine Special Planning

Port Engineering and Coastal Structures

- Planning and Design of Ports
- Design and Construction of Coastal Structures
- Maintenance, Inspection and Repair of Coastal Structures
- New Equipment and Materials for Construction of Coastal Structures
- Hydrography and Dredging

Offshore and Pipeline Engineering

- Design and Construction of Offshore Structures
- Maintenance, Inspection and Repair of Offshore Structures
- Planning and Construction of Submarine Pipelines
- Marine Geotechnics

Marine Environment and Safety

- Ports and Maritime Safety Management
- International Convention, Regulations and Rules
- Pollution and Environmental Impacts of Structures and Marine Transportation
- Coastal and Marine Ecosystems

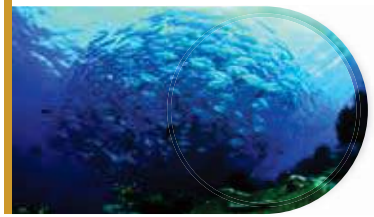

Board of Directors

No.	Organization
1	Managing Director of Ports and Maritime Organization (Conference President)
2	Commander of the Navy of Islamic Republic of Iran Army
3	Commander of the Navy of the Army of the Guardians of the Islamic Revolution
4	Vice president and Head of Environmental Protection Organization
5	Deputy Minister of Defense and Armed Forces Logistics and President of Geographical Organization
6	Deputy Minister of Industries and Business and President of Geological Survey of Iran
7	President of National Cartographic Center
8	Deputy Minister of Road & Urban Development, and President of Meteorological Organization
9	Managing Director of Islamic Republic Of Iran Shipping Lines
10	Vice president and Head of Cultural Heritage and Tourism Organization
11	Deputy Minister of Energy in the Water and Wastewater Affairs
12	Deputy Minister of Jihad-e-Agriculture and President of Iran's Fishery Organization
13	Managing Director of Iranian Oil Terminals Company
14	President of Islamic Azad University
15	President of Hormozgan University
16	President of Iran University of Science and Technology
17	President of Chabahar University of Maritime and Marine Science
18	President of K.N. Toosi University of Technology
19	President of Iranian Offshore Engineering and Construction Company

Foreign Scientific Committee

No.	Name	Affiliation
1	Ergin, Aysen	Middle East Technical University, Turkey
2	Higelin, Gerald	University of Applied Science Furtwangen, Germany
3	Ioan, Nistor	University of Ottawa, Canada
4	Kirby, Robert	Ravensrodd Consultants Ltd - U.K
5	Kosyan, Ruben	Southern Branch of the P.P.Shirshov Institute of Oceanology. RAS
6	Larson, Magnus	Lund University, Sweden
7	Ligteringen, Han	DelftUniversityofTechnologyandUNESCOIHE–TheNetherland
8	Mammadov, Ramiz	Institute of Geography, Azerbaijan
9	Michel, Jacqueline	Research Planning, Inc., USA
10	Nemazie, David	University of Maryland Center for Environmental Science, USA
11	Oumeraci, Hocine	TU Braunschweig - Germany
12	Pattiaratchi, Charitha B.	The University of Western Australia, Australia
13	Rahman, MD. Ataur	Bangladesh University of Engineering and Technology (BUET), Bangladesh
14	Risk, Michael J.	McMaster University, Canada
15	Roelvink, Dano	UNESCO_IHE, The Netherlands
16	Sanford, Lawrence	University of Maryland Center of Environmental Science, USA
17	Sasaki, Jun	The University of Tokyo, Japan
18	Shibayama, Tomoya	Waseda University, Japan
19	Subramaniam, Neelamani	Kuwait Institute for Scientific Research, KUWAIT
20	Tomasicchio, Giuseppe Roberto	University of Salento, Italy
21	Van Breugel, Klaas	Delft University, Netherlands

Iranian Scientific Committee

No.	Name	Affiliation
1	Abaee, Hamidreza	Port & Maritime Organization (PMO)
2	Ahmadian, Reza	Islamic Azad University, Iran
3	Alam, Mohammad Reza	University of California – USA
4	Aliakbari Bidokhti, Abbas Ali	Institute of Geophysics
5	Ale Sheikh, Ali Asghar	K.N. Toosi University of Technology, Iran
6	Allahyar, Mohammad Reza	Ports and Maritime Organization, Iran
7	Badiee, Seyed Peyman	University of Tehran, Iran
8	Bahari, Mohammad Reza	Consulting Engineer, Iran
9	Banijamali, Babak	Consulting Engineer, Iran
10	Bargi, Khosro	University of Tehran, Iran
11	Daghigh, Mohammad	University of Tehran, Iran
12	Dibajnia, Mohammad	Baird Company – Canada
13	Estiri, Seyed Ali	Consulting Engineer, Iran
14	Farshchi, Parvin	Department of Environment , Iran
15	Gatmiri, Behrouz	University of Tehran, Iran
16	Ghader, Sarmad	University of Tehran, Iran
17	Ghaderi, Seyed Mohammad Reza	Ports and Maritime Organization, Iran
18	Golshani, Ali Asghar	Islamic Azad University, Iran
19	Hajizadeh Zaker, Nasser	University of Tehran, Iran
20	Hakimzadeh, Habib	Sahand University of Technology, Iran
21	Hejazi, Kourosh	K.N.Toosi University of Technology, Iran
22	Jandaghi Alaee, Majid	Consulting Engineer, Iran
23	Kamalian, Reza	Ministry of Energy Water Research Institute
24	Kebriaee, Alireza	Ports & Maritime Organization, Iran
25	Ketabdari, Mohammad Javad	Amirkabir University of Technology, Iran
26	Khayyer, Abbas	Kyoto University, Japan
27	Khedmati, Mohammad Reza	Amirkabir University of Technology, Iran
28	Khoshravan, Homayoun	water research institute / Caspian Sea National Research Center
29	Mazaheri, Saeed	Iranian National Center for Oceanography
30	Moradi, Masoud	Iranian National Center for Oceanography
31	Gharabaghi, Ahmadreza	Sahand University of Technology, Iran
32	Naimi, Babak	University of Copenhagen, Denmark
33	Nakhaei, Ali	University of Tehran, Iran
34	Panahi, Roozbeh	Tarbait Modarres University, Iran
35	Pirasteh, Saeed	Waterlo Institute, Canada
36	Rahimipour, Hamid	Consulting Engineer, Iran
37	Rahmani, Iraj	Building and Housing Research Center
38	Ramezanianpour, Ali Akbar	Amirkabir University of Technology, Iran
39	Rasti Ardakani, Reza	Shahid Beheshti University, Iran
40	Razazan, Abdolkarim	Ports & Maritime Organization, Iran
41	Sadeghi, Kabir	Near East University, Cyprus
42	Shafieefar, Mahdi	Tarbait Modarres University, Iran
43	Shayan, Siavosh	Tarbait Modarres University, Iran
44	Soltanpour, Mohsen	K.N. Toosi University of Technology, Iran
45	Yeganeh Bakhtiari, Abbas	University of Science and Technology, Iran
46	Zaker, Homayoun	Consulting Engineer, Iran

Chair of Scientific Committee

- **Mohsen Soltanpour**

Exhibition Plan

For further enquiries please contact the secretariat via email: icopmas@pmo.ir

Registration Fees (Euro)

Title	Before 21 May	After 21 May
Authors of the accepted papers	-	150
Professors	300	400
Students	150	200
Other participants	500	600
Accompanying Persons	200	300

Note

- Registration fees cover the conference materials, lunch and coffee break.
- To register for ICOPMAS 2016, please Visit http://icopmas.pmo.ir or contact the secretariat via email: icopmas@pmo.ir

Organization

President	Saeidnejad, Mohammad
Vice President	Aliabadi, Nooreddin
Secretary	Allahyar, Mohammadreza
Vice Secretary	Alvand, Behzad

Executive committee

No.	Name	Designation
1	Sohrabi, Reza	Chief Executive
2	Khansari, Farhad	Announcement Consultant
3	Shoghian, Somayeh	Website Expert
4	Khaleghi, Afshan	International Affairs Expert
5	Mirzaei, Mansour	Coordinator
6	Monadi, Mehdi	EDI Expert
7	Kalantari, Farzad	Formalities Expert
8	Kiani, Mahmoud	Formalities Expert
9	Mousavi, Seyed Mohammad	Hardware Expert
10	Lak Aliabadi, Asghar	Public Relations Expert
11	Ghanbari, Rasoul	Coordinator
12	Zare' , Ebrahim	Public Relations Expert
13	Hosseininejad, Seyed Mohammad	International Announcement Expert
14	Mohammadnejad, Hamed	Internal Announcement Expert
15	Tavakol, Aneseh	Coordinator

Moral Sponsors

- The World Association for Waterborne Transport Infrastructure (PIANC)
- International Association of Ports and Harbors (IAPH)
- World Meteorological Organization (WMO)
- International Association for Hydro-Environment Engineering and Research (IAHR)
- Coordinating Committee on Hydrometeorology & Pollution Monitoring of the Caspian Sea (CASPCOM)
- International Association of Marine Aids to Navigation and Lighthouse Authorities (IALA –AISM)
- Iranian National Commission for UNESCO
- Iranian Association of Geomorphology
- Iranian Coastal & Marine Structural Engineering Association (ICOMSEA)
- Iranian Association of Naval Architecture and Marine Engineering

Financial sponsors

LIEBHERR

MCS INTERNATIONAL KALMAR Continental Siwertell NOVATECH

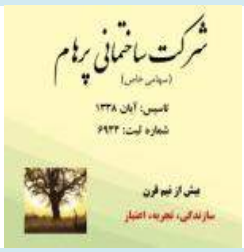


مهندسین مشاور
پویا طرح پارس


شرکت سازه اهواز
SAZEH AHVAZ CO.


هندسه پارس
مهندسین مشاور


TADBIR SAHEL PARS
تدبیر ساحل پارس


مهندسان مشاور خاک بافت
Khakbaft Consulting Engineers


تایدواتر خاورمیانه
شرکت سهامی عام


RAHAD OXIN


نگین سبز
Negin Sabz


دریابندر
مهندسین مشاور
DB
DARYABANDAR
engineering consultants


TFA


مهندسان مشاوراوج پژوهش صنعت
Awdge Pazhoohesh Sanaat
(Consulting Engineers)
APS


مشاور عمران ایران


شرکت خدمات دریایی هدایت کشتی خلیج فارس (سهامی خاص)
Persian Gulf PILOT Maritime Services Co.

Media Sponsors

Media Sponsors

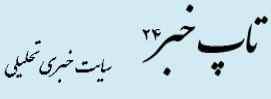

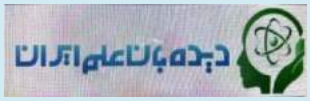

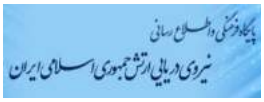

Contents

- Metocean Measurements and Analysis

- GIS and Remote Sensing

- Port's Technologies and Management

- Maintenance, Inspection and Repair of Offshore Structures

- Planning and Construction of Submarine Pipelines

- Marine Geotechnics

- International Convention, Regulation and Rules

- Pollution and Environmental Impacts of Structures and Marine Transportation

- **Coastal and Marine Ecosystems**

IMPLEMENTATION OF VISCOELASTIC MUD-INDUCED WAVE DISSIPATION IN SWAN

Mostafa Beiramzadeh[1], Seyed Mostafa Siadatmousavi [2]

1) Civil engineering Department, Iran University of Science and Technology, mostafabeiramzadeh@yahoo.com
2) Civil engineering Department, Iran University of science and Technology, siadatmousavi@iust.ac.ir

1. Introduction

The absence of wave-mud interaction in wave models forced researchers to calibrate their models by increasing sand friction coefficient in the model. However; this approach would result in more dissipation in low-frequency part of the spectrum while the field observations designate more damping in high-frequency part of the spectrum. To remedy this problem, researchers were persuaded to include the correct mechanism in the models[1].

Mud-induced relative dissipation was implemented for first time in SWAN model and validated for Guyana coast. Generally two important results were found: (1) large wave height existed in the absence of mud-induced relative dissipation in model results; and (2) the mean wave period decreased strongly over the fluid mud layers, due to strong dissipation of the low-frequency waves[2].

In some field cases lack of in situ data forced researchers to do inverse modeling, i.e. to choose values for unknown data such that model outputs were more compatible with observations[3]. This approach was performed on Casino beach, Brazil. It was shown that wave height was overestimated if wave-mud interaction was ignored. It proved mud existence in the region. Then, they considered 40 cm thickness for mud layer over the region. Inclusion of wave-mud interaction mitigated the overestimation in wave height but using a uniform 40 cm mud thickness resulted in high mud-induced dissipation, and they concluded that patchy mud layer exist in some points in this region[3].

2. Viscoelastic mud-induced dissipation

Two different models are used here to describe the mud behavior.

2.1. Liu-Chan viscoelastic model

Nonlinear advection terms and shear stress in horizontal momentum equation for sediment and water layer are ignored in this model. Nonlinear advection terms, vertical acceleration and shear stress in vertical momentum equation for sediment water layer were also considered negligible[4]. Boundary conditions included in model are kinematic condition for water surface, and equality of shear stress, vertical pressure and vertical velocity at interface of water and mud, kinematic condition for the interface and also zero vertical and horizontal velocities at bed.

The resulted dispersion equation is:

$$\omega^2 = gktanh(kH_{w0})\frac{1+\Omega\, coth(kH_{w0})}{1+\Omega\, tanh(kH_{w0})} \quad (1)$$

$$\Omega = ik\gamma\left[H_{m0} - \frac{tanh(\alpha H_{m0})}{\alpha}\right] \quad (2)$$

$$\alpha = (1-i)\sqrt{\frac{\omega}{2\nu_{me}}}, deltam = \delta_{me} = \sqrt{\frac{2|\nu_{me}|}{\omega}} \quad (3)$$

$$\nu_{me} = \nu_m + \frac{iG}{\omega\,\rho_m} \quad (4)$$

in which $\omega = 2\pi/T$, $k = k_r + ik_i$, T is wave period, G is mud elasticity, ρ_m, ρ_w are mud and water densities, H_{w0} and H_{m0} are water depth and mud thickness respectively.

It can be shown that the relative mud-induced dissipation for Liu-Chan method: $2C_g k_i$ in which C_g is the group velocity. Note that Eq. (1) is implicit and needs a trial-error procedure to solve.

2.2. Macpherson viscoelastic model

In this model, the nonlinear advection terms in the horizontal and vertical momentum equations for sediment layer were ignored[5]. Boundary conditions are the same as section 2.1. The resulted dispersion equation is:

$$\frac{\rho_w(\omega^4 - g^2k^2)\ tanh(kH_{w0})}{gktan\,h(kH_{w0}) - \omega^2} + \rho_m gk + Tk^3 + \rho_m(2k^2\nu_{me} - i\omega)^2\left[\frac{\left(2k^2 - \frac{i\omega}{\nu_{me}}\right)[lC_mC_l - kS_mS_l] - 2k^2l}{\left(2k^2 - \frac{i\omega}{\nu_{me}}\right)[lS_mC_l - kC_mS_l]}\right] - 4\rho_m k^3 {\nu_{me}}^2 l\left[\frac{\left(2k^2 - \frac{i\omega}{\nu_{me}}\right) - 2k[kC_mC_l - lS_mS_l]}{2k[lS_mC_l - kC_mS_l]}\right] = 0 \quad (5)$$

in which $C_m = cosh(kH_{m0})$, $C_l = cosh(lH_{m0})$, $S_m = sinh(kH_{m0})$, $S_l = sinh(lH_{m0})$, $l = (k^2 - \frac{i\omega}{\nu_{me}})^{\frac{1}{2}}$.

Moreover, T is surface tension. The relative Mud-induced dissipation for Macpherson model is:

$$\frac{-\frac{1}{2}\rho_w g\left(be^{-k_i x}\right)^2 \omega\, Im\left(\left[\frac{\omega^2(gk\,cosh(kH_{w0}) - \omega^2\,sinh(kH_{w0}))}{gk(gk\,sinh(kH_{w0}) - \omega^2\,cosh(kH_{w0}))}\right]\right)}{\frac{1}{2}\rho_w g\left(ae^{-k_i x}\right)^2 + \frac{1}{2}(\rho_m - \rho_w)g\left(be^{-k_i x}\right)^2} \quad (6)$$

in which b is: mud and water interface amplitude

$$b = |cosh(k*h) - (g*k)/\omega^2 * sinh(k*h)| \quad (7)$$

It is clear that if G=0, the viscoelastic model performs similar to a viscous model. Note that Eq. (5) is also an implicit equation and needs trial-error procedure to solve.

3. Results

Figure1and Figure2 indicates that in case of G=0 (viscous condition) Liu-Chan and Macpherson methods are in good agreement with a well-known viscous model proposed by Ng [6]. Figure1 shown mud-induced dissipation for water depth of 4m while Figure2 is for water depth of 1m.

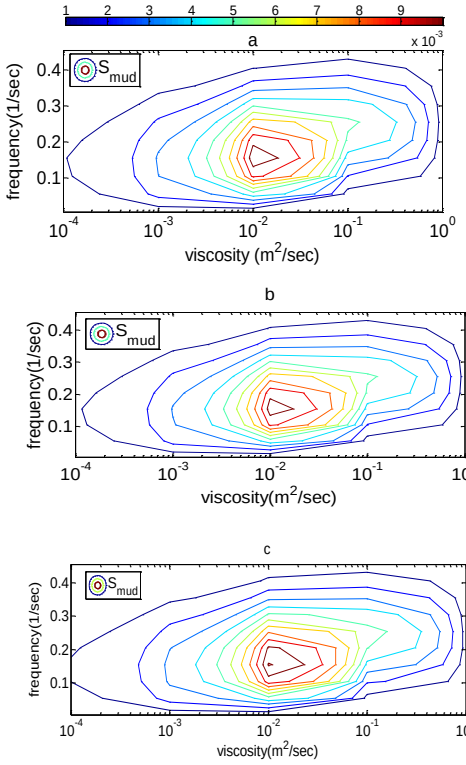

Figure1.a(Liu-Chan in viscous manner), b(Macpherson in viscous manner), c(Ng (2000)). $H_w = 4$, $H_w = 0.2$

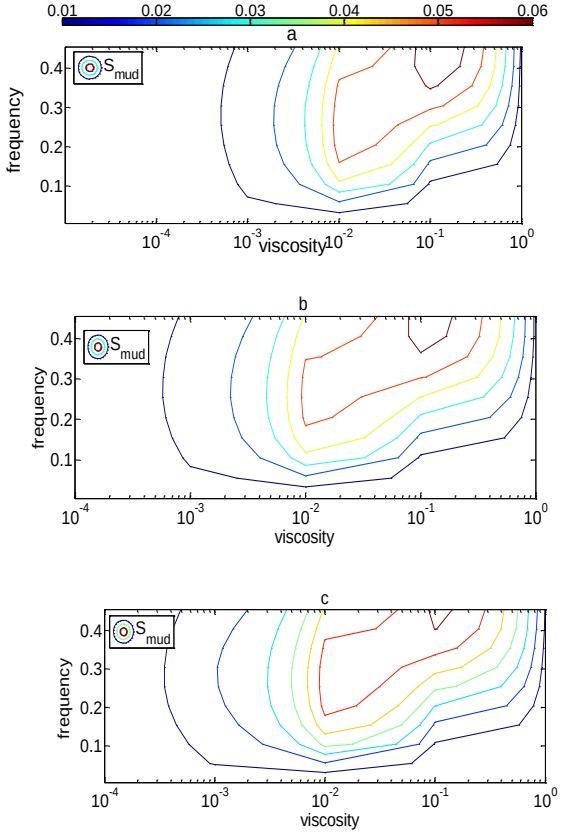

Figure2.a(Liu-Chan in viscous manner), b(Macpherson in viscous manner), c(Ng (2000)). $H_w = 1$, $H_w = 0.2$

Figure3 shows that for a constant frequency, increasing elasticity coefficient would decrease wave dissipation rate. Moreover, for a specific viscosity value, the dissipation rate is the maximum.

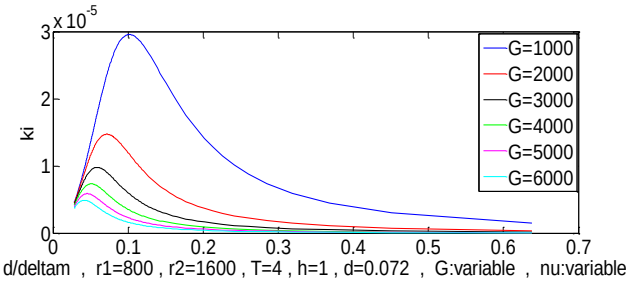

Figure 3. Liu-Chan dissipation rate due to G change

In Figure4, two methods were applied to field measurement in Surinam coast[7]. It is clear that neglecting mud-effects would result to overestimation of energy content in wave frequencies higher than 0.2 Hz. Both viscoelastic models were successful; however Macpherson model keeps wave energy for frequencies bigger than 0.2 but Liu-Chan method completely dissipates wave energy for these frequencies.

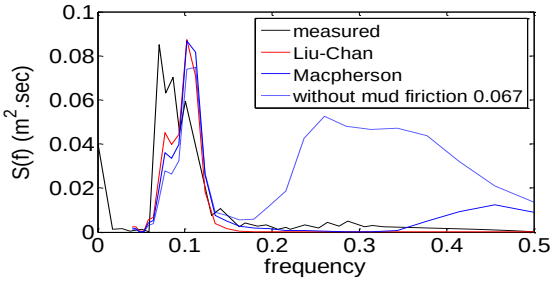

Figure4. Modeled and measured wave spectrum. G=4000 was used for both models

4. References

[1] Sheremet, A. and G. Stone, *Observations of nearshore wave dissipation over muddy sea beds.* Journal of Geophysical Research: Oceans, 2003. 108(C11).

[2] Winterwerp, J.C., et al., *Modelling of wave damping at Guyana mud coast.* Coastal Engineering, 2007. 54(3): p. 249-261.

[3] Rogers, W.E. and K.T. Holland, *A study of dissipation of wind-waves by mud at Cassino Beach, Brazil: Prediction and inversion.* Continental Shelf Research, 2009. 29(3): p. 676-690.

[4] Liu, P.L.-F. and I.-C. Chan, *A note on the effects of a thin visco-elastic mud layer on small amplitude water-wave propagation.* Coastal engineering, 2007. 54(3): p. 233-247.

[5] Macpherson, H., *The attenuation of water waves over a non-rigid bed.* Journal of Fluid Mechanics, 1980. 97(04): p. 721-742.

[6] Ng, C.-O., *Water waves over a muddy bed: a two-layer Stokes' boundary layer model.* Coastal Engineering, 2000. 40(3): p. 221-242.

[7] Wells, J.T. and G.P. Kemp, *Interaction of surface waves and cohesive sediments: field observations and geologic significance*, in *Estuarine cohesive sediment dynamics*. 1986, Springer. p. 43-65.

A COMPARISION AMONG DIFFERENT AVAILABLE MARINE FORECASTING SYSTEMS IN IRANIAN SEAS

Aliasghar Golshani[1], Alireza Vaselali[2] and Said Mazaheri[3]

1) Beta Group, Tehran, Iran, a.golshani@betagroupco.com
2) Beta Group, Tehran, Iran, a.vaselali@betagroupco.com
3) Iranian National Institute for Oceanography and Atmospheric Science, Tehran, Iran, said.mazaheri@inio.ac.ir

1. Introduction

The marine forecasting is of great importance for several reasons including planning marine operations, scheduling shipping movements, dredging, survey, berth maintenance or construction. There are several global marine forecast systems based on large scale regional data which do not consider the localized effects of seabed and land topography on local wave and wind climate. They are also several local marine forecast systems in Iranian waters. This paper aims to perform an inter-comparison among different marine forecasting systems in Iranian seas in order to evaluate the accuracy and difference between their figures and give a proper ground for further investigation and research in this crucial issue.

2. Global Marine Forecast Project Covering Iranian Seas

MetOcean Solutions Ltd (MSL) operates a GIS tool for a 3-hourly 10-days wave forecasting namely WXTiles which does not include closed seas such as the Caspian Sea [1].

NOAA Environmental Modeling Center operates a 3-hourly 7-days wave forecast project using WWIII wave model and 0.5 degree GFS wind boundary conditions in Indian Ocean including Oman Sea and half of the Persian Gulf [2]. This project provides wind sea, primary and secondary swell parameters separately as output as well as spectrum, sources and bulletin in several point in Indian Ocean.

ECMWF Company provides three global wave forecast projects namely HRES-WAM (10 days, 0.25 degree), HRES-SAW (10 days, 0.125 degree) and ENS-WAM (15 days, 0.5 degree) by running WAM Cy41r1 model which are not freely available [3]. They do forecast every 3 hrs for the first 6 days and every 6 hrs afterwards.

3. Iranian Authorities Forecasts in Iranian Seas

Currently, there are three different authorities which are performing wave forecasts in Iranian Seas.

Iranian Meteorological Organization (IRIMO) runs a 6-hourly 4-days wind and wave forecast system in Iranian seas. They first run a WRF local wind model with resolution of 10 km using GFS boundary condition and the output is the input to a SWAN wave model with resolution of 2.5km to generate wave field [4]. There is two open boundaries in Oman Sea wave model (18N, 66E) without applying any boundary conditions.

Iranian National Center for Ocean Hazards (INCOH) at Iranian National Institute for Oceanography (INIO) runs a 6–hourly 4-days wave forecast system in Iranian seas using WWIII wave model (spatial resolution 0.05 degree) forced by GFS wind boundary condition [5]. There is an open boundary at 15N without applying any boundary condition.

Isfahan Technical University (ITU) performs a 6-hourly 4-days wave forecast system for Ports and Maritime Organization (PMO) in Iranian seas using WWIII wave model forced by GFS wind boundary condition which uses the same method that INCOH uses for wave forecasting [6]. They have validated their forecast model by comparison with those of DHI forecast in Persian Gulf [7].

K.N. Toosi University (KNTU) with cooperation of Institute of Geophysics (IG) is currently working on a wave and 3D current forecast system in the Persian Gulf for PMO. They plan to run a WRF local atmospheric model with resolution of 0.1 degree and the wind and pressure output will be forced to PMO-Dynamics in-house wave and 3D current models [8].

4. Foreign Companies Forecasts in Iranian Seas

MSL operates a local 3-hourly 7-days wave forecasting namely SwellMap for Persian Gulf which provides swell wave parameters for recreational activities [9].

Based on PERGOS hindcast project, Danish Hydraulic Institute (DHI) with cooperation of OceanWeather Inc (OWI) runs a 3-hourly 7-days wave and current forecast in the Persian Gulf and Strait of Hormuz [10]. They use a modified NCEP wind field with spatial resolution of 0.75 degree as boundary condition which is adjusted using ship observations, QuikSCAT wind data and synoptic wind stations. Mike21 SW is run for wave forecasting and Mike21 HD 3D model for current and water level forecasting. The spatial resolution varies from 8 km offshore to 1 km near-shore. The output includes wave parameters, current speed and direction in different depth layers, and water surface level. Their results with coarse

resolution is available on its website in time series, animation and tabular formats.

Turkish State Metrological Service (TSMS) runs a 3-hourly 5-days wind and wave forecast project in Caspian Sea [11]. They first run a MM5 local wind model with resolution of 4.5km (inner domain), 13.5 km (outer domain) using 0.15 degree ECMWF IFS boundary condition and the output is the input to METU3 in-house wave model with resolution of 3 km.

5. Conclusion

We can categorizes all above-mentioned forecasting systems in four main groups as below:

The first group is global forecast systems which uses coarse wind fields as input and run wave models with relatively coarse resolution (MSL, NOAA, and ECWMF). Their results are not accurate in closed seas like Caspian Sea and Persian Gulf especially when there are surrounded by high mountain ranges like south of Caspian sea, however they work well in the open oceans.

The second group is local systems which use coarse global wind fields as input to local wave models with fine resolution (INCOH, PMO-ITU). Wind field as the main driving input for wave model is not improved in these systems therefore, the wave results are still not accurate despite the implementation of finer mesh resolution and better bathymetry resolving in the wave model.

The third group is the local systems which use modified global wind fields as input to local wave models (DHI-OWI).

The fourth group is the local systems which run both wind model and wave model with fine resolution (IRIMO, TSMS, KNTU-IG). They use global wind forecasts (GFS, IFS) as boundary condition for the local wind models.

The 3rd and 4th groups are the most accurate systems in our area and it is recommended to use them for forecasting purpose (IRIMO for all Iranian seas, DHI-OWI for Persian Gulf, TSMS for Caspian Sea).

For instance, Fig.1 illustrates the comparison between DHI (belongs to G3) and INCOH (belongs to G2) forecasts in south of Qeshm Island and vicinity of Bushehr port areas. DHI forecast is higher in Qeshm, as DHI's wind in Strait of Hormuz is higher and more accurate. INCOH's coarse GFS wind field is underestimated as this island is not well resolved in the wind model due to coarse land-sea mask and as a result high and unreal surface roughnesses in both sides of the strait. As for Bushehr Port, although two comparison points are 15 km away but results look very different and the reason for such a difference needs to be investigated. This implies the necessity of application of a well-calibrated fine resolution model in Iranian waters via improvement of available forecasting systems for operational purposes.

For forecasting in Oman Sea, it is recommended to apply spectral or parametric wave boundary condition in open boundary or alternatively extending the Oman Sea mesh to cover the whole Indian Ocean to be able to capture properly the swells coming from the South Pole. Neither of the local forecasts have considered the open boundary conditions. NOAA Indian Ocean forecast model is extended to South Pole and has no open boundary.

It is also suggested to plot the buoys data in a graph together with forecast data and put them in the forecasting website for comparison between "the forecast results and what is happening in reality in the seas" purpose. It is worthy to mention that IRIMO and PMO has 10 and 7 operating buoys in Iranian Seas, respectively [12, 13] which can be used in this regards.

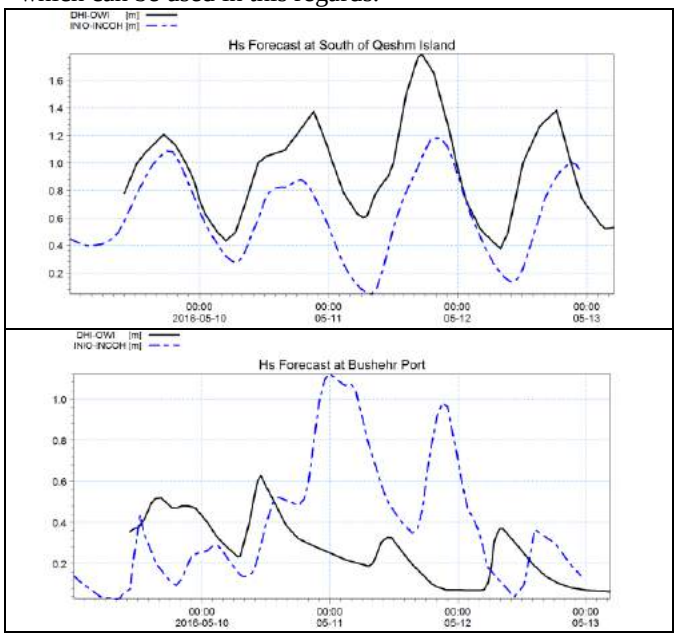

Figure 1. Comparison between DHI and INCOH forecasts at Qeshm (top) and Bushehr (bottom)

6. References

[1] http://www.wxtiles.com

[2] http://polar.ncep.noaa.gov/waves

[3] http://www.ecmwf.int

[4] http://www.irimo.ir

[5] http://www.inio.ir

[6] http://waveforecast.pmo.ir/

[7] Saeidi, D., Zamani, A.R., Sedaghat, A., and Saghafian, M.," Validation of short-time wave forecasting in Persian Gulf , Oman Sea and part of Indian Ocean by using Iranian numerical wave prediction model", Proceeding of ICOPMAS2014.

[8] http://www.pmo.ir

[9] http://www.swellmap.co.nz/

[10]http://gulf.waterforecast.com/dbm/DashboardEngine.aspx?DashboardID=Gulf\Home

[11] http://www.mgm.gov.tr/en-us/marine-metu3-detail.aspx?g=p&b=Hazar

[12] http://buoy.irimo.ir/

[13] http://marinedata.pmo.ir/

OPTIMIZATION OF THE WEIGHT MATRIX IN DATA ASSIMILATION FOR WAVE DATA IN PERSIAN GULF USING WAVEWATCH-III MODEL

Hamidreza Moazzami [1], Seyed Mostafa Siadatmousavi [2]

1) Civil engineering Department, Iran university of science and technology, Tehran, Iran, hamid.moazzami@gmail.com
2) Civil engineering Department, Iran university of science and technology, Tehran, Iran, siadatmousavi@iust.ac.ir

1. Introduction

Decreasing the errors of calculating the meteorological and oceanographic parameters is of great importance. One of the efficient methods to do this is Data Assimilation. In this method, observational data and statistical assumptions are applied to make the calculation of the parameters more precise than that of the mode which model runs without Data Assimilation. One of the crucial phenomena in oceanography is wave. Data Assimilation have been studied extensively in meteorology but it is still a new subject in wave modeling; especially in Iranian waters. Furthermore, the wave model used in limited available researches on application of Data Assimilation in wave modeling have been done using SWAN and WAM models, and not using WAVEWATCH-III. Since this model is very efficient in oceanic scales, in this research the original code of WAVEWATCH-III was enhanced to include Data Assimilation routines effectively, and the enhanced model was employed in in Persian Gulf.

2. Data Assimilation

Data Assimilation is a method which decreases the errors of meteorological and oceanographic models based on statistical assumptions and observational data and prevents the errors to be accumulated in time. Data Assimilation methods are divided into two main groups. Variational and sequential methods. Optimal Interpolation[1] is the method which is used in this study. Equation (1) is the main formula of this method.

$$\boldsymbol{x}^{a} = \boldsymbol{x}^{f} + \boldsymbol{W}(\boldsymbol{y} - \boldsymbol{H}\boldsymbol{x}^{f}) \quad (1)$$

In this equation, $\boldsymbol{x}^{f}$ is the vector of model outputs without using Data Assimilation, called model vector. $\boldsymbol{y}$ is the observational vector, $\boldsymbol{H}$ and $\boldsymbol{W}$ are interpolation and weight matrixes respectively. $\boldsymbol{x}^{a}$ is the vector of model outputs after using Data Assimilation called analysis vector.

Data Assimilation can be applied on spectrum or mean parameters such as weight height or period. In this study, it is used for significant wave height parameter.

3. Modeling the Persian Gulf using WAVEWATCH-III

Five different packages of wind input and deep water wave dissipation in WAVEWATCH-III model are used for time period from January to March 2013. No Data Assimilation was used and as shown in the Table 1, WAM4 was the best one that showed the minimum root mean square error (RMSE) compared to observations close to Farsi Island. So this package was used for the case that the Data Assimilation code was applied in the model.

Table1.packages comparison

package	WAM4	WAM3	Ardhuin	Tolman	BYDRZ
RMSE (m)	0.5652	0.6145	0.5868	0.6949	0.7575

4. Weight Matrix

The most challenging parameter in Equation (1) is the weight matrix which is calculated as follows [2].

$$\mathrm{P(i,j)} = \frac{v^{f}}{v^{f}+v^{o}}\left(1+\frac{r_{ij}}{L}\right)\exp\left(\frac{-r_{ij}}{L}\right) \quad (2)$$

P(i,j) is the covariance between points i and j, L is the correlation length scale, v^{f} is model variance vector without using Data Assimilation, v^{o} is observation variance vector which is used in Data Assimilation procedure and r_{ij} is the distance between points i and j. Measurements of an ADCP close to Farsi Island were employed for applying Data Assimilation in the model. The i point refers to ADCP point and j is all other different grid points in the model. Using Equation (3), the weight of any grid point is obtained based on the distance between the grid point and ADCP. Determination of L parameter has a crucial effect on the performance of Data Assimilation and wave field promotion. Most of the previous studies considered an empirical value for L but in this research, the Quick Canadian method (QC) [3] was used to obtain the most optimized value for this parameter. It is concluded from QC method that L=125 km is the

optimized value which improves the wave field forecasting.

Because the correlation between shallow water and deep water points is low, in this study, Equation (3) was used to consider the effects of shallow water on the performance of Data Assimilation.

$$\exp\left[-\left(\left[30-\frac{d_j}{13}\right]\right)^4\right] \qquad d_j < 30\ m \qquad (3)$$

For depths under 30m, the effect of Data Assimilation is decreased by this formula [4]. The Data Assimilation method was used for wave height parameter but because the WAVEWATCH-III analyses the wave field in spectral form, the results of assimilated wave heights must be transferred into energy and wave action spectrum in each time step. After that, the wave action spectrum was numerically solved in the model and the effects of Data Assimilation were seen in all spaces and times.

5. Results and Discussion

In this research, the Persian Gulf was modeled in two cases in WAVEWATCH-III. In the first case, it was modeled normally and in the second one, the Data Assimilation method was applied in the model. An ADCP data were used as in situ observation in the Data Assimilation procedure. The model results were compared in two cases and the improvement of results using Data Assimilation was assessed.

Model outputs in 2 cases were compared to available SAR-derived significant wave height data inside the Persian Gulf. The results confirmed L=125 as the best value for L. Figure(1) is the comparison of model wave height results with/without Data Assimilation with SAR data for the wave heights.

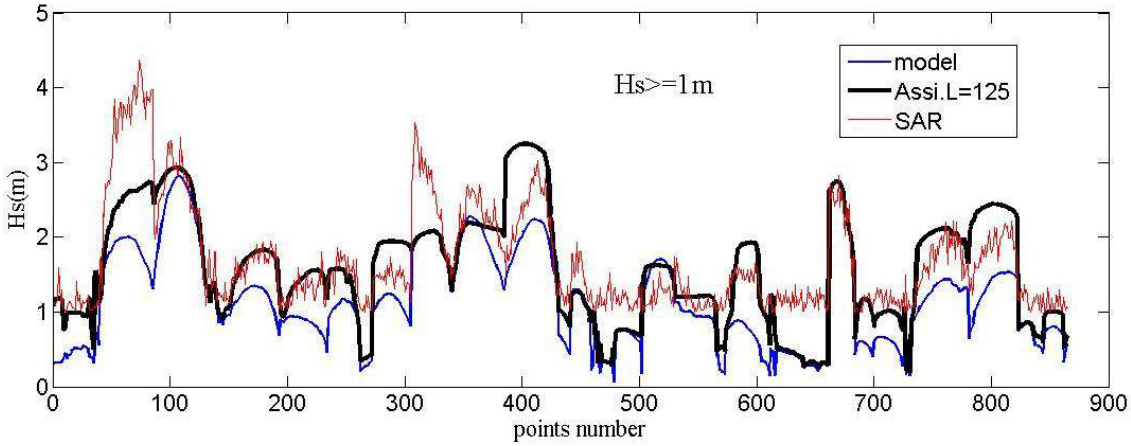

Figure1. Comparison of model, Data Assimilation and SAR outputs for wave heights more than 1m in Persian Gulf

The performance of the used Data Assimilation method was assessed in different cases such as for all wave heights in the whole domain, weight heights more than 1m, for the points with distance under 100 km from Assimilation point (ADCP) and in different values for L parameter.

The results showed 26.3 percent reduction in the RMSE value after applying Data Assimilation and 24.85 percent for wave heights more than 1m.

It was observed that for points closer to Assimilation point, lower values for L shows better performance in Data Assimilation but L=125 km is the best one for the whole domain of this case study.

The effect of Data Assimilation method in the time steps in which there is no observation data for Assimilation point shows the effect of the method comes from previous time steps so the Data Assimilation code which is applied in the model implements a complete temporal and special Data Assimilation for wave field in the WAVEWATCH-III model.

6. References

[1] L. S. Gandin and R. Hardin, *Objective analysis of meteorological fields* vol. 242: Israel program for scientific translations Jerusalem, 1965.

[2] S. Hasselmann, P. Lionello, and K. Hasselmann, "An optimal interpolation scheme for the assimilation of spectral wave data," *Journal of Geophysical Research: Oceans (1978–2012)*, vol. 102, pp. 15823-15836, 1997.

[3] S. Polavarapu, S. Ren, Y. Rochon, D. Sankey, N. Ek, J. Koshyk, *et al.*, "Data assimilation with the Canadian middle atmosphere model," *Atmosphere-Ocean*, vol. 43, pp. 77-100, 2005.

[4] J. Waters, L. R. Wyatt, J. Wolf, and A. Hines, "Data assimilation of partitioned HF radar wave data into Wavewatch III," *Ocean Modelling*, vol. 72, pp. 17-31, 2013.

THE RELATION BETWEEN CURRENT AND WIND IN UPWELLING AREA IN THE EASTERN COASTAL OF CASPIAN SEA USING NUMERICAL SIMULATION

Maryam Shiea[1], Ali-Akbari Bidokhti[2]

1) Faculty of Marine Science and Technology, Science and Research Branch, Islamic Azad University, Tehran, Iran, mshiea@gmail.com
2) Institute of Geophysics, University of Tehran, Tehran, Iran, bidokhti@ut.ac.ir

1. Introduction

The Caspian Sea is the largest inland body of water on the planet and consists of three basins: the northern, middle and southern basins. The sea is located on the northern hemisphere between 36.5 N to 47.2N and 46.5E to 54.1E and receives a yearly input of about 300 $km^3$of fresh water from approximately 130 rivers [1, 2]. In the summer the eastern coast of the middle part of the Caspian Sea experiences an upwelling that is considered to be the most important thermal and dynamical phenomenon. The upwelling area is a region of 20 km wide and extends 10s of km along the coast; also the timescale of such phenomena was about a few weeks. From June to August the advection of cold upwelling waters occur from eastern area of the Caspian Sea [3, 4].

In this study, the relation between surface current and the wind in the eastern coast of middle of the Caspian Sea for 2004 was studied using the three-dimensional ocean model COHERENS (Coupled Hydrodynamical Ecological model for Regional Shelf seas).

2. Methods and Data

The COHERENS model is based on the hydrostatic version of the Navier-Stokes equations. The hydrodynamic part of the model uses the equations of temperature and salinity, and the momentum equations use the Boussinesq approximation, the assumption of vertical hydrostatic equilibrium, and the in compressible continuity equation. The equations of the model are discretised on an Arakawa C-grid. The equations of momentum and continuity that are solved numerically use the mode-splitting technique [5]. The model is run with a 0.046 degrees horizontal resolution and 30 vertical sigma levels. Bathymetry and coastline locations are based on GEBCO data (0.5˚ ×0.5˚), that has been interpolated and slightly smoothed. The model was forced by climatologic six hourly atmospheric forcing. The air temperature and air pressure (0.5˚ ×0.5˚) derived from Reanalyses (ERA- Interim) ECMWF data, wind velocity derived from modification of ECMWF (0.5˚ ×0.5˚) and precipitation rate, cloud cover and relative humidity (2.5˚×2.5˚) derived from NCEP/NCAR re-analysis data. There are three major rivers used in the model and the monthly mean values of the flows for the Volga (has three locations for discharge into the Caspian Sea in the model), Ural, and Kura are given. The salinity of river flow waters was considered to be 0‰. Monthly mean discharge value for each river was obtained from the GRDC (The Global Runoff Data Centre). The model was initialized in winter (January) using monthly mean temperature and salinity climatologies obtained from Kara et al [6]. Total simulation time of the model was five years. The model was first run for four years with six hourly varying climatologic forcing at the sea surface boundaries until a quasi steady state was reached and then extended for another year (2004).

3. Results

During the summer, along the eastern coastal areas of the Caspian Sea, persistent winds blow the north; the effect of wind (speed and direction) plus earth's rotation or the coriolis effects and restriction lateral movements of water cause net movements of surface water at about 90 degree of the right of the wind direction. In fact, Ekman transport moves surface waters away from the coast. Simulation results show that this phenomenon well (Figures 1 and 2). Figures 1 and 2, show the mean monthly current and wind that obtained from simulation results. According these Figures velocity of current and wind have good agreement to each other. Also the ratio of current velocity to wind speed is about 1/50 (~ 0.02) or less than 1/50.

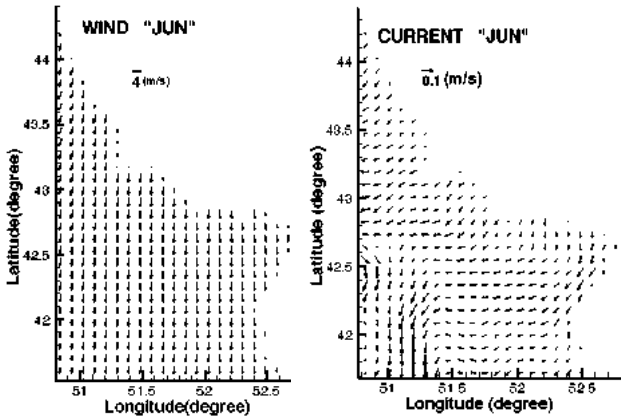

Figure 1. Monthly mean sea surface current (m/s) (right) and wind (left) for the month of Jun.

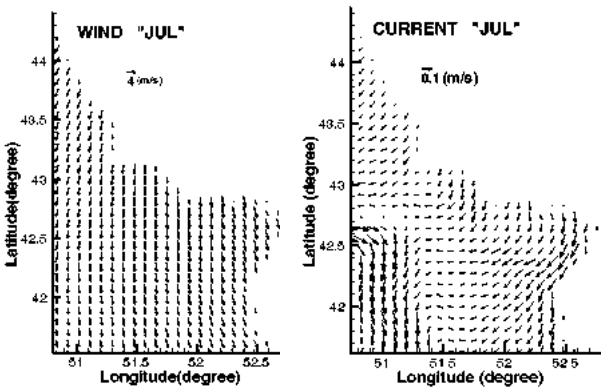

Figure 2. Monthly mean sea surface current (m/s) (right) and wind (left) for the month of July.

On the other hand, due to the surface water moves away from the eastern coast of middle Caspian Sea; surface waters are replaced by waters that well up from below. So the sea surface temperature in this area is considerable reduction. Figure 3 shows the mean monthly sea surface temperature in eastern coast of the middle Caspian Sea for Jun and July, obtained from simulation results. According Figure 3, the sea surface temperature is cooler in eastern coast that represent the upwelling phenomenon in this area.

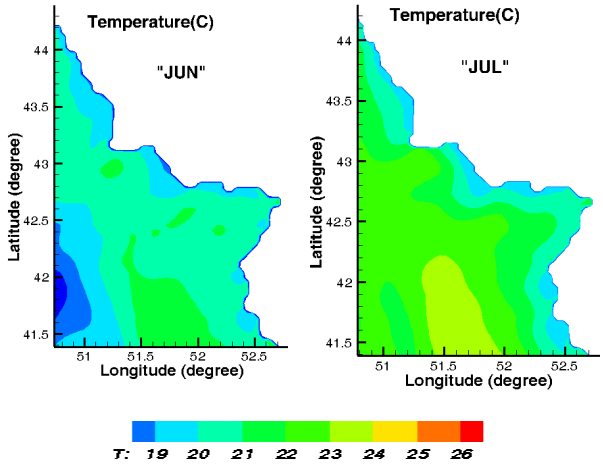

Figure 3. Monthly mean sea surface temperature for the months of Jun (left) and July (right).

Figure 4 shows the sea surface temperature (SST) on the first of July 2004, using the model results and Satellite SST photos (GHRSST level 4 AVHRR) often show relatively colder waters along the coast with filaments penetrating offshore from the upwelling region and these have a relatively good coordination with simulation results on the same day.

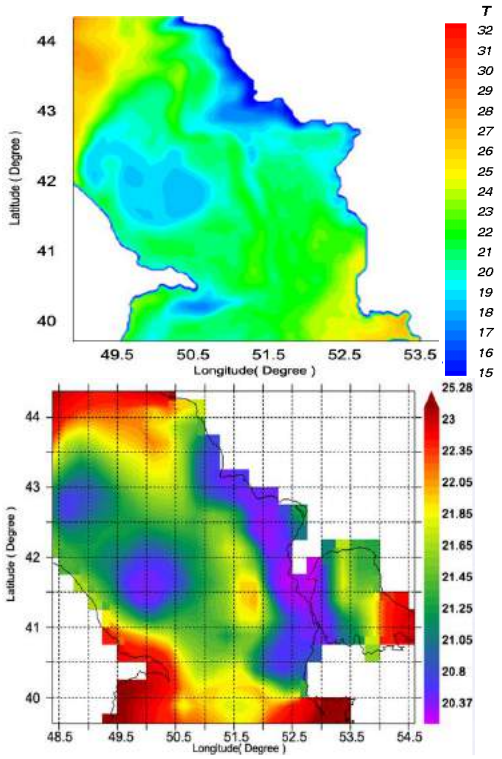

Figure 4. The mean monthly of horizontal temperature for the first day of July (2004) in model (right) and satellite (GHRSST level 4 AVHRR) photos (left).

4. References

[1] Aubrey, D. G. Glushko, T. A. Ivanov, V. A., "North Caspian Basin: Environmental status and oil and gas operational issues, " *Report for Mobil-oil*, 1994.

[2] Aubrey, D.G., "Conservation of biological diversity of the Caspian Sea and its coastal zone, " A proposal the Global Environment Facility", *Report to GEF*, 1994.

[3] Tuzhilkin, V. S. Kosarev, A. N., "Thermohaline Structure and General Circulation of the Caspian Sea Waters, ". In A. G. Kostianov and A. N. Kosarev [editors], *The Caspian Sea Environment (Handbook of Environmental Chemistry)*, p 33-58, 2005.

[4] Shiea, M. Bidokhti, A., "The study of upwelling in the eastern coast of the Caspian Sea using numerical simulation, " *Journal of the Earth and Space Physics*, 41(3), 2015, pp 535-545(in Persian).

[5] Luyten, P. J. Jones, J.E. Proctor, R. Tabor, A. Tett, P. and Wild-Allen, K., "COHERENS- A coupled hydrodynamical-ecological model for regional and shelf seas: user documentation, " *MUMM Rep., Management Unit of the Mathematical Models of the North Sea*, 1999.

[6] Kara, A. B. WallcraftAlan, J. and Metzer E. J. Cunduz, M., "Impacts of freshwater on the seasonal variations of surface salinity and circulation in the Caspian Sea, " *Continental Shelf Research.*, 2010, 30, pp1211-1225.

VEVIFICATION OF ISWM WIND DATA IN THE SOUTHERN CASPIAN SEA

Fereshte Komijani

School of Marine Science and Technology, Khoramshahr Marine Science and Technology University (KMSU), Khoramshahr, IR Iran, Email: fereshtehkomijani@gmail.com

1. Introduction

The Caspian Sea (CS) wave hindcasts has been done in project called Iranian Seas Wave Modeling (ISWM) phase II [2] by forcing a wave model with ECMWF-Operational wind data with grid spacing and temporal resolution of 0.5 degree and 6 hourly, respectively. The ECMWF wind data is calibrated by comparing with wind measurements from synoptic stations and Quikscat satellite and produced ISWM wind filed.

2. Material and Methods

The present study is generally focused on verifying of ISWM wind field and investigating its ability to predict wave characteristics of Southern Caspian Sea' (SCS) by simulating of wave generation with SWAN model.

The CS' bathymetry data was obtained from the GEBCO dataset [6] and computational grid' resolution was considered equal to bathymetry' grid file. Model is forced by ISWM wind data in spatial resolution of 0.5×0.5 deg. Since using the theory of Komen et al. (1984) [4], yields more accurate results for the wave height predictions [3], Komen option was used in the simulation. Collins formulation was used for computing bottom friction and wave growth term of Cavaleri and Malanotte-Rizzoli (1981) [1] was activated. Dissipation due to white-capping, breaking and friction were also included firstly with default values and then, were optimized in the calibration process. Simulations were implemented in several selected periods from 2005 to 2011 years that contained high measured wave. Results were analyzed by comparing time series of modeled and measured wave height, period and directions. For quantitative assessment of the calibration results, error indices (correlation coefficient (CC), scatter index (SI), root mean square error (RMSE)) and Bias were calculated according to the Eqs. (1)–(4) [5]:

$$CC = \frac{\Sigma(x_i - \bar{x})(y_i - \bar{y})}{\sqrt{\Sigma(x_i - \bar{x})^2 \Sigma(y_i - \bar{y})^2}} \quad (1)$$

$$RMSE = \sqrt{\frac{1}{n}\Sigma(y_i - x_i)^2} \quad (2)$$

$$SI = \frac{RMSE}{\bar{x}} \times 100 \quad (3)$$

$$Bias = \bar{y} - \bar{x} \quad (4)$$

in which, x and y are the measured and modeled values, respectively and (¯) is average symbol.

The in-situ wave data used in this study were obtained from four shallow to deep water observational stations. Measured wave height, period and direction data were provided from Buoy sites, which distributed in eastern to western parts of SCS, for calibration and verification of the numerical modeling results. One of these site was located in Neka' nearshore in a depth of about 9 m (at 51.95 E and 37.60 N), also Nushahr sites in middle (51.62 E, 36.70 N and depth of 61 m) and deep water (51.51 E, 37.78 N and depth of 738 m) were in center of SCS as shown in Fig.1. Other buoy was located in 49.52 E and 37.54 N near the Anzali port in depth of 46 m that measured wave height without wave period. The wave height field is represented by Hs and wave period is represented by TM02.

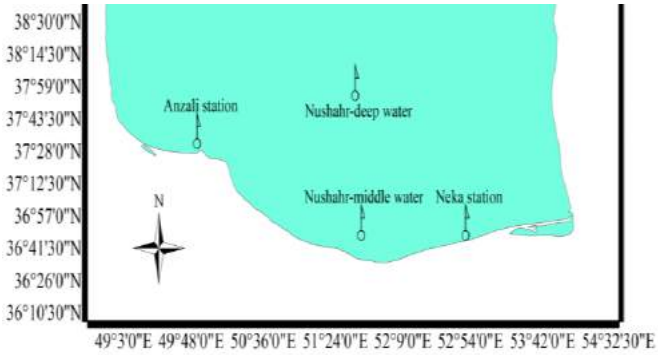

Figure 1. Location of wave observational sites in the SCS

3. Results and Discussions

Time series of measured and modeled wave characteristics in calibration steps are shown in Fig.2 and their computed statistical error indices are given in table 1. Results represent that there is an acceptable correlation (more than %90) between the hindcasted and measured wave height for measured Hs less than 1m. But it underestimated the peak of wave height about %18 (by 1.5m, Fig.2a) in deep water to about %35 (about 1m) in middle water (Fig.2c) and shallow water (Fig.2b) of central and eastern stations by utilizing of ISWM wind data. As shown in Fig.2, while simulated wave period (red dashed lines) has same trend as measurement (red dotted lines), it is underestimating about 1.5 to 2s with Bias more than 1.5s

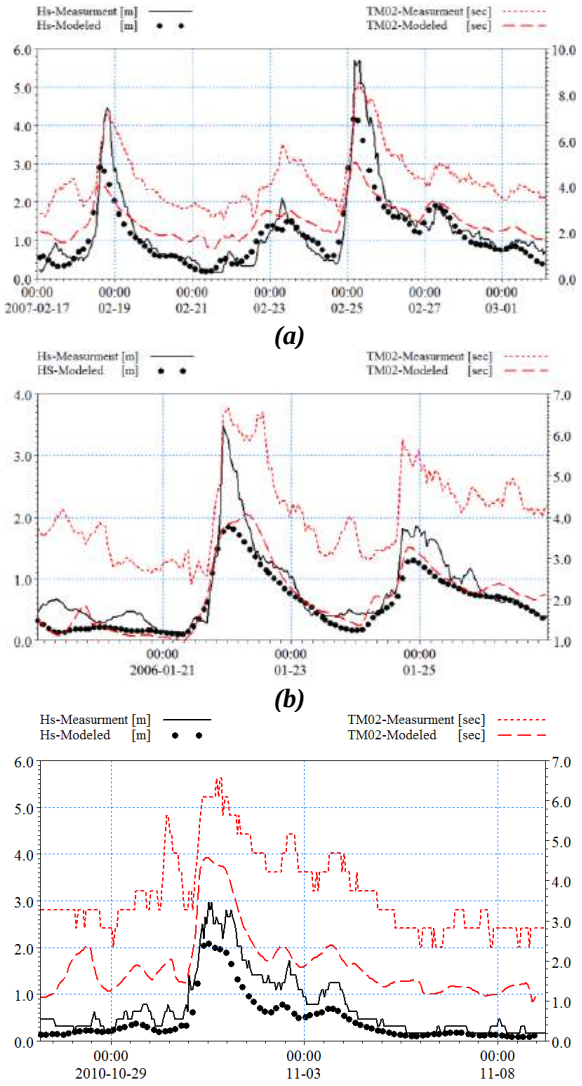

Figure 2. Time series of modeled and measured Hs and TM02, calibration period: (a) in Nushahr deep water, (b) Neka shallow water (c) Nushahr middle water.

Based on results, model' coefficient variations does not have signification effect on wave direction changes (not shown) and reveals wave direction with deviation less than 20 deg from observational wave direction. So simulated dominant wave blows from northwest- north direction, which is same as what shown in measured wave roses. After calibrating the model, it is verified to confirm its reliability. For this purpose, time series of wave characteristics are selected for the period of Feb., 11, 2011 to Feb., 15, in western part of SCS. The results of model verification are indicated in Fig.3 and table 1, shown that SWAN wave model performed well in westen SCS with the lowest Bias (table 1) by using of ISWM wind database. It is concluded duo to this fact that Anzali station' synoptic wind data was used for calibrarating of ISWM wind data in ISWM project [2], directly. It forecasts a rapid Hs increase from less than 0.7 m to exceed 2 m during the measured strong event in Anzali port (as shown in Fig.3). So ISWM wind production increases model accuracy to simulate wave characteristic and picks in western site.

Based on results, coarse spatial and temporal resolutions of ISWM wind filed precisely simulated Hs as waves height is less than 1.5 m but underestimated during storm even. Consequently, using this wind data in extreme event modeling (such as storm surge), will predict low result of wave force and energy and could not simulate extreme wave height, correctly.

Table 1. Statistics of the SWAN model wave parameters in the calibration and verification periods.

Period	Parameter	CC	Bias	RMSE	SI
Calibration 1	Hs (m)	0.92	-0.22	0.48	43
	TM02 (s)	0.86	-1.87	1.97	46
Calibration 2	Hs (m)	0.90	-0.22	0.35	46
	TM02 (s)	0.89	-1.97	2.08	50
Calibration 3	Hs (m)	0.96	-0.29	0.38	51
	TM02 (s)	0.86	-1.84	1.61	50
verification	Hs (m)	0.83	0.11	0.33	47

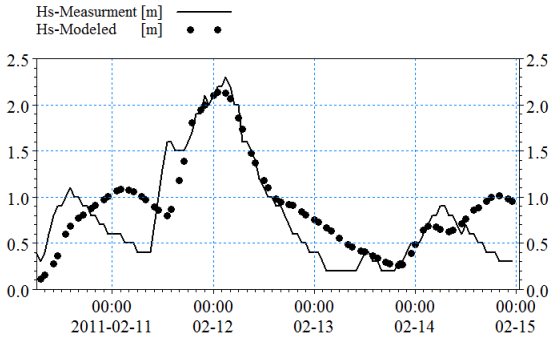

Figure 3. Time series of Hs in Anzali site

4. References

[1] Cavaleri, L., Malanotte-Rizzoli, P., Wind wave prediction in shallow water: theory and applications. J. Geophys. Res. vol. 86 (C11), 10, pp. 961–10, 973-10, 1981.

[2] Mazaheri, s., Hajivaliee, F., Kamranzad, B., Wave Atlas of Persian Gulf, Oman Sea and Caspian Sea, Phase II, Iranian national Institute for Oceanography and Atmospheric Science. ISSN: 392.105.01. P 74, 2013.

[3] Moeini, M.H., Etemad-Shahidi, A., Application of two numerical models for wave hindcasting in Lake Erie. Appl. Ocean Res, vol. 29, pp. 137–145, 2007.

[4] Moeini, M.H., Etemad-Shahidi, A., Chegini, V., Rahmani, I., Wave data assimilation using a hybrid approach in the Persian Gulf. Ocean Dynamics, vol. 62, pp. 785–797, 2012.

[5] Zanaganeh, M., Mousav, S.M., and EtemadShahidi, A.F., "A hybrid genetic algorithm–adaptive network-based fuzzy inference system in prediction of wave parameters", Engineering Applications of Artificial Intelligence, Vol. 22, pp. 1194–1202, 2009.

[6] http://www.gebco.net/.

NUMERICAL SIMULATION OF WIND-INDUCED WAVES DURING SUMMER MONSOON IN THE NORTH-WESTERN INDIAN OCEAN

Farrokh Alavian Ghavanini [1], Mohammad Hossein Kazeminezhad [2]

1) Iranian National Institute for Oceanography and Atmospheric Science, Tehran, IRAN, ghavanini@inio.ac.ir
2) Iranian National Institute for Oceanography and Atmospheric Science, Tehran, IRAN, mkazeminezhad@inio.ac.ir

1. Introduction

In ocean state forecasting, the most important subject is to forecast the status of ocean waves which are mainly driven by the effect of wind over the ocean surface. Needless to say that ocean state forecasting - for a specific period of time - is almost impossible without using the high computational power of today's computers. One of the well-known computational models for modelling and predicting deep water waves is NOAA's WAVEWATCH III™ (WWIII). Different methods and parametrizations can be employed in WWIII for modelling of the wind-sea interaction and wave dissipation in deep water such as WAM3 (WAMDI Group, 1988), Tolman and Chalikov (Tolman et al., 1996), WAM4 (Komen et al., 1994) and BJA (Bidlot et al., 2005).

Several studies have been carried out to investigate the capability of these parameterizations in the wave simulation over different water bodies which indicate that the BJA parametrization results in better simulation of ocean waves. WWIII manual (Tolman et al., 2014) also expresses that the BJA parametrization is generally better than the others and mentions that "A more recent modification [BJA], strongly improved the model results for Pacific swells, at the price of an underestimation of the highest sea states".

The main goal of this study is to evaluate the capability of WWIII model in the wave forecasting of the Arabian Sea. To do so, Indian Ocean and Arabian Sea region were selected as the main computational domain with coordination of 15 S and 31 N, 31 E and 80 E. In this region the most severe waves are generated during the monsoon period. The summer monsoon in the region extends from June to September and also generates higher waves than winter monsoon. Therefore, model validation has been carried out for the summer monsoon. As for input of the model, NOAA's NCEP/GFS global forecast system wind with resolution of 0.5x0.5 degrees and 3-hour time steps has been used. Numerical simulation has been performed for the period of June 20th to August 2nd 2015. Also 1-Minute Gridded Global Relief Data (ETOPO1) has been used for bathymetry data. The computational grid was set to rectangular (considering spherical coordination) with resolution of 0.1x0.1 degrees. 29 frequencies discretized the spectral space ranging from 0.035 to 0.55 Hz with resolution of 15 degrees (24 directions). The time steps amounts were also set as 1200, 600, 600 and 15 seconds for the global, intra-spectral, spatial and source term integration, respectively. At the end, to examine the model's accuracy, the simulated results were compared with the Ku-Band's significant wave heights (SWH) measured by JASON-2 satellite from its three swept tracks (55,131,207). Figure 1 shows significant wave height (Hs) obtained from a satellite pass on track 55 in addition to Hs values calculated from different model settings which indicates that WWIII model results have a good conformity with the trend of altimetry data although with different settings. As another assessment, Figure 2 is represented to show the correlation between accumulations of data generated by model with BJA setting versus JASON-2 altimetry data from multiple tracks ($r = 0.9246$). As result, and by analysis of the data obtained from satellite together with data calculated from different model settings, WWIII model, with BJA setting, has a better consistency in simulation of wave-induced ocean waves on the selected region and conditions.

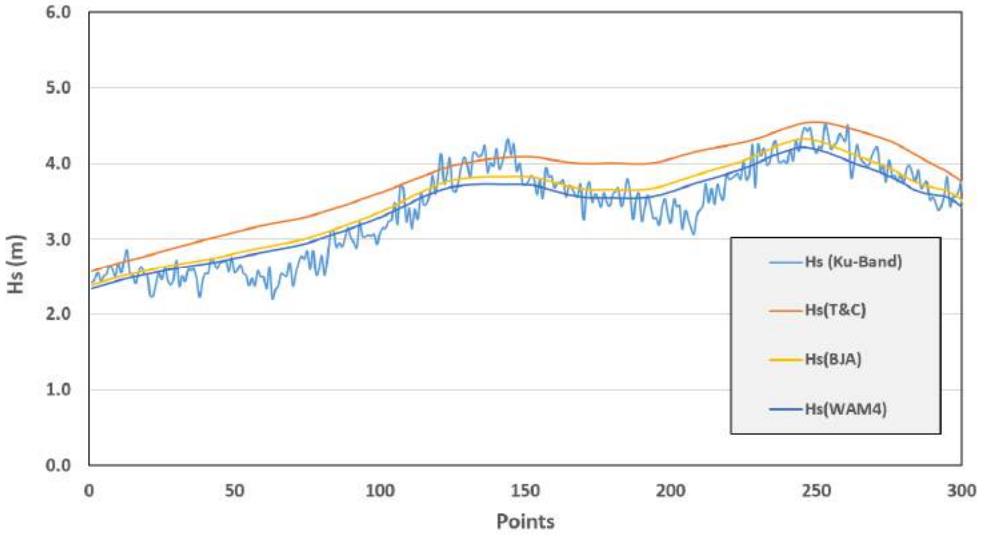

Figure 1. Comparison of altimetry data with model computed data.

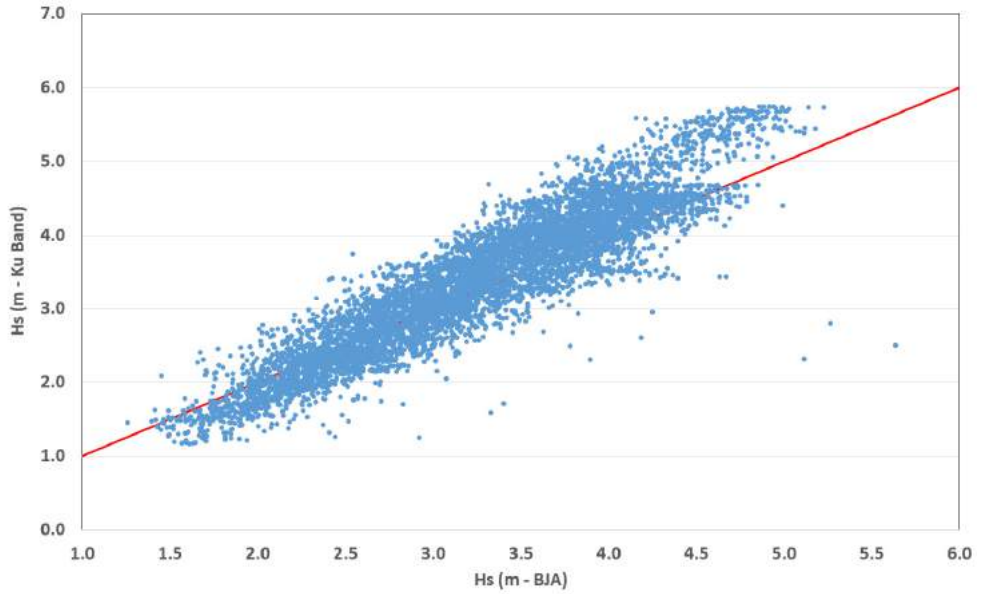

Figure 2. Correlation between altimetry data and computed data from model with BJA setting.

2. References

[1] Komen, G.J., Cavaleri, L., Donelan, M., Hasselmann, K., Hasselmann, S., Janssen, P.A.E.M. "*Dynamics and Modelling of Ocean Waves*", Cambridge University Press, 532 pp., 1994.

[2] Tolman H.L., "*User manual and system documentation of WAVEWATCH III™ Version 4.18. Technical Note*", Available from: ⟨http://polar.ncep.noaa.gov/waves⟩, 2014.

[3] Tolman H.L., Chalikov D.V., "Source terms in a third-generation wind-wave model", *Journal of Physical Oceanography*. 26 (2), 497–518, 1996.

[4] WAMDI Group, "The WAM model-A third generation ocean wave prediction model", *Journal of Physical Oceanography*, 18, 1775-1810. 1988

HYDRAULIC MODEL TESTS ON WAVE ATTENUATION BY COASTAL VEGETATION

Sanaz Hadadpour[1], Andreas Kortenhaus[2], Hocine Oumeraci[3] and Hisham Elsafti[4]

1) Leichtweiss-Institute for Hydraulic Engineering and Water Resources (LWI), Department of Hydromechanics and Coastal Engineering, Technische Universität Braunschweig, Braunschweig, Germany, s.hadadpour@tu-braunschweig.de
2) Faculty of Engineering and Architecture, Department of Civil engineering, Ghent University, Zwijnaarde/Ghent, Belgium, Andreas.Kortenhaus@UGent.be
3) Leichtweiss-Institute for Hydraulic Engineering and Water Resources (LWI), Department of Hydromechanics and Coastal Engineering, Technische Universität Braunschweig, Braunschweig, Germany, h.oumeraci@tu-braunschweig.de
4) Leichtweiss-Institute for Hydraulic Engineering and Water Resources (LWI), Department of Hydromechanics and Coastal Engineering, Technische Universität Braunschweig, Braunschweig, Germany, h.el-safti@tu-braunschweig.de

1. Introduction

Coastal areas are very complex and sensitive regions, which are extremely important in terms of economic, social and environmental value. Hence, providing protection against coastal erosion becomes one of the most significant current issues and a large amount of studies have been conducted on the development of shore protection concepts and approaches. In addition to structures such as jetties and breakwaters, which can protect the shoreline by dissipating and reflecting wave energy, vegetation role in shore protection is recently considered. Coastal vegetation is able to enhance wave attenuation [1-2] and hence, there is a potential to use vegetation for coastal protection purposes.

Although it was found that coastal vegetation plays a major role in wave energy attenuation and thus in natural shore protection, engineering evaluation or design related information regarding plants exposed to waves are still lacking. Therefore, this study aims to focus on some types of coastal vegetation, seaweeds, due to their applications in different industries as well as for coastal protection, and to investigate their interactions with waves and their wave attenuation performance.

2. Methodology

Hydraulic model tests have been carried out in the 1-m wide flume of Twin Wave Flume (TWF) at the Leichtweiss Institute (LWI), TU Braunschweig to study the effect of vegetation parameters (density and flexibility) and wave parameters (wave height and period) on wave attenuation. A series of experiments was performed for regular waves propagating over an artificial seaweed field, with a length of 4.2 m, in order to reproduce wave conditions of the North Sea. For this purpose, two different types of materials (rigid and flexible) were used for preparing the artificial seaweeds. Moreover, two different densities of the seaweed field (i.e. 10 lines and 5 lines of artificial seaweeds) were considered. Figure 1 shows the model set-up in the TWF of LWI.

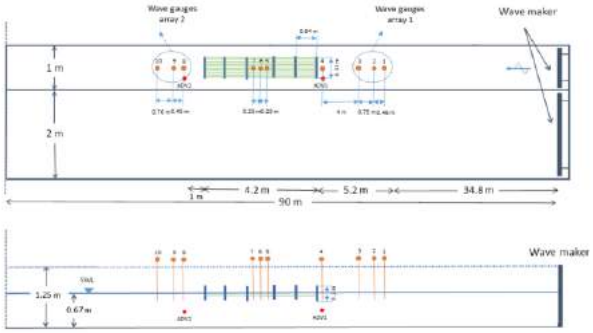

Figure 1. The experimental set-up in the TWF of LWI: (a) Plan view (b) Longitudinal cross section view.

3. Results

The wave analysis was performed on each time series measured in the wave flume using L-Davis (LWI Data Analysis and Visualization Software) tools. The percentage of wave height reduction within the seaweed field was determined as:

$$\%\ \text{Reduction} = \left(\frac{H_{i,behind} - H_{i,front}}{H_{i,front}} \right) \times 100 \qquad (1)$$

where $H_{i,front}$ and $H_{i,behind}$ are the measured wave height in front of and behind the seaweed field, respectively.

To investigate the influence of vegetation characteristics on wave damping, the percentage of wave height reduction versus two different materials used for preparing artificial seaweed was plotted. Figure 2 show these graphs for 5 lines and 10 lines of seaweed including eight different combinations of wave heights and periods.

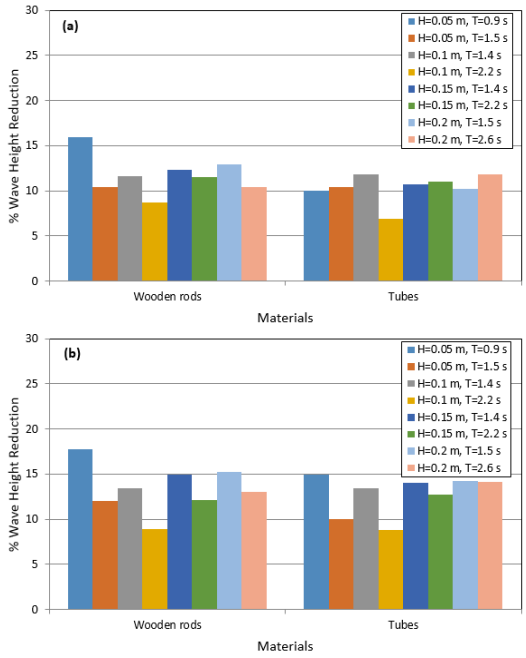

Figure 2. The percentage of wave height reduction for (a) 5 lines and (b) 10 lines of seaweed.

The energy attenuation through the first half and last half of the seaweed field, as well as the total energy loss for two different materials, including two densities (i.e. 5 lines and 10 lines of seaweed) is summarized below in Tables 1.

Table 1. Wave height reduction through the first and last half of seaweed field.

Density	H_{m0}	T_p	Wooden rods			Tubes		
			First Half	Last Half	Total	First Half	Last Half	Total
5 Lines	0.05	0.9	10.75	7.63	15.95	6.94	4.39	10.02
		1.5	8.66	2.14	10.42	7.27	3.51	10.42
	0.10	1.4	8.60	3.44	11.58	8.71	3.59	11.83
		2.2	6.76	2.10	8.75	5.53	1.43	6.90
	0.15	1.4	9.56	3.41	12.35	9.72	1.53	10.72
		2.2	9.71	1.95	11.53	8.25	2.84	10.99
	0.20	1.5	10.37	3.21	12.95	9.28	1.43	10.26
		2.6	9.83	0.66	10.40	9.30	2.69	11.86
10 Lines	0.05	0.9	12.07	8.45	17.71	10.65	6.52	14.93
		1.5	8.43	4.03	12.00	8.43	1.92	10.00
	0.10	1.4	10.21	3.79	13.40	10.21	3.79	13.40
		2.2	6.83	2.18	8.90	7.09	1.82	8.80
	0.15	1.4	10.16	5.57	14.92	12.53	2.32	14.07
		2.2	11.19	1.10	12.17	10.32	2.61	12.76
	0.20	1.5	10.99	5.07	15.26	13.29	1.62	14.21
		2.6	11.28	1.89	13.00	10.06	4.25	14.11

To investigate the effect of the field width on attenuation, the percentage of wave height reduction is plotted against relative field width, B/L, for 10 lines of different materials, which are shown in Figure 3.

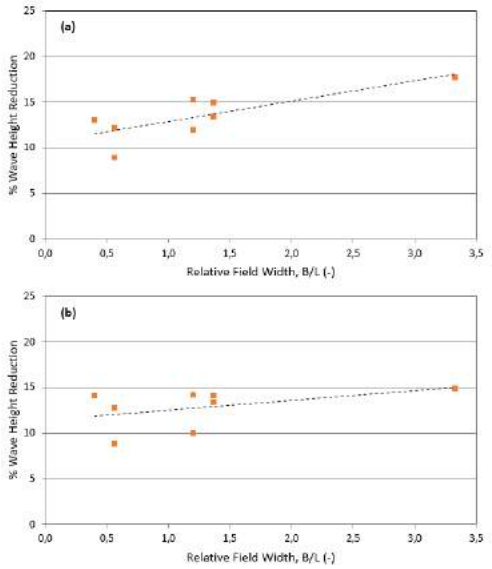

Figure 3. Wave attenuation (determination of relative field width) for 10 lines of (a) Wooden rods and (b) Tubes.

4. Conclusions

The wave height reduction showed the same trends for both materials (rigid and flexible), which were used for preparing the artificial seaweeds. The results show how the vegetation density affects wave attenuation: with the higher vegetation density (10 lines of seaweeds) the wave height decreases only by 1- 4% more than the lower density with 5 lines of seaweeds. In addition, it was found that the vegetation stiffness also affects the amount of wave height damping: with rigid members, in most cases, the wave height is reduced by an extra 1- 3% compared to flexible members. As expected, the longer vegetation field resulted in the higher wave energy attenuation.

The experimental results show a total wave height reduction of nearly 7- 16% through the total length of the seaweed field. About 6- 13% reduction occurred in the first half of the seaweed field, while in the last half the decrease of the wave height was only around 1- 8%.

5. Acknowledgments

The authors would like to gratefully acknowledge the financial support of this study by the EU within the MERMAID project (FP7-OCEAN.2011-1 "Multi-use offshore platforms"). We also gratefully acknowledge the continuous support and help of Jan-Joost Schouten from Deltares and Dr. Maike Paul through this project.

6. References

[1] Augustin, L. N., Irish, J. L. and Lynett, P., "Laboratory and numerical studies of wave damping by emergent and near-emergent wetland vegetation", *Coastal Engineering*, 56, 2009, pp. 332-340.

[2] Méndez, F. J. and Losada, I. J., "An empirical model to estimate the propagation of random breaking and nonbreaking waves", *Coastal Engineering*, 51(2), 2004, pp. 103-118.

VOLUME TRANSPORT ALONG KIMBERLEY SHELF IN NORTH-WEST AUSTRALIA

Mohammad Hadi Bahmanpour[1], Charitha Pattiaratchi[1], E.M.S Wijeratne[1], Craig Steinberg[2] and Nick D'Adamo[3]

1) School of Civil, Environmental and Mining Engineering & UWA Oceans Institute, The University of Western Australia, Perth, Australia, mohammadhadi.bahmanpour@research.uwa.edu.au
2) Australian Institute of Marine Science, Townsville, Australia, C.Steinberg@aims.gov.au
3) Intergovernmental Oceanographic commission, Perth Regional Programme Office of the UNESCO, Perth, Australia, N.D'Adamo@bom.gov.au

1. INTRODUCTION

North West shelf of Australia (NWS) is a relatively wide shelf compared to other shelves of Australia and covers the area between Timor Sea and North West Cape [*6*]. NWS is named as an oceanographically complex region and knowledge of its circulation is limited [*2*]. This study presents the results of multi-year observation of current profiles and volume transport across Kimberley transect in North-West Australia (Figure 1).

Previous works on the circulation of NWS have identified a mean annual flow of ~1 Sv to the south-west, i.e., Holloway Current [4, 1], confined to the southern parts of the shelf. In this study, we seek to answer whether the same flow is observable in our data in the middle of the shelf.

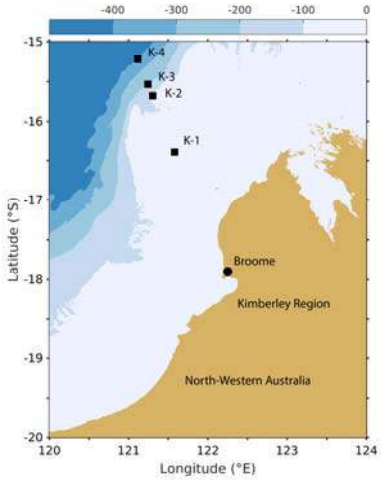

Figure 1. Map of the study area and mooring locations

2. DATA AND METHODS

Data used in this study comes from 4 moorings installed at depths 50,100, 200 and 400 m. Mooring data are part of IMOS (Integrated Marine Observing System) mooring network in North West Australia to study boundary currents within the shelf edge. Each mooring has an Upward-looking ADCP near the bottom and measures current profiles in eastward (u) and northward (v) direction. The data is freely available to the scientific community for scientific research and is available from http://thredds.aodn.org.au/thredds/catalog/IMOS/ANMN/QLD/catalog.html.

Spectral analysis of hourly original time series shows that the data is highly tidal and have a peak at semi-diurnal frequency (~12 h) (Figure 2). There is also significant variance in the seasonal band (period of several months). Since the aim of this study is to analyze mean flow, a low-pass filter with cut-off frequency of 40 h was used to remove inertial and higher frequency variability. The data is then rotated ~40° to get the alongshore and cross-shore component of the flow. The data were then sub-sampled at daily intervals for further analysis. Monthly averages are constructed if there is more than 15 days of data available in a month. Volume transport calculations were performed by first integrating the velocities vertically and then horizontally across the transect similar to the method of *Holloway* [3]. Volume transport calculations were performed for months when all moorings across the transect had returned useful data.

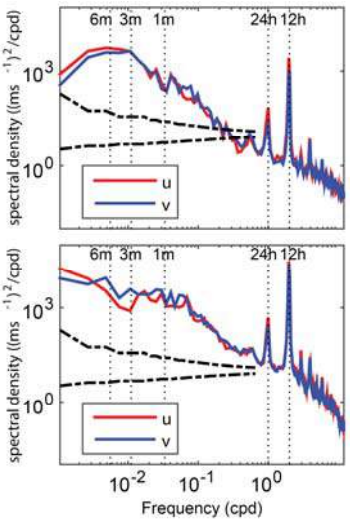

Figure 2. Spectral analysis of K-4 (top) and K-2 (Bottom) stations. Dashed line shows 95% confidence intervals for spectral estimates.

3. RESULTS AND DISCUSSION

Daily velocity stick plots show a general feature among all 3 stations to have south-westward flow which is at times stronger (Figure 3). The same feature is not evident in the KIM-400 station (not shown). The south-westward flow is more evident in the 2 middle stations (K-2 and K-3). The very strong flow observed in the shallowest station near Jan 2014 is due to the passage of a tropical cyclone (Figure 3c).

Maps of monthly alongshore velocities are presented in Figure 4. The negative south-westward flow is stronger in Autumn (Apr-Jun) with its core centered on the shelf edge (Holloway Current). At this time, Holloway current velocity reaches 0.1-0.15 m/s. There is a secondary peak in Oct-Nov which is located offshore of the first peak. There is a relatively strong undercurrent at depths>200 m which at times reaches the surface (Jul-Sep) when the winds have a strong southerly component.

Volume transport calculations show an annual mean net transport of 0.5 Sv to the south-west (Figure 5). South-westward transport reaches 1.2 and 1 Sv in Jun 2013 and Mar 2014, respectively and shows strong inter-annual variations. There is also a peak of 1 Sv in Oct 2012 which is related to the secondary peak mentioned earlier in the text. The reason for smaller transports compared to what reported by *Bahmanpour et al*. [1] is in the existence of the undercurrent seen in Figure 4 in the calculations that tend to cancel out the flow to the south-west.

The observed seasonality of Holloway current which is stronger in Austral Autumn is in phase with the passage of an anomalous high sea level pulse that seems to be originated in the Gulf of Carpentaria [5]. Each year, sea level builds up in Gulf of Carpentaria due to monsoon winds and when winds relax in March, sea level pulse releases south-westward along the shelf edge wave guide and causes the currents to respond consecutively. The same mechanism is proposed for the southern transect in the work of *Bahmanpour et al.* [1]. Therefore, these two transects seem to be connected and acts like a unified system in the low-frequency band, although they are more than 700 km apart.

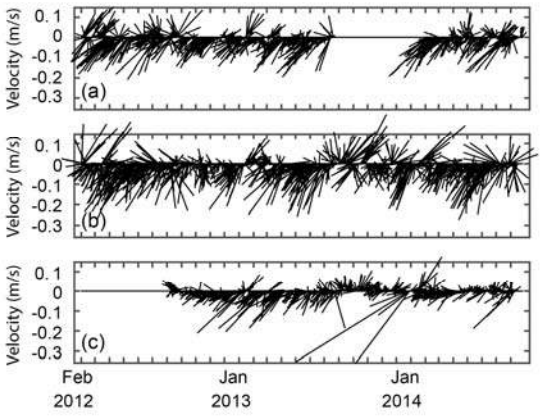

Figure 3. Daily velocity stick plots for K-3 (a), K-2 (b) and K-1 (c) stations.

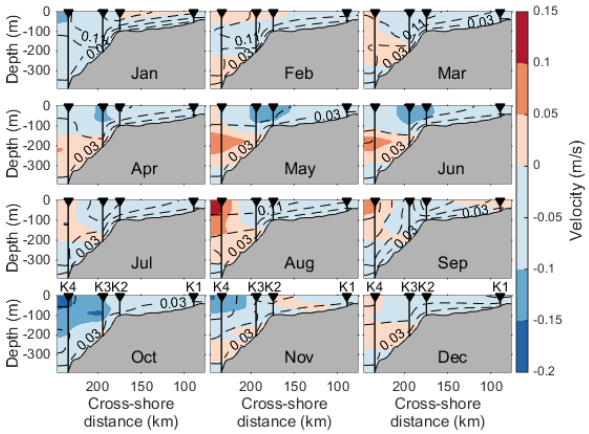

Figure 4. Maps of monthly alongshore velocities. Negative is toward south-west. Dashed contour represent standard deviation values.

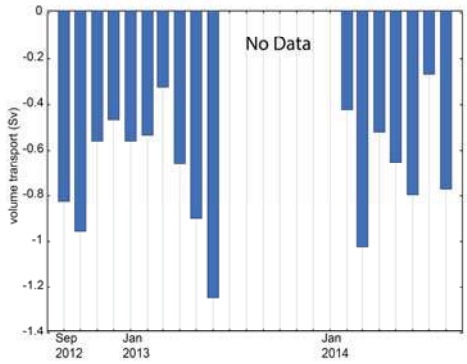

Figure 5. Alongshore volume transport across Kimberley transect. Negative is toward south-west.

4. REFERENCES

[1] Bahmanpour, M. H., Pattiaratchi, C., Wijeratne, E.M.S., Steinberg, C., and D'Adamo, N., "Multi-Year Observation of Holloway Current along the Shelf Edge of North Western Australia", *Journal of Coastal Research.*, 2016, 517-521.

[2] Godfrey, J. S., and Mansbridge, J.V., "Ekman transports, tidal mixing, and the control of temperature structure in Australia's northwest waters", *Journal of Geophysical Research*, 105(C10), 2000, 24021-24044.

[3] Holloway, P. E., "Leeuwin current observations on the Australian North West Shelf, May–June 1993", *Deep Sea Research Part I: Oceanographic Research Papers*, 42(3), 1995, 285-305.

[4] Holloway, P. E., and Nye, H., "Leeuwin current and wind distributions on the southern part of the Australian North West Shelf between January 1982 and July 1983", *Marine and Freshwater Research*, 36(2), 1985, 123-137.

[5] Ridgway, K. R., and Godfrey, J.S., "The source of the Leeuwin Current seasonality", *Journal of Geophysical Research: Oceans*, 120, 2015, 6843-6864.

[6] Webster, I., "Wind-Driven Circulation on the North West Shelf of Australia", *Journal of Physical Oceanography*, 15(11), 1985, 1357-1368.

NEAR-SHORE CIRCULATION AND WATER MASS STRUCTURE IN THE SOUTH-EASTERN PART OF THE BALTIC SEA

Alexander Demidov[1], Nikita Rykov[2]

1) Department of Oceanology, Moscow State University, Moscow, Russia, alik1@mail.ru
2) Atlantic branch, P.P. Shirshov Institute of Oceanology, Kaliningrad, Russia, tin2006@inbox.ru

The water in the Baltic Sea is composed by a two-layer structure - the deep layer and the surface one. There are, however, differences in the near shore zone associated with bottom relief, seasonality and weather conditions. During joint expeditions of Moscow State University, Moscow Institute of Physics and Technology and Baltic Federal University in 2009-2016, we carried out ADCP measurements in more than 1000 CTD stations along the shore of Sambian peninsula near Kaliningrad (See Figure 1).

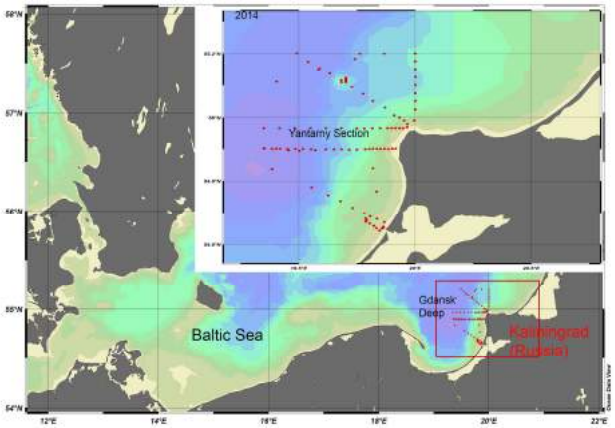

Figure 1. Map of work area

The main characteristic of the hydrological structure of the Baltic Sea water, is a flow of warm and salty water from the North Sea in the bottom layer. The thermohaline structure of coastal waters is influenced by factors such as heat input from the atmosphere, river runoff, heat transfer processes of vertical mixing. Meteorological processes also plays an important role on the thermohaline structure of coastal waters.

The thermohaline structure of the waters of this region, discovered during the expeditions (See Figure 2), consists of three layers: the top of the stratified warm layer, cold intermediate layer and the lower layer of saltier waters of the North Sea.

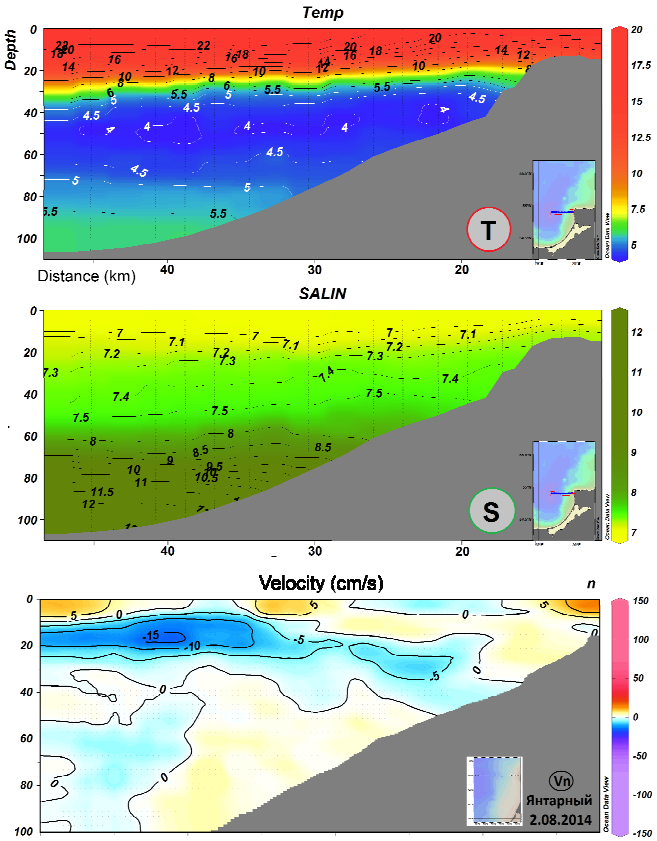

Figure 2. Temperature, salinity and current velocity distribution in the "Yantarny" section (2.8.2014)

On the TS-diagram (See Figure 3) is well represented the variability of the hydrological structure of the waters in the region: we see the presence of the cold intermediate layer with temperature of 4° C, the flow of relatively warm and salty waters of the North Sea and the warm surface layer, characterized by low salinity values.

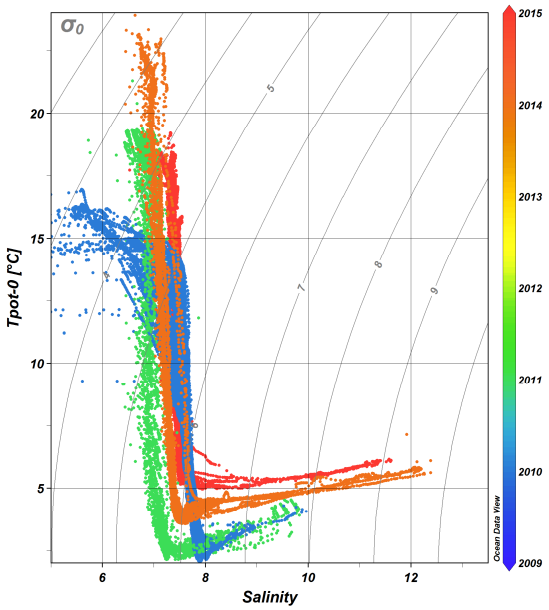

Figure 3. T,S- diagram for 2009-2015 measurements

In 2014, at the core of the cold intermediate layer the temperature was of about 4° C, this is 2° C higher than found in previous expeditions in 2009-2011, due to the interannual variability of temperatures during the cold season, found during the formation of the cold intermediate layer. In 2015 there was an extremely change in the depth of this layer (below 50 m).

Halocline was observed in deep-water sections at 60-80 m. At the sea bottom, salinity values in some cases reach 13 psu, this lower more salty layer originates advection processes of North Sea waters movements. Measurements done in 2014-15 years, confirm the presence of a Major Baltic Inflow, which is accompanied by the absence of H_2S.

Direction of surface currents depends on prevailing wind direction. In general, there is north transfer along the western coast of the peninsula. Therefore, we described the summer vertical structure of coastal waters in the south-eastern Baltic Sea and create coastal current scheme for each year (See Figure 4).

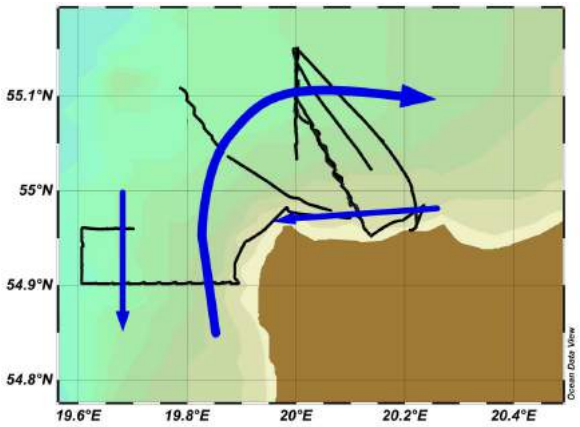

Figure 4. Scheme of coastal currents in August 2015 based on ADCP data

The work was supported by Russian Geographical Society.

SIMULATION OF SOLITARY WAVES CAUSED BY PADDLE WAVE-MAKER USING MODIFIED MOVING PARTICLE SEMI IMPLICIT METHOD

Masoud Arami-Fadafan[1], Masoud-Reza Hessami-Kermani[2]

1) Ph.D. Student, Department of Engineering, Faculty of Civil Engineering, Shahid Bahonar University of Kerman, Kerman, Iran, Aramimasoud@Eng.uk.ac.ir
2) Assistant Professor, Department of Engineering, Shahid Bahonar University of Kerman, Kerman, Iran. Hessami@uk.ac.ir

1. Introduction

Numerical methods may be classified into two generally mesh based methods and particle methods. Utilizing MPS method , originally developed by Koshizuka and Oka [1], similar to other mesh-free methods, problem of mesh adaptability and connectivity eliminated; because in this methods, the state of a system is represented by a set of discrete particles, without a fixed connectivity [2]; hence, such methods are inherently well suited for the analysis of large deformations and fragmentations. The original form of MPS method suffers from spurious oscillations in pressure and density fields. Therefore, different modifications are suggested to improve the computational pressure fields [2-8]. In this study a modified incompressible MPS method is used to simulate a solitary wave rushing inland and collapse near the shoreline. Proposed MPS method utilizes one row of wall boundary condition (no dummy/ ghost particle defined in wall boundary condition). Moreover, proposed Poisson equation of pressure is very similar to original one and is similar to the second term of PPE defined in [6] except in the dominator of the equation. This matter proves our suggested method. Actually our method may be consider as a special case of PPE in [6].

2. Governing equations

The governing equations of viscous fluid flows that are mass and momentum conservation equations are presented in the following:

$$\frac{1}{\rho}\frac{D\rho}{Dt}+\nabla.\mathbf{u}=0 \tag{1}$$

$$\frac{D\mathbf{u}}{Dt}=-\frac{1}{\rho}\nabla P+\frac{\mu}{\rho}\nabla^2\mathbf{u}+\vec{g} \tag{2}$$

Where ρ is the density, $\mathbf{u}$ is the velocity vector, t is the time, P is the pressure, μ is the dynamic viscosity and g is the gravitational acceleration.

3. Kernel function

In Lagrangian method such as MPS, an interpolation kernel function with a support size is implemented to represent any field of quantity utilizing its values on a set of disordered neighbor particles. It is possible to use any kernel function in the calculations with following specific properties such as positivity, compact support, unity, monotonically decreasing and delta function behavior [9]. In this study, the following weight functions was used:

$$w(r_{ij},r_e)=\begin{cases}\dfrac{r_e}{r_{ij}}-1 & 0\le r_{ij}<r_e\\ 0 & r_{ij}\ge r_e\end{cases} \tag{3}$$

4. Temporal discretization

Each time step is divided into two steps namely prediction and correction steps. In the first step, the provisional velocity and position of particles are calculated using governing equations considering MPS discretization. In the second step effect of the pressure is considered following chart depicts algorithm of the modified MPS method.

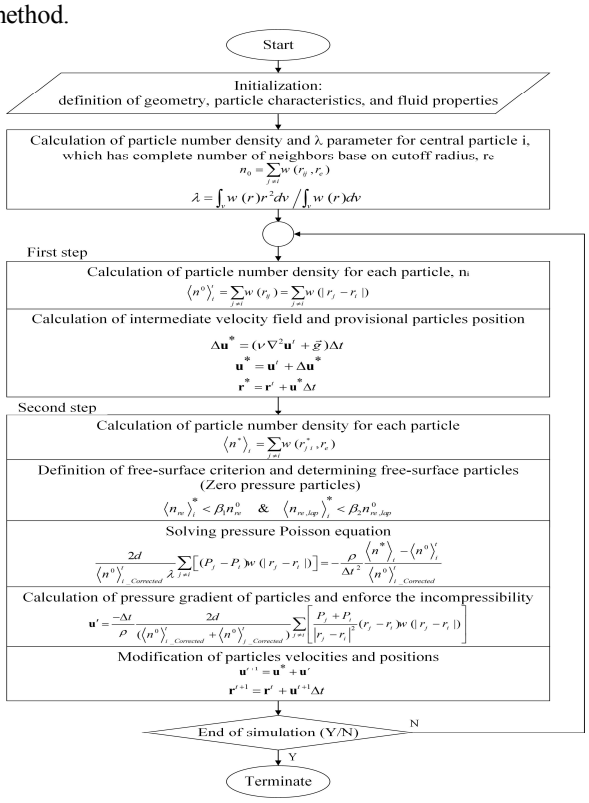

Figure. 2. Proposed MPS algorithm

5. Model Application

In this example, a solitary wave caused by a paddle wave-maker is simulated using proposed I-MPS method. Experimental measurements of Hsiao and Lin [10] are used to compare with the simulated problem results. In the experiment, beach has a slope of 1:20 and a trapezoidal caisson with seaward 1:4 and landward 1:1.8 slopes is considered as a breakwater. The seawall was starting at a horizontal distance of 3.6 m from the beach toe. Initial geometry of the problem is shown in Fig. 3. Initial particle spacing is selected equal to 0.015 m and a constant time step size of 0.0015 s is used to solve the problem.

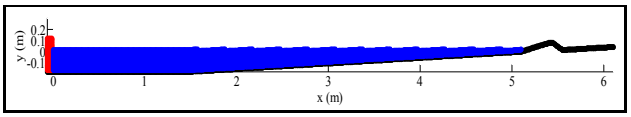

Figure 3. Initial geometry of paddle wave-maker problem

History times of velocity and displacement of wave-maker paddle for a wave height of 0.07 m and water depth of 0.2 m are depicted in Fig. 4.

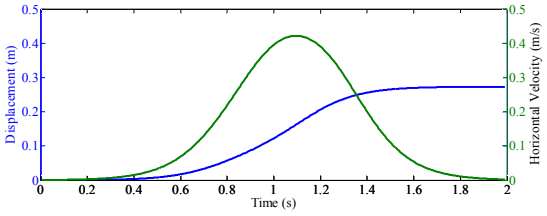

Figure 4. Time series of the displacement and horizontal velocity of the paddle wave-maker

In this problem, generated wave rushing inland and collapses near the shoreline due to near-shore breakwater and overtopping the seawall. In the experiment free-surface elevation was recorded using several gauges at different places along the flume and a reference wave gauge was fixed at 1.1 m in front of the beach toe. Results of the mentioned gauge are used to compare between experimental and numerical wave height. Fig.5 shows these comparisons.

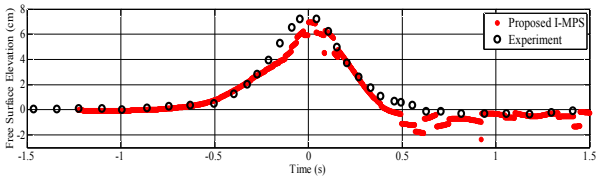

Figure 5. Comparison between experimental and numerical wave height at reference wave gage

Fig. 6 shows spatial snapshots of the solitary wave during its movement. Propagated wave is perspicuous at the beach toe in top part of this figure, which maximum pressure occurred in this area.

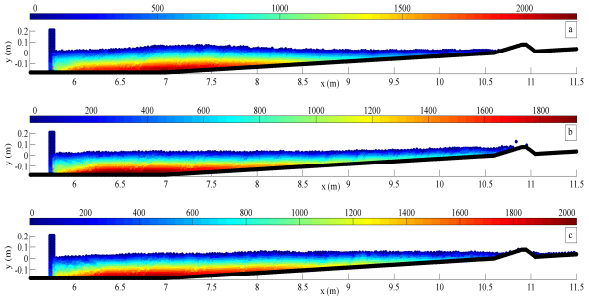

Figure. 6. Computational pressure fields using proposed I-MPS at a) t=0.87, b) t=3.01 and c) t= 5.67 s

6. References

[1] Koshizuka, S., and Oka, Y., "Moving Particle Semi-implicit method for fragmentation of incompressible fluid", *Journal of Nuclear Science and Engineering*, Vol. 123, 1999, pp. 421-434.

[2] Asai, M., Aly, A.M., Sonoda, Y., and Sakai, Y., "A Stabilized Incompressible SPH Method by Relaxing the Density Invariance Condition", *Journal of Applied Mathematics*, 2012, Article ID 139583, 24 pages.

[3] Gotoh. H., Khayyer, A., Ikari, H., Arikawa, T. and Shimosako, K. "On enhancement of Incompressible SPH method for simulation of violent sloshing flows", *Journal of Applied Ocean Research*, Vol. 46, 2014, pp. 104-115.

[4] Khayyer, A., and Gotoh, H. "Modified Moving Particle Semi-implicit methods for the prediction of 2D wave impact pressure", *Journal of Coastal Engineering*, Vol. 56, 2009, pp. 419-440.

[5] Khayyer, A. and Gotoh, H. "A higher order Laplacian model for enhancement and stabilization of pressure calculation by the MPS method", *Journal of Applied Ocean Research*, Vol. 32, 2010, pp. 124-131.

[6] Kondo, M., and Koshizuka, S. "Improvement of stability in moving particle semi-implicit method", *International Journal for Numerical Methods in Fluids*, Vol. 65, 2011, pp.638-654.

[7] Kondo, M., Suto, K., Sakai, M., and Koshizuka, S. "Incompressible free surface flow analysis using moving particle semi-implicit method", *Joint International Workshop: Nuclear Technology and Society- Needs for next generation*, Berkeley, California, Januar 6-8, Berkeley Faculty Club, UC Berkeley Campus, 2008.

[8] Shakibaeinia, A., and Jin, Y.C. "A weakly compressible MPS method for modeling of open-boundary free-surface flow", *International Journal for Numerical Methods in Fluids*, Vol. 63, 2010, pp. 1208-1232.

[9]. Liu, G.R., Mesh Free Methods: Moving Beyond the Finite Element Method. 2nd Edition, CRC Press, Boca Raton, FL 33487-2742.

[10] Hsiao, S.C., and Lin, T.C. "Tsunami-like solitary waves impinging and overtopping an impermeable seawall: Experiment and RANS modeling", *Journal of Coastal Engineering,* Vol. 57, 2010, pp. 1-18.

EVALUATING THE VALIDITY OF ISWM PROJECT RESULTS IN THE CASPIAN SEA USING RECENT FIELD MEASURMENT DATA

Hadi Sadeghian[1], Aghil Hajmomeni[2] and Ali Pak[3]

1) Senior Coastal Engineer, Sazeh Pardazi Iran Consulting Eng. Co., Tehran, Iran, h.sadeghian@sazehpardazi.com
2) Head of Coastal Process and Hydraulic Discipline, Sazeh Pardazi Iran Consulting Eng. Co., Tehran, Iran, hajmomeni@sazehpardazi.com
3) Professor, Department of Civil Engineering, Sharif University of Technology, Tehran, Iran, pak@sharif.edu

1. Introduction

Wave hindcasting projects for Iranian seas started about fifteen years ago under supervision and management of Ports and Maritime Organization (PMO). During the recent years, several other hindcasting projects have also been carried out by different marine consultants for complementing previous studies, improving the hindcasting results and establishment of a reliable wave climate for the Iranian seas. The validity of wind field pattern is one of the key factors affecting the accuracy of wave hindcasting results.

The first wave hindcasting project entitled "Iranian Seas Wave Modeling (ISWM)" has been performed by Iranian National Center for Oceanography (INCO) with the assistance of DHI Water and Environment in the Caspian Sea, Persian Gulf and Oman Sea. Wind dataset used in ISWM Project is based on ECMWF (European Center for Medium range Weather Forecasting) wind field but with modification in the southern part of the Caspian Sea. Although a relatively long time has passed from the completion of this project, its results are still reliable and are utilized by researchers and consultants for design of marine structures. Despite comprehensive utilization of ISWM project results during the last decade, there have been some ambiguities regarding the accuracy of the applied wind field and the modification procedure that was exerted to it. There has been a good consistency between the wave measurement data and the ISWM project results especially in the Caspian Sea. Nevertheless, the re-analysis of ECMWF wind data and re-examining the proposed procedure for modification of ECMWF wind dataset is a suitable measure for verification of ISWM project outcome for applying this data in the future projects. It should be noted that short period of ISWM project data (12 years) is one of its weakness when applied for extreme value analysis which is expected to be resolved by complementary hindcasting projects.

In this paper, the accuracy of ECMWF wind data and the proposed procedure for its modification in ISWM project has been investigated through numerical modeling results comparison with field measurement data in Ramsar coastal area. Wave parameters in Ramsar coastal zone has been measured in a location of about 10 meters depth for about four months in 2012 during metocean studies of coastal bypass road project of Ramsar.

The methodology adopted for the current research is that in the first step, ECMWF 2D wind field over the Caspian Sea has been collected in the field measurement period. Then the provided ECMWF wind data has been corrected according to the procedure applied in ISWM project. In the Following, the generation of the wind waves in the Caspian Sea has been simulated using MIKE 21 Spectral Waves FM (SW) numerical model. The calibration parameters for this modeling have been considered on the basis of ISWM project results. Finally the time series of modeled significant wave height, peak wave period and mean wave direction have been compared to the wave measurement data.

2. Numerical Modeling

2.1. Modeling Domain

The modeling domain for wave generation simulation covers the entire of the Caspian Sea. The modeling domain, the computational mesh and bathymetry for wave generation simulation has been shown in *Figure 1*. The Location of AWAC wave recorder installed in the depth of about 10 meters is also presented in *Figure 1* [4].

2.2. Simulation Duration

The simulation period is corresponding to the field measurement duration which was about four months from September to December 2012 [1].

2.3. Calibration Parameters

The model calibration parameters have been considered on the basis of final calibration parameters utilized in the ISWM project as follows [2]:

- White capping coefficient for wave height, $C_{dis} = 2$
- White capping coefficient for wave period, $\delta_{dis} = 0.8$
- Depth-induced wave breaking factor, $\gamma = 0.8$
- Bottom friction as Nikuradse roughness, $k_N = 0.002$

The ECMWF 2D wind field in the duration of field measurement has also been modified in the southern part of the Caspian Sea on the basis of modification procedure performed in the ISWM Project. Graphical modification

procedure adopted for ECMWF wind dataset has been illustrated in *Figure 2* [2].

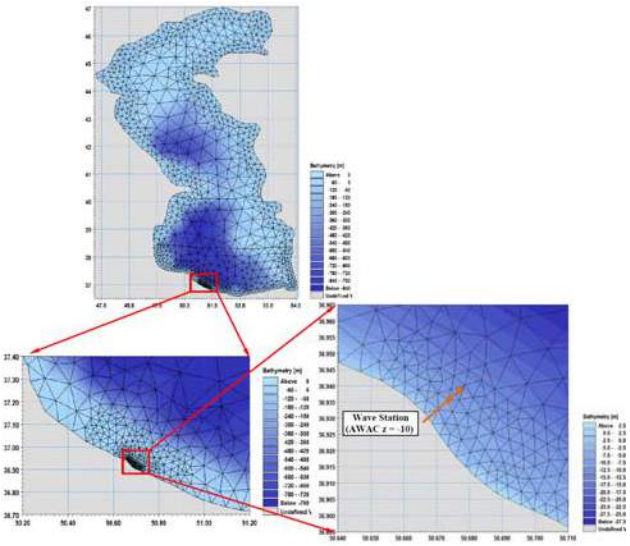

Figure 1. The modeling domain, computational mesh and bathymetry for wave simulation.

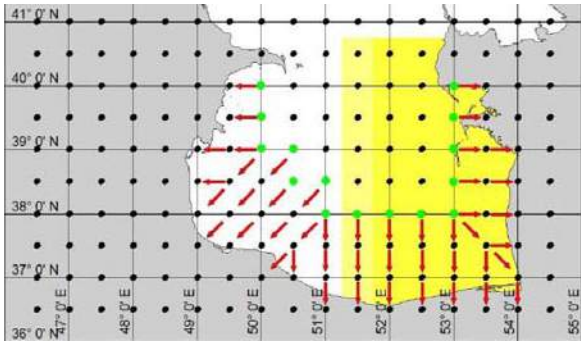

Figure 2. Modification pattern of ECMWF wind dataset in the southern part of the Caspian Sea

2.4. Modeling Results

In order to evaluate the quality of the wave simulation results, a comparison is made between the time series of wave parameters based on numerical modeling and wave measurement data in the location of AWAC wave recorder. The comparison results for significant wave height (H_s), peak wave period (T_p) and mean wave direction (MWD) are presented in *Figure 3* [4]. The comparisons results demonstrate that the numerical model predictions are in very good agreement with the measurement data.

3. Conclusion

By comparison of simulation results with field measurement data in the depth of about 10 meters in Ramsar coastal zone, it is seen that the wave parameters are well captured by the numerical model. Reasonable agreement between recorded and simulated wave data shows that the ECMWF 2D wind source with the modification proposed in ISWM project would be a suitable and reliable wind source for the southern part of the Caspian Sea. The ISWM project calibration parameters have also been approved by re-analyzing of the calibrated wave model using four-month wave measurement data in the Ramsar area. In other words, the ISWM Project wave model, which is calibrated against buoys measurements in Anzali, Amirabad and Neka during project implementation, is re-validated based on field data in another measurement duration and location. Thus it could be concluded that ISWM project wave data would be reliable for the southern part of the Caspian Sea and could be applied by researcher and engineers in future oceanography and engineering projects.

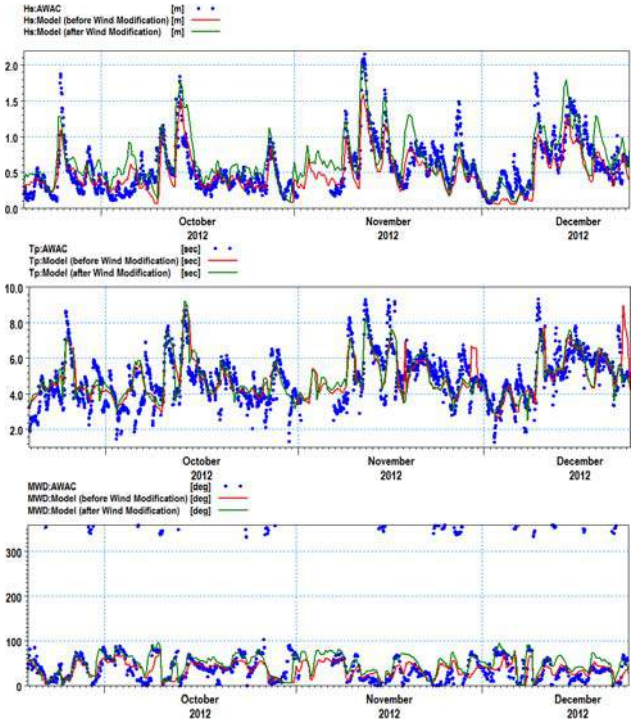

Figure 3. Time series of significant wave height, peak wave period and mean wave direction based on numerical modeling and wave measurement data.

4. References

[1] Darya Negar Pars Consulting Engineers, "Metocean Field Measurement Data Gathering and Processing Report in Ramsar Area", *Ramsar Coastal Bypass Project, Fourth Edition*, 2012.

[2] General Directorate for Coasts and Ports Engineering, "Iranian Seas Wave Modeling, Vol.1: Caspian Sea", *Ports and Maritime Organization, First Edition*, 2009.

[3] "MIKE 21 Spectral Waves FM Module User Guide", *Danish Hydraulic Institute (DHI) Water and Environment*, 2009.

[4] Sazeh Pardazi Iran consulting Eng. Co., "Complementary Hydrodynamic, Sediment and Design of Protection Structures Studies", *Ramsar Coastal Bypass Project, First Edition*, 2012.

STUDY OF CURRENT BEHAVIOR ON THE SOUTHERN SHELF OF THE CASPIAN SEA BASE ON FIELD MEASUREMENTS

Ehsan Shad[1], U. Reza Kamalian[2]

1) MSc. Student of Coastal Engineering, Qom University, Qom, Iran, Ehsan.shad@ymail.com
2) Qom University, Qom, Iran, ulrich.kamalian@cardiffalumni.org.uk

1. Introduction

The Caspian Sea (CS) is the largest internal drainage body of water on earth. The southern coast of the CS has a subtropical climate characterized by warm humid summers and mild, wet winters [9]. The CS surface circulation consists of cyclonic (counter clockwise) eddies in the southern, middle, and northern regions [7]. The mesoscale eddy features have a seasonal evolution [8]. The middle and southern CS has northerly northwesterly winds during summer, with easterly southeasterly winds in winter [2]. Two groups classified atmospheric circulation patterns which determine the wind field over the CS, the first one includes those patterns that are characterized by strong northerly winds [1].

The second group comprises atmospheric circulation patterns with strong southerly wind [6]. Currents on the northern shallow shelf are especially influenced by wind [3]. Along the western coast of the middle CS, the prevailing currents are southeastward and southward. Other types of currents, such as baroclinic currents and seiches, also play an important role in local circulation patterns [2]. It has been suggested that low-frequency motions are responsible for the large-scale sedimentary features of natural beaches [4]. Field investigations of low-frequency motions in the surf zone have dealt primarily with their physical properties, e.g., alongshore and cross-shore structure, secondary circulation patterns, runup and potential forcing [5].

In this study, comprehensive field measurements, 2D modeling and data analysis have been used. We tried to shed some light on the flow pattern and Its correlation with the wind and waves. A series of comprehensive field measurements were carried out by Iranian Ports & Maritime Organization (IRPMO) in south coast of CS. Wind data is extracted from the simulation of wind fields using WRF model by IRPMO.

2. Field measurement

Met-ocean data from 7 AWCAC units and 2 Aqua-Doppler profilers have been analyzed along the Iranian shoreline which cover November 2012 to June 2014. Field sites location and flow pattern as illustrated in Figure. 1. The instruments are located at positions with water depth of 10 and 25 meters. Some temporary measurements are also available at 5m depth. The studied parameters here are wind, wave and current velocity. Current velocity profile has been recorded by 10-minute intervals throughout 2.5 minutes continues measurements at 2 Hz. It has been averaged into 1-hr intervals.

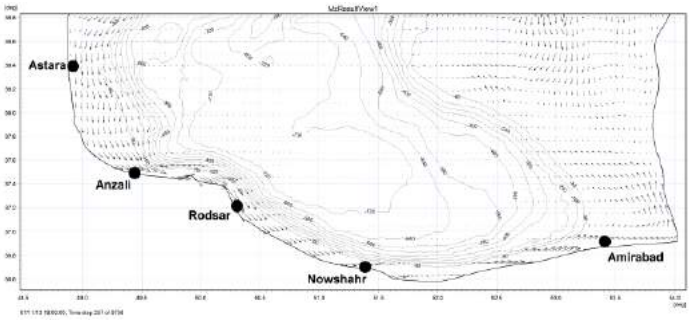

Figure. 1. Location map showing field sites and flow pattern

3. Data analysis

Prior to conducting the analysis, both the original wind and current data have been projected to alongshore components. A quality control procedure was performed to eliminate obvious errors. Then the data were checked for date, changes in references and spikes.

The time series have been filtered based on the frequency bands of the effective natural phenomena. The current data on hourly intervals have been averaged. Factors caused by tides and other forces within the same frequencies have been removed, in order to relate the current to particular wind conditions. The time series of alongshore current have been filtered for periods of less than 36 hours, in order to illustrate the weather-induced forces, including surge and long wave fluctuations. The essential requirement for applying a FFT method is the continuity of the data record [1]. Therefore, the time series of the current and wave components were inspected for gaps using the instruments included in the CMGTOOLS and then it is filling linearly or spectrally. Spectral analyses were performed on the current and wind time series at all stations using existing instruments in CMGTOOLS in order to showing correlation between data.

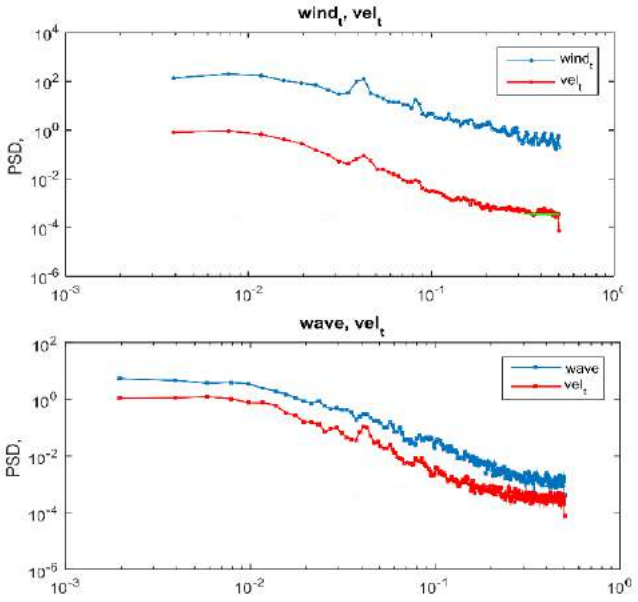

Figure. 2. Power spectral density of alongshore current, wind and wave based on hourly filtered data sets for whole recording period (Nov 2012 to June 2014)

4. Results and discussion

The alongshore velocity at all the stations have a periodical behavior. However, it is not symmetric everywhere. The velocity at Astara is mainly southward. At Anzali it is mainly eastward. At Rodsar it is more or less symmetric, except for spring where it is mainly northward. At Nowshahr it is symmetric in winter and spring but mainly eastward during summer and fall. The alongshore velocity at Amirabad is nearly symmetric. However, there are high speed eastward peaks that are followed by gentler but longer-lasting westward flows.

Figure. 2 illustrates correlations between current, wind and wave at Astara station. Periodograms have been drawn for odder station too. The spectral analysis between the alongshore currents, wind and wave for all stations have been done. According to Figure. 2 there is relatively small energy at the tidal frequencies band. Common energetic periods are visible at most of the stations. By comparing the correlation between wind and alongshore currents, it is obvious that most current velocity caused by wind.

Alongshore current has oscillatory behavior with periods far longer than the storms duration. Therefore, the current direction does not change during the storm (see Figure. 3). Due to the effects of general current (caused by low-frequency motions) on coastal phenomena such as sediment transport, cooling water systems, water desalination systems etc., it is necessary to apply the current in calculations. So wave and current relationship have been provided by comprehensive field measurements over a period of 15 months. Figure 4. illustrates relationship between wave and current at Astara station by bubble chart. Such relationship is also provided for the rest of the stations. Also The regression line have been drawn, which is useful for extracting proportional current form each wave condition.

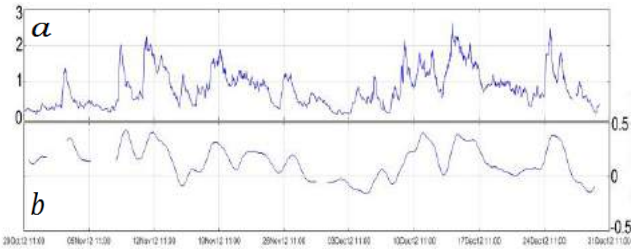

Figure. 2. wave and alongshore Current time series during Nov and June 2012 at Astara station. (a) Wave height; (b) Alongshore current

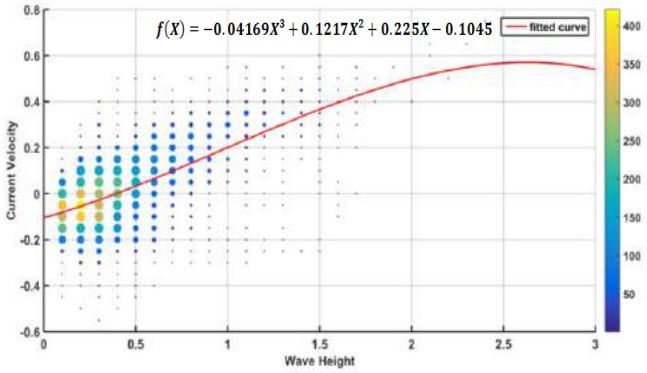

Figure. 4. Relationship between wave and current (Nov 2012 to June 2014)

5. References

[1] Ghaffari, P., & Chegini, V. (2010). Acoustic Doppler Current Profiler observations in the southern Caspian Sea: shelf currents and flow field off Feridoonkenar Bay, Iran. Ocean Science, 6(3), 737-748.

[2] Sur, H., Ozsoy, E., & Ibrayev , R. (2000). Satellite-derived flow characteristics of the Caspian Sea. (D. Halpern, Ed.) Satellites, Oceanography and Society.

[3] Bondarenko, A. (1993). Currents of the Caspian Sea and Formation of Salinity Field of the Waters of the North Caspian Sea. Nauka, Moscow.

[4] Bowen, A. J., & Inman, D. L. (1971). Edge waves and crescentic bars. ournal of Geophysical Research, 76(36), 8662-8671.

[5] Bowen, A., & Huntley, D. (1984). Waves, long waves and nearshore morphology. Marine Geology, 60(1-4), 1-13.

[6] Rodionov, S. (1994). Global and regional climate interaction: the Caspian Sea experience. London, UK: Kluwer Academic,Dordrecht.

[7] Terziev, F. S., & Kosarev, A. N. (1992). Hydrometeorology and Hydrochemistry of Seas. (A. A. Kerimov, Ed.) Caspian Sea(Hydrometeorological Conditions), Petersburg,359pp.

[8] Trukhchev, D., Kosarev, A., Ivanova, D., & Tuzhilkin, V. (1995). Numerical analysis of the general circulation in the Caspian Sea. Comptes Rendus de l'AcadÉmie Bulgare des Sciences,sofia,48, 35-38.

[9] Tuzhilkin, V. S., & Kosarev, A. N. (2005). The Caspian Sea Environment. Berlin Heidelberg: Springer.

STUDY OF WATER FLOW EFFECT ON RESPONSE OF PLATES SUBJECTED TO UNDER WATER EXPLOSION

S. Jalili[1,2], E. Shad[2,3], and M. Biglarkhani[2]

1) PhD Candidate, Mechanical Engineering, Tehran University, Tehran, Iran, sinajalili@ut.ac.ir
2) Orooj Gostar Aria, Tehran, Iran, info@oga_group.com
3) MSc. Student, Coastal Engineering, Qom University, Qom, Iran, Ehsan.shad@ymail.com

1.INTRODUCTION

Plates and thin walled structures are generally main elements that are used for fabricating of shell-plating of marine and submarine vessels. As being must exterior parts of vessels that are in contact with water they are prone to various threats that under water explosion is one of main dangerous and unavoidable ones. Extensive studies concerning this phenomenon are available [1], [2], [3]. Various methods are employed for investigation of plate responses subjected to under water explosion (UNDEX). Due to its inherent complexity of problem returns to interaction of fluid and structure (FSI), analytical solutions are very limited and deviations from experiment are considerable. In other hand experimental studies are really expensive and dangerous while their fulfillments require extensive substructures that are not available in every research center. In recent years by development of powerful computer codes are named hydrocodes in particular for handling of high rate mechanics problems, numerical methods approved their capabilities in study of this research area. To the best knowledge of authors all of works devoted to this research field are concerning that the fluid (Water) is calm and in stand situation before detonation of explosive charge and a published study with flowing water effect on the UNDEX phenomenon and its interaction with structure cannot be found.

In this paper, using powerful and professional hydrocode ANSYS-AUTODYN, effect of water flow on UNDEX response of rectangular plates is considered. Flow is in tangential direction of plates and velocity of current is in a feasible order to cover regular ocean streams and marine moving objects [4]. High fidelity numerical studies illustrate that effect of flow on distribution of UNDEX overpressure are tangible and maximum deflection of plates may be affected by this phenomenon.

2.NUMERICAL MODEL ASSESSMENT

While numerical procedures are indeed powerful in modeling disparate complicated problems, it is needed to be aware of subtleties of these methods and shortages in their implementations. Explosion phenomena due to massive energy conversion from chemical to mechanical one, is really an elaborate problem and its modeling requires especial tools are not available in ordinary numerical codes. Interaction of fluid and solid is another complicacy that must be considered here. For appropriate numerical assessment of problem, both of water (Sea environment) and structure (plate) must be modeled simultaneously. Large deformation of water medium needs Eulerian approach to be grasped with suitable care and shell elements are implemented in construction of plate model. In Figure 1 schematic of proposed problem and its numerical equivalent are depicted. Due to symmetry in plane normal to flow direction only half of problem is needed to be modeled.

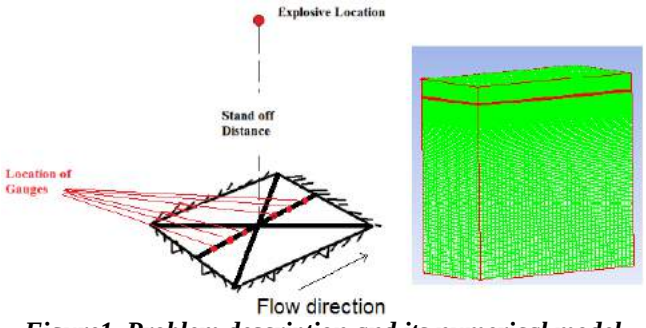

Figure1. Problem description and its numerical model.

It is assumed that TNT is explosive charge and JWL equation of state is implemented for its modeling. 4340 steel as an accepted alloy for structures are threatened by explosive and ballistic loads is used as plate constructing material. Plate dimensions are: 1000*500*2 mm and flow is in longitudinal direction.

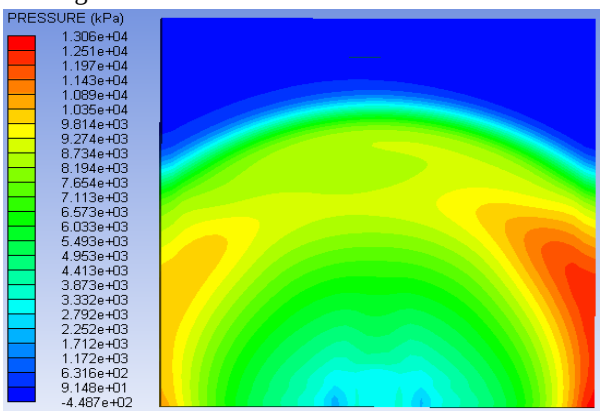

Figure 2. Shock wave pressure field due to UNDEX in 3-D environment (flow from right to left).

For achieving more careful simulation of detonation process, a 1-D wedge model with highly fined grid is used to model the incipient moments of explosion. By a little propagation of detonation and in its consequence shock waves in water medium, results of 1-D model are remapped into 3-D model to be utilized in remaining portion of simulation. Figure 2 shows propagation of shock wave pressure field in water in three dimensional model.

3. RESULTS AND DISCUSSION

After conducting numerical studies with mentioned above assumptions, results of variation of UNDEX overpressure along the flow direction are graphed in Figure 3 for 1 m stand-off. Mass of explosive charge is 23 gram of TNT. This amount of charge is enough for making permanent visible plastic deformations on plate.

Distribution of pressure on the plate according to numerical surveys is complicated and depends on flow velocity. Up to 4 m/s, pressure profile has two extremes that are occurred in both sides of plate but after reaching to 5 m/s, the profile is changed significantly and its lone apex migrates to flow direction. This behavior may be result of intricate interaction of Mach front and reflective waves and conversion process of flow hydrodynamic pressure to hydrostatic one.

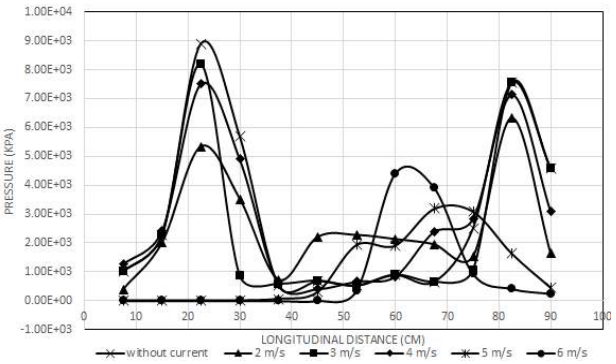

Figure 3. Variation of overpressure along the flow, tangent to plate for 1 m stand-off.

For more scrutinizing the event, numerical simulations are performed in two different stand-offs. In Figures 4 and 5, variation of deflection of plate along the flow direction is illustrated for 1 and 1.5 m stand-offs respectively and all deflections are recorded in instance that maximum deflection of plate is occurred.

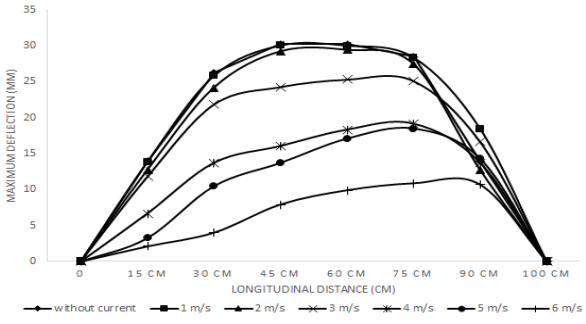

Figure 4. Deflection variation along the flow direction for various flow velocities (1 m-stand-off).

Results show that by increasing flow velocity, deflection profile deviates from symmetry configuration of flow-less problem. Maximum point of deflection migrates to the direction of flow from center. Another main observed note construed from deflection graphs are reduced amplitudes of deflection by enhancement of current velocity. This can be elicited from this fact that some portion of explosion energy can be absorbed by water flow in counter direction.

By addition to stand-off distant of charge, symmetry disturbing effect on deflection profile is deteriorated nominally. But still deflections are reduced due to flow velocity.

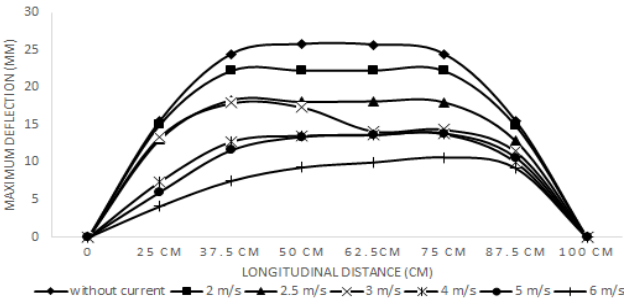

Figure 5. Deflection variation along the flow direction for various flow velocities (1.5 m-stand-off).

In figure 6, a caption from plate's final permanent deformation due to UNDEX effect is illustrated.

Consideration of mentioned results, this fact that effect of water flow on distribution of pressure and deflection of plates may be tangible is revealed. Extensive numerical studies show that this phenomenon is rigorous in low mass explosive charges and also thinner structures. These conclusions may be useful for underwater explosive forming purposes also.

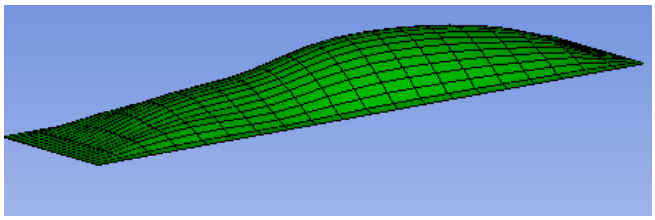

Figure 6. Permanent Deformation of plate subjected to UNDEX and 6 m/s vel. (1 m-stand-off).

4.REFERENCES

[1] Hung C.F., Hsu P.Y., Hwang Fu, J.|J.,(2005): Elastic shock response of an air-backed plate to underwater explosion, Int. J. of Impact Engineering, 31, pp. 151-168.

[2] Chunliang X., Gengguang X..,(2008): Numerical Simulation of Underwater Explosion Loads,Tianjin Univ. and Springer, 14, pp. 519-522.

[3] Ramajeyathilagam K., Vendham C.P., Bhujanga Rao V.,(2000): Non-linear transient dynamic response of rectangular plates under shock loading, Int. J. of Impact Engineering, 24, pp. 999-1015.

[4] T.J. Sherwin.,(1988): Measurements of current speed using an Aanderaa RCM4 current meter in the presence of surface waves, Continental Shelf Research, Volume 8, Issue 2, pp.131-144

NUMERICAL MODELING OF CYCLONE GONU WAVES CRASH ON RAMIN PORT BREAKWATERS

Fatemeh Hajivalie[1] and Ahmad Arabzadeh[2]

1) Ocean Engineering and Technology Research Center, Iranian National Institute for Oceanography and Atmospheric Science (INIOAS), Tehran, IRAN, hajivalie@inio.ac.ir
2) Persian Gulf Center- Boushehr, Iranian National Institute for Oceanography and Atmospheric Science (INIOAS), Boushehr, IRAN, ahmadarabzadeh@inio.ac.ir

1. Introduction

High waves are considered as an important coastal hazard which impact and overtop coastal structures and inundate coastal region during storm condition. To prevent the disastrous effect of the wave run-up and overtopping, many physical tests have been performed to derive empirical formulas and design curves to estimate wave run-up and overtopping over the coastal structures (i.e. De Waal and Van Der Meer [1]; Owen [2]. These empirical tools have been very useful in the design of coastal structures. However they are only based on the special condition in wave flumes with limited wave conditions.

By developing numerical method, researchers started to simulate wave run-up and overtopping using numerical methods. Hubbard and Dodd presented a two dimensional numerical model of wave run-up and overtopping based in the 2D nonlinear shallow water (NLSW) and investigated the overtopping of a seawall by long-crested waves [3].

In this research, TELEMAC-3D has been hired to simulate and study the wave run-up and wave overtopping for high waves induced by so called Cyclone Gonu happened in 2007 in the Indian Ocean, over Ramin port breakwaters, located in Southeast of Iran (Fig. 1). The results then have been compared with the videos and photos taken during the cyclone in Ramin port.

Figure 1. Ramin fishing port (Google earth)

2. Numerical model

2.1. Mathematical formulation

The TELEMAC-3D software is part of the TELEMAC modeling system developed by the LNHE of EDF R&D. TELEMAC-3D solves the RANS equations by the finite elements method through the vertical integration of the continuity equation and momentum equations. The turbulent viscosity can be estimated from a *k-ε* model. Thereafter the governing equations are:

$$\frac{\partial U_j}{\partial x_j} = 0 \tag{1}$$

$$\frac{\partial U_j}{\partial t} + U_i \frac{\partial U_j}{\partial x_i} = -\frac{1}{\rho}\frac{\partial p}{\partial x_j} - g_j + \upsilon\Delta(U_j) + F_j \tag{2}$$

$$\frac{\partial k}{\partial t} + U_j \frac{\partial}{\partial x_j} k = \frac{\partial}{\partial x_j}\left(\frac{\nu_t}{\sigma_k}\frac{\partial k}{\partial x_j}\right) + p - G - \varepsilon \tag{3}$$

$$\frac{\partial \varepsilon}{\partial t} + U_j \frac{\partial}{\partial x_j} \varepsilon = \frac{\partial}{\partial x_j}\left[\frac{\nu_t}{\sigma_\varepsilon}\frac{\partial \varepsilon}{\partial x_j}\right] + C_{1\varepsilon}\frac{\varepsilon}{k}\left[P + (1 - C_{3\varepsilon})G\right] - C_{2\varepsilon}\frac{\varepsilon^2}{k} \tag{4}$$

$$P = \nu_t \frac{\partial \overline{U_i}}{\partial x_j}\left[\left(\frac{\partial \overline{U_i}}{\partial x_j} + \frac{\partial \overline{U_j}}{\partial x_i}\right)\right] \tag{5}$$

$$G = -\frac{\nu_t}{\mathrm{Pr}_t}\frac{g}{\rho}\frac{\partial \rho}{\partial z} \tag{6}$$

$$\nu_t = C_\mu \frac{k^2}{\varepsilon} \tag{7}$$

U_i and U_j are velocity component in ith and jth coordinate directions (for three dimensional equations i and j =1, 2, 3), p is pressure, g_j= gravity acceleration in jth direction, ν_t kinetic eddy viscosity, ρ is water density. k is the turbulence kinetic energy, ε is the kinetic energy dissipation rate. P is a turbulence energy production term and G is a source term due to the gravitational forces. C_μ, Pr_t, $C_{1\varepsilon}$, $C_{2\varepsilon}$, $C_{3\varepsilon}$, σ_k and σ_ε are *k-ε* model contestants.

2.2. Model setup

Model setup is based on Ramin port geometry and Gonu Cyclone hydrodynamic situation. The Gonu tropical cyclone is the strongest storm in the Arabian Sea which has caused severe damages in the Iranian Southeast coastlines in 2007.

The numerical domain is discretized to 10 m triangular grids at the entire domain and 1 m grids around the port as illustrated in Fig. 2. The bed, coastline and breakwaters are introduced to model as rough solid boundary. The East and West boundary are open boundary and at the South, the inlet boundary, a wave generator is defined by introducing a time varying free surface elevation at the inlet boundary. Fig. 3 shows the inlet waves derived from Mashhadi et al. who simulated the waves' characteristics as well as the storm surge during the Gonu Cyclone [4].

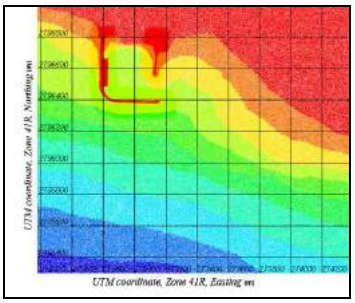

Figure 2. Mesh and bathymetry of Ramin port

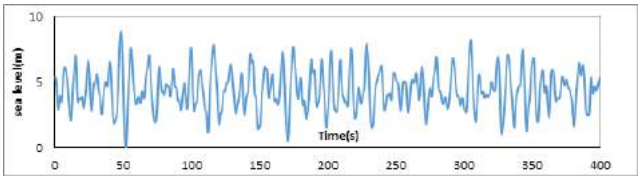

Figure 3. Random waves generated based on Mashhadi et al. (2013)

3. Results and dissections

The wave maker boundary condition generated the random waves of the worst situation near Ramin port during the Cyclone. Fig.4 shows the wave propagation around the Ramin port in four different time steps during the simulation time. As it could be seen in these figures, the port stays safe enough for the moored vessels during the event which is in agreement with the videos taken by Iran Fisheries Organization.

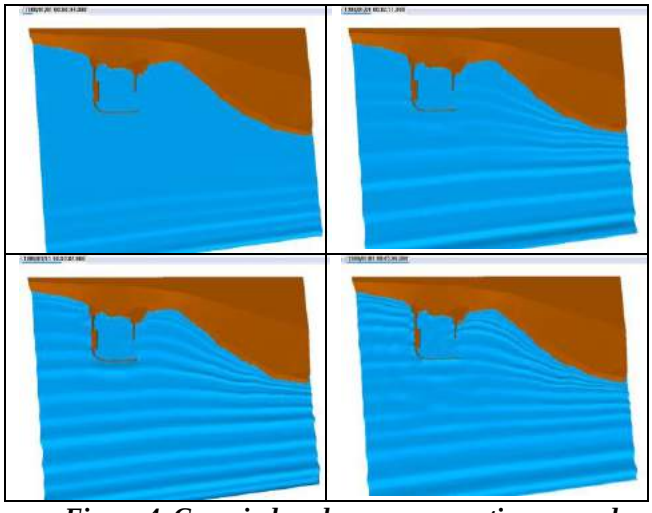

Figure 4. Gonu induced wave propagation around Ramin port

Both simulation and the event videos show huge wave overtopping over main breakwater which has caused damages to the breakwater as illustrated in Fig 5 a and b. Fig. 6 shows a time series graph for wave overtopping in the middle of main breakwater during the simulation, according to this figure, the maximum overtopping discharge in this section is about 1.4 $m^3/m\times s$. No measurement has been undertaken during the event, therefore only qualitative verification is possible.

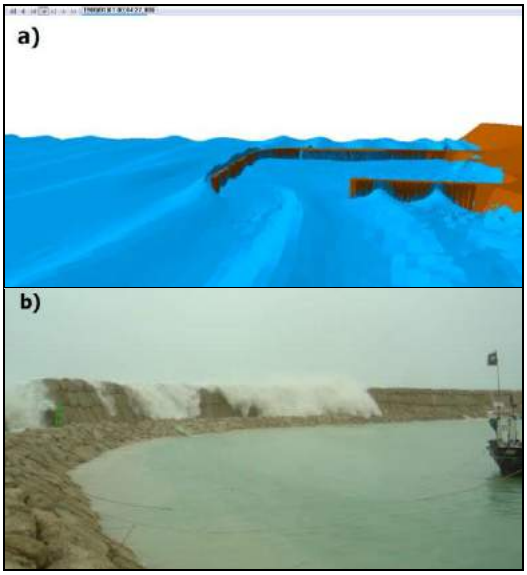

Figure 5. wave overtopping over main breakwater, a) in numerical simulation, b) in the incident images

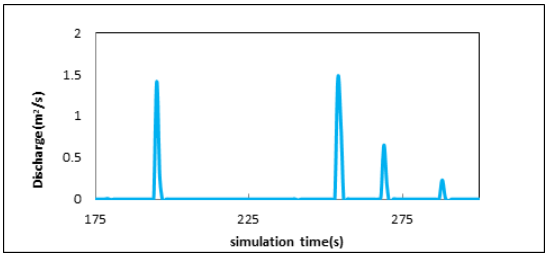

Figure 6. Time series of overtopping discharge over the main breakwater

4. References

[1] De Waal, J.P., Van Der Meer, J.W., 1992: Wave runup and overtopping on coastal structures. Proc. 23rd Int. Conf. Coastal Eng. A.S.C.E., Venice, pp. 1758– 1771.

[2] Owen, M., 1980: Design of seawalls allowing for wave overtopping, Tech. Rep. EX 924. Hydraulics Research Wallingford.

[3] Hubbard, M.E., Dodd, N., 2002: A 2D numerical model of wave runup and overtopping. Coastal Engineering, 47, 1-26.

[4] Mashhadi, L., Hajizadeh-Zaker, N., Soltanpour, M. Moghimi, S., 2013: Numerical simulation of waves and storm surge induced by the Gonu Tropical Cyclone in the Chahbahar bay area. Journal of Marine Engineering, 17, 37-50, (in Persian).

SIMULATION OF THE SEA WATER CIRCULATION AND COASTAL CURRENTS IN THE CASPIAN SEA

M.H. Moeini[1], E. Jafari[2], M. Bali[3], M.J. Alaee[4] and C. Pattiaratchi[5]

1) Pouya Tarh Pars Consulting Engineering Company, Tehran, Iran, mhmoeini@gmail.com
2) Pouya Tarh Pars Consulting Engineering Company, Tehran, Iran, e.jafari@ptpco.com
3) Pouya Tarh Pars Consulting Engineering Company, Tehran, Iran, meysam_baali@yahoo.com
4) Pouya Tarh Pars Consulting Engineering Company, Tehran, Iran, m.j.alaee@ptpco.com
5) University of Western Australia, Australia. chari.pattiaratchi@uwa.edu.au

1. Introduction

The Caspian Sea is the largest enclosed water body in the world. It is located in the west Asia and surrounded by the five countries of Russia, Kazakhstan, Turkmenistan, Iran and Azerbaijan. It is about 1300 km long and its width varies between 200 and 450 km in different regions. The bathymetry of the Caspian basin shows that the basin can be divided into the flat northern part, the middle bowl shape, and southern Caspian containing a depression reaching a maximum depth of 1025 meters, with an abrupt western slope and a gentler eastern slope (Figure 1). The physical oceanographic characteristics of this basin are of the great importance, particularly for Iran which has more than 800 km coastline and significant natural resources at the sea.

The simulation of flow patterns in the Caspian Sea was the subject of different studies during recent decades. Primarily, numerical investigations did not result in reliable findings, mainly due to numerical model weaknesses as well as inadequate initial and boundary conditions. Later on, more sophisticated numerical models such as three-dimensional models were employed to simulate circulation in the Caspian Sea (e.g. [1-3]). These studies revealed that there are relatively strong coastal currents along the southwestern coasts of the Caspian Sea. None of the previous studies on the Caspian Sea flow regimes focused on local currents along the Iranian coastal areas. Therefore, the Iranian Port and Maritime Organization (PMO) initiated a project, led by Pouya Tarh Pars Consulting Engineers to examine the physical processes along the Iranian sector of the Caspian Sea through the use of field measurements and numerical modeling. In this paper the results of these studies with regard to coastal currents are presented.

2. Field observations

In this study, extensive field observations of coastal currents were performed for more than a year from the end of 2012 to the beginning of 2014. For this purpose, ADCP devices including AWACs and AQUADOPPs were deployed at 5, 10 and 25m depth in six different locations (Astara, Anzali, Roodsar, Noushahr, Amirabad and Gomishan; Figure 1).These observations were analyzed to evaluate the various flow regimes and their corresponding flow structure in the Caspian Sea, especially Iranian coasts.

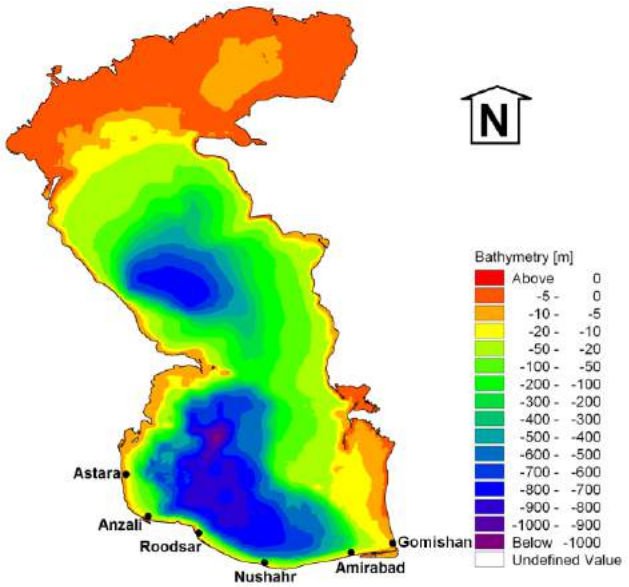

Figure 1. The Caspian Sea bathymetry and the stations of measurements.

The observations show that there are relatively strong coastal currents along the southern coasts of the Caspian Sea. The main circulation flows from north to south in front of Astara and it continues to the east from Anzali to Amirabad. The comparison of the measurements in different levels also shows that the current speed is almost uniform in depth near the coastal areas.

3. Simulation and results

This paper also demonstrates the results of 2D & 3D numerical simulations of the sea currents in the Caspian Sea for the period of the field observations. The numerical simulations were performed considering all effective parameters on the circulation, including wind, air pressure, river discharges, precipitation, evaporation and ice coverage. In 2D model, no density gradient was taken into account and the model ran in barotropic mode; while in 3D

one, the density considered as a function of temperature and salinity. The simulations were conducted using an unstructured horizontal mesh in which the mesh dimensions were between 0.03˚ and 0.25˚. For the wind forcing, the hourly results of the Weather Research and Forecast (WRF) model with the resolution of 0.1°×0.1° was used which produced in this project.

Figure 2 shows the comparisons of the 3D modeled alongshore currents against observations in different stations for a sample month. As seen, the simulations are in a good agreement with the field measurements and the model results follow the observations well.

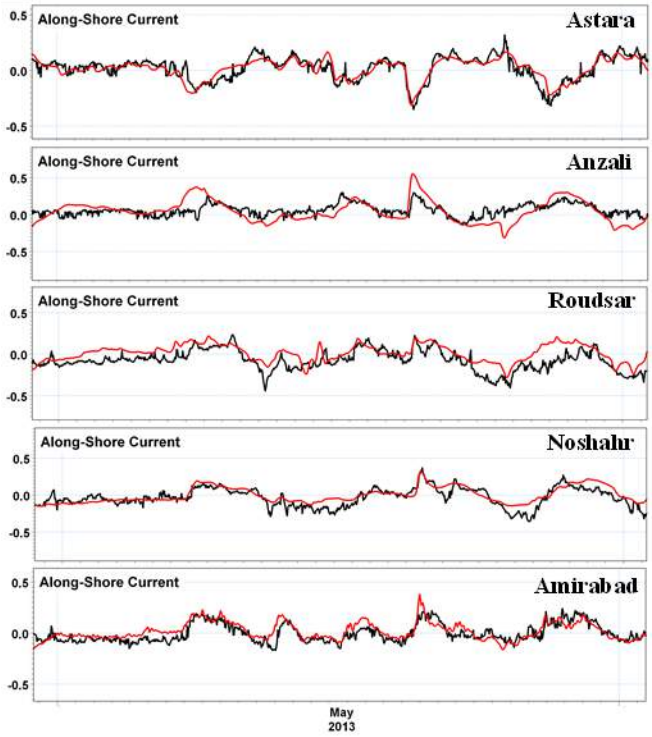

Figure 2. Comparisons of the modeled alongshore currents against observations in different stations for a sample month. (black line: observation, red line: model results)

For quantitative evaluation of the model results, error indicators such as model skill, *BIAS* parameter and root mean square error (*RMSE*) were used:

$$Model\ Skill = 1 - \frac{\sum (S_i - O_i)^2}{\sum \left(|S_i - \overline{O_i}| + |O_i - \overline{O_i}| \right)^2} \quad (1)$$

$$BIAS = \frac{1}{N} \sum (S_i - O_i) \quad (2)$$

$$RMSE = \sqrt{\frac{1}{N} \sum (S_i - O_i)^2} \quad (3)$$

where N is total number of data, O_i and S_i are respectively the observed and simulated data, and $\overline{O_i}$ is the average of observed data. The calculations of these parameters for the estimated currents are shown in Table 1. As seen in the Table, the statistics also indicated that the model outperforms the current simulation in the southern Caspian Sea.

Table 1. The summary of statistical analysis for current simulation in the Caspian Sea

Error Indicator	Astara	Anzali	Roodsar	Noushahr	Amirabad
Model Skill	0.86	0.80	0.74	0.83	0.80
BIAS	0.02	-0.019	0.04	0.002	-0.016
RMSE	0.09	0.13	0.12	0.12	0.09

Based on the simulation results and analysis of the measurements, current speed is often uniform in depth at all of the observation stations. On the other hand, it was found that most of the strong sea currents in the Caspian Sea are wind driven currents and other factors have not significant effects on the water circulation.

4. References

[1] Ibrayev, R., Ozsoy, E., Schrum, C., and Sur, H. (2009) "Seasonal variability of the Caspian Sea three-dimensional circulation, sea level and air-sea interaction". Ocean Science Discussions, 6, 1913–1970.

[2] Birol Kara, A., Wallcraft, A., Joseph Metzger, E., and Gunduz, M. (2010). "Impacts of freshwater on the seasonal variations of surface salinity and circulation in the Caspian Sea". Continental Shelf Research, 30(10-11), 1211–1225.

[3] Turuncoglu, U. U., Giuliani, G., Elguindi, N., and Giorgi. F. (2013) "Modelling the Caspian Sea and its catchment area using a coupled regional atmosphere-ocean model (RegCM4-ROMS): model design and preliminary results". Geoscientific Model Development, 6(2), 283-299.

INVESTIGATION OF KERNEL FUNCTION EFFECT ON THE STABILITY OF CORRECTED MOVING PARTICLE SEMI-IMPLICIT (CMPS) METHOD

Afsharpour, T.[1], Kolahdoozan, M.[2], and Rezaee Mazyak, A.[3]

1) Hydraulic Structures Department, Amirkabir University, Tehran, Iran, t.afsharpour@yahoo.com
2) Hydraulic Structures Department, Amirkabir University, Tehran, Iran, mklhdzan@aut.ac.ir
3) Marine Structures Department, Tarbiat Modares University, Tehran, Iran, a.rezaeemazyak@modares.ac.ir

1. Introduction

In the recent decades, Particle-based Lagrangian methods have been developed in various fields of studies (i.e. astronomy, fluid dynamics, etc.). Moving Particle Semi - Implicit (MPS) Method is a particle-based lagrangian method with robust capability for numerical representation.

The MPS method was applied to hydrodynamic problems for the numerical simulation of the free surface flows due to breaking waves [1, 3]. Also, other studies have been carried out on the improvement of the accuracy and performance of MPS method [3, 4, 5].

In this study, in order to assess the stability of CMPS method, effect of different kernel functions and types of advanced operators in the Lagrangian modeling, have been tested. In the developed numerical model, the hydrostatic pressure and wave run-up is approximated by the static reservoir model and the impact of wave to the wall, respectively. Comparison of the numerical model results with laboratory measurements and analytical relationships reveal that the stability of developed model is increased by using corrected gradient term for a new kernel functions.

2. Numerical Modeling

2.1. Governing Equation

The motion of an incompressible viscous fluid flow is described by the continuity and Navier-Stokes equations written as follows:

$$\frac{1}{\rho}\frac{D\rho}{Dt} + \nabla.u = 0.0 \qquad (1)$$

$$\frac{Du}{Dt} = \frac{1}{\rho}\nabla p + g + \nu\nabla^2 u \qquad (2)$$

where u = particle velocity vector; t = time; ρ = fluid density; p = particle pressure; g = gravitational acceleration vector and ν = laminar kinematic viscosity.

2.2. Solution Process

The overall calculation algorithm of CMPS is described in Fig. 1. At the first stage of computation, calculation parameters such as kernel function, corrected gradient and laplacian operators are defined. Then in each time step, source terms are explicitly calculated to obtain temporal velocities u_i^*. Next, motion of particles is calculated, and temporal coordinates r_i^* are obtained. The Poisson equation of pressure is solved by ICCG with the temporal particle number densities and then pressure is calculated based on the corrected gradient operators (CMPS method). Finally new velocities and co-ordinates are obtained from the corrected pressure gradient terms.

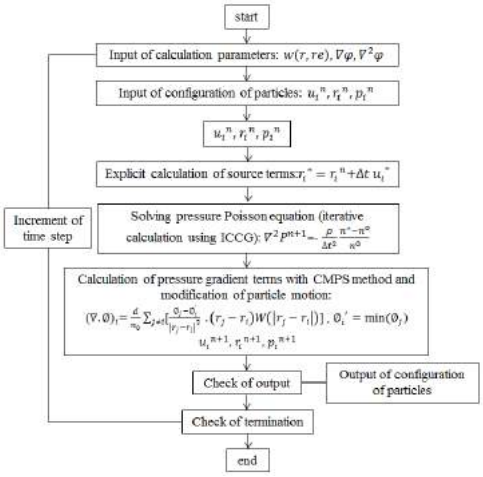

Figure 1. Calculation algorithm of CMPS

2.2.1. Kernel Function

The kernel function is utilized to smooth (approximate) the physical quantities around each particle and it is controlled the stability of CMPS method. In previous studies, three types of kernel (weight) functions are used [1, 5, 6]. These functions are shown below:

$$w(r) = \begin{cases} \frac{r_e}{r} - 1 & 0 \le r < r_e \\ 0 & r_e \le r \end{cases} \qquad \text{(KF1)} \qquad (3)$$

$$w(r) = \begin{cases} (1 - \frac{r}{r_e})^2 & 0 \le r < r_e \\ 0 & r_e \le r \end{cases} \qquad \text{(KF2)} \qquad (4)$$

$$w(r) = \begin{cases} (1 - \frac{r}{r_e})^3 & 0 \le r < r_e \\ 0 & r_e \le r \end{cases} \qquad \text{(KF3)} \qquad (5)$$

Based on the various requirements for the smoothing functions, in this study for improvement the stability of CMPS method, three kernel functions are defined as below:

$$w(r)=\begin{cases}(1-\frac{r}{r_e})^{2.5} & 0\le r<r_e\\ 0 & r_e\le r\end{cases} \quad \text{(KF4)} \quad (6)$$

$$w(r)=\begin{cases}(1-\frac{r}{r_e})^{3.5} & 0\le r<r_e\\ 0 & r_e\le r\end{cases} \quad \text{(KF5)} \quad (7)$$

$$w(r)=\begin{cases}(1-\frac{r}{r_e})^{4} & 0\le r<r_e\\ 0 & r_e\le r\end{cases} \quad \text{(KF6)} \quad (8)$$

3. Validation

By considering the advantages of the meshless particle methods in modeling of free surface flow and pressure fields, in this section, two simple tests are carried out to validate the above introduced kernel functions in the CMPS method. In these tests, the time variation of hydrostatic pressure in the stationary water tank and the amount of wave run-up due to propagation of solitary wave are investigated.

3.1. Hydrostatic Pressure

Fig. 2, illustrates the snapshots of pressure field at t = 0.5 s for the CMPS method. The shown error indices in the table 1, that obtained based on the comparison of numerical model and theoretical results, are used for the assessment of the numerical modeling results.

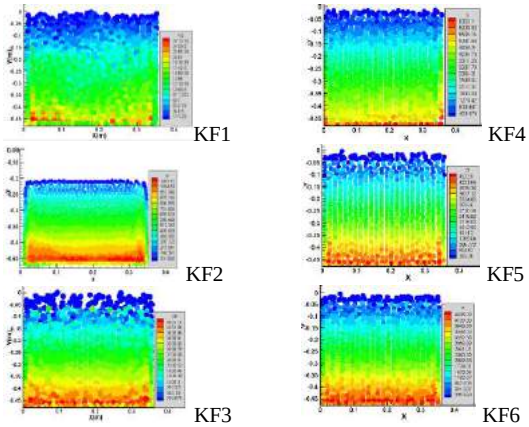

Figure 2. Pressure field in the stationary tank (t=0.5s)

Table 1. Error indices of the hydrostatic pressure

Kernel Functions	MAE (pa)	RMSE (pa)
KF1	670.0895	0.346
KF2	989.192	0.077
KF3	253.388	0.027
KF4	402.087	0.043
KF5	262.490	0.0337
KF6	255.080	0.0305

3.2. Wave Run-up

Fig. 3. demonstrates the pressure field and wave run-up for propagation of the solitary wave at The relative wave height=0.8, which is defined as the ratio of wave height (=H) to water depth (=h). The shown error indices in the table 2 , that obtained based on the comparison of numerical model and experimental results, are used for the appraisal of the numerical modeling results.

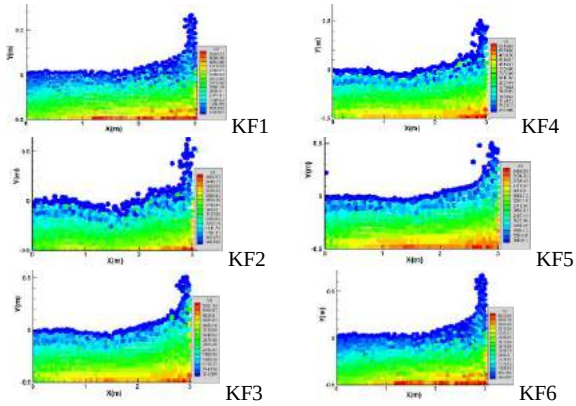

Figure 3. Solitary wave run-up, (H/h=0.38)

Table 2. Error indices of the amount of wave run-up

Kernel Functions	MAE (m)	RMSE (m)
KF1	0.2614	0.2871
KF2	0.2331	0.2698
KF3	0.0984	0.1102
KF4	0.1975	0.2329
KF5	0.1611	0.2042
KF6	0.2269	0.2518

4. Conclusion

Investigation of the modified gradient operators and the high-order kernel functions are novelty of this study. Also according to the numerical model results can be concluded that using of the KF3 kernel function (introduced in the [6]) in the CMPS method leading to the lowest error.

5. References

[1] Koshizuka, S. and Oka, Y., "Moving-Particle Semi-Implicit Method for Fragmentation of Incompressible Fluid", Nuclear Science and Engineering: 123,1996, pp 421-434.

[2] Ataie-Ashtiani B, Farhadi L. "A stable moving-particle semi-implicit method for free surface flows", Fluid Dynamic. Research, 38(4), 2006, pp 241–256.

[3] Suzuki, Y., Koshizuka, S and Oka, Y., "Hamiltonian moving-particle semi-implicit (HMPS) method for incompressible fluid flows", Computer Methods in Applied Mechanics and Engineering, 196, 2007, pp 2876-2894.

[4] Khayyer A. and Gotoh, H., "Modified Moving Particle Semi-implicit methods for the prediction of 2D wave impact pressure", Coastal Engineering, 56, 2009, pp 419-440.

[5] Shakibaeinia, A. and Jin, Y.C., "A weakly compressible MPS method for modeling of open-boundary free-surface flow", Int. J. for Numerical Methods in Fluids, 63, 2010, pp 1208-1232.

[6] Kondo, M. and Koshizuka, S., "Improvement of stability in moving particle semi-implicit method", Int. J. for Numerical Methods in Fluids, 65 (6), 2011,pp 638-654.

EVALUATION OF ERA-INTERIM WAVE CHARACTERISTICS IN SOUTHERN CASPIAN SEA

Hasan Imani[1], Bahareh Kamranzad[2]

1) Mechanical Engineering, Sharif University of Technology, Tehran, Iran, hasan.imani@mech.sharif.ir
2) Ocean Engineering and Technology Research Center, Iranian National Institute for Oceanography and Atmospheric Science, Tehran, Iran, kamranzad@inio.ac.ir

1. Introduction

Environmental data specially wave and wind data are the most important phenomenon to be considered among the other potential factors affecting marine and coastal activities like construction, maintenance, transportation, fishing, etc. Since obtaining environmental data by measuring devices or satellites is time consuming and very expensive, numerical models are utilized in order to predict the sea wave characteristics.

The results of numerical wave hindcast models mainly depend on the quality of the wind data used to drive the model [1-4]. Therefore, using an appropriate wind field is essential and the most problematic task for wave modeling. Although, there are various wind sources to predict the wave characteristics, a couple of attempts have been undertaken within the last few years on the performance of reanalyzed data in wave modeling. ECMWF's ERA-Interim is more recent reanalyzes which provides better resolution and description of the wind fields. Therefore, the aim of this work is to evaluate the wave characteristics of the new assimilated dataset, ERA-Interim in the southern Caspian Sea. Therefore, at first, a numerical simulation of sea wave characteristics was carried out based on ERA-Interim wind data. In this regard, the SWAN spectral model was implemented and validated against measured data. Regarding to calibration, a combination of appropriate white-capping dissipation and bottom friction factors was used to calibrate the model. Then, the model results were compared to the wave characteristics obtained from ERA-Interim.

2. Study area and datasets

Caspian Sea is the biggest enclosed body of water on Earth, with approximately 7000 km coastline, a surface area of 371,000 km², and a volume of 78,200 km^3. It is located between latitudes 47.07'N and 36.33N and longitudes 45.43 E and 54.20E and also bordered by five countries including Iran. The Caspian Sea can be divided into three distinct physical parts, the northern, middle and southern parts. The southern and middle parts are characterized as deep water, with a depth more than 1000 m in the southern region and 500 m in the central region. The Northern part is also known as shallow water with average depths of less than 5m [5-8].

2.1. Measured datasets

In this study, buoy measurements near Noshahr (deployed by Port and Maritime Organization (PMO)) was considered in order to evaluate the wave characteristics of the new assimilated dataset, ERA-Interim, in the southern Caspian Sea.

2.2. Assimilated datasets

ERA-Interim is a third generation reanalysis dataset produced by much improved atmospheric model and assimilation system from those used in ERA-40 with a temporal resolution of 6 hour [9]. Time series of measured and assimilated significant wave height are shown in Fig 2.1. It can be seen that the assimilated significant wave height (H_s) agrees well with the measured ones while some peaks are slightly underestimated. It was quite predictable from the negative bias in ERA-Interim data (Table 2.1).

In addition, Fig 2.2 illustrates the wave-rose diagrams. It is clear from the Fig 2.2 that the direction of the southern wind-waves is to the north east. Table 2.2 shows the statistical analysis of the Measured and ERA-Interim data. Although the assimilated data underestimate the results, two data group has a good agreement on mean and standard values.

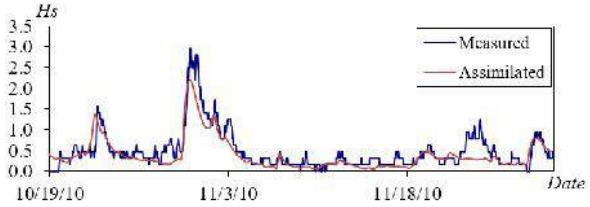

Fig 2.1. Time series of the wave height (m)

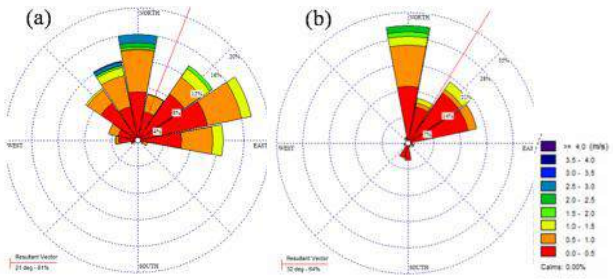

Fig 2.2. (a) Measured and (b) assimilated data wave-rose

diagrams, respectively.

Table 2.1. Error indices of buoy and assimilated wave height data

Error index	Significant wave height
Bias (m)	-0.09
R	0.88
MSE	0.06
SI	0.51

Table 2.2. Buoy and assimilated wave parameter statistics

Wave parameters	Buoy		ERA-Interim	
	$H_{1/3}$ [m]	WD [deg]	$H_{1/3}$ [m]	WD [deg]
Min	0.16	0.0	0.065	0.652
Max	3.281	357.19	2.198	359.62
Average	0.5	119.29	0.393	98.549
Stdv	0.384	119.1	0.377	114.227

Note: $H_{1/3}$=Significant wave height; T= wave period and WD=Wave direction.

2.3. Modeled wave characteristics

Third generation numerical model, SWAN, was used to produce the time series of wave characteristics over a month for a location in the southern Caspian Sea. This model is based on wave spectrum concept (in all frequencies and all directions). In this study, a nonstationary two-dimensional model with a 30 min time step and a spherical scale was used. In addition, a uniform, regular computational grid with 0.1° resolutions in x and y directions was considered as scale grid for the model. Furthermore, the bathymetry had a resolution of 0.0083^{o} in x and y directions, respectively.

3. Results and discussions

The model calibration was carried out based on the minimization of simulation error of significant wave height comparing to the measured one. Then, the calibrated model was verified using the measured data. Comparison of the time series of the measured, assimilated, and modeled wave height is illustrated in Fig 3.1. As can be seen, there is an acceptable agreement between the measured and modeled data. The model's performance was also quantified by computing some standard statistics shown in Table 3.1.

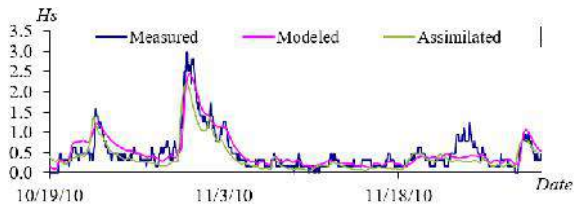

Fig 3.1. Time series of the wave height (m)

Table 3.1. Error indices of buoy and modeled wave height data

Error index	Significant wave height
Bias (m)	0.03
R	0.90
MSE	0.04
SI	0.42

All the error indices show that the simulated wave height using SWAN and buoy recorded data are nearly similar and the model performs well.

4. Conclusion

In this study, the new reanalyzed dataset, ERA-Interim, was investigated in Noshahr, southern Caspian Sea. The wave model SWAN was utilized to simulate wave characteristics. After calibration and verification of the model, wave height assessment between modeled, assimilated, and observed data showed a very good agreement. Moreover, wave parameters investigation indicates that the majority of wave heights are lower than 1.5 m and the dominant wave direction was also found from NE. Finally, it can be concluded that the ERA-Interim wave height underestimate the H_s, while the wind field can give a more accurate wave hindcasting by appropriate implementation of the numerical model.

5. References

[1] Hubertz, J. M., Driver, D. B. & Reinhard, R. D. [1991] "Wind waves on the Great Lakes: A 32-year hindcast," Journal of Coastal Research 7(4), 945–967.

[2] Teixeira, J. C., Abreu, M. P., and Guedes Soares, C., 1995. Uncertainty of Ocean Wave Hindcasts due to Wind Modelling. Journal of Offshore Mechanics and Arctic Engineering, 117, 294-297.

[3] Holthuijsen, L. H., Booji, N., and Bertotti, L., 1996. The propagation of wind errors through ocean wave hindcasts. Journal of Offshore Mechanics and Arctic Engineering, 118, 184-189.

[4] Rusu, L., Pilar, P., and Guedes Soares, C., 2008. Hindcast of the wave conditions along the west Iberian coast. Coastal Engineering, 55, 906-919.

[5] Kostianoy A, Kosarev AN. The Caspian Sea environment. Springer; 2008.

[6] Eugen Rusu, Florin Onea, Evaluation of the wind and wave energy along the Caspian Sea, Energy, Volume 50, 1 February 2013, Pages 1-14.

[7] Hadadpour, S., Etemad-Shahidi, A., Jabbari, E., Kamranzad, B., Wave energy and hot spots in Anzali port, Energy, Volume 74, 1 September 2014, Pages 529-536.

[8] Zounemat-Kermani, M., Kisi, O., Time series analysis on marine wind-wave characteristics using chaos theory, Ocean Engineering, Volume 100, 15 May 2015, Pages 46-53.

[9] Dee DP, Uppala SM, Simmons AJ, Berrisford P, Poli P, Kobayashi S, et al. The ERA-Interim reanalysis: configuration and performance of the data assimilation system. Quart JR Meteorol Soc 2011; 137:553e97.

NUMERICAL MODELING OF NUTRIENT ASSIMILATIVE CAPACITY OF ANZALI WETLAND

Zahra mohagheghe hazrati, Naser Hajizade zaker, Fahime Rostami
1) Department of Environmental Engineering, Tehran university, Tehran, Iran, z.m.hazrati@ut.ac.ir
2) Department of Environmental Engineering, Tehran university, Tehran, Iran, nhzaker@ut.ac.ir
3) Department of Environmental Engineering, Tehran university, Tehran, Iran, f.rostami1985@ut.ac.ir

1. INTRODUCTION

Wetlands are vital for human survival. They are among the world's most productive environments; cradles of biological diversity that provide the water and productivity upon which countless species of plants and animals depend for survival.

Anzali wetland located in the southwestern part of the Caspian Sea. The big cities consists of Rasht, Some-e-sara and rezvan- shahr are located in the vicinity of this wetland. Therefore, marine pollution due to discharge of domestic sewage and industrial activities causes serious problems for this precious ecosystem environmental. In this paper, nutrient assimilative capacity of The Anzali wetland during a month in summer was studied. In order to perform any engineering project or marine environmental study related to Anzali wetland, the prediction of currents is an essential task. Therefore, MIKE 21 HD FM hydrodynamic and quality model was used to simulate nutrients and chlorophyll a concentrations.

2. STUDY AREA

The Anzali Wetland covers an area of 193 km2 in Guilan Province of Iran on the southern coast of the Caspian Sea. The northern open boundary of the Anzali wetland interacts with the Caspian sea, while is enriched by 9 sources of rivers from the southern part. The water quality of the wetland is deteriorating due to the inflow of wastewater and solid waste from neighboring cities, including the provincial capital, Rasht**.** Aquaculture is an especially important economic activity in Anzali wetland. Aquaculture interacts with the environment. It utilizes resources and causes environmental changes. The release of soluble inorganic nutrients (nitrogen and phosphorus) has the potential to cause nutrient enrichment possibly followed by eutrophication (increase of primary production) of a water body. Related changes in phytoplankton ecology may result in algal blooms, which can be harmful to wild and farmed organisms. High concentrations of nutrient components like nitrate and nitrite have been reported by Nippon Koie (2005) in Anzali wetland.

3. METHOD

MIKE 21 HD hydrodynamic and quality model was used to simulate nutrient and chlorophyll a concentrations within Anzali wetland. The Hydrodynamic module is the basic computational component of the entire MIKE 21 FM modeling system providing the hydrodynamic basis for the ECO Lab Module.

4. MODEL INPUT

HYDRODYNAMIC (HD) MODULE

Anzali wetland hydrodynamic model was forced by considering: wind forcing, water surface changes at open sea boundary, impact of river discharges, surface shear stress, Precipitation and evaporation and bottom friction. The number of horizontal cells was 4623. A time step of 5 s was required to satisfy the Courant–Friedrichs–Lewis (CFL) criterion and avoid divergence. The boundary condition information including surface elevation, river discharges data and wind speed put into the model. Various sensitivity tests were carried out to analyze the effect of variations of different parameters on the results including bed resistance and eddy viscosity. after Calibration which is the comparisons of measured and simulated surface elevation time series at a point located near the Ghazian boundary a very good agreement has been observed.

ECOLAB MODULE

Initially, the current condition of Anzali wetland with the existing load of nutrients was modeled. Chlorophyll a was used as the metric of primary production and results were compared with OECD open boundary index (OECD 1982), which is shown in fig.1, to categorize the water into different trophic states. Based on the water trophic state, 6 scenarios were defined and simulated. Through these scenarios, the amount of nutrient load from existing sources increased regularly. Finally, simulation was stopped when the trophic state of the wetland became predominantly eutrophic.

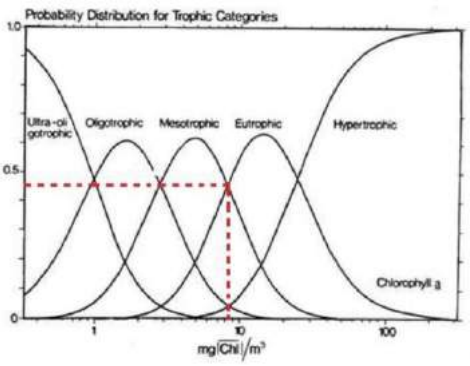

Figure 1: OECD open boundary index (OECD 1982), probability distribution curve for the average chlorophyll a used for controlling the trophic status in simulation. The probability that the water will be within a particular classification is taken from the probability curve

5. RESULT AND DISCUTTION

HD

Simulation was conducted under the typical condition of one month in summer. The results indicated that wind forcing is the major forcing factor in Anzali wetland. The Depth-averaged current pattern due to northwestern wind (prevailing wind) of 4m/s simulated by Mike 21-FM and is shown in fig.2. The current velocity ranged between 0.1 and 0.3m s−1 with the highest velocities at the Ghazian(open boundary). According to the results of model, currents flow from north to south in the Ghazian (the wind direction). The currents flow from south to north near the Shanbe bazar impressed by currents coming from the Ghazian. Currents in other parts of the wetland have very low velocity with clockwise direction.

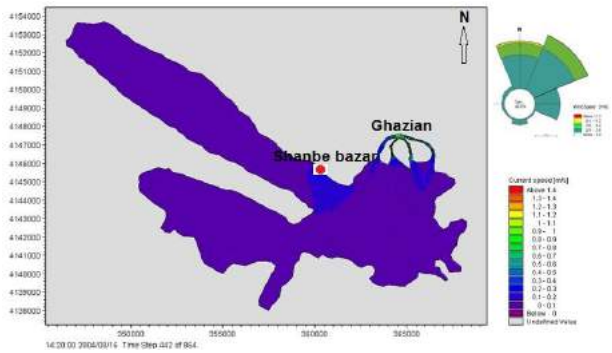

Figure 2: Overview of current in the surface layer

ECOLAB

The main objective of the current study was the estimation of the nutrient assimilative capacity of Anzali wetland. The water quality and chlorophyll a modeling in the study area was conducted for a 1-month period under current condition and also assumed scenarios of nutrient loadings. The average Chlorophyll a was used to determine the trophic status Probabilities based on OECD (1982) index. Under current condition, the Anzali wetland is mainly mesotrophic which means that it is receiving moderate rates of nutrient inputs(Fig.3). Under the mesotrophic dominant state of the current condition, the maximum assimilative capacity was estimated by increasing nutrient loads based on different scenarios.

Different scenarios were defined and nutrient load increased gradually until the eutrophic state was predominant(Fig.4). In this step, simulation was stopped and the total load of nutrients in the last scenario was selected as the maximum nutrient assimilative capacity. Total load of nutrients in scenario 6 was considered as nutrient assimilative capacity of Anzali wetland.. Distribution of total nitrogen, phosphorous, and chlorophyll a under different nutrient loads was studied numerically. It was found that the Anzali wetland can assimilate 9,554 kg/day TN and 1,236.5 kg/day TP in its capacity. Restrictions of N and P loading to Anzali wetland should be accomplished by implementing advanced wastewater treatment in the watershed to maintain chlorophyll a concentrations in Anzali wetland permanently in mesotrophic condition. Anzali wetland needs to build on methods and practices that have been proven to be effective and also work on ways to develop enforceable alternative accountability frameworks or provide reasonable assurance that point and non-point pollution source controls are achieving desired results.

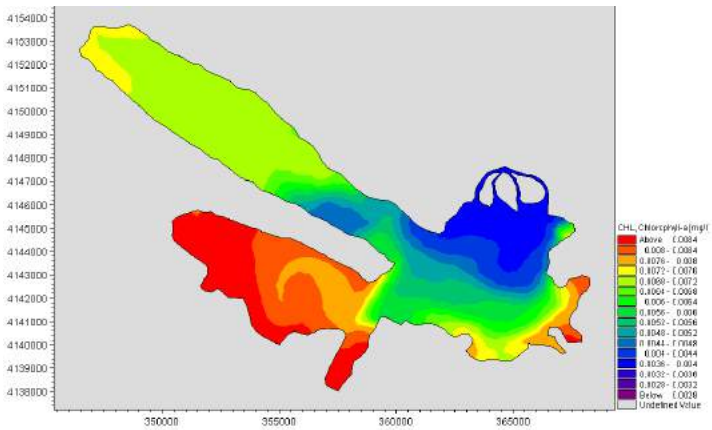

Fig. 3 Distribution of time-averaged chlorophyll a concentrations within Anzali wetland under current condition

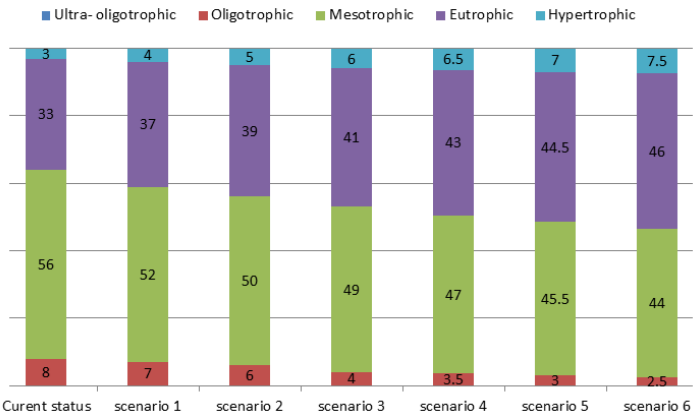

Fig. 4 Trophic status probability in Anzali wetland under all scenarios based on oecd(1982)

6. REFERENCES

[1] Nippon Koie Co., Ltd, 2005. "The Study on Integrated Management for Ecosystem Conservation of the Anzali Wetland in the Islamic Republic of Iran".

[2] OECD, 1982. Eutrophication of waters: monitoring, assessment and control. Organisation for economic and cooperative development, Paris, France

[3] DHI, (2007). MIKE 3 Flow Model User Guide and Scientific
Documentation, Danish Hydraulic Institute.

NUMERICAL MODELING OF WAVE-CURRENT COMBINED MOTION USING TWO-EQUATION TURBULENCE MODELS

Ahmad Sana

Department of Civil and Architectural Engineering, Sultan Qaboos University, Muscat, Oman,
sana@squ.edu.om

1. Introduction

In the coastal environments both waves and currents coexist to affect the bottom boundary layer characteristics. In the past analytical models were used to analyze the bottom boundary layers under wave-current combined motion. In general, these analytical models assumed different variations of the cross-stream eddy viscosity. These models have been useful for a general understanding of the bottom boundary layers properties. However, in the past three decades the availability of efficient computational resources has prompted the use of numerical models to study the coastal bottom boundary layers. In the recent years a number of studies have been carried out using two equation turbulence models to study steady and wave boundary layers. The most popular two-equation models thus far are k-ε model and k-ω model. For wave-current combined motion, the capabilities of these are not fully explored as yet.

The present study was carried out to examine the applicability of this low Reynolds number k-ε model to one-dimensional wave-current collinear motion.

2. Methodology

2.1. Governing Equations

Using the eddy viscosity concept, the equation of motion, for one dimensional oscillatory boundary layer, may be written as;

$$\frac{\partial u}{\partial t} = \left(\Delta p_S + \frac{\partial U}{\partial t} \right) + \frac{\partial}{\partial y} \left\{ (\nu + \nu_t) \frac{\partial u}{\partial y} \right\} \qquad (1)$$

where, u; the velocity in x-direction, Δp_s; steady pressure gradient, U; free-stream velocity, t; time, y; cross-stream dimension and ν_t; eddy viscosity. According to the general form of low Reynolds number k-ε model the eddy viscosity is expressed as;

$$\nu_t = C_\mu f_\mu \frac{k^2}{\tilde{\varepsilon}} \qquad (2)$$

Where, C_μ is a constant (=0.09 for the models considered here) and f_μ is the damping function. The turbulent kinetic energy, k transport equation is;

$$\frac{\partial k}{\partial t} = \frac{\partial}{\partial y} \left\{ \left(\nu + \frac{\nu_t}{\sigma_k} \right) \frac{\partial k}{\partial y} \right\} + \nu_t \left(\frac{\partial u}{\partial y} \right)^2 - \tilde{\varepsilon} - D \qquad (3)$$

And the transport equation of turbulent kinetic energy dissipation rate, $\tilde{\varepsilon}$ is;

$$\frac{\partial \tilde{\varepsilon}}{\partial t} = \frac{\partial}{\partial y} \left\{ \left(\nu + \frac{\nu_t}{\sigma_\varepsilon} \right) \frac{\partial \tilde{\varepsilon}}{\partial y} \right\} + C_1 f_1 \nu_t \frac{\tilde{\varepsilon}}{k} \left(\frac{\partial u}{\partial y} \right)^2 - C_2 f_2 \frac{\tilde{\varepsilon}^2}{k} + E \qquad (4)$$

Here, C_1, C_2, σ_k and σ_ε are model constants and f_1, f_2, D and E are model functions.

Jones and Launder [1] (JL model) proposed an expression based on turbulence Reynolds number only. But, Myong and Kasagi [2] (MK model) and Nagano and Tagawa [3] (NT model) used wall coordinate ($y^+ = yu_*/\nu$, u_* = shear velocity) in the expression for the damping function. MK model and NT model perform better than the JL model, depicting the importance of the distance in the damping function.

2.2. Numerical Method

All the governing equations (Eq. 1, 3 and 4) were made dimensionless using the kinematic viscosity of the fluid ν, amplitude of the free-stream velocity U_0 , angular frequency χ (=$2\pi/T$, T = period of oscillation), fluid density ρ, and the distance from the wall to the free-stream y_h. In the dimensionless form, governing equations require wave Reynolds number R_w (=$U_0^2/(\chi\nu)$) and the reciprocal of Strouhal number S (=$U_0/(\chi y_h)$) as input values. The steady pressure gradient has to be found by trials to produce the same steady velocity magnitude u_c as in the experimental data.

At the solid boundary, no slip boundary condition and at the free-stream, gradients of velocity, turbulent kinetic energy and its dissipation rate were equated to zero. The wall boundary condition for turbulent kinetic energy dissipation rate $\tilde{\varepsilon}_0$ is given in Table 1. It may be observed that this boundary condition involves second derivative of the turbulent kinetic energy and therefore numerically rigid. A mathematically equivalent boundary condition may be derived as follows:

$$\tilde{\varepsilon}_0 = \nu \frac{\partial^2 k}{\partial y^2} = \nu \frac{\partial^2}{\partial y^2}\left(\sqrt{k}\right)^2 = 2\nu\left(\frac{\partial \sqrt{k}}{\partial y}\right)^2 + 2\nu\sqrt{k}\frac{\partial^2 \sqrt{k}}{\partial y^2} \quad (5)$$

But at the wall, k=0, so the second term on the right hand side vanishes and we get;

$$\tilde{\varepsilon}_0 = 2\nu\left(\frac{\partial \sqrt{k}}{\partial y}\right)^2 \quad (6)$$

In the present study this mathematically equivalent wall boundary condition for $\tilde{\varepsilon}$ was used instead of the one with second derivative of k.

A Crank-Nicolson type implicit finite difference scheme was used here. The grid spacing near the wall was varied exponentially in order to achieve better accuracy. In space 100 and in time 6000 steps per wave cycle were used. The convergence was based primarily on velocity, k and ε and then on maximum wall shear stress. The convergence limit was set to 1×10^{-6} in the present study. A detail of the finite difference method and the solution procedure is given by [4].

2.3. Experimental Data

Here the experimental data by [4] was used for comparison with the model prediction. The experiment was performed in a U-shaped oscillating tunnel equipped with a centrifugal pump to generate the uniform flow. The velocity was measured using one component LDV in forward scatter mode. The wall shear stress was computed by assuming the logarithmic velocity profile in the near-wall region. Main parameters of this experiment are; R_w= 5.4×10^5, R_c (= $u_c y_h/\nu$) = 2345, y_h = 3cm, u_c= 8.9cm/s, U_0=116.8cm/s, T = 2.84s.

3. Results

From Fig.1, it is clear that JL model underestimated the velocity gradient in the near wall region, however, the overall predictive ability is satisfactory, in this regard. Especially the velocity over-shooting is predicted very well, and the agreement far from the wall is excellent.

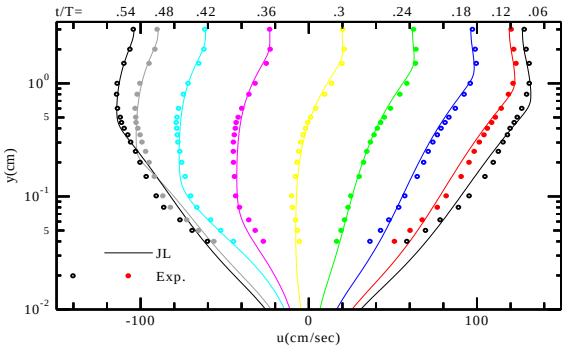

Figure 1. Velocity Profile

Figure 2 depicts that MK and NT models are superior to JL model in predicting period averaged fluctuating velocity <u'>. The cross-stream variation of <u'> shows a peak at distance of 0.04cm from the wall and a change in the curvature at a distance of about 0.5cm which corresponds to the boundary layer thickness as observed from Fig.1. Figure 3 shows that the wall shear stress prediction by MK and NT is much more close to the experimental value in magnitude, as compared to that by JL model. The reason for the underestimation by JL model is in fact due to the underestimation of turbulence fluctuations. The experimental data shows stepping of the wall shear within phases of about 45° and 135° and then from 270° to 310°.

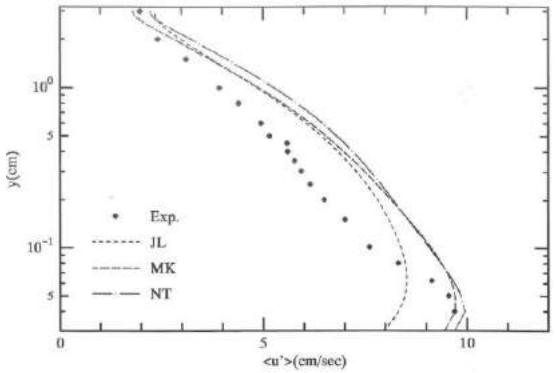

Figure 2. Fluctuating velocity

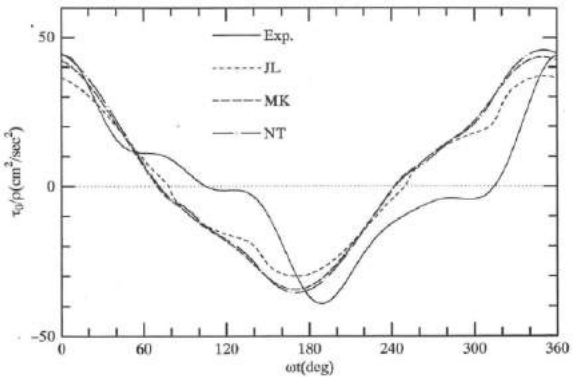

Figure 3. Bottom shear stress

4. References

[1] Jones, W. P. and Launder, B. E., "The prediction of laminarization with a two-equation model of turbulence", *Int. J. Heat Mass Transfer*, 15, 1972, pp. 301-314.

[2] Myong, H. K. and Kasagi, N., "A new approach to the improvement of k-ε turbulence model for wall-bounded shear flows", *JSME Int. J., Series II*, 33, 1, 1990, pp. 63-72.

[3] Nagano, Y. and Tagawa, M. J., "An improved k-ε model for boundary layer flows", *J. Fluids Eng. ASME*, 112, 1990, pp. 33-39.

[4] Sana, A., *Experimental and Numerical Study on Turbulent Oscillatory Boundary Layers*, Tohoku University, Sendai, Japan, Doctoral thesis, 1997.

INVESTIGATION OF COASTAL TRAPPED WAVES ON THE SOUTHERN CONTINENTAL SHELF OF CASPIAN SEA OF BABOLSAR, OFF MAZAZDARAN

Mina Masoud, Nasser Hajizadeh[2]

1) PhD student, School of civil engineering, University of Tehran, Tehran, Iran, mina_masoud@ut.ac.ir
2) Associate Professor, Faculty of Environment, University of Tehran, Tehran, Iran, nhzaker@ut.ac.ir

1. Introduction

The Caspian Sea, as the largest inland water body on the Earth has a unique marine environment and is of great importance for the world and the lateral countries around it.

The continental shelf is one of the most important and diverse ecosystems economically and ecologically. There is no doubt that coastal trapped waves are a major feature of most shallow shelves. Coastal trapped waves can make a significant contribution to the observed variability of sea level and currents on the shelf and it is essential to include them in a discussion of the coastal ocean.

One of the common tools for investigating coastal trapped waves is numerical modeling. Brink model is the set of Matlab mfiles can be used to calculate coastal trapped wave modal structures and dispersion curves under very general circumstances. A complex frequency is allowed, so that instability and damping can be accounted for directly.

According to previous investigation about currents on continental shelf off Babolsar, alongshore currents were uniform across the depth and were dominated by low frequencies less than 0.33 cycle per day with peak energy at 7-9 days periods. The results showed a low relationship between low frequency dominated alongshore currents and local wind forcing and raised the hypotheses of the existence of west to east traveling coastal trapped waves along the southern coast of the Caspian Sea [1].

In this paper, existence of trapped waves which produce currents on continental shelf off Babolsar are investigated by the Brink model. Therefore, comparison between results of model and field measurements is performed to prove this hypothesis. Also, the type and characteristics of trapped waves in summer and winter on Babolsar shelf are identified by principle formulas.

2. Study Area

The study area is located at approximately N 36o, 41', 54" latitude and E 52o, 33', 23" longitude. The shelf in the study area has a width of about 10 km. The depth gradually increases to about 45 m near the shelf break, after that the depth sharply increases to 400 m at about 18 km from the coastline [1].

3. Methodology

3.1. Model Description

In this study, the topographically trapped wave model (MATLAB version, Brink, 2010) developed by Dr.K.Brink based on Brink and Chapman (1987) are used [2]. The model provides a free wave solution for linearized topographically trapped waves. This model can be used to calculate coastal trapped wave modal structures and dispersion curves under very general circumstances. A complex frequency is allowed, so that instability and damping can be accounted for directly. Modal structures and energy diagnostics are provided.

3.2. Empirical Formulas

There are some formulas which are resulted from coastal trapped wave theories. These formulas can determine the type of costal trapped waves.

A general criterion for barotropic shelf water response for wind forcing frequencies in the "weather" band (2π/few weeks to 2π/few days) can be derived. For the purpose of rapid calculation, this criterion reduced, approximately, to

$$N_s^2 \alpha^2 f^{-2} \ll 1$$

Where N_s^2 is a shelf-averaged value of the buoyancy frequency squared, α is an averaged shelf bottom slope and f is the Coriolis parameter. Under the more restrictive condition, this criterion will be reduced to $N_s \alpha f^{-1} \ll 1$. Analysis shows that the shelf edge pressure is zero and essentially all the wind-driven fluctuation flow occurs on the shelf [3].

Another criterion is stratification parameter or burger number. Wang and Moors (1976) have presented the $S = (N_{max} H_T)/fL$ formula as the burger number [4]. Also, Mysak (1980) has presented the $S = \left(\frac{NH}{fL}\right)^2$ formula as the burger number [5].

The last criterion is the effective baroclinic radius of deformation (L_D) which is determined by $\bar{N}\bar{H}/f$, where $\bar{N}$ and $\bar{H}$ are the mean stratification and local depth, respectively. Wang and Moores have presented the below relation

$$\left(\frac{H_s}{\bar{H}}\right) \sim \frac{f^2 L_s^2}{\bar{N}^2 \bar{H}^2} \sim \left(\frac{L_s}{L_D}\right)^2$$

Where L_s is the offshore length scale of the wave (i.e., the shelf width for the case of long waves), and H_s is the "trapping'' height of the wave. Therefore, motions are

barotropic ($H_s/\overline{H} \gg 1$) where the baroclinic radius of deformation is small ($L_D \ll L_s$) [4].

4. Results

The shelf in the study area has a width of about 10 km and its depth gradually increases to about 45 m near the shelf break, after that the depth sharply increases to 400 m at about 18 km from the coastline [1]. Its maximum depth (H) is 400 m and its length (L) is 19.5 km.

The Maximum of N^2 in summer is $1.2e^{-3}$ and the mean of N^2 in summer is $0.467e^{-4}$ according to field measurements [5]. There is no stratification in winter, so the amount of N^2 is assumed to be 10^{-6} in winter.

Coriolis parameter in this study area is 0.875e-4 and the mean shelf slope (α) is 0.02.

In this model, a free surface approximation is chosen. Because, the rigid lid criterion ($f^2L^2/(gH) \ll 1$) is not satisfied and the amount of $f^2L^2/(gH)$ is about 1000 in this study area.

4.1. Investigation about the hypothesis of the existence of Trapped waves

The results of simulation indicate that frequency ranges are between $8e^{-6}$ to $10e^{-6}$. Dominated wave periods is 7-9 days considering the dispersion curve (not shown here). Also, results of Zaker et al. (2011) have presented that the dominate period is 7-9 days. Therefore, the results of simulation and field measurements are fully compatible.

Furthermore, one of the characteristics of currents were driven by coastal trapped waves is that they propagate to the east in one direction in the northern hemisphere [5]. It is in compatible with the results of Zaker et al. (2011).

Another characteristic of currents driven by coastal trapped waves is that the strongest velocities occur near shelf break and slope. Also, currents become weak near the coast and in the deep water [6]. According to the measurements of Zaker et al. (2011), currents on the shelf break station is stronger than ones on the station which is near the coast. So, it is another compatibility with the results of Zaker et al. (2011).

Therefore, it is concluded that coastal trapped waves exist on the continental shelf of Babolsar.

4.2. Determination of type of coastal trapped waves

In this study area, the amount of $N_s^2\alpha^2f^{-2}$ is $5.2e^{-8}$ in winter. Therefor, there are barotropic shelf waves on the Babolsar shelf in winter. In addition, the amount of $N_s\alpha f^{-1}$ is 2.3e-4. Thus, the shelf edge pressure is zero and essentially all the wind-driven fluctuation flow occurs on the shelf in winter.

In the case study, the burger numbers are 2.3 and 2.3e-4 in summer and winter respectively. Based on these criterions, stratifications are intermediate and low in summer and winter respectively. Therefore, there are internal kelvin waves along the barotropic shelf waves in summer and barotropic shelf waves in summer.

According to the effective baroclinic radius of deformation, L_s is 18000 m and the amount of L_D is $5e^4$ in summer. So, there are bottom trapped and baroclinic kelvin motions in summer. In addition, the amount of L_D is 4.5 m apparently; L_D is less than L_S so there are motions are barotropic in winter. Additionally, the amounts of trapping height (H_S) are 78 m and 1742.2 m in summer and winter, respectively.

5. Summary and Conclusion

Dominated periods are 7 to 9 days according to the results of the simulation by Brink model which is compatible with observed dominated periods.

Also, one of the characteristics of coastal trapped waves is propagation to east from west in northern hemisphere which is compatible with observed currents direction.

Therefore, the existence of coastal trapped waves is proved in Babolsar so probably dominated currents are due to these waves.

With using three criterion for determination of the type of coastal trapped waves, there are brotropic kelvin waves along barotropic shelf waves (coastal trapped waves) in summer and barotropic shelf waves in winter.

6. References

[1] Zaker, N. H., Ghaffari, P., and Nouranian, M.: Currents on the Southern Continental Shelf of the Caspian Sea off Babolsar, Mazandaran, Iran, Journal of Coastal Research, Special Issue 64, 2011.

[2] Brink K.H. and Chapman D.C., 1987, Programs for computing properties of CTW and wind-driven motions over the continental shelf and slope, Technical Report WHOI-87-24, Woods Hole Oceanographic Institution.

[3] Clarke, A. J., Brink, K. H., The response of stratified, frictional flow of shelf and slope waters to fluctuating large scale low-frequency wind forcing. J. Phys. Oceanogr.15:439-53,1985.

[4] Wang, D.-P., and C. N. K. Mooers, Coastal trapped waves in a continuously stratified ocean, J. Phys. Oceanogr., 6, 853-863, 1976.

[5] Mysak, L. A., Recent advances in shelf wave dynamics. Rev. Geophys. SpacePhys, 1980.

[6] Zaker, N. H., Ghaffari, P., and Jamshidi, S.: Physical Study of the Southern Coastal Waters of the Caspian Sea, off Babolsar, Mazandaran in Iran, J. Coastal R., Special Issue, 50, 564–569, 2007.

[7] Codiga, D. L, Renouard. D. P. and Fincham A., Experi-ments on waves trapped over the continental slope and shelf in a continuously stratified rotating ocean, and their incidence on a canyon. J. Mar. Res., 57, 585-612, 1999.

ESIMATION OF CHABAHAR BAY FLUSHING TIME BY A TWO DIMENSIONAL HYDRODYNAMIC MODEL

Morteza Zanganeh[1]

1) Department of technical engineering , Golestan University, Gorgan, Iran, E-mail: m.zanganeh @gu.ac.ir

1. Introduction

Estimation of flushing time or turnover time is an essential issue in design of coastal infrastructures in enclosed water bodies. This subject is highlighted more in restricted water bodies for the layout of outfall systems of desalination factories or design of artificial islands for recreational activities. One of the most important bays in Iran is Chabahar bay where recently many economical activists have decided to invest at it. Due to the important role of Chabahar Bay in the region, many marine projects were constructed in this bay. In addition, one of the largest marine projects of the country, i.e. Shahid Beheshti Port Complex located at the east end of the bay. Therefore, the bay must be under a comprehensive monitoring and modeling study including an extensive field measurement program. Most of these investments at this area go back either to the petrochemical activities or power plant systems which may increase the potential damage for pollution of this environmentally sensitive area. So, it is advantageous to develop a model to estimate the flushing time for the semi-enclosed coastal embayment in order to estimate their flushing capability.

Various activities have been devoted so far to estimate flushing time in water bodies. Stamou et al. (1999) presented an analytical method to appraise the flushing time of Saraya wetland at Aqoba gulf. Their results showed the flushing time for the study area on average 5 days which is important to remove pollutants from the water bodies [1]. Also, Stamou et al. (2007) presented an algorithm to estimate flushing time on the back of Durrat Alkhobar artificial islands. Their findings prove tidal currents disability to remove water pollutants from the back of the artificial islands and some modifications to increase the study area flushing. Based on their research, considered modifications can bring the flushing time in the order of 15 days which is a tolerable period for the residents living around the region not to feel the bad smell [2]. In another research, Stamou et al. (2007) evaluated different remedies to decrease the flushing time of the Salman bay. They concluded that among dredging, widening water entrance channel and increasing bottom level of the channel the thirt action has shown the best performance by decreasing the flushing time from 48.6 days to 12.8 days for tidal currents. However, this action has increased flushing time from 13 days to 34 day for stormy condition [3]. Brenes et al. (2007) did some researches to estimate the flushing time of Perlas wetland and Blufield gulf. Their findings showed the flushing time for the first water body is about 14 to 17 days while this factor reported about 2 to 4 days for Blufield gulf [4]. More recently, Zanganeh and Hajmomeni presented a method based on FM module of MIKE 21 to estimate the flushing time of an enclosed water body surrendered by artificial islands which themselves were connected with some causeways [5]. Their research was based on Stamou work and was applied for a case study in Iran. In their study only storm-induced currents were considered. Their final results showed a flushing time about 14 day with 100 percent reliability while for 96.7 percent reliability the flushing time was estimated about 4 days. In this paper, the FM module of MIKE 21 is applied to develop a model to estimate flushing time of Chabahar bay in which only tidal currents as the stimulus for flow pattern are taken in to account.

2. Study area

Chabahar crenulated shape bay is located in the southeast of Iran, near to Iran-Pakistan border. It is the largest bay of Iran bordering Oman Sea with a 13.5 km wide entrance and 17 km length in south-north direction (Figure 1). As this part of the Iranian coastline faces the open sea, most of the coasts receive persistent swell waves from south direction. SE and W directions are the most predominant wind directions according to long-term wind data of synoptic stations. The Indian Ocean monsoon has a strong seasonal effect on the currents of the Oman Sea.

The water depth outside of the Chabahar Bay is about 30 m. The average tidal range is about 1.7 m. The bathymetry of Chabahar bay and the considered mesh for the fluid flow model in the MIKE 21 software have been indicated in Figure 2. Based on the bathymetry of the study area the volume of the water body is MSL water level is about 2260000000 m^3.

3. Flushing time

The flushing time defines the amount of time required to exchange the water in a semi-enclosed water body by new

Figure 1: The Chabahar bay

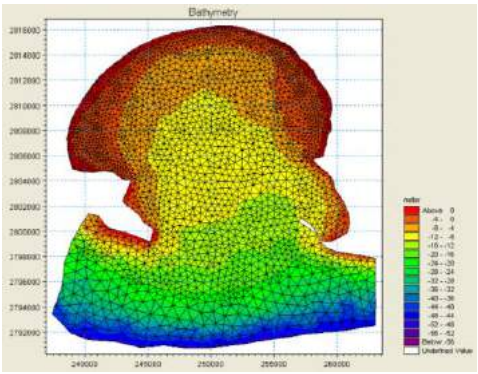

Figure 2: The Chabahar bay bathymetry

water. Water renewal of semi-enclosed coastal lagoons (SECL) is vital for oxygen supply and the removal of pollution. There are various indicators to estimate how fast the water of a SECL is renewed via transport and mixing. In this paper, the formula employed by Stamou et al. at Durrat Alkhobar artificial islands project is used to estimate the flushing time (Θ). The formula is expressed as follows:

$$\Theta = \frac{V_{waterbody}}{Q_{ex}}$$

in which $V_{waterbody}$ is the volume of water body for Mean Sea Level (MSL) condition and Q_{ex} is avrage discharge leaving the waterbody.

4. MIKE 21-FM module

In order to capture the flow pattern at the study area, the FM module of MIKE 21 model was applied. The FM module of MIKE 21 package is a two-dimensional module to model coastal currents based on solving depth-averaged equations by unstructured finite volume method. This is one of the DHI software and its governing equations are the continuity equation, the motion equation in the x- axis direction and the motion equation in the y- axis direction. In this software water depth, current velocity in x direction and current velocity in y direction are obtained by solving the equations.

To capture the flow pattern, registered tidal levels near Chabahar bay are assigned as the boundary condition of the model. Solving the governing equations in the study area, leaving discharge from the bay entrance is calculated. According to the flushing time relation now this parameter can be estimated.

5. Results

Following to the development of numerical model for the studied area, results for the current speed at a time step along with time series of water discharge at the entry of Chabahar bay have been reported in Figure 1 and Figure 2, respectively. Based on these results the flushing time at the studied area is estimated about 2 to 4 days.

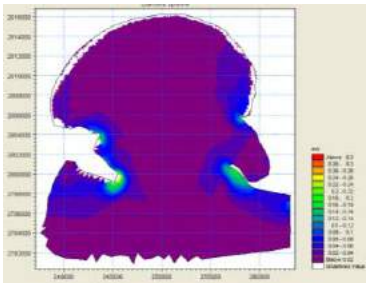

Figure 3: Distribution of coastal current velocities at Chabahar bay for a time step

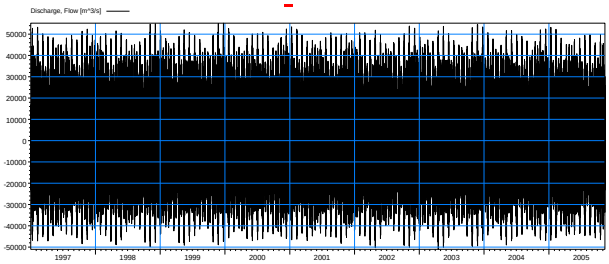

Figure 4: Discharge time series at the Chabahar bay entry (m^3/s)

6. References

[1] Stamou A. I., Memos K. and Pipilis K.(1999b). “Mathematical Modelling of Thermal Discharges in Coastal Regions”, 28th IAHR Congress, Graz, Austria.

[2] Stamou, A., Memos, C. and Spanoudkis, K.. Estimating water renewal time in semi-enclosed coastal areas of complicated geometry using a hydrodynamic model, ICS 2007, Journal of Coastal research. pp. 282-286, 2007

[3] Stamou, A. I., C. D. Memos, and M. E. Kapetanaki. "Modelling water renewal in a coastal embayment." Proceedings of the ICE-Maritime Engineering 160.3. 93-104. 2007

[4] Brenes, Carlos L., Aldo Hernández, and Daniel Ballestero. "Flushing time in Perlas Lagoon and Bluefields Bay, Nicaragua." Investigaciones Marinas 35.1 (2007): 89-96.

[5] Zanganeh, M. and Hajmomeni, A. "estimation of flushing time for enclosed water bodies by artificial islands in causeways " Third International Symposium on Environmental and Water Resources Engineering, KhajehNasir university, 2015

SIMULATION OF QESHM STRAIT TIDAL CURRENTS USING PMO-DYNAMICS AND MIKE21

Mohammad Javad Ketabdari[1], Amir Hossein Parvin Ashtiani[2]

1) Associate Professor, Amirkabir University of Technology, Tehran, Iran, ketabdar@aut.ac.ir
2) MSc, Amirkabir University of Technology, Tehran, Iran, ahparvin@aut.ac.ir

1. Introduction

Nowadays recent coastal ocean models are capable of numerically simulating a variety of coastal, estuarine and marine phenomena. One of these is maritime currents that have important impact on marine and coastal environment. Usually comprehensive models have several computational modules to perform various tasks such as hydrodynamics, waves and morphology. Generally main task undertakes to hydrodynamics module that solves basic governing equations. Mahmoudov simulated currents on Qeshm strait by 3D open source COHERENCE model [1]. Sadeghi et al. reviewed tidal currents in nearby khouran starait [2]. Momen-nia et al. studied numerical modeling for propagation of oil pollution at Qeshm channel [3]. Sharifi et al. modeled wind generated waves with WAVEWATCH III in Hormoz Strait [4]. Bakhtiari et al. investigated on PMO-Dynamics wind waves result in Bousehr Gulf [5]. Aghaganloo et al. presented results of 2D PMO-Dynamics model for the tidal currents simulation in Persian Gulf [6]. In this essay Qeshm Strait and Shahid Rajaei port that is one of the most important ports of Iran is determined for case study. The aim of this study was hydrodynamic modeling and simulation of current patterns in this area [7].

2. PMO-Dynamics[1]

Persian Model for Ocean Dynamics, is an Iranian numerical model developed for coastal engineering studies by internal experts. Due to the growth in the needs of related coastal engineering software and according to some difficulties such as lack of transfer of technical knowledge, and considering the requirement of a valid native numerical model, the Ports and Maritime Organization (PMO) decided to invest for development of such a model. The model is applicable in different fields of coastal engineering. This software is composed by tree coupled elements: a spectral wave model, a hydrodynamics model and a morphology module. It can performs simulations in tidal currents, wind-driven currents; coriolis induced currents, simulating the currents in large scale environments (oceans), wave generated currents, large and small scale wave generation and wave propagation simulations, coastal morphology, sediment transportation and tidal analysis and tidal parameters extraction. Hydrodynamic module can perform calculations in 2DH Nested Structured and Unstructured Grid, Cartesian and Spherical Coordination and be able to consider bed friction, turbulence, flood/drying, wave, wind and coriolis terms. The user interface was implemented using C# 4.0 programming language and Net Framework 4.0. SQLite was used as database engine which communicates with main program through system. To achieve a better modular design and simpler debugging process, the software was developed in form of various libraries which can be viewed as DLLs in final distribution.

[1] The public version of PMODynamics can be downloaded by the users after logging in this Link: www.pmodynamics.pmo.ir

3. Governing Equations

The 2DH flow model solves the over depth integrated horizontal equations for momentum and continuity. Following 2D shallow water equations in Cartesian Co-ordinates as [8, 9]:

$$\frac{\partial u}{\partial x}+\frac{\partial y}{\partial x}+\frac{\partial w}{\partial x}=S \tag{1}$$

$$\frac{\partial u}{\partial t}+\frac{\partial u^2}{\partial x}+\frac{\partial uv}{\partial y}+\frac{\partial wu}{\partial z}=fv-g\frac{\partial \eta}{\partial x}-\frac{1}{\rho_0}\frac{\partial p_a}{\partial x} -\frac{g}{\rho_0}\int_z^{\eta}\frac{\partial p}{\partial x}dz-\frac{1}{\rho_{0h}}\left(\frac{\partial s_{xx}}{\partial y}+\frac{\partial s_{yy}}{\partial z}\right)+F_v+\frac{\partial}{\partial t}\left(v_t\frac{\partial u}{\partial z}\right)+u_sS \tag{2}$$

$$\frac{\partial v}{\partial t}+\frac{\partial v^2}{\partial y}+\frac{\partial uv}{\partial x}+\frac{\partial wv}{\partial z}=-fv-g\frac{\partial \eta}{\partial y}-\frac{1}{\rho_0}\frac{\partial p_a}{\partial y} -\frac{g}{\rho_0}\int_z^{\eta}\frac{\partial p}{\partial y}dz-\frac{1}{\rho_{0h}}\left(\frac{\partial s_{xx}}{\partial y}+\frac{\partial s_{yy}}{\partial z}\right)+F_v+\frac{\partial}{\partial t}\left(v_t\frac{\partial v}{\partial z}\right)+v_sS \tag{3}$$

where t is the time; x, y and z are the Cartesian co-ordinates; η is the surface elevation; d is the still water depth; h= η +d is the total water depth; u, v and w are the velocity components in the x, y and z direction; f=2ΩsinØ is the Coriolis parameter (Ω is the angular rate of revolution and Ø the geographic latitude); g is the gravitational acceleration; ρ is the density of water; s_{xx}, s_{xy} , s_{yx} and s_{yy} are components of the radiation stress tensor; v_t is the vertical turbulent (or eddy) viscosity; p_a is the atmospheric pressure; p_0 is the reference density of water, S is the magnitude of the

discharge due to point sources and (u_s, v_s) is the velocity by which the water is discharged into the ambient water.

4. Qeshm Strait and Comparison Methods

Qeshm strait located in Southern Iran, Eastern-Western belonged between Qeshm Island and mainland. This case study damain limited with approximate length over 70Km among 55°45′ to 56°27′ longitude. The different tidal head and phase between Eastern and Western boundary points cause the main local currents in this region. Water fluctuation in the study period was obtained using stations' data from Bandar-e-Abbas, Shahid Rajaei Port, Bahman port, Hormoz Island and Pohl Quay. For comparison, data from two ADCP mounted in Shahid Rajaei and Dargahan stations were used. Furthermore, the results from well-known MIKE21 FM HD software in similar and unique conditions were used. Fig. 1 compares the PMO and MIKE 21 results with measured data. Fig. 2 shows the water level variation simulated by PMO model. Fig.3 shows the directional current results (current rose) by measurement and PMO model. This figure shows that despite all the differences, the dominant current direction was estimated properly by the model.Comparison of water level changes in Shahid Rajaei Port is showed in Fig.4. This figure illustrates a good agreement between model results and measurement data.

5. Conclusions

In this study water level changes and current velocity in Shahid Rajaei port was estimated using PMO-Dynamics and Mike 21. The survey of estimated results against measured data by PMO-Dynamics shows that these parameters have been estimated more accurately than Mike 21 model. Also using this model it is possible to simulate the circulation currents within and outside of Shahid Rajaei port basin.

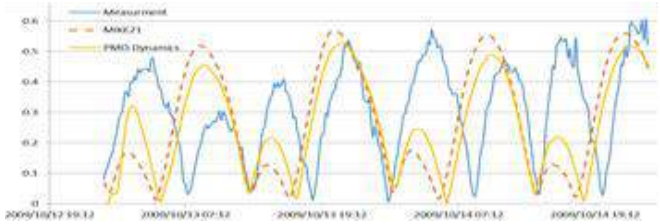

Figure 1 - Comparison of MIKE21 and PMO results with current measurement in Shahid Rajaei Port

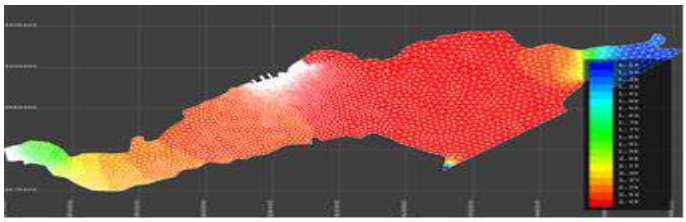

Figure 2 - Water level variation in a time step and domain meshing.

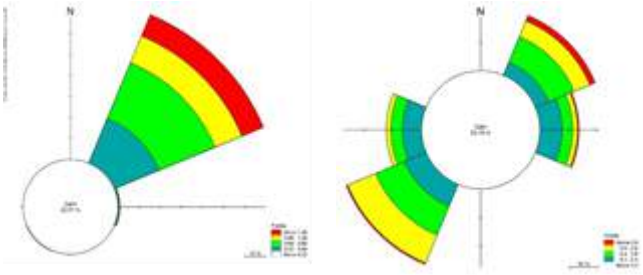

a **b**

Figure 3 - Current rose in Shahid Rajaei station for a) Measured data and b) PMO results

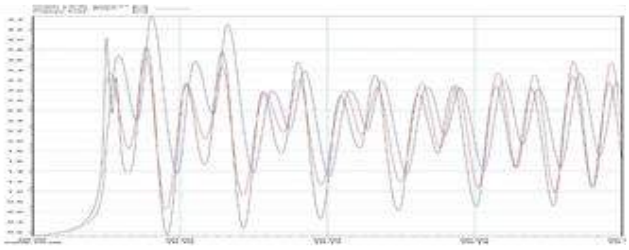

Figure 1 - Comparison of level changes, PMO and Mike21 modeling with measured

4. References

[1] Mahmoudov, M, "*Numerical modelling of Qeshm channel currents by 3D Hydrodynamics Model*",M.sc thesis. Homozgan Univ., Supervisor: Montazeri Namin, M (in Persian), 2007

[2] Sadeghi, A., Tajziechi. M., and Chegini. V., "*Modelling tidal current in Khouran strait*", 11th maritime industry Conference, Kish, Iran, 2009, (in Persian)

[3] Momen-nia. S., Madihi. M., and Ataee.A, B., *"Numerical modelling for propagation of oil pollution (case study: Qeshm channel)"*, 13th maritime industry Conference, Kish, Iran,2011, (in Persian)

[4] Sharifi, F., Ezam, M., and Karami Khaniki, A., *"Numerical modeling of wind waves in the Strait of Hormuz with WAVEWATCHIII"*, 14th ICOPMAS,Tehran,iran,2012,(in Persian)

[5] Bakhtiari, A., Komijani, F., Allahyar, M.R., Tavakoli, M. *"PMO Dynamics check in Boushehr gulf"*, *Journal of oceanography*, Vol. 4, No.14, pages 13-18,,2013,(in Persian)

[6] Aghajanloo, A., Dolatshahi Pirouz, M., Montazeri Namin, M. , *"Numerical Simulation of Tidal Currents in Persian Gulf"*, *Journal of World Academy of Science, Engineering and Technology*, Vol.5,2011, pp. 677-684.

[7] Parvin A.A.H, "*Estimation of sediment transport rate in Hormozgan coastal zone*". M.Sc thesis. AmirKabir Univ., Supervised by Ketabdari, M.J, 2013

[8] DHI, HD Manual MIKE3 and MIKE21 Flow model FM: Hydrodynamic and Transport Model: Scientific documentation,2007

[9] Van Rijn, L.C., *"Principles of sediment transport in rivers, estuaries and coastal seas", AQUA Publication*,1993, pp.12-16

LONG-TERM SEA LEVEL VARIABILITY IN THE SOUTHERN CASPIAN SEA

Mostafa Nazarali[1], Charitha Pattiaratchi[2], Parham Pad[1], and Mohammad Hossein Nemati[3]

1) Pouya Tarh Pars consulting engineers company, Tehran, Iran, mostafa.nazarali@gmail.com
2) University of Western Australia, Perth, Australia, chari.pattiaratchi@uwa.edu.au
3) Port and Maritime Organization, Tehran, Iran, mhn1982@gmail.com

1. Introduction

At the border of Asia and Europe, the Caspian Sea (CS) is the world's largest inland basin. Coastal regions of southern CS experience different types of sea level fluctuations. The timescale of these fluctuations vary from hours to months and years. In this study a good understanding of the Caspian Sea level (CSL) variation is reached through both field observation and numerical modeling.

The CSL variation is due to various factors; these fluctuations could be divided into long-term and short-term categories. The long term CSL variability depends on sea water balance and is dominated by Volga river discharge. The other contributing components for this type of CSL variability include surface evaporation, precipitation, discharge to Kara Bogaz Gol bay and ground water input/output. The next category is short-term CSL variability which is caused mostly by the effect of wind, waves, atmospheric pressure, and tide. These fluctuations have the time scales less than 2-3 days, but the long-term CSL variability acts as seasonal and inter-annual variation. The following figure shows the seasonal CSL cycles from 2009 to 2011 in a coastal station in the southern region of the CS. The reason for sea level rise in the summer times is the higher rivers' discharge which is mostly flows into the CS by Volga River.

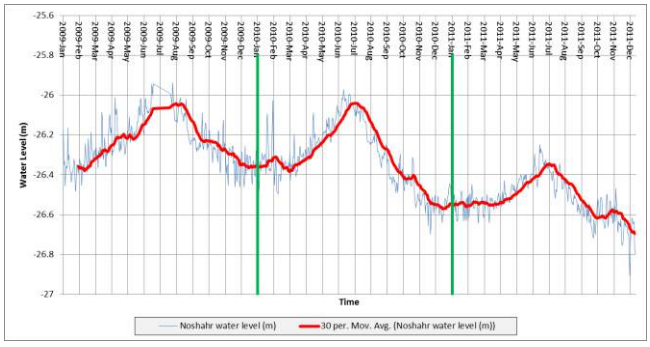

Figure 1. Time series of CSL variation and the seasonal cycles (2009-2011).

2. Methodolody

In this study we tried to investigate the effective hydrological parameters controlling long-term CSL fluctuations. The 0.125 degree gridded evaporation and precipitation data sets were obtained from ERA-Interim ECMWF in which both of them have 12 hourly accumulated values. These data covers the period between 1979 and 2015 including some yearly gaps.

The river discharge data was acquired from Global Runoff Data Centre (GRDC). The largest river coming in to CS is Volga River which accounts for 80 percent of riverine in flow to this lake. Also the outflow to Kara Bogaz Gol is also gathered from the studies of Kostianoy et al. (2007).

In order to study the water budget components and correlation between them and the CSL, an overlap period of 1979 till 2010 was selected. The annual cumulative values of evaporation, precipitation and river input are illustrated in figure 2. In this plot the contribution of each factor in terms of sea level change is expressed in meter. According to this plot absolute annual evaporation rate is higher than other two factors, precipitation and river input. Also it seems that all influencing factors acts together to decrease CSL, during the study period. As it is shown below the annual evaporation rate is increasing with the slope of 0.43 percent and precipitation rate is increasing by 0.23 percent. However the river discharges does not have specific behavior. This is due to the fact that most rivers inflow is regulated by construction of many dams in the upstream regions.

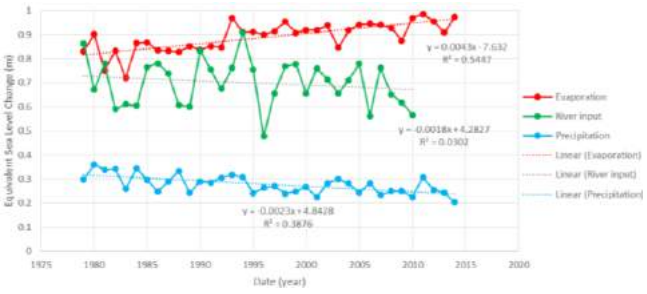

Figure 2. Time series of annual precipitation, evaporation, and river discharge in to the CS.

3. Numerical Simulation

In the next step in order to simulate long term Caspian Sea level variation, DHI MIKE21 2D hydrodynamic model was employed. This model was forced by ECMWF derived evaporation and precipitation data, discharge to Kara Bogaz Gol bay and all river discharges. The simulation period was selected between 1992 and 2005 when all influencing parameters were available.

Due to the purpose of the modeling, a coarse mesh was generated to decrease computational costs. The time series of sea level fluctuation in Anzali port station were extracted and compared to mean monthly observed sea level in this station (Figure 3). It seems that the model could successfully simulate the seasonal sea level variation and also it captures the inter-annual variation of the CSL. As it is shown below the highest peak of mid 1995 and the following gentle decrease of CSL in the next years is also simulated by this model.

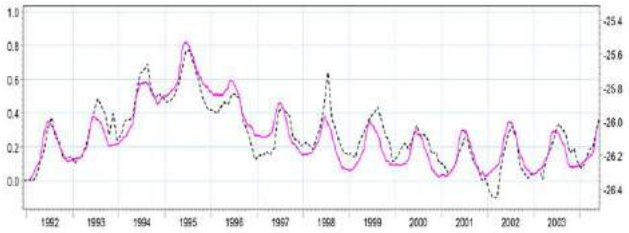

Figure 3. Comparison between observed (solid pink line) and simulated (dotted black line) CSL fluctuations.

4. Conclusion

According to these simulations, the CSL fluctuations during 1992–2005 resulted from climate-forced model have a very strong correlation with corresponding CSL observation. The result of this study also indicates that geological factors and ground water influx/outflux play an insignificant role in the generation of water level change of this lake and the main water budget components are surface evaporation, precipitation, and river discharges.

5. Acknowledgements

The authors would like to thank Iranian Ports and Maritime Organizations (PMO) for their sincere technical and administrative supports, and funding the study.

6. References

[1] Pouya Tarh Pars consulting engineers (2015), *Long-term Caspian Sea water level report*, Under the project entitled: Monitoring and Modeling Study of Northern Coasts of Iran, funded by: Port and Maritime Organization of Iran.

[2] Global Runoff Data Centre (2015): *Long-Term Mean Monthly Discharges, Global Runoff Data Centre*. Koblenz, Federal Institute of Hydrology (BfG).

NUMERICAL MODELLING OF WAVE-DRIVEN CURRENTS IN SHALLOW WATER; A CASE STUDY FROM NOSHAHR COASTS

Marzieh Hajiarabderkani[1], Seyed Mostafa Siadatmousavi[2], Seyed Masoud Mahmoudov[3]

1) School of Civil Engineering, Iran University of Science and Technology, Tehran, Iran, M_Hajiarabderkani@civileng.iust.ac.ir
2) School of Civil Engineering, Iran University of Science and Technology, Tehran, Iran, siadatmousavi@iust.ac.ir
3) School of Civil Engineering, University of Tehran, Tehran, Iran, m_mahmoudov@yahoo.com

1. Abstract

In situ measurements of wave and current close to Noshahr was used to estimate the longshore current within the surf zone close to Noshahr port. The third generation wave model, SWAN[1] was used to simulate wave propagation from offshore boundary to coastline. A 1D model for wave-induced current was developed. The model successfully reproduced alongshore current measured by ADCP[2] during storm event.

2. Introduction

Wave induced longshore currents are assumed to be responsible for changes in the shoreline plan-shape on extend of kilometers [1, 4, 10]. However, the cross-shore currents action should be taken into account for predicting detailed bathymetry variations; for instance when appraising the impact nearby coastal structures [7, 11]. In this study performance of a 1D model for estimating the wave-driven longshore currents is evaluated.

3. Field of Study and Instrumentation

An ADCP close to 5 m isobaths was used to measure wave and current from March 13th to 16th, 2014 at sandy coast of Noshahr, located at the Southern Caspian Sea (Figure 1). A storm with significant wave height of approximately 1.4 m was observed during the measurement period.

Figure 1. Noshahr port and the study area.

[1] Simulating WAves Nearshore.

[2] Acoustic Doppler Current Profiler.

4. Method

The numerical modelling was done along a shore-perpendicular transect crossing ADCP location. Wave transformation from ADCP location to the coastline was simulated using SWAN wave model. This third-generation wave model solves the wave action balance equation with sources and sinks. The wave action (N) is defined as:

$$N \equiv E/\sigma \tag{1}$$

Where E and σ denote wave energy and relative frequency respectively. The wave action balance equation is:

$$\frac{\mathrm{DN}}{\mathrm{Dt}} = \frac{S}{\sigma} \tag{2}$$

DN/Dt represents the total time derivative and S is composed of any energy source or sink, such as wind energy input, wave interactions or dissipation.

The mean alongshore current is computed using equations that assume a balance between the alongshore component of cross-shore energy flux gradient and a current-opposing bottom stress [6, 12]. The alongshore current is found by solving an alongshore momentum balance [9].

$$-\frac{\sin[\theta(x,\bar{t})]}{\rho c(x,\bar{t})} D_r(x,\bar{t}) + \mu \frac{\partial}{\partial x}[d(x,\bar{t}) \frac{\partial}{\partial x} \bar{v}(x,\bar{t})] = c_f[\bar{v}^2(x,\bar{t}) + \alpha^2 \sigma_u^2(x,\bar{t})]^{1/2} \bar{v}(x,\bar{t}) \tag{3}$$

where c is the local wave celerity, c_f is an empirical drag coefficient (assumed to be a constant, and estimated using bed particle size), α is correction parameter associated with the correlation between alongshore and cross-shore components of the instantaneous velocity field [2] (suggested as α = 1.16 as an optimum value), and μ is an empirical eddy diffusion coefficient, which is an adjustable parameter [9].

The roller energy dissipation is used as forcing. The roller energy (E_r) and its dissipation (D_r) are computed as

$$D_r(x,\bar{t}) = 2gE_r(x,\bar{t})\beta / c(x,\bar{t}) \tag{5}$$

$$\frac{\partial}{\partial x}[2c(x,\bar{t})\cos\theta(x,\bar{t})E_r(x,\bar{t})] = D_w(x,\bar{t}) - D_r(x,\bar{t}) \quad (6)$$

Where β was set to 0.1 as a standard value [5, 9]. The wave energy dissipation rate, D_w, is described by [8]:

$$D_w(x,\bar{t}) = \frac{3\rho g\beta^3\gamma^2\sqrt{\pi}f}{16} H_{rms}^2(x,\bar{t})\Gamma^3(x,\bar{t}) .\{1-[1+\Gamma^2(x,\bar{t})/\gamma^2]^{-\frac{5}{2}}\} \quad (4)$$

Where B is a description of breaking wave geometry, Γ and γ are the normalized wave height and its critical value, and f is the peak frequency of the incident waves. The parameters B and γ are typically used to tune the wave model to give optimum estimates of the wave height, and here they were set to 1.0 and 0.36 [3, 5].

5. Results

Figure 2 designates the depth and the significant wave height variation at 20:00 March 13th along transect.

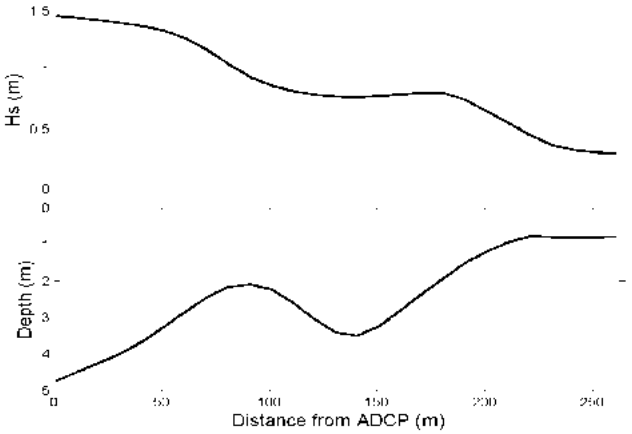

Figure 2. Significant wave height and depth variations along transect.

Figure 3 compares the recorded and estimated alongshore current velocity. The results show that the numerical modelling presented here properly estimates alongshore current velocity. The correlation coefficient of this estimations is ~0.78 and root mean square deviation is ~0.06 m/s compared to recorded data.

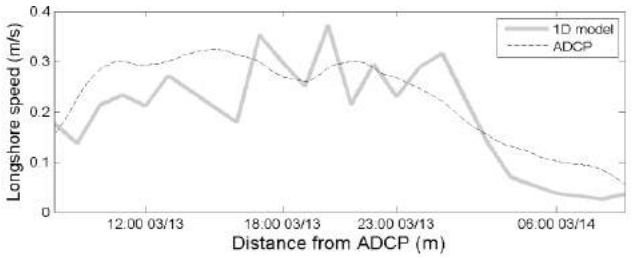

Figure 3. The recorded and estimated alongshore current velocity (m/s) at ADCP location.

An example of distribution of mean alongshore current along transect is depicted in Figure 4.

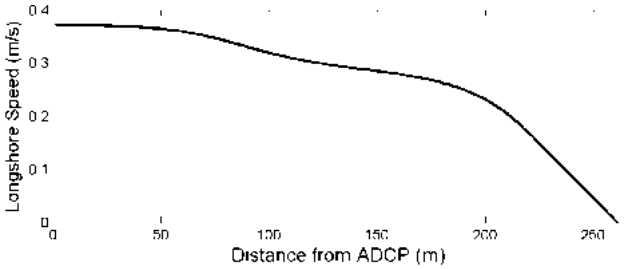

Figure 4. Estimated alongshore current velocity (m/s) at 20:00 March 13th, 2014.

6. References

[1] Coeffe, Y. and Pechon, P. "Modelling of Sea-Bed Evolution under Waves Action." Coastal Engineering, pp. 1149-1160. 1982.

[2] Feddersen, Falk, R. T. Guza, Steve Elgar, and T. H. C. Herbers. "Velocity moments in alongshore bottom stress parameterizations." Journal of Geophysical Research: Oceans 105, no. C4 (2000): 8673-8686.

[3] Haines, John W., and Asbury H. Sallenger. "Vertical structure of mean cross-shore currents across a barred surf zone." Journal of Geophysical Research: Oceans 99, no. C7 (1994): 14223-14242.

[4] Horikawa, Kiyoshi, ed. Nearshore dynamics and coastal processes: Theory, measurement, and predictive models. University of Tokyo press, 1988.

[5] Lippmann, T. C., A. H. Brookins, and E. B. Thornton. "Wave energy transformation on natural profiles." Coastal Engineering 27, no. 1 (1996): 1-20.

[6] Longuet-Higgins, Michael S. "Longshore currents generated by obliquely incident sea waves, 1." J. geophys. Res 75, no. 33 (1970): 6778-6789.

[7] Okayasu, Akio. "Characteristics of turbulence structure and undertow in the surf zone." (1989).

[8] Plant, Nathaniel G., K. Todd Holland, Jack A. Puleo, and Edith L. Gallagher. "Prediction skill of nearshore profile evolution models." Journal of Geophysical Research: Oceans 109, no. C1 (2004).

[9] Ruessink, B. G., J. R. Miles, F. Feddersen, R. T. Guza, and Steve Elgar. "Modeling the alongshore current on barred beaches." Journal of Geophysical Research 106, no. C10 (2001): 22451-22463.

[10] Southgate, Howard N. "A one-dimensional model of wave-current interaction." In Coastal Hydrodynamics, pp. 79-92. ASCE, 1987.

[11] Svendsen, Ib A. "Wave heights and set-up in a surf zone." Coastal Engineering 8, no. 4 (1984): 303-329.

[12] Thornton, Edward B., and R. T. Guza. "Surf zone longshore currents and random waves: Field data and models." Journal of Physical Oceanography 16, no. 7 (1986): 1165-1178.

NUMERICAL MODELING FOCUSED ON EFFECTS OF THE POROUS MEDIAON THE WAVES IMPINGING RUBBLE MOUND BREAKWATERS

Sahameddin Mahmoudi Kurdistani [1],Giuseppe Roberto Tomasicchio[2]and Antonio Francone [3]

1) Department of Engineering for Innovation, University of Salento, Ecotekne, Lecce, Italy, s.m.kurdistani@unisalento.it
2) Department of Engineering for Innovation, University of Salento, Ecotekne,Lecce, Italy, roberto.tomasicchio@unisalento.it
3) Department of Engineering for Innovation, University of Salento, Ecotekne,Lecce, Italy, antonio.francone@studenti.unisalento.it

1. Introduction

The permeability of the core material influences armour stability, wave run-up and wave overtopping. The main problem related to the scaling of filter layer and core materials in physical models is that the hydraulic gradient and the pore velocity are varying in space and time. This makes it impossible to reach a fully correct scaling.

CFD models based on the Reynolds Averaged Navier-Stokes (RANS) equations are becoming extremely important in maritime and coastal engineering due to their capabilities, robustness and extensive validation for both surf zone hydrodynamics and the stability and functionality of conventional or non-conventional coastal structures. In the recent years, complex numerical simulations of breakwater behavior have been made possible, especially for rubble mounds, composed by blocks of concrete or rock in which water flows through complex geometry, such as: Van der Meer et al. (1992), Hsu et al. (2002), Lara et al. (2006), Chopakatla et al. (2008) and Dentale et al. (2015).

However, there is still a need for practical empirical formula to estimate the pore velocities in filter layers and core avoiding the use of complex and time-consuming numerical models.

2. Materials and Methods

The present study has adopted the Crablock unit. As it is shown in Figure 1, this type of very recently appeared unit (Almasaood & Sons. Co. 2016 [7]) is used as a single layer amour.

Figure 1. Crablocks as rubble mound breakwaters.

Figure 2, shows the details and dimensions of the selected Crablock and dimensions values are presented in the table 1.

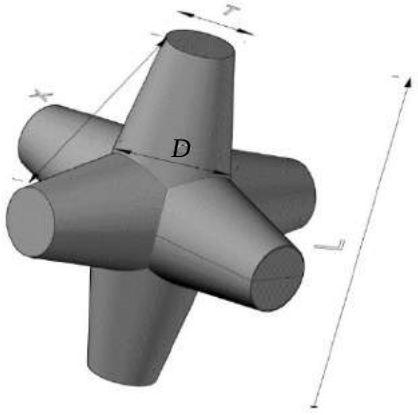

Figure 2. geometry of Crablock.

Table 1. dimensions of Crablock.

T (mm)	D (mm)	L (mm)	X (mm)
385	600	1880	1570

Two different scenarios have been selected for preparing the CFD model. The first scenario consists of an impermeable breakwater armoured with Crablocks; the second scenario considers the presence of a permeable inner layer.

Both scenarios have been simulated in a virtual channel 10 meters wide, 50 meters long and 6 meters high. The side slope of the breakwater has been considered $z = 2$. The mesh included 5000000 cells. The wave height of 0.8 m and wave period of 5.5 seconds have been used to simulate.

3. Results and Discussions

A fifth-order Stokes wave has been generated at a mesh boundary. The model is based on the fifth-order Stokes

wavetheory developed by Fenton[6]. Itallows higher wave amplitude than the linear wave theory.

Figure 3 shows the maximum run-up elevation of the wave impinging rubble mound breakwater when breakwater is completely impermeable. Figure 4 depicts that considering a porosity of 35% for the breakwater leads to decrease the maximum run-up elevation. The coordinates of the points of the maximum run-up have been presented in the table 2. The toe of the breakwater (point G in Figure 3) is the reference point of these coordinates.

Table 2. coordinates of therun-up elevations for the two scenarios.

Scenario	X (m)	Y (m)	Z (m)
Impermeable	9.7	19	5.07
Permeable	8.1	19	4.05

Y, is the selected position of the longitudinal profile. Table 2 clearly shows that in case of impermeable model, the wave run-up reaches the point (X=9.7 m, Z=5.07 m), while in the case of permeable model, the maximum wave run-up elevation is at the point (X=8.1 m, Z=4.05 m) therefore results to the 1.02 m less height of run-up.

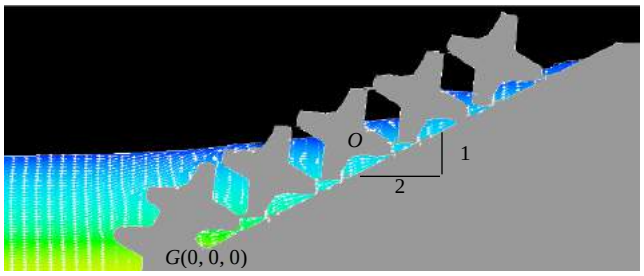

Figure 3. maximum run-up elavationt for impermeable breakwater.

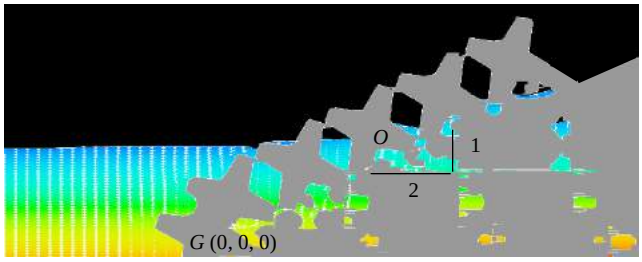

Figure 4. maximum run-up elevation height for permeable breakwater.

At the point *O* (X=6.12 m, Y=19 m and Z=3 m) in Figure 3, the pressure (Pa) at the rubble mound during the 17 seconds of simulation has been compared in Figure 5 (a, b). It shows well that the maximum pressure decreases while the permeable breakwater is used.

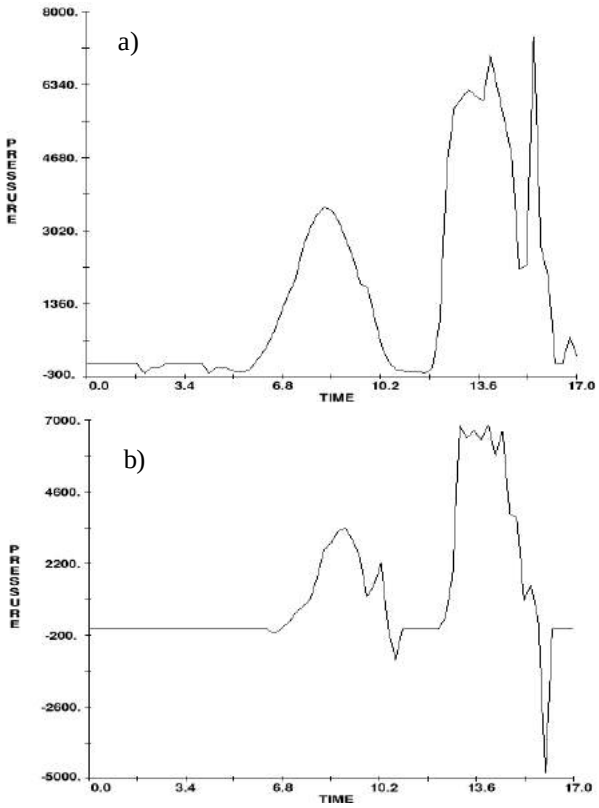

Figure 5. the maximum pressure on the Crablocks, a) impermeable breakwater b) permeable breakwater.

4. References

[1] Chopakatla, S.C., Lippmann,T.C., and Richardson, J.E., "Field verification of a computational fluid dynamics model for wave transformation and breaking in the surf zone", Journal of Waterway, Port, Coastal and Ocean Engineering, Vol.2, No.134, 2008, pp. 71-81.

[2] Dentale, F., Donnarumma, G., Pugliese Carratelli, E., and Reale, F."A numerical method to analyze the interaction between sea waves and rubble mound emerged breakwaters ",WSEAS TRANSACTIONS on FLUID MECHANICS, Vol.10, pp. 106-116, 2015.

[3] Fenton, J. D., "A fifth-order stokes theory for steady waves", Journal of Waterway, Port, Coastal, and Ocean Engineering, 111(2):216–234, 1985.

[4] Hsu, T.J., Sakakiyama,T. and Liu,P.L.F., "A numerical model for wave motions and turbulence flows in front of a composite breakwater", Coastal Engineering, Vol.46, No.1, 2002, pp. 25-50.

[5] Lara, J.L., Garcia,N. and Losada,I.J., "RANS modeling applied to random wave interaction with submerged permeable structures", Coastal Engineering, Vol.53, No.5-6, 2006, pp. 395-417.

[6] Van der Meer, J.W. and Stam, C.J.M., "Wave run up on smooth and rock slopes of coastal structures", Journal of Waterway, Port, Coastal and Ocean Engineering, Vol.118, No.5, 1992.

[7] Almasaood& Sons Co., "Development support Crablocks Artificial Armouring", Abu Dhabi, http://www.cdr-international.nl , 2016.

MODELLING OF OCEAN CURRENTS AND SURGE ALONG THE IRANIAN MAKRAN COASTLINE ON THE OMAN SEA

Mohammad Dibajnia[1] Morteza Jedari Attari[2], Arash Bakhtiari[3], Mohammad Hossein Nemati[4], S. Abbas Haghshenas[5]

1) Collaborating Researcher, Inst. of Geophysics, Univ. of Tehran, Iran, Email: dibajnia@gmail.com
2) Project engineer, Middle East Water and Environment Co., Tehran, Iran, Email: mortezajedariattari@yahoo.com
3) Project engineer, ditto, Email: arash.bakhtiary@gmail.com
4) Iranian Ports and Maritime Organization, Tehran, Iran, Email: mhn1982@gmail.com
5) Inst. of Geophysics, Univ. of Tehran, Iran, Email: sahaghshenas@ut.ac.ir

1. INTRODUCTION

The southeast coast of Iran bordering the western Makran region is exposed to the Indian Ocean (see Figure 1) and is directly affected by the climate and hydrodynamic processes of this ocean. Measurements of currents by the Port and Maritime Organization (PMO) in 2006-7 around Chabahar and by the Iranian Fishery Organization in 2008 at Zarabad, have shown the presence of oscillating ocean currents along this coastline. The oscillation period of these currents varies approximately from 3 days to a week. They are typically strong through the water column with the near-bed current velocity reaching up to 0.5 m/s at 20~30 m depth.

In 2014, the Iranian Makran coastline was selected by the PMO to be studied as the Phase 6 in the series of Monitoring and Modelling Studies of Iranian Coasts. Makran Coast plays an important role in country's future navigation and trade due to its accessibility.

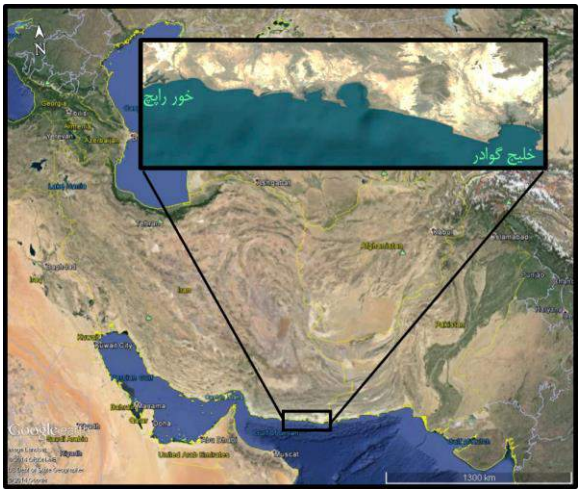

Figure 1. Study area

The present paper presents the results of a 3D modelling effort to simulate the hydrodynamics of Makran ocean currents as well as their corresponding water level variations. Sea levels in the Oman Sea are impacted by water temperature and air pressure in the Indian Ocean in addition to the classical surge in water level due wind stresses. The data used for model calibration and verification were recorded in approximately 30 m depth which falls in the shallower edge of the continental shelf just before the beginning of the transition zone to coastal currents.

2. MEASURED DATA

An invaluable data set recorded during the first phase of the monitoring projects (by PMO) [1]. includes current profile measurements in 30 m depth at a location outside Chabahar Bay. Measurements at this location cover the period from September 2006 until early June 2007 immediately after the Cyclone Gonu event. The oscillating ocean currents have been captured in this data set. The deployed current profiler device (i.e. bottom-mounted AWAC) also recorded water temperature near the seabed. A number of tide gauges deployed inside and outside of Chabahar Bay measured the water level. Figure 2 shows locations of the current profiler (AW2, E60.65 N25.26) and Tiss tide gauge (E60.594 N25.35).

In addition to the measured current data, daily surface current, water level, and temperature data from HYCOM assimilative global model developed by the USACE in collaboration of NASA, NOAA and several universities worldwide, were also collected for the last three months of 2006. The data is available at 1/12 degree spatial resolution.

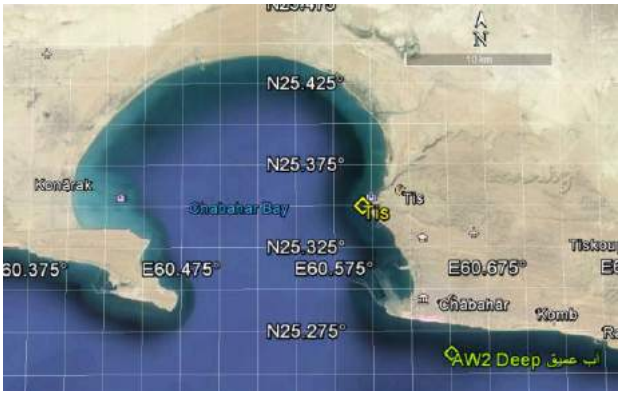

Figure 2. Locations of the measurement stations

3. METHODOLOGY

Due to importance of geostrophic currents and the relatively deep water conditions in the Makran area, a 3-dimensional hydrodynamic model had to be used for proper simulation of oceanic currents. Required initial and boundary conditions data for currents, water level, and temperature/salinity fields as well as the wind and pressure field data were obtained from publicly available sources such as C-GLORS ocean parameters and CFSR global wind field.

4. NUMERICAL MODELING

The MIKE3 package by DHI was used in the present work. Finding the most appropriate model configuration that can properly simulate large scale oceanic processes was a matter of trial and error. Applying various domains showed that obtaining reasonable results requires adopting a domain far larger than the study area boundaries. The mesh size, number and form of vertical layers also play significant role in the validity of the model results. Figure 3 shows the final selected model domain which extends to the southern hemisphere.

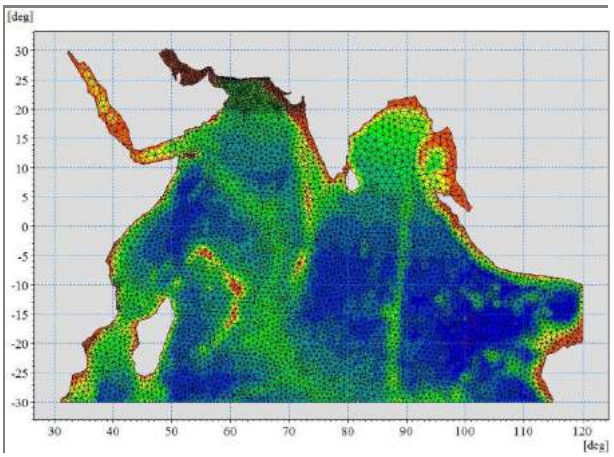

Figure 3. Computational domain

4. SAMPLE RESULTS and DISCUSSION

Current speed and direction, sea surface elevation and temperature are the main outputs of the model which were compared to the collected data. An example comparison between the AW2 current profiler data and model results is presented in Figure 4. The figure provides comparison between surface currents and indicates that the model can reasonably reproduce the ocean current regime in Makran area. The oscillating nature of ocean currents is well reproduced. Current speeds are also reasonably simulated (a perfect match is not expected due to the extremely complex nature of the problem). The bottom panel in Figure 6 depicts the simulated temperature fluctuations near the seabed showing good consistency with the measured data.

Cyclone Gonu was an extreme event that took place in early June 2007. This event was recorded by the AW2 sensor. Figure 5 depicts comparisons between a selected section of the recorded data (black dots) and model results, demonstrating a great performance by the model in reproducing ocean currents along the Makran coastline. Simulations started from the beginning of 2006 to allow model warm up and convergence of the temperature field. At the beginning of 2007 simulations were continued in two versions using two different temperature fields. The red line shows the results with the temperature field taken from the end of 2006 simulation, i.e., the simulation continued without any changes. The blue line was produced by a simulation whose initial temperature field was replaced with the data from C-GLORS (with other parameters such as velocity and water surface levels from the end of 2006). Details will be discussed in the full paper.

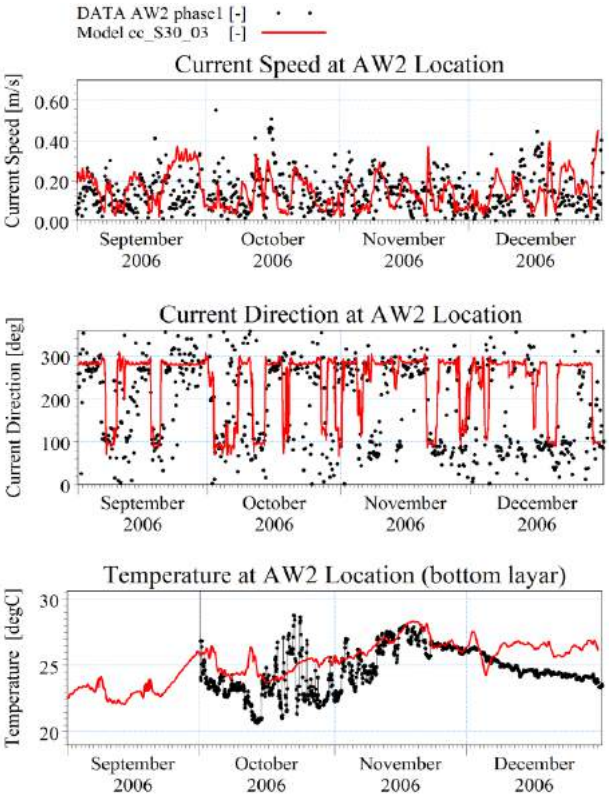

Figure 4. Comparisons between AW2 data (black) and model results (red).

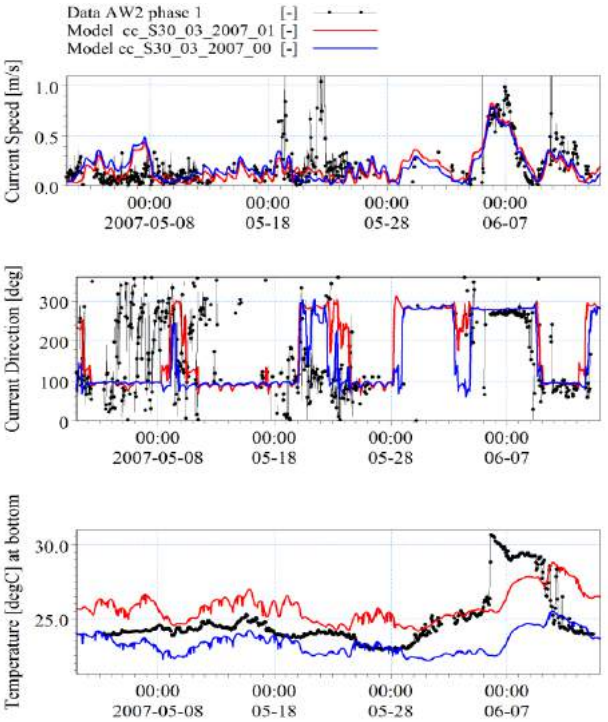

Figure 5. Comparisons between AW2 data (black) and model results (red) during cyclone Gonu.

6.REFERENCES

[1] Jahad Water and Energy Research Company (JWERC): Study reports of "Monitoring and Modelling Studies of Parts of Sistan, Balouchestan and Boushehr Provinces", Ports and Maritime Organization (PMO), 2008.

EXPERIMENTAL STUDY OF PIPE DIAMETER EFFECT TO THE VORTEX INDUCED VIBRATION OF TWO-DEGREE-OF-FREEDOM PIPE DUE TO WAVES

S.M. Mousavi[1], A.R. M.Gharabaghi[2] and M.H. Sedaaghi[3]

1) Civil Eng. Department, Sahand University of Technology, Tabriz, Iran, musavi6889@yahoo.com
2) Civil Eng. Department, Sahand University of Technology, Tabriz, Iran, mgharabaghi@sut.ac.ir
3) Electrical Eng. Department, Sahand University of Technology, Tabriz, Iran, sedaaghi@sut.ac.ir

1. Introduction

When an object like a pipe is located in a flow or wave, the flow regime would be changed around it which leads to the increment of shear stress and turbulence intensity. As a result, in special conditions we will see flow separation and vortex shedding in lee-side of the pipe. These vortexes impose the periodic forces on the cylinder which may lead the pipe to vibrate. These vibrations are named Vortex Induced Vibrations (VIVs) [1]. VIV's studies are mostly around Cross-Flow (CF) pipe vibrations (one-degree-of-freedom pipes) and somewhat both In-Line (IL) and CF pipe vibrations (two-degree-of-freedom pipes), Fig. 1. Two-degree-of-freedom vortex-induced vibration of a pipe in waves has been less studied which it is investigated experimentally in this case and the pipe diameter effect is considered.

2. Dimensionless parameters

Relative dimensionless parameters are classified in three categories: 1) Flow parameters such as Re and KC; 2) Structural parameterslike mass ratio (m^*) and structural damping ζ ; 3) Fluid-structure Interaction parameters like nondimensional amplitudes and reduced velocity (Ur). Reduced velocity can be defined as following:

$$U_r = U / (Df_n) \quad (1)$$

where U, D, and f_n are maximum value of the oscillatory-flow velocity, pipe diameter and natural frequency respectively.

3. Details of laboratory model

3.1. Laboratory set-up

Experiments all had done in Sahand University of technology's wave maker flume. The length, depth and width of the flume are 10, 0.5 and 0.3 meters respectively. A Plexiglas supporting frame and four springs arranged like a cross (X- with the angel of 45° to the horizon) at each side of the pipe were used to provide 2dof vibrations of the pipe. To install the frames, flume width has been reduced to 25cm by security glasses. Two Plexiglas square plates were provided at the end sides of the pipe for spring's supports. Pipes were made from Plexiglas which were smooth (pipes properties are allowable at Table 1). Despite the deficiency of some previous works [2], in this set-up, equal natural frequencies in the both degrees of freedom were obtained.

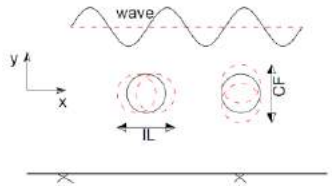

Figure 1. In-Line and Cross-Flow motions

Table 1. Pipe properties

NO.	Pipe's name	Outer diameter, D	m*
1	P20	20 (mm)	1.10
2	P30	30 (mm)	1.11

At Table 1, m* indicates mass ratio which is defined as the ratio of the cylinder mass per unit length, m, over ρD^2, where ρ and D, are water density and pipe outer diameter respectively.

A high-speed camera was 1m far from the pipe, has been located perpendicular to the pipe central axis to record its vibrations. Three 500-Watt-spotlights provided the suitable illumination. By recording the suspension colored particle's movements in the flume, wave induced velocities were measured.

3.2. Experiments description

455 experiments were hold in this research to recognize the vortex-induced vibration of the pipe in wave and effective parameters. At the beginning of each test, pipe and springs system were being installed in the supporting frames and then they have been located in the flume. After that the pipe and the flume were slowly filled with water till water depth reached the height of 25cm in flume. Then wave's properties recording sensors were installed in their locations and transformed the information to a computer. Finally, wave maker machine started to generate regular waves listed at Table 2, when its software was running.

A minute of pipe's vibrations were recorded at least twice by the camera. If there were no same results, third or other records were taken to get the same records. In that case it could be sure enough that there are no accidental errors like camera shakes, lightening changes or other unexpected errors. An image processing program was developed in MATLAB to analyze the films. Similarly, this technique

was employed for suspension colored particles to measure the wave induced velocities at pipe level.

Table 2. Waves properties generated in flume

Wave name	Wave height (mm)	Wave frequency (Hz)
1	67	f1-H67
0.90	41	f0.9-H41
0.80	64	f0.8-H64
0.70	39	f0.7-H39
0.60	49	f0.6-H49

To calculate the natural frequency of pipe-spring system, we benefited the free-vibration test which pipe was located in the filled flume far enough from bed and free surface. Then a known initial excitation was imposed to the pipe and its response was recorded and analyzed. Next the envelope curve on its response was fitted and its equation was extracted. By comparing the extracted equation to the theories, the structural damping ζ and natural frequencies (f_{nx} and f_{ny}) have been calculated. Damping frequencies (f_x or f_y) were also determined by the power spectra from image processing and Fast Fourier Transform technique (FFT).

4. Discussion

Two-degree-of-freedom vortex-induced vibrations of a pipe in waves was studied experimentally. In this study data were smoothed by Moving Average filter in MATLAB to eliminate the desultory ones. Pipe's vibrations amplitudes and corresponding frequencies were extracted. They were plotted in dimensionless parameters such as A_{mx}/D, A_{my}/D, f_x/f_n, and f_y/f_n which A_{mx}, A_{my}, f_x, and f_y are pipe's vibrations amplitudes in IL and CF directions and corresponding frequencies respectively.

Fig. 3 shows relative pipe's vibrations amplitudes in IL and CF directions (A_{mx}/D and A_{my}/D) against U_r. It can be observed that by increasing the pipe diameter, the nondimensional parameters of A_{mx}/D and A_{my}/D are increased in this range of reduced velocity ($0.6 \prec U_r \prec 2.4$). It should be mentioned that in this figures, the center longitudinal axis of the two pipes are at the same height.

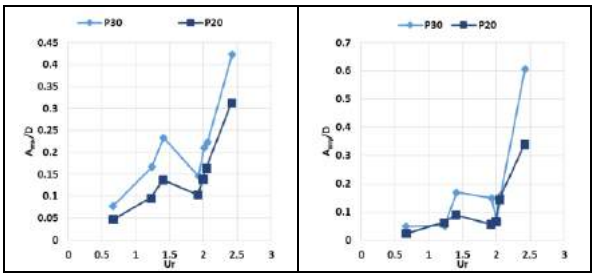

Figure 2. Relative pipe's vibrations amplitudes in IL and CF directions (Amx/D and Amy/D) against reduced velocity ($0.6 \prec U_r \prec 2.4$) for a pipe which diameter is: a) 20(mm) ■, b) 30(mm) ◆.

To avoid the accidental results and figure out the pipe response in other ranges of reduced velocities, second set of experiments were hold by new system of springs. Again it was observed that, the dimensionless parameters of A_{mx}/D and A_{my}/D are bigger for the pipe with diameter of 30mm rather than the 20mm one.

Till now it was observed that two dimensionless parameters (A_{mx}/D and A_{my}/D) were increased when pipe diameter was increased. In continue, the frequencies changes are considered. For this aim, relative pipe's vibrations frequencies in IL and CF directions (f_x/f_n and f_y/f_n) were plotted against reduced velocity ($0.6 \prec U_r \prec 2.4$) in Fig. 5.

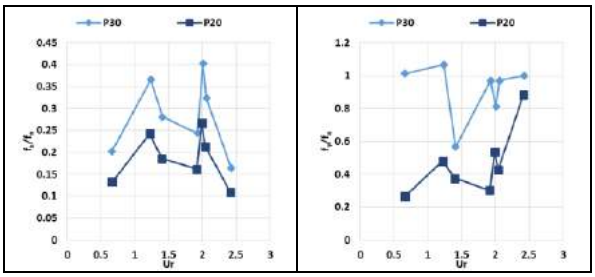

Figure 3. Relative pipe's vibrations frequencies in IL and CF directions (fx/fn and fy/fn) against reduced velocity ($0.6 \prec U_r \prec 2.4$) for a pipe which diameter is: a) 20(mm) ■, b) 30(mm) ◆.

Considering diagrams in Fig. 5, again this could be concluded that using a pipe with bigger diameter would lead to the bigger dimensionless parameters of f_x/f_n and f_y/f_n which are important in fatigue damages. As it mentioned previously, second set of experiments were hold by new sets of springs. The same as the previous manner, the relative pipe's vibrations frequencies (fx/fn and fy/fn) were in touch to the pipe diameter that they would increase by increasing of the pipe diameter.

5. conclusions

Pipe diameter effect to the vortex-induced vibration of two-degree-of-freedom pipe due to waves was investigated experimentally. More than 455 experiments were held (including free vibration tests to get the pipe's natural frequencies). To increase the accuracy, each of the experiments were repeated at least twice till the same results observed. All of them were analyzed by an image processing code which was developed in MATLAB. The data were filtered by Moving Average filtering method in MATLAB. They were plotted in several diagrams against the nondimensional parameters. In addition of theories, using the flow visualization technique, showed the vortex shedding phenomena in experiments. It was concluded that, both the pipe's vibrations amplitudes and frequencies are affected by pipe diameter. In other words, the dimensionless parameters of A_{mx}/D, A_{my}/D, f_x/f_n and f_y/f_n were increased when the pipe diameter was increased.

6. References

[1] Sumer, B.M., Fredsoe, J., (2006), "Hydrodynamics around cylindrical structures," World Scientific Publishing, Singapore.

[2] Jauvtis, N., Williamson, C.H.K., (2003), "Vortex-induced vibration of a cylinder with two degrees of freedom," Fluids and Structures, vol. 17, p.p. 1035-1042.

AN ANALYTIC MODEL FOR THE STRUCTURE OF THE GRAVITY CURRENT FROM THE MIDDLE TO THE SOUTHERN BASIN OF THE CASPIAN SEA

Javad Babagoli Matikolaei [1], Abbasali Aliakbbari Bidokhti [2], Maryam Shiea[3], Sarmad Ghader [4]

1) Student, Physical Oceanography, Institute of Geophysics, javadbabagoli@ut.ac.ir
2) Professor, Institute of Geophysics, University of Tehran, bidokhti@ut.ac.ir
3) Islamic Azad University, Tehran, m.shiea@gmail.com
4) Associate Professor, Institute of Geophysics, University of Tehran, sghader@ut.ac.ir

1. Introduction

Bottom-trapped currents play an integral role in thermohaline circulation and are a vehicle for the transport of heat, salt, oxygen and nutrients over long distances [3]. The ability of abyssal flows to transport and deposit sediment is also of geological interest [6].

The density difference between the deeper water of the middle basin and that of southern basin of the Caspian Sea leads to an overflow gravity current over the Abshoran sill. This difference is mainly due to the temperature difference between these two basins as a result of cold water sinking in the northern part of this Sea, at about 48 degrees latitude. Similar outflow from the semi-enclosed sea, as that from the Persian Gulf to the Oman Sea, but mainly due to salinity difference, also exist [1, 5].

In this study an analytic model for the overflow gravity current over the Abshouran sill, with inertial and frictional effect is presented. The deep baroclinic flow is over the inclined surface is then studied using this model. The dynamical characteristics of the flow are investigated with different initial and boundary conditions. These conditions are taken from the physical oceanographic and hydrographic data.

2. Materials and Methods

2-1 The analytical model

As the gravity current starts to flow over the incline sill, it adjusts itself under the gravitational, rotational and frictional forces [4, 7]. The zonal and meridional components of the current are given by:

$$\frac{du}{dt} = g'i - fv - ru$$
$$\frac{dv}{dt} = -fu - rv \qquad \textbf{(1)}$$

Where u and v are zonal and meridional components of velocity, *f* is the Coriolis parameter (= 2Ω sin θ, were Ω is the earth angular speed, and θ is the latitude angle), i is the slope, *g'* is the reduce gravity and *r* is the fiction coefficient.

The solutions of these differential equations are as follows: (where *x* and *y* are location parameters and $C_1$and C_2 are constants to be found from boundary conditions).

$$u(t) = C_1 e^{-rt}\cos(ft) - C_2 e^{-rt}\sin(ft) - \frac{g'ir}{f^2 + r^2} \qquad \textbf{(2)}$$

$$v(t) = C_1 e^{-rt}\sin(ft) + C_2 e^{-rt}\cos(ft) + \frac{g'if}{f^2 + r^2}$$

$$x(t) = \frac{fC_2 - rC_1}{f^2 + r^2}e^{-rt}\sin(ft) - \frac{fC_1 + rC_2}{f^2 + r^2}e^{-rt}\cos(ft) - \frac{g'irt}{f^2 + r^2} + \frac{fC_1 + rC_2}{f^2 + r^2} \qquad \textbf{(3)}$$

$$y(t) = \frac{fC_1 + rC_2}{f^2 + r^2}e^{-rt}\sin(ft) + \frac{fC_2 - rC_1}{f^2 + r^2}e^{-rt}\cos(ft) - \frac{g'if}{f^2 + r^2}t + \frac{rC_1 - fC_2}{f^2 + r^2}$$

$$C_1 = -\frac{ig'f}{f^2 + r^2}$$

$$C_2 = u_p + \frac{g'ir}{f^2 + r^2}$$

As the flow develops with time is shows some oscillations (see below), and after a long time it acquires a steady state, moving parallel to the sloped bed in which in this situation *u* and *v* are obtain from the following equation which α is the angle between the two velocity components.

$$u = \frac{-g'ir}{f^2 + r^2}, v = \frac{g'if}{f^2 + r^2}$$

$$\tan\alpha = \frac{u}{v}, \alpha = \arctan(-\frac{r}{f})$$

2-2 *The main parameters of the flow*

As the field observations are scarce, the flow parameters are obtained from numerical simulations of the Caspian Sea circulation using COHERENS (Shiea, et al, 20015, [6]). The model has been applied on grids of 0.046 × 0.046 degrees along the horizontal directions (081×229 grid), which gives a grid size of about 5 km, and 30 sigma layers. Bathymetry and coastline locations are based on GEBCO

data (0.5˚ ×0.5˚) that has been interpolated and slightly smoothed. Figure 1 shows a transect of the isopycnal lines across the Absoran sill for Sept., an example of the overflow simulations. The sloping bed as well as the slopes of those of the isopycnal lines of the overflow is shown. From such results the model boundary conditions are extracted.

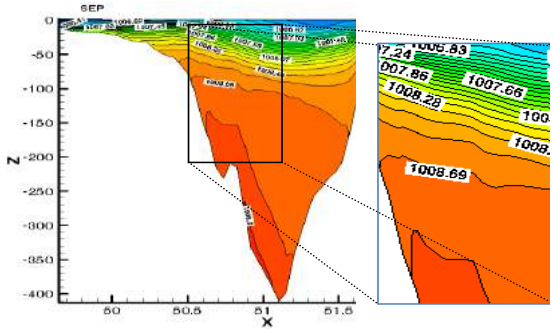

Figure 1. A transect of density field in the Abshoran Strait in September (2004), based on numerical simulations. The position of the current is highlighted.

3. Characteristics of the overflow

The gravity current overflow characteristics are obtained from the numerical simulations. The outflow (as overflow towards the southern basin of the Caspian Sea) appears to have higher velocity (e. g. Sept.) as the isopycnal slopes and particularly the reduced gravity, are higher for these months.

Using the analytical model we calculated the flow charactrestics. Figure 2 shows the paths of the initiial stage of the outflow over the sloped bed for different months, indicating that it varies with seasons. Figure 3 also shows the very initial stage of the flow speed, indicating that it has an oscillation of inertial type with varying strengths for different months.

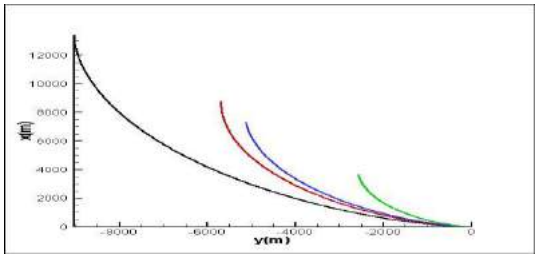

Figure 2. The paths of the flow in different months after t=9h, the black color shows September, the red color indicates May, the blue color indicates November, the green color January.

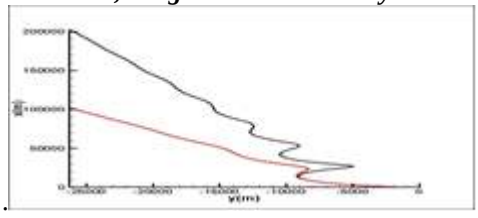

Figure 4. The comparison of the path of the flow with friction coefficient 0.00001 and 0.00002 (s^{-1}) in September

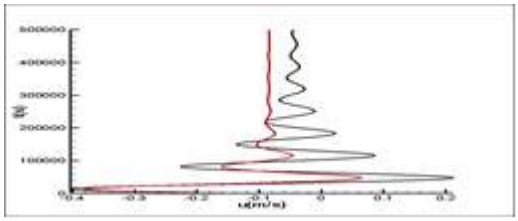

Figure 5. The comparison of the speed of flow with friction coefficient 0.00001 and 0.00002 (s^{-1}) in September (long-time).

Table 2 shows the values the components of the flow velocity for typical isopycnal slopes and two different frictional coefficients.

Table 2. Some results of the analytical model (long-time integration).

parameter	$r = 10^{-5}(s^{-1})$	$r = 2\times10^{-5}(s^{-1})$
α (deg)	6.17	12.2
u(m/s)	-0.04	-0.084
v(m/s)	-0.4	-0.39

4. Conclusions

The results of an analytical model for a gravity driven flow over a sloped bed, between the middle and southern basins of the Caspian Sea have been presented. The model includes inertial, Coriolis and frictional forces. In its initial stage the flow has oscillations of inertial types (as also observed in down sloped valley winds, [2]) with typical inertial period at this latitude. After a long time the flow adjust itself moving as a gravity driven topographically trapped current. Typical steady state velocity of the flow is about 0.1 m/s. Such flow is important in the abyssal circulation and ventilation of the deep southern basin of the Caspian Sea.

4. References

[1] Bidokhti A. A. and Ezam M, "The structure of the Persian Gulf outflow subjected to density variations "., 2009, Ocean Sci., Vol. **5**, 1–12.

[2] Bastin, S. and Drobenski, P. “temperature and wind velocity oscillations along a gentle slope during sea-breeze events”, Bound. Lay. Met. (2005) 114: 573–594.

[3] Dickson, R. R., Gmitrowics E. M., and Watson A. J., "Deep water renewal in the northern, North Atlantic",. Nature, 1990, 344, 848-850.

[4] Mateusz K.R. and Gordon E. S., "Dynamics of bottom trapped currents with application to the strait of Georgia",. J.Math. quarterly, 2001,Vol. **9**, 127-157.

[5] Price, J. F. and Baringer, M. O., 1994, "Outflows and deep water production by marginal seas",.Progress in Oceanography, 33, 161-200.

[6] Shiea, M., Ali-Akbari Bidokhti, A., A., and Chegini, V. A study of the roles of important forcing mechanisms on the circulation of the Caspian Sea using numerical simulations, Iranian Journal of Geophysics Vol. 9, No. 3, 2015, 118-142.

[7] Smith, P.C., "A stream-tube model for bottom boundary currents in the ocean". Deep-Sea Res. 22 (1975), 853 873.

SIMULTANEOUS EFFECTS OF WAVE AND TIDE ON THE COSATAL CURRENTS ALONG HORMOZGAN PROVINCE COASTLINES (CASE STUDY: PARSIAN AREA)

Hadi Sadeghian[1], Mohammadreza Allahyar[2], Aghil Hajmomeni[3] and S. Majid Tavakolani[4]

1) Senior Coastal Engineer, Sazeh Pardazi Iran Consulting Eng. Co., Tehran, Iran, h.sadeghian@sazehpardazi.com
2) General Director of Coastal and Port Engineering Department of Ports and Maritime Organization (PMO), Tehran, Iran, allahyar@pmo.ir
3) Head of Coastal Process and Hydraulic Discipline, Sazeh Pardazi Iran Consulting Eng. Co., Tehran, Iran, hajmomeni@sazehpardazi.com
4) Deputy of Coastal and Port Engineering Department of Ports and Maritime Organization (PMO), Tehran, Iran, mtavakolani@pmo.ir

1. Introduction

Coastal currents are one of the important hydrodynamic factors in the near shore zone which play a key role in sediment transport as well as in pollution dispersion. Thus, accurate and precise predictions of coastal currents in the near shore area are quite important which provides valuable data for engineering projects and coastal management purposes.

This paper investigates the simultaneous effects of wave and tide on the current pattern in the near shore zone along Hormozgan province coastlines in the Persian Gulf. Accordingly, two different numerical modeling scenarios have been considered to study the current patterns in the near shore area; tide only condition and tide and wave combination condition. In this paper the results of the numerical modeling have only been presented for Parsian region at the end of the western part of Hormozgan province. This work has been done as a part of Hormozgan Integrated Coastal Zone Management (ICZM) project and the results have been used for shoreline management plan (SMP) studies.

In this study, the coastal currents simulation has been performed using Hydrodynamic (HD) and Spectral Waves (SW) modules of MIKE 21/3 Coupled Model FM.

2. Numerical Modeling

2.1. Modeling Domain

The modeling domain for coastal current simulation covers the entire Hormozgan province coastlines. As mentioned above, this study focuses only to Parsian area between Nayband bay and Bandar-e Javad Alaemmeh as a case study. The modeling domain, computational mesh and bathymetry for the current simulation have been shown in *Figure 1* [3].

2.2. Simulation Duration

The modeling has been carried out for a one-year period from January to December 2005. This year has been selected as representative year for the western part of the Hormozgan province from Nayband bay to Kong port [3].

2.3. Other Parameters

Two different modeling scenarios have been considered to investigate the near shore current patterns. In tide only scenario, tide is the only deriving force whereas in tide and wave combination scenario, the radiation stresses due to wave breaking have been incorporated in the simulations. The radiation stresses act as another driving force and have been used to calculate the wave-induced currents. The radiation stresses have been included by reading values from a coupled SW simulation. It should be noted that in the second scenario, wave-current interaction has been considered in the simulation [3].

In both scenarios, the Flather (1976) boundary condition has been considered in all open HD boundaries [2]. The boundaries information has been extracted from global tidal model in the Persian Gulf and Oman Sea. In the second scenario, the lateral boundary condition in the side open SW boundaries and wave parameters boundary condition in the other open SW boundaries have been considered. The boundaries information has been extracted from the results of "Monitoring and Modeling Studies of Coastal Zone of Hormozgan Province" project [1].

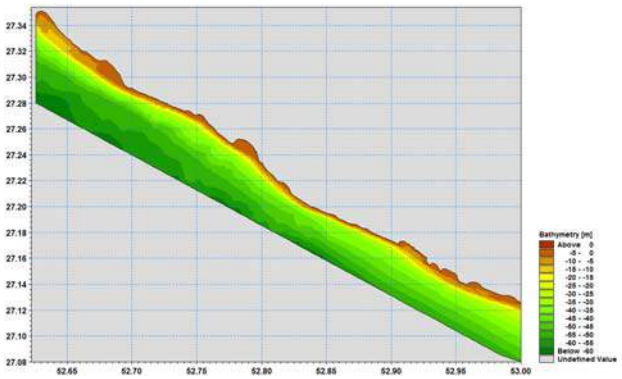

Figure 1. The modeling domain, computational mesh and bathymetry for coastal current modeling.

2.4. Modeling Results

In order to investigate the simultaneous effects of wave and tide on the coastal currents along Hormozgan province coastline, time series of current speed and direction has

been extracted in the water depth of 1 meters due to CD. Then a comparison is made between modeling results in two different scenarios. The current roses at the Parsian area for two different scenarios are presented in *Figure 2*. Typical example of the combined tidal and wave induced current patterns in the vicinity of the future Parsian port has been shown in *Figure 3*. The maximum current speed in the modeling domain during the simulation period for two different scenarios are presented in *Figure 4* [3].

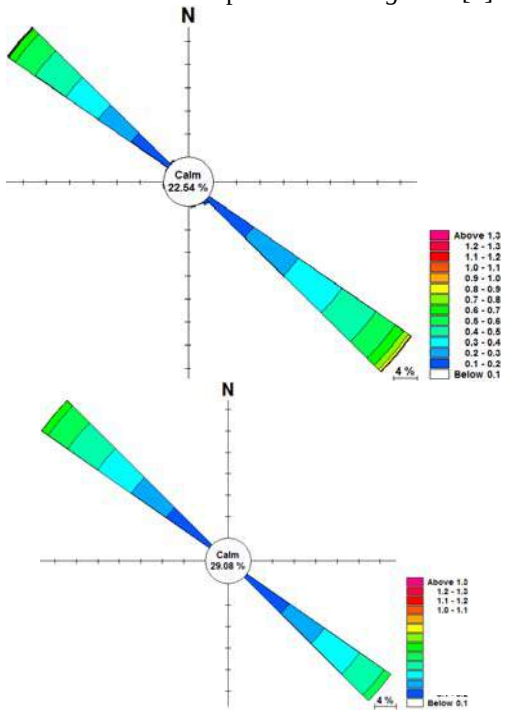

Figure 2. The modeling result as current roses comparison in Parsian area (top: tide and wave condition, bottom: tide only condition).

3. Conclusion

In this study the simultaneous effects of the wave and tide on coastal currents regime in the area between Nayband bay and Bandar-e Javad Alaemmeh has been examined through numerical modeling. The simulation results show that waves are of great importance for coastal currents pattern in the study area because of some reasons. Firstly, the maximum current speed in the presence of waves is almost two times greater than current speed in the absence of waves. Secondly, the north westerly prevailing tidal currents have been altered to south easterly currents in the presence of waves. Finally, the percentage of clam conditions has been decreased in the presence of waves. This study clearly demonstrates that coupled simulation of wave and tide may impose drastic changes on the hydrodynamic characteristic of the currents.

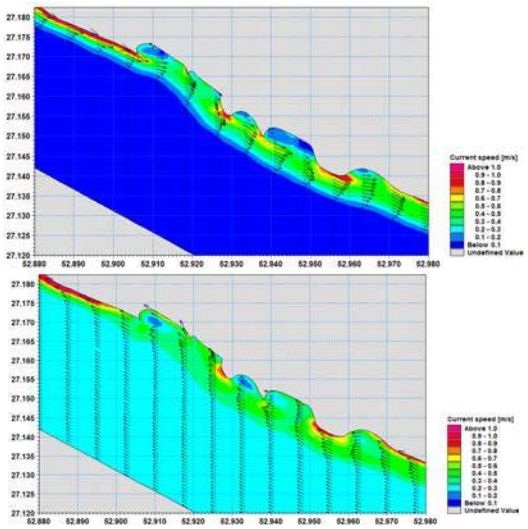

Figure 3. Combined tidal and wave induced current pattern in the vicinity of future Parsian port.

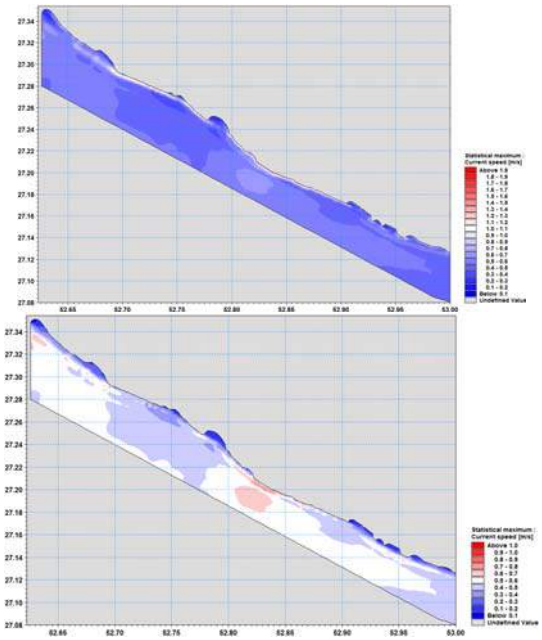

Figure 4. Maximum current speed in the modeling domain during the simulation period (top: tide and wave condition, bottom: tide only condition)

4. References

[1] Fara Darya Arsheh Consultants., "Local wave propagation modeling studies", *Monitoring and Modeling Studies of Coastal Zone of Hormozgan Province, Forth Edition*, February 2013.

[2] Flatehr, R. A., "A tidal model for the northwest European continental shelf", *Memories de la Societe Royale des Sciences Liege*, 6 10, 1976, pp.141-164.

[3] Sazeh Pardazi Iran consulting Eng. Co., "Coastal Current Hydrodynamic Studies Report", *Hormozgan Integrated Coastal Zone Management Project, First Edition*, March 2016.

NUMERICAL MODELING OF TIDAL CIRCULATION IN THE KHURAN STRAIT

Shafieefar, M.[1], Rezaee Mazyak, A.[2] and Mosayebi, S.[3],

1) Civil Engineering Department, Tarbiat Modares University, Tehran, Iran, shafiee@modares.ac.ir
2) Civil Engineering Department, Tarbiat Modares University, Tehran, Iran, a.rezaeemazyak@modares.ac.ir
3) Marine Structures Group, Pars Geometry Consultant, Tehran, Iran, sa.mosayebi.84@gmail.com

1. Introduction

Information on tidal circulation in coastal waters is essential for planning and monitoring of coastal construction activities and resource exploration, etc.

Several researchers have studied and modelled tidal flows in the Persian Gulf over the years, but this studies have not focused on the tidal circulation in the strait of Khuran [1, 2, 3]. Several ports such as Shahid Rajaee and desalination plants and other infrastructures is located between Qeshm Island and the southern Iranian coast in Hormozgan Province (Khuran Strait), But only some studies are carried out about the circulation in this area [4, 5].

In the summer of 2015 for calibration the numerical model and understanding the tidal circulation pattern in the khuran strait, an extensive 60 days field measurement was conducted. The measurement data include time series of currents and surface elevation.

This paper describes the development of a high-resolution hydrodynamic model of tidal flows in the Khuran strait, and its application for the assessment of tidal circulation pattern.

2. Study Area

The Khuran Strait is a narrow strait separating the Iranian island of Qeshm from the Iranian mainland. It is the much smaller counterpart to the Strait of Hormuz. The Fig. 1 shows the study area.

Figure 1. Study area.

3. The Model

In his study MIKE 21 Flow Model (FM)-HD has been used for simulating currents in the Strait of Khuran. This model simulates the water level variations and flows in response to a variety of forcing functions in oceans and coastal areas.

The model is based on the two-dimensional incompressible Reynolds averaged Navier-Stokes equations, subject to the assumptions of Boussinesq approximation and hydrostatic pressure.

3.1. Bathymetry and Mesh

The bathymetry of Khuran strait is shown in Fig. 2. Also mesh file is generated in the MIKE Zero Mesh Generator. Optimized final mesh includes 5912 elements and 3384 nodes.

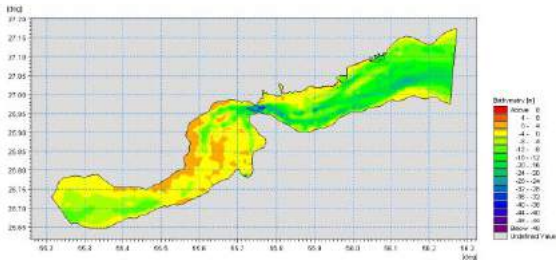

Figure 2. Bathymetry of the modeling area.

3.2. Boundary Conditions

As shown in Fig. 3, there are two open boundaries in the west and the east side of the modeling area that are named code 10 and code 20 respectively. For producing the boundary conditions in the west and east side of the modeling area, tidal elevation time history have been predicted based on the Basaidu and the Bandar Bahman tidal harmonic constituents information (N.C.C Station) for the year of 2015.

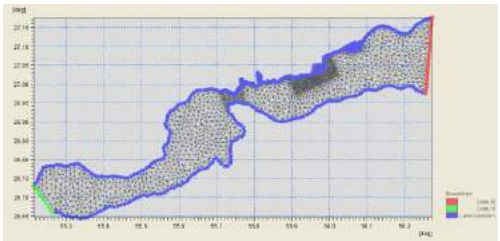

Figure 3. The open boundaries of the model

4. Field Measurements

Current velocity and direction were collected with Acoustic Doppler Current Profiler (ADCP) at 2 stations (Fig. 4). The RBR is located in the Isoico port and collected time series of surface elevations.

Figure 4. Scatter plot of current components

5. Results and Discussion

5.1. Calibration

The calibration is achieving the best fit between simulated results and available measured data by changing the empirical parameters such as bed resistance.

The comparisons between the measurement data and calibrated model results including current speed and surface elevation for one month duration (23 Jun- 22 Jul) have been shown in **Error! Reference source not found.** and **Error! Reference source not found.**.

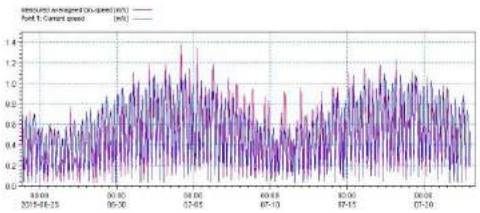

Figure 5. Measured and Modeled Current Speed (Jun-Jul)

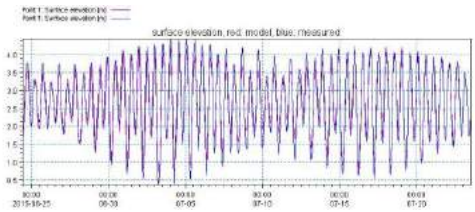

Figure 6. Measured and Modeled Surface Elevation (Jun- Jul)

Moreover for better comparison between modeled and measured data the statistical parameters including Bias, Root Mean Square Error (RMSE), Scatter Index (SI) and correlation coefficient (CC) have been calculated and presented in Table 1.

Table 1. Statistical Parameters for Comparison Modeled and Measured Data

Time duration	parameter	Bias	RMSE	SI	CC
Jun- Jul	Current speed	0.07	0.19	0.38	0.79
Jun- Jul	Surface elevation	0.005	0.24	0.09	0.97
Jul- Aug	Current speed	0.09	0.19	0.37	0.81
Jul- Aug	Surface elevation	0.04	0.59	0.23	0.80

5.2. Results

Based on the results of calibrated model, the mean and the maximum tidal current velocity in the strait of Khuran is shown in Fig. 7.

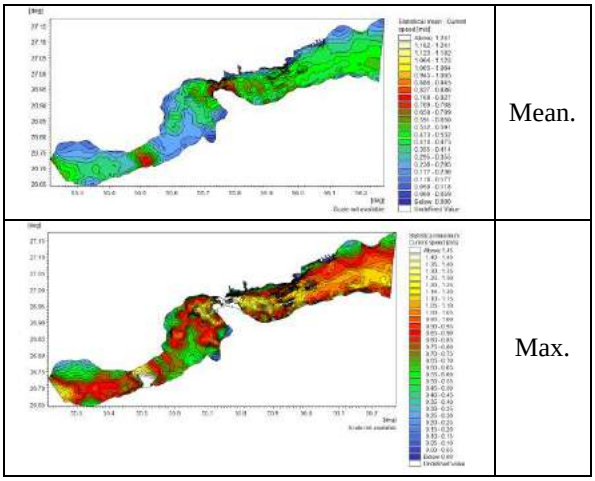

Figure 7. The mean and the maximum tidal current velocity in the strait of khuran

6. Conclusion

The results indicated that the mean of tidal current velocity in the most area of the Khuran strait is greater than 0.5 m/s. Also in the some part the maximum tidal current velocity is greater than 2 m/s.

7. References

[1] Pous, S., et al., "A Process Study of the Tidal Circulation in the Persian Gulf.", *Open Journal of Marine Science*, 2, 2012, 131-140.

[2] Kampf, J. and Sadrinasab. M., "The circulation of the Persian Gulf: a numerical study.", *Ocean Science Discussions*, 2(3), 2005, 129-164.

[3] Aghajanloo, A., et al., "Numerical Simulation of Tidal Currents in Persian Gulf.", *Journal of Environmental, Chemical, Ecological, Geological and Geophysical Engineering* 5(1), 2011, 613-620.

[4] Zaker, N. H., et al., "Dynamics of the Currents in the Strait of Khuran in the Persian Gulf.", *Journal of Shipping and Ocean Engineering* 1, 2011, 109-115.

[5] Mahmoudov, M., et al. (2011). "Three-Dimensional Simulation of Qeshm Channel Currents." *Journal of Persian Gulf* ,2(3), 2011, 9-16.

NUMERICAL SIMULATION OF TIDAL WAVE OVER WAVY BED

Maryam Ziaadini-Dashtekhaki[1], Mahnaz Ghaeini-Hessaroeyeh[2]

1. Department of Civil Engineering, Faculty of Engineering, Shahid Bahonar University of Kerman, Kerman, Iran, m.ziaadini@eng.uk.ac.ir
2. Department of Civil Engineering, Faculty of Engineering, Shahid Bahonar University of Kerman, Kerman, Iran, mghaeini@uk.ac.ir

1. INTRODUCTION

A commonly used approach for modeling water flows with free surface is to solve the shallow water equations, which can be obtained from depth averaging of the Navier Stokes equations. To date, many studies have been done on tidal flow modeling [1, 2, 3]. In the present work, the 1D shallow water equations are used and the HLLC method is selected for flux modeling. To achieve the second-order accuracy, the WAF method is selected and the tidal wave flow presented by Bermudez[4] was chosen to demonstrate the capability of the present model.

2. NUMERICAL MODEL

2.1. GOVERNING EQUATIONS

The one-dimensional shallow water equations with bottom topography expressed in the conservation law form are given by:

$$\frac{\partial h}{\partial t}+\frac{\partial}{\partial x}(hu)=0$$

$$\frac{\partial}{\partial t}(hu)+\frac{\partial}{\partial x}(hu^2+\frac{1}{2}gh^2)=-gh\frac{dB}{dx} \quad (1)$$

Where t denotes the time, x is the distance, h(x,t) is the water depth above bottom, u(x,t) is the water velocity averaged across the water depth in the x-direction, and g is the acceleration due to gravity, given by the constant value g=9.81m/s^2. B=B(x) is the bottom elevation.

The free surface elevation is:

$$\eta(x,t)=h(x,t)+B(x) \quad (2)$$

2.2 DISCRETISATION

Shallow-water equations (1) in the form of hyperbolic conservation equations can be written as:

$$\frac{\partial U}{\partial t}+\frac{\partial F}{\partial x}=S \quad (3)$$

The discretisation of Eq. (3) is as follows:

$$U_i^p=U_i^m-\frac{\Delta t(F_{i+1/2}-F_{i-1/2})^m}{\Delta x} \quad (4)$$

Where Δt is the time step, Δx is the spatial step, m is the time step index; p represents the state updated from Eq. (3), and $F_{i+1/2}$ and $F_{i-1/2}$ are the interface fluxes. The Harten-Lax-van Leer-Contact (HLLC) approximate Riemann solver[5] is adopted in the present model. $F_{i+1/2}$ evaluated as follows:

$$F_{i+1/2}=\begin{cases}F_L & if \quad s_L\geq 0\\ F_{*L} & if \quad s_L\leq 0\leq s_*\\ F_{*R} & if \quad s_*\leq 0\leq s_R\\ F_R & if \quad s_R\leq 0\end{cases} \quad (5)$$

Where $F_L=F(U_L)$, $F_R=F(U_R)$, U_L, U_R are the left and right Riemann states of a local cell interface, respectively, F_{*L} and F_{*R} are the numerical fluxes in the left and right sides of the star region. S_L, S_* and S_R are the speed of the left, contact and right waves, respectively. There are several possible options for these wave speeds. The approach proposed by Toro [6] is:

$$S_R=\max(u_R+\sqrt{gh_R},u^*+\sqrt{gh^*})$$
$$S_L=\min(u_L-\sqrt{gh_L},u^*-\sqrt{gh^*}) \quad (6)$$

In above expressions h^* and u^* are the flow depth and flow velocity in the intermediate region of the wave structure. One can evaluate these flow variables as follows [6]:

$$h^*=\frac{1}{g}\left[\frac{1}{2}(\sqrt{gh_L}+\sqrt{gh_R})+\frac{1}{4}(u_L-u_R)\right]^2$$
$$u^*=\frac{1}{2}(u_L+u_R)+\sqrt{gh_L}-\sqrt{gh_R} \quad (7)$$

In order to achieve second-order accuracy the Weighted Average Flux (WAF) method which was introduced by Toro [6] is employed in the present model.

The WAF scheme, as being second-order accurate in space and time, produces spurious oscillations near steep gradients, and so needs TVD stabilization [6]:

$$F_{i+1/2}^{TVDWAF}=\frac{1}{2}(F_i+F_{i+1})-\frac{1}{2}\sum_{k=1}^{3}sign(c_k)A_{i+\frac{1}{2}}^{(k)}\Delta F_{i+\frac{1}{2}}^{(k)}$$
$$F_i=F(U),\ \Delta F_{i+\frac{1}{2}}^{(k)}=F_{i+\frac{1}{2}}^{(k+1)}-F_{i+\frac{1}{2}}^{(k)},\ c_k=(\frac{\Delta t}{\Delta x})s_k \quad (8)$$

Where $A^{(k)}_{i+1/2}$ is a WAF flux limiter function. Some suitable choices for limiter function are reported. The Van Leer limiter has been used in the present applications [6].

3. MODEL TESTING

Tidal waves often have to be considered in coastal engineering. In the present work, the problem that the analytical solution is reported by Bermudez and Vazquez [4] is selected. The bed topography defined by:

$$H(x) = 50.5 - \frac{40x}{L} - 10\sin\left[\pi\left(\frac{4x}{L} - \frac{1}{2}\right)\right] \quad (9)$$

Where L=14000m is the channel length. The initial and boundary conditions are:

$$h(x,0) = H(x) \quad (10)$$
$$u(x,0) = 0$$

And

$$h(0,t) = H(0) + 4 - 4\sin\left[\pi\left(\frac{4t}{86400} + \frac{1}{2}\right)\right] \quad (11)$$
$$u(L,t) = 0$$

The same bed and flow condition were also used by Bermudez and Vazquez [4]. Bermudez suggested the asymptotic analytical solution for this test as following:

$$h(x,t) = H(x) + 4 - 4\sin\left[\pi\left(\frac{4t}{86400} + \frac{1}{2}\right)\right] \quad (12)$$
$$u(x,t) = \frac{(x-L)\pi}{5400h(x,t)}\cos\left[\pi\left(\frac{4t}{86400} + \frac{1}{2}\right)\right]$$

A comparison of the numerical results with the asymptotic analytical solution at t=7552.13S is shown in figure 1 and 2.

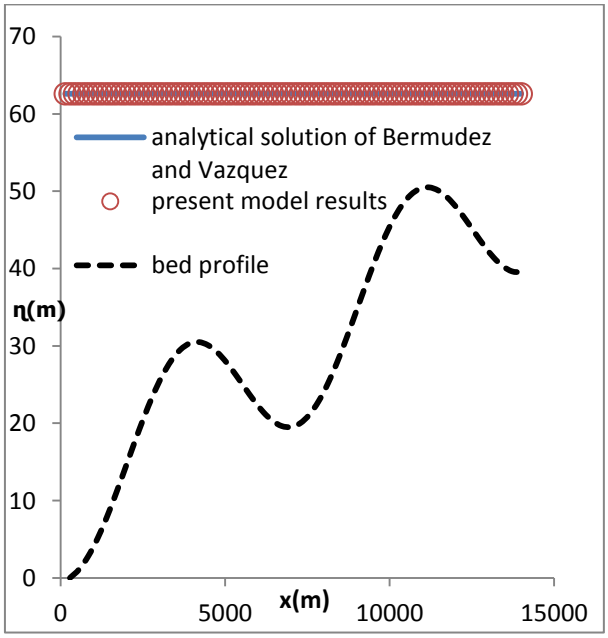

Figure 1. Comparison of the result of present model and analytical solution of Bermudez and Vazquez for water surface

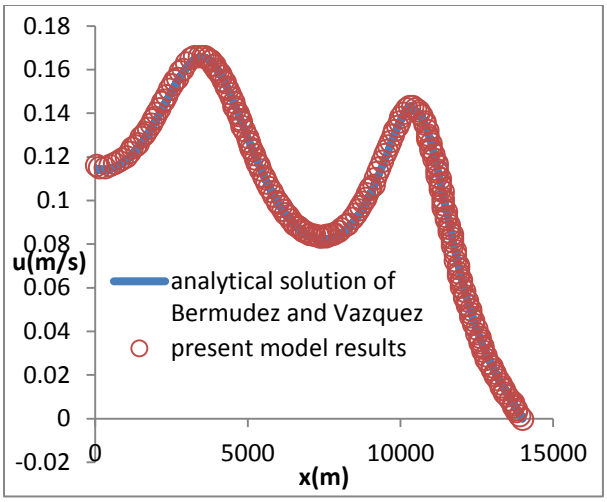

Figure 2. Comparison of the result of present model and analytical solution of Bermudez and Vazquez for velocity

The figures show the good agreement between the analytical results and the results of the present model for both the water surface and velocity profile.

4. CONCLUSIONS

The study reported in this paper has focused on the tidal flow using the 1D shallow water equations. Model verification has been made by comparison of the model results with analytical solution. Comparison of results shows that the present model is able to model tidal wave flow.

5. REFERENCES

[1] Pu, J. H., Cheng, N., Tan, S. K., Shao, S., "Source term treatment of SWEs using surface gradient upwind method", *journal of Hydraulic Research*, 2012, 50, 2, pp. 145-153.

[2] Devkota, J., Fang, X., "Numerical simulation of flow dynamics in a tidal river under various upstream hydrologic conditions", Hydrological Sciences Journal, 2015, 60, 10, pp. 1666-1689.

[3] Huang, J., Zhang, X., Chua, V., "Numerical modeling of longitudinal dispersion in tidal flows with submerged vegetation", *journal of Hydraulic Research*, 2015, 53, 6, pp. 728-746.

[4] Bermudez, A., Vazquez-Cendon, M. E., "Upwind methods for hyperbolic conservation laws with source term", *Comput. Fluids*, 23, 7, 1994, pp. 1049-1071.

[5] Toro, E. F., Spruce, M., Speares, W.,"Restoration of the contact surface in the HLL Riemann solver", *Shock Waves*, 4, 1, 1994, pp. 25-34.

[6] Toro, E. F., "Shock Capturing Method For Free Surface Shallow Flows", *John Wiley and Sons*, 2001.

NUMERICAL MODELING OF WAVE PROPAGATION OVER IRREGULAR TOPOGRAPHY

Maryam Ziaadini-Dashtekhaki[1], Mahnaz Ghaeini-Hessaroeyeh[2]

1. Department of Civil Engineering, Faculty of Engineering, Shahid Bahonar University of Kerman, Kerman, Iran, m.ziaadini@eng.uk.ac.ir
2. Department of Civil Engineering, Faculty of Engineering, Shahid Bahonar University of Kerman, Kerman, Iran, mghaeini@uk.ac.ir

1. INTRODUCTION

The shallow water equations have wide applications in the ocean and hydraulic engineering. Several techniques have been published to solve the shallow water equations to model free surface flows. In recent years numerical model of flow over an irregular bed has been considered [1]. In the present work, the 1D shallow water equations for flow over arbitrary bottom topography is used and the HLLC method is selected for flux modeling. To achieve the second-order accuracy, the WAF method is selected and a quasi-stationary test case presented by Leveque[2] was chosen to demonstrate the capability of the present model for computation involving small perturbations of the water surface.

2. GOVERNING EQUATIONS

Under the assumption of hydrostatic pressure, the obtained one-dimensional model of depth averaged shallow water equations appears as:

$$\frac{\partial U}{\partial t}+\frac{\partial F}{\partial x}=S \tag{1}$$

The vector of conserved variables U, the flux vector F, and the source term S are defined as:

$$U=\begin{bmatrix} h \\ hu \end{bmatrix},\ F(U)=\begin{bmatrix} hu \\ hu^2+\frac{1}{2}gh^2 \end{bmatrix}$$

$$S(U)=\begin{bmatrix} 0 \\ gh(s_0-s_f) \end{bmatrix} \tag{2}$$

In the above equations, t denotes time, x is the longitudinal distance, h(x,t) is the water depth, u(x,t) is the depth-averaged velocity along x-direction and g is the gravitational acceleration.The bottom slope is given by:

$$S_0=-\frac{dZ_b}{dx} \tag{3}$$

Where Z_b is the bottom elevation. The friction slope s_f is calculated using the Manning's resistance law:

$$S_f=\frac{n_{Manning}^2 u|u|}{h^{4/3}} \tag{4}$$

Where $n_{Manning}$ is the Manning's friction coefficient. The free surface elevation is:

$$\eta(x,t)=h(x,t)+Z_b(x) \tag{5}$$

3. NUMERICAL MODEL

The discretisation of Eq. (1) is as follows:

$$U_i^p=U_i^m-\frac{\Delta t(F_{i+1/2}-F_{i-1/2})^m}{\Delta x} \tag{6}$$

Where Δt is the time step, Δx is the spatial step, m is the time step index; p represents the state updated from Eq. (1), and $F_{i+1/2}$ and $F_{i-1/2}$ are the interface fluxes. The Harten-Lax-van Leer-Contact (HLLC) approximate Riemann solver[3] is adopted in the present model. $F_{i+1/2}$ evaluated as follows:

$$F_{i+1/2}=\begin{cases} F_L & if \quad s_L\geq 0 \\ F_{*L} & if \quad s_L\leq 0\leq s_* \\ F_{*R} & if \quad s_*\leq 0\leq s_R \\ F_R & if \quad s_R\leq 0 \end{cases} \tag{7}$$

Where S_L, S_* and S_R are the speed of the left, contact and right waves, respectively, and $F_L=F(U_L)$, $F_R=F(U_R)$, U_L, U_R are the left and right Riemann states of a local cell interface, respectively, F_{*L} and F_{*R} are the numerical fluxes in the left and right sides of the star region [3].In order to achieve second-order accuracy the Weighted Average Flux (WAF) method which was introduced by Toro [4] is employed in the present model.

The WAF scheme, as being second-order accurate in space and time, produces spurious oscillations near steep gradients, and so needs TVD stabilization [4]:

$$F_{i+1/2}^{TVDWAF}=\frac{1}{2}(F_i+F_{i+1})-\frac{1}{2}\sum_{k=1}^{3}sign(c_k)A_{i+\frac{1}{2}}^{(k)}\Delta F_{i+\frac{1}{2}}^{(k)} \tag{8}$$

$$F_i=F(U),\ \Delta F_{i+\frac{1}{2}}^{(k)}=F_{i+\frac{1}{2}}^{(k+1)}-F_{i+\frac{1}{2}}^{(k)},\ c_k=(\frac{\Delta t}{\Delta x})s_k$$

Where $A^{(k)}_{i+1/2}$ is a WAF flux limiter function. Some suitable choices for limiter function are reported. The Minbee limiter has been used in the present applications [5].

4. MODEL TESTING

To demonstrate the accuracy of the model, we performed a numerical test for which the analytical solution is reported in the literature.

As the bottom topography takes:

$$Z_b = \begin{cases} 0.25[\cos(\pi - 0.5)/0.1) + 1] & if \ |x - 0.5| < 0.1 \\ 0 & otherwise \end{cases} \quad (9)$$

On $0 < x < 1$ with $h(0) = 1$ and g=1. The initial conditions are the stationary solution u=0 and:

$$\eta(x, 0) = \begin{cases} h(0) + \varepsilon & if \ 0.1 < x < 0.2 \\ h(0) & \text{otherwise} \end{cases} \quad (10)$$

Figure 1 shows the computed surface with the present model at t=0.7s. The results are shown for both $\varepsilon = 0.2$ and $\varepsilon = 0.01$ and compared to the exact solution in figure 2 and 3 , respectively.

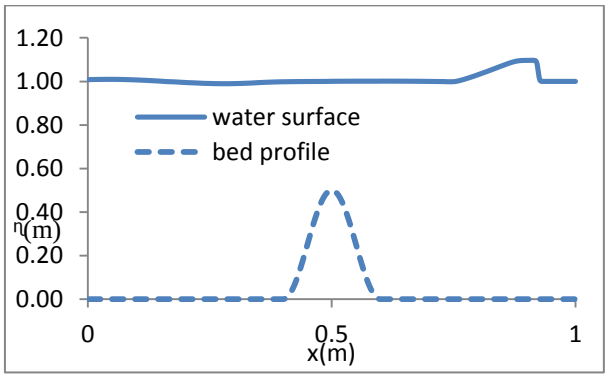

Figure 1. The bottom topography and calculated water surface at t=0.7s

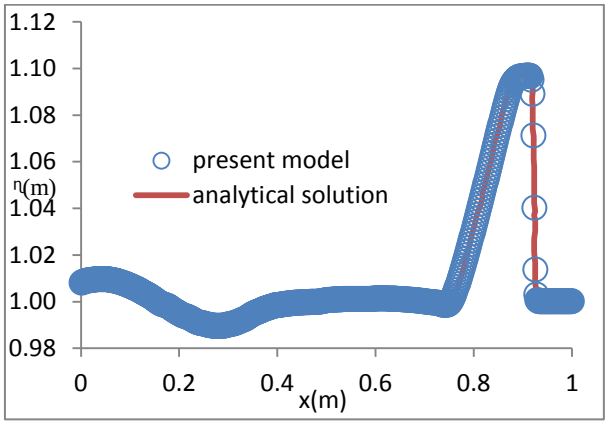

Figure 2. The present model results of the water surface at t=0.7s for the the initial perturbation of ε=0.2.

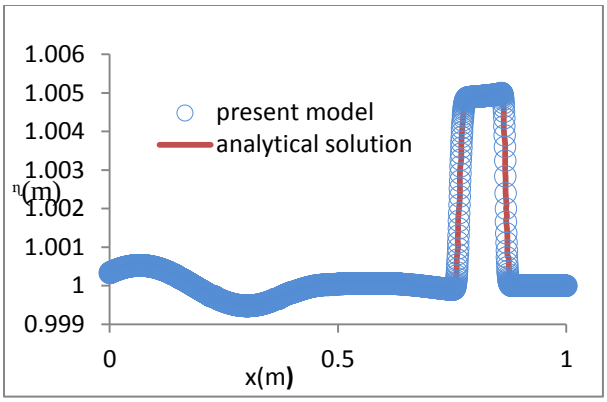

Figure 3. The present model results of the water surface at t=0.7s for the the initial perturbation of ε=0.01.

A magnified view of water surface is shown in figures 2 and 3. The figures show that the present model is able to model small-perturbations on water surface and problems related to wave propagation in shallow water flows.

5. CONCLUSIONS

A shock capturing numerical scheme was applied to one-dimensional non-linear shallow water equations for flow modeling over arbitrary bottom topography. Model verification has been made by comparison of the model results with analytical solution. Comparison of these two sets of data shows that the present model is able to model wave propagation and small-perturbation problems occurring in shallow water flows.

6. REFERENCES

[1] Pu, J. H., Cheng, N., Tan, S. K., Shao, S., "Source term treatment of SWEs using surface gradient upwind method", *journal of Hydraulic Research*, 2012, 50, 2, pp. 145-153.

[2] Leveque, R. J., "Balancing source term and flux gradients in high-resolution Godunov methods: the quasi-steady wave-propagation algorithm", *Journal of computational physics*, 146, 1, 1998, pp. 346-365.

[3] Toro, E. F., Spruce, M., Speares, W.,"Restoration of the contact surface in the HLL Riemann solver", *Shock Waves*, 4, 1, 1994, pp. 25-34.

[4] Toro, E. F., "Riemann Problem and the WAF Method for Solving the Two-Dimensional Shallow Water Equations", *Philosophical Transactions of the Royal Society*, A338, London, 1992, pp. 43-68.

[5] Toro, E. F., "Shock Capturing Method For Free Surface Shallow Flows", *John Wiley and Sons*, 2001.

ANALYTICAL SOLUTION FOR GROUNDWATER HEAD IN UNCONFINED COASTAL AQUIFER USING VARIATIONAL ITERATION METHOD

Seyed Mahmood Hamze-Ziabari[1], Abbas Yeganeh-Bakhtiary[2] and Seyed Mostafa Siadatmousavi [3]

[1)] PhD candidate, School of Civil Eng., IUST, Tehran, Iran, ziabari@civileng.iust.ac.ir
[2)] School of Civil Engineering, IUST, Tehran, Iran, yeganeh@iust.ac.ir
[3)] School of Civil Engineering, IUST, Tehran, Iran, siadatmousavi@iust.ac.ir

1. Introduction

Tides or other long waves induce a considerable oscillation in the groundwater table or head in a coastal aquifer system. These fluctuations are important for many environmental and engineering problems. For example, the variation of groundwater table remarkably affects the cross-shore sediment transport and may cause beach erosion. A high water table accelerates the beach erosion; conversely a low groundwater table may result in accretion at the beach foreshore [1]. Therefore, the proper modeling of groundwater hydraulics in coastal zone is vital.

In the modeling of the flow in an unconfined-aquifer, the governing equations are nonlinear. In some of the previous studies, the reduced linear form of the governing equations for underground flow was used, assuming negligible error in the solution due to linearization. However; it has been shown that the nonlinearity of the governing equation has an important influence on the tide-induced fluctuations in unconfined aquifers [2]. Most recently, the perturbation methods have been widely used to solve the nonlinear Boussinesq equation for water table fluctuations in an unconfined coastal aquifer. However; like other techniques for solving nonlinear equations, a perturbation method has its own limitations [3]. The main limitation of a perturbation method is the fact that it is based on "small" values for some pre-determined parameters.

In the present study, an analytical solution is presented to estimate water table fluctuations induced by tidal waves in an unconfined coastal aquifer with vertical slope. A one-dimensional non-linear Boussinesq equation was solved by means of the so-called variational iteration method, which has been widely applied to solve the strongly nonlinear systems without any linearization or with small perturbations. The validation of the new solutions was then verified against several previous studies, e.g. Parlange et al. [2], Barry et al. [4] and the experimental data of Cartwright et al. [5].

2. The Variational Iteration Method

The variational iteration method (VIM) has been used recently to solve engineering problems with nonlinear governing equation. The solution for partial differential equations governing an engineering problem is often not unique or it is difficult to find. There are many standard methods to solve nonlinear differential equations, e.g. Adomian's decomposition method, inverse scattering method and etc. The main advantages of VIM compared to the other methods are its flexibility, convenience of implementation and the accuracy of the solution. The VIM method usually leads to an accurate solution by a few iterations, if the initial solution is carefully chosen [2].

3. Application of VIM for aquifers

A homogeneous and isotropic unconfined aquifer with vertical section perpendicular to the shoreline is assumed. By neglecting the effects of vertical flow and capillarity, the ground water table fluctuation in a horizontal and impermeable unconfined aquifer can be simulated based on the classic Boussinesq equation. It is convenient to define the following non-dimensional quantities:

$$H = \frac{h}{h_z},\ X = \frac{x}{l},\ T = \omega t,\ A = \frac{a}{h_z},\ \delta = \frac{h_z}{l} \quad (1)$$

where h_z is the average height of mean sea water level, a is the amplitude of tidal fluctuations, ω is the tidal wave frequency and l is the decay length along the x direction. Substituting non-dimensional

quantities into Boussinesq equation, the following equation can be obtained.

$$\frac{\partial H}{\partial T} = \frac{1}{2}\left(\left(\frac{\partial H}{\partial X}\right)^2 + H\frac{\partial^2 H}{\partial X^2}\right) \quad (2)$$

To solve Eq. (2) by means of VIM, a correction function can be written as follows:

$$H_{n+1} = H_n + \int_0^t \lambda\left[\frac{\partial H_n(\mathrm{X},\mathrm{S})}{\partial S} - \frac{1}{2}\left(e_1\left(\frac{\partial \tilde{H}_n}{\partial X}\right)^2 + e_2\tilde{H}_n\frac{\partial^2 \tilde{H}_n}{\partial X^2}\right)\right]dS \quad (3)$$

4. Comparison

To skill-asses the VIM results, the experimental data from Cartwright et al. [5] were used. The bottom of aquifer is horizontal; the beach slope is vertical, and the other conditions are as follows: k=40.6 m/day, a=0.235 m, wave period T=772 s and aquifer thickness h_z=1.094 m. Fig. 1 shows the comparison between the results of VIM and experimental data. The prediction of Parlange et al. [2] equation is also presented. When the calibration coefficients were selected as e_1=0.8 and e_2=0. 01, the VIM solution closely agrees with the experimental data. Therefore, these coefficients are used for vertical beaches. Another comparison of the VIM solution with mentioned calibration coefficients for vertical beaches against Cartwright et al., [5] is given in Fig. 2. It is clear that the VIM yields to a satisfactory result with similar trends.

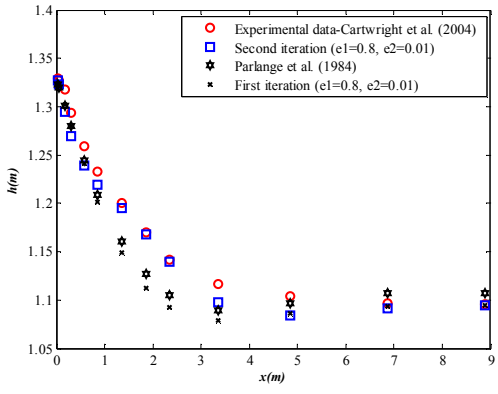

Fig.1. Comparison between the results of VIM, Parlange et al.[2] and the experimental data

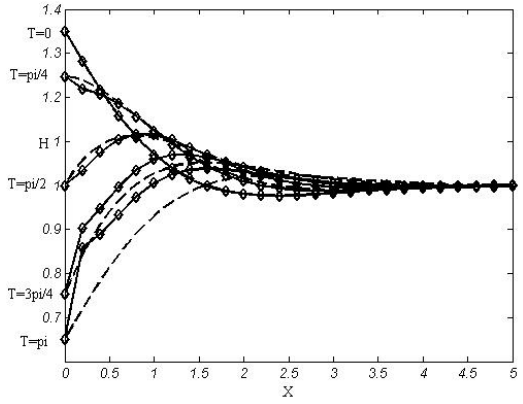

Fig. 2. Comparison between the VIM (-o-) and Barry et al. (--)

5. Conclusion

The performance and accuracy of the variational iteration method (VIM) technique was numerically evaluated by comparing the obtained solution with that of the Cartwright et al. [5] experiments for vertical beaches. The results were also compared with other analytical solutions in the literature. It was shown that the VIM used here is a flexible and an accurate approach and it can effectively converge to the same results obtained by the other approaches.

References

[1] Nielsen, P., "Tidal dynamics of the water table in beaches", Water Resource. Res. Vol. 26 (9), pp. 2127–2134, 1990.

[2] Parlange, J.Y., Stagnitti, F., Starr, J.L. & Braddock, R.D., "Free-surface flow in porous media and periodic solution of the shallow-flow approximation", J. Hydrology. Vol. 70, pp. 251–263, 1984.

[3] He, J.H. & Wu, X. H., "Variational iteration method: New development and applications", Computers and Mathematics with Applications Vol. 54, pp.881–894, 2007.

[4] Barry, D.A., Stagnitti, F., Parlange, J.Y. & Jeng, D.S., "Beach water table fluctuations due to spring-neap tides: moving boundary effects", Adv. Water Resource Vol. 23, pp. 817–824, 2000.

[5] Cartwright, N., Nielsen, P. & Li, L., "Experimental observations of water table waves in an unconfined aquifer with a sloping boundary", Adv. Water Resource, Vol. 27, pp. 991–1004, 2004.

NUMERICAL INVESTIGATION OF WAVE INTERACTION WITH A GROUP OF PILES USING WCSPH METHOD

Mohammad Hadi Shabani[1] and Mahmoud Rostami Varnousfaaderani[2]

1) Faculty of Marine Engineering, Malek-Ashtar University of Technology, Shahin shahr, Iran, mhadishabani@gmail.com
2) Faculty of Marine Engineering, Malek-Ashtar University of Technology, Shahin shahr, Iran, rostamivf@aut.ac.ir

1. Introduction

Cylindrical piles are commonly used in coastal and offshore engineering as support structures for piers, offshore platforms and wind turbines. Thus it is important to understand the interaction of waves with a group of piles and to compute wave forces acting on the cylinders accurately. Weakly Compressible Smoothed Particle Hydrodynamic (WCSPH) method is a Lagrangian meshless method, introduced by Monaghan [1]. In this method, a computational domain is represented by particles, which possess fluid properties. SPH method has been widely used for many applications such as modeling dam break, fluid-structure interaction, and solitary wave breaking.

2. Governing Equations

The governing equations in transient, viscous, and compressible flow are continuity and momentum conservation equations as:

$$\frac{1}{\rho}\frac{D\rho}{Dt} + \nabla.\mathbf{u} = 0 \tag{1}$$

$$\frac{D\mathbf{u}}{Dt} = -\frac{1}{\rho}\nabla P + \mathbf{g} + \Theta \tag{2}$$

where t is time; ρ is fluid density; $\boldsymbol{u}$ is velocity vector; P is pressure; $\boldsymbol{g}$ is the gravitational acceleration vector; and Θ refers to diffusion terms. Two different options can be used for diffusion terms: (i) artificial viscosity [1] and (ii) laminar viscosity and SPS turbulence model [2].

3. Basic SPH Concepts

In SPH, any arbitrary function $A(r)$ for particle a is approximated by following summation over fluid domain:

$$A(r_a) = \sum_b m_b \frac{A_b}{\rho_b} W_{ab} \tag{3}$$

where m_b and ρ_b are mass and density, respectively. $W_{ab} = W(|\mathbf{r}_a - \mathbf{r}_b|, h)$ is the kernel function and h is the smoothing length of it. In this study, cubic B-spline kernel, repulsive boundary condition, and predictor-corrector scheme were used. All simulation were done by SPHysics_3D_v2.2.001 open-source code.

4. Pressure Field Correction

There are large fluctuations in pressure field of WCSPH method. To remove these unphysical fluctuations, some modifications should be applied on pressure field. When artificial viscosity was used as diffusion terms, Moving-Least-Square (MLS) density filter [3] and XSPH scheme were applied (henceforth referred as SPH-MLS). When laminar viscosity and SPS turbulence model were used, nonconservative Riemann solver [4] was applied and gradients of kernels [5] were corrected (henceforth referred as SPH-T-RG).

5. Validation of Horizontal Force Values

Yeh and Petroff's [6] experiment was used to validate numerical method. In this experiment, a dam-break hydraulic bore was generated in a tank and collide a rectangular column. The time histories of the horizontal force acting on the column of numerical simulations and experimental results [6] are shown in Figure 1.

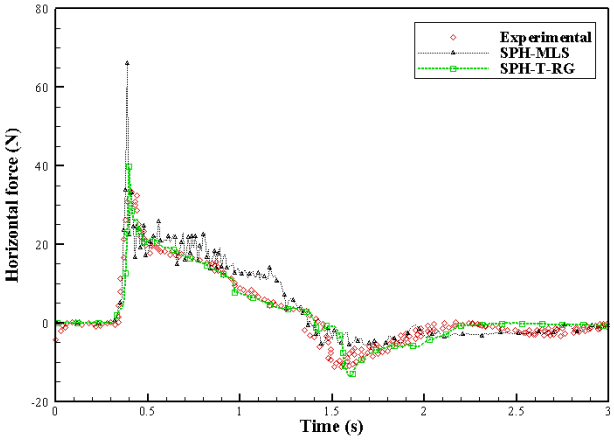

Figure 1. Comparison between numerical and experimental data [6] of exerted force on an obstacle

It can be seen that the results of SPH-MLS is highly fluctuating and it is entirely unreliable. But thanks to using Riemann solvers, the computed force by SPH-T-RG was obtained accurately. Simulating viscosity in a realistic manner is another advantage of this method.

6. Wave interaction with single cylinder

Linear waves of height H=0.08 m, Period T=1.2 s, and wavelength L=2.065 m were generated in a numerical wave tank with 14.43 m length, 4.42 m width and 0.52 m depth. A cylinder with diameter of 0.39 m was placed 5.20 m downstream of the wavemaker. A snapshot of wave interaction with a cylinder is shown in Figure 2. Minimum and maximum of wave force which is obtained by SPH-T-RG was compared with Airy theory. These errors were reported in table 1 and they were 5.80% and 19.79% for minimum and maximum of wave force respectively.

Table 1. Comparison of maximum and minimum wave force obtained by computation and Airy theory.

	Airy theory (N)	SPH-T-RG (N)	Error (%)
Maximum	144.38	136.46	5.80
Minimum	55.22	66.15	19.79

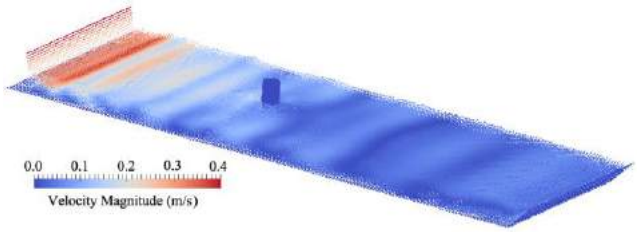

Figure 2. A snapshot of wave interaction with a cylinder at t=9.5 s

7. Wave interaction with nine cylinder

Nine cylinders with a diameter of D=0.39 m in 3*3 square array was placed in a wave tank with a water depth d=0.52 m. Linear waves of height H=0.08 m, Period T=1.2 s, and wavelength L=2.065 m were incident on the cylinders. Figure 3 shows the schematic of problem and a snapshot of wave interaction with the cylinders.

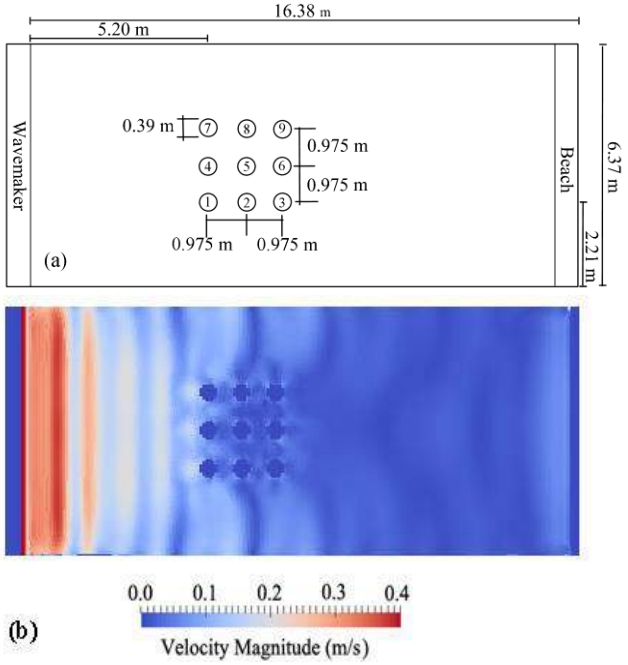

Figure 3. (a) Schematic of wave tank and piles; and (b) a snapshot of wave interaction with the cylinders at t=9.5 s

Since maximum wave forces were acted on the first row cylinders and maximum water surface elevations were observed in front of this row, only their time histories are shown in this paper and they are depicted in Figure 4 and Figure 5 respectively. In the downstream rows, these values decreased gradually.

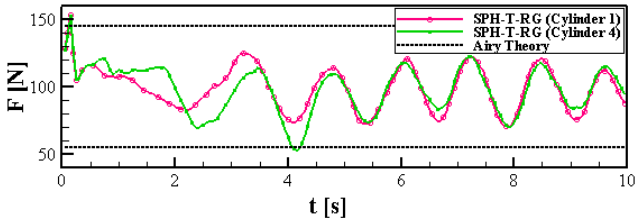

Figure 4. Time histories of wave forces on Cylinder 1 and Cylinder 4

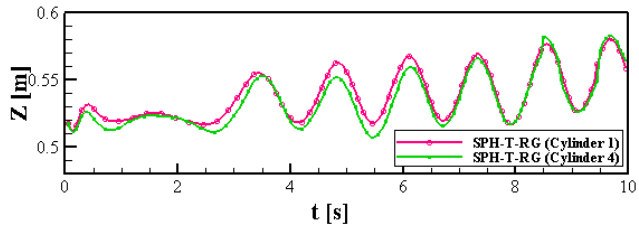

Figure 5. Free surface elevation in front of Cylinder 1 and Cylinder 4

There are some noises at initial seconds which are due to weakly compressible assumption. These oscillations diminish gradually and at t=3 s wave arrives at the cylinders. Cylinders in this array experiences less forces compared to a single cylinder (Dashed line in Figure 4 is related to predicted force obtained by Airy theory for a single cylinder). Maximum run-up occurs in front of cylinder 1 and this cylinder experiences the highest force in this array. The central cylinder in the first row (cylinder 4) experiences less force in comparison with cylinder 1. The reason of this event is related to trapped waves between cylinder 4 and 5 which neutralize the incidence wave force.

8. References

[1] Monaghan, J. J. "Simulating Free Surface Flows with SPH", Journal of Computational Physics, 110, 1994, pp. 399-406.

[2] Dalrymple, R. A. and Rogers, B. D. "Numerical Modeling of Water Waves with the SPH Method", Coastal Engineering, 53, 2–3, 2006, p. 141–147.

[3] Colagrossi, A. and Landrini, M. "Numerical simulation of interfacial flows by smoothed particle hydrodynamics", Journal of Computational Physics, 191, 2003, p. 448–475.

[4] Parshikov, A. N. and Medin, S. A. "Smoothed particle hydrodynamics using Inter-particle contact algorithms", Journal of Computational Physics, 180, 2002, p. 358–382.

[5] Bonet, J. and Lok, T. –S. L. "Variational and momentum preservation aspects of smoothed particle hydrodynamic formulations", Computer Methods in Applied Mechanical Engineering, 180, 1999, p. 97–115.

[6] Gomez-Gesteira, M. "SPHERIC SPH benchmark test cases: Test 1", 2006.

NUMERICAL MODELING OF MUD-INDUCED WAVE DAMPING

Mohammad Reza Dorri[1] and Kourosh Hejazi[2]

1) Department of Civil Engineering, K. N. Toosi University of Technology, Tehran, Iran, Dori1364@mail.kntu.ac.ir
2) Department of Civil Engineering, K. N. Toosi University of Technology, Tehran, Iran, HejaziK@ kntu.ac.ir

1. Introduction

Progressive water waves can be severely damped over muddy beds. This damping is assigned to the bottom pressure of the wave deforming the viscous mud, creating a wave on the interface between the water and the mud, defined as the lutocline. The movement of lutocline can cause mud migration through Stokes drift [1]. For prediction of damping mechanism, several theoretical, experimental and numerical studies have been carried out. In this research, ALES-VOF method has been implemented in the WISE 2DV non-hydrostatic numerical model [2] for simulation of wave-mud interaction. For a more accurate simulation of water free surface and interface of mud and water, advantages of ALES and VOF methods are integrated.

2. Governing equations

Conventional turbulence models may be deployed in RANS equations. In WISE, the two-equation *k-ε* turbulence model with buoyancy terms are utilized and implemented in the numerical model. The conservative forms of 2DV equations deployed in the model are as follows:

$$\frac{\partial u}{\partial x}+\frac{\partial w}{\partial z}=0 \tag{1}$$

$$\frac{\partial u}{\partial t}+\frac{\partial u^2}{\partial x}+\frac{\partial uw}{\partial z}-w_g\frac{\partial u}{\partial z}= -\frac{\partial P^*}{\partial x}+\frac{\partial}{\partial x}\left(\nu_T\frac{\partial u}{\partial x}\right)+\frac{\partial}{\partial z}\left(\nu_T\frac{\partial u}{\partial z}\right) \tag{2}$$

$$\frac{\partial w}{\partial t}+\frac{\partial uw}{\partial x}+\frac{\partial w^2}{\partial z}-w_g\frac{\partial w}{\partial z}= -\frac{\partial P^*}{\partial z}+\frac{\partial}{\partial x}\left(\nu_T\frac{\partial u}{\partial x}\right)+\frac{\partial}{\partial z}\left(\nu_T\frac{\partial u}{\partial z}\right)-\frac{\rho-\rho_0}{\rho_0}g \tag{3}$$

where *t* is time; *x* and *z* are coordinates in horizontal and vertical directions respectively, *u* and *w* are horizontal and vertical velocity components respectively, *P** is the pressure with the exclusion of the hydrostatic pressure divided by the reference density of water; ρ is water density and ρ_0 is the reference density. *g* is the acceleration of gravity, w_g is the grid velocity and v_t is the eddy viscosity coefficient. In this model, a hybrid formulation based on a pseudo-plastic rheology model has been used to show the relationship between the effective viscosity of mud, shear rate, and volumetric concentration, which is presented as follows [3]:

$$\mu_e=A\dot{\gamma}^B+C\dot{\gamma}^D+\mu_w \tag{4}$$

where $A=a_1\varphi^{a_2}$, $B=b_1\varphi+b_2$, $C=c_1\varphi^{c_2}$ and $D=d_1\varphi+d_2$.The empirical coefficients in Eq. (4) are determined as follows[3]:

a_1 = 59.1026, a_2 = 2.9378, b_1 = -1.2438, b_2 = -0.6332, c_1 = 1207.5846×10^4, c_2 = 12.5729, d_1 = 2.9643, d_2 = -1.1972.

3. Numerical Method

Spatial discretization was based on the finite volume method, which utilizes a staggered grid. The temporal discretization of the equations was based on fractional step method, which resembles a projection method. In the VOF method, the free surface is represented by a volume function known as the color function. The color function, *C*, is considered to determinate a cell volume which is occupied by the fluid. The method was devised to solve the advection part of the N-S equations, presented in equation (5)

$$\frac{\partial C}{\partial t}+\nabla.(UC)=0 \tag{5}$$

The concept of Youngs method [4] was utilized for volume function advection in the present model. The advantage of the Youngs method is that it possesses an easy implementation, with a reasonable accuracy.

4. Numerical Simulations

In this section, propagation of water waves over non-Newtonian muddy bed has been simulated. The experimental test conducted by Hsu et al. [3] has been numerically modeled herein. The test was performed in a flume with 20 m length, 0.5 m width and 0.8 m depth. Figure 1 illustrates the schematic of the flume and waves gages. The mud layer was placed along 8.77 m length and with a depth of 0.06 m and a bulk density of 1420 kg/m^3. The wave height was set equal to 0.04 m, the wave length was 1.77 m and the wave period was 1.2 s. The computational domain was discretized by grids sizing $\Delta x = \Delta z$ = 0.015 m. The results of the numerical

simulations of the present model are compared with the experimental measurements in Fig. 2.

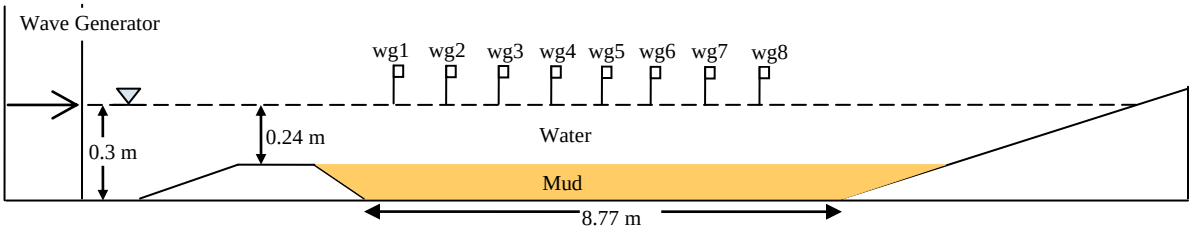

Figure 1. The schematic of experimental setup and locations of wave gages [3]

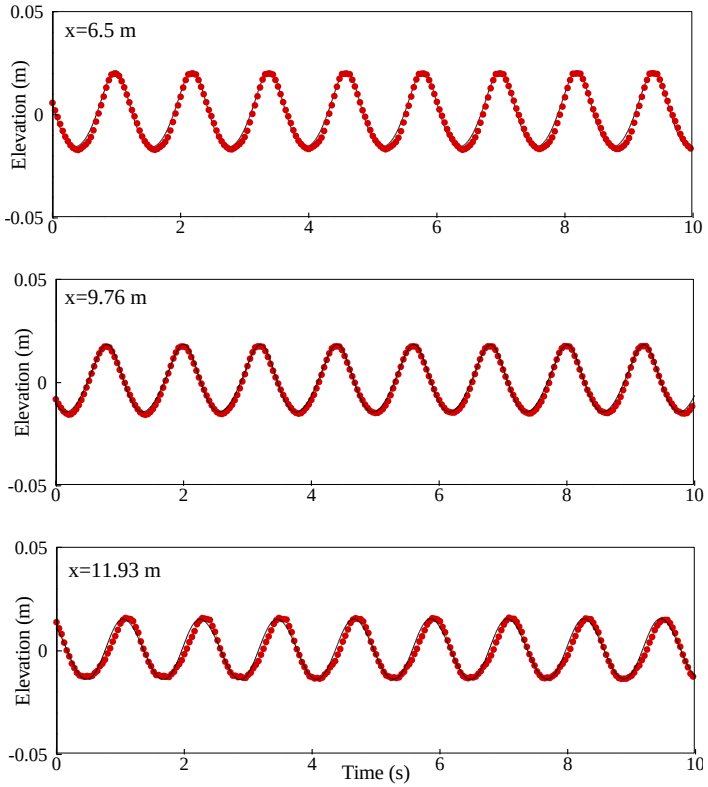

Figure 2. Comparison of surface elevation time series of measured values (solid circle) and predicted results (solid line)

5. Conclusions

In this paper, ALES-VOF method has been used for capturing the free surface and the interface of water and non-Newtonian mud layer. Numerical simulation of wave-mud interaction shows good agreements between predicted values and experimental measurements, which confirms the capability of integrated ALES-VOF methods for the present application..

.

6. References

[1] Hu, Y., Guo, X., Lu, X., Liu, Y., Dalrymple, R. A., & Shen, L. (2012). Idealized numerical simulation of breaking water wave propagating over a viscous mud layer. *Physics of Fluids (1994-present)*,*24*(11), 112104.

[2] Hejazi, K., Soltanpour, M., & Sami, S. (2013). Numerical modeling of wave–mud interaction using projection method. *Ocean Dynamics*, *63*(9-10), 1093-1111.

[3] Hsu, W. Y., Hwung, H. H., Hsu, T. J., Torres-Freyermuth, A., & Yang, R. Y. (2013). An experimental and numerical investigation on wave-mud interactions. *Journal of Geophysical Research: Oceans*, *118*(3), 1126-1141.

[4] Rudman, M. (1997). Volume-tracking methods for interfacial flow calculations. *International journal for numerical methods in fluids*, *24*(7), 671-691.

DEVELOPING THE PERSIAN GULF WAVE FORECAST SYSTEM

Morteza Jedari Attari[1], S. Abbas Haghshenas[2], Mohsen Soltanpour[3], Azadeh Razavi Arab[4], Zohreh Hajisalimi[5], S. Jaafar Ahmadi[6], Arash Zarkani[7], Mohammad Reza Allahyar[8] Arash Bakhtiari[9] and Edris Delkhosh[10]

1) Inst. of Geophysics, Univ. of Tehran, Iran, Email: mortezajedariattari@yahoo.com
2) Inst. of Geophysics, Univ. of Tehran, Iran, Email: sahaghshenas@ut.ac.ir
3) K. N. Toosi University of Technology, Tehran, Iran, Email: soltanpour@kntu.ac.ir
4) Inst. of Geophysics, Univ. of Tehran, Iran, Email: azadeh_razavi_1981@yahoo.com
5) Port and Maritime Organization, Tehran, Iran, Email: hajisalimi.zohreh@yahoo.com
6) Inst. of Geophysics, Univ. of Tehran, Iran, Email: jaafarahmadi@yahoo.com
7) Inst. of Geophysics, Univ. of Tehran, Iran, Email: arash_zarkani@yahoo.com
8) Port and Maritime Organization, Tehran, Iran, Email: mallahyar@yahoo.com
9) K. N. Toosi Univ. of Technology, Tehran, Iran, Email: arash.bakhtiary@gmail.com
10) Inst. of Geophysics, Univ. of Tehran, Iran, Email: edrisdelkhosh@ut.ac.ir

1. Introduction

The Persian Gulf is one the most crowded navigation corridors which hosts a significant portion of world's energy and cargo transports. Considering the numerous offshore and onshore constructions, drillings and oil and gas platforms in the region, the demand for a reliable met-ocean forecast system has been highly increased in recent years. Thus, Port and Maritime Organization (PMO) of Iran, as the authorized and responsible entity to meet the marine and coastal needs of the country, introduced the Persian Gulf Forecasting System project in 2014. The project, which includes the state of art modeling of wind field, waves and currents in the Persian Gulf, was awarded to K. N. Toosi University of Technology and Institute of Geophysics (University of Tehran). The waves are simulated by introducing the modelled wind field to the wave generation/propagation model. The present paper offers the development of the wave forecast system which has been calibrated and verified for the Persian Gulf. Figure 1 illustrates the study area and available measured data.

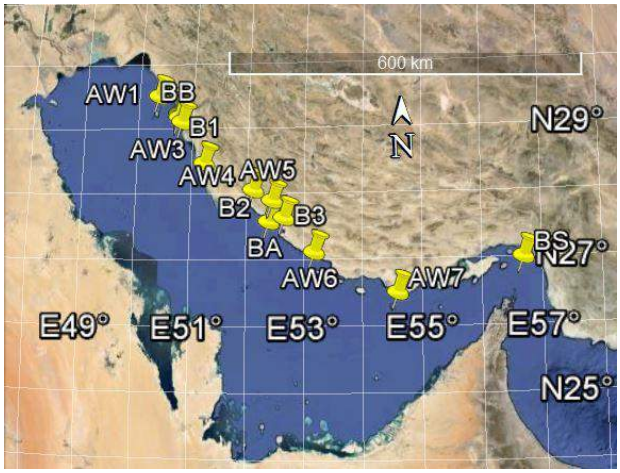

Figure 1. The Persian Gulf and Data Collection stations

2. Data Gathering

As illustrated in Figure 1, the existing data of 10 stations were collected in this study. The waves have been mainly recorded by PMO through different phases of Monitoring and Modelling Projects of Iranian coasts [1]. Furthermore, the data of 3 active buoys are regularly collected and used to improve the accuracy of the model predictions.

Wind field is provided by Institute of Geophysics, University of Tehran. The obtained global GFS data is implemented in WRF [2] model in order to resolve the meso-scale phenomena.

The bathymetry of the Persian Gulf was developed collecting various data sources of ETOPO1 for deep waters [3] and local data sets of PMO, National Cartographic Center (NCC) of Iran and Iranian Fishery Organization (IFO) for shallow areas (Fig. 2).

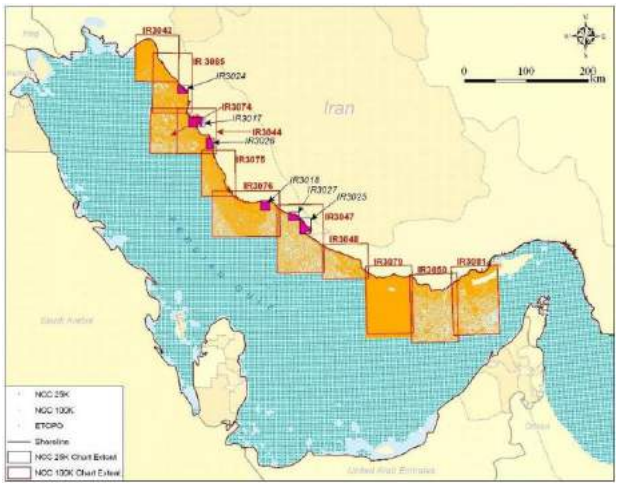

Figure 2. Hydrography data

3. Methodology

The outputs of wind modelling is applied in the third generation WAVEWATCH III (WW3) model to simulate the wave characteristics over the domain of the Persian Gulf. Both wind field and wave forecasting systems are updated every 12 hours.

WW3 was selected for the numerical modelling, in comparisons to other wave generation models such as, SWAN, MIKE-SW, PMO-Dynamics, because of its high performance and accessibility to the source code, which enables the implementations of necessary

modifications and required developments within a unified automatic system.

4. Numerical Modeling

Version 4.18 of the third generation WW3 model was implemented for the generation and propagation of waves in the Persian Gulf [4].

The source term consists of three parts, i.e. wind-wave interaction, nonlinear wave-wave interactions and dissipation ('whitecapping') in deep waters, but additional processes including the effective wave-bottom interactions, need to be considered in shallow waters. In extremely shallow areas, depth-induced wave breaking and wave-wave interactions become important too.

A structured mesh is developed to resolve the bathymetry within the computational domain (Figure 3). The mesh size is 0.05°×0.05° and general time-step was set to be 12 minutes. The main parameters of the model were assigned based on comprehensive sensitivity analyses. Calibration and verification of the model was performed for about 30 individual selected events, based on the available historical and new data.

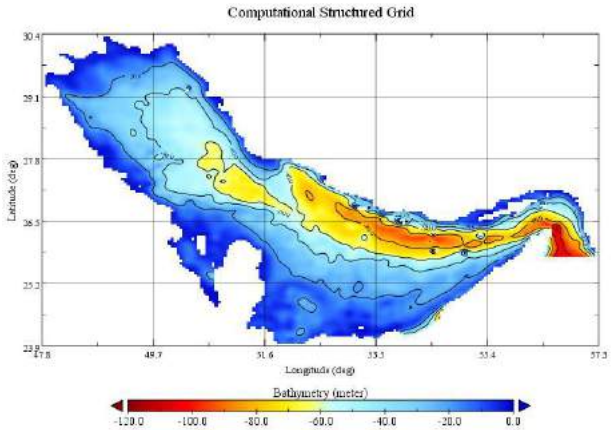

Figure 3. Bathymetry and computational domain of the Persian Gulf

5. Discussion and Conclusion

Figure 4 illustrates the comparisons between model results and recorded data of AW6 from 18th of March to 7th April, 2010. As AW6 was located in the middle of the Persian Gulf, the recorded waves are generally higher than other parts. Blue dots present the measured data, which include significant wave heights (top panel), wave periods (middle panel) and mean wave directions (bottom panel).

The statistical tests on model performance shows a high rate of consistency with the general correlation coefficient of significant wave heights of more than 80% and the average root mean square of errors of less than 0.35 m. The accuracy of the prediction of wave periods are reasonable too, with the average correlation coefficient of 70% and the root mean square of errors in the order of 0.8 seconds. The simulation of mean wave directions also shows no crucial problem.

Regarding the peak wave heights, the model showed a very good performance for 65% of the high waves but 23% of the peaks were overestimated (up to 20% of the recorded wave heights) and the remaining 12% of simulated results were about 20% lower than the recorded values. Altogether, it can be concluded that the results of the forecast system for the Persian Gulf are reliable for practical applications.

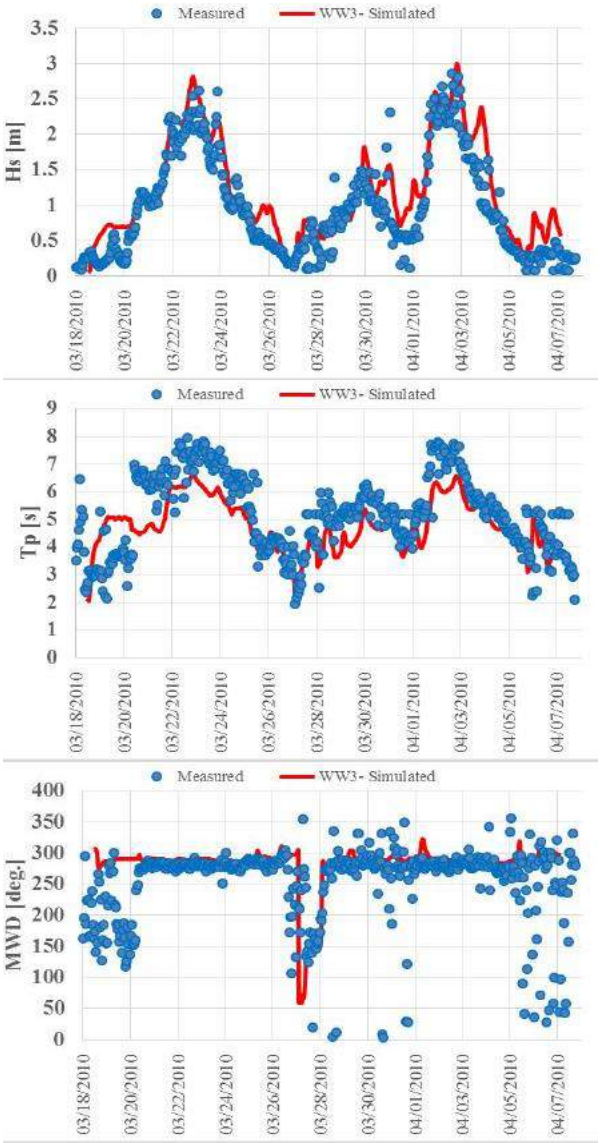

Figure 4. Comparisons between the recorded data of AW6 and WW3 model results

6. References

[1] Ports and Maritime Organization (PMO) (2012): Monitoring and Modelling Projects of Iranian coasts, *Phase II & III reports*. JWERC.

[2] Michalakes, J., J. Dudhia, D. Gill, J. Klemp and W. Skamarock (1998) Design of a next-generation regional weather research and forecast model: Towards Teracomputing, *World Scientific*, River Edge, New Jersey, pp. 117-124.

[3] Amante, & Eakins. (2009). ETOPO1 1 Arc-Minute Global Relief Model: Procedures, Data Sources and Analysis. *NOAA Technical Memorandum* NESDIS NGDC 24. National Geophysical Data Center, NOAA. doi:10.7289/V5C8276M

[4] Tolman, H. (1991). A third-generation model for wind waves on slowly varying, unsteady and inhomogeneous depths and currents. *J. Phys. Oceanogr*, 21, 782–797.

FVM MODELING OF STRATIFIEDFLOWS USING A NON-LINEAR K-ε TURBULENCE CLOSURE

HamidReza Shirkavand[1] and Kourosh Hejazi[2]

1) Civil Eng. Dept., K. N. Toosi University of Technology, Tehran, Iran, hshirkavand@mail.kntu.ac.ir
2) Civil Eng. Dept., K. N. Toosi University of Technology, Tehran, Iran, hejazik@kntu.ac.ir

1. Introduction

Buoyancy forces caused by stratification have substantial impacts on propagation of currents, turbulent mixing processes, production and dissipation of turbulence eddies. They also play a major role in the transportation of sediments and contaminants in these flows. In stratified flows, due to the presence of buoyancy forces, the stresses caused by turbulence are anisotropic and the implementation of this anisotropy may have a significant impact on the predicted results. The accuracy of the numerical simulation of such flows is highly dependent on the turbulence model and the treatment of the buoyancy forces in the model. Despite the intensive research efforts to develop more complete turbulence models, *k-ε* models, still remain the most widely used approach by engineers and scientists for the solution of practical problems. The main advantage of a *k-ε* turbulence model is its reasonable computational time in comparison with the more complicated models, while reserving satisfactory results. The linear *k-ε* turbulence model is usually incapable of accurate prediction of turbulent flows, where the non-isotropy is considerable. The hydrodynamic model WISE (Width Integrated Stratified Environments) used herein is a 2DV numerical model developed by Hejazi (2013). WISE is a free surface numerical model based on the time-dependent Reynolds averaged Navier-Stokes equations. For the development of the non-linear k-ε turbulence model, the model proposed by Speziale [3], and for the Reynolds scalar fluxes, the flux equations suggested have been implemented [4]. The new model has been simulated for several lock-release type tests, and saline water jets discharging into an ambient flow, for which the laboratory experimental values are reported in the literature. Simulated velocity and concentration profiles have been compared with the measured values, as well as two- and three-dimensional numerical simulations reported in the literature along with the predictions of the linear *k-ε* turbulence model.

2. Governing Equations

The model developed herein is an extension to WISE 2DV numerical model [1]. WISE uses a structured non-orthogonal curvilinear staggered mesh based on ALE description. The discretization of the flow and transport equations has been based on finite volume method. For modeling the turbulence, the two-equation *k-ε* turbulence model with buoyancy terms has been deployed in the original numerical model. The model is also capable of simulating non-homogeneous (i.e., variable density) stratified flow fields. The conservative equations of mass and momentum and the transport equation of species concentration are as follows:

$$\frac{\partial u_i}{\partial x_i} = 0. \tag{1}$$

$$\frac{\partial U_i}{\partial t} + U_j \frac{\partial U_i}{\partial x_j} - w_g \frac{\partial U_i}{\partial z} = -\frac{1}{\rho_r}\frac{\partial P}{\partial x_i} + \frac{\partial}{\partial x_j}\left(\nu \frac{\partial U_i}{\partial x_j} - \overline{u_i' u_j'}\right) + g_i \frac{\rho - \rho_r}{\rho_r} \tag{2}$$

$$\frac{\partial \varphi}{\partial t} + U_i \frac{\partial \varphi}{\partial x_i} - w_g \frac{\partial \varphi}{\partial z} = \frac{\partial}{\partial x_i}\left(\lambda \frac{\partial \varphi}{\partial x_i} - \overline{u_i' \varphi'}\right) + s_\varphi \tag{3}$$

where, *x* and *z* are the horizontal and vertical directions in Cartesian coordinate system, respectively, *u* and *w* the horizontal and vertical velocity components respectively, *p* the pressure, ρ_r and ρ the reference density and density of the fluid respectively, *v* the kinematic viscosity, and *g* the gravitational acceleration.

3. Non-linear k-ε turbulence model

Non-linear equations for the Reynolds stresses are as follows, where τ_{ij} represents the Reynolds stresses [3].

$$\tau_{ij} = -\rho \overline{u_i' u_j'} = -\frac{2}{3} k \delta_{ij} - 2C_\mu \frac{k^2}{\varepsilon} \bar{S}_{ij} \tag{9}$$

$$- 4C_D C_\mu^2 \frac{k^3}{\varepsilon^2}\left(\bar{S}_{ik}\bar{S}_{kj} - \frac{1}{3}\bar{S}_{mn}\bar{S}_{mn}\delta_{ij}\right) - 4C_E C_\mu^2 \frac{k^3}{\varepsilon^2}\left(\bar{S}'_{ij} - \frac{1}{3}\bar{S}'_{mn}\delta_{ij}\right)$$

$$- \overline{u_i c} = \beta_1 \frac{\partial c}{\partial x_i} + \beta_2 \frac{k^3}{\varepsilon^2}\left(\frac{\partial u_i}{\partial x_k} - \frac{\partial u_k}{\partial x_i}\right)\frac{\partial c}{\partial x_k} \tag{10}$$

3. Numerical simulations

The first test is the simulation of a lock-release flow which was conducted by zhu et al [5].The experiments were carried out in a rectangular Perspex channel of 200 mm width, 400 mm depth and 2590 mm length. The flume was filled with fresh water to a depth of 100 mm and a Perspex gate were positioned vertically at a distance 200 mm away from the left end of the channel to form a lock. Densities of ρ_0=1009.5 and ρ_a =999.5 kg/m^3 were used for saline and fresh waters, respectively. The numerical grid size in the *x*-direction was equal to 1cm with 15 layers in *z*-direction and a time step of 0.01 s was considered ($t^* = t/t_c$, $t_c = x_0/(g'h_0)^{0.5}$) [5]. The simulated results are presented in figure (1).

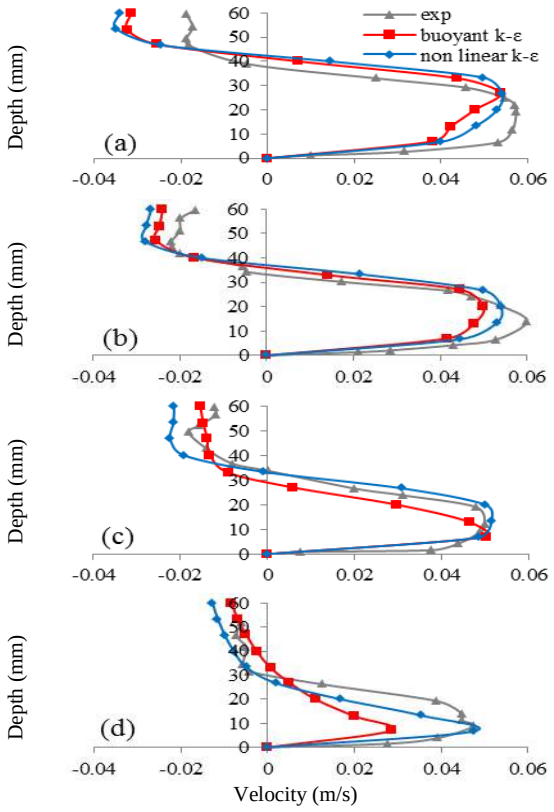

Figure 1. Horizontal velocity profiles at different positions when t* = 12.28 and (a) x = 1020 mm; (b) x = 1040 mm; (c) x = 1060 mm; (d) x = 1080 mm.

The second test presented herein is the lock-release experiments reported by Sutherland et al (2004). The experiments were conducted in a flume with 197.1 cm length, 17.6 cm width and 48.5 cm height. The lock-length (l) behind the gate was fixed at 18.6 cm and the total water depth (H) was set equal to 20 cm. Figure 2 shows Set-up and definition of parameters for intrusion experiments where $h_0=h_1$, ρ_0=1000 , ρ_1=1020 and ρ_d=1010 kg/m^3 . The grid size was set to Δx=0.005 and the number of layers in z direction was equal to 15where a time step of 0.01 sec was considered [6]. The results are illustrated in figure (3).

4. Discussion

Simulated results show good agreements with experimental measured values. While the linear *k-ε* model with buoyancy terms retards compared with the measured values and retardation increases with the evolution of the current, the non-linear model provides better predictions for velocity profiles especially in the far zone from the bed and forehead (front head position). The second test shows that the numerical model predictions describe the dynamics of intrusive gravity current with a symmetrical condition. It is also evident that the numerical model resolves the fine scales associated with the mixing that occurs in the vicinity of the gravity current head. The formation of Kelvin-Helmholtz billows that show the vertical structure behind the head of intrusive gravity current is reproduced well by both closure schemes. After the collapse of the lock, the emergence of the Kelvin-Helmholtz instabilities appears in the interaction between fluid volumes. This instability is clearly seen at all times.

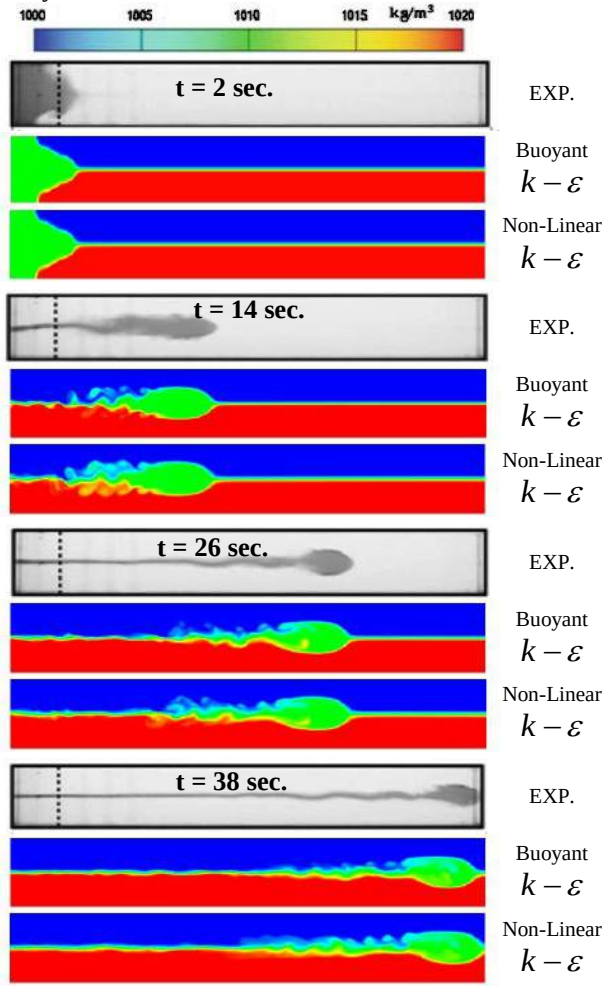

Figure 2 . Temporal evolutions of an intrusive gravity current for experimental results of Sutherland et al (2004).

5. References

[1] Hejazi, K., Soltanpour M. and Sami, S. (2014), "Numerical modeling of wave–mud interaction using projection method," Ocean Dynamics, DOI 10.1007/s10236-013-0637-x.

[2] Rodi, W,H., 1987, Examples of Calculation Methods for Flow and Mixing in Stratified Fluids, Journal of Geophysical Research, Vol. 92, No. C5, pp. 5305-5328.

[3] Speziale, C. G., 1987. On nonlinear k-l and k-ε models of turbulence. Journal of Fluid Mechanics, 178: 459-475.

[4] Jones, W, P., Lentini, D., 2007, A Realisable Non-Linear Eddy Viscosity/Diffusivity Model for confined swirling flows, J. Heat Fluid Flow.

[5] Zhu, J. B., Lee, C. B., Chen, G. Q., and Lee, J. H. W. (2006), " PIV observation of instantaneous velocity structure of lock release gravity currents in the slumping phase," Communications in Nonlinear Science and Numerical Simulations, 11, 262-270.

[6] Sutherland, B.R., Kyba, P.J. and Flynn, M.R. (2004), "Intrusive gravity currents in two-layer fluids," Journal of Fluid Mechanics, 514, 327-353.

2D HYDRODYNAMIC MODELING AND DEVELOPMENT OF CO-TIDAL/CO-RANGE CHARTS OF THE PERSIAN GULF

S. Mahya Hoseini[1], Mohsen Soltanpour[2] and Zahra Ranji[3]

1) K.N. Toosi University of Technology, Tehran, IRAN, sm.hoseini@mail.kntu.ac.ir
2) K.N. Toosi University of Technology, Tehran, IRAN, soltanpour@kntu.ac.ir
3) K.N. Toosi University of Technology, Tehran, IRAN, zranji@mail.kntu.ac.ir

1. Introduction

Tidal waves propagation are mainly controlled by the Coriolis, reflection, shoaling and friction effects, which the last two factors are restricted to shallow water basins. On the other hand, the boundaries of basin geometry and the Coriolis effect result to the development of amphidromic systems with zero tidal range at amphidromic points. These can be depicted by co-tidal lines, which link all the points with the same tidal phase, and co-range lines which connect points having the same tidal range [1].

Literature shows few derived co-tidal and co-range maps for the Persian Gulf. One series of the well-known maps, based on direct observations over the sea and shallow waters, has been provided by the United Kingdom hydrographic office (Admiralty) [2]. These charts are not the outputs of the propagation of the tidal waves and they have been developed by applying the well-established mathematical relations between stream and surface-gradient [3]. Applying the water level data of Admiralty at the open boundary of Hormuz Strait, Sabbagh-Yazdi et al (2007) used NASIR model to extract the co-tidal charts of the Persian Gulf [4]. Pous et al (2012) also applied a 2D shallow water model over the northwestern Indian Ocean, forced by 7 tidal components at the southern boundary, to derive the co-tidal and co-range maps of harmonic constituents [5]. Using a state of art hydrodynamic model with a detailed bathymetry and shoreline, the present study offers the tidal regime and co-tidal/co-range maps of the Persian Gulf.

2. Numerical Modeling and Field Measurement

Based on the depth averaged equations of shallow water, the numerical model has been developed using Flow Model (FM) module of MIKE 21 [6]. The fine unstructured mesh comprises 31239 elements and 16664 nodes (Figure 1) with coastline data extracted from ICZM database, ESRI information database, and aerial photos of Landsat. Bathymetric data was developed by combining the maps of National Cartographic Center (NCC) of Iran and ETOPO two-minute gridded dataset. The location of open boundary was selected at a straight line connecting Jask in Iran and Almasnaeh in Oman [7]. The water level at open boundary was adopted from TPXO global tide model [8]. Model verification was performed by comparing the simulated tidal elevations and measured water levels at ten stations along the Iranian coastline (Figure 2).

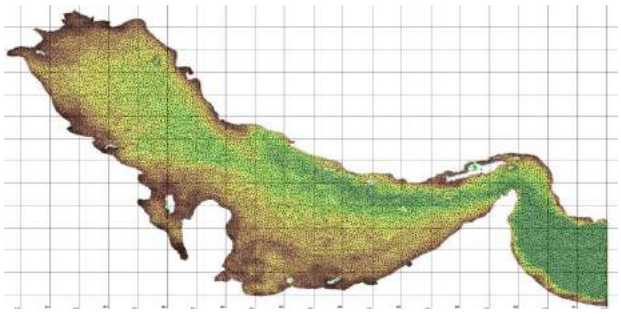

Figure 1. Computational grid.

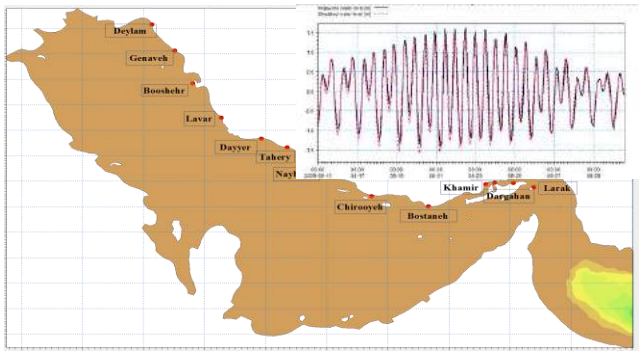

Figure 2. Field measurement stations and comparison between measured and simulated water levels at Larak.

3. Harmonic Analysis

Harmonic analysis is one of the widely used approaches for tidal analysis and prediction, wherein the energy at specific tidal frequencies is determined by a mathematical fitting procedure, usually least squares. Foreman et al (2007) assumed a one-dimensional time series with tidal and non-tidal energies can be expressed as:

$$h(t_j) = z_0 + at_j + \sum_{k=1}^{n} f_k(t_j) A_K \cos[V_K(t_j) + u_k(t_j) - g_k] + R(t_j) \quad (1)$$

where $h(t_j)$ is the measurement at time t_j, z_0 is a constant background value; $f_k(t_0)$ and $u_k(t_0)$ are the nodal corrections to amplitude and phase, respectively, at some reference time t_0 for major constituent k with frequency ω_k; A_k and g_k $(k=1, n)$ are the amplitude and phase lag of constituent k, respectively; $v_k(t_0)$ is the astronomical argument for constituent k at time t_0; $R(t_j)$ is the nodal residual; and n is the number of tidal constituents. A least squares approach is usually employed to solve for z_0, A_k and g_k. The amplitude and phase of constituents are derived here from one year simulated water level using Foreman code (F77) based on IOS method [9]. A MATLAB interface was also written to assist deriving the results.

4. Results and Discussion

Tides in the Persian Gulf are mostly very complex and the dominant pattern varies from primarily semi-diurnal to diurnal [10]. The results of major semi-diurnal and diurnal tidal constituents, M_2, S_2, K_1 and O_1 are discussed in this section. Figure 3 presents the modeling results of co-tidal and co-range maps of M_2 and K_1 constituents where Kriging method is applied for interpolation of 1097 simulation output points in the Persian Gulf using ArcMap 10.3 [11].

Assuming an average depth of 35 m for the Persian Gulf, the wavelength of diurnal and semi-diurnal constituents can be approximated of about 1700 m and 880 m, respectively. Therefore, it is expected that the standing waves generate two nodes for semi-diurnal constituents and one node for diurnal constituents in the approximately 805 km long basin of the Persian Gulf, which is in accordance with the number of simulated amphidromic points in Figure 3.

Figure 4 shows the changes of tide form number over the Persian Gulf. As illustrated, the type of tides is mixed ($0.25<F<1.5$) in most parts of the Persian Gulf. However, the tides show semi-diurnal characteristics near two semi-diurnal amphidromic points ($F<0.25$) and present diurnal behavior approaching diurnal amphidromic point ($F>1.5$), respectively.

References

[1] Wright, J., Colling, A., Park, D., Open University Course Team, "*Waves, Tides and Shallow-Water Processes*", 2005.

[2] United Kingdom Hydrographic Office, "*Admiralty Co-Tidal Atlas-Persian Gulf (NP 214)*", 2nd edition, 1999.

[3] United Kingdom Hydrographic Office, "*The Admiralty Manual of Tides (NP120)*", 1941.

[4] Sabbagh-Yazdi S. R., et al, "Solution of Depth-averaged Tidal Currents in Persian Gulf on Unstructured Overlapping Finite Volumes", *International Journal for Numerical Methods in Fluids*, 21, February 2007, pp. 81-101.

[5] Pous S., et al, "A Process Study of The Tidal Circulation in The Persian Gulf", *Open Journal of Marine Science*, 18, June 2012, pp. 131-140.

[6] DHI Water & Environment., User Guide and Scientific Documentation of Flow Model, *Danish Hydraulic Institute*, 2012, pp. 3-4

[7] K. N. Toosi University of Technology, Development of a forecast system for the Persian Gulf, Study Report of 2D Modeling Persian Gulf Using PMO Dynamics, Iran, Tehran, 2015.

[8] Egbert, G. D., Erofeva, S. Y., "Efficient Inverse Modeling of Baratropic Ocean", *Journal of Atmospheric and Oceanic Technology*, 19, February 2002, pp. 183-204.

[9] Foreman, M. G. G., et al, "Versatile Harmonic Tidal Analysis: Improvements and Applications", *Journal of Atmospheric and Oceanic Technology*, 26, 21, August 2008, pp. 801-817

[10] Reynolds, R. M., "Physical Oceanography of the Gulf, Strait of Hormoz, and the Gulf of Oman-Results from the Mt Mitchell expedition", *Marine Pollution Bulletin*, 27, 1993, pp. 35-59.

[11] "Oliver, M. A. ",Kriging: A Method of Interpolation for Geographical Information Systems" , *International Journal of Geographic Systems*, 4, 1990, pp. 313-332.

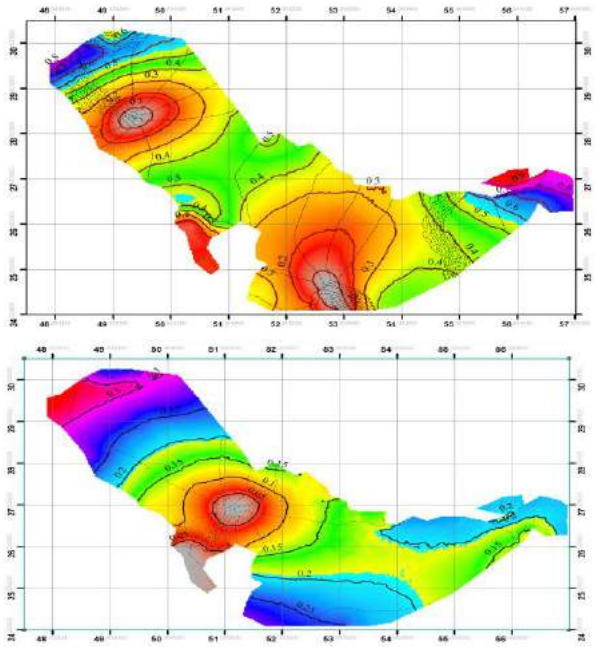

Figure 3. Co-tidal and co-range map for M_2 (top) and K_1 (bottom), dash-line indicates co-tidal contours and solid-line indicates co-range contours

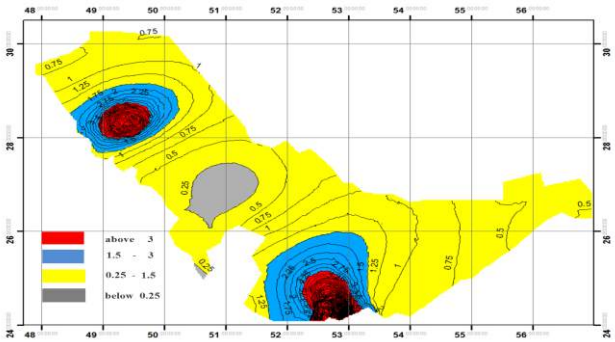

Figure 4. Changes of Tide form number in the Persian Gulf.

NUMERICAL SIMULATION OF WAVE INDUCED FLOW IN THE VICNINITY OF SUBMERGED BREAKWATERS USING DELFT3D

S. Mojabi, H.Oumeraci

Leichtweiß-Institute for Hydraulic Engineering and Water Resources
, TU-Braunschweig, Braunschweig, Germany, s.mojabi@tu-bs.de

1. Introduction

The main objective of the present study is to evaluate the capabilities of DELFT3D to simulate the wave induced flow in the lee of submerged breakwaters (Hereafter SBW). This is especially important, as the application of DELFT3D to reproduce wave induced flow field leeward of SBW has not yet been validated quantitatively. For this purpose, the laboratory study performed by Haller et al (2000) on the near-shore flow pattern in the lee of fixed submerged bars has been selected for simulation using DELFT3D. The experimental configuration consisted of one full SBW and two partial SBWs to reproduce a multiple SBW system in the basin. Among all tests performed in this experimental study, ***test B*** has been selected, as it contains the most extensive flow measurements.

2. Description of the Laboratory Study

The laboratory tests were performed in the wave basin located in the Ocean Engineering Laboratory in the University of Delaware. The internal dimensions of the wave basin are approximately 17 m in length and 18.2 m in width. The plan view and cross section of the basin are respectively shown in Figs 1a and 1b. Fig. 1a also shows the coordinates, in which the origin is located in the left upper corner of the basin where the wave maker meets the side walls . The beach consists of a steep (1 : 5) toe located between 1.5 m and 3 m from the wave maker followed by a milder (1 : 30) sloping section extended to the wall of the basin opposite to the wave maker. Three submerged barriers were made from sheets of high-density polyethylene (HDP). The wave conditions are given by Table 1 in which H_{bar} denotes wave height measured at the offshore edge of the central bar, H_0 deep water wave height, T wave period, Θ angle of incidence measured in counter clockwise direction, h_c average water depth at the bar crest and X_{swl} cross-shore location of the still water line.

Table 1. Experimental Condition in Test B

H_{bar} (cm)	H_0 (cm)	T (s)	Θ (degree)	h_c (cm)	X_{swl} (cm)
4.41	5.12	1	0	4.73	1490

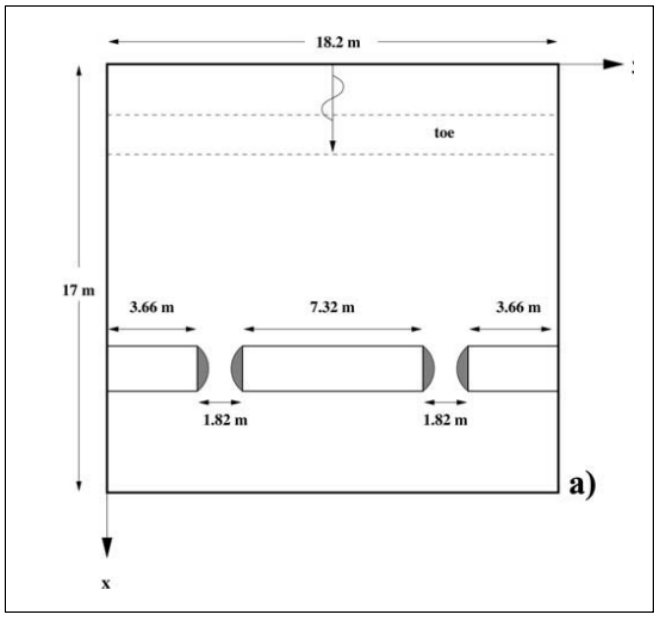

Figure 1. a) Plan view and (b) cross section of the Wave basin-SBW configuration (From Hallet et al , 2000)

Ten wave gauges were used to measure the wave height all over the basin. Three two-dimensional acoustic Doppler velocimeters (ADVs) were used to record horizontal currents. In general, the ADV measurements were installed 3 cm from the bottom. For further information on the details of laboratory tests the reader should reffer to Haller et al(2000).

3. Numerical Simulation

In order to reproduce the measured waves and wave induced flow fields in the vicinity of the submerged breakwater, DELFT3D has been employed in the depth-averaged (2DH) mode. In 2DH mode, DELFT3D modelling system uses SWAN as the wave generation module which works simultaneously with the flow module to simulate the wave driven flow field. In order to quantify the accuracy of the modelled waves and flow field, the index of agreement proposed by Wilmott (1981) is utilized:

$$d = 1 - \frac{\sum_{j=1}^{n}[y(j)-x(j)]^2}{\sum_{j=1}^{n}[|y(j)-\bar{x}|+|x(j)-\bar{x}|]^2} \qquad (1)$$

where x(j) are the measured data, y(j) are the computed data, and $\bar{x}$ is the mean of x(j). A value of d = 1 indicates perfect agreement, and a value of d = 0 indicates total disagreement.

SWAN is originally developed to simulate random irregular waves propagation. However, as suggested by Holthuijsen (2003), the incident monochromatic waves, such as incident waves in the laboratory tests considered in this study, could be approximated by the delta spectrum. The delta spectrum is the wave spectrum with one frequency and a very narrow Gaussian directional distribution around the mean direction (Holthuijsen, 2003). The model grid spacing is selected to be dx = 10 cm and dy = 10 cm, and the time step is dt = 0.01 s corresponding to a maximum courant number of 0.3. It was found that further mesh refinement does not significantly affect the numerical simulation results. Some comparisons between the numerical simulation results and the measurements are shown by Fig. 3.

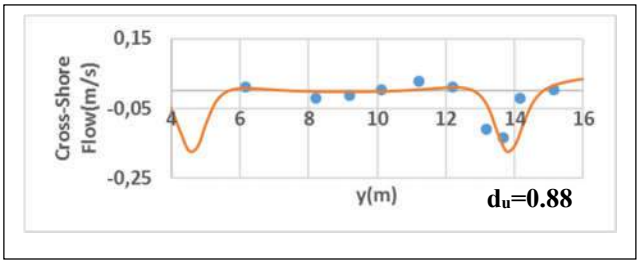

Figure 3. a) Comparison between measured and simulated cross-shore flow velocity at x=12.2m

As can be seen in Fig 3a,b, generally there is a relatively good agreement between numerical simulation results and measured flow velocities, with an index of agreement du=0.88 for cross-shore flow velocity *u* and dv=0.89 for longshore flow velocity *v*.

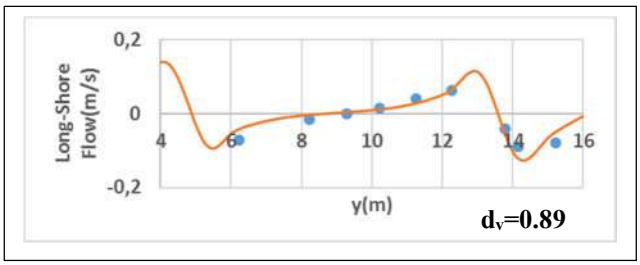

Figure 3. b) Comparison between measured and simulated Long-shore flow velocity at x=12.2m

4. Concluding Remarks

The present study is carried out to evaluate the capability of DELFT3D to reproduce the wave-induced flow in the lee of submerged breakwaters. Accordingly, the laboratory study carried by Haller et al (2000) to investigate the flow field leeward of the fixed submerged bars is selected for simulation using DELFT3D. on the near-shore flow pattern in the lee of fixed submerged bars. The relatively good agreement between numerical simulation results and laboratory measurements confirms the applicability of DELFT3D for the numerical simulation of the wave induced flow field leeward of submerged barriers (e.g. submerged breakwaters)

Acknowledgements

This research is a part of the PhD study of the first author which is supported by the DAAD in the frame of the Exceed-Swindon Project at Technische Universität Braunschweig. This support is gratefully aknowledged.

5. References

[1] Haller, Merrick C., Robert A. Dalrymple, and Ib A. Svendsen. *Experiments on rip currents and nearshore circulation: Data report*. University of Delaware, Ocean Engineering Laboratory, Center for Applied Coastal Research, 2000.

[2] Willmott, Cort J. "On the validation of models." *Physical geography* 2, no. 2 (1981): 184-194.

[3] Holthuijsen, L. H., A. Herman, and N. Booij. "Phase-decoupled refraction–diffraction for spectral wave models." *Coastal Engineering* 49, no. 4 (2003): 291-305.

NUMERICAL MODELING OF INTERNAL SOLITARY WAVES PROPAGATION IN A TWO LAYER SYSTEM

Mohammad Reza Dorri[1] and Kourosh Hejazi[2]

1) Dept. of Civil Engineering, K. N. Toosi University of Technology, Tehran, Iran, Dori1364@mail.kntu.ac.ir
2) Dept. of Civil Engineering, K. N. Toosi University of Technology, Tehran, Iran, HejaziK@kntu.ac.ir

1. Introduction

Internal waves play an important role in driving mixing in oceans and lakes. The balance between nonlinearity and dispersion causes propagation of internal solitary waves. These waves have been studied by means of experimental observations and Korteweg-de Vries equation [1]. Nonlinear internal waves have also been investigated experimentally by Horn et al [2]. To this end, several numerical models have been developed [3, 4]. In this paper an integrated VOF-ALE numerical model has been developed, such that the VOF (Volume of Fluid) method has been implemented in WISE (Width Integrated Stratified Environments) 2DV ALE (Arbitrary Lagranigan-Eulerian) non-hydrostatic model [5] for simulation of interfacial waves.

2. Governing Equations

The conservative form of 2DV RANS equations is as follows:

$$\frac{\partial u}{\partial x}+\frac{\partial w}{\partial z}=0 \tag{1}$$

$$\frac{\partial u}{\partial t}+\frac{\partial u^{2}}{\partial x}+\frac{\partial uw}{\partial z}-w_{g}\frac{\partial u}{\partial z}= -\frac{\partial P^{*}}{\partial x}+\frac{\partial}{\partial x}\left(\nu_{T}\frac{\partial u}{\partial x}\right)+\frac{\partial}{\partial z}\left(\nu_{T}\frac{\partial u}{\partial z}\right) \tag{2}$$

$$\frac{\partial w}{\partial t}+\frac{\partial uw}{\partial x}+\frac{\partial w^{2}}{\partial z}-w_{g}\frac{\partial w}{\partial z}= -\frac{\partial P^{*}}{\partial z}+\frac{\partial}{\partial x}\left(\nu_{T}\frac{\partial u}{\partial x}\right)+\frac{\partial}{\partial z}\left(\nu_{T}\frac{\partial u}{\partial z}\right)-\frac{\rho-\rho_{0}}{\rho_{0}}g \tag{3}$$

where t is time, x and z are coordinates in horizontal and vertical directions respectively, u and w are horizontal and vertical velocity components respectively, P^* is the pressure with the exclusion of the hydrostatic pressure divided by the reference density of water, ρ is water density and ρ_0 is the reference density, g is the acceleration of gravity, w_g presents the mesh velocity and v_t is the eddy viscosity coefficient. In the hydrodynamic model, the two-equation k-ε turbulence model with buoyancy terms has been included.

3. Numerical Method

Spatial discretization of the governing equations was based on finite volume method. For the temporal procedure a fractional step method has been deployed. The free surface is represented by a volume function known as the color function. This function, C, is considered to determine cell volumes which are occupied by the fluid. This method was devised to solve the advection contribution (Eq. 4) of the Navier-Stokes equations.

$$\frac{\partial C}{\partial t}+\nabla.(UC)=0 \tag{4}$$

The fluid density in each cell can be obtained from Eq. (5) as follows:

$$\rho=C\rho_{1}+(1-C)\rho_{2} \tag{5}$$

The concept of Youngs method [6] was utilized for volume function advection in the newly developed model.

4. Numerical Simulations and Results

Numerical simulation results have been compared with experimental measured values of Horn et al. [2]. The experimental tests were conducted in an acrylic tank with length of L=6 m, depth of H=0.29 m and width of W=30 cm. The upper fresh water layer was added after the lower saline layer was filled in the tank. An initial tilt of interface was made with rotation of tank about horizontal axis. Figure 1 shows schematic illustration of the tank and ultrasonic wave gauges. Figure 2 compares time series of interface displacement in the center of the tank for numerical predictions and experimental measurements, which show good agreements. Also figure (3) demonstrates the comparison of the simulated internal solitary wave propagation with the experimental measurements of Horn et al. [2]. The internal solitary waves originate from cascade of energy into shorter waves. In these interfacial waves viscosity, nonlinearity and dispersivity effects play an important role. The superior results of present model have verified capability of integrated ALE-VOF model for prediction of non-hydrostatic nonlinear interfacial waves.

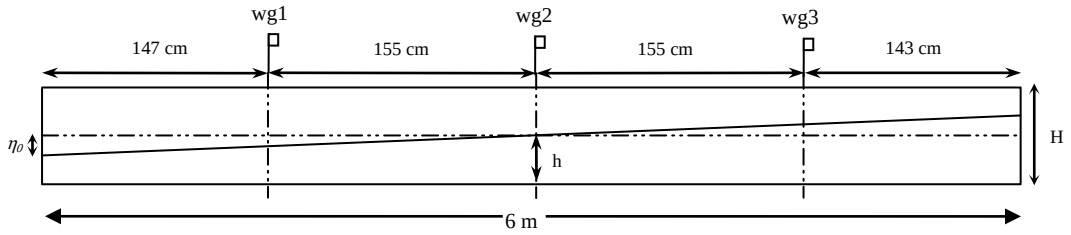

Figure 1. Schematic illustration of the experimental setup and locations of ultrasonic wave gages [2]

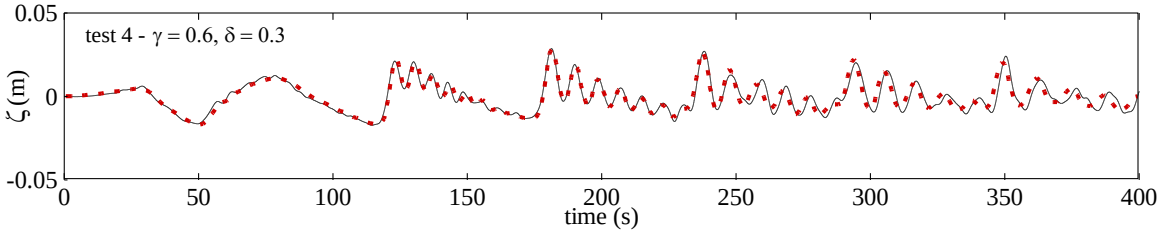

Figure 2. Comparison of surface elevation time series of experimental measurements (solid circle) and present model results (solid line)

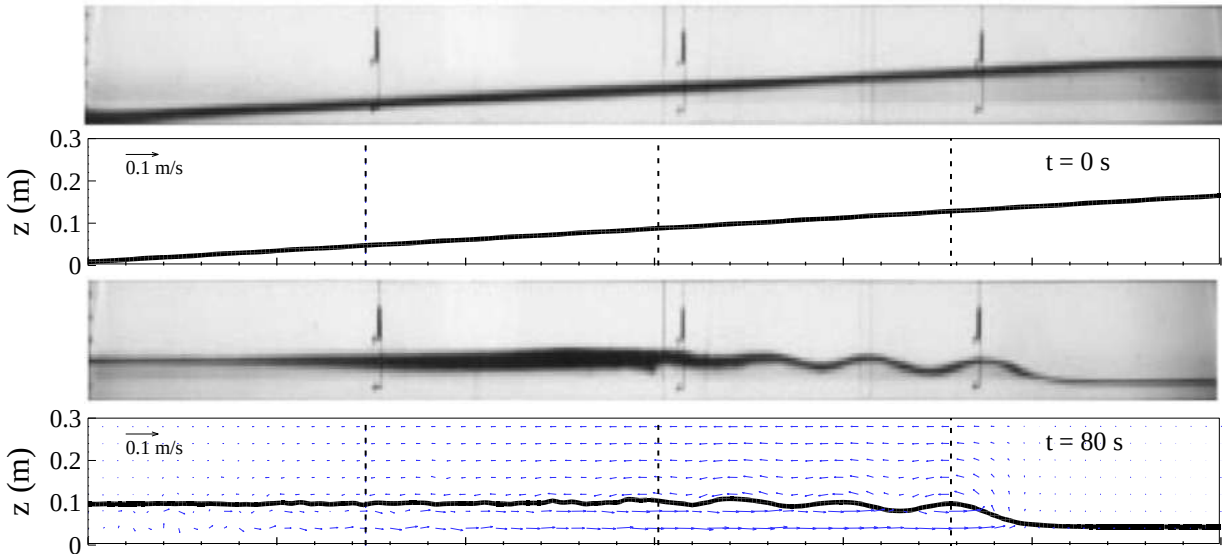

Figure 3. Comparison of internal solitary wave propagation for experimental measurements of Horn et al. [2] and predictions of the present numerical model

5. References

[1] Koop, C. G., & Butler, G. (1981). An investigation of internal solitary waves in a two-fluid system.*Journal of Fluid Mechanics*, *112*, 225-251.

[2] Horn, D. A., Imberger, J., & Ivey, G. N. (2001). The degeneration of large-scale interfacial gravity waves in lakes. *Journal of Fluid Mechanics*, *434*, 181-207.

[3] Kanarska, Y., Shchepetkin, A., & McWilliams, J. C. (2007). Algorithm for non-hydrostatic dynamics in the regional oceanic modeling system. *Ocean Modelling*, *18*(3), 143-174.

[4] Vitousek, S., & Fringer, O. B. (2014). A nonhydrostatic, isopycnal-coordinate ocean model for internal waves. *Ocean Modelling*, *83*, 118-144.

[5] Hejazi, K., Soltanpour, M., & Sami, S. (2013). Numerical modeling of wave–mud interaction using projection method. *Ocean Dynamics*, *63*(9-10), 1093-1111.

[6] Rudman, M. (1997). Volume-tracking methods for interfacial flow calculations. *International journal for numerical methods in fluids*, *24*(7), 671-691.

A GP-BASED APPROACH FOR IMPROVING WIND-WAVE SIMULATIONS OVER THE PERSIAN GULF

S. Abbas Haghshenas[1], Azadeh Razavi Arab[2], Ali Haghighi[3], and Sarmad Ghader[4]

1) Institute of Geophysics, University of Tehran, Tehran, Iran, Email: sahaghshenas@ut.ac.ir
2) Institute of Geophysics, University of Tehran, Tehran, Iran, Email: azadeh_razavi_1981@yahoo.com
3) Shahid Chamran University of Ahvaz, Iran, Email: a.haghighi@scu.ac.ir
4) Institute of Geophysics, University of Tehran, Tehran, Iran, Email: sghader@ut.ac.ir

1. Introduction

Reliable coastal structure design, sediment transport predictions and future planning all depend on the use of accurate long-term wave data. Wave measurements are not usually available everywhere and on a long-term basis; hence, numerical simulations are to be adopted to obtain such data in locations of interest. It is while the most important role in obtaining reliable simulated wave data is played by well-established and reliable simulated wind field data sets over the study area. Numerical weather prediction models can be used as a tool to estimate marine surface winds and for providing input parameters to the sea surface wave and ocean circulation numerical models (e.g., Chen et al., 2005; Schulz, et al., 2007, Sousa, et al., 2013; Liu, et al., 2011). In addition, the model results which are to be verified with observational data usually show remarkable bias from the real situation which can be attributed to the very dynamic and unstable nature of the atmospheric phenomena affecting simulation results.

The present study aims to reproduce measured wind data from an offshore wave buoy in the central Persian Gulf. The simulated wind data are modified through a Genetic Programing (GP) framework to obtain an optimum correlation factor between the simulated results and observations. This data is used to provide input parameters to the sea surface wave model. The native and modified wind data sets are introduced to the 3rd generation WaveWatch III wave model to simulate the time series of wave characteristics at the buoy location. The output wave data are compared with the observations to evaluate the efficiency of GP-based method for improving wind/wave simulations over the Persian Gulf.

2. Wind-Wave Simulations

In order to provide a reliable assessment of the wave condition simulations for the study area, a one month time series of wind and wave measurements at Assaluyeh Buoy was collected for which wind and wave simulations are performed. The wave buoy, owned by Iranian Ports and Maritime Organization, is located near Naiband Bay and adjacent to one the areas with highest waves in the Persian Gulf. Five major storms with wave heights in the order of 2m and higher are captured during this period. The wind field is reproduced using a meso-scale numerical weather prediction model, namely, Weather Research and Forecast (WRF) model. A Genetic Programing (GP) based strategy is applied to modify simulated wind speeds to improve the correlation factor between simulations and observation data. This scheme improved the correlation factor between simulated and measured data for about 15%. Figure 1 shows the comparison between modified simulated wind speed data and observations.

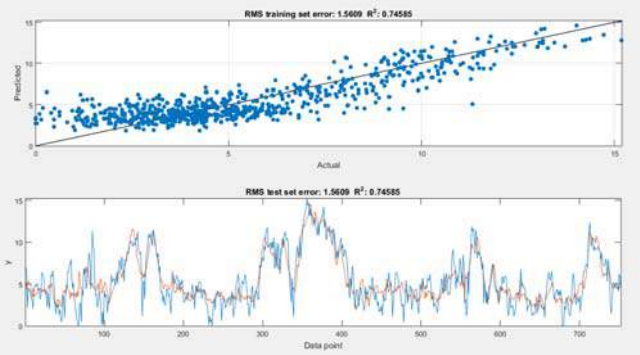

Figure 1. GP-Based modified wind speed data in comparison with measured wind data

Both sets of the wind data are introduced to the wave generation model to hindcast wave characteristics for the whole period of available wave data at Assaluyeh Buoy.

The third-generation spectral wave model WaveWatch III was employed in the present study to simulate wave generation and propagation over the physical model domain. Model runs were carried out for a one month period including the observational studies. The WW3 computations are presented and compared with the observed wave parameters recorded at the study site for original wind simulation results and GP-Based modified results in Figures 2 and 3, respectively. As it is observed, the modified input wind data has improved the accuracy of simulated wave data at the buoy location, especially for capturing extreme storm events. The correlation coefficient is increased from 69% to 85% with the modification applied to the model results.

3. Summary

A combination of WRF and WW3 modeling activities are adopted to simulate and regenerate a one-month wind and wave data set in the Persian Gulf. Model setup for WRF model is selected by using more than 25 major storm events happened in the Persian Gulf since 1998. Regenerated wind field for a one-month period in November and December 2015 was modified through a GP-Based framework and then introduced to WW3 wave model and wave parameters were hindcasted at Assaluyeh Buoy over Iranian Coastline of the Persian Gulf. It is concluded that the GP-Based approach is an effective method to improve wind-wave simulations in the study area.

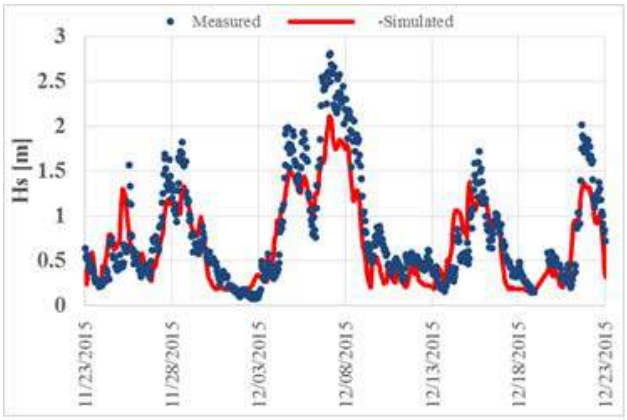

Figure 2. Simulated wave data using the unmodified wind speed data at Assaluyeh Buoy Location

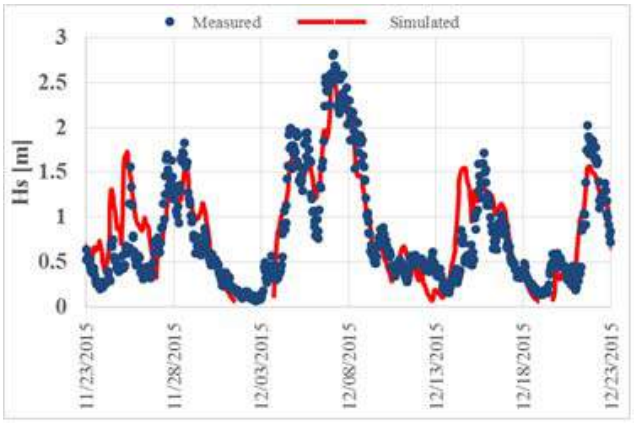

Figure 3. Simulated wave data using the GP-Based modified wind speed data at Assaluyeh Buoy Location

4. References

Chen, C., Beardsley, R. C., Hu, S., Xu, Q., Lin, H., 2005. Using MM5 to hindcast the ccean surface forcing fields over the gulf of Maine and Georges bank region, Journal of Atmospheric and Oceanic Technology, 22, 131-145.

Liu, B., Liu, H., Xie, L., Guan, C., Zhao, D., 2011. A coupled atmosphere–wave–ocean modeling system: Simulation of the intensity of an idealized tropical cyclone, Mon. Wea. Rev., 139, 132-152.

Schulz, Eric W., Jeffrey D. Kepert, Diana J. M. Greenslade, 2007., An assessment of marine surface winds from the Australian bureau of meteorology numerical weather prediction systems, Weather and Forecasting, 22,613-636.

Sousa, M. C., I. Alvarez, N. Vaz, M. Gomez-Gesteira, J. M. Dias, 2013. Assessment of wind pattern accuracy from the Quikscat satellite and the WRF model along the Galician coast (northwest Iberian Peninsula), Monthly Weather Review, 141, 742-753.

NUMERICAL MODELING OF NON-NEWTONIAN FLUID MUD FLOW USING FINITE VOLUME METHOD

HamidReza Shirkavand[1] and Kourosh Hejazi[2]

1) Civil Eng. Dept., K. N. Toosi University of Technology, Tehran, Iran, hshirkavand@mail.kntu.ac.ir
2) Civil Eng. Dept., K. N. Toosi University of Technology, Tehran, Iran, hejazik@kntu.ac.ir

1. Introduction

Stratified flows influenced by buoyancy forces are due to the density difference between one fluid and the surrounding fluid. In many coastal areas and estuaries, especially in the areas near large rivers, fine cohesive sediments are present. The stratified flows due to sediments exhibit a non-Newtonian rheological behavior, and numerical simulation of such flows for perception of their behavior, and management of the dense and mud stratified flows is of great importance. In this paper a non-linear *k-ε* turbulence model has been developed and included in the existing hydrodynamic model WISE (Width Integrated Stratified Environments). The implementation of non-isotropy and non-Newtonian rheological behavior is included in the turbulence model. WISE is a 2DV ALE RANS free surface width integrated numerical model and employs a staggered non-orthogonal curvilinear coordinate system (Hejazi et al., 2013). The new model has been verified against the experimental data for several lock-release tests. The numerical predictions of the velocity and density profiles show good agreements with the measured values.

2. Governing Equations

The model developed herein is an extension to an existing 2DV numerical model [1], which uses a structured non-orthogonal curvilinear staggered mesh based on ALE description. The discretization of the flow and transport equations has been based on finite volume method, providing flexibility for defining control volumes in a staggered grid system, especially near the bed and water surface, where rapid changes of the bathymetry and free surface may have a significant effect on the prediction of flow field. The model is also capable of simulating non-homogeneous (i.e., variable density) stratified flow fields. The conservative equations of mass and momentum and the transport equation of species concentration are as follows:

$$\frac{\partial u_i}{\partial x_i} = 0. \tag{1}$$

$$\frac{\partial U_i}{\partial t} + U_j \frac{\partial U_i}{\partial x_j} - w_g \frac{\partial U_i}{\partial z} = -\frac{1}{\rho_r}\frac{\partial P}{\partial x_i} + \frac{\partial}{\partial x_j}\left(\nu \frac{\partial U_i}{\partial x_j} - \overline{u_i' u_j'}\right) + g_i \frac{\rho - \rho_r}{\rho_r} \tag{2}$$

$$\frac{\partial \varphi}{\partial t} + U_i \frac{\partial \varphi}{\partial x_i} - w_g \frac{\partial \varphi}{\partial z} = \frac{\partial}{\partial x_i}\left(\lambda \frac{\partial \varphi}{\partial x_i} - \overline{u_i' \varphi'}\right) + s_\varphi \tag{3}$$

Where, *x* and *z* are the horizontal and vertical directions in Cartesian coordinate system respectively, *u* and *w* are the horizontal and vertical velocity components respectively, *p* is the pressure, ρ_r and ρ are the reference density and density of the fluid respectively, *v* is the kinematic viscosity, and *g* is the gravitational acceleration.

2.1. Non-Newtonian rheological behavior

In the following flow equations (Eqs. 4-5), and for the Newtonian fluids, the α coefficients are equal and constant. But these coefficients are not constant in non-Newtonian fluids and are determined based on fluid momentum [2].

$$\frac{\partial u}{\partial t} + \frac{\partial u^2}{\partial x} + \frac{\partial uw}{\partial z} - w_g \frac{\partial u}{\partial z} = -\frac{1}{\rho_r}\frac{\partial P}{\partial z} + \frac{\partial}{\partial x}\left(2\alpha \frac{\partial u}{\partial x}\right) + \frac{\partial}{\partial z}\left(\alpha \frac{\partial u}{\partial z} + \alpha \frac{\partial w}{\partial x}\right) \tag{4}$$

$$\frac{\partial w}{\partial t} + \frac{\partial uw}{\partial x} + \frac{\partial w^2}{\partial z} - w_g \frac{\partial w}{\partial z} = -\frac{1}{\rho_r}\frac{\partial P}{\partial z} + \frac{\partial}{\partial x}\left(\alpha \frac{\partial w}{\partial x} + \alpha \frac{\partial u}{\partial z}\right) + \frac{\partial}{\partial z}\left(2\alpha \frac{\partial w}{\partial z}\right) - g\frac{\rho - \rho_r}{\rho_r} \tag{5}$$

In power-law Model α may be obtained by equation (6) in which $|\dot{\gamma}|$ is the second invariant of the rate of the deformation tensor, *D* is the deformation tensor, *m* is the consistency index and *n* is the fluid behavior index, where $n = 1$ presents a Newtonian fluid. For a fluid with $n > 1$, the effective viscosity increases with the shear rate, and the fluid is called the shear-thickening or dilatant fluid. For a fluid with $n < 1$, the effective viscosity decreases with the shear rate, and the fluid is called the shear-thinning or pseudo plastic fluid [3]. For the Bingham Model α is presented by equation (7), where τ_y is the yield stress and μ_B is the Bingham viscosity [4].

$$\alpha = m\left(|\dot{\gamma}|\right)^{n-1} \tag{6}$$

$$\alpha = \mu_B + \tau_y / |\dot{\gamma}| \tag{7}$$

$$|\dot{\gamma}| = \sqrt{2tr(D^2)} = \sqrt{2\left(\frac{\partial u}{\partial x}\right)^2 + \left(\frac{\partial u}{\partial z} + \frac{\partial w}{\partial x}\right)^2 + 2\left(\frac{\partial w}{\partial z}\right)^2} \tag{8}$$

3. Validation tests and simulation results

The simulation cases are performed to identify the propagation dynamics of intrusive mud flow with Non-Newtonian rheological behavior. The simulations are compared with the experimental measurements of Chowdhury and Testik [5]. The laboratory experiments were carried out in a rectangular Plexiglas lock-exchange

tank (430 cm length, 25 cm width and 50 cm height). A removable vertical gate located at a distance, x_0=24.5cm, from one end of the tank serves as the lock-gate, to avoid exchange of the fluids between the two reservoirs (i.e., water and fluid mud reservoirs), before the commencement of the experiments. The various status for concentrations of fluid mud suspensions which were used, are tabulated in Table (1). Fluid mud suspensions were prepared by vigorously stirring cohesive Kaolinite clay particles (mean particle diameter, $d = 0.7\mu m$ and particle density, $\rho_p = 2.62\, g/cm^3$). The grid size was set to be equal to Δx=0.005 and the number of layers to be n=15, where a time step of 0.04 s was considered [5]. The simulation results are demonstrated in figure (1).

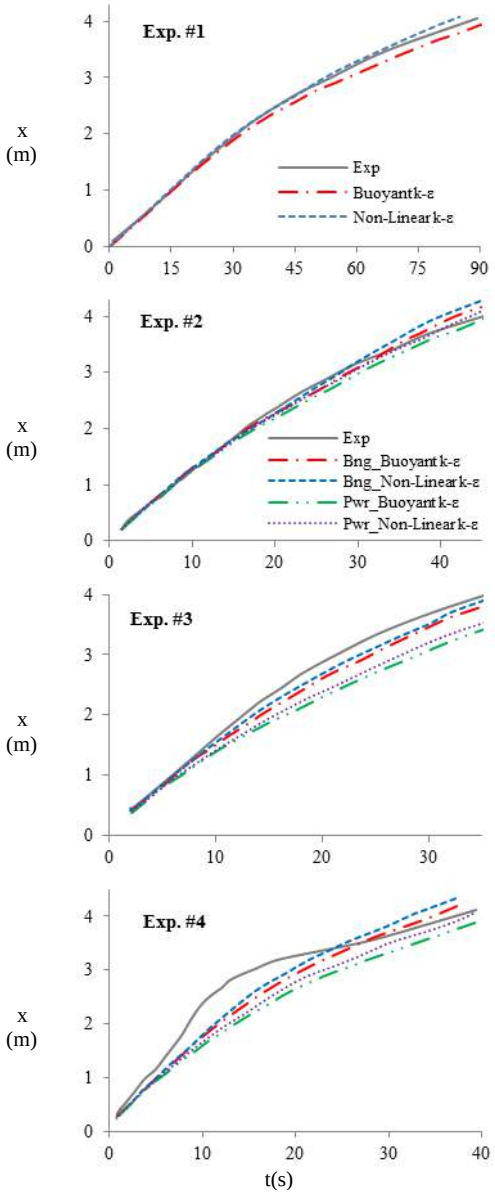

Figure 2 . Comparison of the simulated front position for buoyant k-ε and nonlinear k-ε turbulence model with the experimental data of Chowdhury and Testik (2011).

Table 2. Parameters of experiments of Adduce et al. (2010)

Exp.No.	ρ_c(g/cm^3)	Rheological properties		
		$m(pa\ s^n)$	n	$\tau_y(pa)$
1	1.015	-	-	-
2	1.06	0.067	0.381	0.0421
3	1.09	0.285	0.285	0.131
4	1.14	1.224	0.1989	0.547

4. Results

The simulated results show that the discrepancies grow when the density differences are larger where also the two turbulence closures exhibit larger differences. Non-isotropic Reynolds stress is raised by increase in density difference between two fluids, and as it is expected the nonlinear turbulence model leads to closer agreements than the linear model. As long as the non-Newtonian behavior is limited in scope the fluid fairly acts like a Newtonian fluid, and the difference between the rheological models will be small, however the nonlinear turbulence model displays slightly superior simulations compared to the linear model. On the other hand the growth in the concentration and non-Newtonian behavior causes more disagreements among rheological models. Experimental data show that when the concentration and non-Newtonian behavior of fluid are beyond a certain limit, it takes less time for fluid to enter the viscous phase and the numerical models would fail to predict this phenomenon. Nevertheless, Bingham model gives more preferable results in terms of quantity and the power-law model exhibits superior qualitative results. .

5. References

[1] Hejazi, K., Soltanpour M. and Sami, S. (2013), "Numerical modeling of wave–mud interaction using projection method," Ocean Dynamics, DOI 10.1007/s10236-013-0637-x.

[2] Markovitz, H. (1968), "Film notes for rheological behavior of fluids," Mollen Institute, No.21613.

[3] Beverly, C. and Tanner, R. (1992), "Numerical analysis of three-dimensional Bingham plastic flow," Journal of Non-Newtonian fluid mechanics, 42, 85–115.

[4] Gao, W. and Liu, R. (2009), "A hybrid finite volume/finite element method for incompressible generalized Newtonian fluid flows on unstructured triangular meshes," Acta Mechanica Sinica, 25, 747–760.

[5] Chowdhury, M. and Testik, F. "Laboratory testing of mathematical models for high-concentration fluid mud turbidity currents," Ocean Engineering, 38, 256 – 270, 2011.

A THREE-DIMENSIONAL NON-HYDROSTATIC NUMERICAL MODEL FOR PREDICTION OF OCEAN CURRENTS

Saeideh Sami[1] and Kourosh Hejazi[2]

1) Civil Eng. Dept., K.N. Toosi University of Tech., Tehran, Iran, sami@dena.kntu.ac.ir
2) Civil Eng. Dept., K.N. Toosi University of Tech., Tehran, Iran, hejazik@kntu.ac.ir

1. INTROUDUCTION

Modeling of flow and transport in oceanic water bodies is of great importance for hydraulic and coastal engineering, environmental protection, and disaster planning. A number of numerical models based on the hydrostatic assumption and the depth integrated shallow water equations have been developed. Although these assumptions are usually employed to reduce the complexity and computational burden of full pressure–velocity coupling problems of the 3D free-surface hydrodynamic models, they are no longer valid for flows over abruptly-changing bed topographies, flows with sharp density gradients or current-wave interactions, for which the ratio of the vertical to horizontal scale of motion is not small. In this paper a three-dimensional free surface numerical model is developed to simulate the oceanic and coastal hydrodynamics based on the fully three-dimensional Navier-Stokes equations.

2. THE UNSTRUCTURED GRID DESCRIPTION

To overcome the geometric complexity of the regions of interest of this research project, a triangular unstructured grid system has been utilized for the numerical model developed herein. The σ-coordinate system has been deployed and the governing equations were transformed vertically to obtain an accurate representation of the moving free surface and bottom topographies.

The unsteady Navier-Stokes equations were solved in a 3D mesh which consisted of an unstructured two-dimensional horizontal non-overlapping triangular grid and horizontal layers over the water depth.

The scalar quantities, the pressure values for example, were defined at the vertexes and the containment node-dual finite volumes were employed around a vertex. The horizontal velocities are located at the midpoint of each edge, and the vertical velocities are at the vertices, at the top and bottom of each polygon cell.

3. NUMERICAL SOLUTION

Finite volume method was deployed to discretize the governing equations using a cell-vertex-edge grid, which preserves the local conservation property.

The factional step method with semi-implicit schemes is employed following the algorithm presented by Casulli and Cattani [1]. The method consists of two major steps. During the first step, the momentum equations are solved with the omission of pressure terms. This yields an approximate velocity field, which, in general, is not divergence free. To discretize the horizontal advection and diffusion terms, Perot's scheme [2] was applied, which converts the face-centered calculation of the horizontal advection or diffusion terms to their cell-centered computations. The free-surface equation was solved by substitution of the discrete horizontal momentum equation. This yields a 2D symmetric, diagonally dominated matrix for the intermediate free surface elevation, where the linear system was solved with the preconditioned conjugate gradient algorithm. In the second step, a correction with the non-hydrostatic pressure is applied to the velocity field. Imposing the continuity constraint, yields to the pressure Poisson equation. The matrix of unknown pressures is then solved by the bi-conjugate gradient squared stabilized (BiCGSTAB) algorithm together with the modified incomplete lower upper pre-conditioner (MILU) [3]. The solution of the non-hydrostatic pressure updates the intermediate velocity field and then the water elevation.

4. RESULTS

.

Firstly, to verify the solution of the advection terms, a two-dimensional bell-shape distribution of concentration is applied to 600 x 600 m horizontal and vertical planes for examining the horizontal and vertical advection. The former is subjected to a rotational velocity field and the latter experiences a constant velocity field only in the z direction. The results of these two numerical tests have been presented in **Error! Reference source not found.** and 2 respectively.

Secondly, to demonstrate the validity of the pressure solver, a two-dimensional square plate is subjected to prescribed constant temperature boundary conditions, while at $x = 0$, $T = 1^{o}$ C and on three other edges T is set equal to zero. The solution of the Laplace's equation determines temperature distribution on the plate. In **Error! Reference source not found.** analytical solution is compared with the model predictions.

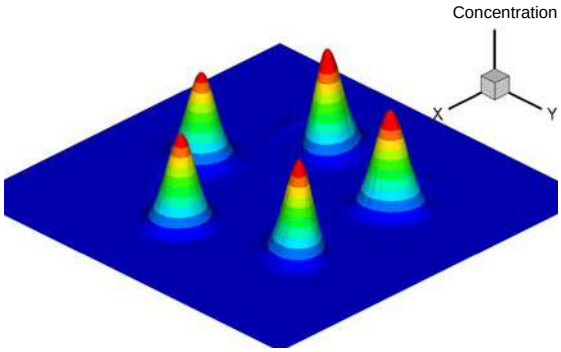

Figure 1. Advection of normal distribution of concentration in horizontal surface.

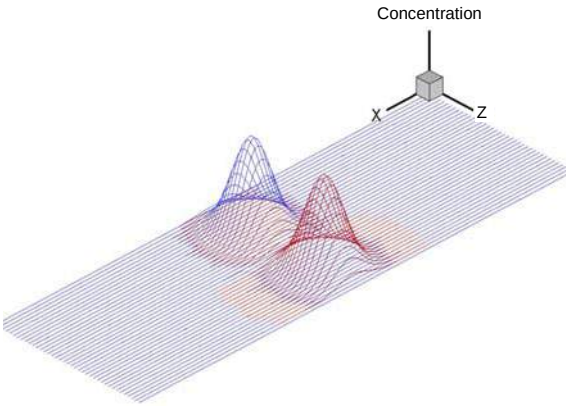

Figure 2. Advection of normal distribution of concentration in vertical surface.

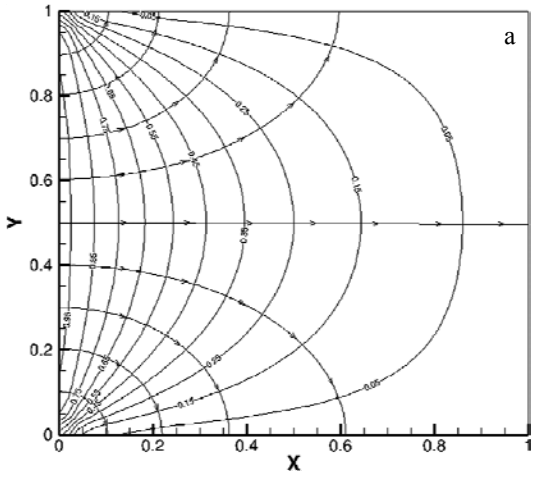

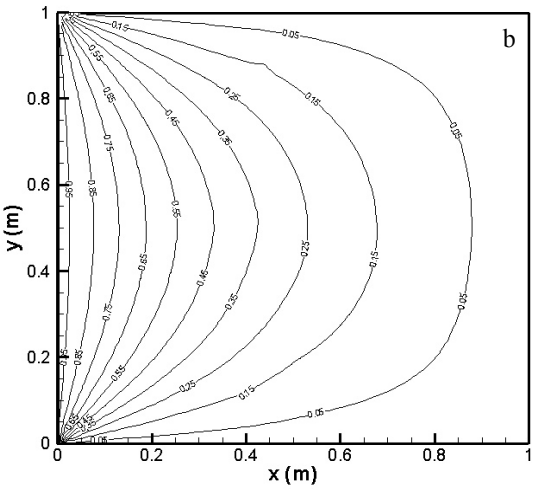

Figure 3. Temperature distribution, a) analytical solution, b) predcited.

5. CONCLUSIONS

The three dimensional, non-hydrostatic, finite volume model has been developed using an unstructured triangular grid based on σ-coordinate description. The numerical tests, show that the model gives satisfactory results in comparison with analytical solutions.

6. REFERENCES

[1] Casulli, V., and Cattani, E., "Stability, accuracy and efficiency of a semi-implicit method for three-dimensional shallow water flow", *Computers and Mathematics with Applications*, 1994, 27 (4), pp. 99-112.

[2] Perot, B., "Conservation properties of unstructured staggered mesh schemes", *Journal of Computational Physics*, 2000, 159 (1), pp. 58-89.

[3] Chan, T. F., and Van der Vorst, H. A., "Approximate and Incomplete Factorizations", *Parallel Numerical Algorithms*, 1997, 4, pp. 167-202

THREE DIMENSIONAL MODELING OF GENERAL CIRCULATION IN THE PERSIAN GULF USING FVCOM NUMERICAL MODEL

Mohammad Kazem Sharifian[1], Kourosh Hejazi[2], Mohsen Soltanpour[2], Mohammad Hosein Nemati[3], Zohreh HajiSalimi[3] and Arash Zarkani[3]

1) University of Tabriz, Tabriz, IRAN, m.sharifian@tabrizu.ac.ir
2) K.N. Toosi University of Technology, Tehran, IRAN, hejazik@kntu.ac.ir
3) PMO, Tehran, IRAN

1. Introduction

The Persian Gulf is a shallow, semi-enclosed marginal sea with average depth of about 35 m, characterized by significant evaporation which is connected to the Gulf of Oman and the Arabian Sea through the Strait of Hormuz. High evaporation and strong surface heat loss in the Persian Gulf during winter combined with restricted exchange with the open ocean lead to the convective formation of the saltier and denser Persian Gulf water (PGW) mass. The PGW flushes out of the Persian Gulf as a deep outflow and induces a surface inflow of the Indian Ocean Surface Water (IOSW), driving an inverse-estuarine type water exchange through the Strait of Hormuz. In this study a high-resolution model of the Persian Gulf is presented and validated against the data reported from field measurements using the FVCOM numerical model. The predictions are then used to describe the circulation, the thermohaline structures and water mass transformation processes in the Persian Gulf in response to the atmospheric forcing. A sensitivity study for the settings of the numerical model, in particular vertical mixing parameterizations, has been performed in order to provide a favorable comparison with the available data from the observations.

2. Model Description

This study has employed FVCOM (Finite-Volume Coastal Ocean Model), which is an unstructured-grid, finite-volume, three-dimensional primitive equation, coastal ocean model. The governing equations consist of momentum, continuity, temperature, salinity, and density equations [1]. For the simulations 10 sigma levels have been considered, and the domain was discretized into 6526 elements and 3458 nodes in a triangular mesh (Figure 1). The coastline data were extracted from ICZM database, ESRI information database, and aerial photos of Landsat. The bathymetric data are developed by combining the maps of National Cartographic Center (NCC) of Iran and ETOPO two-minute gridded dataset and have been interpolated and slightly smoothed onto the grid. In the eastern open boundary, the temperature and salinity are relaxed toward the HYCOM + NCODA Global 1/12° analysis. Due to the uncertainties in river discharge, simulations were performed without taking the river discharges into the computations. The water level at open boundary was adopted from TPXO global tide model. The simulations started from rest on 1st January 2009 for two years and were initialized with temperature and salinity from the HYCOM analysis. The model was driven by fields of 10-m wind speed, vector wind stress, 2-m air temperature, 2-m atmospheric humidity, sea level pressure, surface shortwave and longwave heat fluxes, and precipitation. These fields were extracted from the 6-hourly NCEP DOE reanalysis product.

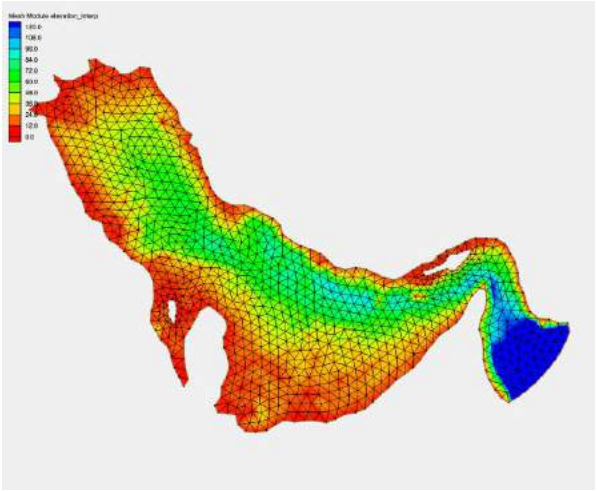

Figure 1. Computational grid.

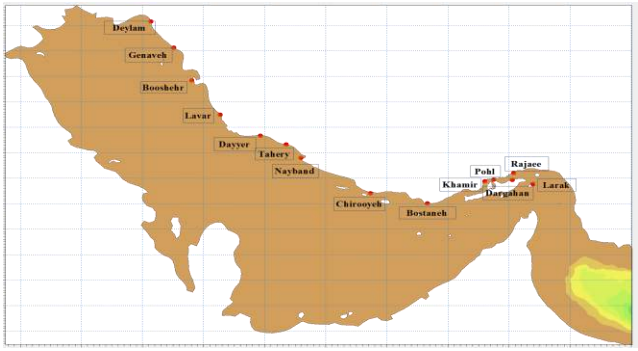

Figure 2. Surface elevation and current measurement stations.

3. Results and Discussion

Model verification for surface elevation and currents was performed by comparing the simulated results with measured data at different stations along the Iranian coastline (Figure 2).

Figure (3) presents the modeling results of free surface elevation and current velocity at two sample stations, in comparison with the observations. It can be seen that the model predictions are in close agreement with the in-situ measurements. In the case of current velocity, due to the fluctuations in the observed values, there are some discrepancies but the trend has been captured well.

The circulation and thermohaline structures in the Persian Gulf are well reproduced by the model, both for the mean state and for the seasonal variability. Figure (4) shows the comparison between surface salinity distributions simulated by the model and observed values published by Swift and Bower [2] during January–June. The difference of surface salinity between the model simulation and the observation is small over most of the Persian Gulf during the January–June. Consistent with Reynolds' observation [3], two isolated salinity maxima are found, one in the northern, and one in the southern gulf along the UAE coast, both with salinity >41 psu. Figure (5) shows the comparison between the simulated surface temperature and their observed counterparts published by Reynolds [3] in winter. The model predictions of the temperature spatial distribution are in a good agreement with Reynolds' observations [3]. The flow of IOSW into the Gulf Persian, forming a low-salinity surface layer, peaks in May–June. Water masses of the deep ocean are also well reproduced by the model (not shown here). A permanent southeastward deep current advects dense water from the northwest towards the Strait of Hormuz all year long, while dense water formed in the southern banks only reaches Hormuz from November to April. A seasonal decrease in salinity in the Persian Gulf is related with the increased inflow of IOSW through the Strait of Hormuz.

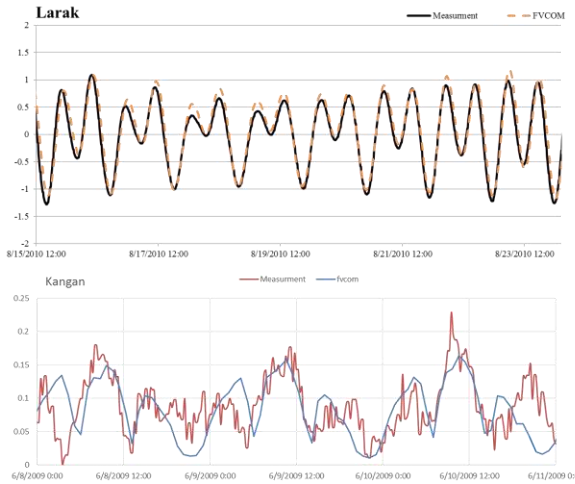

Figure 3. Comparison between results of FVCOM and observations for time evolution of the free surface elevation for Larak station (top) and magnitude of current velocity at Kangan station (bottom).

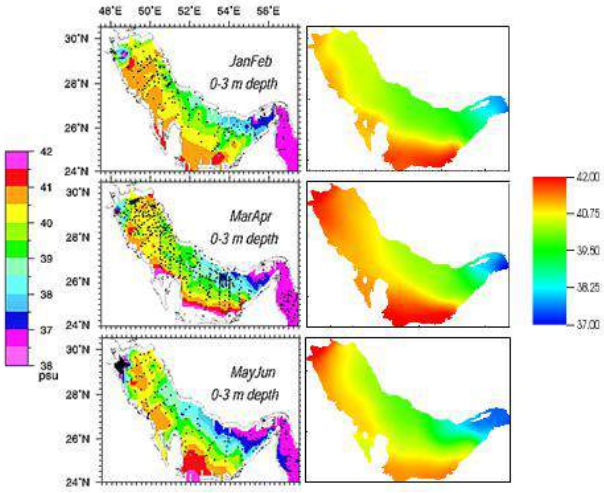

Figure 4. Comparison between the observed salinity [2] (left) and simulated salinity by the model (right) at the surface layer during the January–June.

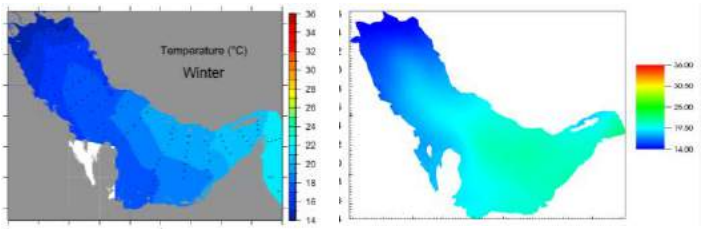

Figure 5. Comparison between surface fields of temperature during Reynolds' [3] winter survey (left) and simulated temperature by the model (right).

References

[1] Chen, C. S., Beardsley, R. C., and Cowles, G., (2006): An unstructured grid, finite-volume coastal ocean model–FVCOM user manual, School for Marine Science and Technology, University of Massachusetts Dart-mouth, New Bedford, Second Edition. Technical Report SMAST/UMASSD-06-0602, 318pp.

[2] S.A. Swift, A.S. Bower, Formation and circulation of dense water in the Persian Gulf, J. Geophys. Res. 108 (C1) (2003) 1–2.

[3] R.M. Reynolds, Physical oceanography of the Gulf, Strait of Hormuz, and the Gulf Oman – result from the Mt. Mitchel expedition, Mar. Pol. Bull. 27 (1993) 35–59.

NUMERICAL MODELLING OF WAVE-NON NEWTONIAN MUD INTERACTION USING INCOMPRESSIBLE SMOOTHED PARTICLE HYDRODYNAMICS (ISPH)

Kourosh Hejazi[1], Mohsen Soltanpour[2] and Abolfazl Aslani Kordkandi[3]

1) K.N. Toosi University of Technology, Tehran, IRAN, hejazik@kntu.ac.ir
2) K.N. Toosi University of Technology, Tehran, IRAN, soltanpour@kntu.ac.ir
3) K.N. Toosi University of Technology, Tehran, IRAN, a.aslani@mail.kntu.ac.ir

1. Introduction

Attenuation of wave height while it propagates over muddy beds is a typical phenomenon and is of interest to coastal researchers. The dissipation of waves propagating over muddy beds has been investigated theoretically and experimentally in several studies, but very few numerical model developments for simulation of the wave–mud interaction have been reported in the literature. In this paper, incompressible smoothed particle hydrodynamics (ISPH) method has been deployed to simulate wave-non Newtonian mud interaction. The SPH method overcomes limitations associated with mesh-based methods and provides a high degree of accuracy for the free surface and interface predictions. The projection method has been utilised for the solution of Navier-Stokes equations whereby the divergence-free velocity enforces the incompressibility of SPH.

2. Governing equations and the SPH formulation

The two-dimensional governing equations of mass and momentum conservation, written in Lagrangian form are presented as follows [1]:

$$\frac{d\rho}{dt} = \sum_b m_b(\vec{u}_a - \vec{u}_b)\vec{\nabla}_a W_{ab} \tag{1}$$

$$\frac{\Delta(\vec{u}_* + \vec{u}_{**})}{\Delta t} = \left[\vec{g} + \sum_b \frac{4m_b(\mu_a+\mu_b)\vec{r}_{ab}.\nabla_a W_{ab}}{(\rho_a+\rho_b)^2(|r_{ab}|^2+\eta^2)}(\vec{u}_a - \vec{u}_b)\right] - \sum_b m_b\left(\frac{P_b}{\rho_b^2}+\frac{P_a}{\rho_a^2}\right).\vec{\nabla}_a W_{ab} \tag{2}$$

where a and b indices indicate the reference and neighbouring particles respectively, m_b and ρ represent mass and density respectively, W is the interpolation kernel, h is the smoothing length, $\vec{u}_*$ and $\vec{u}_{**}$ are the velocity in the prediction and correction steps respectively, $\vec{r}_{ab} = \vec{r}_a - \vec{r}_b$ is the distance between the particles a and b, t is time, $\vec{u}$ the particle velocity, P the pressure, $\vec{g}$ the gravitational acceleration, $P_{ab} = P_a - P_b$ and η are equal to $0.1h$.

In this study water and mud are considered as Newtonian and non-Newtonian fluids respectively. Effective viscosity (μ_{eff}) for mud is obtained by combining the Cross and Bingham models as presented in the following equation [1]:

$$\mu_{eff} = \frac{1000(\mu_B + \frac{\mu_B^2}{\tau_B}\dot{\gamma})}{1+\frac{1000\mu_B}{\tau_B}\dot{\gamma}} \tag{3}$$

where τ_B , μ_B and $\dot{\gamma}$ are the Bingham yield stress, the Bingham viscosity and the shear rate respectively. The solution method is comprised of two steps. The first step is the prediction step in which the velocity field is computed without the inclusion of the pressure gradient term in the momentum equations. Incompressibility is not satisfied in this step and the fluid density calculated based on the temporary particle positions deviates from the initial constant density. In the second correction step, the pressure term is calculated to enforce the incompressibility constraint using the Poisson equation. The Poisson equation is obtained from the integration of the continuity equation and the pressure gradient term in the momentum equations. The new velocity values and positions of the particles are then computed. In this study the iterative technique Sparse- Gauss–Seidel solver with successive over relaxation (SOR) accelerator has been deployed. The relaxation factor was found to lie between 1.8 and 1.95 and the criterion to stop the repetitions was set as $\varepsilon = 10^{-8}$ ($\varepsilon = \max\left|p^{(n+1)} - p^{(n)}\right| \le 10^{-8}$).

3. Model verification and application

In order to validate the numerical scheme of the ISPH model, the propagation of a sinusoidal wave is simulated. Fig.1 shows the numerical results which are in a good agreement with the analytical solution. For the wave-mud interaction a two-dimensional simulation of wave–non Newtonian mud is presented. Fig. 2 shows the schematic of the simulation set-up and the attenuation of the wave. A piston wave maker type formulation was implemented to generate sinusoidal waves at the entrance of a channel with the length of 10 m. The number of particles employed in the computation was about 36000 and the initial spacing for the particles and the time step were set equal to 0.01 m and 0.001 s respectively. The predicted wave attenuation is compared against the

simulated results of Hejazi et al. [2], the experimental results of Sakakiyama and Bijker [3] and the theoretical solution of Dalrymple and Liu [4] and An [5].

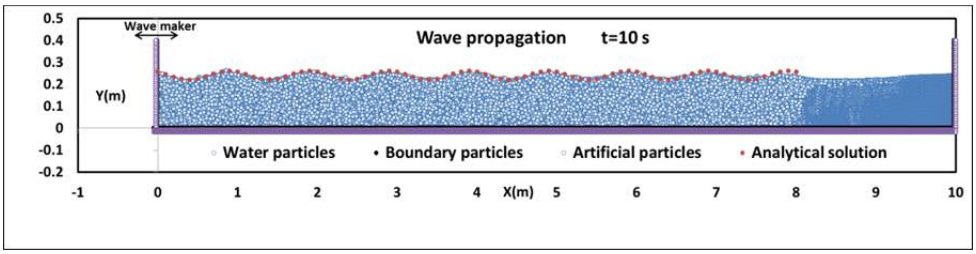

Fig.1 Comparison of the simulated and analytical wave profiles

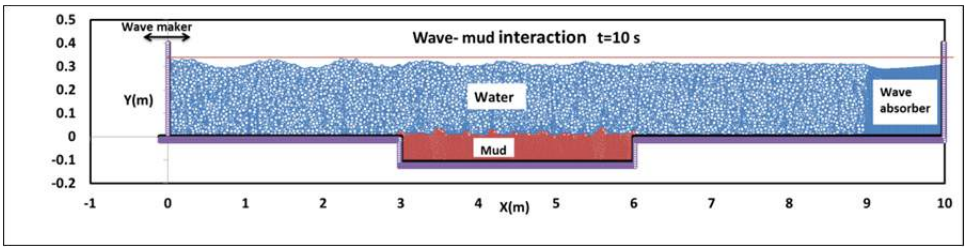

Fig.2 wave-mud interaction
wave period =1s , H_0 = 3.2 cm
water density =1000 kg/m^3
mud density =1300 kg/m^3

4. Results and Discussion

The relation between the wave height (H), initial wave height (H_0) and wave damping coefficient (k_i) is presented as follows [4]:

$$H = H_0 e^{-k_i x} \quad (4)$$

The simulated results of wave attenuation have been compared against the measured values of Sakakiyama and Bijker [3] in Fig.3. The properties of wave and mud have been also presented in Fig.2.

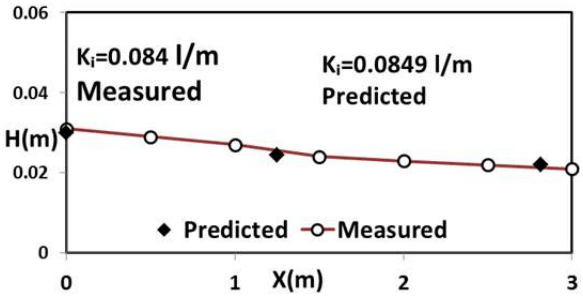

Fig.3 wave attenuation; comparison between the ISPH model, experimental results of Sakakiyama and Bijker (1989) H_0=3.2 cm, Water density =1000 kg/m^3 , Mud density=1300 kg/m^3

For a wave with a period of 1s and height of 3.2 cm k_i was computed 0.0849 1/m using the simulated results of the present ISPH model. This value for the theoretical results of Dalrymple and Liu (1978) and An (1993) was 0.089 and 0.109 1/m respectively, and for the experiments of Sakakiyama and Bijker [3] and simulated results of Hejazi et al. [2] which considered mud as Newtonian fluid was reported 0.084 1/m and 0.0829 l/m respectively. The results show that predicted value of the present SPH method is much closer to the experimental results than theoretical and numerical results considering linear approximation or Newtonian mud in the governing equations.

5. References

[1] Shao, S. and Lo, E.Y., ″Incompressible SPH method for simulating Newtonian and non-Newtonian flows with a free surface″ Advances in water resources, 2003 26(7), pp.787-800.

[2] Hejazi, K., Soltanpour, M., Sami, S., ″Numerical modeling of wave-mud interaction using projection method″ Ocean Dynamics, 2013 Vol. 63, pp. 1093-1111.

[3] Sakakiyama T., Bijker E.W., ″Mass transport velocity in mud layer due to progressive waves.″ J Waterway Port Coast Ocean Eng ASCE 1989 115(5):614–633.

[4] Dalrymple R.A., Liu PL-F., ″Waves over soft muds, a two-layer fluid model.″ J Phys Oceanogr 1978 8:1121–1131.

[5] An N.N., ″Mud mass transport under wave and current.″, Department of Civil Engineering, Yokohama National University, Yokohama Ph.D. dissertation, 1993.

ENTROPY DEFICIT DURING TROPICAL CYCLONE HAIYAN

Nafiseh Pegahfar
Assistant Professor, Atmospheric Research Center, Iranian National Institute for Oceanography and Atmospheric Science, Tehran, Iran,
pegahfar@inio.ac.ir;pegahfar@ut.ac.ir

1. Introduction

Various environmental factors affecting formation and intensification of tropical cyclone (TC) contribute in challenges of TC prediction. So different approaches and empirical indexes have been established to investigate influence of these factors on TC. Meanwhile, those related to the thermodynamic parameter of entropy have been considered further, because variation of this long-lasting parameter can preclude incipient dispersion development to a tropical cyclone. Moreover, outward eddy flux of entropy along with its advection into a TC play significant role in TC intensification and weakening. In addition, infiltration of low entropy air into a TC can decrease the efficiency of TC heat engine ([1]). The schematic view of infiltration of low-entropy air into a TC has been shown in Figure1.

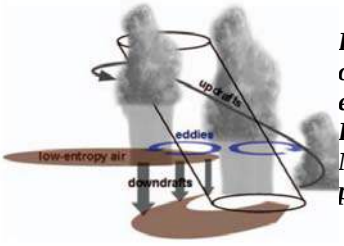

Figure 1. An illustration of infiltration of low-entropy air into a TC. Figure adapted from Michael riemer with permission.

Recently, Tang and Emanuel ([2]) developed a simple framework including vertically variation of entropy, and studied ventilation effect on TC intensity. They showed that non-dimensional entropy deficit plays a significant and discussable role in ventilation. Hence in the current research, entropy deficit will be investigated for an intense tropical cyclone to evaluate its applicability as a TC predicator.

2. Methodology

In the current work, entropy deficit has been calculated based on the relation of

$$\chi_m = \frac{s_m^* - s_m}{s_{SST}^* - s_b}, \qquad (1)$$

where s_m^*, s_m, s_{SST}^* and s_b denote the saturation entropy at 600 hPa in the inner core of the TC, the environmental entropy at 600 hPa, the saturation entropy at the sea surface temperature, and the entropy of the boundary layer, in that order. For this aim, the pseudo-adiabatic entropy relation, calculated by Emanuel ([3]) and modified by Lopez and Raymond ([4]), as

$$s = (c_{pd} + c_l r_t)\ln(T/T_R) - R_d \ln(p_d/p_0) + \frac{L_{vo}\, r_v}{T} - R_v\, r_v \ln(H), \qquad (2)$$

$$p_d = \rho_d \times R_d \times T, \quad \rho_d = 1.2,$$

has been used. Here, the constants of c_{pd} = 1005 J/kg/K, c_l = 428 J/kg/K and $L_{vo} = 2.55\times10^6$ J/kg are the specific heat for dry air at constant pressure, specific heat for liquid water and latent heat, respectively. The gas constants for water vapor and dry air have been included as R_v = 461.51 J/kg/K and R_d = 287.05J/kg/K, in that order. Constants of T_R = 273.15 K and P_R = 1000 hPa denote freezing point of water and reference pressure, correspondingly. Also the variables of T, P_d, H, and r_v show temperature, partial pressure, humidity and water vapor mixing ratio, respectively. Cloud-base height has been calculated as the height of boundary layer based on Lawrence ([5]) formula.

Three domains of $1^o\times1^o$, $2^o\times2^o$ and $10^o\times10^o$, all surrounding the selected TC eye location at each time step, have been designed to represent the radius of maximum wind, inner core and environment of the selected TC, correspondingly.

3. Data and Tropical Cyclone Haiyan

NCEP-GFS reanalysis data (with $0.5^o \times 0.5^o$ horizontal resolution at 26 pressure levels with 6-h intervals) and data produced by Japan Meteorology Agency (JMA) have been used during 03-11 November 2013. In the present research, tropical cyclone Haiyan (TCH) has been focused which was the most intensive TC formed over the West Pacific Ocean basin to 2014 and devastated southeast Asia, especially the Philippine Islands. TCH has been analyzed by Pegahfar and Ghafarian ([6]) from different points of view, based on dynamic and thermodynamic aspects at various scales. They showed that not only lower-tropospheric forcings but also upper-tropospheric ones play significant roles on TCH amplification and dilution. The above forcings affect TCH with lag or lead time, comparing with TCH maximum activity time.

4. Results and discussion

Entropy deficit with considerable effect in ventilation index, which is the anti-fuel for a TC, has been calculated during TCH and the results have been shown in Figure 2.

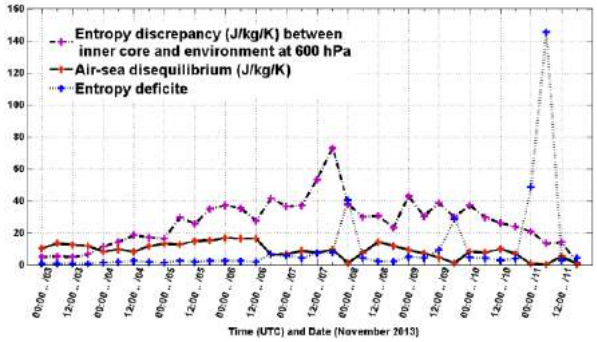

Figure 2. Time series of (I) entropy discrepancy (J/kg/K) between inner core and environment at 600 hPa (dashed-dotted line marked with purple plus), (II) air-sea disequilibrium (J/kg/K) (solid line marked with red plus) and (III) entropy deficit (dotted line marked with blue plus).

To distinguish the contribution of the difference in entropy between TCH and the environment at 600 hPa as the midlevel (using the numerator of Eq. 1) from the role of air–sea disequilibrium (using the denominator of Eq. 1), the numerator and denominator of Eq. 1 have been plotted individually in Figure 2. The denominator of entropy deficit ratio has been computed using the averaged values over the innermost domain surrounding TCH, while the nominator terms have been calculated via the averaged values over the inner core and environment of TCH, respectively. Figure 2 shows that the discrepancy of entropy between the inner core and the environment of TCH has been increased by TCH intensification and decreased during TCH weakening, however containing some rises and falls. Also the maximum value of this difference occurred simultaneously with the time TCH peak intensity. While, air-sea disequilibrium maximized at about 30 hours earlier than TCH maximum intensity time, and reached its first minimum value at 6 hours later than the time of TCH peak activity.

To 1200 UTC 06 November, the increase of air-sea disequilibrium has been balanced by the rise of the entropy difference between the inner core and environment of TCH. Hence, no entropy deficit occurred. Afterward, air-sea disequilibrium has been declined and entropy deficit has been increased. So, further ventilation led to TCH weakening. The first maximum value of entropy deficit occurred due to small value of air-sea disequilibrium, while the second and third maximum ones happened because of Asia continental effect on averaging process and also landfall effect on TCH.

5. Conclusions

In the current work, entropy deficit and its numerator-denominator elements have been focused during TCH as the most intensive tropical cyclone formed over the West Pacific Ocean. For this aim, the components of entropy deficit as (1) discrepancy between the inner core and environment at 600 hPa and (2) air-sea disequilibrium have been analyzed during TCH life cycle. The results indicated that the numerator of entropy deficit ratio has been maximized simultaneously with TCH peak intensity time. While, the denominator of entropy deficit ratio reached the maximum value at about 30 hours earlier than TCH peak activity time and then decreased until the end of TCH lifetime, including some rise and fall. The most considerable finding is three maximum values of entropy deficit that the first one is simultaneous with TCH maximum intensity time and second and third ones occurred later than that. Before TCH peak activity time, relatively monotonic behaviour of entropy deficit with small values indicates that TCH is intensifying. While, increase of entropy deficit in the second half of TCH life span guaranteed that TCH will be weakened. Although, occurrence of the greatest value of entropy deficit after entering the Asia illustrates the effect of entropy deficit on TCH weakening. Conclusively, it can be acclaimed that entropy deficit is worthwhile to be used as a relevant proxy parameter in TC research.

6. References

[1] Simpson, R. H., and Riehl, H., "Mid-tropospheric ventilation as a constraint on hurricane development and maintenance", *Proc. Tech. Conf. on Hurricanes, Miami Beach, FL, Amer. Meteor. Soc., D4-1–D4-10*, 1958.

[2] Tang, B., and Emanuel, K., "Midlevel ventilation's constraint on tropical cyclone intensity", *J. Atmos. Sci*., 67, 2010, pp. 1817–1830.

[3] Emanuel, K., *The physics of tropical cyclogenesis over the eastern Pacific*. In Tropical Cyclone Disasters, ed. JZ Lighthill, Z. Holland, G. and Emanuel, K., editors., 588 pp. Beijing: Peking Univ. Press, 1994.

[4] Lopez C. C., and Raymond, D. J., "Moisture tendency equations in a tropical atmosphere", *J. Atmos. Sci*., 62, 2005, pp. 1601–1613, doi:10.1175/JAS3424.1.

[5] Lawrence, M. G., "The relationship between relative humidity and the dewpoint temperature in moist air: A simple conversion and applications", Bull. Amer. Meteor. Soc., 86, 2005, pp. 225–233.

[6] Pegahfar, N., Ghafarian, P., "*Analysis of Two Dynamic Parameters of CAPE & Helicity for Haiyan Tropical Cyclone*", *The 11th International Conference on Coasts, Ports and Marine Structures (ICOPMAS), Tehran, Iran, 24-26 Nov*, 2014.

EXPERIMENTAL AND NUMERICAL ANALYSES OF TSUNAMI JET FLOWS IN FRONT OF AN UPRIGHT BREAKWATER

Akio NAGAYAMA[1], Kenji ISHIMOTO[2], Iyan E.MULIA[3], Toshiyuki ASANO[4]

1) Department of Ocean Civil Engineering, Kagoshima University,Kagoshima,Japan,nagayama@oce.kagoshima-u.ac.jp
2) ECOH CORPORATION, Tokyo, Japan, ishimoto@ecoh.co.jp
3) Faculty of Engineering, Tokyo University,Tokyo,Japan,iyane.m@gmail.com
4) Department of Ocean Civil Engineering, Kagoshima University,Kagoshima,Japan,asano@oce.kagoshima-u.ac.jp

1. Introduction

The 2011 Great East Japan Tsunami demolished a number of breakwaters. This raised concerns amongst coastal engineers/practitioners regarding the three-dimensional characteristics of a tsunami flow over a breakwater. When a large tsunami strikes a caisson-type breakwater, the tip of the tsunami runs vertically up the front face of the structure. Herein, this phenomenon is called the tsunami jet flow. However, little understanding has been derived on such violent motion, either through experimental or numerical studies.

2. Objectives

This study aimed to clarify the behavior of a tsunami jet flow by measuring water surface motion using capacitance-type wave gauges and through visual analysis of sequential photographs. Numerical analysis was conducted using OpenFOAM, an advanced numerical software package that can reproduce three-dimensional free-surface flows. The spatial and temporal characteristics of the transient flow are discussed based on comparisons between the experimental and numerical results.

3. Method

3.1. Experiments

The experiments were conducted in a two-dimensional wave tank (Figure. 1) owned by Kagoshima University. The width (shoreline direction), length (on/offshore direction), and offshore depth of the wave tank were 14.0, 30.0, and 0.5 m, respectively. A uniformly sloped beach made of concrete was developed with a gradient of 1/9. On the slope, a 2-m-long and 3-m-wide horizontal concrete stage was built, to which a rectangular concrete bar (70 × 70 × 800 mm) was fixed to represent the breakwater model. To generate a solitary wave as a model tsunami, a plunger-type wave generator was installed at the offshore end of the tank.

3.2. Numerical Analysis

OpenFOAM is an open software package that can be used to analyze three-dimensional multi-phase flows.

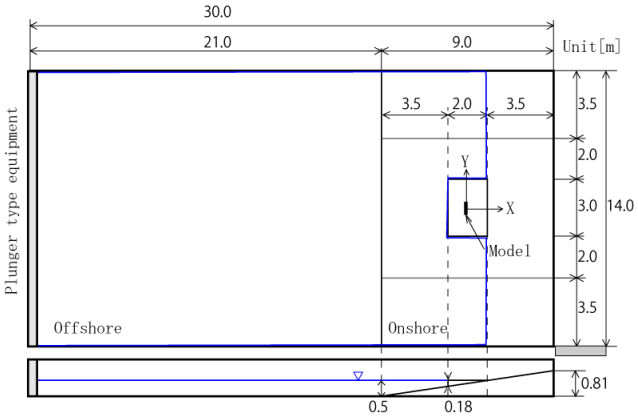

Figure 1. Experimental set-up

For the numerical analysis, we used the interFoam solver, which is able to reproduce free-surface flows. The boundary conditions of wave generation and absorption were handled using ihForm, which is an improved solver of interFoam. At the wave-generation boundary, the time sequence of a solitary wave with cnoidal form was introduced as the incident tsunami wave.

4. Results

Figure 2 shows the sequential motions of a wave colliding against the model breakwater. Figure 2(b) shows the solitary wave colliding with the breakwater. In Figure. 2(c), the water mass is shown jumping upward, and in Figure. 2(d), some of the elevated water mass can be seen forming an upward jet flow, while the remaining water mass moves horizontally and flows over the breakwater. Figure 2(e) shows that the generated upward jet flow is pushed by the water behind and is transformed into a curved jet in the air. In Figure. 2(f), the elevated jet flow is shown falling in front of the breakwater.

Figure 3 illustrates the corresponding flow motions to the experimental results (shown in Figure. 2), as computed by OpenFOAM. The numerical and experimental results are similar regarding the impinging flow and upward jet

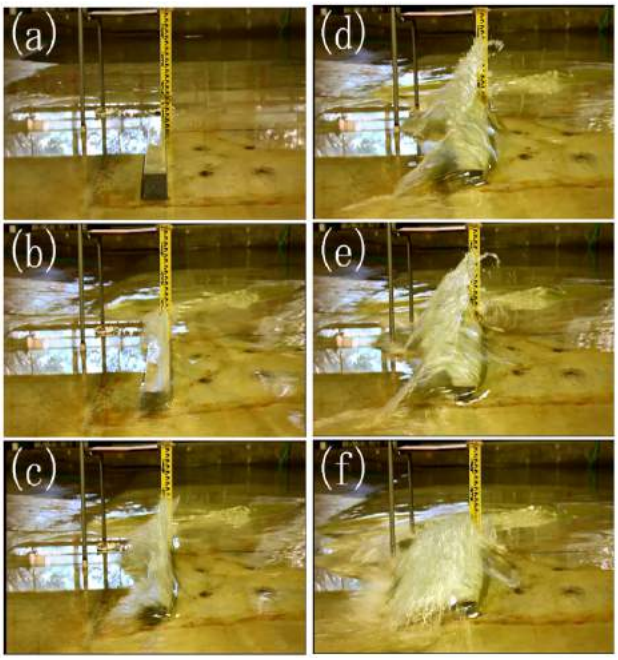

Figure 2. Successive photographic images of water surface motion

flow patterns, although there are some differences, e.g., the jet flow run-up angle.

Concerning the temporal motions of the water surface overflowing the breakwater, Figure. 4 shows comparisons of the three analyses: the experimental results measured by the capacitance-type wave gauges, sequential photographic images, and numerical computations. The photographic image analysis shows the highest run-up height (35 cm); the maximum run-up height based on the numerical calculation is about 23 cm, and that derived from the wave gauge is 18 cm (half that observed in the photographic images). Because the upward jet flow is a transient mixed air–water flow, the capacitance-type wave gauges, which measure the electrical capacity of a water mass between the sensor threads, are unable to detect the flow motion properly.

5. Conclusions

This study investigated the behavior of the tsunami jet flow generated in front of the vertical face of a breakwater. The photographic image analysis was found capable of capturing the intense motions of the mixed air–water tsunami jet flow. It was found that the tsunami jet flow rose to almost five times the height of the breakwater. Experiments using capacitance-type wave gauges were found to provide poor results, because the equipment was incapable of detecting the motion of the air–water mixture accurately. The numerical model was found to be able to reproduce the motion of the collision and run-up of the tsunami jet flow, including the jet flow shape, although some disagreements remain with the results obtained from the photographic image analysis.

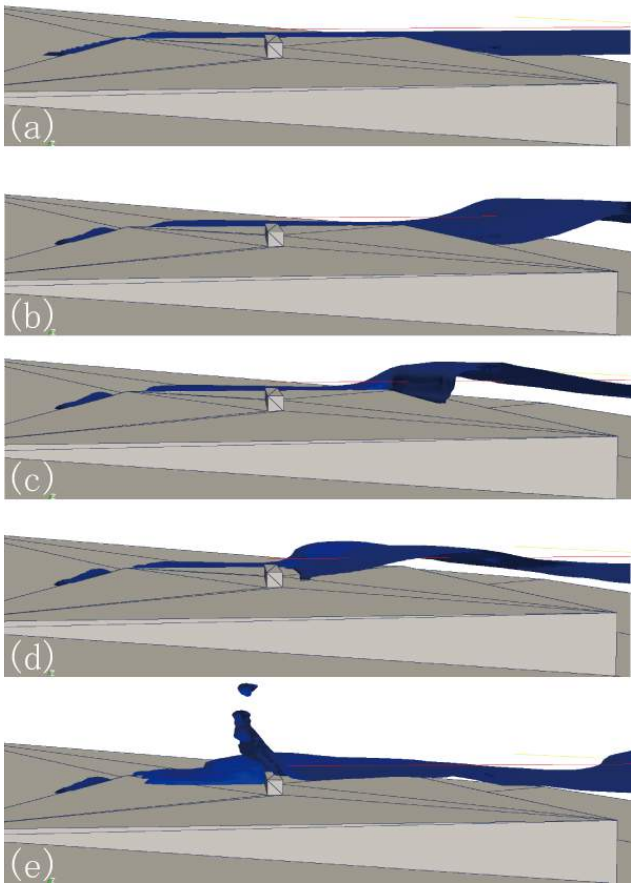

Figure 3. 3D water surface motion by OpenFOAM computation

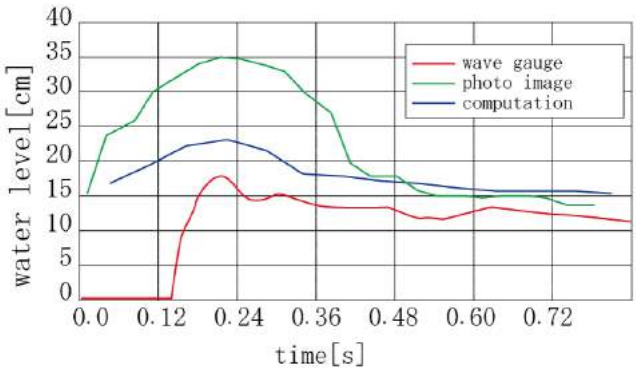

Figure 4. Comparisons of experimental and numerical results on water surface motions

6. References

[1] Higuera P,Lara J, Losada I:Realistic wave generation and active wave absorption for navier-stokes models:Application to openfoam, Coastal Engineering,vol.71,pp.102-118,2013.

[2] Higuera P,Lara J,Losada I: Simulating coastal engineering processes with openfoam.,Coastal Engineering, vol.71,pp119-134,2013.

EFFECTS OF TOPOGRAPHIC OBSTACLES ON TSUNAMI PROPAGATION OVER A CONTINENTAL SHELF

Toshiyuki Asano[1], Iyan Ekka Mulia[2] and Ryo Kobaru[3]

1) Dept. of Ocean Civil Engrg., Kagoshima Univ., Kagoshima, JAPAN, asano@oce.kagoshima-u.ac.jp
2) Dept. of Earth Planetary Science, Univ. of Tokyo, JAPAN, iyan@oa.u-tokyo.ac.jp
3) ECOH Corporation, JAPAN, kobaru@ecoh.co.jp

1. Introduction

At the 2011 Tohoku tsunami, the southern limit where people were victimized extended to Asahi city, Chiba Prefecture. At Iioka coast of the city, the maximum tsunami run-up height 7.6m was recorded around 3 hours after the occurrence of the earthquake. Judging from the far propagation and long duration of the tsunami fluctuations, edge-wave mechanism could governed the event. A distinct continental shelf topography is observed in front of the coastal area which may facilitate the edge wave generation. There are, however, several protuberance geometries like capes, which may affect the edge wave propagations. Both the width and slope of the continental shelf in this site are not constant, therefore, the hypothesis that the edge wave would contribute the generation of far field disaster should be carefully examined.

This study investigates the influence of the topographic obstacles on the propagation/generation of edge waves.

2. Simulation to reproduce 2011 Tohoku tsunami propagation

A calculation domain was taken to cover the range of 28°N～48°N, 134°E～158°E as the entire domain. The calculations were conducted from the largest scale grid (ΔL=90 arc sec) to the smallest scale grid (ΔL=100m) using 4 nesting levels. A computer program COMCOT based on the shallow water equations was adopted, which was developed by the group of Cornel University [2].

Fig.2 shows the initial sea surface deformation of 2011 Tohoku tsunami, which was obtained by an inverse analysis utilizing computational intelligence techniques[1].

The tsunami wave trapping in the continental shelf area and the effect of the existence of a topographic obstacle; Inubo-saki cape on the alongshore propagation of the tsunami are observed in the calculated results (Fig. 3). Distinction between a propagating mode edge wave and standing wave mode edge wave was not clear in the calculating results in the real field, because several disturbance effects such as on-offshore standing mode waves and bay oscillations may contaminate the edge wave results.

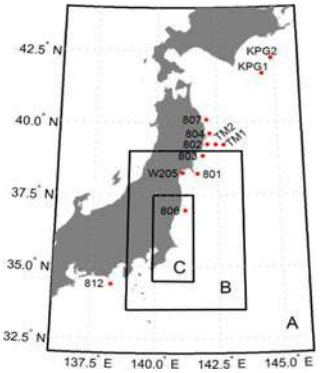

Fig.1 Calculation domain

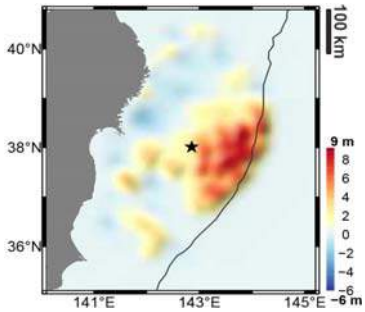

Fig.2 Initial sea surface deformation

3. Edge wave simulation over an idealized continental shelf

We next examined the edge wave behavior over an idealized continental shelf topography. A simple shape bathymetry model; a step type beach in the on-offshore direction, a curved coastal line with a radius of 156.8km and a curved continental shelf of 12.8km width, both of which make concentric circles, was adopted as illustrated in Fig. 4. A jetty type obstacle was set at the coastal line. Numerical analyses were conducted by making a tsunamigenic solitary wave incident with angle $\theta_0 = \pi / 4$ into the domain. A parametric study by varying wave parameters or topographic parameters was conducted. The alterations of edge wave mode from progressive to standing mode with increase of the jetty's length were investigated.

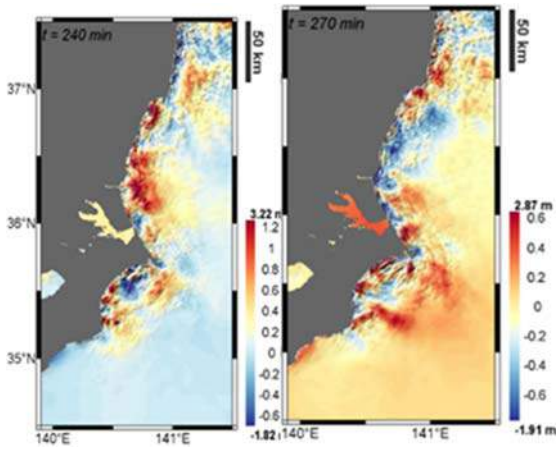

Fig. 3 Tsunami propagation along the coast
(left: after 4hrs, right: after 4.5hrs of the earthquake occurrence)

4. Results and Discussion

From 2-D contour plots of water level in Fig.5, the propagating waves are trapped in the shelf region as the edge waves. In the early stage calculation, direct incident waves from the tsunami source and the reflected waves made complex 2-D distributions, and after such fluctuations were attenuated, clear edge wave propagations were observed which was around after 1600s from the calculation start. The blocking effect by the jetty on the alongshore propagating waves were slightly observed.

Fig. 6 illustrates the on-offshore distributions of the water surface fluctuations. The red broken vertical line indicates the shelf edge. In the offshore region from the line, exponential decays are observed. In the onshore region, the loop and node structure is found. The estimated wave number from the loop and node is $\mu_1 = 3.68\times10^{-4}(m^{-1})$, which nearly agrees with the theoretical value. The jetty slightly affects the loop-node structure, because the length of jetty assumed here is restricted (maximum 3km).

Alongshore distributions with time passes are shown in Fig.7. The phase speed in the alongshore direction can be estimated by tracing the crests of each curve. The obtained speed c=71m/s is found to satisfy the theoretical relationship $\sqrt{gh_1} < c < \sqrt{gh_2}$, in which h_1 is the shelf depth (we assume here h_1=200m) and h_2 is the ocean depth (h_2=1000m).

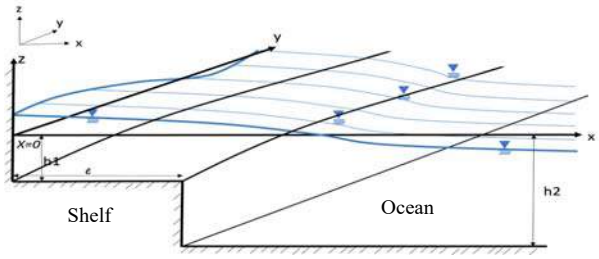

Fig.4 Step type continental shelf model

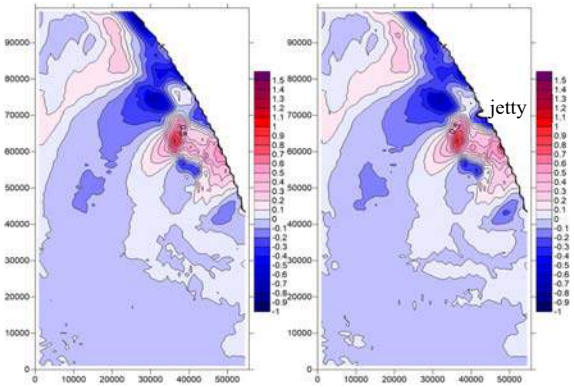

Fig.5 Snap shots of two-dimensional propagations along the coast (left: without jetty, right: with jetty)

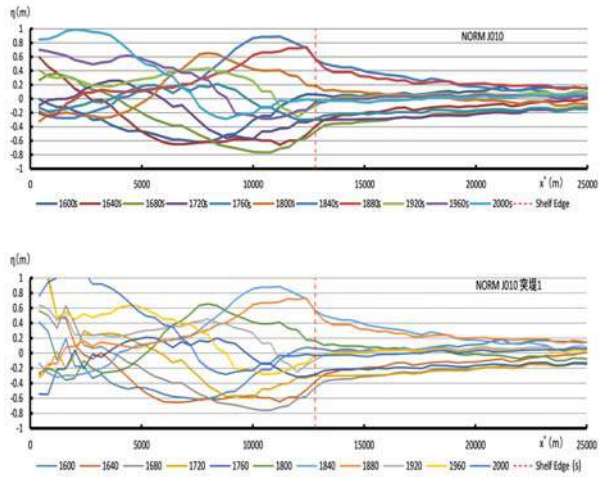

Fig.6 Water surface fluctuation in the on-off shore direction (upper: without jetty, lower: with jetty)

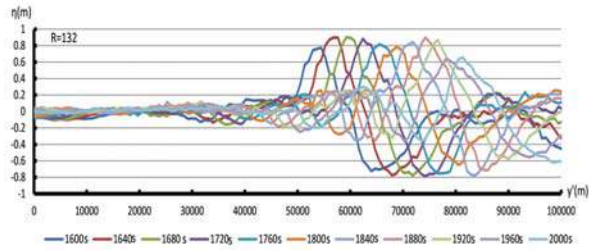

Fig.7 Water surface fluctuations in the alongshore direction

5. References

[1] Mulia, I.E. and T. Asano: Randomly distributed unit sources to enhance optimization in tsunami waveform inversion, Natural Hazards and Earth System Sciences, Vol. 15, pp.187-196, 2015.
[2] Liu, P.L.F., S-B. Woo and Y-S Cho : Computer programs for tsunami propagation and inundation, Technical report, Cornell University, 1998.

ON THE USE OF AN ENSEMBLE FORECASTING SYSTEM FOR PREDICTION OF SURFACE WIND OVER THE PERSIAN GULF

Sarmad Ghader[1], Daniel Yazgi[2], Mohsen Soltanpour[3]and Mohammad H. Nemati[4]

1) Institute of Geophysics, University of Tehran, Tehran, Iran, sghader@ut.ac.ir
2) Institute of Geophysics, University of Tehran, Tehran, Iran, daniel.yazgi@ut.ac.ir
3) Faculty of Civil Engineering, Khaje Nasir Toosi University of Technology, Tehran, Iran, soltanpour@kntu.ac.ir
4) Ports and Maritime Organization, Tehran, Iran, mhn1982@gmail.com

1. Introduction

In this article, results of an ensemble forecasting system developed for the Weather Research and Forecasting (WRF) model to predict surface wind over the Persian Gulf, is presented. It is well established that numerical weather prediction models and in particular meso-scale models such as WRF, can be employed to forecast and hindcast of marine surface winds (e.g., [1-5]). Furthermore, prediction of marine surface winds is an essential data for many marine activities such as costal management and ship routing. On the other hand, surface wind forecasts are a key input parameter to the wave and ocean circulation numerical models.

Since early 1990s, operational weather forecasting centers (such as The European Centre for Medium-Range Weather Forecasts and US National Center for Environmental Prediction) started to use ensemble forecasting to response to limitations imposed by the uncertainties of the numerical weather prediction process (e.g., initial condition and model uncertainties). In ensemble forecasting, instead of generating a single forecast form a numerical weather prediction model (deterministic prediction) a group or ensemble of forecasts which are generated by using perturbations in some way, are used [6,7].

In the present work, an ensemble prediction system developed for the WRF model is used to predict the surface wind over the Persian Gulf. The ensemble mean is used to assess the performance of the system against observational data (including in situ and satellite data).

2. WRF Model

The Advanced Research WRF (ARW) model developed at US National Center for Atmospheric Research (NCAR) which is a fully compressible, Euler non-hydrostatic mesoscale numerical weather prediction model is the [8,9]. In this article, the ARW dynamical core of the WRF model version 3.4.1 is used. The model is configured with two nests with 0.3 degree and 0.1 degree horizontal grid resolutions in a Latitude-Longitude projection. Figure 1 presents domains and shows that the finer (inner, d02) domain covers the Persian Gulf. Outer and inner domains have 88×41 and 235×94 grid points, respectively. In both domains 49 terrain following vertical levels are used.

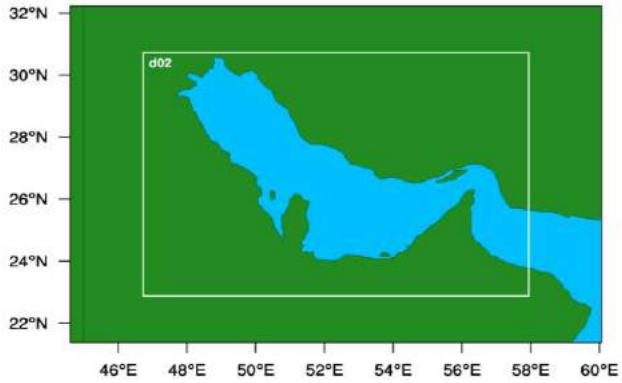

Figure 1. Domains used in WRF model simulations.

To find the candidate configurations of the WRF model based on physical parametrizations, different choices are used to create 13 WRF model configurations. Then, to find the candidate WRF model configurations, the model is run with these 13 different physics configurations. Finally, three of these configurations are selected to be more suitable for wind predictions over water based on statistical analysis against observational data.

The selected parameterization schemes for physical processes in WRF model are as follows. Configuration 1 (Phys01): The Lin method for the microphysics, the rapid radiative transfer model (RRTM) scheme for the longwave radiation, Goddard method for the shortwave radiation, the MRF scheme for the planetary boundary layer (PBL), Kain Fritsch for the cumulus parametrization, the revised MM5 method for the surface layer and the Noah method for the land surface. Configuration 2 (Phys02): The Lin method for the microphysics, the RRTM scheme for the longwave radiation, Goddard method for the shortwave radiation, the MYNN2.5 schemes for the PBL, the Kain Fritsch for the cumulus parametrization, the MM5, the MYNN method for the surface layer and the Noah method for the land surface. Configuration 3 (Phys03): The Ferrier method for the microphysics, the RRTM scheme for the longwave radiation, the Dudhia method for the shortwave radiation, the YSU schemes for the PBL, the BMJ for the cumulus

parametrization, the MM5 method for the surface layer and the Noah method for the land surface. More details regarding the physical parametrization schemes are given in Refs. [8,9].

In addition, the Global Forecast System (GFS) data of the US National Center for Environmental Prediction are used to provide the initial and boundary data for WRF model control forecast.

3. Ensemble System

To construct the ensemble members a combination of perturbed initial condition and model perturbations (using three physical parametrization schemes) is employed. A Monte Carlo approach is used to add perturbations to the control initial condition (e.g., [10]). Here, an ensemble prediction system with 15 members (three physical parametrization schemes and five initial condition perturbations for each one including control initial data) is employed to conduct forecasts.

4. Results

Figure 2 presents a 15 day time series of the ensemble mean predictions of surface wind speed at Boushehr buoy location. In figure observational data are also shown.

In addition, to evaluate the ensemble system predictions, the ensemble mean is compared against the observational in situ and satellite (e.g., ASCAT and QuikSCAT) data. At observational stations that have valid observation, the corresponding predicted wind field are interpolated from ensemble mean forecasts. Then, the root mean squared error (RMSE) and correlation coefficient (CC) are calculated.

The correlation coefficient and RMSE of the surface wind vector and its components at satellite point observations over the Persian Gulf, are presented in Table 1. It can be seen that the performance of the ensemble system is promising and there is a good agreement between the model predictions and observational data.

5. References

[1] Chen, C., Beardsley, R. C., Hu, S., Xu, Q., Lin, H., "Using MM5 to hindcast the ccean surface forcing fields over the gulf of Maine and Georges bank region", Journal of Atmospheric and Oceanic Technology, 22, 2005, 131-145.

[2] Schulz, E W., Kepert, J. D., Greenslade, D., "An assessment of marine surface winds from the Australian bureau of meteorology numerical weather prediction systems", Weather and Forecasting, 22, 2007, 613-636.

[3] Sousa, M. C., Alvarez, I., Vaz, N., Gomez-Gesteira, M., Dias J. M., "Assessment of wind pattern accuracy from the Quikscat satellite and the WRF model along the Galician coast (northwest Iberian Peninsula)", Monthly Weather Review, 141, 2013, 742-753.

[4] Ghader, S., Montazeri-Namin, M., Chegini, F., Bohluly A., "Hindcast of surface wind field over the Caspian Sea using WRF model", in *Proceedings of the 11th International Conference on Coasts, Ports and Marine Structures*, Tehran, Iran, 24-26 November, 2014.

[5] Ghader, S.; Yazgi, D.; Haghshenas , S.A.; Razavi Arab, A., Jedari Attari, M., Bakhtiari, A., Zinsazboroujerdi, H., "Hindcasting tropical storm events in the Oman sea", Journal of Coastal Research, Special Issue, No. 75, 2016, pp. 1087-1091.

[6] Leutbecher, M., Palmer, T.N., "Ensemble forecasting", Journal of Computational Physics, 227, 2008, pp. 3515-3539.

[7] Inness, P., Dorling, S., *Operational Weather Forecasting*, Wiley-Blackwell, 2013.

[8] Skamarock, W. C., Klemp, J. B., Dudhia, J., Gill, D. O., Barker, D. M., Wang, W., Powers, J. G., *A description of the advanced research WRF version 3*. NCAR Tech. NCAR/TN–475+STR, 2008.

[9] Wang, W., Bruyère C., Duda M., Dudhia J., Gill D., Lin H., Michalakes J., Rizvi S. Zhang X., Beezley J. D., Coen J. L., and Mandel J., *User's guide for the advanced research WRF (ARW) Version 3.5*, NCAR (http: //www.mmm.ucar.edu/wrf/), 2010.

[10] Stensrud, D. J., Bao, J., Warner, T., "Using initial condition and model physics perturbations in short-range ensemble simulations of mesoscale convective systems", Monthly Weather Review, 128, 2000, 2077-2107.

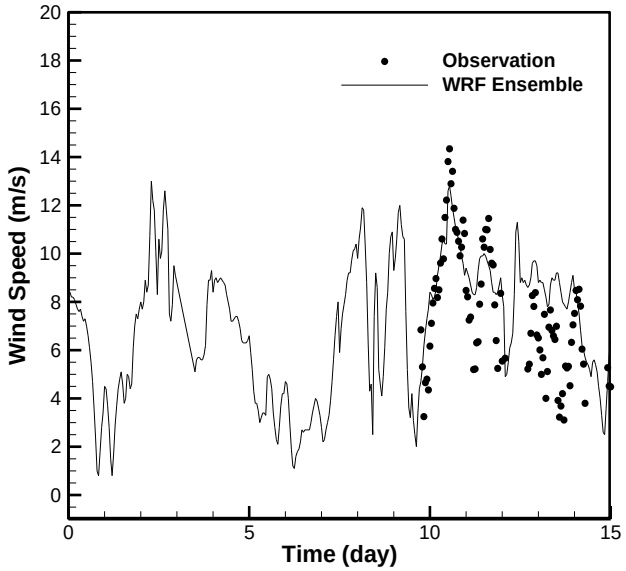

Figure 2. Time series (15 days, started at 12 UTC of 19-03-2016) of the ensemble mean predictions for wind speed at Bousher buoy (Lat: 28.828, Lon: 50.739). Observational data are also shown in figure.

Table 1. Values of CC and RMSE of surface wind speed (SPD) vector and its components for different dates.

Satellite	Date	SPD CC	SPD RMSE	U CC	V CC
OuikSCAT	10/2/2009	0.91	1.83	0.94	0.92
OuikSCAT	13/2/2009	0.88	1.56	0.73	0.68
OuikSCAT	16/9/2008	0.70	1.88	0.75	0.88
ASCAT	14/9/2008	0.94	1.32	0.95	0.69
ASCAT	16/9/2008	0.91	1.49	0.89	0.80
ASCAT	10/2/2009	0.89	0.76	0.89	0.97
ASCAT	21/2/2011	0.83	1.04	0.74	0.70
ASCAT	13/2/2009	0.74	1.18	0.64	0.79

MECHANISMS OF COASTAL FLOODS IN JAKARTA: THE NEED FOR IMMEDIATE ACTION AGAINST LAND SUBSIDENCE

Hiroshi Takagi[1], Miguel Esteban[2], Takahito Mikami[3], Daisuke Fujii[1], and Shota Kurobe[1]

1) School of Environment and Society, Tokyo Institute of Technology, Tokyo, Japan, takagi@ide.titech.ac.jp
2) Graduate School of Frontier Sciences, The University of Tokyo, Tokyo, Japan, esteban.fagan@gmail.com
3) Dep. of Civil and Environmental Engineering, Waseda University, Tokyo, Japan, takahito8765@gmail.com

1. Introduction

Jakarta, the capital of Indonesia, is one of the largest coastal megacities in the planet. Although Jakarta has been facing many urban development issues, the issue of land subsidence appears to have become especially serious over the last couple of decades. Recently, Takagi *et al.* investigated two distinctive mechanisms of coastal floods in Jakarta, hereinafter referred to as *widespread coastal flood* [1] and *dyke-break induced tsunami* [2], both of which are exacerbated by land subsidence. The present work will introduce both of these studies, and discuss how rapid land subsidence could have serious impacts on unprepared parts of Jakarta city.

2. Land Subsidence in Jakarta

The occurrence of land subsidence in Jakarta was clearly recognized as far back as 1978, when substantial cracks were found in buildings and a bridge in downtown Jakarta. The subsidence continues, with rates of 9.5 to 21.5 cm/year being measured along the coastline of the city in the period between 2007 and 2009, with groundwater extraction appearing to be the main cause for the lowering of the land. In particular, the extraction of water for industrial uses is a widespread practice which can induce rapid rates of land subsidence. Such subsidence can lead to severe damage to buildings and infrastructures, increase the extent of flooded areas, destroy local ground water systems or increase seawater intrusion [*e.g.* 3, 4, 5].

3. Widespread Coastal Flood

The extent of coastal floods by the year 2050 in Jakarta was projected using a coastal hydrodynamic model that considers sea-level rise (SLR), land subsidence, astronomical and abnormal tides [1]. The simulations demonstrate that by the middle of this century extensive floods could potentially reach several kilometers inland in Jakarta (Fig.1). Land subsidence is clearly one of the major challenges facing the city, as considering only the influence of SLR indicates that such floods may be limited to within a few hundred meters of the coastline. From 2000 to 2050 the potential flood extent is estimated to increase by 110.5 km^2 in the Jakarta Metropolitan Area.

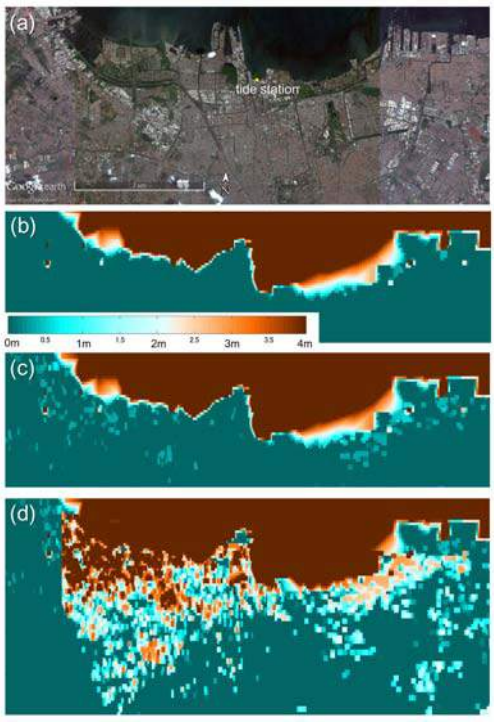

Figure 1. Potential inundation areas and depths, (a) satellite image of Jakarta, from Google Earth, (b) extent of coastal floods at the beginning of the 21st century, simulating the 2007 abnormal high tide, (c), (d) potential expansion of flood area in 2050 due to only SLR and SLR + land subsidence scenarios, respectively.

4. Dyke Break Induced Tsunami

Thin coastal dykes typically found in developing countries may suddenly collapse due to rapid land subsidence, material aging, SLR, high wave attack or a collision with vessels. Such a failure could trigger a *dyke-break induced tsunami*, a possibility which has so far been overlooked in the field of coastal disaster science and management [2, 6]. To analyze the potential consequences of one such flooding event caused by a dyke failure, a detailed hydrodynamic model was constructed based on the authors' field surveys of a vulnerable coastal location in Jakarta (Fig.2). Under a 2-m land subsidence scenario –

which is expected to take place in the study area after only 10 years, the model results show that the flood waters could rapidly rise to a height of nearly 3 m, resembling the flooding pattern of earthquake-induced tsunamis. The depth–velocity product criteria suggests that many of the narrow pedestrian paths behind the dyke could experience strong flows, which are far greater than the safe limits that would allow pedestrian evacuation [2, 7].

Figure 2. Pluit District is situated below sea level. The thin dyke protecting the settlement was raised by about a meter after the 2007 high tide event. The bay serves as a port for many fishing and work vessels (Photo: May 13, 2016).

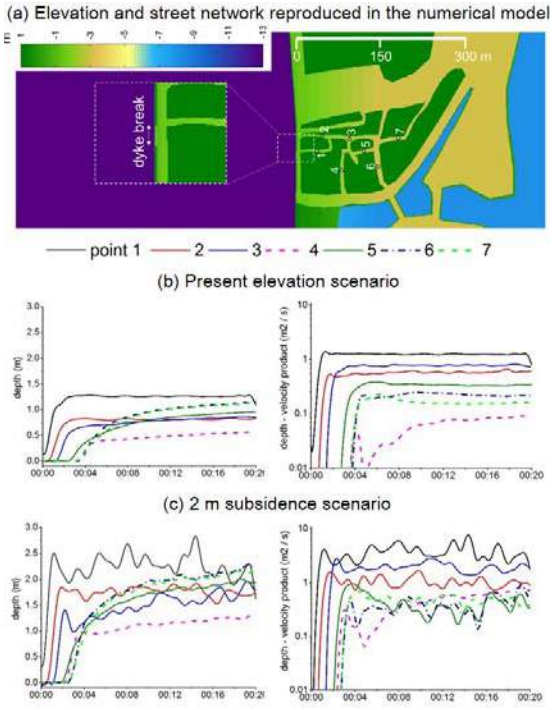

Figure 3. (a) Elevation map, measured from the maximum sea level. The numbers 1 through to 7 indicate the output points of the computational results. (b), (c) Simulated water depth (left) and depth – velocity product (right) for present elevations and 2-m land subsidence scenario, respectively.

5. Discussion and Conclusions

The numerical analysis suggests that land subsidence is responsible for 88% of the potential coastal flooding [1]. The results also indicate that the rate of expansion in the area that could be potentially flooded in the 2025–2050 period would be 3.4 times faster than during the 2000–2025 period, demonstrating a non-linear exponential increase in flood risk with the passage of time.

The possibility of a dyke-break induced tsunami is far more likely than that of a regular earthquake tsunamis. In the 2-m subsidence scenario, expected to be reached within the next 10 years, the depth-velocity products exceed the pedestrian evacuation limit of 1 m^2/s throughout the town, and could seriously endanger the life of any resident in the streets [2, 7].

The results of the authors' recent studies [2, 6, 7] clearly highlight that effective actions against land subsidence need to be implemented as a matter of urgency. Although some coastal engineering countermeasures such as raising dykes or floodgate construction could provide some immediate relief to mitigate the likelihood of flooding taking place, their effectiveness will quickly reduce if land subsidence is not stopped.

6. Acknowledgements

Funding for this research was supported by the Environment Research and Technology Development Fund (S-14) of the Ministry of the Environment, Japan.

7. References

[1] Takagi H., Esteban M., Mikami T., Fujii D. Projection of coastal floods in 2050 Jakarta, *Urban Climate*, 2016.

[2] Takagi H., Mikami T., Fujii D., Esteban M. Mangrove forest against dyke-break induced tsunami in rapidly subsiding coasts, *Nat. Hazards Earth Syst. Sci. Discuss.*, 2016.

[3] Djaja R., Rais J., Abidin Z. H., Wedyanto K. (2004) Land subsidence of Jakarta Metropolitan Area, *3rd FIG Regional Conference*, Jakarta, Indonesia, 14p., 2004.

[4] Chaussard E., Amelung F., Adibin H., Hong S-H. Sinking cities in Indonesia: ALOS PALSAR detects rapid subsidence due to groundwater and gas extraction, *Remote Sensing of Environment*, 128, pp.150-161., 2013.

[5] Ng A.H-M., Ge L., Li X., Abidin H. Z., Andreas H., Zhang K. Mapping land subsidence in Jakarta, Indonesia using persistent scatterer interferometry (PSI) technique with ALOS PALSAR, *International Journal of Applied Earth Observation and Geoinformation*, 18, pp.232-242., 2012.

[6] Esteban M., Takagi H., Mikami T., Aprilia A., Fujii D., Kurobe S. Awareness about tsunamis and dyke-break induced tsunami in low-lying coastal communities in Jakarta, *The proceedings of the ICOPMAS 2016*, Tehran, Iran, 2016. (submitted)

[7] Mikami T., Takagi H., Esteban M., Fujii D., Kurobe S. Evacuation simulation for a vulnerable coastal community in Jakarta, *The proceedings of the ICOPMAS 2016*, Tehran, Iran, 2016. (submitted)

MODELLING OF LAST RECENT TROPICAL STORMS IN THE ARABIAN SEA

Arash Bakhtiari[1], Mohammad Reza Allahyar[2], Morteza Jedari Attari [3], Syed Abbas Haghshenas[4], Mohammad Bagheri[5] Shima Droudi[6]

1) Project engineer, Middle East Water and Environment Co., Tehran, Iran, Email: arash.bakhtiary@gmail.com
2) Iranian Ports and Maritime Organization, Tehran, Iran, Email: allahyar@pmo.ir
3) Project engineer, Middle East Water and Environment Co., Tehran, Iran, Email: mortezajedariattari@yahoo.com
4) Assistant Professor, Institute of Geophysics, University of Tehran, Iran, Email: sahaghshenas@ut.ac.ir
5) Iranian Ports and Maritime Organization, Tehran, Iran, Email: mbagheri@pmo.ir
6) Project engineer, Middle East Water and Environment Co., Tehran, Iran, Email: Shima.doroudi@modares.ac.ir

1. INTRODUCTION

The Oman Sea waters and coastline is subjected to tropical cyclones (TC) influence on an infrequent basis; however, these cyclones can generate relatively large sea states. At many locations along this coastline, particularly in the southern and northern central and eastern parts or areas of the coast, tropical cyclone waves are the dominant coastal design wave condition as the wave heights can exceed those generated from other meteorological phenomena, such as the monsoon and the northerly Shamals.

Thereupon, a better understanding of tropical cyclones (TC) and hurricane hazards in this area will help to make a more informed decision on your risk and what actions to take.

In this study, as part of the sixth phase of Monitoring and Modeling Study of Iranian Coasts, the assessment of tropical cyclone risks along the Iranian coasts of Arabian Sea and Gulf of Oman have been studied.

The study aims to improve the understanding of hazards posed by tropical cyclones to ports and harbors of the Makran coastline. The resulting risk information will allow beneficiaries and the government to better integrate risk considerations into infrastructure development and ex-ante disaster planning.

2. STUDY AREA

The regions to be studied in this study are coastal areas of Sistan & Baluchesan province. This coastline which is also called Makran Coasts is about 350 km stretching from Gwadar Bay at the border with Pakistan to Rapch Estuary at the border with Hormozgan Province (Figure 1).

Figure 1. Study area

3. MEASURED DATA

An invaluable data set recorded during the first phase of Monitoring and Modeling Study of Iranian Coasts (by PMO) includes wave characteristics measurements in 30 m depth at a location outside Chabahar Bay. Measurements at this location cover the period from September 2006 until early June 2007 immediately after the Cyclone Gonu event. The oscillating ocean currents have been captured in this data set. Moreover, wind and wave measurements were carried out offshore of Chabahar in 20 m water depth from 1998, and the effects of a cyclones that occurred from this were detected. A synoptic wind station in Chabahar area, also recorded winds characteristics.

4. HISTORICAL TROPICAL CYCLONES

For this project, we used the International Best-Track Archive for Climate Stewardship (IBTrACS) global tropical cyclone database to represent historical TC activity [2]. The IBTrACS database collates information on TC tracks and intensity from reporting agencies around the globe and provides a single authoritative database that can be used for climate analysis. Figure 2 shows the tracks contained within the IBTrACS dataset for the period 1974-2014 which are within 500 km of the Eastern End of the Oman Sea Coastline.

In addition to this set of data, TC tracks of India Meteorological Department (IMD) and re-analysed wind data extracted from ECMWF (ERA-Interim) data centre were also considered and analysed.

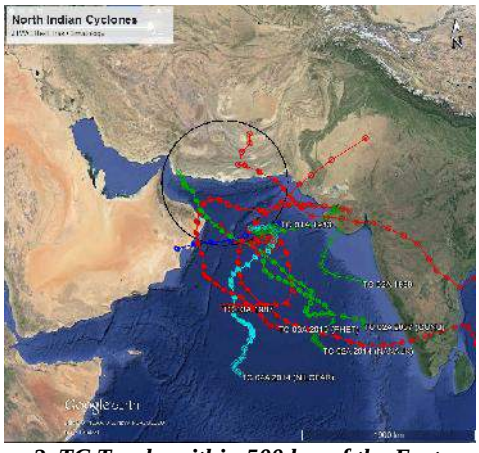

Figure 2. TC Tracks within 500 km of the Eastern End of the Oman Sea Coastline

5. NUMERICAL MODELING

The MIKE21-SW and Cyclone Wind Generation (CWG) package by DHI were used in the present work. Finding the most appropriate model configuration that can properly simulate large scale oceanic processes was a matter of trial and error. Applying various domains showed that obtaining reasonable results requires adopting a domain far larger than the study area boundaries. The mesh size, and models parameters also play significant role in the validity of the model results. Figure 3 shows the final selected model domain which extends to the southern hemisphere.

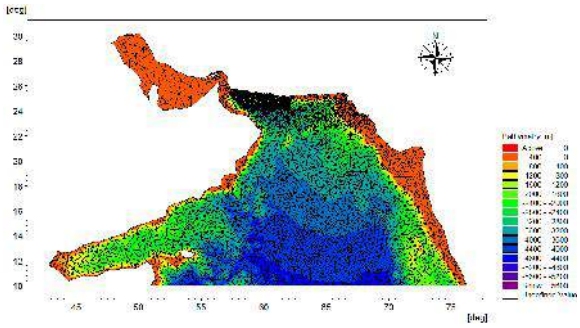

Figure 3. Computational domain

4. SAMPLE RESULTS and DISCUSSION

A detailed investigation of wind and waves generated by tropical cyclones has been carried out for the Oman Sea coastline of Iran. Model setup for CWG model is selected by using three major tropical storms happened in the Oman Sea and the Indian Ocean since 2007 including GoNu, Phet, and Niloufar cyclones. Generated winds were calibrated against measured wind data (Figure 4). Regenerated wind field for all storm (2007) was introduced to MIKE21-SW model and wave parameters were hindcasted at Chabahar measurements over Iranian Coastline of the Oman Sea. Figure 5 depicted comparison of modelled and measured wave characteristics of Gonu Cyclone. Regenerated waves are in reasonable agreement with observations in height and direction, but more attention should be paid for improving the accuracy of simulated wave periods.

The following conclusions and recommendations were developed based on the analyses and modeling performed in this study:

1. Based on measured wind data, IBTrACS data are the most appropriate data set to regenerating of recorded TC in this study area.
2. Regenerated wind field of each cyclone were slightly under estimated rather than measured data.
3. Wave height and direction were reasonably compatible with recorded data in the study area.
4. Wave periods need to be investigated more carefully in order to achieve an adequate accuracy.
5. Reanalysis wind field data such as ERA-Interim (obtained from ECMWF) are not appropriate for wind field of cyclonic winds.

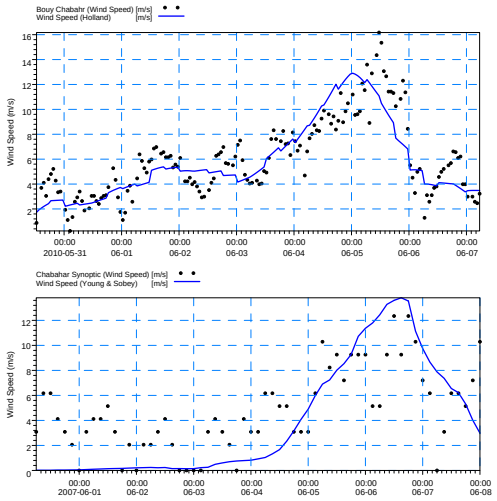

Figure 4. Comparisons between wind speed of Chabahr Buoy data (black points) and Wind Generation model results (blue solid line) during cyclones Phet (above) and Gonu (below).

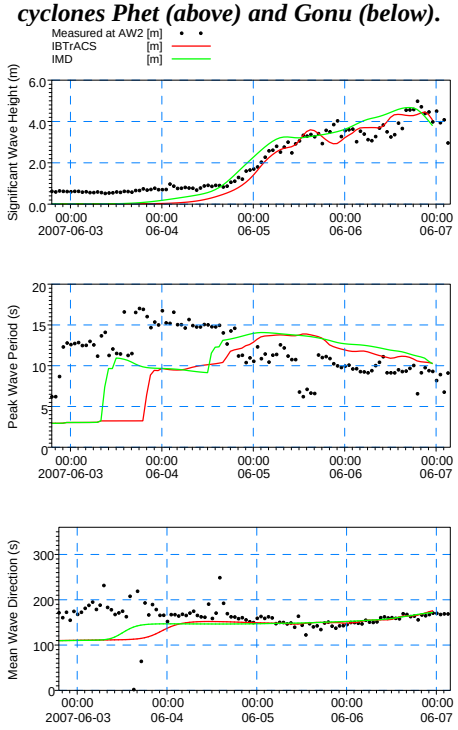

Figure 5. Comparisons between wave characteristics of AW2 data (black points) and SW model results (solid lines) during cyclone Gonu for two wind track sources.

5. ACKNOWLEDGEMENTS

The present work has been supported by the Port and maritime Organization (PMO).

6. REFERENCES

[1] Jahad Water and Energy Research Company (JWERC): Study reports of "Monitoring and Modelling Studies of Parts of Sistan, Balouchestan and Boushehr Provinces", Ports and Maritime Organization (PMO), 2008.

[1] Knapp, K. R., M. C. Kruk, D. H. Levinson, H. J. Diamond, and C. J. Neumann, 2010: The International Best Track Archive for Climate Stewardship (IBTrACS): Unifying tropical cyclone best track data. Bulletin of the American Meteorological Society, 91, 363-376.

MULTI-SCALE ANALYSIS OF AIR-SEA THERMODYNAMIC DISEQUILIBRIUM DURING TROPICAL CYCLONE (A CASE STUDY)

Nafiseh Pegahfar[1], Parvin Ghafarian[2]

[1,2]*Assistant Professor, Atmospheric Research Center, Iranian National Institute for Oceanography and Atmospheric Science, Tehran, Iran,*

[1]*pegahfar@inio.ac.ir; pegahfar@ut.ac.ir*

[2] p.ghafarian@inio.ac.ir

1. Introduction

Tropical cyclone (TC) has devastating impacts in the global tropics and sub-tropics. Hence, various physical parameters including dynamic and thermodynamic ones have been defined to show TC characteristics. Meanwhile, the role of enthalpy flux from the ocean in TC intensification has been marked ([1, 2]) and proved by observations, indicating that a TC (I) only develops where significant potential heat flux from sea exists, and (II) also decays over land even when plentiful amount of moisture and instability exist. The other thermodynamic parameter focused during TC lifetime is air-sea thermodynamic disequilibrium (ASTD) that has been applied in the calculation of potential intensity ([3]). In addition, ASTD can change radiative forcing affecting TC ([4]). Emanuel [4] also concluded that ASTD does not have any significant role in difference between potential intensity calculated using NCEP/NCAR and ERA40 dataset. This result emphasizes on the little variability of this parameter calculated using different datasets, as an advantageous of this parameter.

In the current study, ASTD has been calculated and analyzed in various scales during Haiyan tropical cyclone (TCH) nominated as a Category-6 TC ([5]). In the rest of this paper, at first the applied methods are presented. Afterward, data and TCH descriptions are explained. Finally, results and conclusions are discussed.

2. Methods

In the present study, ASTD parameter has been calculated using the relations suggested by Emanuel [4] as:

$$\mathrm{ASTD} = \mathrm{s}_0^* - \mathrm{s}_{600}^* \quad (1)$$

and

$$\mathrm{ASTD} = \mathrm{k}_0^* - \mathrm{k}_{10} = \frac{-\mathrm{F}_{\mathrm{rad}_0} + \mathrm{E}}{\mathrm{C}_\mathrm{k}\rho_{10}|\mathrm{V}_{10}|} \quad (2)$$

Here, s and k denote entropy and enthalpy, respectively. The asterisk belongs to saturated values and the subscripts of "0" and "10" denote values at surface and 10-m height, respectively. The enthalpy exchange coefficient has been shown by C_k. The energy source supplied by ocean and the energy flux produced by radiation have been shown by E and F_{rad}, in that order. To calculate entropy and enthalpy parameters, the relation defined by Bryan [6] for pseudo-adiabatic entropy has been used as:

$$s = \left(c_{pd} + c_l r_t\right)\ln(T/T_R) - R_d \ln(p_d/p_0) + \frac{L_{v0} r_v}{T} - R_v r_v \ln(H), \quad (3)$$

$$p_d = \rho_d R_d T, \quad \rho_d = 1.2.$$

Where the constants of $c_{pd} = 1005\, J/(kgK)$, $c_l = 4218\, J/(kgK)$ and $L_{v0} = 2.55 \times 10^{-6}\ J/kg$ are the specific heat at constant pressure for dry air, specific heat for liquid water and latent heat, respectively. The gas constants for water vapor and dry air have been included as $R_v = 461.51\, J/(kgK)$ and $R_d = 287.05\, J/(kgK)$, which the constants of $T_R = 273.15\, K$ and $p_R = 1000\, hPa$ denote freezing point of water and reference pressure, respectively. Also, the variables of T, p_d, H and r_v show temperature, partial pressure, humidity and water vapor mixing ratio, correspondingly. In addition, multi-scale analysis of ASTD has been done through focusing on various different-sized domains. For this aim, four domains of $1^o \times 1^0$, $2^o \times 2^0$, $4^o \times 4^0$ and $10^o \times 10^0$ have been designed surrounding the TCH eye location. The above domains represent eye, inner core, mesoscale features and environment of TCH, in that order. Reasons of choosing such dimensions have be proved by Dvorak [7], Weatherfort and Gray [8], Marin et al., [9] and Tang [10], correspondingly.

3. Data

In the current work, two dataset produced by (I) Japan Meteorology Agency and (II) NCEP-GFS have been used. The first dataset includes TCH eye location (latitude and longitude), while the second group consists of the global meteorological reanalysis data with $0.5^o \times 0.5^o$ horizontal resolution at 26 pressure levels with 6-h intervals. All data have been used during 03-11 November 2013.

4. Tropical cyclone Haiyan, TCH

TCH with the extra-ordinary intensity of 170 kts intensified as the highest ever observed TCs globally and reached 35 kts well above the threshold of 135 kts as the existing highest value for category-5 ([5]). Figure 1 shows 10-m wind vector at 1800 UTC 07 November 2013, before reaching the Philippines Islands.

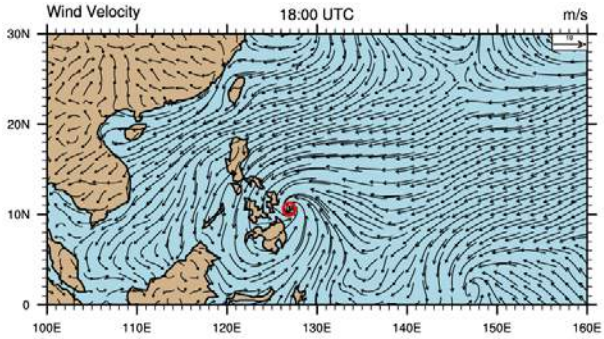

Figure 1. 10-m wind vector at 1800 UTC 07 November 2013. The red circle shows TCH eye location.

5. Results and discussion

ASTD parameter during TCH has been calculated and averaged over four domain areas of $1^o \times 1^o$, $2^o \times 2^o$, $4^o \times 4^o$ and $10^o \times 10^o$. Time series of averaged values for each domain has been depicted in figure 2a-d, respectively.

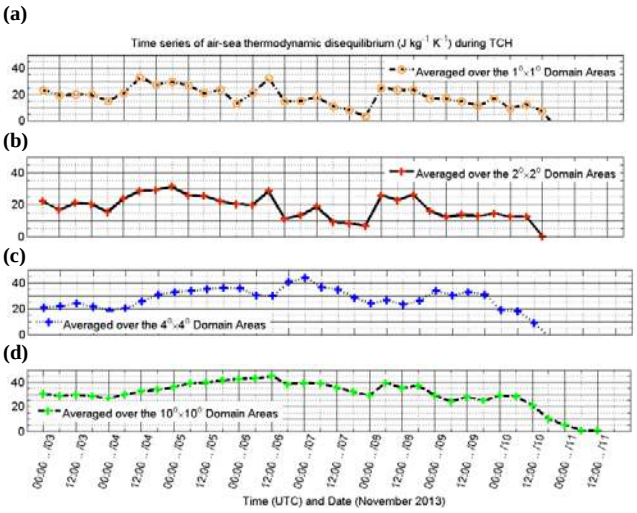

Figure 2. Time series of air sea thermodynamic disequilibrium values, averaged over the $1^o \times 1^o$, $2^o \times 2^o$, $4^o \times 4^o$ and $10^o \times 10^o$ domain areas.

The averaged values of ASTD over the two larger domains reached around 45 J/(K kg) with smoother behaviour, while those over the two smaller domains gained 35 J/(K kg). Also, trends for two smaller domains are similar. the latest time for zero value occurrence belongs to the largest domain. In addition, all subplots show an increasing-decreasing trend before TCH maximum intensity time (1800 UTC 07 November 2013). It is worthwhile to note that averaged values of ASTD over all mentioned domains maximized before TCH peak activity time, however with different time differences. For example, the maximum value of ASTD averaged over $10^o \times 10^o$ domain areas had about 42 hours lag, comparing with corresponding value over $1^o \times 1^o$ domain area. While the maximum and relative minimum values between $10^o \times 10^o$ and $4^o \times 4^o$ domains showed about 18 hours time difference. It is noteworthy that the earliest time of occurrence for the extreme values belongs to $1^o \times 1^o$ domain area, while the latest ones took place in $10^o \times 10^o$ domain area.

6. Conclusions

In the current work, ASTD parameter averaged over four different-sized domains ($1^o \times 1^0$, $2^o \times 2^0$, $4^o \times 4^0$ and $10^o \times 10^0$) have been analyzed during TCH (03-11 November 2013). The defined domains cover eye, inner core, mesoscale features and environment of TCH, respectively. This multi-scale analysis indicated that ASTD parameter averaged over all domains maximized before TCH peak activity time. Hopefully time difference between occurrence of TC peak activity and maximum of ASTD values averaged over various different-sized domains can be extended as a predicator for time of maximum intensity in a TC.

7. References

[1] Riehl, H., "A model for hurricane formation", *J. Appl. Phys.*, 21, 1950, pp. 917–925.

[2] Kleinschmidt, E., Jr., "Grundlagen einer theorie der tropischen zyklonen", *Arch. Meteor. Geophys. Bioklimatol*., 4A, 1951, pp. 53–72.

[3] Emanuel, K. A., "Sensitivity of tropical cyclones to surface exchange coefficients and a revised steady-state model incorporating eye dynamics", *J. Atmos. Sci*., 52, 1995, pp. 3969–3976.

[4] Emanuel, K., "Tropical cyclone activity downscaled from NOAA\CIRES reanalysis, 1908–1958", J*ournal of Advances in Modeling Earth Systems*, 2, 1, 2010.

[5] Lin, I. I., Pun, I. F., and Lien, C. C., " "Category-6" supertyphoon Haiyan in global warming hiatus: Contribution from subsurface ocean warming", *Geophysical Research Letters*, 41, 23, 2014, pp. 8547-8553.

[6] Bryan, G. H., "On the computation of pseudoadiabatic entropy and equivalent potential temperature", *Monthly Weather Review*, 136, 12, 2008, pp. 5239-5245.

[7] Dvorak, V. F., "Tropical cyclone intensity analysis and forecasting from satellite imagery", *Monthly Weather Review*, 103(5), 1975, pp. 420-430.

[8] Weatherford, C., and Gray, W.M., "Typhoon structure as revealed by aircraft reconnaissance. Part II: Structural variability", *Mon. Wea. Rev*., 116, 1988, pp. 1044-1056.

[9] Marin, J., Raymond, D., and Raga, G., "Intensification of tropical cyclones in the GFS model", *Atmos. Chem. Phys*., 9, 2009, pp. 1407–1417.

[10] Tang, B. H. A., "*Midlevel ventilation's constraint on tropical cyclone intensity*", Doctoral Thesis, Massachusetts Institute of Technology, 2010.

INVESTIGATION OF TSUNAMI HAZARD IN JASK PORT DUE TO LARGEST POSSIBLE EARTHQUAKES OF MAKRAN SUBDUCTION ZONE

Ehsan Rastgoftar, Mahmood Reza Akbarpour Jannat, Rasoul Ghanbari, and Mani Moghadam

1) Iranian National Institute for Oceanography and Atmospheric Science, Tehran, Iran, e.rastgoftar@inio.ac.ir
2) Iranian National Institute for Oceanography and Atmospheric Science, Tehran, Iran, akbarpour@inio.ac.ir
3) Ports and Maritime Organization, Tehran, Iran, rasoul.ghanbari@yahoo.com
4) Ports and Maritime Organization, Tehran, Iran, mani.moghadamm@gmail.com

1. Introduction

Two huge tsunamis of the present century have attracted the attention of researchers to this oceanic phenomenon. Although tsunamis can be generated by variety of different sources like earthquakes, submarine landslides, volcanic eruptions and meteorite impacts, but subduction zones earthquakes are known as the most common source of tsunamis. One of the earth's subduction zones is Makran Subduction Zone (MSZ) that is located at the northwest of Indian Ocean near southern coasts of Iran and Pakistan. The results of the research carried out recently based on thermal modeling of the MSZ, have shown that past assumptions may have significantly underestimated the earthquake and tsunami hazard in the MSZ; and it is potentially capable of producing major earthquakes, up to Mw 8.7-9.2 [1]. Hence, the probability of recurrence of seismic tsunami in the Makran zone is relatively high and it can be considered as an obvious hazard for neighboring countries, like Iran.

Jask Port is one of the most important coastal areas of Iran, regarding to its population and strategic situation. It is located at the west of Makran zone and can be affected by possible tsunamis. In order to assess tsunami hazard, the impact and run-up of MSZ seismic tsunamis, caused by largest possible earthquakes, on Jask Port is simulated in this study. For this purpose, GEOWAVE known as a comprehensive numerical tsunami model is applied.

2. Earthquake Scenarios

For tsunami modeling, earthquakes having magnitude of 9.1Mw and 8.7Mw are considered. During the 9.1Mw earthquake, the MSZ should experience the full rupture to obtain relevant seismic moment; while in order to produce the moment magnitude of 8.7Mw about half of the plate boundary should be faulted. In the latter case, the western or eastern part of the MSZ can be faulted, according to the earthquake epicenter. Since estimation of future earthquakes place is impossible, the 8.7Mw earthquake is considered both at the western and eastern segments of the MSZ in the intended scenarios (see Table 1). In each scenario, the source parameters defining faulted area dimensions are estimated using empirical relationships [2].

Table 1. Considered scenarios for MSZ earthquakes.

Scenario	Earthquake magnitude and faulted area	Faulted area dimensions		
		L (km)	W (km)	S (m)
1	9.1 Mw All part of MSZ	900	70	25
2	8.7 Mw Western part of MSZ	500	50	14
3	8.7 Mw Eastern part of MSZ	500	50	14

3. Numerical modeling

In the beginning of numerical simulations, TOPICS, tsunami generator model of GEOWAVE, calculates initial disturbance of ocean surface using Okada's elastic deformation source model [3], as shown in Figure 1a.

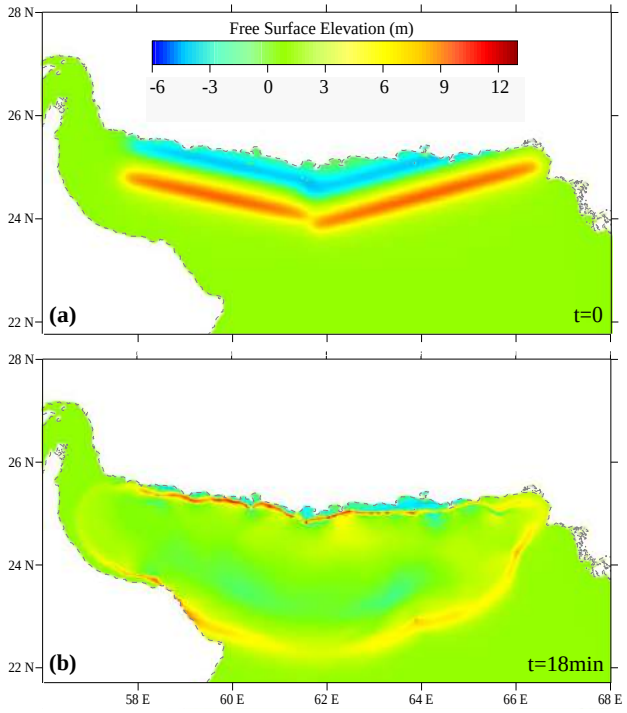

Figure 1. Snapshots of tsunami waves under scenario 1 a) immediately after earthquake b) on the verge of impact on Jask Port.

Free surface elevations obtained from TOPICS provide initial condition of the tsunami propagation model, FUNWAVE; which is based on fully nonlinear and dispersive Boussinesq equations developed by Wei et al. [4]. Numerical simulations in this study are performed in two distinguish models, i.e. global and local models. The global model encompasses throughout of the MSZ; while the local one, based on 3-arc sec resolution topography and hydrographic data, focuses on Jask Port and its surrounding areas. Firstly, in the global model initial wave of tsunami is generated and it propagates from the faulted area to the coastlines. Then, when the waves reach to in vicinity of Jask Port coasts (Figure 1b), the local model is started to capture tsunami impact on coastal area and possible inundation.

4. Conclusion

According to results of numerical wave gauges, as expected, the maximum wave heights are observed in scenario 1 that represents the largest earthquake. During scenario 3 tsunami waves appear at the gauges much smaller than two other scenarios. For example, one gauge has recorded about 14 and 10 meters height waves in scenario 1 and 2, respectively. While the maximum wave height observed in this gauge in scenario 3 is less than 0.4 meter. The reason is that when earthquake occurs at the eastern part of MSZ, the tsunami waves reaches slightly along the western coasts of the Makran zone, like Jask Port; because the tsunamis caused by earthquakes spread perpendicular to the source fault, i.e. in the north-south direction in MSZ.

Maximum tsunami heights recorded during scenarios 1 and 3 are presented in Figure 2, which also displays the tsunami inundation extent for all the scenarios. It is observed that the waves due to the 8.7Mw eastern Makran earthquake (scenario 3) cannot run-up on Jask Port at all. However, the waves caused by the 9.1Mw earthquake (scenario 1) and the 8.7Mw western Makran earthquake (scenario 2) not only inundate the port completely, but also attack on farther inland areas. Therefore, it can be concluded that the most crucial factor determining the tsunami risk in the Jask Port is the location of the Makran earthquakes. In other words, the huge earthquakes occur at east of MSZ can be considered as small hazard for Jask Port, while the occurrence of earthquakes having less magnitudes at west of MSZ leads to the high waves able to devastate the port seriously. While it was previously thought that the tsunami effect depends essentially on the earthquake magnitude.

Figure 2 also shows although the most coastal areas around the Jask Port are inundated by the tsunami waves in scenarios 1 and 2, but there are also regions where are safe against the tsunami waves (shown by circles). As adjacent areas of the Jask Port are considered for development in future plans of Makran zone, the estimated safe regions seems advisable regarding to tsunami threat.

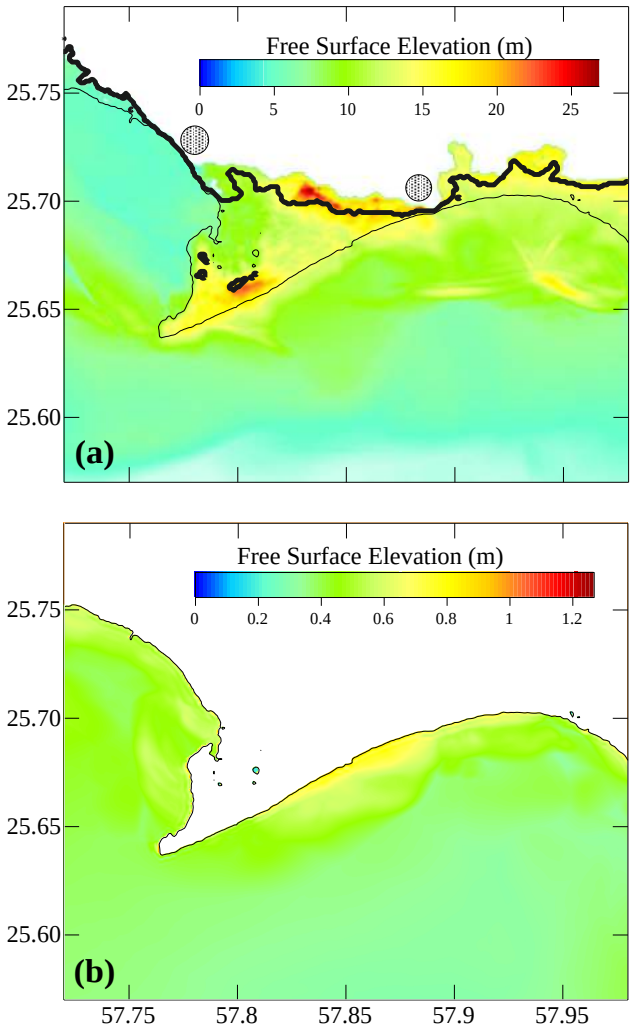

Figure 2. Maximum tsunami heights under a) scenario 1 b) scenario 3. Bold line represents the inundation line of scenario 2. The circles mark the regions are safe against the tsunami waves.

5. References

[1] Smith, G. L., McNeill, L.C., Wang, K., He, J., and Henstock, T.J., "Thermal structure and megathrust seismogenic potential of the Makran subduction zone", *Geophysical Research Letters*, 40, pp. 1528-1533, 2013.

[2] Wells, D. L., and Coppersmith, K. J., "New empirical relationships among magnitude, rupture length, rupture width, rupture area, and surface displacement", *Bulletin of the Seismological Society of America*, 84, 4, pp. 974-1002, 1994.

[3] Okada, Y., "Surface deformation due to shear and tensile faults in a half space", *Bulletin of the Seismological Society of America*, 75, 4, pp. 1135-1154, 1985.

[4] Wei, G., Kirby, J.T., Grilli, S.T., and Subramanya, R., "A fully nonlinear Boussinesq model for free surface waves. Part 1: Highly Nonlinear Unsteady Waves", *Journal of Fluid Mechanics*, 294, pp. 71-92, 1995.

AWARENESS ABOUT TSUNAMIS AND DYKE-BREAK INDUCED TSUNAMI IN LOW-LYING COASTAL COMMUNITIES IN JAKARTA

Miguel Esteban[1], Hiroshi Takagi[2], Takahito Mikami[3], Aretha Aprilia[4], Daisuke Fujii[2], and Shota Kurobe[2]

1) Graduate School of Frontier Sciences, The University of Tokyo, Tokyo, Japan, esteban.fagan@gmail.com
2) School of Environment and Society, Tokyo Institute of Technology, Tokyo, Japan, takagi@ide.titech.ac.jp
3) Dep. of Civil and Environmental Engineering, Waseda University, Tokyo, Japan, takahito8765@gmail.com
4) CDM Smith, Mr 21 Bldg. , Jakarta, Indonesia, aretha.a@gmail.com

1. Introduction

Jakarta is one of the largest coastal megacities in the planet. Due to decades of groundwater extraction, large parts of its coastal zone are currently below mean water level, creating a variety of problems for municipal authorities [1, 2]. Actually, land subsidence in the city was recognized as far back as 1978, when substantial cracks were found in buildings and a bridge in the downtown area. This subsidence continues nowadays, with rates of around 9.5 to 21.5 cm/year being measured along the coastline of the city in the period between 2007 and 2009. In particular, the extraction of water for industrial uses is a widespread practice, which can typically lead to rapid rates of land subsidence. Such subsidence can result in severe damage to buildings and infrastructures, increase the extent of flooded areas, destroy local ground water systems and increase seawater intrusion [1, 2, 3].

One of the worst flooding events took place in 2007, when abnormally high tides brought about the flooding of many coastal areas [4,5], including the Pluit District, which is situated below sea level. As a result, the dyke protecting this settlement was raised by about one metre (see Fig. 1). However, these dykes appear extremely fragile and, given their current size, if they were to break they could create a *dyke-break induced tsunami* [5]. Simulations show that, for a 2-m land subsidence scenario (which can be expected in the area in the next 10 years), flood waters could rapidly rise to a height of nearly 3 m, resembling the flooding pattern of earthquake-induced tsunamis [6]. The depth–velocity product criteria suggests that many of the narrow pedestrian paths behind the dyke could experience strong flows, which are far greater than the safe limits that would allow pedestrian evacuation [5, 7].

Residents of these areas have experienced many coastal flooding events in recent times, though the authors of this paper fear that as land continues to subside and dykes are built to higher levels, the possibility of a catastrophic *dyke-break induced tsunami* will increase. This will be extremely dangerous as the time available for evacuation and turbulence of the water would be much greater than what residents have been exposed to in the past. To ascertain the level of awareness of residents about such issues, the authors conducted questionnaire surveys to in one of the areas that could be worst affected. Such research is particularly important given that the area is one of the most impoverished in Jakarta, and the link between resilience and inequality, and resilience to infrastructure is one that has received comparative little attention in the past [8].

Figure 1. Thin concrete dyke protecting the Pluit District in Jakarta. Photo was taken at low tide, showing how water is already above the ground level in the district. (Photo: May 13, 2016).

2. Methodology

The authors, together with 3 local enumerators, conducted a structured questionnaire survey amongst local residents of the Pluit area, with the intention of measuring the level of awareness to tsunamis, storm surges, and *dyke-break induced tsunami*. The interviews were conducted on the 13-14th May 2016, and resulted in a collection of 200 valid responses (n=200). The structured questionnaire was originally drafted in English and then translated into Bahasa Indonesia, the national language of Indonesia. The questionnaire was then administered by the enumerators to individuals encountered in the Pluit area on an opportunistic basis, taking about 10 minutes per individual to complete.

3. Results

85.5% of respondents had experienced some form of damage that was caused by coastal flooding, and 44% of indicated that this coastal flooding occurs once every few years. It was thus clear that respondents had strong awareness and frequent exposure to the types of hazards present in the area.

However, awareness about the strength of the dykes seemed somehow misplaced. Visual inspections and professional judgement by the authors indicated that these dykes were rather weak, and could catastrophically fail if overtopped, especially under high overtopping flow rates. Nevertheless, when asked to rate the strength of the dykes on a 5-point Likert scale (from "very weak" to "very strong"), 56.5% and 24.5% of respondents rated them as "very strong" or "somewhat strong".

If the dykes in the area were broken, 73.5% of respondents stated that the flood water would reach the settlement within less than 1 minute; and 24% that the flood water would reach them within 2-10 minutes. This would appear to be an accurate assessment, as computer simulations show that the area would indeed be flooded within just a few minutes [5]. Thus, it appears that respondents were acutely aware that seawater is only a few dozen metres away from their houses, despite the dyke obstructing their vision of the water behind it.

Also, it appears that many respondents understood that if the dykes were broken water could reach a height of 2-3 m (the approximate height of a one-storey house, 41% of respondents). However, worryingly 39% of respondents stated that such levels would only be 1-2m. This might have been true in the past, though due to ongoing land subsidence levels are almost certain to be much higher.

Again, it is concerning that 27.5% of respondents stated that water flow speed would be moderate, and that it would possible to swim in it. While this was probably true for past events, the more that land subsides the higher the speed the water will reach in the event of a dyke break. However, it is worth noting that 51.5% of respondents stated that the water flow would be impossible to swim in.

Regarding evacuation in case the dykes were breached, 36% of respondents stated that they would go inside the nearest building and climb as high as they could; go towards their houses and try to find their family members (40.5%); try to walk to the higher regions in the nearby areas (29%); try to get into their car, motorcycles, or bicycles, for evacuation (6%); with a variety of other answers provided (including "do not know", "evacuate", "ride a ship" (22%)).

Regarding adaptation measures, respondents indicated that the local government should strengthen the existing dykes by making them stronger and bigger (91.5%); Build the Giant Sea Wall in the Jakarta Bay (49%); Plant mangroves in front of the dykes (8%); Elevate the entire area in all districts (4%); Build higher and stronger buildings for disaster evacuations (9%); Relocate all houses and people to safer locations (2%); and other answers, such as garbage clean-ups, improve drainage system, irrigation, construction of dams (3%).

4. Discussion and Conclusions

The possibility of a dyke-break induced tsunami in the case study area could be potentially very dangerous. If the area sinks by another 2m (likely to happen within the next 10 years), the depth-velocity products would exceed the pedestrian evacuation limit of 1 m^2/s throughout the settlement of Pluit, which could seriously endanger the life of any resident caught in the streets [4, 5, 7].

However, given a number of relatively recent flooding events which caused comparatively little damage, residents appear unaware about the extreme danger that they could face if the fragile dykes were to fail. In order to solve this problem it is imperative that significant remedial action is taken, to ensure the safety of residents and their property. First and foremost pumping of groundwater should be stopped to prevent future subsidence, though higher dykes and the elevation of entire coastal areas would probably also be necessary for placed like Pluit.

5. Acknowledgements

Funding for this research was supported by the Environment Research and Technology Development Fund (S-14) of the Ministry of the Environment, Japan.

6. References

[1] Djaja R., Rais J., Abidin Z. H., Wedyanto K. (2004) Land subsidence of Jakarta Metropolitan Area, *3rd FIG Regional Conference*, Jakarta, Indonesia, 14p., 2004.

[2] Chaussard E., Amelung F., Adibin H., Hong S-H. Sinking cities in Indonesia: ALOS PALSAR detects rapid subsidence due to groundwater and gas extraction, *Remote Sensing of Environment*, 128, pp.150-161., 2013.

[3] Ng A.H-M., Ge L., Li X., Abidin H. Z., Andreas H., Zhang K. Mapping land subsidence in Jakarta, Indonesia using persistent scatterer interferometry (PSI) technique with ALOS PALSAR, *International Journal of Applied Earth Observation and Geoinformation*, 18, pp.232-242., 2012.

[4] Takagi H., Esteban M., Mikami T., Fujii D. Projection of coastal floods in 2050 Jakarta, *Urban Climate*, 2016.

[5] Takagi H., Mikami T., Fujii D., Esteban M. Mangrove forest against dyke-break induced tsunami in rapidly subsiding coasts, *Nat. Hazards Earth Syst. Sci. Discuss.*, 2016.

[6] Takagi H., Esteban, M., Mikami T., Fujii D., Kurobe, S. Mechanisms of Coastal Floods in Jakarta: The Need fof Immediate Action Against Land Subsidence. *The proceedings of the ICOPMAS 2016*, Tehran, Iran, 2016. (submitted)

[7] Mikami T., Takagi H., Esteban, M., Fujii D., Kurobe, S. Evacuation Simulation for a Vulnerable Coastal Community in Jakarta. *The proceedings of the ICOPMAS 2016*, Tehran, Iran, 2016. (submitted)

[8] Le Blanc, D., Freire, C., Jussila, R., Vaturi, T. Chapter 2: The infrastructure - inequality - resilience nexus. Global Sustainable Development Report, 2016.

CASPIAN RAPID SEA LEVEL CHANGING IMPACT ON EROSION HAZARD OF ASTARA

Homayoun Khoshravan[1]

Coastal management Group, Caspian Sea research center, Sari, Country, Email: h_khoshravan@yahoo.com

1. Introduction

Global warming have been caused sea level rising since the past centurey and erosion events were concentrated in coastal area as high destructive beach zone[1]. The intensity of erosion vulnerability is associated to waves regime, currents development and beach type in coastal zone[2]. Caspian Sea rapid sea level changing has caused the sea level fluctuation about 6 meter between 1930- 1995 and vast shore line displacement had been happened during this period[3]. Caspian Sea level fluctuation trend likely is 100 time more than other open seas and ocean in the world[4]. So hydrological behaviour of Caspian Sea is different to ocean hydrodynamic[5].the evaluating of erosion hazard risk in Astara coast is the main target. Infact it is vital question how did the Astara beach behave to Caspian rapid sea level changing? And how can calculate the erosion vulnerability intensity in Astara port? And what are the most important morphodynamic formation near the Astara port? So by use the GIS and RS technology and field survey along the beach and shore and laboratory tests, the main result have been obtained.

.

2. Material and Method:

2.1. Study area

Astara city was located in the South- western coasts of the Caspian sea and it is vital port territory in the Gilan province(fig 1). This area was situated in wetern Gilan morphological zone[4]. The important landuse spreading in the Astara have been caused more govermnet economic attention and coastal zone engineering program has implemented in this region since 1980. The last sea level arise of the Caspian Sea has damaged some economic vital territories of Astara city and vast coastal zone was annundated by sea flooding. Now there are vast lowland beach in Astara which is too vulnerable to erosion hazard.

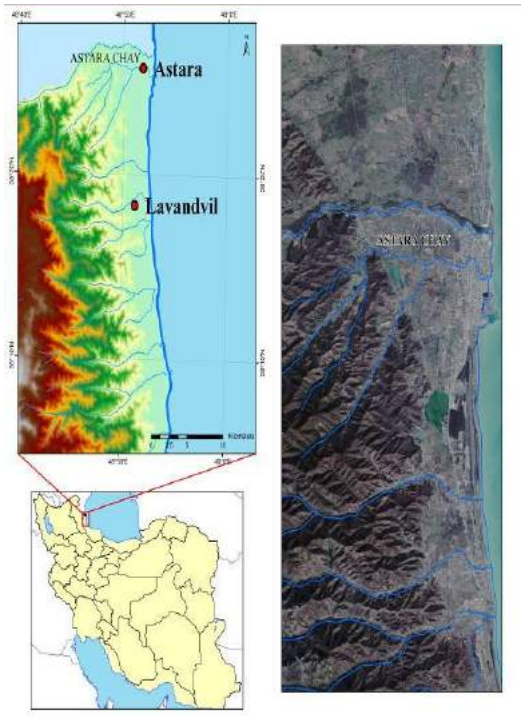

Fig1- Astara morphology and geography location map

2.2. Method

The morphological formations were determined with sattellite image interpretation and sedimentary morphodynamic condition was monitored. Beach profile geometry was measured by maping and Hydrography method

and sedimentry texture has been studied in laboratory. Shorelind displacement and erosion rate has been calculated in Arc- GIS with periodic sattelite images during 1966- 2015. Then by overlaying Caspian sea level changing data on digital elevation model map of study area (DEM), the fluctuation senarios were created and several morphodynamic changing have been simulated.

3. Result and discussion

3.1. beach structure geometry

Beach geometry and profiling survey in Astara shows a gentel steepness on the shore(fig 2) and the sea floor sediments contain fine to very fine sand. Accretion process has dominated near to north(fig 3-left) of port and eroding has been developed at the south beach(fig 3- right).

Fig 2. Beach profile of Astara

Fig 3. Morphodynamic condition in the Astara beach

3.2. shoreline displacement

The sattelite image comparing between 1966-2015 shows the different response of shoreline and shoreline displacement trend is unique in Astara coast due to high gentle beach steepness and beach erosion vulnerability have been increased during the Caspian sea level rose. So the degree of erosion vulnerability and erosion hazard is so high in Astara and antropogenic impact due to harbor construction caused erosion rate increasing in southern part of Astara port. The obtained results of DEM map in GIS confirmed that increasing sea level of the caspian Sea about two meter may cause anunduation and flooding of coast area land use approximately 300000 m^2 and it will be the huge economic issue along the Caspian sea coasts(table 1). and next increasing of the Caspian sea level may be dangerous events.

Table1- Caspian sea level fluctuation senario model

Annundation grade(m^2)		Accretion grade(m^2)	
96347	**1 meter incease**	**186465**	**1 meter decrease**
202898	**1.5 meter increase**	**352253**	**1.5 meter decrease**
312503	**2 meter increase**	**504395**	**2 meter decraese**

4. References

[1]Feng., S. et al, 2014, Projected climate regime shift under future global warming from multi- model and multi scenario CMIP5 simulation, Global and planetary change, Vol 112, PP 41- 52

[2]Rogers, J., Jarratt, O., Astle, G. 2007. national coastal erosion risk mapping user verification, international conference on coastal management, thomas telford, London, PP 89- 108

[3]Kroonenberg., S. B. et al, 2000, A full sea level cycle in 65 years: barrier dynamics along Caspian shores, sedimentary Geology, Vol 134, PP 257- 274

[4]Khoshravan, H. 2007. Beach sediments, Morphodynamics, and risk assessment Caspian Sea coast, Iran, Quaternary international journal, 167-168, pages 35-39

[5]Rychgov., G.I., 1997, Holocene oscillation of the Caspian Sea, and frocast based on paleogeographical reconstruction, Quaternary international, Vol 41/42, PP 167- 172

CLASSIFICATION OF BARRED AND UNBARRED BEACH PROFILES IN THE CASPIAN SEA

S. Ataei H.[1], M. A. Lashteh Neshaei[2] and M. Adjami[3]

[1] MSc of Coastal Engineering, Shahrood University of Technology, Shahrood and Center of Young Geniuses Support, Tehran, Iran, ataei.h.s@gmail.com
[2] Associate Professor of Civil Engineering Department, Guilan University, Rasht, Iran, maln@guilan.ac.ir
[3] Assistant Professor of Faculty of Civil Engineering, Shahrood University of Technology, Shahrood, Iran, adjami@shahroodut.ac.ir

1. Introduction

Nearshore bars are ubiquitous morphological features along many of the world's beaches. They are the main expression of hydrodynamic and sediment transport gradients, with bars developing as a result of sediment convergence and troughs forming in areas of sediment divergence. Nearshore bars are the most dynamic morphological element of the surf zone and hence they are a major topic of coastal research.

The separation between barred and non-barred profiles is generally related to the direction of cross-shore sediment transport. Offshore sediment transport results in erosion of the beach and the formation of barred profiles, whereas onshore sediment transport causes beach accretion and non-barred profiles (Figure1).

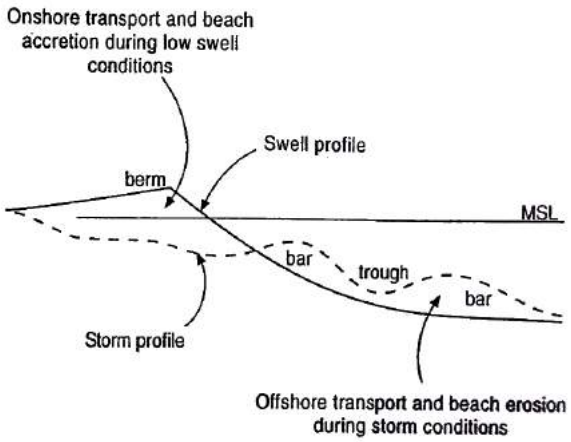

Figure 1. Idealized barred and non-barred beach profiles (AD Short, 1999).

2. Barred and Unbarred Beaches

Based on laboratory experiments according to equation (1), Gourlay (1980) introduced the dimensionless fall velocity to distinguish between non-barred beaches ($\Omega < 1$) and barred beaches ($\Omega > 1$).

$$\Omega = \frac{H_0}{w_s T} \tag{1}$$

A similar parameter to the dimensionless fall velocity was derived by Sunamura (1984):

$$K = \frac{H_b^2}{gT^2 D_{50}} \tag{2}$$

A K value of 10 separates barred and non-barred beaches. With $K > 10$ resulting in bar formation (Sunamura, 1989). Further analysis of large-scale laboratory data and also field data resulted in the formulation of a new profile parameter P (Dalrymple, 1992):

$$P = \frac{gH_0^2}{w_s^3 T} \tag{3}$$

For $P > 9000$ barred profiles develop and non-barred profiles from when $P < 9000$.

3. Bar Morphologies

Short and Aagaard (1993) reviewed the literature on multi-barred beaches and introduced a bar parameter (B_*) to predict the number of bars on nearshore profiles that can be approximated by a linear slope $\tan\beta$, terminating at a constant depth at a distance x_s from the shoreline:

$$B_* = \frac{x_s}{gT^2 \tan\beta} \tag{4}$$

On the basis of field data, Short and Aagaard (1993) suggested that no bars occur when $B_* < 20$, one bar occurs for $B_* = 20 - 50$, tow bars for $B_* = 50 - 100$, three bars for $B_* = 100 - 400$ and four bars for $B_* > 400$. The formulation of the bar parameter is based on the premise that standing infragravity waves are responsible for bar formation.

4. The Southern Coasts of the Caspian Sea

The southern coasts of the Caspian Sea were studied in this research. Necessary information such as the mean sediment particle size (D_{50}) and etc. of the southern coasts from Anzali, Dastak, Namakabrood, Mahmoodabad, Larim and also from Miankaleh were calculated by Ataei et al. (2016).

5. Analysis and Discussion

With regards to the proposed parameters for recognizing and categorizing the southern coasts of the Caspian Sea, the results of the equations (1) to (4) are illustrated in table 1.

Table 1 - Calculated data from Caspian Sea Parameters.

Parameter/Zone	Anzali	Dastak	Namakabrood	Mahmoodabad	Larim	Miankaleh
Ω	5.7	6.1	4.9	6.4	7.1	7.1
K	9.9	10.5	10.3	12.5	11.7	11.7
P	59920	75446	31487	72310	117072	117072
B_*	177.6	176.3	141.7	111.2	208.2	810.5

Considering the probability of cross-shore profiles formation in a period of one year, the related specifications to waves average were used in order to investigate the Caspian Sea's balanced nature of trends. According to table 1, the calculated values out of equations (1) to (3) for the coasts under study show that the cross-shore profiles of southern coasts of Caspian Sea are of the type of coast with the possibility of bar formation. Upon investigating the B_* value of the coasts under study, it is inferred that the value of this parameter is between 100 to 400 for coasts of Anzali, Dastak, Namakabrood, Mahmoodabad and Larim, which according to the aforementioned subjects, would observe the formation of three bars. Moreover, the value of this parameter is more than 400 for Miankaleh coast which means the cross-shore costs of Miankaleh would have four of more bars. In figure 2, the measured profiles of coasts under study are illustrated.

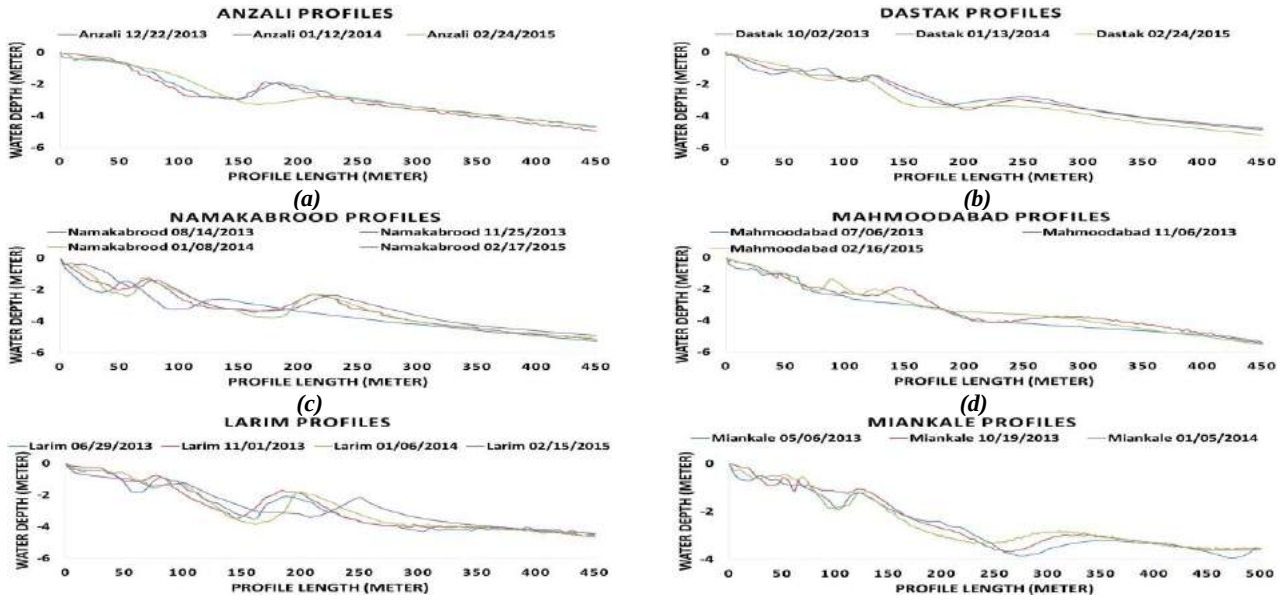

Figure 2. Caspian Sea coasts profiles (Caspian Sea National Research Center, 2015)

As it is observed in figure 2, in most of the profiles of Dastak, Namakabrood, Mahmoodabad and Larim coasts three bars have been formed. In addition, in most of Miankaleh's profiles, four bars have been formed. The only contrary trend to the predictions belongs to Anzali's profile, where only two profiles were formed.

6. Conclusion

Regarding the investigations done on the presented equations, the cross-shore profiles of Caspian Sea are of the coastal type with the possibility of bar formation.

The cross-shore profiles of Dastak, Namakabrood, Mahmoodabad and Larim belong to the type of coast with formation possibility of three bars, and cross-shore profile of Miankaleh is of the type of coast with formation possibility of four bars. Anzali's cross-shore profile, based on the calculations, is categorized as those of coasts with formation possibility of three bars; but the measured profiles only show the formation of two bars.

Bearing all the investigations in mind, the southern coasts of Caspian Sea is considered as the type of coast with possibility of bar formation and under storm conditions, three bars would be formed in most of its coasts.

7. Acknowledgment

We would like to thank the center of young Geniuses support for the moral support of this research.

8. References

[1] Dalrymple, R. A. (1992). Prediction of storm/normal beach profiles. Journal of waterway, port, coastal, and ocean engineering, 118(2), 193-200.

[2] Gourlay, M. R. (1980). Beaches: profiles, processes and permeability. Dept. of Civil Engineering, University of Queensland.

[3] Iran. Caspian Sea National Research Center. Data center.

[4] S. Ataei, H., M. Adjami, M. A. Lashteh Neshaei, & S. H. Ya'asubi, (2016). Investigation of sea level fluctuation on beach profile evolution of sandy coasts. MSc. Thesis, Faculty of Civil Engineering, Shahrood University of Technology.

[5] Short, A. D. (1999). Handbook of beach and shoreface morphodynamics. John Wiley & Sons.

[6] Short, A. D., & Aagaard, T. (1993). Single and multi-bar beach change models. Journal of Coastal Research, 141-157.

[7] Sunamura, T. (1984). Onshore-offshore sediment transport rate in the swash zone of laboratory beaches. Coastal Engineering, 27, 205-212.

[8] Sunamura, T. (1989). Sandy beach geomorphology elucidated by laboratory modeling. Elsevier Oceanography Series, 49, 159-213.

POTENTIALITY OF LAND RECLAMATION NEAR THE MOUTH OF MEGHNA ESTUARY OFF BANGLADESH THROUGH SATELLITE IMAGERY AND MATHEMATICAL MODELLING

G. M. Jahid Hasan[1]

1) Department of Civil Engineering, Military Institute of Science and Technology, Dhaka-1216, Bangladesh, jahid@ce.mist.ac.bd

1. Introduction

Land reclamation is the process to create new land from sea or riverbeds. Land accretion and erosion in the Meghna Estuary is a continuous and gradual natural process. The net average annual natural accretion is quite significant in the estuary mouth ranging 1200 ha/yr to 1900 ha/yr. In Bangladesh, land reclamation by closure or cross-dam construction in order to accelerate the natural accretion process started in mid-nineties. Physical intervention is required to accelerate the rate and area recovered. Regularly received satellite images and other tangible supporting evidences suggest that Bangladesh is about to receive of huge land areas from its adjoining coastal areas particularly near the mouth of Meghna Estuary. Last 40~50 years, several char islands (ie, Sandwip, Urir Char, Jahaizzer Char etc) has been formed by accretion of sediment carrying through the River Meghna. Aim of this study is to check the potentiality of gaining land areas through analysis of recent satellite images and numerical model development.

2. Location

Jahizzer Char is a newly accreted island located near the mouth of the Meghna Estuary bordering the Bay of Bengal to the south (Figure 1). Urir Char and Sandwip are located in the east and north of the Jahizzer Char. Urir Char and Sandwip are more stable as they formed relatively earlier than Jahizzer Char. Jahizzer Char has been fast expanding in south-west, south and south-east direction in to the Bay of Bengal. The char area is morphologically very dynamic and become entirely submerged during spring flood tide of monsoon and a large portion of it becomes bare during ebb tide of winter period.

3. Satellite Image Analysis

Several Landsat images of the year 1993, 2000, 2005, 2008, 2011, 2015 and also high resolution Rapid Eye images for the year 2011 and 2015 were collected to analyze. All the images were digitized to identify boundary between land and water, and trends of erosion-accretion. Analysis of images shows that the area has been experiencing huge erosion and accretion over the years and made the estuary mouth morphologically very dynamic as depicted in Figure 1. In the year 1990, Jahizzer Char did not exist, but in 2015 it covers approximately 300 km^2. From 2011 to 2015 about 5,310 ha land is accreted around the southern side of Jahizzer char. Also about 2576 ha land is eroded along the south and north-west side of the char. In 1993 Urir Char was divided into three parts but now it becomes one single char. The erosion-accretion pattern are summarized in Figure 2 and Table 1 as well.

4. Mathematical Modelling

The Bay of Bengal model has been developed to analyze the hydrodynamics around this region. The model extends from Chandpur on the Lower Meghna river in the north to about 160 Latitude in the Bay of Bengal in the south. The model is forced by discharges at Chandpur (northern boundary) and major tidal constituents in the Bay of Bengal (southern boundary). The model bathymetry based on charts and recent survey around Jahaizzer Char, Urir Char and Sandwip area. The southern part of the Bay of Bengal is quite deep and the maximum depth varies more than 3,000 m near open boundaries. Size of the computational grid decreases towards the coastlines and islands. The model includes flooding scheme to cover the inter-tidal areas. Recently surveyed data of water levels and currents were used to validate the model. The model produces very good agreement between field data and model data, and reflects the tidal dynamics around the area.

Table 1. Rate of accretion (+ve) and erosion (-ve) near the Meghna Estuary between 2011 to 2015 obtained through the analysis of satellite images.

Area	Erosion (ha)	Accretion (ha)	Net Change (ha)	Net Change/yr (ha)
Jahizzer Char	2576	5310	2734	683.5
Sandwip	0	743	743	185.75
Urir Char	435	1175	740	185
Noakhali Coast	4212	0	(-4212)	(-1053)

5. Concluding Remarks

Already, a substantial land mass has surfaced off the shore of Bangladesh, on some of these completely surfaced

land masses and human habitations are growing, while others emerge during the ebbing of the tide and go under water during the flood tides. The natural process of accretion being slow and can be accelerated by engineering, which is neither prohibitive in terms of cost nor complex, in technology terms. For Bangladesh, it would require establishment of structures like cross-dams to speed up the silt deposition pace in already accreted or nearly accreted areas. The hydrodynamic model identifies couple of tidal meeting zones around the study area, which could be potential places to construct cross-dams to speed up the natural accretion processes of land reclamation.

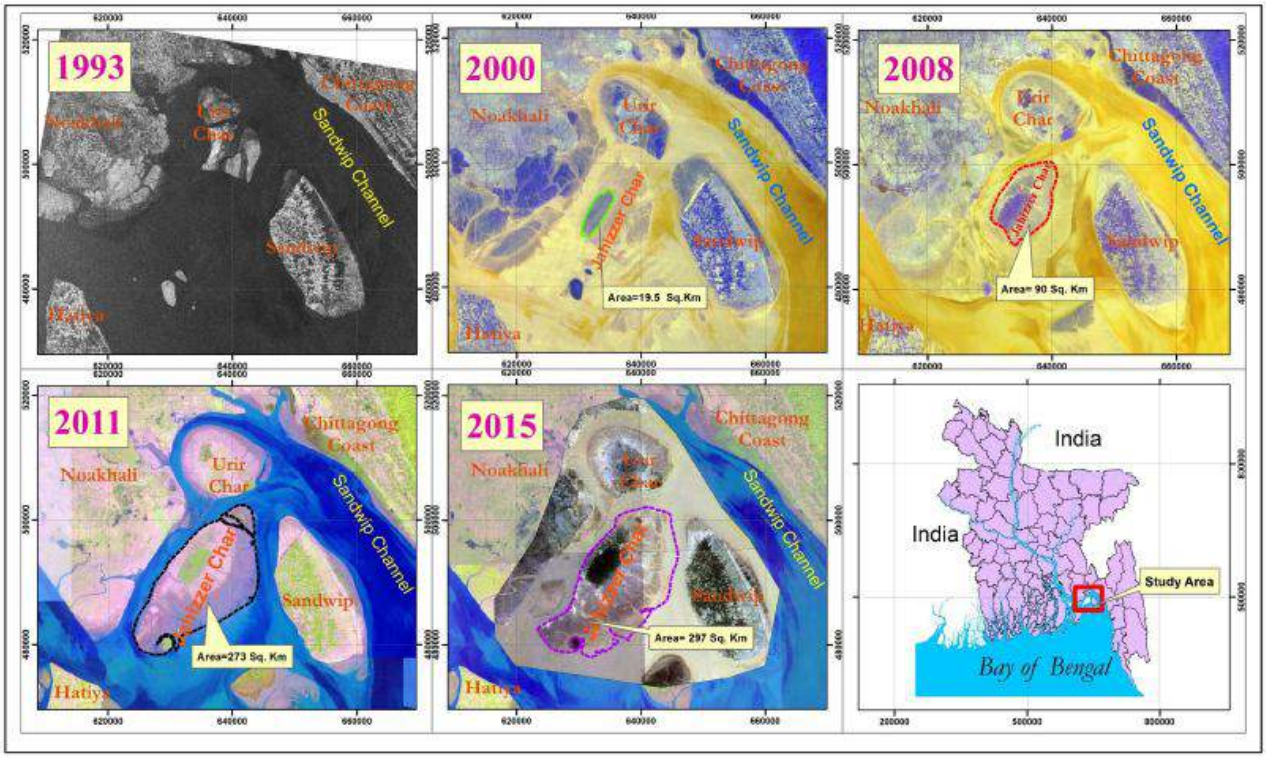

Figure 1. Evolution of different islands through satellite images in Meghna Estuary.

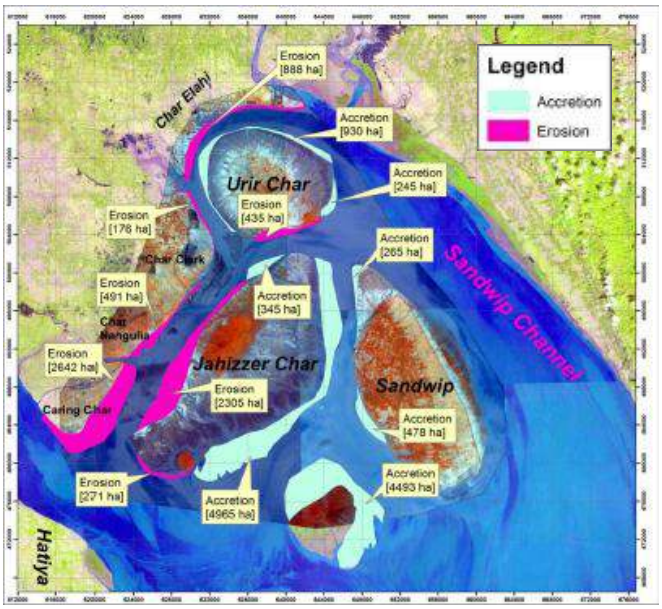

Figure 2. Net accretion and erosion between 2011 and 2015 obtained through satellite images.

COMPARISON BETWEEN BIJKER AND LEONT'YEV LONGSHORE SEDIMENT TRANSORT FORMULAE

Masoumeh Ebrahimi [1], Peyman Badiei [2]

1) Master Student, University of Tehran, Tehran, Iran, ebrahimi_masoomeh70@yahoo.com
2) Assistant Professor, University of Tehran, Tehran, Iran, pbadiei@ut.ac.ir

1. Introduction

Longshore sediment transport (LST) rate induced by waves and current is an important element in coastal management, morphology and design of coastal structures. When LST is determined, shoreline changes, caused by nature or human constructions can be predicted. LST is mainly calculated either by applying a bulk or detailed approach. Formulas such as CERC uses a bulk approach and estimates an integral LST amount across surf zone. Many researchers have worked on the calibration coefficient of this formula. One of the most recent formulas for CERC coefficient is proposed by Leont'yev [1]. An example of a detailed LST calculation method is proposed by Bijker [2]. In the present paper the results obtained by a simplified Bijker method and CERC formula based on Leont'yev proposed coefficient are compared and evaluated against field data.

2. LST calculation methods

Bijker [2] calculates LST at a location with specific depth, wave height, wave period and current velocity. Bed and suspended load transport modes are calculated using the following formulae:

$$q_{sb,cw} = 5D_{50}\frac{U}{C}\sqrt{g}\exp(-0.27\frac{\Delta D_{50}\rho g}{\mu\tau_{cw}}) \qquad (1)$$

$$q_{ss} = 1.83\ q_{sb}\left(J_1 \ln\left[\frac{33\ h}{r}\right] + J_2\right) \qquad (2)$$

where $q_{sb,cw}$, q_{ss}: bed and suspended load volume flux rates ; D_{50}: median grain size diameter; U: depth averaged longshore current velocity; C: Chezy coefficient;; μ: ripple factor; ρ_s, ρ: sediment and water densities; τ_{cw}: combined shear stress caused by wave and current; J_1, J_2:Einstein integrals which are calculated by Guo and Julien [3] Analytical approximations; h =depth; r :bed roughness; $\Delta = \rho_s - \rho/\rho$;

If the distribution of sediment transport rate is assumed approximately linear in the surf zone, the total LST in m^3/s is determined as follows:

$$Q_y = \frac{1}{2}x_B(q_{ss} + q_{sb,cw}) \qquad x_B = h_B / m \qquad (3)$$

where Q_y :LST; x_B :surf zone length; m :bed slope; h_B :breaker depth.

$$h_B = (\frac{1}{4\pi\gamma^2})^{2/5} H_0^{4/5}(gT_p^2)^{1/5}(\frac{\cos\theta_0}{\cos\theta_B})^{2/5} \qquad (4)$$

where γ :breaker index; H_0 :significant wave heights in deep water; T_p : the wave spectrum peak period; θ: the angle between the wave direction and the normal to the shore; B subscript refers to breaking point. In the model of Leont'yev h_B corresponds to breaking of waves of 1% exceedance.

CERC formula calculates the LST rate based on the longshore energy flux component F_{yB} in the surf zone[4]:

$$Q_y = \mu K F_{yB} \qquad F_{yB} = (EC_g\cos\theta\sin\theta)_B \qquad (5)$$

$$\mu = 3600/[g\cdot\Delta\cdot(1-n)] \quad C_g = \sqrt{gh}$$

where n **:**porosity of the sediments;

Leont'yev [1] proposed K coefficient when using H_{rms} in the CERC formula reads:

$$K_{rms} = 0.04(0.8 + 0.02\frac{\sqrt{gh_B}}{w_g}) \qquad (6)$$

where w_g is fall velocity.

3. Comparison between formulae and field data

Three arrays of data were used to compare the result of calculations over a relatively wide range of transport rates (table 1). The measurements of Voitsekhovich [5] and Leont'yev [6] were made in the Black Sea and the data of Miller [7] were made in the Atlantic coast of the US (Duck, NC). Bijker method shows a better conformity with field measurements except for Leont'yev's field data. The calculated results are compared based on root mean square error so that it is dimensionless as shown in table 2.

Table 1. LST rate calculated by Bijker and Leont'yev models and field data.

$\bar{H}$, m	$\bar{T}$, s	θ0	dg, mm	sediment transport rate m³/h		
				measue--rments	Leont'yev estimate	Bijker estimate
Voitsekhovich						
0.4	4	10	0.25	6.7	3.1	7.2
0.4	3.8	15	0.25	6.7	4.4	10.6
0.5	5.7	10	0.32	5.9	5.1	10.2
0.4	3.8	10	0.36	3	2.3	4.1
1	6	30	0.43	101	66.1	111.0
1	5.4	18	0.34	85.1	52.2	92.2
0.6	4.8	10	0.25	22.2	9.7	18.1
1.1	5.9	25	0.36	76.6	85.8	144.9
0.6	5.8	25	0.36	16.6	16.8	32.4
0.5	5.9	18	0.32	15.2	8.8	17.4
0.5	4.2	20	0.28	21.1	9.5	22.3
0.6	3.8	10	0.3	17	7.6	18.0
0.8	5	5	0.28	8.9	9.8	17.3
0.6	4.2	5	0.4	3.7	3.3	3.0
0.8	6.2	5	0.37	4.4	8.4	14.4
1	5.8	20	0.28	121	68.7	108.3
0.8	5.3	30	0.28	67.3	47.9	88.7
0.5	4.1	5	0.29	4.4	2.5	5.9
0.6	5.4	10	0.32	10.4	8.9	16.0
0.9	4.5	30	0.25	176	69.6	126.8
0.5	4.3	35	0.7	11.8	8.1	41.6
0.6	5.9	15	0.48	7	10.3	22.4
0.5	3.6	15	0.5	4.1	4.9	18.8
0.4	4.3	10	0.47	1.5	2	7.5
0.5	3.8	10	0.28	4.4	4.9	12.0
0.9	4.7	10	0.32	42.9	23.1	43.2
1.2	5.7	20	0.23	186	137.2	184.3
0.4	3.3	20	0.24	5.2	7.1	14.2
0.6	4.2	30	0.22	34.8	25.8	49.9
0.9	4.7	25	0.23	95.8	69	113.2
Leont'yev						
0.5	4.2	30	0.4	7.8	9.7	30.0
0.7	4.8	30	0.3	48.8	30.5	64.2
0.6	4.2	30	0.4	13.7	15.8	27.1
1.1	4.8	30	0.4	68.4	83.3	168.8
1.4	6.1	10	0.4	45.1	70.3	103.2
1.2	6.9	10	0.4	48.8	48.4	69.7
1.4	6	10	0.3	129	87.6	122.0
Miller						
1.9	6.3	20	0.17	530	778	641.6
2.8	5.8	13	0.17	1780	1518	1072.0
1.8	5.6	33	0.17	560	886	826.1
1.7	5.8	35	0.17	670	782	736.1

Table 2. RMS calculations for Bijker and Leont'yev models

field data	Voitsekhovich	Leont'yev	Miller
Leont'yev estimate	0.0856	0.0903	0.0897
Bijker estimate	0.0541	0.128	0.0698

1. Conclusion

Bijker model gives more accurate values of LST in comparison with Leont'yev formula. This method yields higher values of LST in 98% of cases as compared with field measurement, so it gives conservative estimates. However for deep sea wave heights greater than 2 m Biker model underestimates the LST and not recommended. There remains a skepticism against Leont'yev's field data due to its mismatch with the other two sets of data presented and applied in this paper.

4. References

[1] Leont'yev, I.O., (2014)."Calculation of Longshore Sediment Transport". Journal of Oceanology, 54(2), pp 205-211.

[2] Bijker, E.W. (1971). *"Longshore Transport Computations"*, Journal of Waterways, Harbors and Coastal Engineering Division, American Society of Civil Engineers, 97(4), pp 687-701.

[3] Guo, J. and Julien, P. (2004). *"Efficient Algorithm for Computing Einstein Integrals"*, Journal of Hydraulic Engineering, American Society of Civil Engineers, 130, pp 1198-1201

[4] Bagnold, R., (1966).*"An approach of sediment transport model from general physics".* US Geol. Survey Prof. Paper 422-I

[5] O. V. Voitsekhovich, "Transportation of drifts along the shore: general principles and real data," Vodn. Resur., No. 5, 108–116 (1986)

[6] I. O. Leont'yev, Dynamics of Surf Zone (Shirshov Insti tute of oceanology, USSR Science Academy, Moscow, 1989).

[7] H. C. Miller, "Field measurements of longshore sedi_ ment transport during storms," Coastal Eng. **36**, 301–321 (1999).

NUMERICAL STUDY OF SEDIMENTATION IN ANZALI HARBOR DUE TO NORTHWEST WAVES WITH RESPECT TO THE EXTENDED BREAKWATERS

Hamed mohammadnejad[1], Habib hakimzadeh[2]
1) Expert Ports and Maritime Organization, Tehran, Iran, Hamed.m.tce@gmail.com
2) Professor in Coastal Engineering, Faculty of Civil Engineering, Sahand University of Technology, Tabriz, Iran, hakimzadeh@sut.ac.ir

Introduction

In this research study, sedimentation in Anzali harbor due to northwest waves has numerically been investigated with respect to the extended breakwaters. First, it was tried with considering the study region and collecting the required data for this research, a comprehensive study has been conducted. The obtained data includes two series of information. The first series, the data used as input for the numerical wave simulation models including bathymetry maps, the wind and wave data, etc. The second group of the data has been used for calibration and verification of the numerical model.

One of the most important aims of constructing a harbor is providing favorable conditions for berthing, loading and unloading of vessels. According to the development plan of Anzali port for improving the berthing capacity and unloading of large vessels in the Caspian Sea, the necessity of a mathematical model study to determine the transport rate and accumulation of sediments in the previous and current basins is more clarified and this can be undertaken using a mathematical software such as MIKE.

The purpose of this study was to investigate the effects of extended western and eastern breakwaters of Anzali harbor (breakwaters extension project) on the basin and lagoon. Exact recognition of the hydrodynamics and sedimentation processes using field measurements and numerical simulation and also analysis of wave penetration rate into the harbor basin before and after extension of the breakwaters were the other aims.

Boundary Conditions and Bathymetry

The boundary conditions used in the wave model to the regional model with dimensions of nine kilometers along the coast and sixteen kilometers perpendicular to the coastline are shown in Figure 1 (a). Also deep water wave data received from the PMO was set for the northern boundary of the regional model in MIKE 21-Spectral Waves FM module, the eastern and western boundaries were defined as lateral boundaries and finally boundary conditions for the northern boundary of the local model were extracted from the numerical results of regional wave model [1].

In Figure 1 (b) regional model and the output wave model boundary conditions as the northern boundary the local model shown

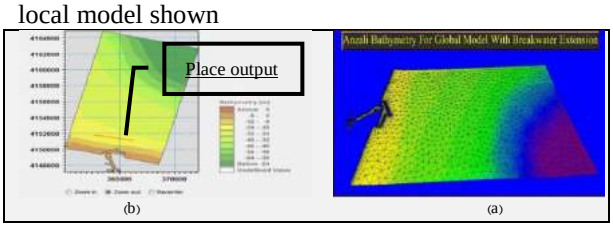

Figure 1. study area of regional model and the local model output along the northern boundary

Utilized Software in Modeling

In this research study the wave transmission process from deep water to shallow water within Anzali Harbor (after construction of the new breakwaters) has been simulated using hydrodynamic model of MIKE21.

The FM module of MIKE21 software enables the user to use triangular grids with various areas within and outside of the basin and meshing is carried out based on the required accuracy of the numerical results for the study area.

Figure 2 shows an example of the triangular used mesh for two different models with and without breakwaters extension.

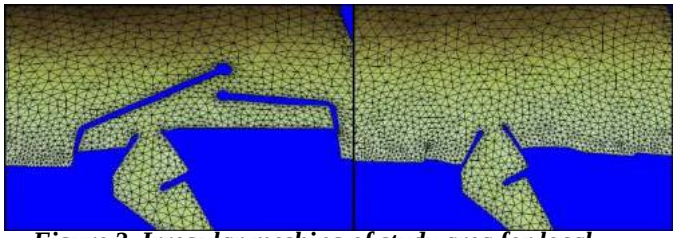

Figure 2. Irregular meshing of study area for local model

Figure 3 shows the satellite/aerial photographs and the bathymetries of study area (before and after extension of breakwaters) that have been made using MIKE21 and hydrographic data for local model.

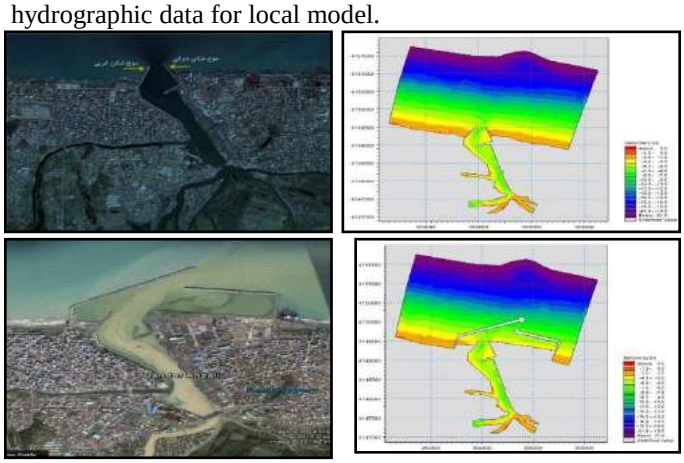

Figure 3. Aerial photographs and the bathymetries of study area used for the local model

Modes of Sediment Transport

The sediment transported in the coastal zone usually contains particles ranging from gravel or sand down to very small particles classified as silt or clay. The very fine fractions are carried as wash load. [2]

With respect to the results of field measurements in Anzali based on USDA[1] classification, sediments in the

[1] U.S. Department of Agriculture

study area are divided into the following three categories:

1. Silt
2. Very Fine Sand
3. Fine Sand

Based on a triangular diagram, the genera of sediments are Silt Clay Loam and Loam [3].

The sources of sediment particles within harbor basin are the marine and lagoon sediments, respectively. It has already been shown that based on the numerical model results as well as dredging statistics, the portion of two sources from marine and lagoon were about 80 and 20 percents, respectively. Based on this, annually the average magnitude of 130 to 160 thousand cubic meters of marine sediments and 30 to 40 thousand cubic meters of river fine sediments from both the north and south were arrived in to the harbor basin and were deposited at various points [4].

Results

In this section after providing the bathymetries of study area, model set up and calibrating of the wave module for local model and also extraction of boundary conditions have been made from regional model to deploy for the numerical simulation of the local model. In the following part, the numerical model results with respect to the dominant wind direction (i.e., northwest) will be examined both before and after extension of the breakwaters in Anzali harbor.

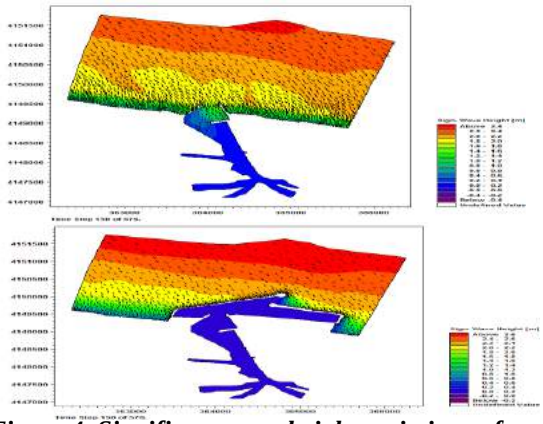

Figure 4. Significant wave height variations after eight days of the model running, the scenario in which wind is blowing from the North West at two states before and after extension of the breakwaters

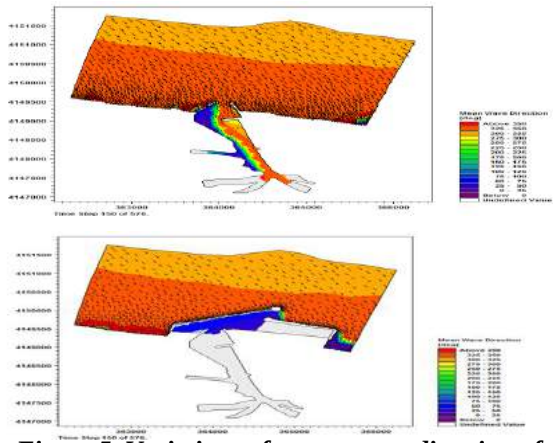

Figure 5. Variations of mean waves direction after eight days of the model running, the scenario in which wind is blowing from the North West at two states before and after extension of the breakwaters

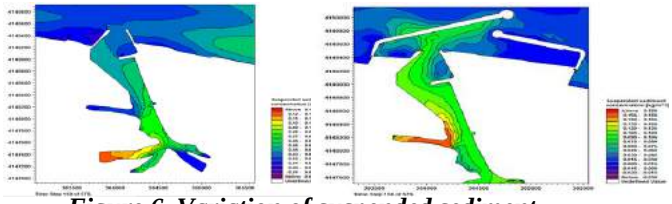

Figure 6. Variation of suspended sediment concentration after eight days of running the model, the scenario in which wind is blowing from the North West at two states before and after extension of the breakwaters

As may be observed from the results, the pattern of waves in the basin at two conditions before and after the development is such a way that height of waves after development plan is mainly lower than that before-development plan so that wave heights ranges between 0.6 -1.4 meters before development plan were reduced to 0.1 -1.0 meters after development plan. In other words, with extension of harbor breakwaters, the aim of development and rest ensuring of the harbor have relatively been achieved. These conditions show existence of the fairly good resting within the harbor after development plan which is also in good agreement with field observations.

Before the construction of new breakwaters, the large amounts of sediments that entered to the channel, discharged through two old breakwaters to the sea due to opening passage and the initial hydraulic gradient. During the rivers flooding, the effects of mud pollutant were visible to a distance of a few kilometers in the sea. But in practice with construction and development of the breakwaters in Anzali harbor, it can be seen that the movements of sediments from lagoon to the basin were controlled and deposited within the harbor and channel.

The above discussion can also be inferred from the sediment concentration output whereas the concentration after development was more than that before development, so that concentration range before development was between 0.030 – 0.055 kilograms per cubic meter and after development of the breakwaters the range was between 0.075 - 0.135 kilograms per cubic meter. Further, currently dragging activities tentatively confirm the results of this research study.

Numerical simulation results of the current study indicate that with development of breakwaters the conditions have been made that the harbor environment became relatively still and this relative still water condition within basin provides conditions for sediment deposition. Now, with construction of the new breakwaters, a part of the sediments that have naturally discharged into the sea before these structures were built up, were trapped, in other words the extended part of the basin acts as a sedimentation trap.

References

[1] DHI Software, complete package of MIKE ZERO & MIKE 21-Spectral Waves FM ,Hydrodynamic Module,User Guide,(2005,2007.2011)

[2] Fredsoe, J., Deigaard, R. (1992), Mechanics of coastal sediment transport, Institute of Hydrodynamics and Hydraulic Engineering Technical University of Denmark, Vol. 3, No. 2, pages 194-195.

[3] Das, B. M. (2003), principles of geotechnical engineering, No. 7, pages 95-97.

[4] Maritime Studies and Numerical Modeling of Anzali Port, (2005), Ports & Shipping Organization, Coasts and Ports Engineering Department, Chapter Eight (Sedimentation studies in basin harbor), In Persian.

MONSOON WAVE-ANGEL OSCILLATION AND ITS EFFECT ON SEDIMENT TRANSPORT AT MAKRAN COASTLINE

Vahid khorsandifar[1], Reza kamalian[2]

1. Master of coastal and marine engineering, College of Engineering, University of Qom,Qom,Iran, Email: v.khorsandifar@gmail.com

2. Assistant professor of coastal and marine engineering, College of Engineering, University of Qom,Qom-Iran- Email: ulrich.kamalian@cardiffalumni.org.uk

Introduction

Monsoon wave is the main factor of littoral drift at Makran beaches. Summer and Winter Monsoons are caused by annual temperature difference between sea and land. The summer monsoon waves usually start from middle of June until the end of September. The most part of annual sedimentation happens during this times frame. In order to calculate harbor sedimentation in this area, usually a fixed averaged monsoon wave direction is used. Recently (2015) waves have been measured for several months at seven locations in front of the Makran shoreline which include directional wave energy spectrum. These instruments show that the monsoon wave direction is not constant. This paper focuses on the oscillation of the monsoon wave direction, its reason and its effect on long shore sediment transport. There are very limited research works in this regard in the literature. A research in California recently studied on the longshore sediment transport sensitivity to deep water wave direction variability (Adams, Inman, & Lovering, 2011). Ignoring monsoon wave direction undulation when calculating littoral drift, may cause inaccuracy in Qnet and error in sediment transport of the secondary direction (here; west to east). If a fixed wave direction is taken, the long shore sediment transport always remains in one direction. When the wave angle is more or less perpendicular to the coast line, sometimes sed. transport from the other direction also happens. This study compares the difference between fixed and variable wave direction (as in the time-series) effect on littoral drift calculation.

The study area

The area studied in this research is the Iranian continental shelf of Makran between longitudes E57 to E61.61. Three beaches have been studied in particular, where continuous monsoon wave measurements exist at 25 meters depth. They are Tang, Ramin and Rodik. (See Figure 1)

Methodology

Wave characteristics (2D spectrum, height, period, directional variations) and current speed have been measured by ADCP devices from Nortek.

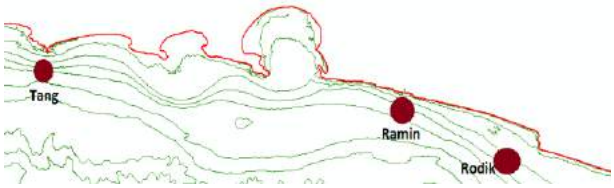

Figure 1. Three ADCP locations at 25 meter depth

Data measured for a period of 122 days from June to September 2015. The swell waves (periods greater than 8 seconds) have been analyzed. The correlation between swell directions and the alongshore current have been studied via FFT cross-spectrum analysis. The potential long shore drift have been calculated every 1 hours by Kamphuis formula (Kamphuis, 2000). Previous studies show that Kamphuis formula is more accurate than CERC on the southern coasts (Afshar kave & Soltanpoor, 2010). The irregularity of the bottom contours have been taken into account, while calculating wave transmission from the measurement locations to the breaking points.

Results and Conclusions

The results show that the summer Monsoon wave has variable direction with more than 10 degrees. It involves both stochastic and oscillatory variations (see Fig. 2). Monsoon waves – because of oscillating direction – may cause longshore sediment transport from both directions at some beaches (Figure 3). According to Table 1, monsoon littoral drift from west (Q_R) is as large as 30% of the net drift (Q_{net}) at Ramin, while it is not so much at Rodik. The oscillatory behavior of the monsoon waves should be considered into account when designing small harbors, because they have small secondary breakwaters.

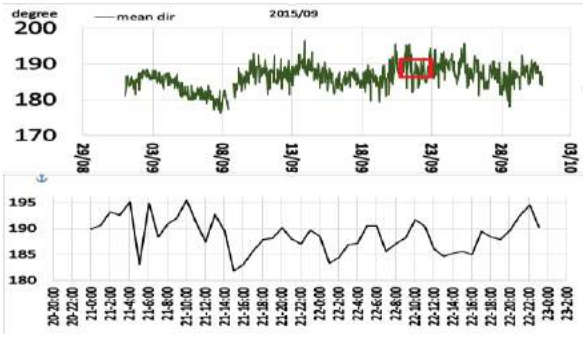

Figure 2. Variation of wave direction in front of Ramin

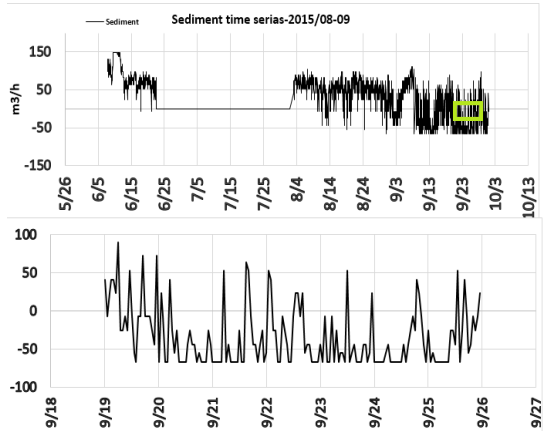

Figure 3. Sediment transport from both directions (Ramin)

The net annual drift is also affected by the monsoon wave direction variability. The net value (Q_{net}) over-estimated by 30% & 20% at Ramin and Rodik respectively, when the average wave direction is used. The reason of wave-angle oscillations have been studied too. Numerical modelling and FFT cross-spectral analysis show that the general currents of Oman Sea can affect the swell mean wave directions (see Fig. 4). Details will be presented in another paper.

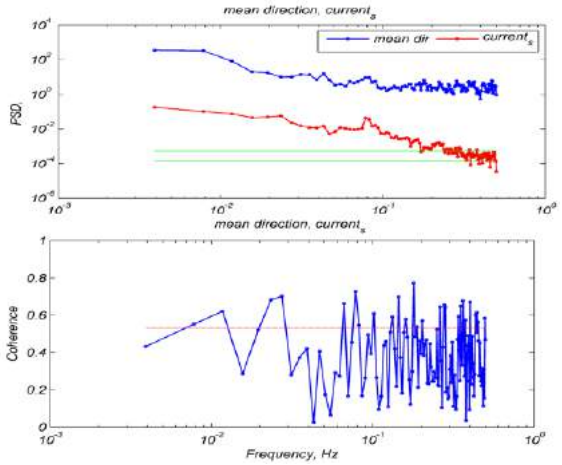

Figure 4. Cross-spectra and coherency between current and wave direction (Ramin station)

Table 1. Monsoon-2015 littoral drift (m3) using variable wave direction

Site	Q_{net}	Q_{gross}	Q_{Left}	Q_{Right}
Ramin	61522	99082	80402	18880
Rodik	41286	51897	45397	2055

Table 2. Monsoon-2015 littoral drift (m3) using averaged wave direction

Site	Q_{net}	Q_{gross}	Q_{Left}	Q_{Right}
Ramin	92646	92646	92646	0
Rodik	51897	51897	51897	0

Coherence between the general parallel shore flows with the wave direction oscillatory behavior analyzed with FFT strategy and the results show the intense relationship between these parameters which is investigating in another research.(see Figure 4)

References

1. Adams, p., Inman, D., & Lovering, J. (2011). Effects of climate change and wave direction on longshore sediment transport patterns in Southern California. *Springer Science+Business Media*.

2. Afshar kave, N., & Soltanpoor, M. (July 21, 2010). Verification of the relationship between the longshore sediment transport rate in the number of beaches. *College of Civil Engineering and Surveying. Technical College,*.

3. habibi, f. (March 20, 2001). Examining the impact of the Indian monsoon on Iran. *Geographic research*.

4. Kamphuis, J. (2000). *Introduction to Coastal Engineering and Management.* Worfd Scientific Pubiishing.

5. Reeve, D., Chadwick, A., & Fleming, C. (2004). Coastal engineering-processes, theory and design practice. *New York spon press.*

STUDY OF BED MATERIAL EFFECTS ON SCOUR PATTERN IN FRONT OF A VERTICAL BREAKWATER BY A TWO-PHASE FLOW MODEL

Hamid Houshangi[1], Abbas Yeganeh-Bakhtiary[2,3] and Ebrahim Jabbari[4]

1) School of Civil Engineering, IUST, Tehran, Iran, houshangi@iust.ac.ir
2) Faculty of Engineering, UniversitiTeknologi Brunei (UTB), Brunei Darussalam, yeganeh@utb.ac.bn
3) School of Civil Engineering, IUST, Tehran, Iran, yeganeh@iust.ac.ir
4) School of Civil Engineering, IUST, Tehran, Iran, jabbari@iust.ac.ir

1. Introduction

Scour in front of vertical breakwaters (VBs) under the action of standing waves induces serious potential risks to the stability of such structures. The recorded history of the VBs confirms many failures due to occurrence of scour [1, 2]. The scour problem has been studied by many researchers, which indicate that the key mechanism for scour under action of standing waves in front of VBs is the field of steady streaming pattern, consisting of bottom and top re-circulating cells [3, 4].

Bed materials (bed sediment particles) essentially respond to the top and the bottom re-circulating cells; in which the fine and coarse materials are picked up respectively by the top and bottom cells. Coarse or fine materials may considerably influence on scour/deposition pattern in front of VBs and act on the stability of such structures.

In this study a Lagrangian two-phase flow model was developed to simulate the scour process and to describe the sediment transport processes in front of a VB with different bed materials. The fluid phase was simulated via the solution of two-dimensional Navier-Stokes equations based on WCSPH method in conjunction with the SPS turbulence closure model. The sediment phase was simulated using the MBS-3D code [5] to calculate the effects of interparticle and particle-wall collisions. The MBS-3D code is based on Distinct Element Method that using a spring/dashpot system to simulate the contact forces between each contacting particle.

The numerical two-phase model is developed and implemented for simulation of scour/deposition process in front of a vertical breakwater with different bed materials. To avoid any disagreement between the experiment and the numerical simulation, Shields parameter in the numerical simulations was considered equivalent to that of the experiments. At the end of every numerical simulation, different scour pattern was observed due to the effect of fine and coarse bed materials. Both scour patterns from numerical results were separately verified by the experimental data. Xie[6] and Sumer &Fredsoe[7] experimental values were used for verification.

2. Governing Equations

The governing equations for fluid particles include mass and momentum equations as follow:

$$\frac{1}{\rho}\frac{d\rho}{dt} + \nabla.\vec{u} = 0 \quad (1)$$

$$\frac{d\vec{u}}{dt} = -\frac{1}{\rho}\nabla P + \frac{1}{\rho}\nabla(\mu.\nabla\vec{u}) + \frac{1}{\rho}\nabla.\tau + \vec{g} + \vec{F}_{sf} \quad (2)$$

where $\vec{u}$, ρ, P, and μ are the velocity vector, density, pressure, and dynamic viscosity of a fluid particle, respectively, ∇P is the pressure force, $\nabla(\mu.\nabla\vec{u})$ and $\nabla.\tau$ are the viscosity forces between fluid particles, respectively, τ is the SPS stress tensor, $\vec{F}_{sf}$ is the interaction force between fluid and sediment phases, and $\vec{g}$ is the gravity acceleration vector.

The governing equations for sediment particles based on Newton second law are

$$m_i\frac{d\vec{u}_i}{dt} = \sum_j \vec{F}_{c,ij} + \vec{F}_{fs,i} + m_i\vec{g} \quad (3)$$

$$I_i\frac{d\vec{\omega}_i}{dt} = -\sum_j R_i\vec{n}_{ij} \times \vec{F}_{c,ij} \quad (4)$$

$$\frac{d\vec{r}_i}{dt} = \vec{u}_i \quad (5)$$

here subscripts i and j are for identifying particles, m and $\vec{u}$ are the mass and the velocity vector of the mass center, respectively, $\vec{\omega}$ is the angular velocity vector, $\vec{r}$ is the particle position, R is the particle radius, $\vec{F}_{c,ij}$ is the contact force of particle $j$acting on i, $\vec{F}_{fs,i}$ is the fluid–sediment interaction force assumed to act at the mass center of particles, I_i is the inertia moment of a sediment particle equal to $\pi R^4/2$, and $\vec{n}_{ij}$ is the normal direction of the contact pointing to particle i from j.

3. Numerical Simulation

The numerical two-phase flow model has been developed and implemented for simulation of scour/deposition process in front of vertical breakwaters. The numerical results are compared with Sumer &Fredsoe[7] and Xie [6]experiments. Table 1 describes the numerical configuration and summaries the physical

characteristics of the incident wave and sediment bed. The sand grains are relatively fine and coarse. Figure 1 shows a schematic view of numerical domain in current study.

Table 1. Test cases of numerical simulation based on Sumer & Fredsoe[7] and Xie[6] experiments

Test No.	Slope	h (cm)	H (cm)	T (s)	L (m)	$d_{50}(mm)$	Sand type	S (cm)	Experimental data
1	vertical	0.30	5.0	1.17	1.714	4	fine	1.3	Xie (1981)
2	vertical	0.31	9.7	3	5.13	5	coarse	7.9	Sumer & Fredsoe (2000)

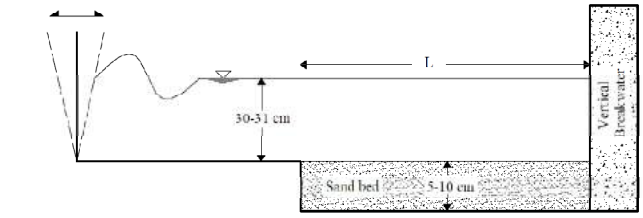

Figure 1. Schematic view of numerical domain in current study

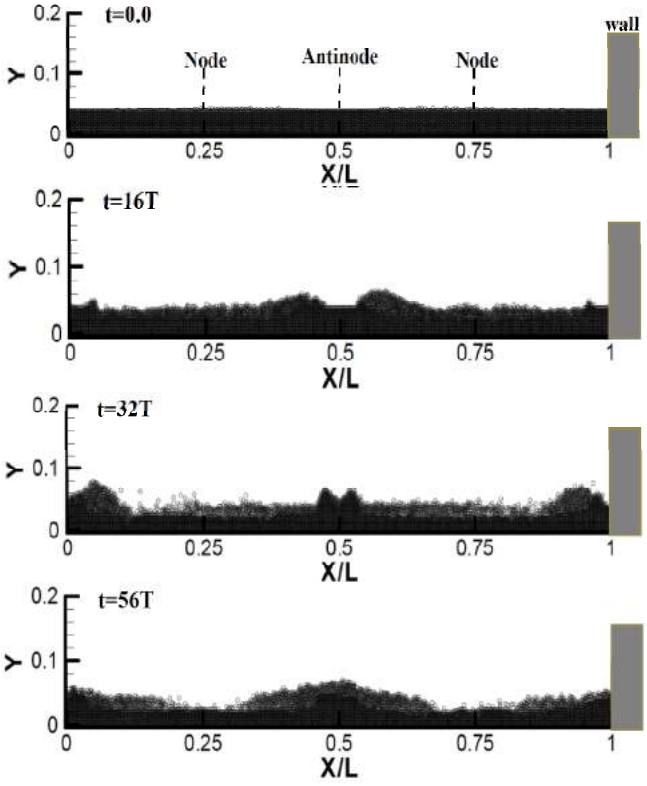

Figure 2. Scour/deposition Pattern in front of VB with relatively fine materials

Figure 2 shows the snapshots of the scour/deposition formation in front of a vertical breakwater for test No. 1 with relatively fine sand. The sediment particles are influenced by the top re-circulating cells and after few wave periods, sand bars and scour holes started to form in the domain. Figure 3 compares the numerical results for the bed profile with that of the Sumer &Fredsoe[7] and Xie[6] experiments for test No. 1 and test No. 2. Figure 3 indicates that the scour pattern from the model fitted well with the experimental results, In the case of coarse bed materials, the sand particles deposited at the vicinity of the breakwater, the distance of $L/4$ from the breakwater (at nodes); accordingly, the scour hole occurred between nodes and antinodes at nearly $L/8$ from the breakwater. This expression is approximately vice versa in the case of fine sand which the scour hole occurred at nodes and the sand particles deposited at near the antinodes.

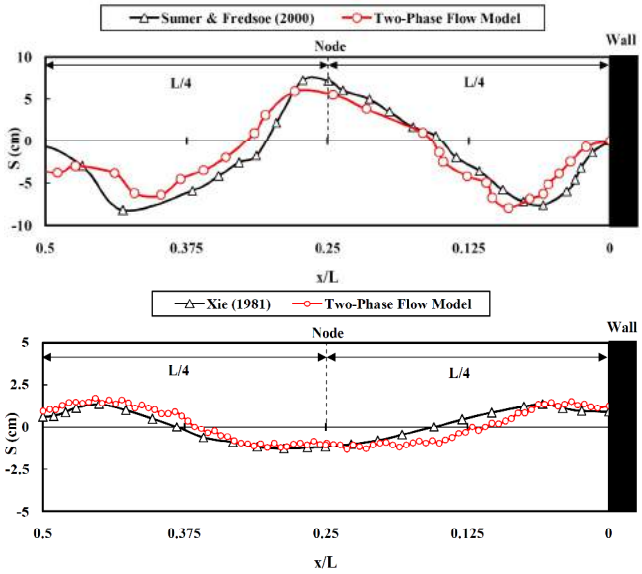

Figure 3.Comparison of scour profiles between numerical and experimental values with coarse material (top figure) and with relatively fine material (bottom figure)

4. References

[1]Oumeraci, H.,"Review and analysis of vertical breakwater failures — lessons learned",*Coastal Engineering, Special Issue on Vertical Breakwaters*. Vol. 22, pp. 3–29, 1994a.

[2] Sumer, B. M. & Fredsøe, J., "The Mechanics of Scour in the Marine Environment",*World Scientific Publication Co.*, Singapore, xiv + 536 p, 2002.

[3] Yeganeh-Bakhtiary, A., Hajivalie, F. & Hashemi-Javan, A., "Steady streaming and flow turbulence in front of vertical breakwater with wave overtopping",*Applied Ocean Research*. Vol. 32 (1), pp. 91–102, 2010.

[4] Hajivalie, F., Yeganeh-Bakhtiary, A., Houshangi, H. & Gotoh, H., "Euler–Lagrange model for scour in front of vertical breakwater",*Applied Ocean Research*. Vol. 34, pp. 96–106, 2012.

[5] Yeganeh-Bakhtiary, A., Shabani, B., Gotoh, H. & Wang, S. S. Y. "A three-dimensional distinct element model for bed-load transport," *Hydraulic Research.*Vol 47(2), pp. 203–12, 2009.

[6] Xie, S. L., "Scouring pattern in front of vertical breakwaters and their influence on the stability of the foundation of the breakwaters", *Report, Department of Civil Engineering, Delft University of technology, Delft, Netherlands*, September, 61 p, 1981.

[7] Sumer, B.M., & Fredsøe, J., "Experimental study of 2D scour and its protection at a rubble-mound breakwater", *Coastal Engneering*, Vol. 40, pp. 59–87, 2000.

NUMERICAL MODELING OF DIKE BREACHING USING SPH METHOD

Rasoul Memarzadeh[1], Gholamabbas Barani[2] and Mahnaz Ghaeini-Hessaroeyeh[3]

1) Department of Civil Engineering, Shahid Bahonar University of Kerman, Kerman, Iran, rasoul.memarzadeh@eng.uk.ac.ir
2) Department of Civil Engineering, Shahid Bahonar University of Kerman, Kerman, Iran, gab@mail.uk.ac.ir
3) Department of Civil Engineering, Shahid Bahonar University of Kerman, Kerman, Iran, mghaeini@mail.uk.ac.ir

1. Introduction

Soil dikes along coasts are designed to protect harbors and cities from waves such as tsunami. However, overtopping from these structures is an old concern and still a number of events occur yearly causing both monetary and human losses. In this phenomenon, flood flows and bed changes occur simultaneously. The main difficulty in simulating the embankment erosion process is related to the modeling of solid transport, because there are intricacies between fluid flow and bed evolution. In the last few decades, many one-dimensional and two-dimensional numerical models have been developed to simulate the embankment breaching (e.g. [1, 2]). In this paper, a multi-phase model based on SPH method has been developed to simulate the dike erosion process.

2. SPH Method

SPH method represents the continuum domain by discrete particles. The idea of SPH method is to follow the particles in their motion. The particles can be considered as the material points carrying the physical properties of it (e.g. mass and density) and quantities of flow (e.g. velocity and pressure). The SPH interpolation procedure is based on the position of particles using a kernel function. The kernel (or weighting) function, W, depends on the distance between the central particle (i) and other particles in its vicinity (j), either in same phase or different phases, and smoothing length (h) controls the support domain around the central particle [3].

3. Numerical Model

This is hypothesized that the multi-phase system of embankment breaching problem can be considered as a multi-density multi-viscosity fluid. Therefore, the mass and momentum conservation equations are used to express the multi-phase system:

$$\frac{D\rho}{Dt} + \rho(\nabla \cdot \mathbf{u}) = 0 \tag{1}$$

$$\rho \frac{D\mathbf{u}}{Dt} = -\nabla P + \mu(\nabla^2 \mathbf{u}) + \mathbf{g} \tag{2}$$

Where ρ is the density, $\mathbf{u}$ is the flow velocity, P is the pressure, μ is the dynamic viscosity, $\mathbf{g}$ is gravitational acceleration and t is the time.

By applying the SPH interpolation to the governing equations (1) and (2), the following relations are obtained:

$$(\frac{D\rho}{Dt})_i = -\rho^2{}_i \sum_j m_j (\frac{\mathbf{u}_j}{\rho_j^2} + \frac{\mathbf{u}_i}{\rho_i^2}).\nabla_i W_{ij} \tag{3}$$

$$(\frac{D\mathbf{u}}{Dt})_i = -\sum_j m_j (\frac{P_j}{\rho_j^2} + \frac{P_i}{\rho_i^2}).\nabla_i W_{ij} + \sum_j \frac{2m_j (\frac{\mu_i}{\rho_i} + \frac{\mu_j}{\rho_j})\mathbf{r}_{ij}.\nabla_i W_{ij}}{(\rho_i + \rho_j)(|\mathbf{r}_{ij}|^2 + (0.01h)^2)}(\mathbf{u}_i - \mathbf{u}_j) + \mathbf{g} \tag{4}$$

4. Multi-Phase Model

The present multi-phase model has two parts for the simulation of sediment particles. When the sediment acts as a rigid material, only the force due to the shear stress is considered to move the sediment particles. Otherwise, the sediment particles are considered like the water particles, and all the force terms in the Navier-Stokes equations are used to simulate the movement of them. The Bingham non-Newtonian constitutive model is used to obtain the threshold between the rigid or Newtonian behavior of the sediment particles.

5. Results

In this section, the breaching of a dike which is made of uniform non-cohesive sand is modeled to study the efficiency and accuracy of the multi-phase SPH model. The laboratory experiment of Schmoker & Hager [4] is used to evaluate the accuracy of computations. The initial geometry of this experiment is shown in Figure 1. In the present simulation w is 0.2 m, L_K is 0.1 m, L is 0.9 m, S_0 is 2 and Q_0 is 11.31 L/s.

The comparison between the computed bed evolution profiles by WCSPH multi-phase model and experimental data are shown in Figure 2 at two different times after the overtopping being started. It is seen that the entire dike

breaching process is well modeled by the Multi-phase ISPH model with relatively good agreement in the bed profile.

6. Conclusion

A multi-phase SPH model is developed for simulation of dike breaching. It is considered the flow system to be multi-density and multi-viscosity and solved the flow equations on the computational domain which is represented by particles. The model simulates the movements of sediment particles in two-part. Application of the model to the test case of this study shows the capabilities of the present model in the simulation of dike breaching.

7. References

[1] Faeh, R., "Numerical modeling of breach erosion of river embankments", Journal of Hydraulic Engineering, 133, 9, 2007.pp. 1000–1009.

[2] Pontillo, M., Schmoker, L., Greco, M. and Hager, W. H. "1D numerical evaluation of dike erosion due to overtopping", Journal of Hydraulic Research, 48, 5, 2010, pp. 573-582.

[3] Memarzadeh, R. and Hejazi, K., "ISPH Numerical Modeling of Nonlinear Wave Run-up on Steep Slopes", Journal of the Persian Gulf (Marine Science), 3, 10, 2012, pp.17-26.

[4] Schmoker, L. and Hager, W.H., "Modelling dike breaching due to overtopping", Journal of Hydraulic Research, 47, 5, 2009, pp. 585-597.

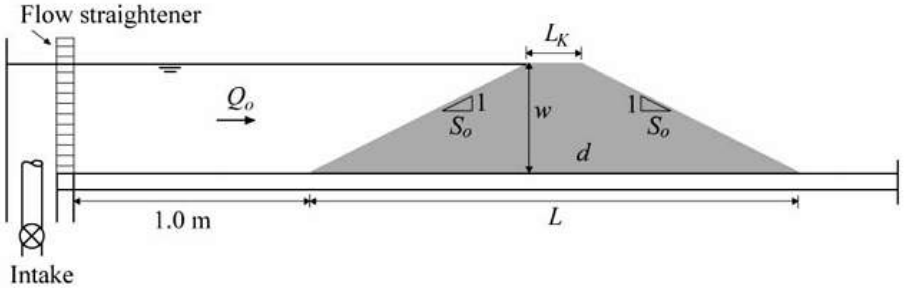

Figure 1. Initial geometry of dike breaching experiment [4].

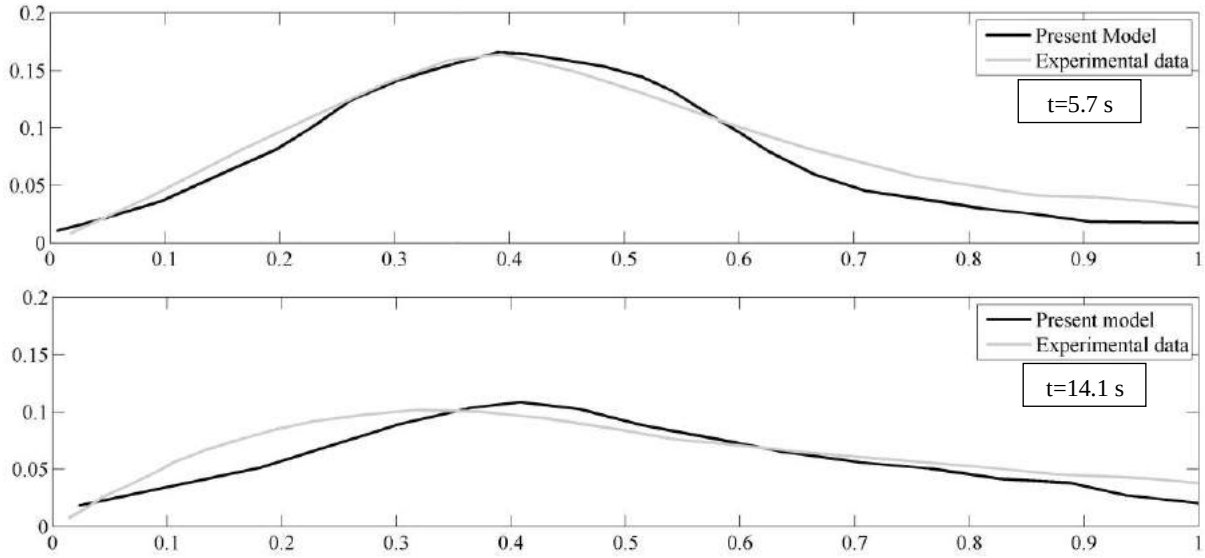

Figure 2. Comparison of the longitudinal embankment profile of present model and experimental data of Schmoker and Hager [4] at various times (The horizontal and vertical units are meters).

SUDY AND ANALYSIS OF THE TANG ESTUARY MOUTH BY REMOTE SENSING

Amirpouya Bakhtiari[1], Reza Kamalian[2], Maryam Rashtbari[3]

1) Department Of Civil Engineering, Qom Univeristy, Qom, Iran, A.p.bakhtiary@gmail.com
2) Department Of Civil Engineering, Qom Univeristy, Qom, Iran, Ur.kamalian@gmail.com
3) Water Research Institute, Tehran, Iran, Mr.6088@yahoo.com

Introduction

Estuaries are among the most important coastal landforms that could be utilized with adequate understanding of their hydrodynamic and morphological conditions as well as their interactions with seas. The research objective was to study variations in Tang Estuary (in Sistan and Baluchestan) over the past years, analyze causes of the variations, and predict/propose a general plot of changes of these estuaries. Tang Estuary is an active hydrodynamic estuary, whose mouth undergoes various changes every 7 or 8 years on average. The mouth of this estuary opens westward during some years and during some years opens eastward.

Figure 1. Bay modeling in mepbay.

Methodology

Landsat satellite images from 1985 to 2016 were used in this research. ENVI was used to process and recreate the images. Using these images, it is possible to observe changes in bed geometry and coastline, while analysis of these changes results in adequate understanding of morphodynamics of the inlet of Tang Estuary. To examine the trend of depth changes at the estuary mouth, bathymetric operations were conducted on both sides of the estuary using ENVI. Mepbay was also employed to examine static stability of the west bay of the estuary and obtain wave components (see Figure 1).

Using the Dynlet feature of Cedas, variations in depth and velocity of inflow and outflow caused by tidal currents were studied (see Figure 2).

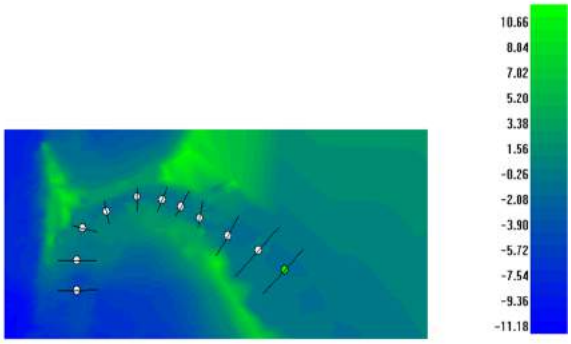

Figure 2. Modeling in cedas software.

Results

The following results were obtained from satellite images:

- When the estuary mouth opens toward east, the inflow of sediments from east to

west leads to settlement of sediments at the mouth over time, and the narrowing process leads to an increase in water inflow and outflow velocity in the region. During this process, the shear stress of water and sedimentary wall escalates and results in erosion of wall and a decrease in the wall width. Over time, width of this wall reduces to the point that an adequately storm from the southwest ruins and washes the sediments away through waves, and the eastern mouth closes due to settlement of sediments(cross-shore sediment) and eventually the mouth opens westward (see Figure 3).

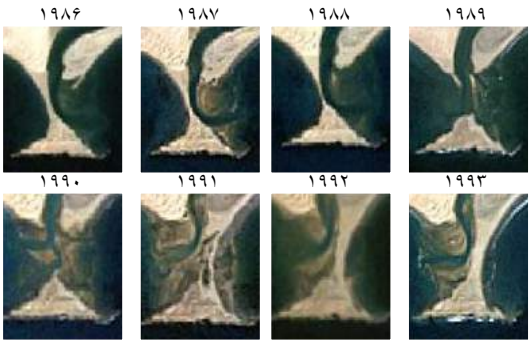

Figure 3. landsat images.

- When the estuary mouth opens toward west, using the modeling in Mepbay it is found that a delta forms over time due to separation and dispersion on top of the mouth. As the delta expands gradually, the mouth becomes narrower and adds to the water-wall shear stress in the eastern side. Hence, the wall narrows from the inside until an adequately strong storm from the east completely washes the wall away and eventually the western mouth closes. With settlement of sediments in the western side of the mouth and a decrease in depth of this region, which was revealed by bathymetric analysis of Landsat images, the estuary mouth opens eastward. The inlet instability is confirmed by Dynlet. This process occurred twice in the past 31 years (1985 to 2003) and it is predicted to occur in future (see Figure 4).

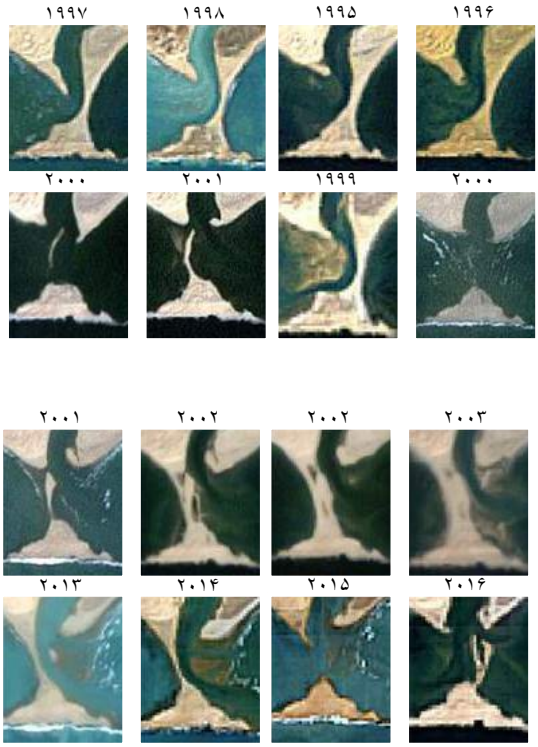

Figure 4. changing process of the Tang estuary mouth direction.

Refrences

[1] Seto,K.C., et al .2002. Monitoring land-use change in the Pearl River Delta using Landsat TM,International Journal of Remote Sensing , 8(6), 460－473.

[2] Di, K., 1999. Shallow water depth extraction and chart production from ETM+ image in Nansha islands and nearby sea area. *Remote Sensing for Land & Resources,* 41(3), pp. 59-64.

[3]Kamphius, J.W., "introduction to coastal engineering and management",Advance series on ocean engineering ,Volume 16, PP. 257-297.

[4] USGS: Landsat 8 band designations.(2014). http://landsat.usgs.gov/band_designations_landsat_satelites.php

[5]Mangor, K., "shoreline management guidelines", (2004), DHI Water & Environment, PP.49-65.

[6]Banijamali**,** Report of Tang harbor, bed morphology, Daryabandar Consulting Engineers, 2008

ANALYTICAL STUDY ON THE SEDIMENTATION OCCURRENCE AT THE ENTRANCE OF PORTS AND NAVIGATION CHANNELS (CASE STUDY: ASTARA PORT)

Shapur Tahouni[1], Maryam Nikkhah[2], Majid Safehian[3] and Mohammad Khalaji[4]

1) Assistant Professor, Dept. of Civil and Environmental Engineering, Amirkabir University of Technology, Tehran, Iran, stahouni@aut.ac.ir
2) Ports and Marine Structures Dept. in Tadbir Sahel Pars Consultant, Tehran, Iran, nikkhah.mari@gmail.com
3) Assistant Professor, Dept. of Construction Management, Science and Research Branch Islamic Azad University, Tehran, Iran, safehian@yahoo.com
4) Ports and Marine Structures Dept. in Tadbir Sahel Pars Consultant, Tehran, Iran, khalaj.mo@gmail.com

1. Introduction

Sedimentation is a common problem in harbors, which reduces the required navigation depth and disturbs vessels passage. In order to provide a safe passage for vessels, frequent maintenance dredging in harbors is needed. The amount of maintenance dredging which is the most expensive item in the running costs of harbors depends on the rate of sedimentation in harbor basins. For example, the annual dredging costs of marinas of the Netherlands are estimated about €500,000,000, as reported in [1]. As another case in point, the average annual dredging costs of federal navigation projects in the United States between 1995 and 2000 were estimated to be about M$500, as reported in [2]. Therefore, minimizing sedimentation in harbors is one of the major considerations in port design. Generally, sediments transported into harbors by currents and waves, are deposited in parts of the harbor where currents and waves are not strong enough to keep sediments in motion and reduce water depth.

Recently, many attempts have been made to study sediment transport and measures for the reduction of sedimentation in harbor basins. Winterwerp [3] gives a summary of measures for the reduction of sediment deposition reduction measures in harbors for various environmental conditions. Kuijper et al [4] discussed the effects of harbor geometry on sediment deposition in harbor basins, together with the application of CDW (Current Deflection Wall) as a type of geometrical modification to reduce sediment deposition in a harbor basin of the port of Hamburg (Germany). Yüksek [5] conducted an experimental study on the effects of layouts of breakwaters on sedimentation patterns in harbor basins and suggested some design criteria in the form of dimensionless geometrical parameters of breakwaters.

In this paper, current, wave and sediment transport of Astara port has been studied by numerical modeling in MIKE-21 software. Results of simulation have shown good agreements compared with field measurements and numerical results. Then, four variants for reduction of sedimentation are proposed and finally the best solution is determined.

2. Study Area

Astara port is located in the western coast of Caspian Sea at latitude 38°25'45" N and longitude 48°52'19" E. This port was built in 1996 and its development was started in 2010 which included the extension of the breakwaters, constructing docks and dredging (see Figure 1). These variations are resulted to the high amount of sedimentation in the entrance of harbor.

Figure 1. Location of Astara Port and its development

3. Sedimentation Processes

Owing to the fact that they are relatively quiescent, basins are susceptible to muddy siltation. Basin water is exchanged with sediment-laden waters from outside the basin through the harbour entrance. Once the sediment-rich water enters the basin, sediments tend to settle due to low basin flow velocities. Keep the sediment out strategies focus on minimizing penetration of a basin and/or navigation channels by sediment laden waters.

4. Model Setup

Mike 21/3 Coupled Model FM is a dynamic modeling system which is used in coastal and estuarine zones. In this

research, a two-dimensional model in HD Module is used to investigate the wave-induced currents. The most important of these phenomena are growth and advance of waves in deep waters, wave breaks, wind waves, white capping, nonlinear wave-wave interactions, longshore current and width of surf zone. The agreements of the numerical model results and bed level change at the entrance of Astara port indicate the consistency of the model and the true physics.

Model grids are generated by Mike mesh generator, using bathymetry data and user defined grid limits as shown in Figure 2.

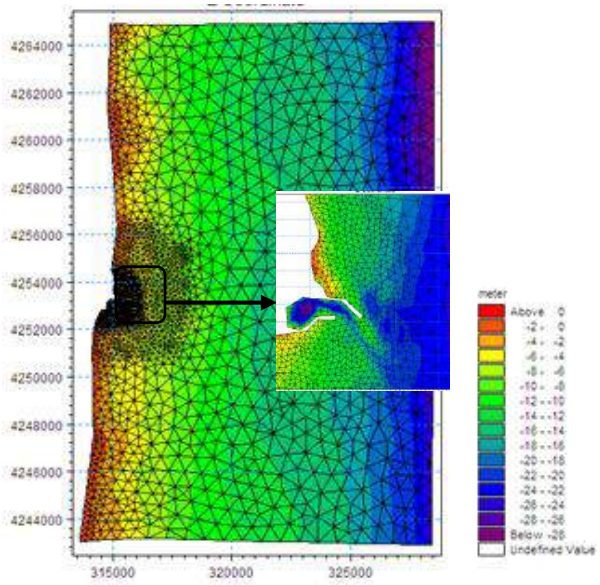

Figure 2. Mesh of used for numerical modeling

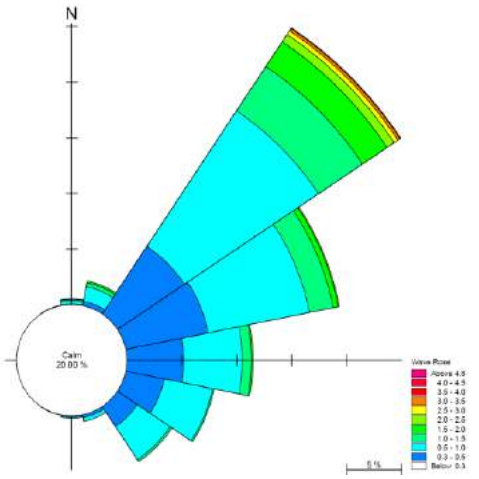

Figure 3. Wave rose used for boundary condition of SW Model.

5. Model Results

In the Figure 4, sedimentation occurrence in the entrance of port has been shown. As approximately after passing one year, the bed level is changed in entrance port about one meter by sedimentation. As well as scour of head of northern break water.

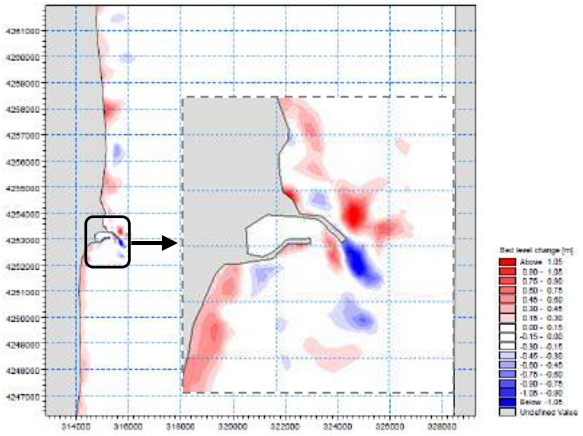

Figure 4. Sedimentation pattern at the entrance of Port.

6. Conclusion

The study shows in the vicinity of coastal breakwater and port layout, the current pattern principally different. Breakwaters form a shadow to harbour and generate circulating nearshore current adjacent of the Astara Port entrance. The northern breakwater (primarily arm) is not long enough; therefore sand will be carried along the entrance of the harbour forming a localized spit in the entrance. In Figure 5, the northern breakwater extended about 400 meter and then investigated the sedimentation and results. As it is shown in figure 5, the problem of sedimentation of entrance of port has been reduced.

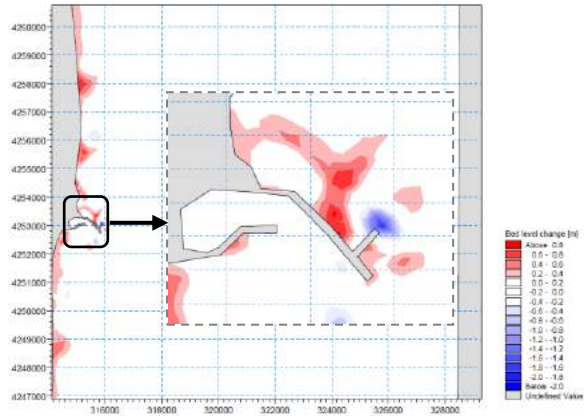

Figure 5. The best solution for minimizing sedimentation

7. References

[1] Ommen H. C., Schaap G., (1995), Nautical dredging problems in marinas: Rep. O. N. 44.03151, 1192 Grontmij Environment, De Bilt, The Netherlands.

[2] Parchure T.M., Teeter A.M., (2002), Lesson Learned from existing projects on shoaling in harbors and navigation channels, 2002, US Army Corps of Engineers.

[3] Winterwerp J.C, (2005), Reducing Harbor Siltation. I: Methodology., Journal of Waterway, Port, Coastal, and Ocean Engineering, ASCE, Vol.131 Issue.6, 258-266.

[4] Kuijper C., et al. (2005), Reducing Harbor Siltation.II: Case Study of Parkhafen in Hamburg. Journal of Waterway, Port, Coastal and Ocean Engineering, ASCE, Vol.121 Issue6.

[5] MarCom Working Group 102(2008), Minimising Harbour Siltation, World Association for Waterborne Infrastructures.

PREDICTION OF LIQUFICATION USING GROUP METHOD OF DATA HANDLING

Farshid Rafiei[1], Mojtaba Ghasemi[2] …

1) Ms. C. student, Department of Civil Engineering, Faculty of Engineering, Shahid Bahonar University of Kerman, Kerman, Iran
2) Assistant Prof , Department of Civil Engineering Graduate University of Advanced Technology-Kerman, Kerman, Iran

1. Introduction

Caissons are massive structures which are used for anchor or foundation of marine facilities. During large earthquakes, liquefaction is occurred and caissons may be completely collapsed. Several researchers performed studies on liquefaction [1-5]. In recent years, artificial intelligent methods were applied to predict liquefaction. Rahman and Wang, (2002) used Fuzzy Logic for liquefaction predication. Jeng et al.,(2003) applied Artificial Neural Network to predict liquefaction[6,7] GMDH based on neural network neurons and these neurons makes it possible to predict complex system modeling. Recently, some researchers have been done about GMDH prediction in engineering problems. In this method in training period, weights are calculated by Least Square Estimation (LSE) method. Recently, some researches have been used GMDH for solving engineering problems [8-10] In this study, Group Method Handling was used to predict liquefaction in sand due to experimental database. They have compared GMDH correlation coefficient with genetic programming and neural network correlation coefficients. The results showed that GMDH is better than above mentioned methods.

2. Group data method handling

The Group Method Data Handling (GMDH) is one of soft computing method that has been used in complex and multivariate variable systems modeling. This method was introduced by Ivanenko in 1970. GMDH is based on kolmcogruph – Gabour statement [11].

$$y = a_0 + \sum_{i=1}^{N} a_i x_i + \sum_{i=1}^{N}\sum_{j\geq i}^{N} a_{ij} x_i x_j + \sum_{i=1}^{N}\sum_{j\geq i}^{N}\sum_{k\geq i} a_{ijk} x_i x_j x_k + \ldots \quad (1)$$

In GMDH, a two-variable function was used for calculating outputs in each neuron. Number of neurons was related to number of input variables. For example, if a problem have m input variable, number of neurons in first layer will become $m(m-1)/2$.

$$y_{acual} = w_{11} + w_{12}x_1 + w_{13}x_2 + w_{14}x_1^2 + w_{15}x_2^2 + w_{16}x_1x_2 \quad (2)$$

w_{11} to w_{16} was calculated using Least Square model.

In GMDH, in each layer, weights and outputs of each neurons were calculated and output of neurons with best correlation coefficient formed next layer. The schematic of GMDH is shown in Fig .1

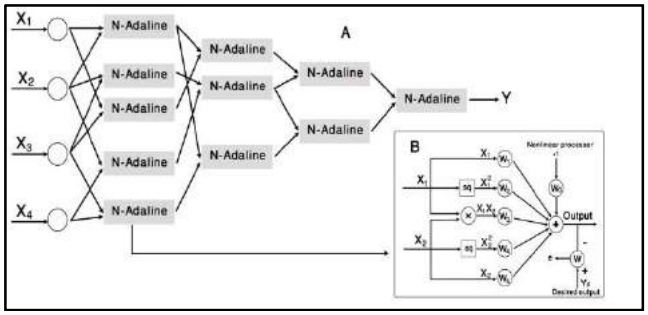

Fig. 1. GMDH structure schematic diagram [11].

3. Liquefaction definition

During earthquakes pore water pressures is increased and effective stress of soil due to dynamic loading is decreased. So, liquefaction is occurred. It is a phenomenon in which the strength and stiffness of a soil is reduced by earthquake shaking or other rapid loading. Liquefaction occurs in saturated soils and saturated soils are the soils in which the space between individual particles is completely filled with water. This water exerts a pressure on the soil particles that. CSR is output and it is a function of $\sigma_v, \sigma_v^{'}$, depth and magnitude of earthquake and $a_{\max}$ and it is defined as Eq. (3)

$$CSR = 0.65\frac{\sigma_v}{\sigma_v^{'}}\frac{a_{\max}}{g}\frac{\gamma_d}{MSF} \quad (3)$$

Where g is acceleration due to gravity. γ_d is stress reduction factor and MSF is magnitude scaling factor .

4. Data from Earthquake

In this study, there were 226 data sets of laboratory measurement were collected from published literature. The data set used in this research for liquefaction prediction is similar to [5,12-13]. 151 of these data sets were used for training and the rest were used for testing the applied model. These data sets were gathered by Goh and Goh. (2007) and also used by other researchers for liquefaction prediction. Input variable including Cone tip resistance (q_c), sleeve

friction ratio (R_f), effective stress ($\sigma_v^{'}$), total stress (σ_v), maximum horizontal ground surface acceleration ($a_{\max}$) and earthquake moment magnitude (M_w) [5].

5. Results and discussion

In this paper, in first layer there are seven in depended variables. Therefore, in first layer, therefore in first layer there were 21 neurons. Because of the GMDH convergence 6 of neurons with best correlation coefficient were selected to form second layer this process was continued until only one neuron was remained. One drawback of the commonly used neural network approach is the time consuming iterative (trial and error). The Group Method of Data Handling (GMDH) calculated weights and relationship between the variables. Further research into producing interpretable results with confidence measures is needed

6. Conclusion

This study presents an alternative algorithm, the GMDH that can be considered to analyze classification-type problems. The GMDH has been successfully applied to assess liquefaction potential. This paper has demonstrated the viability of the GMDH to model the complex relationship between the seismic and soil parameters, and the liquefaction potential using in situ measurements based on the CPT. The overall classification success rate for the entire data set is 96% and is comparable with those calculated using neural networks. The GMDH used For liquefaction assessment are available from the writers. A further development currently being considered is a Probabilistic based approach to assess liquefaction potential by the integration of Bayesian statistics with the GMDH..

7. References

[1] Bjerrum, J., 1973. Geotechnical problem involved in foundations of structures in the North Sea. Geotechnique 23 (3), 319–358.

[2] Nataraja, M.S., Singh, H., Maloney, D., 1980. Ocean wave-induced liquefaction analysis: a simplified procedure. In: Proceedings of an International Symposium on Soils under Cyclic and Transient Loadings, pp. 509–516..

[3] Sassa, S., Sekiguchi, H., 2001. Analysis of wave-induced liquefaction of sand beds. Geotechnique 51 (2), 115–126..

[4] Juang CH, Yuan H, Lee D-H, Lin P-S. Simplified cone penetration test-based method for evaluating liquefaction resistance of soils. JGeotech Geoenviron Eng ASCE 2003;129(11):66–80.

[5] Goh, A. T. C., & Goh, S. H. (2007). Support vector machines: Their use in geotechnical engineering as illustrated using seismic liquefaction data. Computers and Geotechnics, 34, 410–421

[6] Rahman MS, Wang J. Fuzzy neural network models for liquefaction prediction. Soil dynamics and earthquake engineering. 2002 Sep 30; 22(8):685-94.

[7] Jeng DS, Cha DF, Blumenstein M. Neural network model for the prediction of wave-induced liquefaction potential. Ocean Engineering. 2004 Dec 31; 31(17):2073-86.

[8] Abdel-Aal RE, Elhadidy MA, Shaahid SM. Modeling and forecasting the mean hourly wind speed time series using GMDH-based abductive networks. Renewable Energy. 2009 Jul 31;34(7):1686-99.

[9] Qaderi, K., Arab., D. R., Teshnelab, M, Ghazagh, A. Intelligence operation modeling of reservoir using group method of data handling (GMDH). Iran-Water Resources Research, 2011(Issue 3), 52-65. (In Persian).

[10] Pournemat, R. N., Qaderi, K., Karimi, Gh. Sh. Rainfall-Runoff modeling using Artificial Neural Network (ANN) and Group Method Data handling. Watershed management research, 2004 Issue5 (10), 68-84(In Persian).

[11] Ivakhnenko, A.G. The group method of data handling – a rival of the method of stochastic approximation. Soviet Automatic Control c/c of Avtomatika, 1968;1(3), pp. 43-55.

[12] Kalantary F, MolaAbasi H, Salahi M, Veiskarami M. Prediction of liquefaction induced lateral displacements using robust optimization model. Scientia Iranica. 2013 Apr 30;20(2):242-50.

[13] Rahmani A, Fare OG, Pak A. Investigation of the influence of permeability coefficient on the numerical modeling of the liquefaction phenomenon. Scientia Iranica. 2012 Apr 30;19(2):179-87.

VERIFICATION IMPACT OF ARVAND RIVER SEDIMENT ON KHUZESTAN PROVINCE SHORELINE

Ardalan Hamedi[1], Ali Nasrollahi[2] and Ali Asghar Hodaiee[3]

1) Pishahangan Amayesh Consultant Engineering , Tehran, Iran, ardalan.hamedi@gmail.com
2) Jahad Water Resource Consultant Engineering, Tehran, Iran, Nasrollahi_a@yahoo.com
3) Pishahangan Amayesh Consultant Engineering, Tehran, Iran, hodaeiaa@gmail.com

1. Introduction

Current geomorphology of Khuzestan Province coasts is the results of morphogenesis ruling of the onshore and offshore environments. These systems are active simultaneously but their impact is not equal and regarding to regional circumstances, one of them is the predominant factor. Two existence factors of large rivers and strong currents caused by tides play vital roles.

2. Formation of Khuzestan Province Shoreline

Rivers have a fundamental role in progressing of shorelines and tidal currents are effective of coasts erosion.

Generally, coastal region of Khuzestan Province, in terms of morphology predominance systems can be divided into three zones. In the east and west areas, as shown in figure 1, land environmental system is governing system and land has been developing towards the sea shore. In central part of the province, the marine environmental system is ruling system. Figure 1 shows the effect of morphology systems in this area.

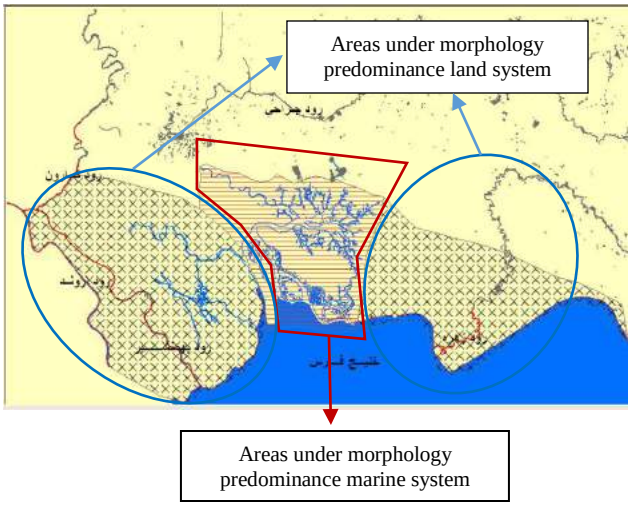

Fig1: Areas under morphology predominance land and marine systems

As can be seen in Figure1, west of the province affected by Arvand River sediments. The enormous volume of Arvand sediments impact on shorelines by wide delta formation. Deposits of this delta are silt and clay. Consideration of development this Delta shows that, its morphological status is not equal and has experienced changes over time, especially in recent years due to lots of changes in upstream and tributaries of Arvand River, rate of progress Arvand Delta River has decreased.

3. Simulation

The mathematical model is used to simulate Khuzestan Province shoreline changes due to progress of Arvand River Delta.

Given that sediments of this area are fine-grained and the mean diameter of them are less than 0.02 mm, mud transport module of Mike21 mathematical model is used for simulations.

In this research, because of having the same sediment characteristic of Khuzestan Province, model Parameters achieved from data measurements in other parts of Province, similar project and returning to the existing references. Table 1 illustrated lists and assumed values of sediment parameters that used in model.

Table 1. Sediment parameters used in the model

Parameters	Symbols	Value	Unit
Erosion Coefficient	E	0.005	g/m2/s
Fall Velocity	W	0.0004	m/s
Critical shear stress of erosion	τ_{ce}	0.1	N/m2
Critical shear stress of sedimentation	τ_{cd}	0.01	N/m2
Diffusion Coefficient	D	1	m 2/s

Before implementation of sediment model, it needs to run and calibrate hydrodynamic model. For this purpose, hydrodynamic module (HD FM) of Mike21 mathematical model is used for simulations. Also for model calibration measurements of water level in vicinity of arvandkenar port (located in eastern shore of Arvand River) is used. Figure 2 illustrates position of extracted model results.

Moreover, figure 3 displays comparison of measured tidal levels and extracted model results.

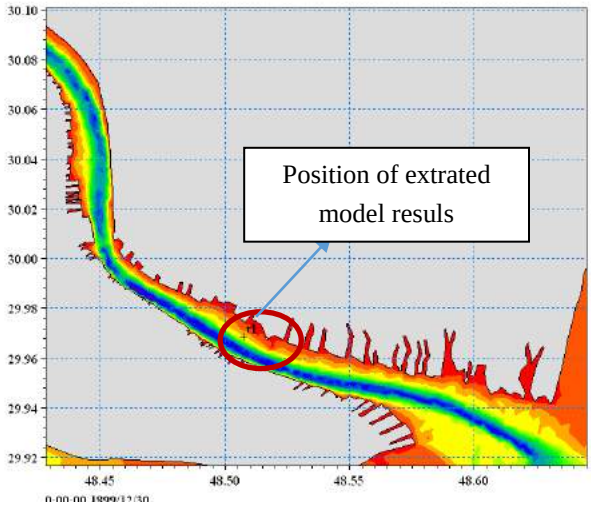

Fig 2: Position of extracted model results

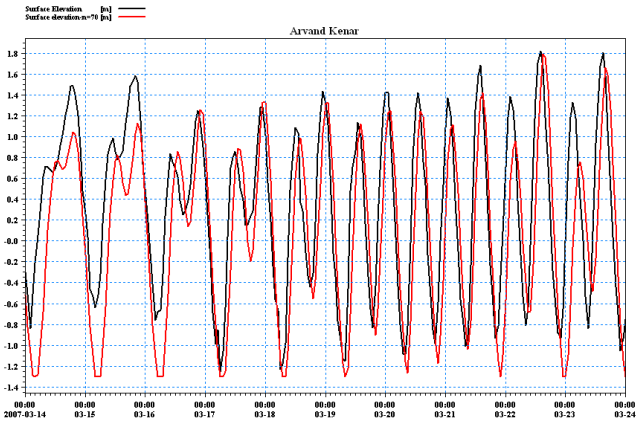

Fig 3: comparison of measured tidal levels and extracted model results

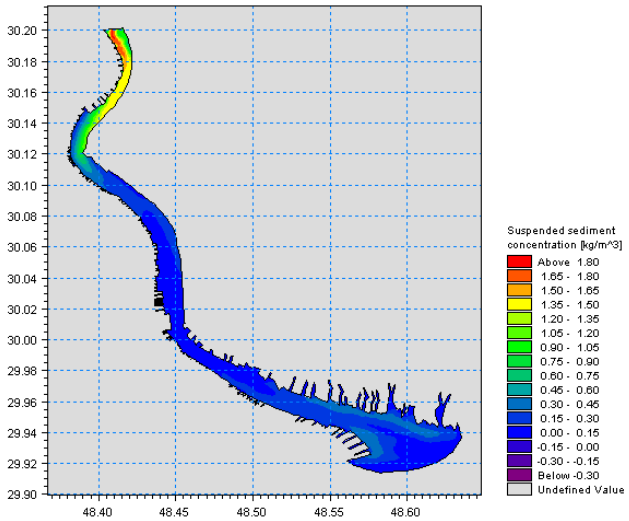

Fig 4: Suspended sediment concentration in the case of natural Arvand River discharge

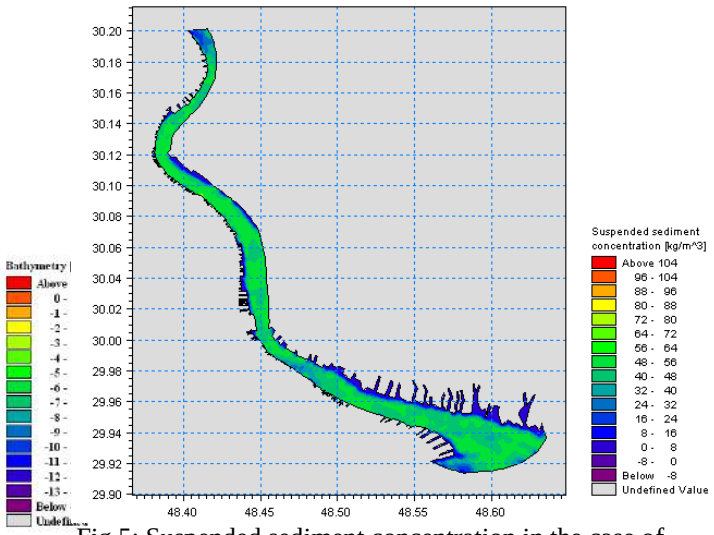

Fig 5: Suspended sediment concentration in the case of flood Arvand River discharge

4. Results

As can be seen in Figures 4 and 5, after decreasing of Arvand River discharge in the recent years, Arvand river has not capability of transporting sediments into Persian Gulf in the case of natural Arvand River discharge but in the case of flood Arvand River discharge, the Arvand river entered large amount of sediments into Persian Gulf that is making progress of Arvand Delta River.

For a better conclusion, take advantage of comparison between Satellite Image and aerial photos in the different periods. Comparison of these photos show that Arvand River during 1973 to 2015 has a large development into the sea.

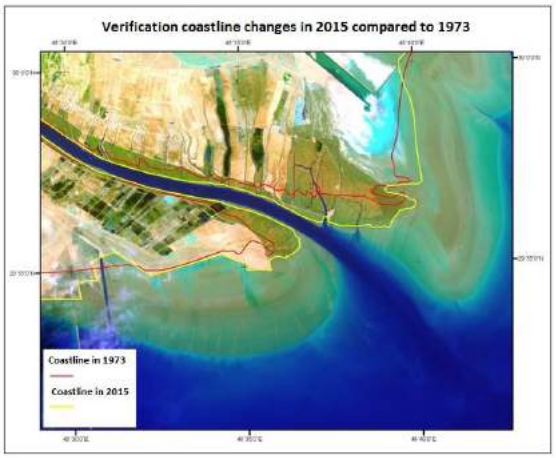

Fig 4: Coastline changes in 2015 compared to 1973

5. References

[1] Van Rijn..,"Principle of sediment transport in rivers, estuaries and coastal seas", 1993.

[2] Dezab consultant engineering report." Hydrology studies of Kuzestan Construction Control Line project", April 1999.

[3] Manual on MIKE21 Hydrodynamic Module FM.

[4] Manual on MIKE21 Mud Transport Module.

MATHEMATICAL MODELLING OF SEDIMENTATION IN THE PORT OF DEYLAM

Ali Nasrollahi[1]

1) Jahad Water and Energy Research Company, Tehran, Iran, Nasrollahi_a@yahoo.com

1. Introduction

Siltation of harbor basins and navigational channels is a serious problem all over the world. Because of siltation, basins and channels require frequent maintenance dredging which its costs are fairly high.

The port of Deylam is located in the northwest of the port of Bushehr where locates in coast of Hendijan bay which involves a shallow water region. The large part of the Hendijan bay covered by very fine material and cohesive sediment too. Figure 1 indicates location of the port of Deylam as well as a snapshot which shows a seaward view of its jetties. This port has two jetties to protect navigational channel against sedimentation in order to have a suitable navigational depth.

This Paper is aimed to study on mathematical modelling of sedimentation using MIKE21-MT [2]. The results of model are verified and calibrated using field measurements. The model results show that sedimentation between jetties and harbor basin, respectively, is about 45000 and 16000 cubic meter per year.

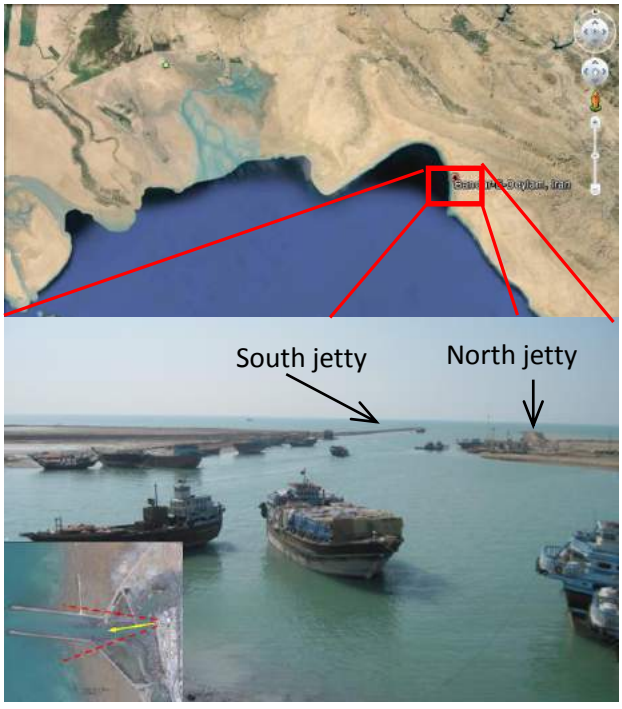

Figure 1.Location map of Deylam port and a seaward view of north and south jetties of the port [1]

2. Data

To study siltation and mud transport needs some data such as, hydrodynamics and sediment properties. Current and water surface level are most important in order to study sediment transport. Hydrodynamic characteristics in front of the port of Deylam obtained from a global model results which contained whole Persian Gulf and calibrated using water elevations in location of some ports extracted from tide tables. Furthermore, sediment characteristics such as mean diameter grain, critical shear stress for deposition and erosion as well as fall velocity are crucial to simulate sedimentation. Unfortunately, there is not any information about critical shear stresses, therefore in this study, these factors are used as calibration parameters.

Two hydrographic surveys were performed in the basin as well as between two jetties at 1392 and 1393[1]. The difference between two hydrographic data which indicates bed level changes in the area during a year, shows in figure 2. As it is shown that between two jetties there are lots of sedimentation especially in entrance where sedimentation rate is about 1 m/year and toward the basin its rate gradually reduces. However, in the basin the rate of sedimentation reduces drastically so that in many location bed level changes are negligible.

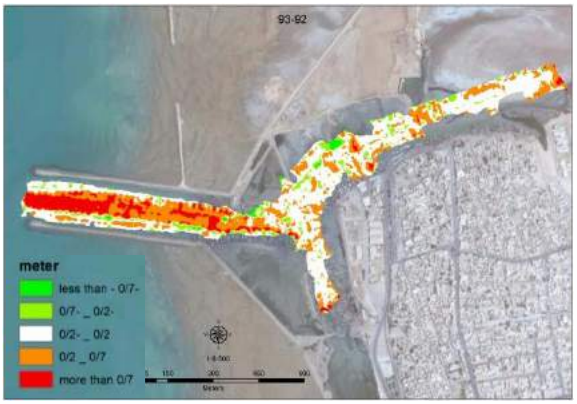

Figure 2. Bed level changes during a year between 1392 and 1393 [1]

3. Model setup

As said above, the MIKE21 MT was used to determine the hydrodynamics and simulation of bed level changes just in navigational channel and harbor basin. Firstly, the most important parameter to setup a model is bathymetry and preparing its file well enough is a crucial activity in

modelling process. So, in this study we used hydrographic survey performed in 1392. Figure 3 indicates bathymetry and its simulation area.

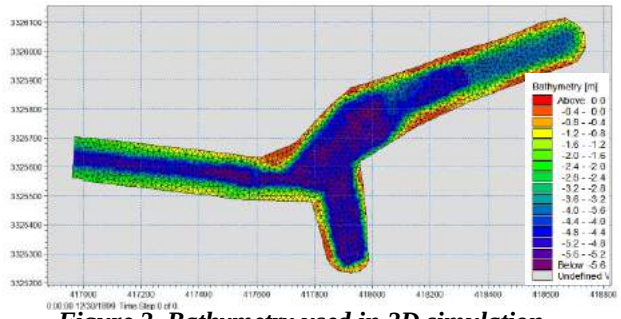

Figure 3. Bathymetry used in 2D simulation

Formerly, the hydrodynamic properties such as water levels, currents and other parameters were simulated in Persian Gulf as global model using flow model. Therefore, flow properties in front of the port as boundary conditions of local model were extracted from global model. Sediment properties were used from measurements performing in the area at the end of year 1393 [1]. Moreover, in MT model default values of parameters were used for parameters which there is no information.

4. Results analysis

It must be noted that simulation period took account about one year in order to compare with bed level changes, as in figure 3.

Figure 4 shows pattern of flow and current speed in ebb condition. In this condition, flow pattern is quite uniformly distributed especially between jetties. However, in the harbor basin the amount of current speed is negligible.
Figure 5 indicates flow pattern and current speed in flood condition. As it seen, the main part of flow approaches to north jetty and enters to harbor basin. Although, near south jetty, there is not quite flow. The maximum of current speed, in this situation, is about 0.2 m/s.

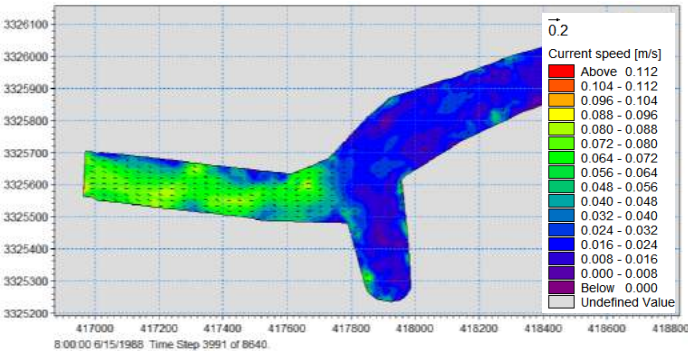

Figure 4. Pattern of tidal current in ebb condition

The result of siltation was represented in figure 6. As it shows, maximum sedimentation occurred in the entrance of the port and it was about 1 m that equaled by real situation. The results show that by decreasing the amount of critical shear stress for deposition, sedimentation reduced and approached to measurements so that D=0.002 model results have best agreement with field data.

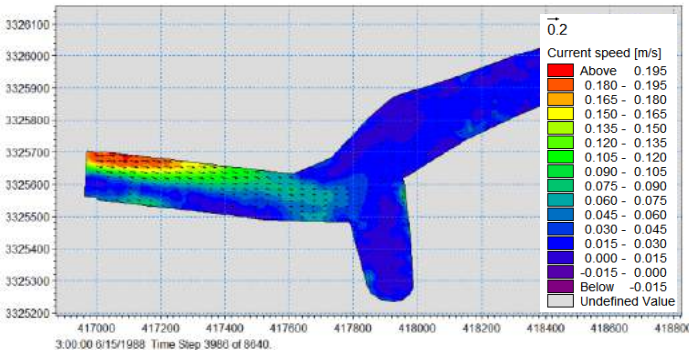

Figure 5. Pattern of tidal current in flood condition

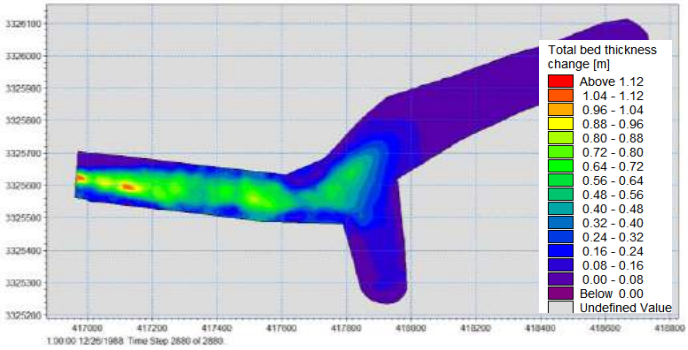

Figure 6. Modelled annual sedimentation rate

5. Conclusion

In this study, sedimentation phenomenon was simulated by MIKE21 MT and the results were calibrated and verified. Mathematical models were used to gain profound understanding about hydrodynamic and sedimentation processes. Based on results some conclusions can be drown. First of all current speed in flood condition was more than ebb one. Although, Flow pattern between jetties in ebb condition was quite more uniform than in flood condition.

Calibration values for critical shear stress for deposition is D=0.002 and for erosion in soft and hard layers are, respectively, 0.1 and 0.2. Calibrated MT model indicated that sedimentation between jetties and harbor basin, respectively, was about 45000 and 16000 cubic meter per year while hydrographic surveys showed that those amounts were about 42000 and 25000 cubic meter per year.

6. References

[1] JWERC, 1394,"Sedimentation study in the port of Deylam"
[2] DHI, 2011, "Mud transport Module, User Guide"

EVALUATION OF SEDIMENT TRANSPORT IN ACCESS CHANNEL OF SHAHID RAJAEE PORT

Amir Hossein Parvin Ashtiani[1], Mohammad Javad Ketabdari[2]

1) MSc, Faculty of Marine Technology, Amirkabir University of Technology, Tehran, Iran, ahparvin@aut.ac.ir
2) Associate Professor, Faculty of Marine Technology, Amirkabir University of Technology, Tehran, Iran, ketabdari@aut.ac.ir

1. Introduction

Sedimentation and erosion are the most important issues which cause serious problems in the port areas. The consequences of these phenomena are reduction of the service life of the port and unavoidable continual and costly dredging. Shahid Rajaei port (located at 56º04'E, 27º05'N near Bandar-e-Abbas in south of Iran.) is one of the most important ports and export and import gate of Iran. The aim of this study was to set up the hydrodynamic modeling of the area to estimate the sedimentation rate using MIKE21 ST. The main focus was investigation of the effectiveness of the rip-rap layer protection and addition of small external branches to the left and right arms of the breakwater on the sedimentation rate in the area.

2. Analysis of the Sediment Behavior of the Area

One of the most influential factors in determination of the sediment transport rate is the bed material properties. Unfortunately in this area the information of the type of the materials is only limited to the grading curve. Therefore due to lack of the complete data the most appropriate way to considering the problem is base studies and the engineering judgment. For example using *Figure 1* the general properties including cohesive condition could be predicted with regard to the constitutive materials of the bed clay, sand and gravel [1, 2]. These studies show that for this area, despite the fine aggregate nature of the bed, due to the low proportion of clay the dominant sediment of the area is non-cohesive.

3. Hydrodynamic Properties of the Area

Usually waves and tides are assumed as the main influencing factors in marine hydrodynamics Shahid Rajaei Port are located in the Qeshm Strait. According to the previous studies, the phase and level gradient of the tides cause some major local currents in this region. Also, based on the collected data of this region, in comparison with tides the wave impact is negligible. Thus an area of approximately 70 Km which is stretched from Bandar e Abbas and Hormuz Island to Khouran Strait was considered to investigating the sediment transport rate in the area due to tidal currents.

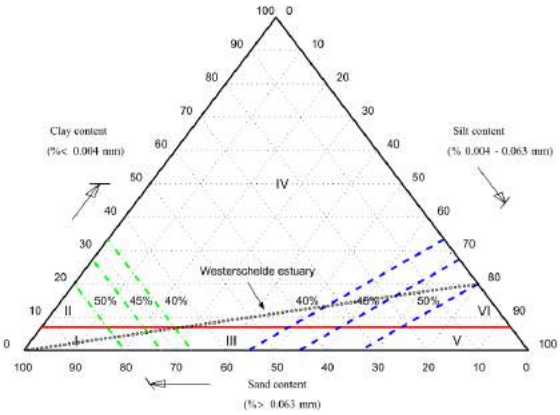

Figure 1. Sand-silt-clay digram with transition for cohesion and network structure [1]

4. Bed Roughness Effects

Roughness of the bed is a major factor influencing the current formation and its speed [3]. It also affects the form of the bed and the grading [4]. Bed roughness indicates the bed resistance against flow motion [5]. Considering the complicated conditions in the sea due to existence of different marine currents and waves, it is necessary to protect against erosion in most susceptible places. Such protection against erosion can be performed in special locations such as around piles, culverts and platform foundations using rip rap layers. This can increase the boundary layer thickness equivalent to roughness increase where the shear stress displaces the bed to the theoretical one above the real bottom [6]. The aim of this study was simulation and evaluation of effectiveness of the rip rap layer protection by different roughness on sedimentation rate in the area. Figure 2 shows the modeled area with different roughness. In this section, in the erodible areas

around the port, roughness increased by rip rap with Manning Number of 28 and 33 (equivalent roughness of 0.5, 0.2 m respectively). In other parts the natural bed with Manning of 55 (equivalent roughness of 0.01 m) were used. In addition to the bed surfaces changes 13 points were considered as benchmark in different locations of the area to monitor the bed changes. Figure 3 shows the results for point 1.

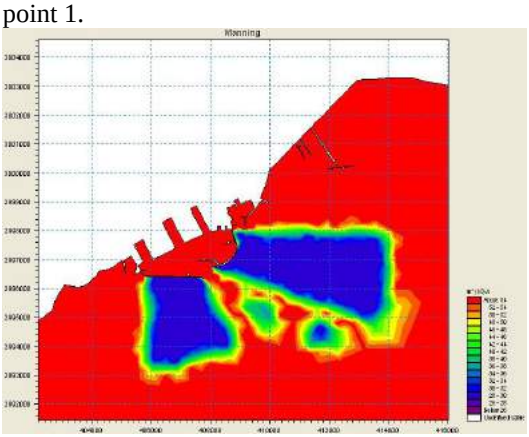

Figure 2. Simulated area with rip rap covered bed

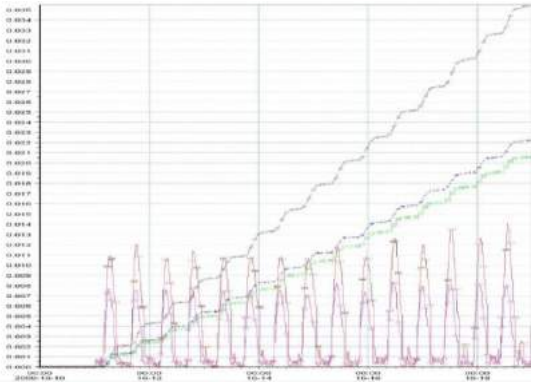

Figure 3. Comparison of bed level changes in Point 1 due to bed roughness changes.

5. Influences of Adding Branches to the Arms of the Breakwater

Figure 4 shows the breakwater after adding external Small branches to its left and right arms and flow pattern in this vicinity. This figure clearly shows that the construction of these two branches could greatly effects the tidal currents pattern in the region. The model output reveals that erosion is reduces at breakwater head. Furthermore the erosion zones location moves away from the edges of the main body of the breakwater. It can be seen in results that sedimentation zone moves downward and its severity decreases. However a part of the sediment load has been accumulated behind the arms. Therefore due to the generation of vortex flows in the access channel vicinity, local sedimentation occurred. Nevertheless overall results show that the average sedimentation in the basin and the access channel has been reduced.

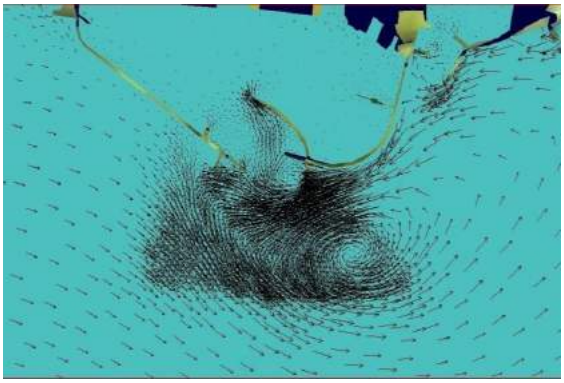

Figure 4. Pattern of the induced circulation currents in breakwater entrance after addition of external branches

6. Conclusions

In this case study Shahid Rajaei Port was numerically investigated for sediment situation. The results showed that the areas of close to arms and out of the breakwater are mostly erodible. However the access channel is susceptible for deposition. The average depth of deposition was about 0.03 m during 8 days of running the model. The rate of sedimentation in the basin was negligible. By increasing the bed roughness to 28 in the erodible areas around the port, a 30% decrease of sedimentation and erosion in surrounding areas and access channel occurred. By constructing of two external arms perpendicular to the both arms of the breakwaters, main changes are obtained in the current circulation pattern leading to reduction of the average sedimentation in the basin and the access channel.

7. Acknowledgement

The authors would like to thank the General Director of Coastal and Port Engineering Department of Ports and Maritime Organization (PMO) for it help and support of this research.

8. References

[1] Van Ledden, M., Van Kesteren, W.G.M., Winterwerp, J.C.," A conceptual framework for the erosion behavior of sand–mud mixtures", *Continental Shelf Research 24*,2004, pp. 1-11.

[2] Jacobs, W., Hir, P.L., Van Kesteren, W., Cann, P.," Erosion threshold of sand–mud mixtures", *Continental Shelf Research 31*, 2011, pp. 11-25.

[3] Van Rijn, L.C., "*Principles of sediment transport in rivers, estuaries and coastal seas*", *AQUA Publication*,1993

[4] Soulsby, R., "Dynamics of marine sands: A manual practical application", *Pub. Telford*,1997

[5] Parvin A.A.H, "*Estimation of sediment transport rate in Hormozgan coastal zone*". M.Sc thesis. AmirKabir Univ., Supervised by Ketabdari, M.J, 2013

[6] Dixen, M., Hatipoglu, F., Sumer, M., Fredsoe, J., "Wave boundary layer over a stone-covered bed", *Coastal Engineering 55*, 2008, pp. 1-11.

EXPERIMENTAL STUDY ON THE EFFECT OF SEDIMENT SHAPE ON JUMP LENGTH UNDER ASYMMETRICAL WAVES

Mohammad Moradi[1] and Ahmad shanehsazzadeh[2]

1) Department of Engineering, University of Isfahan, Isfahan, Iran, mmoradi@eng.ui.ac.ir
2) Department of Engineering, University of Isfahan, Isfahan, Iran, a.shanehsazzdeh@eng.ui.ac.ir

1. Introduction

In the coastal zone, sediment transport is one of the most important processes that have direct impact on sediment transport and overall morphological evolution of coastline. The part of a beach that is frequently covered by uprushes and exposed by return of water seaward is named swash zone. It is the boundary condition for the integrated domain of models of the coastal zone [1].

The flow regime in the swash zone contains a number of highly asymmetric waves. For attaining insight to the swash zone sediment transport, it is necessary to develop an extensive series of experimental and field measurements in such flow condition to verify the computational results of sediment transport [2].

Studies on the effect of the shape of particles on the rate of sediment transport are more focused on unidirectional currents [3, 4]. However, the influence of the particle shape on the sediment response to the waves and in particular asymmetric waves that experience in the swash zone is questionable.

Scope of the present study is an experimental study on the effect of the sediment shape on the particle jump length under highly asymmetrical single waves for implication in the swash zone.

2. Experiments

In order to generate a single, very highly accelerated asymmetric wave in the laboratory, similar to the flow over the surf and swash zone, a mechanical apparatus called Single Asymmetric Wave Generator (SAWG) that has been used in Shanehsazzadeh and Holmes (2013) is redesigned and developed (Figure 1) [5].

Three particle sizes namely 2.9, 3.1 and 4.1 mm are considered for study. In orther to recognize the motion and jump lengh of the sediments, selected particles are marked by different colors according to their shape, as follows (Figure 2):

Green: low sphericity and very rounded
Blue: high sphericity and angular
Yellow: high sphericity and very rounded
Orange: mid sphericity and sub-rounded

Figure 2. Sediments marked by colors

Figure 3. colored sediments on the bed

The jump length of marked particles are monitored by eye. Then the original and new positions of each one were recorded before and after the each wave event.

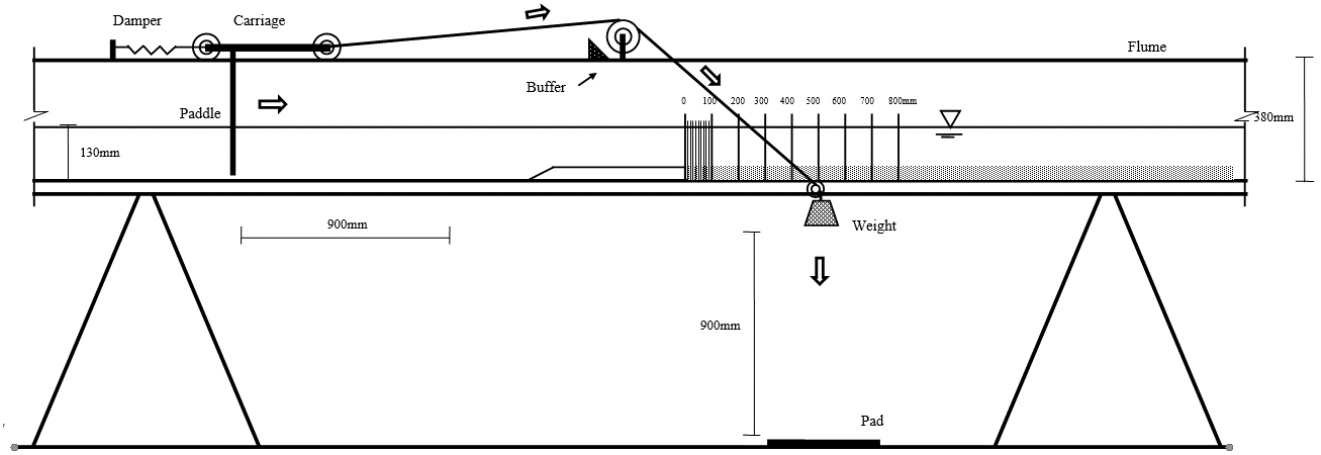

Figure 1. The Single Asymmetric Wave Generator (SAWG)

3. Experimental results

Since there is difference between particles that firstly dropped on the surface and particles naturally lay inside the surface, the first two or three jumps do not represent the real condition. Figure 4 shows the average of the jump lengths in two flow regimes. The first, second and third jumps are not in the natural condition. Therefore, in this study, fourth and fifth jumps that have more natural behavior are considered.

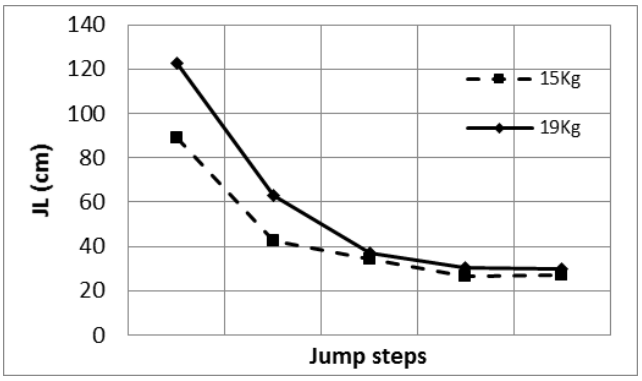

Figure 4. The average of the jump lengths in the same enargy

The jump length is a stochastic phenomenon due to the geometry of the sediment and position of the sediment at the bed. Distribution of the jump length due to a single asymmetric wave is presented in Figure 5. As shown in the figure, the vast range of jump length is occurred for an identical flow condition. In this study the average of more than 500 jump length of the particles are considered for each asymmetric single wave.

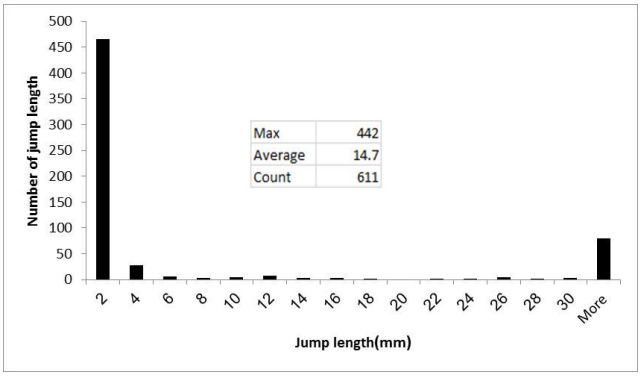

Figure 5. Distribution of Jump length

The average jump length of particle in different flow conditions for various shapes of particles is presented in Figure 6. The maximum velocity is considered as the representative of the flow regime. As can be seen in the figure, in the same flow velocity, the spherical sediments have more Jump length (Blue and yellow sediments). On the other hands, low sphericity shape (green) sediment clearly has the shortest Jump length. As presented in the Figure, the results of yellow and blue sediments are very close; demonstrating that rounded and angular shape of these two particles is of less effective. Among sediments with different diameters, low sphericity sediment (green) has the lowest jump length. In general, the results show the overall shape of sediment is effective on the jump length.

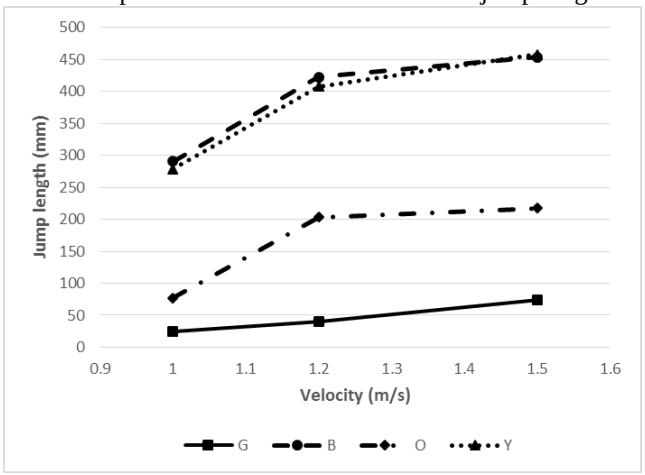

Figure 6. The average jump length of 3.1 mm sediment particles of various shapes

4. Conclusion

In this article, the effect of particle shape on the behavior of sediments under a single asymmetric wave is experimentally studied. The results show that the shape of the particles highly influences the jump length, whereas the jump length of high sphericity particles (rounded and angular) in some conditions is 5 times more than particles with low sphericity.

High asymmetric waves generated in this study present the flow regime in the swash zone. Thus, the present study improves the insight to the problem of sediment transport in the swash zone.

5. Reference

[1] Longo, S., Petti, M., and Losada. I.J., "Turbulence in the swash and surf zones: a review", *Coastal Engineering*, 45, 3, May 2002, pp.129-47.

[2] Bakhtyar, R., Barry, D.A., Li, L., Jeng, D.S., and Yeganeh-Bakhtiary, A., "Modeling sediment transport in the swash zone: A review". *Ocean Engineering*, 36, 9, 2009, pp.767-783.

[3] Lane, E.W., and Carlson, E.J., "Some observations on the effect of particle shape on the movement of coarse sediments", *Eos, Transactions American Geophysical Union*, 35, 3, 1954, pp.453-462.

[4] Van Rijn, L.C., "Sediment transport, part I: bed load transport", *Journal of hydraulic engineering*, 110, 10, 1984, pp.1431-1456.

[5] Shanehsazzadeh, A., and Holmes, P., "Coarse sediment particle motion under highly asymmetrical waves with implications for swash zone sediment transport", *Coastal Engineering*, 71, 2013, pp.60-67.

FALLING SEDIMENT PARTICLES UNDER PROGRESSIVE WAVE

Hanifeh Imanian[1], Mina Zakipour[2] and Morteza Kolahdoozan[2]

1) Engineering Department, Alzahra University, Tehran, Iran, h.imanian@alzahra.ac.ir
2) Department of Environmental and Civil Engineering, Amirkabir University of Technology, Tehran, Iran

1. Introduction

Coastal areas are a typical example of multi-phase environment, which sediments and marine waters interact another during time.

Herein, a two-phase numerical lagrangian model using MPS method is developed which precisely simulate sediment particles motion in flow domains.

The developed two-phase model is applied in a calm water tank and sediment falling is studied. Calculated results are in accordance with experimental data and the ability of developed model in sediment motion prediction is approved.

In the next step, the developed model is applies in a wave flume and sediment motion under progressive wave is predicted.

2. Governing Equations and MPS Discretization

The governing equations of incompressible viscous fluid flow are the continuity and momentum conversation equations:

$$1/\rho \, D\rho/Dt + \nabla . \mathbf{u} = 0 \quad (1)$$

$$D\mathbf{u}/Dt = -1/\rho \nabla P + \nabla . (\nu_t \nabla \mathbf{u}) + \mathbf{g} \quad (2)$$

where u= velocity vector, t= time, ρ= fluid density, P= pressure, ν_t= fluid eddy-viscosity and g= gravitational acceleration.

In the MPS method, the governing equations are converted to interaction equations of particles using different operators. All interactions between particles are limited to a specific distance known as efficient radius. The weighting of different neighboring particles within the efficient radius on the desired particle is calculated based on Kernel functions:

$$w(r) = \begin{cases} r_e/r - 1 & 0 < r/r_e \le 1 \\ 0 & 1 < r/r_e \end{cases} \quad (3)$$

where r= distance between two particles i and j, r_e= efficient radius and w= Kernel function.

The particle number density can be computed as:

$$\langle n \rangle_i = \sum_{j \neq i} w(|r_j - r_i|) \quad (4)$$

where n_i= particle number density of i in location r_i. The continuity equation is satisfied if the particle number density is constant in incompressible fluids, which is denoted by n^0 and is called standard density.

A gradient operator is obtained as the average of gradient vectors which are determined between two neighboring particles. It is modelled as:

$$\langle \nabla \phi \rangle_i = d/n^0 \sum_{j \neq i} \left[\frac{\phi_j - \phi_i'}{|r_j - r_i|^2} (r_j - r_i) w(|r_j - r_i|) \right] \quad (5)$$

where ϕ= arbitrary physical quantity, d= number of dimension (for 2D is replaced with 2), r_i= location vector for particle i, and ϕ'= minimum amount of ϕ belongs to the neighbouring particles in the efficient radius:

$$\phi_i' = \min(\phi_j) \quad \text{for} \quad \{w(|r_j - r_i|) \neq 0\} \quad (6)$$

The Laplacian operator is derived from the physical concept of diffusion. It has a conservative form since the quantity lost by particle i is attracted by particles j. This operator can be written as follows:

$$\langle \nabla^2 \phi \rangle_i = 2d/n^0 \lambda \sum_{j \neq i} [(\phi_j - \phi_i) w(|r_j - r_i|)] \quad (7)$$

3. Falling Sediment Particle in Calm Tank

A sediment particle is placed in a calm water tank. Falling path and its velocity are simulated using developed MPS numerical model.

The water tank is closed and has no free surface, with a height of 6 cm and 2 cm wide (Figure 1) [1].

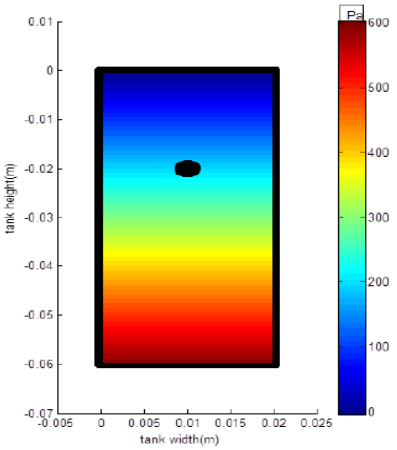

Figure 1. Fluid initial pressure in calm tank

Numerical modeling specifications are presented in Table 1.

Table 1. Falling sediment particle in calm tank

Sediment density (kg/m^3)	1500

Water density(kg/m^3)	1000
Sediment particle diameter (mm)	1.25
Water particle diameter (mm)	0.1
Number of particles	120000
Time step (s)	0.001
Sediment initial position	4 cm above bed 1 cm from side wall

In numerical simulation, sediment is released and falling down in calm water tank. Comparison of calculated non-dimensional sediment falling velocity with experimental data [2] is presented in Figures 2, which is in good agreement. These results approve precise ability of developed MPS model in simulating multi-phase cases.

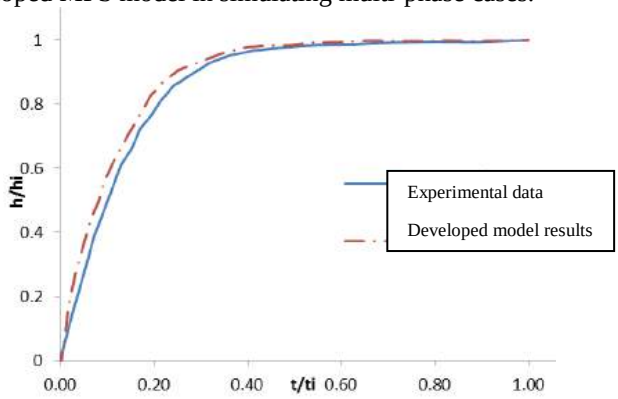

Figure 2. Comparison of experimental data of falling sediment velocity during time and numerical results

4. Sediment Motion in a Wave Channel

4.1. One-Phase Wave Simulation

To model a wave flume, a channel with 1.5 m height and 36 m length with initial water depth 0.65 m is assumed. A total number of 22000 particles with a diameter of 4 cm are considered in the computational domain. The time step was selected equal to 0.002 seconds. A piston-type wave maker considered to have sweep motion to generate waves, which are propagated along channel.

Calculated results of developed MPS model in a section 7 m away from flume beginning are compared with experimental data [3] in Figure 3. It can be seen that present model can predict water surface changes during time accurately.

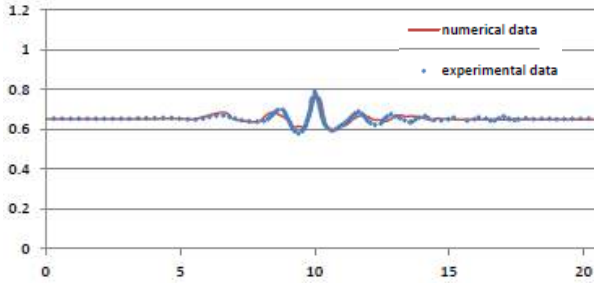

Figure 3. Water level changes during time (section x=7m)

4.2. Two-Phase Sediment Motion Simulation under Progressive Wave

To simulate sediment motion under wave propagation, a wave channel with 8 m length and initial water depth of 0.65 m is assumed. A piston-type wave maker applied to have sweep motion and generate waves. A sediment particle is placed 5.5 m away from flume beginning and 0.54 m above channel datum.

Numerical modeling specifications are presented in Table 2.

Table 2. Sediment particle motion in wave channel

Sediment density (kg/m^3)	1500
Water density(kg/m^3)	1000
Sediment particle diameter (mm)	10
Water particle diameter (mm)	2.5
Sediment initial position	x= 5.5 m y= 0.54 m

Produced waves propagates along channel and sediment particle gradually displaces downward. Sediment Vertical and horizontal position changes are illustrated in Figure 4. This figure shows that developed two-phase numerical is able to predict sediment displacement under different complicated flow domains.

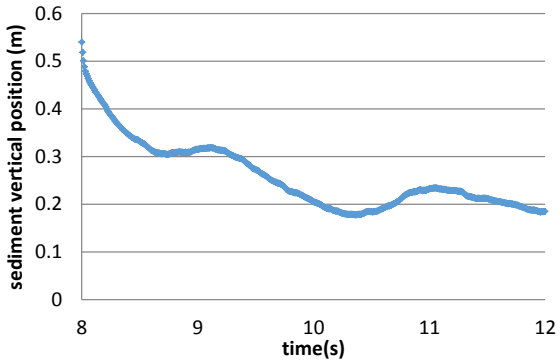

Figure 4. Vertical sediment displacement during time under wave propagation

5. Conclusion

A two-phase lagrangian numerical model using MPS method is developed. The model applying in different normal and complicated flow situations show that present two-phase numerical is able to predict sediment displacement with an acceptable precision.

6. References

[1] Zakipour, M., *Multi-Phase Modelling of Sediment Particle Motion in Fluid Using MPS*, Amirkabir University of Technology, Tehran, Iran, M.S. thesis, 2015, p. 116.

[2] R. Glowinski, T. Pan, T. Hesla, D. Joseph, and J. Periaux, "*A fictitious domain approach to the direct numerical simulation of incompressible viscous flow past moving rigid bodies: application to particulate flow*", Journal of Computational Physics, vol. 169, pp. 363-426, 2001

[3] D.T. Cox and J. Ortega, "*Technical Note Laboratory observations of green water overtopping a fixed deck*", Ocean Engineering, vol. 29(14), pp. 1827-1840, 2002

COASTAL EROSION POTENTIAL AT HORMOZGAN PROVINCE THROUGH SATELLITE IMAGE ANALYSIS

Arefi, R.[1], Siadatmousavi, S.M. [2], Hajmomeni, A.[3], Khalili, H.[4] and KouroshNia, A.[5]

1) Senior Engineer, Sazeh Pardazi Iran Consulting Eng. Co., Tehran, Iran, r.arefi@sazehpardazi.com
2) Assistant Professor, Iran University of Science and Technology, Narmak, Tehran, Iran, siadatmousavi@iust.ac.ir
3) Head of Coastal Process and Hydraulic Discipline, Sazeh Pardazi Iran Consulting Eng. Co., Tehran, Iran, a.hajmomeni@sazehpardazi.com
4) Head of Coastal Management Department of Ports and Maritime Organization (PMO), Tehran, Iran, hkhalili@pmo.ir
5) Senior Engineer of Coastal and Port Engineering Department of Ports and Maritime Organization (PMO), Tehran, Iran, akouroshnia@pmo.ir

1. Introduction

Information on the rates of erosion or sedimentation and trends of shoreline change would be used to improve our understanding of the underlying causes of coastal erosion and the potential effects on coastal populations and infrastructure. This information can improve coastal management decisions [1]. Long-term beach erosion is aggravated locally by engineering works, such as breakwaters and long jetties. Construction of seawalls results in shifting of erosion sites from one place to another adjacent place, whereas, breakwaters act as barriers for littoral drift [2] and cause accretion of sediment in the immediate vicinity of the structure and erosion on its downstream side.

The erosion induced by man-made structures is studied for coastal zone of Hormozgan province in Iran as a part of Hormozgan ICZM project. In this regard, all the existing marine structures (60 structures) along the Hormozgan province shoreline and their nearby erosion and sedimentation phenomena are studied. Identification of potential coastal erosion due to construction of coastal structures is very important for shoreline management plans (SMP) that are part of the integrated coastal zone management plan. For this study satellite images over a period of 40 years have been analyzed along the 1000 km coastlines of Hormozgan province and for the first time the effects of water level variations have been included on extraction of the shoreline position.

2. Shoreline extraction

Shoreline change is investigated by comparing the shoreline position over a period of time. To study the accretion or erosion near the structures, the shoreline positions before and after the construction of the structure have been examined using satellite images. In recent decades, satellite imagery has been widely used in the coastal engineering. Among many different available resources, Landsat satellite imagery is selected for this study.

Some phenomena such as tide, wind and wave setup cause water level changes and these variations also affect the shoreline position. To reduce these effects, two images from summer seasons (calm conditions in Persian Gulf to avoid wind/wave setup) are selected which have the same tidal elevations (with tidal level variation below 20cm compare to the reference image of 2015). As shown in Figure 1, several images are required to cover the entire province. Flowchart of coastline monitoring by satellite remote sensing technology is shown in Figure 2. Shoreline position is detected by calculating Normalized Difference Water Index (NDWI), extracting the edge, and smoothing the results. NDWI uses two near-infrared channels; one centered at a wavelength of approximately 0.86 μm (band 3 in Landsat-8 images), and the other at 1.24 μm (band 6 in Landsat-8 images) [3]:

$$NDWI = \frac{B_3 - B_6}{B_3 + B_6} \quad (1)$$

Landsat satellite images consist of eight spectral bands with a spatial resolution of 30 m. After georeferencing and vectorizing the maps, the extracted shorelines are checked visually and the results are smoothed manually near the coastal constructions as shown in Figure 3.

Figure 1. Image exploring in the data bank

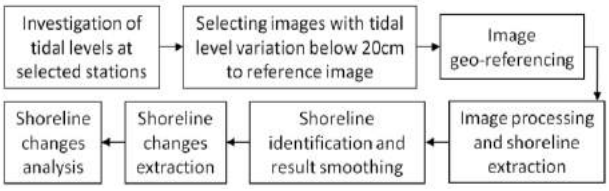

Figure 2. Flowchart of coastline monitoring

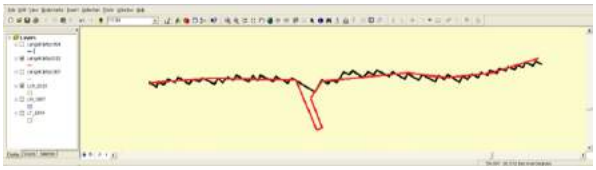

Figure 3. Shoreline vectorizing and result smoothing

3. Shoreline change analysis

As mentioned above, the coastline erosion due to construction of future structures could be estimated using the analysis of the shoreline position before and after the construction of the existing coastal structures. As shown in Figure 4, the downstream coastline near the Bostaneh is erosive, while there is no erosion around the Kalat-e-Aftab port.

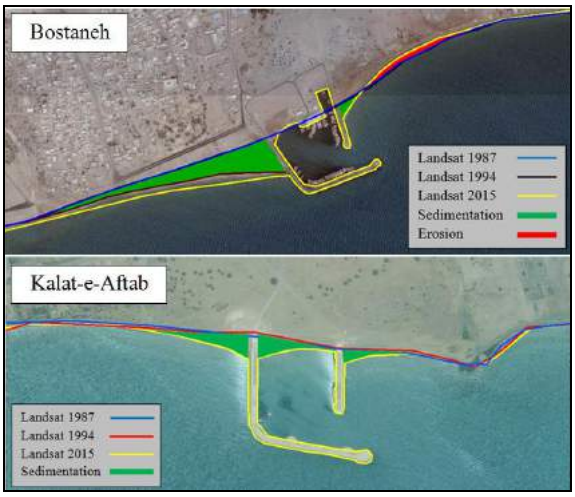

Figure 4. Sedimentation and erosion around the Bostaneh and Kalat-e-Aftab ports

In addition to satellite images, site visits, interview with local stakeholders and other resources such as technical reports are used to investigate the morphodynamics of Hormozgan coastlines. Figure 5 shows that at the downstream of the Shioo port, erosion is occurred due to the construction of the breakwater, which has been recorded during the extensive site visits.

Figure 5. Erosion (left) and protection (right) at the downstream of Shioo port

4. Conclusion

Study of shoreline changes is important for a wide range of coastal studies, such as hazard zoning, MIU (Morphological Impact Assessment), and etc studies [4]. In this study potential of coastal erosion due to construction of future coastal structures is detected based on the history of the shoreline changes. In this regard, all 60 existing structures along the Hormozgan province shoreline have been studied. According to sedimentation and erosion regimes around these structures, the coastline has been divided into three groups (erosive, likely erosive, and stable). Figure 6 shows the coastal erosion susceptibility along the Hormozgan shoreline. Detailed figures regarding the erodability of Hormozgan coastlines are available from the Coasts and Ports Engineering Department of PMO via the reports of Hormozgan ICZM project [5].

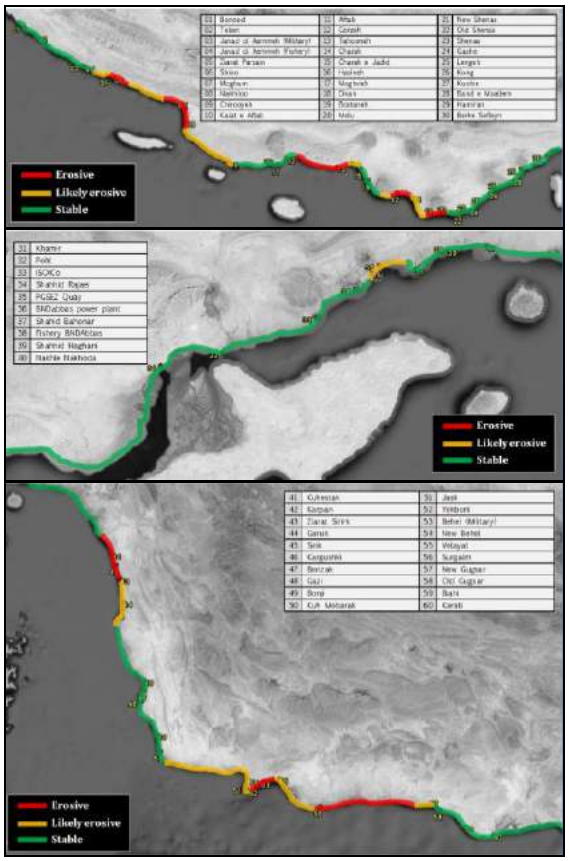

Figure 6. Potential coastal erosion due to future structures in the Hormozgan province

5. References

[1] Thieler, E.R., Smith, T.L., Knisel, J.M., and Sampson, D.W., *Massachusetts Shoreline Change Mapping and Analysis Project, 2013 Update*,

[2] Shetty, A., Jayappa, K.S., Mitra, D., *Shoreline Change Analysis of Mangalore Coast and Morphometric Analysis of Netravathi-Gurupur and Mulky-pavanje Spits*, ICWRCOE, V.4, p.182-189, 2015.

[3] Gao, B., *NDWI-A normalized difference water index for remote sensing of vegetation liquid water from space*, Remote Sensing of Environment, 1996.

[4] Maiti, S., Bhattacharaya, A.K., *Shoreline change analysis and its application to prediction: A remote sensing and statistics based approach*, Marine Geology, 257, 11-23, 2009.

[5] Sazeh Pardazi Iran C.E., *Investigation of shoreline changes of Hormozgan province and sediment study around the coastal structures*, Technical report, Hormozgan ICZM Project, 363p. 2016. (In Persian).

DETERMINATION OF THE ACTUAL LITTORAL SEDIMENT TRANSPORT RATES ALONG HORMOZGAN PROVINCE SHORELINE, IRAN

Ansari, Sh.[1], Arefi, R.[2], Hajmomeni, A.[3], Tavakolani, S.M.[4], and Khalili, H.[5]

1) Senior Engineer, Sazeh Pardazi Iran (SPI) Consulting Eng. Co., Tehran, Iran, sh.ansari@sazehpardazi.com
2) Senior Engineer, Sazeh Pardazi Iran Consulting Eng. Co., Tehran, Iran, r.arefi@sazehpardazi.com
3) Head of Coastal Process Discipline, SPI Consulting Eng. Co., Tehran, Iran, a.hajmomeni@sazehpardazi.com
4) Deputy of Coastal and Port Engineering Department of Ports and Maritime Organization (PMO), Tehran, Iran, mtavakolani@pmo.ir
5) Head of Coastal Management Department of Ports and Maritime Organization (PMO), Tehran, Iran, hkhalili@pmo.ir

1. Introduction

Longshore sediment transport (LST) refers to the movement of beach and nearshore sand parallel to the shore through the longshore currents produced by tides, wind and waves. Identification of the LST rate is essential for sustainable coastal zone management and site selection for marine structures. Analytical expressions for determination of LST rate assume that there are infinite amounts of sand along the shoreline. This assumption is not valid at most locations and it is necessary to distinguish between potential and actual alongshore sediment transport [1].

In this study, the longshore sediment transport rate for Hormozgan province coastline is determined by using LITDRIFT developed by DHI. Considering the long length of Hormozgan coastline (1000 km), the coastline is divided into a number of segments. The model is calibrated based on the actual rate of sedimentation around the existing structures such as breakwaters and long jetties. Although the periodic hydrography is the best source to determine the actual sedimentation rate, it is not available for all existing structures. Hence, the satellite images are used to investigate the shoreline changes and estimating the sedimentation volume. In addition to the actual littoral sediment transport rate, calibration parameter (bed roughness) along the Hormozgan province coastline is presented in this paper for the first time. This study is part of Hormozgan ICZM project [2].

2. Estimation of actual sedimentation rates

The littoral sediment transport rate is estimated at locations of the existing coastal structures. The deposited sediment volume in the vicinity of these structures is estimated based on one-line theory, where the sedimentation area is multiplied by the closure depth [3].

2.1. Sedimentation area

To determine the sedimentation area in the vicinity of the coastal structures, shoreline changes are investigated by comparing the shoreline position over a period of time and have been examined using satellite images. In this study Landsat satellite is selected among many different resources.

2.2. Depth of closure

Depth of closure is widely used by coastal engineers as an empirical measure of the seaward limit of significant cross-shore and long shore sediment transport on sandy beaches. From Hallermeier (1981) [4]:

$$d_c = 2.28H_{te} - 68.5H_{te}^2 / gT_{te}^2 \quad (1)$$

Where H_{te} is the effective wave height just seaward of the breaker zone that is exceeded for 12 hours per year, T_{te} is the wave period associated with H_{te}, and g is the acceleration of gravity.

2.3. Special notes

At this study some special notes are considered for determination of actual LST rate as follows:

- Exact construction dates are achieved by exploring the satellite images at different time periods.
- The date of sediment bypassing over the coastal structures (for Hasineh and Bostaneh ports) is estimated by comparing the shoreline position at different period of time.
- For some structures which are very close to each other, sedimentation volume is calculated for all structures as a group (e.g. Mogham, Charak and Bahl ports).
- At certain locations in which periodic hydrographies were available, LST rate is calculated by comparing the periodic hydrographies (Karati, Biahi and Surgalm ports).

3. Longshore sediment transport modeling

Calculation of LST rates are performed using LITDRIFT module of LITPACK tool. LITDRIFT model is developed by the DHI Water & Environment. The model is calibrated based on the estimated actual LST rates in the vicinity of existing structures. The results of the littoral sediment calculations are presented as active surf zone width in different directions parallel to shoreline, transport rate in each direction, net and gross rate of longshore sedimentation and its distribution pattern along the cross-shore profile.

3.1. Identification of the shoreline segments

In order to calculate the LST rate along the Hormozgan shoreline, the coastline is divided into 36 segments. General uniformity and similarity in coastline direction, shoreline general landform, and hydrodynamic conditions are the main factors for determination of the segments. (Fig. 1). Sediment and sub-sediment cell boundaries which were identified in the previous studies [5, 6] have also been used for this purpose.

3.2. Calibration of LST model

As mentioned above, the model is calibrated based on the actual LST rates estimated in vicinity of the existing structures. At the areas where the model calibration was not possible (due to the lack of distinct marine structures and other morphological evidences), the results of other similar adjacent segments are applied. Assuming the validity of the sediment model, the calibration coefficient, which is normally bed roughness, has been used for the other locations of the segment shoreline.

3.3. Results of longshore transport model

In Figure 2, a sample of calculated sedimentation volumes around Nakhiloo port and the modeling results of the LITDRIFT model (accumulated net and gross sediment transport, etc) are presented. Such an analysis and corresponding numerical simulations have been carried out for all the existing marine structures in the course of Hormozgan ICZM project

4. Conclusion

In this paper, the littoral sedimentation modeling results of Hormozgan coastlines are presented. Due to the lengthy shorelines of the province and different marine climate along these coasts, the shorelines are divided into segments based on the general shoreline direction and morphology. The geomorphologic formation and marine climate are assumed to be the same for each segment, despite their variation along the shoreline. The LST model is calibrated using the calculated sedimentation rates around the existing coastal structures. Finally actual rates of longshore sediment transport are calculated for all segments. Because the calculated rates are actual (not potential), the results of the study can be used efficiently in shoreline management studies.

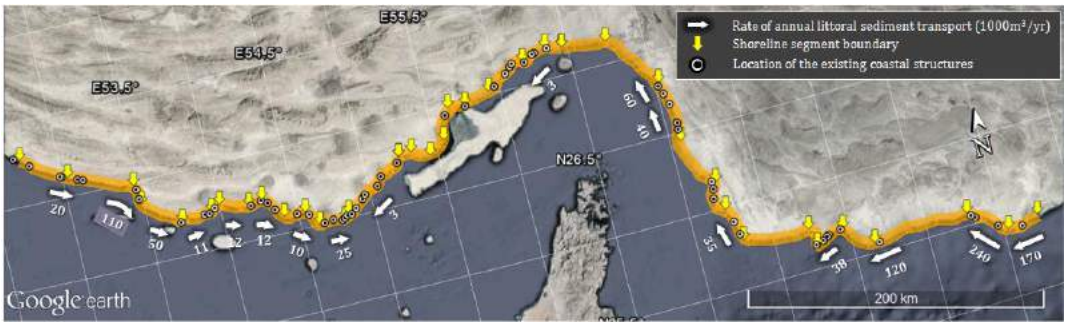

Figure 1. Estimated actual LST rate along the Hormozgan coastline and the LST rate at location of existing structures.

Table 1. Summary of modeling results for Nakhiloo and Soorgalm port.

Shoreline No.	Control Coastal structure	direction of sediment transport	Accum. Net [1000 m^3/y]	Accum. Gross [1000 m^3/y]	Surf zone 90% (+)	Surf zone 90% (-)	Roughness
W-3	Nakhiloo	North to South	55	65	-2.4	-1.3	$2.5\times d_{50}$
E-11	Soorgalm	East to West	122	287	-2.7	-1.6	$50\times d_{50}$

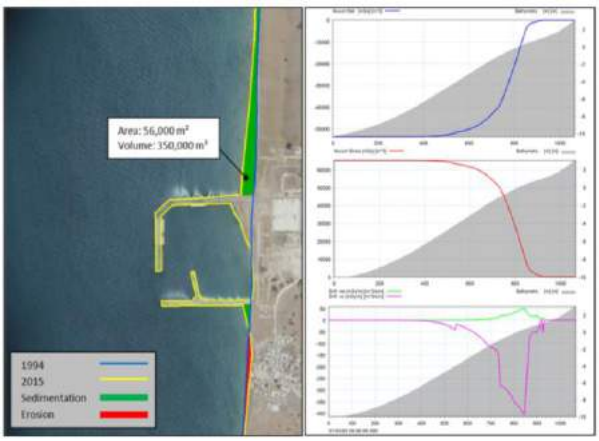

Figure 2. Modeling outputs for Nakhiloo port.

5. References

[1] Kamphuis, J.W., *Introduction to Coastal Engineering and Management*, Advanced Series on Ocean Engineering, Vol. 30.

[2] Sazeh Pardazi Iran C.E., *Investigation of shoreline changes of Hormozgan province and sediment study around the coastal structures*, Technical report, Hormozgan ICZM Project, 363p. 2016. (In Persian).

[3] *CEM - Coastal Engineering Manual*, US Army corps of Engineers, 2006.

[4] Hallermeier, R.J., *A profile zonation for seasonal sand beaches from wave climate*, Coastal Engineering, Vol. 4, 1981.

[5] *Sedimentary cell*, Technical report, Studies of Integrated Coastal Zone Management, ICZM, 2008.

[6] *Determination of Sediment Cells and Sub-Cells*, Technical report, Monitoring and Modeling Study of Coastal Zone of Hormozgan Province Project, 2012.

SEDIMENT TRANSPORT SIMULATION IN TIDAL RIVER BY SPH METHOD

Mahdi Kamfiroozi[1], Seyed Abbas Hossini[2]

1) Department of Civil Engineering, Science and Research Branch, Islamic Azad University, Tehran, Iran, Email:Kamfiroozi.m@gmail.com
2) Department of Civil Engineering, Science and Research Branch, Islamic Azad University, Tehran, Iran, Email:abbas_hoseyni@srbiau.ac.ir

1. Introduction

A Tidal River is a river that connected to sea or ocean and whose flow and level are influenced by tides. Suspended sediment moving along with the rivers has complex behaviors. In here, the two-dimensional numerical simulation of sediment behavior was performed using SPH[1] Method.

2. SPH Method

Smoothed Particle Hydrodynamics (SPH), a mesh free method, is based on integral interpolation. In this method, all fluid parameters such as density, pressure and speed is carried on fluid particles. All the variables in each particle, by adding on a series of neighbor particles and using an interpolation function (kernel) are calculated. Mass and momentum conservation equations are the equations of fluid flow, are as follows.

$$\frac{1}{\rho}\frac{d\rho}{dt} + \nabla\vec{u} = 0 \quad (1)$$

$$\frac{D\vec{u}}{Dt} = -\frac{1}{\rho}\nabla p + \vec{g} + \vec{F} \quad (2)$$

In this equation ρ, u, P, t, g, and F consecutively represent density, velocity, pressure, time, gravitational acceleration and a source term. [5] Actually the SPH method is a weighted averaging method for estimating a parameter.

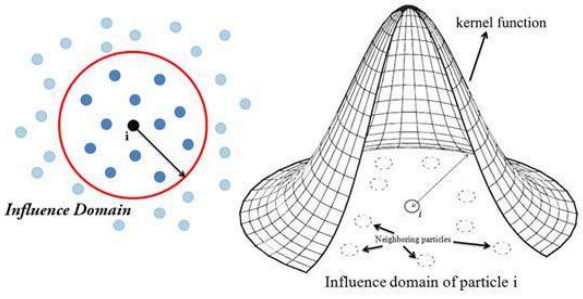

Figure 1. Influence Domain.

To estimate the quantity of one parameter at a certain point, it is assumed that neighboring areas, according to an interpolation function, contribute in estimating the value of this parameter to the desired point. The area around a particle that particles in this area contribute in interpolation is influence domain.

[1] Smoothed Particle Hydrodynamics

3. Boundary Condition (BC)

In SPH method, solid boundaries can be simulated by particles that position is fixed over the time. Solid border apply repulsive force to the fluid particles located near the solid border to preventing them from infiltrating inside walls. In other words, the equation of state solving for particles, prevents the accumulation of fluid particles near the solid border. In addition, several rows of solid particles placed outside the boundaries that called dummy particles.

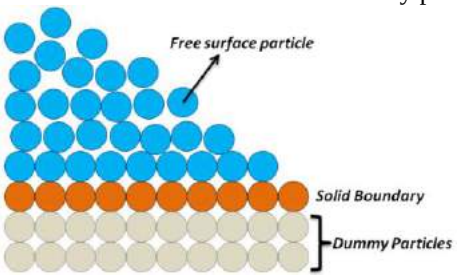

Figure 2. Particles close to the borders.

4. Tidal River Sediment Simulation

For tidal rivers modeling, the model in Figure 3 has been used. Movable walls, according to a sinusoidal form, simulate tidal flow.

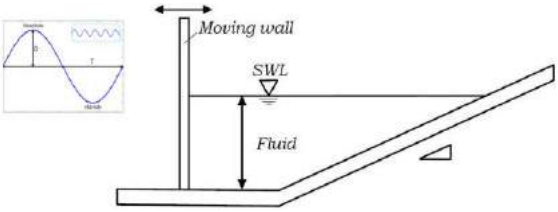

Figure 3. Tidal River 2-D modeling.

Suspended sediment particle density is assumed 2.65 g/cm^3. Coordinate are shown below in the sediment

Table 1. Sediment Coordinates.

	X	Y
Particle 1	3.2	1.3
Particle 2	4.2	1.5
Particle 3	5.2	1.7

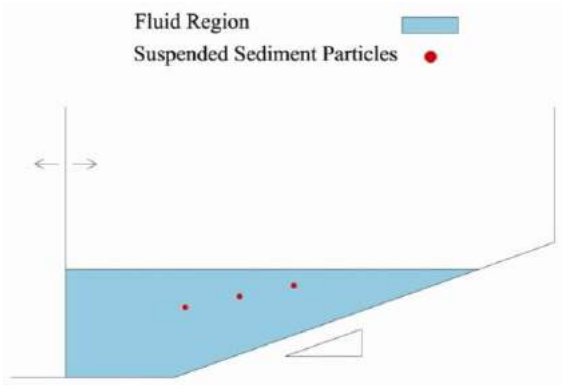

Figure 4. The location of the sediment.

Other parameters that used in this simulation is shown in the table 2.

Table 2. Simulation Parameters.

Smooth bed before ramp (m)	3
The ramp angle (degrees)	20
How to Create a tide moving	piston
The initial position of movable wall(m)	1
Left wall motion phase	0
Step Time (seconds)	0.0005
Smoothly length factor	1.3
Water density (kg per cubic meter)	1000
Sediment density (kg per cubic meter)	2650

5. The Results

To consider better, a dimensionless number has been shown in equation (3) that T_{Period} stand for tidal period time.

$$T_i = \frac{t_i}{T_{Period}} \tag{3}$$

In Figure 5 sediment particles positions during the tide period are shown.

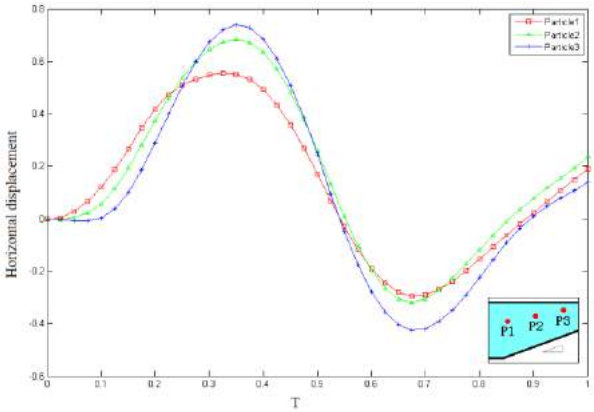

Figure 5. Sediment positions during the tide period.

In 2009 a research on the sediment behavior in a river of Argentina was performed. Bahia Blanca River entrance to the Atlantic Ocean in a 13-hour tidal cycle, had been studied at several different points. Measuring velocity of sediment, at three points of the river, are shown in Figure 6. [2]

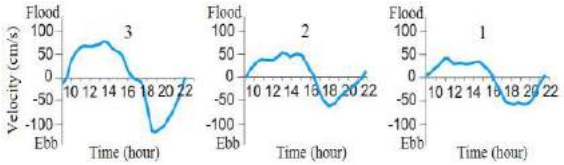

Figure 6. Curve of 3-point horizontal velocity in river.

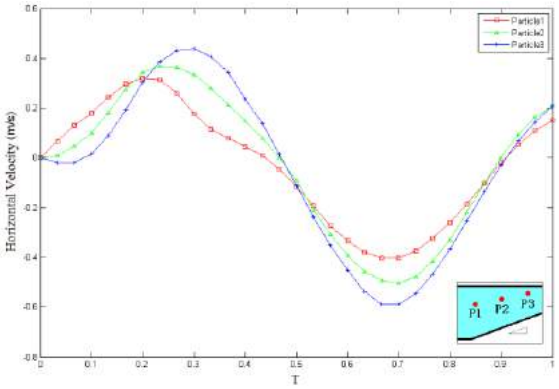

Figure 7. Curve of 3-point horizontal velocity in modeling.

Compare trends in numerical simulation and river sedimentation rate reflects the high similarity between them.

6. References

[1] Gomez-Gesteria M, Rogers B.D, Dalrymple R.A, Crespo A.J.C, "State-of-the-art of classical SPH for free-surface flows", Journal of Hydraulic Research, Vol(48) Extra Issue, 2010, pp. 6-27

[2] Ginsberg S.S, Aliotta S, "Sediment Transport Circulation Pattern through Mesotidal Channels System", Latin American Journal of Aquatic Research, 2009, ISSN 0718-560X, pp. 231-245

[3] Lucy L.B, "A numerical approach to the testing of the fission hypothesis", Astron J., Vol 82(12), 1977, pp. 1013-1024.

[4] Monaghan J.J, "Fluid motion Generated by impact", J.Waterway, Port, Coastal, Ocean Eng., Vol 196(6), 2003, pp. 250–259.

[5] Shao S, Edmond Y.M.L, "Incompressible SPH method for simulating Newtonian and non-Newtonian flows with a free surface", Advances in Water Resources, 2003, pp. 787-800.

MINIMISING SEDIMENT DEPOSITION AT BASIN AND ENTRANCE OF NOSHAHR PORT VIA DEFLECTING WALL

Ali Shoushtarizadeh Naseri[1], Afshan Khaleghi[2] and Behzad Alvand[3]

1) P.M.O, Ports and coastal Engineering Dep., Tehran,Iran, ali.s.naseri@gmail.com
2) P.M.O, Ports and coastal Engineering Dep., Tehran,Iran, afshan.khaleghi@yahoo.com
3) P.M.O, Ports and coastal Engineering Dep., Tehran,Iran, behzad.alvand@yahoo.com

1. Introduction

Sediment deposition at the basin and the entrance of Noshahr Port (South of Caspian Sea) become a serious challenge for operation and cost efficiency.

So far, different solutions have been suggested to solve this problem, including breakwater extension, groin construction, by pass and also increasing the reflection coefficient of the western breakwater of the port. However, in order to find the optimal solution, a comprehensive study on sediment transport regime is required.

Harbor sedimentation is an important problem to be addressed, especially within the access channel. Noshahr harbor (from 1939) had no sedimentation problem until 1988. Then dredging became necessary at the harbor entrance. The dredging rate was about 100'000 to 120'000 m3/year for several years. However, it has been increased to about 200'000 m3/y in the last three years [1]. Several factors have been studied in order to describe the specific trend of sedimentation along Noshahr Harbor lifetime. Among them are the sea level change, modifications in the harbor layout, and the effect of road construction along Chaloos River near the harbor [2].

2. Study Area

Caspian Sea is the largest enclosed inland body of water on Earth by area, variously classed as the world's largest lake or a full-fledged sea located between Europe and Asia.

Noshahr Harbor, located at the mid side of southern shorelines, has been constructed during the years 1930 to 1939 (Fig.2). The harbor layout has been modified during the years 1993 to 1997 by extension of the main breakwater and shifting the eastern shoreline towards the sea (Fig.1).

There are 5 rivers in the vicinity of Noshahr port. Among them Chaloos River play an important role in port sedimentation (picture1).

The dominant wind direction is north-west. The wind rose shows that the western storms have the highest intensity. Although some sever eastern storms occur in the region.

Waves approach the harbor mostly from north-west and north. The maximum wave height at the depth of 10 and 5 meters are respectively about 3.7 and 1.94 m.

There are no or seldom studies which address specifically the effect of Caspian Sea level changes on sedimentation behaviors at the harbors, including Noshahr. The sea level has been decreased Continuously from 1930 to 1977 by more than 3 meters. Then it has been increased continuously to 1995 by 2.5 meters. It is not possible to describe the trend of harbor entrance siltation and the annual dredging reports without taking the effect of sea level change into account [1].

Figure 1. Noshahr port location at Caspian Sea

The satellite images show a considerable accretion at the western side and erosion at the eastern. In addition, a large amount of sediments deposit at the basin and entrance of the port which disrupt the safe navigation.

3. Field Measurements

A set of field measurements was performed at the field site from 2013 to 2014. Directional wave spectra and vertical current profiles were simultaneously recorded at two stations, i.e. nearshore (5 m deep) and offshore (10 m deep) via ADCPs. Wind speed and direction was recorded in 10m high on the eastern breakwater.

Sediment samples were also collected at different points of the coast to define the sediment sources and particle size distributions. The results show that the sediments consist mainly of fine sand with a median grain diameter of 0.1-0.3 mm. Also the seasonal sea bed profiles were measured during a year.

4. Sediment transport pattern

The sediment transport is dominantly west to east in Noshahr coastal region and deposition behind the western breakwater shows that. Previous studies indicate the eddies formation on the entrance and off the port's eastern breakwater, which have influence on sediment transport pattern around the port. In accordance with the effect of eddies on sediment movement pattern, the solutions based on move or dislocate the eddies have been considered. Among the potential solutions, due to the implementation coast and required time, deflecting wall (deflecting littoral drift) could be a distinguished way out.

At present, deposition of sediment at the port entrance and basin cause relocation of access channel and also difficulties for navigation which requires quick measures.

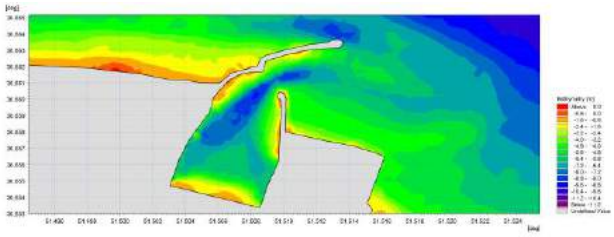

Figure 2 . Noshahr port bathymetry

5. Deflecting Wall

Different solutions have been suggested to solve Noshahr port sediment problem including breakwater extension, groin construction, by pass and also increasing the reflection coefficient of the western breakwater except for the deflecting wall. In order to find the effect of deflecting wall on eddies dislocation and consequently on sediment transport, MIKE 21 ST model is applied. The results showed that eddies dislocation is sensitive to the deflecting wall layout (length, orientation and situation), so the model applied for quite a few scenarios to find the appropriate solution.

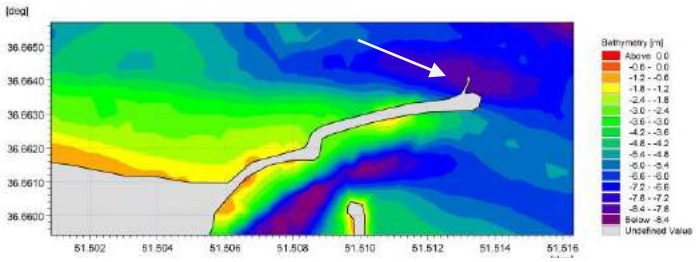

Figure 3. Example for deflecting wall

6. References

[1] Kamalian R. (2011), "Hydrodynamic and Sedimentation Study Report of Nowshahr", Tehran Berkeley Eng. Co.

[2] Kamalian R. (2012), " The Effect of Caspian Sea Water Level Changes on Nowshahr Harbor Sedimentation ", in *Proceedings 10th ICOPMAS International Conference on Coasts, Ports and Marine Structures*, Tehran, Iran, November 19-21 2012.

[3] "Minimizing harbor siltation", PIANC, WG 150.

MODELING OF HEAVY METAL POLLUTANT IN SARBAZ TRIBUTARY WITH FINITE VOLUME METHOD (CASE STUDY PISHIN DAM)

Seyed Arman Hashemi Monfared[1], Seyed Reza Elyas Langaran[2], Golsa sadat Elyasi[3]
1) Civil Eng. Department, University of Sistan &Baluchestan, Zahedan, Iran, hashemi@eng.usb.ac.ir
2) Civil Eng. Department, University of Sistan &Baluchestan, Zahedan, Iran, sr.elyas@gmail.com
3) Chemical Eng. Department, University of Zanjan, Zanjan, Iran, gs.elyasi@gmail.com

1. Introduction

In this research hydrodynamic flow of pollutant concentration with finite volume method basis, was analyzed by using MIKE21 software [1]. For this reason, Numerical solution with computational fluid dynamic analyzing was selected, for coupling of hydrodynamic flow and concentration changes during the process [2]. Spatial discretization in numerical solution and shallow water equations for hydrodynamic flow model applied. Case study should have appropriate data's for modeling the hydrodynamic flow [3] In this case, the whole area of the dam is separated in two main parts, 1) Sarbaz river, which it carry the large amount of discharge, 2) the outlet of Pishin Dam that plays major role for fate and transport of contaminant. Finally, output data's compared with observed data's for accurate discussion [4].

2. Governing equations

The basis of the equations is Finite Volume Method and shallow water equations that described as below;

2.1. Numerical Solution

The discretization in solution domain is performed using a finite volume method. This type of modeling is considered by shallow water equations, which functioned in MIKE21 software simulation. Integration of the horizontal momentum equations and the continuity equation (1) over depth h=η+d, the two dimensional shallow water equations obtained [3].

$$\frac{\partial h}{\partial t}+\frac{\partial h\bar{u}}{\partial x}+\frac{\partial h\bar{v}}{\partial y}=hS \quad (1)$$

$$\frac{\partial U}{\partial t}+\nabla.\mathrm{F(U)}=\mathrm{S(U)} \quad (2)$$

Where $(\bar{u}\,.\,\bar{v})$ is the depth – averaged velocities The integral form of the system of shallow water equations can in general form be written as (2), Where U is the vector of conserved variables, F is the flux vector function and S is the vector of source terms [3].

3. Case study

Area of study is located in southeast of Iran, Zahedan province with geographical description of $60^o56'$ to $61^o35'$ longitude and $26^o01'$ to $27^o05'$ Latitude (Figure 1).

4. Bathymetry

Simulation of the Sarbaz tributary in the Pishin dam is processed in regard of heavy metal concentration changes. The whole area is between $61^o37'$ to $61^o41'$ Longitude and $26^o02'$ to $26^o04'$ Latitude (Figure 2), Interchange of water volumes between rivers and dam are taking into account in the modeling. So each entry of rivers introduced as an open source beside the outlet of the dam that is discharged.

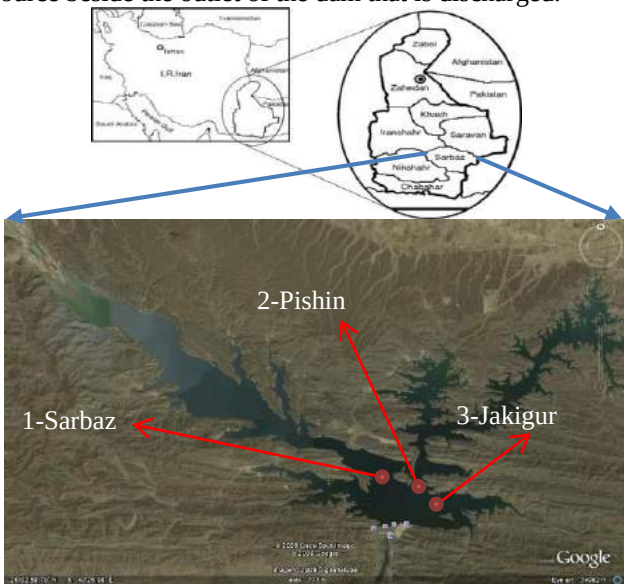

Figure 1. position of Pishin dam catchment stations [5]

Pishin dam is located in the joint of Sarbaz and Pishin rivers. Earth fill dam that contains 250 million (m^3) of capacity and bed rock of 6930 (Km^2) area (Figure 1). Pishin dam outlet contribute for 7000 acre of agricultural water usage that plays key role for vital and economical aspect of the region especially in drought and hot season (Figure 2).

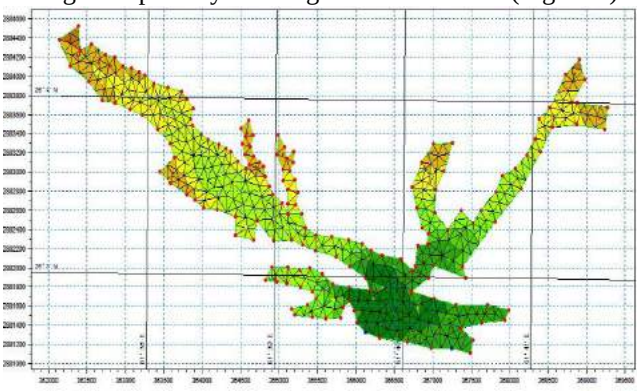

Figure2. Pishin dam mesh generator in simulation

5. Simulation

Observation stations are: 1- Pishin, 2- Sarbaz and 3- Jakigur (Figure 1). Each data that gathers from these stations are evaluated for gaps in registration and then by

comparison of the information trends, the appropriate nonlinear equation in time series interpolation of the software has used in which operates as an soft start in the simulation [3]. Table 1, shows the stations description and their coordinates positions.

Table1. Stations of 1 to 3 and geographical coordinates

No of Stations	Longitude	Latitude
1- Sarbaz	$26^0 2' 4.4"$	$61^0 41' 11"$
2- Pishin	$26^0 1' 58.5"$	$61^0 41' 34"$
3- Jakigur	$26^0 1' 46"$	$61^0 41' 49"$

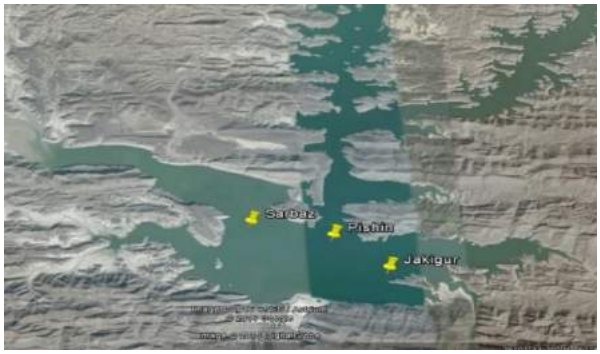

Figure 3. Location of the stations and samples [5]

Stations of 1 to 3 are considered as an open source items due to finite volume method simulation (Figure 3).

6. Results and Conclusion

The outlet of Pishin Dam is attending different mesh for two parts by the same qualification method. In Figure 4 variation of Cd pollutant is shown. By considering soft start for simulation, the gaps in first month of the simulation can be neglected. We estimate the initial condition near to zero and let the simulation to estimate the amount for the initial condition in the term of the modeling which is more compatible with the outcome [3]. Figure 5 shows that in hot season such as May we face with large index of pollution. Less participation and huge amount of evaporation beside domestic usage of water lead to high part per million (ppm) changes. Figure 5 demonstrate compatibility of observed data and outcome of the simulation. In first time steps of the modeling there are gaps in outcome. Although the frequency of hot season and the duration of them are not negligible but the management of the floods runoff and over loaded agricultural water consumption is the key factor of water loss in spite of evapotranspiration in semi-arid region. Figure 6 shows the concentration changes of Ni pollutant and the different amount of results. In correspondence of hot start for the simulation in one-year time step, there is one gap in the first month of the simulation in regard of zero initial but as the simulation goes throw the running the compatibility of the system is close to the data of the study. Ni concentration changes in contrast of Cu and Cd is that the amount of Ni is increasing after cold season, on the other side, Cd and Cu is near to reach the equilibrium in hot season. The topography of the district is not well enough for agricultural usage in Jakigur and North of the Pishin basin, so the water loss in these zones are less than Sarbaz river.

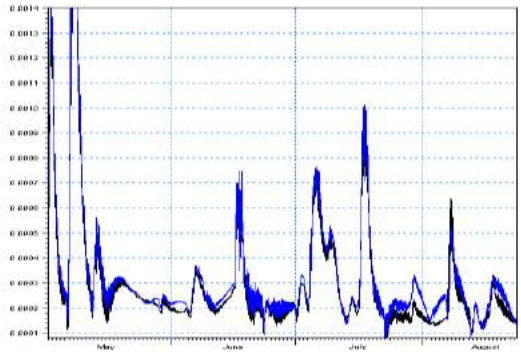

Figure 4. Cd changes (ppm) per month, Sarbaz station

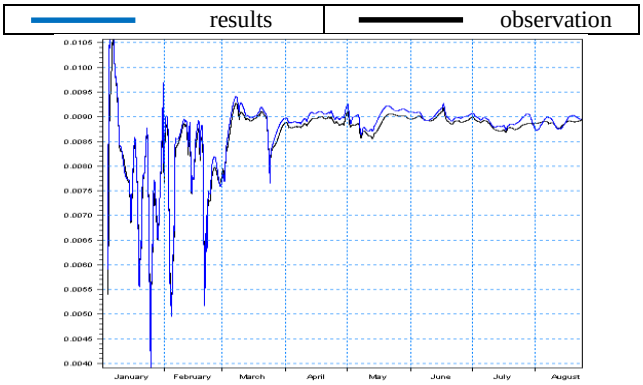

Figure 5. Cu changes (ppm) per month, Pishin station

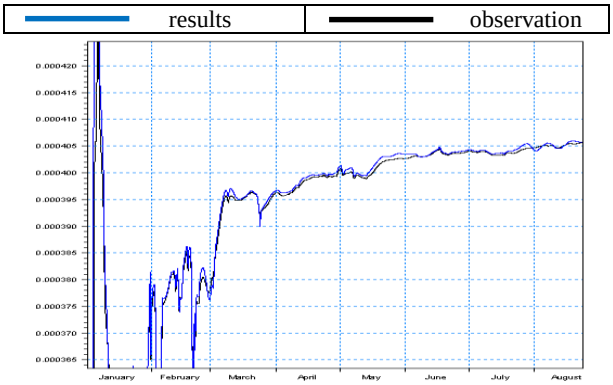

Figure 6. Ni changes (ppm) month, Jakigur station

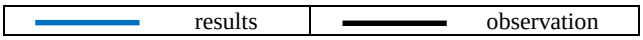

7. References

[1] Elyas Langaran, S. Reza., "*Modeling of heavy metal concentration changes in reservoirs case study Zyqlab dam*", Master of Science Thesis, February 2011.

[2] Hashemi Monfared, S. Arman., Elyas Langaran, S. Reza., *"Fluid dynamics modeling for concentration variation in Kondok tributary using MIKE11"*, 7th National Congress on civil Engineering, Zahedan, Iran

[3] Danish Hydraulic Institute, MIKE collection software manual, scientific document. 2007 edition

[4] Hashemi Monfared, S.A, Elyas Langaran, S.R, "*Applied Modeling of Computational Fluid Dynamic for Eco-Lab concentration changes with sediment transport (Case Study Shadegan Lake)"* The 10th International Conference on Coasts, Ports and Marine Structures ICOPMAS 2012..

[5] http://earth.google.com.

[6] Akbari, Gholamhossein., Elyas Langaran, S. Reza., "*Risk of contaminants modelling errors in Middle East waters*", Technical Journal of Engineering and Applied Sciences, TJEAS Journal-2013-3-14/1441-1446

INVESTIGATING MORPHODYNAMIC CHANGES OF TANG ESTUARY INLET, IRANIAN COASTLINE OF THE OMAN SEA

Aref Farhangmehr[1], S. Abbas Haghshenas[2], Mohammad Dibajnia[3] and Ali Naeimi[4]

1) Visiting Researcher, Institute of Geophysics, University of Tehran, Iran, Email: aref.farhangmehr@gmail.com
2) Assistant Professor, Institute of Geophysics, University of Tehran, Iran, Email: sahaghshenas@ut.ac.ir
3) Collaborating Scientist, Institute of Geophysics, University of Tehran, Iran, dibajnia@gmail.com
4) Assistant Professor, Islamic Azad University, Saveh Branch, Email: ali.naaeimi@gmail.com

1. Introduction

Tang Inlet with its complex morphodynamic behavior is of high interest not only from a theoretical coastal engineering perspective, but also it deserves attention due to its potential for development on the Iranian Makran Coastline. The estuary is located approximately 75 km east of Chabahar Port. It is a tidal estuary formed landward of a crescentic bay on the Oman Sea. The estuary's inlet is located at the end of this bay in an area sheltered by an approximately 1.7 km long island (Figure 1). This island acts as a natural offshore breakwater, which results in formation of a tombolo connecting the estuary's inlet to the island. An important feature of the system is the migration of the inlet and its alternative opening to the west and east sides of the tombolo feature behind the island. This phenomenon has occurred at least three times during the past 50 years.

Tang Estuary experiences infrequent flood events during occasional intense rainy periods. The upstream watershed is not large; however, it supplies the narrow estuary with moderate sediment load once a year and heavy sediment load once every five years, on average. Tang estuary lies on riverine remains of a major flood channel of the region experiencing considerable floods during rare but intense rainy periods.

In the current study, morphodynamic changes of Tang Estuary are investigated by analyzing 33 historical Landsat satellite images taken over the period of 1966 to 2016. All the images were analyzed in a GIS framework to investigate the evolution of Tang Estuary over the past three decades. Three inlet migration events were detected which occurred in 1987, 1998 and 2015. Figure 1 shows 2015 events on its corresponding satellite image.

Figure 1. Sample inlet migration event captured through historic shoreline change analysis for the Tang area [1].

2. Probable Effects of wave Characteristics and Rain Fall on Migration Inlet

Considering the importance of this dynamic system and corresponding wave and current characteristics, physiography and watershed analysis of Tang Estuary is a matter of importance. The average annual precipitation of the study area is estimated to be about 100 mm/year, while the maximum daily precipitation during the past 30 years is recorded 116 mm in January 1998, the year that one of the inlet migrations had occurred.

On the other hand, Figure 2 shows annual wave roses for the period of 1996 to 1999 adopted ISWM (2002) data [2]. The wave roses for 1998 and 1999 show remarkable difference in direction comparing with those for 1996 and 1997. The dominate orientation of waves changed from South and South-East in 1997 and before to South-East in 1998 and later (See Figure 2.). This may be considered as another reason for the captured migration in 1998.

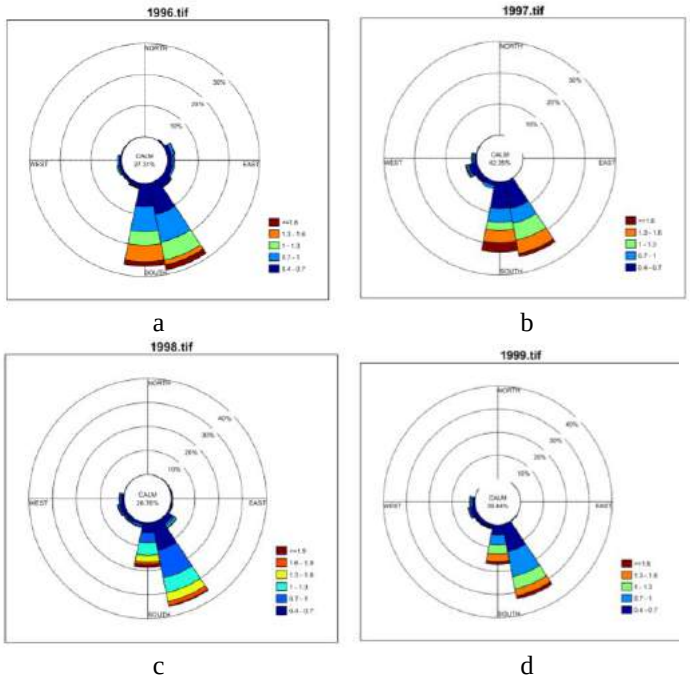

***Figure 2. Yearly wave rose in front of estuary at depth of 30m*. (a) 1996, (b) 1997, (c) 1998 and (d) 1999 [2]**

3. Discussion

Tang inlet is characterized by a migrating tidal channel which demonstrates two semi-stable westerly and easterly orientations. It seems that the inlet has been opening alternatively to the west and to the east every 10~15 years. The switching from the westerly to easterly channel orientation seems to be predominantly caused by floods and diffraction currents caused by the dominant southerly and south-easterly waves diffracted around the rocky headland. It is while another possibility refers to the inlet response to decadal variations in alongshore sediment transport. Generally, inlet stability is a result of balance between tidal prism volume and longshore transport rate. If easterly transport is strong, then it closes off the inlet and it has to breach/open to the west. When there is strong westerly events, then easterly transport closes off the inlet and it opens up towards the east. These two possibilities are examined in this paper.

4. References

[1] Haghshenas (2015): Morphodynamic Changes of Tang Estuary Inlet. Researh Report, Institute of Geophysics, University of Tehran. 63p.

[2] Technical report, ISWM Iranian sea wave modeling. Phase 3, ports and maritime organization. See URL:, http://coastseng.pmo.ir/coastalengineeringoffice-proj17-proj19-fa.html; 2008.

EFFECT OF SEDIMENT POROSITY, GENERAL ALONGSHORE, WIND AND FALL VELOCITY ON LITTORAL DRIFT AT SOUTHWEST COAST OF CASPIAN SEA

Mostafa Tangsiri[1], Reza Kamalian[2] and Aghil Haaj-Momeni [3]

1) Master of Coastal and Marine Engineering, Dept. of Engineering, Univ. of Qom, Qom, Iran, Email: tangsiri@yahoo.com
2) Assistant Professor of Coastal and Marine Engineering, Dept. of Engineering, Univ. of Qom, Qom, Iran, Email: ur.kamalian@gmail.com
3) Master of Coastal and Marine Engineering, Saze Pardazy Company, Tehran, Iran, Email: hajmomeni@sazehpardazi.com

1. INTRODUCTION

Pare-Sar power-plant is located on the southwest coast of Caspian Sea (Figure 1). Its intake basin (for cooling water) has been constructed on 2007. Longshore sediment bypassing started after 5 years, and caused deposition at the entrance. Based on the initial estimations, it was expected that sediment bypass would not be started before 2027. The difference is too large to be addressed just by a calibration factor. The estimated value was based on usual engineering algorithms, including substantial numerical models, engineering formula and field measurements. Figure 2 illustrates the offshore wave rose in the area.

This study addresses the main factors which have caused so much difference between the calculated and the actual littoral drift. Several factors have been studied, including sediment porosity, general alongshore velocity out of the surf-zone, accuracy of the wave data, wind speed and fall velocity. The sediment in the area is a mixture of sand and chip (wood). There are few available papers that address the mentioned factors in the literature. For example see Farhadzadeh, 2012 [1], Noble, 2015 [2] and Schoen, 2014 [3].

Figure 1 location of Pare-Sar & length of breakwater

The effect of each parameter – on increasing the littoral drift - have been controlled. Simulation results have been compared to the field measurements and to each other. Comprehensive data have been used, including four hydrography within seven years, continuous wave and current measurements for one month at three locations (with 20, 6 and 3 meters depth), and continuous wave-current time series for seven years in front of Pare-Sar shoreline (calculated by global Caspian Sea models). The mix effect of these parameters has been checked too.

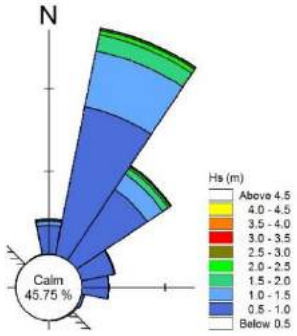

Figure 2 Wave rose offshore Pare-Sar

2. METHODOLOGY

The effect of several parameters -on the sediment transport- has been analyzed via simulation. The actual drift and sediment transport pattern has been obtained by comparing annual hydrography data from 2012 to 2014. The longshore sediment transport has been calculated by Kamphuis formula (1991) [4] and a numerical model like Litpack [5]. The wooden chip in sediment mixture has been addressed by changing the porosity. Fall velocity decrease has also checked.

The general current and wind in the area are far from symmetry; they are usually from left to right parallel to the shoreline (see Figure 3). Stormy waves usually coexist together with left-to-right alongshore current. Therefore the effect of current and wind has been controlled by two scenarios.

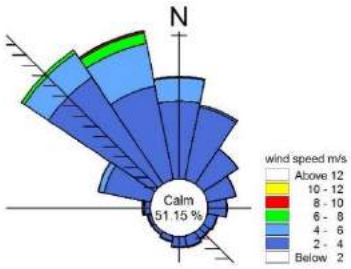

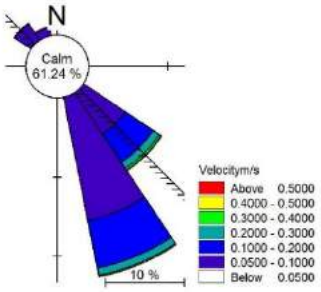

Figure 3 Wind & current rose offshore Paresar

Table (1) illustrates some of the studied scenarios. The numerical model has been calibrated using measured wave and current data by three ADCPs at 20m, 6m and 3m depth in front of the study area (before construction). The model estimates longshore sediment transport time series in hourly intervals. Wave, current and wind time-series are available at the same interval. The accumulated sand has been obtained via integration over the surf zone from each hydrography's date up to the next one.

Table 1 Some of the simulated scenarios

Type	scenario
Fall Velocity 0.025m/s	1
50% Increase in Porosity	2
Wind added	3
General current added	4
Current & wind added	5

3. RESULTS AND DISCUSSION

The net littoral drift in the area is from left (west) to right. Comparing the annual hydrography data (from 2012 to 2014) shows that the net longshore sediment transport is about 146,000 m^3⁄year [6]. Table (2) illustrates the results for some selected scenarios. It shows that both the general current and porosity correction increases the accuracy considerably.

Table 2 Selected results

Accuracy of model	
Scenario 5	97%
Scenario 4	92%
Scenario 2	75%

Taking the effect of general current into account, was not easy. Numerical models such as litpack can take general current as input. But it seems that they can not handle this parameter correctly. Based on their simulations, the general current speed outside the surf-zone decreases dramatically as the distance to the coastline decreases. So they under-estimate the effect of general current on the littoral drift. However, field measurements at Pare-Sar prove that the general current speed usually remains nearly the at positions with 20m, 6m and 3 meters depth (see Figure 4).

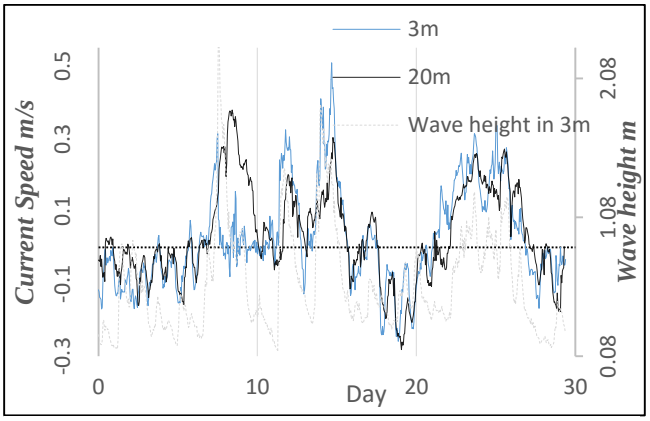

Figure 4 Current speed at 3 & 20m with wave height at 3m depth

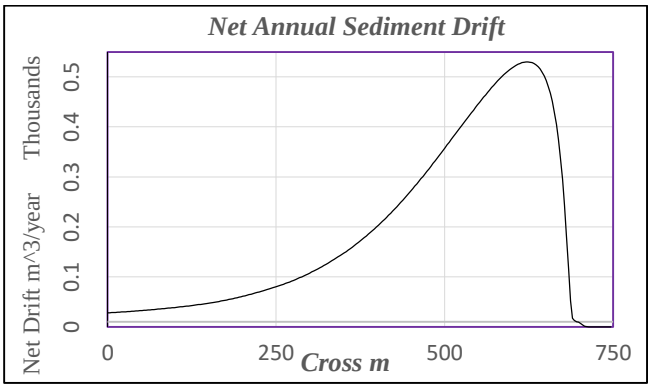

Figure5. Sample simulated Drift distribution along the surf-zone

4. Reference

[1] "Report of Sedimention", Saze Pardazy Company, Tehran, 2007-2011.

[2] J. W. Kamphuis, "Introduction to Coastal Engineering and Management".

[3] J. F. &. R. Deigaard, "Mechanics of Coastal Sediment Transport".

[4] A. Farhadzadeh, "Effect of Breaking Waves and External Current on Longshore Sediment Transport," *Journal of Waterway, Port, Coastal, and Ocean Engineering*, 2012.

[5] M. A. Noble, "Strongly-sheared wind-forced currents in the nearshore regions," *Continental Shelf Research*, 2015.

[6] J. Schoen, "Estuarine , Coastal and Shelf Science Wind-driven circulation patterns in a shallow estuarine lake : St Lucia , South Africa," *Estuarine, Coastal and Shelf Science*, 2014.

FINGER PRINTS OF HYDRODYNAMIC CONDITIONS OF THE NORTH- WESTERN PERSIAN GULF IN THE OOLITIC BANKS – CASE STUDY OF BUSHEHR BAY

Sahar Soltani[1], Mohsen Soltanpour[2], and S. Abbas Haghshenas[3]

1) K. N. Toosi University of Technology, Tehran, Iran, saharsoltani@email.kntu.ac.ir
2) K. N. Toosi University of Technology, Tehran, Iran, soltanpour@kntu.ac.ir
3) Institute of Geophysics, University of Tehran, Tehran, Iran, sahaghshenas@ut.ac.ir

1. Introduction

The Persian Gulf is an important shallow water body with an average depth of about 35 m. Sediments in the Persian Gulf are mainly composed of two different origins; bio-clastic or clastic sediments. Bio-clastic sediments are composed of organic debris, i.e. the remains of marine organisms, and belong to the regions where they were created in, while clastic sediments are generally composed of broken rocks and are transferred to the sea from land.

The types of sediments can be related to the hydrology, hydrodynamics, climate conditions and marine habitats of the study area. Oolitic sediments are one of the particular sediments that are formed in shallow water bodies. These sediments are the result of carbonate precipitation in the water column during hot seasons.

As one of the shallowest water bodies of the world, especially in the north-western part, and because of the very high temperature during summer, the Persian Gulf is a text book example for carbonate sediments, generated in the water column. It encompasses many oolite factories along the north-western coastal parts as well as some certain locations in the south.

Although the general aspects of oolitic depositional systems are well documented, the details of processes acting on these systems are not well understood and quantified [1]. The present study aims to investigate hydrodynamic-related impacts on the formation of oolitic deposits at the case study of Bushehr Bay. The sediments and hydrodynamic conditions of the bay are examined and the relation between the ambient flows and sediment characteristics is presented.

2. Oolite Sediments – Origin and Formation

Oolitic grains are composed of cemented ooids. Ooids are generally spherical and small grains with a diameter less than 2 mm, composed of concentric laminae of carbonate, that are usually formed around a nuclei. Ooid accumulations normally form in shallow, warm and supersaturated environments. Three conditions are often necessary for the formation of ooids, i.e. supersaturated water, a source of nuclei and some sources of agitation such as waves and tides.

Shoals of vast marine ooids exist in many locations all over the world, including Bahamas, Yucatan and Shark Bay [2]. Many locations in the Persian Gulf have aslo been covered with pure oolitic deposits (Fig. 1)

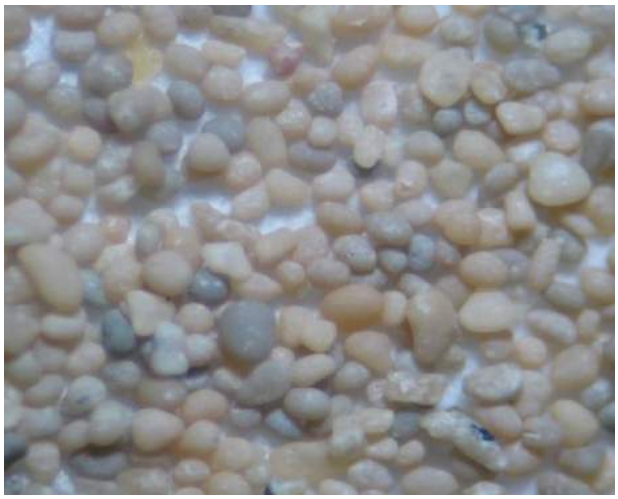

Figure 1. An example of oolite sediments from Deylam Port, the PersianGulf [3]

Ooids are either formed from the remains of marine organisms such as corals, shells, molluscs, etc., or directly formed from the solved calcium carbonate of the sea water. For the direct formation, an intense evaporation in the shallow marine environments under high temperature is necessary. If a large volume of water exited from the system, the supersaturated water layers are formed. Then, a small flip is enough for the sediments to be precipitated and then deposited on the sea floor.

The effective parameters for the formation of ooids include hypersaline layer formation and current/wave induced turbulence as a flip for precipitation. Some of the important observations in the formation of oolite sediments are:

- Oolitic sands and shoals are formed and shaped by the hydrodynamic processes [4].
- Ooids are most abundant on the shoal crests and the percentage of ooids abruptly decreases off the shoal [4].
- The relations among different processes of sedimentology, geomorphology and stratigraphy

may illustrate a clear distinction between wave-dominated and tide-dominated accumulations [5].

- A lower agitation energy results to the smaller sizes of oolite grains [5].

3. Study Area and Field Measurements

The north-western parts of the Persian Gulf are rich in oolitic sediments; where pure oolite grains can be observed in locations such as Bushehr Bay, Jazireh-shomali, Emam-Hassan Port, Leilatein Estuary and Deylam Port. The northern part of Bushehr Bay is mostly covered by oolitic shoals and muddy deposits where the waves are small and the area is flooded and dried during the periodic tidal cycles.

A comprehensive field program of sediment sampling was planned at the site. Figure 2 shows the results of the grain sizes and the percentages of oolitic vs. non-oolitic originated grains of the sediment samples, taken from the Bushehr Bay. The detail examination of sediment samples were done with a microscope, based on visual assessment.

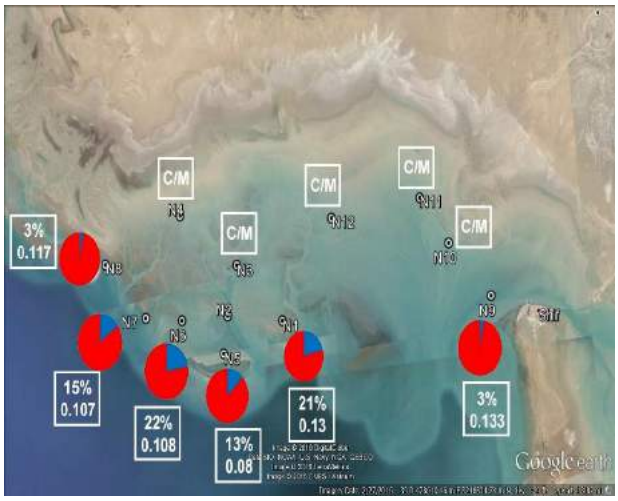

Figure 2. Oolitic sediment percentage in the samples from Bushehr Bay

4. Numerical Modeling

2D hydrodynamic modeling of waves and currents were conducted by using the SW module and Flow Model of MIKE21, respectively, to investigate the wave patterns and flow conditions in the study area [6]. Figure 3 shows an example of the transformation of significant wave heights in the bay during the ebb tide.

5. Summary and Conclusion

A comprehensive field, laboratory and modeling studies were conducted to correlate the grain size and oolite percentage in sediments to the hydrodynamic characteristics at Bushehr Bay. Comparing the modeling results with the field and laboratory measurements, it was concluded that the size of the grains are increased with the increase of the current velocity. Moreover, the percentage of oolite sediments are higher in the areas with low currents.

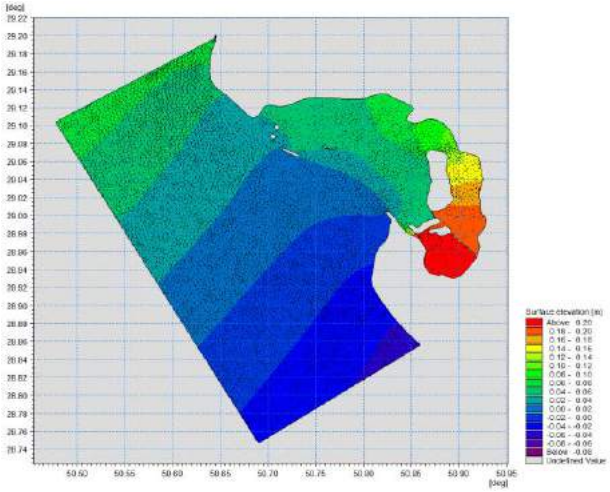

Figure 3. Vectors of significant wave heights in Bushehr Bay

6. References

[1] Rankey, E.C., Riegl, B., and Steffen, K., " Form, function and feedbacks in a tidally dominated ooid shoal, Bahamas." *Sedimentology*, 2006 Dec 1;53(6), PP.1191-210.

[2] Diaz, M.R., Swart, P.K., Eberli, G.P., Oehlert, A.M., Devlin, Q., Saeid, A., and Altabet, M.A., "Geochemical evidence of microbial activity within ooids." *Sedimentology*. 2015 Dec 1;62(7), PP. 2090-112.

[3] Haghshenas, S. A., Samsami, F., Razavi Arab, A., Soltanpour, M., and Risk, M. J., "Sediment Constituent Analysis; Application of a New 'Toolbox' for the Study of Iranian Coastlines". *10th International Conference on Coasts, Ports & Marine Structures, ICOPMAS 2012*, Tehran, Iran, CD.

[4] Reeder, S.L., and Rankey, E.C., " Interactions between tidal flows and ooid shoals, northern Bahamas." *Journal of Sedimentary Research*. 2008;78(3), PP. 175-86.

[5] Rankey E.C., " Contrasts between wave-and tide-dominated oolitic systems: Holocene of Crooked–Acklins Platform, southern Bahamas." *Facies*. 2014 Apr 1;60(2), PP. 405-28.

[6] Danish Hydraulic Institute (DHI), " MIKE 21 & MIKE 3 FLOW MODEL FM, Hydrodynamic and transport module." *User Manual*, Hørsholm, 2011.

SEDIMENTATION PROBLEMS OF NAHR GHASR AND IDEAS FOR SOLUTION AND METHODS FOR INCREASE SPEED OF MORPHOLOGICAL SIMULATION

Reza kamalian, Seyed mojtaba hoseini chavooshi

1) Assistant Professor of Qom University, faculty of civil engineering, department of marine structure
2) Master student of Qom University

1. INTRODUCTION

Nahre-ghasr is a natural tidal stream at arvand kenar beach, which is derived from Arvand River. It is located in front of Faw city (48 ˚ 31′ E and 29 ˚58′ N). Bed material in the area is cohesive mud. A fishery harbor has been constructed in Nahre-ghasr by 2009. During the construction of the port, the width and depth of the natural channel has been increased in order to allow operation of vessels. After 4 years the bed was stricken to 1.5 m sedimentation in the entire length of the channel (1800m) while the initial guess was 0.5 m sedimentation for this period of time. The target of this paper is to investigate the sedimentation problem and its solution as well as to provide methods to reduce regarding 2d-simulation time. Another study have been done previously in this regard (Orooghi-2015). But is has focused on sedimentation at the intersection of Nahre-ghasr and Arvand River. This paper studies the entire channel length. To reduce sedimentation of fine-grained material in a tidal creek, several technics have been studied. Some of them are (bailard-1987), (CC Inglis Allen FH &-1957) and (Komura-1966). The basic idea is increasing the current speed by decreasing the cross section or by increasing the water discharge. Real-world solutions need numerical simulation for optimization. One- and two-dimensional models may be used in this regard.some of them are **(**Cayocca, F-2001**)**, **(**R., Alfageme, S., and Irish, J. L-2003**)**.

2. CAUSE OF PROBLEMS

During the construction of the port - by increasing the width and depth of the channel – the cross-section area has been increased by 5times (or more at the harbor), but tidal discharge through the cross section has been remained constant. For cohesive materia, deposition/erosion depends on the relation between the shear velocity and the critical shear stresses for deposition and erosion. Before harbor construction, the longitudinal bed slope and the cross section along the channel was in balance with the tidal discharge. So the near-bed velocity was not less than the critical sedimentation speed (according to the sediment cohesiveness). Therefore no net sedimentation was available averagely after some tidal cycles. So the channel was morphologically stable. After widening the channel, tidal current speed reduced by a factor of 5 and acute deposition started. Suspended sediment comes into the channel from Arvand by every tidal cycle and partly deposits. Deposition trend continues until the cross section area decreases sufficiently and the current speed returns back to the balanced values.

3. NUMERICAL SIMULATIONS

To simulate the long-term morphology of Nahre-ghasr Harbor, a one-dimensional model (MIKE 11) and a two-dimensional one (MIKE 21 FM) have been used. The tidal level at al-Faw has been applied as the hydrodynamic B.C. Measured suspended sediment –at the intersection of Arvand and Nahr ghasr- has been applied as suspended sediment B.C. The hydrodynamic and sediment transport model have been calibrated by measured water level and suspended sediment at a point near to the harbor for 1 month (two Neap-Spring cycles). Then the model simulated one complete year. Numerical simulation show that there was no considerable sedimentation/erosion before construction of the harbor (equilibrium condition). Then the after-construction condition simulated for four years using the calibrated model. Results show that 1.5m deposition occurs along the access channel and harbor after 4 years.

4. SPPEDUP 2D-MORPHOLOGICAL SIMULATION

Two-dimensional morphological simulations need long computational time. Speedup algorithms are needed to increase the speed of simulation. For this purpose, the flow and sediment models are used for limited tidal cycles (neap to spring). Then the erosion/deposition pattern is averaged and is extended for several months. After specified bed level change, the procedure is repeated by hydrodynamic and sediment transport simulation using the new bathymetry. This procedure is repeated until the end of simulation time.

Another algorithm that is suitable for the quasi-stationary flow condition, is the scaling factor algorithm (see Mike 21 curvilinear). In this way, each time step is divided by a factor (SF) in order to relax the restrictions due to the courant number. At the end of simulation, any change in time duration and bed level change is multiplied by the factor to show the actual results. The first algorithm have been used in this paper.

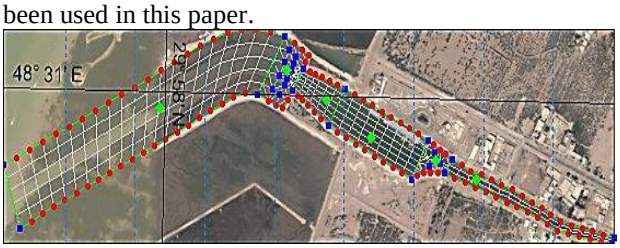

F***igure1: 2D rectangular mesh for flow model***

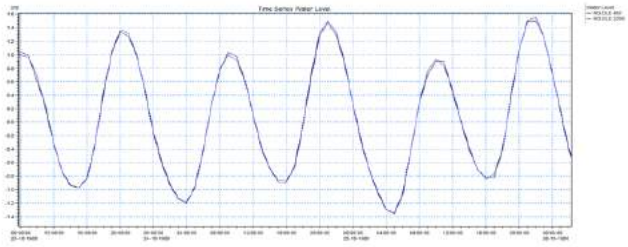

Figure2: measured and computed water level at harbor station in spring time

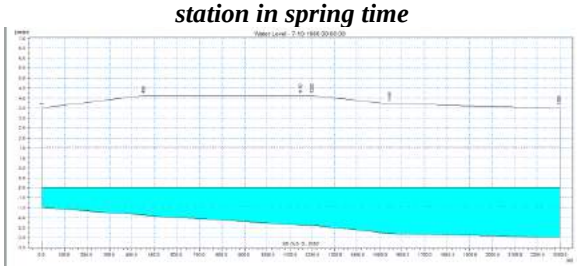

Figure3: result of mike11 for discharge

5. CONCLUSIONS AND SOLUTIONS

The simulation results prove that the cause of sedimentation is disruption in the primary balance. To solve this problem, the near bed velocity in Nahre-ghasr should be returned to the previous condition. Three solution concepts are available in this regard:

1. Decrease the channel cross section (below CD)
2. Increase the area that receives water by tide
3. Any mixture of the methods 1 & 2

For the first concept, it is efficient to decrease the cross section area particularly below the chart datum. This is the way how Nature acts.

For the second concept, the tidal flats around the main channel or any available area at the end of Nahre-ghasr water way may be used. In fact part of the tidal flats were supportive before widening the channel and constructing dikes on its sides.

Figure4: Before construction that inlets have been existed

Figure5: After construction that inlets have been destroyed

Narrowing the channel and decreasing its cross-sections may cause problems for navigation and vessels cannot pass each other. However, increasing the tidal water flux is available. Considering that the current speed has been decreased up to 0.2 of the initial value (by harbor construction), an extra reservoir is needed with area of approximately 350000 square meters. Such area is available as shown in Figure (6). Numerical simulations prove that this concept can eliminate deposition problem in the harbor and along the access channel. For the implementation of this plan, limited part of the land near the harbor-channel should be dredged.

Some dikes or gates are needed at the boundary between the illustrated tidal reservoir (Fig. 6) and Arvand River. If one-way gates are used (to be opened during flood and closed during ebb), then more efficient conditions may be available (less reservoir area is needed). In this way, the water comes from Arvand into the reservoir by flood-tide. But during the ebb condition, the water must out-flow from an outfall at the upper part of the channel. This concept will increases out-flow current speed sufficiently more than the critical deposition stress. Therefore a new natural balance by the new cross section is achieved. Numerical simulations show that even natural dredging may be planned.

Figure6: location of reservoir and its valves

6. REFERENCES

[1] **Bailard JA** 1987 Controlling Sedimentation in Harbor Berthing Areas, in Sedimentation Control to Reduce Maintenance Dredging of Navigational Facilities in Estuaries. Report and Symposium Proceedings, Marine Board, Commission on Engineering and Technical Systems, National Research Council, National Academy Press, Washington, D.C,

[2] **Cayocca, F. (2001).** Long-term morphological modeling of a tidal inlet: the Arcachon Basin, France. *Coastal Engineering*

[3] **Dr. Mohsen Soltanpour & Mehrdad Orooghi Amidi** 2015 Study and analysis of siltation in Nahr Ghasr Fishery port

[4] **Inglis CC & Allen FH** 1957 .The regimen of the Thames Estuary as affected by currents, salinities and river flow. Proc. Inst. Civ. Engrs., Vol 7, p 827-878.

[5] **Komura, S. (1966).** "Equilibrium depth of scour in long constrictions." Journal of Hydraulic Engineering, ASCE, 92(HY5), pp. 17-37**.**

[6] ***MIKE BY DHI (2012)***. Curvelinear Model for River Morphology.

[7] **R., Alfageme, S., and Irish, J. L. (2003)**. Modeling of morphological changes at Shinnecock Inlet, New York, USA. *Proc. Coastal Sediments 2003*, Florida, Paper IV-B-5.

ANALYSIS AND NUMERICAL MODELING CROSS-SHORE PROFILES IN THE SOUTH AND NORTH COASTS

Ahmad.Ghasemi [1]and U. Reza.Kamalian[2]

1. MSc. Student, Dept. of Civil Eng. Qom University, Qom, Iran, ahmad.ghasemi29@yahoo.com
2. Assistant Professor, Dept. of Civil Eng. Qom University, Qom, Iran, ur.kamalian@gmail.com

1. INTRODUCTION

Precise knowledge about cross-shore sediment transport and beach profile seasonal change is crucial in coastal engineering. This phenomenon affects the quantity and characteristics of longshore sediment transport. It also influences the interaction between sediment and the coastal structures. For example, swell-induced cross shore sediment transport after storm impact's deposition behind the head of the breakwater at harbor entrance. This is the time when the storm-induces sand bar moves back toward the shoreline. Coastal morphology is highly sensitive to the cycles of storm-swell impacts.

There are several relevant papers in the literature. Among them are Sallenger (2003), Houser et al. (2008), van Rijn et al. (2003), Lashte Neshaei et al. (2007), Judge et al. (2003), and Masselink (2008). However, still more research is needed to understand the sand-bar migration during and after storm.

This paper addresses cross-shore sediment transport and beach-profile variations at two representative Iranian shorelines; Nowshahr (Caspian Sea) and Zarabad (Makran). Figures (1) and (2) illustrates the shorelines and the studied profiles. Lots of measured profiles have been studied with the corresponding wave time series (measured). The wave climates at the two selected sites are different, including monsoonal wave behavior at Zarabad and irregular frequent storms with steep waves at Nowshahr. Seasonal profile types have been studied and compared. Two numerical models -Litpack and SBeach- have been tested.

2. Methodology

Several measured beach profiles have been studied and traced considering the wave T.S. into account. They have been simulated too, and the results have been compared to the measurements. The capability of numerical models Litpack and SBeach have been tested not only sand bar development during storm, but also for sand-bar migration after storm.

Many profiles at Nowshahr have been studied, ten of them corresponding to two months. Nearly one hundred profiles have been studied at Zarabad corresponding to seven years. Fourteen profiles belong to a specific line by six-month intervals. Both monsoon and off-monsoon profiles are available. Figures (1) and (2) illustrate the hydrography dates at Nowshahr and Zarabad.

Monsoon profiles have been compared to each other in order to determine their variance. By Zarabad, several measurement lines are available along the shoreline. Simultaneous profiles have been compared in order to check homogeneity along the shoreline.

A quantitative criterion is needed to compare the simulated profiles and the measured ones (in addition to the visual observation). Van Rijn et al. (2003) proposed a statistical parameter "Brier Skill Score (BSS)" in this regard. It can be defined has.

$$(\mathrm{BSS}) = 1 - \frac{\langle(|z_{b,c} - z_{b,m}| - \partial)^2\rangle}{\langle(z_{b,o} - z_{b,m})^2\rangle}$$

Where $z_{b,c}$ belongs to the simulated profile, $z_{b,m}$ to the measured one, and $z_{b,o}$ to the initial profile. ∂ Stands for the measuring error. Van Rijn's classification can be seen in Table 1.

Table 1. Goodness of bed profile simulation

Classification	Excellent	good	Reasonable
BSS	1.0 – 0.8	0.8 – 0.6	0.6 – 0.3

Figure 1. Study beach near Nowshahr port - Caspian Sea

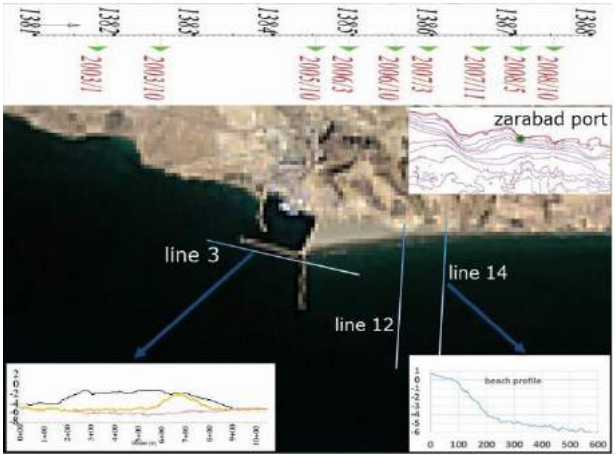

Figure 2. Study beach at Zarabad port - Oman Sea.

3. RESULTS

Figures 3 and 4 illustrate the time rulers for successive measured profiles at Nowshahr and Zarabad respectively. The corresponding wave time series are also illustrated. Fig. (4) Shows that the sand bars are formed at a distance of 100 to 150 meters from the shoreline during every summer monsoon, with water depth 1 to 2 meters over them. This condition repeats every year due to the wave repetitively. Fig. (3) Illustrates that the situation is completely different at Nowshahr, where severe changes occur with multiple rapidly moving sandbars and irregular abrupt storms. All the Zarabad profiles are similar after the monsoon. However, profile similarity before it is subjected to wave conditions. At Makran, monsoon wave climate usually develops only one sandbar, while numerous sandbars are developed by Nowshahr storms. Makran beach is gentler than Nowshahr. The bed slope outside the Makran surf zone has been increased to a new stable condition after the Gonu event (2 June 2007).

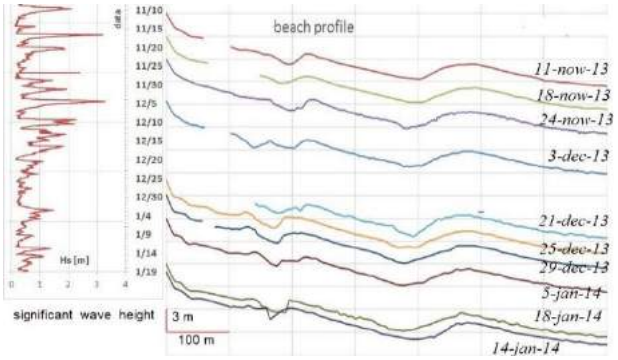

Figure 3. Beach profiles and wave heights - Noshahr - winter

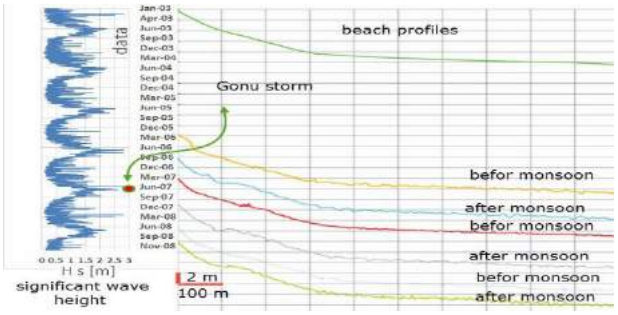

Figure 4: Beach profiles and wave heights - Zarabad -line 14

Sequence analysis of Nowshahr profiles and wave time series indicates that numerous irregular storms occur during a short time. It causes disordered bed with numerous incomplete sandbars (Fig. 3).

Numerical modeling and data analysis prove that the frequent irregular storms at Nowshahr and its wave steepness cause irregularity in the beach profile.

Comparing simultaneous profiles on different lines at Zarabad shows that profile conditions are similar along the coastline, while it is not the case in other seasons. The nearby profiles are also different at Nowshahr. Therefore, one-dimensional models such as Litpack & NMLong are closer to the reality in monsoon condition.

During Zarabad measurements, consecutive profiles have been taken as a line parallel to the shoreline in front of the main breakwater (Line 3 in Fig. 2). The measured profiles on this line are shown in Figure (5). It shows that sand bypass has been started and the deposition front moves forward towards the harbor by about 150 meters per year.

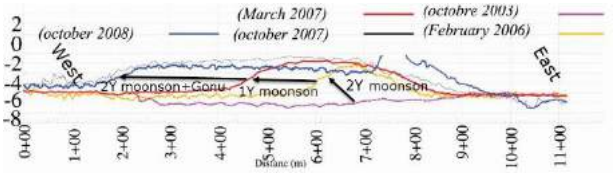

Figure 5 parallel profiles (Line 3), bypassed sand moves towards harbour entrance.

Numerical modeling shows that the simulation algorithm of Litpack is able to predict the monsoon profile with good agreement (see Fig. 6). The BSS factor is equal to 0.75, which is good according to Table 2. However, Litpack and SBeach have difficulties in predicting Nowshahr profiles. They have serious problems in modeling the situation after storm when the sand-bar disappears and sand moves back to the shoreline.

The numerical model set-up is sensitive to wave breaking parameter (the coefficient for energy loss; γ_2), turbulence parameters (β) and scale parameter are also important and require high precision. The best values for Makran are 0.53, 0.5 and 7.8 respectively.

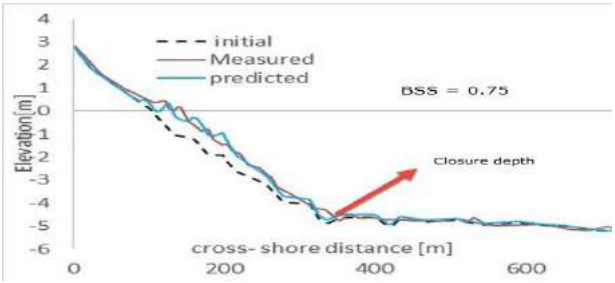

Figure 6: Sample a simulation result Zarabad

4. REFERENCES

M. A.Lashteh Neshaei and et al, 2007. Investigation of cross shore sediment transport using physical and numerical methods.

Morton, R.A. and Sallenger, A.H., Jr.2003. Morphological impacts of extreme storms on sandy beaches and barriers.

Oliveira, F.S.B.F. and Contente, J., 2013. Scale effects in numerical modeling of beach profile erosion.

Tim Scott, Gerhard Masselink, Paul Russell, 2010. Morphodynamic characteristics and classification of beaches in England and Wales.

Masselink, G.; Auger, N.; Russel, P., and O'Hare, T., 2007. Short-term morphological change and sediment dynamics in the intertidal zone of a macro tidal beach. Sedimentology.

STUDY AND NUMERICAL MODELING OF TANG REMIGRATING INLET

Ahmadreza Palizvan[1], Mansoure Mashhadi[2], Mohsen Soltanpour[3]and Babak Banijamali[4]

1) K.N. Toosi University of Technology, Tehran, Iran و Ar.palizvan@email.kntu.ac.ir
2) K.N. Toosi University of Technology, Tehran, Iran, mmashhady@email.kntu.ac.ir
3) K.N. Toosi University of Technology, Tehran, Iran, soltanpour@kntu.ac.ir
4) Daryabandar Consulting Engineers, Tehran, Iran, babak.banijamali@dbc.ir

1. Introduction

Tang inlet is located in the south Iranian border at Gulf of Oman, connecting a seasonal river to the open sea (Fig. 1). The local people use the tide-dominant Tang inlet as a natural fishery harbor, where the offshore reef protects the entrance against large waves [1]. A pier has also been constructed in the lagoon.

Existing aerial and satellite images from 1967 up to the present and the interviews with local people reveals that the tombolo behind the reef has experienced interesting natural periodic migrations in time spans of about 8-15 years (Fig. 2). The periodic shifts of port entrance has resulted to the suffering of the fishermen and in particular, the shallow water depth and the rocky bed of west entrance is highly dangerous and undesirable for navigation.

Figure 1. Tang inlet [3]

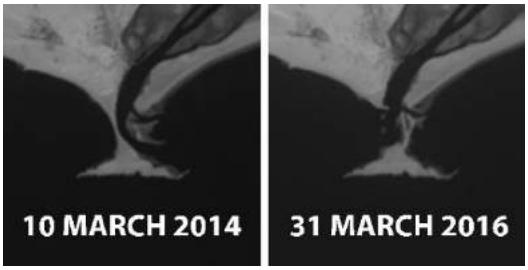

Figure 2. Tang inlet migration [4]

2. Field Measurements

A bathymetry survey has been conducted in 2009 (Fig. 3). A one-month water level measurement was also performed in 2010. The analyses of five disturbed sediment samples, taken at different locations of the site, show that the bed materials consist of sand particles.

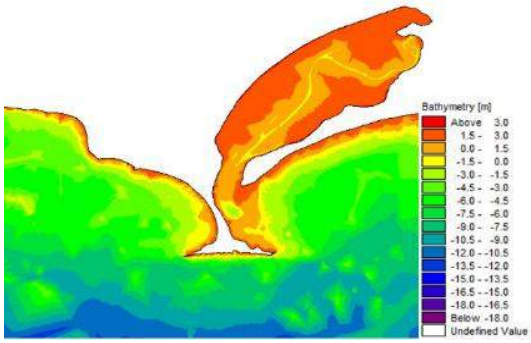

Figure 3. Bathymetry of Tang Inlet

3. Arial and Satellite Images

Landsat satellite images [4] and valuable old aerial photos of 60s and 70s were studied to derive the approximate times of inlet migrations. The images reveal that the channel opening was westward from 1967 to 1975 before changing to eastward. Due to lack of any aerial photo from 1987 to 1995, the time of next westward inlet migration is not clear. However, it is clear that a westward migration has happened in this period because another eastward migration happened in the beginning of 1998. Analysis of Landsat 8 satellite images, taken every two weeks, shows a breaching at the left bank of the mouth, coincided with an intense rainfall on March 13th, 2015 (Fig. 4). The detailed process of widening of the breach and transition can also be observed in the series of Landsat images.

4. Modelling Studies

Admiralty Tide Table provides four main constituents of M_2, S_2, O_1 and K_1 [6]. Figure 5 shows the favorable agreement between the measured data in 2010 and the predicted water surface level using the Admiralty method. Applying the simulated time series of water level at open boundaries, the hydrodynamic model of Tang Inlet was conducted by FM module of MIKE 21, at which the wave-induced currents, due to radiation stresses, were included from the outputs of SW module [5]. The offshore input wave at south boundary was adopted from the hindcast data

of Iranian Seas Wave Modeling (ISWM). Wave diffraction was also included in SW module because of the importance of wave modeling behind the offshore reef. Figure 6 shows the offshore wave rose and a sample of SW modeling.

The modeled tidal ranges at offshore, gorge and middle of the bay are 2.4 m, 2.25 m and 1.9 m, respectively. Tang is thus categorized as a meso-tidal estuary [2]. Moreover, about 80 minutes time shift is observed between the tides at open sea and in the bay, which results in the development of residual currents and the consequent accretions in the channel (Fig. 7).

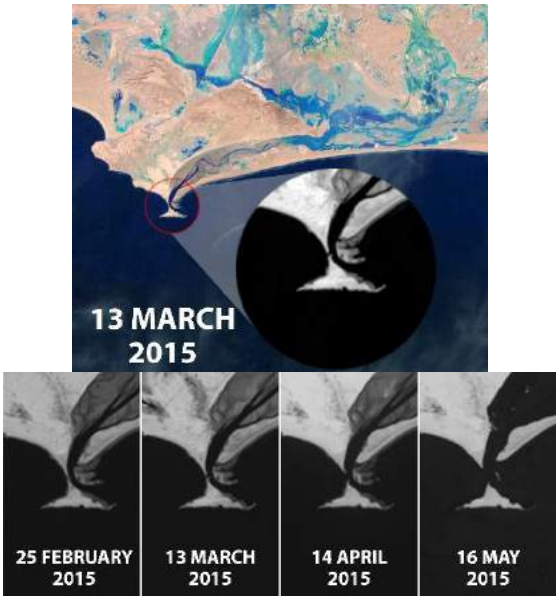

Figure 4. Breaching of the west bank (top), transition process (Bottom) [4]

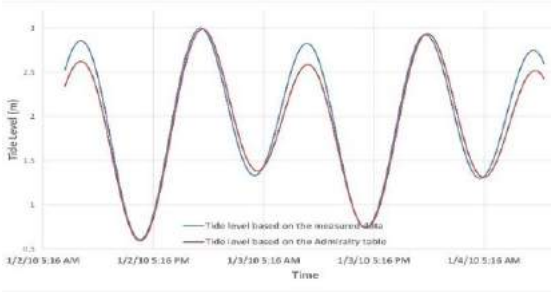

Figure 5. Tide level comparison

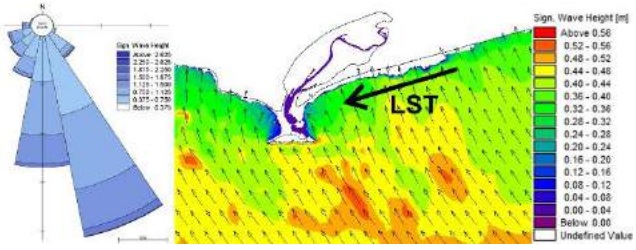

Figure 6. Offshore ISWM hindcast wave-rose (1992-2002) (left), SW wave transformation (right)

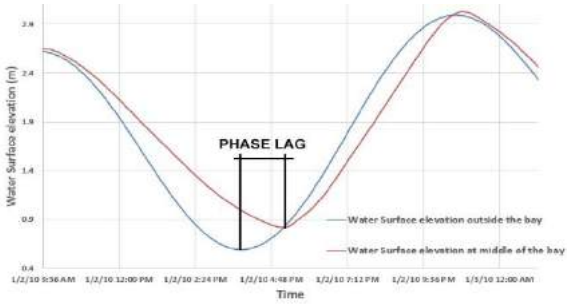

Figure 7. Phase lag between tides at open sea and inlet

5. Discussion and Conclusion

The remigration of the Tang Inlet is due to the combined effects of tidal currents, floods, longshore currents and diffraction currents. The dominant southeastern waves result to a net westward longshore sediment transport (LST) at Tang (Fig. 6). While the tidal currents can keep the minimum depth and width of the opening, LST rate results in the long-term sedimentation at the east entrance. Sedimentation can also happen at the west opening due to the diffraction currents. On the long term, these sedimentations reduce the hydraulic efficiency of estuary. Thus, a breaching may occur when the channel is not capable of passing the excess flow of flood. After breaching, the channel is open at both east and west sides, i.e. transition, in a relatively short time interval. The upstream flow and tidal currents lead to a wider breach at this stage. Then the sedimentation, either due to LST at east entrance or diffraction currents at west entrance, gradually blocks the other entrance and the shift between two entrances completes.

As discussed before, a shift was monitored during the large flood of March 13th, 2015. The rainfall records prove that flood was also the main reason of the migration Tang Inlet from west to east, as this migration coincided with a severe rainfall in the early of 1998.

6. Acknowledgment

The authors wish to thank Iran Fisheries Organization for providing the data of Tang Inlet.

7. References

[1] Sorourian, S., & Banijamali, B., "A Case Study of Hydrodynamics and Morphological Modeling of a Re-migrating Inlet", *Coastal Engineering Proceedings,* Jan 31 2011.

[2] Bird, E., *Coastal Geomorphology: an Introductio*n, Second Edition, John Wiley, 2008, pp.411.

[3] URL: https://earth.google.com/

[4] URL: http://earthexplorer.usgs.gov

[5] Danish Hydraulic Institute (DHI), "MIKE 21 & MIKE 3 FLOW MODEL FM, Hydrodynamic and transport module." *User Manual*, Hørsholm, 2011.

[6] The United Kingdom Hydrographic Office, "Admiralty Tide Table", *Indian Ocean and South China Sea,* Volume 3, 2005.

The General Model for the Estimation of Longshore Transport

Giuseppe Roberto Tomasicchio[1], Felice D'Alessandro[2] and Sahameddin Mahmoudi Kurdistani[3]
1) Department of Engineering for Innovation, University of Salento, Ecotekne, Lecce, Italy, roberto.tomasicchio@unisalento.it
2) Department of Engineering for Innovation, University of Salento, Ecotekne, Lecce, Italy, felice.dalessandro@unisalento.it
3) Department of Engineering for Innovation, University of Salento, Ecotekne, Lecce, Italy, s.m.kurdistani@unisalento.it

1. Introduction

The formulation of a reliable estimate of the longshore transport (LT) rate is important in coastal engineering problems. Indeed, practical applications such as the design of dynamically stable reshaping or berm breakwaters, dispersion of the beach-fill and placed dredged material, beach nourishment projects, sedimentation rates in navigation channels, they all require accurate predictions of the LT. Such estimates should be made only with valuable sediment transport models formulated on the ba-sis of reliable transport measurements (Van Wellen et al., 1998).

To date, sand beaches have received most of the attention. The number of documented studies and available data on sand beaches is, therefore, considerable and ranges from analytical/numerical mod-els and laboratory tests to large scale field experiments. In strong contrast is the moderate attention which coarser grained (i.e. shingle) and, in particular, gravel beaches and pebble beaches have received.

Presently, there is a growing interest in properly defining the morphological processes of a gravel or pebble beach due to the increased use of coarser sediments in the artificial nourishment of eroded beaches, as they are characterized by higher hydraulic roughness and provide a better defense to the forcing processes induced during storm events. Because of the limited range of validity in the exist-ing models (e.g. CERC formula, USACE 1984; Kamphuis 1991) a valuable goal in the LT modeling is to make available a simple but 'general' model valid for a wider interval of units composing the struc-ture, from stones to sands.

2. Materials and Methods

The General Longshore Transport model (Tomasicchio et al., 2013; Tomasicchio et al., 2015) represents a practical tool for the estimation of longshore transport (LT) for a large range of conditions, from sandy beaches till reshaping breakwaters (Figure 1). The GLT model is based on an energy flux approach combined with an empirical relationship between the wave induced forcing and the number of moving elements. In the present paper, the suitability of the GLT model is assessed by means of the comparison between the LT predictions and the observations from different data sets covering a wide mobility range of the units: from stones to sands.

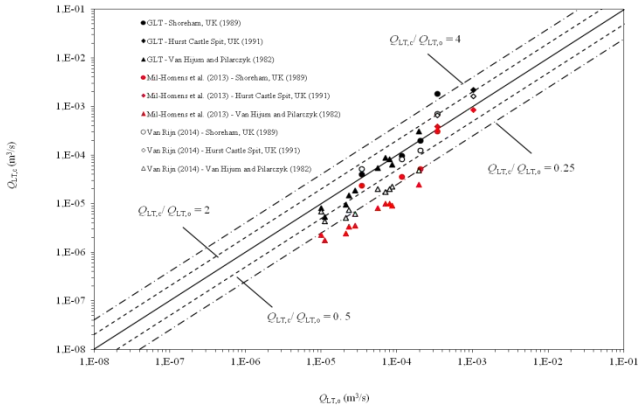

Figure 1. Observed and calculated longshore transport rates

3. Results and Discussions

The General Longshore Transport (GLT) model and the Van Rijn (2014) expression represent the only two general formulae in literature for the estimation of LT at sand, gravel and shingle beaches. In par-ticular, the GLT model is based on an energy flux approach combined with an empirical relationship between the wave induced forcing and the number of moving elements.

In the present paper, a large database consisting of observations from field and laboratory experiments is adopted to verify the ability of the proposed general model in calculating the LT rate for a wide mobility range of the units: from stone to sand. In particular, three types of coastal structures have been considered in the comparisons: reshaping berm breakwaters, gravel and sandy beaches.

Without any further calibration, the suitability of the GLT model is assessed by means of the comparison between the LT prediction and the observation from laboratory and field experiments. With reference to the

range of variation of the stability number Ns**, three different regions can be observed in Figure 2, where $\theta_{k,b}$ represents the wave obliquity at breaking. The first region, with 2 0 < Ns** < 6, refers to the berm breakwaters; the second refers to the shingle beaches (6 < Ns** < 23); the third considers sandy beaches (Ns** > 23).

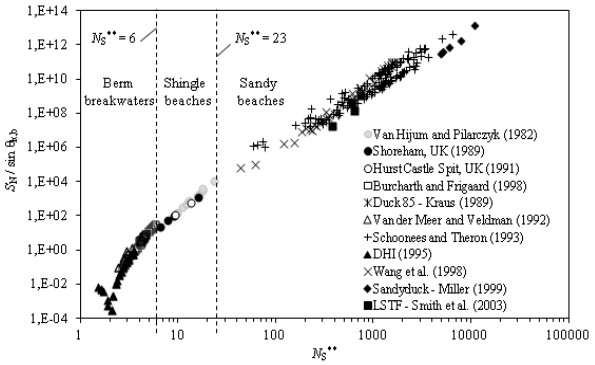

Figure 2. Calculated SN/sinθk,b versus Ns**.

4. References

[1] Kamphuis, J.W.,"Alongshore sediment transport rate", Journal of Waterway, Port, Coastal and Ocean Engineering, 117, 624-640, 1991.

[2] Tomasicchio, G.R., D'Alessandro, F., Barbaro, G., Malara, G." General longshore transport model",Coastal Engineering, 71, 28-36, 2013.

[3] Tomasicchio, G.R., D'Alessandro, F., Barbaro, G., Musci, E., De Giosa, T.M. " General longshoretran sport model at shingle beaches: an independent verification", Coastal Engineering, 104,69-75, 2015.

[4] U.S. Army Corps of Engineers (USACE)," Shore Protection Manual", Research and Development Center. Coastal and Hydraulics Laboratory, Vicksburg,1984.

[5] Van Rijn, L.C." A simple general expression for longshore transport of sand, gravel and shingle", Coastal Engineering, 90, 23-39,2014.

[6] Van Wellen, E., Chadwick, A.J., Lee, M., Baily, B., Morfett, J."Evaluation of longshore sediment transport models on coarse-grained beaches using field data: a preliminary investigation", Proceedings 26th International Conference on Coastal Engineering, Copenhagen, 2640-2653, 1998.

PECULIARITIES OF THE SUSPENDED SEDIMENT CONCENTRATION MEASUREMENT IN THE COASTAL ZONE

Kosyan R.D., Divinskiy B.V. and Krylenko M.V.

P.P. Shirshov Institute of Oceanology, RAS. 1g, Prostornaya, 353467 Gelendzhik, Russia. rkosyan@hotmail.com

1. Intoduction

The ultimate purpose of sediment transport studies is the prediction of bottom relief in the zone of active wave effect accompanied by transport of significant sand volumes. The energetic longshore currents induced by the oblique wave approach, transport large amounts of sand lifted by waves from the sea bottom. This mass sediment transport and its longshore variations finally determine the shore-line configuration and the location of accumulative and erosion areas on the underwater slope.

Because of great practical significance, the problem of longshore sediment transport has attracted much attention. When constructing theoretical models of suspended sediment mass transport by water flows, investigators have to face a number of difficulties.

Modeling of the sediment transport is limited by the absence of clear physical mechanisms of sediment suspension. Due to difficulties in making measurements in real marine conditions quantitative assessment of sediment distribution in the coastal zone has been done by modeling with laboratory-scale empirical parameters.

Real processes of sediment suspension are more complex than mechanisms which are put into the models. Detailed measurement of mechanisms and time scales of sand suspension by irregular waves were carried out during field experiments at the Black, North and Mediterranean seas and in a biggest in Europe wave channel of the Hannover University. The processes which control the temporal variations in suspended sediment concentrations near the sand bottom have been examined by using field measurements of the suspended sand concentration and the horizontal current components.

Measurements during experiments, revealed, that there were fluctuations of concentration in a broad band of frequencies near the bottom. On the basis of experimental data it is confirmed that the turbulent kinetic energy is a significant factor influencing the formation of suspended sediment concentration. The macroturbulent vortexes that are generated under plunging and spilling breakers are the driving forces for the mechanism of sand suspension in the surf zone.

It is shown that to improve the accuracy of measurement it is necessary to take into account the convective mechanism of the sediment suspention, as well as the size, the direction of the rotation axis and other parameters of the turbulent vortices transporting sand sediments.

2. Some Results

It was produced an analysis of the impact of the frequency distribution of wave energy on the suspension dynamics:

1. At the same integral characteristics of the irregular surface wave, specificity of wave action on the sandy bottom is especially determined by frequency distribution of wave energy.

2. The concentration of wave energy in the area of the main peak of the spectrum promotes the growth of the ripples linear dimensions and promotes more active injection of sediments in the upper layers.

3. With decreasing of the surface waves spectrum width the depth of the sediment erosion increases, contributing to the transition of more suspension (Fig. 1).

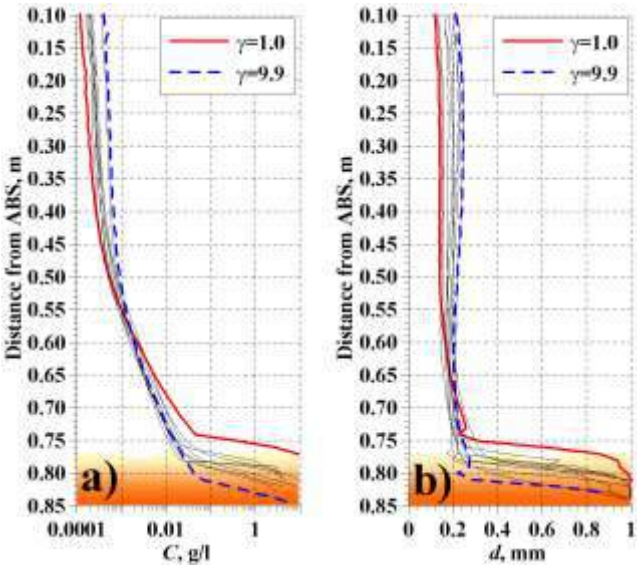

Figure 1. Vertical profiles of concentration (a) and mean diameter of suspended particles (b)

γ – JONSWAP spectrum's shape parameter

An investigation of the features of sediment suspension during the passing of waves groups of different forms and intensity was performed.

The geometrical characteristics of waves groups affecting the bottom sediment suspension are the following: the height of individual waves, forming the group; position of maximum wave within the group (spatial asymmetry); the number of waves in the group (group length).

Based on the geometrical characteristics four types of groups are allocated:

- 1 - positive horizontal asymmetry (maximum wave at the beginning of the group);
- 2 - negative horizontal asymmetry (maximum wave at the end of the group);
- 3 - symmetric (maximum wave in the middle group);
- 4 - constant (wave height in the group are almost identical).

Analysis of experimental data revealed the common to all groups suspension patterns, and differences in the dynamics of suspended material:

- Common features. The instantaneous concentration at the forefront of the waves group envelope of the free surface elevation is less than average, averaged over the group. The solitary waves, forming a group are responsible for the suspension during the initial stage. With the passage of waves group instantaneous concentrations in the upper layers begin to be comparable to the near-bottom values.
- Differences. The vertical distribution of suspended sediment concentration closest to the exponential during the passage of a wave group of type 3 with a symmetric spatial form. The passage of waves groups of type 1 delivers the bottom sediment to higher levels from the bottom and forms a more uniform field of suspended sediment.

The vertical distribution of the average particle diameter and normalized concentrations of suspended sediment, specific to different types of wave groups is shown in Fig. 2.

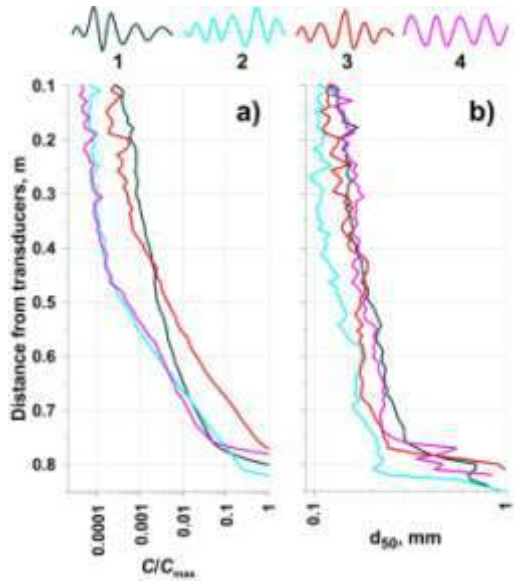

Figure 2. The vertical distribution of the normalized concentrations of suspended sediment (a) and an average particle diameter (b) for different types of wave groups

The fulfilled research allowed to draw some conclusions:

- the initial process of suspension within the boundary layer occurs on the scale of single waves. Redistribution in the water column - in the scale of wave groups;
- patterns of suspension within the wave group are mainly determined by the parameters of bottom roughness and the presence (absence) of ripples;
- in the case of symmetrical wave group passing with the same characteristics of individual waves for the first and second halves of the group the concentration of suspended sediment in the second half of the group always is more than in the first one;
- there may be situations when the result of the passage of a wave group the concentration of suspended sediment in the wave boundary layer is reduced. This mechanism is implemented in the event of restructuring bottom microforms, namely erasing steep ripple and reduce the vortex shedding effect in the lee of the ripples;
- an important factor is the energy characteristics of the groups. In the case of weak surface waves the concentration of suspended sediment during the passing the wave group of type 2 is greater than during the passing the wave group of type 1, and under the influence of more strong waves the situation is reversed. This is due to differences in horizontal wave velocities and, consequently, different characteristics of roughness of the bottom.

Thus, the suspension of the bottom material under the influence of groups of waves is characterized by a combination of hydro and lithodynamic factors: the wave power, sequence of waves in the group, the length of the groups, the size and stability of relief forms. The initial process of engagement within the boundary layer occurs on the scale of single waves, redistribution in the water column - on the scale of wave groups.

Recommendations on the optimal location of equipment for measurement of the suspended sediment concentration are made. The obtained information will help to improve the quality of analysis of experimental data.

Collection of data, the office data processing and analysis of the literature and archive data were supported by the Russian Scientific Foundation (grant no. 14-50-00095).

MODELING OF RETURN SEAWATER OUTFALL FROM AN INDUSTRIAL PORT IN OMAN

Mahad Baawain[1] and Anton Purnama[2]

1) Department of Civil & Architectural Engineering, Sultan Qaboos University, Muscat, Oman, Email: msab@squ.edu.om
2) Department of Mathematics, Sultan Qaboos University, Muscat, Oman, Email: antonp@squ.edu.om

1. Introduction

Seawater is used as the cooling medium to remove heat from processes or equipment of various industrial plants at Sohar Industrial Port Area (SIPA). This water is supplied by Majis Industrial Services (Majis) from the first Seawater Intake Pumping Station (SWIPS 1). In 2016 Majis will be commissioning the second Seawater Intake Pumping Station (SWIPS 2). The used cooling water at an increased temperature is then returned via an open channel (Figure 1) and eventually discharged to the sea through an outfall (Outfall 1) which was constructed as part of SWIPS 1. Options other than building a new outfall (Outfall 2, which is about 500 m south of Outfall 1 and to be constructed as part of SWIPS 2) are being investigated to reduce the potential negative socioeconomic impact on the nearby Majees village, where the peak discharge capacity will be increased from 334,000 m^3/h to 708,000 m^3/h (max. 800,000 m^3/h).

Figure 1. Areal view of the outfall at SIPA.

2. Background and Objectives

In order to assess the potential changes in temperature in the receiving coastal waters due to heated water discharges from the outfall channel at SIPA, and to demonstrate the compliance with the Ministry of Environment and Climate Affairs (MECA) regulations, CORMIX simulations were carried out in this modelling study. The MECA regulations, in particular, specify a circular mixing zone of a 300 m radius around the outfall channel as the initial mitigating area (Majis has been granted an extension of a mixing zone of 500 m radius), and beyond this mixing zone, the water temperature must not be increased by more than 1 oC (weekly average), and the salinity change should not be changed by more than 2 parts per thousand (daily average).

The main objectives are to demonstrate the compliance with MECA regulations within the specified circular mixing zone of 300 m radius around the outfall channel (and its extension to 500 m radius), to estimate the excess recirculation temperature near the intake channel of SWIPS 1 at 1000 m north of Outfall 1, and to show a small temperature rise near the Majees village 2000 m south of Outfall 1. Four scenarios are considered:

1. Outfall 1 with (weekly average and peak) discharge and future discharge capacities,
2. Outfall 2 with a peak discharge capacity,
3. Modifications of Outfall 1 with a future (weekly average) discharge capacity, and
4. Extending Outfall 1 channel 1500 m from the shoreline.

3. Model Inputs

The CORMIX model for shoreline (positively) buoyant heated water discharges through an open channel has three different types of inflow discharge configuration that can be specified as (i) flush with the bank, (ii) protruding from the bank, and (iii) co-flowing along the bank. The input data for CORMIX simulations of heated water discharge flushed from open channels at the shoreline is given in Table 1. The location of the nearest bank is assumed to be on the right side as seen by an observer looking downstream in the direction of the flow, and a Darcy-Weisbach friction factor of 0.025 is specified for the roughness characteristics of the coastal area.

4. Results

Figure 2 shows a typical CORMIX3 simulated surface heated water plume for Scenario 1. The discharge plume is rapidly deflected by the ambient current and remains attached to the downstream shoreline. Since the discharge density is always less than the ambient density, the plume

is positively buoyant and will stay and spread at the surface. Beyond the specified 300 m regulatory mixing zone, the plume thickness is less than 3 m (below the surface).

Table 1. Input data for Scenario 1.

Parameter	Summer	Winter
Ambient (unbounded coastal environment)	Weekly average	Peak
Velocity of the currents (m/s)	0.3	0.3
Depth at discharge (m)	6	6
Wind speed (m/s)	3	5
Temperature (^oC)	34	23
Salinity (ppt)	37	37
(Uniform) Density (kg/m^3)	1021.8	1025.5
Effluent characterization		
Heat loss coefficient (W/m^2 ^oC)	62	76
Width of the outfall channel (m)	84	84
Depth of the outfall channel (m)	4.25	4.25
Local depth at discharge outlet (m)	4.5	4.5
Bottom slope (degree)	0.3	0.3
Horizontal angle of discharge (degree)	90	90
Flow rate (m^3/s)	72.22	92.78
Temperature (^oC above ambient)	7	7
Salinity (ppt above ambient)	1	1
(Uniform) Density (kg/m^3)	1019.8	1024.0
Mixing zone		
Water Quality Standard (WQS), (^oC above ambient)	1	1
Regulatory Mixing Zone (RMZ), m	300	300
Region of Interest (ROI) , m	2000	2000

As shown in Figure 3, the surface water temperature rise is greater than 4.7 ^oC (above ambient) at the extended regulatory mixing zone at 500 m radius, which is well above the maximum permissible limits set by the Omani government. At the end of the simulation at 2000 m downstream (Majees village), the excess temperature is about 2.37 ^oC (above ambient).

The seawater intake channel of SWIPS1 (600 offshore) is located at 1000 m (upstream) of Outfall 1. Assuming a (tidal) flow reversal, Figure 3 also shows that the excess recirculation temperature at 1000 m (upstream and within 100 m from the shoreline) is about 3.79 ^oC (above ambient). However, since the overall plume lateral extend is less than 300 m offshore, CORMIX predictions are not directly applicable to evaluate the effect of recirculation at the surrounding intake areas.

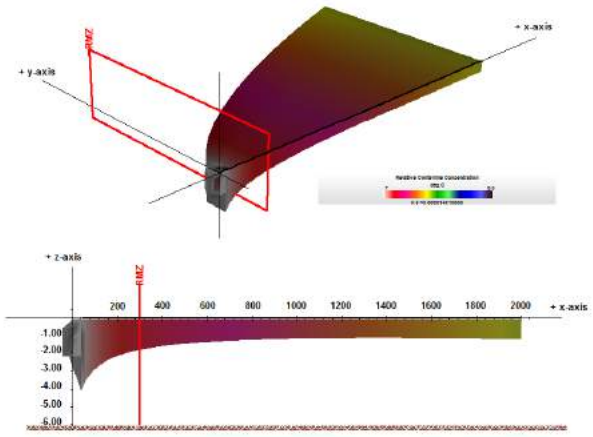

Figure 2. Heated water (weekly average) discharge plume from Outfall 1 (Summer); 3D view (top) and side view (bottom).

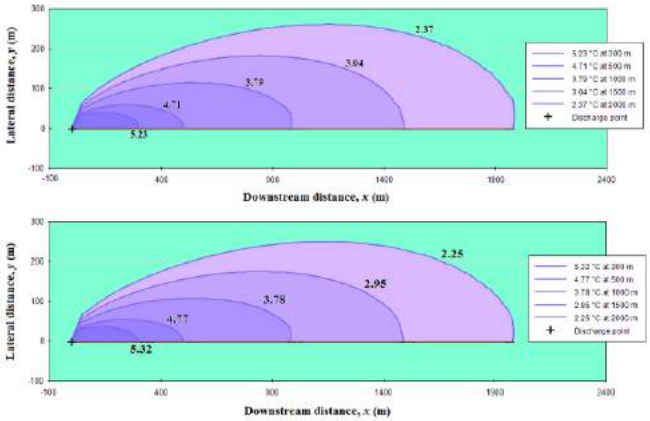

Figure 3. Contours of excess temperature for Scenario 1 (Weekly average discharge); summer (top) and winter (bottom).

5. Conclusions

CORMIX simulation results show that the overall temperature rise due to the present operational (weekly average) surface heated water discharges from Outfall is above 5 ^oC (above ambient) at the end of the Regulatory Mixing Zone (RMZ) of 300 m. At the nearby residential village, 2000 m south of Outfall 1, temperature excess is about 2 ^oC (above ambient). If discharge capacity of Outfall 1 is increased to the projected future peak rate of 708,000 m^3/h, CORMIX simulation estimates a temperature rise of 4 ^oC (above ambient) at Majees village. Finally, by extending the outfall channel to 1300 m offshore, CORMIX simulation results show that, only for the future (weekly average) discharge, temperature rise is below the specified Water Quality Standard (WQS) of 1 ^oC (above ambient) for stronger ambient velocities 1.3 m/s.

THE EFFECTS OF PRECIPITATION AND EVAPORATION ON THE CASPIAN SEA LEVEL

S. Ataei H.[1], A. M. Khakpour[2a], A. Jabari Kh[3b] and M. A. Lashteh Neshaei[4]

[1] MSc. of Coastal Engineering, Shahrood University of Technology, Shahrood, Iran, ataei.h.s@gmail.com
[2,3] MSc. Student of Coastal Engineering, Shahrood University of Technology, Shahrood, Iran,
[a]amirmohammad.khakpour@gmail.com, [b]amir.jabarikh@gmail.com
[4] Associate Professor of Civil Engineering Department, Guilan University, Rasht, Iran, maln@guilan.ac.ir

1. Introduction

It is believed that the rise of sea level over the past century is due to climate warming resulting in the melting of ice masses and the expansion of sea water. There are predictions regarding the faster uplift of the general sea level over the next century. If this happens, there will be a significant impact on the coastline (Nicholls, R. J., & Cazenave, A., 2010; Warrick, R. A., & Oerlemans, J., 1990).

Changes of the Caspian Sea may be the result of several factors such as climate change, changing river flows, regional precipitation, evaporation, wind stress, changes in seabed morphology, changes in the pattern of atmospheric transport and human activities such as construction of dams on main rivers.

2. Precipitation and Evaporation

Evaporation and precipitation, are the most important factors in sea level's change. The evaporation process is so high that without rainfall's runoff and groundwater areas' discharge, almost all oceans will be empty. Most of the water that evaporates from the oceans, returns to the ocean through rain and snow (Eghtesadi, Sh., and Zahedi, R., 2012).

3. The Caspian Sea

The Caspian Sea is situated in a semi-arid area between southern Russia, Kazakhstan, Turkmenistan, Iran and Azerbaijan (36–47N, 47–54E). Its sea level lies about 25 to 29 *m* during the last 150 years, below the mean sea level of the oceans (Arpe, K., & Leroy, S. A., 2007). The Caspian Sea area is about 436000 km2 (world lakes, 2016). The Caspian Sea Geographical position is shown in Figure 1.

Figure 1. The Caspian Sea Geographical position.

As the data show, free waters are continuously experiencing rises in their levels, while in the Caspian Sea, there are periods of both sea level rise and fall. From 1977 to 1995, the sea had a level rise of 2.4 meters, while from 1995 to 2014, it has had a 0.8 m level fall (Ports and Marine Administrations of Guilan Province, 2015). These sea level changes are shown in figure 2.

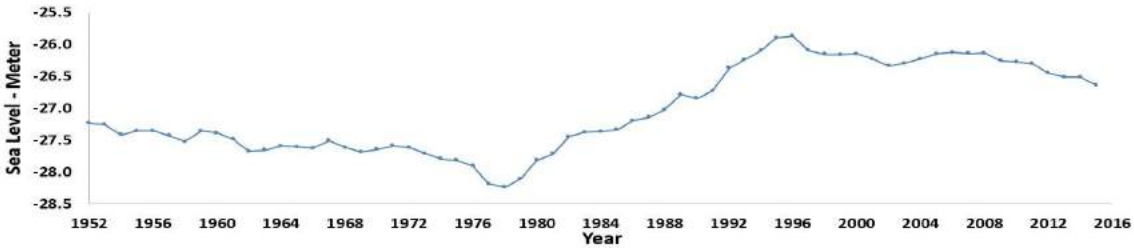

Figure 2. 60 years of the Caspian Sea level changes according to the high seas level (Ports and Marine Administrations of Guilan province, 2015).

4. Analysis of Precipitation and Evaporation processes in the Caspian Sea

In order to analyze the precipitation and evaporation, ERA Interim's data from a subset of Categories of information of European Centre for Medium-Range Weather Forecasts (ECMWF) are used.

In this study, information of Evaporation and Total Precipitation that contain rain and snow statistics have been analyzed during 2000 to the end of 2015. In order to have higher accuracy of the analysis, the level of the Caspian Sea has been divided into 4 sections (Figure 1); In total, the Caspian Sea is divided into 184 levels and each year 134320 Data has been collected from the surface of the sea. In Table 1, the average precipitation and evaporation are shown per year and according to millimeters of water column.

Table 1 – Average of Precipitation and Evaporation in each year (in millimeter – ECMWF, 2016)

Year	2000	2001	2002	2003	2004	2005	2006	2007	2008	2009	2010	2011	2012	2013	2014	2015
Precipitation	288	276	316	331	299	261	304	261	265	281	245	304	259	266	208	292
Evaporation	727	681	700	648	692	698	691	712	688	662	716	708	695	669	700	700

As data on precipitation from Table 1 show, Precipitation trend has not changed much during the 16 years, mostly it has increased or decreased for periods of one-year. The maximum of the precipitation in 2003 amounted to 144.316 cubic kilometers (331 *mm*) and the minimum was in 2014 at a rate of 90.470 cubic kilometers (208 *mm*); even in 2015, according to El-Nino phenomenon, the precipitation has not reached the maximum which occurred in 2003 and the amount was 127.203 cubic kilometers (292 *mm*).

Evaporation rate has been approximately the same over 16 years and was alternately rising and falling each year (Table 1). The least evaporation rate was in 2003 with an amount of 282.637 cubic kilometers (648 *mm*); the remarkable thing is that in 2003, the maximum rainfall was observed. The highest rate of evaporation was in the Year 2000 in the amount of 316.972 cubic kilometers (727 *mm*). In the 2014 and 2015, while the lowest rainfall in the last 16 years and the El-Nino phenomenon occurred, respectively, the evaporation rate remained at the same level.

5. Data analysis and discussion

In order to assess and analyze the snowfall, rainfall, evaporation and scientific measurements between these two factors, the histogram in Figure 3 have been included for 2000 and 2015.

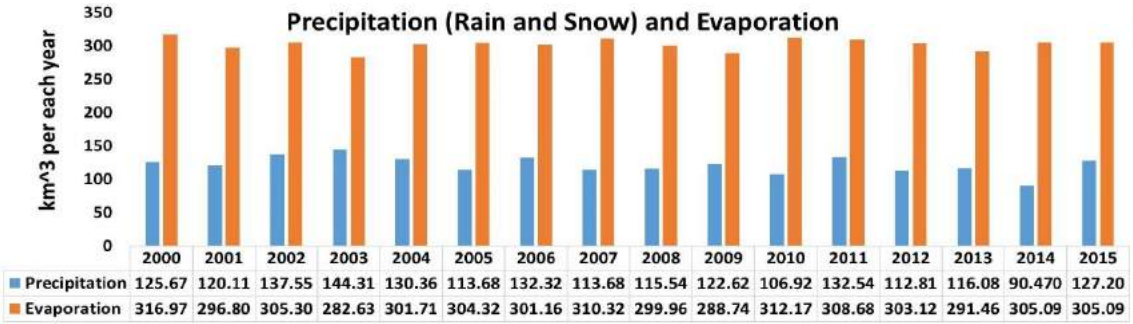

Figure 3. Comparison annual volume of Precipitation and Evaporation in the Caspian Sea.

As can be seen in Figure 3, the evaporation of the Caspian Sea is much more than precipitation in most years – it has been more than doubled. For controlling the water level of the Caspian Sea should learn that the annual precipitation of the Caspian Sea is not the same as the amount of evaporation that occurs each year; accordingly, every year the water level of the Caspian Sea gradually lessens and in the future, the Caspian Sea would dry.

According to the level changes of the Caspian Sea (Figure 2) show that from 2000 to 2015 (except 2001 and 2005) level changes were reduced. This suggests that evaporation have impacted the sea level and decreases it every year. In the 2001 and 2005 due to a reduction in the rise of the water level, other factors such as input water of the rivers may have had more impact one the water level.

Considering the falling process of water level of the Caspian Sea, to maintain biological areas in the north of the country (Iran) and the future of the Caspian Sea, any water extraction and transferring of it out of the sea, especially in the plan to transfer Caspian Sea's water to desert regions of Iran, comprehensive evaluations should be conducted to prevent crisis in the northern cities of Iran.

6. Conclusion

Evaporation and precipitation are counted as the most important factors affecting the change in sea level. Due to global warming, the amount of precipitation (snow and rain) has been reduced and the evaporation rate has increased.

During previous years, evaporation level has been almost doubled compared to the precipitation in the Caspian Sea; the current climate, have caused the decreasing trend of steadily water level of the Caspian Sea. Even, due to the phenomenon of El-Nino and consequently more rainfall in 2015, still the evaporation of rainfalls was more.

Accordingly, any extraction of water from the Caspian Sea in the future needs to be comprehensively researched so that the biological future of coastal cities of countries bordering this sea, especially Iran, are not endangered.

7. References

[1] Arpe, K., & Leroy, S. A. (2007). The Caspian Sea Level forced by the atmospheric circulation, as observed and modelled. Quaternary International,173, 144-152.

[2] Eghtesadi, Sh., & Zahedi, R. (2012). Study of factors affecting the South Caspian Sea level fluctuations. Journal of Marine Science and Technology, 10 (3), 4-13 (*In Persian*).

[3] Iran. Ports and Marine Administrations of Guilan province. Data center.

[4] Nicholls, R. J., & Cazenave, A. (2010). Sea-level rise and its impact on coastal zones. science, 328(5985), 1517-1520.

[5] Precipitation and Evaporation in the Caspian Sea. (2016). European Centre for Medium-Range Weather Forecasts (ECMWF), http://www.ecmwf.int.

[6] Warrick, R. A., & Oerlemans, J. (1990). Sea level rise.

[7] World Lakes, Caspian Sea. (2016). http://www.worldlakes.org/index.asp.

STATISTICAL DOWNSCALING of CMIP5 MODEL for CLIMATE CHANGE IMPACT ASSESSMENT in the PERSIAN GULF

Tahereh Alinejhad Tabrizi[1], Nasser Hadjizadeh Zaker[2], Bahareh Kamranzad[3],
1) Graduate Faculty of Environment, University of Tehran ,Tehran, Iran, t.alinejhad@ut.ac.ir
2) Graduate Faculty of Environment, University of Tehran, Tehran, Iran, nhzaker@ut.ac.ir
3) Iranian National Institute for Oceanography and Atmospheric Science, Tehran, Iran, kamranzad@inio.ac.ir

1. Introduction

Climate change is any long-term change in the patterns of average weather of a specific region or the whole Earth, which reflects abnormal variations to the climate and subsequent effects on other parts of the Earth. Excessive use of fossil fuels will increase the concentration of greenhouse gases which cause global temperature to rise. This phenomenon cause change in ocean circulation, sea ice and glacial melt, species extinction, sea level rise and changing weather patterns etc. Life of people in coastal areas highly depends on the sea and the beach and therefore, predicted effects will impose a number of challenges to them.

The main tools used to project climate are General Circulation Model (GCMs), which are computer models that mathematically represent various physical processes of the global climate system. These processes are generally well known but often cannot be fully represented in the models due to limitations on computing resources and input data [1]. In order to derive climate projections at scales that are desirable for the researchers and decision makers, a process termed downscaling has been developed.

Many studies have been assessed different models of CMIP5 -the last framework for climate change modeling published by the Intergovernmental Panel on Climate Change (IPCC) - in different areas such as Australia [2] and the Persian Gulf [3], which showed that the GCM data are required to be downscaled. Moreover, some studies have also performed downscaling of the data in different areas [4, 5]. As mentioned by Alinejhad et al. [3], CMIP5 wind data in the Persian Gulf must be downscaled and localized.

This paper represent the results of two statistical methods of downscaling for wind speed data in the Persian Gulf, which can be utilized to assess the effects of climate change there.

2. Methodology

2.1. Study Area

Downscaling is performed on the wind data of a point, located in the Persian Gulf; where the data was available, based on the spatial resolution of IPSL-CM5A model (figure 1). The point is located far from the coastal areas where numerical models have limited ability to produce the reliable data due to complicated orography.

The Persian Gulf lies between Iran to the northeast and the Arabian Peninsula to the southwest. It is the world's largest source of crude oil, and related industries have dominated the region. Therefore, understanding the variation of wind parameters during the long time caused by climate change and assessing its impact is necessary in this area in order to better planning for the future development.

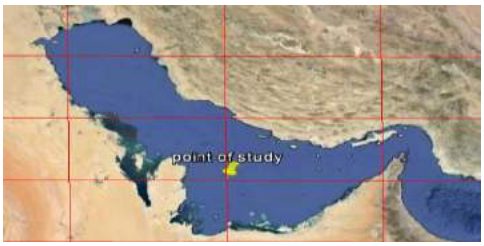

Figure 1. Study Area and CMIP5 grid in domain

2.2. Data Resources and Methods of Downscaling

Assessment of CMIP5 in the Persian Gulf shows that the wind field obtained from the GCM models need to be downscaled for using in assessment of impact of climate change [3].

Two fundamental approaches exist for downscaling of large-scale GCM output to a finer spatial resolution. The first one is dynamical approach while the second approach is to use statistical methods to establish empirical relationships between the GCM climate variables and local climate [5]. One of the simplest ways to statistically downscale GCM projections is to use the delta (or change factor) method. The change factor is the ratio between GCM simulations of the future and current climate and is used as a multiplicative factor to obtain the future regional conditions [1]. A simple linear

regression is another widely used method that establishes a linear relationship between one large-scale atmospheric predictor, e.g., GCM-simulated wind speed, and one local predictand, e.g., local-scale wind speed. Once a relationship is established, it can be applied to derive projected local conditions using GCM simulations of the future climate as input [1].

In this paper, downscaling of wind data in the Persian Gulf is carried out using two methods: Delta Method, and Simple and Multiple Linear Regression. For this purpose, local wind field was obtained from the European Centre for Medium-Range Weather Forecasts (ECMWF) which contains the wind vector at 10 meters from the sea level with 0.5 degree and 6-hourly spatial and temporal resolutions, respectively. Global wind field also was obtained from the IPSL-CM5A model with 6-hourly temporal resolution and spatial resolutions of 3.75 degrees in longitude and about 1.875 degrees in latitude, prepared by the Pierre Simon Laplace Institute (IPSL), based on the new scenarios called Representative Concentration Pathways (RCPs).

3. Results & Discussion

3.1. Delta Method

The ratio (α) between GCM simulations of future and current wind speed calculated using all four RCPs and historical experience for the 25-year interval. Results are presented in table 1.

Table 1. The ratio between GCM simulations of future and current wind speed (α)

RCPs	α_{spring}	α_{summer}	α_{autumn}	α_{winter}
2.6	0.98	1.01	0.94	0.98
4.5	0.97	1.02	0.89	0.98
6	0.95	1.03	0.89	0.97
8.5	0.96	1.06	0.89	0.98

According to table 1, the change factor is less than one for spring, autumn and winter, while it shows a ratio more than 1 in summer for all four RCPs. In addition, the highest and lowest factors belong to RCPs 2.6 and 6.0 respectively, which implies that the highest and lowest variations will be caused by RCPs 6.0 and 2.6, respectively.

3.2. Simple and Multiple Linear Regression

Wind speed distribution of ECMWF model as local data and IPSL CM5A model as global model, for the period of 1980 to 2005 (figure 2) shows that a linear relationship between two models is not established. For example, the distribution of the wind speed among spring is provided in figure 2. According to this figure, establishing a linear relationship between GCM-simulated wind speed and local wind speed is unexpected.

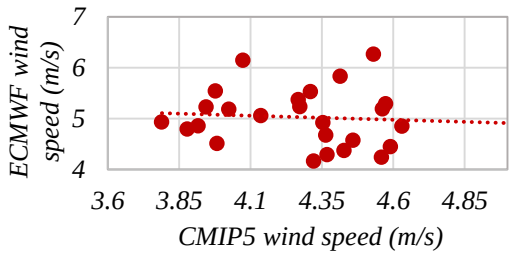

Figure 2. Wind speed data distribution of local & global model in spring

Therefore, a constant that is the ratio between local and global models was considered in order to be applied to GCM simulations of the future climate to drive projected local conditions. These constants are presented in Table 2.

Table 2. Seasonal coefficient between local and global data

season	spring	summer	autumn	winter
ECMWF/CMIP	1.17	1.28	1.18	1.39

4. Summery and Conclusion

Statistical downscaling of wind data in the Persian Gulf is conducted using two methods. The results of delta method shows that the change factor is less than 1 in all seasons except in summer.

Moreover, according to wind speed distribution of ECMWF model and IPSL-CM5A model, establishing a linear relationship between these two data is unexpected.

5. References

[1] Trzaska, S and Schnarr, E. A Review of Downscaling Methods for Climate Change Projections. 2014. USAID Contract No. AID-EPP-I-00-06-00008.

[2] Mehrotra, R, Sharma, A, Bari, M. Tuteja, N, Amirthanathan, G. 2014. An assessment of CMIP5 multi-model decadal hindcasts over Australia from a hydrological viewpoint. Journal of Hydrology, 2932–2951.

[3] Alinejhad, T, Hadjizadeh Zaker, N, Kamranzad, B. 2016. Assessment of CMIP5 Wind Field in the Persian Gulf. Under review.

[4] Ahmed, K.F, Wang, G, Silander, J, Wilson, A.M, Allen, J. M, Horton, R, Anyah, R. 2013. Statistical downscaling and bias correction of climate model outputs for climate change impact assessment in the U.S. northeast. Global and Planetary Change 100, 320–332.

[5] Storch, H, Zorita, E and Cubasch, U. 2009. Downscaling of Global Climate Change Estimates to Regional Scales: An Application to Iberian Rainfall in wintertime.

ASSESSMENT of CMIP5 WIND FIELD IN THE PERSIAN GULF

Tahereh Alinejhad Tabrizi[1], Nasser Hadjizadeh Zaker[2], Bahareh Kamranzad[3]
1) Graduate Faculty of Environment, University of Tehran ,Tehran, Iran, t.alinejhad@ut.ac.ir
2) Graduate Faculty of Environment, University of Tehran, Tehran, Iran, nhzaker@ut.ac.ir
3) Iranian National Institute for Oceanography and Atmospheric Science, Tehran, Iran, kamranzad@inio.ac.ir

1. Introduction

Climate research and observations of global climatic conditions have shown that many future climate conditions will differ from historical and current trends [1]. Excessive usage of fossil fuels has increased the concentration of greenhouse gases which cause the global temperature rise. This phenomenon has resulted in change in ocean circulation, sea ice and glacial melt, species extinction, sea level rise and changing weather patterns etc., which can also in turn lead to fundamental effects in the coastal conditions, such as change in the rate of erosion and sedimentation, etc.

The effects of climate change will impose a number of challenges to people who live along the coasts. At these areas, people life is related to sea and beach. Hence, they need to protect the coastal area in order to protect the beaches [1].

Projections of future climate changes are based on the application of emissions scenarios or representative concentration pathways (RCPs) obtaining from the Global Climate Models (GCMs) that have been developed based on assumptions of different kinds of future human behavior. The future climate can be forecasted and the past climate can be hindcasted to some extent using these models [2]. Some studies assessed different global circulation models in different areas such as northern Eurasia and Australia [3, 4].

Assessment of climate change impact in the Persian Gulf is important. In the Persian Gulf, a study has been done to evaluate the climate change based on the previous scenarios [5]. However, considering the development of RCPs, no studies have been conducted in the Persian Gulf in order to investigate the new dataset. This paper assesses the performance of the Coupled Model Intercomparison Project phase 5 (CMIP5) in simulating wind field over the Persian Gulf for the period of 1980 to 2005, by comparing it to a local reliable wind field (ECMWF).

2. Methodology

2.1. Study Area

Assessment of wind speed variations due to climate changes was carried out in a location in the middle Persian Gulf (figure 1) where the data was available. This point was selected based on the spatial resolution of IPSL-CM5A model (figure 1). The point is located far from the coastal areas where numerical models have limited ability to produce the reliable data due to the complicated orography. The Persian Gulf is an extension of the Indian Ocean through the Strait of Hormuz and it lies between Iran to the northeast and the Arabian Peninsula to the southwest. The Persian Gulf has many fishing grounds, extensive coral reefs, and abundant pearl oysters. It is the world's largest source of crude oil, and oil industries dominate the region. Therefore, understanding the variation of wind parameters during the long time period caused by climate change is necessary in this area.

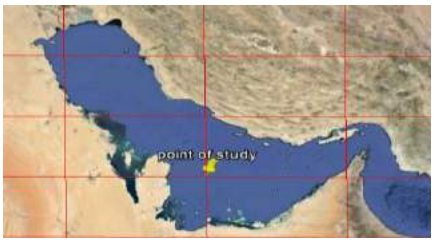

Figure 1. Study Area

2.1. Data Resources

The Fifth Assessment Report (AR5) of Intergovernmental Panel on Climate Change (IPCC) is based on a new set of scenarios that replace the Special Report on Emissions Scenarios (SRES) standards employed in two previous reports. The new scenarios called Representative Concentration Pathways (RCPs) contain four pathways: RCP8.5, RCP6, RCP4.5 and RCP2.6 which includes: one high pathway in which radiative forcing reaches >8.5 W/m2 by 2100 and continues to rise until a certain time; two intermediate stabilization; and one pathway where radiative forcing peaks at approximately 3 W/m2 before 2100 and then declines [2].

In order to evaluate the impact of climate change on the variation of wind field over the Persian Gulf, the IPSL-CM5A model with 6-hourly temporal resolution and spatial resolutions of 3.75 degrees longitude and 1.875 latitude, prepared by the Pierre Simon Laplace Institute (IPSL) were used [6].

In order to assess the CMIP5 wind field, local wind field was obtained from the European Centre for Medium-Range Weather Forecasts (ECMWF). It

contains the wind vector at 10 meters above the sea level with 0.5 degree and 6-hourly spatial and temporal resolutions, respectively.

3. Results & Discussion

CMIP5 and ECMWF wind fields were compared in a point in the Persian Gulf, for the period of 1980 to 2005 in order to assess CMIP5 to be used in interpolation approaches.

Seasonal average wind speed were obtained and shown in figure 2. According to this figure, in comparison to ECMWF, CMIP5 wind speeds are underestimated. However, the trend of both wind data seems to be similar.

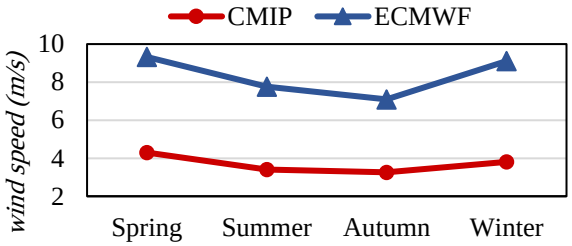

Figure 2. Seasonal average wind speed (1980-2005)

In addition, wind direction were assessed using wind roses as shown in figure 3, which illustrates that CMIP5 wind direction is consistent with that of ECMWF, while the amount of wind speed is required to be modified.

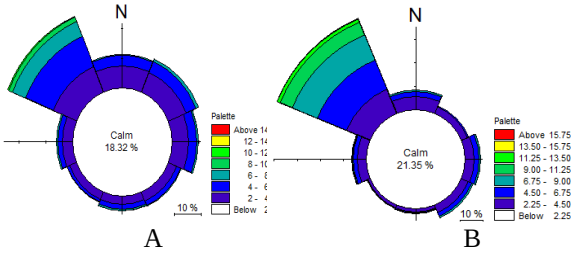

Figure 3. Wind roses for A) CMIP5 and B) ECMWF

According to figure 4 which shows the monthly average of CMIP5 and ECMWF wind speeds from 1980 to 2005, CMIP5 show the highest wind speed in April and June whereas the highest wind speed for ECMWF occur in February and June which implies the winter and summer-time Shamal winds, respectively in the study area. Shamal is the most well-known wind in the Persian Gulf which blows from the North West (NW). The winter Shamal is related to synoptic weather systems to the NW. The summer shamal is practically continues from early Jun through July. [7]

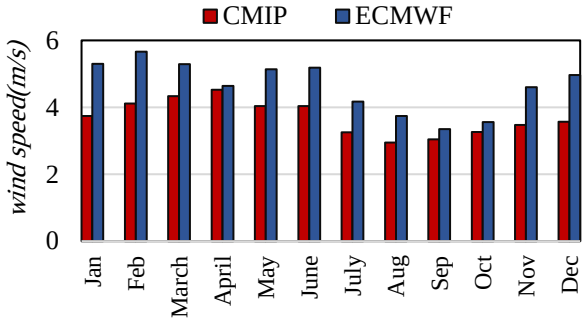

Figure 4. The monthly mean wind speed (1980-2005)

Regarding the mentioned difference between CMIP5 and local wind data, CMIP5 wind speed requires modification before being used in this area for climate change impact assessments.

4. Summery and Conclusion

Wind field from IPSL model of CMIP5 are examined to determine its accuracy in the Persian Gulf wind field comparing with ECMWF. Results show that CMIP5 wind speeds are underestimated in accordance to ECMWF and it needs an overall correction in the amount of wind speed while the dominant wind direction is somewhat similar for both wind fields.

5. References

[1] Erichsen, A, Rugbjerg, M, Mangor, K, Deigaard, R. 2011. Marine climate change guidelines Prepared for DHI-Project No 11098602.

[2] IPCC expert meeting report. 2007. Noordwijkerhout, the Netherlands.

[3] Miao, Ch, Duan, Q, Sun, Q, Huang, Y, Kong, D, Yang, T, Ye, A, Di, Zh and Gong, W. 2014. Assessment of CMIP5 climate models and projected temperature changes over Northern Eurasia. Environmental Research Letters, Volume 9.

[4] Mehrotra, R, Sharma, A, Bari, M. Tuteja, N, Amirthanathan, G. 2014. An assessment of CMIP5 multi-model decadal hindcasts over Australia from a hydrological viewpoint. Journal of Hydrology, 2932–2951.

[5] Kamranzad, B, Etemad-Shahidi, A, Chegini, V, Hadadpour, S. 2013. Assessment of CGCM 3.1 wind field in the Persian Gulf, Journal of Coastal Research, SI65, 249-253.

[6] CMIP5 Coupled Model Intercomparison Project, http://cmip-pcmdi.llnl.gov/cmip5/

[7] Reynolds, R.M. 1993. Physical Oceanography of the Persian Gulf, Strait of Hormuz, and the Gulf of Oman - Results from the Mt. Mitchell Expedition.

SEA WATER TEMPERATURE OBSERVATION AND SIMULATION IN THE CASPIAN SEA

E. Jafari[1], M.H. Moeini[2], M.J. Alaee[3], M. Nazarali[4] and M. Bali[5]

1) Pouya Tarh Pars Consulting Engineering Company, Tehran, Iran, e.jafari@ptpco.com
2) Pouya Tarh Pars Consulting Engineering Company, Tehran, Iran, mhmoeini@gmail.com
3) Pouya Tarh Pars Consulting Engineering Company, Tehran, Iran, m.j.alaee@ptpco.com
4) Pouya Tarh Pars Consulting Engineering Company, Tehran, Iran, mostafa.nazarali@gmail.com
5) Pouya Tarh Pars Consulting Engineering Company, Tehran, Iran, meysam_baali@yahoo.com

1. Introduction

The Caspian Sea is the world's largest enclosed water body in both area (380,000 km^2) and volume (78,000 km^3). It contains 44% of the global volume of inland waters. It has dimensions of 1300 km in length from north to south and width of 200–450 km from east to west. The water depth of the Caspian Sea reaches to more than 1000 m in the southern areas.

Based on the physical oceanographic studies, the temperature of the sea water varies with the location as well as along the water column. Previous studies and field observations show that the temperature of the surface mixed layers varies along the day and night and also in different seasons; while in the deep sea, the temperature only has small seasonal variations. In addition, due to approximately 1200 km north-south extension of the Caspian Sea, there is a horizontal variation of the temperature between northern and southern parts of the sea [1-4].

The Iranian Port and Maritime Organization (PMO) initiated a project, led by Pouya Tarh Pars Consulting Engineers to examine the physical processes along the Iranian sector of the Caspian Sea through the use of field measurements and numerical modeling. In this paper the results of these studies with regard to sea water temperature is presented.

2. Field Observations

In this study, satellite observations alongside the field observations are used to evaluate the model results of sea water temperature.

A Group for High Resolution Sea Surface Temperature (GHRSST) is produced by the JPL OurOcean group using a multi-scale two-dimensional variational (MS-2DVAR) blending algorithm on a global 0.009 degree grid. This Global 1 km SST (G1SST) analysis uses various satellite data from different sensors (AVHRR, AATSR, SEVIRI, AMSRE, TMI, MODIS, GOES Imager, MTSAT-1R radiometer) and also in situ data from drifting and moored buoys.

On the other hands, ADCP devices including AWACs and AQUADOPPs were deployed at 5, 10 and 25m depth in six different locations (Astara, Anzali, Roodsar, Noushahr, Amirabad and Gomishan). In these locations, sea temperature is observed in the depth of device installation. In addition, physical properties of the sea water are measured in various locations and in different depths (5 to 60 m) using RCM9 and RBR-Tu devices.

These observations were analyzed to evaluate the sea water temperature variation patterns in the Caspian Sea, especially Iranian coasts.

3. Model Setup

3D simulation of water circulation and temperature variation in the Caspian Sea was performed using MIKE3-flow model. The study area covered the whole area of the Caspian Sea, located between the longitude of 46.5°-54° E and the latitude of 36.5°-47° N. The model was executed considering all effective parameters, including wind, air pressure, air temperature, relative humidity, sunshine duration and etc. The simulation was conducted using an unstructured horizontal mesh in which the mesh dimensions were between 0.03˚ and 0.25˚. For the vertical layers, a combination of sigma coordinate and z-level coordinate system was used. For the air temperature data, the Modern Era Retrospective-analysis for Research and Applications (MERRA) reanalysis data was used. The model was calibrated using field measurements in different locations at the southern parts of the Caspian Sea.

4. Simulation Results

The results show good agreement between simulations and observations. For example, Figure 1 displays comparisons of the numerical modeling sea surface temperature results against the observations in Astara, Anzali, Roodsar, Noshahr and Amirabad in south of the Caspian Sea for 2013. As seen, the simulations are in a good agreement with the field measurements and the model results follow the observations in the seasonal and annual variations of the sea surface temperature in the Caspian Sea.

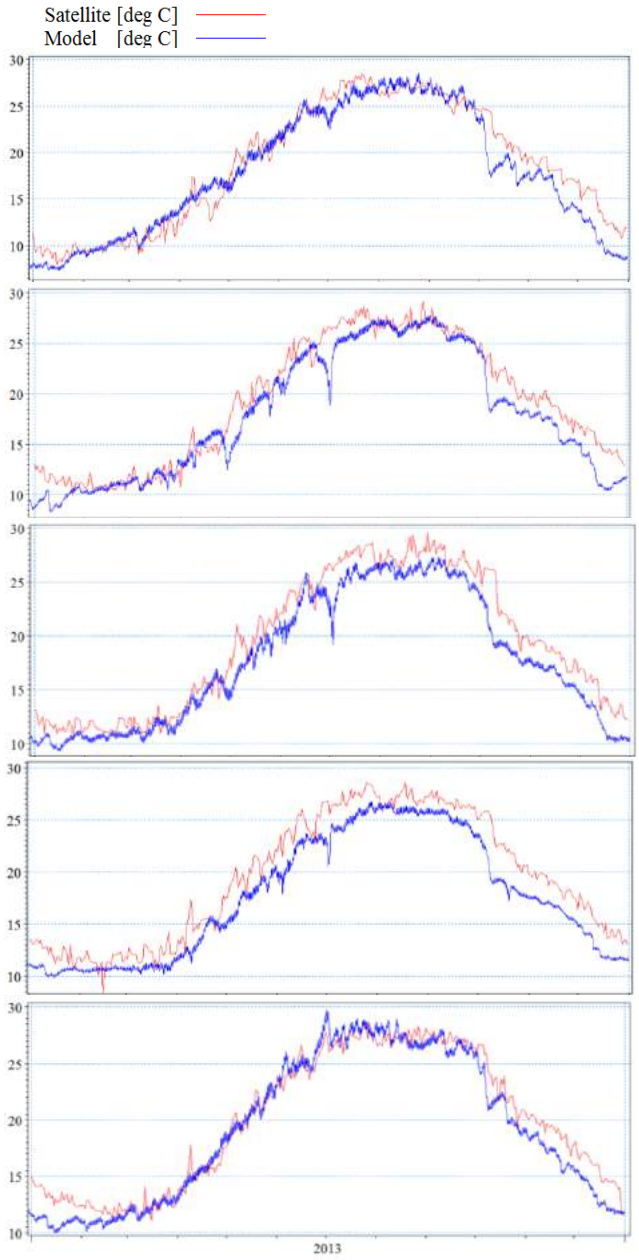

Figure 1. Comparisons of the numerically modeled SST against the observations in (from top to bottom) Astara, Anzali, Roodsar, Noshahr and Amirabad for 2013. Red line is the satellite observation and the black line is the modeling result.

The comparisons of the results with the ADCP water temperature measurements in different depths also show the same results.

In order to evaluate the model performance in the prediction of water temperature profile in depth, a comparison between model results and CTD observations is presented in the Figure 2.

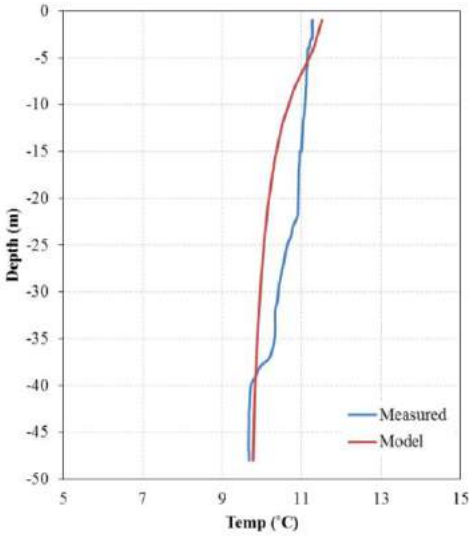

Figure 2. Comparison between measured water temperature profile and model results.

The results demonstrate that the model can simulate the water temperature quit well not only on the sea surface, but also in different depths of the sea.

5. References

[1] Jamshidi, S., &Bakar, N. A. (2012). Seasonal variations in temperature, salinity and density in the southern coastal waters of the Caspian Sea. *Oceanology*, 52(3), 380-396.

[2] Zaker, N. H., Ghaffari, P., & Jamshidi, S. (2007). Physical study of the southern coastal waters of the Caspian Sea, off Babolsar, Mazandaran in Iran. *Journal of Coastal Research*. SI, 50, 564-569.

[3] Jamshidi, S., Bakar, A., &Noordin, M. (2010). Temperature, Salinity and Density Measurements in the Coastal Waters of the Rudsar, South Caspian Sea. *Journal of the Persian Gulf*, 1(1), 27-36.

[4] Oktaee, R. (1999). The analysis of the physiochemical parameters of the Caspian Sea water. *Caspian Sea National Research Center, Iran Water Resources Management Company*.

INTRODUCING a MATHEMATICAL MODEL for HYDRODYNAMICS of SURF ZONE and in VICINITY of SEAWALLS, USING PROBABILITY DENSITY FUNCTIONS of WAVE HEIGHT

A. Jalali Gilani, S. K. Gharachorloo, M. A. Mehrdad, and M. A. Lashteh Neshaei
Department of Civil Engineering, University of Guilan, Rasht, Iran, pr@guilan.ac.ir

Abstract

In reality, sea waves are random and so does sediment transport. Today statistical and probabilistic view for this concept has grown rapidly among researchers and coastal engineers. Specifically in vicinity of shore protection structures, such as seawalls; that induce reflection which leads to creation of standing waves and these phenomena drastically change surf zone flow regime and also the mentioned surf zone sediment transport. In this study a mathematical model is introduced that can transform wave height probability density function to horizontal velocity probability density function near seabed, in surf zone and in vicinity of seawalls. Afterwards this model is verified by experimental data obtained from coastal laboratory of Imperial College University.

1 Horizontal Velocity PDF

1.1. Natural Beach

The method used to build velocity PDF from wave height PDF is by transforming wave height mean and standard deviation to velocity mean and standard deviation. Having the corresponding mean and standard deviation, velocity PDF can be built. A Gaussian distribution is used for describing velocity PDF as it is the best fitting function on experimental velocity data. More details on this investigation are explained later in chapter 1.3.

First the standard deviation of particle velocities are built and then the mean. The long-wave equation for calculating horizontal velocity is as follows [Guza and Thornton, 1980 (1)]:

$$u = \frac{H}{2}\sqrt{\frac{g}{d}}\cos(kx-\sigma t) \qquad (1)$$

where u= horizontal particle velocity; H= wave height; g= gravitational acceleration; d= water depth; k= wave number; x= horizontal distance from origin used for observation; σ = wave angular frequency; t= time.

By assuming the origin as the observation point, x=0 and $A=\cos(-\sigma t)$, equation (8) turns to this equation:

$$u = \frac{H}{2}\sqrt{\frac{g}{d}}A \qquad (2)$$

The standard deviation of horizontal particle velocities will be proved as [Goodman, 1960 (2); Grimmett and Stirzaker, 1992 (3)]:

$$\sigma_u = \frac{\sqrt{2}}{4}\sqrt{\frac{g}{d}}\bar{H} \qquad (3)$$

And the mean of horizontal velocity will be proved as [Kobayashi, 1998 (4)]:

$$\bar{u} \approx -\frac{1}{8}\sqrt{gd}\left(\frac{\bar{H}}{d}\right)^2 \qquad (4)$$

Now, having the standard deviation (equation 3) and the mean (equation 4) a probability density function can be defined. If the function would be a Guassian one the equation would be as follows:

$$p(u) = \frac{1}{\sigma_u\sqrt{2\pi}}\exp\left(-\frac{(u-\bar{u})^2}{2\sigma_u{}^2}\right) \qquad (5)$$

1.2. In Front of Seawall

A concise description of the method to incorporate the reflection phenomenon in natural beach velocity PDF model is that for each of the incident waves and reflected waves standard deviation and mean for particle velocity is calculated separately and later these standard deviation and mean are combined to obtain velocity PDF in front of the seawall [Rakha and Kamphuis, 1997 (5); Neshaei, 2009 (6)].

To achieve this purpose, firstly standard deviation and mean of reflected wave height are estimated using the reflection coefficient equation as follows:

$$H_r = C_r H_i \qquad (6)$$

$$\bar{H}_r = \frac{\sum_{i=1}^{n} H_{r_i}}{n} = \frac{\sum_{i=1}^{n} C_r H_i}{n} = C_r\bar{H}_i \qquad (7)$$

$$\sigma_{H_r} = \sqrt{\frac{\sum_{i=1}^{n}(H_{r_i}-\bar{H}_r)^2}{n}} = \sqrt{\frac{\sum_{i=1}^{n}(C_r H_i - C_r\bar{H}_i)}{n}} = C_r\sigma_{H_i} \qquad (8)$$

where H_r = reflected wave height; C_r = reflection coefficient; H_i = incident wave height; $\bar{H}_r$ = reflected wave height mean; $\bar{H}_i$ = incident wave height mean; σ_{H_r} = reflected wave height standard deviation; σ_{H_i} = incident wave height standard deviation.

Using the equations (3) and (4) standard deviation and mean of incident and reflected waves of near seabed particle velocity are calculated as follows:

$$\sigma_{u_i} = \frac{\sqrt{2}}{4}\sqrt{\frac{g}{d}}\bar{H}_i \qquad (9)$$

$$\bar{u}_i \approx -\frac{1}{8}\sqrt{gd}\left(\frac{\bar{H}_i}{d}\right)^2 \qquad (10)$$

$$\sigma_{u_r} = \frac{\sqrt{2}}{4}\sqrt{\frac{g}{d}}\bar{H}_r \qquad (11)$$

$$\bar{u}_r \approx -\frac{1}{8}\sqrt{gd}\left(\frac{\bar{H}_r}{d}\right)^2 \qquad (12)$$

where σ_{u_i} = standard deviation of particle velocity induced by incident waves; $\bar{u}_i$ = mean of particle velocity induced by incident waves; σ_{u_r} = standard deviation of particle velocity induced by reflected

waves; $\bar{u}_r$ = standard deviation of particle velocity induced by reflected waves.

Using the propagation of errors and as for every incident wave there is a reflected wave, standard deviation and mean of particle velocity in front of the seawall are:

$$\sigma_{u_W} = \sqrt{\sigma_{u_i}^{\ 2} + \sigma_{u_r}^{\ 2}} \qquad (13)$$

$$\bar{u}_W = 0.5(\bar{u}_i + \bar{u}_r) \qquad (14)$$

where σ_{u_W} = standard deviation of particle velocity in front of the seawall; $\bar{u}_i$ = mean of particle velocity in front of the seawall by incident waves.

Now, having the standard deviation (equation 13) and the mean (equation 14) a probability density function can be defined. If the function would be a Guassian one, the equation would be as follows:

$$p(u_W) = \frac{1}{\sigma_{u_W}\sqrt{2\pi}} \exp\left(-\frac{(u_W - \bar{u}_W)^2}{2\sigma_{u_W}^{\ 2}}\right) \qquad (15)$$

In order to make comparison between PDFs, root mean square error of the predicted and Gaussian fit of measured PDF is calculated and then normalized and presented in Table 4. The following equation is used to calculate the normalized root mean square error:

$$NRMSE = 1 - \frac{RMSE_i}{P_{\max} - P_{\min}} \qquad (34)$$

where $RMSE_i$ = root mean square error of predicted PDF and best fit Gaussian of measured PDF; $P_{\max}$ = maximum value of predicted PDF; $P_{\min}$ = minimum value of predicted PDF.

Table 1 yields two fundamental results, firstly the math model prediction of PDF is more precise in natural beach than in front of seawall; this decrease in precision is expected because the hydrodynamics of wave reflection is modeled and not straightly used, secondly the math model precision generally decreases as the distance from shoreline increases. This is also expected as linear progressive long-wave theory accuracy diminishes as the water depth increases. All in all as it can be seen in Table 4, the math model method is in good agreement with the measured data.

Table 1. NRMSE of predicted PDF and measured PDF

Distance from shoreline(mm)	Natural beach	In front of seawall
900	0.968	0.921
1200	0.961	0.944
1800	0.947	0.953

1.3. PDF determination

To find the best PDF function for describing the velocity PDF an investigation was done on different PDF functions in consideration of the method presented in this study. The PDF functions must have the following two criteria:

1. The PDF function domain must encompass negative and positive numbers, $[-\infty, +\infty]$.

2. The PDF function must come into existence by having a mean and a standard deviation as inputs.

After an exploration in a set of forty nine PDF functions, five functions satisfied the criteria. These functions were, Caushy, Gumble, Hyperbolic Secant, Logistic and Gaussian distributions. Afterwards these five functions were fed by mean and standard deviation of calculated particle velocity from the method presented in sections 1.1 and 1.2 and a goodness of fit exam of Kolmogorov-Smirnov was used to find the best fitting function.

The result of the exams on all measured data is that Gaussian distribution is the best fitting function for the math model. Fig 1 and Fig 2 show the five qualified distributions which are fed by standard deviation and mean of modeled horizontal particle velocity and measured PDF of particle velocity for a particular point in surf zone.

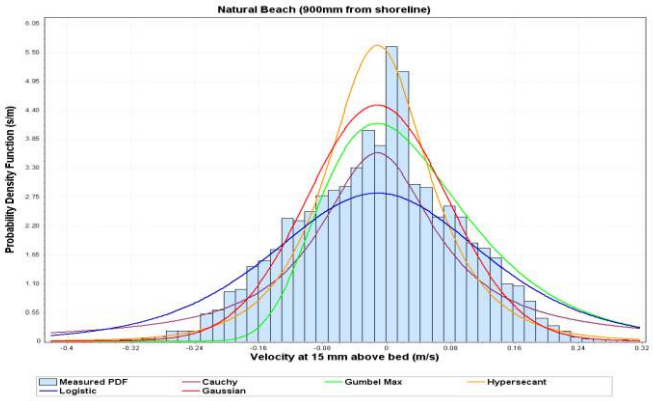

Figure 1. Measured PDF and final five qualified PDF distributions used by model- Natural Beach

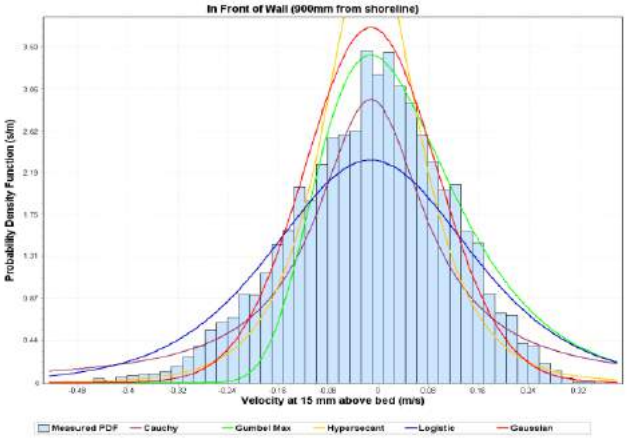

Figure 2. Measured PDF and final five qualified PDF distributions used by model- In front of seawall

References

1- Guza, R.T., Thornton E.B., 1980. Local and shoaled comparisons of sea surface elevations, pressures and velocities. Journal of Geophys. Res., 85(C3), pp. 1524-1530.

2- Goodman L., 1960. On the Exact Variance of Products, Journal of the American Statistical Association 55(292): pp.708-713.

3- Grimmett G.R., Stirzaker D.R., 1992. Probability and Random Processes, 2nd edition, Clarendon Press, Oxford.

4- Kobayashi, N., Herrman, M.N., Johnson, B.D., Orzech, M.D., 1998. A probability distribution of surface elevation in surf and swash zones. Journal of waterway port, coastal, and ocean engineering. Vol 124, No. 3, pp. 99-107.

5- Rakha, K.A., Kamphuis, J.W., 1997a. Wave induced currents in the vicinity of a seawall. Coastal Engineering 30, pp. 23–52.

6- Neshaei, M.A.L., Mehrdad, M.A., Veiskarami, M., 2009. The effect of beach reflection on undertow. Iranian Journal of Science & Technology, Transaction B, Engineering. Shiraz University 33 (B1), pp. 49–60.

INTERCOMPARISON OF SIX PLANETARY BOUNDARY LAYER SCHEMES IN THE WRF-ARW MODEL ON SURFACE WIND SIMULATIONS OF PERSIAN GULF

Siavash Gholami[1], Sarmad Ghader[2], Hasan Khaleghi-Zavareh[3] and Parvin Ghafarian[4]

1) Iranian National Institute for Oceanography and Atmospheric Science, Tehran, Iran, s.gholami@inio.ac.ir
2) Institute of Geophysics, University of Tehran, Tehran, Iran, sghader@ut.ac.ir
3) Iranian National Institute for Oceanography and Atmospheric Science, Tehran, Iran, hkzavareh@gmail.com
4) Iranian National Institute for Oceanography and Atmospheric Science, Tehran, Iran, p.ghafarian@inio.ac.ir

1. Introduction

The study of Persian Gulf as one of the largest energy sources in the world and one of the connection paths between marginal countries with the other regions of the world has a special importance. Wind over sea and ocean is one of the effective factors on economic activities in every region but unfortunately atmospheric observation data in overseas area is in intense shortage in compare with overland data. In order to maintain the safety of life in overseas and coastal areas and construction of needed offshore and onshore structures there must be enough knowledge about the wind variability and the waves caused by wind[1]. On the other hand the most common effects of wind on ocean is seen in wind driven currents, swells and oceanic circulations (upwelling and down welling)[2]. Also wind has an key role in the modeling of phenomenon caused by the interaction between atmosphere and ocean (e.g. Drag coefficient)[3]. In other words uncertainty in the determination of surface wind could cause a large difference in the output of atmospheric and oceanic models.

2. Model composition and data

The 3.4.1 version of WRF model as one of the limited area models with ARW dynamic core is used for wind field simulation over Persian Gulf area in 24 hours forecast horizon. The simulation domain is assumed as three nested grids with grid resolution of 36, 12 and 4 km, for parent, first nest and innermost domains respectively (Figure1). In this simulation the parameterization schemes are used for different physical processes that for microphysics the Lin method, Goddard scheme for short wave radiation, RRTM scheme for long wave radiation, Noah method for land surface and Kain-Fritsch scheme for convection are used. But for planetary boundary layer and surface layer six boundary layer schemes of YSU ،ACM2 ،MYJ ،MYNN ، BouLac and QNSE along with their coupled surface layer schemes are used. More details about parameterization are explained in by Skamarock et al., and Wang et al.,[4,5] . In this study for providing initial and boundary conditions for WRF model in order to simulate wind field for 24 hours in Persian Gulf area two datasets are used:

1) Reanalysis dataset of ERA-Interim from ECMWF with $0.75^{\circ} \times 0.75^{\circ}$ horizontal resolution for Geographic latitude and longitude[6].
2) NCEP-FNL dataset from National center for environmental prediction with $1^{\circ} \times 1^{\circ}$ horizontal resolution for Geographic latitude and longitude.

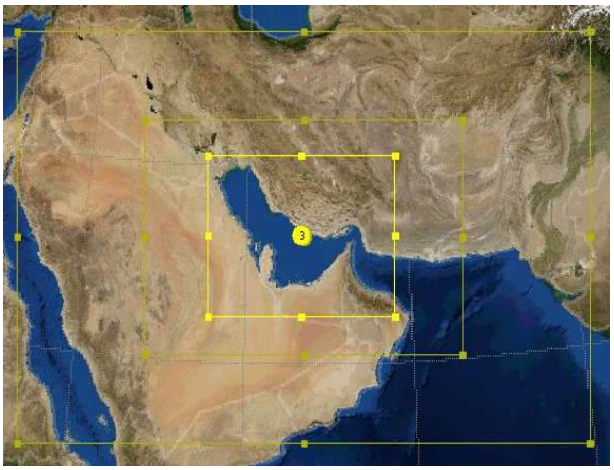

Figure 1. Domains used in WRF model simulations.

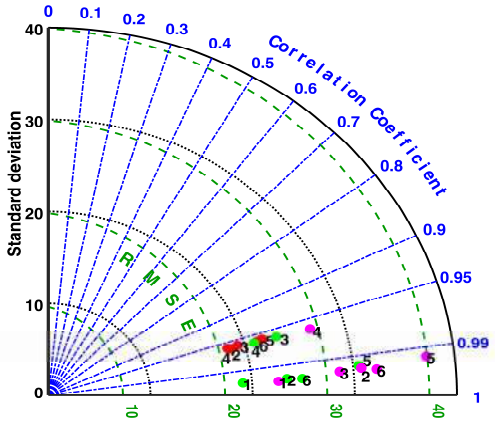

Figure 2. Pattern statistics describing the wind direction over Persian Gulf simulated by WRF models compared with the synoptic observations.

3. Results

In this study the simulation of wind field using WRF model is being verified in compare with observation data from synoptic stations and the data collected by QuikSCAT satellite. The statistical results (e.g. R, RMSE, STDE) for wind speed and direction under the PBL schemes are given in table 1 and table 2 in summery. Overall the ACM2 scheme has a better performance in compare with other schemes.

For instance the Taylor diagram [7] that has the ability to simultaneously show the statistical parameters for simulated wind direction using FNL as initial condition is shown in figure 2. In figure 2, red, green and pink marks are belonging to parent, first nest and innermost domains of simulation respectively. 1 to 6 numbers are belonging to ACM2, BouLac , MYJ , MYNN , QNSE and YSU schemes respectively.

Tablel 1. Statistics of the comparison between synoptic stations and simulated wind data .

variable	scheme	R	RMSE	STDE
wind speed	ACM2	0.63	1.18	0.8
	BouLac	0.62	1.29	0.92
	MYJ	0.56	1.39	1.05
	MYNN	0.53	1.27	0.94
	QNSE	0.58	1.38	1.03
	YSU	0.56	1.34	1
wind direction	ACM2	0.99	22.65	19.99
	BouLac	0.98	26.92	24.26
	MYJ	0.97	26.36	23.73
	MYNN	0.96	24.56	21.95
	QNSE	0.98	32.52	29.87
	YSU	0.98	28.81	26.15

Table 2. Statistics of the comparison between QuikSCAT and simulated wind data .

variable	scheme	R	RMSE	STDE
wind speed	ACM2	0.86	1.44	0.98
	BouLac	0.71	1.77	1.38
	MYJ	0.74	1.73	1.33
	MYNN	0.76	1.69	1.28
	QNSE	0.75	1.71	1.31
	YSU	0.70	1.79	1.40
wind direction	ACM2	0.94	13.87	13.02
	BouLac	0.92	17.35	16.52
	MYJ	0.94	12.96	12.11
	MYNN	0.93	17.56	16.71
	QNSE	0.92	15.45	14.62
	YSU	0.94	16.56	15.71

.

4. References

[1] Caires, S., Sterl, A., Bidlot, J.R., Graham, N., and Swail, V., "Intercomparison of different wind-wave reanalyses", *Journal of Climate*, pp.1893-1913 , 2004.

[2] Carvalho, D., Rocha, A. and Gómez-Gesteira, M., "Ocean surface wind simulation forced by different reanalyses: Comparison with observed data along the Iberian Peninsula coast", *Ocean Modelling*, 2012, pp.31-42.

[3] Deng, Zengan, Lian Xie, Bin Liu, Kejian Wu, Dongliang Zhao, and Ting Yu., "Coupling winds to ocean surface currents over the global ocean", *Ocean Modelling*, 2009, pp. 261-268.

[4] Skamarock, W.C., Klemp, J.B., Dudhia, J., Gill, D.O., Barker, D.M., Duda, M.G., Huang, X.Y., Wang, W. and Powers, J.G., "A description of the advanced research WRF Version 3", NCAR tech note NCAR/TN 475 STR, 125., 2008, pp. *Available from: UCAR Communications, PO Box*, *3000*.

[5] Wang, W., Bruyére, C., Duda, M., Dudhia, J., Gill, D., Kavulich, M., et al., "ARW Version 3 Modeling System User's Guide January 2014", National Center for Atmospheric Research, Boulder, CO, *http://www2 Mmm Ucar edu/wrf/users/docs/user_guide_V3 2014*.

[6] Dee, D.P., Uppala, S.M., Simmons, A.J., Berrisford, P., Poli, P., Kobayashi, S., et al., "The ERA-Interim reanalysis: Configuration and performance of the data assimilation system, *Quarterly Journal of the Royal Meteorological Society,* 2011, pp. 553–597.

[7] Taylor, K.E., "Summarizing multiple aspects of model performance in a single diagram", *Journal of Geophysical Research: Atmospheres*, 2001, pp. 7183-7192.

THE CASPIAN SEA WATER LEVEL FLUCTUATIONS, A MAJOR THREAT TO GORGAN BAY

Majid Jandaghi Alaee[1], Mostafa Nazarali[2], Faraz Mohseni[3], and Mohammad Reza Allahyar[4]

1) Pouya Tarh Pars consulting engineers, Tehran, Iran, m.j.alaee@ptpco.com
2) Pouya Tarh Pars consulting engineers, Tehran, Iran, mostafa.nazarali@gmail.com
3) Pouya Tarh Pars consulting engineers, Tehran, Iran, f.mohseni1362@yahoo.com
4) Port and Maritime Organization, Tehran, Iran, mallahyar@yahoo.com

1. Introduction

The Caspian Sea is the largest closed sea in the world, with area of 360,000 Km^2 has no significant tide, less than 10 cm. The Caspian Sea water level is about -27 m, below the free surface of the oceans, with annual fluctuation of about 0.4 m and interdecadal oscillation of 3 m during last century. Gorgan inlet which is known as Gorgan Bay (GB) is located adjacent to the southeast corner of the Caspian Sea. GB is 60km long, 10km wide and connected to the Caspian Sea through a relatively wide but very shallow channel. GB plays important roles in various aspects of its surrounding region hence it is a must to recognize its existing situation, monitor its changes, and to predict its behavior in different conditions. The main threat to the life of GB can be simply described: the average precipitation in the area is about 0.5 m/year while the average evaporation is around 1.5 m/year, therefore with no noticeable river discharge, it can be estimated that water depth of GB is facing a decrease of 1 m/year. On this basis and knowing that the average water depth of GB around 3 m, it can be easily estimated that GB will disappear in only three years, if its connection to the Caspian Sea is cut!

2. Methodology

In order to recognize the present condition of GB and effective parameters in how GB can be fed by the Caspian Sea waters, a review on available technical reports was performed, and a set of field observations together with the 2D and 3D numerical modeling were carried out. Primary results of the study indicated that during 1979, GB was completely separated from the Caspian Sea, corresponding to the time that the Caspian Sea water level was around -28. It was also shown that during wet years, while the Caspian Sea level reached its upper limits, GB was connected to the Caspian Sea not only through the abovementioned channel but also via a new channel, called Khozeini Channel. Therefore, it was obvious that the main task of the study must be to investigate the relationship between the fluctuations of the Caspian Sea level and the hydraulics of the channel.

Figure 1. (left) The Caspian Sea, (right-top) connecting channel between GB and the Caspian Sea in the water level rise and (right-bottom) fall condition

3. Field Observations

Three tide gauges, a current meter, monthly bathymetry survey and monthly CTD survey have been carried out from September 2014 till July 2015. Since the GB waters were about 15 to 20 percent more saline than the Caspian Sea waters, the CTD data enabled the authors to employ the conductivity as a tracer and depict the three-dimensional structure of the flow at various conditions. It was clearly shown that during storm, the wind set-up pushes up the water, at the coast and the resulting pressure gradient cause a relatively strong current, up to 0.5 m/s, into the GB. This inflow rises the water level in GB so that when storm is over, the connecting channels experience the return flow with relatively lower speeds (Figure 2).

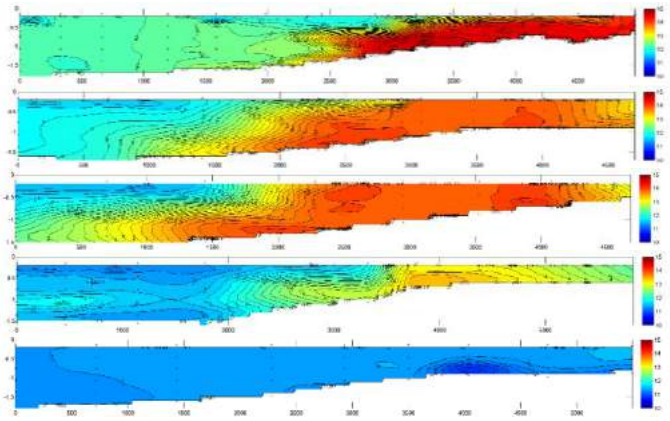

Figure 2. Intrusion of the Caspian Sea waters to GB (left: Caspian Sea, right: GB)

4. Numerical Modeling

What seen in the field data was examined by a three dimensional numerical model with two domains. In the first, the whole Caspian Sea was considered as the main domain and wind forcing was applied to the whole domain. In another set of runs, a smaller domain containing a part of GB, the connecting channels and southeast of the Caspian Sea was selected. The main purpose of the first was to recognize the behavior of the connecting channel in response to the actual meteorological conditions, while in the later, the main purpose was to investigate how important would be the pressure gradient in feeding GB.

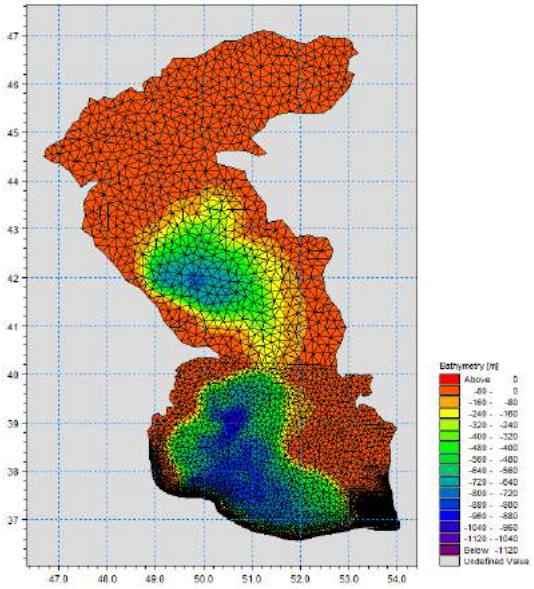

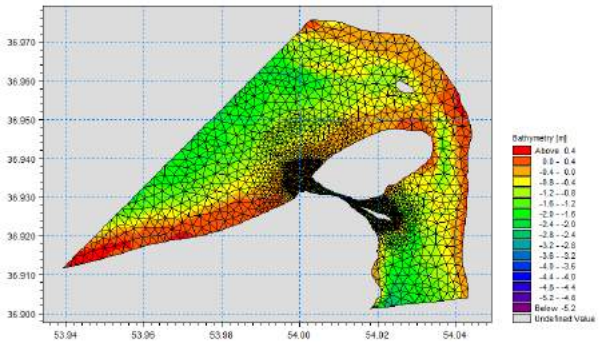

Figure 3. Domains selected for two model setups

5. Conclusion

The results of the field study and numerical modeling confirmed that the pressure gradient plays the key role of in feeding GB and keeping the connecting channel open. They also clearly showed that with small amount of dredging (about 1m deepening), particularly at the mouth of the main channel, the inflow to GB during storms enhances noticeably which helps the water quality in GB and secures the channels to be open. The solution was proposed to Ports and Maritime Organization in Iran (PMO) and it is expected that the dredging starts, soon.

6. Acknowledgement

This study was funded by PMO and the authors would like to thank the funding and their sincere cooperation.

7. References

[1] Pouya Tarh Pars consulting engineers co., "*Gorgan Bay hotspot report- Monitoring and Modeling studies of southern Caspian Sea coasts"*, Port and Maritime Organization of Iran, January 2016.

[2] DHI MIKE software package (2012), *2D- HD Flexible mesh module*, Denmark , 2012.

[3] Pugh, D.T. (1987), *Tides, surges and mean sea-level: a handbook for engineers and scientists.* Wiley, Chichester, 472pp.

[4] MATLAB and Statistics Toolbox Release 2014a, *The MathWorks, Inc.*, Natick, Massachusetts, United States.

DYANAMICS OF GORGAN BAY CHANNELS, VITAL CONNECTIONS TO THE CASPIAN SEA

Majid Jandaghi Alaee[1], Mustafa Nazar Ali[2] and Mohammad Hadi Moeeni[3]

1) Pouya Tarh Pars Consulting Engineers, Tehran, Iran, mja@ptpco.com
2) Pouya Tarh Pars Consulting Engineers, Tehran, Iran, mna@ptpco.com
3) Pouya Tarh Pars Consulting Engineers, Tehran, Iran, mhm@ptpco.com

1. Introduction

The Caspian Sea is the largest closed sea in the world, with area of 360,000 Km2 and no significant tide, less than 10 cm. The Caspian Sea water level is about 27m below the open seas, with 0.4m yearly fluctuation and 3m during last century. Gorgan Inlet which is known as Gorgan Bay (GB) is located adjacent to the southeastern corner of the Caspian Sea (Figure 1-a). GB is 60km long, 10km wide and connected to the Caspian Sea through a relatively wide and very shallow channel. GB plays important roles in various aspects of its surrounding region hence it is a must to recognize its existing situation, monitor its changes, and to predict its behavior at different conditions. The main problem is that the average precipitation in the area is about 0.5 m/year while the average evaporation is around 1.5 m/year, therefore with no noticeable river discharge, GB is facing a decrease of 1 m/year, of course if it is not fed by the Caspian Sea through the above mentioned channel. GB with maximum depth of around 3m will disappear in only three years!

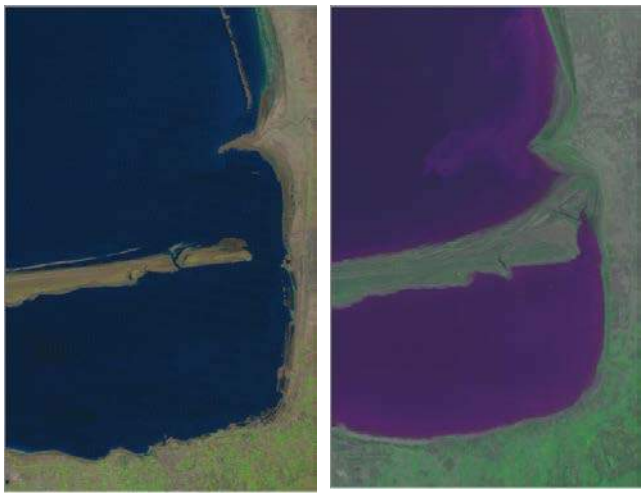

Figure 1: Connecting channel between GB and the Caspian Sea during the years with high sea water level (left) and lower (right).

2. Methodology

In order to know about the dynamics of the GB channels and effective parameters in how GB can be fed by the Caspian Sea waters, a set of field observations were planned. Historical data, particularly the long record of the Caspian Sea water level and various satellite images, contain important information about the channels reaction to the sea water fluctuations.

Bathymetry survey of the GB channels together with various beach profiles in the vicinity of the GB mouth helped to obtain a three dimensional picture of the study area. Using salinity difference between GB waters and the Caspian Sea waters, a set of monthly CTD survey was designed for one year, to trace the water movement during various Caspian-GB states.

Figure 2: CTD sampling stations

Three gauges for recording water elevations and one ADCP for having time series and corresponding vertical profile of current velocity in the main channel were deployed. Wind data was also collected from the met stations at Bandar Torkman and Amir Abad. In order to complete our understanding about the dynamics of the GB channels, number of 2D and 3D numerical modeling were carried out.

3. Results

Primary results of the study indicated that during 1979, GB was completely separated from the Caspian Sea (Figure 1- right), corresponding to the time that the Caspian Sea water level was around -28m. It was also shown that during wet years, while the Caspian Sea level reached its upper limits, GB was connected to the Caspian Sea not only through the above mentioned channel but also via a new channel, called Khozini Channel (Figure 1- left).

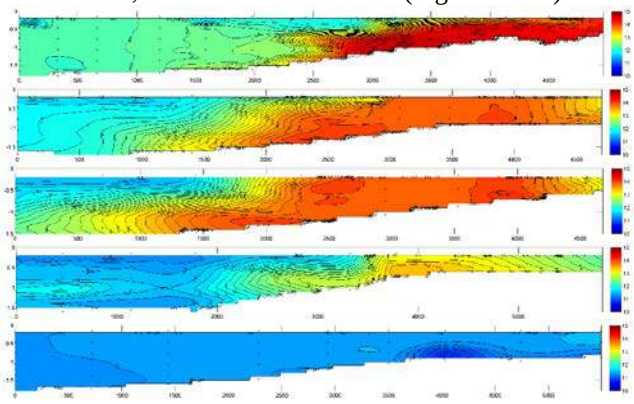

Figure 3. Interaction of the Caspian Sea (left) and GB (right) waters at different conditions.

From the results it was clearly shown that during storm, the wind set-up pushes up the water, at the coast and the resulting pressure gradient cause a relatively strong current, up to 0.5 m/s, into the GB. This inflow rises the water level in GB so that when storm is over, the connecting channels experience the return flow with relatively lower speeds (Figure 3).

What seen in the field data was examined by a three dimensional numerical model with two domains. In the first, the whole Caspian Sea was considered as the main domain and wind forcing was applied to the whole domain.

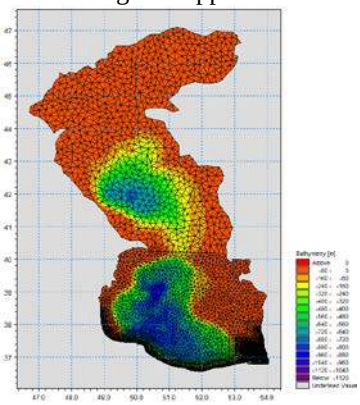

Figure 4. Numerical mesh for regional model

In another set of runs, a smaller domain containing a part of GB, the connecting channels and southeast of the Caspian Sea was selected. The main purpose of the first was to recognize the behavior of the connecting channel in response to the actual conditions, while in the later, the main purpose was to investigate how important would be the pressure gradient in feeding GB.

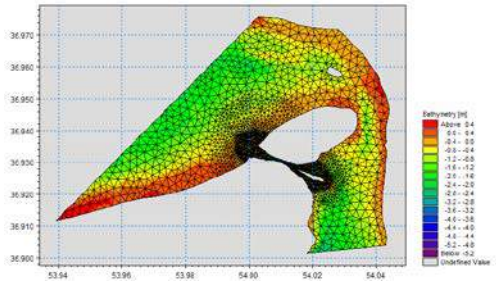

Figure 4. Numerical mesh for local model with fine grids for the GB channels

The field study and numerical modeling results supported the hypothesis that the pressure gradient plays the key role in feeding GB and keeping the connecting channels open. It was also examined that with small amount of dredging (about 1m deepening) particularly at the mouth of the main channel, the inflow to GB during storms enhances noticeably, that not only helps the self-wash of the channel but also strengthen the water circulation in the GB and consequently, by exchanging the GB and Caspian waters plays positive role in the GB water quality. The solution was proposed to Ports and Maritime Organization in Iran (PMO).

4. Acknowledgement

This study was funded by PMO and the authors would like to thank the funding and sincere cooperation.

CALCULATION OF FINITE SIZE LYAPUNOV EXPONENTS AND LAGRANGIAN COHERENT STRUCTURES IN THE ADRIATIC SEA

Saeed Hariri[1] [2]

1) Department of Civil, Chemical and Environmental Engineering (DICCA), University of Genoa, Genoa, Italy.
2) National Institute of Oceanography and Experimental Physics (OGS), Trieste, Italy. saeed.hariri@edu.unige.it

1. Introduction

Ocean is a complex system because of its movement patterns, since it changes from thousands of kilometers to the sub-mesoscales. Transport by Surface Ocean is an important issue that has become an area of intensive research (see for instance, [1-3]). In addition, the processes of mass transport depend strongly on the conditions of motion of the ambient fluid. The fundamental basis for the study of the mixing processes is related to the Eulerian flow field. Considering that the mass transport is a Lagrangian phenomenon and associated with coherent structures, it is necessary the preparation of tools for dispersion modeling based on Lagrangian quantities.

During last decade powerful tools have been introduced to better understanding of transport barriers in ocean; and one of the useful methods for describing local dispersion properties in time dependence flows is Finite-Size Lyapunov Exponent (FSLE) which is based on the time dependent velocity field with good accuracy. It should be noted that the fundamental definition of Lyapunov exponent is a global measure of the diverge rates of nearby trajectories. Furthermore, hyperbolic Lagrangian Coherent Structures (LCSs), that define transport pathways in ocean, especially over the mesoscale range, would be defined as ridges of the Finite-Size Lyapunov Exponent (FSLE) fields, although mathematical link between the FSLE and LCSs has been missing. Investigating relative dispersion based on Finite Scale Lyapunov Exponents (FSLEs) has been addressed in many works such as [4-8].

2. Data and Methods

In this paper, we study mixing structures and transport properties of the surface layer of Adriatic Sea, a semi-enclosed basin of the Mediterranean, during selected years (2006-2011). Lagrangian transport models have been used to simulate synthetic trajectories from the mean flow obtained by the MIT general circulation model implemented in the Adriatic Sea.

The classical definition of Lyapunov exponent is based on the exponential rate of separation of nearby trajectories that averaged over infinite time; so if $\delta X(t_0)$ is the initial distance between two neighbor trajectories and $\delta X(t)$ is defined as a distance between the same particles at time t, the global Lyapunov exponent is [7]:

$$\lambda = \lim_{t\to\infty} \lim_{\delta X(t_0)\to 0} \frac{1}{t} Ln \frac{|\delta X(t)|}{|\delta X(t_0)|} \quad (1)$$

Additionally, Finite-Size Lyapunov Exponents (FSLEs) depend on the two length scales: initial separation distance δ_0, assumed as a model resolution $1/32^0$, and the final separation δ_f. Considering that in this paper we are interested to study the structures mostly related to mesoscale range, the value of 1^0 has been taken for δ_f. So we define FSLE at time t_0 as:

$$\Lambda\left(X, t_0, \delta_0, \delta_f\right) = \frac{1}{|\tau|} Ln \frac{\delta_f}{\delta_0} \quad (2)$$

τ is the time which is required for two particles of fluid to separate from a distance of δ_0 to δ_f.

3. Results and Discussions

The first part of results presents the Adriatic mean surface circulation in 2008 derived from synthetic trajectories (Figure 1). As the flow map (Figure 1) clearly show recirculation cells are in correspondence of the Palagruza sill, the mid Adriatic pit in front of Split and south of the Istrian Peninsula [12, 13]. Strong currents along the eastern and western flanks of Adriatic have been detected in the mentioned periods (2006-2011) which indicate the energetic flows along EAC and the Italian coastline, although during 2008 is more visible. In the north end of Adriatic as numerical results show under the influence of seasonal wind-stress curl, the fourth isolated anticlockwise cyclonic gyre in the north of Po River is generated which has an important role on movement and transit of numerical particles located in this area.

On the other side of northern Adriatic an anticyclonic pattern which is located off the Istria between a cyclonic structure in the northern basin up to the Po River delta and the branch of the EAC recirculation [9] doesn't appear in the mean circulation maps generated by the model; however the FTLE (Finite Time Lyapunov Exponent) and FSLE (Finite Size Lyapunov Exponent) maps obviously show the effects of this pattern on dispersion of numerical particles (Figure 1).

FSLE map in March 2007 (Figure 2) presents different types of vortices in the Center, Southern and some parts of the Northern Adriatic Sea especially close to the Eastern and Western Boundary Currents. Generally, these unstable lines organize the transport properties of the surface flow. The maximum values of FSLE are at vortex edges, while in the core of eddy FSLE has low values. Along the Italian coastlines, in the North and South of Conero Promontory, we have obtained the highest values of FSLE because of strong currents generated by Po River during March 2007. As well as, our observations show that eddies produced by strong circulation cell in the Southern Adriatic have an important role in increasing of mixing activities and dispersion of pair particles. As expected this pattern increases the values of residence time corresponded to particles located in the core of SAP.

FSLE filaments, which are defined as unstable manifolds of hyperbolic material lines, have been detected in the center of Adriatic close to the Croatian coast. Because of low energy flow fields in the northern Adriatic (lack of strong circulation cells), FSLEs are negligible, which are ranging between 0.05-0.15 1 *day*− ; it means that the time is needed for the pair particles to separate and disperse away, is higher in the Northern Adriatic compared to the other parts of basin, since the highest values of time separation cause the lowest values of FSLE with less mixing activities and Kinetic Energy.

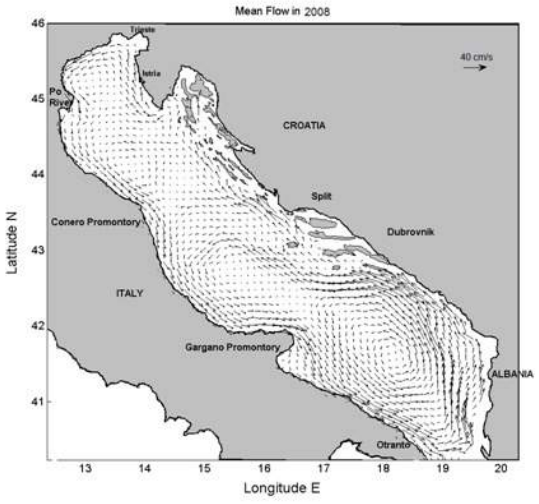

Figure 1. Mean flow field in the Adriatic Sea in 2008

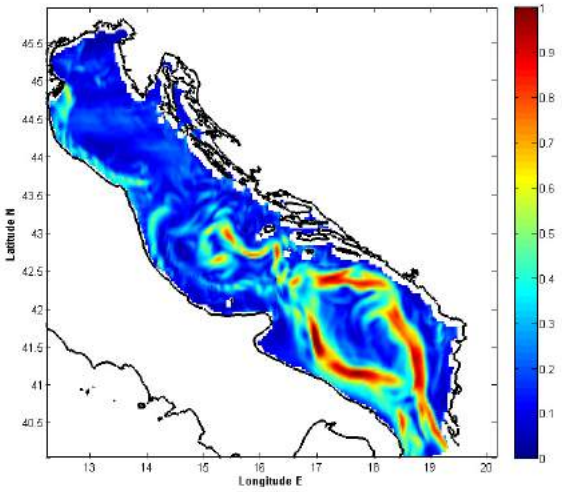

Figure 2. Time averaged FSLEs during March 2007 (The colorbar has units of day^{-1} ***)***

4. References

[1] Davidson, F.J.M., Allen, A., Brassington, G.B., Breivik, O., Daniel, P., Kamachi, M., Sato, S., King, B., Lefevre, F. Sutton M. and Kaneko K.: Applications of GODAE ocean current forecasts to search and rescue and ship routing, *Oceanogr.,* 22, 176-181, 2009.

[2] Hays, G.C., Fossette, S., Katselidis, K.A., Mariani P. and Schofield, G.: Ontogenetic development of migration: Lagrangian drift trajectories suggest a new paradigm for sea turtles, *J. R. Soc. Interface*, 7, 1319–1327, 2010.

[3] Poulain, P.-M., Hariri, S. Transit and residence times in the Adriatic Sea surface as derived from drifter data and Lagrangian numerical simulations, *Ocean Sci.*, vol.9, pp.713-720, 2013.

[4] LaCasce, J. H. and A. *Bower.*, Relative dispersion in the subsurface North Atlantic. *J. Mar. Res.*, 58, 863–94, 2000.

[5] Artale, V., Boffetta, G., Celani, A., Cencini, M., Vulpiani, A., Dispersion of passive tracers in closed basins: beyond the diffusion coefficient, *Phys. Fluids.,* 9 (11), 3162–3171, 1997.

[6] Haza, A. C., Poje, A.C., Ozgokmen, T., Martin, P., Relative dispersion from a high-resolution coastal model of the Adriatic Sea, *Ocean Modelling.,* 22, 48–65, 2008.

[7] Lumpkin, R., and S. Elipot ,Surface drifter pair spreading in the North Atlantic, *J. Geophys. Res.,* 115, C12017, 2010, doi:10.1029/2010JC006338.

[8] Peikert, R., Pobitzer, A., Sadlo, F., and Schindler, B., A Comparison of Finite-Time and Finite-Size Lyapunov Exponents, *Topological Methods in Data Analysis and Visualization III Mathematics and Visualization*, pp. 187-200, 2014.

[9] Ursella, L., Poulain, P.-M. and Signell R.P.: Surface drifter derived circulation in the northern and middle Adriatic Sea: Response to wind regime and season, *J. Geophys.* Res., 111, C03S04, doi: 10.1029/2005JC003177, 2006. [Printed 112(C3), 2007].

NUMERICAL ANALYSIS OF WAVE-STRUCTURE DYNAMIC INTERACTION CAUSED BY DIFFERENT GEOMETRIES OF GRAVITY PLATFORMS

Elham Mina[1], Mohammad Amin Kalantari [2], Saleh Neishaburi[3]

1) Hydraulic Structures , Tarbiat Modarres University,Tehran,Iran, E.mina@modares.ac.ir
2) FacultyOf Marine Technology, AmirKabir University Of Technology, kalantari@aut.ac.ir
3) Hydraulic Structures , Tarbiat Modarres University,Tehran,Iran, salehi@modares.ac.ir

1.Introduction

Given that the gravity platforms are supported by the sea bed but not attached to the ground, the motion of them is known as a rocking fluctuation. During the fluctuations, the platform maybe overturned if the angle is large. In this study, using Ansys Aqwa hydrodynamic software and analytical methods with regard to the performance, the dynamic interaction of platform's geometry on hydrodynamic forces have been simulated. The objective of this study was to analyze the hydrodynamic parameters of the sea and rocking fluctuations of gravity platforms under the impact of regular wave's moment considering the soil mechanics and hydrodynamic features of the structure. In order to achieve the objective the hydrodynamic forces using numerical simulations and analytical methods[7] of Mac Cami[3] foch and Chakrabarty[6]for monopod and tripod platforms were analyzed. Finally, responses of the platform to irregular waves were studied using numerical simulation.

2. Methodology

In this study, using Ansys Aqwa software, the equations of fluid flow including the equations of continuity and momentum were simulated regarding the non-compressibility by boundary element method.The effects of the sea bed on the depreciation of the rocking fluctuation of the construct and hydrodynamic properties were considered for a gravity construct with wavelengths larger than the diameter of the structure using scattering theory around the structure. The study is based on the following assumptions and if other conditions are considered, mathematical relationships need to be corrected. Linear wave theory, harmonic regular waves, rigid gravity platform of monopod and tripod bases are regarded. The gravity platform is not attached to the soil [1] and wave-induced force is obtained using Erie linear wave theory [2],[4],[5] for a regular wave. Since the geographical location of platforms is located in the North Sea, the environmental conditions and specifications are as follows:

$\rho = 1025\,{}^{kg}/_{m^3},\ g = 9.81\,{}^{m}/_{s^2},\ H_0 = 6m,$

$d = 150m,\ T = 8s, \lambda = 100m)$

$k = \frac{2\pi}{\lambda} = 0.062\ m^{-1}, \omega = \frac{2\pi}{T} = 0.7853\ \left(\frac{rad}{s}\right)$

3.Analysis

3.1. The analysis of the hydrodynamic force for monopod and tripod platform

According to the analysis result of the hydrodynamic force for monopod and tripod platform:

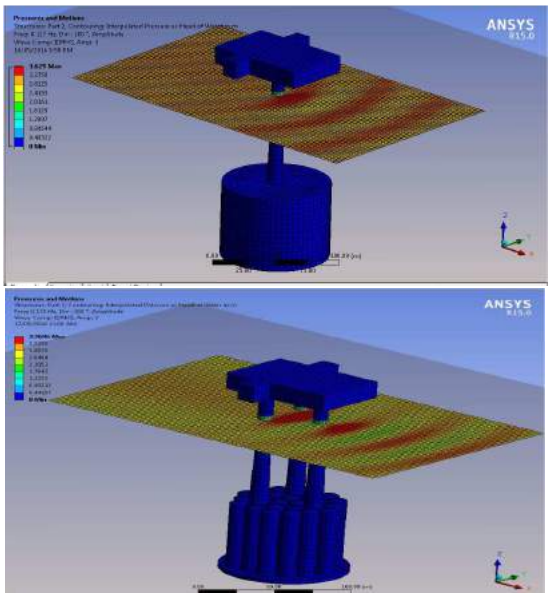

Figure 1: A view of the pressure caused by hydrodynamic forces in the frequency domain

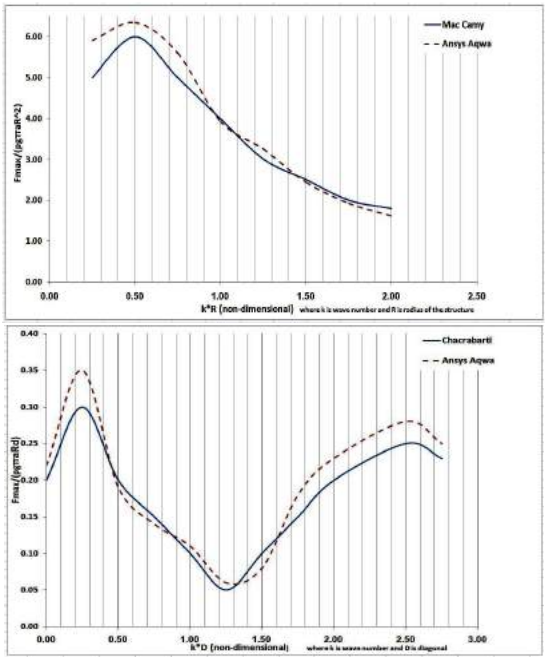

Figure 2: the Graph of maximum hydrodynamic force of wave based on k.D parameters for monopod and tripod platform

3.2. The analysis of platform stability index

According to the analysis result of platform stability for tripod platform:

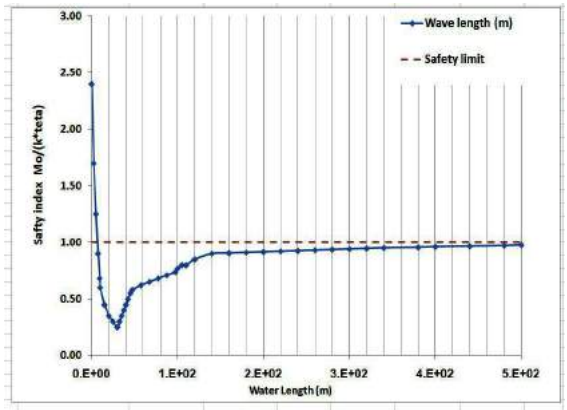

Figure 3. Structural changes of the frequency of the fluctuation angle

Finally, in order to analyze the stability of the platform across the range of wave changes, the stability index of the platform was defined as the ratio of the overturning moment to restoring moment.

4.Conclusion

The results showed that with the increasing of the depth, the impact of wave's force and moment on the base of platform are reduced through exponential relationship. The amount of force and total moment are inclined to a fixed value. The reductions are due to the effective depth that is equal to half the wavelength; so that it reduces the amount of force and moment to a small amount. Based on the maximum amount of non-dimensional hydrodynamics force in the tripod platform, the maximum and the minimum amounts of free water level happen in the moments of t = T/2 and t = 0 and in the monopod platform, the maximum and the minimum amounts of free water level happen in the moments of t =T/4. Also, the maximum and the minimum values, in the force curve are attributed to waves whose half the wavelength is a multiplication of the distance between the bases of the platform. The results also suggest that the response of the rocking motion of gravity platform shows significant changes in relation to height and wavelength. Based on the curves fitted to the data of the fluctuation angle, sustainability of the platform in the rocking motion can be thoroughly and completely investigated. Regarding the regular waves, different analytical methods in the different structural conditions had good agreement with numerical data. So we can use the numerical methods for analyzing the structural response to irregular waves in dealing with gravity platform

5.References

[1] Dean, E. T. R., "Offshore Geotechnical Engineering", 1st edition, Thomas Telford Limited, 2010.

[2] Wilson, J. F., "Dynamics of Offshore Structures", John Wiley & Sons, 2003.

[3] McCormick, M. E., "Ocean Engineering Mechanics", Cambridge University Press, 2010.

[4] Mogridge, G. R., Jamieson, W. W., "Wave Forces on Large Circular Cylinders:A Design Method", Hydraulics Laboratory, National Research Council of Canada, Report MH-111, 1976.

[5] Stansberg, C. T., Baarholm, R., Fokk, T., Gudmestad, O. T., Haver, S., "Wave amplification and possible deck impact on gravity based structure in probability extreme crest heights", 23rd international conference on offshore mechanics and arctic engineering, 2004.

[6] Chacrabarti S.K.,"Hydrodynamics Of Offshore Structures ",(1994),Mechanics Publication.

[7] Barati M.," Numerical model diffraction waves around the base of calculation force of the waves offshore platforms ",(2002),Thesis of Tehran University.

AN ARTIFICIAL NEURAL NETWORK STRATEGY TO IMPROVE WIND SPEED HINDCASTING

Nabiallah Rashedi[1], Sarmad Ghader[2], S. Abbas Haghshenas[3]

1) Institute of Geophysics, University of Tehran, Tehran, Iran, Email: nabi.rashedi@ut.ac.ir
2) Institute of Geophysics, University of Tehran, Tehran, Iran, Email: sghader@ut.ac.ir
3) Institute of Geophysics, University of Tehran, Tehran, Iran, Email: sahaghshenas@ut.ac.ir

1. Introduction

The veracious forecasts of wind waves are of great importance in ocean and coastal engineering applications as well as in managing oceanic resources. Accurate predictions of wind waves with different lead times are necessary for a large scope of coastal and open ocean activities. Attempts to improve wave short-term forecasts based on artificial neural networks are reported by different researchers.

Due to the lack of wind wave measured data, predicted wind waves data are used to determine wave climate in many regions. Nowadays spectral wind waves model are the most practical tool for wave prediction. Since the outputs of these models generally contain some errors, their results should modify based on the measured data. In this study, a new approach based on the error prediction of simulated wind data at the observing stations and distributing the errors in the computational domain was implemented for updating of the model outputs. To do so, wind simulation of meteorological model (WRF) was carried out over the Persian Gulf and the results were compared with the measured data. In this study, artificial neural networks are used to find out the relationship between the output of the WRF and measured data.

2. Outline of artificial neural networks

Artificial neural network (ANN) method is applied to establish a proper correlation between the measured wind speed data and data obtained from the simulation model (WRF) in Persian Gulf. ANN is one of the most wellknown machine learning methods which is used for many different purposes. It is inspired by how our brain processes data through neurons. The basis of an artificial neural network is the concept of the neuron considered as a unit. The unit takes an argument formed as a sum of a weighted input and bias, and produces an output by means of some transfer (activation) function, which is typically the step or sigmoid function. There can be many inputweight products to form a unique argument of the transfer function in the j^{th} neuron, where j¼ 1; . . . ; R and R are the number of neurons in the hidden layer. Several such neurons can be combined into a layer, whereas a particular network can contain one or more interconnected layers of neurons. The pattern of these interconnections is called the architecture.

Non-linear activation functions (like the log sigmoid or the hyperbolic tangent sigmoid) for the hidden units are needed to make artificial neural networks capable of representing non-linear dependencies. For the output units, one should choose an activation function suited to the distribution of the target values.

The method of determining the weights and biases is called learning. The learning process requires a set of patterns ‘‘input–target output’’. During the learning process, the weights and biases of a network are iteratively adjusted to minimize the network performance function (the averaged squared error between the network outputs and the target outputs is the default one for the feedforward networks) making the entire network to perform in some expected way. The amount by which the weights change is the learning rate parameter. Each representation of a training set to a net is called an epoch.

3. Neural networks involved

The commonly used three-layer feed-forward networks with a non-linear differentiable log–sigmoid transfer function in the hidden layer and a linear transfer function in the output layer were employed in this study.

4. Data used

The wind data is adopted from the study performed by Ghader, et al. (2016). They applied WRF model to the whole Persian Gulf area and simulated the relevant wind field data. Figure l presents a time series data of wind speed at the observation point of Assaluyeh Port and the WRF out put data.

5. Summary

Applying the collected set of data and examining different combinations of wind speed as input data with the measured data as the target vector in Matlab neural network toolbox, it is tried to obtain a high correlation between WRF outputs and measured data. Therefore, by applying a neural network with 2 layers and 10 neurons per layer, an R value of 0.82 is obtained between modified simulation results and the observations. The training result for the applied network is presented in Figure 2. It seems that this method is of high efficiency in improving wind simulation results for being introduced to wave and hydrodynamic models.

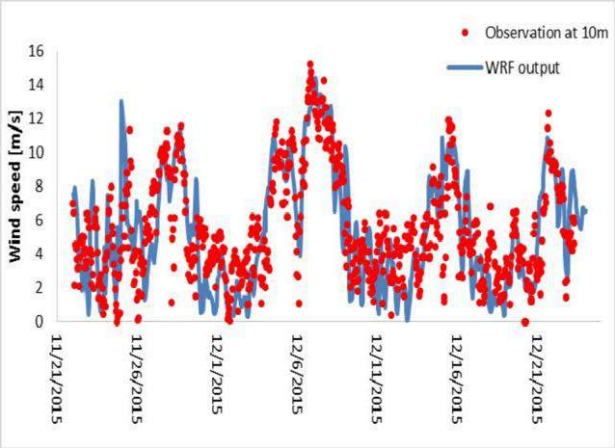

Figure 1: Wind speed output of WRF model at Assaluyeh Buoy location for the period of measurements

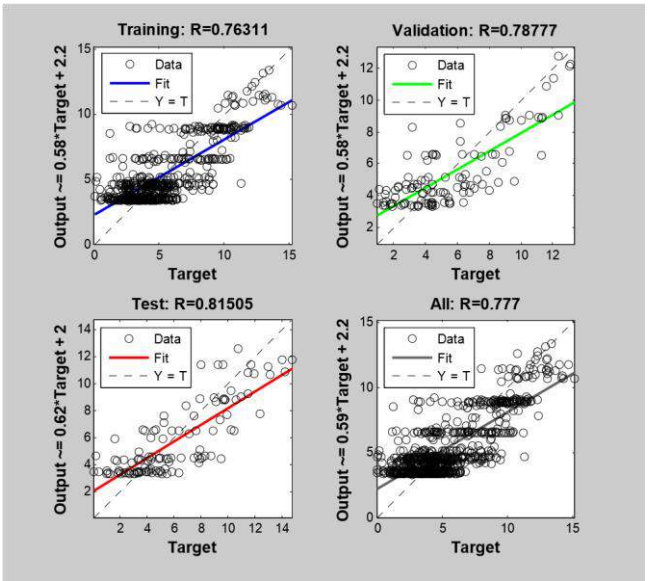

Figure 2. Training results of the applied neural network

6. References

[1] Agrawal JD, Deo MC, 2002: On-line wave prediction. Marine Structures 15 (1):57-74.

[2] Cheggaga, Nawal., 2013: New Neural Networks Strategy Used to Improve Wind Speed Forecasting, Wind Engineering, 37(4), 369-380.

[3] Demuth, Howard., 2002: Neural Network Toolbox, Networks, 24(1), 1-8.

[4] Makarynskyy O., 2004: Improving wave predictions with artificial neural networks, Ocean Engineering, 31(5-6), 709-724.

[5] Mandal, S. Rao, Subba Raju, D. H., 2005: Ocean wave parameters estimation using backpropagation neural networks, Marine Structures, 18(3), 301-318.

[6] Ghader, S., Yazigi, D., Soltanpur, M., Nemati, M. H. 2016: Wind field forecasting over the Persian Gulf using an ensemble system developed for WRF, *3rd International Conference on the Persian Gulf Oceanography*, Tehran, Iran.

AN EXPLORATORY ANALYSIS OF FACTORS AFFECTING SEDIMENT ERODIBILITY

Ebrahim Hamidian Jahromi[1], Farhang Ahmadi Givi [2], Lawrence P. Sanford[3], and S. Abbas Haghshenas [4]

1) Institute of Geophysics, University of Tehran, Tehran, Iran, Email: eb_hamidian@ut.ac.ir
2) Institute of Geophysics, University of Tehran, Tehran, Iran, Email: ahmadig@ut.ac.ir
3) Horn Point Laboratory, University of Maryland Center for Environmental Science, Cambridge, MD, Email: lsanford@umces.edu
4) Institute of Geophysics, University of Tehran, Tehran, Iran, Email: sahaghshenas@ut.ac.ir

1. Introduction

Erosion is one of the most significant coastal and estuarine processes which may lead drastic geomorphological changes, dispersing contaminants and fine grain material in to the water column and surrounding areas, and resultant probable habitat loss and environmental problems. The prediction of sediment erosion is an important issue while dealing with estuarine dynamics. The erosion resistance of sediments is characterized by introducing critical shear stress and erodibility. These two parameters, as the major sediment erosion properties, are dependent on many parameters which should be identified through an exploratory analysis of factors affecting sediment erodibility.

Although understanding of erosion especially in cohesive sediments is not thoroughly obtained, for gaining a better understanding of erosion and analysis of erodibility data, paying attention to some parameters affecting on erosion is inevitable; parameters such as: sediment grain size, clay content, organic content, tidal fluctuations, Atterberg limits, water content, plastic index, etc. Many researchers have tried to correlate sediment erodibility with these sediment properties, including Winterwerp et al. (2012), Jacobs et al. (2011), Van Prooijen and Winterwerp (2010), Winterwerp and van Kesteren (2004), and Parchure and Mehta (1985); however, the relations they have suggested for correlating sediment erodibility and other sediment properties are highly dependent on location and sediment origin. Hence, erosion like many other natural processes depends on many factors which makes it a complicated problem. This issue makes ordinary statistical methods less effective to interpret and analyze such data. Moreover, it is so probable that there would be a gap in our measured dataset which will influence on the statistical analysis results.

This study aims to propose a conceptual framework for analyzing erosion data of cohesive/non-cohesive/mixed sediment beds using soft computing techniques in order to 1) determine effective parameters and evaluating the level of effectiveness, and 2) establish a general framework to correlate physical parameters of the sediment to the erodibility parameter.

2. Case Study

As a case study, the erosion data set provide by Kimiaghalam *et al* (2014), encapsulated in Table 1, is adopted to find an appropriate correlation between critical shear stress and other sediment properties. According to Kimiaghalam *et al* (2014) several undisturbed natural soil samples were taken from different river banks in Manitoba, Canada. The samples mainly contained clay and silt with 24–94% clay content. For each sample 13 different physical, mechanical, and electrochemical properties were measured.

Artificial neural network (ANN) method is applied to establish a proper correlation between critical bed shear stress and a number of other sediment properties. ANN is one of the most well-known machine learning methods which is used for many different purposes. It is inspired by how our brain processes data through neurons. As the capability of each neuron for data process is so limited, it is so common to make various networks in order to cope with complicated problems. It goes without saying that in networks, the output of one neuron is the input for next neuron. It has been proved that parallel arrangement of neurons in a network increases process capability. Optimization, data training and finding the relationship between different parameters are some of the most important applications of artificial neural network.

As regular statistical regressions are not usually fitted on the majority of data points and ususally do not consider more than two variables in every try, such artificial intelligence methods are getting more and more popular in recent decades. Hence, applying the mentioned set of data and examining different combinations of sediment properties as input data with critical shear stress as the target vector in Matlab neural network toolbox, it is tried to perform as much run eventually led to a high correlation between critical shear stress and a selective set of other properties. Taking all the parameters except material dependent coefficient (k_d) in to account, and using a neural

network with 2 layers and 10 neurons per layer, eventually a high correlated set off variables were obtained after a couple of iterations with a R value of 0.98. The training result for the applied network is presented in Figure 1.

Table 1. Sediment sample characteristics and properties Kimiaghalam et al. (2015).

Sample ID	CEC (meq/100gr)	EC (ds/cm)	OM (%)	SAR	d50 (mm)	ρ dry (kg/m^3)	C (kN/m^2)	tan (ϕ)	W (%)	PI (%)	τ_c (pa)
Red 1	30.7	0.72	2.2	0.992	0.015	1312	9.5	0.597	39	29	9.38
Red 2	17.2	0.352	1	0.89	0.045	1415	2.37	0.731	29	12	0.98
Red 3	31.29	0.855	9	0.92	0.0056	1209	10.4	0.624	44	34	9.55
Red 4	30.28	0.888	6.6	1.16	0.0081	1133	1.16	0.743	54	40	1.72
2M (2-1)	23.6	0.446	1.1	1.071	0.002	1567	8.3	0.551	28	21	7.81
2M (2-2)	23.1	0.462	1	1.075	0.002	1542	11	0.435	34	24	10.25
8M (1-1)	29.2	0.406	1.4	1.621	0.0004	1419	8.5	0.551	35	27	4.85
M (2-1)	28.2	0.284	1.4	1.373	0.0011	1512	10	0.572	27	17	8.57
8M (2-2)	27.1	0.288	1.9	0.28	0.0013	1445	1.7	0.74	23	14	1.62
8M (3-1)	28.1	0.314	2.8	0.639	0.0015	1378	2	0.738	40	24	2.68
8M (3-2)	24.7	0.386	2.1	1.035	0.0017	1605	2.9	0.75	38	18	2.74
8M (6-1)	21.6	0.204	1.2	0.239	0.02	1843	2.4	0.897	17	13	1.6
8M (7-1)	26.3	0.206	1	0.358	0.0074	1747	1	0.869	22	5	0.31

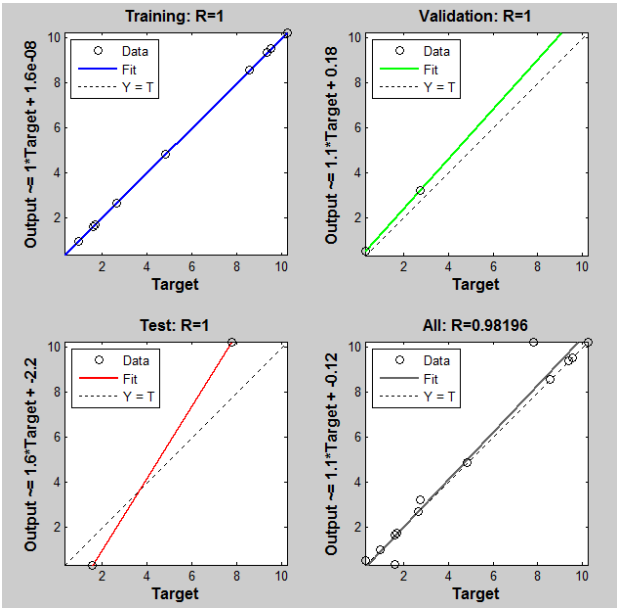

Figure 1. Training results of the applied neural network

3. Summary

Due to indisputable importance of erosion in estuaries and coastal areas, it is vital to have a good understanding of critical shear stress and erosion rate as two fundamental parameters to evaluate sediment erosion. As these two parameters are intensely affected by many other physical and chemical sediment properties, ANN or such other methods can be used as an effective tool to find out how much effective is every sediment property on these two. Although some researchers did their best to correlate erodibility with other sediment properties, just very few of these efforts really did work. In this study artificial neural network method was used for a set of sediment properties and unlike two variable common statistical regression, a high correlation among most of parameters was obtained. Hence, it seems that artificial intelligence methods are capable to be applied for analysis of parameters affecting sediment erodibility in marine and estuarine environments. Moreover, according to our trial and errors, it seems that Sodium Adsorption Ratio and Cohesion are more correspondent to the critical shear stress values.

4. References

Jacobs, W., P. Le Hir, W. G. M. Van Kesteren, and P. Cann (2011), Erosion threshold of sand-mud mixtures, Cont. Shelf Res., 31, 14–25, doi:10.1016/j.csr.2010.05.012.

Kimiaghalam, N., et al. An experimental study on the effects of physical, mechanical, and electrochemical properties of natural cohesive soils.... International Journal of Sediment Research (2015), http://dx.doi.org/10.1016/j.ijsrc.2015.01.001i

Parchure, T. M., and A. J. Mehta (1985), Erosion of soft cohesive sediment deposits, J. Hydraul. Eng., 111(10), 1308–1326, doi:10.1061/(ASCE) 0733-9429(1985)111:10(1308).

Van Prooijen, B. C., and J. C. Winterwerp (2010), A stochastic formulation for erosion of cohesive sediments, J. Geophys. Res., 115, C01005, doi:10.1029/2008JC005189.

Winterwerp, J. C., W. G. M. van Kesteren, B. van Prooijen, and W. Jacobs (2012), A conceptual framework for shear flow–induced erosion of soft cohesive sediment beds, J. Geophys. Res., 117, C10020, doi:10.1029/2012JC008072.

Winterwerp, J. C., and W. G. M. van Kesteren (2004), Introduction to the Physics of Cohesive Sediments in the Marine Environment, Dev. Sedimentol., vol. 56, Elsevier, New York.

NUMERICAL STUDY OF THE EFFECT OF CURRENT VELOCITY ON THE POWER PRODUCTION BY A HORIZONTAL AXIS MARINE CURRENT TURBINE AND FEASIBILITY OF USING IT IN THE STRAIT of HORMUZ

Amir Honaryar[1], Mahmoud Ghiasi[2]

1) Faculty of Marine Technology, Amirkabir University of Technology, Tehran, Iran, Yarehonar@aut.ac.ir
2) Faculty of Marine Technology, Amirkabir University of Technology, Tehran, Iran, Mghiasi@aut.ac.ir

1. Introduction

World energy consumption has increased by sixty percent for thirty years (1980-2010) and it reached to about 16000 GW in 2010[1]. According to increasing global population growth this demand will continue in the future. In the other hand, due to the rate of increase in pollutants and greenhouse gas emissions, the need for renewable energy has increased in the world. Considerable portion of this energy can be extracted from the sea. Marine renewable energy can be divided into several types, including wave energy, tidal energy, ocean thermal energy, ocean current energy and salinity gradient energy. The tidal energy is also divided to tidal potential energy and tidal kinetic energy.

Due to its special geographical position and climate conditions, there is a good potential for exploitation of marine renewable energy in Iran. This country has a marine boundary of about 2700 km in its southern and northern regions, including 1259 km with the Persian Gulf, 784 km with the Gulf of Oman, and 657 km with the Caspian Sea[2]. Thus the need for further research on marine renewable energy resources and their extraction sites in Iran has increased more than before.

2. Marine Current Turbine

Marine current power converters are divided into three main categories: 1) horizontal axis turbine, 2) vertical axis turbine and 3) oscillating hydrofoil. Horizontal axis marine current turbine is the most appropriate marine turbine which is used widely[3]. Figure 1 shows a horizontal axis marine current turbine which is brought to the surface for inspection. Predictability is one of the benefits of tidal current energy and also is one of the advantages of marine turbine to the wind turbine[4].

Figure 1. Horizontal axis marine current turbine [5].

3. Tidal Current Energy Potentials in Iran

According to its position, between the seas in Iran, the Persian Gulf is the best one for tidal current energy extraction. It has 1000 km long, 350 km wide and an average depth of 40 m[6]. As shown in Figure 2 the current speed exceeds 1 m/s in the Strait of Hormuz and in some areas it reaches to 2 m/s. Including appropriate areas in terms of tidal current speed, Qeshm, Hengam and Tonb-e Bozorg Islands and Bandarabbas can be noted. In these areas the current speed is between 1 to 1.5 m/s [2]. Among these, a region in Qeshm channel with the width of 2600 m and the maximum depth of 29 m that is shown in Figure 3 is very suitable for exploitation of tidal kinetic energy. The tidal water-level in this region varies between 3-3.5 m leading to a tidal current velocity of about 3 m/s[7].

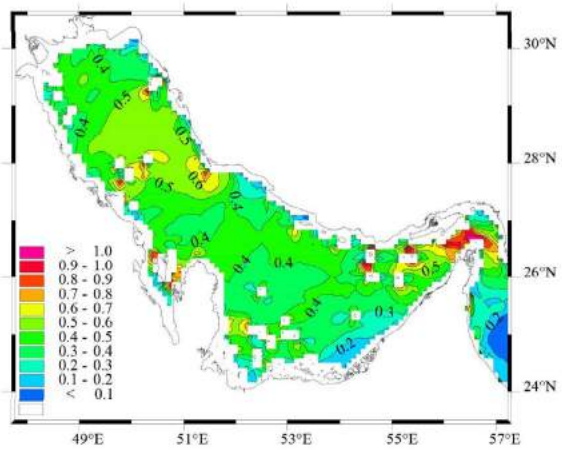

Figure 2. Tidal current velocity distribution in the Persian Gulf [6].

Figure 3. Qeshm channel in the Strait of Hormuz.

4. Numerical Analysis

Among the factors contributing to efficiency of marine current turbine can be noted in the current velocity, current angle of attack and geometry of turbine blades. In this paper the effect of current velocity on the power production by a horizontal axis marine current turbine has studied numerically.

4.1. Governing Equations

To study the efficiency of marine current turbine, it is necessary to obtain hydrodynamic torque which yields power produced by turbine. This torque can be calculated by velocity and pressure distribution. To obtain velocity and pressure distribution, governing equations for fluid flow i.e. mass conservation and Navier-Stokes equations are solved. By applying RANS method, theses equations can be written as follows:

$$\frac{\partial \rho}{\partial t} + \frac{\partial}{\partial x_i}\left(\rho U_i\right) = 0 \quad (1)$$

$$\frac{\partial \rho U_j}{Dt} + \frac{\partial}{\partial x_i}\left(\rho U_j U_i\right) = -\frac{\partial p}{\partial x_j} + \frac{\partial}{\partial x_i}\left(\tau_{ji} - \rho u_j u_i\right) + S_M \quad (2)$$

where p is pressure and U is velocity vector.

4.2. Geometric modeling

Designed blade geometry with cross section of NACA63$_I$-424 and the radius of 9 m is shown in Figure 4.

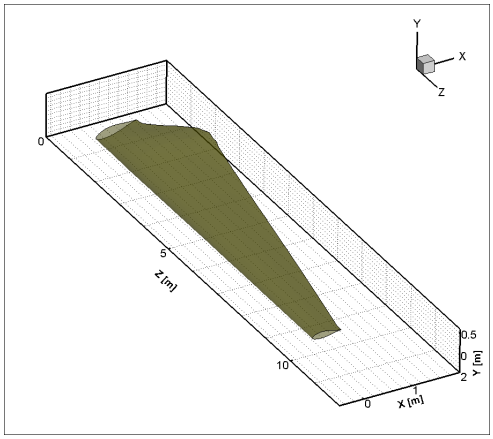

Figure 4. Designed turbine blade geometry.

4.3. Numerical method

According to computational fluid dynamic (CFD), an element based finite volume code is used to solve RANS equations. Among turbulence models, (SST) $k-\omega$ has selected. Where k and ω are turbulence kinetic energy and dissipation rate in transport equations respectively.

5. Results and Discussions

Finally by solving RANS equations, the pressure and velocity fields have obtained numerically. Figure 5 shows the pressure distribution on the turbine blade and also the nods and element shape on it.

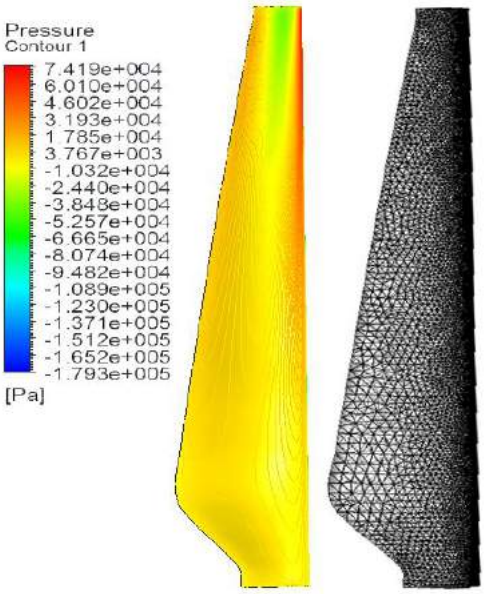

Figure 5. Pressure field and the elements on the Blade.

In this paper, the feasibility of extracting tidal current energy in Iran has investigated and Qeshm channel as a good place to install horizontal marine current turbine has introduced. In addition, effect of current velocity on power produced by turbine has numerically studied. Finally it has been concluded that by installing this turbine in Qeshm channel can produced 500 W. Thus with the installation of 10 systems, which has two turbines, can be produced 10 MW.

6. References

[1] F. Zabihian and A. S. Fung, "Review of marine renewable energies : Case study of Iran," *Renew. Sustain. Energy Rev.*, vol. 15, no. 5, pp. 2461–2474, 2011.

[2] G. of Authors, "RED SEA AND THE PERSIAN," *National geospatial-intelligence agency*, vol. 172, 2014.

[3] R. Noruzi, M. Vahidzadeh, and A. Riasi, "Design , analysis and predicting hydrokinetic performance of a horizontal marine current axial turbine by consideration of turbine installation depth," *Ocean Eng.*, vol. 108, pp. 789–798, 2015.

[4] F. Sculiller, T. Tang, Z. Zhou, M. Benbouzid, and J. Fre, "A review of energy storage technologies for marine current energy systems," *Renew. Sustain. Energy Rev.*, vol. 18, pp. 390–400, 2013.

[5] Y. Li, "On the definition of the power coefficient of tidal current turbines and efficiency of tidal current turbine farms," *Renew. Energy*, vol. 68, pp. 868–875, 2014.

[6] S. Pous, X. Carton, and P. Lazure, "A process study of the tidal circulation in the Persian Gulf," *Open J. Mar. Sci.*, vol. 2, no. October, pp. 131–140, 2012.

[7] K. Soleimani, M. J. Ketabdare, and F. Khorasani, "Feasibility study on tidal and wave energy conversion in Iranian seas," *Sustain. ENERGY Technol. ASSESSMENTS*, vol. 11, pp. 77–86, 2015.

ON THE TIME-VARIABILITY OF ADDED MASS AND DAMPING OF A FLAP TYPE WAVE ENERGY CONVERTER

Saghy Saeidtehrani[1], Giorgio Bellotti[1], Leopoldo Franco[1], Pedro Lomonaco[2]

1)Dipartimento di Ingegneria, Università degli Studi Roma Tre, Rome, Italy,
Email: saeidtes@oregonstate.edu
2)Dipartimento di Ingegneria, Università degli Studi Roma Tre, Rome, Italy,
Email: giorgio.bellotti@uniroma3.it
3)Dipartimento di Ingegneria, Università degli Studi Roma Tre, Rome, Italy,
Email: leopoldo.franco@uniroma3.it
4) O.H. Hinsdale Wave Research Laboratory, Oregon State University, Corvallis, Oregon, United States
Email: Pedro.Lomonaco@oregonstate.edu

1. Introduction

Almost most of mathematical models of fluid-body interaction represent the radiation effect as two frequency dependent components proportional to acceleration and velocity. This approach originally comes from strip theory of ship motions [1]. Mathematical models for simulating body motion also suggest to include another damping term proportional to a higher power of velocity [2], for fluid-body interaction, it could compensate the nonlinearities and viscous effects [3]. In this paper, radiation damping, added mass and the quadratic damping coefficient are extracted from the free decay experimental results. Different approaches have been used for extracting these parameters, based on the stages of time dependency. The parameters are used to investigate the ability and applicability of the above-mentioned models for simulation of a flap type wave energy converter, patented by [4]. The numerical results will be compared with the experimental measurements. It will be shown that due to the rapid motions of this device and the interactions between flaps in an array, considering constant damping and added mass could not effectively model the motion of this type of wave energy converter.

2. Theory and mathematical background

This section briefly presents the important theoretical background and the simplifications for the simulation of fluid- body interaction. To make a clear picture of the object, first the physical model is explained.

The experimental tests were carried out in a flume at the laboratory of Roma Tre University. The flume is 9 m long, 0.27 m wide, and 0.3 m deep. A 1:40 Froude scaled model of the device was build which comprises of five flaps hinged to the breakwater [4] (see Figure 1).

The general equation of motion for a free decay oscillation of a floating body could be expressed as [3, 5]:

$$M\ddot{X} + KX = F_{Rad} + F_V \quad (1)$$

X, $\dot{X}$, and $\ddot{X}$ are displacement, velocity and acceleration vectors with the number of rows equal to the degree of freedom.

M and K are mass and stiffness matrixes, respectively,

F_{Rad} is the radiation force

F_V is the force simulating the viscous effects,

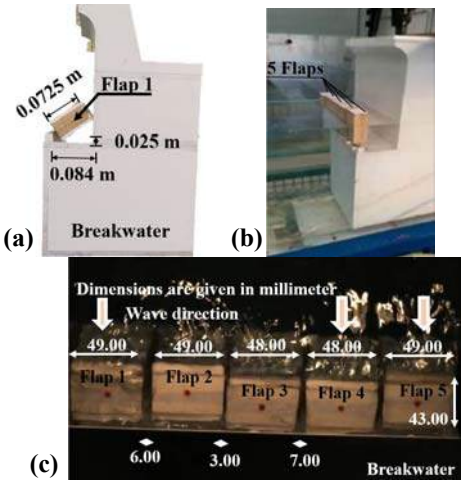

Figure 1. Geometry of the wave energy device (a) Cross section, (b) Side view, (c) Top view

Radiation force is representing the fluid pushed away by the body movement, it can be mathematically modeled by considering two components proportional to acceleration and velocity of the structure:

$$F_{Rad} = -(m\ddot{X} + C\dot{X}) \quad (2)$$

Where

m is the added mass

C is the radiation damping

F_V adds the nonlinear term to the equation. It could be simulated as a quadratic damping force [3, 6, 7]:

$$F_V = -\frac{1}{2}\rho C_D A_D \dot{X}\left|\dot{X}\right| \quad (3)$$

Where

C_D is the drag coefficient,

A_D projected area normal to motion/flow direction,

ρ is the water density

Since the flaps are rigid, and hinged to the breakwater, the equation of motion could be solved for one degree of freedom, i.e. pitch motion of the flap. Therefore, the mass matrix and stiffness which are used for the equation; are moment of inertia, and pitch hydrostatic stiffness, respectively. Equation (1) could be rewritten in the following forms to represent the linear and nonlinear models.

$$(M+m)\ddot{X} + C\dot{X} + KX = 0 \quad (4)$$

$$(M+m)\ddot{X} + C\dot{X} + \frac{1}{2}\rho C_D A_D \left|\dot{X}\right|\dot{X} + KX = 0 \quad (5)$$

In this paper, m, C, and C_D are extracted from the time series responses by assuming both linear and nonlinear model. Two main approaches for extracting the coefficients are used: in the first approach, different time series' windows are selected. It is assumed that the coefficients are constant in each window. The windows have different lengths: time step, period of the response, and finally the whole time series. These approaches hereafter will be called A11, A12, A13, for the abovementioned windows.

The second approach (A2) takes advantage from the perpendicularity of the signals of velocity and acceleration. As a result, it is acceptable to consider that the acceleration is zero in the maximum of velocity and vice versa. Therefore, in this approach, first the negative and positive maximums in acceleration are identified, then the corresponding parameter is calculated. For example, in the maximums of acceleration, we only have one component which is acceleration dependent. Therefore, added mass could be calculated by equation (6).

$$m = \frac{M\ddot{X} + KX}{\ddot{X}} \qquad t = t_{\ddot{X}_{Max}} \quad (6)$$

Some of the results are presented in the following figures.

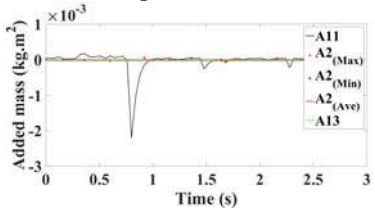

Figure 2 Linear model coefficients

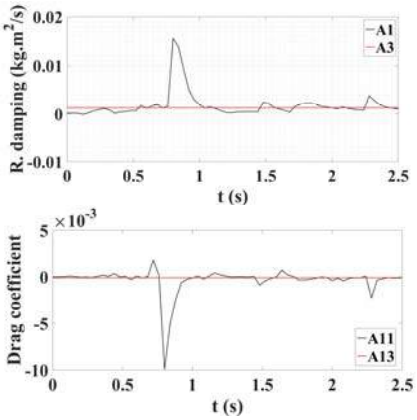

Figure 3 Nonlinear model coefficients

Complete set of results and the detailed explanation will be provided in final paper.

3. Numerical simulation

This section presents the numerical results for linear and nonlinear models by using the extracted coefficients. It will be followed by the comparison of numerical results with the experimental tests.

Figure 4 shows the Comparison between results of both numerical models with constant coefficients and experimental measurements.

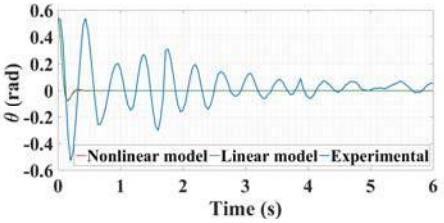

Figure 4 Time series response

It could be seen that the constant parameters cause the response to vanish in the first cycle.

Adding nonlinear term doesn't make a lot differences in the model.

4. Conclusion

The results show that for this type of wave energy converter, which has rapid motions in time, and is supposed to work in an array, the estimation of added mass ,radiation damping and drag coefficient as a constant value cause remarkable change in both period and pattern of the response.

5. References

[1] Ogilvie, T.F. , Tuck , E.O "A rational strip theory of ship motions: part I" , Department of naval architecture and marine engineering, college of engineering, The University of Michigan, Ann Arbor, Michigan, 1969.

[2] Rayleigh JWS， "The theory of sound", Section 68a, 2nd revised edn. Mineola, NY: Dover Publications Inc, . 1945

[3] Babarit, A., Hals, J. , Muliawan, M.J., Kurniawan, A. , Moan, T. , and Krokstad, J., "Numerical Benchmarking Study of a Selection of Wave Energy Converters". Renewable Energy, 41:44–63, 2012

[4] Sammarco, P., Simone michele, S., D'errico, M., " syncres: wave energy converter", Universita degli Studi di Roma Tor Vergata, Italy, 2015

[5] Mei, C.C., Stiassnie, M. & Yue, D.K.-P. Theory and applications of ocean surface waves, World Scientific, USA, 2005.

[6] Environmental Conditions and Environmental Loads, DNV-RP-C205, 2007.

[7] Modelling and Analysis of Marine Operations, DNV-RP-H103, 2014.

ASSESSMENT OF TIDAL STREAM ENERGY RESOURCES IN THE PERSIAN GULF

Sadegh Yari[1], Maziar Khosravi[2]

1) Iranian National Institute for Oceanography and Atmospheric Science, Tehran, Iran, syari@inio.ac.ir
2) Iranian National Institute for Oceanography and Atmospheric Science, Tehran, Iran, mazyar.khosravi@inio.ac.ir

Abstract

Tidal stream systems make use of the kinetic energy of tidal movement to power turbines, in a similar manner to the way in which windmills extract energy from the wind. The predictability of tides makes it a reliable energy resource. Energy extraction using tidal current energy technologies offers a vast and predictable energy resource. This paper reviews the tidal current energy resource assessment for the Persian Gulf. In this study the potential energy of tidal stream in the various sites of the Persian Gulf is evaluated. Currents are measured in different locations in the Persian Gulf. A series on analysis are applied to the measurements to estimate the potential energy and extractable electrical energy. The assessment of tidal stream energy in few locations of the Persian Gulf is presented in this abstract.

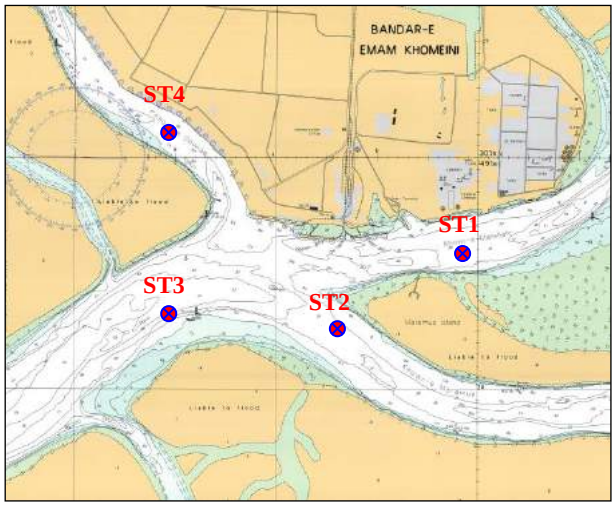

Figure 1. Khur e Musa area and current measurement stations

The characteristics of the currents are investigated applying a sort of analysis. A set of current measurements are carried out in Khur e Musa in the framework of sediment transport study (1996) by PMO. The measurements in the Khur e Musa show a high velocity up to 1.95 m/s (Fig. 2).

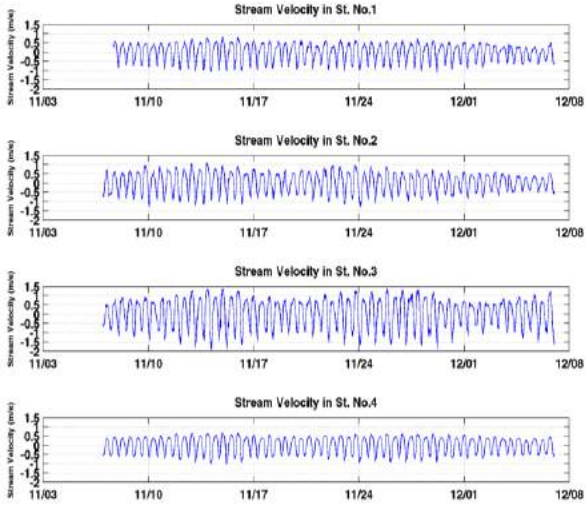

Figure 2. tidal stream in 4 stations in Khur e Musa

Velocity distribution is calculated to show the availability of appropriate currents to extract the energy (Fig. 2).

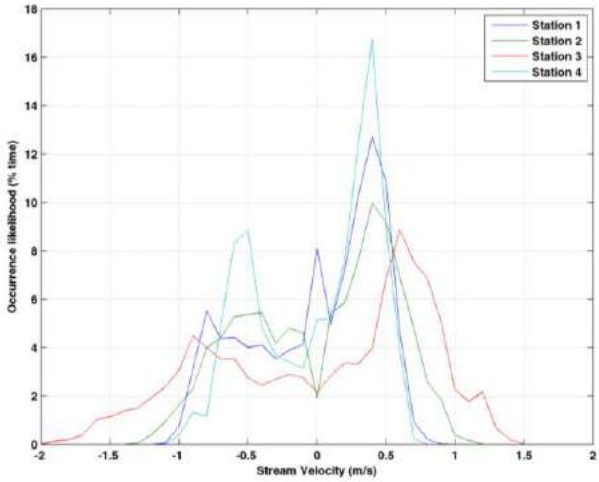

Figure 2. Velocity distribution of tidal stream in 4 stations in Khur e Musa

The contribution of different components of measured current such as tidal part and background currents are calculated using spectral analysis (Fig 3.). The results show that a strong tidal current system is governed in the area as it has channel shape geometry.

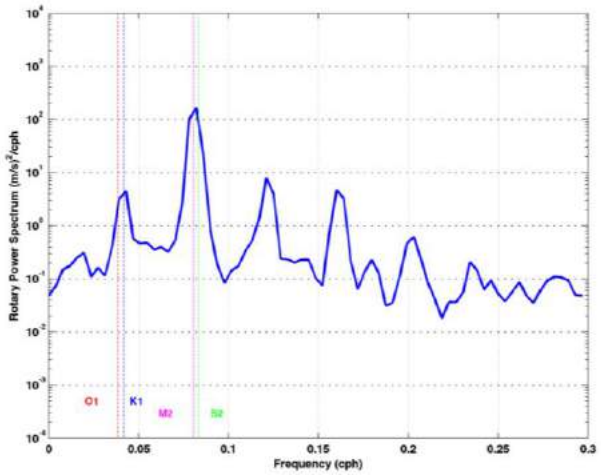

Figure 1. Spectral analysis of tidal stream in station3 in Khur e Musa

A harmonic analysis is applied to calculate the harmonic constituents of tidal currents. Long-term (annual) tidal currents are predicted using harmonic constituents to evaluate annual potential energy. The correlation of the predicted currents with measured ones is examined.

The average power density (APD) of the annual predicted currents is calculated to estimate the potential energy using:

$$APD = \frac{1}{2}.\rho.A.\sum_{i=1}^{N}\left(U_i^3.f(U_i)\right) \qquad Wm^{-2}$$

U is stream velocity (ms^{-1}), ρ is seawater density (kgm^{-3}), A is turbine area (m^2) and $f(U)$ is velocity distribution.

The current observations in other sites are analyzed in a similar manner. The results improve the potential sites for the extractable energy. For instance, the results of the energy calculation in the Khuran Strait shows a potential energy of 248 KWm^{-2}.

References

- Foreman, M.G.G., 1978. Manual for Tidal Currents Analysis and Predition. Pacific Marine Science Report 78-6, Institute of Ocean Sciences, Patricia Bay, Sidney, B.C., 57 pp. (2004 revision(.
- R. Pawlowicz, B. Beardsley, and S. Lentz, "Classical tidal harmonic analysis including error estimates in MATLAB using T_TIDE", Computers and Geosciences 28 (2002), 929-937.
- Xia, J.Q.; Falconer, R.A.; Lin, B.L. Impact of different tidal power projects on the hydrodynamic processes in the Severn Estuary. Ocean Model. 2010, 32, 86–104.
- Gorban', A.N., Gorlov, A.M. and Silantyev, V.M. 2001. Limits of the Turbine Efficiency for Free Fluid Flow. Journal of Energy Resources Technology 123(4), p. 311.
- EMEC (The European Marine Energy Centre Ltd), 2009. Assessment of Tidal Energy Resource, ISBN 978-0-580-65642-2.
- Physical oceanography group, university of Malaga, 2012. Assessment of tidal energy resource in the strait of Gibraltar. Technical report of the project: Energy flux maps in the Strait of Gibraltar as potential source of renewable energies based on marine currents (FLEGER).

FLEXIBLE SEA FLOOR CARPET WAVE ENERGY CONVERTOR AND ITS PERFORMANCE IN PERSIAN GULF

Aref Hossein Moalemi[1] Mohamad Javad Ketabdari[2]
1) BSc student, Amirkabir University, of Technology, Tehran, Iran, rfmoalemi@aut.ac.ir
2) Associate Professor, Amirkabir University of Technology, Tehran, Iran, ketabdar@aut.ac.ir

1. Introduction

Gade, 1958 reports a place in the Gulf of Mexico known to locals as mud hole [1] where accretion of mud banks is considerable during storms (Figure 1),. Within the mud hole the interaction of surface waves with the mud is very strong such that waves completely damped out within a few wavelengths [2]. Observations of strong wave damping due to the coupling with the bottom mud are not limited to the gulf, but almost anywhere with a muddy seafloor. Inspired by the natural phenomenon of strong attenuation of oceanic surface waves by muddy seafloors, a mud-resembling synthetic compliant seabed carpet known as Wave Carpet, was proposed composed of linear springs and generators that can be used as an efficient wave energy conversion device. The presented wave energy conversion device is completely under the water surface. The carpet is survivable against high momentum of storm surges and in fact can perform even better under very energetic (e.g. stormy) sea conditions, when most existing wave energy devices are needed to shelter themselves by going into an idle mode. The proposed idea and its variations may also be used to create localized safe havens for fishermen and sailors in open seas, or if implemented in large scales to protect shores and harbors against strong storm waves.

Figure 1: Surface waves attenuation by a small strip of muddy seabed (darker part of the sea from center to the right)

2. Sea Waves condition in Persian Gulf

The stored energy in the waves has a direct relationship with the wave height. As indicated in Figure 2, shows the waves height in Persian Gulf and Oman Sea Areas. Based on this figure close to the coastline of Iran the waves are higher than other points.

Furthermore the west regions of the Persian Gulf up to the Gheshm Island and particularly Hormoz Channel with wave height of 4.5-5 m, up to 5 km of the shore are suitable regions for installing wave energy convertors [3]. In this region ship traffic is too high and surface wave energy convertors witch usually need widespread area to generate desired electrical energy. For this reason cannot be used. Nevertheless the use of submerged wave energy convertors in this area is a suitable option. It should be noted that depth of water over 10 km of the shore in Persian Gulf is not larger than 10 m. This is the reason that most parts are not suitable for installing usual heaving deep water wave energy convertors. Therefore it is needed to use a kind of convertor in Persian Gulf that can have good performance in shallow water and small amplitudes of the waves.

Advantages of the wave carpet can be expressed as follows:

- Wave Carpet is more efficient in shallow waters.
- It is an Omni-directional device.
- it is completely under the water surface hence imposes minimal danger to ships and the sea life (no mammal entanglement), and also causes no visual pollution,
- Its variations may also be used to create localized safe havens for fisher- men and sailors in open seas, or if implemented in large scales to protect shores and harbors against strong storm waves.

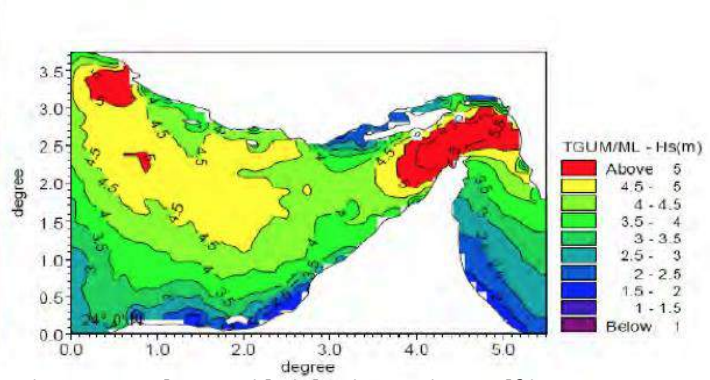

Figure 2. Peak waves' heights in Persian Gulf in 100-year period

3. Stored Energy Estimation in Wave Carpet

The fluid assumed to be homogeneous inviscid incompressible with irrotational motion. The bottom at the mean depth z = -h is regarded as viscoelastic, the surface and bottom elevations are η_s and η_b (Figure 3) and surface tension is neglected [4].

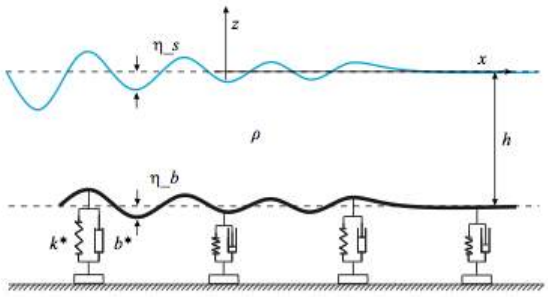

Figure 3. Schematic of a synthetic viscoelastic carpet on the seafloor

The energy stored in the carpet per unit area for an undamped system is described as

$$E_{tot} = E_{kin} + E_{pot} = \frac{1}{2}\rho g a_s^2 D \qquad (1)$$

and the dimensionless constant D

$$D = \frac{sinh2kh}{2}\left(\frac{\omega^2}{gk} + \frac{gk}{\omega^2}\right) - 2sinh^2(kh) + \frac{a_s^2 - a_b^2}{a_s^2} + \frac{k^* a_b^2}{2\rho g a_s^2}$$

$$E_{tot} = \frac{1}{2}\rho g a_s^2 \left\{\frac{sinh2kh}{2}\left(\frac{\omega^2}{gk} + \frac{gk}{\omega^2}\right) - 2sinh^2(kh) + \rho g(a_s^2 - a_b^2) + k^* a_b^2\right\} \qquad (2)$$

The solution of the dispersion relation in dimensionless form (3) gains an imaginary part of dimensionless frequency $\Omega = \Omega_r + i\Omega_i$ if damping is presented.

$$\gamma\Omega^4 \tanh(\mu) + i\mu\gamma\zeta\Omega^3 - \mu\Omega^2 - i\mu^2\gamma\zeta\Omega \tanh(\mu) + \mu^2(1-\gamma)\tanh(\mu) = 0 \quad (3)$$

With a_s, a_b are surface and the bottom amplitudes and respectively, Ω, ζ and γ are the dimensionless frequency, damping ratio and restoring force ($\omega\sqrt{g/h}$), ($\frac{b^*}{\rho\sqrt{g/h}}$) and ($\frac{\rho g}{k^*}$) respectively. $\mu = kh$ is the shallowness parameter.

Considering $a_S(t) = a_{S0}\, e^{\omega i t}$ the energy in of dimensionless form is then written as

$$\epsilon = \frac{E}{E_0} = \frac{1}{2} e^{2\Omega_i \tau} D_d \qquad (4)$$

The dimensionless constant D is then written as D_d

$$D_d = \frac{1}{2}\left(\frac{\sinh(2\mu)}{2}\left(\frac{\Omega_r^2}{\mu} + \frac{\mu}{\Omega_r^2}\right) - 2\sinh(\mu)^2\right) + \frac{1-\alpha}{\alpha} + \frac{2\alpha}{\gamma} \qquad (5)$$

where Ω_r is the real part of the dimensionless Ω. The dimensionless amplitude ratio of bottom to surface is:

$$\alpha = \frac{a_s^2}{a_b^2} = cosh^2\left(1 - \frac{\mu tanh\mu}{\Omega^2}\right) \qquad (6)$$

with $E_0 = 1/2\rho g a_s^2$ and $\tau = t\sqrt{\frac{g}{h}}$

The stored energy in Carpet for one period of time is then:

$$E_c = \frac{1}{2}\rho g a_s^2\, \epsilon A_c \qquad (7)$$

where A_c represents the carpet area.

4. Device performance in Persian Gulf

By using equation 7, and assuming average waves in Persian Gulf with H=1-1.5 m and T=4s (λ=86 m), the peak of the stored energy in Carpet for one period of time in southern Iranian coastal region is estimated between 16.46 and 23.73 kW/m. To go far from the beach stronger waves may occur. However the transfer cost will affect the efficiency of the system.

References

[1] Gade, H. G., "Effects of a non-rigid, impermeable bottom on plane surface waves in shallow water". *Journal of Marine Research, 1958.* **16**, pp. 61–82.

[2] Elgar, S., and Raubenheimer, B., "Wave dissipation by muddy seafloors". *Geophysical Research Letters, 2008.* **35**(7), Apr., p. L07611.

[3] Jawad Faiz, M. Ebrahimi-salari.'' Wave Power Resource in Iran for Electrical Power Generation'' World Renewable Energy Congress 2011-sweden

[4] Alam, M.-R., Marcus Lehmann., Ryan Elandt, Mostafa Shakeri,'' The Wave Carpet: Development of a Submerged Pressure Differential Wave Energy Converter'', 30th Symposium on Naval Hydrodynamics Hobart, Tasmania, Australia, 2-7 November 2014

[5] Macpherson, H., and Kurup, P. G., "Wave damping at the Kerala mud banks, southwest India". *Indian J. of Mar. Sci., 1981.* **10**, pp. 154–160.

NUMERICAL SIMULATION OF FULLY NON-LINEAR IRREGULAR WAVE BY FLAP TYPE WAVE MAKER

Saadati-Nasab .Mehran[1], Passandideh-Fard. Mohammad[2] and Anbarsooz. Morteza[3]

1) Mechanical Engineering, Ferdowsi of Mashhad, Mashhad, Iran, saadati.mehran@gmail.com
2) Mechanical Engineering, Ferdowsi of Mashhad, Mashhad, Iran, mpfard@um.ac.ir
3) Mechanical Engineering, Advanced Technologies Engineering, Quchan, Iran, m.anbarsooz@gmail.com

1. Introduction

Sea waves are usually irregular and of random nature. Therefore, no two waves are of the same wave height and period and move at different speeds. Investigating the effect of sea waves on offshore structures as well as absorbing energy from sea waves requires a thorough recognition of the waves and their features. Using numerical wave substrates being developed over the last two decades is an effective technique to simulate waves in different situations.

For the first time Havelock (1929) [1] and Hieu (1976) [2] assuming the non-viscous flow through using linear wave theory provided an analytical solution for flap and piston wave generators. However, Ursell (1960) [3], after conducting numerous experiments and examining waves with different sharpness, showed that the height of the waves generated by the piston wave generator is 10 percent less than the values obtained from analytical solutions based on the linear theory. Inability of analytical solutions for modeling waves in solid objects led high-order numerical models be presented based on the stream function wave theory to simulate the waves.

In one of the leading research studies conducted in 2008, Lee and Elanggovan [4] modeled linear regular waves by finite volume method. In 2015, Finnegan and Goggins [5], using the same method and Fast Fourier transformation, modeled linear irregular waves.

All afore-mentioned research studies used linear boundary conditions and problems are solved in a nonlinear form. Especially, in cases considering the wave contact with moving objects and absorbing their energy and when the drag force acting on the object cannot be ignored, linear boundary conditions will reduce the accuracy for the free surface. Thus, using non-linear theories to simulate waves and to track the free surface of the liquid is inevitable.

For the first time in 1965, Harlow and Welch [6] introduced marker and cell (MAC) method for free surface flows. In 1970, Chan and Street [7] improved this method at the Stanford University Modified Marker and Cell SUMMAC.

In 2005, Suea et al. [8], through solving the Navier-Stokes equations and boundary conditions by volume of fluid method, investigated the impact of non-linear waves on cubic structures submerged in the water.

For the actual mechanism of generating waves, height and wavelength are a function of range and course of the wave-generator motion as well as water depth. To this end, the linear wave-generating theory proposed by Dean and Darimpel [9] in 1984 and second-order wave-generating theory proposed by Madson [10] in 1971 were employed.

Accordingly, the development of a numerical model by assuming the viscous flow which models the actual conditions of the wave-generator seems necessary. In this study, Anbarsooz et al. numerical model [11] is used to model the real conditions of irregular nonlinear waves are produced flap wave generator.

2. The Governing Equations and Boundary Conditions

The schematic of the wave generation by flap type wave generator is shown in Figure 1.

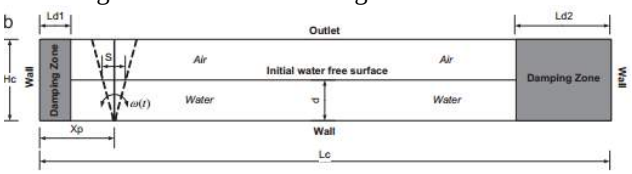

Figure 1. The area of the numerical solution and the boundary conditions

The equation governing the fluid flow is the Navier-Stokes' equation is two-dimensional with laminar, incompressible, and Newtonic flow:

$$\nabla.\vec{V} = 0 \tag{1}$$

$$\frac{\partial \vec{V}}{\partial t} + \vec{V}.\nabla\vec{V} = -\frac{1}{\rho}\nabla P + \frac{1}{\rho}\nabla.\vec{\tau} + \vec{g} + \frac{1}{\rho}\vec{F}_b \tag{2}$$

$$\vec{\tau} = \mu\left[(\nabla\vec{V}) + (\nabla\vec{V})^T\right] \tag{3}$$

Where, $\vec{V}$ is the velocity vector, ρ density, μ the dynamic viscosity, p the pressure, $\vec{\tau}$ stress tensor and $\overrightarrow{F_b}$ external forces applied on the fluid. To track the free surface of fluid, the volume of fluid method is used and defined as follows:

$$F = \begin{bmatrix} 0 & \text{in the gas phase} \\ 0 <, < 1 & \text{in the liquid} - \text{gas interface} \\ 1 & \text{in the liquid phase} \end{bmatrix} \tag{4}$$

In this method, the solid in the solution is specified by using the scalar quantity below:

$$\emptyset = \begin{bmatrix} 0 & \text{Out of the solid} \\ 0 <, < 1 & \text{Solid boundary} \\ 1 & \text{within the solid} \end{bmatrix} \quad (5)$$

3. Numerical Solution Method

To discretize the governing equations, the three-stage analysis method is used for the equations of continuity and momentum proposed in 2012 Mirzaii and Passandideh-Fard [12]. This method can be used for the Euler's constant networking in the simulation of free surface flows with surface tension. The momentum equation (2) is rewritten as follows.

$$\frac{\vec{V}^{n+1} - \vec{V}^{n}}{\Delta t} = -\left(\vec{V}.\vec{\nabla}\vec{V}\right)^{n} - \frac{1}{\rho^{n}}\nabla p^{n+1} + \frac{1}{\rho^{n}}\vec{\nabla}.\vec{\tau} + \vec{g}^{n} + \frac{1}{\rho^{n}}\vec{F}_{b}^{n} \quad (6)$$

4. Results

In this section, the capabilities of the method presented in this study to model non-linear irregular waves through comparing the numerical results with experimental and numerical results obtained by other researchers are discussed.

According to what mentioned earlier, in order to generate the wave in the developed context of numerical wave, the height and the courses of wave-generating movement are only required and other parameters and related phenomena are obtained by solving the Navier-Stokes equation. To this end, using Fast Fourier transformation method, harmonic waves of the experimental and numerical wave proposed by Liang et al. [13]. This numerical wave possesses 20 harmonics and 10 of its main harmonics are used for numerical modeling.

The periodicity of flap type wave-generating motion is equivalent to the periodicity of the harmonic waves and its motion course is calculated by using the following equation:

$$\theta(t) = \frac{\Delta\theta}{2}\cos\left(\frac{2\pi}{T}t\right) \quad (7)$$

$$S = 2d \times \tan\left(\frac{\Delta\theta}{2}\right) \quad (8)$$

To avoid sudden wave-generating movement at the beginning of the resolution and sharp waves, the ramp function is used for the first second. Figure 2 shows the process of forming waves by flap type wave generator. Figure 3 shows the changes in water level or the length of the waves generated in 2 m distance from wave generator. As it can be seen, the results of the model presented in this study are pretty much consistent with experimental and analytical results extracted from the study conducted by Liang et al. [19]. Accuracy of the results has provided conditions for investigating different waves with various H/L ratios and different sharpness and provides the opportunity for modeling solid objects and investigating the interaction of waves with these objects.

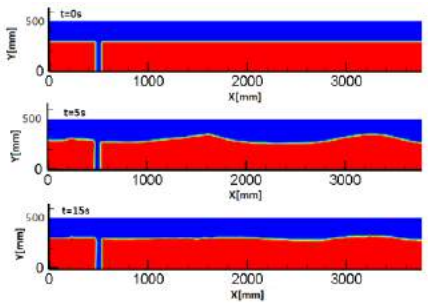

Figure 2. Latitude changes and periodicity of irregular wave generated by the finned wave-generator

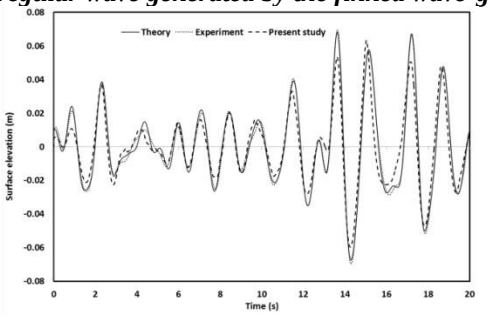

Figure 3. Changes in the water level at x = 2 m

5. References

[1] Havelock, T.H., 1929. Forced Surface Wave on Water. Philos. Mag. 8 (7), 569–576.

[2] Hieu, P.D., Tanimoto, K., 2006. Verification of a VOF-based two-phase flow model for wave breaking and wave-structure interactions. Ocean Eng. 33 (11–12), 1565–1588.

[3] Ursell, F., Dean, R.G., Yu, Y.S., 1960. Forced small-amplitude water waves: A comparison of theory and experiment. J. Fluid Mech. 7, 32–53.

[4] Lai, A., M., Elanggovan, CFD Simulation and Validation of Flap Type Wave Maker, International Journal of Mathematical, Computational, Physical, Electrical and Computer Engineering Vol:2, No:10, 2008

[5] Finnegan, W., Goggins, J., 2015. Linear irregular wave generation in a numerical wave tank. Applied Ocean Research 52 (2015) 188–200

[6] Harlow, F.H., Welch, J.E., 1965. Numerical calculation of time-dependent viscous incompressible flow of fluid with free surface. Phys. Fluids 8, 2182–2189

[7] Chan, R.K.C., Street, R.L., 1970. A computer study of finite-amplitude water waves. J. Comput. Phys. 6 (1), 68–94.

[8] Suea, Y.C., Chernb, M.J., Hwanga, R.R., 2005. Interaction of nonlinear progressive viscous waves with a submerged obstacle. Ocean Eng. 32, 893–923

[9] Dean, R.G., Dalrymple, R.A., 1984. Water Wave Mechanics for Engineers and Scientists. World Scientific Publishing Co. Re. ttd., Singapore

[10] Madsen, O.S., 1971. On the Generation of Long Waves. J. Geophys. Res. 76, 8672–8683

[11] Anbarsooz.M., Passandideh-Fard.M., Moghiman.M., Numerical simulation of a submerged cylindrical wave energy converter, Renewable Energy 64 (2014) 132–143.

[12] Mirzaii I, Passandideh-Fard M. Modeling free surfaceflows in presence of an arbitrary moving object. Int J Multiphase Flow 39 (2012) 216-242

[13] Liang.X. F., Yang.J. M., Li.J., Xiao.L. F., Li.X., Numerical simulation of irregular wave-simulating irregular wave train, Journal of Hydrodynamics, 2010, 22(4):537-545

FEASIBILITY STUDY of OFFSHORE SOLAR POWER PLANT in PERSIAN GULF

Morteza Bahadori [1], Hassan Ghassemi[2]

1) Department of Maritime Engineering, Amirkabir University of Technology (Tehran Polytechnic), Tehran, Iran, m.bahadori@aut.ac.ir.
2) Department of Maritime Engineering, Amirkabir University of Technology (Tehran Polytechnic), Tehran, Iran, gasemi@aut.ac.ir.

1. Introduction

Large flat land surfaces, where direct normal irradiance (DNI) is high enough for concentrating solar power (CSP), are scarce in some countries. Floating offshore solar power plants in these areas could increase the countries and island's solar power resources significantly. Building offshore solar power plants offers two technical advantages. First, sun-tracking around a vertical axis can be implemented easily. Secondly unlimited cooling water is available, which can increase the efficiency of the thermodynamic cycle [1].

In this paper, a solar platform is investigated, where individual platform segments are supported by several air chambers formed by cylindrical flexible membrane skirts. From experimental data gained from a 4x4 m physical model [1], we have obtained the general characteristics of the platform which extended to a 20x30 m numerical model. By using wave data of the Persian Gulf, the motion of the platform in different sea states is calculated.

2. Model Setup

The platform motion at different sea states is described by experimental data and the environmental conditions at the Persian Gulf are gained from a wave atlas and satellite data which were used in PVSYST software [2].

2.1. Environmental Conditions

According to [3, 4], 80% of the sea states have a *Hs* smaller than 2 m and a *Tm* smaller than 6 s. The main wave direction is between 90° and 135°. In this paper, results for a sea state with *Hs* = 2 m and *Tm* = 6 s, which should model typical operating conditions, and for a sea state with *Hs* = 4 m and *Tm* = 8 s are presented. *Hs* = 4 m and *Tm* = 8 s equate to storm conditions and only 3% of the sea states are worse than the one mentioned for Persian Gulf.

2.2. Platform Motion

Response amplitude operators (RAOs) for the six degrees of freedom and three deformation modes of the platform were obtained from the measurements. Only the rotational degrees of freedom are considered in the model, as the translational degrees of freedom have no influence on the power plant performance.

To calculate the platform motion under ocean wave influence, a random wave signal is generated. First, a JONSWAP energy density spectrum **S** (f) as a function of wave frequency f for desired *Hs* and *Tm* is calculated. Fig. 1 shows an example of the rotational RAOs and a wave spectrum **S** (f) with a mean wave period of 6 s.

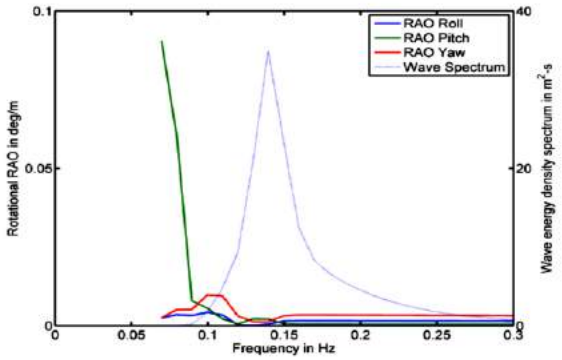

Figure 1. Rotational RAOs and wave spectrum.

According to equation (1) [5], the energy density spectrum is converted to a wave height spectrum $H(f)$ where Δf is the bandwidth of the discretization.

$$H(f) = 2\sqrt{2S(f)\Delta_f} \quad (1)$$

By adding the phase angles to $H(f)$, a random wave signal is defined with the desired spectral parameters. The phase angles are added according to equation (2).

$$\underline{H}(f) = H(f)e^{i\theta} \quad (2)$$

The complex height spectrum $\underline{H}(f)$ of the wave signal is multiplied with the RAOs to obtain the complex response height spectra$\underline{H_R}(f)$. For each degree of freedom and deformation mode, a response height spectrum is calculated. From the complex response height spectra, the platform motion in time domain can be derived by equation (3).

$$\eta(t) = \sum_n \left|\frac{H_R(f_n)}{2}\right| \cos(2\pi f_n t + \Theta_{Rn}) \quad (3)$$

In equation (3) η(t) is the platform deflection for the considered degree of freedom or deformation mode at time *t*, f_n is the frequency, and Θ_{Rn} is the response phase angle of the Fourier component *n*.

Fig. 2 presents an example of the model process. It is a cutout of a pitch motion signal of the platform and

the corresponding water elevation. The motion of the degrees of freedoms and deformation modes are superposed to get the total platform motion.

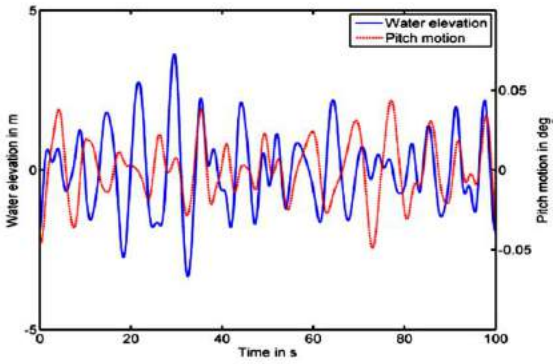

Figure 2. Water elevation and pitch motion.

3. Solar Performance

The solar simulation program (PVSYST) is used to analyze the performance of solar platform. To take advantage of the highest efficiency of solar panels in the Persian Gulf, the region of Dayyer port with geographical coordinates has been chosen. Fig. 3 shows the sun height relation with azimuth during different periods of the year [6].

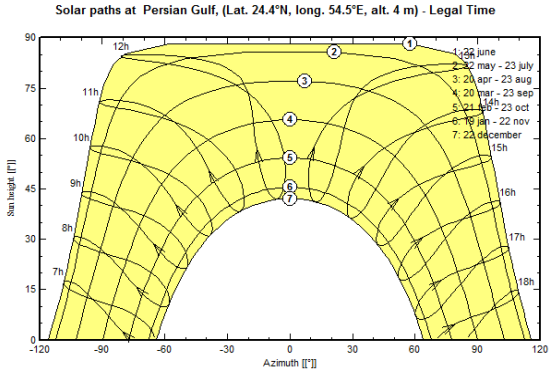

Figure 3. Sun paths diagram at Dayyer region.

3.1. Solar Panels

According to the environmental conditions of the selected region, 52 SunPower all-back contact monocrystalline solar cells were utilized in simulation.

3.2. Solar Inverter

The inverter should be a transformer less, 3-phase Inverter for grid connected PV power plants (SINVERT 2000 MS TL) with efficiency > 98% and 1000V system voltage.

3.3. Output Energy

By the simulation of the solar platform with solar data and platform deflection characteristics, the performance ratio and normalized production has been calculated.

Fig. 4 shows the normalized power production from January to December.

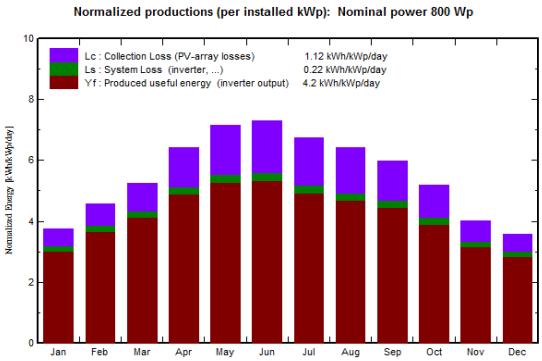

Figure 4. Normalized power production of platform.

4. Conclusions

In this paper, the influence of sea wave excitation on the performance and final energy output of floating offshore solar power plants is investigated. The avoidance of platform motion is essential for an economic platform design, as the efficiency of solar concentrator's decreases significantly for even small misalignments [1]. Therefore a platform design was developed which reduces the platform response to wave excitation to a minimum. It is demonstrated that wave motion and direction theoretically have an influence on the performance, However since the effect is very small for the presented design, we conclude that it can be neglected in further investigations.

Due to the environmental condition of Persian Gulf and simulation of the solar platform, the system production would be 1225 $^{kwh}/_{yr}$ which can support the energy demands of coastal regions.

5. References

[1] Diendorfer C, Haider M, Lauermann M. Numerical simulation of the optical performance of offshore solar power plants. Solar Paces Proceedings 2012.

[2] Bishop J, Rossow W, Dutton E. Surface solar irradiance from the International Satellite Cloude Climatology Project 1993-1991. Journal of Geophysical Research, Vol. 102, 1997.

[3] A A. Golshani. "A 60 Years Wave Hindcast Study In The South Of Persian Gulf Using Swan Model & Semi-Time Domain Method", International Journal of Maritime Technology. Vol. 12, pp. 73-87, 2010.

[4] S, Taebi. A, Golshani. V, Chegini. "An Approach Towards Wave Climate Study In The Persian Gulf And The Gulf Of Oman: Simulate Io N and Validation", Journal of Marine Engineering. Vol. 4, No. 7, spring, 2008

[5] Chakrabarti S. Handbook of Offshore Engineering Volume 1. Elsevier, 2005.

[6] Rigollier C, Lefèvre M, Wald L. The method Heliosat-2 for deriving shortwave solar radiation data from satellite images. Solar Energy, 77(2), 159-169, 2004.

AN EXPERIMENTAL STUDY OF YAW MOTIONS OF SPAR-TYPE FOWT

Fatemeh Tavakoli[1], Rouzbeh Shafaghat[2] and Rezvan Alamian[3]

1) Department of Naval Architecting, Babol Noshirvani University of Technology, Babol, Iran, Fatemeh.tavakoli70@gmail.com
2) Department of Mechanical Engineering, Babol Noshirvani University of Technology, Babol, Iran, rshafaghat@nit.ac.ir
3) Department of Mechanical Engineering, Babol Noshirvani University of Technology, Babol, Iran, r.alamian@stu.nit.ac.ir

1. Introduction

The offshore wind energy is one of the most important renewable energy resources which can cover worldwide energy demand. The wind turbines are devices that can convert wind energy to electrical energy. Noting that the wind energy is stronger on offshore regions, the floating offshore wind turbines (FOWTs) can be a proper choice for generating electricity. Therefore, analyzing various forces on these devices including hydrodynamic and aerodynamic forces can be vital in the FOWTs design process.

Existence of rotating blade in the FOWTs system makes the gyroscopic effect as a substantial parameter in the hydrodynamic studies. If the rotation of turbine blades around an axis leads to the oscillation of the system around another axis, these movements will make the system oscillate around the third axis which is perpendicular to the previous axes; this effect is called the gyroscopic effect. As an example, if the spinning turbine rotor has an angular momentum (torque) around the surge axis and this motion results in platform oscillation in pitch direction, the spinning rotor creates a new component of angular momentum yaw. This new component of angular momentum may either enhance or decrease the yaw motion of platform. Similarly, initial yaw motions can also induce torque and motions in pitch.

Several studies have been carried out concerning the dynamic behavior of SPAR-type FOWTs both experimentally and numerically. Suzuki and Sato [1] investigated the load on turbine blade induced by motion of floating platforms and design requirement for them. They analyzed the effect of stabilizing the fin attached to the base of the FOWT on reducing the pitch motion of the floating SPAR-type wind turbine. Matsukuma and Utsunomiya [2] performed a motion analysis of a SPAR-type FOWT under steady wind considering rotor rotation. The wind loads acting on the rotor blade were calculated using the blade element momentum theory. As a result, yaw, sway and roll motions are generated due to the effect of gyro moment for the rotor rotation. N. Mostafa et al [3] investigated the interaction between the change of rotational speed as well as inertia momentum of the blade and the motion of the FOWT in regular waves. They also studied the interaction between the rotary motion of the wind turbine blade and the dynamic motion of the SPAR-type FOWT at small angel of inclination in regular waves and they conclude that change of gyroscopic effect does not affect the surge, heave, and pitch motions, but its effect is observed on yaw motion.

In the current study, to investigate the effects of the gyro moment on yaw motion, a 1:100 FOWT model was designed and constructed in the Hydrodynamic, Acoustic and Marine Propulsion Laboratory of Babol Noshirvani University of Technology. For observing the performance of this system and also studying the gyro effect of the blades rotation, the system was tested for three different waves. The results show that wavelength increment will lead to increase in rotating oscillations which makes the system relatively unstable.

2. Equation of Motion

The motion of the FOWT in waves can be presented by equation of motion with six degrees of freedom including three translational and three angular motions(see Figure 1).

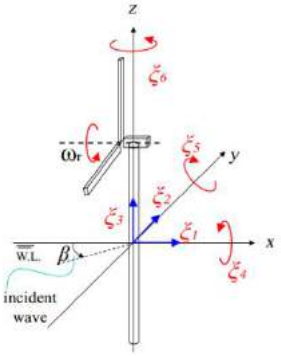

Figure 1. Coordinate system of the FOWT with respect to center of water plan of FOWT [3].

The translational displacements in the x, y, z directions are ξ_1, ξ_2, ξ_3, respectively, where ξ_1 is surge, ξ_2 is sway, and ξ_3 is heave motion. Furthermore, the angular displacement of the motion about the x, y, z axes are ξ_4, ξ_5

, ξ_6 respectively, where ξ_4 is roll, ξ_5 is pith and ξ_6 is yaw rotation.

The dynamic equation of motion of a FOWT in waves can be written as follows in frequency domain:

$$\left[(M+m)\ddot{\xi}+N\dot{\xi}+C\xi\right]=F \quad (1)$$

Where M is inertia matrix, m is added mass matrix, N is damping matrix, C is restoring force matrix, F is wave exciting force vector and ξ is motion response vector.

3. Experiment in Wave Tank

The experiments were carried out in the wave tank of Hydrodynamic, Acoustic and Marine Propulsion Laboratory of Babol Noshirvani University of Technology with dimensions of 11m length, 3m width, and 3m depth. With regard to the power extracting considerations and with using the Froude law of similarity, a 1:100 model of the designed FOWT was constructed which can be seen in Figure 2.

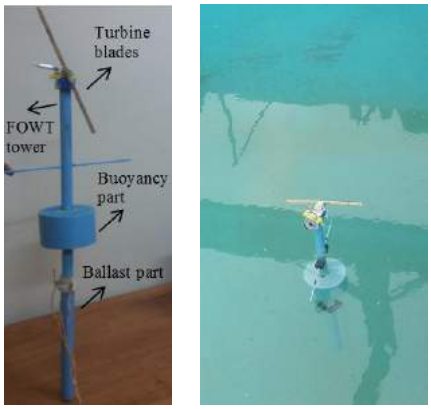

Figure 2. Experimental model, left: descriptions of different parts, right: model placed in wave tank

The specifications of the model are listed in Table 1. It is worth noted that a flat blade was used as the rotor in experimental model in order to neglect the thrust force.

Table 1. Specifications of the model

	parameter	Dimensions (cm)
FOWT tower	Height	22.6
	Diameter	2
Buoyancy part	Depth	6
	Diameter	10
Ballast part	Depth	40
	Diameter	2

4. Discussion and Results

Wave calibration tests are performed in the first series of experiments. In the next step, the model was placed the wave tank and wave-maker was ran to generate the desired waves (Figure 2 right). In order to prevent the model from drifting, it was moored by two mooring lines. A sample time series motion of the model in yaw direction is shown in Figure 3. The vertical axis in this figure is RAO which is defined as the ratio of Yaw amplitude (in radian) and wave amplitude times by wave number. It can be seen that the yaw oscillation of the model is relatively regular.

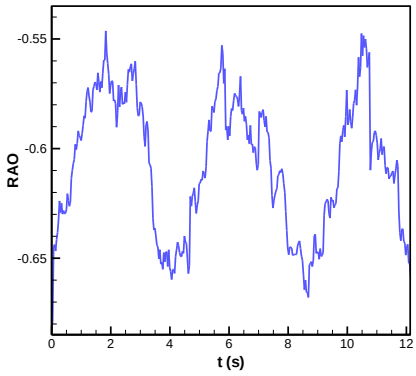

Fig 3. Oscillation of the FOWT in Yaw direction for wave period of 1.7s

The experiment was implemented for three different periods including 1.7, 2 and 2.4s which was leaded in Yaw rotation of the FOWT with the magnitudes of 0.194, 0.188 and 0.083 radian, respectively. Looking at the results, it can be concluded that increasing the wavelength will lead to increment in the amplitude of yaw oscillation.

For the future studies, noting that the gyro moment has major effects on the FOWT Yaw motion, the blades will be optimized. Moreover, the experiment will be implemented for a wide range of waves with the wave specifications of the desired sea.

5. Conclusion

According to previous studies it was observed that the gyroscopic effect caused by the rotation of flat blades has a major effect on yaw motion of FOWTs and in this study this effect was observed for different waves. The effect of thrust force was ignored in this study. It was also seen that the motions of FOWT in different wave periods were regular; moreover, the results showed that increasing the wavelength will lead to increment in the amplitude of Yaw oscillation.

6. References

[1] Suzuki,H. And Sato.,"Load on Turbine Blade Induced by Motion of Floating Platform and Design Requirement for the Platform", Proceeding of 26th International Conference on Offshore Mechanics and Arctic Engineering, California, USA, 2007

[2]Matsukuma, H. and Utsunomiya,T. " Motion Analysis of a Floating Offshore Wind Turbine Considering Rotor Rotation", The IES Journal Part A: Civil and Structural Engineering, pp.268-279, 2008

[3] Md. Nur-E-Mostafa. "A Study on Dynamic Response of Spar-type Floating Wind Turbine in Waves Using 3-D Green Function Method Considering Rotation of Windmill Blades" Japan, Doctoral Thesis, 2012.

ENERGY ABSORPTION OF FULLY NON-LINEAR IRREGULAR WAVE BY BRISTOL CYLINDER WAVE ENERGY CONVERTER

Saadati-Nasab .Mehran[1], Passandideh-Fard. Mohammad[2] and Anbarsooz. Morteza[3]

1) Mechanical Engineering, Ferdowsi of Mashhad, Mashhad, Iran, saadati.mehran@gmail.com
2) Mechanical Engineering, Ferdowsi of Mashhad, Mashhad, Iran, mpfard@um.ac.ir
3) Mechanical Engineering, Advanced Technologies Engineering, Quchan, Iran, m.anbarsooz@gmail.com

1. Introduction

Various types of wave energy absorption equipment work based on a swing or a submerged buoy to a fixed reference. The efficiency of this equipment can vary based on the depth of water in which they are installed. One of the equipment that can effectively use both components of wave forces in x and y direction is Bristol cylinder which was first introduced by Evans from the University of Bristol in 1976 [1].

Evans provided a linear theory to predict the performance of this group of wave energy absorption equipment and indicated that, in theory, there is a possibility of 100% absorption for wave energy using the cylinder [1]. He also showed that passing waves can be eliminated and the total wave energy can be absorbed for certain values of the spring constant and damping factor in each frequency of incident wave. Recently, Heikkinen et al. [2], through providing a theoretical analysis based on potential flow theory, investigated the effect of various parameters such as height, wave periodicity, and the cylinder diameter on the cylindrical Bristol efficiency.

Evans [3] and Davis [4] experimentally showed that linear theory quite loses its accuracy in calculating the Bristol cylindrical efficiency for waves with high sharpness. This is due to limiting assumptions of linear theory which ignore the effects of viscosity and assumes the non-rotating flow and linear waves.

A common method for considering the effects of viscosity in non-viscous fluid simulations is adding a sentence of similar force with the drag force in the well-known Morison's equation [5]. This method has been used by many researchers, including Davis [4] and Babarit et al. [6]. Regarding the Bristol cylinder, Davis [4] showed that the use of this method for predicting efficiency does not provide acceptable results. In fact, because of the cylinder movement, the drag coefficient is different at any given moment and considering a fixed amount for the drag coefficient cannot accurately predict wave forces.

Hence, providing a method for predicting the performance of the Bristol cylinder in various conditions, including against irregular non-linear waves, seems essential. In this study, using a method based on the unmatched and fixed networking (fast fictitious domain method), the performance of this wave energy absorbent in different conditions is simulated.

2. The Governing Equations and Boundary Conditions

The schematic of the wave energy absorption mechanism by the Bristol cylinder is shown in Figure 1.

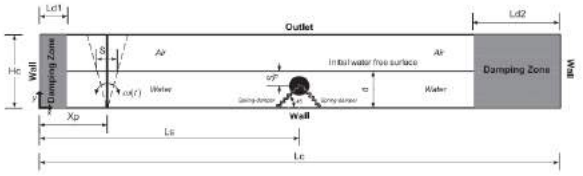

Figure 1. The area of the numerical solution and the boundary conditions

The equation governing the fluid flow is the Navier-Stokes' equation is two-dimensional with laminar, incompressible, and Newtonic flow:

$$\nabla.\vec{V} = 0 \tag{1}$$

$$\frac{\partial \vec{V}}{\partial t} + \vec{V}.\nabla\vec{V} = -\frac{1}{\rho}\nabla P + \frac{1}{\rho}\nabla.\vec{\tau} + \vec{g} + \frac{1}{\rho}\vec{F}_b \tag{2}$$

$$\vec{\tau} = \mu\left[(\nabla\vec{V}) + (\nabla\vec{V})^T\right] \tag{3}$$

Where, $\vec{V}$ is the velocity vector, ρ density, μ the dynamic viscosity, p the pressure, $\vec{\tau}$ stress tensor and $\overrightarrow{F_b}$ external forces applied on the fluid. To track the free surface of fluid, the volume of fluid method is used and defined as follows:

$$F = \begin{bmatrix} 0 & \text{in the gas phase} \\ 0 <, < 1 & \text{in the liquid} - \text{gas interface} \\ 1 & \text{in the liquid phase} \end{bmatrix} \tag{4}$$

In the taken computational steps, after calculating the velocity based on the momentum equation, F values are replaced based on the following transfer equation in the solution area:

$$\frac{\mathrm{dF}}{\mathrm{dt}} = \frac{\partial \mathrm{F}}{\partial \mathrm{t}} + \vec{\mathrm{V}}.\nabla \mathrm{F} = 0 \tag{5}$$

In this method, the solid in the solution is specified by using the scalar quantity below:

$$\emptyset = \begin{bmatrix} 0 & \text{Out of the solid} \\ 0 <, < 1 & \text{Solid boundary} \\ 1 & \text{within the solid} \end{bmatrix} \tag{6}$$

3. Efficiency of Energy Absorption

The overall force applied on the cylinder, in addition to wave forces, includes external forces (spring and damper forces) as well as the buoyancy force. According to Newton's second law:

$$\vec{F}_{tot}(t) = \vec{F}_{spring}(t) + \vec{F}_{damper}(t) + \vec{F}_{bouyancy}(t) + \vec{F}_{wave}(t) = M_s \frac{d\,\vec{V}_s(t)}{dt} \quad (7)$$

The energy absorption efficiency which is defined as the ratio of the average power absorbed, $\bar{P}_{abs}$, to the average total energy of the wave, $\bar{P}_w$, can be introduced by using the following equation [7]:

$$\eta = \frac{\frac{1}{T}\left[\int_t^{t+T} -\vec{F}_{damper}(t).\vec{V}_s dt\right]}{\frac{1}{T}\left[\int_t^{t+T}\int_{-h}^{\gamma} P_D.udzdt\right]} \quad (8)$$

4. Numerical Solution Method

To discretize the governing equations, the three-stage analysis method is used for the equations of continuity and momentum proposed in 2012 Passandideh-Fard and Mirzaii [8]. This method can be used for the Euler's constant networking in the simulation of free surface flows with surface tension. The momentum equation (2) is rewritten as follows.

$$\frac{\vec{V}^{n+1} - \vec{V}^n}{\Delta t} = -\left(\vec{V}.\vec{\nabla}\vec{V}\right)^n - \frac{1}{\rho^n}\nabla p^{n+1} + \frac{1}{\rho^n}\vec{\nabla}.\vec{\tau} + \vec{g}^n + \frac{1}{\rho^n}\vec{F}_b^n \quad (9)$$

5. Results

Potentials of the method proposed in this research are indicated in this section for Bristol cylinder modeling and absorption of energy from sea waves.

Figure (2) shows the Bristol cylinder in the solution domain. Spatial displacements of the cylinder and wave maker are clearly depicted in the latter figure over time. To absorb energy from the cylinder deep in water a spring with a constant of 826 N/m and a damper with a damping factor of 20 Ns/m were used. The free spring length is 30 cm and the cylinder is static when the solution begins. As the wave travels over the cylinder with irregular movements, part of the wave energy is dissipated by the cylinder and damper.

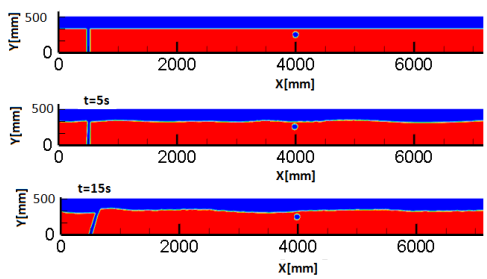

Figure (2): Spatial displacements

Due to the absorption of wave energy by the cylinder in the x and y directions, the amount of energy absorbed by the cylinder in the aforementioned two directions is depicted in Figure (3). The energy absorbed by the cylinder is insignificant and varies in the 0.1-0.45 W/m range because of irregularity of waves hitting the cylinder. As seen in figure (4), efficiency of energy absorption by the cylinder varies from 20 to 60%. Therefore, the cylinder should be optimized for maximum absorption of energy, and this could be the subject of future research.

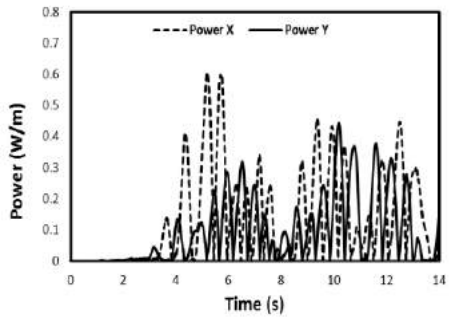

Figure (3): Power absorbed by cylinder

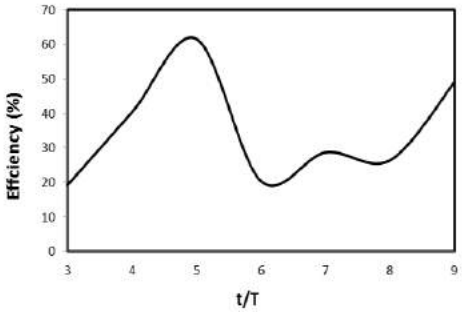

Figure (4): Variations of efficiency of energy absorption by the Bristol cylinder

6. References

[1] Evans.D. V., A theory for wave-power absorption by oscillating bodies, Journal of Fluid Mechanic, 77 (1976) 1–25.

[2] Heikkinen.H.,Lampinen.M.J., Boling.J., Analytical study of the interaction between waves and cylindrical wave energy converters oscillating in tow modes, Renewable Energy, 50 (2013) 150–160.

[3] Evans.D. V., Jeffrey.D. C., Salter.S. H., Taylor. J. R. M., Submerged cylinder wave energy device: theory and experiment, Applied Ocean Research, 1 (1979) 3-12

[4] Davis.J. P., Wave energy absorption by the Bristol Cylinder-linear and non-linear effects, Proceeding of the institution of Civil Engineers, part2, 89 (1990) 317–340.

[5] Morison.J.R.,O'Brien.M.P., Johnson.J.W., Schaaf.S.A., The force exerted by surface waves on piles, Journal of petroleum Technology, 2 (1950) 149–154.

[6] Babarit.A.,Hals.J., Muliawan.M.J., Kurniawan.A., Moam.T., Krokstad.J., Numerical benchmarking study of a selection of wave energy converters, Renewable Energy, 41 (2012) 44–63.

[7] Dean RG, Dalrymple RA. Water wave mechanics for engineers and scientists. New Jersey: Prentice Hall; 1984.

[8] Mirzaii I, Passandideh-Fard M. Modeling free surfaceflows in presence of an arbitrary moving object. Int J Multiphase Flow 39 (2012) 216-242

INVESTIGATION ON PERFORMANCE AND ARRAY OPTIMIZATION OF AN OPERATING MARINE HYDROKINETIC (MHK) TURBINE FARM IN GREAT-TONB OF IRAN

Soheil Radfar[1], Roozbeh Panahi[2,*], Amir Teymour Javaherchi Mozafari[3], Hamed Khalilpur

1) Civil and Environmental Engineering Department, Tarbiat Modares University, Tehran, Iran, soheil.radfar@modares.ac.ir
2) Civil and Environmental Engineering Department, Tarbiat Modares University, Tehran, Iran, rpanahi@modares.ac.ir
3) Mechanical Engineering Department, University of Washington, Seattle, United States, teymourj@uw.edu
4) Civil and Environmental Engineering Department, Tarbiat Modares University, Tehran, Iran, sh.khalilpur@modares.ac.ir

1. Introduction

During last five decades the sky-rocketing demand for energy production parallel to the limited resources of fossil fuels, with proven harmful side effects, around the world led into the search for alternative resources of energy. Among available alternative energy resources, the renewable energy resources have attracted the attention of many scientists and engineers. One type of renewable energy is the Marine Hydrokinetic (MHK) energy, which also is referred to as Tidal Energy. The most important advantage of MHK resources over other renewable energy resources, such as solar, wind, geothermal and etc. is it's high level of predictability. There are numerous narrow estuaries and MHK sites around the world, where has large energy density to be captured and used to produce energy, that made MHK resources to be promising renewable energy resource.

The goal of the present study is to investigate the feasibility of implementation of an array of Tidal Energy Converters (TECs), methods of array optimization and its potential effect on one of these promising location, Great-Tonb, connecting the Persian Gulf to the Gulf of Oman in south of Iran.

2. Tidal Site Selection and Characterization

Previous detail numerical investigations [1] on the flow field of the narrow connection between the Persian Gulf to the Gulf of Oman confirmed that there are multiple regions of strong tidal currents with maximum speed of 1.5 [m/s] as visualized in figure 1.

Beside the evidence for existence of strong tides in this MHK site, it was confirmed that the variation of the water depth in this region is mild and has average value of 55 [m]. These two factors therefore made this MHK site a perfect candidate to implement a farm of TECs. In the current study the geometry of this MHK site is approximated as a flat seabed rectangular cube with the corresponding relevant realistic dimensions of the site [1, 2].

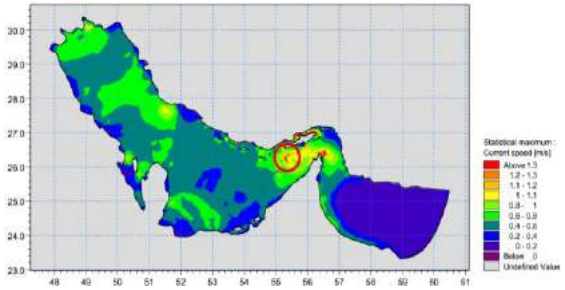

Figure 1. Zonation of maximum tidal current speed in the Persian Gulf

3. Numerical Model

The operation and effect of each TEC within the array is simulated using the Virtual Blade Model (VBM). The VBM is an implementation of the Blade Element Method (BEM) within ANSYS FLUENT commercial CFD-package [cite the original paper by developer of VBM, available in my work citations].

In BEM the entire blade span is divided into small sub-elements from the root to the tip. The lift and drag forces on each of the element will be computed using calculated velocity field estimated by solving Reynolds Averaged Navier-Stokes (RANS) equations coupled with a turbulence closure model and the provided lift and drag coefficients as a function of Angle of Attack for each section as follows:

$$f_{L,D} = c_{L,D}(\alpha, Ma, \mathrm{Re}) c\,(r/R).\frac{\rho V_{tot}^{2}}{2} \qquad (1)$$

In this equation $c_{L,D}$ is the lift or drag coefficient, $c(r/R)$ is the chord length of the element, ρ is the fluid density, V_{tot} is the total fluid velocity relative to the blade. The elemental lift and drag forces are then averaged over a full revolution to calculate the total body force components at each cell in the discretied CFD domain by:

$$F_{L,D_{cell}} = N_b.\frac{dr.d\theta}{2\pi}.f_{L,D} \qquad (2)$$

$$\vec{S}_{cell} = -\frac{\vec{F}_{cell}}{V_{cell}} \quad (3)$$

Here N_b is number of blades, r is the radial position of the blade section from the center of the turbine, θ is the azimuthal coordinate and V_{cell} is the volume of the grid cell. The flow field data is then updated with the estimated body forces and this process is repeated until a converged solution is obtained.

Assessment of the VBM shows that the general fluid mechanics of the flow, such as performance of the device and flow filed around and in the wake of the device, can be simulated accurately with this model. However, VBM is limited to capture the detail of the flow in the near wake region (i.e. right after the blade), since it is averaging the aerodynamic effects of the blade over the whole swept area of the rotor disk. To summarize the VBM simulates the flow crossing a turbine in a good agreement with other models, such as Sliding Mesh and Rotating Reference models, while decreasing the computational time and the effort for the geometry creation and meshing process significantly [3, 4].

4. Model Setup

4.1. Turbine Geometry and Design

The turbine used in this study is the DOE Reference Model 1 (DOE RM1). The creation of the DOE RM1, as an open access design, allows for direct comparison of results and analysis from different research groups. The turbine rotor consists of two blades formed from NACA 60240 foils, and has a diameter of 20 meters. This geometry has been proposed and tested in previous numerical simulations [5-7].

4.2. Computational Domain/s

In this study, so far two different Tidal Energy Converters (TECs) configurations were created and meshed as shown in figure 2. The basic domains were sized at 650 [m] long (Z-axis) by 400 [m] wide (X-axis) by 55 [m] deep (Y-axis). Mesh was created with GAMBIT (ANSYS, Inc. Cannonsburg, PA.) software.

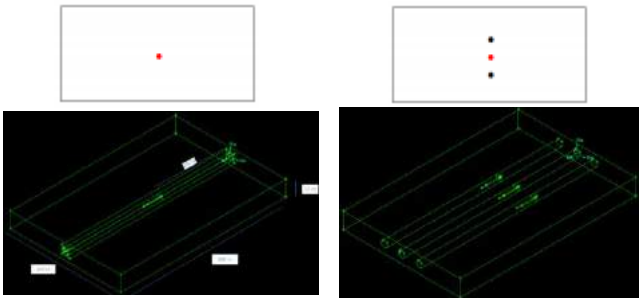

Layout 1: Base Case Layout 2: One Row Array

Figure 2. TECs layouts

5. Results

Currently the main part of the research progress is focused on finalizing the simulation setup of the base case. After validation of the simulation for the base case, simulation of the flow field in an array of TECs (i.e. layout 2) will be conducted. The results of these simulations will define the guidelines to create alternative TECs configuration to investigate the performance of each device and overall performance of different configurations and the flow field around them.

Furthermore base on fundamental fluid mechanics it is believed that variation of the lateral spacing between TECs in an aligned configuration could lead into either lowering, not effecting or increasing, the performance of middle TEC. It is hoped that the results of previous simulations complimented with simulation of the flow field in computational domain with variable lateral distances and other configurations will provide general guidelines and answer to this class of open questions about the feasibility of implementation of TECs and their optimum configurations in the proposed MHK site in this and other similar regions.

6. References

[1] Radfar, S., Panahi, R. and Rezaee Mazyaki, A., "Feasibility study and characterization of potential sites for tidal energy extraction in Persian Gulf using zonation in Mike21", *18th Marine Industries Conference*, Kish Island, December 22-25 2015, p. 129.

[2] Bai, L., Spence, R. R. G. and Dudziak, G., "Investigation of the Influence of Array Arrangement and Spacing on Tidal Energy Converter (TEC) Performance using a 3-Dimensional CFD Model", *8th European Wave and Tidal Energy Conference*, Uppsala, Sweden, 2009, pp. 654-660.

[3] Javaherchi Mozafari, A. T., "Numerical Modeling of Tidal Turbines: Methodology Development and Potential Physical Environmental Effects". *Master thesis*, University of Washington, November 2010.

[4] Javaherchi Mozafari, A. T., "Numerical investigation of Marine Hydrokinetic Turbines: methodology development for single turbine and small array simulation, and application to flume and full-scale reference models". *PhD thesis*, University of Washington, 2014.

[5] Tessier, M. and Tomasini, N., "Numerical Study of Horizontal Axis Hydrokinetic Turbines: Performance Analysis and Array Optimization", *Report*, University of Washington, 2010.

[6] Cerisola, A., "Numerical Analysis of Tidal Turbines using Virtual Blade Model and Single Rotating Reference Frame", *Report*, University of Washington, 2012.

[7] Lawson, M., Li, Y. and Sale, D., "Development and verification of a computational fluid dynamics model of a horizontal-axis tidal current turbine". *Proceedings of the 30th International Conference on Ocean, Offshore, and Arctic Engineering*, Rotterdam, The Netherlands, 2011.

RENEWABLE ENERGY CONCEPTS FOR OFFSHORE STRUCTURES

Gerald Higelin[1]

1) University of Applied Sciences Furtwangen, Germany

Abstract

International recognized studies for market data on energy consumption state an annual growth of 1,7 % for the next two decades /1/. Regions with exceptional high growth rates are Middle East, China and India.

Worldwide increasing demand for energy cannot be satisfied by exploration of fossil energy carriers /2/.

Environmental impacts, which are less tolerated by the society of the 21st century, promote climate policy for significant reduction of emission of climate harmful greenhouse gases. United nations climate conferences in the past 20 years stated repeatedly the aims for climate change /3/.

As experienced in Europe and North America during the past 20 years the increase of energy consumption will be more and more satisfied by renewable energies. Renewable energy sources, such as solar energy, wind, hydro , tidal , or geothermal will have more importance in future.

A major drawback of renewable energy economy is the misfit of location of availability and of demand. Interesting areas for solar energy are in tropical and subtropical zones and landscapes with desert character. Hydro power is available in mountainous areas, and wind energy mainly in costal and offshore sites.

In comparison to fossil energy processing renewable energy plants use much more land and need to be in distance to residential areas because of environmental deficits.

So far most of renewable energy plants are based on land, but the highest potentials are near coastal areas or offshore sites. In future offshore sites will have a strategic advantage over land- based sites in terms of technical, economical, and environmental reasons.

Even floating platforms are in consideration, with the advantage of flexibility of construction and maintenance near the coast and operation in far offshore sites. These concepts can be scaled and flexible adopted to regional demand and developments.

Another challenge with renewable energy comes from the requirement of storage and transport over long distances. Solar power, wind and hydropower are subjected to daily, seasonal variations and other inestimable conditions.

The most promising renewable energy source for coastal and offshore sites is wind, where due to less friction high wind velocities and very constant conditions are to be expected. Rotors with airfoil lift blades can be adjusted to varying wind velocities or directions, and offer high efficiencies (80-90%) . Technology is sophisticated available and continuously scaled up to higher power. Today the most powerful systems have maximum generator power of 10MW /5/.

Hydrogen gas production and storage promises high potential with a specific energy of 3,54 kWh/m^3 , in terms of weight 33,3 kwh/kg /4/ , so H_2 is almost three times more concentrated than diesel (12,6 kWh/kg) and the advantage of transformation into any other usable form of energy without emission of CO_2 or other harmful substances. Liquid Hydrogen can be stored in large scale tanks, under pressure, or in solid state metalhydride container. In fuel cells it can be transformed directly into electric energy with high efficiency. Fuel cells can be applied stationary or mobile and can be scaled for any application.

The technical concepts that have to be mastered are construction of high reliable and reasonably maintainable systems for wind and tidal power plants. Construction of long distance undersea transmission for high voltage electrical transmission. For ultra high distance transport, e.g more than 2000 km where electrical transmission is not reasonable. The development of offshore energy conversion and transport concepts have to be considered.

In this paper three different concepts are presented and discussed in terms of technological feasibility, typical scenario for applications, and economic rating.

- An offshore wind park with high voltage underwater electrical transmission to land is the most conventional concept that has already been realized in the North Sea for installed power of 9000 MW(Doggerbank, UK). Technological feasibility is guaranteed, it is scalable, but still limited near coastal areas with distances up to 50 km in sea areas with reasonable low water depth preferable up to 40-50m.

- A more flexible and innovative concept aims to floating platform wind generators where energy is converted by power-to-gas concept. Power-to-gas is already in use for land based energy transport into existing gas pipeline grids. For offshore application it is considered to produce hydrogen by electrolysis, here electric power from wind rotors connected with synchronous generators is used with high efficiency, as no transformation adaption to public grids are necessary. Hydrogen will be stored in gas

tanks and transported by ships to gas terminal near coast to fed the gas into existing long distance pipeline grids.

- The most advanced concepts use ocean stream or tidal power stations for energy harvesting, storage, and transport. In deep sea areas, water tanks fixed on ground can be pumped out if extra energy is available. So high energy amounts can be stored with no loss and side effects. In times of high demand the tanks are refilled with water powering a turbine with reasonable high head. Special emphasis is given to the requirements and innovations needed to systems.

In this paper also a methodology is presented for assessment and rating of different concepts in terms of feasibility, risc, and overall potential.

References

[1] BP Energy Outlook 2035, 2015
[2] International Energy Agency (IEA) , World Energy outlook, 2015
[3] United Nations Paris Agreement , COP 21 Paris 2015
[4] Energie, B.Diekmann, E Rosenthal, 3.Auflage ,Springer Spektrum Verlag, 2014
[5] Siemens AG, Industry Sector, Bestell-Nr.: E20001-A70-P550 , 2012

AN UNCERTAINTY-BASED DECISION MODEL FOR MANAGING COASTAL GROUNDWATER RESOURCES

Mohammad Mahdi Rajabi[1], Hamed Ketabchi[2] and Behzad Ataie-Ashtiani[3]

1) Civil Engineering Department, Sharif University of Technology, Tehran, Iran, mmrajabi@alum.sharif.edu
2) Department of Water Resources Engineering, Tarbiat Modares University, Tehran, Iran, h.ketabchi@modares.ac.ir
3) Civil Engineering Department, Sharif University of Technology, Tehran, Iran, ataie@sharif.edu

1. Introduction

As highlighted by the Barcelona convention [1], an important objective of integrated coastal zone management (ICZM) is to ensure the *sustainable use of natural resources, particularly with regard to water use*. Groundwater is an important, and in some cases the only source of freshwater in coastal areas and communities living in these areas highly depend on groundwater abstraction for drinking water, irrigation and industrial use [2]. However, in many coastal areas around the world, overexploitation of groundwater has resulted in lowering of the water table which in turn has induced seawater intrusion (SWI). SWI is the most prominent type of groundwater pollution in coastal aquifers through the world and many examples of SWI have been reported in the literature [2, 3]. So the sustainable use of groundwater in coastal areas requires particular attention to the pollution risks associated with SWI.

A novel approach to developing sustainable coastal groundwater extraction schemes is to combine SWI models with optimization algorithms. Often the objective is to increase fresh groundwater extraction while reducing SWI, considering the optimum combination of well locations and pumping rates. This approach has been applied by a number of previous studies, which were reviewed by [3]. The outcome of these simulation-optimization schemes can then be used as a basis for land use planning and shoreline management in ICZM. However, what is missing in previous studies is the lack of attention to the uncertainty inherently embedded in SWI model outputs. As argued by a number of previous studies [e.g. 3, 4], this ignorance of uncertainty can lead to faulty decisions in the development of coastal groundwater extraction plans.

The main objective of the present study is to develop a new uncertainty-based simulation-optimization model which can act as a decision tool in the selection of optimal coastal aquifer extraction schemes. Some of the main building blocks of the proposed approach are based on previous work described in a number of references including [4-6], but the objective function and the approach use in the handling of the computational burden are unique in the current study.

2. Methodology

The uncertainty-based simulation-optimization model described in this paper is based on an array of concepts and ideas. In this section, we briefly review these concepts and refer the interested reader to more extensive descriptions in the cited literature.

a) Numerical Simulation: The three-dimensional simulation of SWI described in this paper is based on the application of the USGS code SUTRA [7]. The model employs a finite element approximation of the governing equations in space, and an implicit finite difference approximation in time. The numerical model has been calibrated using the PEST inverse code [8].

b) Continuous Ant Colony Optimization (CACO): CACO is utilized as the optimization tools in this study. CACO is a meta-heuristic optimization method which is inspired by the foraging behavior of ant colonies [6].

c) Monte Carlo Simulations (MCSs): This study employs MCSs to quantify the uncertainty in model outputs. MCS is carried out by using an optimized Latin hypercube sampling (OLHS) strategy based on the centered L_2-discrepency (CLD) criterion and the enhanced stochastic evolutionary (ESE) optimization algorithm [9].

d) Artificial Neural Networks (ANNs): MCSs require large numbers of model simulations, and so the computational burden has long been a key obstacle in applying Monte Carlo-based simulation-optimization algorithms in similar applications. In order to solve this problem, ANNs are used as a surrogate modeling tool to replace the numerical model in MCSs.

e) The decision model: The proposed decision model is characterized by an objective function and a constraint. The objective function is maximizing the total groundwater extraction rate, which is alternatively represented here as minimizing the net recharge rate in a number of proposed management zones. This objective is represented as:

$$\min\ Z = \sum_{j=1}^{n_z} R_j \times S_j \qquad (1)$$

Where Z is total net recharge to the coastal aquifer system, R_j is net recharge per surface area in the j^{th} so-called groundwater management zone (GMZ), S_j is the surface area of the j^{th} GMZ, and n_z is the number of GMZs in the coastal aquifer system.

The above objective function is subjected to:

$$P_{exd}^{i} < P_{exd}^{max} \; for \; i = 1 \; to \; n_{obs} \qquad (2)$$

Were P_{exd}^{i} is the probability of exceedance for salinity in the i^{th} monitoring wells from a specified threshold value, P_{exd}^{max} is the maximum allowable probability of exceedance, and n_{obs} is the number of observation wells in the island. P_{exd}^{i} values are estimated by employing the SWI model within the framework of MCSs.

3. Case Study

The proposed approach is applied to the real-world test case of Kish Island, located in the Persian Gulf. The island is divided into 11 GMZs based on similarities in land use and water consumption (see Figure 1), and these GMZs are used as the basis for planning the groundwater extraction schemes [5]. Details regarding the numerical modeling of Kish Island are available in [8]. In this study the key uncertain input parameter of the Kish island model is assumed to be the net recharge rate which includes the uncertainties of both precipitation and extractions.

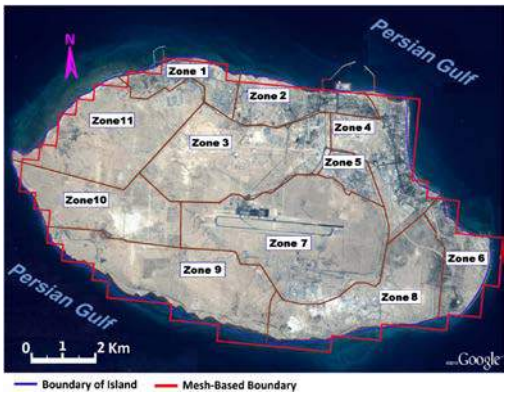

Figure 1. Aerial map of Kish Island and the boundaries of the 11 management zones (see [5, 6]).

4. Results and Conclusions

As the initial step, the numerical model of Kish Island is constructed and subsequently calibrated using the PEST inverse code. Figure 2 illustrates the resulting three-dimensional numerical modeling outputs at the start of the planning period. Then a total of 5,000 input-output patterns of the net recharge rates and the associated salinity values in the observation wells, obtained from the numerical model, are used to train the ANN. A feed-forward back-propagation ANN with an architecture consisting of 11 input-layer neurons, 40 hidden-layer neurons, and 20 output-layer neurons with sigmoid transfer functions is considered. The best training performance of 0.0004220 is obtained at 830 epochs.

These trained ANNs are then employed within the framework of the proposed simulation-optimization algorithm to estimate the set of optimal extraction rates (from the 11 GMZs) that limit the probability of SWI occurrence into the island freshwater aquifer system. The total sum of these extraction rates is the sustainable extraction rate from the island`s aquifer system. The suitable CACO population size and the number of generations are found based on the convergence rate of the objective function and are set equal to 30 and 100 respectively. The number of MCSs is set to 100, resulting in a total of 9 million simulations for the 30 independent runs of simulation-optimization algorithm. The study shows that by employing ANNs and an efficient sampling strategy in MCSs, the amount of computational resources spent on the decision model can be strictly reduced. The use of ANNs instead of the original numerical model reduces the required computational time of the simulation-optimization algorithm from 775 hours to less than 2.5 hours. The results also show that the uncertainties of the Kish Island test case are effectively integrated into simulation-optimization algorithm to provide the means to estimate optimum groundwater extraction rates.

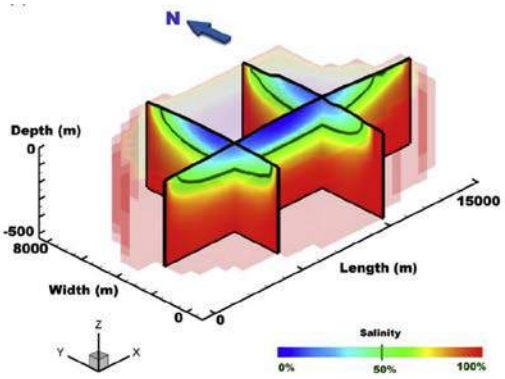

Figure 2. Three-dimensional view of simulated salinity of Kish Island

5. References

[1] EU, "Protocol on integrated coastal zone management in the Mediterranean, Barcelona", 1995.

[2] Werner, A.D., et al. "Seawater intrusion processes, investigation and management: recent advances and future challenges." Advances in Water Resources 51 2013, 3-26.

[3] Ketabchi, H, Ataie-Ashtiani, B., "Review: Coastal groundwater optimization—advances, challenges, and practical solutions." Hydrogeology Journal 23.6 2015, 1129-1154.

[4] Sreekanth, J., Datta, B., "Stochastic and robust multi-objective optimal management of pumping from coastal aquifers under parameter uncertainty." Water resources management 28.7 2014, 2005-2019.

[5] Ataie-Ashtiani, B., Ketabchi, H., Rajabi, M.M., "Optimal management of a freshwater lens in a small island using surrogate models and evolutionary algorithms." Journal of Hydrologic Engineering 19.2 2013, 339-354.

[6] Ketabchi, H., Ataie-Ashtiani, B., "Assessment of a parallel evolutionary optimization approach for efficient management of coastal aquifers." Environmental Modelling & Software 74 2015, 21-38.

[7] Voss, C. I, Provost, A.M., "SUTRA, a model for saturated-unsaturated variable-density ground-water flow with solute or energy transport", U.S. Geological Survey, Water-Resources Investigations, Open-File Report 02-4231, 2010.

[8] Ataie-Ashtiani, B., Rajabi, M.M., Ketabchi, H., "Inverse modelling for freshwater lens in small islands: Kish Island, Persian Gulf." Hydrological Processes 27.19 2013, 2759-2773.

[9] Rajabi, M.M., Ataie-Ashtiani, B., "Sampling efficiency in Monte Carlo based uncertainty propagation strategies: application in seawater intrusion simulations", Advances in Water Resources, 67, 2014, 46-64.

ANALYSIS OF THE PLANNERS' EXPECTATIONS TO FUTURE CLIMATE CHANGE IN COASTAL PROVINCES OF IRAN

Davood Mafi Gholami[1], Afshin Danehkar[2] and Akram Nouri Kamari[3]

1) Assistant professor, Department of forest sciences, Faculty of natural resources and earth science, Shahrekord University, Shahrekord, Iran , d.mafigholami@nres.sku.ac.ir
2) Associated professor, Department of environment, Faculty of natural resources, University of Tehran, Karaj, Iran, danehkar@ut.ac.ir
3) Ph. D. Student, department of environment, Faculty of natural resources, University of Tehran, Karaj, Iran, a.nourikamari@ut.ac.ir

1. Introduction

Climate variability and change have emerged as additional issues influencing planning strategies, especially in coastal environments that are susceptible flooding and erosion [1,6]. Planners must consider the rate and magnitude of climate change, range of uncertainty, and likelihood of potential impacts in assessing adaptation priorities and strategies [2]. These expectations of climate change are related to perceptions of risk; however, the magnitude of the event or range uncertainty is only one dimension of feeling at risk. Diverse expectations of the nature of climate change complicate reaching a working level of agreement and are major barriers to climate change adaptation (CCA) planning [4]. Differences in planner expectations and scientific projections of change may also impede mediated modeling or facilitated planning activities. This paper addresses the following question: "How do coastal planners' expectations of climate change compare to published projections of climate change?" The paper focuses on assessing expectations of the magnitude and uncertainty of global temperature and sea level change by 2030 and the likelihood of four climate impacts by the mid- to late 21st century.

2. Method

This study targets three groups of coastal planners. The first group which represents "local" planners includes city planners and engineers, county planners, natural resource planners, town administrators, and zoning administrators. The second group, representing "province" perspectives, includes section and division heads of key province agencies. The third group, entitled "NGOs", includes heads of NGOs and non-profit organizations. NGOs include both grassroots and local organizations and national-level organizations. These groups were selected because they have received limited attention in survey-based research [5]. Bushehr, Hormozgan and Sistan va Baluchestan provinces were selected as the study areas given their diversity of coastal management challenges and differences in projections of climate change. Twenty coastal planners across Bushehr, Hormozgan and Sistan va Baluchestan provinces were interviewed during the spring and summer of 2015 to inform the development of a questionnaire. Interviewees were selected using a maximum variation purposeful sampling technique. This sample of interviewees contained planners at different levels of government and along different regions of each province coastline. The questionnaire was administered between April and August 2015, based on Dillman's (2000) Tailored Design Method [3].Participants were asked to provide low-end, best estimate, and high-end estimates for changes in temperature and sea level in whole numbers (°C and centimeter, respectively). The year 2030 was selected for analysis because it represents the upper limit of coastal planning time frames and it is a period just prior to projected divergence of global temperature change. Global temperature and sea level change estimates were assessed based on the magnitude of change and range of uncertainty. The range of uncertainty was measured as the distance between low- and high-end estimates. Estimates of global temperature and sea level change were then compared to values in the peer-reviewed literature across three dimensions: point estimates of the magnitude of change, interval estimates of the range of uncertainty, and overlap of interval estimates

3. Results

3.1 Estimation of Change of Global Temperature

Thirty-eight participants (38%) provided low-end, best, and high-end estimates of the magnitude of global temperature change by 2030. The remaining 62% of respondents indicated that they did not know the magnitude of change. Of the respondents who provided estimates, the median best estimate global temperature was 3.16 °C. 75% estimated that temperature would rise 3.26 or 3.16 °C and all participants indicated that global temperature would rise. Of those participants that did not know magnitude of temperature change, 71.5% believed that temperature was going to increase, 22.5% were not sure the direction of change, and 6% believed there would be no change. Coastal planner median best estimates of global temperature change were approximately 3.26°C

higher than the IPCC AR4. 28% of participants provided estimates similar to the IPCC (3.26°C), while 33% and 39% of planner estimates were 3.26°C and 3.16°C or greater than the IPCC, respectively. Planners in Hormozgan were the only sub-group of planners whose median best estimates were similar to the IPCC. Median best estimates of temperature change were significantly higher for planners in Bushehr (2.95°C) than in Hormozgan and Sistan va Baluchestan (3.16°C) ($p = 0.009$ and 0.006, respectively).

3.2. Estimation of Sea Level Rise

Thirty-six participants (52%) provided low-end, best, and high-end estimates of global sea level change by 2030. Best estimates generally followed a bimodal distribution of 5 and 10 centimeters, and high-end estimates centered on 15 and 30 centimeters. The median best estimate of sea level rise was 10 centimeters. All of these participants believed that global sea level would rise, and 47% of participant best estimates of sea level rise were 15 centimeters or greater. Of the participants who "did not know" low-end, best, and high-end magnitude of future sea level by 2030 (64%; n =80), 76.6% believed that sea level would rise, 3.4% believed there would be no change, and 20% were not sure the direction of change. Participant best estimates of sea level rise by 2030 are approximately twice as high as the high-end estimates of climate science projections assumed in this study. Only 22 participants (31%) provided best estimates that were similar to, or less than, the high-end estimate (5 cm) of climate science projections. 27% and 35% of participant best guess estimates were 8 centimeters greater than or 10 or more centimeters greater than the high-end estimates of climate science projections, respectively. Best estimates of the magnitude of sea level rise by 2030 were the highest in Sistan va Baluchestan (15 centimeters) and the lowest in Bushehr (10 centimeters).

3.3. Estimation of Sea Level Rise

Four questions measured estimates of the likelihood of climate change impacts by the mid- to late 21st century. Overall, 82% to 89% of participants believed that the likelihood for each of these impacts was "more likely than not" (>50% chance) or greater (Table 1). Of participants that stated they did not know the likelihood of each statement (n ranged from 15 to 18 across the 4 questions), 65 to 72% of participants were local planners from Hormozgan. However, there were a few significant differences in the estimated likelihood of different climate change impacts across levels of management and study areas. NGOs estimated a significantly higher likelihood of warmer and more frequent hot days and nights over most land areas than local planners ($p \leq 0.00$). Planners in Hormozgan estimated a significantly higher likelihood of an increase in the intensity of hurricane activity than planners in Bushehr ($p \leq 0.05$). Finally, the likelihood of an increase in the frequency of heavy precipitation events over most areas was significantly higher for planners in Sistan va Baluchestan than in Hormozgan and was significantly lower for local planners than state and NGO planners.

Table 1. Estimates of the likelihood of climate change impacts by the mid to late 21st century (2050-2100): n (%).

Likelihood Statement	Increased incidence of extreme high sea level due to regional weather systems	An increase in the frequency of heavy precipitation events over most areas	An increase in the intensity of hurricane activity	Warmer and more frequent hot days and nights over most land areas
Virtually Certain (>99% chance)	21 (15)	16 (12)	21 (15)	**25 (18)**
Very Likely (>90% chance)	30 (22)	**29 (21)**	30 (22)	34 (25)
Likely (>66% chance)	**32 (23)**	33 (24)	**35 (26)**	27 (20)
More Likely than Not (>50% chance)	26 (19)	31 (23)	28 (20)	30 (22)
Unlikely (<33% chance)	8 (6)	8 (6)	7 (5)	3 (2)
Very Unlikely (<10% chance)	3 (2)	4 (3)	2 (1)	2 (1)
Exceptionally Unlikely (<1% hance)	1 (1)	1 (1)	1 (1)	1 (1)
Not aware of	16 (12)	15 (11)	13 (9)	15 (11)
Hit Rates (%)	32 (23)	29 (21)	35 (26)	25 (18)
Exact ± 1 Ordinal Interval	88 (64)	78 (57)	93 (68)	59 (43)

Bold values represent IPCC estimates for each likelihood statement

4. Discussion

This study assessed how coastal planner expectations of climate change compare to widely published and referenced climate science projections. The major findings are:

- 62% and 57% of planners reported that they were not aware of the magnitude of global temperature and SLR change by 2030, respectively.
- Planners expect a greater increase in global temperature change by 2030 and greater range of uncertainty than model projections in the IPCC AR4.
    - Planners expect a greater increase in global sea level rise by 2030 and a greater range of uncertainty than climate science projections.
    - Planner's expectations of climate change impacts are similar to estimates provided in the IPCC AR4. 82 to 89% of participants believed that the likelihood of each of the four climate impacts were "more likely or not" or greater, and 62 to 89% of participants were calibrated within one ordinal interval of the IPCC likelihood statements across the 4 questions.

5. References

[1] CAKE. 2012. C*limate Adaptation Knowledge Exchange: Case study database 2012*. Available from http://www.cakex.org/case-studies.

[2] De Schiller, S., and J. M. Evans. 1996. Training architects and planners to design with urban microclimates. *Atmospheric Environment* 30 (3):449-454.

[3] Dillman, D. A. 2000. *Mail and internet surveys: the tailored design method*. 2nd Ed. New York: John Wiley and Sons, Inc.

[4] Moser, S. C., and J. A. Ekstrom. 2010. A framework to diagnose barriers to climate change adaptation. *roceedings of the National Academy of Science*, 107(51): 22026-22031.

[5] MRAG. 2009. Systematic review of the needs and issues of the U.S. coastal resource management community, 53. Charleston, *SC: NOAA Coastal Services Center*.

[6] NOAA CSC. 2008. Climate-Related Needs Assessment Synthesis for Coastal Management, 29. Charleston, *SC: NOAA Coastal Services Center*.

ENVIRONMENTAL PROTECTION DURING DREDGING AND LAND RECLAMATION OPERATIONS IN KISH COMMERCIAL PORT

MahtabMoalemi[1], HamidehTaheri[2]

1) Pars Geometry Consultants, Tehran, Iran, m_moalemi@parsgc.com
2) Pars Geometry Consultants, Tehran, Iran S.H_taheri@parsgc.com

1. Introduction

The presented paper describes the severe environmental mitigation plan, which was conducted prior to commencement and during the dredging and land reclamation operation in Kish Island in year 2012.

Kish is a 91.5 km2 resort island situated 18 km from southern coastline of Iran and 200 km north-west of Dubai. Kish Island with its strategic location, magnificent nature and rich cultural heritage is one of the main tourism destinations in Iran. Being a free trade zone Kish Island is the destination of approximately one million tourists annually.

Kish Commercial Port with cargo throughput of around 1,000,000 tons in year 2005 and cargo throughput of around 2,000,000 tons in year 2010 is one of the growing ports in the country (the records do not include the number of imported and exported vehicles). Land has always been considered as a high-valued commodity in this developing region. Therefore, land reclamation has always been included in the perspective of Kish development plans. During year 2012 as a part of the development plan of the island, a dredging operation was conducted in Kish Commercial Port. The work comprised the removal of 700,000 m3 of materials from the depth of -3.0 to -6.0 m CD inside the harbor. The port is bounded to the west by a natural habitat of few sensitive benthic marine resources. Based on thorough studies [2] this area was identified as the most appropriate site for deposition of the dredged material and the most optimal site for land reclamation.

In accordance with sustainable development policy in Iran, and the environmental impact assessment (EIA) studies a comprehensive environmental mitigation plan was carried out which was consisted of several actions including (a) coral relocation and (b) turbidity management. This paper describes the indicated exercises in detail.

2. CORAL REEF RELOCATION

Prior to commencement of the dredging campaign a coral relocation exercise was conducted in order to preserve the benthic marine resources and improve their health condition. An assessment of coral cover and general benthic health was conducted. A brief description of the sensitive species at the deposition site is as follows [3]:

- Some sensitive species were identified in the area including hard coral, soft coral and sponges
- The dominant coral species in the work area were identified as Porites and Acropora (see Figure 1)
- Coral cover was as high as 13%
- Five colonies of Porites species with the colony diameter of more than 1 m and five other colonies of Acropora species with colony diameter of 30 cm were the biggest colonies diagnosed in the work area

Figure 1. a seemingly dead Porites coral

Challenges ahead were related to considering the most appropriate harvesting, transporting, reattaching and monitoring methods and choice of the best reattachment site. The reception site was predetermined based on similarities in water depth and movement, (possible) reef type, and location (exposed or sheltered) [1]. Signs of growth of new

corals have been witnessed at the reattachment area. The success rate of the operation can be determined by conducting survey campaigns and monitoring the current coral cover, healthiness of the corals, and growth rate of different species.

3. TURBIDITY MANAGEMENT

Coastal development projects, including dredging and land reclamation could come with sever environmental constraints and require mitigation measures [4]. In this project, the work area was located in the vicinity of the intake of Kish desalination plant. Thus, turbidity management was of high importance. In addition, in order to limit spreading of turbidity silt screens were installed around the reclamation area. Also an online turbidity measurement station was set-up by at the desalination intake location. By regular monitoring, in case turbidity passed trigger levels specific management plans were applied or the operation was suspended.

This paper includes detailed description on practical and operation phases of the project. Also environmental and engineering achievements of the project are described. This project has been the first reef relocation project in the country and achievements from this project could be applied in future similar situations.

4. REFERENCES

[1] Marsalek D.S., *Impact of dredging on a subtropical reef community*, Southeast Florida, USA,1981.

[2] Pars Geometry Consultants, "Environmental Impact Assessment", Kish free zone authority, Tehran, Iran, 2009, pp35-49

[3] Rezayi H. "Studies on health situation of the coral reefs in the deposition site at the north east of Kish Island", 2012.

[4] Van der Schrieck G.L.M., *Dredging Technology*, Delft, The Netherlands, 2009.

A DECISION SUPPORT SYSTEM for ANALYZING the PORT CAPACITY by SYSTEM DYNAMICS APPROACH

Rassam Moshrefi[1], Bahare Ansari[2]

1) Department of Economics, Shahid Beheshti University, Tehran, Iran, r-moshrefi@sbu.ac.ir
2) The university of economic science, Tehran, Iran, bahare_ansari@yahoo.com

1. Introduction

In recent decades, globalization has increased trade volume. As a result, the importance of transportation infrastructures has improved so that the governments take advantage of globalization. Seaports, as crucial nodes in converting efficient marine transportation to other modes, are vital infrastructure that should be managed wisely. Keeping up ports capacity to the ongoing demand always is a need. But port capacity is a complex issue. On one hand, there are different types of cargos and ships to be load and handled. On the other hand, Port operation for each type of cargo depends on many different elements and there are feedback relations among them. Therefore port capacity is a complex nonlinear dynamics concept that should be studied by an appropriate approach. [1]

In this paper, the general aspects of SD modeling and its consistency with the port's decision environment have been discussed. Moreover, an integrated system dynamics model which simulates the seaport transportation system has been developed.

2. System thinking

A considerable part of academic sciences, heretofore, have been formed on the basis of analytic thinking. According to this approach, the first step in problem solving is decomposition of the problem into its building parts. Afterward, it is assumed that solving the problem in every part would lead us to solving the whole problem. But success in this procedure is totally depended on two prerequisites. The first is that those decomposed parts have not any bilateral or multi-lateral interconnections. And the second is that relationships between parts should be linear. Just based on these two prerequisites, it is logical and mathematically rational to apply decomposition of the problem for solving it.

But these prerequisites do not exist in the phenomena called system, an interdependent and interrelated purposeful structure. Considering their operational and management mechanism, port are typical examples of systems, therefore system thinking is needed in case to appropriately manage them. [2]

In spite of just about 60 years of introduction of system thinking in academic area, this approach, because of its effectiveness to improve the quality of organization management has gradually dominated the studies of organizations. A brief review of most attractive consultancy services- BSC, Strategic management, TQM, management flights simulators to just mention - shows the need of management consultancy market to these system thinking based services. [3]

3. The Seaport System

System Dynamics (SD), as Peter Senge defines it in its well-known book fifth discipline "a necessity for learning organizations", is a major field evolved based on system thinking. [4]

Considering the dynamic interconnection between the port's subsystems, it seems to be a typical example of an interconnected and complex system that creates a suitable platform for this modeling methodology to be applied at decision making levels.

Much of the art of system dynamics modeling is representing the feedback loops of a system which is the source of dynamicity in it. The maritime transportation system has to support the trade relations in a country and these relations are also influenced by maritime capacity. This is the major feedback loop that determines the dynamics of the ports' system. [5]

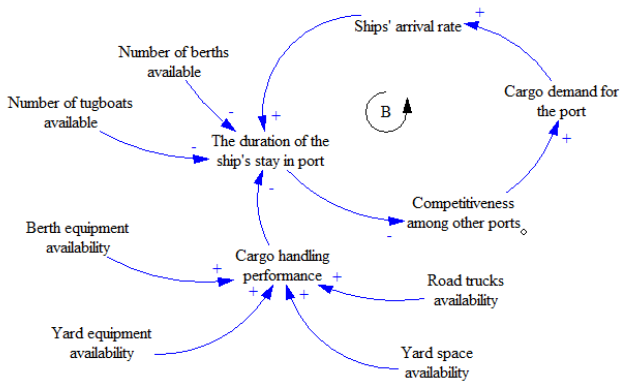

Figure 1. Causal loop diagram of the port performance

As Khaled and Bell (1994) has stated, system dynamics provides an entire system approach to transport management and offers particularly designed tools for calibration, optimization and policy analysis which all contribute to the underlying transport system. [6]

4. Model description

The main questions that the ports and maritime mangers confront with, is that whether the ports are able to satisfy the estimated demand or not? And if not, what is responsible for that and what investment can lead us to achieve the goals and implement the strategies? Which facility and how many of it is required for satisfying the demand? Is the infrastructure can support the new facilities and estimated demand? If not, how should it be improved? How does the changes in ship size or cargo packing influence the port's operation? How does the improvement of the productivity in one module affect the whole system?

To build the model, 87 stocks, 100 flows and 257 converters has been employed in seven modules that are Ship Arrival, Tugboats and Pilots, Berths, Berth Cranes, Yard Cranes, Yard-Warehouse Spaces and Gates. The model can be applied as a Decision Support System for the commercial ports of Iran.

The fundamental flow in the model is the flow of cargoes which goes throughout the port. The cargo flows have different formats in each section of the model and these formats can be converted into each other. Ships flow is the major format of cargo flow that is employed for modeling the process of anchoring, berthing and departure of the ships. Trucks flow is another format of cargo flow that is employed for modeling the process of cargo transportation toward and away from the port.

For ease of use, the model contains a dashboard layer to be used in the process of sensitivity analysis. By this means, the model can be used for finding gaps between real and desired capacity and modify port investment plan more efficiently and proactively so that it can satisfy the demand of cargo handling in coming years.

5. References

[1] Christiansen, Marielle, et al. "Maritime transportation." Transportation 14 (2006): 189-284.

[2] Gharajedaghi Jamshid, 1999, System Thinking, Managing Chaos And Complexity, A Platform For Designing Business Architecture, Butterworth- Heinemann

[3] Coyle, R, 1985, The Practice of System Dynamics: Milestones, Lessons and Ideas from 30 Years of Experience, System Dynamic Review, 1(1), 81-91

[4] Belly and P. Senge, 1980, System Dynamics and Scientific Method in Renders, Walthman, MA: Pegasus Communication

[5] Sterman John, 2000, Business Dynamics: System Thinking and Modeling For Complex World, Mc Graw Hill Higher Education

[6] Abbas, Khaled A., and Michael GH Bell. "System dynamics applicability to transportation modeling." Transportation Research Part A: Policy and Practice 28.5 (1994): 373-390.

HORMOZGAN PROVINCE BEACH AND SHOREFACE MORPHODYNAMIC CLASSIFICATION

M. Raghebi[1], M. Allahyar[2], H. Sadeghian[3], S.M. Siadatmousavi[4] and M. Haghighat[5]

1) Coastal Engineer, Sazeh Pardazi Iran Consulting Eng. Co., Tehran, Iran, m.raghebi@sazehpardazi.com
2) General Director of Coastal and Port Engineering Department of Ports and Maritime Organization (PMO), Tehran, Iran, allahyar@pmo.ir
3) Senior Coastal Engineer, Sazeh Pardazi Iran Consulting Eng. Co., Tehran, Iran, h.sadeghian@sazehpardazi.com
4) Assistant Professor, Iran University of Science and Technology, Narmak, Tehran, Iran, siadatmousavi@iust.ac.ir
5) Expert of Coastal and Port Engineering Department of Ports and Maritime Organization (PMO), Tehran, Iran, mhaghighat@pmo.ir

1. Introduction

The study of coastal systems evolution is an important issue for a proper coastal management and planning of beaches. For this reason, morphodynamic classification of the beach plays a crucial role in forecasting changes in beach morphology, when dealing with coastal management.

The classification should be based on the mutual interaction of all hydrodynamic and morphological parameters (i.e. wave climate, tidal range, mean grain size of sediments, and beach shape) in order to provide a complete description of the physical processes occurring in the coastal areas and affecting the beach response. Indeed, the beach is a system that dynamically responds to a wide range of hydrodynamic and morphologic processes.

The aim of this study is to determine the beach types that occur in Hormozgan Province coasts. Accordingly, the beach types in some sample points along the Hormozgan Province coastlines have been reported in this article.

Based on field measurements in Australia, Wright and Short (1984) presented a model of shoreface morphodynamic. The dimensionless fall velocity Ω is utilized in their model to classify wave-dominated microtidal beaches [7]:

$$\Omega = \frac{H_b}{w_s T} \quad (1)$$

Where H_b = breaking wave height, w_s = sediment fall velocity, and T = wave period. The Ω parameter indicates whether reflective ($\Omega < 1$), intermediate ($1 < \Omega < 6$), and dissipative ($\Omega > 6$) surf zone conditions prevails. Intermediate beaches are subdivided into four distinct types: (1) longshore bar-trough; (2) rhythmic bar and beach; (3) transverse bar and beach; (4) ridge and runnel or low tide terrace [7].

Masselink and Short (1993) presented another model based on both Ω and the non-dimensional relative tide range parameter (RTR) to classify more tide dominated beaches [2]:

$$RTR = \frac{TR}{H_b} \quad (2)$$

Where TR = spring tide range. The RTR parameter indicates the relative importance of swash, surf zone and shoaling wave processes in determining profile morphology [2].

The Masselink and Hegge (1995) presented morphodynamic characteristics of the mixed wave – tide beaches (meso- and macrotidal beaches, $3 < RTR < 15$) that generally fall into three types [1].

Short (1999) presented a simplified version of the model proposed by Messelink and Short (1993) and consists of seven major beach types that fall into three broad groups, depending on the value of RTR [4].

Short (2006) based on parameter RTR classified the Australian coast into three beach types: (1) Wave-dominated; (2) Tide-modified; (3) Tide-dominated. Wave-dominated beaches occur where $RTR < 3$. They consist of the six wave-dominated beaches types of Wright and Short (1984). Tide-modified beaches occur in areas of higher tide range exposed to persistent waves. These beaches are with an RTR range of between 3 to 4 and 10 to 12, which is in general agreement with the 3 to 15 range suggested by Masselink and Short (1993). They can be classified into three beach types: reflective plus low-tide terrace, reflective plus low-tide bar, and rips and ultradissipative.

Tide-dominated beaches occur in areas of higher tide range and very low waves, with a lower RTR boundary of about 12 and an upper boundary of about 50, beyond which they grade into tidal flats. They can be classified into four beach types: reflective plus sand ridges, reflective plus sand flats, reflective plus tidal sand flats, and reflective plus tidal mud flats [5].

Based on tidal range, the beaches are classified into two general categories in CEM (2006): high tidal range (>2m) and low tidal range (<2m) coasts. Macrotidal beaches (>2m) are divided into three groups based on gradient, topography, and relative sea-swell energy: Group 1 - High wave, planar, uniform slope; Group 2 - Moderate wave, multi-bar; and Group 3 - Low wave beach and tidal flat. Microtidal beaches (<2m) are divided into two different categories. Where wave breaker height is greater than 0.5m, the microtiadal beaches are classified based on Wright and Short (1984) model. Where $H_b < 0.5m$,

This article is retrieved from scrutinizing the ICZM plan for Hormozgan Province

microtiadal beaches are entitled as “Reflective beach and tidal (sand) flat”. Beach type classification in CEM (2006) is illustrated in ***Figure 1*** [6].

2. Methods and Data

In this study, Hormozgan province beach types are determined according to CEM (2006) and Short (2006) classifications. The results of the Hormozgan province beach and shoreface morphodynamic classification are presented here in five sample points. The study area and locations of sample points along the Hormozgan province coastlines are presented in ***Figure 2***. This study has been done as part of the Hormozgan Integrated Coastal Zone Management (ICZM) project and its results are used for shoreline management plan (SMP) studies. The required data including mean tidal level, wave climate, cross-shore profile and the sediment grain size were obtained from the results of “Monitoring and Modeling Studies of Coastal Zone of Hormozgan Province” project [3].

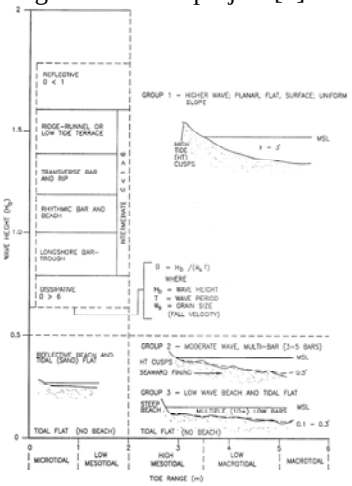

Figure 1. Micro - to macrotidal beach and tidal flat systems [6]

Figure 2. The study area and the location of the sample points investigated along the Hormozgan province coastlines

3. Results and discussion

Hormozgan province beaches have been classified depending on wave, tide, and sediment characteristics. The low mesotidal ($1<TR<2$) and high mesotidal ($2<TR<3.5$) beaches predominate along the Hormozgan province coasts. Based on CEM (2006) classification, Javad Al-Aemmeh beach with $TR<2$ and $H_b>0.5$ is of dissipative type ($\Omega>6$), whereas Lengeh with $TR<2$ and $H_b<0.5$ is a reflective beach and tidal (sand) flat. Besides, Bahl beach with $TR>2$ and $H_b>0.5$ is of Group 1 type, whereas Sirik and Khamir beaches with $TR>2$ and $H_b<0.5$ are categorized in Group 2 and Group 3, respectively. It should be mentioned that as wave energy decreases, macrotidal beaches (>2m) eventually grad into tide-dominated tidal flat. Accordingly, Khamir beach with a very low wave breaking height could also be considered as tidal flat (no beach) type. Based on Short (2006) classification, Javad Al-Aemmeh and Bahl beaches with $RTR<3$ are of wave-dominated types, whereas Lengeh and Sirik beaches with $3<RTR<12$ are tide-modified ones. Besides, Khamir beach with $RTR>12$ is a tide-dominated one. The summary results for five sample points are presented in ***Table 1***.

Table 1. Beach types in some sample points

Location	TR (m)	H_b (m)	D_{50} (mm)	$\Omega = H_b/W_s T$	Beach Type (CEM, 2006)	$RTR = TR/H_b$	Beach Type (Short, 2006)
Javad Al-Aemmeh	1.26	0.59	0.141	6.40	Dissipative	2.11	Wave-dominated
Lengeh	1.73	0.38	0.166	-	Reflective Beach and Tidal (Sand) Flat	4.53	Tide-modified
Khamir	3.36	0.16	0.066	-	Group 3	21	Tide-dominated
Sirik	2.37	0.46	0.074	-	Group 2	5.1	Tide-modified
Bahl	2.1	0.83	0.140	-	Group 1	2.5	Wave-dominated

4. Conclusion

Hormozgan province beaches have been classified based on wave, tide, and sediment characteristics. According to the results of the Hormozgan province beach and shoreface morphodynamic classification, different beach types have been identified that cover the entire Hormozgan province coasts. The length of the Hormozgan province coast and its wide range of wave, tide and sedimentary regimes have resulted in the formation of different beach types. They can be classified into four main categories ($TR<2$ and $H_b>0.5$; $TR<2$ and $H_b<0.5$; $TR>2$ and $H_b>0.5$; $TR>2$ and $H_b<0.5$) based on CEM (2006) and three categories of wave-dominated, tide-modified and tide-dominated beaches based on Short (2006). These beach types can occur in similar wave-tide-sediment environments. The framework presented in this paper can be employed for identifying the beach types throughout the Persian Gulf and Oman Sea coastlines. Besides, the results of this study can be used for coastal management and spatial planning of beaches such as shoreline management plan (SMP).

5. References

[1] Masselink, G. and Hegge, B J., "Morphodynamics of meso- and macrotidal beaches: examples from central Queensland, Australia", *Marine Geology*, 129, 1995, pp. 1-23.

[2] Masselink, G. and Short, A.D., "The effect of tide range on beach morphodynamics and morphology: a conceptual model", *Journal of Coastal Research*, 9, 1993, pp. 785–800.

[3] Sazeh Pardazi Iran consulting Eng. Co., "Hormozgan province coasts classification based on hydrodynamic characteristics", *Hormozgan Integrated Coastal Zone Management Project, First Edition*, March 2016.

[4] Short, A.D. (ed.)., "Beach and shoreface morphodynamics", *Chichester, United Kingdom: John Wiley & Sons*, 1999, p. 379.

[5] Short, A.D., "Australian beach systems-nature and distribution", *Journal of Coastal Research*, 22, 2006, pp.11–27.

[6] US Army Corps of Engineers., "Coastal Engineering Manual (CEM)", 2006.

[7] Wright, L.D. and Short, A.D., "Morphodynamic variability of surf zones and beaches: a synthesis", *Marine Geology*, 56, 1984, pp. 93–118.

This article is retrieved from scrutinizing the ICZM plan for Hormozgan Province

INTEGRATING MONITORING DATA INTO ENVIRONMENTAL HEALTH REPORT CARDS IN THE US AND BRAZIL

David A. Nemazie and William C. Dennison

University of Maryland Center for Environmental Science, Cambridge, Maryland, USA 21613
Tel: +1.410.221.2006 Fax: +1.410.228.3843
e-mail: nemazie@umces.edu, presenting author

1. Introduction

Based upon monitoring data, environmental report cards are an emerging technique used to assess and report on the ecosystem health of a region. Providing rigorous, quantitative assessments provides an accountability that is increasingly required by various funders that support environmental protection and restoration efforts. In addition, the transparency that is created by generating color-coded metrics, maps, graphs and diagrams used in environmental report cards is also a growing expectation on behalf of funders, government and non-government organizations, and the public.

A five step process of developing report cards can be used to assess progress in achieving these objectives: 1) conceptualization, 2) choosing indicators based on monitoring data availability, 3) defining relevant thresholds, 4) calculating scores and 5) communicating results. Each of these steps will be discussed in turn using the Chesapeake Bay and Guanabara Bay as examples of water bodies that include large ports.

Chesapeake Bay is the largest estuary in North America with an extensive watershed that includes a population of 16 million people who live in a portion of five States, and includes two major ports – the Port of Norfolk and the Port of Baltimore. The Chesapeake Bay report card has been done annually for the last 10 years and while scores were calculated back to when the Chesapeake Bay Program monitoring system was established in the mid1980's. Guanabara Bay has a watershed population of six million people, all within the State of Rio de Janerio - the third largest port in Brazil. We are currently working with a group of partners from multiple sectors to develop the first Guanabara Bay report card which is expected to be released in late 2016.

2. Methods

Conceptualization: Report cards need a conceptual framework to underpin the reporting effort. Conceptual diagrams can be used to communicate this framework and these diagrams used in the communication of report card results. Some crucial decisions need to be made at the outset of a report card program, including the geographic size and scope of the reporting regions, the reporting time intervals and integration periods for reporting and the types of indicators (e.g., environmental pressures, state of environment, management responses).

The Chesapeake Bay report card uses 15 reporting regions including several tributaries while the Guanabara Bay has six watershed and five Bay reporting regions (Figure 1), for a total of 11 reporting regions. The geographic data density is a consideration in creating reporting regions.

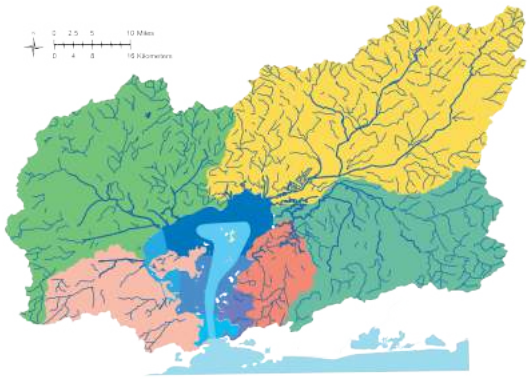

Figure 1. Guanabara Bay reporting regions

Choosing indicators: Selecting indicators that convey meaningful information and be measured reliably typically involves an iterative process. Streamlining the data collection and analyses to make them timely and useful requires a concerted effort.

The Chesapeake Bay report card uses data from 180 monitoring stations and has 11 indicators (Table 1). The initial Guanabara Bay report card will likely have at least 8 indicators while a few more are still being reviewed (PAH concentration, litter collected by eco-barriers and eco-boats).

Defining thresholds: After selecting indicators, several decisions are required for developing a report card. Pass/fail thresholds require large data sets and multiple thresholds appear to work better where using limited data sets. There are ecological thresholds that can be determined through scientific studies, but also there are various management thresholds that can be used based on goals and objectives created by the regulatory agencies or by conservation targets.

Table 1. Indicators for Chesapeake and Guanabara Bays.

Indicator	Chesapeake Bay	Guanabara Bay
DO	mg/l	mg/l
BOD		mg/l
N	mg/l (TN)	mg/l (DIN)
P	mg/l (TP)	mg/l (orthoP, TP)
Chl a	µg/l	
Water Clarity	Secchi depth	NTU
Aquatic Grass	% of goal	
Benthic comm	meets IBI	
Blue crab	% of goal	
Bay anchovy	% of goal	
Stripped bass	% of goal	
Fecal Coliform		MPN
Total Dissolved Solids		mg/l

Calculating scores: Indicator scores can be calculated by comparing the indicator metrics to the various thresholds established. The percent attainment of indicators provides a common reporting framework that allows various water quality, living resources or habitat indicators to be compared with one another. These individual scores then need to be rolled up into an overall index. The method of aggregating data needs to be clearly defined, and often in developing report cards, back-calculating scores using historical data helps test and refine the indices.

Communicating results: Communication of report card results provides a regular opportunity to engage with a wide public audience on the status of a region. This communication can be effective using mass media outlets and events, elected officials and designated science communicators. The communication strategy needs to established to maintain credibility through a rigorous and transparent process of developing and communicating results. The printed and online materials for environmental report cards use a variety of color schemes, rating systems, diagrams, maps and photographs to communicate to a broad audience, based on principles of effective science communication (Dennison et al. 2007).

A hierarchy of report card communication products can be instituted to address different audiences. A relatively simple report card with overall grades or scores can provide key messages to a broad public audience. A more detailed regional analysis and indicator by indicator comparison can target resource managers, agencies and non-government organizations. And finally, the data used to provide the assessments with the analytical methods can be made available through online or printed documents that allows scientific and media scrutiny.

3. Results

Report card credibility relies on independent rigorous assessments by environmental scientists. UMCES has been collaborating with a wide variety of partners on developing various report cards.

Chesapeake Bay, USA: This report cards has tracked 15 reporting regions since 2006, with interactive trend graphics for indicators and reporting regions. Results for previous years have been back calculated. It takes several months after the monitoring year is completed to calculate scores and finalize the report card (Figure 2).

Figure 2. Chesapeake Bay reporting regions and scores

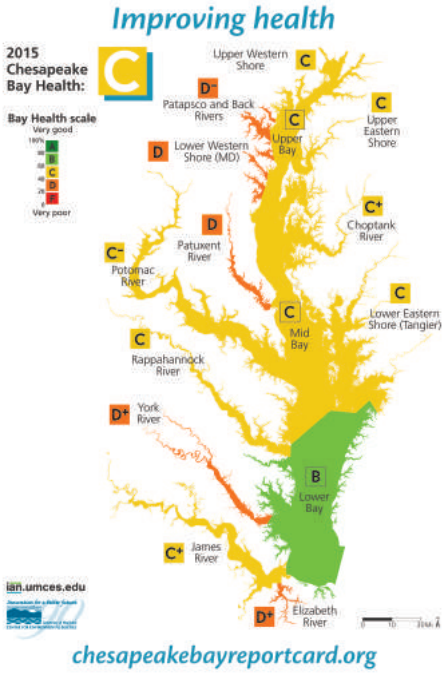

Guanabara Bay, Rio de Janeiro, Brazil: This inaugural report card is currently in development with at least eight indicators and 11 reporting regions. A series fo workshops have been conducted with key stakeholders including resource managers, scientists, and NGOs.

4. Conclusions

Environmental report cards can be an important tool for effective management of natural resources. Report cards utilize environmental monitoring data and can guide the prioritization of ongoing monitoring efforts. The goal of environmental reporting is to provide effective feedback as to the efficacy of management actions so that the often considerable resources devoted to environmental protection and restoration are used efficiently (Dennison, 2008). The annual release of the Chesapeake Bay report card has been an important tool that helps resources managers and the public calibrate their restoration planning and communication efforts.

References

Dennison, WC, Lookingbill, TR, Carruthers, TJB et al., 2007. An eye-opening approach to developing and communicating integrated environmental assessments. Front. Ecol. Environ. 5(6): 307-315

Dennison WC (2008) Environmental problem solving in coastal ecosystems: A paradigm shift to sustainability. Estuarine, Coastal and Shelf Science 77(2):185–196

EVACUATION SIMULATION FOR A VULNERABLE COASTAL COMMUNITY IN JAKARTA

Takahito Mikami[1], Hiroshi Takagi[2], Miguel Esteban[3], Daisuke Fujii[2], and Shota Kurobe[2]

1) Dept. of Civil and Environmental Engineering, Waseda University, Tokyo, Japan, t.mikami@aoni.waseda.jp
2) School of Environment and Society, Tokyo Institute of Technology, Tokyo, Japan, takagi@ide.titech.ac.jp
3) Graduate School of Frontier Sciences, The University of Tokyo, Chiba, Japan, esteban.fagan@gmail.com

1. Introduction

Coastal communities in developing countries are faced with an increasing risk of coastal floods because of various factors, such as sea level rise, coastal erosion, poor defense structures, and land subsidence (see Figure 1). In addition, an increase in the number of coastal residents due to population growth means that the number of residents without disaster experience and awareness is also increasing. To mitigate the potential damage due to future flood events it is necessary for coastal engineers and planners to evaluate the risk to each coastal community and inform local residents of the results of such exercises.

The authors have been investigating one coastal community in Jakarta, the capital city of Indonesia, as a typical coastal community which is at risk of coastal floods (see [1] and [2]). The results of the investigation so far show that proper actions against possible flood scenarios, such as raising dykes, planting mangroves, and preparing evacuation plans, are needed to lower the potential overall risks. In the present paper, an evacuation simulation of how residents of the community are likely to behave in the event of flooding was carried out, which can be considered as a useful tool for evacuation planning.

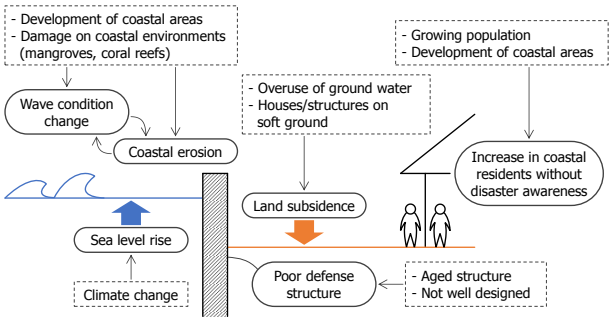

Figure 1. Various factors behind the increasing risk of coastal floods to coastal communities in developing countries.

2. Survey of Pedestrian Paths

The community investigated is located in Pluit District in the northern part of Jakarta city. Rapid coastal and port development can be observed in this district, but the community still preserves original characteristics of poor settlements in the city: high population density and low-rise houses and stores. According to the authors' own topographical survey, the ground level of the community is more than 2 m lower than the high tide level [2]. However, the community is only protected by a thin concrete coastal dyke (see Figure 2(a)). The authors fear that if unusual high tides occur and/or the dyke is breached the community could be affected by severe coastal flooding. One of the actions required for mitigating the consequences of such an event is to develop an efficient evacuation plan.

To analyze the evacuation behavior of the residents in this community, the authors first surveyed the network of pedestrian paths. It is difficult to construct an actual pedestrian path network using a satellite image, such as an image from Google Earth, because some of the paths are covered by roofs or are too narrow to show (see Figure 2(b)). Thus, the authors constructed the paths network by surveying the entire network with a handheld GPS instrument (Montana 650, Garmin). Since the width of the paths is expected to influence evacuation behavior, the width of each path was measured using surveying staffs.

Figure 2. Community Investigated, (a) Coastal dyke protecting the settlement, (b) Narrow pedestrian paths inside the settlement.

Figure 3 shows the pedestrian paths network obtained from the authors' field survey. The network contains 71

nodes (representing an intersection or a point where a path curves) and 88 links (representing a pedestrian path with a constant width). The paths in the west and north sides are relatively wide (widths of 4.5-5.5 m), which allow cars to pass. On the other hand, the paths inside the community are very narrow (0.5-2.5 m), and often have many obstacles preventing the smooth movement of pedestrians, such as bikes, barrels, or grocery supplies.

Figure 3. Pedestrian paths network overlaid on a satellite image from Google Earth.

3. Evacuation Simulation

In this study a multi-agent simulation platform, artisoc [3], was used for conducting the evacuation simulation. With artisoc the evacuation behavior of the residents can be modeled by putting moving agents on the pedestrian path network.

In the evacuation simulation 65 of the nodes which faced houses were selected as initial locations for the residents. Then, 5 agents representing residents were created at each of the selected nodes. Finally, the time required for all these agents to evacuate from the initial locations to an evacuation building was measured. A relatively strong building located in the southern end of the community was selected as the evacuation building.

According to Wills et al. [4], the mean walking speed of individuals is 1.47 m/s. However, the actual walking speed varies due to physical conditions (gender, age, etc.), group conditions (group members, moving direction, etc.), psychological conditions, and environmental conditions. Thus, it is necessary to include these conditions in the evacuation simulation. In the present simulation the crowd density (person/m^2) was considered to be an important factor for the walking speed, and the relationship of the crowd density and the walking speed used in Kimura and Kobayashi [5] was applied.

4. Results and Discussion

The time required for the evacuation using the surveyed widths of the pedestrian paths was measured to be 609 seconds. It was found that a high crowd density made the walking speed lower in the paths in the east side of the community. Simulations with more limited effective widths of the paths (because of the obstacles present) were also carried out by assuming a 0.25 m and 0.5 m in the effective width of each that was over 1.0 m wide. The time required for the evacuation with these limited widths was 643 and 769 seconds, respectively. Thus, the results show that it is important to make sure that pedestrian paths are clear of any obstacles to facilitate evacuation in the case of coastal flooding in this community.

5. Conclusions

Evacuation simulations can be a useful tool to determine the appropriateness of evacuation routes and shelters, and identify specific problems related to evacuation in a given coastal community. Further studies for different scenarios considering different age composition, time frame (daytime or night), etc. together with the findings from the authors' other recent research in the area [6 and 7], are needed to illustrate proper countermeasures that can increase the overall resilience of the community to coastal flooding.

6. Acknowledgement

Funding for this research was supported by the Environment Research and Technology Development Fund (S-14) of the Ministry of the Environment, Japan.

7. References

[1] Takagi, H., Esteban, M., Mikami, T., and Fujii, D., "Projection of coastal floods in 2050 Jakarta", *Urban Climate*, 2016.

[2] Takagi, H., Mikami, T., Fujii, D., and Esteban, M., "Mangrove forest against dyke-break induced tsunami in rapidly subsiding coasts", *Nat. Hazards Earth Syst. Sci. Discuss.*, 2016.

[3] Yamakage, S., *Modeling and Expanding Artificial Societies: Introduction to Multi-Agent Simulation with artisoc*, Kozo Keikaku Engineering Inc., 2009.

[4] Willis, A. et al., "Human movement behavior in urban spaces: implications for the design and modelling of effective pedestrian environments", *Environmental Planning B: Planning and Design*, 31, 2004, pp. 805-828.

[5] Kimura, K and Kobayashi, K., "Analysis of the Nishinomiya large scale tsunami evacuation exercise using a multi-agent model", *Journal of Japan Society of Civil Engineers, Ser. B1 (Hydraulic Engineering)*, 71, 4, 2015, pp. I_1375- I_1380.

[6] Takagi, H., Esteban, M., Mikami, T., Fujii, D., and Kurobe, S., "Mechanism of coastal floods in Jakarta: the need for immediate action against land subsidence", *The Proceedings of the ICOPMAS 2016*, Tehran, Iran, 2016. (submitted)

[7] Esteban, M., Takagi, H., Mikami, T., Aprilla, A. Fujii, D., and Kurobe, S., "Awareness about tsunamis and dyke-break induced tsunami in low-lying coastal communities in Jakarta", *The Proceedings of the ICOPMAS 2016*, Tehran, Iran, 2016. (submitted)

A METHOD OF CELLULAR PHONE MEDICAL EXPERT SYSTEM BASED ON WIRELESS SENSOR NETWORKS FOR OFFSHORE APPLICATIONS IN IRAN

Mohammad Reza Hedayati[1], Hamid Reza Najafi kapourchali[2]

1) University of applied and science, Faculty of applied post and Telecommunication ,Tehran,Iran,hedayati.rov@gmail.com

2) University of applied and science, Faculty of applied post and Telecommunication ,Tehran,Iran,ha22132004@yahoo.com

ABSTRACT

Offshore healthcare access affordability and quality are common problems all over the world.

The present work surveys the principals and criterion off Ehealth applications incorporating Mobile technology and expert systems for offshore and near to the shore applications. In this paper we look at specific application and proposed innovation on remotely accessed medical services based on mobile phone networks in Iran and also discusses how mobile can transfer healthcare in the proposed architecture for offshore applications. The nodes of the proposed experimental wireless sensor network are created by using a combination of Continuous Glucose Monitoring (CGM) sensors and Blood Pressure (BP) Sensor. The proposed remote monitoring system is a wireless sensor network with the nodes of the network installed in the patients' work place through dedicated mobile phones. These nodes are then connected to a central node located at a hospital through an Internet connection. In this paper it has been argued that m-health can helps frontline offshore workers health and also discuss how healthcare providers expend their rich and interactions**.**

1.INTRODUCTION

Offshore installations are characterised by the symbiosis of workers of different fields in a surrounding and condition that is isolated and hazardous. Prevention of major accidents is vital to effective management of risks in this type of environment. Healthcare technology has been identified as a means to improve quality, efficiency and patient safety in Health organizations and hospitals. Detailed measurements related to the path physiologic state of each patient are provided by an impressive array of technologically sophisticated instrumentation, in order to identify problems early and to monitor patients remotely through new technologies. Global mobile traffic approximately has doubled for the fourth year in a row at the same time wireless sensor networks (WSN) increasingly attracted attention for health care application. Device sales in I.R.Iran are expected to grow from 75 million clients in 2016 to 112 million clients in the next two years.

Ehealth supports services and activities facilitating the supply of health-related goods and services.

EHealth also encompasses the provision of health related knowledge infrastructure and collaboration platforms and is dependent upon the existence of the necessary Information Technology (IT) infrastructure [1].

Accordingly, the ICT applications and tools for health maybe distinguished as following:

a) Better support and services for hardware and software in the field of health in the offshore.

b) Effects e-health in the offshore medical services.

c) Training health professionals in this field work and use of professionals to link health system and information technology.

d) IT infrastructure for the deployment of e-health, namely the physical networks allowing connectivity, the devices supporting 'interoperability' of systems and technologies, as well as the necessary legal and regulatory framework related to security and confidentiality issues (secure transmission, secure processing, secure storage, authentication and data integrity)[1-4].

Compared to conventional health services the costs and cost effectiveness of Healthcare technology applications are understandably central concerns of decision makers. Remote Patient Monitoring RPM systems enable healthcare organizations to remotely monitor and manage pati ents with chronic conditions. RPM requires various sensors that transmit and store physiological data for review such as heart rate, blood pressure, body and skin temperature, oxygen saturation, respiration rate and ECG.

The sensor sends data using Ethernet, Bluetooth, Zigbee,Wi-Fi or 3G/GPRS protocols dependingon the specific contexts and requirements (distance, bandwidth and energy). In addition to distance and power limitations, Bluetooth master node can only control up to seven active slaves simultaneously in RPM systems. Since both Bluetooth and IEEE 802.11 devices use the same frequency 2.4 GHz ISM band, interference may lead to significant performan -ce degradation. These limitations may also affect RPM System Performance [1-4].

2.DEVELOPMENT OF EXPERT SYSTEM

Knowledge built in to an expert system may originate from different sources. The prime source of knowledge for developing an expert system should be the domain expert. To design and develop knowledge based expert system, the specific knowledge domain or the subject domain must be acquired. The knowledge domain is to be organized so that the information can be structured in the computer program for effective use. In this respect, a knowledge engineer usually obtains knowledge through direct interaction with the expert. A typical diagnosis system shown as below consists of a sensor assembly which provides the fault signal to a signal processing unit, which further sends its result to be analyzed by expert systems, where the corresponding fault is ultimately detected (see figure 1, 2).

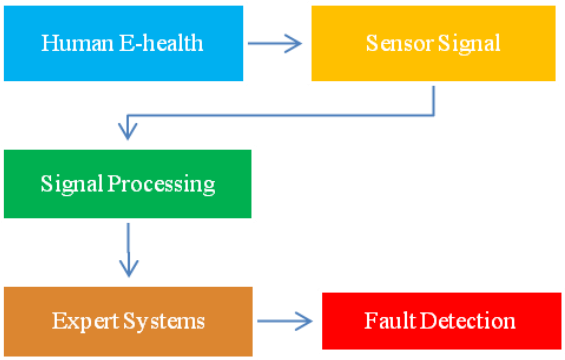

Figure 1.The fellow diagram of proposed expert systems of explanation fin health care application

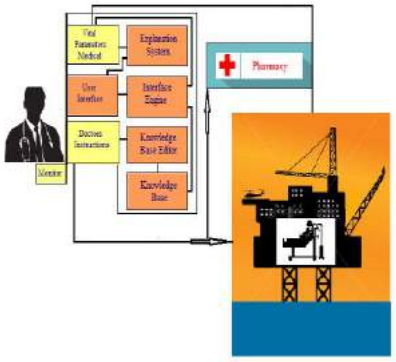

Figure2.Development of cellular phone medical expert system for a typical offshore application

3.E-HEALTH EXPERT SYSTEMS

Ehealth is the cost effective and secure use of information and communications technologies in support of health and health-related fields, including healthcare services, health surveillance, health literature, and health education, knowledge and research "Ehealth is an emerging field of medical informatics, referring to the organisation and delivery of health services and information using the Internet and related technologies. In a broader sense, the term characterizes not only a technical development, but also a new way of working, an attitude, and a commitment for networked, global thinking, to improve health care locally, regionally, and worldwide by using information and communication technology [1, 5].

Ehealth=Medicine+Communication+Information+ Society

Ehealth Expert Systems are expected to improve various aspects of healthcare like quality, cost efficiency, accessing by Improving diagnostic accuracy and treatment appropriateness Improving access to effective healthcare by reducing barriers created, for example, by physical location or disability;

- Facilitating patient empowerment for self-care and health decision making;
- Supporting the delivery of care tailored to individual patients, which enables more informed decision making based both on evidence and patient-specific data;
- Improving transparency and accountability of care processes and facilitating shared care across boundaries;
- Aiding evidence-based practice and error reduction;
- Improving cost- efficiency by streamlining processes, reducing waiting times and waste.

4.REFERENCES

[1] K. Vijaya Lakshmi1, Prof. M.Padmavathamma2 *1,2 Department of Computer Science, S.V. University, Tirupati, INDIA.* Diagnosis through Secured e-health Expert System International Journal of Recent Development in Engineering and Technology Website: www.ijrdet.com (ISSN 2347-6435(Online), Volume 1, Issue 3, December 2013)

[2] Erin Larsen-Cooper,etc "Scale Matters: A Cost-Outcome Analysis of an m-Health Intervention in Malawi" mary ann liebert,inc._vol.22.no.4_April2016 Telemedicine and E-health.

WATER EFFECTS ON HYSTERESIS CURVE WITH SEISMIC SOIL-STRUCTURE-INTERACTION

M. Shahmohammadi Mehrjardi[1], S.T. Tabatabaei Aghda[2]

1) M.Sc student, Islamic Azad University of Maybod, Iran, mohammadshahmohammad@gmail.com
2) Member of Road, Housing & Urban Development Research Center (BHRC), Bandarabas, Iran, taha.taba@gmail.com

1. Introduction

Hysteresis curve during earthquakes is affected by nonlinear Soil-Structure-Interaction (SSI). Regard to water can have a change result of soil, the effect of water on SSI for the marine structures is the fascinating subject.

In present paper, the Hysteresis curve of pile with superstructure is investigated by comparing with saturated soil and dried one. For these goals, analyses of a single pile in cohesive soil with nonlinear pier to ground motion have been performed and the consequences in Hysteresis curve have been exhibited. This complex system has been produced using Open System for Earthquake Engineering Simulation (OPENSEES) Software. By comparison to Soil-Structure-Water-Interaction, structure analysis parameters are changed by considering water.

2. Methods and Numerical Modeling

For the column structure, the section of a beam-column element is used. Fiber Element Section is available in OPENSEES, whose detailed information can be found in the OPENSEES User Manual [1].

2.1. Column-pile properties

A column-pile height is 40 meters, which is embedded in one layer of soft clay to a height of 30. Table 1 presents information for the column-pile examined in this study.

Table 1. ***Column-Pile Specifications***

Dimension and Reinforcement Properties	Longitudinal Rebar	Spiral (lateral reinforcement)
	38ф25	ф12@4cm
	Column Diameter (m)	Cover (cm)
	1.5	7
Material Properties (kg/cm2)	Unconfined concrete strength	Yield strength of steel
	280	2700

2.2. Ground Motion description

For dynamic analyses, Tabas 1978 (Dayhook station) set of record is selected with 0.32 PGA (g) and set contains the record without forward directivity. It has been recorded far to the strike-slip mechanism. Horizontal acceleration time history, which is used in this study, are shown in Figure 1.

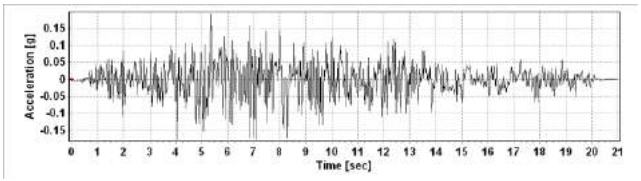

Figure 1. Ground motion Time history used in the analyses

2.3. The constitutive model of soft clay:

Yield by soil clay statuettes of multi-model simulation of the column-pile, the clay conducted as nonlinear hysteretic materials and has Mise's multi-faceted plastic deformation, which is demonstrated in Figure 2 [3-2].

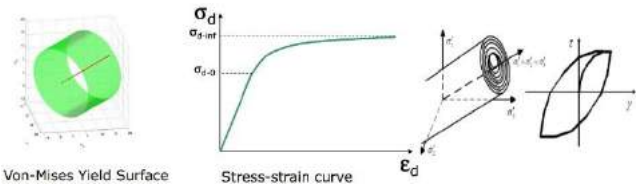

Figure 2. Von Mises multi-surface kinematic plasticity model

3. Soil-pile-structure system and adopted model

The mass at the center of the deck is 60 ton and the bedrock is confronted at -50 meters and is presumed to be rigid (figure 3).

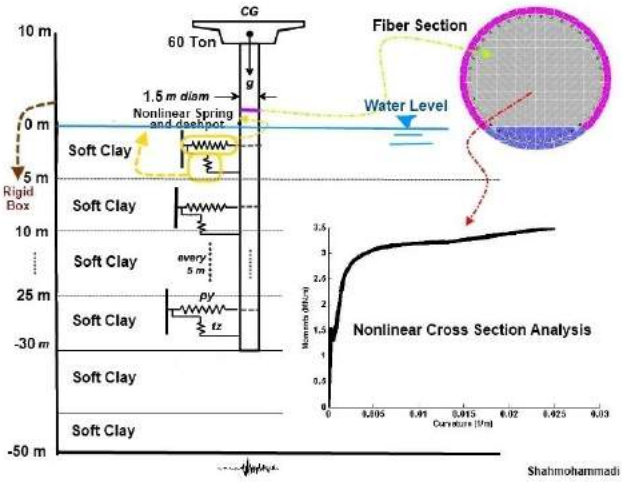

Figure 3. Assumed model in OPENSEES

4. Summary and conclusions

In this study, the numerical model has been used to replicate the soil-water-structure-interaction. The proposed model, which is based on the finite element method with the OPENSEES software, is applied.

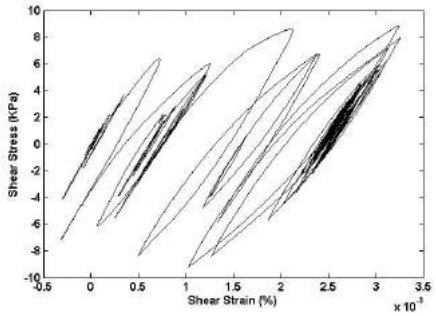

Figure 4. Shear stress vs. shear strain hysteretic response at dried clay at the depth of 38 meters

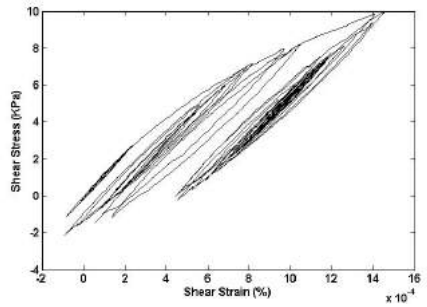

Figure 5. Shear stress vs. shear strain hysteretic response at saturated soil at the depth of 38 meters

Two typical shear stress versus shear strain of clay at the 38 meters depth are shown in Fig 4 and 5. Failure happened at a smaller maximum displacement, but with more cycles. Comparing two curves, the lateral axis of dried clay had less amount, and hence had smaller hysteresis loop. At the end of the analyses, the residual displacement corresponds to 400% agreement between saturated analysis values and dried analysis. In dried soil, the hysteresis loops are wide and the residual responses are separated (figure 4) but in saturated soil, the hysteresis loops are narrow and the residual responses are continued (figure 5).

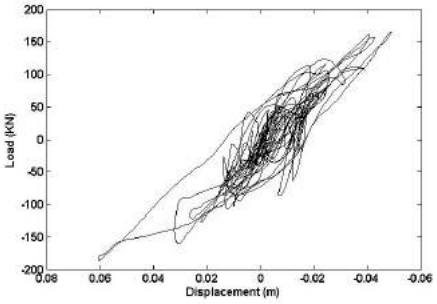

Figure 6. The load displacement hysteresis curve for the column-pile in dried clay

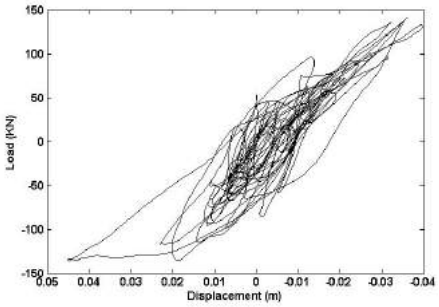

Figure 7. The load displacement hysteresis curve for the column-pile in saturated clay

Figure 6 and 7 plot the axial load-displacement response for the column. Figure 6 corresponds to the analysis with dried soil and the figure 7 corresponds to the saturated one. The maximum displacement of the bridge deck to the base of the column in dried clay is 6 cm and the maximum load is 160 KN (fig 6) but the maximum displacement of bridge deck in saturated clay is 4.5 cm and the maximum load is 149 KN (fig 7).

The following results were made based on the analyses obtained in this paper.

- When the cohesion soil is saturated, the residual displacement of soil is increased.
- Saturated soil brought the displacement and the load of the hysteresis down and changed hysteresis curve results.
- Considering water, displacement and load of structure are decreased, however, strain and stress of soil are increased.

5. References

[1] Mazzoni, S., McKenna, F., & Fenves, G. (2006). Open System for Earthquake Engineering Simulation User Manual. California: Pacific Earthquake Engineering Research Center, Berkeley University.

[2] Elgamal, A., Yan, L., Yang, Z., & Conte, J. (2008). Three-dimensional seismic response of bridge foundation-ground system. Journal of Structural Engineering, ASCE, 134(7), 1165-1176.

[3] Maula, B., XianZhang, L., Liang, T., & Pengju, X. (2011). 3D FEM Numerical Simulation of Seismic Pile-supported Bridge Structure Reaction in Liquefying Ground. Research Journal of Applied Sciences, Engineering and Technology 3(4): 344-355.

SURVEY RISK-BASED PRIORITIZATION METHODOLOGY IN CASE OF ACCIDENTAL SPIIL AT SEA OF HAZARDOUS AND NOXIOUS SUBSTANCES (CASE OF STUDY ASALUYEH PORT)

Moradpour Tayebi Emran[1], Atabak Nasrin[2]

1) Deputy of Marine Affairs, Asaluyeh ports and maritime authority, e.tayebi89@gmail.com
2) Pollution control officer, Bushehr port and maritime authority, nasrin.atabak@gmail.com

1. Introduction

For the purposes of the OPRC-HNS Protocol, HNS means any substance other than oil which, if introduced into the marine environment, is likely to create hazards to human health, to harm living resources and marine life, to damage amenities, or to interfere with legitimate uses of the sea. Such a definition will include:

- Noxious liquid substances described in Annex II of MARPOL 73/78 and the International Bulk Chemical Code (IBC Code).
- Dangerous goods described in the IMO Dangerous Goods Code (IMDG Code).
- Solid cargoes covered by the Code of Safe Practice for Solid Bulk Cargoes (BC Code)

Current estimates indicate some 2000 hazardous and noxious substances (HNS) are carried regularly by sea with bulk trade of 165 million tonnes per year worldwide. Incidents occurring in a port or coastal area can have potential and actual public health implications. A methodology has been developed for prioritization of HNS, based upon potential public health risks. The work, undertaken for the, aims to provide information for Asaluyeh port contingency planning and preparedness. HNS were assessed using conventional methodology based upon acute toxicity, behavior and reactivity. Tonnage was used as a proxy for likelihood, although other factors such as shipping frequency and local navigation may also contribute.

Analysis of 32 individual HNS identified the highest priority HNS as being those that present an inhalation risk. In conclusion a risk prioritization matrix has been developed to assess the acute risks to public health from the transportation of HNS. The study has developed a method for rapid prioritization of the acute public health risks from the transportation of HNS. The process can provide useful information for port operators, emergency planners and maritime agencies when developing strategic plans and contingency measures, such as response resources and training programmers

2. Methods

A risk prioritization process was developed based upon potential acute public health risks from HNS and aimed to provide strategic risk information for public health planning and preparedness. Acute health impacts were chosen as the key risk driver in order to reflect the type of incident scenario envisaged and because the principal aim of chemical incident planning and response is focused on immediate acute effects, which can have catastrophic impacts and make significant demands upon emergency services and resources. The risk prioritization process used conventional risk assessment Methodology, which can be described as: (Haimes, 2009)

Risk = Severity x Likelihood

Where: Severity is expressed as a function of toxicity and behavior of the chemical, whilst the Likelihood is expressed as a function of the (annual) tonnage. For the prioritization work undertaken, the terms of the equation comprised the following:

(Relative) Risk = (Chemical Toxicity) x (Behavior) x (Annual Tonnage shipped):

Similar risk assessments have included shipping frequency (CEDRE, 2004; CEFAS, 2009) and this was included as a function of likelihood leading to a revised risk prioritization equation as below;

(Relative) Risk = (Toxicity x Behavior) x (Annual Tonnage x Frequency shipped)

Table 1. Likelihood scores (based upon tonnage shipped) (CEDRE, 2004; National Contingency Plan for Marine Pollution from Shipping and Offshore Installations).

Annual tonnage (or cubic meters for gases)	Score
>1,000,000	**5**
100,000-1,000,000	**4**
10,000-100,000	**3**
1000-10,000	**2**
<1000 or no data	**1**

Table 2. Behavior scores for HNS (CEDRE, 2004), based upon Standard European BehaviourClassification System for Accidentally Spilled Chemicals (SEBC, 1991; (National Contingency Plan for Marine Pollution from Shipping and Offshore Installations)).

Category	Score	vapor pressure (kpa)^2	Solubility (mg/l)
Gas	**10**	**>101.3**	**<100,000**
Gas-dissolver	**9**	**>101.3**	**>100,000**
Evaporator	**8**	**> 3**	**<10,000**
Evaporator-floater	**7**	**>0.3**	**<1000**
Eva-dissolver- floater	**6**	**>0.3**	**1000-50,000**
Eva- dissolver	**5**	**>3**	**10.000-50,000**
Floater	**4**	**<0.3**	**<1000**
Floater-dissolver	**3**	**<0.3**	**<1000**
Dissolver	**2**	**<10**	**>50,000**
Sinker	**1**	**<0.3**	**<10,00**

3. Results

A total of 32 HNS have been assessed using this risk prioritization matrix and a top 13 priority chemical list has been established for the Asaluyeh port (Table 3). Many of the highest priority chemicals are those that are volatile or gaseous, reflecting their potential to result in wide dispersion in the environment and result widespread public health exposure. Several HNS also fell within the top 13 priority chemicals based upon their reaction products. For example several metal halides react with water to produce acids, increasing their subsequent severity rating as a result of increased toxicity and exposure risk from the daughter products. The majority of the top 13 HNS for the Asaluyeh port were also found to relate to chemicals transported in relatively large amounts (i.e.scoring 5 on the tonnage score).However, none of the highest scoring HNS for tonnage made the top 13, but were in the top 100.This was because such HNS typically scored lower for severity, for example methanol scores high for tonnage but only has moderate toxicity and dissolves in water which further reduces the potential for widespread public exposure. This illustrates that in terms of public health it is severity as a function of toxicity and the potential for exposure that are more important than tonnage.

Table 3. Top 13 priority HNS for Asaluyeh port based upon acute public health impact.

Chemical name	Toxicity Score	Behavior Score	Tonnage Score	Final risk score
Butene	**8**	**10**	**5**	**400**
Propion	**6**	**10**	**5**	**300**
Ethylene	**6**	**10**	**5**	**300**
Monomer styrene	**6**	**8**	**5**	**240**
Ammonia	**8**	**5**	**5**	**200**
Benzene	**6**	**4**	**5**	**120**
P-xylene	**6**	**4**	**5**	**120**
Methanol	**4**	**5**	**5**	**100**
Condensate	**6**	**2**	**5**	**60**
Mono-ethylene-glycol	**6**	**2**	**5**	**60**
Di- ethylene-glycol	**6**	**2**	**5**	**60**
Urea	**4**	**2**	**5**	**40**
Tri-ethylene-glycol	**6**	**2**	**3**	**36**

4.Thank

This Paper Published With Financial and Spiritual Support of Iranian Ports and Maritime Organization

4. References

[1] IMO. OPRC HNS Protocol. http://www.imo.org/OurWork/Environment/PollutionResponse/HNSPollutionResources/Documents/12605%20OPRC-HNS%20enviro%20LR.pdf, 2000

[2] Campbell D, Cox D, Crum J, Foster K, Riley A. "Initial effects of the grounding of the tanker Braer on health in Shetland". *BMJ 1993*;307:1251–5

[3] Haimes, Y. "On the complex definition of risk: a systems-based approach". *Risk Anal* 2009; 29:1647–54.

[4] CEDRE (Centre of Documentation, Research and Experimentation on Accidental Water Pollution). " Review of chemical spills at sea and lessons learnt". *A technical appendix to white paper for the interspill conference and 4th IMO R&D forum*;2009.[http://www.itopf.com/information-services/publications/papers/HNSpapers.html].

[5] Erkut Erhan, Ingolfsson Armann. " Transport risk models for hazardous materials": *revisited.Oper Res Le*tt 2005;33:81–9. [www.elsevier.com/locate/dsw].

[6] Mullai A, Paulsson U. "A grounded theory model for analysis of marine accidents". *Accid Anal Prev* 2011;43:1590–603.

[7] Mullai A, Larsson E, Norrman A. " A study of marine incidents databases in the Baltic Sea Region". *Int J Mar Navig Saf Sea Transp* 2009;3(3).

[8] CEFAS. "UK Risk Assessment for Hazardous and Noxious Substances"; 2009.

PROVIDE OF A GIS-BASED TOOL FOR SUPPORTING DECISION MAKING IN PORT DEVELOPMENT AND INFRASTRUCTURE PROTECTION - SAFEPORT

Jalal Karimi[1] , Mohammad Reza Allahyar[2]

1) Ports and Maritime Organization (PMO), Tehran, Iran, Jkarimi@pmo.ir
2) Ports and Maritime Organization (PMO), Tehran, Iran, mallahyar@pmo.ir

1. Introduction

Ports Critical Infrastructure consist of Mechanical and Electrical Infrastructure such as Energy, Water, Transport, and Chemical industry, Telecommunications and Research facilities. The main phases of Critical Infrastructure emergency management are referred to as Preparedness, Mitigation, Response and Recovery.

This paper presents a system for analysis of Port Critical Infrastructures, which offers integrated tools for target analysis, hazard scenario simulations and spatial analysis within a remotely accessible Web-based Geographic Information System. The system has been applied to research conducted in the port of Shahid Rajaee with the aid of blast accident or attack, chemical leakage and flood hazard scenarios, as well as a spatial density algorithm, which highlights events in which the proximity of infrastructures influences their susceptibility to an accident or attack. The paper also discusses the way in which the tools provided by the system aim to assist in the processes of infrastructure vulnerability assessment, mitigating discovered risks as well as strategic planning of port development.

2. Analysis of infrastructure vulnerability to a blast accident or attack

Thermal explosions are complex processes which involve chemical and physical reactions such as heating, expansion, and phase transition as well as transfer of heat and momentum. When appropriate data regarding the placed charges has been input, the Web GIS client sends it to the blast simulation module. The module generates a vector layer representing areas with different exposures to the pressure generated by the explosion. The results are shown in the window in the right part of Fig. 1.

Figure 1. Explosion in example point and that effects in adjacent areas.

3. Analysis of the effects of a chemical vapor cloud on the neighborhood of a chemical plant or storehouse

The behavior of a cloud of chemicals over a given terrain and under specific weather conditions may be forecast with the use of dedicated atmospheric dispersion models.

The following analysis depicts a hypothetical scenario of a cloud of toxic fumes rising from a chemical plant or storehouse near the oil terminal of port. The simulation is modeled after a virtual accident in which some amounts of non-toxic waste were released from the nearby storehouse. Whether this amount of toxins poses any real threat depends on the type of released substance. Such simulations may constitute a valid argument when making decisions regarding the allowed localizations of storage warehouses and chemical plants on port development plans (Fig.2.).

Figure .2. Chemical accident in example point and effects in adjacent areas.

4. Analysis of the port's vulnerability to a flooding hazard

Because of unstable weather conditions in a changing climate, these port are under a constant risk of being flooded. The port of Shahid Rajaee lies in north side of the Khoran bay, near the coast of the Oman sea. In the Safe

Port hazard simulation module, flood zone mapping requires the user to define a given set of modeling criteria. These include the amount by which the simulated water level is increased over its standard value and the extent of the area for which the simulation will be executed.

Fig. 3 shows two results of a simulated increase of the water level in the adjacent seasonal rivers, which crosses near the port of Shahid Rajaee in several areas, by two meters. The performed analysis shows that, according to detailed DTM data, the recent investments in flood countermeasures ought to prove sufficient to protect the port should the worst-case scenario be enacted.

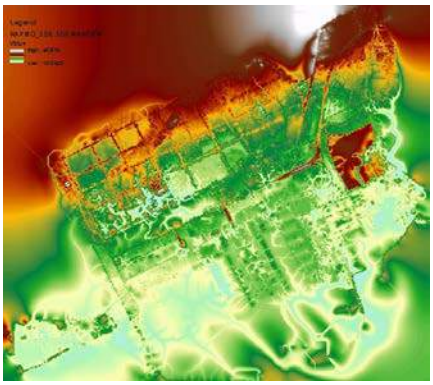

Figure 3.areas of be affected by flood in port

5. Analysis of Critical Infrastructure spatial density distribution

As prior analyses have shown, geographic diversification of Critical Infrastructure localizations is an important factor in ensuring proper and continued operation of a port. However, with the increasing number of infrastructures requiring protection, planning their spatial arrangement becomes increasingly difficult. In order to support this process, Safe Port offers a tool for investigating the spread of infrastructures with different levels of criticality over an area, available through its spatial analysis module. The analysis clearly shows a large concentration of highly vulnerable infrastructures in the area between districts 1, 3 and 5. Incidentally, the area also denotes the administrative zone of the port. Such a situation causes an unnecessary danger to the ports human force which should be minimized, optimally by moving some infrastructures into other areas. Also according to the analysis, the district's 4, 7 and 6 denote large areas with low criticality and therefore could be designated in land use and port development plans as good places for locating (or relocating) Critical Infrastructures. Fig. 4.

Figure 4. Shows a large concentration of highly vulnerable infrastructures in the area between districts 1, 3 and 5

6. Conclusion

The presented system offers tools which have been designed for specific purposes related to modeling and spatial analysis of different types of hazards in port regions. The algorithms employed by these tools operate in a spatial context and produce thematic layers representing either the outcome of a possible hazard (in the case of models) or the results of spatial risk analysis. On the basis of the type of produced analysis, each algorithm may be applied to different phases of the emergency management process. In particular, the hazard simulation algorithms may be applied to creation of hazard scenarios during the Preparedness phase, mapping of identified threats in the Response phase as well as simulating the geographical impact of threats during the Mitigation phase.

It should be pointed out that the use of both the presented software and methodology is in no way limited to the described case of the Port of Shahid Rajaee, but may be easily applied to any port situated in Iran, in Middle east or quite likely any other part of the world which possesses a basic IT infrastructure. This, in particular, applies to big and medium-sized ports which cannot afford an extensive infrastructure security policy. The outcome of the presented study shows that the quality of Critical Infrastructure protection in such ports may be substantially improved at virtually no additional costs.

7. References

[1] M. Kulawiak, Z. Lubniewski, SafeCity — A GIS-based tool profiled for supporting decision making in urban development and infrastructure protection, Technol. Forecast. Soc. Change (2013), http://dx.doi.org/10.1016/j.techfore.2013.08.031

[2] R. Hanson, Perspectives on Urban Infrastructure, National Academies Press, 1984.

[3] M. Bulu, O. Ozben, I.H. Eraslan, Clusters in Turkish Textile Industry— A Case Study in Bayrampasa District, II, International Istanbul Textile Congress (IITC), Istanbul, 2004.

DETECTING THE CHANGES OF LAND USE IN KANGAN COUNTY USING RS AND GIS

Kouroshniya A.[1], Mashhadi N.[2], Feghhi J.[3] and Ashrafi A.[4]
1) Faculty of Natural Resources, University of Tehran /Expert of ICZM project, PMO, Tehran, Iran, ali_kooroshnia@yahoo.com
2, 3) Faculty of Natural Resources, University of Tehran, Tehran, Iran, nmashhad@ut.ac.ir, jfeghhi@ut.ac.ir
4) Faculty of Geography, University of Tehran, Tehran, Iran, ashrafi852@yahoo.com

1. Introduction

The results of the studies indicate the fact that different areas of our country's natural resources, uneven conditions and suffered numerous problems. Certainly one of the important issues, and in a sense the most important issue in the field of protection of natural resources, land, natural resources and agricultural land use changes and prevent other applications and monitoring changes in these areas as the first step in the planning and management of natural resources in the world. Why desertification, increasing erosion and problems of coastal zone or forest lands as a result of human activities are illegal, always as serious challenges and constraints to achieving sustainable development objectives of the country were discussed.

RS and GIS for the convenience, speed and low cost compared to other methods, now have become a powerful tools in the hands of professionals and scientists, the way many things are in this world. The applications of this science, the use of natural resources and is in studies and researches. So that the evidence of past experience, the easiest and most economical method for such studies, the use of remote sensing and GIS is the science and has the potential to be very economical.

The aim of this study is detecting changes in landuse of coastal area by post classification method in area of Kangan town in end east of Bushehr (border of Bushehr city). Due to the location of special place of Parse-Jonubi and Nayband national park, this area is known as a critical natural environment and makes it more essential to study its land changes

2. Study Area, Data and Methodology

2.1 Study Area and Data

The coastal area in this study would be Kangan County in the 27¿ 39N 52 ¿ 31E that located in the northern of Nayband gulf in eastern end of Bushehr province (border of Hormozgan province-Figure 1).

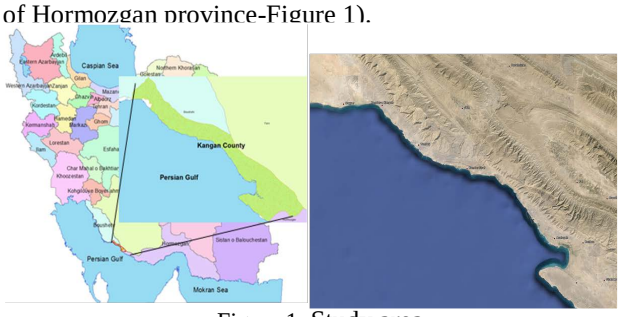

Figure 1: Study area

In this study following data have been used:

- One image of ETM Landsat 7 of 27th of December 2000
- One image of ETM Landsat 8 of 26th of December 2014
- Topographic maps of National Cartographic Center in scale of 1:25000
- ICZM Land use maps in scale of 1:25000

The reason to use satellite image in the mentioned date is that lack of water is the main reason for limited plant growth in the study area. On the other hand, according to local climate and concentration of precipitation in winter, usually most of the vegetation can be seen at this season. So, after reviewing the archives of available satellite images and with necessity of coincidence of two images due to the change detection method (with use of post-classification), images in mentioned dates were chosen in this study.

2.2 Methodology

To carry out this study, after receiving satellite images geometrical pre-analysis were done and images were prepared for processing. Training Samples were gathered carefully from the area and the classes of landuse were classified. With regard to considered classes of use, different identifiable classes on the map in final framework of classes were mixed.

Before starting the main analysis and comparison of the maps, geometrical corrections were done on them. In this process Landsat8 image of 2014 was considered as the reference and Landsat7 image of 2000 was corrected geometrically based on that through first grade equations. In order to determine the minimum field check necessary control points for geometric correction based on Polynomial function, Wolberg 1990 [3] was used.

$$K= (N+1) (N=2)/2$$

K=minimum of necessary points (Formula 1)
N= Polynomial function

After geometrical correction, in order to create a new image, re-sampling should be done. Used method is the method of the nearest neighbor. This method used for measuring grade of pixel brightness of new image; it uses the brightness of neighbor pixels and spectral value of the nearest pixel. This method avoids the change of value of initial pixels [2]. Finally image of year 2000 have been geometric correction compared to 2014 year image with RMSE less than a fourth (1/4) pixel image and was rewritten by the nearest neighbor method. Then training samples of the region were made through field check and

also with application of maps of land use in scale of 1:25000 produce in ICZM[1] plan and topographic maps developed by NCC in scale of 1:25000 and satellite images of Google Earth.

In this study with the use of digital interpretation and other information resources and analysis for classification of satellite images, land use classes were classified in 6 classes of agriculture, built area, rangeland and forest, wet and salt land area, bare land area, and finally water bodies. After specifying the amount of separation of classes, supervised classification and with the Maximum Likelihood was done.

Before using the results of classification of satellite images for detecting the changes, estimating the validity of produced maps with earth reality is necessary. If the needed validity does not exist, classification should be repeated. The commonest method for estimating the validity in use of RS data measurement is producing Error Matrix or Contingency Matrix [1]. With the use of Error Matrix, the quality of separation of images pixel and devoting them to their suitable classes can be specified. This matrix is the result of pixel to pixel comparison in which known pixels or earth reality with their correspondents exists.

According to results of the study by Jensen Congaltonand 250 control points (50 points for each class) are necessary for assessing the validity of data. With regard to 6 main defined classes in this study, 50 control points for each use point and totally 300 points were considered randomly. Earth reality in this study includes field check (with regard to being near the time of field supervision), visual analysis on false color images and usage of satellite data in software of Google Earth. But considering the lack of enough data from the past situation of the area in 2000, validity of this map was analyzed through visual interpretation. Stages of the study have been shown in figure (2) and all stages are discussed in detail in the following.

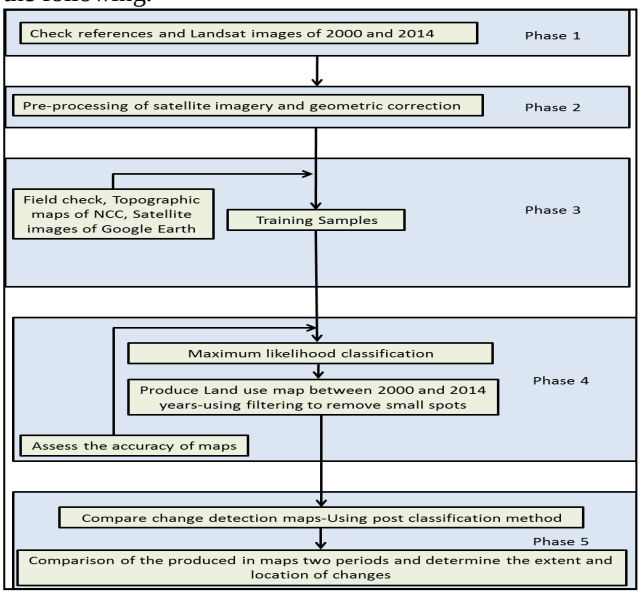

[1] Integrated Coastal Zone Management

Figure 2-Methodology Flowchart

3. Results

In figure (2) landuse of Kangan which was analyzed in two different periods of time were observed. As it is obvious in maps, most use of this area is rangeland and forest. From the features of this area mangrove forests in end east of the region in Nayband bay can be named. On the other hand, installations of Parse Jonubi as a land class are visible. Other classes which are the second in size are wetland and saltland which cover a big area of the coast because of being beside the sea.

Results of land use in 2014 shows the expansion of built land class compared to year 2000. This is affected of buildings as the result of expansion of region installations specially Parse Jonubi for exploiting the big resources of petrol and gas. In generated map of 2000 the most exact map is for bare lands and the most number of mistakes is for lands of rangeland and forests. Also, in generated map of 2014, the most exact map is for wet and salt lands and the most number of mistakes is for water areas. Table (1) shows the changes in areas in two years of 2000 and 2014.

The accuracy of the land use map produced in 2000, with kappa and the overall accuracy and 85%, respectively, 88/0. The correct use map produced from satellite images 2014 have 86/0 kappa and overall accuracy of 82% is calculated.

Table (1): Area (ha) of Land use and among of changes in 2000 and 2014

Changes	2014	2000	CLASS	No.
-921.96	14499.9	15421.86	Bare Land Area	1
16021.71	18028.71	2007	Built Area	2
23.4	6385.41	6362.01	Farming Area	3
-7541.82	70420.59	77962.41	Rangeland Area	4
-1008.72	1373.4	2382.12	Water Area	5
-6572.61	10207.98	16780.59	Wet/Salt land Area	6

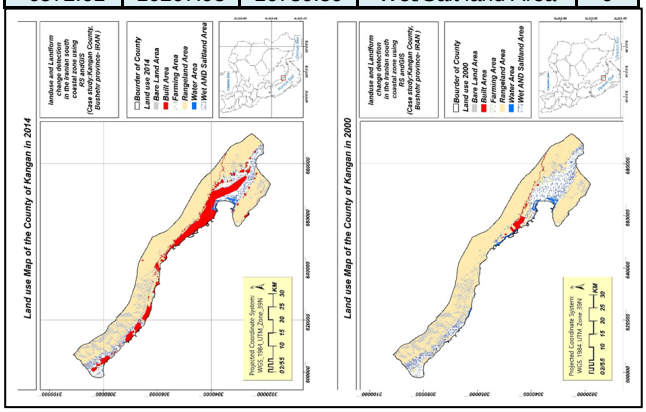

Figure 2-Land use maps of study area (2000/2014).

4. References

[1] Foody, G. 2002. Status of land cover classification accuracy assessment. Remote sensing ofenvironment. 1: 185-201

[2] Yang, X., And Lo, C.P., 2002.Using A Time Series Of Satelite Imagery To Detect Land Use And Land Cover Change In The Atlanta ,Georgia Metropolitan Area. International Journal of Remote Sensing . 29:1775-1798.

[3] Wolberg, G. 1990. Digital image warping. Los Alamitos, CA: IEEE Computer Society Press, 318p

DESIGN AND PREPARATION A SPATIAL DECISION SUPPORT SYSTEMS (SDSS) FOR INTEGRATED COASTAL ZONE MANAGEMENT (ICZM) OF IRAN

Kouroshniya A.[1], Haghighat M.[2]

1) Ports and Maritime Organization, Department of Ports and Coast Eng., Tehran, Iran, ali_kooroshnia@yahoo.com
2) Ports and Maritime Organization, Department of Ports and Coast Eng., Tehran, Iran, monir_haghighat@yahoo.com

1. Introduction

Integrated Coastal Zone Management (ICZM) refers to a dynamic, multidisciplinary and iterative process to promote sustainable management of coastal zones. This approach has been identified as a solution to overcome the complexity of the coastal area management where diverse resources provide the most productive yet highly threatened systems in the world. Diverse viewpoints as well as conflicts among stakeholders in these areas imply difficulties in the decision making process that can result in conflict over current and future uses of the coast. ICZM is therefore concerned with providing a balance between different goals that set by stakeholders within the sustainable development framework and illustrates a general trend toward more interactive policymaking and stakeholder involvement (Van Kouwen et al. 2007). For this purpose, decision support systems (DSS) become more common to support decision making at various institutional levels.

A DSS is a set of computer tools for finding alternative solutions for a decision problem. Kouwen et al. (2007) defined بICZM-DSSپ as a computer system that design information about ICZM issues and is designed to perform analysis to help coastal managers in decision-making. Furthermore, the application of DSS in ICZM requires the integration of different modelling systems and tools (Varghese et al. 2008). Typically different organizations produce relevant data and information with different structures (StojanovicGreen and Lymbery 2010) and use different software tools which cannot be integrated as is needed in the ICZM framework (Hansen and Fuglsang 2014). Modular design can be considered as a solution when a system is complex and include different but related (sub-) systems. Modular programming is a software design technique that emphasizes separating the functionality of a program into independent, interchangeable modules, such that each contains everything necessary to execute only one aspect of the desired functionality.

This paper aims to discuss a modular spatial decision support system as an appropriate approach for implementing a DSS for ICZM. Moreover, ICZM_DSS software is introduced in this paper which was implemented based on the modular approach and provides a set of valuable tools to coastal managers and planners in data management.

2. Methodology

The ICZM_DSS software was designed using modular approach which requires software packages (libraries) that can perform different kinds of computations on different aspects of the ICZM framework. This allows for interoperability or joint usage of the different modules. We used open source technology due to the availability of the standard libraries for this purpose. It has been reported that the open source technology for spatial data is mature enough to creating a spatial data infrastructure (Moreno Sanchez et al. 2007). Python was used as the core programming language for development of ICZM_DSS because it provides excellent facilities for interoperating modules. Several standard libraries were used for different functionalities in the software including gdal, proj, mapnik and arcpy for spatial data input/output, coordinate system management, spatial mapping and interfacing with ArcGIS, respectively. A new module, named ICZM tools, was implemented to provide specific functionalities required in the coastal area including coastal zoning visualization, risk assessment, opportunities/threats, and ecological capacities (Figure 1). An extendible graphical user interface (GUI) was designed using QT platform (http://qt.nokia.com/).

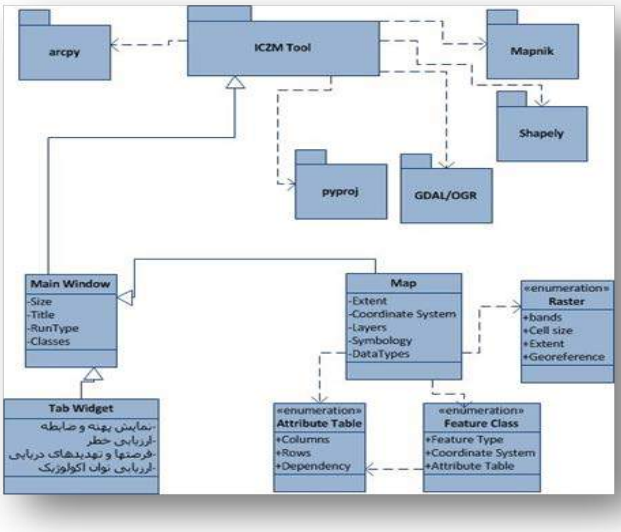

Figure 1) Modules and their interaction in ICZM_DSS software

3. Result

Figure 2 illustrates the main ICZM_DSS user interface. This interface follows the standard well know GIS software such as ArcGIS and QGIS. The interface provides the capability of including/excluding different tools (modules).

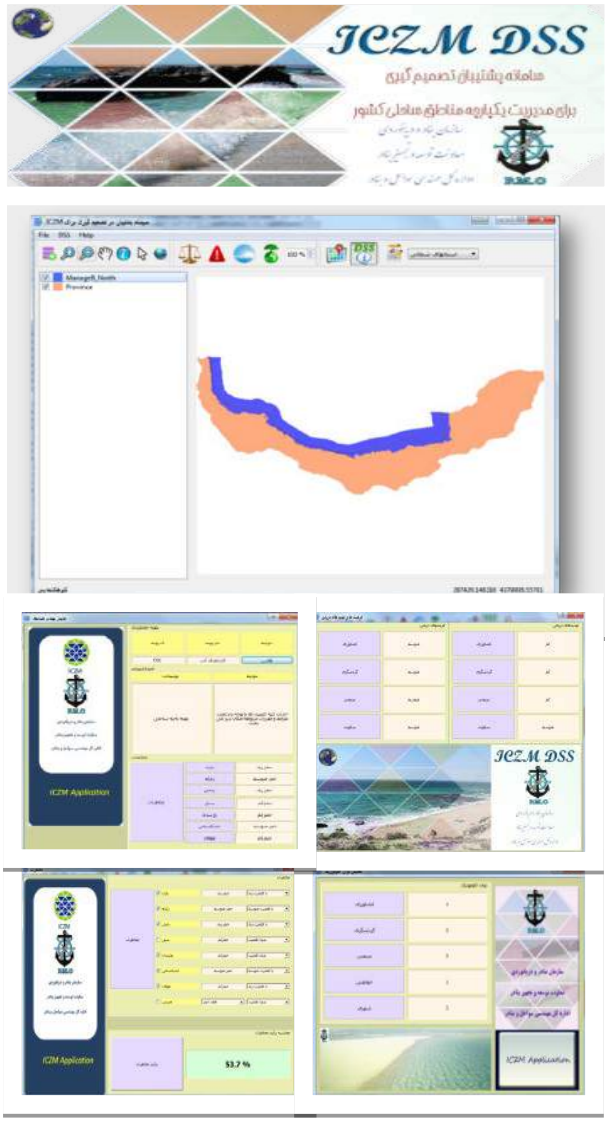

Figure 2. Graphical user interface of ICZM_DSS software

4. Conclusion

This paper introduces ICZM_DSS software that is designed using a modular approach. The software is extendible and provides a framework to integrate modules that may be developed for different purposes by different organizations. This approach can be considered as a solution to interoperable the tools are needed by the stakeholders in coastal area.

5. References

[1] Fabbri. P. karan. (1998) A Methodology for supporting decision making in integrated costal zone manegment, (JRC) European commission Italy

[2] Geertman, S. C. M. (2006). Potentials for planning support: a planning-conceptual approach. Environment and Planning B: Planning and Design, 33(6), 863-880. doi: 10.1068/b31129

[3] Guariso, G., & Werthner, H. (1989). Environmental Decision Support Systems. New York: Chichester Halsted Press.

[4] Hansen, H. S. & M. Fuglsang (2014) An Operational Web-Based Indicator System for Integrated Coastal Zone Management. ISPRS International Journal of Geo-Information, 3, 326-344.

[5] Moreno,Sanchez, R., G. Anderson, J. Cruz & M. Hayden (2007) The potential for the use of Open Source Software and Open Specifications in creating Web-based cross-border health spatial information systems. International Journal of Geographical Information Science, 21, 1135-1163.

[6] Rafael Sarda, Conxita Avila, Joan Mora. (2005) A methodological approach to be used in integrated coastal zone management processes: the case of the Catalan Coast (Catalonia, Spain) Centre d'Estudis Avancxats de Blanes (CSIC), Carrer d'Acces a la Cala Sant Francesc, 14, 17300-Blanes, Girona, Spain.

[3] Sharifi, M. A. (2003) Integrated Planning and Decision Support Systems for Sustainable, Water Resources Management: Concepts, Potentials and Limitations, Seminar on Water Resources Management for Sustainable Agricultural Productivity, Lahore, Pakistan

[4] Sharifi, A., van Herwijnen, M., van den Toorn, W. (2004) Spatial Decision Support Systems, Institute of Geo-Information Science and Earth Observations (ITC), The Netherlands

[9] Stojanovic, T., D. R. Green & G. Lymbery (2010) Approaches to knowledge sharing and capacity building: The role of local information systems in marine and coastal management. Ocean & Coastal Management, 53, 805-815.

[10] Van Kouwen, F., C. Dieperink, P. Schot & M. Wassen (2007) Applicability of decision support systems for integrated coastal zone management. Coastal Management, 36, 19-34.

[11] Varghese, K., L. Ganesh, M. Mani, P. Anilkumar, R. Murthy & B. Subramaniam (2008) Identifying critical variables for coastal profiling in ICZM planning: A systems approach. Ocean & Coastal Management, 51, 73-94.

DEVELOPING AN AUTOMATIC MONITORING METHOD USING SATELLITE IMAGERY TO DETECT DUST STORMS IN COASTAL AREAS

M.Samadi*[1], S.K.Alavipanah[1] and A.Darvishi[1]

1) Department of Remote sensing and GIS, University of Tehran, Tehran, Iran (*M.Samadi@ut.ac.ir)

1. Introduction

Every year in Iran, several natural hazards occur which cause social, economic and environmental damages. Over the past decades, Middle East dust storms have caused many problems for the residents of South and Southwest regions of Iran. During the recent years, there has been an increase in the trend of dust storm activities in this region, especially in spring and summer [1]. Now, this trend is changing into the main persistent environmental problem in Iran and the Middle East region. Detecting dust phenomena, identifying their sources and surveying about their movements and situation can help planners and decision makers in planning and controlling to reduce damages of this phenomena. Remote sensing allows for better tracking of regional and global distribution of aerosols, which are extremely dynamic in nature [2].

Several studies have been done about identifying dust source regions using satellite imagery [3-5]. Also in case of using remote sensing and satellite imagery for detecting dust storms several methods have been developed since 1970. By considering almost all developed methodologies, there are common limitations in them. First, while they have good abilities for dust detection over lands, they cannot do the same over water bodies. Second, they have problems with seasonal changes and they need different thresholds. Third, they almost have problems with dust discrimination from other objects like clouds, water and land soil surface. Therefore, the main objective of this research is the development of a new methodology which resolves mentioned problems.

2. Data and Methods

2.1. Study area

Study area of this research is western part of Iran which is close to internal and transboundary sources of dust which are exposed to several dust systems and many dust storms occur in these areas every year. Surveying meteorological data from 2000 - 2011 indicates that in some cities like Ahwaz, Dezful, Susangerd, Bostan and Shush the annual average of days with dust is more than 31 days. In these days the visibility was less than 1000m. Figure 1 shows the average of days with annual dust events which happened in western part of Iran.

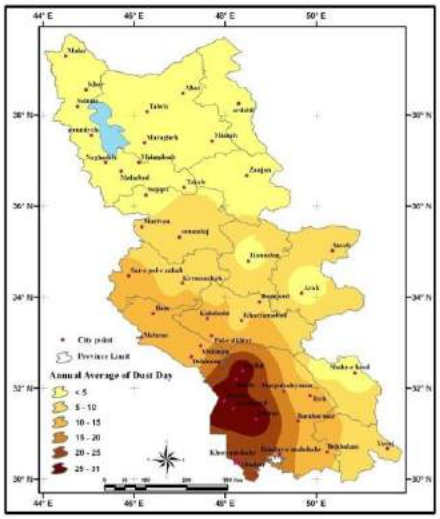

Figure 1. Study area and annual distribution of dust during 2000-2011[6].

2.2. Data

Almost all western and south western parts of Iran which are affected by local, regional and global dust storms are considered in this study. The synoptic data from 27 stations are provided by the Islamic Republic of Iran Meteorological Organization (IRIMO). Dusts are identified based on two criteria: first, to be measured in three stations simultaneously and second visibilities less than 1000 meter is reported. Dust phenomena can be detected by remote sensing in different spectral channels. Data from the Moderate Resolution Imaging Spectroradiometer (MODIS) were used in this study.

2.3. Detecting of dust storm

As the behavior of dust storms is not the same over different land covers and water bodies, first the land cover map of the study area must be produced. Using MODIS images, in clear days, three main land cover classes were separated: bright land cover, dark land cover and water bodies. In addition to the map of water bodies, based on an equation (Equ. 1) from Remer et al., (2005) [7] these two land cover classes (bright and dark surfaces) were separated.

$$0.01 \leq Ref_{2.13} \leq 0.25 \quad (1)$$

In this equation, $Ref_{2.13}$ is the reflectance of 2.13 µm of MODIS data. If the equation be true, the surface is dark.

To achieve and modeling the spectral behavior of different objects and also discriminating them from each other, the training pixels were collected. In this procedure the dusty pixels over different land covers i.e. bright and dark land covers were collected. This procedure was carried out for all images, separately and almost all MODIS bands were used. Then, the statistical mean and standard deviation of samples for seven classes, i.e. clouds, bright surfaces, dust over bright surfaces, dark surface and dust over dark surfaces were calculated and spectral curve of these classes were drawn. Based on these spectral behaviors, some indices were defined to separate them from each other. Figure 2 shows dust storm detection procedure.

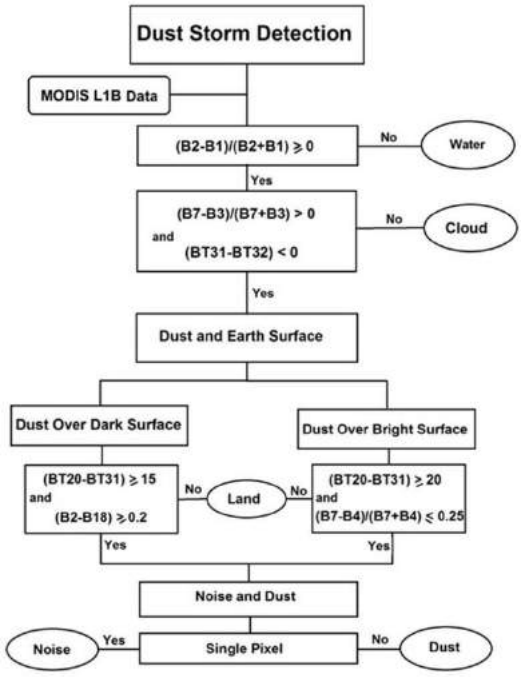

Figure 2. Dust storm detection procedure

3. Results

Totally to investigate the capability of developed method, we used two dust events happened in the west part of Iran: 5th July 2009 and 13th April 2011(figures 3 and 4).

4. Conclusion

In this study we developed an automatic dust storm detection method using satellite imagery of MODIS. It uses the optical and thermal portions of the electromagnetic spectrum. In comparison to previous methodologies for detection of dust, the developed method has no need of threshold. Being able to work in all climatic conditions is another characteristic of this method which makes it preferable.

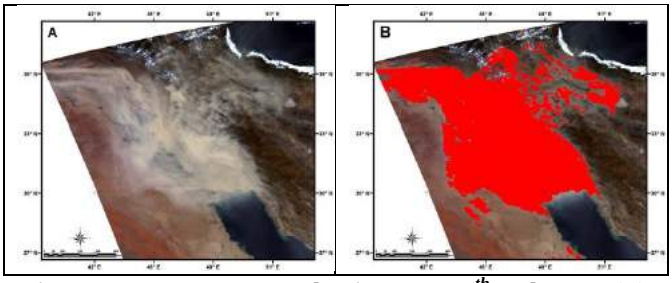

Figure 3. MODIS true color image at 5th July 2009(A), detected dust storm by using developed model, red color,(B).

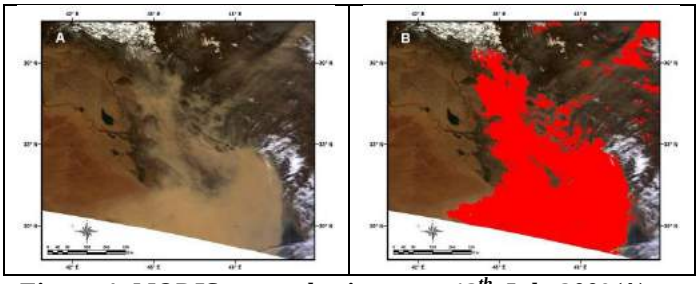

Figure 4. MODIS true color image at 13th July 2009(A), detected dust storm by using developed model, red color,(B).

4. References

[1] Khoshakhlagh F, Najafi MS, Samadi M: An analysis on synoptic patterns of springtime dust occurrence in West of Iran. *Physical Geography ResearchQuarterly* 2012, 2(80):99–124. (In Persian)

[2] Ichoku C, Kaufman YJ, Remer LA, Levy R: Global aerosol remote sensing from MODIS. *Adv Space Res* 2004, 34:820–827.

[3] Baddock MC, Bullard JE, Bryant GR: Dust source identification using MODIS: A comparison of techniques applied to the Lake Eyre Basin, Australia. *Remote Sensing Environment* 2009, 113:1511–1528.

[4] Lee JA, Gill TE, Mulligan KR, Miguel Dominguez A, Perez AE: Land use/land cover and point sources of the 15 December 2003 dust storm in southwestern North America. *Geophys J Roy Astron Soc* 2008. doi:10.1016/j.geomorph.2007.12.016.

[5] Wang X, Huang J, Ji M, Higuchi K: Variability of East Asia dust events and their long-term trend. *Atmos Environ* 2008, 42:3156–3165.

[6] Samadi M, Darvishi A, Alavipanah SK, Mohamadi H, Najafi MS: Global Dust Detection Index (GDDI); A New Remotely Sensed Methodology for Dust Storms Detection, *Journal of Environmental Health Science & Engineering* 2014, 12:20.

[7] Remer LA, Kaufman YJ, Tanre D, Mattoo S, Chu DA, Martins JV, Li RR, Ichoku C, Levy RC, Kleidman RG, Eck TF, Vermote E, Holben BN: The MODIS Aerosol Algorithm, Products, and Validation. *Journal of the Atmospheric Sciences—Special Section* 2005, 62:947–973.

LAND CHANGE DETECTION FOR COASTAL AREA USING REMOTE SENSING (A CASE STUDY OF THE SOUTHERN COASTS OF IRAN)

Bahman Saei
Ports & Maritime Organization

1. Introduction

Development of technology, significant progress in improving image quality sensors, remote sensing spectral and spatial resolution of the sensor data has so largely increased. This advances the way for the introduction of new applications and exploit the opportunities provided by the sensors, is opened. A general idea of image analysis, remote sensing, and land surface changes on the coast is clear. The importance of this idea, when it is clear that we can use it to estimate the amount of malicious destruction of many natural disasters and identify modified areas, relief and reconstruction operations we speed. For countries such as Iran's bitter experience in Rudbar earthquake, Bam, Zarand and ... And war is still not vanished from their memories, the importance of this issue is more tangible. Coastal change detection on the other hand, many applications in surveillance and monitoring of coastal sedimentation regime and sediment sampling in the coastal region is [1] that due to geographical and strategic position of our country, with most coastal areas in the Persian Gulf and Oman Sea Caspian Lake, is the research in this field can be of great importance.

2. The data used

The study area in this study, Bandar Imam Khomeini, part of the south coast of the country. The famous port of Imam Khomeini who was called before the Islamic Revolution, namely Bandar Shahpour and Bandar Khor Musa is located. The area in the southern province of Khuzestan in southwestern Iran, in the Northwest of the Persian Gulf is located in the Khor Musa. A picture taken from Google to general introduction of the study area is given below. Coordinates Bandar Imam Khomeini, 30 degrees 26 minutes north and 49 degrees east longitude is 5 minutes. Bandar Imam, from the north to the surgical area, to the south Khor Musa and the Persian Gulf, from the West to the East to the city of Abadan and Mahshahr limited [2]. Bandar Mahshahr 15 km away from the city, Ahvaz (Center of Province) 90 km until Tehran (the capital) is 1000 km. According to the 2004 population of about 80,000 and about 17,000 people daily movement of the float in this area.

3.3. The proposed algorithm (based change detection Decision Fusion)

Si =Total pixels class i in first image
Sci = Total the i column of C3
Si-SCi=nCi = The number of i class pixels in the class i (unchanged) left
Substituting nCi in position (i, i) in the matrix C3, we have:

$$C4 = \begin{bmatrix} nC_1 & a_{21} & \\ a_{12} & nC_i & \vdots \\ \vdots & \vdots & nC_n \end{bmatrix}_{n\times n} \quad (4)$$

The maximum integration method to vote, in the absence of correct diagnosis of pixels class, the last class to class ambiguity, was considered. By subtracting the transformation matrix C3, Any method of transformation matrix changes similar $C3_{GTM}$, errors can be eliminated, redundancy, producers and users of each method carefully obtained.

$$C3 - C3_{GTM} = \quad (5)$$

In this matrix the sum of positive numbers with a total of column matrix $C3_{GTM}$ redundancy error and the sum of negative numbers with a total of columns matrix $C3_{GTM}$ error of omission as well as the relationship of these errors, the accuracy is achieved using and producing. C4 any way by subtracting the transformation matrix changes the transformation matrix changes $C4_{GTM}$ similarly, other evaluations of each method can be obtained

.

$$C4 - C4_{GTM} = \quad (6)$$

4.1. Quantitative assessment

Using formulas 1-6 and implementation of two methods, maximum votes and Dempster Shaeffer, we have:

4.2. Visual assessment

The visual assessment and the data cover images, just as qualitative evaluation and conversion to other classes is as simple to interpret.

4.3. New findings on the implementation of the algorithm:

The implementation method based on Dempster Shaeffer method, the matrix coefficients obtained plausibility.

To calculate the plausibility of each i class and Normalization m_p for i class are:

$$m_p(:,i) = \begin{bmatrix} nC1 \\ a_{1,2} \\ \vdots \\ a_{1,n} \end{bmatrix} \quad (7)$$

m_p To normalization, we have:

$$m_{p_n} = \frac{m_p(:,i)}{\sum m_p(:,i)} \quad (8)$$

As a result of this research, m_p normalized matrix based on formulas (7) and (8), to predict and examine the trend of events in the period studied (in the same environmental conditions and the absence of unforeseen events) creates. This means that if stationary stochastic process, we can assume what happened (in the current study, the process of conversion to other classes in the study period) to predict the next and the next. For example, seven classes defined in image classification can be used to plot changes in the years 2002.2009 possible. Below are a few examples of the charts has been the desire transformation (conversion desire) each class to other classes, shows...

According to the survey data available from the study area, the process of withdrawal and full conversion of sea water and estuary and desire transformation class (sea) water, shallow, muddy pond (class two and four), has been approved .

5. Conclusion

The integration algorithms implemented in this study and the method of voting methods Dempster Shaeffer was used. The results showed that the integration of methods with higher accuracy and reliability. Dempster Shaeffer method in detection of changes due to maximum use of evidence-based data model and its initial detection, provides better results. With the use of neural networks and fuzzy logic models such as educable as a combination of data integration algorithms implemented, the advantages of these methods, to improve the accuracy and reliability results benefited. Extraction and determination of the matrix converter drive together into classes as an outcome of this study, change and estimates of future changes can be detected using methods of integration and using estimation methods, the researcher in monitoring and surveillance in coastal sedimentation and sediment sampling, ... Trends can be identified.

6. References

[1]. *Bishop, Peter WT Yuen & Gray.Hyperspectral Algorithm Development for Military Applications: A Multiple Fusion Approach. Edinburgh 2006: s.n., 3rd EMRS DTC Technical Conference – Edinburgh 2006.*

[2]. *Mandatory Dr Bahador, the history of eighty years, Bandar Imam Khomeini؛ 2009. 978-964-7829-40-3.*

[3]. *MACLEOD, R. D., CONGALTON, R. G, A quantitative comparison of change detection algorithms for monitoring eelgrass from remotely sensed data. Hotogrammetric Engineering and Remote Sensing, Vol. 64, pp. 207–216. 2011.*

[4]. *LAMBIN, E. F., STRAHLER, A. H., Indicators of land-cover change for changevector analysis in multitemporal space at coarse spatial scales. International Journal of Remote Sensing, Vol. 15, pp. 2099-2119. 2009.*

5]. *Barbara Zitova, Jan Flusser. Image registration methods: a survey. 2009.*

[6]. *MORAN, D. LU & P. MAUSEL & E. BRONDI´ZIO & E.MORAN. Change detection techniques. International Journal of Remote Sensing, 2004.*

[7]. *Jiang Dong, Dafang Zhuang, Yaohuan Huang and Jingying Fu. Advances in Multi-Sensor Data Fusion: Algorithms and Applications. ISSN 1424-8220. 2009.*

[8]. *Hong, Gang. IMAGE FUSION, IMAGE REGISTRATION, AND RADIOMETRIC NORMALIZATION FOR HIGH RESOLUTION IMAGE PROCESSING. Canada: Geodesy and Geometrics Engineering (UNB), 2011.*

[9].Rashidi, Ali Jabbar, making integration of remote sensing multiple systems; doctoral dissertation, Faculty of Electrical Engineering, Tarbiat Modarres University.2004

[10]. Oort, P.A.J. van. Interpreting the change detection error matrix.Wageningen University, Centre for Geo-Information, The Netherlands: s.n., , Remote Sensing of Environment. 2006.

COASTLINE EXTRACTION USING ALOS PALSAR DUAL-POLARIZATION DATA, IN ANZALI REGION, NORTH IRAN

Saeed A.jafari[1], Ali Soltanpour[1], Ahmad Hojati Malekshah[2] and Mahmood Pirooznia[1]

1) Hydrography and Tidal affairs, National Cartographic Center, Tehran, Iran, aminjafari@alumni.ut.ac.ir
1) Hydrography and Tidal affairs, National Cartographic Center, Tehran, Iran, asoltanpour@yahoo.com
2) School of Surveying and Geospatial Engineering, University of Tehran, Tehran Iran, hojjati.ahmad@ut.ac.ir
1) Hydrography and Tidal affairs, National Cartographic Center, Tehran, Iran, ma.pirooznia@gmail.com

1. Introduction

Determination of coastline is extremely essential especially in coastal cities where there are harbors and ship transportation. In addition, the monitoring of coastline would be helpful to gain valuable information about sea level variations during the years. As conventional methods including RTK GPS are manpower, cost and time consuming, the aim of this study is to utilize the pairs of polarimetric SAR images for water and land distinction in Anzali region. This approach is an effective, precise and fast way which requires less money and manpower. In this study polarimetric SAR images of ALOS sensor have been used which belongs to Japan. SAR images are in HH and HV mode.

2. Materials and Methods

The microwave polarization refers to the orientation of the electric field vector of the transmitted beam with respect to the horizontal direction. If the electric field vector oscillates along a direction parallel to the horizontal direction, the beam is said to be "H" polarized. On the other hand, if the electric field vector oscillates along a direction perpendicular to the horizontal direction, the beam is "V" polarized. After interacting with the earth surface, the polarization state may be altered. So the backscattered microwave energy usually has a mixture of the two polarization states. The SAR sensor may be designed to detect the H or the V component of the backscattered radiation. Hence, there are four possible polarization configurations for a SAR system: "HH", "VV", "HV" and "VH" depending on the polarization states of the transmitted and received microwave signals. For instance, the SAR onboard the ERS satellite transmits V polarized and receives only the V polarized microwave pulses, so it is a "VV" polarized SAR. In comparison, the SAR onboard the ALOS satellite is both "HH" and "HV" polarized SAR [1]. Therefor the complex back scatter matrix of SAR is written as a complex back scatter vector:

$$u = [\, E_{HH}\ E_{HV}\ E_{VV}\ ]^T \quad (1)$$

The covariance matrix of radar pixels is:

$$C = u(u)^+ \quad (2)$$

In equation 2 the sign (+) means Hermitian matrix (transposed complex conjugate).

One of the most challenging problems in coastline extraction is the speckle noise of SAR images. In this paper the SAR images have been multilooked to reduce the speckle noise. In other words, neighbor pixels are averaged in a direction:

$$Z = \frac{1}{n}\sum_{k=1}^{n} u(k)\,[u(k)]^+ \quad (3)$$

Anzali region and location of SAR image have been shown in Fig 1. This image is acquired on 5th October 2009. The SAR images have been multilooked with n=7 and georeferenced using Digital Elevation Model (DEM) of ASTER sensor (These data are distributed by the Land Processes Distributed Active Archive Center (LP DAAC), located at the U.S. Geological Survey (USGS) Center for Earth Resources Observation and Science (EROS) http://LPDAAC.usgs.gov.).

Figure 1. Anzali region and location of SAR image

Coastline determination was done through three main steps: first of all, the pairs (HH and HV) are averaged, multilooked and become speckle noise free by Speckle Reducing Anisotropic Diffusion (SRAD) method [2]. In

SRAD a set of smoothed images of the base image are obtained from a partial differential equation.

Secondly, During the SRAD process a parameter named Instantaneous Coefficient Of Variation (ICOV) is calculated which is the combination of normalized gradient magnitude and normalized Laplacian operators. ICOV distinguishes edge image from the noise contaminated image [3].

Finally, a watershed transform is applied on ICOV [4]. Watershed transform divides image domain to M subdomains. In order to remove non coastal regions a region merging algorithm is used. This algorithm relies on similarity metric of radar brightness, which is computed by equation 4:

$$S = \frac{N_i N_j}{N_i + N_j}\left(< \ln(I) >_i + < \ln(I) >_j \right) \quad (4)$$

N_i and N_j are the pixel numbers in two adjacent regions R_i and R_j. To merge the regions, Region Adjacency Graph method is used [5]. Suppose $\{R_k\}$ consists of M partitions, every two regions with high similarity metric would merge. Hence M-1 regions should be left. This method is repeated and the variables are updated frequently until just land and water regions remain. If there is just one coastline then M=2 is the stopping criterion, and if there are m coastlines then M=m+1 is the stopping criterion [3].

3. Results

The base image and the result of SRAD filter have been demonstrated in fig 2. These images are not geocoded.

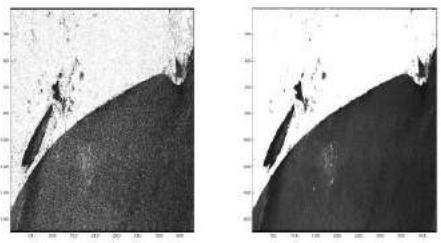

Figure 2. Left: multilooked image, Right: SRAD filtered image.

The regions which are extracted from watershed transform have been illustrated in fig 3.

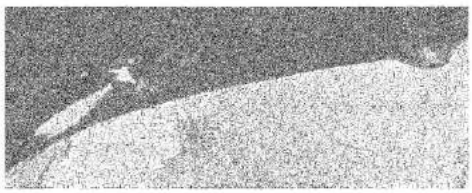

Figure 3. Watershed transformed image.

Fig 4 shows geocoded image merging results. Three main regions are determined. Two of them are related to the Anzali lagoon and the other one is the coastline of the Caspian Sea. However, some small regions could be seen in the figure because of remained noise in the images. Also a region has been focused in the figure that shows both the coastline obtained from ALOS images (blue line) and collected GPS points (red line).

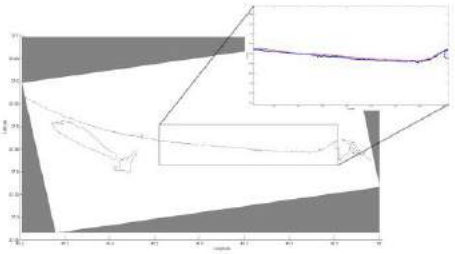

Figure 4. Coastline obtained from ALOS images. In the focused area our results (blue line) are compared with collected GPS points (red line).

4. Discussion and Conclusion

As enormous cost, time and manpower which are needed for coastline determination, we used SAR dual-polarization method to explore the coastline more effective and faster. In this study ALOS PALSAR images were acquired to extract the edge between Caspian Sea and land in Anzali region. The images were multilooked and filtered by SRAD approach to reduce the speckle noise. Then watershed transform was applied to divide the images into some non-coastal regions. Finally, non-coastal regions were merged using RAG algorithm. The results showed the boundaries between land and water in Anzali Pond and coastline of Caspian Sea. The results were compared with obtained GPS points. There was a uniformed shift between coastline acquired from ALOS images and GPS points. This shift is probably because of inaccurate geocoding, remained speckle noises and the state of sea water in time of images capturing.

5. References

[1] Dr. S. C. Liew., 2001, PRINCIPLES OF REMOTE SENSING. Centre for Remote Imaging, Sensing and Processing.

[2] YU, Y., and ACTON, S. T., 2002, Speckle reducing anisotropic diffusion. IEEE Transactions on Image Processing, 11, 1260–1270.

[3] Y. Yu & S. T. Acton Corresponding author (2004): Automated delineation of coastline from polarimetric SAR imagery, International Journal of Remote Sensing, 25:17, 3423-3438

[4] VINCENT, L., and SOILLE, P., 1991, Watersheds in digital spaces: an efficient algorithm based on immersion simulations. IEEE Transactions on Pattern Analysis and Machine Intelligence, 13, 583–593.

[5] HARIS, K., EFSTRATIADIS, S. N., MAGLAVERAS, N., and KATSAGGELOS, A. K., 1998, Hybrid segmentation using watershed and fast region merging. IEEE Transactions on Image Processing, 7, 1684–1699.

MORPHOLOGICAL CHANGES OF BARRIER-LAGOON COMPLEXES ASSOCIATED WITH SEA LEVEL FLUCTUATIONS IN NORTHEAST OF CASPIAN SEA

Ashrafi Ali[1], Isaie moghaddam Ehsan [2]

1) Faculty of Geography, University of Birjand, Birjand, Iran, aashrafi@birjand.ac.ir
2) Faculty of Civil Engineering, Sahand University of Technology, Tabriz, Iran, e_isaie@sut.ac.ir

1. Introduction

The Caspian Sea (CS), whose main characteristic is isolation from open oceans, as the world's greatest enclosed water basin revealed a complete sea-level cycle with an amplitude of around three meters over the last century, which included stages of regression (1929-1977) and transgression (1978-1995) [1,2]. Based on satellite altimetry data, the CS basin is experiencing a decreasing trend in water level during the recent years (Fig. 1). Shoreline evolution patterns, morphological changes of barrier-lagoon systems and beach-ridge emergence/submergence are the most common coastal responses to water level fluctuations at low-lying coastal segments [3]. The Gorgan bay and Gomishan lagoon, the major geomorphologic features in the southeastern of the CS, are formed behind the barrier-spit and recognized as areas of high terrestrial biodiversity, rich marine, natural habitat for migratory shorebirds, and social tourist value. The southeastern Caspian coast is characterized by beach with very mild slope both offshore and onshore that prevents high waves from approaching the shore and hence fine-grained sediments mainly consist the composition of bed material of the beach.

The present paper aims to investigate the shoreline changes of Gorgan bay and Gomishan lagoon as places protected by the Ramsar Convention in terms of size and areal extents using remote sensing-image processing techniques integrated with Geographic Information System (GIS) during 1994-2015.

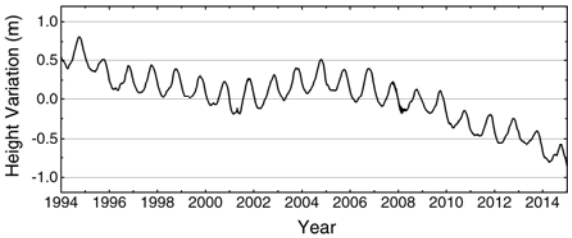

Fig. 1. Long-term water level variation of the Caspian Sea based on TOPEX/POSEIDON, JASON-1 and JASON-2/OSTM altimetry data between 1994 and 2015

2. Materials and Methods

The geomorphological changes over the study area were analyzed with satellite images including Landsat 4 and 5 TM, Landsat 7 ETM+SLC-on, and Landsat 8 OLI. In this study, a series of images were adopted from the U.S. Geological Survey with a pixel size of 30 m. (http://earthexplorer.usgs.gov). The data products employed in this study were corrected with the aid of Standard Terrain Correction, and finally changed to radiometrically and geometrically terrain corrected data (Level 1T). Steps of the study are shown in Fig. 2.

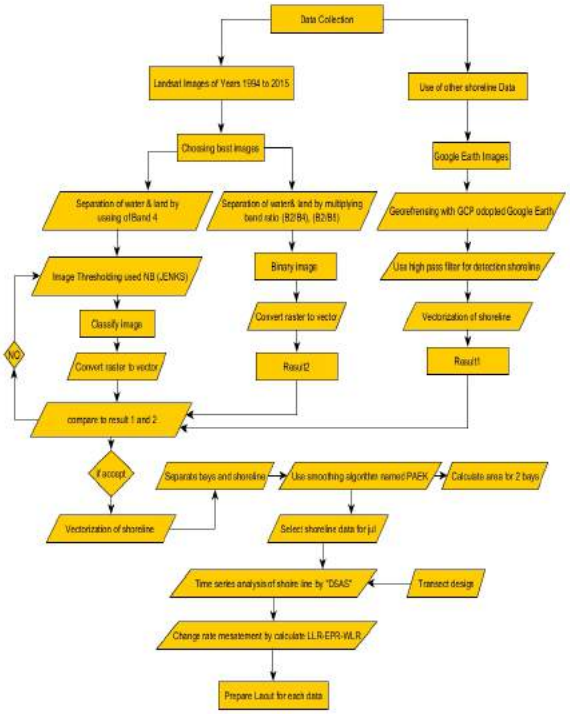

Fig. 3. Methodology Flowchart

3. Results and Discussion

Shorelines derived from Landsat imagery were analyzed in order to determine the degree of evolution between different time intervals within the selected areas

of interest. Based on the study conducted by Kakroodi, A. A. et al. [4], during sea-level fall the Gorgan bay areal extent decreased to 323 km^2 in 1975. Followed by rising the CS water level, Gorgan bay grew and covered an area of about 523 km^2 in 1998. Since 1998 onwards contemporaneous with sea level changes, the bay surface area has demonstrated a dynamic trend as well (Fig. 4). The areal extent of the bay has reduced by losing the total area of ~151 km^2 through the study period to ~372 km^2 in 2015. The calculated measures of changes in areal extents of Gomishan area has indicated a high degree of similarity to Gorgan bay evolutionary trend (Fig. 4). The surface area of the Gomishan lagoon was ~148 km^2 in 1994, reached up to ~155 km^2 in 1998 and then decreased to ~15.5 km^2 in 2015 drastically. Coastal morphology of the southeastern CS coastal zone correlates strongly with water level fluctuations. As illustrated in Fig. 5, most substantial changes within the study area occurred in recent years due to rapid fall in CS water level

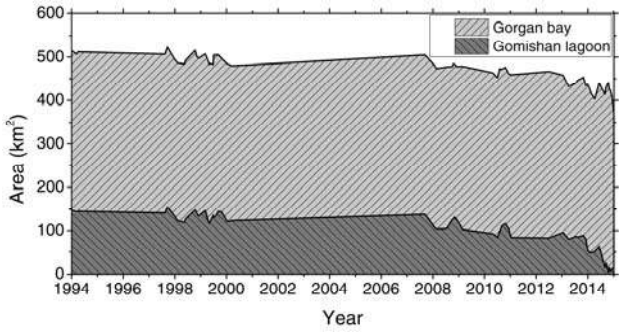

Fig. 4. Variations in areal extents of study area during 1994-2015.

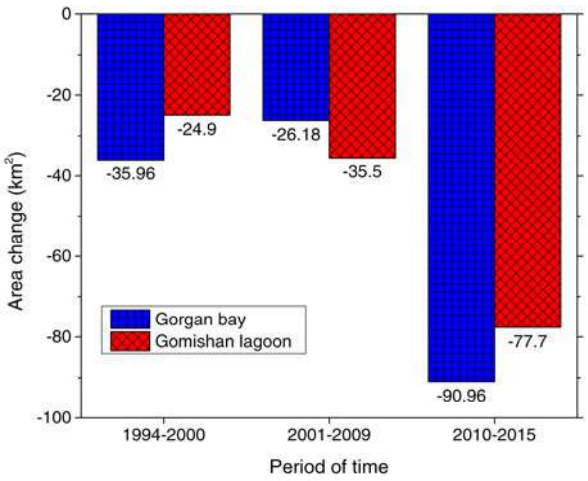

Fig. 5. Changes in surface area of study region over the specified time period.

Analyzing the data on rate of changes in areal extents employing linear regression approach shows a negative trend both in Gorgan bay and Gomishan lagoon (Fig. **6**).The Gorgan bay and Gomishan area have reduced in size by 0.01084 km^2/year and 0.01312 km^2/year respectively over a 22 year period.

4. Conclusions

The response of the barrier-lagoon systems in the southeastern CS coastal segment to sea level changes have been examined by using the satellite derived products. Our findings suggest that coastal variability of the study area is largely affected by water level fluctuations in the CS. Both Gorgan bay and Gomishan lagoon undergo significant reduction in their areal extents as a consequence of fall in CS water level during recent years. Accelerated water level decrease in the CS is a particular threat to low-lying, shallow-gradient coastal ecosystem dynamics, like the selected areas of interest and will lead to disappearing and drying up the coastal lagoons eventually.

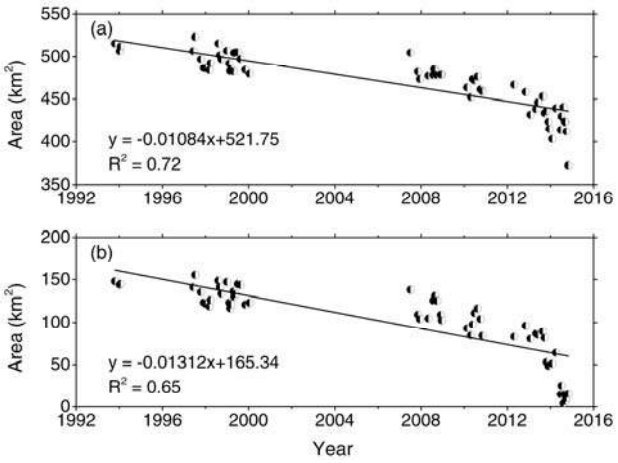

Fig. 6. Linear regression analysis determined by plotting the amount of areal extents with respect to time for: (a) Gorgan bay and (b) Gomishan lagoon.

5. References

[1] Lebedev, S. A., Ostroumova, L. P., and Sirota, A. M., "Seasonal and Interannual Variability of the Caspian Sea Evaporation on Remote Sensing Data", in European Geosciences Union (EGU) General Assembly, Vienna, Austria, April 13-18 2008.

[2] Kasimov, N. S., and Lychagin, M. Yu., "Environmental Geochemistry of the Caspian Coastal Zone", in Proceedings the Caspian Region: Environmental Consequences of the Climate Change, Moscow, Russia, October 14-16 2010, pp. 21-23.

[3] Kaplin, P. A., and Selivanov, A. O., "Recent Coastal Evolution of the Caspian Sea as a Natural Model for Coastal Responses to the Possible Acceleration of Global Sea-Level Rise ", Marine Geology, 124, 1-4, May 1995, pp. 161-175.

[4] Kakroodi, A. A., Kroonenberg, S. B., Hoogendoorn, R. M., Mohammad Khani, H., Yamani, M., Ghassemi, M. R., and Lahijani, H. A. K., "Rapid Holocena Sea-Level Changes along the Iranian Caspian Coast", Quaternary International, 263, June 2012, pp. 93-103.

A ROBUST APPROACH FOR BERTH SCHEDULING PROBLEM IN SHAHID RAJAEE CONTAINER PORT

Ali Dadashi[1], Aborreza Sheikholeslami[2], Erfan Babaee Tirkolaee[3], Mani Bakhshi Sasi[4]

1) M.Sc. Transportation Planning, Iran University of Science and Technology, ali.dadashi1990@gmail.com
2) Assistant Professor, Iran University of Science and Technology, Civil Engineering Faculty, Sheikh@iust.ac.ir
3) PhD Candidate, Industrial Engineering, Mazandaran University of Science and Technology, e.babaee@in.iut.ac.ir
4) M.Sc. Industrial Engineering, Isfahan University of Technology, m.bakhshi@in.iut.ac.ir

Abstract

Berth scheduling is one of the most important problem in container terminals. Any change of berth plan may lead to significant changes of other operations, deteriorating the reliability and efficiency of terminal operations. In this paper, a robust berth scheduling problem (RBSP) which considers the uncertainty of vessel arrival delay and handling time is studied. Slack times are inserted between the vessels occupying the same berthing location to give room for uncertain delays. The results have shown the proposed approach has significant effect in absorbing delays caused by uncertainty.

1. Introduction

Berth Scheduling Problem (BSP) refers to the problem of allocating berth space for set of vessels within a specific time horizon in container terminal. Most past research on the BSP concerns how to obtain an initial schedule (baseline schedule, or berth allocation template) in a static and deterministic environment complete information [1]. There are few research that considers uncertainty in model [2-4]. However, in reality, there are a lot of uncertain factors and unexpected events, e.g., deviation of arrival time and operation time from the initial baseline schedule. Ignoring uncertainties in making berth allocation plans may result in last minute scrambling and changes of plans, which include berthing plans, quay crane assignment plans, yard storage allocation plans, etc. Therefore, port planners have to protect the initial baseline schedule from adverse effects of possible disruptions. For detailed research review, we refer readers to Beirwirth and Meisel [1, 5].

Robust Berth Scheduling Problem

In this paper a dynamic berth scheduling model is proposed to schedule multiple separate terminals with continuous wharf space in Shahid-Rajaee container port. We consider uncertainty in arrival and handling time by inserting time buffers between the vessels occupying the same berthing location to give room for uncertain delays. Total departure delay of vessels is used as the service measure. We added a buffer time for each vessel's handling time to consider uncertainties. The quantity of proposed buffer time is as below:

$$\theta_i = \max(\alpha h_i, c_i) \tag{1}$$

θ_i, h_i, α respectively denote buffer and handeling time of vessel i, percent of handeling time that is considered for buffer time of vessel i, and c is minimum quantity of a buffer time.

2. Mathematical Model

Before we present the mathematical formulation, we present the notation used in Mathematical Model. $V = \{1,...,n\}; i, j \in V$ and $Q = \{1,...,K\}; k \in Q$ are set of vessels and terminals, respectively. $a_i, R_i, D_k, d_i, h_i, l_i$ L, L_k, and M are estimated arrival time of vessel i, requested departure time of vessel i, quay depth of terminal k, draft of vessel i, estimated operation time of vessel i, length of vessel i, length of wharf, the coordinate of ending edge of terminal k, and a Large number, respectively.

$$Min\ f = \sum_{i \in V} (y_i + h_i - R_i) \tag{2}$$

Subject to:

$$y_i + h_i \le y_j + M(1-\alpha_{ij}) \qquad \forall i, j \in V, i \ne j \tag{3}$$

$$x_i + l_i \le x_j + M(1-\beta_{ij}) \qquad \forall i, j \in V, i \ne j \tag{4}$$

$$\beta_{ij} + \beta_{ji} + \alpha_{ij} + \alpha_{ji} \ge 1 \qquad \forall i, j \in V, i \ne j \tag{5}$$

$$y_i \ge a_i \qquad \forall i \in V \tag{6}$$

$$\sum_{k \in Q} \delta_{ik} = 1 \qquad \forall i \in V \tag{7}$$

$$x_i \ge (\delta_{ik}) \times L_{k-1} \qquad \forall i \in V, \forall k \in Q, k > 0 \tag{8}$$

$$x_i + l_i \le \sum_{k \in Q} \delta_{ik} \times L_k \qquad \forall i \in V \tag{9}$$

$$(d_i - D_k) \times \delta_{ik} \le 0 \qquad \forall i \in V, \forall k \in Q \tag{10}$$

$$\delta_{ik} \in \{0,1\} \qquad \forall i \in V, \forall k \in Q \tag{11}$$

$$\beta_{ij}, \alpha_{ij} \in \{0,1\} \qquad \forall i, j \in V, \mathrm{i} \neq \mathrm{j} \qquad (12)$$

Objective function (2) minimizes the total departure delay time of all the vessels. Constraints set (3) to (5) ensure that there is not an overlap between vessels in time-space dimension. Constraints (6) ensure that each vessel cannot be berthed before arrival. Constraints (7) ensure that each vessel is served at one terminal. Constraints set (8) and (9) ensure that the full length of the vessel is accommodated at the terminal served. Constraints (10) guarantees that the draft of each vessel is less than the berthing terminal's depth. Finally, constraints (11) and (12) show the domain for decision variables.

3. Evaluating the Robustness of Model

In this section, the robustness of model is investigated by adding buffer time to handling time of each vessel. For this purpose, 10 data samples are selected from Shahid-Rajaee container port. We randomly generate 10 scenario for each data sample to simulate the uncertainties in arrival and handling time. We assume the arrival time and handling time respectively belong to $[a_i - 20, a_i + 20]$ and $[0.9\ h_i, 1.1h_i]$ (the time unit is 15 minute). For berth reallocation problem, we have borrowed the approach proposed by Zeng et al. [6]. Results of this the experiment has been implemented for $\theta_i = \max(0.1h_i, 4)$. The mathematical model is encoded in CPLEX. Mean absolute value of deviation for departure time and vessel's berthing position in proposed scenarios of each sample is shown respectively in figures (1) and (2) for Robust Berth Scheduling Problem (RBSP) and Deterministic Berth Scheduling Problem (DBSP). As the figures are shown, by adding proposed buffer time, terminal planners are able to reduce the deviation in departure time and berthing position significantly, and this buffer time inserting can absorb the negative effects of uncertainty in arrival and handling time and improve the robustness of the model significantly.

4. Conclusion

In this paper, we have presented a hybrid berth scheduling problem with uncertain arrival times and handling times of vessels. We have proposed an approach based on adding buffer time to each vessel handling time to absorb existing uncertainties. The results has been shown both the actual departure delay and berthing position deviation achieved by the RBSA solutions are reduced significantly.

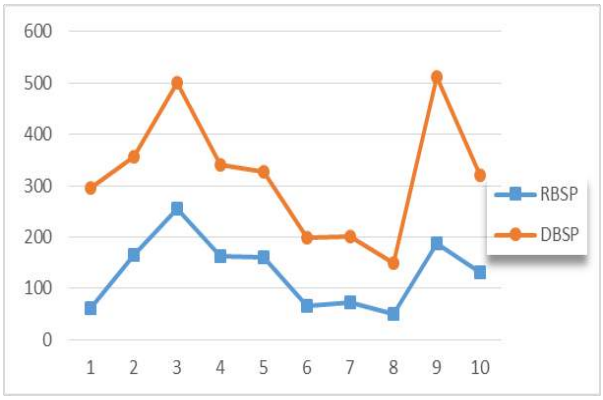

Figure 1. Mean absolute value of deviation in the departure time of vessels for each sample

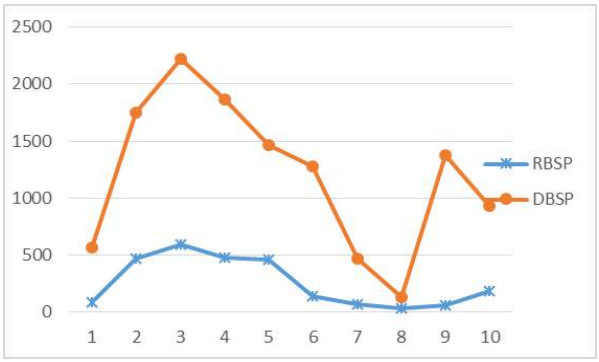

Figure 2. Mean absolute value of deviation in berthing location of vessels for each sample

5. References

[1] C. Bierwirth and F. Meisel, "A survey of berth allocation and quay crane scheduling problems in container terminals," European Journal of Operational Research, vol. 202, pp. 615-627, 2010.

[2] M. Golias, I. Portal, D. Konur, E. Kaisar, and G. Kolomvos, "Robust berth scheduling at marine container terminals via hierarchical optimization," Computers & Operations Research, vol. 41, pp. 412-422, 2014.

[3] C. Q. Xu Y, Quan X, "Robust berth scheduling with uncertain vessel delay and handling time," Annals of Operations Research, vol. 192, pp. 123-140, 2012.

[4] D.-F. C. Lu Zhen "A bi-objective model for robust berth allocation scheduling" Computers & Industrial Engineering, vol. 63, pp. 262–273, 2012.

[5] C. Bierwirth and F. Meisel, "A follow-up survey of berth allocation and quay crane scheduling problems in container terminals," European Journal of Operational Research, vol. 244, pp. 675-689, 2015.

[6] Q. Zeng, X. Hu, W. Wang, and Y. Fang, "Disruption Management Model and Its Algorithms for Berth Allocation Problem in Container Terminals," International Journal of Innovative Computing, Information and Control, vol. 7, pp. 2130-2142, 2011.

MARICULTURE SITE-SELECTION STUDY ALONG MAKRAN COAST VIA A SPATIAL MULTI-CRITERIA DECISION MAKING MODEL

Babak Banijamali[1]& Amirhamed Alviri[2]

1) Head of Coastal Engineering Division, Darya-Bandar Consulting Engineers, Tehran, Iran, babak.banijamali.babak@daryabandar.com
2) Senior Coastal & Marine Structural Engineer, Darya-Bandar Consulting Engineers, Tehran, Iran, amir.hamed.alviri@daryabandar.com

1. Introduction

Consensually, the rising trend of utilizing mariculture potential around the world is deemed an absolute necessity in the quest by mankind to address crucial food security issues faced by the ever-increasing population of the planet earth, in addition to partaking of the significant economical rewards of this relatively new industry, not only in wealth creation for the sea-bordering states, but also in creating long-term employment to empower the underprivileged in coastal communities. Moreover, re-stocking of endangered marine species is another environmentally beneficial application of mariculture. Consequently, as preliminary studies for the Iranian Fisheries Organization (IFO) by international experts emphasize the fact that in terms of generating revenue, this industry has tremendous prospects, potentially being second only to the petroleum sector, therefore, mariculture has been allocated a vital role as stipulated within the sixth national four-yearly development plan. Accordingly, to ensure an environmentally sustainable yet economically advantageous approach to developing this industry, identifying suitable marine aquaculture sites within the Exclusive Economic Zones (EEZ) of Iran is of paramount importance so as to pin-point suitable locations as well as derive an estimate of the carrying capacities of nearshore marine aquaculture yield which can tremendously boost the national gross domestic product [1].

In order to ensure that environmental sustainability and social justice concerns are soundly taken into account, thereby, avoiding the pitfalls which have often hampered the sound development of other industries, the approach to coastal aquaculture as adopted by this manuscript shall be within a Marine Spatial Planning (MSP) scheme, whereby, the relative compatibility of all perceived present and planned future human activities in the marine realm as well as their associated land-bases are holistically evaluated within a spatial & temporal system [2, 3].

As a result, IFO has defined projects to undertake mariculture site-selection study as well as other specialized fish-cage related studies for all Iranian coasts, with the region delimited by Jask cape on the East to the Gowater bay by the Pakistan border on the West within the so-called Makran coast being the subject of this article (see Figure 1).

2. Methodology

2.1. Makran Study Area

Makran region neighboring the North-Western Indian Ocean extends eastward from the Western edge of the Strait of Hormoz inside Iran to near Karachi within Pakistan with a linear expanse of about 900 km, owing its name to the well-known tsunami-genic Makran Fault-line.

A multitude of factors inter-play within such a site-selection study in this area with its own particular characteristics, such as annual Monsoon swells, the possibility of tropical cyclones resulting in sustained wind speeds reaching beyound 204 (km/h) generating sea-waves of heights over 7 (m), annual sea surface temperature ranges between 21 to 35 (^{o}C), and mean annual sea-water salinity of about 37 (ppt). Albeit, an significant point to bear in mind for planning ahead in all aspects of this study including the choice of the species to use in fish-cages is the climate change.

Notably, there are many coastal and marine engineering aspects such as water waves, currents, wind speeds as wells as phenomena inter-alia tsunamis which are to be investigated before a properly constructed fish-cage structure, as an offshore structure at times designed by the same engineers who design offshore platforms for the petroleum industry, can be safely moored at the right location in the sea to ensure minimal environmental risks to the fish stock to be grown while maximizing the expected financial yield for the investor.

2.2. Conceptual Analysis Model

For the sake of data processing & modelling, the Remote Sensing (RS) & Geographical Information System (GIS) software utilised in this study were SeaDAS 7.2 and ArcGIS 10.3, respectively. The model structure as adopted for identifying relative suitability of mariculture sites was devised based on the well-known hierarchical structures philosophy, breaking down all inter-playing criteria into smaller groups. At the highest level, the most general objectives are set which can still be defined at lower levels, with the lowest level of the hierarchy being the attributes [4]. Based on existing scientific literature, the present study identified 13 criteria, divided into three sub-models (biophysical, social-infrastructural and constrains), to fulfill

suitability requirements for marine aquaculture (see Figure 2).

Figure 1. The Study area: Makran Coast

Firstly, all pertinent data were acquired either via specialized modeling or from remote-sensing data repositories. Secondly, these were integrated into the spatial database for the sake of reclassification in order to create a standard scoring method. Subsequently, a relative weight for each criterion and factor were established. Thereupon, the pairwise comparison method as originally developed by Saaty (1977) [5] in the context of the Analytic Hierarchy Process (AHP) was employed to derive a set of relative weights for each parameter. Notably, the 'constraints' constitute a Boolean Algebra filtering, typically, characterizing the regions deemed off-limit to aquaculture. It is strived to incorporate all potential uses of the coastal area for the energy sector, tourism, and so-forth in the decision-making process.

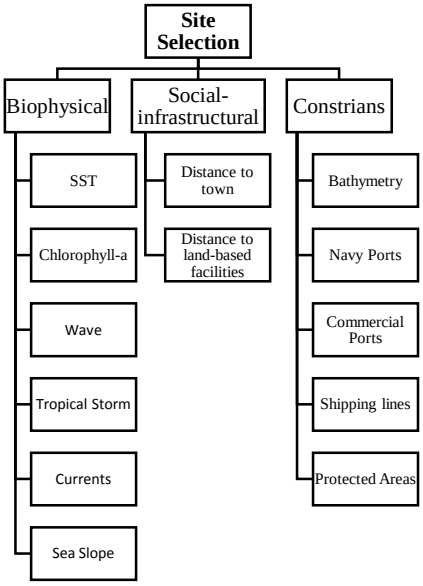

Figure 2. A Hierarchical Modeling Scheme to Identify Suitable Sites for deploying Fish-Cages

3. Results & Conclusions

The study focused on the selection of the most suitable areas for mariculture along the Makran coasts, where different criteria were grouped into two sub-models. For instance, as depicted in the following two plots (see Figure 3 & 4), where the permitted range for the sea-bed depths are set to from 20 to 60 (m), the devised model classified marine areas to possess most suitable, fairly suitable, least suitable, and unsuitable mariculture potential, with the latter being denoted in the colour black.

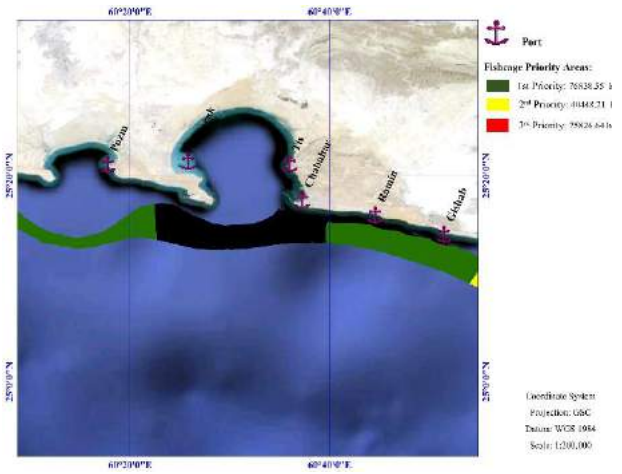

Figure 3. Mariculture Suitability Maps (Chabahar Bay)

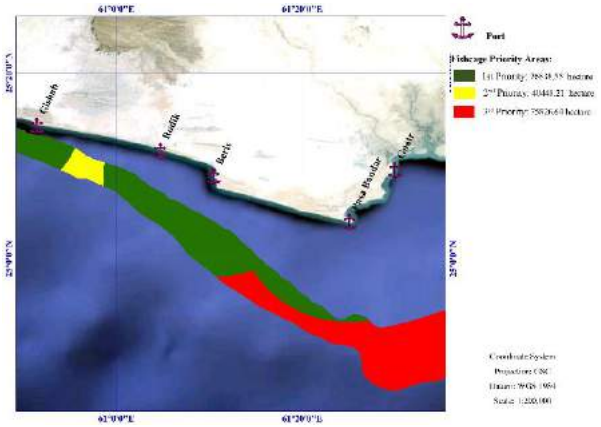

Figure 4. Mariculture Suitability Maps (Gowater Bay)

4. References

[1] GESAMP (IMO/FAO/UNESCO/WMO/WHO/IAEA/UN/UNEP Joint Group of Expert on the Scientific Aspects of Marine Pollution), *The contribution of science to integrated Coastal management*, 1996, Reports and Studies GESAMP, 61.

[2] UNESCO, *Marine spatial planning: a step-by-step toward approach,* 2009, IOC Manual and Guides, No. 53.

[3] UNESCO, *A guide to evaluating Marine Spatial Plans,* 2014, IOC Manual and Guides, No. 70.

[4] Malczewski, J., 2000. *On the use of weighted linear combination method in GIS*: common and best practice approach. Trans. GIS 4, pp. 5–22.

[5] Saaty, T.L., *A scaling method for priorities in hierarchical structures*, 1977, J. Math Psychol. 15, pp. 234–281.

UTILIZATION OF MOBILE GIS TECHNOLOGY, AN EFFECTIVE STEP TOWARDS ESTABLISHING MOBILE GOVERNMENT IN PMO (PORTS AND MARITIME ORGANIZATION)

Hamed Sartipi [1],Jalal Karimi [2] and Behzad Alvand[3]

1) Fara Omran Negar Engineering Company, Tehran, Iran, hamedsartipi@yahoo.com
2) Port and Maritime Organization (PMO), Tehran, Iran, jkarimi@pmo.ir
3) Port and Maritime Organization (PMO), Tehran, Iran, balvand@pmo.ir

1. Introduction

One of the lingering issues of the governments from past, has been interacting with organizations, institutes and people of a country.

Offering fair services, optimized application of government resources, effective relationship with segments and subsets of the government, interacting with private sector and increase of civil partnership in managing the country, are all prerequisites of modern governments.

Expansion of communication and information technologies, made it possible for governments to pursue the idea of Electronic Government, thus manage the limited government resources in an optimized way and increase the quality and scope of their various services and fulfil their inclusive growth.

In recent years with the expansion of wireless technologies, the ability to accelerate making the idea of Electronic Government a reality using the infrastructure of mobile phones, has been welcomed more than ever.

Ease of usage, high penetration factor, flexibility in providing services, awareness of audience characteristics, having no need for special trainings and infrastructure and continual access are all the reasons encouraging goverments to welcome the idea of Mobile Government.

Mobile spatial information management systems or simply Mobile GIS, are information systems which are accessible in wireless networks using cellular devices and are based on using position of these cellular devices.

These definitions, describe Mobile GIS as the intersection point of three technologies. These technologies are NICTs: New Information and Communication Technologies (including cellular communication systems and cellular devices), Internet Technology and Geographic Information System (GIS).

Due to the shores of the country being spread in a vast geographic bed and the necessity of doing inspection and monitoring operations on the shores and ports of the country, utilization of Mobile GIS technology in order to improve the quality of monitoring and governmental activities of PMO has been addressed in this article.

2. Research Questions

Monitoring and inspection are inseparable parts of every government's responsibilities. Providing appropriate methods of improving and increasing the efficiency of monitoring systems is an effective step towards making governments capable followed by development and prosperity of the country.

Hereon, at PMO which is responsible for monitoring the shores and providing services to the people at ports, appropriate operating of the organization under constant monitoring is an undeniable necessity.

Implementation of Mobile GIS technology as a fitting method of carrying out monitoring operations has been suggested in this article.

Implementing this technology makes monitoring operations on the shores and the facilities present at the ports mechanized in addition to, making the inspection job of inspectors more feasible.

Moreover, maintenance and repair managers will have a more appropriate means of monitoring the personnel by gaining the ability to observe their location on a map online using Mobile GIS technology.

3. Methods

In order to present the suggested method of tackling the issues in operation of monitoring the facilities and personnel in private sector companies, we summarize the applications of Mobile GIS technology.

3.1. Applications of Mobile GIS

Mobile GIS structurally consists of components that are shown in diagram 1 below.

Diagram 1. *Components and their relationships in Mobile GIS*

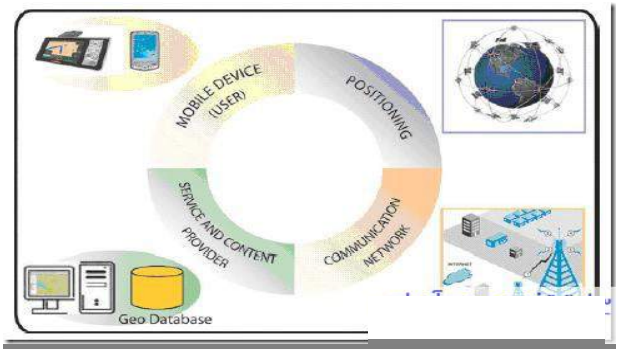

Afterwards the specifications of the methods based on Mobile GIS technology are presented:

- The ability to use both online and offline maps in order to access data
- The ability to use regular basic maps (Google Map, Bing, etc.)
- The ability to use two technologies for positioning (GPS in tablet devices and positioning using GPRS)
- The ability to send and receive data on various communication infrastructure such as: GPRS, WIFI, SMS, etc.
- The ability to perform scheduled field monitorings
- The ability to send online inspection orders to the dispatched teams
- The ability to save recorded spatial data with proper accuracy in a user friendly way
- The ability to save recorded descriptive data and inspection check lists based on dynamic forms
- The ability to implement restrictions on the allowed radius for recording data
- The ability to provide recording users with spatial guidance using basic and geographical positioning maps

Diagram 2. *The ability to guide the inspectors to gain access to the inspection site*

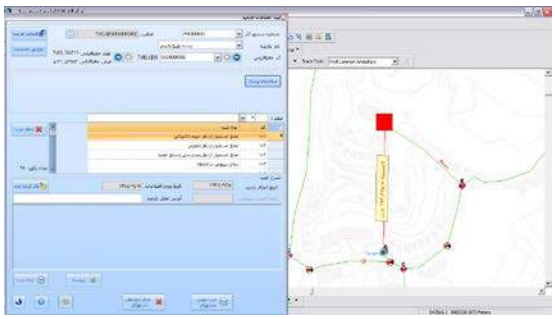

- The ability to observe spatial and descriptive data of online or offline maps required for recording data (sent from a central position based system)
- The ability to track the inspecting personnel
- The ability to generate various forms of reports

Diagram 3. *The ability to generate various forms of reports*

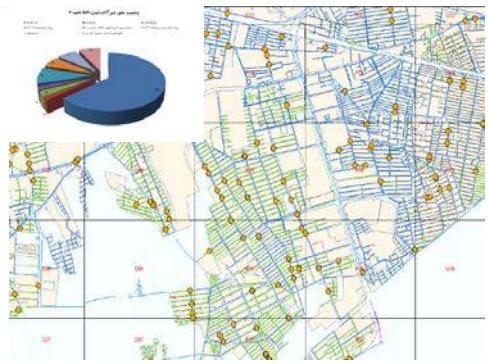

4. Discussions and Conclusion

Mobile GIS technology, is a type information technology accessible through the use of cellular devices on wireless networks and based on application of positioning of these devices.

Utilizing this technology in inspection operations performed by respective personnel of PMO is suggested as a fitting method in this article.

Implementing this technology in addition to making the monitoring process mechanized, helps the personnel perform the respective monitoring operation with more ease and less errors.

Also, the managers will have a more appropriate means of controlling their personnel through having the ability to monitor them online on a map using Mobile GIS technology.

5. References

[1] Paul, A., (2001). Geographic Information Systems and Science, LONGLEY

[2] Sartipi, H., Beiralvand, B. and Fath'ali M., Systems of Maintenance and Repair Using GIS, Fifth Confrence of Maintenance and Repair

[3] Sartipi, H., Khodchiani, R. and Asl Alinejad Fard, M., Increasing Efficiency in Inspection and Manoeuvre of Water Supply System Components using LBS Services, Nineth Confrence of Maintenance and Repair

[4] Billinton, R. and Allan, Ronald N., Reliability Evaluation of Power Systems, Plenum Press, New York, 1996.

A NAVIGATION ALGORITHM FOR AN UNMANNED BOAT

Hossein Mousazadeh[1*], Hamid Jafarbiglu[2], Hamid Abdolmaleki[2], Elham Omrani[2], Farshid Monhaseri[3], Mohammad-reza Abdollahzadeh[3], Aref Mohammadi-Aghdam[3], Ali Kiapei[4], Hossein Azimi[5], Mohammad-ali Mousapour-Gorji[6], Yousef Salmani-Zakaria[3], Ashkan Makhsos[3]

1-Assistant Pro. Mechanical Engineering of Biosystems. University of Tehran. hmousazade@ut.ac.ir

2 -Ph.D. candidate, Mechanical Engineering of Biosystems. University of Tehran

3-M.Sc. student, Mechanical Engineering of Biosystems. University of Tehran

4-Engineer in Mechanical of Biosystems and expert of ports and maritime organization. Iran.

5-Deputy of Research & Development in Amirabad Port Special Economic Zone

6- Head of Studies and Planning in Amirabad Port Special Economic Zone

*Corresponding author: Assistant Pro. Mechanical Engineering of Biosystems. University of Tehran. Telefax: 0098-26-32801011. Email: hmousazade@ut.ac.ir

1. Introduction

USV technology is rather new in contrast to autonomous underwater vehicles (AUVs) which has already reached its maturity. [1]. USVs are robots for operation at lakes, canals, harbors and even open sea that are characterized by small size, good hiding capability, high mobility, and low price [2],[3]. Liu et al., (2015) introduced a path planning algorithm for the USV formation navigation based on the fast marching (FM) method, which has features of fast computation speed and low computation complexity [4].

2. Materials and Methods

This manuscript explains a part of a complete scientific project (Morvarid [1]) that is pending for tracing the hydrography map of a harbour in the bureau using an USV. The Morvarid is a plug-in hybrid solar powered USV, equipped with two thrusting motor each with 133 N thrust force. This boat length, width and height approximately are 3.8, 2.4 and 1.5 m respectively. Its overall weight is about 600 kg. An 8 kWh high technology Li-ion battery pack can extend its stability for more than three continues cloudy days. To perform the defined duty, it is equipped with some local perception and global monitoring sensors as; a simple GPS, pack of state sensor (IMU, compass and air pressure), range finder Lidar, a set of ultrasonic sensors, stereoscopic vision system and four single beam echo-sounders. The 3D CAD model of the Morvarid is shown in the Figure(1-a) and its first test in the Persian Gulf lack, suburban of Tehran is illustrated in Figure(1-b).

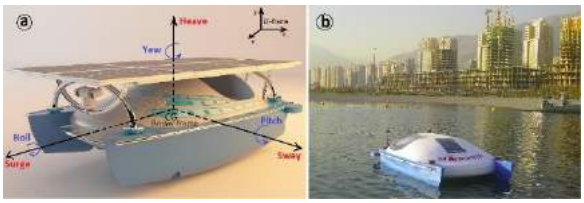

Figure 1. a) The Morvarid 3D CAD model b) The first test of Morvarid in the Persian Gulf lack, Tehran.

This USV can operate in four modes by a priority as: a) manual operation by a joystick on the vehicle, b) remote control by a handheld unit c) control from office using a GUI and d) fully automatic path following.

According to Fossen (1996) [25] dynamic model of the marine vehicle in six degrees of freedom (DOF) is derived that is explained in full text.

To best estimate the statues of the vehicle, extended Kalman filter (EKF) is used.

Between path following algorithms, potential field method is one of the most well-known algorithm that operate according to magnetic potential field. Approximately in all developed algorithms the destination point is a single point that attract the vehicle. Due to this, the main drawback with potential field techniques is their susceptibility to local minima. To dissolve this problem, an algorithm is developed based on the combination of potential field and

[1] Emorvarid.ut.ac.ir

research ball algorithms [5]. This concept, is illustrated in the Fig. (2), as NGC algorithm.

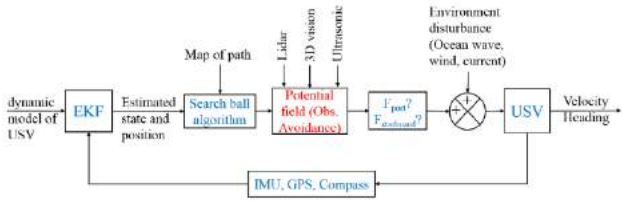

Figure 2. The architecture of navigation, guidance and control

To detect obstacles, three set of sensors were used. According to Fig. (3), a Lidar (Hokuyo's UXM series) is used in front of the boat that covers 190^{o}. To cover the rear area, stereoscopic system is under development using two CCD cameras and finally a set of ultrasonic sensors using 14 waterproof modules (JSN-SR04T) is used that detect near obstacles approximately all-around of the vehicle.

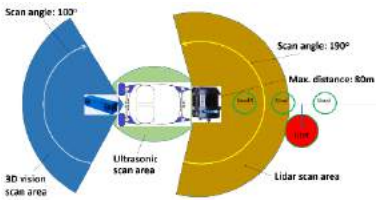

Figure 3. Obstacle avoidance senores and cover area of each system

For Morvarid USV the first test is performed in real situation and useful experimental data is obtained for some sensors e.g. GPS. However to evaluate the robustness and confidantes of the developed NGC algorithm, before second test, it is simulated as hardware-in-the-loop by using Lidar, GPS, IMU/compass and ultrasonic sensors as a real data acquisition sources. The algorithm is programmed and developed using visual C# in Microsoft Visual Studio software.

3. Results and discussions

To plot the hydrography map of purpose port, all area is divided to straight lines that connect at end by U turns. Many points on the lines are regarded and 2D position of points are defined in earth fixed frame. Figure (4) illustrates three of these lines. As shown in the figure, the lines are 800 m in length and with 150 m distance to each other. The predefined path is drawed by blue line and GPS data is pointed by green, while the estimated positions are shown by red line. For careful illustration, the GPS data is drawed by multiplying data to 10 in y direction.

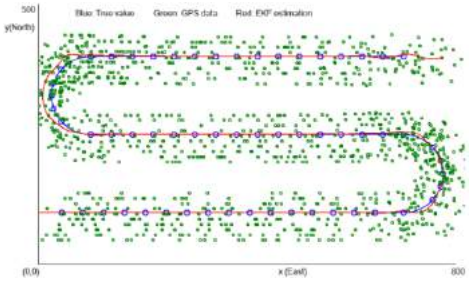

Figure 4. Path following by EKF estimator and combination of search ball and potential field algorithm

According to Fig. (5), the developed algorithm follow the straight paths very precisely, while some errors are present for U turns.

Result of obstacle avoidance algorithm is shown in the Fig. (5). Two different obstacles in two different positions are regarded. The algorithm is evaluated, changing position and size of obstacle in different cases. Results are discussed completely in the full text.

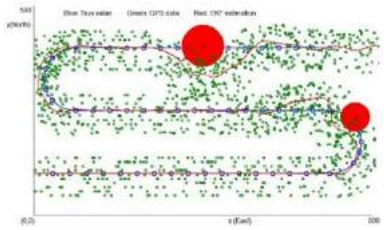

Figure5. Obstacle avoidance with two obstacles

Acknowledgment: Authors would like to acknowledge the Ports and Maritime Organization for funding the Morvarid Project No. 20S/7509. 2015.

4. References

[1] Naeem W., Xu T., Sutton R. Chudley J. 2007. Design of an unmanned catamaran with pollutant tracking and surveying capabilities. Published by the Institution of Engineering and Technology. 99-113.

[2] Tang P., Zhang R., Liu D., Huang L., Liu G., Deng T. 2015. Local reactive obstacle avoidance approach for high-speed unmanned surface vehicle. Ocean Engineering.106, 128–140.

[3] Campbell S., Naeem W., Irwin G.W. 2012. A review on improving the autonomy of unmanned surface vehicles through intelligent collision avoidance manoeuvres. Annual Reviews in Control. 36, 267–283.

[4] Liu Y., Bucknall R. 2015. Path planning algorithm for unmanned surface vehicle formations in a practical maritime environment. Ocean engineering. 97, 126–144.

[5] Más F.R., Zhang Q., Hansen A.C. 2010. Mechatronics and intelligent systems for off-road vehicles. Springer. 62-65.

FORECASTING CONTAINER CAPACITY USING ARTIFICIAL NEURAL NETWORK ALGORITHM AT RAJAIE SEAPORT

Amin Karimi Jashni, Sobhan Iranshahi
1) Hormozgan Province Maritime & Ports Authority, Bandar Abbas, Iran, a.jashni@gmail.com
2) Hormozgan Province Maritime & Ports Authority, Bandar Abbas, Iran, Sbn.iranshahi@gmail.com

1. Introduction

In this research Artificial Neural Network (ANN) as a main tool calculations was used for container capacity prediction at Rajaie seaport. The ANNs are a learner trainee network base on the samples, like the human. The ANNs could be arranged for different tasks, such as pattern recognition, information categorizing, prediction, and etc. [1]. This application many times were used as a powerful calculations tool for estimation and prediction based on the input data [2]. These tools included two important part; trainee, and test.

First, the network trained using the input data, then this network will be used for simulation in the second step (test). On the other hand performance of these process are non-simultaneously. Forasmuch as, ANNs are accurate for estimations therefore used in this project to estimate the container capacity in Rajaie seaport.

2. INPUTS AND OUTPUTS

Several parameters which have effects on the estimation, explained as below [2]:

1- Gross Domestic Production (GDP)
2- Fuel Price
3- Transit of the container ship number for a determined period in Rajaie Port
4- Loading and un-loading of the container in Rajaie Port (TEU)
5- Iran Inflation Rate.
6- Power workload of the Rajaie port (Velocity of the loading and un-loading (Tons/hour).

These parameters were collected for 10 years (2002-2011). Of course, this simulation could be applied for other system parameters. Also, the results are more accurate if further parameters were used for network training.

3. ANN TYPE AND STRUCTURE

There are different type of artificial networks so that, simulation times and accuracy depend on upon the input or middle layer of the network, number of cells in the layers. Reducing the layers and cells number will be reduced the simulation time and network complexity. However, network efficiency is dependent on the trade-off between the number of layers, cells, results accuracy, and simulation time. MATLAB software was used to train a multi-layer perceptron (MLP) with two-layer as a feed-forward ANN model to map the set of input data onto an appropriate output estimation for container prediction. The uncertainty of simulation results were less than 1e-3.

Linear regression give graphs for network output that is a forecasting function for port capacity (figure 1).

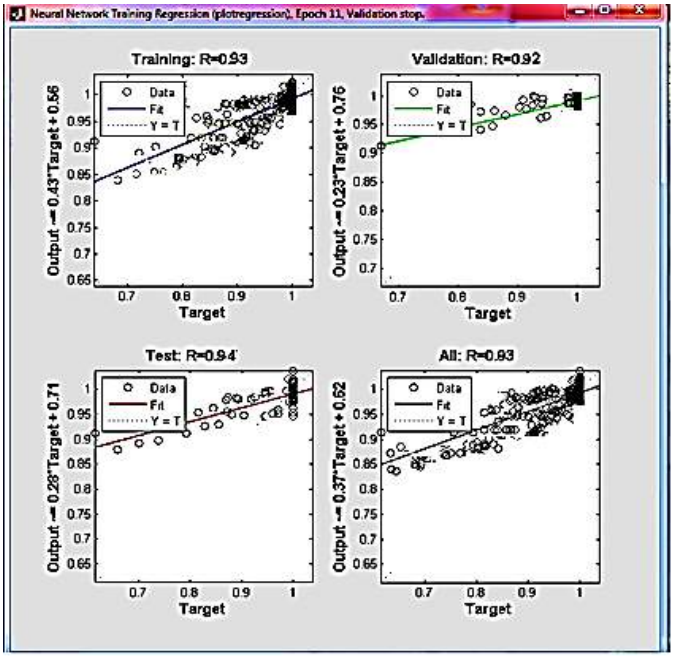

Figure1: Observation of training, Testing and evaluation of data for forecasting port capacity with accurately 93%.

4. RESULTS AND DISCUSSION

In Figure 1, compared the ANN model results and the actual value during 10 years from 2002 to 2011 as one can see the model track the actual value, very well. For example, this model predict a container number of 700000 at 2600000 TEU in year, while the actual value were 2011[4]. Also,

the average difference between the model results and the actual value were less than 4%. Therefore, this model can be used to estimate the container capacity for the future based on the input data library to reduce the costs. In this project, the ANNs computation tool was used to estimate the container capacity at the Rajaie port. To do this, database and documents for 10 years were extracted and used as an input source of ANN. The maximum difference between the model and actual data was 4%. However, using further information for a longer duration (i.e. 10 years) the prediction is more accurate. This application can apply for other seaports, to reduce the costs, and increase the productivity.

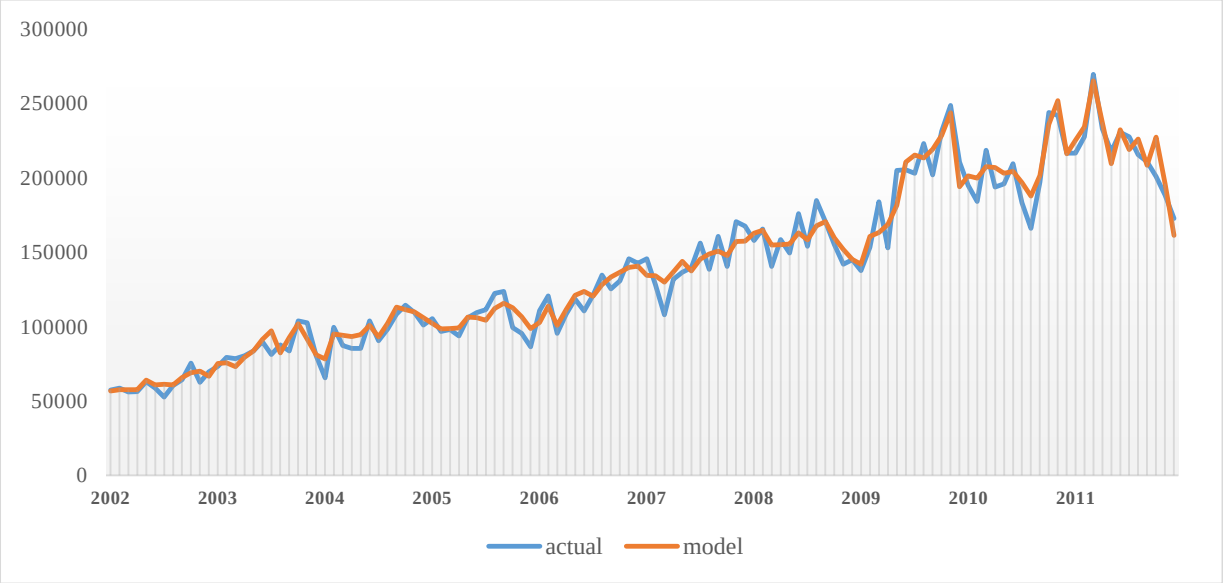

Figure 1: Comparison between model and actual value for loading (a), and unloading (b), for 12 months per year to 10 years.

5. Reference:

[1]. Gosasang, V. Chandraprakaikul, W. & Supaporn Kiattisin, "An Application of Neural Networks for Forecasting Container Throughput at Bangkok Port", *2010. July 2, London, U.K.*

[2]. Poularikas, A. "Handbook of neural network signal processing", CRC Press LLC, 2002.

[3]. Rodriguez, T. Gonzalez, G. & Soler, F. "Forecasting Models in Ports Transport Systems", *the 2nd Electronic International Interdisciplinary Conference*, 2013.

[4]. http://www.pmo.ir/en/statistics/annualreport, *access time*: 2014.11.23, 10:25.

SOLUTIONS TO SOME CHALLENGES FOR THE IMPLEMENTATION OF THE SMARTPORT STRATEGIES

Francisco Sarrias
Marina System Iberica, http://www.MSI.Barcelona, Spain, info@msicom.net

INTRODUCTION

The SmartPort strategies include all kinds of initiatives and projects that improve the operation efficiency and the sustainability of the activities in the ports.

The main targets for these strategies usually are the energy consumption reduction, the port operators carbon footprint decrease, the increase in the use of clean energies, the security increase and the reduction of the port activities impact in the urban environments, among others.

On the one hand, savings that can allow the return on the investment are sought, on the other hand, we want to improve the people quality of life.

THE FIRST CHALLENGE: THE INTEGRATED MANAGEMENT

It is essential to know what is happening in the port in real time to increase the port efficiency [3] .

In a port we usually have traffic control platforms that control through the AIS systems and radars the large size vessels state in the docks and the activity of the pilots, the tug boats, the maritime rescue service, the military police, the customs, the Red Crescent Movement, etc…

There are also the maritime navigation systems that inform about the marine lights and buoys state.

The geographic information systems (GIS) inform about the location of the different static port assets pictured in a cartographic way.

The energy measurement and control systems allow us to control the lighting, the energy consumption for buildings and storage areas, the moored boats with connection to the quay, the energy production of solar panels or wind mills or other generation sources, etc…

The security cameras, access barriers, smoke and gas detectors, weather stations, sonometers and measurement buoys also monitor the port environmental state (air quality, water, winds, noise levels, rain volume, tides, etc...).

Finally, the on-board GPS in the port police land vehicles, mooring crew, supply trucks, container trucks and mobile cranes show us what is happening in the docks at all times.

Our main challenge consists in integrating all this information in a single management platform since they come from different departments of the port authority or from third party contractors.

This platform should show all the relevant information related to each department and be fully integrated in order to know exactly the results of the decisions taken on it.

Spain has a pioneering role in the development of this kind of open-source platforms and has a strong financial support from the public administrations. The main platforms in the Smart Cities field are Sentilo.io [1] and Fiware [2] , well known for their maturity and presence.

Figure 1: Sentilo SmartCity platform

THE SECOND CHALLENGE: THE NON-ELECTRICALLY SUPPLIED ASSETS

Another challenge that should be settled to assure that the SmartPort strategy we are implementing is complete consists in including the non-electrically port assets, that is to say, the objects that don´t have their own power supply (connected to the main electrical network, battery or solar panel) and therefore cannot inform our control platform about their state or position.

These assets can be containers, platforms, barges, provisional fences, air compressors, hoists, ro-ro ramps, waste collection tanks, etc…

The increasing deployment of the communications network for IoT (Internet of Things) can fill this gap because it allows the development of small hardware devices provided with sensors and low consumption GPS that can easily be added to the objects in the port in order to inform our control platform about their state without worrying about the power supply.

These sensors include long-live batteries that can keep them active during a whole year or more without any service or maintenance needed.

In this area the main standards [4] are SigFox and LoRa that use very low power consumption communications standards. Many times the port does not need to invest in implementing its own infrastructure because there are telecommunications companies that offer this service with a pay per use model.

SOLUTIONS TO SOME CHALLENGES FOR THE IMPLEMENTATION OF THE SMARTPORT STRATEGIES

Francisco Sarrias
Marina System Iberica, http://www.MSI.Barcelona, Spain, info@msicom.net

Figure 2: Long live GPS tracker

CONCLUSIONS

The SmartPort strategies look for the efficiency of port operations, but at the same time they need to minimize the negative impacts that the port activity cause on the environment and human life.

The only way to make these two opposite objectives compatible is through technological platforms that permit to integrate all the information coming from the different systems and deploy a new generation of sensors and devices to control all the assets that so far has been difficult to get real time information so far.

The port community can use the new management systems for Smart Cities and the progress in the Internet of Things to achieve these goals.

Figure 3: 3D view of a Fi-Ware port platform

REFERENCES

[1] IMI, Barcelona., "Sentilo - Sensor and Actuator Platform for smart Cities", JoinUp: Share and reuse interoperability solutions for public administrations May 22, 2014.

[2] SmartPort: a visualization and information management system for the Port de la Luz de las Palmas (Canary Islands – Spain). J.P. Suárez Rivero (1), A. Trujillo Pino (2), C. Domínguez Trujillo (3), P. Fernandez Moniz (1), J. Santana Almeida (4) , A. Sánchez Medina (4) , S. Ortega Trujillo (4) , J.M. Santana Nuñez (2) (1) Division of Mathematics, Graphics and Computation (MAGiC). IUMA, Information and Communication Systems. Universidad de Las Palmas de G.C. josepablo.suarez@ulpgc.es; pablo.fernandez@ulpgc.es (2) Imaging Technology Center (CTIM). Universidad de Las Palmas de G.C. agustin.trujillo@ulpgc.es; josemiguel.santana@ulpgc.es (3) Gerencia de la Universidad de Las Palmas de G.C. gerente@ulpgc.es (4) Equipo de Fi-Ware de la Universidad de Las Palmas de G.C. fiware@ulpgc.es

[3] Description of the current situation of MED ports regarding the Smart Port criteria. Med-Maritime Integrated Projects consortium. 30/4/2015.

[4] Sigfox, LoRa : quelles différences entre les réseaux M2M pour objets connectés ? Thibaut Watrigant. 22/04/2015

Figure 4: Yacht harbour control application

INVESTIGATION AND FEASIBILITY STUDY OF ONSHORE POWER SUPPLY IN PORTS (CASE STUDY: AMIRABAD PORT)

Abdolreza Esmaeli[1] , Majid Rohipour asrami[2],Mahyar Zanjani[3]

1) Plasma and nuclear fusion research school, Nuclear science and technology research institute, Tehran, Iran, aesmaeli@aeoi.org.ir
2) Shahid Beheshti University PHD student ,Department of Electrical Engineering ,Tehran,Iran & Ports and Maritime Organization Electerical Expert, Amirabad port, Mazandaran, Iran, Rohipour.Asrami@gmail.com
3) Saveh Branch Islamic Azad University MSC student, Department of Electrical Engineering, Saveh,Iran zanjani.eng@gmail.com

1. Introduction

The increasing use of fossil fuels in recent decades and creating a variety of hazardous and toxic pollutants and its distribution in human environment, are serious concerns for humanity now and in the future. The use of fossil fuels for diesel engines providing power and energy requirements of ships in ports of the world to meet domestic requirements with the highest and most dangerous level of pollution among other factors will change the environment into the dustbin in which there will be no room for the human being which requires global consensus to reduce the use of fossil fuels. The scientific and practical suggestion tailored specifically for this application with the maximum proficiency, Power Supply of vessels in ports using the local electricity network according to international law and standards (IEEE, IMO, IAPH ...) to supply power supply requirements of ships docked at ports [1].

In this article the investigation and feasibility study of onshore power supply in ports of Iran with the case study of Amirabad port (one of the largest ports in the north of the country) is evaluated. Amirabad port is a multipurpose port located in the north of the country bordering Caspian Sea as one of the three major ports in the north along with Anzali and Noshahr (Figure 1).

Figure 1. Study area at Amirabad Port

The purpose of this article: maximum reduction of environmental pollution in ports, using the potential and actual power supply capacity in Iranian ports, updating and modernizing the Iranian ports in line with international standards, and transferring power supply with high quality and stability to vessels. At first, investigating the required power supply based on the Amirabad port electricity power network and various vessels and their specifications, including technical and environmental studies of ships during their berthing and unberthing period, statistical study of environmental pollutants, studying the cost and maximum revenue from the sale of energy, study and feasibility of building a system after designing in Iran, and finally submitting the final suggestions in order to implement the plan.

2.The Electerical Distribution Network in Amirabad Port

The double-fed distribution network of power supply in Amirabad port constitutes two separate feeders, one from the main key of 75-megawatt DG power plant and the other from the air network of regional distribution plants, with dispatching management and the high-voltage substation deployed in the area suppliers in 3-level 230/63/20 kV, provides a reliable and stable electrical power for all investors and strategic equipment and heavy consumption of operations in the port area using medium-voltage air and ground lines and 19 distribution substation with a primary voltage of 20 kV.

3. Technical, Economic, Envirnomental Examination and Project Results

In this article motor vessel TIBA with IMO Number: 8879275 has been selected and analyzed, considering that this ship has three 68-kilowatt diesel generators to create a 204 kW electrical power in total. By applying coefficients (concurrency, etc.) and considering one equipment as a spinning capacity, the total of delivered power would be 136 kW, and with applying all the technical and non-technical parameters, the required demand of the vessel has been calculated and the initial demand at peak will be equal to 1600 kW. Ultimately with a detailed analysis of the costs and revenues of the project, the results indicate that investment in this project in addition to the maximum resolution of environmental problems that its pollution rate and resolution is shown in Table 1 based on the pollution, with creating green and modernized ports, According to international conventions allow maximum profitability and revenues from the sale of energy in these projects. Also listed in Table 2 is a Summary of costs and return of investments as a result of the implementation of this project. It is observed from Table 2, that the ratio of

profits to investment in the first year digit is greater than 1 (100%), which indicates that the performance of all port investment cost of the project in the first year is reversible and since the latter has Substantial profit after deduction of operating costs will be approximately 561,000 $, that it shown high benefits in this investment [2,3,4,5].

4.Results and Discussion

The results of the shorepower design and feasibility study shows its effectiveness in environment, Port attractive to vessels owner and for people who want to investment in port or like to do trade over there. This paper results shows the acceptable cost-benefit in shorepower investment in Amirabad port.

Table 1: Annual emissions of gases given off by the Tiba vessel motors during its operation time in Amirabad port (working hours in port: 24 h,300 days of year, Engine numbers: 2) **[6,7,8].**

Type of pollution	Gr/(hp*h)	Emissions (kg)	The volume of annual emissions 1000(kg/(hp*h))
Total hydrocarbons burned (HC)	0.1	0.442	2.25
NO_X	6	26.5	135.1
CO	0.5	2.2	11.2
PM Particulate matter	0.25	1.77	9
SO_2	0.5	2.2	11.2

Table 2: The total biennial financial estimate the cost - benefit

Capital expenditures and current of Project			**First Year ($)**	**Second Year ($)**
1	The cost of the initial investment		432,858	
2	The cost of maintenance	Per year	17,715	21,258
3	Consumed Energy cost	Per year	103,874	109,068
Income tax and Investment costs				
4	Value-added investment costs	9%	38,958	
5	Energy consumption tax expense	5%	5,194	5,454
6	Financial investments 20% annual interest expense on bank plan	20%	94,363	
7	Plans to invest 1% of annual insurance costs and repairs	1%	4,506	4,731
8	Total costs in the first year		697,465	
9	Total expenses in the second year			140,509
10	Revenue from the sale of electricity to vessels	Per year		738,302
Income tax		5%		36,916
11	Profit after tax			701,386
12	The ratio profits from the sale of investment and running costs		1.005623	
13	The pure profits from the sale in the second year at constant load energy prices			560,877

5.References

[1] International standard *" ISO/IEC/IEEE 80005~1:2012 Utility connection in ports " for high voltage shore connection (HVSC) systems.*

[2] Papoutsoglou G.theodoros *"A Cold Ironing Study on Modern Ports, Implementation and Benefits Thriving for Worldwide Ports " , thesis , School of Naval Architecture & Marine Engineering National Technical University of Athens , 2012.*

[3] Ballini F, *"Air Pollution from Ships in Danish Harbours: Feasibility Study of Cold-ironing Technology in Copenhagen ", Doctoral Dissertation, University of Genoa ,2013.*

[4] Danish Environmental Protection Agency, *" Reducing Air Pollution from Ships, - a cost benefit analysis and feasibility study on possible means for further reduction of emissions ", Environmental Project no. 1421, 2012.*

[5] "The impact of international shipping on European air quality and climate forcing ", EEA Technical report No 4/2013.

[6].Jean-florent helfre,Pedro andre Couto boot, *" Emission Reduction in the Shipping Industry: Regulations,Exposure and Solutions" .july 2013.*

[7].Application Engineering- *T-030: Liquid-cooled Generator Set Application Manual.*

[8]. John C.Y. Lee, Peter Lau, Thomas Teo, *" Sustainable Application of Reciprocating Gas Engines Operating on Alternative Fuels".*

NEW TECHNOLOGY OF DATA TRANSMISSION INSIDE BUOY BETWEEN THE UNDERWATER PROFILER AND THE FOOATING BODY

Soudabeh Khabaz sabet[1]

1) Export Comunication,Boushehr ports and maritime organization, BPMO of Bushehr, Bushehr, Iran, Soudabeh.khabazsabet@yahoo.com

1. Introduction

The anchor mooring profile monitoring bouy is one of the best method to obtain data from under water in recent years. The data transmission between the under water profiler and the floating body. The advanteges of an anchor mooring profile monitoring buoy based are long-term, fixed-point and high vertical resolution vertical profile monitoring data of specific sea area . we use two-point mooring design above of floating body and blew is the anchorage.

The underwater profiler can move up and down for acquiring the profiler monitoring data. After obtain monitoring data by profiler transmitted to the foating body. Data will be sended by data a radio station or communication satellite to the on shore data center.

For sending data between under water profiler and the floating body, they can be used two kinds of communication: wired or wireless communication. If wired communication is choosen we have some problem because communication distance is variable with the reciprocation so difficult. Wireless communication is better than wired mode, the reason of used is reliability and safety. In all of underwater data transmission mode, acoustic communication is the best because it have high transmission rate, but acoustic communication device is very expensive and high power consumption. The underwater-laser communication is well but the structure is so complex and has high cost.

To solve this problem in the data transmission between the underwater profiler and the floating body, the method implemented in this paper is to use the underwater wireless communication system based on electromagnetic induction coupling. Using of this system has some advantages such as: low cost, low power consumption, low directionality demand, reliable and short-distance data transmission.

The buoy presented in this paper how to transfer the profile monitoring underwater acquisition data and self-contained storage when profiler move up and down, data profile monitoring save on floating body and send by dara radio station or communication satellite.

2. system function

the anchor mooring profile monitoring buoy is consists of antenna, floating body, profile data for resending, wireless communication with electromagnetic induction coupling, under water profiler, sensor, underwater profile data acquisition and stroge system, unidirectional switch, mooring cable and matching block. The structure is shown in figure 1.

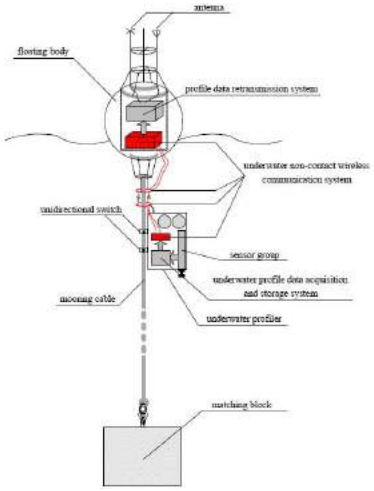

Figure1.the structure buoy presented in this paper

The operation of this system is to transmit to the underwater profile data acquisition and storage system for self-contained stroge by specific interface sensor in the rising or falling profiler performance: when the profiler move up to down of floating body and establish stable link between the underwater non-contact wireless communication based on electromagnetic induction couplingin the profiler and floating body. When the profiler stop and the profile monitoring data save in the underwater profile data acquisition and stroge system will be transmitted to the profile data retransmission system on the floating body by the the coupling signal transceiver modules, the underwater profile data will be saved in the SD card or USB storage device on the profile data retransmission system and then the retransmission will be performed by the data radio station or communication satellite, the profiler sink again after the retransmission of the profile data and a new round of the data acquisition starts.

3. Coupling signal transceiver module

This system divides into three parts: 1) coupling signal transmitter 2)coupling signal receiver 3) coupling coil. The diagram of the coupling signal transceiver is shown in fig2

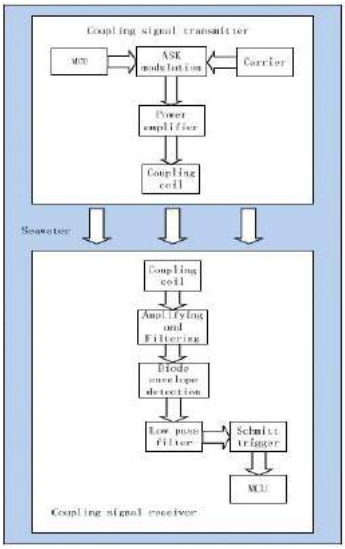

Figure2: diagram of the coupling signal transceiver moudle

Coupling signal transmitter: coupling signal transmitter is composed of three parts: data interface, moudulation circuit and power amplifier circuit. The performance of data interface in the coupling signal transmitter is to receive the profile data from the underwater profile data acquisition and storage system and use serial port RS232. The modulation circuit use ASK mode and the carrier frequency is about 200kHz based on the electromagnetic transmission.The class B push-pull power ampilifier circuit amplify the modulated profile data for coupling transmission.

Coupling signal receiver : coupling receiver is composed of four parts such as:amplifying and filtering circuit, demodulation circuit, digital signal recovery circuit and data interface. Voltage Amplifier according to Integrated Operational Amplifier amplify the micro voltage signal recived from recived coil. For removing that the noise whose frequency is higher than carrier frequency by the active low pass filter based on IOA. Diode envelop detection circuit combined with active low pass filter is used asdemodulation circuitto recover the baseband signal. Schmitt trigger recover the digital signal from baseband signal. The data interface in the coupling signal receiver is RS232 to send the recoverd profile data to the profile data retransmission system.

Coupling coil : L-C Parallel resonance circuit choose in this article for receiveing the electromagnetic induction signal such as shown in fig 3. This L-C circuit has been used on coupling signal transmitter and coupling signal receiver. After doing various testing, the shape of the coupling coil is selected as circle whose picture is shown in fig 4.

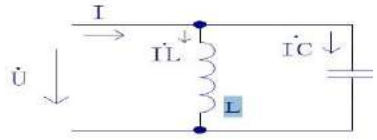

Figure3: L-c parallel resonance circuit

Figure4: the picture of the coupling coil

4. Conclusion

To assemble the circumstance, coupling signal transmitter and and coupling signal recever are integrated with profile data retransmission system and underwater profile data acquisition and storage system. The intergrated electronic system is put underwater and waterproof system and test. When the distance and the axial direction between the two coupling coils are lessthan 20cm and 60 degree that we have the reliable halfduplex non-contact wireless communication at9600bps. The power consumption of the coupling signal transceiver is about 250mW. The integrate electronic system fix on the profiler or floating body to realize the anchor mooring profile monitoring buoy. Final assembly of the buoy is shown in fig6. To use this system have some advantages such as: low cost, low power consumption, low directionality demand, short-distance transmission.

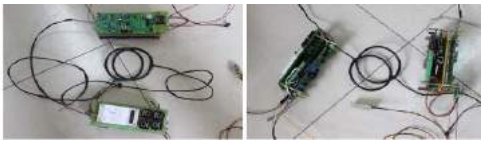

Figure5:The integrated electronic system

Figure6:Final assembly of the buoy

5. Thank

This Paper Published With Financial and Spiritual Support of Iranian Ports and Maritime Organization

6. References

[1] Ayano. H, Yamamoto. K, Hino. N (2002), "Highly efficient contaacless electrical energy transmission system". Proceedings of IEEE IECON, 2002"62-68.

[2] Byeong-Mun Song. R, Gurol. S, (2002), "Contactless inductive power pick up system for Maglev application" , Proceeding of IEEE IAS, 2002:34-39

[3] J. Clerk Maxwell. ATreatise on Electricity and Magnetism,3rd ed, vol.

[4] Garrod. D, Lehtomaki. Luk. Neudorfer. (1999) "Synthetic aperture sonar an evolving technology". Sea Technology, 1999,40(6):17-23.

[5] Jingbiao Liu, Guang Zhang , Haibin Yu , Xueting Zhang; (2010) , "An Anchor Mooring Profile Monitoring Buoy based on Underwater Non-contact Wireless Communicatio" . IEEE Int. Conf. OCEANS 2010 IEEE - Sydney.

ENVIRONMENTAL SENSITIVITY INDEX (ESI) MAPPING – APPLICATIONS FOR MANAGING OIL SPILL RESPONSE, PROTECTION OF NATURAL RESOURCES, AND MARINE SPATIAL PLANNING

Linos Cotsapas[1], Jacqueline Michel[2], and Jason Hale[3]

1) Research Planning, Inc., Columbia, SC, USA and Pandion Technology, Ltd., Limassol, Cyprus, lcotsapas@researchplanning.com
2) Research Planning, Inc., Columbia, SC, USA, jmichel@researchplanning.com
3) Pandion Technology, Ltd., Limassol, Cyprus, jhale@pandiontech.com

1. Introduction

The first environmental sensitivity index (ESI) maps were prepared days in advance of the arrival of the oil slicks from the Ixtoc 1 well blowout in the Gulf of Mexico in 1979. For almost 40 years, ESI maps have been specially developed for oil spill planning and response, with the first ESI maps in the Persian Gulf area developed for Kuwait in 1985.

ESI maps incorporate a range of critical environmental data such as coastal and marine habitats, but ESI maps are not "coastal habitat maps" because: 1) the fundamental ESI shoreline classification is an integration of geomorphological and ecological states, and 2) ESI maps summarize data contained in a relational geodatabase, and thus can be used to analyse and display a much wider range of information than maps of coastal habitats.

Worldwide, ESI maps have proven to be invaluable planning and conservation tools during oil spills and other marine emergencies by providing concise summaries of coastal resources that are at risk at a given time. However, design and use of ESI maps requires experience and expertise in coastal processes, ecology, and conservation and development planning so that the widest possible range of relevant information is effectively integrated.

2. Components of ESI Maps

An ESI system is composed of two basic components: 1) maps, which may be digital or printed in hard copy, and 2) an underlying relational geodatabase, which is the heart of the system.

Development of the relational geodatabase begins by collection and evaluation (QA/QC) of available physical, environmental, and socio-economic data. The experience of local biologists, geologists, engineers, and planners is critical at this stage for two reasons. First, information from each of these disciplines is necessary to create a complete and effective ESI system. Second, data gaps can be identified, and a plan developed to collect remaining critical information. Thus, all data and supporting observations are carefully screened and vetted to determine: 1) reliability and 2) completeness before they are incorporated in the database.

After the relational geodatabase is complete, ESI maps for particular uses and areas can be produced. ESI maps will contain and highlight information that is of greatest use for a particular application. In the case of oil spill response, ESI maps and data can be used to identify:

- Sensitive shoreline type, to guide deployment of spill response equipment
- Locations and levels of environmental sensitivity, key fauna, flora, and fisheries species at the time of the spill
- Details of features designated as critical for socio-economic needs (e.g. seawater intake)

ESI maps feature color-coded shorelines to show their sensitivity to oiling (Figure 1). The color-coded shoreline classification follows an established oiling sensitivity scale developed by RPI scientists, which has been in use worldwide for decades. This time-proven method has helped oil spill responders quickly and efficiently deploy equipment such as booms, skimmers, and vacuum trucks.

Some environmental and socio-economic data are best represented unique symbols, and standard icons are used to mark specific locations of sensitive resources (Figure 2). Examples of the types of resources best represented by symbols include concentrations of bird species when feeding or nesting, water intakes, aquaculture facilities, and beach and recreational areas.

The underlying relational geodatabase as well as customized software coding are then used to produce an ESI map of a specific location and optimized for a specific use (example, Figure 3). To produce such a map, all relevant information on shoreline types, sensitive habitats, important biological resources, and human-use features, must be presented in a way that is clear, accurate, and fit-for-purpose. The most efficient way to manage this information is with a relational geodatabase.

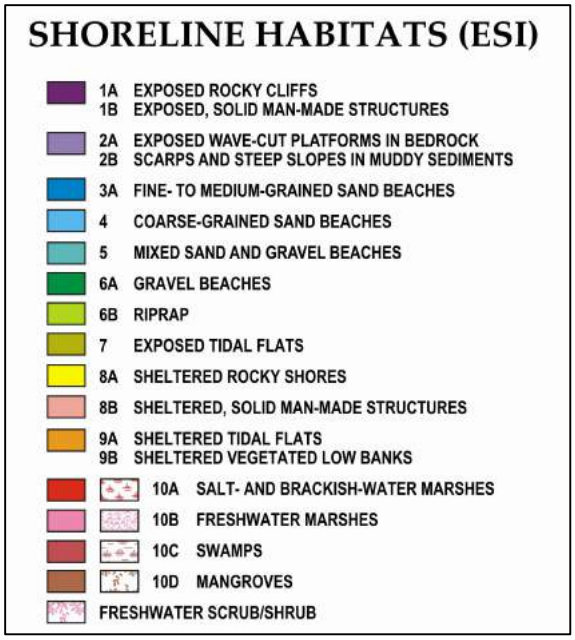

Figure 1. ESI shoreline classification.

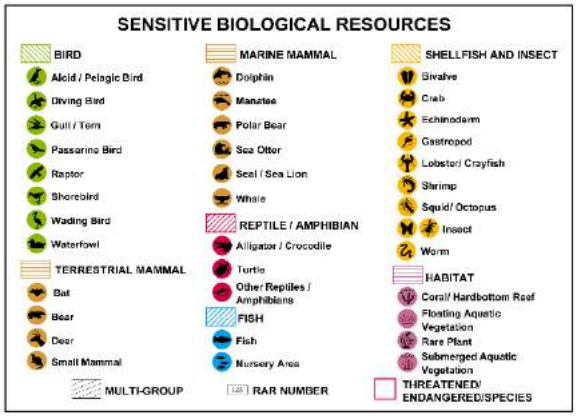

Figure 2. Biological resources depicted on ESI maps.

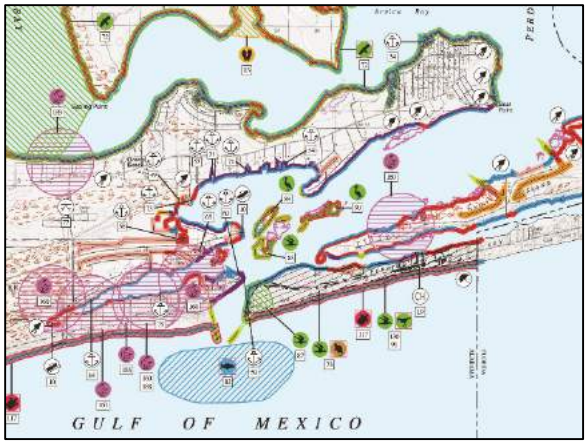

Figure 3. Example from an ESI map page.

An important feature that supplements the graphical information shown in Figure 3 is a table (or tables) of information often printed on the back of hardcopy ESI maps. Such tables provide additional details of the information summarized in "map" format and may include: concentrations of individual species of fauna present and seasons of the most sensitive life history; specific characteristics of water intakes or discharges (e.g. timing or content of discharge); and expert or competent authority contact information. Thus, ESI maps provide a complete set of relevant information that can be used during small or large oil spill response situations.

3. Beyond Oil: Additional Uses for ESI Maps and Databases

Because the information used in ESI maps is managed by a relational geodatabase, many other applications requiring summaries of spatially explicit data from a range of sources have been discovered and developed. In the region, ESI maps have contributed to the following types of programs:

- Integrated Coastal Zone Management (ICZM) plan development and assessment
- Marine Environmental High Risk Areas (MEHRA) and Places of Refuge (POR) planning.
- Natural resource management, including fisheries and aquaculture resources
- Environmental impact studies and assessments, environmental mitigation and offset planning, and marine spatial planning.

4. Summary

Though ESI maps were created to support oil spill response, they are currently used to support may other applications. Key features of an ESI include high-quality maps summarizing critical information and companion tables including important supporting details. A comprehensive relational geodatabase is used to extract relevant data from geomorphological, environmental, and socio-economic datasets. By providing relevant data in an easy-to-understand format, ESI maps are a valuable resource for oil spill responders, natural resource managers, scientists, and conservation and development planners.

5. References for Further Reading

Peterson, J., Michel, J., Zengel, S., White, M., Lord, C, and Plank, C. 2002. *Environmental Sensitivity Index Guidelines, Version 3.0*, NOAA Technical Memorandum NOS OR&R 11. National Oceanic and Atmospheric Administration, Seattle, WA, 89 pp + appendices.

MATARÓ MARINA BARCELONA. SUPERYACHT MARINA. A SUCCESSFUL CASE OF TRANSFORMING OLD BASINS FOR NEW PURPOSES.

Marc Cucurella Vilà [1]

1) OCEANS Civil Engineering Ltd., Roses (Girona), Spain. marc@oceans-eng.com

1. Introduction

This successful case of study is located in Mataró city, 30km far from Barcelona to the north. The city of Mataró has a marina called Port Mataró and a fishing basin beside this marina.

Figure.1. Mataró in the map. ICC.

Figure. 2. Mataró port (Font Google Maps)

Port Mataró marina has over 1.000 moorings and over 7.000sqm for commercial activities. The size of the moorings are from 7 up to 18m length. The strategy of this marina wasn't include greater moorings. Geometrically, this marina is limited.

Next to this marina we can find a fishing area in clear decline: every time few fishing boats due to the retirement of fishermen, less fish captures, and an increase of the aging of infrastructures. A completely general decline. The result of all this, is that nowadays this fishing area has only 5 fishing boats of 5m length, in a basin of 12.000m^2 water surface.

The image of this fishing basin inside the Mataró port before the transformation is as it follows:

Figure. 3. Fishing basin in 2009.

As we can see in the above figure, the basin is completely in a very low use: only small fishing boats, and one bigger abandoned ship. Also, in this area there's a building, without use. Initially was the fish market and Dutch auctions of fish.

After manage this marina privately for 3 years, Ports de la Generalitat, the port authority of Catalonia Government, published a public tender to manage, through a government concession, this basin for 10+5 years. Varador 2000 won this tender in 2014 and inverted over €1.5 million for manage this fishing marina and reconvert it from fishing marina to Superyacht marina; this mean yachts form 25m to 60m length.

2. Objective

The objective of this document is to explain the transformation of this basin, from a fishing basin to a modern superyacht marina, a case of success, with the analysis of weaknesses, opportunities, threats and technical aspects.

3. Relevant conflicts and accidents occurred

Apart of refurbish all the basin, including wharfs, buildings and infrastructures, the tender compelled to maintain 5 fishing boats in the marina, due to they are still active, and actively fishing.
This might cause problems of image: beside luxurious yachts we have trash and refuse products on the quay from fishermen. Also during works we had to manage and fight against the surfaces occupation: all time they need a lot of space for their fishing gadgets. This issue, obliged to manage with accuracy and speak with fishermen to maintain cleat its area.

Another important point is that we had to dredge the bottom of the basin, because the depth was insufficient for the expected yachts.

4. Strengths

This project is very attractive because as we had already done all the big infrastructure of docks, breakwaters, pavements, buildings etc., civil works were very few. So, initial investment wasn't in big amount.
This marina can give good mooring prices to yacht owners, and the distance from Barcelona is saved by very good highways and trains every 5min to Barcelona. This make Mataró very interesting to escape from the mass use of the marinas in Barcelona city and escape also from the high prices they apply to moorings.

5. Weaknesses

The weaknesses of this project are that we had to adapt to the existent geometry and dimensions. We didn't any modification to the initial geometry, so in consequence, we can be home to determinate sizes and determinate number of yachts. We had to adapt yacht to existing quays and not the reverse, as when we design a new marina that we have more flexibility and variety of yacht dimensions.

The existing fishing fleet is a weakness due to the image we may give.

6. Threats

A threat could be the success. A big success will demand more moorings, and this will be impossible in short time. Medium term or long term, and with big investments, it's possible to increase moorings with an expansion to the south of the port. Actual Special Plan of the port and the city allow to grow to the south. This will mean more buildings, new wharfs, dredging … another level of investment, higher.

7. Opportunities.

This was an opportunity for Varador 2000 S.A., a private company, that in 2011 begun to manage this area with an agreement with government.
Today is an opportunity for buy or rent a mooring for mega yacht very close to Barcelona, with all the advantages of having a yacht in a city, with an international airport, and less than 25 min from Barcelona, and with low prices than Barcelona. A good opportunity.

8. Conclusions

This is a very good example of a successful case of the transformation of an existing old and deteriorated basin to a modern marina for superyachts, and this case of study can be exported to any other area of the world, with similar characteristics, but always adapting moorings to specific demand of each part of the world, and country, and also depending on the coast they might have. Exportable also to different uses of port and kind of vessels we are going to adapt to that basin.

Figure 4. Mataró Marina Barcelona in 2016.

This marina has been inaugurated this past April 2016.

APPLICATION OF PLACE ATTACHMENT THEORY IN COASTAL PLANNING

Arman Jahangiri[1], Sahar Fereidouni[2], Maziar Jahangiri[3]

1) Ph.D. Candidate, Department of Art and Architecture, Science and Research Branch, Islamic Azad University, Tehran, Iran , arman.jahangiri@gmail.com
2) M.Sc. Student, Science and Research Branch, Islamic Azad University, Bushehr, Iran, shrfereidouni@yahoo.com
3) Bushehr Port and Maritime Organization, Bushehr, Iran, jahangiri.bpmo@googlemail.com

1. Introduction

One of the current key issues in coastal planning and design is the specific human emotional approaches toward environment at psychological perspective. The question of how and in what framework one individual finds him/herself in an emotional link with the coastal environment is what urban researchers have been always trying to find an appropriate answer for. Identifying the main structure of the process of creating emotional bonds to places would reveal a lot of crucial questions which by answering them, coastal planners or designers would be able to apply proper strategies to their design practices which may be leaded to improved urban areas by sustaining the effective components of this structure. Many researches emphasize on the role of place attachment in making social ties and personal and public identity [1]; [2]; [3]. Moreover, studies have shown open urban spaces are most important contexts in shaping place attachment because of their various desirable physical especially coastal areas. (Natural and Man-made) and their activity features [4], [5], [6]. Therefore, identifying the real structural essence of interactions and inter relationships between coastal environment and individuals is indispensable for the researchers in the context of coastal planning and design.

2. Theory of Place Attachment

The concept of place attachment has been originated from the notion of the sense of place which is related to how people make a connection with their surrounding environment. Proshansky et al. assert that sense of place is an emotional or cognitional attachment to geographical environments [7], and similarly, Tuan defines it as an emotional, meaningful and deep rooted relationship between one person and a particular place and defines place as a significant meaningful context for individual experiences in the environment [8]. Despite all various definitions that have been presented so far and the absence of a comprehensive agreement among researchers, in a simple definition, based on Low and Altman and Giuliani, Scannell and Gifford defined place attachment as an emotional link between human and the environment (both objective and subjective) [9], [10], [11]. Definition of place attachment as an emotional link is widely common in literature of environmental studies, especially in tourism management and coastal areas [12] and in short, it is related to the this fact that humans would be attached to one place during their lives as they might be attached to their family members, friends, gifts and memories.

3. Place Attachment Dimensions in Coastal Planning and Design

Many researches on planning coastal and waterfront areas has revealed that place attachment can be identified as two dimensional concept: place dependence and place identity [13], [14] ,[15], and valid this two-dimensional definition have been used as a framework for place attachment evaluation regularly [16], [17]. However, Place dependence is conceptualized as how people are dependent to one place for their specific activities and needs and place identity means those symbolic concepts that are defined as individual's identification in relation to physical environment [18]. This dimension is known as functional bonds that people have with a place, according to their own place perception, and personal assessment about how much one place allow them do their desired activities, [19]. On the other hand, Place identity refers to emotional bonds between the self and the physical environment, rooted from cognitive and affective elements of one place regarding to the values, beliefs, preferences, feelings, goals, and behavioral tendencies of individuals[7].

Studies show place dependence and place identity are basically connected issues and those people who have more place identity, they care more about physical and social features of the place more than others in coastal areas. Shortly, place attachment as two dimensional concept and expected features of each dimension regarding to physical

features of place and activity characteristics are shown in table 1.

Table 1. Dimensions, expected functions in the concept of place attachment in Coastal Areas.

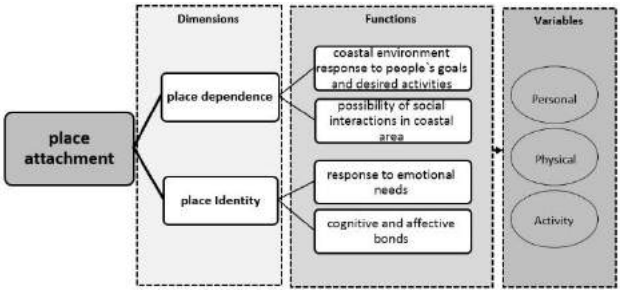

4. Conclusion

In sum, according to the literature reviewed, particularly three areas of activity, physical features and individual characteristics as parts of the most important predictors or factors that directly are affecting the concept of place attachment. These factors which can be categorized on the basis of previous reviewed dimensions of place attachment, place dependence and place Identity, are known as main elements that help attachment development process throughout connecting different urban environments to progress. Obviously at physical level, the type of the environment, whether it is natural, man-made or a combination of both, is essential in the assessment of place attachment as well as factors like compactness, scale, size, etc. Individual's specialization level and the environmental acquired skills and the degree of place possession are effective in generation of this emotional bond. Regarding activity features, the possibility of doing desired activities in the environment are also notable. This subject is related to service level and functionality in physical section. Also the possibility of doing desired activities in environment are crucial either. In short, all factors noted, classified based on their concept and features, are presented in table 2.

Table 2. Effective Variables (factors) in Creating Place Attachment in Coastal Planning.

Physical Features in Coastal Areas	• Type of space (natural, man-made or both) • Type of environment functions (uses) • Physical features (compactness, openness, access, scale, size, …) • Place experience • Ownership, control degree and
Activity Features in Coastal Areas	• The degree of Place control • Length and type of vist (permanent or temporary) • Availability of desired activities and ecpected sevices • Possibility of interaction with other social groups • The existence of covergent social groups
Individual Characteristics of Coastal Ara	• individual characteristics (gender, age, level of education, income, nativity) • Local group memberships • presence of friends and family

5. References

[1] Bailey, N., A. Kearns, and M. Livingston, *Place Attachment in Deprived Neighbourhoods: The Impacts of Population Turnover and Social Mix.* Housing Studies, 2011. **27**(2): p. 208-231.

[2] Baran, P.K., et al., *Park Use Among Youth and Adults: Examination of Individual, Social, and Urban Form Factors.* Environment and Behavior, 2014. **46**(6): p. 768-800.

[3] Kyle, G., et al., *An Examination of Recreationists' Relationships with Activities and Settings.* Leisure Sciences, 2004. **26**(2): p. 123-142.

[4] Amundsen, H., *Place attachment as a driver of adaptation in coastal communities in Northern Norway.* Local Environment, 2015. **20**(3): p. 257-276.

[5] Burley, D., et al., *Place Attachment and Environmental Change in Coastal Louisiana.* Organization & Environment, 2007. **20**(3): p. 347-366.

[6] Devine-Wright, P. and S. Clayton, *Introduction to the special issue: Place, identity and environmental behaviour.* Journal of Environmental Psychology, 2010. **30**(3): p. 267-270.

[7] Proshansky, H.M., A.K. Fabian, and R. Kaminoff, *Place-identity: Physical world socialization of the self.* Journal of Environmental Psychology, 1983. **3**(1): p. 57-83.

[8] Tuan, Y.F., *Topophilia: a study of environmental perception, attitudes, and values*. 1974, Englewood Cliffs, NK: Prentice-Hall.

[9] Altman, I. and S.M. Low, *Place Attachment*. null. 1992, New York: Plenum. null.

[10] Giuliani, M.V., *Theory of attachment and place attachment*, in *Psychological theories for environmental issues*, M. Bonnes, T. Lee, and M. Bonaiuto, Editors. 2003, Ashgate: Aldershot. p. 137-170.

[11] Scannell, L. and R. Gifford, *Defining place attachment: A tripartite organizing framework.* Journal of Environmental Psychology, 2010. **30**(1): p. 1-10.

[12] Relph, E., *Place and placelessness*. 1976, London: Pion.

[13] Bricker, K.S. and D.L. Kerstetter, *Level of Specialization and Place Attachment: An Exploratory Study of Whitewater Recreationists.* Leisure Sciences, 2000. **22**(4): p. 233-257.

[14] Jorgensen, B.S. and R.C. Stedman, *Sense of place as an attitude: Lakeshore owners attitudes toward their properties.* Journal of Environmental Psychology, 2001. **21**(3): p. 233-248.

[15] Kyle, G., et al., *An Examination of the Relationship between Leisure Activity Involvement and Place Attachment among Hikers Along the Appalachian Trail.* 2003, 2003. **35**(3).

[16] Fried, M., *Continuities and Discontinuites of Place.* Journal of Environmental Psychology, 2000. **20**(3): p. 193-205.

[17] Hammitt, W.E., E.A. Backlund, and R.D. Bixler, *Place Bonding for Recreation Places: Conceptual and Empirical Development.* Leisure Studies, 2006. **25**(1): p. 17-41.

[18] Farnum, J., T. Hall, and L.E. Kruger, *Sense of place in natural resource recreation and tourism: An evaluation and assessment of research findings*. 2005, U.S. Department of Agriculture, Forest Service, Pacific Northwest Research Station. p. 56.

[19] Halpenny, E.A., *Pro-environmental behaviours and park visitors: The effect of place attachment.* Journal of Environmental Psychology, 2010. **30**(4): p. 409-421.

GREEN DESIGN' PRINCIPLES DURIND All STAGES of MASTERPLANING

Ali Shoushtarizadeh Naseri[1], Behzad Alvand[2]

1) Ports and Maritime Organization, Ali.s.naseri@gmail.com
2) Ports and Maritime Organization,behzad.alvand@gmail.com

1. Introduction

Existing ports, particularly old commercial ports, are often surrounded by the city precisely because they have developed in this way due to the very presence of the port.
Ports have been the single most important economic driver in many countries, to the extent that most of the major cities of the world have developed alongside a commercial port.
Port and city development has always been very closely related. In most cases, the growth of major coastal cities has been driven by port business. This has been due to the creation of many local companies related to a greater or lesser extent to the operation of the port, direct and indirect job creation and taxes paid to local authorities. As a result, ports have contributed greatly to the wealth of their related city.

2. Ports development

Maritime transport has had a paramount importance on trade. Nowadays, more than 80 % of world trade is based on waterborne transport and this figure is expected to continue or even grow.
Many ports are encountering difficulties in achieving their main objective as a port, which is to efficiently meet service demand. There are several reasons for this:

- Cargo volume has grown very rapidly, often exceeding port capacity
- The size of vessels has increased and some port facilities can no longer serve larger vessels, thus reducing the effective capacity of ports
- Port productivity is poor due to the inefficiency of management systems or the fact that handing equipment is no longer appropriate for current handling requirements
- Stacking yards cannot grow at the same pace as vessel productivity since the existing set-up prevents the expansion of terminals
- Inland transport connections are congested or unable to be provided/expanded (i.e.
supply chain congestion)
- Emerging land use conflicts between port and non-port activities (e.g. sensitive land uses along transport corridors and in close proximity to operational areas)

Figure 1. Boushehr Port in vicinity of urban area, Persian Gulf

3. Some current trends are not sustainable

As we move into the 21st century, nations have become increasingly interdependent. International trade has become commonplace and trade between nations is expected to continue growing at historically high rates. This trade has created challenges for the transportation industry as bottlenecks, congestion, air emissions and other impacts draw the attention of the public and policy makers. It is widely recognized that current patterns in the transportation industry are not sustainable [United Nations Agenda 21]. These industry-wide concerns represent a call to action for the waterborne transportation industry, which provides sustainable benefits for a significant portion of the global transportation network.

4. Ports Industry Challenges

All transport activities have noteworthy environmental impacts. The environmental performance of waterborne transport is superior in energy efficiency and infrastructure impacts and yet, challenges are faced in emissions and discharges from vessels. The main environmental impacts and environmental characteristics of port industry can be categorized as:

• Infrastructure impacts: land take, use of other natural resources, barrier impacts and fragmentation.
• Operational impacts: air pollution, water pollution, noise, waste, transfer of harmful aquatic organisms with ballast water and risks related to accidents.

5. Green port concept

Today's steadily increasing global environmental awareness creates new challenges for the development of ports based on a 'Sustainable Development', recognized under the 'Brundtland Report' released by the United Nations in 1987 which included the widely recognized definition:

"*Sustainable development is development that meets the needs of the present without compromising the ability of future generations to meet their own needs*"

The term 'Green Ports' is widely associated to be 'the answer' to this challenging task. Although many issues in this regard have been studied in great detail, PIANC has recognized that a merged single package concept for an approach to a 'Green Port' does not exist.
In terms of preparing port master plans, it is of critical importance to take into consideration 'green design' principles during all stages of master planning, particularly during the early stages of development.
Issues to be considered should include:

- Land and water area use
- Modalities and connectivity
- Air and noise pollution
- Surface water and sediment
- Soil and groundwater
- Dredging
- Climate change and sea level rise
- Light pollution
- Habitat and species management
- Ship related waste
- Globalization
- Sustainable resources management

The Green Port philosophy can be applied to all ports in the world. Sustainable development and adaptation to climate change are issues that have no boundaries and affect everybody. Creating sustainable Green Ports is a common responsibility and is therefore as relevant for Countries in Transition as any other country, especially when it concerns new port developments
Increasing environmental awareness create new challenges for the development of ports. In addition, climate change calls for adaptation measures that aim at minimizing impacts of e.g. rising sea levels and increased flood water heights but safeguard accessibility of ports and waterways and also safeguard future sustainability for the social and natural environmental conditions. International and national legislation for new ports or extensions of existing ports are incorporating these issues and are increasingly based on strict regulations aiming at creating designs with minimized environmental impact and sustainable operations in the long-term. The regulations are enforced through a system of permits in which certain construction and operation methods are predefined including (large-scale) mitigation and compensation measures. In many cases, the environmental issues and (long-term) impacts of port construction and operation are unknown during the planning and design stages of the port. Assumptions may be made on the basis of worst case scenarios, leading to associated mitigation measures. Furthermore, proposed environmental and sustainability measures in the various planning studies and provided permits are new and have not been tested to their full potential nor is their effectiveness monitored in the field. Green Ports are widely regarded as 'the answer' to the above mentioned challenges. However, there is no clear and comprehensive description of what a Green Port actually is.

Figure 2. Anzali Port in middel of urban area, Caspian Sea

6. Green measures in Masterplans

Green measures should be considered in masterplanning to reduce the side effects especially in case of ports located in the middle of the cities. For instance, anzali and boushehr ports of Iran are located in the middle of the city. Their developments have benefits for ports authority, but environment disadvantages. The green measures could be applied to enhance life quality in vicinity of the ports.

7. References

[1] A practical guide for a sustainable seaport, PIANC WG 150, Envicom
[2] Masterplans for the development of existing ports, PIANC Working Group 158, MarCom
[3] Towards a sustainable waterborne transportation industry, PIANC Working Group 136, Envicom

STRATEGIC DEVELOPMENT AND MANAGEMENT OF GWADER PORT IN PAKISTAN.

Sarmad Salahuddin.

Assistant Professor | University of Management and Technology, Lahore,Pakistan.
Email: Sarmad.Salahuddin@umt.edu.pk

Abstract:

The present study is an effort to explore the importance of development of Gwadar port in Pakistan. The government of Pakistan initiated the construction of the country's third deep sea port, at the start of this century. The port is not only supposed to give stimulus to the development of the city, but also to the entire Baluchistan province and the entire country of Pakistan. In order to coordinate all these future activities, a comprehensive strategy is required to ensure that there are no future conflicts in land use and wastage of scarce resources. The paper will figure the key areas of development such as Land-use, Infrastructure development, Transport and Telecommunications, Tourism, Institutional and Administrative setup for the growth of import and exports. Currently, Pakistan is facing severe problems in the area of Economic Development and the energy crisis. There is a dire need of a comprehensive strategic management plan to execute a project of such geo-strategic importance.

Keywords:*Strategic management, Geo-strategic importance of ports, and project management*.

1. Introduction:

If we take a look into the history of the human development we can see that the geographical environment plays a crucial role in the growth and development of civilization. More than 75 percent of the Earth is covered by seas and oceans and this makes them a very important part of the geographical environment.

2. Literature review:

The paper will review the significance of Gwader port, its concerns and its future prospects for the country of Pakistan. So far many studies have been done, reported in magazines, media and news paper. But none of the studies could throw light on practical execution of a project of this scale. The development of Ports involve a high level of Geo-politics, economic studies and urban development feasibility studies, which is a tumultuous task, bigger than any developmental project for a country. This paper is unique effort to study the historical background, comparing it with a successful ports in the region and coming up with practical solutions.

3. Geo-strategic importance and location:

Pakistan has a coastal frontage of close to 1100kms which spans from Western province right across to the Southeast axis. The coast of Pakistan has close to 36,000 ships moving through the sea belt in the region. The total annual trade of the country comes up to around 38 million tons and roughly 95 % of the total trade happens via the sea routes. There is an expected increase of trade to 91 million tons by 2015 which in turn will create a proportional increase of sea trade. Out of the total trade 68% is handled by Port Karachi while around 32 % comes to Port Qasim.

4. Study area:

Gwadar estimated population, 227,984 spread across a total area of 12,637 sqkms. This makes the Gwadar Port a very robust option not just for the regional stakeholders but also for people from outside. Gwadar also can be the future hub which can serve as an entry and exit point for the Strait of Hurmoz; thereby offering stiff competition to the UAE ports by working to enhance the pathways that help vessels to exit from the Caspian Region,. Thus this will help to establish a clear sea based trade route for the Caspian area which is blocked between bits and pieces of land on all sides. There is also a lot of scope in the future for Gwadar which could become a fully functional regional commercial center and a port for trans-shipment vessels to ply into other regions.The threat is however of conflict especially in today's world where there is lot of animosity and poor relations between countries and such a move could create conflicting interests between the various stakeholders. United Arab Emirates (UAE) may possibly have specific benefits which are contradictory in Gwadar. Central Asian states and China can have huge financial gains from this region while on the other hand Chinese and United States (US) interests completely contradict each other. This could well result in Gwadar being a point of conflict between the different regional as well as external powers in Asia and abroad. Gwadar can act as a strategic vantage point helping Pakistan to keep a close watch over the Sea Lines of Communications (SLOCs) with Persian Gulf as a start and constraining at the Strait of Hormuz.(Chaliand 1994)

See Table 1 for the project details.

Table 1.Source Gwader Port Authority website.

Category	Area in Acres
Residential (Extendable)	19,500
Commercial (Extendable)	200
Recreational (Extendable)	210
Export Processing Zone/ Industrial area includes: a) Ware houses. b) Desalination Plant. c) New International Airport d) Railway Linkages. e) Multiple accesses to port and various urban facilities. Other incentives in Gwader Master Plan includes: a) Economic Free Zone. b) Subsidized Electricity. c) 5 Road connecting Gwader with rest of the country/Afghanistan, China, Secondary access to all Central Asian countries.	10,000
Total	29,910

Figure 1.Source: Gwader Port Authority website.

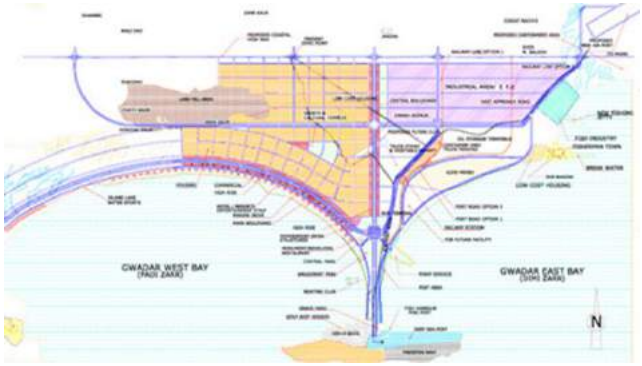

5. Problems:

a) The Government of Pakistan is currently not in a position to bear the financial investment for a project of this scale alone. Private sector companies have however indicated their interest in the project and may get involved in certain non-critical developmental activities.

b) It would be required to call in for investment and support from foreign investors as Pakistan will not be in a position to take up the sole responsibility for the entire financial burden of a project of this scale almost mammoth sized in nature.

6. Research Methodology:

The data was collected from authenticated secondary sources. Moreover, in order to seek practical solutions for the Gwader port, it is required to study the success story of a port having a similar in magnitude in the same geo-strategic location, as a Case study.

7. Research findings and conclusion:

The selected case study will clearly highlight the key aspect of its success, and the draw backs which the government of Pakistan is unable to cover in case of Gwader port. All areas shall be carefully examined and discussed in the paper, to come up with an unbiased conclusion.

8. References

[1] Alexander, G. (2009). Natural Gas as an Instrument of Russain State Power. Carlisle, PA: Strategic Studies Institute , U.S Army War College, U.S.A.

[2] Asad, L. (2007). Between Rising Powers: China Singapore and India. Institute of South Asian Studies, Michigan, USA.

[3] Authority, D. P. W. (2015). "Dubai Ports Wold." from http://web.dpworld.com/our-business/marine-terminals/middle-east- europe-africa/dubai-jebel- ali/

[4] Blank, S. J. (2011). "Central asian security trends views from europe and russia." from http://www.strategicstudiesinstitute.army.mil/pdffiles/pub1063.pdf

[5] Chaliand, F. G. (1994). The Art of War in World History from Antiquity to the Nuclear Age.

[6] Matinuddin, K. (1991). Power Struggle in the Hindu Kush. Lahore, Wajidalis, 1991.

[7] Mumtaz, M. K. (2009). History of Karakoram Highway, Hamza Pervez Printers, Rawalpindi, Pakistan.

[8] Nixon, R. (1992). Seize the Moment. USA, Siman and Schuster, New York , United States of America.

[9] Rahul, B. (2006). The India Security Scope 2006: The New Great Game. New Delhi, India., Gyan Publishing House.

OPTIMUM WHARF TYPE IN SOFT SOILS; A CASE STUDY FOR MAHSHAHR

Hassan Akbari[1], Kamal Soleimani[2]

1) Department of civil engineering, Tarbiat Modarres University, Tehran, Iran, Akbari.h@modares.ac.ir
2) Sahel consultant engineering, Tehran, Iran

1. INTRODUCTION

Selecting the best alternative between different wharf types depends on many items such as hydrodynamic conditions, soil layers, bathymetry of the area, required depth and etc. A gravity quay-wall may be appropriate for an area with high bearing soil strata, yet the selection is not always such simple. It seems that both sheet pile and piled jetty can be used in soft cohesive or sandy soils. Which one is better? Proper answer helps to make a good decision at the initial phases of the project that decrease the project time and costs accordingly.

Because of the coastal sedimentation phenomena, existence of soft soils at the upper layers is a common practice near the shorelines and the north-west part of the Persian Gulf is covered with mud [1]. In this study, numerical method is used to investigate the functionality of sheet pile in soft soils i.e. soft clay and loose sand.

2. FIELD AND GEOTECHNICAL DATA

Upper layers might be composed of soft clay or loose sand depending on the origin of the sedimentations while denser layers are located at a deeper point. The soil parameter at Mahshahr is selected as representatives of soft clay as shown in Table 1.

Table 1. Soil parameters of a soft clay condition

Layer No.	Thickness (m)	Stiffness	Moisture C. (ω) (%)	γ_d (gr/cm^3)	C (gr/cm^2)	ϕ (grade)	Poison (v)	E (kg/cm^2)
1	10	Soft	30	1.5	0.20	0	0.5	50
2	20	Stiff	25	1.6	2.0	0	0.5	400
3	>5	Dense	25	1.8	0.0	34	0.3	500

To study the loose sand condition, the upper layer is replaced by loose sand with properties shown in Table2.

Table 2. Soil parameters of a loose sand condition

Layer No.	Thickness (m)	Stiffness	Moisture C. (ω) (%)	γ_d (gr/cm^3)	C (gr/cm^2)	ϕ (grade)	Poison (v)	E (kg/cm^2)
1	10	Loose	25	1.8	0.0	28	0.3	100
2	20	Stiff	25	1.6	2.0	0	0.5	400
3	>5	Dense	25	1.8	0.0	34	0.3	500

For each soil condition, three different water depths (5, 10, 15m) have been selected and the penetration depth of sheet piles is assumed one-third of their total length to make the comparison of different depths easier. The sketch of the sheet pile is shown in Figure 1.

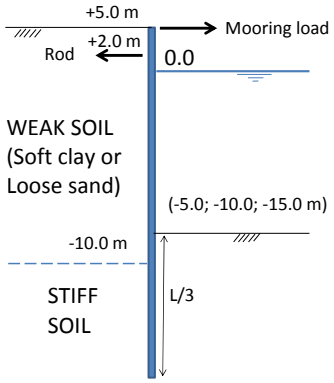

Figure 1. Geometry and loading condition

The sheet pile is analyzed at two ordinary and seismic conditions while mooring load is only applied in the former condition and seismic load is only applied in the latter case. The mooring load is obtained based on the displacement tonnage of a ship that can berth beside the wharf. For each water depth, ship displacement tonnage is obtained from OCDI [2] and then, horizontal mooring load is assumed based on BS6349 [3].

Regional seismic condition is obtained for Mahshahr area based on Iranian code 631[4]. According to this standard, horizontal seismic coefficient is 0.12 as:

$$k = k_{region} \times \mathrm{Im}\, por\, \tan ce\, Coef. \times Soil\, Coef.$$

$$k = 0.08 \times 1.2 \times 1.2 = 0.12$$

To evaluate the earth pressure of sandy or cohesive soil located below water level during earthquake, apparent seismic coefficient k' is used instead of seismic coefficient k.

3. ANALYSIS RESULTS

A sample of results i.e. moment distribution along a sheet pile in 10.0m water depth subjected to seismic load are presented in Figure 2.

According to OCDI [2], in the case of cohesive soil ground, the stability of embedded part is not established unless cohesion of soil at sea bottom be more than one-fourth of the effective soil stress at that point. This limitation may not be satisfied if the sea bottom ground is soft. For the case of 5.0m water depth, cohesion of soil at sea bottom is 20kpa which is less than the required value i.e. approximately 30kpa. Therefore, the sheet pile can not be designed for this condition even by increasing the penetration depth. However, it is interesting that the sheet pile in a 5.0m water depth is stable in the case of loose sand while it was not applicable to the soft clay condition.

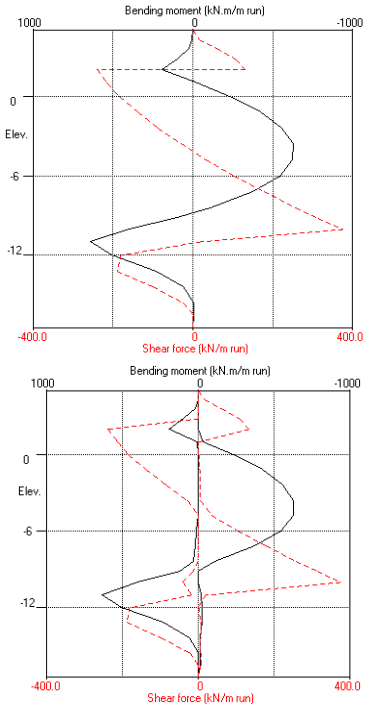

Figure 2. Displacement and bending moment; Up: clay, Down: sand

5. CONCLUSION AND DISCUSSION

Maximum moment along the sheet piles is presented in Figure 3 for different cases.

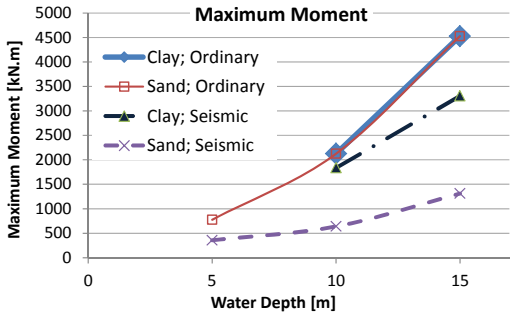

Figure 3. Maximum moments in different cases

According to this figure, in an ordinary condition, maximum moment along the sheet pile are nearly equal for both soft clay and loose sand conditions. However, these parameters are completely different in a seismic condition. The reason is the fact that the upper part of the sheet pile acts as a cantilever and the soil parameters have a negligible effect on the maximum moment.

In a seismic condition, however, the behavior of loose sand is completely different with the behavior of soft clay and their lateral pressures as well as their displacements are not equal any more. According to the results, generated maximum bending moment along the sheet pile driven in loose sand and subjected to the earthquake load is significantly less than the moment generated in the soft clay condition. In addition, the rate of increase in the bending moment versus the water depth is less in a sand condition than in a clay condition. Note that analysis have been done for Mahshahr that is located in a low seismic activity region, therefore, bending moments due to mooring load in ordinary condition is higher than bending moments due to lateral earthquake load in seismic condition.

For each water depth, the maximum bending moment is equal for both sand and clay conditions because ordinary condition has been more critical than seismic condition in evaluating the bending moment for all the analyzed cases. However, a stronger section is required for a sheet pile driven to the soft clay according to Figure 4 that shows the required moment of inertia of sheet pile section for different cases. Actually, the sections are designed based on the requirements for the allowable lateral displacement that have been more dominant than the requirements for bending moment.

As shown in Figure 4, stronger sections shall be used in deeper points for both soft clay and loose sand conditions. However, increase in water depth has a more significant effect on the required section in the soft clay condition.

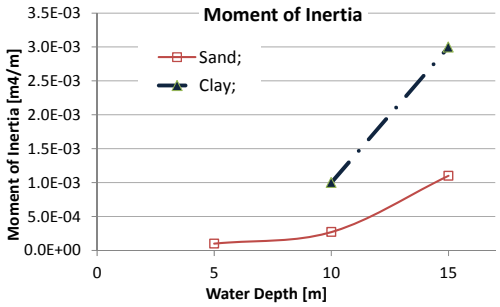

Figure 4. Required moment of Inertia for sheet pile section in different cases

According to the results, it can be concluded that the structural behavior of the sheet pile particularly under seismic condition is better in loose sand condition than in soft clay condition. On the other hand, according to the standards [2,4], for a location with soft clays at the sea bottom, sheet pile is not allowed to be constructed. In these cases, below solutions can be done based on the obtained results:

a) Replacing soft clay with a sand even a loose one
b) Use another type of the structure such as pile and deck structure with less lateral loads.
c) Improve the soil parameters at the sea bottom as suggested by OCDI [2]

6. REFERENCES

[1] Haghshenas S. A., Soltanpour M. (2010): Analysis and modeling of dissipative waves at Hendijan mud coast, the Persian Gulf, Ocean Dynamics, DOI 10.1007/s10236-010-0333-z, 2010.

[2] OCDI (2002); Technical standard and commentaries for port and harbor facilities in japan, The Overseas Coastal Area Development Institute of Japan.

[3] BS6349-4 (1994); British standard, maritime structures-Part 4: Code of practice for design of fendering and mooring systems.

[4] Iranian Code 631, (2013): Design Standard for coastal structures; part2: Design conditions, 1392

PREDICTION OF ROW REDUCTION FACTOR OF PILE GROUPS UNDER LATERAL LOADING

Ali Derakhshani[1], Reza Khoshroo[2]

1) Dept. of Civil Engineering, Engineering Faculty, Shahed University, Tehran, Iran, adera@shahed.ac.ir
2) Dept. of Civil Engineering, Engineering Faculty, Shahed University, Tehran, Iran, reza_khoshroo@yahoo.com

1. Introduction

There are various methods to evaluate the response of piles and pile groups under lateral loading. Rees method is one of the most conventional approaches in which p-y curves are used. One of the most common methods of accounting for the group effects in p-y method is to modify the single pile p–y curves using a p–multiplier, as suggested by Brown et al. (1988) [1]. In this approach, the soil resistance, p, is reduced by multiplying by a constant factor, P, as shown in Figure 1. (Each row has personal reduction factor because of group effects).

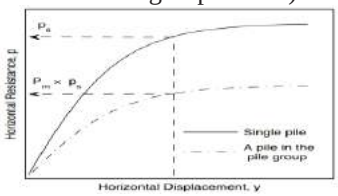

Figure 1. Definition of p-multiplier

In order to estimate row reduction factor, several experimental studies have been carried out such as those conducted by Rollins et al. (1998) [2] about lateral load-displacement behavior of full scale pile group in clay, Rollins et al. (2005) [3] regarding lateral response of pile group in sand and McVay et al. (1998) [4] about centrifuge testing on lateral response of pile group. Main idea of this study is to use tests results to predict row reduction factor. In this regard, all the available relevant datasets were collected. Currently, there is not any correlation to predict reduction factor consisting of all of the effective parameters. There are also two design guidelines that propose the relationships for prediction of the reduction factor, AASHTO [6] and FEMA P-751 [7].

In the current study, among different soft computing methods, Model Tree has been used for prediction of the row reduction factor. Model Tree has been utilized for prediction purposes in civil engineering applications by some researchers e.g. Etemad-shahidi and Mahjoobi, (2009) [5].

2. Model Tree (M5')

Model Tree is one of the robust and suitable methods for prediction and categorizing. MTs have more accuracy than regression trees; they are more understandable than ANN. The MT approach consists of two processes: building the tree and driving knowledge from it. The tree building process involves dividing the input space into several regions using linear regression models (Fig. 2). In the derivation process, a new data record is given into one of the leaves of the tree. This process is done according to dividing condition of the previous process.

Finally, the predicted output is obtained at the leaf of the tree. M5' algorithm is a modified version of M5 algorithm proposed by Wang and Witten (1997) [8] that can deal with missing values.

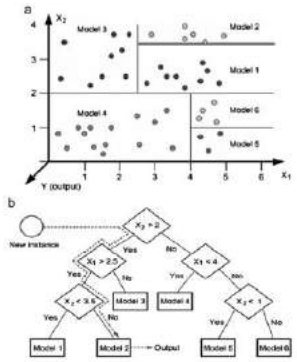

Figure 2. Model Tree mechanism

3. Dataset and modeling

For building the model and increasing the accuracy, all of the published data from different experiments about Pile groups under lateral loading were used. These experiments have been done in sandy and clayey soils with different number of rows and totally 125 data points were collected.

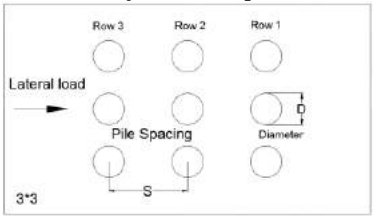

Figure 3. Pile group plan

Various parameters are effective on reduction factor, e.g. the friction angle, row number, pile spacing, number of rows and pile head condition have effect on reduction factor. Input parameters that were employed for training and testing the model are n, S/D, BC, m and ø i.e. row number, normalized pile spacing, pile head condition (free or fixed), number of rows and friction angle respectively. The pile spacing, number of rows and row number are

defined in Fig 3. Output parameter of the model was reduction factor.

4. Results and discussion

The dataset divided into two parts for training and testing, 80% were used for training and 20% were used for testing the model. M5' model tree only presents a linear relationship between input and output variables, while the relation between governing parameters in pile groups under lateral loading and reduction factor is not necessarily linear. Thus the model was developed with Ln (inputs) and Ln (output) to overcome this constraint.
The following equations were obtained using M5':

$$RF = ((n+1)^{-0.0911} \times (S/D)^{0.2408} \times (m)^{0.0686} \times (\cos(45 - \phi/2))^{-0.1024} \times (e)^{0.2465}) - 1 \quad \text{for } n < 2 \qquad (3)$$

$$RF = ((n+1)^{-0.1862} \times (S/D)^{0.3465} \times (\cos(45 - \phi/2))^{-0.4232} \times (e)^{0.128} \quad \text{for } n \geq 2 \qquad (4)$$

The models are compact and have good interpretability. According to equations as friction angle increases, reduction factor decreases and as n increases, reduction factor decreases and as piles spacing increase, reduction factor increases.
Generally, moving from leading row (first row) to trailing rows (end rows), n is increasing and piles mutual influence on each other increase and consequently reduction factor decreases (reduction factor of trailing rows is less than that of leading row).
By the increase of piles spacing (S/D), shadowing effect (piles effect on each other) decreases, so reduction factor increases. By increasing m, pile group becomes larger and group effect increases, so, reduction factor decreases.
Increasing the friction angle, soil strength increases and the soil between rows can better transfer the effect of rows on each other, so piles effect on each other increases and reduction factor decreases.

The results of this study were compared with other equations (AASHTO and FEMA P-751). To compare the performances quantitatively, parameters such as the correlation coefficient (CC), root mean square error (RMSE) were calculated as follows:

$$CC = \frac{\sum(x_i - \bar{x})(y_i - \bar{y})}{\sqrt{\sum(x_i - \bar{x})^2 \sum(y_i - \bar{y})^2}} \qquad (5)$$

$$RMSE = \sqrt{\frac{1}{N}\sum(x_i - y_i)^2} \qquad (6)$$

Where x_i and y_i denote the measured and the predicted values, respectively, and N is the number of measurements. $\bar{x}$ and $\bar{y}$ are the corresponding mean values of the measured and predicted parameters, respectively.
These statistical parameters are given for the test data in Table 1. As shown, the result of Model Tree is more accurate than the other formulas. In AASHTO and FEMA P-751, reduction factor is only function of S/D and n.

Table 1. Performance indices of various methods to predict the reduction factor

	RMSE	CC
Model Tree	0.064	0.96
AASHTO	0.1	0.92
FEMA	0.102	0.92

Table 1. shows the high accuracy of the applied soft computing method in the current study. The most important advantage of Model Tree, compared to other soft computing methods, is giving direct mathematical expressions, which can be used easily for estimating the reduction factor.

5. Summary and conclusion

In this study, M5' model tree was used to predict the row reduction factor. All of existing documented experimental data were collected to build the model. Then, the results of the model tree were compared with AASHTO and FEMA P-751's values. Error measures showed that model tree method is more accurate than the others. Also, model tree was preferred because it has physically sound equations and it considers more parameters than others.

6. References

[1] Brown, D. A., Morrison, C. and Rees, L. C. (1988), 'Lateral load behavior of pile group in sand', Journal of Geotechnical Engineering 114(11), 1261–1276.

[2] Rollins, K. M., Peterson, K. T. and Weaver, T. J. (1998), 'Lateral load behavior of full scale pile group in clay', Journal of Geotechnical and Geoenvironmental Engineering 124(6), 468–478.

[3] Rollins, K. M., Lane, J. D. and Gerber, T. M. (2005), 'Measured and computed lateral response of a pile group in sand', Journal of Geotechnical and Geoenvironmental Engineering 131(1), 103–114.

[4] McVay, M., Zhang, L., Molnit, T., and Lai, P. (1998), 'Centrifuge testing of large laterally loaded pile groups in sands', Journal of Geotechnical and Geoenvironmental Engineering 124(10), 1016–1026.

[5] Etemad-Shahidi, A., Mahjoobi, J., 2009. Comparison between M5' model tree and neural networks for prediction of significant wave height in Lake Superior. Ocean Engineering 36, 1175–1181.

[6] AASHTO (2012), AASHTO LRFD Bridge Design Specifications, sixth edn, American Association of State Highway and Transportation Officials, Washington, D.C.

[7] FEMA P-751 (2012), Foundation analysis and design, in 'NEHRP Recommended Provisions:Design Examples', National Institute of Building Sciences, Building Seismic Safety Council, Washington, D.C., chapter 5.

[8] Wang, Y., Witten, I.H., 1997. Induction of model trees for predicting continuous lasses. In: Proceedings of the Poster Papers of the European Conference on Machine Learning, University of Economics, Faculty of Informatics and Statistics, Prague.

A RELIABLE METHOD FOR DESIGN OF GRAVITY QUAYWALLS; A CASE STUDY FOR SHAHID-BEHESHTI PORT

Hassan Akbari[1], Masoud Hosseini[2]

1) Department of civil engineering, Tarbiat Modarres University, Tehran, Iran, Akbari.h@modares.ac.ir
2) Sahel consultant engineering, Tehran, Iran

1. INTRODUCTION

Gravity quaywalls are commonly used for the location with acceptable soil strengths. To design a gravity type quaywall, several items shall be considered including: sliding of the wall, overturning of the wall, bearing capacity of the foundation, overall stability of the wall, settlement and the amount of eccentricity (e/B) both in the foundation level and between blocks. All of these items depend on the earth pressure acting on the quaywall.

It has been proved that a humpbacked arrangement of blocks make a better response in earthquake condition rather than a regular arrangement. The results of analysis by Sadrekarimi et al. 2007 and Sadrekarimi 2010 show that the earth pressure decreases by a leaning slope at lower elevations [1,2]. Shafiefar and Mirjalili, 2006 utilized an optimistic method for determining the best quaywall geometry [3]. They calculated the earth pressure based on analytical formulations in OCDI, 2002 [4]. However, since simplified analytical equations are used usually for evaluating the earth pressure, the reliability of this method should be investigated. In this study, a design method is introduced for evaluating the earth pressure more accurately. For this purpose, quaywall of Shahid-Beheshti port is selected as a case study and earth pressure is obtained by means of FLAC software as well as analytical formula.

2. GEOMETRY AND LOADING ASSUMPTION

The section of the quaywall for Shahid-Beheshti port is presented in Figure 1. The dimension of blocks has been selected in a way that no tension occurs between blocks by controlling the value of e/B for each block in the allowable range. The parameters of underlying soil are presented in Table 1 according to the performed geotechnical investigations [5].

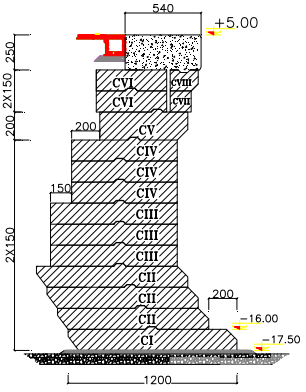

Figure 1. Geometry and loading condition

Table 1. Soil parameters

Layer	Thickness (m)	γ_{sat} (KN/m^3)	γ_d (KN/m^3)	C (kPa)	ϕ (grade)	Poison (v)	E (MPa)
Rock fill	13	17	20	0	40	0.3	80
Silty Sand	17.5	21.8	19.1	10	36	0.3	120
Lean Clay	14	21.6	18.4	175	0	0.45	48
Silty Sand	--	21.8	19.1	0	37	0.3	120

A surcharge equal to 5 ton/m^2 and 2.5 ton/m^2 are applied at the upper elevation of the quaywall in ordinary and seismic conditions, respectively. In addition, the horizontal seismic coefficient for pseudo-static analysis equals to 0.15 for the considered region. A residual water pressure is also applied and the hydrodynamic effect of water in front of quaywall during earthquake has been calculated based on Westergard formula [4].
The mooring load is applied based on a 100,000 DWT vessel, however, berthing load is neglected conservatively because it is exerted in landward direction [6].

3. SIMPLIFIED METHOD

The earth pressure in static condition for sandy soil has been calculated based on Coulomb theory while the earth pressure in seismic condition has been calculated using the Mononobe-Okabe method according to OCDI, 2002 [4]. The load distribution beneath the lowest block of the quaywall is calculated based on the simple equilibrium equations and it is presented in Figure 2. Load distribution is linear because the block is assumed to be rigid in the simple method

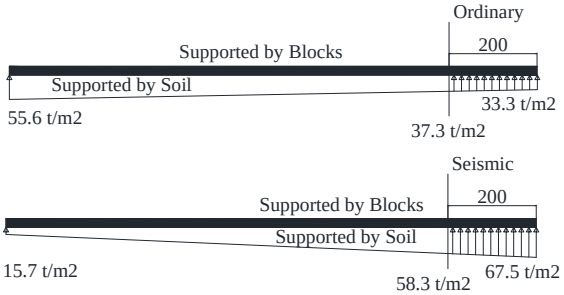

Figure 2. Pressure distribution under the quaywall; Simplified method

It is clear that the pressure at the sea side of the block is higher in the seismic condition while in an ordinary condition, the soil distribution is reversed and the soil

pressure at the sea side is less than the leeside of the quaywall. It should be noted that the humpbacked shape of the quaywall has a big influence of this distribution.

3. NUMERICAL METHOD

The quay wall is analyzed for Two ordinary and seismic cases by utilizing FLAC software. PGA (Peak Ground Acceleration) of the project at base of the structure is 0.15g and therefore, horizontal seismic factor is considered as $K_h=a_{max}/g$ for a_{max}/g <0.2 [7]. The result of analysis is presented in Figure 3 and the soil pressure beneath the quaywall is shown in Figure 4.

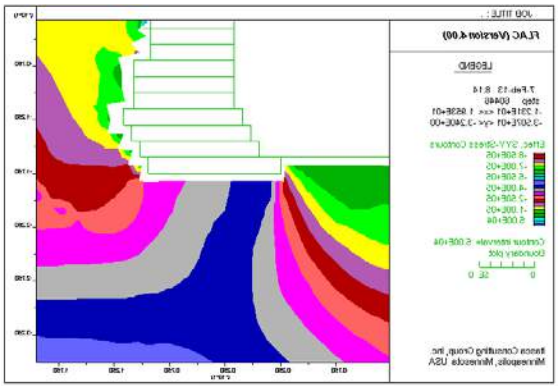

Figure 3. Pressure distribution around the quaywall via numerical method

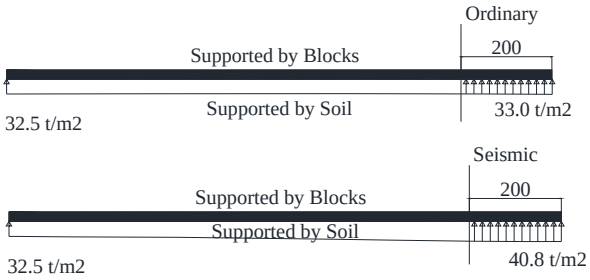

Figure 4. Pressure distribution under the quaywall; Numerical method

5. CONCLUSION AND DISCUSSION

Soil pressure beneath the lowest block of the quaywall is calculated by means of two simplified and numerical methods and the results are compared with each other in Figure 5. Solid lines are the results of the numerical method and dashed lines present the results of simplified method.

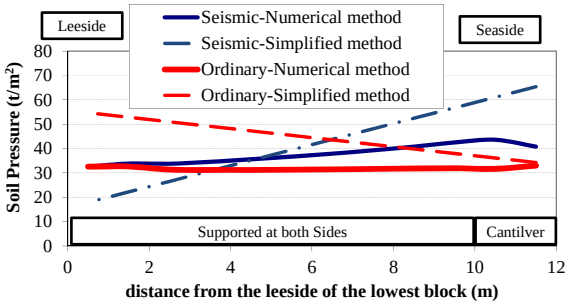

Figure 5. Pressure distribution under quaywall

According to the results, it can be concluded that:

- The load distribution beneath the quaywall is more uniform than the calculated pressure by using the simplified method.
- Simple analytical formula generates higher soil pressure at the sea side of the lowest block than the actual pressure and its utilizing would be conservative particularly in the seismic condition.
- Both simplified and numerical methods generate a similar trend (but different values) in a seismic case. However, the trend is completely different in ordinary condition.
- The mean pressure beneath the quaywall at the ordinary condition is less than the calculated pressure via simplified method, yet the calculated pressure is nearly the same at the toe part of the quaywall. In another case, analytical equations may results in an even less pressure than the actual pressure.
- Since different allowable stresses are used for seismic and ordinary conditions, analytical equations should be used with cautions when an ordinary condition governs the design.
- On the other hands, utilizing analytical equations are conservative for a seismic governing condition.
- As conclusion, it is better and it is more economic to use more reliable methods for evaluating earth pressure instead of making use of simple analytical equations.

6. REFERENCES

[1] Sadrekarimi A, (2010). Pseudo-static lateral earth pressures on broken-back retaining walls. Canadian Geotechnical Journal, J. 47: 1247–1258. doi:10.1139/T10-025.

[2] Sadrekarimi A et al., (2008); Static and dynamic behavior of hunchbacked gravity quay walls. Soil Dynamics and Earthquake Engineering, J 28 (2008) 99–117.

[3] Shafiefar and Mirjalili, (2006); Optimum design of gravity quaywall by means of a Sequential Quadratic Programming Method, Quarterly Journal of Transportation; Third Issue; Fall 1385 (In Persian)

[4] OCDI (2002); Technical standard and commentaries for port and harbor facilities in japan, The Overseas Coastal Area Development Institute of Japan.

[5] Report No.: SCE 10366 OGPD 09 CS RP 405, (2013); Shahid-Beheshti port development. "Structural Design of Multipurpose and Container Berth".

[6] BS6349-4 (1994); British standard, maritime structures-Part 4: Code of practice for design of fendering and mooring systems.

[7] Iranian Code 631, (2013); Design Standard for coastal structures; part2: Design conditions, 1392

[8] PIANC (2006); Seismic Design Guidelines for Port Structures (formerly the Permanent International Association for Navigation Congress); ISBN 90 265 1818 8

MODELLING OF WAVES AROUND POROUS SUBMERGED BREAKWATERS USING DELFT3D

S. Mojabi, H.Oumeraci

Leichtweiß-Institute for Hydraulic Engineering and Water Resources
TU-Braunschweig, Braunschweig, Germany, s.mojabi@tu-bs.de

1. Introduction

A reliable assessment of the transmitted waves is an essential part of the breakwaters design. This paper outlines a new approach for modelling the wave field in the vicinity of porous submerged breakwaters (SPB) using the open source model Delft3D. The implementation of the porous submerged breakwaters (Hereafter SPB) in Delft3D has been elaborated and verified against laboratory measurements.

2. Brief Description of the Numerical Model

Delft3D, an open source numerical model developed by Deltares, has been extensively applied to study wave and flow fields as well as morphological changes in the vicinity on coastal structures, especially submerged breakwaters. Delft3D uses SWAN (Booij et al, 1999) as a wave generation module. Theoretically, Delft3D is capable of representing all the important hydrodynamic processes affecting the wave and flow field in the vicinity of submerged breakwaters. However, regarding the effect of structure porosity and submergence, the model has some limitations which will be discussed in the next sections.

2.1. Implementation of SPB in DELFT3D-SWAN

El Shinawy and Zeidan (2012) showed that, for submerged breakwaters with steeper slopes, DELFT3D-SWAN is not applicable using the original parametrization. Alternatively, porous submerged breakwaters (SPB) could be introduced as an obstacle in the WAVE-module. However, when flow simulation is considered, the bathymetry used in the FLOW-module is transferred to the WAVE-module, resulting in an additional wave dissipation, and thus in an incorrect wave field in the lee of the submerged breakwater. The new approach proposed in this study is based on the local adjustment of wave dissipation over the SPB through adjusting the mesh size and using an artificial obstacle on the leeward toe of the breakwater to take the effect of structure porosity into account. In order to validate the proposed approach, results of the numerical simulations are compared with the results of laboratory studies performed by Kramer et al. (2003). Fig 1 show a schematic description of the SPB implementation using the proposed approach. The computational domain is divided in Region I and Region II.

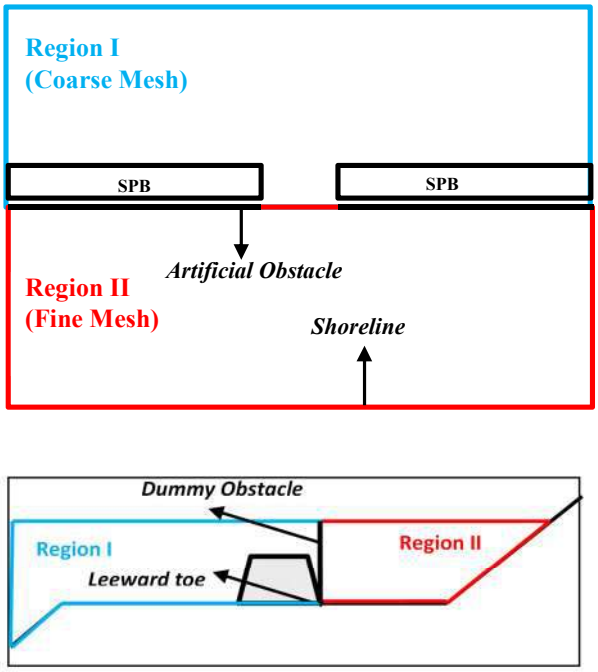

Figure 1. Implementation of porous submerged breakwaters (SPB) in SWAN-DELFT3D

The transmission coefficient of the dummy obstacle is calculated using Eq. 1 for the *Porosity Effect Factor (PEF)* as proposed by Mojabi and Oumeraci (2014), where *Rc* represents the structure freeboard, *H* the wave height, *B* the crest width, *k* the wave number, and *n* the structure porosity.

$$PEF = \begin{cases} 1 - 6.9 \times (n) \times (kB)^{0.144} \exp\left[-1.33 \frac{R_c}{H}\right] & 0 \le n \le 0.1 \\ Linear\ \text{int}erpolation & 0.1 < n < 0.2 \\ 1.22 \times (kB)^{0.29} \times (n) \times \exp\left[-1.53 \frac{R_c}{H}\right] + & \\ \exp\left[\frac{-88.47kB - 81.02}{433.12 R_c/H - 42.91}\right] & 0.2 \le n \le 0.6 \end{cases} \quad (1)$$

3. Results and Concluding Remarks

The schematic representation of the proposed approach is shown by Fig 2, where VDM2003 represents the transmission coefficient (kt) calculated by the empirical formula given Van der Meer et al (2003).

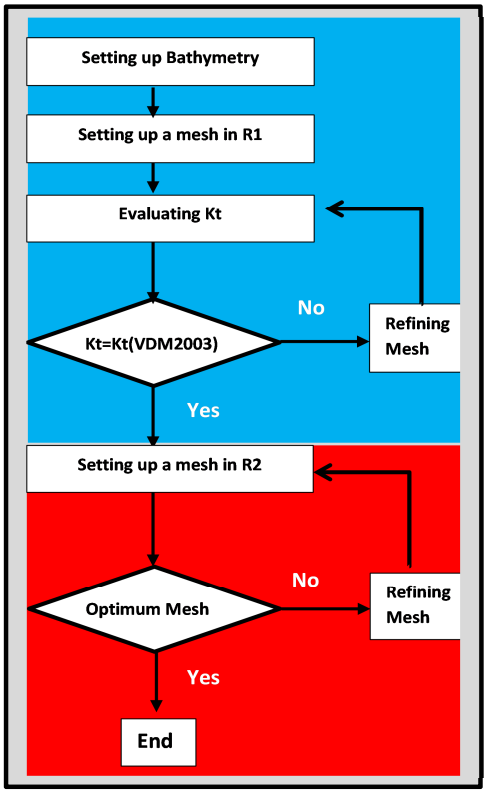

Figure 2. Schematic representation of the proposed approach.

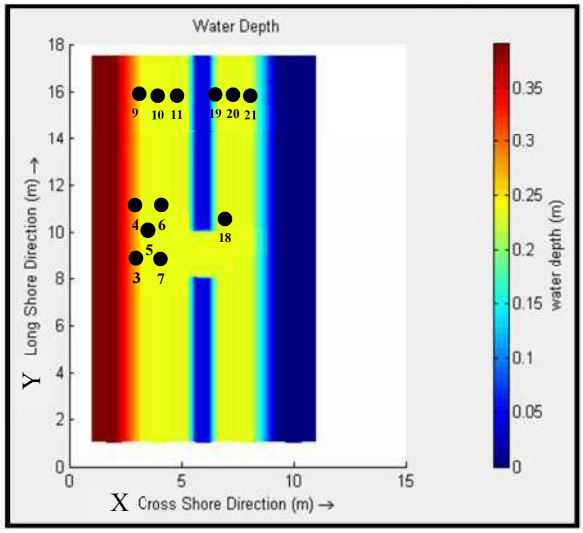

Figure 3. The computation domain. Wave Gauge locations are denoted by G

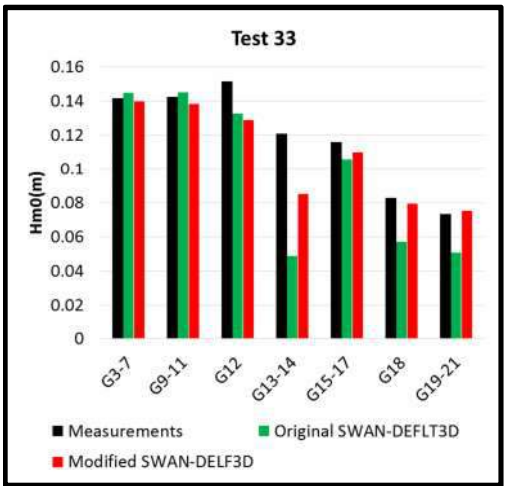

Figure 4. Comparison between numerical simulation results and laboratory measurements.

As shown by Fig 3, the application of the proposed approach to implement SPB in SWAN-DELFT3D modelling system results in a good agreement between numerical simulations and laboratory experiments. Moreover, the present results suggest that the proposed approach noticeably enhances the performance of SWAN-DELFT3D in predicting the wave field in the vicinity of SPB.

4. References

[1] Mojabi,S., Oumeraci. H "An improved wave transmission coefficient formula for submerged porous breakwaters ", *Progress Report2*, July 2015

[2] Van der Meer, J. W., Wang, B., Wolters, A., Zanuttigh, B., ," Oblique wave transmission over low-crested structures ", in *Proceedings Coastal Structures* , 2003.

Acknowledgements

This research is a part of the PhD study of the first author which is supported by the DAAD in the frame of the Exceed-Swindon Project at Technische Universität Braunschweig. This support is gratefully aknowledged.

PERFORMANCE-BASED EARTHQUAKE ENGINEERING OF PILE-SUPPORTED WHARF STRUCTURES AS SEEN THROUGH INCREMENTAL DYNAMIC ANALYSIS

Hamid Heidary-Torkamani[1] and Rouhollah Amirabadi[2]

1) Ph.D. Student, Civil Engineering Department, University of Tehran, Tehran, Iran, Hamid_heidary@ut.ac.ir
2) Associate Professor, Faculty Member of Civil Engineering Department, University of Qom, Qom, Iran, Rohollah@ut.ac.ir

1. Introduction

This study develops the practical application of Incremental Dynamic Analysis (IDA) to pile-supported wharves regarding to Performance-Based earthquake engineering goals.

7th Street terminal at the Port of Oakland (POOAK) was selected as typical wharf structure with batter piles. FLAC2D was used to numerical modeling and performing required analyses. Spectral acceleration (S_a) and displacement ductility factor (μ) were the chosen intensity measure and seismic performance indicator, respectively.

IDA was performed by choosing 8 earthquake records (see Table 1); applying advanced hunt & fill algorithm and using interpolation and summarization techniques to estimate the probability distribution of the structural demand given the seismic intensity. The bounds of damage states were quantified according to PIANC to calculate the corresponding capacities. The results can be integrated with Probabilistic Seismic Hazard Analysis (PSHA) to estimate mean annual frequencies of limit-state exceeding and seismic vulnerability assessment of these structures. The cross section profile of the selected wharf and FLAC numerical model are presented in Figure 1 and Figure 2 respectively.

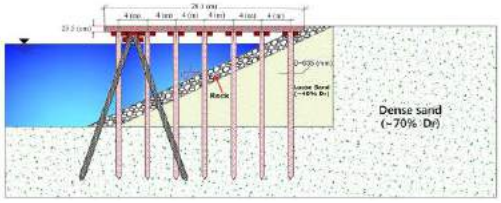

Figure 1. Cross section of Selected Pile-supported Wharf (POLA)

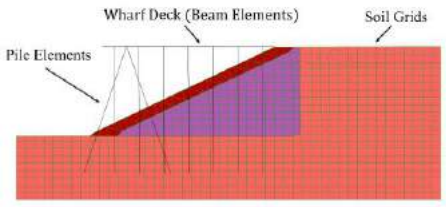

Figure 2. FLAC Numerical Model of the Wharf

Geotechnical properties, used for numerical modeling are presented in Table 1

Table 1. Geotechnical properties of the Wharf

Soil Layer	Dry Mass Density (kg/m3)	Porosity (%)	Friction Angle (deg)	Cohesion (kPa)	Shear Wave Velocity (m/s)	Drained Poisson's Ratio
Pavement Section and Ballast	1958	20	45	0	666	0.20
Rock Fill	1737	35	42	10	262	0.20
Hydraulically Placed Sand	1443	44	30	0	198	0.35
Bay Mud Clay	979	60	0	38	152	0.35
Dense Sand	1752	34	40	0	351	0.30
Stiff Clay and Dense Sand	1701	40	30	12	243	0.35

Table 2. Ground motion records used for seismic analysis

No.	Event	Station	Year	M	R (km)	PGA (g)
1	Imperial Valley	Chihuahua	1979	6.5	28.7	0.270
2	Imperial Valley	Delta	1979	6.5	43.6	0.351
3	Livermore	San Ramon - Eastman Kodak	1980	5.8	17.6	0.154
4	Loma Prieta	APEEL 2E Hayward Muir Sch.	1989	6.9	57.4	0.171
5	Loma Prieta	Palo Alto - SLAC Lab.	1989	6.9	36.3	0.278
6	Loma-Prieta	Sunnyvale - Colton Ave.	1989	6.9	28.8	0.209
7	Morgan Hill	Capitola	1984	6.2	38.1	0.142
8	Northridge	Canyon Country - W Lost Cany	1994	6.7	13.0	0.482

1.1. Validation Analysis

Validation analyses were performed to validate the numerical model. The POOAK modeled during the Loma Prieta earthquake. The horizontal displacement of the rock dike was predicted by the analysis as 33 cm and the vertical settlement as 20 cm at the ground surface, both in agreement with the observed ones of 15-35 cm and 13-30 cm, respectively [1]. In addition, plastic hinge development was predicted by FLAC at the top of the

batter piles. The rest of vertical piles remained elastic behavior throughout the analysis. The predicted behaviors of the piles were consistent with the observations.

1.2. Incremental Dynamic Analysis

Advanced hunt & fill algorithm was used to scale each record to cover the entire range of structural response, from elastic state to yielding and failure [3]. This ensures the record scaling levels are appropriately selected to minimize the number of required runs.

In order to determine the number of required analyses, displacement ductility factor (μ_d) was selected as the seismic response indictor of wharf structure. Analyses were performed at rapidly increasing levels of S_a until structures reach the ultimate state. Herein, "*ultimate state"* is defined as the point which double plastic hinge forms at only one or limited number of piles [4]. Hence, ultimate limit of μ_d is the ratio of ultimate displacement (d_u) to displacement at structure yield point (d_y), driven from push over analysis.

Additional analyses were performed at intermediate S_a-levels to sufficiently bracket the global failure and increase the accuracy at lower levels of S_a.

According to PIANC 2001, extensive damage state of pile-supported wharf structures occurs when double plastic hinge forms at only one or limited number of piles. Hence, ultimate limit of displacement ductility factor was defined as the ratio of ultimate displacement to elastic displacement, driven from push over analysis.

2. Results

The step-by-step practical application of incremental dynamic analysis was demonstrated for 7th Street terminal at the Port of Oakland (POOAK). Spectral acceleration and displacement ductility factor were selected as the IM-EDP pair to assess the seismic performance of these types of structures. Incremental dynamic analyses were performed through application of FLAC2D numerical reference model and advanced hunt & fill tracing algorithm. The resulted IDA curves for 8 ground motion records are illustrated in Figure 3. The summarized IDA curves are presented in Figure 4.

The resulted IDA curves can be used in seismic vulnerability assessment of pile supported wharf structures.

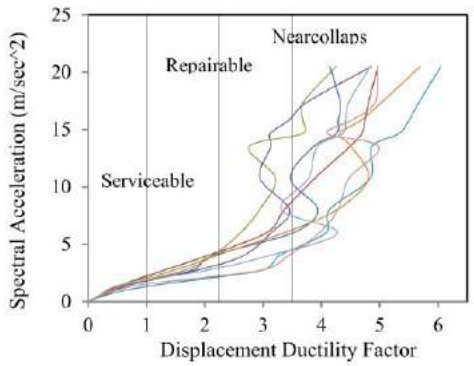

Figure 3. IDA curves and the associated limit-state capacities

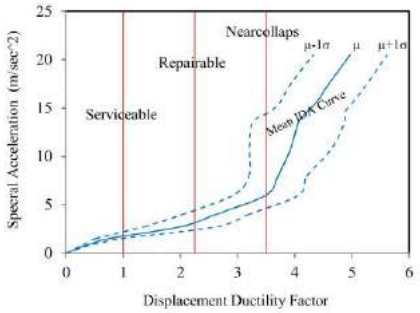

Figure 4. The summary of the IDA curves and Values of IM for each limit-state

The reliability and accuracy of a numerical model, directly depends on the accuracy of desired engineering demand parameters (EDPs) estimation. So, the accurate estimation of EDP values is an important issue in seismic analysis of a wharf structure. Regarding this issue, in this research, instead of static methods with a low level of accuracy, a more accurate and powerful method (i.e. IDA) was used in order to estimate seismic performance assessment of a typical pile-supported wharf.

3. References

[1] Egan J. A., Hayden R. F., Scheibel L. L., Otus M., Serventi G. M. (1992) Seismic repair at seventh street marine terminal. Grouting, Soil Improvement and Geosynthetics. ASCE Geotechnical Special Publication, No. 30, vol. 2, pp. 867 – 878.

[2] Hall, J. F. (Editor). (1995). Northridge Earthquake of January17, 1994 Reconnaissance Report Vol. 1. Earthquake Spectra, Supplement C to Vol. 11.

[3] Vamvatsikos, D. and Cornell, C. A. (2002). Incremental dynamic analysis, Earthquake Engng Struct. Dyn. 31:491-514.

[4] PIANC (2001). Seismic Design Guideline for Port Structure, Working Group NO.34 of the Maritime Navigation Commission, International Navigation Association, Balkema, 474p.

[5] Salton, G., *Automatic Text Processing: The Transformation, Analysis and Retrieval of Information by Computer*, Addison-Wesley, 1989.

DEVELOPING AN INNOVATIVE MODEL TO ESTIMATE THE SERVICE LIFE OF REINFORCED CONCRETE STRUCTURES IN THE PERSIAN GULF USING ARTIFICIAL NEURAL NETWORK

Ali Shojaei[1], Amir Mohammad Ramezanianpour[2], Ali Akbar Ramezanianpour[3]

1) M.Sc Graduated student in Construction Engineering and Management, Faculty of Civil Engineering, University of Tehran, Tehran, Iran, shojaei.ali@ut.ac.ir
2) Assistant Professor, Faculty of Civil Engineering, University of Tehran, Tehran, Iran, ramezanian@ut.ac.ir
3) Professor, Faculty of Civil and Environmental Engineering, Amirkabir University of Technology, Tehran, Iran, aaramce@aut.ac.ir

1. Introduction

One of the main causes of deterioration of reinforced concrete structures exposed to marine environments is steel corrosion due to chloride penetration into concrete. Studies and research in the field of durability models must be based on the special environmental conditions such as temperature, temperature changes, humidity, wind, and locally consumed materials such as cement, additives, pozzolan, etc. On the other hand, using foreign models can be misleading and result in poor decisions due to incompatibility with our country's environmental condition. Based on the significant role of environmental conditions, in the present study, modeling was conducted using data from research sites located in the Persian Gulf in order to improve of the accuracy of the model in estimating the service life of reinforced concrete structures in this region. According to local investigations and examination of structures constructed in different parts of the Persian Gulf, it seems that the effect of environmental conditions of various regions of the Persian Gulf on the durability of concrete is very different [1]. In order to assess concrete durability in these conditions and develop a comprehensive model, it is necessary to consider the results of research in various areas of the region, and results of tests in a particular area are not sufficient. Therefore, results obtained from several research sites in this region were collected and used in this study. Nowadays, inspiration from natural methods has helped mankind to solve complicated real-world problems. One of the most popular and efficient of these methods is artificial neural networks whose role in solving complex problems of today's world cannot be ignored. Developing a model to estimate and evaluate the durability of concrete in the Persian Gulf requires very complex routing of the affecting parameters. Considering the fact that many factors simultaneously affect the durability of concrete in this environment, this route includes examining the impact of each factor on concrete durability, as well as examining the interactions among these factors. This operation is very similar and comparable to the operations of artificial neural networks.

2. Model development

One of the main objectives of this research was to gather the data related to chloride ions penetration from the research sites across the southern coast of the country, and to develop a model applicable to all parts of the Persian Gulf by accumulating the work of researchers along several decades. In this regard, after reviewing the results of past researches and literature in this field, 183 chloride penetration profiles with their concrete mix designs were collected from four research sites in the region.
Then, the apparent diffusion coefficient of chloride ions and the surface chloride calculated by fitting the Fick's second law equation on the chloride penetration profiles were obtained. For this purpose, Curve Fitting Toolbox of MATLAB software was used. In the next step, several artificial neural networks were designed and trained using Improving Generalization methods, early stopping and automated regularization. For this purpose, the MATLAB`s nntool toolbox was used [2]. In this regard, the input and output parameters of the networks were considered according to Table 1, and the networks were trained by different amounts of primary weights, learning functions, number of layers, number of neurons, and transfer functions.

Table1. parameters of artificial neural network

Input parameters	Exposure condition (2= Splash & 1= Tidal)
	Age of concrete (year)
	Water-cementitious materials ratio
	cement content (kg/m^3)
	amount of silica fume (kg/m3)
	amount of metakaolin (kg/m3)
	amount of zeolite (kg/m3)
Output parameters	Chloride diffusion coefficient (mm^2/year)
	surface chloride

Then, by comparing regression and performance charts, the network which had the best performance and also formed a stronger relationship between the output and the available data was chosen to develop the model. Specifications and structure of the selected artificial neural network are presented in Table 2.

Table2 .characteristics of selected artificial neural network

Improving Generalization method	Automated Regularization
learning function	Trainbr
The number of layers	3
The number of neurons in layers	7-20-20-2
Transfer functions	Tansig-logsig-purelin

Moreover, the flowchart of the proposed model, which is based on artificial neural network, is shown in Figure 1.

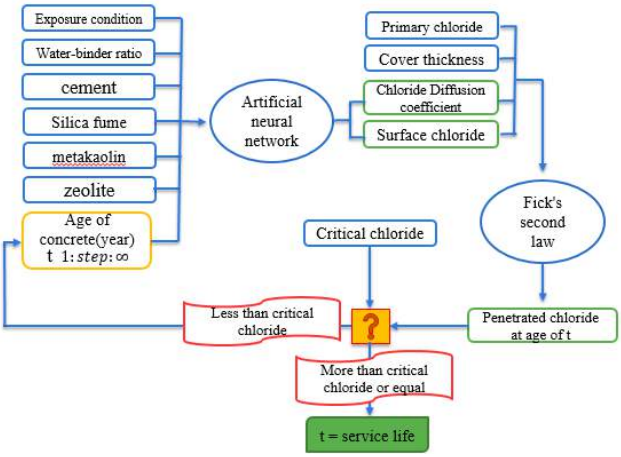

Figure1. Flowchart of the model

3. Model validation

Finally, in order to better evaluate the performance of the developed model, actual and estimated chloride penetration profiles of two real reinforced concrete structure in the Persian Gulf (CICO and PSPC) with the ages 33 and 39 years were compared and the results are presented in Figures 2 and 3.

The actual chloride penetration profiles were extracted from Safehian's researches [3].

As the results suggest, the estimated chloride penetration profiles change with lower slop than actual chloride ion penetration profiles. Sudden changes in amounts of actual chloride ion penetration profiles may be due to testing errors. in general it is clear that the model can properly estimate the overall process of penetrating chloride ions in concrete depth.

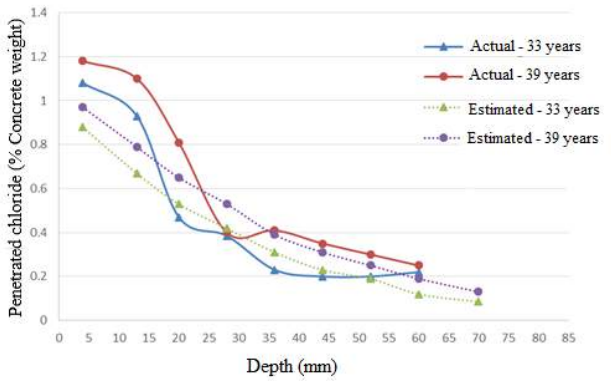

Figure2. Comparison of actual and estimated chloride diffusion profiles for the CICO concrete at the ages of 33 and 39 years

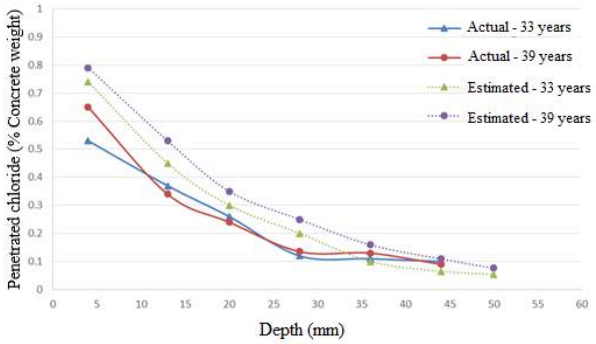

Figure3 .Comparison of actual and estimated chloride diffusion profiles for the PSPC concrete at the ages of 33 and 39 years

4. Conclusion

The results presented in Figures 2 and 3 show that the model developed in this study is capable of estimating the chloride penetration profile and consequently the service life of reinforced concrete structures in the Persian Gulf with very good accuracy. Also, it can properly estimate the overall process of penetrating chloride ions in concrete depth.

5. References

[1] Ramezanianpour AA, Jahangiri E, Moodi F. Assessment of some parameters of corrosion initiation prediction of reinforced concrete in Persian Gulf region. In: 3rd international conference on concrete repair, rehabilitation and retrofitting, ICCRRR-3. South, Africa; 2012

[2] Dimith, H., M. Beale, and M. Hagan, Neural Network ToolboxTM 6-User Guide. The MathWorks, Inc. 3.

[3] Safehian, M . "Assessment of Severe Marine Environments on Durability and Service Life of Reinforced Concrete Members Under Uniform and Variable Flexural Loadings", PhD Thesis, Civil and Environmental Engineering Department, Amirkabir University of Technology, 2014

THE ADVANTAGES OF MULTILAYER BERM BREAKWATERS

Masoud Hosseinii[1], Hassan Akbari[2]

1) Sahel consultant engineering, Tehran, Iran, m.hosseini@sahelce.com
2) Department of civil engineering, Tarbiat Modarres University, Tehran, Iran, Akbari.h@modares.ac.ir

1. Introduction

Berm breakwaters have basically developed in two directions. On one hand are the structures built using a homogenous berm, usually of one stone class, that are allowed to reshape, sometimes referred as dynamic berm breakwaters. On the other hand are the more stable structures with steep upper and lower slopes, built of several stone classes, where only a few stones on the berm are allowed to move. These structures have been referred to as Multilayer type berm breakwaters or well known as Icelandic berm breakwaters.

In this study, homogenous and multilayer Berm Breakwaters are compared regarding to technical and commercial parameters in two case studies. These case studies include construction of breakwater and shore protection of Shahid Beheshti Port locates in Chabahar, south east of Iran.

2. Case study 1: Comparison between Existing Breakwater of Shahid Beheshti Port and Breakwater Extension

The existing breakwater in Shahid Beheshti Port has been built in two phases. The total length of the breakwater is 2050 m. The material for the breakwater was taken from a quarry near the Ramin fishing harbour, about 12 km east of the breakwater which is a sedimentary rock with a density of about 2.1 t/m3. The existing breakwater is a homogenous berm breakwater with armors weighting (3 to 8) tons and berm width about 19 meters. The typical cross section of existing breakwater is presented in Figure 1.

The existing breakwater has been experienced wave height during Gonu 2007 which is close to design wave condition and it is the most intense since 1945. The wave height along the existing Shahid Beheshti breakwater has been modeled with the Mike21 SW refraction model. According to these calculations, the significant wave height varies between 3.2 m to 3.7 m along the breakwater. With reference to [1], with considering these wave heights, classifies the existing breakwater in the regime of Statically stable reshaped berm breakwater. Some reshaping is apparent on the parts of the breakwater. If, on the other hand, the wave had reached the maximum 100-year wave height of 4.73 m, then the existing breakwater would have been well in the region of Dynamically stable reshaped berm breakwater and we would have seen much more reshaping.

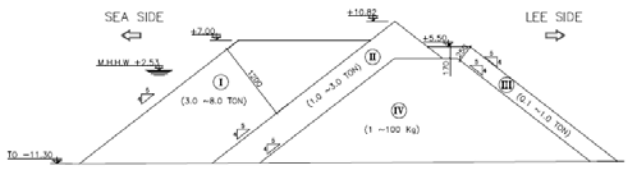

Figure 1. Typical section of existing breakwater

The 1500 m extension of the Shahid Beheshti berm breakwater was constructed in the period 2008 to 2012. As existing breakwater, most part of material for construction is taken from the Ramin quarry. Figure 2 shows cross section design of breakwater trunk. The breakwater is a multilayer berm breakwater with armors class I weighting (8 to 20) tons, armors class II weighting (3 to 8) tons and berm width about 9.5 meters.

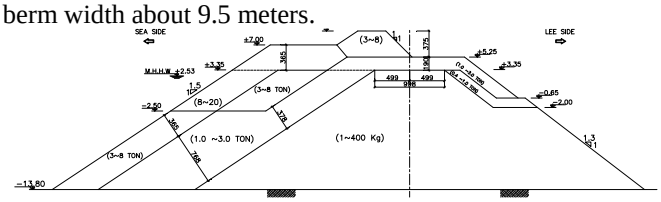

Figure 2. Sectional Design of the Breakwater Extension

In Table 1 various parameters are listed for different sets of stone classes both for the existing breakwater and for the extension of the breakwater. Firstly the stone classes of the existing breakwater are analyzed. Class I is either 3 – 8 ton and Class II is either 1 – 3 ton. It has been estimated that the design wave height is about 4.73 m near the end of the structure. This means that the stability parameter of this breakwater is about 3.4 near the end. With reference to Table 1 this classifies the existing breakwater in the regime of dynamically stable reshaped berm breakwater.

In the lower part of Table 1, the designed stone classes for extension of Shahid Beheshti breakwater are listed. Class I stones as 8 to 20 tonnes leads to result in stability parameters 2.8 at the end and 2.5 at the root. Based on the weighing of the extracted armour, the median mass is more

than 15 tons, considerably higher than the required minimum median mass of 12.8 tonnes. The stability parameters based on the executed Class I armour stones are 2.6 at the end and 2.3 at the root. [1] classifies the breakwater extension in the regime of statically stable reshaped berm breakwater.

For comparison between required material of the existing breakwater and the breakwater extension, volume of different stone classes is presented in Table 1. According to this table the total volume of material in breakwater extension is about 91% of existing breakwater. The Volume of Class I armourstone in the existing breakwater, 3-8 ton, is 35% of total required material. In the other hand the Volume of Class I and II armourstone in the breakwater extension, 3-20 ton, is 23% of total required material. Also the volume of these ranges of material in the breakwater extension is less than 60% of volume of class I existing breakwater for unit length. This means that in spite of the designing heavier class I armour stone in breakwater extension that guarantee more stability, both total required material and class I, II and III are less than of existing breakwater.

Table 1. Stone Classes and Stability Parameter in the Existing Breakwater and Breakwater Extension

Stone Class	W_{max} (ton)	W_{min} (ton)	Volume (m^3/m)	Volume (%)	H_0 $H_s/\Delta D_{50}$
Hs (m)	4.73	Density of Rock (t/m3)	2.11	Density of Sea (t/m3)	1.03
Existing Breakwater					
I	3	8	5729	35%	3.4
II	1	3	2364	14%	4.8
III	0.1	1	1166	7%	7.5
IV	0.001	0.1	7181	44%	16.8
Total Material Volume			16440	100%	
Breakwater Extension					
I	8	20	1354	9%	2.3
II	3	8	2056	14%	3.4
III	1	3	3379	23%	4.8
IV	0.4	1	278	2%	6.7
V	0.001	0.4	7892	53%	10.6
Total Material Volume			14959	100%	

3. Case study 2: Shore protection of Shahid Beheshti port

In the second stage of shore protection project of Shahid Beheshti Port, 1120 m seawall had been designed with rubble mound material. The typical cross section of designed shore protection is presented in figure 3. The designed structure was a homogenous berm with 5 to 10 tons amour materials. The berm width was 14 meters. The required Class 1 amour material was about 55% of total required material. Also there was a gap between selected ranges of material and 1 to 4 tons material was not used in cross section. During Value Engineering studies of this project, Author proposed to modify design based on multilayer berm structure. The modifications allow reducing the required heavy armours and also all range of material to be used (figure 4). These modifications reduce 35% in project cost and approved by client as the result of value engineering workshop.

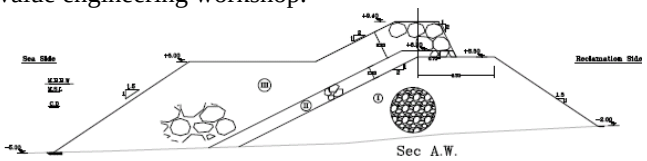

Figure 3: sectional design of the shore protection

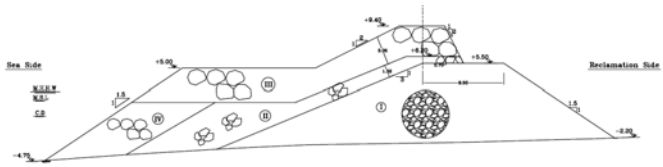

Figure 4: Modified sectional of the shore protection

4. Conclusion

The general method for designing a multilayer berm breakwater is to tailor-make the structure around the design wave load, regarding to possible quarry yield, available equipment, transport routes and required functions. These breakwaters are fairly simple to construct, usually they are built of locally quarried material and quarry yield prediction is used as a tool in the breakwater design procedure. The multilayer berm breakwater, which is a tough structure, has proved to be a cost and technically efficient structure [3]. Compared to homogenous berm breakwater projects, besides providing more stability parameters, required materials and construction prices for the multilayer Berm Breakwater are generally lower. This is due to the fact that the design is developed in close cooperation with construction. Maximizing the utilization of all stone fragmentations from the armourstones quarry is also granted in multilayer berm breakwater for the economy of the structure.

5. References

[1] PIANC. 2003. State-of-the-Art of Designing and Constructing Berm Breakwaters. WG40.

[2] CIRIA, CUR, CETMEF, 2007. The Rock Manual. The use of rock in hydraulic engineering (2nd edtion). CIRIA C683.

[3] Sigurdarson , S, van der Meer , J.W., Tørum, A. and Tomasicchio, R., 2008. Berm Recession of the Icelandic-type Berm Breakwater. ICCE, Hamburg, ASCE.

PIPELINE ROUTE OPTIMIZATION EFFECTS ON SEAWATER INTAKES EFFICIENCY (CASE STUDY: BANDAR ABBAS SAKO DESALINATION PLANT)

Seyede Masoome Sadaghi[1,*], Ali Fakher[2], Zeinab Toorang[3] and Alireza Shafieefar[4]

1) Road, Housing and Urban Development Research Center. Ministry of Road and Urban Development, Tehran, Iran, s.sadaghi@bhrc.ac.ir
2) School of Civil Engineering, University of Tehran, Tehran, Iran, afakher@ut.ac.ir
3) Pars Geometry Consultants, Tehran, Iran, z.toorang@parsgc.com
4) Pars Geometry Consultants, Tehran, Iran, a.shafieefar@parsgc.com

1. Introduction

Seawater is an important source of water for the consumption of power plants, refineries and desalination plants. Water scarcity and the necessity of supplying a portion of water demand from sea, has led to an increase in the need for seawater intakes. Construction of onshore intake basins and supply of water through submarine pipelines is a common method which has been employed in many projects. The intake and discharge pipeline routes are designed to reach the required water quality without recirculation. The environmental criteria shall also be met in selecting the outfall point. In this paper, it has been shown that the selection of the right route for the intake and discharge pipelines has a significant effect on the whole system efficiency. [1]

2. Project Explanation

Bandar Abbas SAKO desalination plant with the seawater intake capacity of four million cubic meters per day (CMD) will be the biggest desalination plant in the world which is under construction west of ISOICO shipyard. Figure 1 shows the project location. [2]

Figure 1. Project location

In the basic design, six intake pipelines (HDPE, D_{in}=2.5m) perpendicular to the intake basin structure, were supposed to supply seawater with the desired quality, from the distance of about 3.1 km offshore (depth of -12m. CD along route 1). Due to the long length of the pipelines, the second alternative as shown in Figure 2 was proposed for the intake route. More investigations revealed a deep area in the vicinity of the project. The third route alternative is considered to reach the mentioned area.

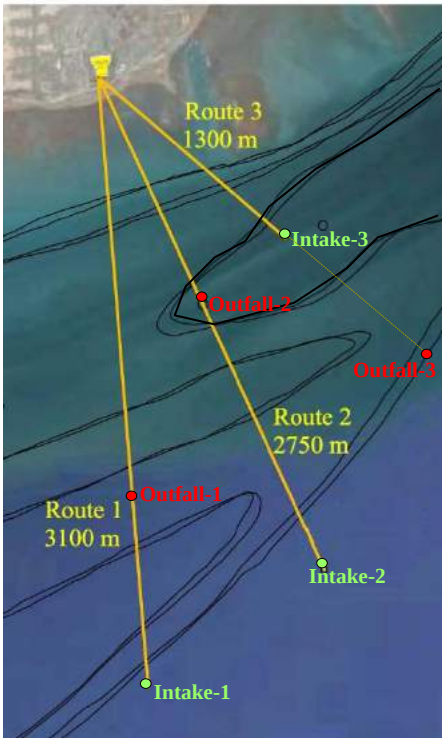

Figure 2. Pipeline route alternatives

The pipe length for each alternative is presented in Table 1.

* Formerly design manager at "Pars Geometry Consultants"

Table 1. Pipe lengths in different alternatives

Alt.	Intake pipe length (m)	Outfall pipe length (m)	Total pipe length (m)
1	6×3100=18600	3×2250=6750	25350
2	6×2750=16500	3×1300=3900	20400
3	6×1300=7800	3×2100=6300	14100

For each alternative the following items were investigated.

2.1. Intake Water Quality

It is assumed that the water quality improves with depth and hence the intake chamber was supposed to be located at a depth of more than 12 m with respect to CD. However, the water quality tests were performed to assure the assumptions. The results proved that there was not a significant difference in the water quality at the intake points of three mentioned routes. [2]

2.2. Intake/Outfall Recirculation

In each alternative, the outfall shall be located in a point where the discharge flow cannot return to the intake line because recirculation can lead to progressive decrease in the desalination system efficiency. In tide dominant regions where the current direction reverses, the outfall is usually located along the intake route so the tidal currents always conduct the brine stream away from the intake. The outfall is usually closer to the shoreline comparing to the intake point. This common practice is proved to be possible for the first and second alternatives in SAKO project by mathematical modeling but for the third alternative, the distance between the intake and shoreline is not long enough to accommodate the discharge point.

2.3. Environmental Considerations

Iran's Department of Environment has some regulations for brine or heated discharges. According to these regulations, the salinity increment at the distance of 200 meters from outfall should not exceed 10 percent of the initial salinity [3]. The required dispersion and mixing is easier to be achieved in deeper waters. Hence, outfall lines usually extend toward deep waters until reaching a point in which the environmental criterion is met.

3. Route Optimization

Considering the above explanations, different numerical models were designed to check the recirculation and environmental criteria for different possible alternatives [4]. A sample dispersion pattern for the 3rd alternative is shown in Figure 3. [4, 5]

The third alternative was proved to fulfill both recirculation and environmental criteria. In this innovative approach, unlike the common practice, the intake is located closer to the shoreline in comparison with the outfall point. The most notable advantages of this approach are summarized below:

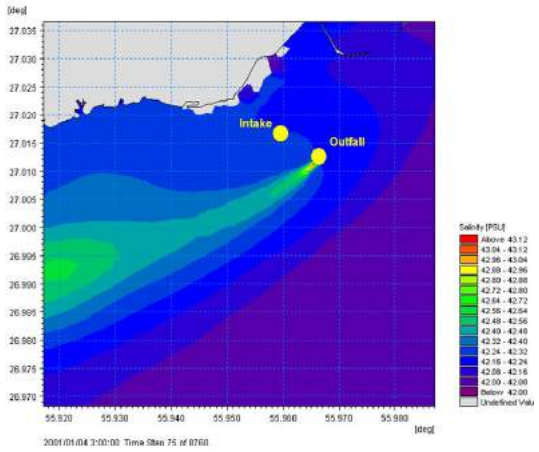

Figure 3. Salinity dispersion pattern for the 3rd alternative

- Due to the decrease in pipes length (decrease of about 11250 m HDPE pipes) and associated dredging volumes, the construction costs attributed to the optimized route were decreased more than 25% compared to the initial plan.
- The reduction of intake pipes length decreases the linear head losses considerably which increases the hydraulic capacity of pipes and the intake basin.
- The increase in the intake capacity leads to higher system availability and reliability especially for extreme conditions.

4. Conclusion

The present study has shown that the route selection for submarine pipelines in seawater intake and outfall systems, has considerable effects on project overall costs and efficiency. In route selection, different aspects shall be considered simultaneously. The shortest routes eventuate the lowest costs but it should be proved to fulfill the required intake water quality and avoid the recirculation between intake and outfall. The environmental criteria shall also be met around outfall point.

5. References

[1]. Pankratz, T., "An Overview of Seawater Intake Facilities for Seawater Desalination". CH2M Hill, Inc.

[2]. Pars Geometry Consultants, SAKO Desalination Plant, "Design general data" report, 2015.

[3]. Iranian Environmental Protection Organization Standard for effluent disposal, Department of Environment of Iran

[4]. Pars Geometry Consultants, SAKO Desalination Plant, "Evaluation of salinity distribution and saline water recirculation" report, 2015.

[5]. Mike 21 User Manual, Danish Hydraulic Engineering (DHI), Denmark, 2014

NUMERICAL MODELLING OF HYDRODYNAMIC RESPONSES OF SINGLE SLOTTED BREAKWATERS

Akbar Ghanei Ardakani[1], Mahdi Shafieefar[2]

1) Department of Civil Engineering, Tarbiat Modares University, Tehran, Iran, a.ghanei@modares.ac.ir
2) Department of Civil Engineering, Tarbiat Modares University, Tehran, Iran, shafiee@modares.ac.ir

1. Introduction

Water circulation near the beach is very important to keep the health of ecosystems in ports and waterways. Creating a natural circulation of water from the sea into the harbor and *vice versa* could well reduce pollution and its damaging effects. In addition to securing watercrafts, permeable breakwaters such as: pile breakwaters and slotted breakwaters, ensure communication and natural circulation between the port and the sea to eliminate environmental pollution in port areas[1]. Many researchers have studied on the reflection, transmission and energy dissipation coefficients of perforated/slotted breakwaters. Many permeable barriers in various designs have been introduced and suggested that their main purpose was to reduce wave transmission and the force exerted on the wall. Most of the modelling that has been conducted to investigate the permeable breakwater, were experimental. Varjavand et al [1] theoretically and experimentally developed analytical model to predict the reflection coefficient, transmission coefficient, the force exerted on the wall and wave run-up on the single and double slotted breakwaters using potential concept. Ahmed et al [2] also investigated hydrodynamic responses of single and double slotted breakwaters theoretically and experimentally. The structure was consist of an impermeable part on top and bottom and the porosity of the middle part was 50%. In this study, using Flow-3D software, regular wave interaction with single slotted breakwaters has been modelled. In order to predict the hydrodynamic responses of slotted walls, reflection, transmission and wave dissipation coefficients, were numerically studied. The reflection, transmission and wave dissipation coefficients, denoted by C_R, C_T and C_E respectively, are defined as the appropriate ratios of wave heights by:

$$C_R = \frac{H_r}{H_i}, C_T = \frac{H_t}{H_i} \quad (1)$$

$$C_E = 1 - {C_R}^2 - {C_T}^2 \quad (2)$$

Where H_t and H_r are the transmitted and reflected wave heights, respectively. Also C_E is the proportion of the incident wave energy flux that is dissipated by the barrier [3].

2. Numerical Model

Mathematical models are powerful tools in solving complex equations in fluid mechanics. Nowadays, by increasing computer processing ability, the application of models is being developed. One of the prevalent mathematical models used for solving complex equations related to hydraulic structures is FLOW-3D. FLOW-3D is a multi-tasks and compatible software uses for complex situations. Solving equations in this application are based on the finite volume method in regular grid[4]. Breakwater geometry and parameters required for numerical modeling, are introduced to the software based on experimental tests. Experimental results used for validating, obtained from Varjavand experimental study at Tehran University in 2014. As shown in Figure 1, breakwater created by AutoCAD software as 3D and moved to FLOW-3D software with storage in STL format. Another experimental data needed for numerical modeling, are wave characteristics generated in the laboratory flume. Incident wave parameters are shown in Table 1.

Table 1. Wave information generated in laboratory flume.

Water Depth [cm]	Wave Height [cm]	Wave Period [s]			
40	2	0.6	0.8	1.2	2.4

As shown in Figure 2 computational domain was considered 300 meters long and consists of 4 mesh blocks. Table 2 shows number of computational cells in every part of the domain.

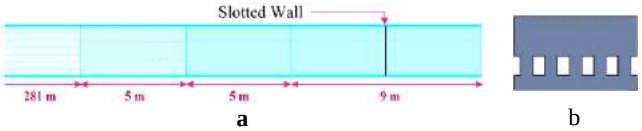

a b

Figure 1 Computational Domain: a) Side view b) Front view of structure

Table 2 Computational Domain Information

Mesh Block	$x_{min[m]}$	$x_{max[m]}$	No. of cells
1	0	9	2700000
2	9	14	187500
3	14	19	22500
4	19	300	147630

3. Results

WaveAR software [5] was used to extract the reflection coefficient. To determine the transmission coefficient or the ratio of the transmitted wave height to the incident wave height, wave heights obtained through analysis of model outputs, was used. Single slotted wavescreen reflection, transmission and wave dissipation coefficients are presented in Figure 3. These coefficients are displayed in a coordinate system in terms of kh that k and h are wave number and water depth respectively.

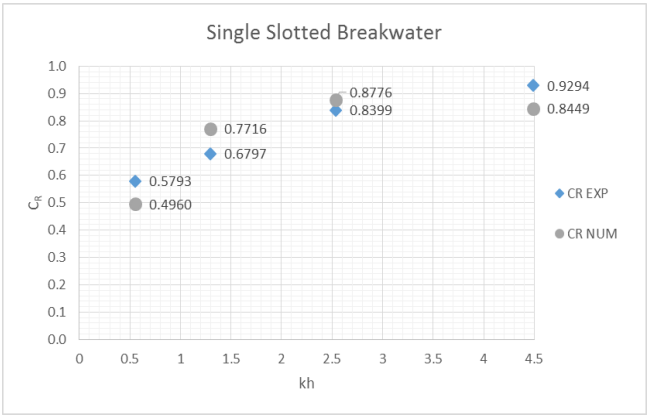

a

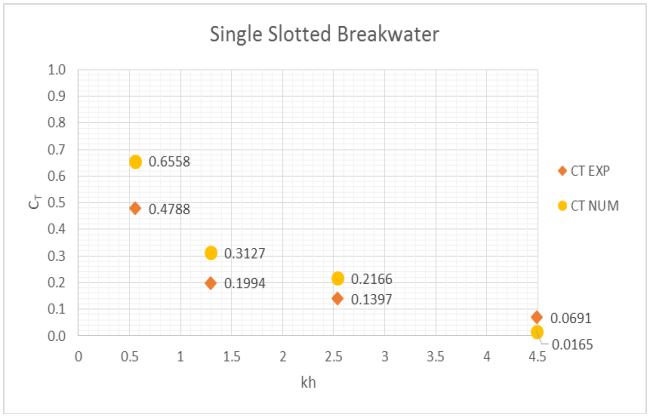

b

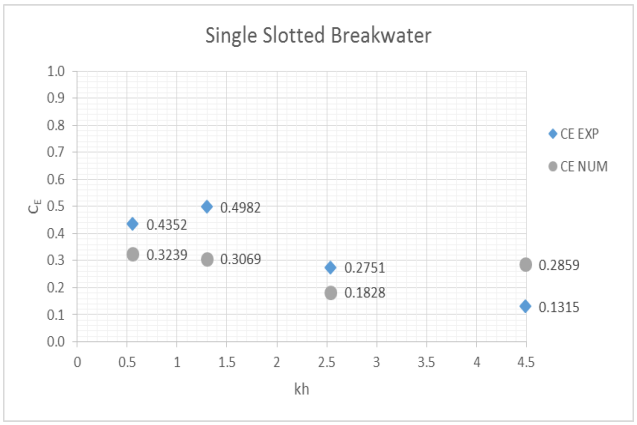

c

Figure 2 Single slotted breakwater numerical and experimental results comparison: a) reflection coefficient b) transmission coefficient c) wave dissipation coefficient

4. Conclusion

The numerical results appear a reasonable similarity with experimental results and these results show that the model is applicable for predicting the hydrodynamic responses of single slotted breakwaters.

5. References

[1] Varjavand, I., "Analytical investigation of interaction of slotted permeable breakwaters and sea waves based on laboratory studies," PhD. Thesis, Tehran University, 2014.

[2] Ahmed, H., "Wave Interaction with Vertical Slotted Walls as a Permeable Breakwater," PhD. Thesis, University of Wuppertal, 2011.

[3] Nejadkazem, O. and Gharabaghi, A. R. M., "Hydrodynamic behavior of curtainwall-pile breakwaters," *China Ocean Engineering*, vol. 26, pp. 685-698, 2012.

[4] *FLOW-3D V11.0.4 User Manual*: Flow Science, Inc, 2015.

[5] Landry, B. J., Hancock, M. J., Mei, C. C., and García, M. H., "WaveAR: A software tool for calculating parameters for water waves with incident and reflected components," *Computers & Geosciences*, vol. 46, pp. 38-43, 2012.

APLICATION OF A MODIFIED WCSPH SCHEME IN SIMULATING WAVE-INDUCED MOTIONS OF A PILE-RESTRAINED FLOATING BREAKWATER

Ehsan Delavari[1], Ahmad Reza Mostafa Gharabaghi[2]

1) Faculty of Civil Engineering, Sahand University of Technlogy, Tabriz, Iran, e_delavari@sut.ac.ir
2) Faculty of Civil Engineering, Sahand University of Technlogy, Tabriz, Iran, mgharabaghi@sut.ac.ir

1. Introduction

Floating breakwater as a special type of breakwater is used predominantly for attenuation of the wave effects. Such a structure cannot dissipate the wave effects completely and therefore, the incident waves are partially transmitted, partially reflected, and partially dissipated. In addition, forces exerted by the propagating waves on the structure cause it to move. These motions can also influence the wave characteristics and affect the stability of the structure. To reduce the wave-induced motions, floating breakwaters are constrained by pile or cable/chain mooring systems.

In literature, there are several numerical studies on the performance of moored floating breakwaters. Most of the numerical methods applied for the investigation of the response of floating breakwaters are generally based on potential flow theory. This is due to the complexity of problems dealing with the wave-structure interaction. Solving these problems using potential theory based methods need some simplifying assumptions that may affect the accuracy of the results. Currently, some simple solver methods for Navier-Stokes' equations such as Smoothed Particle Hydrodynamic (SPH) scheme have been developed. As an example, Manenti and Ruol [1] studied the dynamic response of a pile-moored floating breakwater as a case study for fluid-structure interaction using the SPH method. They used a weakly-compressible SPH scheme for calculating the heave motion of the structure under regular wave action. However, in order to get better results, it needs further research. There are very limited studies performed on the behavior of pile-restrained floating breakwater using the SPH scheme.

In this paper, application of a modified SPH-based equation in simulating the motions of a pile-restrained floating breakwater under regular wave action is investigated.

2. Governing Equations

For simulation of a weakly-compressible, viscous fluid, the well-known Navier-Stokes equations were solved. These equations can be written in a Lagrangian form as:

$$\frac{d\rho}{dt} = -\rho\nabla\cdot\vec{u} \tag{1}$$

$$\frac{d\vec{u}}{dt} = -\frac{1}{\rho}\nabla p + \nu\nabla^2\vec{u} + \vec{g} \tag{2}$$

where $\vec{u}$ is the fluid velocity vector, ρ is the fluid density, p is the pressure, $\vec{g}$ is the body force vector and ν is the kinematic viscosity. For particle i, the discretized SPH form of the governing equations can be written, by exerting a summation on the neighboring particles j, as:

$$\frac{D\rho_i}{Dt} = \sum_{j=1}^{N} m_j\left(\vec{u}_i - \vec{u}_j\right)\cdot\nabla_i W_{ij} \tag{3}$$

$$\frac{D\vec{u}_i}{Dt} = -\sum_{j=1}^{N} m_j\left(\frac{p_i}{\rho_i^2} + \frac{p_j}{\rho_j^2} + R\left(f_{ij}\right)^4\right)\nabla_i W_{ij} + \nu\left(\nabla^2\vec{u}\right)_i + \vec{g}_i \tag{4}$$

Also:

$$\frac{D\vec{r}_i}{Dt} = \vec{u}_i \tag{5}$$

In these equations, m is the mass, $\vec{r}$ is the position vector, and W is a smoothing kernel function. In this paper, the cubic spline kernel was used as the kernel function [2]. Term $R(f_{ij})^4$ in equation (4) is the artificial pressure term introduced by Monaghan [3] to remove the tensile instability problem.

3. Wave-Structure Interaction

Linear and angular momentum equations are given in two-dimensional framework as:

$$M\frac{d\vec{V}_g}{dt} = M\vec{g} + \vec{F}_{fluid-body} \tag{6}$$

$$I_g\frac{d\Omega_g}{dt} = \vec{k}\cdot\vec{T}_{fluid-body} \tag{7}$$

where $\vec{V}_g$ and Ω_g are the velocity vector and the angular velocity of the center of gravity of the studied body, M and I_g are the mass and the moment of inertia of the body with respect to its center of gravity. $\vec{F}_{fluid-body}$ and $\vec{T}_{fluid-body}$ are the vectors of fluid-body hydrodynamic force and torque, respectively, and $\vec{k}$ is the unit vector normal to the xz-plane.

There are different methods for calculating the hydrodynamic forces while using SPH scheme. One of the most common methods is proposed by Monaghan and Kajtar [4]. In this paper, the modified Monaghan and Kajtar's equation which is proposed by the authors is used:

$$\vec{F}_i = \sum_b m_b\left[\sum_i\left(\vec{f}_{bi} - \nu\left(\nabla^2\vec{u}\right)_b\right)\right] \tag{8}$$

$$\vec{f}_{bi} = \frac{\alpha}{\beta} \frac{\vec{r}_{bi}}{\left(r_{bi} - \frac{dp}{\beta} \right)^2} K(r_{bi}/h) \frac{2m_i}{m_b + m_i} + (\vec{g} - \vec{a}_i) W_{bi} \frac{m_i}{\rho_i} \quad (9)$$

In these relations, subscript *i* and *b* are related to the fluid and solid particles, respectively, *dp* is the initial particle spacing, β is ratio of the solid particles' spacing to the fluid particles' spacing, $\vec{f}_{bi}$ is the force on solid particle *b* due to the fluid particle *i* and $K(r_{bi}/h)$ is a 1D kernel function. α is a constant and its value depends on the maximum velocity of fluid in the computational domain. Due to the differences in the velocities of the fluid in *x* and *z* directions in wave domain:

$$\alpha_x = \varphi \alpha_z \quad (10)$$

where φ is considered to be constant and $\varphi \geq 1$.

4. Results

4.1. Test Case 1

As first test case, according to the experimental work performed by Manenti and Ruol [1] on a pontoon-type pile-restrained floating breakwater, a regular wave propagating in a flume with 9 *m* in length, 0.8 *m* in height with a water depth of 0.52 *m* is simulated by a piston-type wave maker. At the far end of the wave flume a sponge layer [5] with a length equal to the incident wave length is placed. The height of the target wave is 0.05 *m* with a period of 0.87 *s*. A rectangular floating body with 0.24 *m* in length, 0.12 *m* in height, static equilibrium draught of 0.06 m, and an average density equal to 500 kg/m^3 is placed at a distance of 2 m from the wave maker. The breakwater has one degree of freedom and it can move only in the vertical direction (heave motion). Figure 1. shows the time history of the free surface elevation (η). In addition, a comparison of the numerical estimated heave motions with the experiments are presented in Figure 2.

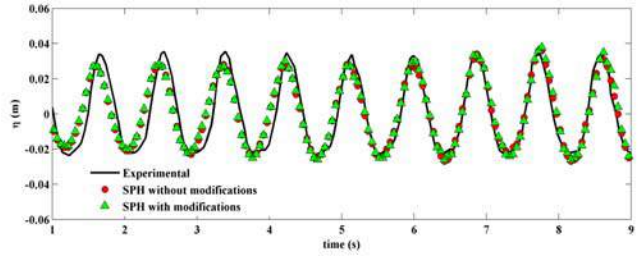

Figure 1. Time history of the free surface elevation

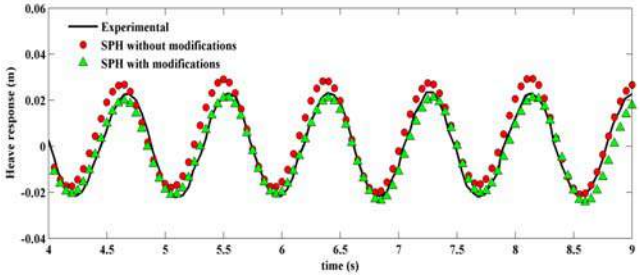

Figure 2. Time history of the heave motion of floating body

4.2. Test Case 2

As second test case, according to experiments performed by Tolba [6], a pontoon-type pile-restrained floating breakwater is simulated in a flume with a water depth (*d*) of 0.3 *m*. Width of the floating breakwater (*B*) is 0.15 *m*. Figure 3. shows regular wave-induced heave motions of the structure as H_h/H_i ratio (where H_h is magnitude of the height of heave motion) with respect to B/L and for $D/d = 1/4$ (*D* is draught of the structure).

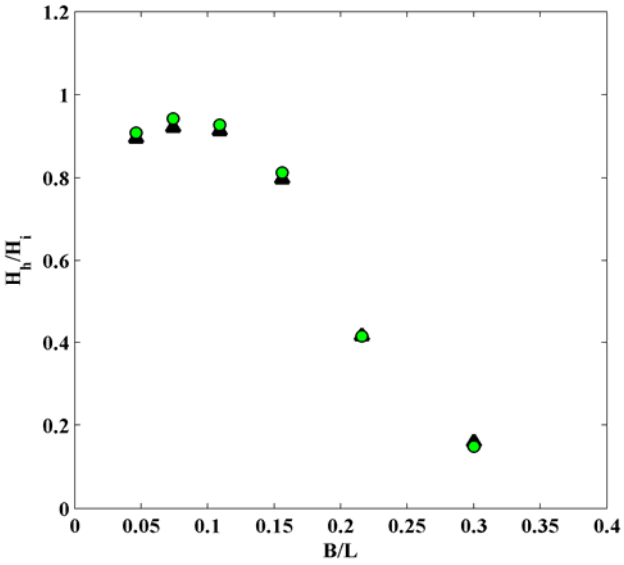

Figure 3. Variation of H_h/H_i against B/L.

5. Conclusion

In this paper, the equation proposed by Monaghan and Kajtar (2009) for fluid-solid interaction is modified and a numerical model is developed based on the Navier-Stokes equations using SPH scheme. In order to investigate the ability of developed model, the behavior of pile-moored floating breakwater is studied. The results show that the proposed modification has developed the accuracy of SPH scheme.

6. References

[1] Manenti, S., and Ruol, P., "Fluid-structure interaction in design of offshore wind turbines: SPH modeling of basic aspects", in *Proceedings of Handling Exceptions in Structural Engineering Conference, November 13-14 2008, Rome, Italy.*

[2] Monaghan, J. J., and Lattanzio, J. C., "A refined particle method for astrophysical problems", *Astronomy and Astrophysics*, 149, 1985, pp. 135-143.

[3] Monaghan, J. J., "SPH without a tensile instability", *Journal of Computational Physics*, 159, 2000, pp. 290-311.

[4] Monaghan, J. J., and Kajtar, J. B., "SPH particle boundary forces for arbitrary boundaries", *Computer Physics Communications*, 180, 2009, pp. 1811-1820.

[5] Delavari, E., and Gharabaghi, A. R., "A modified sponge layer boundary condition for a numerical wave flume based on the SPH scheme", in *Proceedings 11th International Conference on Coasts, Ports and Marine Structures (ICOPMAS), November 24-26 2014, Tehran, Iran.*

[6] Tolba, E. R. A. S., *Behaviour of floating breakwaters under wave action*, Suez Canal University, Panama, PhD Thesis, 1998.

NUMERICAL MODELLING OF SOLITARY WAVE LOADS ON COASTAL BRIDGES USING SPH

Mohammad Sarfaraz[1], Ali Pak[2]

1) Ph.D. Candidate, Civil Engineering Department, Sharif University of Technology, Iran, mohammad.sarfarz@gmail.con
2) Professor, Civil Engineering Department, Sharif University of Technology, Iran, pak@sharif.edu

1. Introduction

Recent tsunamis in Indonesia (2004), Samoa (2009), Chile (2010), and Japan (2011) have caused severe damages both on human lives and coastal structures [1]. In the 2011 Japan tsunami, more than 300 bridges were destroyed [2]. Current methods for estimating wave loads on coastal bridges ([1], [3] and [4]) are presented mainly for normal sinusoidal water waves. Currently, no formula is available for design of bridges that may be subjected to solitary waves [5].

In other words, structural design codes do not consider tsunami forces to these structures. The main goal of this paper is to investigate the tsunami wave loads on bridge superstructures by numerical simulation using the SPH method and proposing applied formulae to calculate forces impinged on these structures. To the authors' best knowledge, this is the first effort which implements the SPH scheme to study this problem.

2. Numerical Method

Appropriate simulation of highly nonlinear flow field of tsunami waves and their complex free surface around a structure is a difficult and challenging task. SPH has shown its ability to simulate these complex flows very well [6]. In SPH, continuum properties of the fluid are replaced with smoothed quantities at discrete Lagrangian locations.

The SPH method in this paper is based on weakly compressible formulation of the Navier-Stokes equations [7]:

$$\frac{d\rho_i}{dt} = -\sum_j m_j \left(\underline{u}_j - \underline{u}_i\right).\nabla_i W_{ij} \qquad (1)$$

$$\frac{d\underline{u}_i}{dt} = -\sum_j m_i \left(\frac{p_i}{\rho_i^2} + \frac{p_j}{\rho_j^2} + \Pi_{ij}\right)\nabla_i W_{ij} + \underline{g} \qquad (2)$$

where ρ is the particle density density, m is the particles mass, u is the particle velocity, $W$is the kernel function, p is the particle pressure, t is time, $\underline{g}$ is the gravity acceleration and π_{ij} stands for viscous effects, which damps out the instability caused by chaotic particle movements and also prevents particle interpenetration.

In this study a deck with two girders is used. Cross-section of the numerical flume and general layout of the domain are depicted in Figure 1.

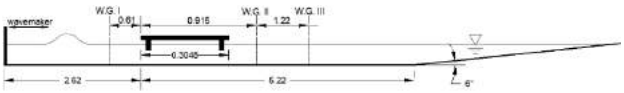

Figure 1. Layout of the numerical wave flume (in meters, not to scale)

Three water depths, three wave amplitudes and three deck elevations are used in the course of numerical simulations.

3. Verification of the Numerical Method

Experimental work of [8] is used to verify the numerical scheme. In that work, a fully submerged deck with six girders was used to study the tsunami loads with h=8.6 cm, a=0.3h and z=0.2h. Comparison between measured horizontal and vertical forces applied to this deck, and computed values by method of SPH is depicted in Figure 2. The SPH code computes the magnitudes for horizontal and vertical forces very well.

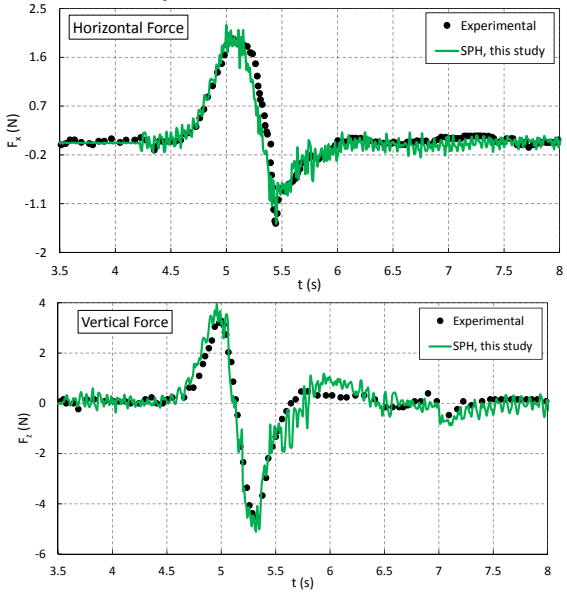

Figure 2. Comparison of measured horizontal and vertical forces with calculated values by methods of SPH

Figure 3 demonstrates the SPH-computed screen capture at the time of the maximum horizontal force applied to the bridge, together with horizontal velocity field. This figure shows that at this time, the solitary wave has reached the

leading edge of the bridge deck and the maximum velocity happens at this location.

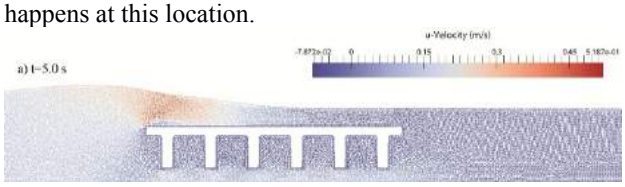

Figure 3. SPH capture of solitary wave impinging on the six girders bridge with horizontal velocity values

4. Results and Discussion

Based on the numerical results, a practical non-dimensional formula with R^2=0.99 to compute the positive horizontal force is proposed as (Figure 4):

$$\left(\frac{+\bar{F}_x}{P_a}\right)^{0.3}\left(\frac{a}{h}\right)(z_2)^3 = 0.3748(z_2)^{2.5}\left(\frac{a}{h}\right)^2 + 0.0004 \qquad (3)$$

where F_x is the horizontal force, a and h are wave amplitude and water depth, respectively. P_a is the atmospheric pressure (100 kPa) and z_2 is defined as:

$$z_2 = \frac{\max\{0, a-(z-t_G)\}}{h} \qquad (4)$$

where z is the distance between top of the deck and the mean water level and t_G is the girder height.

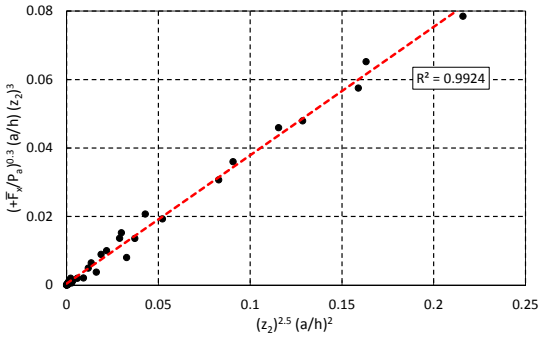

Figure 4. Proposed equation for computing the positive horizontal force applied to a deck with two girders due to a solitary wave

A practical non-dimensional formula with R^2=0.99 to calculate the uplift force is suggested as (Figure 5):

$$\left(\frac{+\bar{F}_z}{a.P_a}\right)^{0.1}\left(\frac{a}{h}\right)^2(z_2)^3 = 0.6212(z_2)^{2.5}\left(\frac{a}{h}\right)^2 - 0.0016 \qquad (5)$$

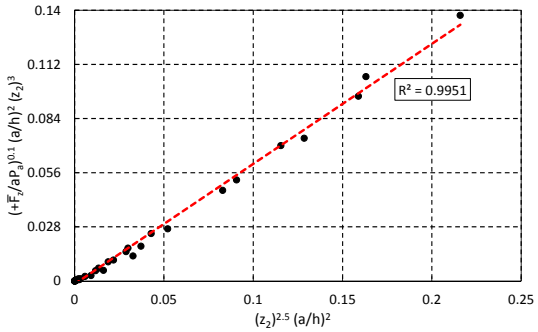

Figure 5. Proposed equation for computing the uplift force applied to a deck with two girders due to a solitary wave

For the bending moment applied to the bridge deck by the tsunami similar formula has been provided, that is presented elsewhere [9].

5. Conclusion

The Lagrangian meshfree method of Smoothed Particle Hydrodynamics (SPH) is used to simulate the solitary wave interaction with superstructures of coastal bridges. The method showed good level of accuracy for predicting the free surface elevation and induced loads on the structures.

Simple non-dimensional formulae were proposed to calculate the maximum horizontal and vertical forces and maximum clockwise and counterclockwise moments applied to deck with two girders due to a solitary wave.

6. References

1 Douglass SL, Chen Q, Olsen,JM, Edge BL, Brown D. Wave forces on Bridge Decks. Office of Bridge Technology, Washington, DC: Technical report, U.S. Department of Transportation; 2006.

2 Wei Z, Dalrymple RA, Hérault A, Bilotta G, Rustico E, Yeh H. SPH Modeling of Dynamic Impact of Tsunami Bore on Bridge Piers. Coastal Engineering. 2015;104:26-42.

3 AASHTO. Guide Specifications for Bridges Vulnerable to Coastal Storms. American Association of State Highway and Transportation Officials; 2008.

4 McPherson RL. Hurricane Induced Wave and Surge Forces on Bridge Decks. M.Sc. Thesis, Texas A&M University; 2008.

5 Hayatdavoodi M, Ertekin RC, Robertson IN, Riggs HR. Vulnerability assessment of Coastal Bridges on Oahu Impacted by Storm Surge and Waves. Natural Hazards. 2015;79:1133-1157.

6 Shao SD, Gotoh H. Turbulence particle Models for Tracking Free Surfaces. Journal of Hydraulic Research. 2005;43(3):276-289.

7 Violeau D, Rogers BD. Smoothed Particle Hydrodynamics (SPH) for Free-Surface Flows: Past, Present and Future. Journal of Hydaulic Research. 2016;54(1):1-26.

8 Hayatdavoodi M, Seiffert B, Ertekin RC. Experiments and Computations of Solitary-Wave Forces on a Coastal-Bridge Deck. Part II: Deck with Girders. Coastal Engineering. 2014;88:210-228.

9 Pak A, Sarfaraz M. SPH Numerical Simulation of Tsunami Wave Forces Impinged on Bridge Superstructures. Submitted to Coastal Engineering.

SPH MODELING OF HEAVE MOTION RESPONSE OF FLOATING BREAKWATER

Kaveh Soleimani[1], Mohammad Javad Ketabdari[2]

1) PhD student, Faculty of Marine Technology, Amirkabir University of Technology, Tehran, Iran, kv.soleimani@aut.ac.ir
2) Associate professor, Faculty of Marine Technology, Amirkabir University of Technology, Tehran, Iran, ketabdar@aut.ac.ir

1. Introduction

The interaction of sea waves and floating bodies is one of the most pioneering fields of study in marine technology. Floating breakwater (FB) is one of the most utilized types of these structures which can be also used in the conditions rather than shallow water, insufficient sea beds and high sedimentation rates in typical wave climates where there is no need to full protection.

In this article, the heave motion response of a single degree of freedom FB was studied. To describe the momentum equation, the laminar viscous stress model and to overcome the pressure oscillation of WCSPH method, the Shepard density filter was used. Also, three different weighting functions including Gaussian, Cubic Spline and Quintic (wendland) were compared. Validation of the results was made by comparison of the obtained data to experimental and numerical work of Ruol and Martinelli [1]. The results demonstrated that the Cubic Spline and Quintic weighting functions are more appropriate to the problem of the interaction of waves with the considered structure. The velocity field near the FB showed that the velocity of water particles is maximum near the sharp edges of the body.

2. Formulation

The SPH method is based on the integral interpolation theory, so that by the use of an interpolation function, the differential equations are converted to integral equations and instead of physical properties, the local derivatives are act on the interpolation function which is an analytical function. So, in SPH method, each function A(r) is estimated by equation (1).

$$A(r) = \int A(r')W(r-r',h)dr' \tag{1}$$

where $W(r-r',h)$ is the weighting function and h is called the smoothing length. The performance of the SPH model is critically dependent on the choice of the weighting functions, since it determines that how the variables are interpolated. The next step, is the approximation of the function *A* from the integral form to the discrete form so that

$$A(r) = \sum_b m_b \frac{A_b}{\rho_b} W_{ab} \tag{2}$$

where the mass and density are denoted by m and ρ, respectively. W_{ab} is the weighting function or kernel.

In this research, three different kernel functions were used:

Gaussian weighting function

$$W(r,h) = \alpha_D \exp(-q^2) \tag{3}$$

Cubic Spline Weighting Function

$$W(r,h) = \alpha_D \begin{cases} 1-\frac{3}{2}q^2+\frac{3}{4}q^3 & 0 \le q \le 1 \\ \frac{1}{4}(2-q)^3 & 1 \le q \le 2 \\ 0 & q \ge 2 \end{cases} \tag{4}$$

Quintic (Wendland)

$$W(r,h) = \alpha_D (1-\frac{q}{2})^4 (2q+1) \quad 0 \le q \le 2 \tag{5}$$

where $\alpha_D = 1/\pi h^2$, $\alpha_D = 10/7\pi h^2$, $\alpha_D = 7/4\pi h^2$ in Gaussian, Cubic Spline and Quintic kernels, respectively [2].

3. Boundary Condition

In the solid boundaries, the Monaghan boundary condition was used to ensure that a water particle could never cross the boundary. In this case, analogous to inter-molecular forces, the particles that constitute the boundary exert central forces on the fluid particles [3].

4. Modeling

To simulate the interaction of wave with the FB, a 2D model was used. The breakwater with a length of 0.24m, a height of 0.12m and a draft of 0.06m was located at a distance of 2 m from the wave maker. A sketch of the experimental setup is shown in figure1. The wave height and period were 0.05 m and 0.87 s, respectively and was propagated in a water of 1.17 m depth. Since this wave was propagated in deep water, the flap type wave maker was used for wave generation. The relation of wave height to the displacement of the wave maker is as [4]:

$$\frac{H}{S} = 4\left(\frac{\sinh kh}{kh}\right)\frac{kh\sinh kh - \cosh kh + 1}{\sinh 2kh + 2kh} \qquad (6)$$

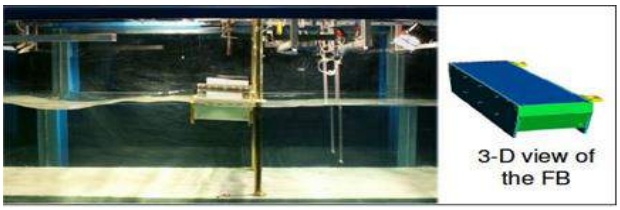

Figure 1. Experimental setup.

To set up the model, 216000 particles with a distance of 0.004m in each direction were used. To describe the momentum equation, laminar viscous stress model and to overcome the pressure oscillation, the Shepard density filter was used. The results were compared with experimental and numerical studies of Ruol and Martinelli [1] which is based on the application of artificial viscosity (Standard model). Generated wave and the displacement and the velocity of the floating body are presented in figures 2-4.

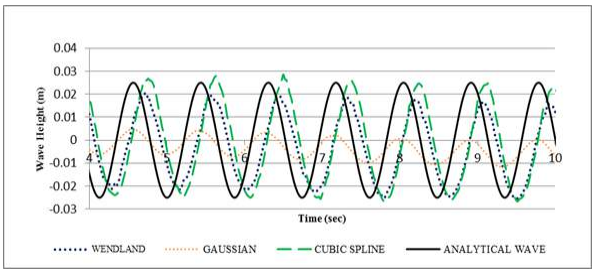

Figure 2. Comparison of wave time histories for different kernels.

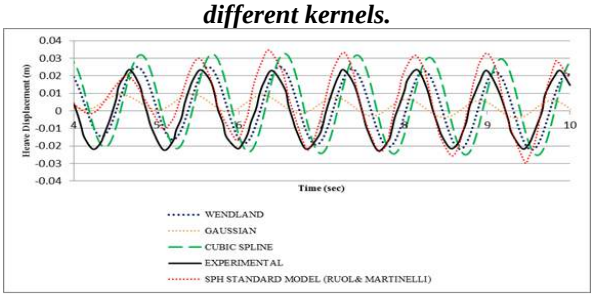

Figure 3. Comparison of heave time histories for different kernels with experimentaldata and SPH standar model.

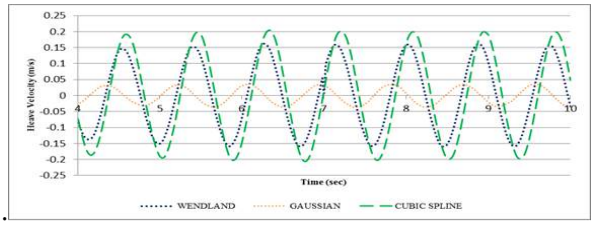

Figure 4. Comparison of heave velocity time histories for different kernels.

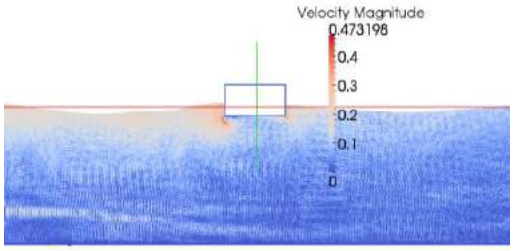

Figure 5. Velocity field around the floating body.

As it is evident from figures 2 and 3, the best results were obtained from Cubic Spline and Wendland kernels, respectively. It should be noted that there is a phase difference between analytical and numerical waves which is due to the wave maker effects. However the values of wave profile and heave displacement amplitudes were almost the same as the analytical and experimental results, respectively. Another point is that the total displacement of the body was about 5 cm which was within the range of wave height.

As it is evident in figure 5 the maximum velocity of water particles occurs near the sharp edges of the floating body with a value of 0.473 m/s which is more than twice of the maximum heave velocity of the floating object. It is expected that for body with round edges, lower maximum water velocities occur. Also, as it is expected, the velocity of water particles has higher amounts at free surface with its maximum at wave crest.

5. Conclusion

In this study, a 2D smoothed particle hydrodynamics code was used to simulate the interaction of a linear wave with a FB. To investigate the effect of the weighting function, three different kernel functions including Gaussian, Cubic Spline and Quintic (Wendland) were used. The results show that the Cubic Spline and Quintic kernel are more eligible to simulate this problem. Also, with sharp edges, the floating body will face higher wave velocities.

6. References

[1] Ruol, P., and Martinelli, L., "Wave flume investigation on different mooring systems for floating breakwaters", *in Proceeding of Coastal Structures Conference*, Venice, Italy, 2007.

[2] Liu, G.R., and Liu, M.B., *Smoothed Particle Hydrodynamics a meshfree method*, World Scientific Publishing Co, 2003.

[3] Gomez-Gesteira, M., Rogers,B.D., Crespo, A.J.C., Dalrymple, R.A., and Narayaswamy, M., "SPHysics – development of a free-surface fluid solver – Part1: Theory",*Computers and Geosciences*, 48, 2012, pp. 289-299.

[4] Dean, R.G., and Dalrymple, R.A., *Water Wave Mechanics for Engineers and Scientists*, World Scientific Publishing Co, 2000.

NUMERICAL AND EXPERIMENTAL STUDY OF SUBMERGED BREAKWATER EFFECT ON WAVE RUN-UP ON STEEP SLOPED SEAWALLS

Naser Abasi[1], Mohammad Ali Lotfollahi Yaghin[2], Morteza Mohamadi Hasan Kiade[3] and Alireza Mojtahedi[4]

1) Phd student of marine structures engineering, Hormozgan University, Bandar Abbas, Iran, n.abasi.phd@hormozgan.ac.ir
2) Professor of marine structures engineering, University of Tabriz, Tabriz, Iran, lotfollahi@tabrizu.ac.ir
3) MSc of marine structures engineering, Tabriz, Iran, m_mohamadi89@ms.tabrizu.ac.ir
4) Assistant professor of marine structures engineering, University of Tabriz, Tabriz, Iran, Mojtahedi@tabrizu.ac.ir

1. Introduction

As a wave breaks, a portion of the remaining energy generates a force that runs up the water on a beach or sloped shore structure. Wave run-up is characterized as the maximum vertical extent of wave uprush above the still water level [1]. In designing maritime structures, hydraulic parameters, such as wave run-up, dictate the geometry and, in particular, elevation of the structure above sea level.

The crest height of most sea dikes in the Netherlands is designed based on a 2% exceedance level of the expected run-up, suggesting a 2% overtopping. Breakwaters and offshore rubble- mound structures are, however, typically designed for more than 2% overtopping. In such cases, allowable overtopping ranges from 5% to 40% of the waves reaching the crest [2].With the water level on the rise, the calculations performed for structures designed for the expected elevation are no longer functional. This causes the run-up to exceed the allowable range, which results in human and financial toll.

An effective strategy for reducing wave run-up height as well as pressure forces on structures concerns constructing sea-facing offshore structures. Over the past decades, few studies have addressed the issue [3]. Drawing on the study of Battjes in 1974, irregular wave run-up on impermeable slopes is described as Equation 1 as follows:

$$Rui\%/H = (A\xi_{op} + C)\ \gamma_f\ \gamma_b\ \gamma_k\ \gamma_\beta \qquad (1)$$

In 1968, van Oorschot and d'Angremond conducted a series of experiments on irregular long crested waves for slopes of 1:4 and 1:6 with $\xi op < 1.2$. In a similar vein, Ahrens (1981) performed studies for slopes of 1:1 and 1:4 with $\xi op > 1.2$. The cited results of these studies for 2% run-up are plotted in Figure 1. Recommended by the US Army Coastal Engineering Manual, the corresponding run-up formulas for smooth, impermeable slopes are shown in Figure 1 [4].

Figure 1. Results of 2% wave run-up on smooth, impermeable slopes [5]

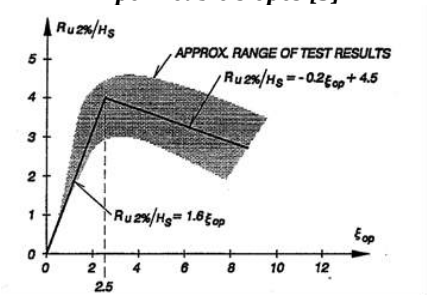

As shown in Figure 1, the data are widely scattered. Given that the data are generated for 100 to 200 waves with $\xi op > 1.2$, such dispersion was highly probable.

Through a laboratory experiment, Neelamani and Muni Reddy (2003) employed an offshore breakwater in front of a vertical seawall, assessing wave force and run-up reduction on seawall [5].

A substantial difference between the experiments conducted by researchers outlined above and the experiments described in this study is that in the former regular waves have been used. To closely simulate the sea conditions, the present study has taken advantage of irregular waves.

2. Experimental Procedures and Numerical Model Setup

To provide the sea conditions for the scale physical models, experiments were carried out in a hydraulic wave flume at the Sea Engineering Laboratory, University of Tabriz, Iran. The wave flume has 14m length and 1.2m wide and a paddle type wave maker. A steal seawall of 1.18×1.2 m and 0.005 m in thickness was used in this study. The submerged breakwater was 0.3m high, with a crest width of 0.16 m and a slope of 2:3, consisting of a 0.19 m high impermeable core and a 0.11 m thick armor layer.

The waves were produced in the flume by the wave generation system according to a JONSWAP spectrum. Geometric properties of the submerged breakwater are shown in Figure 2.

Figure 2. Geometric properties of the submerged breakwater and its distance from the seawall

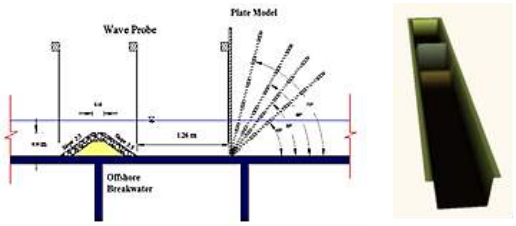

The Mike 21 software package were used for setup numerical model in this study.

3. Verifying the results

In the condition without offshore breakwater, wave run-up on smooth, impermeable slopes is calculated through Equation 1. Thus, the equation was used to estimate wave run-up and to verify the results provided by the experiments. As mentioned before, the data generated by the experiments were recorded as time series. The time series were coded in the MATLAB software using the zero-upcrossing method, yielding a 2% wave run-up. Dividing the 2% run- up by the wave height resulted in the relative wave run-up that is a dimensionless quantity. Finally, a comparison was drawn between the relative run-up yielded by Equation 1 and the experimental results reported by Ahrens (1981). Results of the comparison are illustrated in Figure 4.

Figure 4. Comparison between the results of experiments conducted in this study and those of Ahren's (1981)

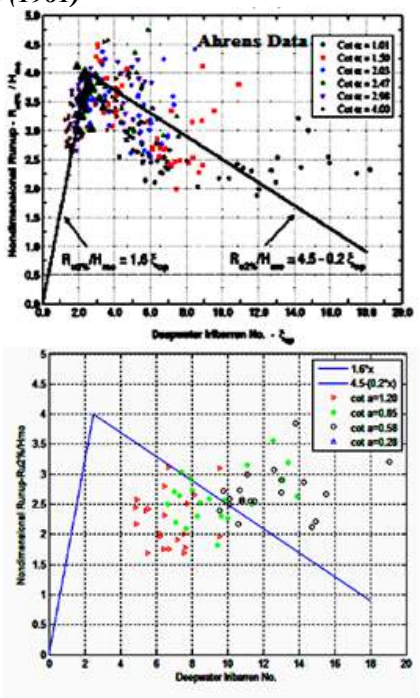

Given the results of the comparison and considering the fact that, due to steeper slopes used in this study, the experiments' data fall in the range of $\xi > 5$, it can be concluded that, within the scope of the study, the data acquired from the experiments at the University of Tabriz are fairly consistent with those reported by Ahrens (1981). It bears noting that the range $\xi > 5$ corresponds to very gentle slopes like beach slopes.

In some data with identical Iribarren numbers, the relative run-up values obtained in this study were slightly lower than those calculated by Ahrens.

This suggests that the steepness of the waves produced by the wave generator at the University of Tabriz is slightly higher than that of waves generated in Ahrens' study. Therefore, it is safe to say that the results of the experiments performed in the present study are valid for estimating the effect of offshore breakwater on wave run-up on a sloping wall.

4. Results

The results produced by the experiments bear witness to the fact that the use of an offshore breakwater in front of sloping walls contributes to a substantial decrease in wave run-up heights. Investigating the laboratory data suggested that the in the presence of offshore breakwater the degree to which wave run-up decreases is dictated by the wave steepness parameter (H/L). Laboratory observations showed that for waves that break on the offshore breakwater, decrease in the wave run-up heights is nearly 20% greater than the condition where waves passes over the breakwater without breaking.

The results further indicated that the effect of the relative height of the offshore breakwater (h/d) on decreasing wave run-up height is significantly reduced after wave breaking.

5. References

[1] Sorensen, R.M., "Basic Coastal Engineering", Chapman and Hall, 1997.

[2] Jentsje W. van der Meer, Cor-Jan M. Stam " Wave run up on smooth and rock slopes of costal structure " , 1992.

[3] Seung Hyun Park, Seung Oh Lee, Tae-Hwa Jung, and Yong-Sik Cho "Effects of Submerged Structure on Rubble-mound Breakwater: Experimental Study" KSCE Journal of Civil Engineering, Vol.11, No.6, 2007.

[4] Hughes S. A.," Estimating Irregular Wave run-up on smooth, impermeable slopes", U.S. Army corps of engineers Washington, ERDC/CHL CHETN-III-68, 2003.

[5] Neelamani, S., MuniReddy, M. G., "Wave Force and run-up reduction on structures defenced by an offshore breakwater", COPDEC VI 2003, Colombo, Sri Lanka, 2003.

A STUDY ON THE PERFORMANCE OF MARINE BRIDGES ON SUPPORTED PILE FOUNDATION UNDER EARTHQUAKE LOAD

Seyed Ehsan Vakili [1], Gholam Reza Nouri[2] and Seyed Amin Vakili[3]

1) Kharazmi University, Tehran, IRAN, std_seyedehsanvakili@khu.ac.ir
2)Civil Engineering Department, Kharazmi University, Tehran, IRAN, r.nouri@khu.ac.ir
3)Mashhad Ferdowsi University ,Mashhad, IRAN , aminvakili@stu.um.ac.ir

1.INTRODUCTION

Earthquake is one of the most destructive phenomena in nature. The country of Iran is located on the high risk zone of world earthquake chain resulting to serious dilemma in every few years. The number of serious earthquakes in coastal area of our country in last few years has been considerable Inclined pile performance against lateral loading is much better than vertical ones. However their design and construction are difficult. Therefore the vertical marine piles are more common structural elements to handle and conduct different environmental loadings through deep sea bed level where the soil provides enough strength as a safe foundation. In this study the nonlinear behavior of vertical marine piles under earthquakes has been investigated, structure and soil has been modeled using Plaxis Software. The soil characteristics such as $E, C, f, g, \ldots$ was obtained by in-situ field study in coastal area of Bandarabbas. Running model for a critical condition of lateral and vertical Dynamic loading for a set of sample marine piles time history of pile displacement was obtained. The decreasing rate of shear stress coefficient respect to bed depth was graphically presented. The results showed promising for optimum and reliable pile design offshore structures .[1]

2.THEORETICAL BACKGRUND

Soil-columns interaction analysis can be performed in following ways:

Method based on maximum lateral soil pressure
Method of bed reaction (vinkler Method)
Method of continuous medium
Finite element method

In first method the ultimate values can be obtained. Hansen (1970) employed this method to obtain the maximum moment as[1]:

$$\sum M = \sum_{z=o}^{z=x} P_z \frac{L}{n}(e+z)B - \sum_{z=x}^{z=l} P_z \frac{L}{n}(c+z)B \qquad (1)$$

$$H_u(e+x) = \int_o^x P_z \frac{L}{n} B(x-z) + \int_x^{x+L} P_z \frac{L}{n} + B(z-x)$$

Fig 1 to 3 show the soil reaction , shear diagram and moment diagram for a typical soil-columns interaction. The method of bed reaction known also as Vinkler Method is a suitable method for soil simulation. This method is able to consider the nonlinearities of soil and radiation damping. According to Vinkler (1876) soil is modeled by a series of separate elastic spring. For a continuous beam on elastic bed the governing equation can be expressed as [2]:

$$\frac{d}{dz^2}(E_p I_p \frac{d^2y}{dz^2}) + \frac{d}{dz}(N_{(2)} \frac{dy}{dz}) - P_{(z-y)} = 0 \qquad (2)$$

In continuous medium method green function which is the base of all boundary integral and boundary element methods is used to determine the displacement due to external loading. The equilibrium of vertical forces acting on the elementary columns segment of fig.4 is written as:

$$\frac{\partial p}{\partial z} + m\frac{\partial^2 U_p}{\partial t^2} + (k + iw\zeta)(U_p - U_{ff}) = 0 \qquad (3)$$

Finite element method is a powerful tool for analyzing soil-columns interaction. In this method volume of soil is divided into separate elements.

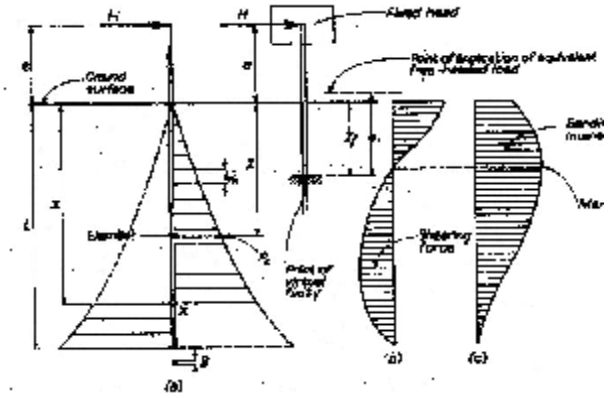

Figure1: Hansen Theory (1961)

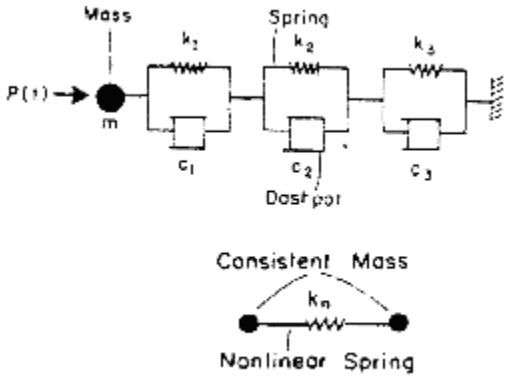

Figure 2 : Nogami & konagi Model (1998)

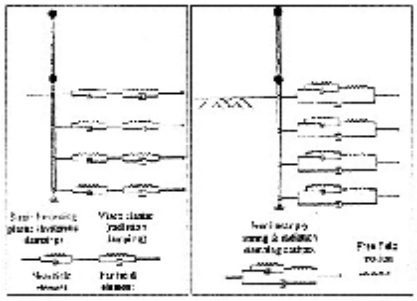

Figure3 : Wang Model (1998)

3.SIMULATION OF NONLINEAR DYNAMIC OF SOIL BEHAVIOUR

One of the difficulties in simulation of pile and soil interaction is separation of pile and soil due to force transmission. In this study Rinterface = 0.6 element was used to model the soil in this complicated interaction. It was assumed that the soil behavior in small deformation domain is elastic- perfect plastic and behavior of concrete material assumed to be linear elastic [2]. Therefore for soil yielding the modified Coulomb criteria was used. Concrete pile was modeled using triangular, 15 node elementsThe results revealed that the parameters of dominant soil layers of the study area are as follow[3]

Layer 1 (Depth=3m):

$E = 12000(kN/m^2)$ $\quad f = 29(deg)$

$g_w = 18.5(kN/m^3)$ $\quad n = 0.3$

$g_d = 15(kN/m^3)$ $\quad C = 0$

Layer 2 (Depth=3m):

$E = 12500(kN/m^2)$ $\quad f = 30(deg)$

$g_w = 17.7(kN/m^3)$ $\quad n = 0.3$

$g_d = 15.2(kN/m^3)$ $\quad C = 0$

Layer 3 (Depth=3m):

$E = 13000(kN/m^2)$ $\quad f = 31(deg)$

$g_w = 17.1(kN/m^3)$ $\quad n = 0.3$

$g_d = 15.8(kN/m^3)$ $\quad C = 0$

Layer 4 (Depth=3m):

$E = 15000(kN/m^2)$ $\quad f = 24(deg)$

$g_w = 16.8(kN/m^3)$ $\quad n = .35$

$g_d = 15.5(kN/m^3)$ $\quad C = 1(KN/m^2)$

4.MODELED PILE PARAMETERS

A typical pile with a diameter of D=1m, lengths of L=20m and 30m, $g = 24kN/m^3$ and $E = 2.1' 10^6 kN/m^2$, $n = 0.2$.

5.LOADING

A dead load of 100 KN applied at top of the pile. For earthquake exiting force the Colorado accelerograph with amax =0.35g

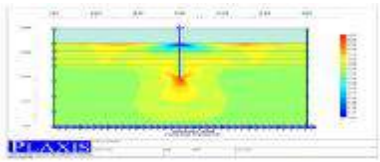

Figure 1: Mesh generated to model soil-columns interaction

6. RESULT

Fig.4 (Comparison of vertical displacement) and Fig.5 (Comparison of lateral displacement) of top two piles with different lengths shows that a decrease of 33% in pile length resulted to an increase in lateral displacement of 19% and vertical displacement of 16%. That the meeting of marine structures under vertical components of earthquake force is proposed in the regulations designed to Iran's Ports and Marine Structures (Publication No. 300-1) Vbnd 11-2-1 - A, the effect of vertical component of earthquake loading is considered.

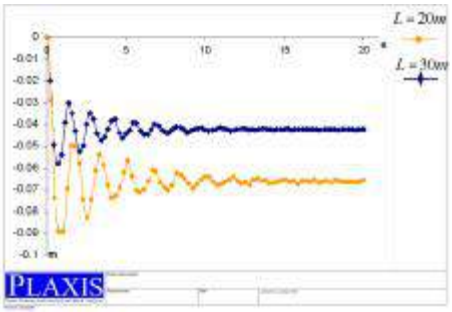

Figure 4: Comparison of Vertical pile Displacement with lengths L=20m and 30m

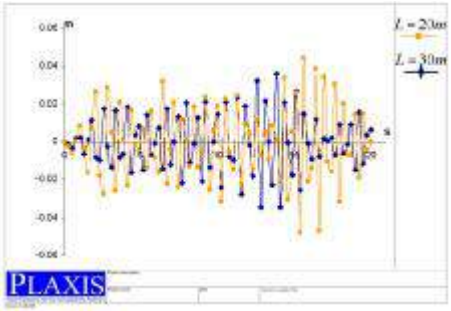

Figure 5: Comparison of lateral pile Displacement with lengths L=20m and 30m

7.REFERENCES

[1]-Melinakis, N. , Gazetas, G.,(2002). "Kinematic pile response to vertical p-wave seismic excitation" 10.1061/(ASCE)1090-0241, 128:10(860)

[2]-Nogami,T., Konagi, k, (1988)."Time domain flexural response of dynamically loaded single pile"; j.Eng. Mechanics. ASCE,114(9).pp. 1512-1525

[3]-S.A.Ashford,T.juirnarongrit,"Evluation of pile dimeter effect on initial modulus of sub grade reaction",j.ofGeotechnical and Geoenvironmental Engng,2003

[4]-Qi, M., Li, J., and Chen, Q. (2016). "Comparison of existing equations for local scour at bridge piers: parameter influence and validation." Natural Hazards, 10.1007/s11069-016-2287-z, 2089-2105.Online publication date: 1-Jul-2016. CrossRef

[5]-Crouzy, B., Bärenbold, F., D'Odorico, P., and Perona, P. (2016). "Ecomorphodynamic approaches to river anabranching patterns." Advances in Water Resources, 10.1016/j.advwatres.2015.07.011, 156-165. Online publication date: 1-Jul-2016.CrossRef

NUMERICAL ANALYSIS OF DEFORMED STIFFENNED CORRODED PLATES BEHAVIOR WITH REGARD TO USE AS THE GATE OF DRY DOCKS

Mohammad Amin Kalantari[1], Mohammad Reza Khedmati[2], Elham Mina[3]

1) M.Sc. in Coastal Engineering, Amirkabir University of Technology, Tehran, Iran, kalantari@aut.ac.ir
2) Marine Technology Department, Amirkabir University of Technology, Tehran, Iran, khedmati@aut.ac.ir
3) PHD in Hydraulic Structures, Tarbiat Modarres University, Tehran, Iran, E.mina@modares.ac.ir

1. Introduction

In this research, the deformation and behavior of stiffened steel plates are investigated benefitting numerical simulation, where the plates are subject to be utilized as the gate of dry docks. In this approach, the analyzed plates are suffering from corrosion on the surface towards to sea water. Aforementioned structure is analyzed under out of plane loads, specifically, hydrostatic and wave loads. A series of finite element analysis is performed on the dry dock gate in both uncorroded and corroded states. The effects of corrosion are introduced into the finite element models using a specially developed computer aided code utilizing Ansys APDL. The effects of different surface corrosion percentages on the plate strength characteristics and its pertinent influences on whole structure characteristics are evaluated. Hence, the main objectives of this research could be included: to find an appropriate method for optimized simulation of the behavior of stiffened corroded plates used in dry dock gates by application of finite element analysis utilizing shell elements by proper boundary condition exerting; and to investigate corrosion effects on the deformation and stress redistribution of plane elements under out of plane compression.

2. Methodology

Newton-Raphson method that is proper to solve nonlinear equations has been applied in this research [1]. In order to achieve the study goals, finite element model created primarily utilizing shell elements that enables to assess analytical model of corroded plates. Corrosion effects were imported to the finite element model benefitting random corrosion distribution, then subsequent influences on deformation and behavior of stiffened plates were investigated. Corrosion were simulated on cylindrically shaped pits [2]. The gate, itself, supposed to be single shell flap gate with overall dimensions of 25m×6.1m. Single shell gates, actually consists of a steel plate that has a series of longitudinal and transversal stiffeners on one side [3]. The various types of gates can be made based on operational circumstances such as terms of opening and closure. In this research, Flap gate as one of regular types of dry dock gate [4], has been considered to be analyzed for assessment of mechanical characteristics. Relevant properties for DH grade steel were applied in software. Modeling of the gate was performed in four different states including uncorroded condition and the geometries that experience DOP of 10%, 20% and 30% respectively, called G0, G3, G6, and G9.

Analysis of the mentioned states were accomplished applying summation of dead load of the gate weight, hydrostatic and dynamic pressures on the plate surface. The height of waves assumed to be 1.15 m in calculation of dynamic loads [5]. The subject loads were applied on the gate surface gradually and examined severally on various heights corresponding to longitudinal stiffeners level. Considering the supporting circumstances in flap gates, for the sake of applying boundary conditions in Ansys software, all degrees of freedom were restricted in bottom and lateral sides of the gate concrete supports. Besides, the flap gates are generally laid on concrete supports laterally in whole sides but the top edge that shall exclusively be free of bonding. Furthermore, frictional surface for contact of concrete and steel were supposed with friction factor equal to 0.3 (see figure 1). The described models were assessed in 12 state of loading, means that 48 various conditions were investigated to gain the most applicable optimization and economization in design of the gate of dry docks, deteriorating from corrosion. Application of proper boundary conditions caused approaching of the most accurate analytical results.

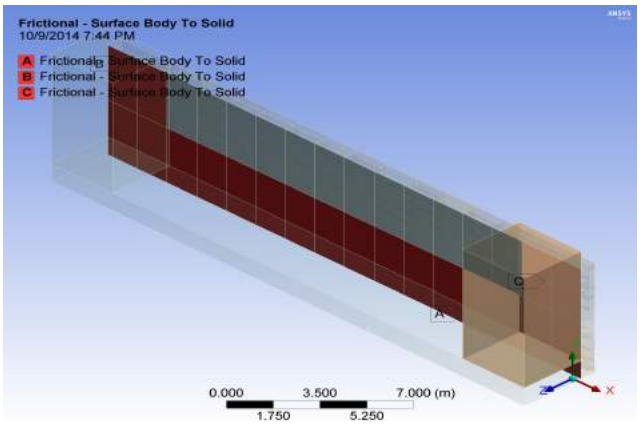

Figure 1. Frictional contact condition of the dry-dock gate.

3. Analysis

3.1. Deformation of the dry dock gate

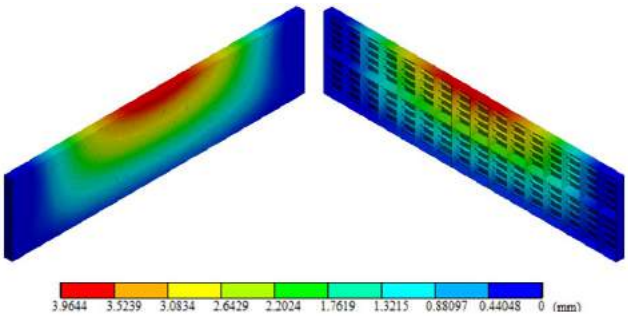

Figure 2. Deformation of the gate for G9 model (DOP=30%, t=9 years, RDP=3.33~125).

3.2. Von-Mises stress distribution on gate elements

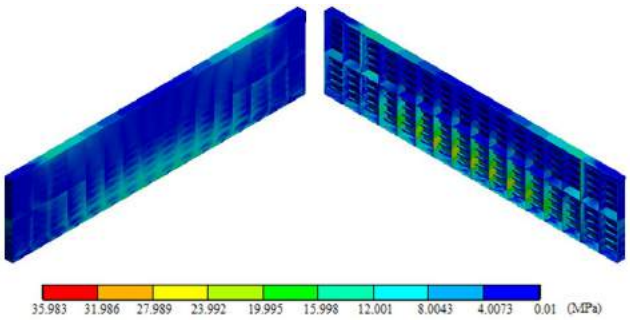

Figure 3. Von-Mises stress distribution of the gate for G0 model (DOP=0%, t=0 year).

3.3. Effects of corrosion growth on structural characteristics of the gate.

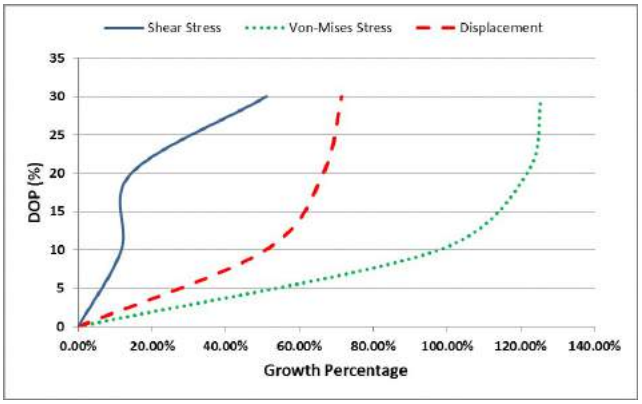

Figure 4. Growth percentage of displacement, shear and Von-Mises stress with DOP.

4. Conclusions

Analytical investigation of the subject study confirms that increased deformations and stresses are observed by alteration of sea level from MSL to MHHW, HHW, and HAT respectively. Whereas, the maximized stresses occur in HHW for waves having maximum height of 1.15 m.

Increasing of the depth and diameter of pitting corrosion, then relative DOP, will conversely effect reduction of the ultimate strength and overall structural capacity, although directly cause on growth of bearing strain and stress. Generally, initiation of corrosion effects on respective increasing of maximum strain and Von-Mises stress in geometries having 10%, 20% and 30% corrosion in comparison with uncorroded model, though initial influence could be caused much sudden increment of the mentioned parameters. Howsoever, maximum stress has been experienced by traversal stiffeners of the gate, in milder level and lower. Free edge of the gate could be considered as the critically distributed stress zone. Where, the transversal stiffeners is connected to the shell plate, could be suitably known as the place of both shear and Von-Mises stresses that achieve its ascending and maximized values. Adversely, aforesaid stresses will be descending in between of transversal stiffeners. Maximum stress occurs where the hydrostatic pressure is maximum. The growth of corrosion surface has maximum influence on variations of Von-Mises stress, strain, and shear stress respectively. Additionally, analysis prove that corrosion and deformation has non-linear relation.

Corrosion is considerably effective on pertinent stresses of the model, emphasizing that the increased percentage of corrosion will cause on growth of incurred stresses, which may negatively effect on safety and stability of the whole structure, and direct to deterioration and demolition. Moreover, ageing of the structure of the gate will conversely and non-linearly effects on related strength properties and mechanical characteristics, specifically, thickness of the main plate will be decreased.

All conclusions concentrate that, thickness loss of the plate by ageing in its lifetime could be properly compensated in design phase of the gate, both in terms of optimization and economization by application of this research findings.

5. References

[1] ANSYS 12.0.1 Reference Manual, ANSYS Inc.

[2] Paik, J.K., Lee, J.M., Ko, M.J., "Ultimate Compressive Strength of Plate Elements with Pit Corrosion Wastage", *Journal of Eng. for Maritime Environment*, 217(M4), pp. 185-200, 2003.

[3] Khedmati, M.R., Bayatfar, A., Rigo, P., "Post-Buckling Behavior and Strength of Multi-Stiffened Aluminum Panels under Combined Axial Compression and Lateral Pressure", *Marine Structures*, Vol. 23, Issue 1, pp. 39-66, 2010.

[4] Heger, R., "DockMaster's Training Manual", *Heger Dry Dock Inc.*, 2005.

[5] Dean, R.G., Dalrymple, R.A., "Water Wave Mechanics for Engineers and Scientists (Advanced Series on Ocean Engineering)", *World Scientific Publishing Co., 1991.*

GEOMETRY AND POSITION OPTIMIZATION OF BREAKWATERS UNDER WAVE FORCING USING GENETIC ALGORITHM

M. Jahangard[1], K. Hejazi[2]

1) MSc Student, K. N. Toosi University of Technology, Tehran, Iran, m.jahangard@kntu.ac.ir
2) Assistant Professor, K. N. Toosi University of Technology, Tehran, Iran, hejazik@kntu.ac.ir

1. INTRODUCTION

The layout of breakwaters, shape and location, is usually designed by assessing several concepts based on the designer engineer experience. The design has not been addressed as a hydrodynamic analysis problem to obtain a solution. This may be due to the difficulty of the hydrodynamic analysis and evaluation of such marine structures regarding their arbitrarily shapes [1].

The purpose of this study is to a achieve an efficient design strategy for the planform of the breakwaters , as such by minimizing the wave heights, comfort and safety are achieved in the coastal zones and harbor access canals. To aim this, a genetic algorithm is developed which incorporates with the REF/DIF numerical model to optimize the geometry and location of breakwaters where the wave height is minimized.

2. OPTIMIZATION PROBLEM

The optimization problem is assumed to be a finite dimensional constrained minimization problem, which symbolically may be considered to find a design variable vector $x \in R$, to minimize the cost function $f(x)$, subject to the m constraints $g_i \leq 0$. A series of x parameters form a new construction, and then upon simulation of hydrodynamic model, the height of the wave is estimated in the harbor according to the planform geometry of the breakwater, which is considered as the objective function.

2.1. PARAMETERIZATION OF THE STRUCTURE

The choice of control parameters is very important for the quality of the optimization. A suitable control space should be defined and the constraints need to be correctly accounted to reach an optimal realistic structure[2]. It is assumed that no definite shape is preferred. The structure is parameterized by 9 points. Each of the points could move within a certain area and therefore form different shapes for the breakwater. The coordinates of these points determine genetic algorithm variables.

2.2. GENETIC ALGORITHM

Genetic algorithm (GA) is primarily based on the principles of natural selection and survival of the fittest elements in the ecosystem. Simple GA (SGA) is robust and is applied in the fields of structural design optimization [3].

Genetic algorithms is a stochastic global search method that operates on a population of the potential solutions to produce better approximations to an optimal solution[1]. The primary population is generated randomly in concordance with the change of variables. For the production of the new generation three main operation are needed; selection, crossover, and mutation. The choice of the parents is made on the basis of their fitness and via tournament method. Each pair of the parents is combined in a random cut point. Then a number of variables are chosen randomly and may change in a certain area, and this is how the new generation is produced. Fig.1 shows the flow chart for the Genetic Algorithm developed for this optimization problem.

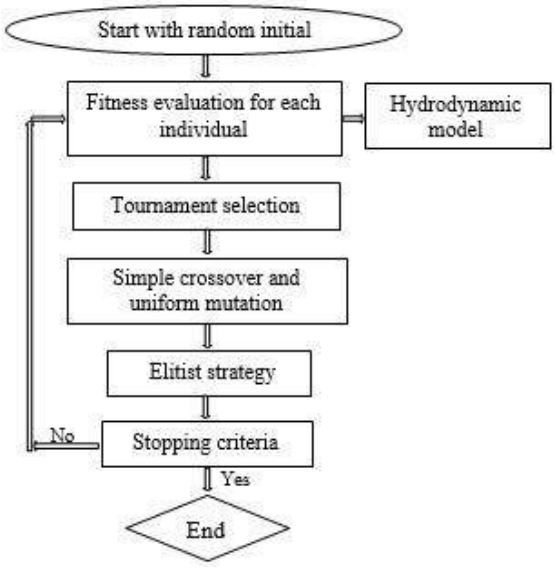

Fig.1. Flow chart for the developed GA

The genetic algorithm operation may be validated by using benchmark functions which are used to assess optimization algorithm such as Ackley's function, Levi function N.13 and McCormick function. Then according to the root-mean-square deviation for the values equal to 0.01, it can be regarded that an algorithm has an acceptable accuracy in determining its optimized amount.

3. HYDRODYNAMIC MODELING

To compute the water wave propagation, the REF/DIF numerical model has been utilized [4]. This model describes

the propagation of water waves over a weakly irregular sea bottom for which shoaling, refraction, diffraction, and energy dissipation are taken into account [2]. The model is a nonlinear combined refraction and diffraction code for the incident wave based on a Stokes expansion of the water wave problem and includes the third order correction to the wave phase speed. The model has been validated on a number of experimental test cases [5].

4. NUMERICAL MODELING

For determining the optimized shapes of breakwaters regarding a minimized wave height in the harbor, the hydrodynamic model, as an objective function, is coupled with optimization algorithm. The genetic algorithm by searching among possible solutions, anticipates different formations for the breakwater whose propriety is determined by considering the waves height in the harbor, which is resulted from the simulation of breakwater by the wave model and by considering a fifteen-percent limit for the length increase of the breakwater. The superior solutions remain in the next generations and finally the algorithm is converged toward the optimized solution and the optimum shape is determined.

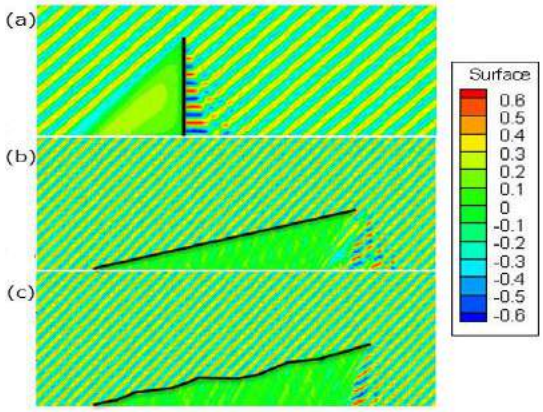

Fig. 2) Water elevations for the NW incoming waves with T= 2s and a= 0.5 m. (a) rectangular structure perpendicular to the horizontal axis. (b) Structures with the same angle as the optimized one but with a straight shape (c) optimized structures with no feasibility constraints.

For validation of the combination of the genetic algorithm and hydrodynamic model, some rectangle-shaped defense structures were considered along the coast and the simulated results of this study are compared with those reported by Isebe et al (Fig.2). For the structure oriented against the wave direction, the wave height decreased by 53% compared to the structure perpendicular to the horizontal axis (Fig. 2a). The wave height of optimized shape (Fig. 2c), shows a decrease of 25% compared to the structure shown in (Fig. 2b). This means that small perturbations around the straight shape are of great importance. The integration of wave model and genetic algorithm was utilized to optimize the shape of breakwater and the simulated results are illustrated in figure 3, which shows the water elevation after the application of the optimization algorithm exhibits a decrease of wave height equal to 20% in the access canal.

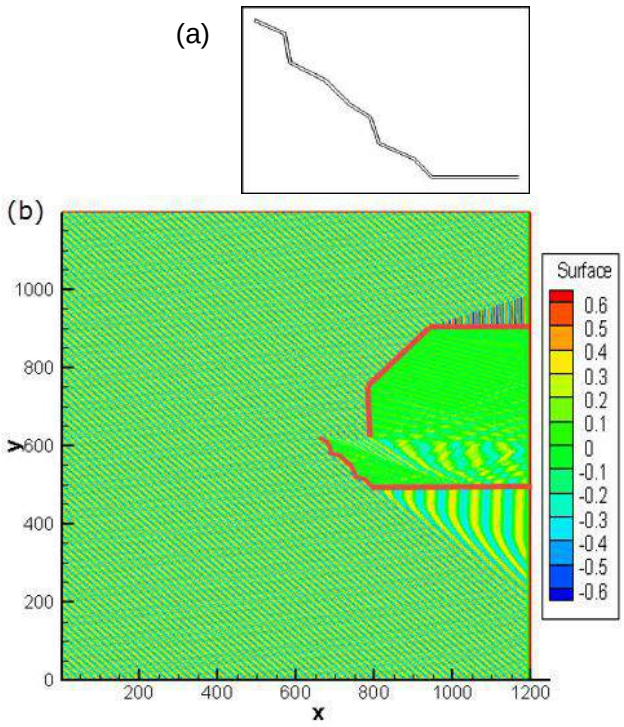

Fig.3) Optimization results (a) Optimized shape structure. (b) water elevation around optimized structure. (NW incoming waves with T=2s and a=0.5m)

5. CONCLUSION

An integrated wave hydrodynamic simulation and genetic algorithm has been deployed to minimize the wave height in the harbor, which results in an optimized geometry and planform for the breakwater. The strategy may be deployed for designing breakwaters in harbors to accommodate sheltered zones in harbors.

6. REFERENCES

[1] Elchahal, G., Younes, R.et al. (2013):"Optimization of Coastal Structures: Application on Detached breakwaters in ports", Ocean Engineering 63(0): 35-43

[2] Isebe, D., Azerad, P., Mohammadi, B., Bouchette, F., 2008b. Optimal shape design of defense structures for minimizing short wave impact. Coastal Eng. 55, 35–46.

[3] Jin, G. G., Genetic Algorithms and Their Applications (in Korean), Kyowoo-sa, 2000.

[4] Kirby JT, Dalrymple RA. (1994), Combined rrefraction/diffraction model ref/dif 1, version 2.5. documentation and user's manual. Research Report No. CACR-94-22, Center for Applied Coastal Research, Department of Civil Engineering, University of Delaware, Newark.

[5] Chawla A, Ozkan-Haller HT, Kirby JT. (1998), Spectral model for wave transformation over irregular bathymetry. Journal of Waterway, Port, Coastal and Ocean Engineering; 124:189–198

PARAMETRIC STUDY OF HYDRODYNAMIC PERFORMANCE OF TWIN-PANTOON FLOATING BREAKWATER

Atena Amiri[1], Roozbeh Panahi[2,*] and Soheil Radfar[3]

1) Civil and Environmental Engineering Department, Tarbiat Modares University, Tehran, Iran, atena.amiri@modares.ac.ir
1) Civil and Environmental Engineering Department, Tarbiat Modares University, Tehran, Iran, rpanahi@modares.ac.ir
1) Civil and Environmental Engineering Department, Tarbiat Modares University, Tehran, Iran, soheil.radfar@modares.ac.ir

1. Introduction

During the past decades, floating breakwater has been studied widely. This type of breakwaters is applicable in regions with calm sea conditions and with the increasing wave period, its performance decreases. In the case of using this type of structure in harsh sea conditions, a wider structure is required, which is not applicable in some cases.

One of the proposed methods to solve this problem is to use floating breakwater with multiple-row arrangement and separate mooring. This study focuses on numerical simulation of double-row floating breakwater and row-distance parameter's effect on system efficiency has been investigated.

The most important effect of floating breakwater like any other breakwater is, reducing incoming wave height. Figure 1 illustrates a simplified sample of this breakwater with mooring lines to sea bed. According to this figure, waves are allowed to pass from the bottom part. [1]

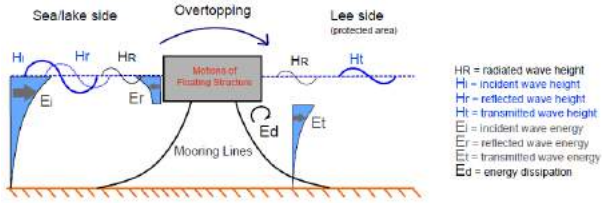

Figure 1. Interaction between wave and floating breakwater

Transmission coefficient (C_t) is one of the important parameters for evaluating the performance of floating breakwater, which is equal with proportion of overtopped wave height to incoming wave height.

2. Experimental study

Pena et al. (2011) performed comprehensive experimental study on four floating breakwater models. Characteristics of the main model which is used as evaluation criterion of numerical results in the present study, are presented in Table 1 [2].

Table 1. Characteristics of the main model

Characteristic	Value
Length	19.9 [m]
Width	4.0 [m]
Height	1.8 [m]
Weight (each pantoon)	40.0 [ton]

The scale of experimental study is 1:15. The final model is provided in depth of 6.75 [m] and with solid connection of five pantoons.

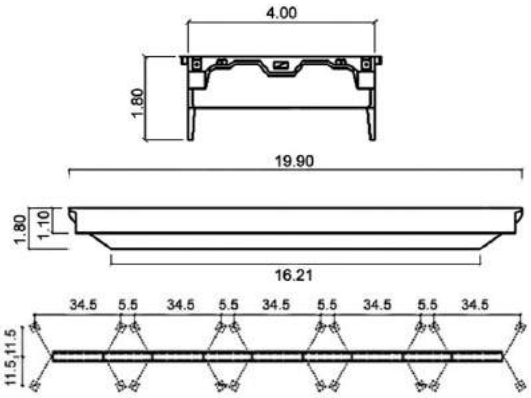

Figure 2. Main dimensions of floating breakwater and mooring lines [2]

Characteristics of existing breakwater are summarized in Table 2. Transmission coefficient of present study is employed to validate the results of numerical simulation. This fact is presented in the following sections [2].

Table 2. Characteristics of existing breakwater

Characteristic	Value
Length	4.0 [m]
Rigidity	30.0 [kN.m]
Constant height of head-on waves	0.6 [m]
Periods of head-on waves	2.25-4.75 [m]

3. Numerical simulation

Frequency and time domain analyses were performed in ANSYS-AQWA software. The ANSYS-AQWA software, which is based on the potential flow theories and utilizes the diffraction theory, solves the equations with respect to the Boundary Element Method (BEM).

Assuming non-viscous and incompressible fluid, and non-rotational flow, fluid motion can be described by velocity potential function (ϕ) which satisfies Laplace's equation. Laplace's equation is as follows:

$$\nabla^2\phi = \frac{\partial^2\phi}{\partial x^2} + \frac{\partial^2\phi}{\partial y^2} + \frac{\partial^2\phi}{\partial z^2} = 0 \qquad (1)$$

where ϕ is compromises from three parts: incident wave (ϕ_i), diffraction wave (ϕ_d) and radiation wave (ϕ_r) [3].

$$\phi = \phi_i + \phi_d + \phi_r$$

Figure 3 shows final model of floating breakwater consisting of five pantoons and mooring system, in ANSYS workbench. Here, 3D geometry has been built in SolidWorks and imported to ANSYS as .(x-t) extension.

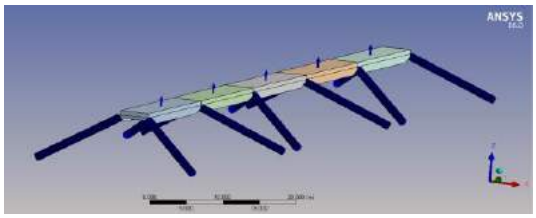

Figure 3. Floating breakwater in AQWA

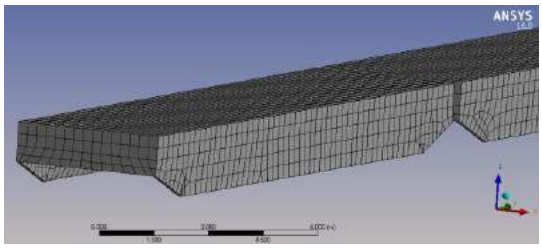

Figure 4. Meshed floating breakwater in AQWA

Comparison between numerical and experimental results showed that the error was less than 10 percent and the numerical model is of well accuracy (Figure 4).

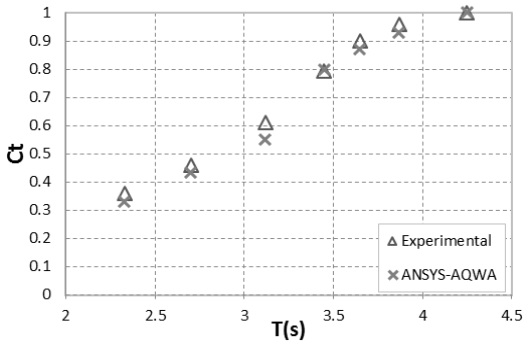

Figure 5. Comparison between transmission coefficient of numerical and experimental results (H_i = 0.6 [m])

Later, double-row arrangement of this breakwater will be studied by radiating waves, present model is being studied at higher wave periods and effect of row distance on transmission coefficient obtained.

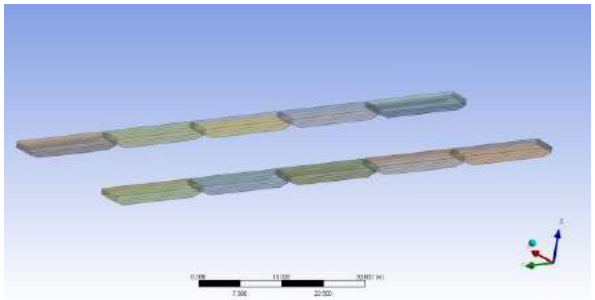

Figure 6. Arrangement of double-row breakwater

4. Conclusions

Numerical model results and their comparison with experimental study show the capability of AQWA software in simulation of moored floating breakwater. As mentioned earlier, one of the important parameters for performance evaluation of floating breakwater is transmission coefficient which value increases in harsh environmental conditions and is a sign for decreasing of breakwater performance.

Here in this study for calm environmental condition of Iranian seas, double-row arrangement breakwater was used and with changing in distance parameter, in each case, breakwater performance evaluated. It should be noted that this software because of employing boundary element method in numerical simulation, has low computational cost and is applicable for similar issues.

5. References

[1] Arie, C. B., "Effectiveness of Floating Breakwaters", Delft University, Master of Science Thesis, 2013.

[2] Pena, E., Ferreras, J., Sanchez, F., "Experimental study on wave transmission coefficient, mooring lines and module connector forces with different designs of floating breakwaters", *Ocean Engineering*, 38, 2011, pp. 1150-1160.

[3] Ioanna, D., Eva, L., Demos. C., "3D Analysis of free and moored twin-pantoon floating breakwaters", in *Proceedings 17th International offshore and polar Engineering Conference*, Portugal, July 1-6 2007.

LAGRANGIAN PARTICLE METHODS FOR COASTAL AND OFFSHORE ENGINEERING - CURRENT ACHIEVEMENTS AND FUTURE PERSPECTIVES

Abbas Khayyer[1] and Hitoshi Gotoh[2]

1) Associate Professor, Laboratory of Applied Mechanics, Department of Civil and Earth Resources Engineering, Kyoto University, Kyoto, Japan, khayyer@particle.kuciv.kyoto-u.ac.jp
2) Professor, Laboratory of Urban Coast Design, Department of Civil and Earth Resources Engineering, Kyoto University, Kyoto, Japan, gotoh@particle.kuciv.kyoto-u.ac.jp

1. Introduction

The paper presents a concise review on the latest achievements made in the context of projection-based particle methods, including MPS and Incompressible SPH (ISPH) methods. The latest achievements corresponding to stability, accuracy, boundary conditions and energy conservation enhancements as well as advancements related to simulations of multiphase flows, fluid-structure interactions, surface tension and heat diffusion are reviewed. The future perspectives for enhancement of applicability and reliability of projection-based particle methods will be also highlighted.

2. Latest Achievements

Projection-based particle methods, including MPS [1] and Incompressible SPH (ISPH) [2] methods, are founded on Helmholtz-Leray decomposition of an intermediate velocity vector field into a solenoidal (divergence-free) one and an irrotational (curl-free) one. These methods potentially result in accurate solutions to the continuity and Navier-Stokes equations, especially in terms of pressure calculation and volume conservation. The latest achievements made in the field of projection-based particle methods are concisely introduced here.

2.1. Stability Enhancement

A distinct category of methods developed for enhancement of both stability and accuracy of particle methods correspond to particle regularization schemes. In this regards, authors have recently proposed an Optimized Particle Shifting (OPS) scheme [3] for consistent implementation of particle shifting for free-surface and multiphase flows. **Figure 1** shows an example of improved performance of OPS with respect to original PS (Particle Shifting) scheme of Lind et al. [4].

2.2. Accuracy Enhancement

For both ISPH and MPS methods refined differential operator models have been proposed to enhance the accuracy of pressure calculation and particle motion. Refined differential operator models have been proposed for discretization of either source term or Laplacian of pressure in the PPE [5,6].

2.3. Improvement of Boundary Conditions

These improvements correspond to wall, free-surface and inflow/outflow boundary conditions.

2.4. Energy Conservation

Khayyer et al. [7] performed a study on energy conservation properties of projection-based particle methods. Their study highlighted the significance of Taylor-series consistent pressure gradient models and enhancing effect of a consistency-related gradient correction in providing enhanced energy conservation.

2.5. Multiphase Flows

Khayyer and Gotoh [8] presented an improved MPS method for multiphase flows characterized by large density ratios. The method was further improved for more accurate consideration of air compressibility effect [9].

2.6. Fluid-Structure Interactions

Khayyer et al. [10] presented an enhanced fully Lagrangian FSI (Fluid-Structure Interaction) solver characterized by several refined schemes. **Figure 2** portrays two snapshots corresponding to a high velocity impact of a deformable aluminum beam and a dam break with an elastic plate by the enhanced MPS-based FSI solver.

2.7. Heat Diffusion

An ISPH-based method is recently proposed for heat diffusion problems encountered in coastal engineering [11]. The method is founded on the solution of continuity, Navier-Stokes and heat diffusion equations in closure with Sub-Particle Scale (SPS) turbulence model.

3. Future Perspectives

In spite of the achieved advancements, rigorous researches should continue to be conducted to further enhance the reliability and accuracy of particle methods for

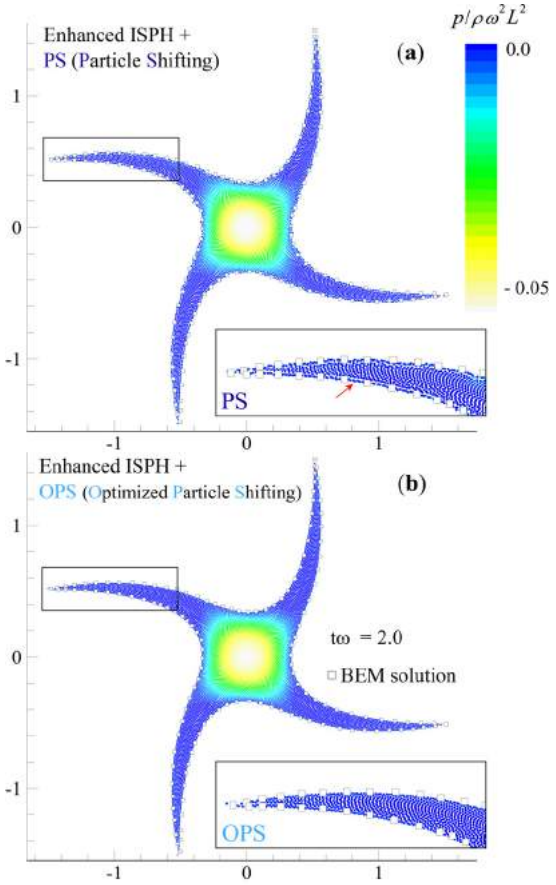

Figure 1. Enhanced Particle Regularization - OPS vs. PS in simulation of a square patch of fluid

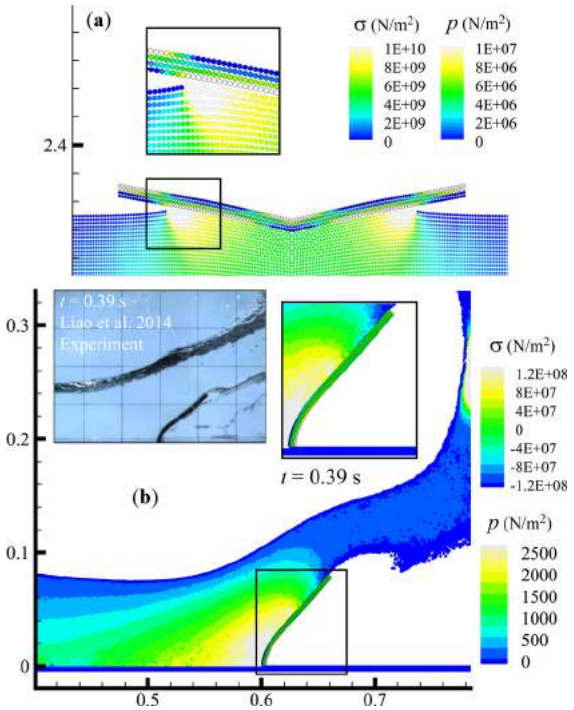

Figure 2. Enhanced MPS methods for refined simulations of FSI (Fluid-Structure Interactions)

practical engineering and scientific purposes. In particular, important issues of stability, conservation, consistency, convergence, boundary conditions, turbulence modeling, multi-scale and multi-physics simulations will be among the future perspectives corresponding to projection-based particle methods.

Further enhancements of stability, accuracy and conservation properties of particle methods along with advancements made in high performance computing will enable particle methods, including projection-based ones, to serve as advanced, reliable and efficient computational methods.

4. References

[1] Koshizuka, S. and Oka, Y. (1996), Moving particle semi-implicit method for fragmentation of incompressible fluid, Nuclear Science and Engineering, 123, 421-434.

[2] Shao, S. and Lo, E.Y.M. (2003), Incompressible SPH method for simulating Newtonian and non-Newtonian flows with a free surface, Adv. Water Resour., 26, 787-800.

[3] Khayyer, A., Gotoh, H. and Shimizu, Y. (2016), Comparative Study on Accuracy and Conservation Properties of Particle Regularization Schemes and Proposal of an Improved Particle Shifting Scheme, Proceedings of 11th international SPHERIC workshop, Munich, Germany.

[4] Lind, S.J., Xu, R., Stansby, P.K. and Rogers, B.D. (2012), Incompressible smoothed particle hydrodynamics for free-surface flows: A generalised diffusion-based algorithm for stability and validations for impulsive flows and propagating waves. J. Comp. Phys., 231, 1499-1523.

[5] Khayyer, A. and Gotoh, H. (2009), Modified Moving Particle Semi-implicit methods for the prediction of 2D wave impact pressure, Coastal Engineering, 56, 419-440.

[6] Khayyer, A. and Gotoh, H. (2011), Enhancement of Stability and Accuracy of the Moving Particle Semi-implicit Method, Journal of Computational Physics, 230, 3093-3118.

[7] Khayyer, A., Gotoh, H., Shimizu, Y. and Gotoh, K. (2015), On Enhancement of Energy Conservation Properties of ISPH and MPS Methods, Proceedings of 10th international SPHERIC workshop, Parma, Italy, 139-146.

[8] Khayyer, A. and Gotoh, H. (2013), Enhancement of performance and stability of MPS meshfree particle method for multiphase flows characterized by high density ratios, Journal of Computational Physics, 242, 211-233.

[9] Khayyer, A. and Gotoh, H. (2016), A multiphase compressible-incompressible particle method for water slamming, International Journal of Offshore and Polar Engineering, 26(1), 20-25.

[10] Khayyer, A., Gotoh, H., Park, J.C., Hwang, S.C and Koga, T. (2015), An enhanced fully Lagrangian coupled MPS-based solver for fluid-structure interactions, Journal of JSCE (Coastal Eng.), 71, 883-888.

[11] Khayyer, A., Gotoh, H., Shimizu, Y. (2016), Development of a SPH-Based Method for Coastal Engineering-Related Heat Diffusion Problems, Journal of JSCE (Coastal Eng.), 72.

DEVELOPING AN IMAGE PROCESSING FILTER AND VERIFYING IT USING IMAGES TAKEN BY AN AUV IN A TOWING TANK

Sayed Ahmadreza Razian [1], Sayed Masoud Beheshti-Maal [2]
1) M.Sc. In Artificial Intelligence, Computer Engineering Department, University of Isfahan, Isfahan, Iran, AhmadrezaRazian@gmail.com
2) B.Eng. in Electronics, Subsea R&D Centre, Isfahan University of Technology, Isfahan, Iran, beheshti@cc.iut.ac.ir

Introduction:

Underwater Robots such as Remotely Operated Vehicle (ROV) or Autonomous Underwater Vehicle (AUV) and even some submarine are equipped with various cameras so as to inspect underwater environment [1]. Due to the inherent murky condition of underwater, images taken from underwater largely differ from those taken outside water. These differences include limitations in viewing depth, viewing angle, sharpness of image due to suspended particles, perceiving object's dimensions and colors to name a few [2].

One of the branches in artificial intelligence is about image processing regarding machine vision. In this branch filters could be designed regarding image enhancement, object segmentation, object detection and object recognition. All these filters are devised considering morphology in spatial or frequency domain in series or in parallel or both, and then implemented on target images [3].

Method:

One of the frequent and the oldest algorithm of image processing which is also used here is the Unsharp Mask. Using this approach higher frequency segments of the image are enhanced, hence better edge detections and image resolutions [4]. Techniques of histogram adjustment and equalization are made use of in this method.

A black & white image is consisted of a 256 histogram array, while an RGB color image includes three 256 histogram arrays each of which is related to the abundance of intensity of the color corresponding to that channel [5].

In this work a recorded video, taken while testing an AUV in the towing tank of the Subsea R&D Centre of the Isfahan University of Technology, is considered. The video as expected was murky and low in resolution in depth viewing (Figure 1).

Figure 1: Sample of a Recorded image for this work experiment taken by AUV's camera

Status of color modes of the image are examined in the first step following which the RGB models are obtained according to the [6] reference for beginning design of the appropriate filter. Parameters such as depth, ampleness of suspended particles, season and time of video recording all affect the way color of objects are viewed underwater [7]. This problem is shown by the histogram of RGB color channels (Figure 2).

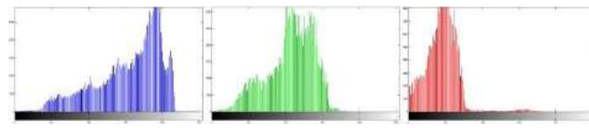

Figure 2: Histogram of the selected image in RGB color channels

In the 2nd step histogram adjustment and equalization of color channels are selected. In this step histogram algorithm is accomplished exponentially according to the reference [8] following which the unsuitable concentrated volume of histograms were improved (Figure 3, Figure 4).

Figure 3 : Result of image after applying the histogram adjusment filter

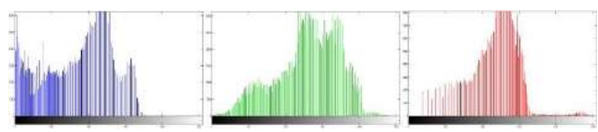

Figure 4: Histogram of figure 3

Implementation of sharpening functions upon each separate color channel is then accomplished so as to enhance the edges following image morphology considerations.

In the last step all color channels are combined and the final image with the RGB format is obtained (Figure 5).

Figure 5 : Final image after running all filter levels

The filter algorithm is shown in Figure 6.

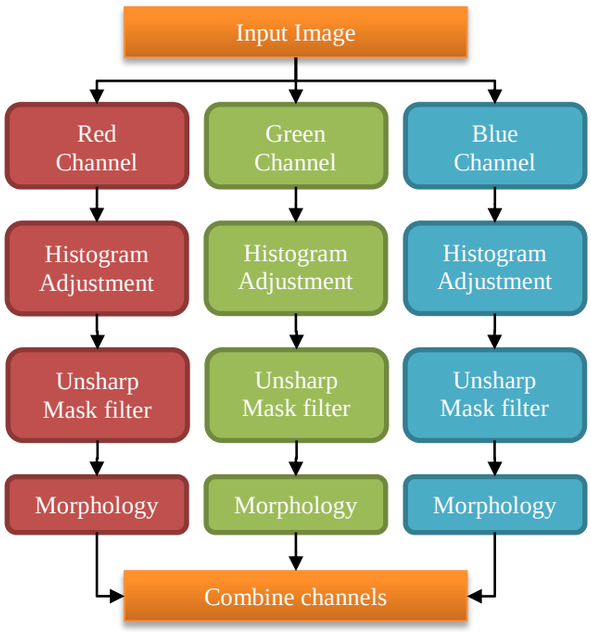

Figure 6 : Algorithm of the designed filter

Results:

Figure 7 (A and B) show the image taken from AUV tests in the towing tank before and after being applied by the designed filter. As it can be seen in the Figure 8, a window and its mirror are clearly visible while it is hardly noticeable in the Figure 9 .

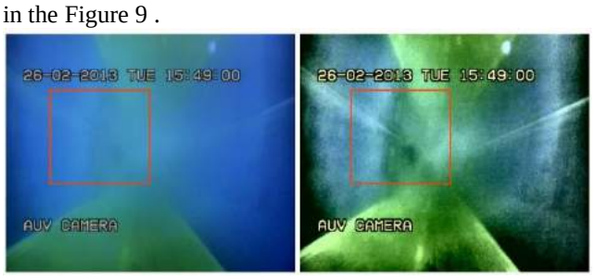

A B

Figure 7 : A:The input image to the filter B:Output image of the filter – Red area is zoomed in figure 8

Figure 8 : Zoomed red area from figure 7B , It's easy to seen the window

Figure 9 : Zoomedf red area from figure 7A , It's hard to seen the window

Discussion:

Suspended particles and its abundance in the water, light penetration behavior and many other parameters all affect the way objects can be viewed underwater.

These would make some hindrances in accomplishing certain jobs underwater by using ROV's or AUV's and would also cause extra time and money expenditures. The filter algorithm proposed in this paper and similar works would greatly enhance the resolution and viewing depth of underwater images especially in perilous operations. Operations such as underwater maintenances, pipeline inspections, mine counter measures, cathode protection inspections and many other tasks could greatly benefit by making use of the filters proposed in this paper.

Complements:

Special thanks are given to Ahmadreza Naghsh Nilchi, Ahmadreza Zamani Forushani, Mohammadreza Allahyar, Mohammad Sakkak and other friends and colleagues who contributed in realizing this work.

References:

[1] J. Elvander and G. Hawkes, "ROVs and AUVs in Support of Marine Renewable Technologies," *IEEE-Oceans*, pp. 1 - 6, 2012.

[2] Y. Schechner and N. Karpel, "Recovery of underwater visibility and structure by polarization analysis," *Oceanic Engineering, IEEE*, vol. 30, no. 3, pp. 570 - 587, 2005.

[3] R. Gonzalez and R. Woods, Digital image processing, 2002.

[4] P. Andrea, G. Ramponi and V. J. Mathews, "Image enhancement via adaptive unsharp masking," *IEEE transactions on image processing*, vol. 9, no. 3, pp. 505-510, 2000.

[5] Smith, J. R. and S.-F. Chang, "Tools and techniques for color image retrieval," *In Electronic Imaging: Science & Technology*, pp. 426-437, 1996.

[6] G. Pass and R. Zabih, "Histogram Refinement for Content-Based Image Retrieval," in *Applications of Computer Vision, 1996. WACV '96., Proceedings 3rd IEEE Workshop on* , Sarasota, FL , 1996.

[7] L. A. Torres-Méndez and G. Dudek, "Color Correction of Underwater Images for Aquatic Robot Inspection," in *Energy Minimization Methods in Computer Vision and Pattern Recognition*, vol. 3757, FL, USA, Springer Berlin Heidelberg, 2005, pp. 60-73.

[8] György Kovács, Attila Fazekas and András Hajdu, "Exponential contrast maximization of intensity images," in *Image and Signal Processing and Analysis (ISPA), 2011 7th International Symposium on,IEEE*, Dubrovnik, 2011.

INPSECTION, MAINTENANCE AND HOSE LIFE ASSESMENT OF OFFSHORE MARINE HOSES

A R Kambiez Zandiyeh ,General Manager

1) Dunlop Oil & Marine Ltd, Moody Lane, Pyewipe, Grimsby, UK, DN31 2SP

1. Introduction

Offshore marine hoses in a Single Point Mooring (SPM) system allow an economical solution in comparison with a Jetty or Dock side facility for import and export crude oil and other Petrochemical products. The design, manufacture and Purchasing of offshore Marine hoses are advised by industry Oil Companies International Marine Forum (OCIMF). The latest guidelines published in 2009 and enforced in 2012 are detailed in Guide to Manufacturing and Purchasing Hoses for Offshore Moorings (GMPHOM 2009). Although these guidelines provide valuable information on the manufacturing, qualification and testing of offshore Marine hoses, it lacks detail on hose service life, maintenance regimes and how the life of these critical components can be extended in a safe and controlled manner.

The aims of this paper are to provide detailed information on the construction of a Marine hose, hose types and their function, submarine system types and design methodologies, factors that may affect marine hose service life, repair/inspection and maintenance techniques and how the life of these critical components can be extended providing economical benefits in a safe and controlled manner.

2. Description of a Single Point Mooring System (SPM)

The concept of a SPM (Figure-1) was introduced in early 1970s with the aim of creating an economical solution in comparison with a Jetty or Dock side for import and/or export of products such as crude oil. The use of SPMs has since become widely accepted with over 390 systems around the World and with over 65 of these concentrated in the Persian Gulf.

Figure 1. Example of a SPM System.

In a SPM system, a floating buoy with a turret system allows a submarine pipeline linked to a refinery to be connected to a loading tanker. The submarine pipeline is connected to the buoy using submarine hoses. Subsequently, floating marine hoses are used to connect the buoy to a loading tanker. The design of both the submarine and floating hose strings is complex and requires detailed dynamic analysis Figure-2, to minimize the loading on the hoses and rigid connections. Furthermore, each string consists of varying hose types and different properties. As part of the system analysis, it is also essential that these properties are optimized.

Figure 2. Example of a SPM System.

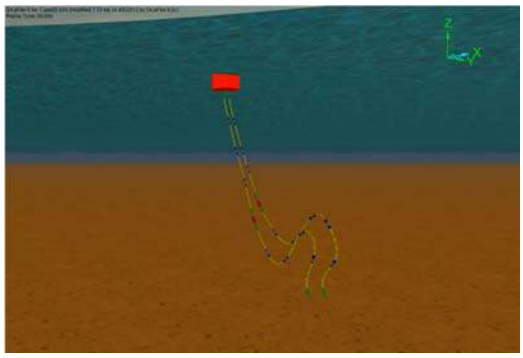

3. Marine Hose Construction

Marine hoses have a complex and composite structure made which is made up of elastomers, textile reinforcement and metallic components. To this extent detailed design analysis using Finite Element Analysis (FEA) Figure-3, have to be performed to arrive at the most optimized solution for any given system.

Figure 3. Typical FEA on the Body of a Marine Hose.

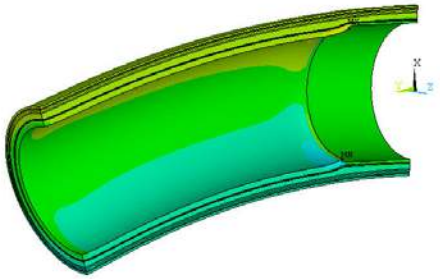

The service life of a marine hose can be affected by many factors and the most critical are detailed below.

1. System Design
2. Hose Design
3. Environmental and Operational conditions
4. Natural and Chemical ageing
5. Poor handling
6. Hose type

In case of a marine hose failure, while in service, product e.g. crude oil, may found its way into the environment with catastrophic consequences. In the formal version of this article each of the critical parameters will be discussed to increase awareness with the aim of mitigating product failure

4. Inspection, Maintenance and Hose Life Assessment

As detailed in section-3, the life of a marine hose can be affected by range of factors. Therefore each operation must develop a regular inspection and maintenance regime for each individual facility to mitigate risks associated with product failure. In the formal version of this paper a bench mark will be made of the best practices across the globe allowing local operators to choose and develop a customized inspection and maintenance regime for their individual operation.

Once the target service of individual marine hoses has been reached, it may be economically viable to extend the life of the existing hoses. This approach needs to be followed in a controlled and safe manner to mitigate risks associated with accidental hose failure. In the formal version of this paper the methodology and approach to increasing marine hose service life will be discussed and beyond this how further optimization could be reached by hose and system design reviews.

5. Conclusions

Marine hoses are designed and manufactured using the guidelines of OCIMF. Despite this hoses can be damaged and subsequently their service life adversely affected if correct inspection and maintenance programs are not adopted. Through a detailed presentation of the guidelines, design and manufacturing processes, system types and factors affecting service life general awareness is raised on these critical products, which are used for offloading. This increased awareness should lead to increased safety, economic and environmental benefits.

6. References

[1] Oil Companies International Forum, "Guide to Manufacturing and Purchasing Hoses for Offshore Moorings", Fifth Edition, 2009.

[2] Oil Companies International Forum, "Guide to Purchasing Manufacturing and Testing of Loading and Discharge Hoses for Offshore Moorings", Fourth Edition 1991.

[3] Oil Companies International Forum, "Single Point Mooring Maintenance and Operation Guide (SMOG)", Third Edition 2015.

[4] API17B, "Recommended Practice for Flexible Pipe, "ISO 13628-11:2007

[5] Zandiyeh, A.R.K, Automatic, “Operational Issues With Rail-Tail Hoses and How to Maximize Service Lives", South Mono Buoy Conference SLOM, 2013.

FIELD AND LABORATORY STUDIES ON THE DURABILITY PROPERTIES OF NEW AND REPAIRED COASTAL STRUCTURES

Majid Safehian[1], Shapur Tahouni[2] and AliAkbar Ramezanianpour[3]

1) Assistant Professor, Dept. of Construction Management, Science and Research Branch Islamic Azad University, Tehran, Iran, safehian@yahoo.com
2) Assistant Professor, Dept. of Civil and Environmental Engineering, Amirkabir University of Technology, Tehran, Iran, stahouni@aut.ac.ir (Engineering Manager of Tadbir Sahel Pars Consultant)
3) Professor, Head of Concrete Technology and Durability Research Center (CTDRC), Amirkabir University of Technology, Tehran, Iran, aaramce@aut.ac.ir

1. Introduction

Reinforced concrete structures are widely constructed in the Persian Gulf region for infrastructures of ports and oil industries. But these structures are increasingly being deteriorated, mainly due to the chloride-induced corrosion of the embedded bars. Consequently, hundreds of million dollars are spent for repair and rehabilitation every year. In marine structures, piles are often subjected to the most severe corrosion due to the permanent wet and dry cycles.

In the majority of previous studies, Fick's 2nd low is often used to predict chloride transport in terms of diffusion [1], because of its convenient and easy calculation with constant values of the apparent diffusion coefficient (D_{app}) and surface chloride content (C_s), which are in fact dependent on concrete mix proportion, production method and degree of contact to severe conditions (e.g. submerged, tidal, splash and atmospheric zones in a marine environment)[2,3]. However these models need to be calibrated with experimental results and surveys of real structures for different climates and exposure conditions all over the world and especially severe conditions like Persian Gulf [4].

Therefore, the main objective of this paper is to study the durability properties of special type of reinforced concrete piles that is called prestressed spun precast concrete piles (PSPC piles). For this purpose, some PSPC piles from concrete jetties in Imam Khomeini Port Complex (see Figure 1) were continuously investigated to assess the chloride penetration and the surface resistivity at 2 to 10 years in tidal exposure conditions. Also, three accelerated durability tests and compressive strength test were performed on standard samples which were made with local materials similar to concrete mixtures of real structures in the laboratory. Finally, corrosion initiation time was estimated by four well known service life prediction models.

2. Description of PSPC Piles

Since 50 years ago; precast, prestressed concrete piles have been the preferred choice for durable and economical foundation, especially in marine environments, due to their good versatility and resistance to corrosion. Also, cylinder piles are used where deep foundation members require exceptionally large axial, buckling and bending capacity. One of the industrial methods for manufacturing these piles is spinning process. During the spinning process as is shown in Figure 2, the concrete is centrifugally compacted, excess water is squeezed out and hence produces a well compacted and dense concrete. After spinning process is completed, the piles are transported to large-scale steam chambers for high temperature heat curing at 8 hours.

Figure 1. Location of under investigated coastal structures in Bandar Imam Khomeini (BIK) zone.

Figure 2. Piles under spinning process in the factory

A summary of the main properties of designed concrete mixture for PSPC piles which is shown in Table 1, are as follows:

a) The employed cementitious materials content is about 550 kg/m^3 and also w/b ratio is 0.30.

b) In addition to type-II Portland cement, silica fume as a supplementary cementitious material is used.

c) An appropriate level of workability is acquired by employing high range water reducer (HRWR) at a dosage of 1.5% of the binder materials weight.

d) Coarse to fine aggregate ratio is above 2 by weight.

e) The concrete density is above 2550 kg/m^3.

Table 1. Properties of concrete mixture

Item	amount	unit
Water	166	kg
Cement	520	kg
Silica fume	36.4	kg
Coarse aggregate	1215	kg
Fine aggregate	600	kg
Super plasticizers	8.3	kg
Air content	3	%
Slump	40	mm

3. Experimental Program and Results

As mentioned before, the mix design of concrete made in the lab and the applied materials were similar to those of real PSPC piles. The experiments in the lab included RCPT (Rapid Chloride Penetration Test), SR (Surface Resistivity), water penetration test, water absorption test and compressive strength at the ages of 7, 14, 28 days. The results of these experiments are shown in Table 2.

Table 2. Laboratory experimental results

Experiment	Standard method	result	unit
Rapid Chloride Penetration Test	ASTM C1202	817	culomb
Surface Resistivity	Wenner test	92	kΩ.cm
Water penetration test	EN-12390-8	5	mm
Water absorption test	BS-1881 part122	1.35	%
Compressive strength (7d)	BS-1881 part116	670	Kg/cm^2
Compressive strength (14d)	BS-1881 part116	820	Kg/cm^2
Compressive strength (28d)	BS-1881 part116	950	Kg/cm^2

The performed experiments on real PSPC piles included surface resistivity (SR) by Wenner test method and extracting concrete core samples (45 mm diameter) to assess chloride penetration. Coring was made to depth of 50 mm or upon reaching prestressing strands.

Chloride ion penetration profile of field-extracted cores were determined according to ASTM C114 and total (acid-soluble) chloride contents at different depths from exposed surface were obtained by potentiometeric titration method. It's noteworthy that the first 1mm powder was excluded in calculations as it might be affected by surface actions such as washout. Figure 3 represents the results of surface resistivity test different ages of the concrete along with its value in the laboratory at 28 days.

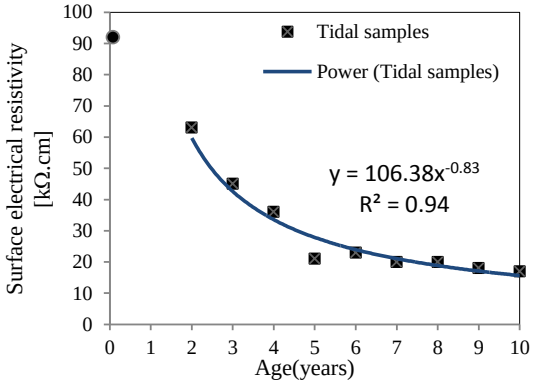

Figure 3. Variation of surface electrical resistivity

4. Estimation of the initiation time of corrosion

In this section, four available models are used to estimate the initiation time of corrosion for PSPC piles considering the exposure conditions. The SLD-SSRC model is developed by Concrete Technology and Durability Research Center in Amirkabir University which has been approved in Iran and is under review to get the International invention certificate.

Table 3. Prediction of corrosion initiation time

Service life models	Exposure conditions	
	Tidal zone	Atmospheric
CTDRC & BHRC	55	>150
DuraPGulf	44	122
Life-365	43	58
SLD-SSRC	40	78

5. Conclusions

As a main conclusion, the combination of dense, high-quality concrete and permanent axial compressive stress results in minimal cracking, very low chloride ion diffusion and high electrical resistivity. Both site investigation and laboratory tests show that PSPC piles are appropriately durable with a high service life under severe conditions. Also, surface resistivity test known as Wenner method provides relatively satisfactory results for estimation of the risk of corrosion in marine structures.

6. References

[1] Petcherdchoo, A. "Time- dependent Models of Apparent Diffusion Coefficients and Surface Chloride for Chloride Transport in Fly Ash Concrete", *Construction and Building Materials*, Vol.38, 2013, pp.497-507.

[2] Safehian, M., Ramezanianpour, AA., Tahouni Sh. "Durability Evaluation of Prestressed Precast Concrete Piles in the Persian Gulf Marine Environment", *1st International Conference on Concrete Sustainaility*, Japan, Tokyo, 2014.

[3] Safehian, M., Ramezanianpour, A.A. "Assessment of Service Life Models for Determination of Chloride Penetration into Silica Fume Concrete in the Severe Marine Environmental Condition", *Construction and Building Materials*, Vol.50, 2013, pp.1-10.

[4] Gjorv, O.D. "Durability Design of Concrete Structures in Severe Environments", Taylor & Francis, London, 2009.

NUMERICAL MODEL FOR PREDICTION OF TIME FROM CORROSION INITIATION TO CRACKING

Mohammad Javad Mirzaee[1], Farshid Jandaghi Alaee[2], Mohammad Hajsadeghi[3]
1) Department of Civil Engineering, Shahrood University of Technology, Shahrood, Iran, m.j_mirzaee@yahoo.com
2) Department of Civil Engineering, Shahrood University of Technology, Shahrood, Iran fjalaee@shahroodut.ac.ir
3) School of Engineering Science, University of Liverpool, Liverpool, UK Mohammad.hajsadeghi@liverpool.ac.uk

1. Introduction

Steel corrosion is one of the most predominant deterioration mechanisms in reinforced concrete structures. The serviceability and durability of concrete structures can be heavily affected by the corrosion of reinforcing steel [1, 2]. After steel de-passivation, corrosion products are formed at the steel/concrete interface. Due to the fact that the volume of the corrosion products is greater than that of the original metal [3-5], the formation of the corrosion products induces a pressure on the surrounding concrete and generates stresses in the concrete cover. As the volume of corrosion products increases, cracks initiate at the steel/concrete interface and propagate outward and eventually spread to the surface of the concrete cover. These cracks in turn provide a path for more rapid ingress of the aggressive agents to the reinforcement, which can accelerate the corrosion process. Therefore, investigation on the corrosion induced cracking process is very important for the prediction of the serviceability and durability of the reinforced concrete structures.

Considerable research has been undertaken on corrosion induced cracking process. These works include experimental, numerical and analytical studies. The experimental studies were mainly focused on testing the critical amount of the steel corrosion needed for cracking concrete cover and developing corresponding empirical model. Numerical studies were mainly based on the use of finite element methods to investigate the corrosion induced cracking process and predict the corrosion of reinforcing steel when the concrete cover has cracks. Several analytical models were also developed for corrosion induced concrete cracking.

In the present study, using an empirical equation proposed in literature and also taking advantage of the developed numerical model, the required time for cover cracking is calculated and compared with the experimental data.

2. Finite Element Modeling

The concrete specimens have been modeled and analyzed using ABAQUS (Standard User's Manual 2010) finite element software. To reduce the computational cost of 3D simulation, a two-dimensional (2D) finite element (FE) model is developed (Fig. 1). The developed 2D model is based on a plane strain finite element formulation. The 4-noded bilinear shell element, i.e. CAX4R, is used for such plane stress simulations.

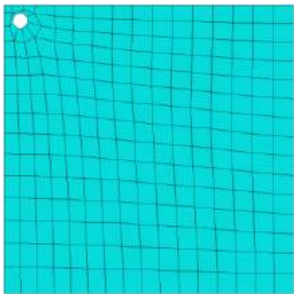

Figure 1. A typical FE model of the concrete specimens

3. Time prediction of concrete cover cracking

To determine the time from corrosion initiation to concrete cover cracking, the empirical equations proposed by Martin-perez [6] is employed that are given below:

$$\Delta V_s = 3.6466\times10^{-11}\,\pi\, d_b\, i_{corr}\,\Delta t$$
$$\Delta M_s = 2.862\times10^{-7}\,\pi\, d_b\, i_{corr}\,\Delta t \quad (1)$$

$$(r_o^2 - r_c^2)\,\gamma = (r_r^2 - r_c^2) \quad (2)$$

where i_{corr} is the rate of corrosion ($\mu A/cm^2$), ΔVs is volume change of steel, ΔMs is mass change of steel, d_b is bar diameter (m), Δt is time (s), r_o is original bar radius (m), r_c is reduced radius of corroded bar (m), r_r is the total bar radius including rust (m), and γ is volumetric ratio of a rust product.

The risk of corrosion is divided into four levels as provided in Table 1. Depending on the iron oxidation level, corrosion leads to varying corrosion current density (i_{corr}) which directly influences the volume increase. The steel reinforcement may have up to six times increase in volume.

Table 1. Risk of corrosion.

i_{corr} ($\mu A/cm^2$)	Risk of Corrosion
$i_{corr} < 0.1$	Negligible
$0.1 < i_{corr} < 0.5$	Low
$0.5 < i_{corr} < 1.0$	Middle
$i_{corr} > 1.0$	High

The procedure how to employ the numerical model to predict the time from corrosion initiation to cover cracking using the empirical equations are shown in Fig. 2.

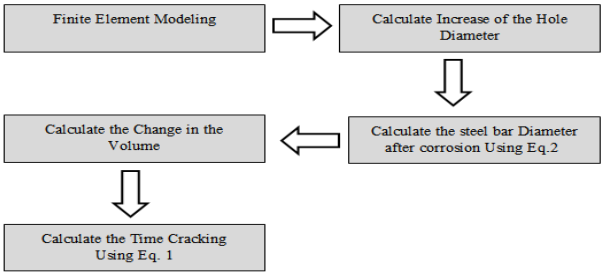

Figure 2. Calculation procedure of the cracking time

Figure 3 shows the concrete cover to bar diameter ratio against time obtained from numerical simulation and the empirical equations for four different values of i_{corr}.

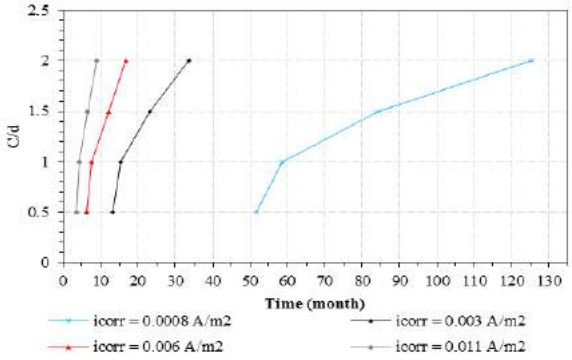

Figure 3. Risk of corrosion

To assess the accuracy of the time estimation, the results from experiments in literature and the estimated data are compared. The experimental specimens' properties (C, d, i_{corr}) are provided in Table 2. In some cases where the actual tensile strength (f_t) and the modulus of elasticity (E_c) were not available, they were estimated by using Equations 3 and 4 in accordance with ACI 318 (2008).

$$f_t = 0.33 \times \sqrt{f_c'} \quad (MPa) \tag{3}$$

$$E_c = 4730 \sqrt{f_c'} \quad (GPa) \tag{4}$$

The estimated times from corrosion initiation to concrete cover cracking are compared to the respective experimental data in Table 3.

Table 2. Experimental specimens' characteristics.

Specimen	d (mm)	C (mm)	i_{corr} ($\mu A/cm^2$)	f_t (MPa)	E_c (GPa)
Andrade et al. [1]	16	20	100	3.55	22
Rodriguez et al. [3]	16	20	100	3.85	22
Maaddawy & Soudki [4]	16	33	150	4.9	28

Table 3. The estimated and experimental time for cracking.

Specimen	Experimental time (h)	Estimated time (h)	Dif. (%)
Andrade et al. [1]	96	117	17.95
Rodriguez et al.[3]	113	153	26.14
Maaddawy & Soudki [4]	95	121	21.48

4. Conclusion

In this paper a numerical model, capable of predicting the time from corrosion initiation to corrosion cracking was developed. A comparison of model's predictions with experimental results published in the literature showed that the model can give reasonable prediction for the time from corrosion initiation to corrosion cracking.

5. References

[1] Andrade, C., Alonso, C., Rodriguez, J. & Garcia, M. 1996. "Cover cracking and amount of rebar corrosion: importance of the current applied accelerated tests", Proceedings of the 5th International Conference on Durability of Building Materials and Components, London, UK..

[2] Oh, B.H., Kim, K.H. & Jang, B.S. 2009. "Critical corrosion amount to cause cracking of reinforced concrete structures", ACI Mater. J., 106(4), 333-339.

[3] Rodriguez, J., Ortega, L.M., Casal, J. & Diez, J.M. 1996. "Corrosion of reinforcement and service life of concrete structures", Proceedings of the 7th International Conference on Durability of Building Materials and Components, London, UK.

[4] Maaddawy, T.E. & Soudki, K. 2007. "A model for prediction of time from corrosion initiation to corrosion cracking", Cem. Concr. Compos., 29, 168-175.

[5] Lu, C.H., Jin, W.L. & Liu, R.G. 2011. "Reinforcement corrosion-induced cover cracking and its time prediction for reinforced concrete structures", Corros. Sci., 53(4), 1337-1347.

[6] Martín-Pérez, B 1999. "Service Life Modelling of R.C. Highway Structures Exposed to Chlorides." Ph.D. thesis, Department of Civil Engineering, University of Toronto, Toronto, Canada.

A STRUCTURAL HEALTH MONITORING STRATEGY FOR OFFSHORE JACKET PLATFORM USING A NOVEL FUZZY BASED METHOD

Mojtahedi Alireza[1]*, Zargarzadeh Ali[2], Shakery Zad Abyaneh Saeed[3]

1) Faculty of Civil Engineering, University of Tabriz, Tabriz, Iran: mojtahedi@tabrizu.ac.ir
2) Faculty of Civil Engineering, University of Tabriz, Tabriz, Iran:zargarzadeh@email.com
3) Faculty of Civil Engineering, University of Tabriz, Tabriz, Iran, shakeryabyaneh @gmail.com

1. Introduction

Structural Health Monitoring method (SHM) has been used to decline the effect of the damages caused by marine environmental conditions. Major parts of offshore structures which are not available for diagnosing, change the monitoring process to a big challenge [1]. However, appropriate detection patterns, based on simulation data, are designed to trace the location and extent of damages [2]. In this study, a new method based on the combination of Krill-Herd group and fuzzy inference system is used to perform structural health monitoring process in a fixed jacket platform. A small scale hydro elastic model of an existing fixed offshore platform (SPD9 located in Persian Gulf) is prepared to obtain modal parameters using vibration behavior. The method is shown to be applicable and appropriate in SHM process and also for handling noisy data.

2. Experimental and numerical model

For this study, ABS hollow tubes, according to the dimensions in the plans, are used for the construction of the experimental model, as shown in Fig. (1). Modulus of elasticity of $2.3\times10^{8}\,N/m^{2}$, has been considered for the experimental model to obtain a scale of $1/100$ of the prototype. Characteristics of platform in the prototype and the experimental model have been listed in table (1). Generally, there are two important ways to stimulate structures. First vibrator method, which a vibrator connects to the structure and applies certain forces to the structure, and second hammer method, which needs a hammer for applying forces. In this study, both of methods have been conducted for comparison.

Table 1. Characteristics of SPD9 prototype and model

Properties	Prototype	Model
Height (m)	74	0.74
Low-level dimensions	36x35	0.36x0.35
High-level dimensions	29x16	0.26X0.16
Platform weight	15500	0.0155

Figure 1. Prototype and scaled experimental model

3. Sensitivity analysis of affective parameters of the dynamic behavior of structure

To perform a sensitivity analysis on changes of modulus of elasticity, 14 members have been chosen for this model, which location of these members are shown in Fig. 2. The same performance of symmetric geometry members on the dynamic behavior of structure is a sign of fuzzy system failure in this research [3]. Sensitivity of structural behavior related to the member's stiffness is compared in Fig. 6. M1 and M2, M3 and M4, M5 and M6, M7 and M8, M9 and M10, M11 and M12 are members of the platform foundation and each couple are located at the same level in the platform. By removing each of the coupled members, same frequency changes are occurred.

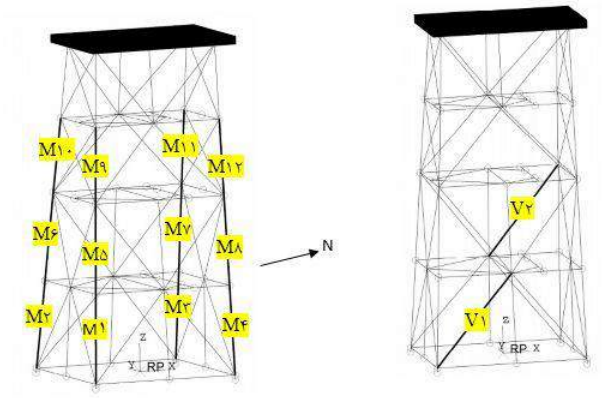

Figure 2. Sensitivity analysis of selected members for modulus of elasticity changes

For more accurate characterization of these members, their changes by increasing failure are shown in Fig. 3.

When the failure rate is less than 75 percent, slope of natural frequency changes is low and by applying more percent of failure rate than 75, slope of frequency changes increases

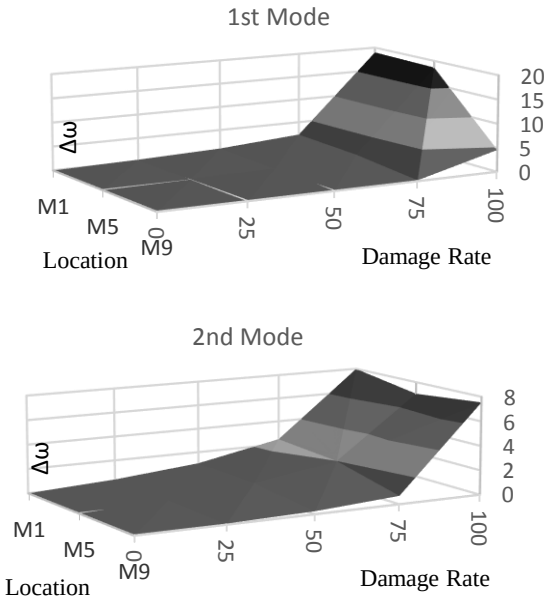

Figure 3. Frequency changes on different modes on axis members

4- Results of fuzzy genetic and Krill herd group

4.1. Comparing system with and without genetic algorithm

The success rate is investigated in this study without using genetic algorithm and with numerical impressions from the finite element model [4]. The average of success rate for both modes is shown in Fig. 4.

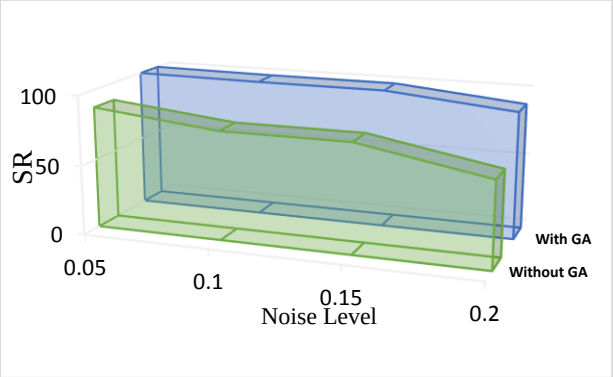

Figure 4. The average success rate in the presence and absence of genetic algorithm

4.2. Krill Herd algorithm

Comparison of the average success rate of genetic algorithm, and Krill herd are shown in Fig. 5. This figure shows same function of both algorithms.

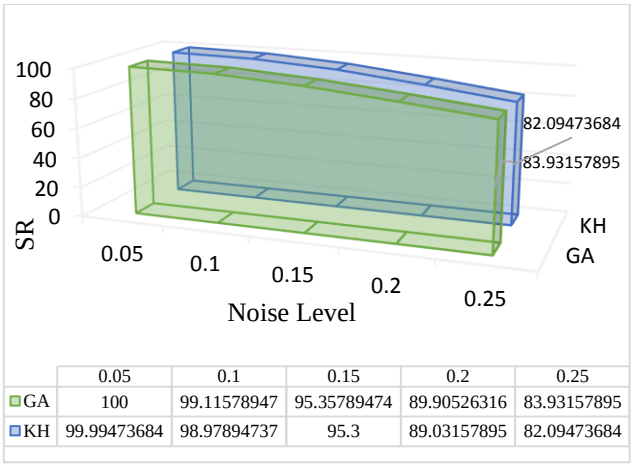

	0.05	0.1	0.15	0.2	0.25
GA	100	99.11578947	95.35789474	89.90526316	83.93157895
KH	99.99473684	98.97894737	95.3	89.03157895	82.09473684

Figure 5. Average success rate of GA and KH optimization

5- Results

Frequency patterns are sensitive on applying different failure scenarios. By using first four natural frequencies, estimating the location and severity of damage are possible. According to the same effects of symmetrical elements failure in natural frequencies, both of symmetry elements must be inspected practically. To consider uncertainties of input data, noise has been included in numerical data and the effects of noise on model is simulated. Based on the results, genetic algorithm shows a better performance by presence of the noise in the input data. According to the success rates of genetic algorithm and krill herd, it can be concluded that for such problems evolutionary algorithms are more efficient.

6- References

[1] Karbhari M, Ansari, F. Structural health monitoring of civil infrastructure systems. New York: Woodhead Publishing Ltd; 2009.

[2] Cheng Y. S., Wang Z. Detecting damage to offshore platform structures using the time-domain data. Journal of Marine Science and Application, 2008; 7(1):7-14.

[3] Kuang K. S. Sensors and actuators a: physical distributed damage detection of offshore steel structures using plastic optical fiber sensors. Sensors and Actuators A: Physical, 2015; 229:59-67.

[4] Mojtahedi A., Lotfollahi Yaghin M., Hassanzadeh Y., Abbasidoust F., Ettefagh M. M., Aminfar M. H. A robust damage detection method developed for offshore jacket platforms using modified artificial immune system algorithm. China Ocean Engineering, 2012; 26(3):379-395.

EFFECT OF POZZOLANS TO IMPROVE THE STRENGTH & LONG-TERM CHLORIDE INGRESS IN CONCRETE IN TIDAL ZONE OF PERSIAN GULF REGION

MohammadHosein Tadayon[1], Mohammad Shekarchi[2] and Mohsen Tadayon[3]

1) Construction Material Institute, University of Tehran, Tehran, Iran, tadayon@ut.ac.ir
2) Road, Housing & Urban Development Research Center (BHRC), Tehran, Iran, shekarch@ut.ac.ir
3) Iranian Concrete Institute, Tehran, Iran, tadayonmoh@yahoo.com

1. Introduction

In general, the use of pozzolans such as silica fume, metakaolin and natural zeolite enhance concrete permeability and durability [6]. This is because of improving the distribution of pore size and structure of concrete matrix, improving interfacial transition zone of the interface between aggregates and the matrix, reducing chloride ingress, and increasing chloride binding [3,4,7-9].

Silica fume and metakaolin are commonly used pozzolans in construction projects. These two pozzolans can sharply increase the compressive strength of concrete and decrease its permeability [3, 6 and 10]. However, recent tendency to use natural pozzolans because of lower cost and accessibility have been led to use natural zeolite, one of the most common natural pozzolanic material [11].

Natural zeolite as cement replacement of 5 to 30% can lead to concrete with a lower permeability and higher compressive strength. However, natural zeolite is not as effective as silica fume in decreasing chloride ion diffusivity or increasing compressive strength [11,12].

Exposure condition of concrete affects greatly on chloride diffusion coefficient. Studies showed that tidal zone and splash zone are the most severe conditions in the case of chloride ingress and steel corrosion in concrete, in compare to atmosphere and immerged zone [3,13].

In the case of durability, long-term measurements can be more valuable and provide better estimations from long-term performance of concrete structures.

In this research, long-time in situ studies are presented to investigate the effect of different w/b ratios and pozzolan replacement on chloride penetration under laboratory and tidal exposure in the field conditions in the Persian Gulf.

2. Experimental

Mix designs are listed in Table 1.

To determine the chloride penetration profile, two sets of specimens containing laboratory specimens 150 mm concrete cubes [14] and field specimens, 150×150×600 mm^3 concrete prisms were prepared. Laboratory specimens cured in the standard conditions, and the field specimens were moist-cured for 2 days in environmental temperature. All the chloride diffusion test specimens were sealed on the five sides using epoxy based coating to expose only top sides to chloride ingress. The field specimens were exposed to tidal conditions in the Qeshm Island in the Persian Gulf, the south of Iran, and laboratory specimens were exposed according to ASTM C1556.

Table 1. Concrete Mix Proportions

Code	w/b	Water (kg/m^3)	Binder, (kg/m^3)			
			PC	SF	MK	ZE
C1	0.35	140	400	-	-	-
C2	0.40	160	400	-	-	-
C3	0.45	180	400	-	-	-
C4	0.50	200	400	-	-	-
SF5	0.40	160	380	20	-	-
MK5	0.40	160	380	-	20	-
ZE10	0.40	160	360	-	-	40

w/b is water-binder ratio, PC is Portland cement, SF is silica fume, MK is metakaolin, ZE is natural zeolite and c_i is initial chloride content.

The compressive strength test were examined on cubes according to EN 12390-3 at the age of 28 days, making and curing the specimens were according to EN 12390-2 [15,16]. The acid-soluble chloride concentration profiles were obtained after 3 months of exposure in the laboratory conditions according to ASTM C1556 [17], and after 3, 9, 27 and 50 months of exposure in the field tidal conditions. Acid-soluble chloride content was determined by ASTM C114, section 19 and ASTM C1152 [18, 19].

3. Summary & Conclusions

Compressive strength of samples are presented in Figure 1. Each result is the average of three specimens.

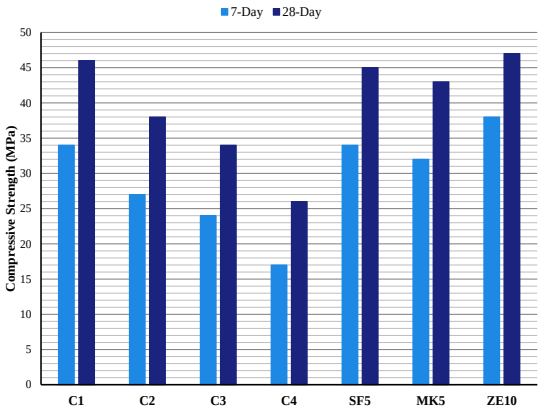

Figure 1. Compressive Strength of Concrete Samples

Figure 2 illustrates diffusion coefficients over the time.

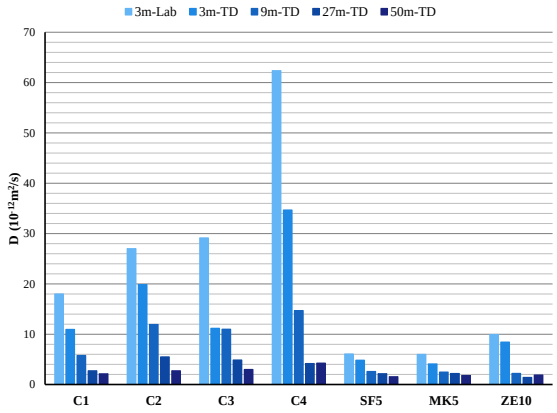

Figure 2. Chloride Diffusion Coefficients of Samples

Figure 3 presents the relationship between compressive strength and laboratory chloride diffusion coefficients.

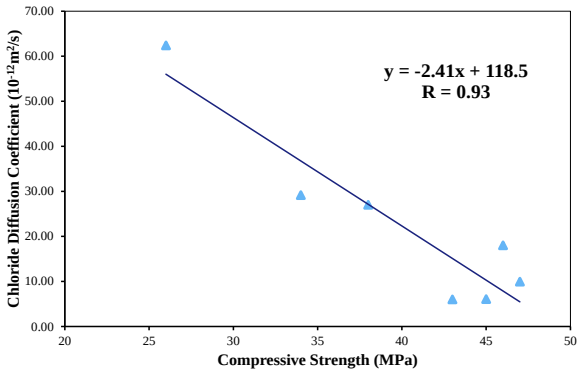

Figure 3. Laboratory Chloride Diffusion Coefficients vs. Compressive strength

The following main conclusions can be drawn from the results of this study:

- Using pozzolans to improve the concrete durability can be much more efficient than reducing the w/b ratio that results in the same improvements in mechanical properties.
- Each 0.05 decrease in w/c ratio can increase 20 percent in compressive strength. Using pozzolans led to same compressive strength improvement.
- At the long time, less permeable mixes show more chloride content at the shallower depths and less chloride content at the deeper depths, and vice versa.
- The mechanical and durability performance of 5% silica fume, 5% metakaolin and 10% natural zeolite as cement replacement are relatively similar.
- Using pozzolans significantly reduced chloride ingress at different times.
- At the long time, chloride diffusion coefficient of all mixes became very close to each other and it seems there would be little or no more improvement in chloride diffusion coefficients after 27 to 50 months.
- At the long time, surface chloride content of the mixes became very close to each other (about 0.9-1%) and it is seen that surface chloride contents of all mixes were increased over the time.
- There is relatively good correlation between compressive strength and laboratory chloride diffusion coefficient.

4. References

[1] Valipour, M., Pargar, F., Shekarchi, M., Khani, "Comparing a natural pozzolan, zeolite, to metakaolin and silica fume in terms of their effect on the durability characteristics of concrete: A laboratory study", Construction and Building Materials, 41, 2013, pp. 879-888.

[2] Valipour, M., Pargar, F., Shekarchi, M., Khani, S., Moradian, M., "In situ study of chloride ingress in concretes containing natural zeolite, metakaolin and silica fume exposed to various exposure conditions in a harsh marine environment", Construction and Building Materials, 46, 2013, pp. 63-70.

[3] Vedalakshmi, R., Rajagopal, K., Palaniswamy, N., "Longterm corrosion performance of rebar embedded in blended cement concrete under macro cell corrosion condition", Construction and Building Materials, 22(3), 2008, pp. 186-199.

[4] Shi, X., Xie, N., Fortune, K., Gong, J., "Durability of steel reinforced concrete in chloride environments: An overview", Construction and Building Materials, 30, 2012, pp. 125-138.

[5] Duan, P., Shui, Z., Chen, W., Shen, C., "Effects of metakaolin, silica fume and slag on pore structure, interfacial transition zone and compressive strength of concrete", Construction and Building Materials, 44, 2013, pp. 1-6.

[6] Dousti, A., Rashetnia, R., Ahmadi, B., Shekarchi, M., "Influence of exposure temperature on chloride diffusion in concretes incorporating silica fume or natural zeolite", Construction and Building Materials, 49, 2013, pp. 393-399.

[7] Poon, C.S., Kou, S.C., Lam, L., "Compressive strength, chloride diffusivity and pore structure of high performance metakaolin and silica fume concrete", Construction and Building Materials, 20, 2006, pp. 858-865.

[8] Shekarchi, M., Ahmadi, B., Najimi, M., "Use of Natural Zeolite as Pozzolanic Material in Cement and Concrete Composites" in Inglezakis, V. J., Zorpas A. A. (Eds.), "Handbook of Natural Zeolites", Bentham Science Publishers, 2012, pp. 665-694.

[9] Ahmadi, B., Shekarchi, M., "Use of natural zeolite as a supplementary cementitious material", Cement & Concrete Composites, 32, 2010, pp. 134-141.

[10] Li, Q., Li, K., Zhou, X., Zhang, Q., Fan, Z., "Model-based durability design of concrete structures in Hong Kong–Zhuhai–Macau sea link project", Structural Safety, 53, 2015, pp. 1-12.

[11] European Committee for Standardization, "Testing hardened concrete - Part 1: Shape, dimensions and other requirements for specimens and moulds", EN 12390-1, 2012.

[12] European Committee for Standardization, "Testing hardened concrete - Part 2: Making and curing specimens for strength tests", EN 12390-2, 2009.

[13] European Committee for Standardization, "Testing hardened concrete - Part 3: Compressive strength of test specimens", EN 12390-3, 2009.

[14] ASTM C1556-11a, "Standard Test Method for Determining the Apparent Chloride Diffusion Coefficient of Cementitious Mixtures by Bulk Diffusion", ASTM International, West Conshohocken, PA, 2011.

[15] ASTM Standard C114-13, "Standard Test Methods for Chemical Analysis of Hydraulic Cement", ASTM International, West Conshohocken, PA, 2013.

[16] ASTM C1152 / C1152M-04(2012)e1, "Standard Test Method for Acid-Soluble Chloride in Mortar and Concrete", ASTM International, West Conshohocken, PA, 2012.

PARAMETRIC STUDY OF STRESS CONCENTRATION FACTORS IN THREE-PLANAR TUBULAR KT-JOINTS SUBJECTED TO OUT-OF-PLANE BENDING LOADS

Esmaeil Zavvar[1], Hamid Ahmadi[2]

1) Faculty of Civil Engineering, University of Tabriz, Tabriz, Iran, esmaeilzavvar@gmail.com
2) Faculty of Civil Engineering, University of Tabriz, Tabriz, Iran, h-ahmadi@tabrizu.ac.ir

1. Introduction

The substructure of a jacket-type offshore platform is a space frame composed of circular hollow section (CHS) members. The intersection of CHS members in which the prepared end of brace members are welded onto the undisturbed surface of the chord member is called a tubular joint. Tubular joints are subjected to wave induced cyclic loads and hence they are susceptible to fatigue damage due to the formation and propagation of cracks. Significant stress concentrations at the vicinity of the welds are highly detrimental to the fatigue life of a tubular connection. For the design purposes, a parameter called the stress concentration factor (SCF) is used to quantify the stress concentration. This calls for greater emphasis in accurate calculation of the SCFs to estimate the fatigue life of offshore structures.

The SCF, defined as the ratio of the local surface stress at the brace/chord intersection to the nominal stress in the brace, exhibits considerable scatter depending on the joint geometry, loading type, weld size and type, and the considered position for the SCF calculation around the weld profile. Critical positions along the weld toe of the brace/chord intersection for the calculation of SCFs in a tubular joint, i.e. saddle, crown, toe and heel.

In order to investigate the behavior of tubular joints and to easily relate this behavior to the geometrical characteristics of the joint, a set of dimensionless geometrical parameters has been defined. depicts tubular KT-joints with the geometrical parameters τ, γ, β, ζ, α, and α_B for chord and brace diameters D and d, and their corresponding wall thicknesses T and t. Geometrically speaking, KT-joint is one of the most common types of tubular joints which is also quite important, since the connection among the jacket leg and bracing members is usually in the form of a KT-joint.

As a result, many parametric design formulas in terms of the joint's geometrical parameters have been proposed providing SCF values at certain positions adjacent to the weld for several loading conditions. The reader is referred for example to Efthymiou [1] and Ahmadi and Zavvar [2].

In the present paper, results of a numerical investigation on the stress concentration in three-planar tubular KT-joints are presented and discussed. In this research program, a set of parametric finite element (FE) stress analyses was carried out on: Three-planar tubular KT-joints subjected to four different types of OPB loadings (Fig. 1).

The analysis results were used to present general remarks on the effect of geometrical parameters including τ, γ, β, and θ on the SCFs at the saddle, crown, toe, and heel positions. In order to study the multi-planarity effect under different types of OPB and IPB loadings, the SCFs obtained from three-planar joints, under each considered loading case, were compared with the SCFs extracted from the corresponding uniplanar connections. The main objective was to detect the critical cases in which the multi-planar SCFs are considerably higher than the corresponding uniplanar SCFs. In such case, the next step was to establish a new SCF parametric equation, based on nonlinear regression analyses, for the fatigue analysis and design. The applicability of proposed equation was evaluated according to the acceptance criteria recommended by the UK DoE [3].

2. Details of FE modeling and analysis

In this study, the welding size along the brace/chord intersection satisfies the AWS D1.1 [4] specifications. Details of weld profile modeling according to AWS D1.1 [4] have been presented by Ahmadi et al. [5].

ANSYS element type SOLID95 was used to model the chord, braces, and the weld profiles. These elements have compatible displacements and are well-suited to model curved boundaries. The element is defined by 20 nodes having three degrees of freedom per node and may have any spatial orientation. Using this type of 3-D brick elements, the weld profile can be modeled as a sharp notch. This method will produce more accurate and detailed stress distribution near the intersection in comparison with a simple shell analysis.

In order to guarantee the mesh quality, a sub-zone mesh generation method was used during the FE modeling. In this method, the entire structure is divided into several different zones according to the computational requirements. The mesh generated by this method for three-planar tubular KT-joints is shown in Fig. 2.

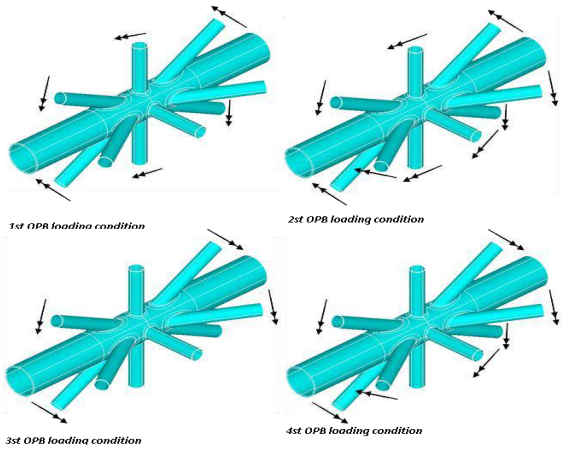

Fig. 1. Four considered out-of-plane bending (OPB) load cases applied to three-planar KT-joints

3. Effect of geometrical parameters on the three-planar SCFs

This section presents the results of investigating the effect of the β on the SCFs. In this study, the interaction of the β with the other geometrical parameters was also investigated. Fig. 3 demonstrates the change of SCFs due to the change in the value of the β and the interaction of this parameter with the γ. However, the amount of SCF change is not considerable. This conclusion is not dependent on the values of other geometrical parameters. It is also evident that, in spite of the parameter β, the parameter γ is quite effective in increasing the SCF values.

4. Parametric design equation for the SCF

The equation was derived based on multiple nonlinear regression analyses performed by the statistical software package, SPSS. Values of dependent variable (i.e. SCF) and independent variables (i.e. β, γ, τ, and θ) constitute the input data imported in the form of a matrix. Each row of this matrix involves the information about the SCF value at the critical saddle position in a three-planar tubular KT-joint having specific geometrical characteristics.

The objective was to investigate the effects of dimensionless geometrical parameters on the chord-side SCFs at the critical saddle position. As mentioned earlier, the other saddle positions were not studied, since at those positions, the multi-planar SCFs were either smaller or only marginally bigger than the corresponding uniplanar SCFs.

$$SCF = (0.888\tau^{1.318}\gamma^{0.926}\beta^{-1.007}\theta^{1.842})(0.008\gamma + 1.896\beta - 0.289\tau - 0.289\theta - 0.004\beta\tau) \quad ; \quad R^2 = 0.992 \tag{1-1}$$

5. Conclusion

In the present research, results extracted from the stress analysis of finite element models, verified against available experimental data, were used to study the chord-side SCFs in three-planar tubular KT-joints subjected to in-plane and out-of-plane bending loads. A geometrically parametric investigation was conducted and then followed by a set of nonlinear regression analyses to derive a SCF parametric equation for the fatigue analysis and design.

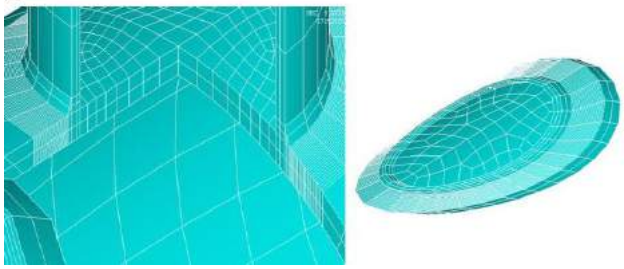

Fig. 2. The mesh generated by the sub-zone method for the region between the weld toe and the second extrapolation point

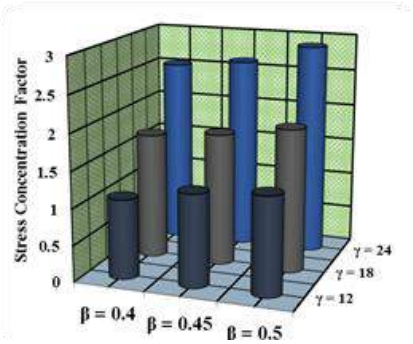

Fig. 3. Effect of the β on the SCFs at the critical saddle position in a three-planar KT-joint subjected to the 4th OPB loading condition: θ = 30°, τ = 0.4

6. References

[1] Efthymiou M. Development of SCF formulae and generalized influence functions for use in fatigue analysis. OTJ 88, Surrey, UK; 1988.

[2] Ahmadi H, Zavvar E. Stress concentration factors induced by out-of-plane bending loads in ring-stiffened tubular KT-joints of jacket structures. Thin-Walled Struct 2015; 91:82–95.

[3] UK Department of Energy. Background notes to the fatigue guidance of offshore tubular joints. London, UK; 1983.

[4] American Welding Society (AWS). Structural welding code: AWS D 1.1. Miami (FL), US; 2002.

[5] Ahmadi H, Lotfollahi-Yaghin MA, Aminfar MH. The development of fatigue design formulas for the outer brace SCFs in offshore three-planar tubular KT-joints. Thin-Walled Struct 2012; 58:67–78.

STATIC STRENGTH OF COLLAR PLATE REINFORCED TUBULAR T/Y-J0INTS SUBJECTED TO TENSILE LOADING

Hossein Nassiraei[1], Mohammad Ali Lotfollahi-Yaghin[2] and Hamid Ahmadi[3]

Faculty of Civil Engineering, University of Tabriz, Tabriz 5166616471, Iran
1) h.nassiraei@tabrizu.ac.ir; 2) lotfollahi@tabrizu.ac.ir; 3) h-ahmadi@tabrizu.ac.ir

1. Introduction

So far, some methods to enhance the static capacity of steel tubular joints have been introduced. Most of these techniques can only be used for structures during the design (e.g. joint can, ring, rack/rib, and doubler plate), But there are only a few methods which can be used during both design and service (e.g. collar plate and FRP). These methods can be valuable methods for such rehabilitation purposes in old and new structures. An existing tubular joint can be reinforced by introducing plates to the outside of the chord resulting in what is called collar plate reinforced joint.

In this study, a set of analyses was performed on 210 steel T- and Y-joint finite element (FE) models subjected to tensile brace loading. Also, failure mechanisms of the reinforced joints are investigated. Based on the results of collar plate reinforced T/Y-joints FE models which verified against experimental data provided by Choo et al. [3], a comprehensive ultimate strength database was prepared and finally through nonlinear regression analysis, a parametric equation was proposed.

2. FE strategy

2.1. Material nonlinearity

The chord, brace, and collar with a Young's modulus of 204 GPa and Poisson's ratio of 0.3 are used. Also, the yield stress of the chord, brace and collar are 300 N/mm^2, 464 N/mm^2, and 300 N/mm^2, respectively.

2.2. Modeling of weld profile

The geometry of the weld along the brace/collar plate intersection and between the collar plate and the chord surface follows the American Welding Society (AWS) recommendations [23].

2.3. Mesh generation procedure

In the present research, ANSYS element types SOLID186 was utilized to model the chord, brace, collar, and weld profile.

2.4. Contact modeling

Nonlinear contact, flexible-to-flexible surface-to-surface contact elements were used to simulate the interaction. The Augmented Lagrange method was used as the contact algorithm and the behavior of the contact surface was defined to be always bonded.

2.5. Analysis

A nonlinear static analysis was carried out to study the behavior of the joints.

4. Verification of FE results based on experimental data

In this paper, the FE software package ANSYS14.0 was utilized for the numerical modeling and analysis of collar plate reinforced and unreinforced T-joints under axially tensile load. The present FE model results were compared with experimental data performed by Choo et al. [1]. The details of validation phase are presented by the authors in Ref [2-4]. Results shown that the developed FE model can successfully predict the static strength of unreinforced and collar plate reinforced tubular joints under axially tensile load.

5. *Effect of the β on the initial stiffness, ultimate strength, and failure mechanisms*

Fig. 1 shows that the initial stiffness and ultimate strength for the joints with intermediate values of the β (say β = 0.5) are smaller than the corresponding initial stiffness and ultimate strength for the joints with big values of the β (say β = 0.6). Also, the initial stiffness for collar plate reinforced joints are bigger than the corresponding initial stiffness for unreinforced joints. Fig. 2 demonstrates the effect of the parameter β on the strength ratio depends on the dimension of the collar plate. Results show for the small values of collar plate size, the strength ratio values for the joints with big values of the β are a little smaller than the corresponding strength ratio values for the joints with intermediate values of the β. However, for intermediate values of collar plate size, both of these joints have the same strength ratio values. Moreover, for big values of the collar plate size, the strength ratio values for the joints with big values of the β are bigger than the corresponding ultimate strength ratio values for the joints with intermediate values of the β.

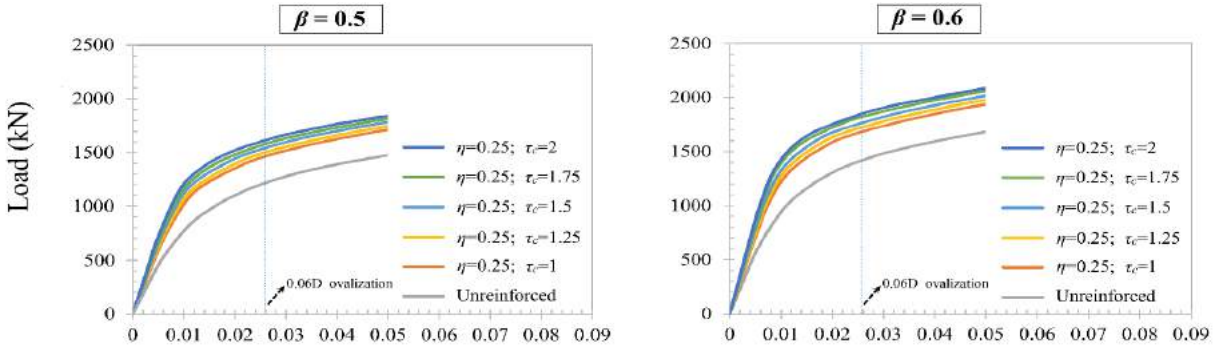

Figure 1. The effect of the β on the initial stiffness and ultimate strength values (θ = 45°, γ = 24, τ = 0.7))(τc= ratio of collar plate thickness to chord thickness; η=(collar plate length-brace diameter/sinθ)/brace diameter))

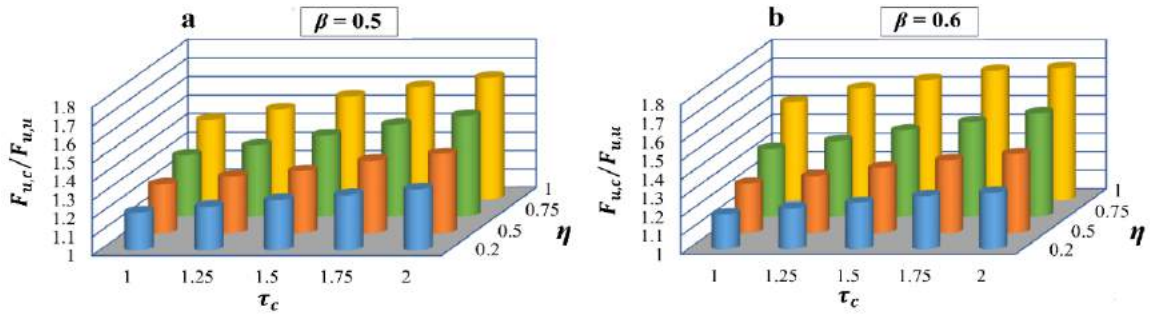

Figure 2. The effect of the β on the strength ratio values (θ = 45˚, γ = 24, τ = 0.7

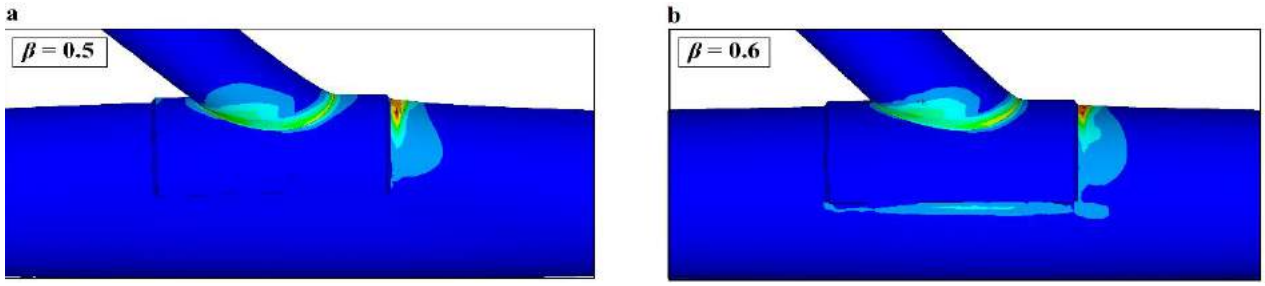

Figure 3. The effect of the β on the equivalent plastic strain. (τ_c = 1.5, η = 0.5, θ = 45˚, τ = 0.7, γ = 24).

Fig. 3 shows the equivalent plastic strain of two reinforced specimens with the different values of the parameter β about the same load (1943 kN). Fig. 13a and 3b show that for both of these joints, the maximum of plastic strain is observed in the vicinity of the toe of the weld between the collar plate and the chord surface.

6. Derivation of the strength ratio function

In the present study, an individual parametric equation is proposed for determining the ultimate strength ratio, i.e. the ratio of reinforced to unreinforced ultimate strength, for tubular T/Y-joints under brace tension.

$$F_{u,c}/F_{u,u} = 0.4\eta^{0.455}\tau_c^{-0.731}\beta^{-0.415}\gamma^{-0.674}\tau^{0.3}\theta^{0.065}(1-0.887\beta)$$
$$.(0.528-0.111\beta\tau)(1+2.854\beta)^{(1+\theta^{-0.059})}\tau_c^{(1-0.192\beta)}(\beta^{\tau}+\beta\gamma$$
$$+\gamma^{(1-0.019\beta-1.276\eta)}+\gamma^{(1-1.408\beta+0.217\theta-0.135\eta)}); \quad R^2 = 0.934 \qquad (1)$$

In Eq. (1), $F_{u,c}/F_{u,u}$ is the ultimate strength ratio of collar plate reinforced to unreinforced joint. The parameter θ in the equation should be inserted in radians. R^2 denotes the coefficient of determination and its value for the developed equation is considered to be acceptable regarding the complex nature of the problem. The validity ranges for the application of Eq. (1) are as follows:

$30^{\circ} \le \theta \le 90^{\circ}$; $0.4 \le \beta \le 0.6$; $0.55 \le \tau \le 1.0$, $12 \le \gamma \le 24$; $0.25 \le \eta \le 1.0$; $1.0 \le \tau_c \le 2.0$.

In Fig. 4, the ultimate strength ratios predicted by proposed equation are compared with the ultimate strength ratio extracted from FE analysis.

7. Conclusions

a) The initial stiffness of the collar plate reinforced joints are bigger than the corresponding initial stiffness of the unreinforced joints. Also, the increase of the collar plate length and collar plate thickness results in the increase of the initial stiffness and ultimate strength values.

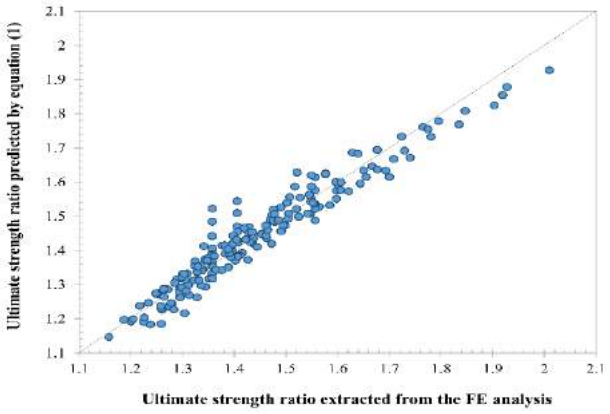

Figure 4. Comparison of the ultimate strength ratios predicted by the proposed equation (Eq. (1)) with the corresponding values extracted from FE analysis of 210 models)

b) A new design equation was proposed for predicting the strength ratio of collar plate reinforced to unreinforced tubular T- and Y-joints subjected to tensile brace loading.

References

[1] Choo YS, van der Vegte GJ, Zettlemoyer N, Li BH, Liew JYR. Static strength of T-joints reinforced with doubler or collar plates. I: Experimental investigations. Journal of Structural Engineering 2005;31(1):119–28.

[2] Nassiraei H, Lotfollahi-Yaghin MA, Ahmadi H. Static strength of offshore tubular T/Y-joints reinforced with collar plate subjected to tensile brace loading. Thin-Walled Structures 2016;103:141-56.

[3] Nassiraei H, Lotfollahi-Yaghin MA, Ahmadi H. structural behavior of tubular T/Y-joints with collar plate under static in-plane bending. . Journal of Constructional Steel Research 2016; 123: 121-34

[4] Nassiraei H, Lotfollahi-Yaghin MA, Ahmadi H. Static strength of collar plate reinforced tubular T/Y-joints under brace compressive loading. Journal of Constructional Steel Research 2016;119:39-49.

A STUDY ON THE LOCAL JOINT FLEXIBILITY (LJF) OF TUBULAR K-JOINTS IN JACKET SUBSTRUCTURE OF OFFSHORE WIND TURBINES UNDER AXIAL LOADING

Ali Ziaei Nejad[1], Hamid Ahmadi[2]

Faculty of Civil Engineering, University of Tabriz, Tabriz, Iran, a.ziyayinejad93@ms.tabrizu.ac.ir
Faculty of Civil Engineering, University of Tabriz, Tabriz, Iran, h-ahmadi@tabrizu.ac.ir

1. Introduction

In recent years, there is a strong trend to shift the wind farm activities to offshore. Offshore wind energy utilization has several attractions. A significant advantage of offshore wind energy is the stronger wind spectra which is stronger and steadier than the onshore wind energy (Li and Ren, 2010). Further, in comparison with the onshore wind turbines there is some different ways to installation offshore wind turbines (OWT) that using a jacket foundation is one of them. So because of some shortages in the marine regulations, knowledge of design techniques for jacket foundation has evidently come to sharp focus today. The local joint flexibility (LJF) in the analysis of tubular structures has been recognized as having an effect on the global static and dynamic responses of offshore structures for decades. This local deformation would lower the strength requirement on the joint by redistributing the member-end loads and moments compared with the conventional rigid joint. For this purpose, it is necessary to determine the local joint flexibility for tubular joints with a reliable method (Gao et al. 2013).

In the present paper finite element (FE) package ANSYS 16 is adopted to simulate the joint with 8-node solid element. An inclusive parametric study is subsequently conducted to investigate the effect of non-dimensional parameters on the LJF. The existing equations to determine LJF mainly focus on simple tubular joints such as T/Y-joint and simple gapped K-joint. These equations may not necessarily be appropriate for the case of two-planar DK-circular hollow section (CHS) joints. To study the behavior of tubular joints and to easily relate this behavior to the geometrical characteristics of the joint, a set of dimensionless geometrical parameters has been defined, as shown in Figure 1, to depict a two-planar DK-joint with the geometrical parameters. Eventually a comprehensive parametric equation to determine the LJF for two-planar DK-joint that is one of the most common joints in the jacket foundation of OWT and also is one of the most important design parameter for this legs subjected to axial loads is presented.

2. Determination of local joint flexibility coefficient

In the FE model, the local deformation at the intersection of chord and brace can be directly measured in the direction normal to the chord axis from the chord ovalization without considering the beam bending movement. It measures the distortion of the circular cross section which is an oval shape under axial loading. The LJF is determined by the local deformation at the crown toe, saddle and crown heel on the surface of the chord and the brace of the joint which subject to a unit compressive load at the end of the brace. Local joint flexibility coefficient (f_{LJF}) is introduced, which is non-dimensional and calculated by the LJF multiplied ED, where E is the young's modulus and D is the chord diameter. As shown in Figure 2, δ_1 and δ_3, and δ_2 and δ_4, are the respective deformations at the crown and the saddle measured perpendicular to the chord axis. The local joint flexibility coefficient of tubular joints under brace end axial load can be determined by equation 1.

$$f_{LJF} = \frac{\delta}{P}\sin\theta(ED) \tag{1}$$

Where P is the brace end axial load; θ is the angle between chord and brace; δ is the average local deformation normal to the chord axis and

$$\delta = \frac{\left(\delta_1 - \delta'_1\right)+\left(\delta_2 - \delta'_2\right)+\left(\delta_3 - \delta'_3\right)+\left(\delta_4 - \delta'_4\right)}{4} \tag{2}$$

3. Parametric study

A comprehensive parametric study is carried out in the current FE analysis of two-planar DK-tubular joints. To preclude the effect of the boundary conditions on the joint itself, the length parameters of α and α_B are set at 16 and 8 respectively and ζ is set at 0.3. In the current analysis, the Young's modulus (E) and the Poisson's ratio (ν) of steel material are assumed 200 kN/mm^2 and 0.3 respectively. The ranges of geometric parameters of the joint are limited as follows:

$$0.4 \le \beta \le 0.6$$
$$12 \le \gamma \le 24$$
$$0.4 \le \tau \le 1 \quad (3)$$
$$30^{\circ} \le \theta \le 60^{\circ}$$

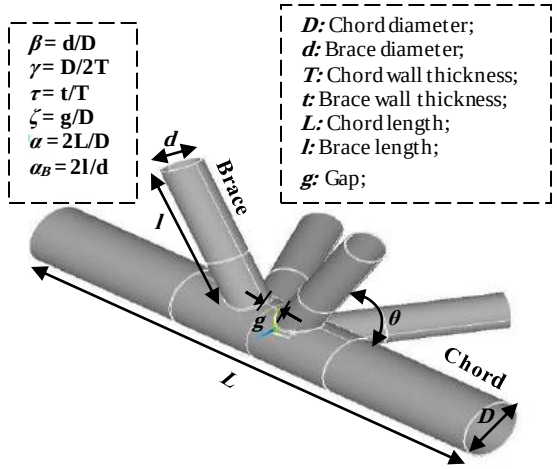

Figure 1. Geometrical notation for a two-planar DK-joint.

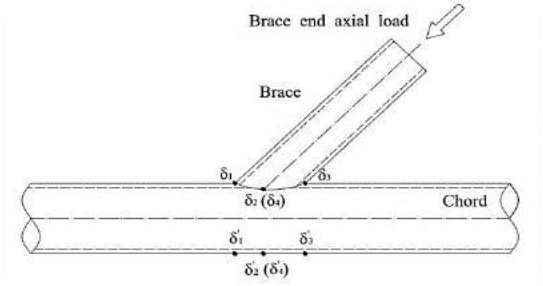

Figure 2. Points of measured deformation at joint.

3.1 Effect of brace-to-chord diameter ratio, β

The effect of β has been shown in Figure 3. As can be seen in this Figure the maximum f_{LJF} occurs at small β and large γ. At small γ, β shows insignificant influence on f_{LJF}. With the increase of β, the diameter of brace increases, which increase the contact area of chord and brace. Thus, the local deformation at the intersection of chord and brace decreases under brace axial loading.

4. Results and discussion

In this paper, the parametric equation is derived to predict the LJF for the two-planar DK-joint. The details of the LJF parametric equation for two-planar DK-tubular joint is listed in equation 4 with high coefficient of determination (R^2). In comparison with simple K-joint, as shown in Figure 5, it can be concluded that there is a Significant gaps between parameter of simple K-joint and two-planar DK-joint.

$$f_{LJF} = 0.0218766e^{\left[\left(\tau^{-0.153}\right)+\left(\beta^{-1.015}\right)+\left(\gamma^{0.486}\right)\right]}\theta^{1.71} \quad (4)$$
$$R^2 = 0.973$$

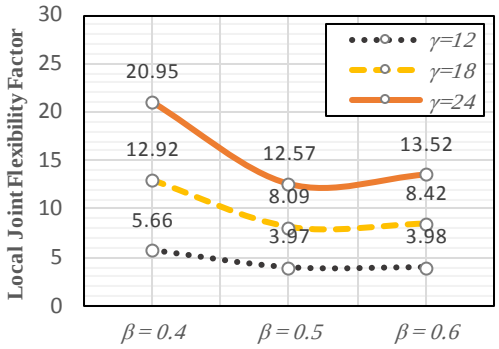

Figure 3. Effect of brace-to-chord diameter ratio, β

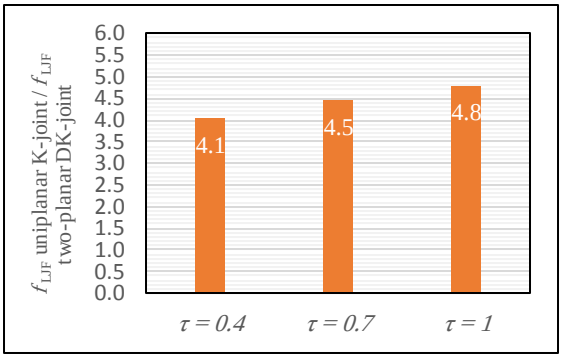

Figure 4. The ratio of f_{LJF} between uniplanar K-joint and two-planar DK-joint.

5. Conclusion

In this paper, the LJF of two-planar DK-joint under axial loading was studied. A total of 81 FE models were generated and analyzed. A comprehensive geometrically parametric study was carried out and based on the extracted data, a parametric equation was proposed for the computation of the LJF.

6. References

[1] Li, L., Ren, J. Offshore wind turbines and their installation. *In Innovative Computing and Communication, International Conference and Information Technology and Ocean Engineering (CICC-ITOE)*, Macao, China, 2010.

[2] Gao, F., Hu, B., Zhu, H. P. Parametric equations to predict LJF of completely overlapped tubular joints under lap brace axial loading. *Journal of Constructional Steel Research*, 2013, pp. 89, 284-292.

ESTIMATION OF VORTEX SHEDDING FREQUENCY AROUND PIPELINES VIA MULTI-RESOLUTION METHOD

Seyede Masoome Sadaghi[1], Seyed Taghi Omid Naeeni[2] and Hassan Yousefi[3]

1) Road, Housing and Urban Development Research Center. Ministry of Road and Urban Development, Tehran, Iran, s.sadaghi@bhrc.ac.ir
2) School of Civil Engineering, University of Tehran, Tehran, Iran, stnaeeni@ut.ac.ir
3) School of Civil Engineering, University of Tehran, Tehran, Iran, hyg_te@yahoo.com

1. Introduction

The vortex shedding from pipelines free span induces alternate hydrodynamic forces on the pipeline. The frequency of vortex shedding is of great importance in view of resonance phenomenon. Vortex shedding in oscillatory flows is more complicated because the near cylinder flow field has to rebuild itself twice per complete cycle as the velocity reverses direction. In this paper, vortex shedding in oscillatory flow has been studied via multi-resolution method in which wavelet transform has been applied on the lift forces to reveal vortex shedding in simultaneous time-frequency domain.

2. Vortex Shedding in Oscillatory Flows

Vortex shedding in oscillatory flows is a function of Keulegan-Carpenter (KC) number. The number of vortex shedding in each half cycle is directly related to the frequency of lift forces according to equation 1. [1].

$$f_v = (N+1)\, f_w \qquad (1)$$

in which N is the number of vortices per half cycle, f_v is the dominant frequency of lift force and f_w is the flow oscillation frequency. This formula is clearly valid for KC<25. However at larger KC values, this simple relationship can only be expected to yield approximate estimate of the overall average lift force frequency [2]. On the other hand, the flow visualization techniques are not easily applicable for investigation of vortex shedding regimes in large KC numbers which shows the necessity of seeking new methods.

3. Experimental Data

The present paper is based on force measurements on a circular cylinder oscillating in still water. The flow is in the subcritical regime with Reynolds number in the range of 9500-26000. The KC numbers for the present study are in the range of 15 to 40 and the cylinder is located at a distance equal to its diameter with respect to the plane bed [3].

4. Wavelet Analysis

Wavelet analysis is an efficient method for feature detection in flows with recognizable coherent structures due to its high resolution nature [4]. Every time a vortex is detached from the cylinder, a sudden change in form of a peak is expected in the lift force trend. The wavelet transform can reveal these peaks in a simultaneous time-frequency domain. The first peak in the wavelet coefficient is related to the return of the most recently shed vortex in the previous half cycle. The rest of the peaks are attributed to the vortex shedding. The number of vortices shed in each half cycle is counted accordingly. This is conceivable due to the simultaneous time-frequency representation of lift force variations by wavelet analysis. The wavelet coefficients for two sample KC numbers are shown in Figure 1 and Figure 2. The approximated numbers of vortex shedding in different KC numbers are compared with those estimated by previous works in Table 1 [1].

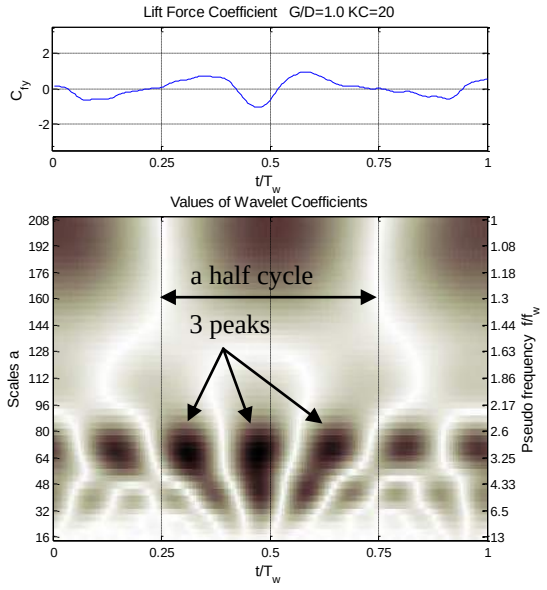

Figure 1. Wavelet coefficients of lift forces for KC=20

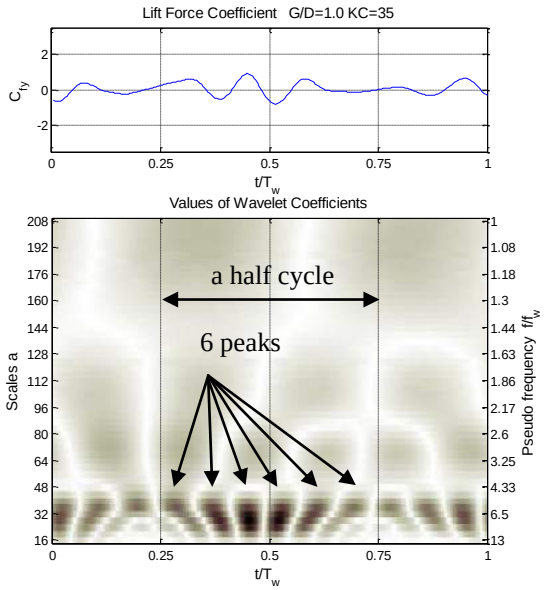

Figure 2. Wavelet coefficients of lift forces for KC=35

Table 1. Comparison of estimation of vortex shedding from former and present approaches

former studies		present study	
KC range	Vortices per half cycle	KC Number	Vortices per half cycle
7<KC<15	1	15	1
15<KC<24	2	20	2
24<KC<32	3	25	3
		30	4
32<KC<40	4	35	5
		40	6

5. Conclusion

Since for larger values of KC number (KC>25), the randomization in the formation and shedding of the vortices increase and flow visualization techniques are hardly applicable to accurately estimate the vortex shedding frequency, the wavelet analysis is proved to be an efficient alternative method to predict the vortex shedding in different flow conditions. The wavelet analyses show more vortex shedding in a half cycle for larger KC numbers in comparison with the estimations of former studies.

6. References

[1] Williamson, C. H. K. (1985), Sinusoidal Flow Relative to Circular Cylinders. J. Fluid Mech., 155, 141-174.

[2] Kenny, J. P. and partners Ltd. (1993), Evaluation of Vortex Shedding Frequency and Dynamic Span Response, Development of Guidelines for Assessment of Submarine Pipeline Spans, Background Document One, OTI93614, Published by Health and Safety Executive.

[3] Naeeni, S.T.O. (2003), Force on Yawed Circular Cylinder Oscillating over a Plane Bed in Current, PhD thesis, UMIST, Manchester, UK.

[4] Addison, P. S. (2002), The Illustrated Wavelet Transform Handbook, Introductory Theory and Applications in Science, Engineering, Medicine and Finance. Institute of Physics Publishing, Bristol and Philadelphia.

COMPARATIVE EVALUATION OF FIXED SUPPORT STRUCTURES FOR OFFSHORE WIND TURBINES IN THE PERSIAN GULF

Parisa Ghahhari[1], Mohammad Reza Bahari[2]

1) School of Civil Engineering, Faculty of Engineering, University of Tehran, Tehran, Iran, parisa_ghahhari@ut.ac.ir
2) School of Civil Engineering, Faculty of Engineering, University of Tehran, Tehran, Iran, mbahari@ut.ac.ir

1. Introduction

In recent years, a lot of attention is paid to the issue of reduction in the use of fossil fuels and utilization of renewable energy sources instead. Wind is one of the major sources of clean energy, which can be converted to electric power via wind turbines. It is proven that the effiency of offshore application of wind turbines is much higher than onshore ones. Therefore, the wind industry is heading through offshore. Yet, the challenging part is to select the most suitable support structure for the wind turbine. Currently, monopile is the most frequently used support structure. Application of this support structure is suitable in water depths less than 25 meters [1]. However, the development of offshore wind industry in deeper waters necessitates examining other types of support structures; because in further offshore, this type of structure may need to be of such dimensions that it becomes economically infeasible. Several studies have been conducted to investigate other configurations of support structures for different wind turbine capacities in different locations of Europe and U.S. such as [2, 3]. There is a clear lack of research in this area in Iran, although since 2012, one of the main research priorities of Renewable Energy Organization of Iran is concerned with offshore wind farms [4]. The goal of this study is to design, compare and evaluate different fixed support structures including monopile, tripod and jacket for a 5 megawatts wind turbine. The inplace, modal and fatigue analyses are conducted in SACS software for design purposes. The final designs of the structures are compared from different aspects and the most reliable structure to use in the Persian Gulf is introduced.

2. Definitions

Main parts of an offshore wind turbine structure are foundation, substructure, tower and turbine (including hub, nacelle and blades). Figure 1 schematically depicts a monopile, a tripod and a jacket including the main parts.

3. Design Basis

The required design inputs for an offshore wind turbine are as follows:

- Site specification data
- Wind turbine specifications
- Loading

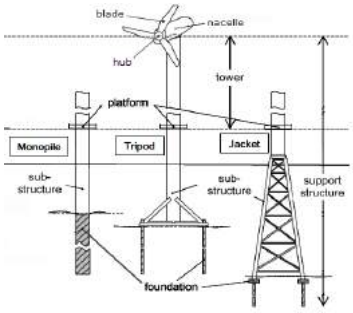

Figure 1. Monopile, tripod and jacket structures with their main parts [5]

As a reference location, Dorood region in the Kharg island district in Persian Gulf is selected. Sufficient soil and environmental data is readily available due to the vast offshore oil and gas projects done in this site.

As a reference wind turbine, the 5 megawatts NREL [6] offshore wind turbine is chosen. According to DNV [1], environmental loads acting on an offshore wind turbine include wind loads on the tower and turbine and hydrodynamic loads due to waves and currents. The horizontal force the turbine exerts on the approaching air flow to reduce its velocity is called thrust force. Equation 1 demonstrates the maximum value of the thrust force acting on the turbine.

$$F_{Thrust,Max} = \frac{1}{2}\rho_{air} A_{disk} V_0^2 (\frac{8}{9}) \quad (1)$$

Where ρ_{air} is the air density, A_{disk} is the area swept by the blades and V_0 is the rated wind speed. Note that all units are metric.

The wind drag force acting on the tower is calculated according to API standard [7]. To compute the hydrodynamic loads induced by waves and currents on slender cylindrical objects, the Morison equation is used.

4. Preliminary Design Process

To model the structure and conduct the necessary analyses, SACS software is used. Instead of modeling the turbine, the corresponding horizontal thrust force and weight force are applied. According to API [7] rules, the soil data is converted into nonlinear p-y, t-z and Q-z springs to model the soil lateral behavior, shaft friction and point resistance of the foundation pile, respectively.

The first step to design an offshore wind turbine's support structure is determining the design levels such as the

platform level. To compute the platform level, the following equation is used.

$$Z_{platform} = HAT + \Delta Z_{surge} + \Delta Z_{air} + 0.65H_{50-yr} \quad (2)$$

Where HAT is the highest astronomical tide, ΔZ_{surge} is the storm surge, ΔZ_{air} is the air gap and H_{50-yr} is the wave height with a 50-year return period.

The next step of the preliminary design process is to determine the structure natural frequency. To prevent resonance, the support structure should be designed such that its first natural frequency does not interfere with the excitation frequencies. In a three-bladed turbine, 1P and 3P stand for the rotation frequency of the rotor and the blades passing frequency, respectively. Given the turbine specifications, these frequencies are obtained. The most safe and economic structure design is achieved when the structure's first natural frequency lies between these two excitation frequencies. Herein, according to 1P and 3P values of 0.21 and 0.327 Hz, the value of 0.28 Hz is chosen as the optimized first natural frequency of the concerned structures. Therefore, the dimensions of the elements are determined such that the specified first natural frequency is gained. Subsequently, the inplace analysis is conducted to evaluate the strength of support structure members and the tower tip displacement under normal and extreme loading conditions.

Meanwhile, the penetration depth of the foundation piles is determined. The penetration depth is governed by several design criteria specified by DNV [1] and API [7] standards.

Afterwards, the spectral fatigue analysis is conducted to ensure that the critical joints are strong enough against wave-induced fatigue. To anticipate the fatigue damage and fatigue lifetime, the Miner's rule is used:

$$D_{fat} = \sum_{i=1}^{k} \frac{n_i}{N_i} \quad (3)$$

Where D_{fat} is the cumulative fatigue damage, n_i is the number of stress cycles in the *i*th stress block, N_i is number of cycles to failure at stress range of the *i*th stress block and k is the total number of stress range blocks.

The joints of the structures are strengthened whenever required and the fatigue analysis is repeated. This procedure continues until no joint fails in the structure.

5. Results

The results of the preliminary design are summarized in table 1.

To design a qualified monopile, the diameter of 6.5 meters and the penetration depth of 38 meters is required. Obviously, such dimensions make monopile a flexible structure in which the tower tip displacement is a point of concern. Special vessels and reliable tools such as grillage system, internal lifting tool, upending system, large sleeve, hammer and handling equipment are needed for monopile installation. Due to the incapability of Iran's rolling factories in manufacturing such large piles and absence of vessels and equipment here, it is economically infeasible to apply monopiles in Iran waters.

Table 1. The results of structures design

Design parameter	Structure type		
	Monopile	Tripod	Jacket
Pile diameter (m)	6.5	1.57	1.016
Penetration depth (m)	38	55	65
Total weight (ton)	1020	855	500
Tower tip displacement (cm)	93	68	78
The 1st natural frequency (Hz)	0.28	0.32	0.3

Strengthening of joints against fatigue damages leads to structures weight uprise of 28.6% in tripod. This demonstrates the high sensitivity of tripod to fatigue. Although possible, but it is costly to utilize the common vessels and equipment of offshore oil and gas industry to install tripods. Compared to the monopile, tripod is stiffer. The advantage of tripod over monopile is that its ordinary-sized foundation piles can be driven by more available and less costly hammers. As the final design shows, the proximity of tripod's first natural frequency to the excitation frequency makes this alternative less attractive. So, the application of tripod in the specific location defined in this study is not recommended. Considering high hydrodynamic transparency, jacket is much less affected by fatigue and the final design leads to a lighter and stiffer structure compared to the tripod. Concerning different stages of fabrication, transportation and installation of jackets in Iran, the presence of experience and trained work force increases the efficiency of the whole procedure. Eventually, selection of the most suitable substructure between these alternatives will be governed by factors such as technical feasibility, availability of vessels and equipment, fabrication capacity, fabrication yard facilities and attained experiences. Considering Iran's local capacity in aforementioned areas, jacket structure is introduced as the best choice to support the 5 megawatts NREL wind turbine in 30 meters water depth in Persian Gulf.

6. References

[1] Veritas, D. D. N. (2010). DNV-OS-J101 offshore standard. *Design of Offshore Wind Turbine Structures*.

[2] Subroto, H., de Vries, W., van der Tempel, J., Salzmanm, D. C., Krolis, V., & Haverkort, T. (2007). Mangrove: offshore wind energy in deeper waters.*Unedited report. sl: sn*.

[3] Fischer, T., De Vries, W. E., & Schmidt, B. (2010). *Upwind design basis (WP4: Offshore foundations and support structures)*. Upwind.

[4] www.suna.org.ir/

[5] Bontempi, F., Gkoumas, K., Manenti, S., & Petrini, F. (2009, May). Basis of design for offshore wind turbines. In Proceedings of the OWEMES 2009 Conference, Brindisi, Italy (pp. 21-23).

[6] Butterfield, S., Musial, W., & Scott, G. (2009). Definition of a 5-MW reference wind turbine for offshore system development.

[7] API, R. (2007). 2A-WSD 2007. Recommended practice for planning, designing and constructing fixed offshore platforms-working stress design.

SCALED BOUNDARY FINITE ELEMENT SOLUTION OF WAVE DIFFRACTION BY A VERTICAL CIRCULAR CYLINDER

Roozbeh Gohari[1], Keyvan Sadeghi[2]

1) Engineering Department, Hormozgan University, Bandar Abbas, Iran, roozbeh.gohari.67@gmail.com
2) Buein-Zahra Technical University, Buein-Zahra, Iran, keyvan.sadeghi@bzte.ac.ir

1. Introduction

Accurate prediction of wave forces acting on offshore structures is important for their design. The vertical circular cylinder is the common hull form in many offshore platforms. For relatively large cylinders wave forces are predicted by diffraction theory, whose boundary value problem (BVP) can be solved analytically or numerically. Experimental results [1] confirmed the analytical solution [2] for diffraction parameters less than 3. In that range, accurate numerical results have been obtained by various numerical methods such as finite element method (FEM) [3], boundary element method (BEM) [4] and scaled boundary finite element method (SBFEM) [5].

In this article, by using the scaled boundary FEM, velocity potential, wave run-up and wave excitation force per unit length are calculated and compared with the analytical results.

2. Introducing the Problem

A vertical circular cylinder extending from the seabed to the above of the free surface is subjected to plane progressive linear waves. The origin of coordinate system is at center of circular water-plane area with z-axis vertically upwards and x-axis in the direction of wave propagation. For cylinder diameters relatively large with respect to the wave length the flow can be assumed potential, governed by Laplace equation. Boundary conditions (BCs) are composed of no-penetration condition at the cylinder surface and the seabed, the common linear wave theory BC at the free surface and a radiation condition far away from the body ensuring that waves scattered by the body are outgoing. In deep water, the semi-unbounded problem domain is bounded by free surface in vertical direction. Using the separation of variables technique and the two BCs of vertical direction the 3-D BVP governed by Laplace equation can be reduced to a 2-D BVP with Helmholtz equation as the governing equation.

3. The Scaled Boundary FEM

The scaled boundary finite element method (SBFEM) is firstly introduced [6] in soil-structure interaction problems where the problem domain is semi-unbounded, although it can be used for bounded domains as well. This method is based on the use of a special coordinate system composed of a radial coordinate and one or two circumferential coordinates in 2-D or 3-D problems. The circumferential coordinates are used to discretize the boundary where the radial coordinate takes unity. The value of the radial coordinate is zero at origin and one at the whole points of the body boundary irrespective of the boundary shape and the origin acts as a scaling center, hence the names scaled boundary coordinates and the scaled boundary FEM. The scaled boundary FEM is a combination of FEM and BEM. Like in BEM the problem domain is only discretized at the boundary, however, instead of using a fundamental solution, the unknowns at discretized nodes are interpolated based on interpolation functions as in FEM. This leads to a semi-analytical formulation where the problem is reduced to an analytical system of ordinary differential equations in the radial direction whose coefficient matrices are obtained from a weighted integral weak formulation in the circumferential directions.

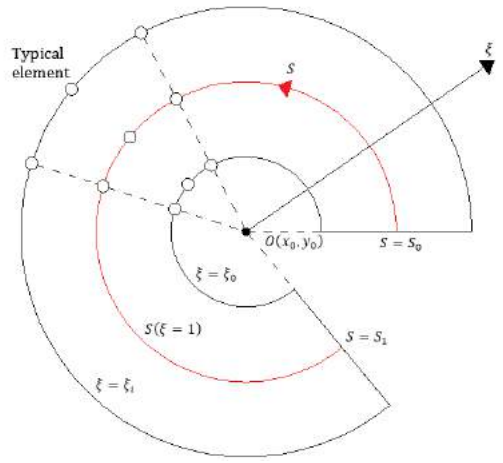

Figure-1. Scaled boundary coordinates

4. Numerical Results

In the present SBFEM scheme, the diffraction problem is solved for a cylinder with 2m radius with diffraction parameter ranging from 1 to 5. The circular boundary is discretized with three node quadratic elements. Due to the problem symmetry only half of the domain is considered. To discretize the half circle three meshes with 18, 24 and

50 elements are used. Numerical results are obtained for total velocity potential, wave run-up and the horizontal component of the wave excitation force per cylinder unit length. These results are shown in figures 2 to 4 where the computed values are compared with analytical solutions. It can be seen from figure 5 that the error in computations is small and for the fine mesh the error is less than 2 percent.

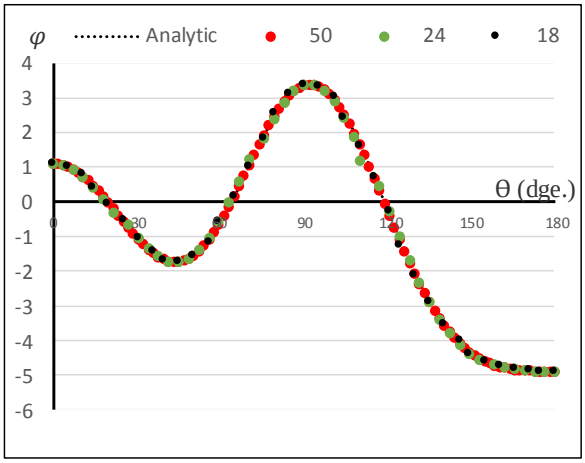

Figure 2. Velocity potential at nodes (kR=3)

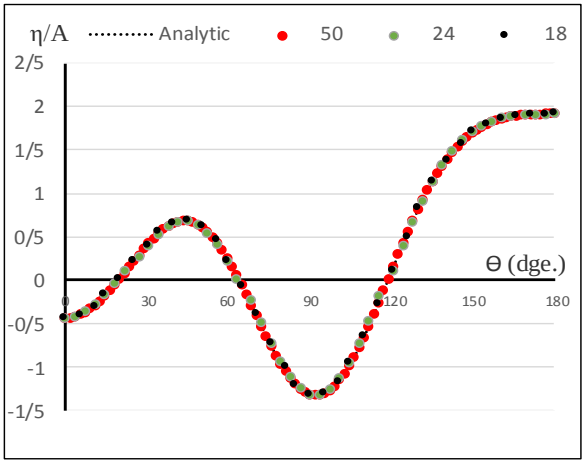

Figure 3. Wave run-up (kR=3)

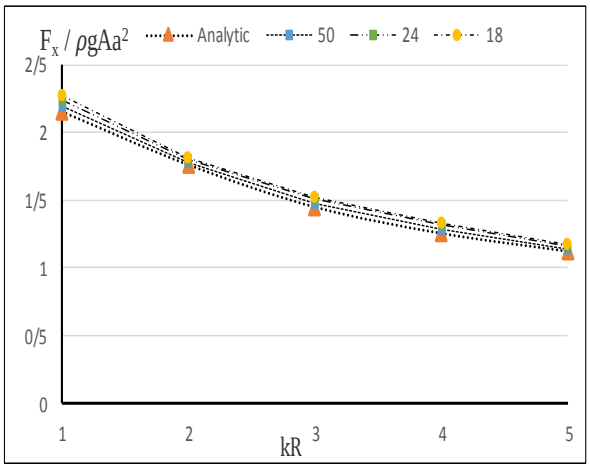

Figure 4. Horizontal component of wave force

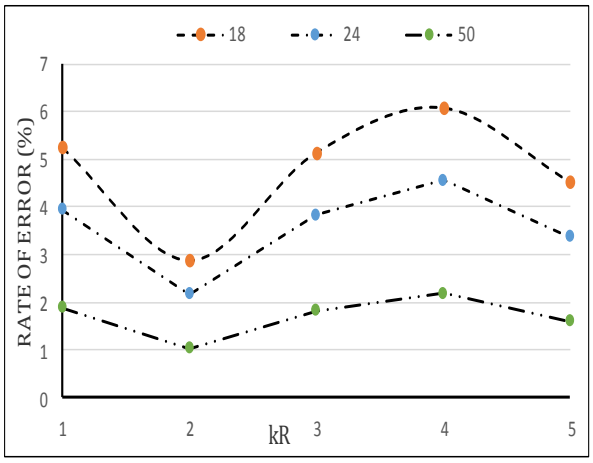

Figure 5. Computational error percentage

5. Conclusions

The semi-analytical scaled boundary finite element method is successfully applied to solve the wave diffraction by a vertical circular cylinder. The BVP is first reduced from 3-D to 2-D with Helmholtz equation as the governing differential equation. The 2-D BVP is then solved by SBFEM for diffraction parameters up to 5. The SBFEM formulation is derived based on a weighted residual approach. Comparisons with analytical solutions indicate that the utilized SBFEM scheme is accurate. The method is free from irregular frequencies often encountered by BEM. The method has the potential to be used to solve more complex wave-structure interaction problems.

6. References

[1] Chakrabarti, S. K., and Tam, W.A., "Interaction of waves with large vertical cylinders", *Journal of Ship Research*, 19, 1, 1975, pp. 23-33.

[2] McCamy, R C., and Fuchs, R. A., "Wave forces on piles: A diffraction theory", *U.S. Army Corps of Engineers, Tech. Memo. No.* 69, Washington D.C., 1954.

[3] Bettess, P., and Zienkiewicz, O. C., "Refraction and diffraction of surface waves using finite and infinite elements", *Int. J. Num. Meth. Eng*, 11, 1977, pp. 1271-1290.

[4] Au, M. and Brebbia, C., "Diffraction of water waves for vertical; cylinders using boundary elements", *Applied Mathematical Modelling*, Portland, 7, 2, 1983, pp. 106-114.

[5] Tao, L., Song, H., and Chakrabarti, S.K., "Scaled boundary FEM solution of short-crested wave diffraction by a Vertical Cylinder", *Comput. Methods Appl. Mech. Engrg*, 197, 2007, pp. 232-242.

[6] Wolf, J. P., *The Scaled Boundary Finite Element Method*, John Wiley and Sons Ltd, Chichester, England, 2003.

ESTIMATION OF NATURAL FREQUENCY OF OFFSHORE MONOPILE WIND TURBINES CONSIDERING FOUNDATION FLEXIBILITY AND TOWER MASS

Saeed Darvishi Alamouti[1], Mohammad Reza Bahaari[2] and Majid Moradi[3]

1) School of Civ. Eng., Faculty of Engineering, University of Tehran, Tehran, Iran, Saeed_darvishi@ut.ac.ir
2) School of Civ. Eng., Faculty of Engineering, University of Tehran, Tehran, Iran, mbahari@ut.ac.ir
3) School of Civ. Eng., Faculty of Engineering, University of Tehran, Tehran, Iran, mmoradi@ut.ac.ir

1. Introduction

With world effort focused on the reducing impact of greenhouse gases, wind (offshore or onshore) has been a serious contender for large-scale, cost-effective and clean source of energy. In offshore wind energy technology, monopiles are the most frequently used substructures to resist lateral cyclic loads produced by wind and waves [1]. Monopiles are the most common sub structure design, especially where turbines of rated capacity less than 5 MW are used in water depths of less than 30m [2]. In offshore wind turbines, support structures are highly sensitive to dynamic loading [3]. Thus, estimation of the structure natural frequency is an important design stage [4]. In offshore wind turbines, dynamic properties of the structural system are strongly influenced by the foundation stiffness, especially in monopile support structures [5]. The aim of this work is to provide an analytical estimation for the natural frequency of monopile supported offshore wind turbines using Rayleigh method. Foundation stiffness effect is simply considered as a rotational spring. Simple equations relating natural frequency to the structural parameters including mass and foundation stiffness are presented which are beneficial in the preliminary stages of the design.

2. Model Framework

The simplified structural model used in this study is illustrated in Figure 1. The rotor nacelle assembly *RNA* is modeled as a lumped mass *M* at the tower top. Tubular substructure (tower + monopile) is modeled as a beam with uniform bending stiffness *EI* and average mass per unit length *m*. Foundation is modeled as a rotational spring with the stiffness K_θ. Rayleigh method is utilized to estimate structure first natural frequency. The basic concept in this method is the principle of conservation of energy [6].

Maximum kinetic energy *K* and potential energy *V* and thereby natural frequency of the system *f* of the system are derived as:

$$V_{\max} = \frac{1}{2}\int_0^L mgu(x)dx + \frac{1}{2}Mgu(L) \tag{1}$$

$$K_{\max} = \frac{\omega^2}{2}[\int_0^L mu^2(x)dx + Mu^2(L)] \tag{2}$$

$$\Rightarrow (\frac{1}{2\pi}f)^2 = \omega^2 = g\frac{\int_0^L mu(x)dx + Mu(L)}{\int_0^L mu^2(x)dx + Mu^2(L)} \tag{3}$$

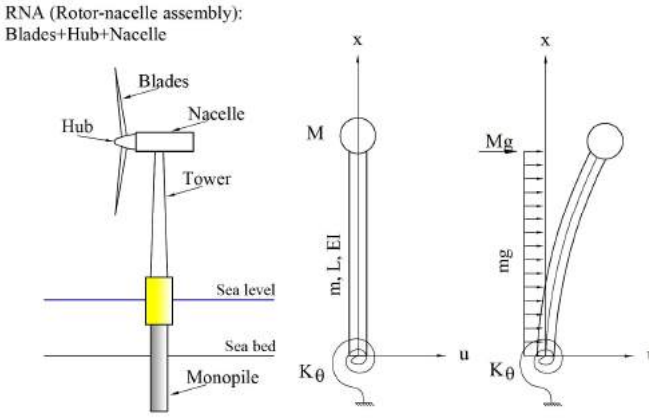

Figure 1. Simplified model for monopile offshore wind turbine

3. Fixed Based Model

In the first step, natural frequency of the system with fixed end boundary condition is derived. By applying the structure weight as lateral loading on the cantilever beam, deflection equation is calculated as follow:

$$\frac{mL}{M} = \alpha \rightarrow u(x) = \frac{Mgx^2}{24EI}[6(2+\alpha)L - 4(1+\alpha)x + \frac{\alpha x^2}{L}] \tag{4}$$

Then then natural frequency is derived using Equation 3:

$$f = \frac{1}{2\pi}\omega = \frac{1}{2\pi}\sqrt{\frac{1}{M}\frac{3EI}{L^3}\frac{8+6\alpha+1.2\alpha^2}{8+\frac{2208}{280}\alpha+\frac{104}{40}\alpha^2+\frac{104}{360}\alpha^3}} \tag{5}$$

$$\alpha << 1 \rightarrow f = \frac{1}{2\pi}\sqrt{\frac{1}{M}\frac{3EI}{L^3}\frac{1}{1+\frac{33}{140}\alpha}} \tag{6}$$

It is possible to examine error of ignoring tower mass *E1* and error of using simplified equation (Equation 6) *E2*.

$$E1 = \frac{f(\alpha=0)}{f(\alpha)} - 1 = \sqrt{\frac{8+\frac{2208}{280}\alpha+\frac{104}{40}\alpha^2+\frac{104}{360}\alpha^3}{8+6\alpha+1.2\alpha^2}} - 1 \tag{7}$$

Remarkable values of errors is anticipated at higher values of α if the tower mass ignored (Figure 2). The values of *E2* for α=1 is less than -0.022% which implies that simplified equation predicts well the natural frequency of OWTs where the ratio α is usually less than 1.

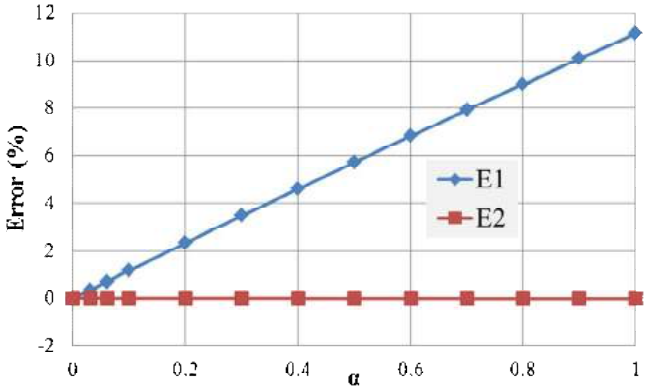

Figure 2. Expected errors E1: for neglecting tower mass, E2: for using simplified equation

4. Model with Flexible Foundation

For convenient, non-dimensional stiffness parameter is defined as:

$$\frac{k_\theta}{EI/L} = \beta \tag{8}$$

$$(\frac{1}{2\pi} f)^2 = \omega^2 = \frac{24EI}{ML^3} \times \frac{A}{B} = \frac{24EI}{ML^3} \times$$
$$\{8 + 6\alpha + 1.2\alpha^2 + \frac{6}{\beta}(2+\alpha)^2\} / \{64 + \frac{2208}{35}\alpha + ...$$
$$... \frac{104}{5}\alpha^2 + \frac{104}{45}\alpha^3 + \alpha[\frac{8\times 24}{\beta^2}(1+\frac{\alpha}{2})^2 + ... \tag{9}$$
$$... \frac{2\times 24}{\beta} \times \frac{33+13\alpha}{15}] + \frac{24^2(1+\frac{\alpha}{2})^2}{\beta^2} + \frac{48}{\beta}(1+\frac{\alpha}{2})(8+3\alpha)\}$$

$$\alpha = 0, \beta >> 1 \rightarrow f = \frac{1}{2\pi}\sqrt{\frac{1}{M}\frac{3EI}{L^3}\frac{1}{1+\frac{3}{\beta}}} \tag{10}$$

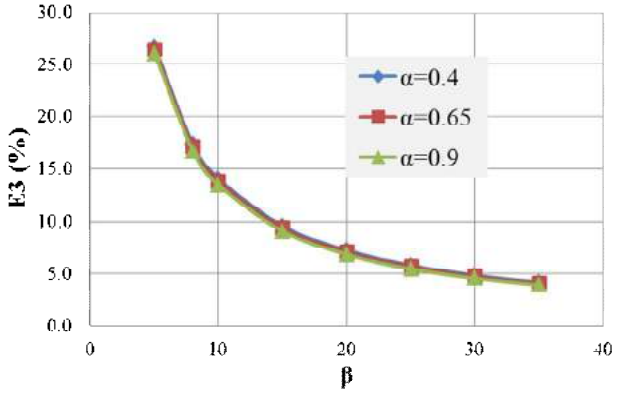

Figure 3. Expected error of estimating the first natural frequency caused by neglecting foundation stiffness

Now the Equation 6 and Equation 10 can be combined together to simply consider the effects of base flexibility and tower mass:

$$\alpha << 0, \beta >> 1 \rightarrow f = \frac{1}{2\pi}\sqrt{\frac{1}{M}\frac{3EI}{L^3}\frac{1}{(1+\frac{3}{\beta})(1+\frac{33}{140}\alpha)}} \tag{11}$$

It is possible to examine the effect of base flexibility on the natural frequency *E3* and the accuracy of the simplified equation *E4* by definition of the error functions. Figure 3 evaluates *E3* errors for different mass ratio α and stiffness parameter β for typical 2MW wind turbines found in the literature [7].

5. Conclusion

The first natural frequency of the monopile supported offshore wind turbines was estimated using Rayleigh method. The structure was modeled as a cantilever beam with concentrated top mass and distributed tower mass. Foundation flexibility was considered as a rotational spring with the stiffness depending on the soil-pile characteristics. Detailed and simplified equations were derived for the first natural frequency. By applying to real OWTs, it is shown that simple framework and derived equations predict the first natural frequency of monopile wind turbines accurate enough suitable for preliminary design stages. Tower mass could affect the natural frequency 4–12%. Foundation flexibility also alters the natural frequency about 4–27% for typical 2 MW OWTs. It is shown that a very simple equation that takes the tower mass and foundation stiffness into account could estimate the natural frequency with very acceptable accuracy.

6. References

[1] EWEA (2016) The European offshore wind industry - key trends and statistics 2015.

[2] Van der Tempel J and Molenaar DP (2002) Wind Turbine Structural Dynamics –A Review of the Principles for Modern Power Generation, Onshore and Offshore. Wind Engineering Vol. 26, NO. 4, 2002 PP 211–220

[3] Arany L, Bhattacharya S, Adhikari S, Macdonald John HG, Hogan S John (2015) An Analytical Model to Predict the Natural Frequency of Offshore Wind Turbines on Three-Spring Flexible Foundations using Two Different Beam Models. Soil Dyn Earthq Eng 2015;74:40–5

[4] DNV (2014) Design of Offshore Wind Turbine Structures. DNV-OS-J101, Det Norske Veritas, Oslo, Norway.

[5] Kühn M (1997) Soft or stiff: A Fundamental Question for Designers of Offshore Wind Energy Converters. In: Proceedings of the European wind energy conference. EWEC. 1997.

[6] Clough RW, Penzien J (2003) Dynamics of Structures. Computers & Structures, Inc.

[7] Bisoi S , Haldar S (2014) Dynamic Analysis of Offshore Wind Turbine in Clay Considering Soil–Monopile–Tower Interaction. Soil Dynamics and Earthquake Engineering 63(2014)19–35

STRESS CONCENTRATION FACTORS OF FRP WRAPPED TUBULAR T-JOINTS OF JACKET TYPE OFFSHORE PLATFORMS UNDER BRACE AXIAL LOADING

A. Sadat Hosseini[1], M. R. Bahaari[2] and M. Lesani[3]

1) School of Civil Engineering, College of Engineering, University of Tehran, P.O. Box 11155-4563, Tehran, Iran, a.sadat@ut.ac.ir
2) School of Civil Engineering, College of Engineering, University of Tehran, P.O. Box 11155-4563, Tehran, Iran, mbahari@ut.ac.ir
3) School of Civil Engineering, College of Engineering, Sadra University, P.O. Box 14875-314, Tehran, Iran, m.lesani@sadra.ac.ir

1. Introduction

Due to the cyclic nature of wave loading on offshore structures, care must be given to their fatigue resistance. Fatigue life of offshore jacket joints is calculated using a parameter called stress concentration factor (SCF). SCF can be computed in un-stiffened and stiffened joints. In un-stiffened joints, many researchers did efforts since the 70s and their main objective was to derive parametric equations for SCF calculation. Ahmadi and Lotfollahi-Yaghin [1] have performed recent studies in this field.

There are some metallic-based methods which are used for strengthening CHS joints in order to decrease the SCF. Lesani et al. [2] reviewed some of these strengthening techniques. There are also some non-metallic external reinforcement schemes such as FRP strengthening method. FRP wrapping method due to its convenience for handling and application, corrosion resistance, potentially high overall durability, light weight, superior strength-to-weight ratio and high specific performance attributes could be easier for application in areas in which using conventional materials may not be feasible due to durability, weight or lack of design flexibility constraints. Lesani et al. [2] reviewed the studies in which this non-metallic reinforcement technique is used. Lesani et al. [2-4] numerically and experimentally studied the performance of this technique on the static strength of steel tubular T and Y-joints. According to these studies, it would be necessary to investigate SCF improvement using the FRP wrapping technique. This paper is aimed to present the relevant findings of such investigations.

2. FE Modeling

All the T-joints in this study have similar un-stiffened geometry which was chosen from JISSP [5], with different FRP materials. They were subjected to axial load applied on top of the brace member. Here in this study, three various types of common FRP materials are used as strengthening material. Table 1 demonstrates the properties of the FRP materials used in the analyses. In this table, subscripts ''1'' and ''2'' stand for the fiber longitudinal and transverse directions respectively.

Table 1: FRP properties [7]

	Glass/ Vinylester	Glass/Epoxy (Scotch ply 1002)	Carbon/Epoxy (T300-5208)
E_1 (Mpa)	28000	38600	132000
E_2 (MPa)	7000	8270	10800
v_{12}	0.29	0.26	0.24
G_{12} (MPa)	4500	4140	5700
G_{13} (MPa)	4500	4140	5700
G_{23} (MPa)	2540	3100	3400

In order to achieve accurate stresses along the chord-brace intersection, the weld profile is modeled accurately as addressed in AWS [8]. Figure 1 shows the weld profile section used in finite element model.

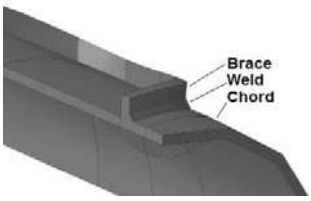

Figure 1. Section of the T-joint including the weld profile

In this study, ABAQUS [9] software package is used for analyses and 3D brick elements (C3D20) are incorporated to model the joint geometry and weld profile. FRP material is modeled using shell elements (S4R) defined as a skin layer on the joint. Different sub-zone mesh generation methods was used for the weld profile, hot spot stress region, FRP wrapping area and other regions of the joint. Here, chord ends were fully restrained (fixed) to represent the actual boundary conditions of the experiment. In order to determine the stress concentration factors in a tubular joint, a linear elastic numerical analysis needs to be performed [10]. The Young's modulus and Poisson's ratio of steel are taken as 207 GPa and 0.3, respectively [5]. To estimate the SCFs, the method introduced by IIW-XV-E [11] is implemented.

In order for validation of the finite element model, Lloyd's Register equations [5] and API [6] equations for

SCF computation together with the test results published in HSE OTH 354 report [5] for JISSP joint "1.3"were used. Table 2 summarizes the verification results at the saddle and crown points. In this table, e_1 and e_2 show the percentage of relative difference of Lloyd's Register [5] and API [6] equations with test results respectively, and e_3 denotes the percentage of relative difference between the results of finite element model and the experiment results. According to Table 2, it is obvious that the finite element model predicts the SCFs at crown and saddle points accurately which is in good agreement with the test results and therefore, the FE model is validated.

Table 2. Comparison of finite element results with experimental data and predictions of LR [5] and API [6] equations.

Position	Test	LR Eq.	API (2014) Eq.	FE	e_1 (%)	e_2 (%)	e_3 (%)
Crown	5.4	3.94	3.85	5.3	27.0	28.7	1.9
Saddle	11.4	10.54	12.13	11.1	7.5	6.4	2.6

3. Parametric Study

Due to the symmetry of stress distribution in a T-joint, results are presented along a 90 degree polar angle (a quarter of Chord-Brace intersection zone) which starts from the Crown point to the Saddle point.

Figure 3. Numerical model of a FRP wrapped T-joint

The three FRP materials with fibers oriented at 0^o (Chord hoop direction), 1 mm in thickness and relative length equal to one times the diameter of the chord member for chord wrapping and one time the diameter of the brace member for brace wrapping. Figure 4 presents the effect of FRP material variation on SCF values for the strengthened T-joint. According to Figure 4, higher mechanical properties of FRP strengthening material lead to more decrease in SCFs. In addition, the maximum effectiveness of FRP strengthening material in SCF reduction is observed at the saddle point, while the least effect is at 30^o polar angle of chord-brace intersection zone. This effectiveness is attributed to the 1mm FRP composed of Carbon-Epoxy material and 0^o fiber orientation and is about 10 percent at the saddle point.

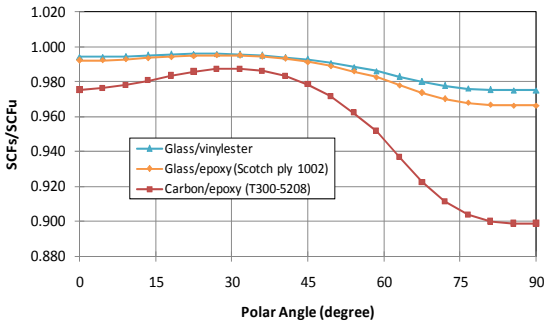

Figure 4. Ratio of SCF distribution in FRP strengthened tubular T-joint with different FRP materials to SCF distribution in un-stiffened joint (Horizontal axis: polar angle from chord to saddle position)

4. Conclusion

Use of FRP material with higher values of mechanical properties shows more effectiveness on decreasing the SCF values. Using carbon-epoxy material has effectiveness of about three times GFRP material in decreasing SCF values in the saddle point. Due to better fatigue performance of CFRP materials in comparison to other materials such as GFRPs, and also better performance of CFRPs in reducing SCF values specially in the saddle region, as per the findings of this study, it would be beneficial to use CFRP as wrapped strengthening material to extend the fatigue life of tubular joints.

5. References

[1] Ahmadi H., Lotfollahi-Yaghin M. A., Stress concentration due to in-plane bending (IPB) loads in ring-stiffened tubular KT-joints of offshore structures: Parametric study and design formulation, *Applied Ocean Research*, 2015; 58: 54-66.

[2] Lesani M., Bahaari M. R., Shokrieh M. M., Numerical investigation of FRP-strengthened tubular T-joints under axial compressive loads, *Composite Structures*, 2013; 100: 71–8.

[3] Lesani M., Bahaari M. R., Shokrieh M. M., Experimental investigation of FRP-strengthened tubular T-joints under axial compressive loads, *Construction and Building Materials*, 2014; 53: 243–52.

[4] Lesani M., Bahaari M. R., Shokrieh M. M., FRP wrapping for the rehabilitation of Circular Hollow Section (CHS) tubular steel connections, *Thin-Walled Structures*, 2015; 90: 216–234.

[5] Health and Safety Executive (UK). OTH 354: Stress concentration factors for simple tubular joints – assessment of existing and development of new parametric formulae, *Lloyd's Register of Shipping*, 1997.

[6] API (American Petroleum Institute), Recommended practice for planning, designing and constructing fixed offshore platforms – working stress design, *API RP 2A WSD*, 22nd edition, November 2014.

[7] Ganesh V. K., Naik N. K., Some strength studies on FRP laminates. *Journal of Composite Structures*, 2005;24, 1993: 51–8.

[8] AWS (American Welding Society), Structural welding code, AWS D 1.1:2010 (22nd Edition). Miami FL (USA): *American Welding Society*, 2010.

[9] ABAQUS/CAE Standard user's manual-Version 6.14-1, 2014.

[10] N'Diaye A, Hariri S, Pluvinage G, Azari Z. Stress concentration factor analysis for notched welded tubular T-joints, *International Journal of Fatigue*, 2007; 29:1554–70.

[11] IIW-XV-E. International institute of welding sub-commission XV-E, recommended fatigue design procedure for welded hollow section joints. IIW Docs. XV-1035-99/XIII-1804-99, *International Institute of Welding*, France; 1999.

USE OF OPENFOAM® IN OFFSHORE ENGINEERING FOR WAVE-STRUCTURE AND WAVE-STRUCTURE-SOIL INTERACTIONS

Hisham Elsafti[1]; Lisham Bonakdar[2] and Hocine Oumeraci[3]

1) PhD, Leichtweiss-Institute, TU Braunschweig, Brunswick, Germany, h.el-safti @tu-braunschweig.de
2) PhD, Leichtweiss-Institute, TU Braunschweig, Brunswick, Germany, l.bonakdar@tu-braunschweig.de
3) Professor, Leichtweiss-Institute, TU Braunschweig, Brunswick, Germany, h.oumeraci@tu-braunschweig.de

1. Introduction

The OpenFOAM®[1] toolbox is an open source software package mainly aimed at CFD simulations. Nevertheless, the high abstraction and modularity of OpenFOAM enables its use as a generic tool for the numerical solution of any set of PDEs, and thus providing a huge potential for studying multi-physics problems. Recently, OpenFOAM has gained a great momentum in coastal and offshore engineering applications with the publication of the *waves2Foam* [1] toolbox for wave generation and absorption in OpenFOAM.

In this paper, the new developments in OpenFOAM to construct a model system for studying wave-structure and wave-structure-soil interaction. The application of this model system to reliably study selected offshore structures in combination with physical model tests is also shown. Finally, recommendations and outlook for the use of OpenFOAM as a numerical wave tank are given.

2. Hydrodynamic Modelling and Wave-Structure Interaction

The CFD solver (*waveVolAvgPorousInterFoam*) is an extension of the incompressible multiphase Eulerian solver of OpenFOAM with *waves2Foam* support and by introducing different seepage laws for non-deformable porous media. Moreover, a term is added in the continuity equation to account for elastic fluid compressibility as volume change. The extended CFD model is successfully applied to reproduce measured breaking wave impact loads including the effect of entrapped air [2].

Further, a hybrid 2D-3D CFD model is developed to provide realistic water waves through coupling *waves2Foam* with other far-field hydrodynamic models. In the hybrid model approach, a one-way link is established between a model for the far-field and another one for studying the fluid-structure interaction in the near field [3]. An overlap zone is introduced to both models, in which fluid kinematics and surface elevation are sampled from the far-field model and introduced via a relaxation function to the overlap zone in the near-field model. In the 3D model, the use of a relaxation approach provides absorption for reflected waves from the structure.

[1] OpenFOAM is a registered trademark of OpenCFD Ltd.

3. Modeling Wave-Structure-Soil Interaction

A new hydro-geotechnical solver (named *geotechFoam*) is developed in [2] to solve the fully coupled, fully dynamic Biot equations. A new approach to solve these equations is implemented taking advantage of the segregated approach and using the PISO algorithm to resolve pore fluid velocity-pressure coupling. Soil-structure interaction is introduced via a frictional contact model that can simulate sliding, separation and reattachment of the structure and the underlying soil. A multi-surface plasticity model is implemented to reproduce the most relevant aspects of the response of the soil beneath a monolithic breakwater (e.g. cyclic mobility). The model is validated against benchmark cases, analytical solutions and laboratory experiments, including one-dimensional consolidation and fluid injection, two-dimensional direct wave loading on seabed, seismic loading of a liquefiable embankment and a plate rocking on a submerged sand box. The model succeeded to reproduce measured wave-induced residual pore pressure buildup and soil densification followed by pore pressure dissipation. A one-way coupling of both CFD and CSD models is implemented, which transforms the CFD model output into input for the CSD model.

4. Combined Use of Numerical and Physical Modelling Approaches

The successful use of numerical modelling as a complementary tool to physical modelling is illustrated via two applications in offshore engineering. The first application is the study of wave-pile group interaction. The second is the study of wave-structure-soil interaction for marine gravity structures. The development of the numerical models aims at reproducing reliably the salient physical processes observed in physical tests. Hence, the models are used to further enhance understanding and interpretation of the physical processes and interactions. Moreover, the models are used to develop simplified empirical relations for practical engineering applications.

4.1. Wave-Pile Group Interaction

The hybrid 2D-3D CFD model system [3] is used to extend the small and large scale laboratory tests conducted in the wave flume of Leichtweiss-Institute (LWI) in

Braunschweig and the Large Wave Flume (GWK) in Hannover, respectively and described in [4]. The numerical model is validated (Fig. 1) and being used to for a systematic parameter study with a focus on the effect of parameters which could not be physically investigated within the fame work of the abovementioned laboratory models.

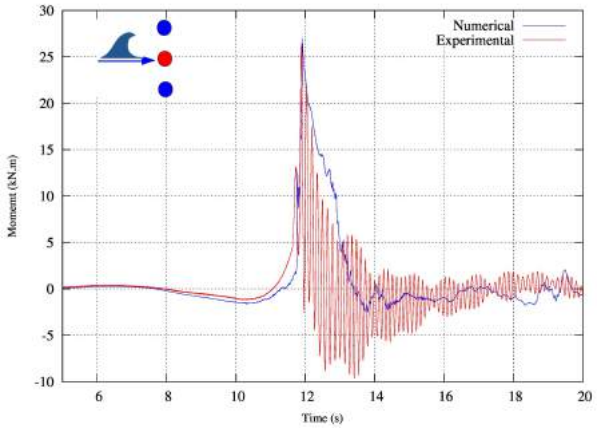

Figure 1. Validation of the hybrid 2D-3D CFD model system with large-scale tests [3].

4.2. Marine Gravity Structures

The semi-coupled CFD-CSD model system is applied successfully to reproduce selected results of a caisson breakwater subject to breaking wave impact loads tested in the Large Wave Flume (GWK). Moreover, the model system is applied to expand the range of conditions tested in GWK for the response of the soil foundation, with a particular focus on the role of transient and residual pore pressure on residual deformations of soil and subsequent residual displacements of the structure. Hence, the toolbox was used successfully to study the stepwise failure of marine gravity structures based on observed relevant physical processes that was reproduced by the model system. This failure mode is associated with plasticity behaviour of the seabed under cyclic loads exerted by the weight of marine structures.

The numerical model system was used in combination with the physical test results to develop the *relative load eccentricity concept* to classify and to interpret stepwise failure of marine gravity structures and develop a simplified dynamic model for engineering use that is validated against the large-scale physical model tests from [5].

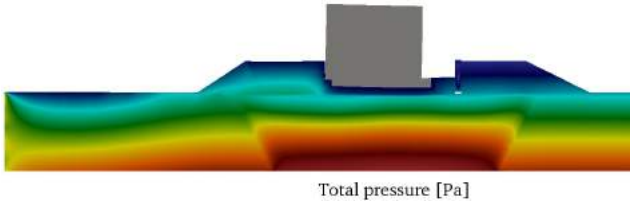

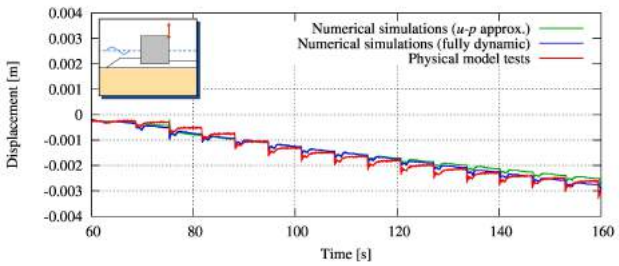

Figure 2. Validation of the CFD-CSD model system with large-scale caisson breakwater physical model [2].

5. Summary and Outlook

OpenFOAM has a great potential for the use in offshore engineering, not only as a CFD tool but also as a complete platform for wave-structure and wave-structure-soil interaction. Recommendations for the application of the toolbox and directions for future developments are drawn from the lessons learned in the process of developing, validating and applying the model system to offshore structures.

Acknowledgment

The authors would like to thank the German Academic Exchange Service (DAAD) for providing financial support for the doctoral studies of the first and second authors. Additionally, the authors would like to thank the German Research Foundation (DFG) for financial support of the WaPiGS (Breaking and Non-Breaking Wave Load on Pile Group-Supported Marine Structures - Knowledge Generation and Model Development) research project (DFG Ou 1/13-1 & DFG Ou 1/13-2).

References

[1] Jacobsen, N. G., Fuhrman, D. R., and Fredsøe, J., "A Wave Generation Toolbox for the Open-Source CFD Library: OpenFoam®". *Int. J. Numerl. Meth. Fluids*, 70(9), 2012, pp. 1073–1088.

[2] Elsafti, H., "Modelling and analysis of wave-structure-foundation interaction for monolithic breakwaters." Ph.D. thesis, *TU Braunschweig,* 2015, Germany.

[3] El Safti, H., Bonakdar, L., and Oumeraci, H., "A hybrid 2D-3D CFD model system for offshore pile groups subject to wave loading." *proceedings of the 33nd International Conference on Ocean, Offshore and Arctic Engineering*, San Francesco, California, USA, 2014, Paper No. OMAE2014-23636

[4] Bonakdar, L., "Pile group effect on the wave loading of a slender pile". PhD thesis, *Technische Universität Braunschweig*, 2014, Germany (ISBN 978-3-86948-383-2).

[5] Kudella, M., Oumeraci, H., De Groot, M., and Meijers, P., "Large-scale experiments on pore pressure generation underneath a caisson breakwater." *Journal of Waterway, Port, Coastal, and Ocean Engineering*, 2006, 132(4), 310–324.

NUMERICAL MODELING OF WAVES ATTENUATION BY USING AIR BUBBLES AND STUDY OF THE BUBBLES EFFECTS ON WAVES DESCRIPTION WITH DIFFERENT WAVELENGTHS

Mojtaba Shegeft[1], Madjid Ghodsi Hasanabad[2] and Mojtaba Ezam[3],

1) MS, Department of Marine Science and Technology, Science and Research Branch, Islamic Azad University, Tehran, Iran, sh_mojtaba@yahoo.com
2) Assistant professor, Department of Marine Science and Technology Science and Research Branch, Islamic Azad University, Tehran, Iran, m.ghodsi@srbiau.ac.ir
3) Assistant professor, Department of Marine Science and Technology Science and Research Branch, Islamic Azad University, Tehran, Iran, m.ezam@srbiau.ac.ir

1. Introduction

In this paper, air bubble breakwater was investigated by 2D modeling. Finite volume method and Ansys Fluent software were used to analyze air bubble breakwater. With regard to the advantages of the breakwater and its good compatibility with environment and its high performance, further study in this field is necessary. The problem is Laboratory works in this field are expensive. Besides, the experimental results and the numerical results of this research were in good accordance. Therefore, it can be concluded that the present numerical method is convenient for air bubble breakwater modeling. In this model the Stokes fifth order equations, the continuity and momentum equations were selected as the governing equations. Also, the interaction between water and air was analyzed with the VOF method.

Air bubble backwater is one of the new methods of breakwaters. Wave energy can be attenuated by air bubble .it can be used instead of some structures which are able to reflect or absorbing wave energy. This breakwater does not need so much space and it does not have negative effects on shipping. This device is installed under the sea level so that it is hidden.

Phillip Brasher was the first one who introduced a method for attenuating waves by forcing compressed air through a submerged perforated pipe in 1907 [1].a Lot of laboratory studies have been done between 1930 and 1950. One of the most significant advances during this period was the development by Taylor [2, 3]. In 1949 Leonard I, did some laboratory studies in the hydrodynamic laboratories California institute of technology. According to his investigation, one aspects of the effectiveness of a single or repeated air bubble screen as a breakwater for gravitational waves in shallow water were considered [4]. So far a lot of laboratory studies have been done however, there aren't enough numerical studies in this field as a result it seems that doing valid study is essential.

2. Numerical model

This device consists of a perforated pipe, usually on the harbor floor, through which compressed air is forced. As the air bubbles rise they move and drag water particles in an upward motion. When this mixture reaches the surface, the air escapes, while the flow of water branches into two horizontal currents, the turbulence induced by this system produces some attenuation of the waves.

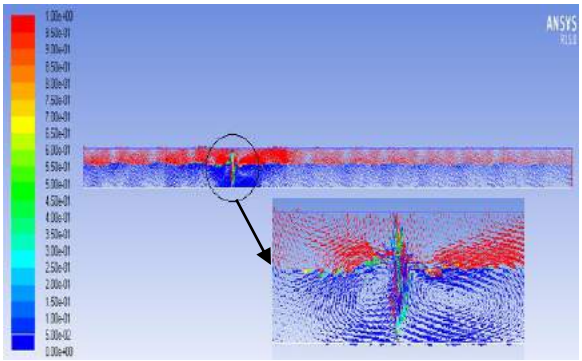

Figure 1. The pattern of velocity vector

For verification of the numerical results we compared them with the Experimental studies which have done by Lorenz G. and his colleagues in ST. Anthony falls hydraulic laboratory [5]. The length of numerical model and the wave parameters and the air amounts are the same as the experimental case.
In the numerical model, Flap type wave generator has been used for making waves with different wavelengths. The wave tank was 0.5 m deep, the depth

of water was 0.3 m, the wave lengths were 0.9, 0.74, 0.85 and the wave steepness was 0.04 m during numerical simulation.

Table 1. The results of numerical simulation (wave length 0.74 m)

Unit Discharge in (m^3/s.m) free air	Wave Steepness (m)	Wave length (m)	attenuation
0.001132	0.04	0.74	0.66
0.000906	0.04	0.74	0.59
0.000708	0.04	0.74	0.53
0.000425	0.04	0.74	0.32

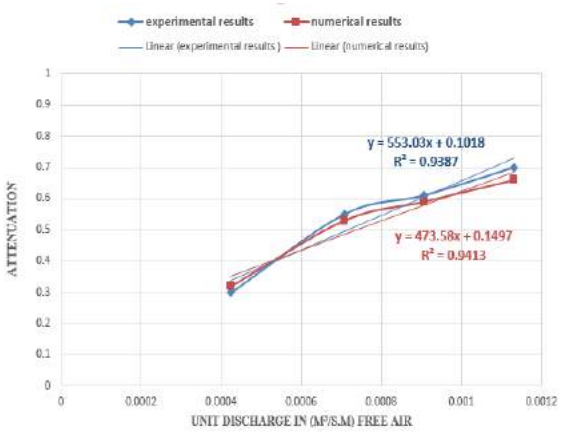

Figure 2. The comparison of wave attenuation between experimental and numerical simulation (Wave length 0.74 m)

Figure 2 show the comparisons of attenuation between experimental and numerical results as u can see the experimental results and numerical results of this research were in good accordance.

3. Mathematics

The generalized expression for wave profile for higher order Stokes theories (second to fifth order) is

(1)

$$\xi(X,t) = A\cos\alpha + A^2\mathrm{k}(b_{22} + A^2k^2b_{24})\cos 2\alpha + A^3k^2(b_{33} + A^2k^2b_{35})\cos 3\alpha + A^4k^3b_{44}\cos 4\alpha + A^5k^4b_{55}\cos 5\alpha$$

The wave frequency ω is defined as

(2)

$$\omega = [gk(1 + A^2k^2c_3 + A^4k^4c_5)\tanh kh]^{1/2}$$

The equation for conservation of mass, or continuity equation, can be written as follows:

(3)

$$\frac{\partial\rho}{\partial t} + \frac{\partial}{\partial x_i} + +(\rho u_i) = S_m$$

The momentum equation was the same with the Reynolds averaging in form as shown in Eq.4.

(4)

$$\frac{\partial}{\partial t}(\rho u_i) + \frac{\partial}{\partial x_j}\left(\rho u_i u_j\right) = -\frac{\partial p}{\partial x_i} + \frac{\partial}{\partial x_j}\left[\mu\left(\frac{\partial u_i}{\partial x_j} + \frac{\partial u_j}{\partial x_i} - \frac{2}{3}\delta_{ij}\frac{\partial u_l}{\partial x_l}\right)\right] + \frac{\partial}{\partial x_j}\left(-\rho\overline{u_i'}\overline{u_j'}\right) - \mu(x)u_i$$

4. Conclusion

According to numerical models, the Wave attenuation depends on the wavelength and the output current of air bubbles. One of the effective factor for the wave attenuation is the horizontal current which has made by air bubble, for getting better attenuation we should increase the horizontal current bye increasing the air bubble discharge. As a result if wave length in constant steepness is increased, air bubble discharge should be increased for achieving the same wave attenuation.

5. References

[1]. Brasher, P. Compressed Air Magazine, p 752.

[2]. Taylor, G. I. Note on Possibility of Stopping Sea Waves by Means of a Curtain of Bubbles. Admiralty Scientific Research Department. 1943.

[3]. Taylor, G. I. The Action of a Surface Current Used as a Breakwater, Proceedings of the Royal Society. 1955

[4]. Leonard I. Schiff. AIR BUBBLE BREAKWATER. Navy Department Bureau of Yards and Docks Contract. . 1949.

[5]. Lorenz G. Straub, C. E. Bowers, and Zals. Tarapore. Experimental studies of pneumatic and hydraulic breakwaters. University of Minnesota. ST. Anthony falls hydraulic laboratory. 1959.

HYDRODYNAMIC ANALYSIS OF MOORING SYSTEM MONITORING USING NUMERICAL METHODS

Mohamad Javad Ketabdari[1] and Hadi Mohamadi Tilenoei[2]

1) Associate Professor, Amirkabir University of Technology, Tehran, Iran, ketabdar@aut.ac.ir
2) Naval Architecture, Amirkabir University, of Technology, Tehran, Iran, hadimohamadi@aut.ac.ir

1. Introduction

There is always a need for continuous development of offshore industries. Several floating structures used in offshore industries, for example crane vessels, semi-submersibles and barges. Relatively, large movements of floating bodies in waves loading cause these vessels to be moored. Mooring of vessels is performed in various ways depending on the floating body geometry, sea state and environmental forces, mooring material, water depth and the junction of mooring lines to the vessel. In the present study, the effect of environmental forces on the mooring lines and mooring of marine vessels was investigated aiming to optimize the mooring system. Floating structures should be able to settle in their operational site using their anchorage. For this purpose, the structure and mooring system for a floating structure envisages to the marine environment is inevitable. Several theoretical studies have been conducted in the field of mooring systems of marine structures.

2. Mooring system

One of the traditional methods for floating object sea keeping is multi segment mooring line [1]. Environmental forces acting on a floating vessel is multidirectional. Multi segment mooring system can be used to keep the floating structure in position. Therefore it is designed and implemented with regard to environmental forces and random loads. However, the method of estimating the loads on floating structures are often more complex than fixed structures. In this study, the most effective environmental forces were considered in modeling of eight symmetrical mooring cable systems.

3. Research method

In this research, by modeling of a floating vessel and analysis of the results, different arrangements for anchorage at different depths were investigated. Since mooring systems are very long, field and laboratory data for them, especially in deep waters are very rare. Therefore using analytics software to model these systems due to advances made in the IT process can provide a fast and accurate preliminary results for designers. In this research mooring lines of multi-component models with different materials in different water depths was performed. While radar-shape charts represents the best behavior of multi segment mooring systems [2]. To study the interaction between waves and mooring system, mean movement and amplitude of motions around the average position were separated.

4. Hydrodynamics of mooring floating vessel

In this study, dynamic motions of moored floating vessel under the effect of waves, currents and wind was were analyzed. The total wave forces on the structure, is consist of impact, diffraction and radiation forces due to waves. The effect of changing parameters on motion of floating structure is presented to monitor the floating structure behavior under different conditions. The results were compared with operational criteria and limits to optimize the operation.

In order to calculate the force of the waves on the floating vessels, if the dimensions of vessels respect to wave length is large, Laplace equation can be used for fluid modeling [3]. The potential function in terms of its constituent components is as [4-5]:

$$\varphi(x,z,t)=\varphi_I(x,z,t)+\varphi_D(x,z,t)+\varphi_R(x,z,t) \quad (1)$$

The Bernoulli equation can calculate the relationship between the pressures on the floating surface:

$$p(t)+\rho\frac{\partial\varphi}{\partial t}+\frac{1}{2}\rho|\nabla\varphi|^2+\rho gz=cte \quad (2)$$

In linear forming and ignoring the ρgz, static pressure just two first terms remain. The total force exerted on the float is:

$$\sum\vec{F}=\int_A p(t)\vec{n}_{in}dA+\vec{F}_h=\int_A-\rho\frac{\partial\varphi}{\partial t}\vec{n}_{in}dA+\vec{F}_h$$
$$=\int_A\rho\frac{\partial\varphi}{\partial t}\vec{n}_{out}dA+\vec{F}_h \quad (4)$$

In the above equation n_{in} and n_{out} are the unit vector perpendicular to the floating body inward and outward respectively. ΣF is the resultant forces acting on the float and F_h, the forces caused by hydrostatic pressure and A is wet surface. The total torque acting on the body is then:

$$\sum\vec{M}=\int_A\rho\frac{\partial\varphi}{\partial t}\vec{r}\times\vec{n}_{out}dA+\vec{M}_h \quad (5)$$

Where r is the location vector of floating body surface from the origin at the center of a flotation and M_h is torque caused by hydrostatic forces around the origin.

5. Results of ship and mooring system modeling

In order to analyze the hydrodynamic of floating body by catenary mooring, Moses software [6] was used and environmental conditions were applied to the model. Floating vessel and mooring systems specifications considered along with environmental conditions in modeling is presented in Table 1 and Figure 1.

Table 1. General information of floating vessel

Length	91.50 m
Breadth	27.50 m
Max. of waterline	5.50 m
Number of anchors	8
Weight	3832 ton
Center of gravity	(51.8,0,4.8) m
Water depth	1000, 500 ,100 m
Max. volume of displaced water	13057 ton

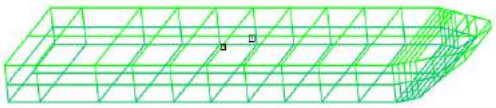

Figure 1. View of modeled vessel

Modeling of floating vessel and their mooring systems was performed at depths of 100, 500 and 1000 m for different wave directions. Figure 2 shows the models of mooring system.

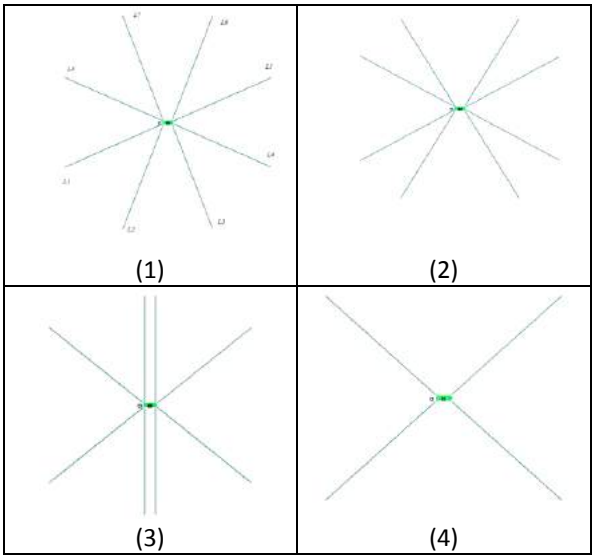

Figure 2. Different arrangements of modeled mooring system

The results of maximum tensions and displacements of mooring line in 500 m depth are presented in Figure 3:

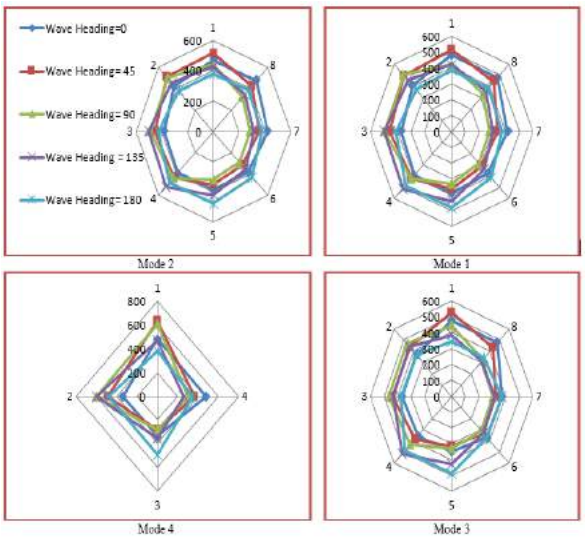

Figure 3. Maximum force of mooring lines (KN) at 500 m depth

6. Conclusion

In the present study, various parameters, which are effective on the behavior of a mooring system, were used in modeling. The most important results are presented as follows:

- Asymmetric patterns show dominant environmental forces over time.
- With reduced stiffness in various depths, mooring forces uniformly distributed among moorings.
- The mean drift waves forces directly controls the average position of the moored floating structure

7. References

[1] Rezvani, A. and Shafieefar, M., "Mooring Optimization of Floating Platforms Using a Genetic Algorithm", Ocean Engineering 34, pp 1413–1421, 2007.

[2] Mazaheri, S. and Incesik, A., "Predicting the Maximum Mooring Force of a Moored Floating Offshore Structure", 23rd International Conference on Offshore Mechanics and Arctic Engineering, Vancouver, British Columbia, Canada, 2004.

[3] Garrett D.L., "Coupled Analysis of Floating Production Systems", Journal of Ocean Engineering , 32, 2005.

[4] Ketabdari, M. J., Rezanejad, K., and Mirzaeian, A., "Hydrodynamic Analysis of Floating Oil Storage Units Using Boundary Element Method", 17th. International Conference on Mechanical Engineering, Tehran, Iran, 2009.

[5] Mirzaei Sefat, S., and Ketabdari, M. J., "Hydrodynami Analysis of Marine Structures Using Diffraction Theory", 9th Conference of Marine Industry, Noor, Iran, 2007.

[6] Ultramarine, Inc., "Reference manual for MOSES", 2005.

NUMERICAL ANALYSIS OF THE EFFECTS OF A SANDGLASS-TYPE FPSO HULL FORM ON HYDRODYNAMIC PERFORMANCE IN REGYLAR WAVES

Adeleh Graylee[1], Mahdi Yousefifard[2]

1) Dept. of Mechanical Engineering, Babol University of Technology, Babol, Iran, a.graylee1365@stu.nit.ac.ir
2) Dept. of Mechanical Engineering, Babol University of Technology, Babol, Iran, yousefifard@aut.ac.i

1. Introduction

Designing an optimum FPSO hull form needs years of experiment and knowledge due to complicated interaction of current, wave, body and many other important factors including inclination angle. Analysis of the problem is very complicated due to nonlinear interactions and the coupled equations. Therefore, many experimental and numerical studies have been carried out to examine the effects of FPSO hull form on hydrodynamic performance in regular and irregular waves. In recent years, sandglass-types of FPSO have been presented as an attractive form for the improvement of hydrodynamics performance in rough seas. References [1] and [2] are examples of experimental and numerical researches on this subject. However, it seems there has not been much attention to inclination effects on hydrodynamic performance of sandglass-type FPSOs.

In this study, numerical simulation of a sandglass-type FPSO is conducted under the effects of small amplitude regular waves, and effects of inclination angle on hydrodynamics performance are studied.

To accomplish this task, frequency-domain numerical simulation method is used in ANSYS/AQWA software. First, Current numerical results of heave and pitch motions of cylindrical FPSO are compared with experimental data of Wang et al. [1], indicating good agreement between the results. Thereafter, effects of hull form parameters on the model linear motions are investigated, and accordingly, the optimized inclining angle is presented. In addition to current effect, the influence of wave direction on sandglass-type FPSO motions is studied.

2. Governing Equations

On the assumption of having small wave heights, the linear wave theory is applicable. Moreover, fluid is inviscid and incompressible, and the flow is considered to be irrotational and all viscous shear forces are neglected. Therefore, the fluid domain is governed by the velocity potential φ satisfying by Laplace equation [3, 4]. These equations and boundary conditions are as follows:

Continuity:

$$\nabla^2\phi = \frac{\partial^2\phi}{\partial x^2} + \frac{\partial^2\phi}{\partial y^2} + \frac{\partial^2\phi}{\partial z^2} = 0 \quad (1)$$

Kinematic and dynamic free surface conditions:

$$\frac{\partial\eta}{\partial t} = -\nabla\phi.\nabla\eta + \frac{\partial\phi}{\partial z}, z = \eta(x,y,t) \quad (2)$$

$$\frac{\partial\phi}{\partial t} = -g\eta - \frac{1}{2}|\nabla\phi|^2, z = \eta(x,y,t) \quad (3)$$

Seabed condition and body conditions:

$$\frac{\partial\phi}{\partial z} = 0, z = -h \quad (4)$$

$$\frac{\partial\phi}{\partial n} = \vec{v}.\vec{n} \quad (5)$$

3. Computational model

Fig.1 shows the schematic of sandglass-type FPSO subjected to regular small amplitude waves. Main principles of sandglass-type FPSO are presented in Table (1).

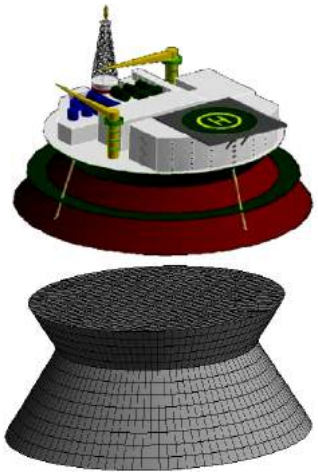

Figure 1. Hydrodynamic model of new sandglass-type FPSO

Table 1. Main dimensions of sandglass FPSO

Under-water section radius	77.151 m
middle section radius	44-64.5 m
deck section radius	64.5 m
Draft	27.151 m
Freeboard	14.49 m
Displacement	358750000 m^3
Inclination angle	30-65 degree

4. Numerical results and discussion

RAOs diagrams of sandglass-type FPSO have been calculated for 6-DOF nodes, and heave and pitch motions in regular wave are presented in Fig.2. These are the prominent motions of a sandglass-type FPSO floats in wave by heading of 180°.

a.

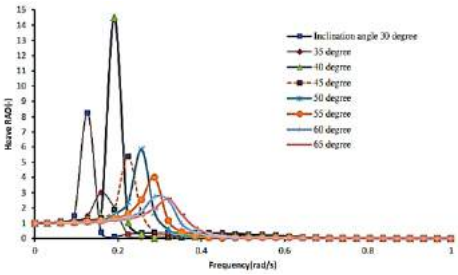

b.

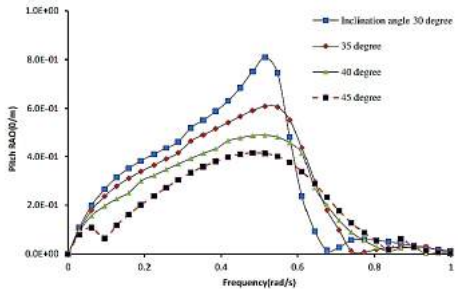

c.

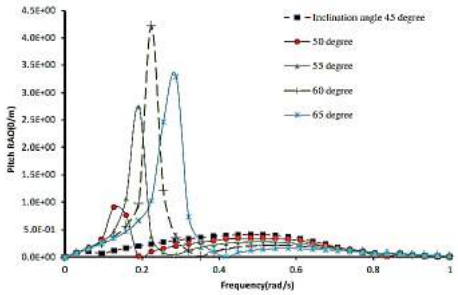

Figure 2 RAO in regular wave with 27.151 m draft: a. heave, b. pitch (1st natural frequency), c. pitch (2nd natural frequency)

It can be seen in (Fig. 2a) that increasing inclining angle leads to small amplitude of motion. But, at high inclining angles, deck effective area is reduced. Moreover, Pitch motion analysis is a little complex. In pitch motion, behavior of structure in two natural frequencies is different (Fig. 2b and 2c). In the second natural frequency, maximum amplitudes of pitch motion decrease by increasing inclination angle (Fig. 2b), while, the pitch motion amplitudes increase suddenly as inclination angle increases in first natural frequency (Fig. 2c). Based on current simulation results, it seems that in 45° inclination angle, both heave and pitch motions have optimum amplitude. As a result, for this angle the effect of different wave directions in 6-DOF motions was examined and base on Fig.3a and Fig.3b, it was obvious that wave direction has more effects on pitch and roll motions. It doesn't have any significant effect on vertical motions.

a.

b.

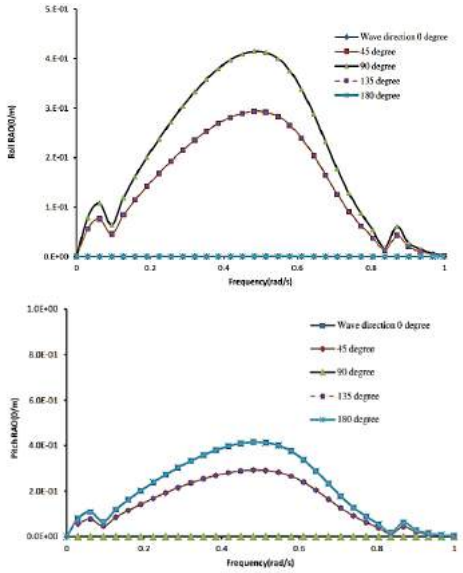

Figure 3 RAOs for 45 degree inclination angle for different wave direction, a. Roll, b. pitch

4. Conclusion

Numerical simulations were carried out to study the hydrodynamic behavior of a novel sandglass-type FPSO form subjected to different conditions. For this purpose, the body motions under the influence of changing the inclination angle that changes the middle part radius were studied. It was observed that, changing inclination angle has the greatest effect on heave and pitch motions. By analyzing both heave and pitch motions together, the best inclination angle was about 45°. Finally, the effect of different wave direction was examined and it was found that oblique waves have significant effects on 4 degrees of freedom. The analyses of the whole body motion have been omitted in the current report and will be presented in full paper.

5. References

[1] Wang, W. H., Wang, L. L., Du, Y. Z., Yao, Y. X., Huang, Y., "numerical and experimental analysis on motion performance of new sandglass-type floating body in waves", Journal of Marine Structures, Vol 46, 2016, PP 56-77.

[2] Yao, Y. X., Wang, W. H., Huang, Y., "Concept design of a new sandglass- type floating production storage and offloading system", J Shanghai Jialo Tong Univ, Vol 48(4), 2014, PP 558-564.

[3] Zhang, X., Bandyk, P., Beck, R. F., "Seakeeping computations using double-body basis flows", Applied Ocean Research, 2010, Vol 32, PP 471-482.

[4] Wang, L., Tang, H., Wu, Y., "Simulation of Wave-body interaction: a desingularized method coupled with acceleration potential", Journal of Fluids and Structures, 2015, Vol 52, PP 37-48.

STUDY OF THE AMOUNT AND DISTRIBUTION OF DECK MASS IN THE ASSESSMENT OF FIXED JACKET PLATFORM USING INCREMENETAL WAVE ANALYSIS

Reza Movahedinia[1], Mir Abdolhamid Mehrdad[2]

1) Department of Civil Engineering, Faculty of Engineering, University of Guilan, Rasht, Iran, rezamovahedinia@yahoo.com
2) Department of Civil Engineering, Faculty of Engineering, University of Guilan, Rasht, Iran, mehrdad@guilan.ac.ir

1. Introduction

Offshore platforms may be exposed to waves and currents greater than design criteria in their lifetime. Due to the permanent wave, current and wind on the platforms,it is very important to study on these environmental load on the existing offshore platforms, to continue the operation of platforms. In order to assessment the performance of fixed jacket platforms against environmental wave, *Golafshani et al.*[1] have established Incremental Wave Analysis (IWA) that is based on Incremental Dynamic Analysis which is used for seismic assessment of building structures. IWA has been done and parameters of assessment were calculated. Moreover CWH accuracy under different deck mass has been studied.

2. Modeling

A 3-D model of FX platform located on Dorood Field in the Persian Gulf was used in this study. FX jacket platform consists of four legs and four battered facesislocated in 50 m water depth. Jacket plan dimension is about 12m×9m as working point. The finite element program ANSYS [2] was applied which has the capability to perform nonlinear analyses of jacket platforms. For considering the mass of deck, structure of deck was modeled by *SACS5.3* software and static analysis was performed to calculate deck reactions which are illustrated in Figure 2.

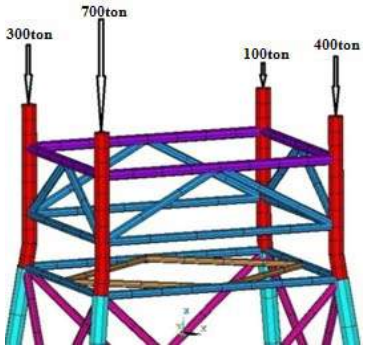

Figure 2. Deck mass distribution (ANSYS)

The pile–soil system was modeled by equivalent elements. This equivalent length (depth) is considered “10D”, where “D” is the pile diameter [4].

3. Methodology

In this study, Incremental Wave Analysis (IWA) which has been introduced by *Golafshani et al.* was used as an advanced approach to obtain the platform's response against wave loading. IWA is useful for estimating the ultimate capacity of jacket platforms against wave loading as well as displacement corresponding to the collapse point and a novel indicator named Collapse Wave Height (CWH).

4. Results

4.1. IWA capacity curves and CWH

In this part, IWA capacity curves for the FX platform were obtained and the corresponding CWH were extracted based on the preceding description provided. The structure was analyzed separately in four main directions and results presented in Figure 3.

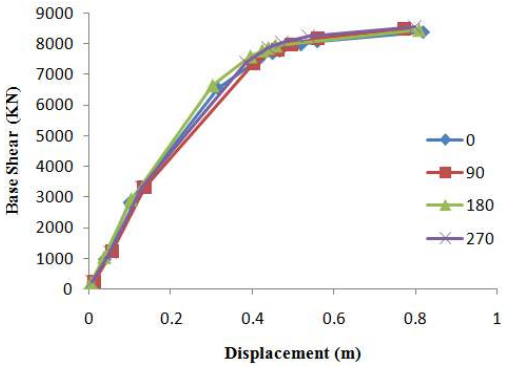

Figure 3. IWA capacity curves for FX platform

Table 1. Results from IWA

Direction	CWH (m)	Wave Period(s)	Displacement (m)	Base Shear(KN)
0	22.5	16.6	0.45	7665
90	21.5	16.23	0.497	7951

Direction	CWH (m)	Wave Period(s)	Displacement (m)	Base Shear(KN)
180	22.75	16.69	0.44	7854
270	21.5	16.23	0.47	8052

4.2. Sensitivity of CWH to the Uniform distribution of mass on the jacket legs

In this part, the deck mass was distributed uniformly on the top of the jacket legs (4 legs) and IWA capacity curves were obtained and the corresponding CWH were extracted.

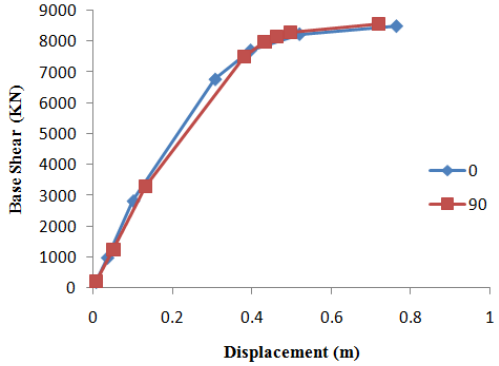

Figure 4. IWA capacity curves for uniformly mass distribution

Table 2. Results from IWA (for uniformly mass distribution)

Direction	CWH (m)	Period (s)	Displacement (m)	Base Shear(KN)
0	22	16.42	0.4	7708
90	21.5	16.23	0.47	8161

4.3. Sensitivity of CWH to the mass of deck

In this part, structure with different states, without deck mass (0M), 0.5M, 1M, 1.5M, 2M and 2.5M, were analyzed and the results were presented as IWA capacity curves (Figure 5). The mass distribution ratio on the platform's leg is based on real ratio which was described in section 2.

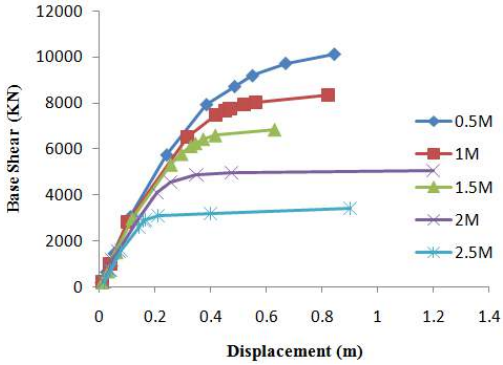

Figure 5. IWA capacity curves for different deck masses

Table 3.CWH accuracy for different deck mass

Deck Mass		CWH (m)
Mass	ton	
0M	0	26
0.5M	750	25
1M	1500	22.5
1.5M	2250	20.5
2M	3000	17
2.5M	3750	14

5. Conclusion

In this study, IWA capacity curves and CWH for FX platform were obtained and the effects of deck mass were studied.

CWH for direction 0 and 180 degree were obtained 22.5m and for direction 90 and 270 degree were obtained 21.5m. According to design wave height (100-year return period) which is 11m for Dorood field, it can be predicted that FX platform would not collapse against wave loading.

Then, deck mass was distributed uniformly on the platform's legs. In this state, CWH be equal with real distribution (withaccuracy of less than 0.5 m),so it can be concluded that distribution of deck mass has a negligible effect on CWH.Obviously, resultsprovide great help for assessment of structural offshore platforms and may saves time and cost.

Finally, structure was studied for 5 different deck masses and according to the results, CWH is affected by the deck mass.

6. References

[1] Golafshani, A., Bagheri, V., Ebrahimian, H., Holmas, T. "Incremental wave analysis and its application to performance-based assessment of jacket platforms". *Journal of Constructional Steel Research 67*, 2011, pp. 759-769.

[2]ANSYS. Mechanical APDL, v.14.5, User's Manuals, 2014.

[3] Hezarjaribi, M., Bahaari, M., Bagheri, V., Ebrahimian, H., "Sensitivity analysis of jacket-type offshore platforms under extreme waves"., *Journal of Constructional Steel Research 83*, 2013, pp. 147-155.

[4] Asgarian, B., Lesani, M., "Pile-soil-structure interaction in pushover analysis of jacket offshore platforms using fiber elements". *Journal of Constructional Steel Research 65*, 2008, pp. 209-218.

[5] Dastan, M., Mohajernassab, S., Seif, M., Tabeshpour, M., Mehdigholi, H., 2014. "Assessment of offshore structures under extreme wave conditions by Modified Endurance Wave Analysis". *Marine Structures 39, 2014*, pp. 50-69.

[6] Matinnikoo, H., Zeinoddini, M., Estekanchi,H., "Probabilistic Estimation of Offshore Jacket Type Platforms Capacity Using Incremental Random Wave Analysis (IRWA)", *Journal of Marine Engineering 16*, 2012, pp.1-18.

PARAMETRIC STUDY ON THE STABILITY ANALYSIS OF OFFSHORE JACKET LAUNCHING OPERATION: A CASE STUDY IN THE PERSIAN GULF

Hamed omdehghiasi[1], alireza mojtahedi[2], mohammad ali lotfollahi-yaghin[3]

1) M.SC. of civil Eng., University of Tabriz, Tabriz, Iran
2) Assist. Prof. of Civil Eng., University of Tabriz, Iran
3) Prof. of civil Eng., University of Tabriz, Tabriz, Iran

1. Introduction

Iran with 5,800 km coastline, important maritime waterways including large and small ports has huge oil and gas resources in the Caspian Sea, Sea of Oman and the Persian Gulf. Considering the enormous energy reserves in the Persian Gulf which are placed in almost shallow waters, emphasizes the importance of construction and operation of jacket structures in this area. The South Pars gas field is the world's largest gas supplier on the border of Iran and Qatar located in the Persian Gulf. Therefore, this area is considered as one of the main sources of fossil energy requirement. Offshore jacket platform is used to oil and gas exploration in shallow water. The jacket platform is transmitted from land to a floating barge and install location is one of the most important phases in implementation of offshore platforms. After jacket transportation by floating barge, jacket should be transmitted in the sea to the site. The sliding of jacket over barge and lift it by crane are two common procedure for this transmission [1, 2].

In this paper, the influence of various parameters such as speed winch, the size of a floating barge, drag coefficient and density of sea water are investigated on launching analysis. Due to the jacket imbalance after launching operation, flotation tanks should be used to stabilizing jacket structure. So, a comparison of the different parameters of analysis should be included spatial, rotational variables and change in jacket velocity. On the other hand, winch speed, rocker arm reaction and maximum rotation of arm have main role in analysis, that the lack of scrutiny of these amounts can cause irreparable losses. 5 different modes of placement and numbers of flotation tank have been suggested, which, the final mode choose by comparing the results of different scenarios to achieve the most appropriate analysis results (table 1 and 2).

Table 1. Primary barge launch specification

Barge height (m)	Barge width (m)	Bottom length of barge (m)	Forward extension of barge (m)	Aft extension of barge (m)	Skid height (m)	Rocker pin location (m)	Rocker arm depth (m)	Winch velocity (m/s)
10	35	72	7	12	3.5	88	4.5	0.1

Table 2. Launching parameter variables

Case	Sea water density (ton/m^3)	Winch speed (m/s)	Drag coefficient	Barge width (m)
Principle case	1.2	0.1	1	35
Parameter variables	1.5	0.3	2	40

2. Governing equations

Hydrodynamic forces exerted on the jacket structures during launch operations could be divided into drag and inertia forces. Flow rate creates drag force that it acts on submerged body of structures and it creates shear stress friction and vertical pressure on structure. It is calculated by eq. 1:

$$F_d = -\frac{1}{2} C_d \rho A_w \overline{v_n} \left|\overline{v_n}\right| \quad (1)$$

In which, c_d is drag coefficient, ρ is fluid density, A_w is flotation area and $\overline{v_n}$ is vertical component of velocity. Acceleration of the structure creates an additional hydrodynamic force. This acceleration or inertia force has two components.

The first component is caused by the pressure difference of flow acceleration field. This difference in pressure around the body creates a net force on the body. Also, when an unsteady flow passes through the body, the added mass of the liquid creates, that it is caused by the presence of an object in motion. The second component of the force of inertia is a function of density, velocity of the liquid, shape of the body and its volume [3]. Inertial force is achieved by eq. 2:

$$F_a = -M'\overline{A_n} - \frac{dM'}{dt}\overline{v_n} \qquad (2)$$

In which, M' is added mass and $\overline{A_n}$ is vertical acceleration.

3. Analysis process

Jacket structures have been modeled and investigated in different scenarios, without and with the use of buoyancy tanks. The first step of model analysis is creation and applying related loads by respect to analysis type. The sections should be assigned after the geometry of the structure is modeled. Buckling length, offset length and rigidity assignment are other important steps that should be considered. Determination of the slenderness ratio (kl/r) for cylindrical compression members should be applied in accordance with the AISC [4]. A rational analysis for defining effective length factors should consider joint fixity and joint movement. Moreover, a rational definition of the reduction factor should consider the character of the cross-section and the loads acting on the member [5].

This jacket is placed on the larger side (side A) on barge. The possibility of placement of platform on funds 2 or 4 axis is not recommended due to symmetry of short and longer spans practically the way the wind. On the other hand, by placing jacket on "A" face, unwanted rotations may be observed during launching process due to asymmetry of the center line perpendicular to the face. This caused to lack of adequate floating offshore jacket and growing movement. To overcome this problem, the buoyancy tanks are used to reduce unwanted movements and to have appropriate flotation. Moreover, the reservoir should be examined in the numbers and different places to achieve an optimal model of economic process. In Table 1, the location, size and number of floating tanks are represented [6].

4. Conclusion

In this article, launching operation of jacket structure is investigated in different conditions and effective parameters in this process is analyzed sensitively. Due to the asymmetry of jacket structures during launching process, use of buoyancy tanks is essential. Multi-pattern tank placement on jacket structure have been studied. Analysis with respect to variable winch speed, the dimensions of the barge floating, drag coefficient and density of sea water and change the parameters of locations, rotations, speeds and specifications of Skid and Rocker arm is comprised with each other. Gravity and buoyancy centers are not considerable discrepancy in different scenarios. Adding flotation tanks will have little effect on the center of gravity and buoyancy. Displacements in x and y direction aren't vary significantly, but, a gap can be seen between jacket by buoyancy tanks and without buoyancy tanks in z displacement.
Maximum pitch and yaw rotation don't vary significantly by adding buoyancy tanks. Also, buoyancy tanks have an important role in reducing maximum roll displacement. Adding buoyancy tanks don't have a considerable impact on jacket velocity in y-direction. Final y and z-velocity are not varied significantly in presence of buoyancy tanks. Final yaw rotation of jacket doesn't vary significantly. Change in launching variables doesn't have feasible effects on center of gravity and buoyancy of jacket. Increasing density has a great impact on the jacket structure roll rotation. Therefore, in high-density areas, other measures should be considered for an appropriate launching analysis. In almost all conditions, the case 3 have the smallest skid velocity, rocker arm angle and its load capacity. These parameters, in case 1, except for barge dimension varying condition are the greatest values.

5. References

[1] Gerwick Ben C. 2007. Construction of marine and offshore structures. Third Edition, p. 435-444.

[2] Jo C.H., Kim K.S., Lee S.H. (2002). Parametric study on offshore jacket launching. Ocean Engineering 29, Elsevier Science Ltd.

[3] Sorensen Robert M. 1997. Basic coastal engineering. Springer Science & Business Media, ISBN 041212341X, 9780412123412.

[4] AISC 360-10. Specification for Structural Steel Buildings. An American National Standard. Specification for Structural Steel Buildings.

[5] API, 2000. Recommended Practice for Planning, Designing and Constructing Fixed Offshore Platforms, Working Stress Design. (API _RP2A-WSD).

[6] Omdehghiasi H., Tavakol A., Mojtahedi A. R., lotfollahi-yaghin M. A. 2015. The SPD8 jacket platform stability analysis in launching process for optimizing the displacement and velocity of the jacket with buoyancy tank. 10th International Congress on Civil Engineering. Tabriz. Iran (in Persian).

OPTIMIZATION OF MOTIONS VERTICAL TRUSS SPAR PLATFORM WITH THE EXACT LAYOUT HEAVE PLATES USING GENETIC ALGORITHM

M.Ezoji[1], A.R.M.Gharabaghi and M.R.Chenaghlou

Marine Infra-Structures Research Center, Sahand University of Technology
1) Mojtaba.ezoji@gmail.com

1. Introduction

Truss spar platforms are the second generation of semi-submersible spar platforms for the extraction of hydrocarbon resources which are installed on deep waters of the Mexican Gulf in the New Gregorian Century. The special feature of these platforms, i.e., the small movement response of spar against environmental loads caused the very deep designing of the waterline.

Knowing that the vertical movements of the platform is mostly influenced by the geometric conditions and according to the outstanding features of heave plates, this article will focus on the optimization of the platform movements with the automatic layout design of these plates.

In order to define the optimization of the platform response in the vertical direction, in this study, the followings shall be done:

- Optimize the template and the layout of the plates in the Truss section of the platform.
- Optimize the space between the plates.
- Automatic design process in order to minimize the time required for the design engineer.

In 2001, through applying the nonlinear programming method and considering the environmental conditions of the sea in short-term and long-term modes and applying different spectra, Clauss dealt with optimizing various offshore structures such as ships, buoys, tension leg platforms, and semi-submerged platforms[1].

The main purpose of this paper was to provide a code of genetic algorithm to minimize the responses of floating platforms in the vertical direction under the waves.

2. Geometry of Truss Spar

This platform includes hard upper tank and lower soft tank which are separated by a truss middle cross section. Generally these plates lead to an increase in the natural period of truss spar platform in addition to increasing the added mass and therefore improve the vertical movement of the platform.

This study focused on finding the exact location of the plates on the truss platform via the genetic code and other original geometric features and parameters of the platform and the number of heave plate were unchanged and in accordance with the relevant reference. For this purpose, we first express the effective parameters on the motion equations of the platform.

The motion equation of the platform is summarized as follows:

$$[M]\{\ddot{X}\}+[B]\{\dot{X}\}+[K]\{X\}=\{F(t)\} \qquad (1)$$

X displacement vector, $\dot{X}$ velocity vector, B is the matrices of damping, K is the matrices of stiffness. By inserting the above parameters in equation 1 and solving and Linearization the equation in the frequency domain equation 3 and also the RAO[1] is obtained[2]. where H_w is height wave.

$$X_i=\left[-\omega^2(M)-i\omega(B)+(K)\right]^{-1}F_i \qquad (2)$$

$$RAO_i=\left|\frac{X_i}{0.5H_w}\right| \qquad (3)$$

3. Genetic Algorithm

This algorithm is an efficient search in the vast area of data which ultimately leads to guidance towards an optimal response.

Like other optimization algorithms, the genetic algorithm begins with defining the optimization variables and the cost function and ends with reviewing the convergence of the algorithm [3]. The optimal amount is obtained through minimizing the cost function 4 per supply constraints 5. The objective function defined here is the response of the platform operator in vertical direction.

$$F(X)=\sum_{i=5}^{14}RAO(i)*w(i) \qquad (4)$$

Where *RAO* is the response amplitude operator of the platform and *w (i)* is the relevant frequency.

In order to prevent the layout and the interference of these plates, the two constraints are defined as follows:

$$\begin{aligned} X_1-X_2 &\le -2 \\ X_2-X_3 &\le -5 \end{aligned} \qquad (5)$$

Where X_1, X_2 and X_3 are the places of the first, second and third heave plates respectively.

4. Process of Optimization and Definition of Design Parameters

The method which was explained in the previous section was modeled and GA code implemented in MATLAB programming language. This code

[1] Response Amplitude Operator

automatically solved the design of the layout of heave plates.

In order to validate the optimized process design approach, first, the primary results of the response amplitude operator of the floating platform in vertical direction were compared to the experimental results in reference [4]. This indicated a good agreement between the results [Fig1].

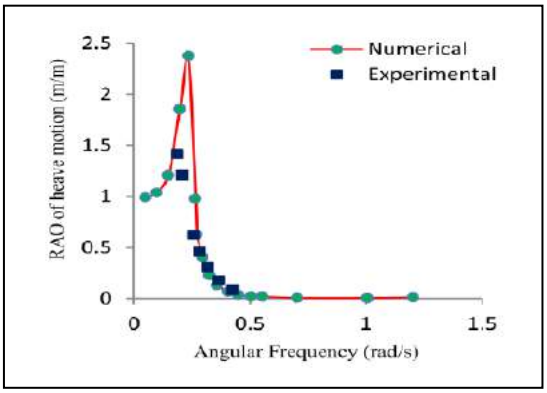

Figure 1. The comparison of the RAO for the heave motion resulted from the present numerical model and the experimental results [4]

The geometric characteristics and environmental conditions of the studied platform are provided in reference[4].

In order to solve the optimization problem, the genetic algorithm is used as an accidental optimization technique.

To begin the setting process of the variables by the genetic algorithm, we define a chromosome as an order of variables that must be optimized. In this equation, according to the number of efficiency parameters and accuracy of the problem, *N=10* chromosomes have been used where each chromosome has three variables.

In this work with the selection rate of $N_{keep} = 4$, the chromosomes which are more appropriate than others, constitute the breeding pool. Selecting the mixing combinations method, four pairs of parents are paired through a random method. Each of the couples produces two children who have the characteristics of both parents. Parents also survive to form a part of the next generation.

After the combining operator, the mutation operator is used in order to improve the performance of the algorithm. In this thesis, using the trial and error mutation method, we selected the mutation rate as 94 percent. This means that 28 variable must be mutated in each phase and new variables are replaced. The first chromosome does not mutate because of elitism. One thing to note here is that through the process of producing new generations the answers gradually tend towards the absolute minimum. In both combination and mutation operators the variable may be out of the [0,1] scope. In this case the main variable will be placed itself. In the present application, the condition of convergence for the end of the program after 5, the index of the successive performance is defined as the same.

Table 1 indicates the optimal values of the design parameters.

Table 1. Values of design parameters for optimal and ordinary model

Design parameters	Ordinary model	Optimal model
X1 (m)	27.1272	35.5664
X2 (m)	49.0728	61.4864
X3 (m)	71.0184	84.9015

Some of the values of the Response Amplitude Operator in each of the frequency points in ordinary and optimal modes are presented in Table 2.

Table 2. Values of RAO for optimal and ordinary model

Frequency (HZ)	Ordinary model	Optimal model
0.042	1.86E+00	1.88E+00
0.043	1.42E+00	1.42E+00
0.045	9.24E-01	8.95E-01
0.046	6.52E-01	6.15E-01
0.048	4.83E-01	4.43E-01
0.056	1.58E-01	1.06E-01
0.072	1.39E-02	2.58E-02

As can be seen in table 2, the platform response in vertical direction and resonance area reduces up to 16% through optimal layout of heave plates in the mentioned platform using genetic optimization algorithm. Therefore engineer can use GA method for reduce most of the costs and laboratory problems to construct a model on a smaller scale.

5. Conclusion

The results indicated that through the dynamic response analysis of truss spar platform in various environmental conditions and the use of genetic inheritance algorithm, the motions behavior of the platform has improved in the vertical direction. This indicates that by displacing these plates, we can control the movements of the platforms even in certain periods. Using this technique allows engineers to obtain the place of these plates in a highly accurate and automated way.

6. References

[1] Birk, L., Clauss, G. F,. "Automated Hull Optimization of Offshore structures Based on Rational Seake eping Criteria " ,*in Proceedings Of 11th ISOPE, Stavanger, 2001.*

[2] Berthelsen, P. A., *"An experimental investigation of motion control devices for truss spars,"*, Marine Technology, University of Newcastle upon Tyne, master of science in offshore Engineering Thesis, 2000.

[3]. Goldberg, D. E., *"Genetic Algorithm in search, optimization and machine learning", Addision Wesley, MA, 1989.*

[4]. Downie.M. J, Graham. J. M. R, Hall. C, Incecik, A, Nygaard, I., "An experimental investigation of motion control devices for truss spars", *Marine Structures, vol. 13 (2000), pp. 75-90.*

DYNAMIC RESPONSE OF JACKET STRUCTURES TO WAVE LOADS: OVERVIEW

Arash Khansari[1] and Hocine Oumeraci[2]

1) Leichtweiß-Institute for Hydraulic Engineering and Water Resources (LWI), Technische Universität Braunschweig, Braunschweig, Germany, a.khansari@tu-braunschweig .de
2) Leichtweiß-Institute for Hydraulic Engineering and Water Resources (LWI), Technische Universität Braunschweig, Braunschweig, Germany, h.oumeraci@tu-braunschweig .de

1. Introduction

Jacket structures have been the most widely used type of structures in the oil and gas industry. They are increasingly becoming competitive, especially in terms of both costs and response to environmental loads, as support structures of wind turbines which are generally built in different water depths. These structures are frequently exposed to breaking and near-breaking waves, especially when they are located in shallow or intermediate water depths. Currently, the wave load models developed for mono-pile structures are also applied for jacket structures. However, considerable uncertainties in the obtained total wave loads might result when applying such approaches. The importance of jacket structures in practice on the one hand, and the complexity and variety of the available approaches implemented for these structures on the other hand, underline the necessity to question the current approaches/models for the assessment of the total wave loading and dynamic response of jacket structures, with the objective to improve the modelling and analysis techniques for this type of structures.

2. Assessment of current approaches/models for the dynamic response of jacket structures

In this research, the overall objective is to improve the understanding of the processes involved in the wave and jacket structure interaction with a particular focus on pile and soil interaction based on available recent experimental, analytical and numerical studies. The best available models and methods for the calculation of the dynamic response of jacket structures exposed to breaking and non-breaking wave loads are evaluated and compared.

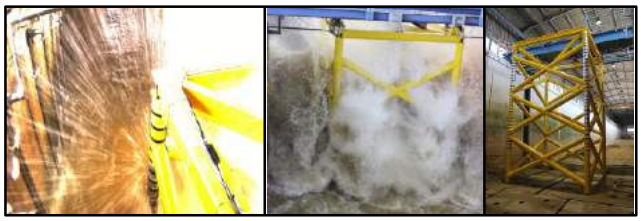

Figure 1. Breaking and non-breaking waves on a truss structure in large scale wave flume (GWK) in Hannover

The main topics to be addressed in the paper are (a) problem statement (b) brief analysis of available analytical and numerical approaches for the calculation of total forces induced by breaking, broken and non-breaking waves on jacket structures based on recently performed experiments on a truss structure in large scale wave flume GWK in Hannover (see Figure 1). (c) pile and soil interaction models for jacket support structures of wind turbines (d) influencing parameters on the dynamic response of jacket structures.

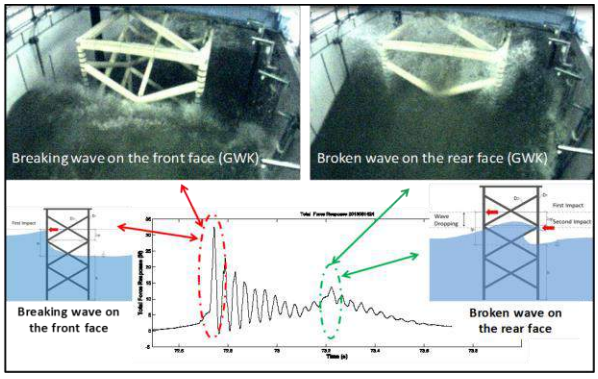

Figure 2. Force response of the truss structure to breaking/broken wave striking the front/rear face as recorded in the GWK tests.

In this study, the effect of the most relevant parameters on the loading and the response of the structure, such as marine growth, jacket members overlapping, joint cans, sealed and unsealed members (see Figure 3), added mass and etc. are investigated and the most influencing parameters on the loading and the dynamic response of the structures are identified. The drawbacks of the current slamming force models are outlined based on the preliminary analysis of available data from the GWK experiments which revealed that the wave slamming force applies not only on the front face of the jacket structure but also the rear face (see Figure 2).

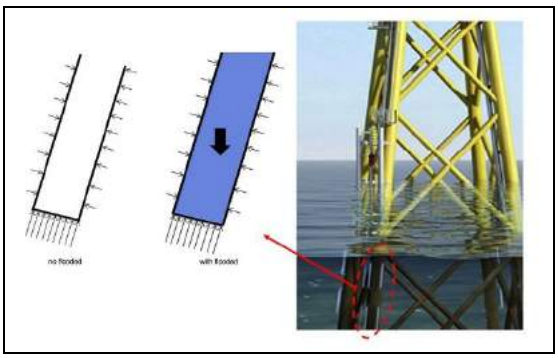

Figure 3. Sealed and unsealed members of the jacket structure [1]

The most appropriate available models and methods to predict the dynamic response of jacket structures are identified. The knowledge gaps related to the processes/approaches involved in the loading and response of jacket structures are determined. Finally, it is shown how the identified knowledge gaps are addressed in the ongoing PhD research study. The paper will also include the first result of a new concept to calculate the loading of such complex structures induced by breaking, broken and non-breaking waves.

3. Results

The results show Lack of proper approach and formula for calculation of breaking wave impact force on jacket structures in guidelines as well as scientific articles. Most of current approaches to calculate impact wave loads on jacket structures are using conventional formula for single piles which means that the total wave slamming forces on truss-type structures are calculated using available methods and models for single slender cylinders. Application of such approaches for truss structures (e.g. Wienke and Oumeraci 2005), would result in a large overestimation of the peak of the slamming force as compared to that obtained in this study based on the performed laboratory tests in large scale wave flume GWK. (see Table1)

Table 1. Measured and calculated slamming forces on the GWK truss structure (H=1.7m ; T=5.55s)

Slamming force model	Impact area λ (m)	Maximum Impact Force (kN)	Maximum slamming coefficient
This Study (Laboratory Tests)	0.66	12.0	1.63
Goda [2]	0.58	21.6	π
Wienke & Oumeraci [3]	0.66	49.7	2π
Campbell-Weynberg [4]	0.72	44.3	5.15

Furthermore there is no simple approach and wave theory to predict water particle kinematics under wave crest while wave is breaking. Therefore application of Morison equation for breaking wave-multimember structures interactions is complicated and needs powerful CFD models. Since breaking waves may release huge amounts of energy, which may severely damage structures it is important to design jacket structures under breaking waves but current available aero-servo-hydro-elastic tools and codes fail to calculate the dynamic response of jacket structures under breaking waves. In addition the majority of available tools do not consider pile-soil foundation and as a result fail to predict accurate values for natural frequencies of jacket structures.

4. Acknowledgments

The support of the Deutsche Akademische Austauschdienst (DAAD) for this study through the DyJaW project is acknowledged.

5. References

[1] Shi, W., Park, H., Han, J., Na, S., & Kim, C., "A study on the effect of different modelling parameters on the dynamic response of a jacket-type offshore wind turbine in the Korean Southwest Sea", 2013, *Renewable Energy*, 58, pp.50-59.

[2] Goda, Y., Haranaka, S., & Kitahata, M., "Study on impulsive breaking wave forces on piles", *Report Port and Harbour Technical Research Institute*,6(5), 1966, pp.1-30.

[3] Wienke, J., & Oumeraci, H., "Breaking wave impact force on a vertical and inclined slender pile—theoretical and large-scale model investigations". *Coastal Engineering*, 2005, 52(5), pp.435-462.

[4] Campbell, I. and Weynberg, P. A., (1980): "Measurement of Parameters Affecting Slamming". *Technology Reports 440*, 1980, Southampton University: Wolfson Unit for Marine Technology.

STRESS ANALYSIS IN BOX BOTTOM OF IRAN AMIRKABIR SEMI-SUBMERSIBLE PLATFORM DUE TO HOOK LOAD CONDITION UNDER ENVIRONMENT LOADS

M.Ezoji[1], A.R.M.Gharabaghi[2], M.R.Chenaghlou[3]

Marine Infra-Structure Research Center, Sahand University of Technology
1) Mojtaba.ezoji@gmail.com 2) mgharabaghi@sut.ac.ir 3) mrchenaghlou@sut.ac.ir

1. Introduction

Semi-submersible rigs are floating multi-hull structures that include a deck, four or more columns, and two submerged pontoons. Columns can also be connected with horizontal bracings. The deck usually consists of three or more levels of upper deck, tween deck, lower deck and box bottom. Regarding the harsh marine environment surrounding these structures, numerous factors can damage them. Therefore, there are always concerns about their integrity and stability as they cannot undergo routine and continuous inspection. On the other hand, inspections of offshore platforms require squad-diving and expensive marine equipment. Development of advanced damage detection methods allows for examination of the structure as a whole before detailed inspections to be investigated at the damaged area, if such damage is detected.

Doebling, et al. [1] provides a comprehensive review of technical literature about the detection, location recognition, and characterization of structural damage via different techniques such as inspection of the changes in measured and estimated structural vibration response.

This paper deals with a part of main study conducted in order to monitor the health of Iran Amirkabir semi-submersible platform. In order to monitor the health of this platform, its complete and accurate model must be first simulated. The numerical model should be then verified by the real platform (current condition) through the in-field measured results. In this paper, the above mentioned procedure which was performed for the platform's box bottom is presented.

2. Description of the Model

In order to simulate the behavior of the studied platform, it was first modeled in complete form with any related details using the finite element method. Then the developed finite element model was used for hydrostatic, hydrodynamic and structural analysis.

The main structural elements of the platform are consisted of shell plating with longitudinal and transverse girders and stiffeners. The main particulars of these elements are described in ref [2].

All girders and stiffeners in the columns, deck and pontoons were modeled using 4-node linear steel beam elements with linear elastic modulus. The shell plating was modeled by layered 8-node shell elements with 6 degrees of freedom. Payloads such as Heli-pad load, weights of generators, tanks, etc. were added to the original model as equipment loads through their exact location by considering the center of gravity of the loads.

The JONSWAP spectrum is applied in the simulation of Caspian Sea waves with 1- year return period.

3. Validation of the Simulation Based on Real Conditions

The purpose of developing a finite element model is to simulate the global structural behavior as realistic as possible. In order to ensure the modeling and confirm the results of analysis, a highly-detailed model of Amirkabir semi-submersible platform was first developed based on layouts and details provided by GVA consultants.

In the next step, the model should be verified through the following procedures:

A) Precise distribution of structural mass based on the real situation in the developed model and exact matching of their centers of gravity (COG) and geometry based on the fixed and variable loading.

The vertical distance from the keel to the COG is calculated by equation 1. Each weight is multiplied with its distance to the keel to create a vertical moment.

$$D_{COG-Pontoon} = \frac{M^P + M^C + M^D + M^E + M^B + ...}{W^P + W^C + W^D + W^E + B^B + ...} \qquad (1)$$

where, $D_{CoG\text{-}Pontoon}$ is vertical distance from keel to COG. M^P,M^C are vertical moment of the pontoons and vertical moment of the columns. W^P,W^C are weight of the pontoons and weight of the columns. Indices *B*, *E*, *C* and *D* are referred to ballast water, equipment, column and deck respectively.

According to Equation 1, the distance between the center of gravity of the whole platform and the pontoon bottom was calculated as 20.23 m.

Table 1 lists the accuracy in modeling of some parts of the platform using the finite element method considering the values of mass (based on the distance between their center of gravity and the pontoon bottom). The mean standard deviation for the centers of gravity was calculated as less than 2 percent.

B) Assessment of the calculated Response Amplitude Operator (RAO) of the platform for different degrees of freedom through hydrodynamic analysis.

Table 1. Values of weight and centers of mass of different parts of the platform in developed finite element model

HULL	Weight (ton)	Center of mass (m) in the model	Designed Center of mass (m)	Standard deviation VCG
Pontoons	3114.46	3.65	3.61	+1.1%
Columns	2001.21	17.144	17.21	-0.4%
Deck	3118.45	32.46	32.39	+0.2%
Diesel oil	1000	3.38	3.4	-0.5%
Drill water	1200	2.04	2.18	-6%
Liquid mud pits	559	30.85	31.17	-1.02%
Displacement tonnage of platform : 29553ton The mean Standard deviation VCG: < 2%				

To ensure that the developed model receives the right hydrodynamic loading, one key step is to verify its response for heave, pitch and roll motion due to wave loading. Figure 1 shows the comparison of RAO for heave motion obtained from the present analysis with the results given by GVA Consultants due to waves approaching from different directions.

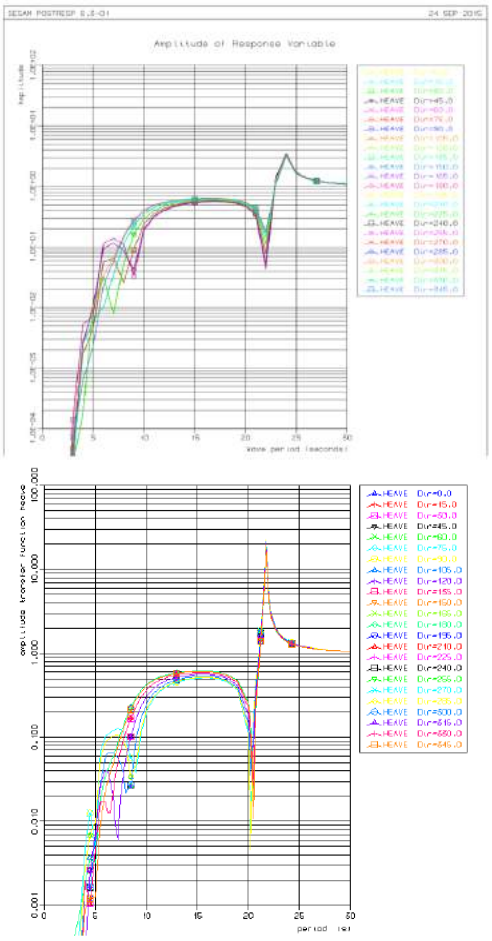

Figure1. Comparison of obtained heave RAO (above) with the results given by GVA Consultants (below)

4. Global Structural Analysis

In the next step, a 650 ton hook load was placed on the top of drilling rig to analyze the structure as a whole under hook load. Fig. 2 shows the distribution of Von Misses stresses in box bottom. It seems that the maximum stress occurs in the moon pool corner (yellow area). However, these values are in the allowable stress range of the box bottom plate. The in-field measured stresses are in god agreement with the calculated results.

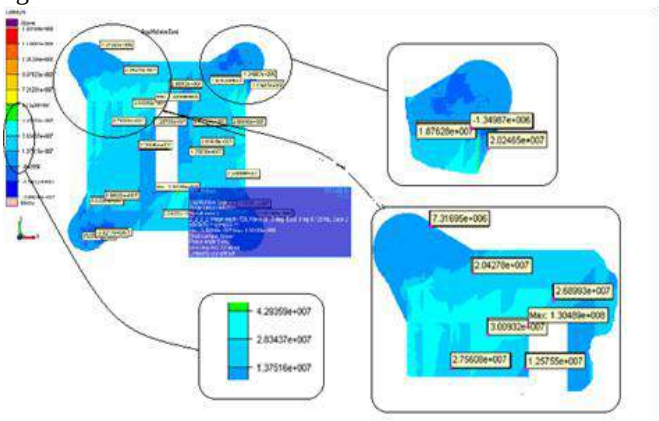

Figure2. The distribution of Von Misses stresses in box bottom

5. Conclusion

The present study showed that it is possible to conduct a full finite element modeling with all the details and structural loads and equipment. It is essential to calculate the center of gravity of each part as well as whole the structure to verify its layout. Equipment layout makes a great impact on the center of gravity which can influence on the results.

In this paper, Iran Amirkabir semi-submersible platform which is under service in Caspian Sea was modeled and verified through different steps. Then, it was analyzed under different expected loads and its integrity was verified. Results can be used to optimize the location of equipment loads. These arrangements can be used to implement in the actual situation. This means that limitations in the stress values are under control.

6. Acknowledgement

Authors would like to acknowledge Khazar Exploration and Production Company for supporting this project.

7. References

[1] Doebling, S. W., et al., "Damage Identification and Health Monitoring of Structural and Mechanical Systems from Changes in their Vibration Characteristics: A literature Review," *Los Alamos National Laboratory report LA-13070-MS. 1996.*

[2] Ezoji, M., Gharabaghi, A. R. M., Gol-Zaroudi, H., "The effects of wave parameters on motion performance of semi-submersible platforms ",*in Proceedings Of Maritime Technology and Engineering, Lisbon, Portugal*, 2015.

ESTIMATIONS OF TLP MOTIONS IN 2D USING ANALYTICAL METHODS

Mohamad Javad Ketabdari[1] , Mohammad Mahdi Abaiee[2]
1) Amirkabir University, of Technology, Tehran, Iran, ketabdar@aut.ac.ir
2) Amirkabir University of Technology, Tehran, Iran, mahdy.abaiee@aut.ac.ir

1. Introduction

Tension leg platform (TLP) is one of the compliant offshore platforms which has designed and implemented in the last couple of decades for oil extraction. Large stiffness in heave, roll and pitch degrees of freedom of TLPs and their stability fit them to be used as the offshore wind turbines leg. Assuming small amplitude of motion for the platform, TLP behavior was modeled in the form of a mass-spring system, in this study. First order wave-induced motion is considered to be a linear combination of oscillations in still water and the motions of excitation forces on the fixed body. For the roll motion this presumption is not valid as the large amount of energy is needed for motion development in most of the offshore structures [1, 2]. Mooring stiffness can be obtained based upon an elastic behavior system [4, 5, 6]. So, Surge stiffness can be derived as follow:

$$k_{11}x = (T_0 + \Delta T)\sin\theta = \left(T_0 + \frac{\left(\sqrt{x^2+l^2}-l\right)AE}{l}\right)\sin\theta = \left(T_0 + \frac{(x^2)AE}{\left(\sqrt{x^2+l^2}+l\right)l}\right)\sin\theta =$$
$$= \frac{T_0 x}{l} + \frac{AE}{2l^2}x^3 = k_1^m x + k_1^b x + k_1^{m'} x^3 \qquad (1)$$

where, T0 and ΔT are initial pre-tension and variation of pre-tension of tendon, respectively. θ is the angle between y axis and the tendon line after surge motion is emerged and its vertex is at the sea level. It can easily found that the stiffness coefficient in this degree is:

$$k_{33}y = \frac{AE}{l}y + \frac{\rho g \pi D^2}{4}y = k_3^m y + k_3^b + k_3^{m'} y^3 \qquad (2)$$

k_i^m، k_i^b and $k_i^{m'}$ are tendon nonlinear stiffness, buoyancy stiffness and linear stiffness of mooring, respectively. Pre-tension is not directly appeared in heave stiffness but is related to the characteristics of tendons pre-tension. Finally, Forced vibration relationships for heave and surge motion states are as follow:

$$\ddot{y} + \frac{k_3}{m_3}y = \frac{F_3}{m_3}\cos\Omega_3 \qquad (3)$$

$$\ddot{x} + \frac{k_1}{m_1}x + \frac{k_1'}{m_1}x^3 = \frac{F_1}{m_1}\cos\Omega_1 t \qquad (4)$$

2. Classic Perturbation Method

Eq. (4) can be written as $\ddot{x} + \omega_n^2 x + \mu x^3 = \frac{F_1}{m_1}\cos\Omega_1 t$ in which the natural frequency of surge motion is $\omega_n = \sqrt{\frac{k_1}{m_1}}$ and perturbation term is $\mu = \frac{k_1'}{m_1}$ resting on what is explained earlier. Responses of the system can be expressed in the first order analysis using perturbation method as follow:

$$x = x_0 + \mu x_1 \qquad (5)$$

In fact, frequency is related to response amplitude and perturbation parameter which varies with natural frequency, structural mass and mooring stiffness as physical properties.

$$\omega^2 = \omega_n^2 + \mu \propto_1 \qquad (6)$$

$\propto_1$ is an unknown function. Substituting equations (5) and (6) in updated equation (4), following relation will be formed:

$$\left(\ddot{x}_0 + \omega^2 x_0 - \frac{F_1}{m_1}\cos\Omega_1 t\right) + \mu\left(\ddot{x}_1 + \omega^2 x_1 - \propto_1 x_0 + x_0^3\right) = 0 \qquad (7)$$

Then, two following equations can be derived:

$$\ddot{x}_0 + \omega^2 x_0 = \frac{F_1}{m_1}\cos\Omega_1 t \qquad (8)$$

$$\ddot{x}_1 + \omega^2 x_1 = \propto_1 x_0 - x_0^3 \qquad (9)$$

Assuming the initial condition of $x_0(0) = A$ and $\dot{x}_0(0) = 0$, homogenous and particular solutions for equation (8) can be expressed as follow:

$$x_0(t) = \beta\cos\Omega_1 t + (A-\beta)\cos\omega t \qquad (10)$$

Where, A is response amplitude of surge motion and β is corresponding parameter for force-mass ratio which can be calculated through $\frac{F_1}{m_1(\omega^2-\Omega_1^2)}$. Replacing equation (10) into (9) and applying required

simplifications by trigonometric expansions and declared equations in reference [7], it yields:

$$\ddot{x}_1 + \omega^2 x_1 = \cos\Omega_1 t\left[\propto_1 \beta + \frac{3}{4}\beta^3 + \frac{3}{2}\beta(A-\beta)^2\right] +$$
$$\cos\omega t\left[\propto_1 (A-\beta) + \frac{3}{4}(A-\beta)^3 + \frac{3}{2}\beta^2(A-\beta)\right] +$$
$$\cos 3\Omega_1 t\left[\frac{\beta^3}{4}\right] + \cos 3\omega t\left[\frac{(A-\beta)^3}{4}\right] +$$
$$\frac{3}{4}\beta^2(A-\beta)\left[\cos(\omega - 2\Omega_1)t + \cos(\omega + 2\Omega_1)t\right] +$$
$$\frac{3}{4}\beta(A-\beta)^2[\cos(2\omega - \Omega_1)t + \cos(2\omega + \Omega_1)t]$$

(11)

$$\propto_1 = -\frac{3}{2}\left[\frac{1}{2}(A-\beta)^2 + \beta^2\right] \qquad (12)$$

Substituting equation (12) in (6), frequency of surge motion can be expressed as:

$$\omega = \sqrt{1 - \frac{3}{2}\frac{\mu}{\omega_n^2}\left[\frac{1}{2}(A-\beta)^2 + \beta^2\right]}\,\omega_n \qquad (13)$$

The solution of equation (11) can be derived as:

$$x(t) = x_0(t) + \mu[x_1^h(t) + x_1^p(t) =$$
$$\beta\cos\Omega_1 t + (A-\beta)\cos\omega t + \mu[B_1\cos\omega t + C_1\cos\Omega_1 t +$$
$$C_2\cos 3\Omega_1 t + C_3\cos 3\omega t + D_1\cos(\omega - 2\Omega_1)t + D_2\cos(\omega + 2\Omega_1)t +$$
$$D_3\cos(2\omega - \Omega_1)t + D_4\cos(2\omega + \Omega_1)t] \qquad (14)$$

Similarly Eq. (3) can be written as $\ddot{y} + \omega_n^2 y = \frac{F_3}{m_3}\cos\Omega_3 t$ in which natural frequency of heave motion is $\omega_n = \sqrt{\frac{k_3}{m_3}}$.

3. Results and Conclusions

In this section, numerical studies on derived equations are presented in figures1 and 2. In the above figures, μ=0 corresponds with infinite depth. In another words, the cubic length of the tendon is going to be infinite ( ) and as a deduction k_1^(m^') will be zero. In relation with figure 1, when exciting force is small enough, the effect of μ=0 can be neglected. Subsequently surge motion equation can be rewritten in the linear form in which nonlinear effects of the mooring structure will be omitted. Although viscosity effects of the fluid seem to be relatively important, in the present study it is neglected. By increasing β, surge motion oscillations become more irregular. Results obtained from the modeling show β, μ and noticeably A parameter effect on structural response and leads to irregular oscillations in the responses. This problem is important for fatigue design in tension leg platform moorings.

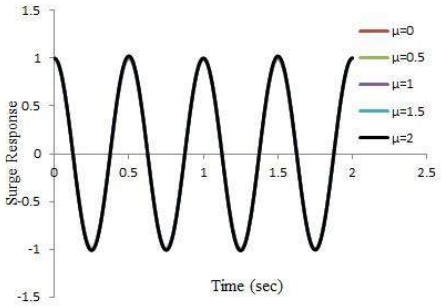

Figure 1. Surge motion response $(\boldsymbol{A = 1, \beta = 1})$

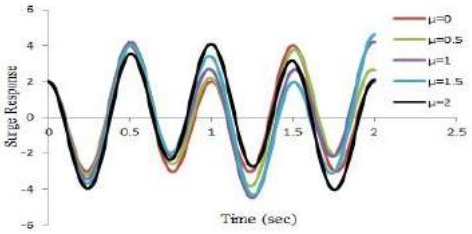

Figure 2. Surge motion response $(\boldsymbol{A = 2, \beta = 3})$

4. References

[1] Faltinsen, O. M., "Sea loads on ships and offshore structures", Cambridge ocean technology series 1991.

[2] Falnes, J., "Ocean waves and oscilating systems", Cambridge university press, 2004.

[3] Journee, J. M. J., and Massie, W. W., "Offshore Hydromechanics", Delft University of Technology, 2001.

[4] Chandrasekaran, S, and Jain, A. K., "Dynamic behavior of square and triangular offshore tension leg platforms under regular wave loads". Ocean Engineering 29, 2002. pp. 279-313.

[5] Tabeshpour, M. R., Golafshani, A. A., and Seif, M., "The effect of added mass fluctuation on heave vibration of TLP". International Journal of Engineering, 18(2),2004, pp. 219-229.

[6] Tabeshpour, M.R., Seif, M.S. and Golafshani, A.A. Vertical response of TLP with the effect of added mass fluctuation, 16th Symposium on Theory and Practice of Shipbuilding, Croatia, 2004.

[7] Abramowitz, M., and Stegun, I., "Handbook of Mathematical Functions", (Dover, New York), 1972.

NUMERICAL FATIGUE ANALYSIS OF JACK UP PLATFORM IN PERSIAN GULF CONDITION

Mohamad Javad Ketabdari[1] , Saeed Jabbari[2]
1) Amirkabir University, of Technology, Tehran, Iran, ketabdar@aut.ac.ir
2) Hormozgan University, Bandarabbas, Iran, j.saeed21@yahoo.com

1. Introduction

Jack-up platforms can experience different environmental situations according to their transport possibility. At the beginning these platforms were used as mobile docks [1] and then as drilling platforms for shallow waters. Time domain approach is mentioned as the most accurate method despite of its difficulties. While frequency domain methods usually are applied on simplified and linearized models. A frequency decomposition of wave forces on the structure shows that even for a regular wave, supper harmonics exist [2].

2. Environment Conditions

Offshore structures experience different loads such as wave, current, wind, earthquake and ice loads. Wave induced loads are the most important dynamic excitations for these structures even for the active seismically areas that design of structure is done based on earthquake excitations [3]. Drag force is a nonlinear second order force and a function of particle velocity. Inertia force is a first order function of particle acceleration. Total force applied on a platform is a composition of distributed force along the height and inundation force . It can be written in modal superposition form as [4]:

$$Q_m = F_m + P_m = \int_{-d}^{0} \Phi_m(z,t) f(z,t) dt + \Phi_m(0)(k_I(0)\dot{u}(0,t) + k_D(0)u(0,t)|u(0,t)|\eta \quad (1)$$

where Fm and Pm are distributed and inundation forces respectively. To predict wave force above the SWL that is an approximation of Taylor series expansion, higher orders are omitted because of their negligible values. For deep water platforms Airy theory can be used for water level prediction, particle acceleration and velocity. So the variable η is Gaussian because of its zero mean value while the applied force is non-Gaussian. For consideration of drag force in a modal frequency analysis various methods are recommended that the simplest choice is linearization leads to removal of higher order harmonics and also structure response will be in the frequency range that exists in the excitation spectrum. Approximation of nonlinear force to a polynomial function of higher orders depends on existence of two important factors, current and inundation force, that in absence of these factors a three order function with odd order terms will be used. Also in absence of current and because of no correlation between the distributed and inundation force there isn't any cross spectrum between them, since respectively the first force is an odd third order polynomial and the second is an even order quadratic polynomial. Polynomial approximations are as the following:

$$|u(z)|u(z) \cong a_1\sigma_u(z)u(z) + \frac{a_3}{\sigma_u(z)}u^3(z) = c_1(z)u(z) + c_3(z)u^3(z) \quad (2)$$

$$\eta u(0,t)|u(0,t) = \eta u_o|u_o| \cong a_0\sigma_\eta\sigma_{u_o}^2 + a_2\sigma_{u_o}u_o\eta + \frac{a_4 u_o^3\eta}{\sigma_{u_o}} = b_0 + b_2u_o\eta + b_4u_o^3\eta \quad (3)$$

$$S_{Q_mQ_n} = S_{F_mF_n} + S_{P_mP_n} \quad (4)$$

LSA method was used to obtain the coefficient of above formulas. Also Fourier series are used to compute the force spectrums.

$$S_{FF}(\omega) = \int R_{FF}(\tau)e^{-i\omega\tau}d\tau \quad (5)$$

That it is defined in statistics like the following [5]:

$$R_{FF}(\tau) = E[F(t)F(t+\tau)] \quad (6)$$

The governing spectrum of the location in Persian Gulf can be modified JONSWAP with a γ value of 2.68 [6]. In order to obtain natural frequencies, modal displacements and tensions of the structure finite element ABAQUS software was used. In modeling of the platform beam elements with pipe sections were used to simulate tubular members. Figs. 1 and 2 show modal displacement, natural frequencies and rack modeling respectively.

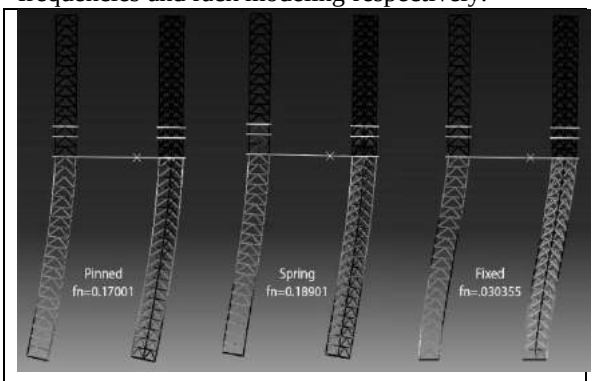

Fig. 1) Second mode displacement and natural frequencies of platform with pinned, fixed and spring modeling

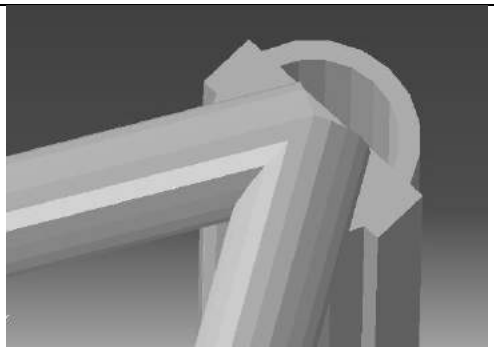

Figure 2. Rack modeling with rectangular section through chord member

3. Response Spectrum Definition

Transfer function Eq. 7 was used to obtain response spectrum Eq. 8:

$$H_{Qy_m}(\omega) = \frac{1}{M_m^*(\omega_m^2 - \omega^2 + 2i\xi_m\omega_m\omega)} \quad (7)$$

$$S_{y_m y_n} = H^*_{Qy_m}(\omega) H_{Qy_n}(\omega) S_{Q_m Q_n}(\omega) \quad (8)$$

4. Tension Prediction

In welded joints of jack up there are two different hot spots for each bracing. one of them is on the weld toe on bracing wall and the other is on the chord wall. For K joints there are four hot spots. Stress concentration coefficient is the ratio of hot spot tension σ_{max} to normal tension:

$$SCF = \frac{\sigma_{max}}{\sigma_N} \quad (9)$$

In this research Efthymiou equations [7] were used for stress concentration coefficient computation. Also the following equation was used to get modal tension spectrums [8].

$$S_{s_k s_k}(\omega) = \sum_{i=1}^{n}\sum_{j=1}^{n} T_{ki} T_{kj} S_{q_i q_j}(\omega) \quad (10)$$

where k is the point location, i and j are the degrees of freedom and Tki shows tension in point k in degree of freedom i. Figure 3 shows the fatigue spectrum of this jack up. For upper parts of legs near deck that are susceptible to fatigue the response fatigue spectrum has a wide band. Therefore calculation was performed using stress strain approach and Dirlik method [9].

5. Conclusion

In this research using nonlinear frequency analysis and transfer functions, structural response spectrum considering wave force including distributed and inundation force were obtained in different sea states of Persian Gulf. Cubic and quartic polynomials were used to approximate drag and inundation force respectively. Frequency analysis was performed with 3D modeling of platform and response spectrums were computed using MATLAB software. Also fatigue calculation was performed by stress-tension theory for pinned, fixed and spring modeling of soil-spudcan interaction. Finally fatigue damage calculation was obtained by Dirlik method and stress-tension approach in upper parts of legs near deck that are susceptible to fatigue

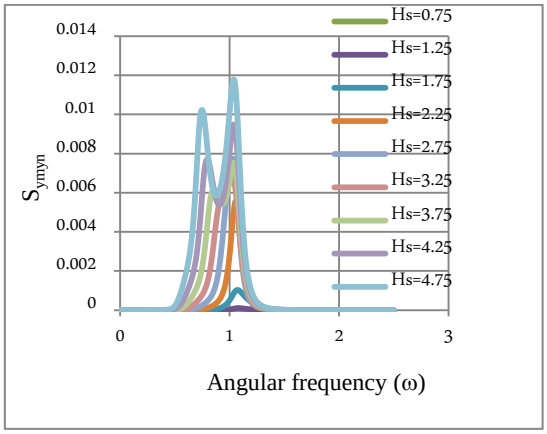

Figure 3. S_{ymyn} for pinned model under wave force considering inundation effect

.References

[1] Cassidy, M., "Non-linear analysis of jack-up structures subjected to random waves", Ph.D. thesis, university of oxford,1999.

[2] Chakrabarti, P., K. Chakrabarti, S., "A practical frequency-domain method for random-wave analysis and its application to jack-up units", OTC 10795,1999.

[3] Zheng, X. Y., "Nonlinear frequency-domain analysis of fixed structures subjected to morison-type wave forces" PhD thesis, National University of Singapore,2003.

[4] Zheng, X. Y., Liaw, C. Y., "Non-linear frequency-domain analysis of jack-up platforms" International Journal of Non-Linear Mechanics 39, 2004, pp 1519-1534.

[5] Newland, D. E., "An introduction to random vibrations spectral and wavelet analysis", United States New York,1993.

[6] Shafie far, M. Hamedi, A., "Proposing a spectral wave model for Northern part of Persian Gulf using available data and assessment of various wave spectral models", 5Th Internation Conference of Coasts, Ports and and Marine Structures, ICOPMAS, 2002.

[7] HSE, Stress concentration factors for simple tubular joints. Lloyd's register of shipping,1997.

[8] Sigurdsson, G., "Stochastic fatigue analysis of jacket type offshore structures", 2nd IFIP WG 7.5 working conference on reliability and optimization of structural systems, 1988.

[9] Halfpenny, A., "A frequency domain approach for fatigue life estimation from Finite Element Analysis" (1999), DAMAS, Dublin, 1999, pp. 401-410.

EFFECT OF COMBINED WAVE AND CURRENTS ON GROUP MARINE RISERS

Mohamad Javad Ketabdari[1] , Alireza Allahverdi[2]
1) Amirkabir University, of Technology, Tehran, Iran, ketabdar@aut.ac.ir
2) Amirkabir University, of Technology, Tehran, Iran, a.allahverdi@aut.ac.ir

1. Introduction

Risers are one of the most important components of offshore structures. The main task of the marine risers is transporting oil from the seabed to water surface. Because of the wave and current forces in the risers various forces affect these components causing their deformation. Marine risers often used in a group and the arrangement of groups risers effect on the drag and lift forces exerted to them due to waves and currents. In this study different variants were examined for modeling wave and riser interaction in order to determine the optimum arrangement for drag and lift forces.

2. Modeling

In order to model the wave, it was assumed that flow is viscous and rotational. Therefore Navier Stokes equations coupled with VOF were used for wave and current modeling. It was also assumed that marine current is uniform. There are different methods for numerical modeling of combined waves and currents. The method used in this article was wave generation by paddle in the wave tank [1]. This method was used to solve the problem employing FLUENT software. The standard k-ϵ model was used for turbulent modeling. The 3D calculation domain should be wide enough in the order of 3-4 wave lengths so that the walls do not influence the study area. The appropriate set up for this problem is seen in Fig.1. In this test a wave with the length of 80m and height of 3m accompanied by 0.6 m/se current reaches the modeled group risers. Four risers with a fixed vertical distance but variable longitudinal distance were used in order to study the influence of this longitudinal distance on risers behaviour. Distances were normalized by riser diameter denoted by D. Some distances were examined such as, 2.5, 2.75, 3, 3.25, 3.5, 4.5 to 7.5 D. First number is the minimum distance due to rules that are used for risers in related rulebooks. The last one is a distance that risers have no effect on each other. Fig 2 shows the geometry of four risers with a distance of 7.5D in flow direction.

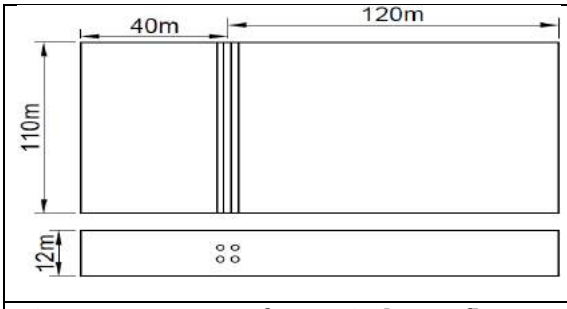

Figure 1. Geometry of numerical wave flume

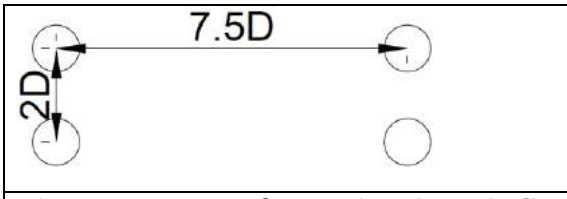

Figure 2. Geometry of group risers in ongitudinal distance of 7.5D

Lift and drag coefficients are determined in every time steps. Fig 3 shows the drag coefficient of the upstream riser and its corresponding downstream riser in distance of 2 diameters apart. As can be seen in this figure the upstream riser has bigger values of drag coefficient.

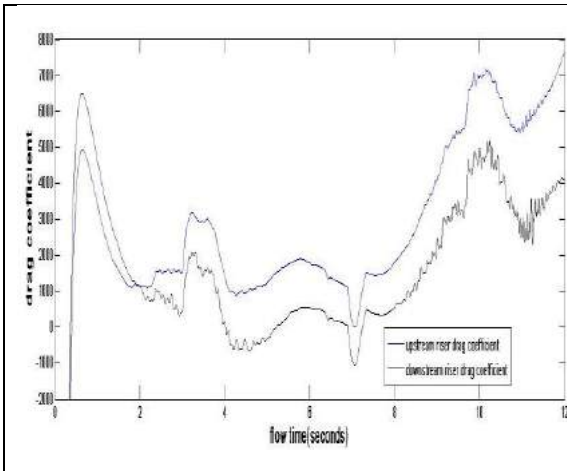

Figure 3. Time histories of drag coefficient of upstream and downstream risers

3. Model validation and results

The results obtained in this research were compared with the regulations and available data related to interaction of marine risers to validate the model [2-4]. Table 1 presents the maximum drag coefficient of upstream and downstream risers based on model. The effect of upstream riser on downstream one for different arrangements is demonstrated in this table in the form of drag coefficient reduction.

Figures 4 and 5 show the ratio of upstream to downstream drag and lift coefficients for different arrangements i.e. distances between risers, respectively. These figures show that longitudinal distance of 3 diameters is the optimum of distances due to maximum reduction of drag forces in this distance. Similar results are evident for lift forces.

Table 1. Maximum drag coefficient for upstream and downstream risers

Longitudinal distance	Maximum drag coefficient of Upstream risers	Maximum drag coefficient of downstream risers
2d	7.19E+03	6.49E+03
2.5d	7.47E+03	9.58E+03
2.75d	7.79E+03	1.04E+04
3.25d	8.47E+03	1.12E+04
3.5d	9.22E+03	1.16E+04
4.5d	1.02E+04	1.20E+04
7.5d	1.23E+04	1.23E+04

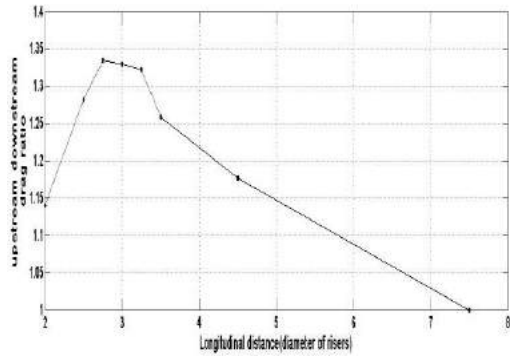

Figure 4. Ratio of upstream to downstream drag forces against longitudinal risers distances

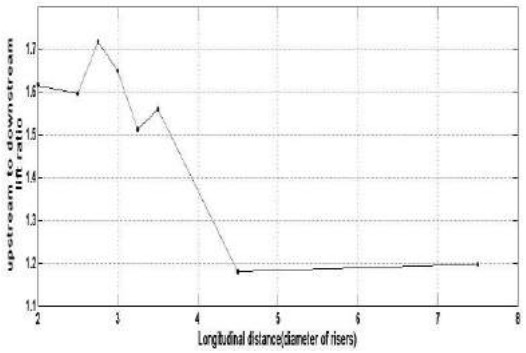

Figure 5. Ratio of upstream to downstream lift forces against longitudinal risers distances

4. Conclusion

Risers are important offshore platform element which their failure may cause serious disaster. In this research, a group of 4 risers were exposed to environmental loading of combined wave and current in a numerical wave flume using FLOW3D model. The optimum arrangement using longitudinal distance between risers was determined. The results showed that the optimum arrangement can reduce the environmental forces on the group risers dramatically. In comparison with rulebooks [5] it is noticed that this is slightly greater than the minimum allowable distance. For further investigation different geometry and number of risers in a group can be considered.

5. References

[1] FLUNET Help Tutorial, "Simulation of Wave Generation in a Tank" ver. 7

[2] DNV-RP-F203, "RISER INTERFERENCE."2011 edition

[3] Wu, W., Huang, S. and Barltrop, N. "Wake-induced large-amplitude low-frequency motions of a vertical riser in the wake of an upstream riser," in ASME 2002 21st International Conference on Offshore Mechanics and Arctic Engineering, 2002, pp. 19–24.

[4] Saint-Marcoux, J. and Blevins, R. "Wake Induced Riser Interference under VIV at 10^ 5 Reynolds," Proceedings of the 22th OMAE Conference Rhodes, Greece, 2012, pp.17–22.

[5] Huang, S., and Wu, W., "Non-dimensional Parameters Governing The Onset of Wake-Induced Marine Riser Collision", Proceedings of OMAE'03, , Cancun, Mexico, 2003, pp.es 1–6.

HEALTH MONITORING OF AN OFFSHORE PLATFORM IN THE PERSIAN GULF USING INVERSE VIBRATION TECHNIQUES

M. Hassan Haeri[1], Kiarash M. Dolatshahi[2], M. Ali Dastan Diznab[3] and Ali Akbar Golafshani[4]

1) Civil Engineering Department, Sharif University of Technology, Tehran, Iran, mh_haeri@mehr.sharif.edu
2) Civil Engineering Department, Sharif University of Technology, Tehran, Iran, dolatshahi@sharif.edu
3) Mechanical Engineering Department, Sharif University of Technology, Tehran, Iran, dastan@mech.sharif.edu
4) Civil Engineering Department, Sharif University of Technology, Tehran, Iran*

1. Inroduction

Offshore jacket-type structures are one of the most expensive and important infrastructures in the economy of countries with oil and gas resources. Environmental operating condition of these kinds of structures is severe, since the steel jacket is always subjected to destructive loads and excitations. Maintenance, optimal and longtime usage of such structures have been of particular interest over the last thirty years.

Many researches have worked on structural health monitoring (SHM) of offshore platforms using vibration data within the last thirty years. On the basis of classification system for damage-identification methods that were introduced by Rytter [1,2], there are four levels for health monitoring procedure:

• Level 1: Determine if damage is present in the structure

• Level 2: Level 1 plus determination of the location of the damage

• Level 3: Level 2 plus quantification of the severity of the damage

• Level 4: Level 3 plus prediction of the remaining service life of the structure

The main aim of this paper is to focus on the level 2 of health monitoring (damage localization) by using modal information data and the fundamental equations of motion and applying Inverse vibration techniques. The advantage of this procedure, comparing to the other studies, is the simplicity and applicability in performing infield health monitoring on jacket platform structures.

The main idea is to create simple lumped mass model as a reference model and trying to recalculate its dynamic characteristics (Fig. 1). As a matter of fact, stiffness of each level is an indicator that can represent the health of the substructures in that level. The role of inverse vibration technique in this situation is to identify the specifications of the reference model. To show the effectiveness of the proposed method, a case study is conducted on an offshore platform in the Persian Gulf, namely Resalat.

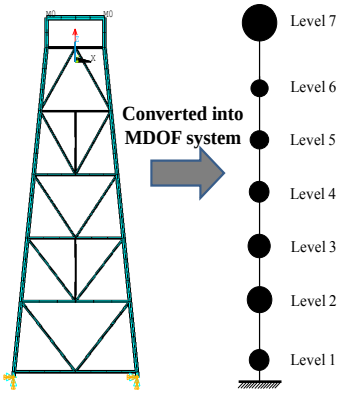

Figure 1. Schematic equivalent MDOF reference model

Inverse problem in vibration began in the former Soviet Union since 1933 in achieving the qualitative properties of the solutions of the Sturm-Liouville Equation. Gladwell introduced a method that finds the characteristics of a mass spring system [3]. In the characteristic equation of a lumped mass, 2-D shear building model (Fig. 2), the eigenvalue problem starts with mass and stiffness matrices. Applying inverse vibration algorithm leads to identification of the natural properties of the system such as mass and stiffness of each level from the modal data.

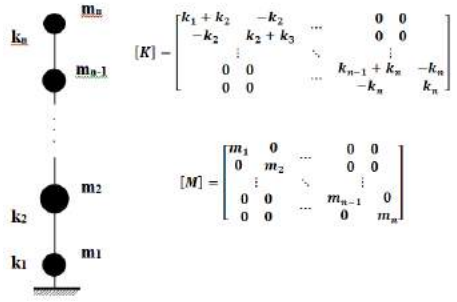

Figure 2. Simple dynamic MDOF lumped mass model

* Date of death:2016-04-11

2. Numerical Case Study

The Resalat platform is an existing offshore jacket platform in the Persian Gulf that is used as the case study in this investigation. Ressalat field is located in the Iranian waters of the Persian Gulf, about 80 Km to the south of Lavan island, in a water depth of 67 m. Ressalat offshore complex (Fig. 3) consists of a drilling platform, a production platform, a service platform and a flare tripod in the field. The field was originally developed and put into production in 1968. The service platform consists of a four leg battered jacket and the topside is located in 67.40 m water depth which is connected to production platform by means of an existing bridge [4].

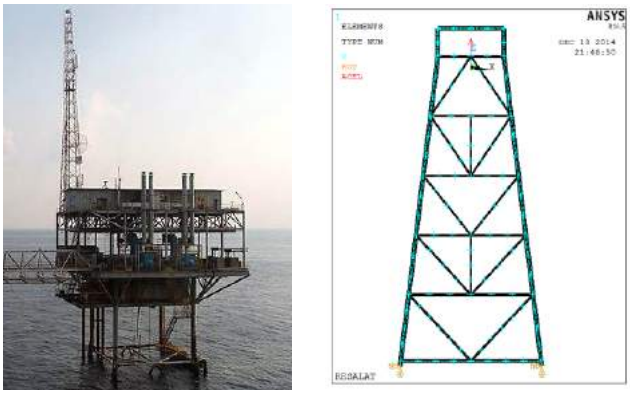

Figure 3. Resalat offshore jacket platform 2D computer model

3. Results and Discussion

To examine the functionality of the introduced procedure, at first it is required to build up the control lumped mass model by means of the first modal information obtained from the original model. The mode shape can be read from horizontal displacement in the first mode shape of 2D model. This operation was conducted to derive the stiffness of each level shown in Table 1. Afterward, some part of the original model is changed representing the induced damage in the system.

The damaged model has two damaged member simultaneously (Fig. 12). In this case two members are damaged in different levels in order to check the efficiency of the proposed damage localization procedure.

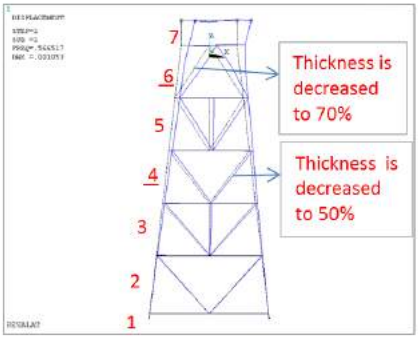

Figure 12. First mode shape of the damaged model

Table 1 compares the stiffness of the original and the damaged structure indicating the capability of this method in finding two damaged levels and the severity of damages.

Table 1. Stiffness of two corresponding lumped mass model of original and second damaged structure

	Intact model stiffness (MN/m)	Damaged model stiffness (MN/m)	Relative difference (%)
k_1	6419	6342	1.20
k_2	209	210	-0.48
k_3	166	169	-1.53
k_4	125	**101**	**18.87**
k_5	111	114	-2.33
k_6	640	**568**	**11.14**
k_7	26	26	1.31

As can be seen, this algorithm provides a practical approach for engineers to find the damaged area in jackets during operative lifetime. The method can be conducted by installing few accelerometers in the main levels of structures. The ambient vibration of the natural environment of the platform is adequate to excite the structure to provide the response of the accelerometers and to extract the data of the first mode of the jacket during the lifetime of the platform. Note that the noise effects in this study are not considered.

By comparing the resultant stiffness of the lumped mass of the corresponding model in each state the damaged level could be found. The main advantage of this method is the simplicity of calculation and convenient applicability. Moreover, the capability of this method in finding the two damaged levels and severity of each damage, can be useful in making decision during operating lifetime of jacket structures. This algorithm has the ability to be improved by changing the reference model to higher dimensions such as 2D or 3D; however, growing the computational cost is inventible.

4. References

[1] Doebling, S. W., Farrar, C. R., and Prime, M. B., 1998, "A summary review of vibration-based damage identification methods", *Shock and vibration digest, 30(2)*, pp. 91-105.

[2] Rytter, A., 1993, "Vibrational based inspection of civil engineering structures", Ph.D. Dissertation, Aalborg University, Denmark.

[3] Gladwell, G. M. L., 2006, "Inverse problems in vibration", Springer Science & Business Media.

[4] Golafshani, A. A., Tabeshpour, M. R., and Komachi, Y., 2009, "FEMA approaches in seismic assessment of jacket platforms (case study: Ressalat jacket of Persian gulf)" *Journal of Constructional Steel Research, 65(10)*, pp. 1979-1986.

[5] API RP2A-WSD, (2007) "American petroleum institute recommended practice for planning, designing and constructing fixed offshore platforms—working stress design", 21st ed. Errata and Supplement, Washington, DC, American Petroleum Institute.

EXPERIMENTAL INVESTIGATIONS ON STABILITY OF THE BANDAR ANZALI RUBBLE MOUND BREAKWATER WITH VARIOUS SIDE SLOPES DUE TO THE CASPIAN SEA SOLITARY WAVES

Amir Houshang Nezamivand Chegini[1], Diyanosh Hedayati[2], Shadi Esmaeeldoost[3]

1) Faculty of Engineering, University of Guilan, Rasht, Iran, chegini@guilan.ac.ir
2) Faculty of Engineering, University of Guilan, Rasht, Iran, Hedayatii@yahoo.com
3) Faculty of engineering ,University of Guilan, Rasht, Iran, esmaeeldoost.sh@gmail.com

1) Introduction

Rubble-mound breakwaters are one of the most important protecting structures in the coast and harbor engineering. Despite of the numerous theoretical and laboratorial investigations of the periodical waves' effect on rubble-mound breakwaters, there are a few investigations on stability of such structures under Tsunami attack. Tsunami is a wave that is mainly generated by underwater earthquakes [1]. In deep waters, these waves have long wavelength and they are very fast but when they reach to the coast, the shoaling occurs that their speed decreases; so wavelengths decrease too and their heights increase severely. Tsunami waves in shallow waters are in the form of Stocks waves and in the coast they are in the form of both Solitary waves and N-waves. Since the southern part of the Caspian Sea is prone to the tsunami attack, it would be noteworthy to study the resistance of the breakwater with different slopes.

2) Setting up laboratory operations

In the present study, the experiments are conducted on rubble mound breakwater in the two dimensional wave flume placed in the hydraulic laboratory of Guilan university in a 12.1 m long ,0.48 m wide and 0.5 m deep to investigate the influence of the Caspian Sea solitary waves on stability and deformation of the so-called breakwater. A total number of seven sets of experiments have been conducted for four different side slopes of the breakwater: 1:1, 1:1.25, 1:1.5, 1:1.75 (as shown in table 1) and in a scale of 1 to 60 of the Bandar Anzali rubble mound breakwater located in the southern zone of the Caspian Sea . The modeling of the Caspian Sea solitary wave (tsunami) in the flume is done by making a certain elevation difference in the two sides of the wave maker and by sudden opening of the gate.Three ultrasonic sensors were used for recording the water elevation changes in the front, backside and above the breakwater, as the same work which is done by Esteban et all [2].

Table 1. Experimental Conditions

Experiment	$d_{1(cm)}$	$d_{2(cm)}$	d_1/d_2	Type of wave generated
1	23	13	1.76	Non-breaking
2	24	13	1.86	Non-breaking
3	30	13	2.30	Bore
4	24	15.8	1.92	Non-breaking
5	25	15.8	2.30	Non-breaking
6	27	15.8	1.70	Non-breaking
7	27	15.8	1.83	Non-breaking

In the above table, d_1 is the water elevation in the back of the gate and d_2 is the water elevation in its front. For the purpose of calculating the dimensions and weights of the modeled breakwaters, the incoming formula is used [3]:

$$\frac{(W_a)_m}{(W_a)_p} = \frac{(\gamma_a)_m}{(\gamma_a)_p}\left(\frac{l_m}{l_p}\right)^3\left[\frac{(S_a)_p - 1}{(S_a)_m - 1}\right]^3 \quad (1)$$

Where W_a is the weight of each unit armor, γ_a is density of armor, $\frac{l_m}{l_p}$ is proposed linear scale and S_a is the ratio of armor's density to water's density. Table 2 shows the weight similarity between models and prototype which are driven from relation (1) and in fig.1 the inclined profile of modeled breakwater for the first slope of 1:1 is shown:

Table 2) Breakwater material weight similarity between models and prototype

	Armor Layer	Filter Layer	Core
Prototype	9 – 14 ton	0.75 – 1.5 ton	1 - 500 kg
Models	40 – 60 gr	3 - 7 gr	Less than 2 gr

Fig .1) Inclined profile of modeled breakwater with slope of 1:1

3) Results and Discussion

Due to the overflow, the drag force overcomes and rapidly makes the armor stones unstable. By failure of the crest material of the breakwater, the condition for ultimate destruction provides. Because of that lack of sufficient superstructure shows the first weakness of breakwaters against Tsunami wave. Since the slope of the model of 1:1 is high, minimum motivation in filter layer leads to breakwater instability. This matter is not sensible in model of other slopes. Consideration of recorded films and final profiles are indicating that destruction initiates from the crest of the breakwater and propagates through the rear area, at the still water level. An example of the breakwater deformation in the slope of 1:1.75 is given in fig.2.

Percentage of destruction of armor layer is calculated by the bellow relation [4]:

$$D = \frac{N_r}{N_T} \quad (2)$$

Which N_r is the replaced armor stones and N_T is the total amount of armor stones in each model.

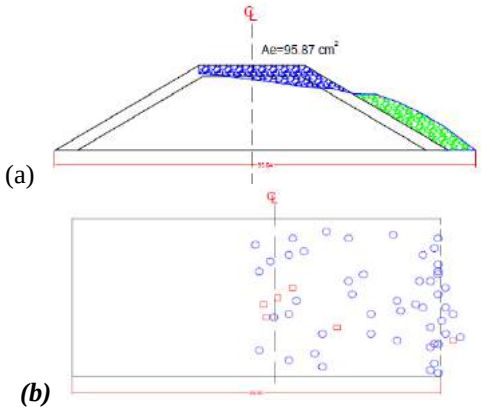

Fig .2) a- Deformed profile of the modeled breakwater with side slope of 1:1.75 (the stones move from the blue part to the green part). b- Displacement of the armor layer stones of the breakwater with slope of 1:1.75

5) Conclusion

The stones on the crest of the structure and the filter layer displaced and the core layer appeared. The destruction initiated from the crest of the breakwater and propagated through still water level in rear area. The final profile of the structure was in the form of S, which corresponds to previous works [5]. It seems that by strengthening the rear area and superstructure the ability of breakwater under tsunami attack increases which needs more investigations in this field. It can be assured from the results that in the case of a non-overflowing stream, the total wave energy made in the laboratory, can be merged by the armor layer. The results of this investigation can be used to strengthen this structure under Tsunami attack.

6) References

[1] Cuypers. I. K, Breakwater Stablility under Tsunami Attack, Report; (2004)

[2]Esteban. M, Morikubo. I, Shibayama. T, Munoz. R. A, Mikami. T, Thao. N. D, Ohira. K, Ohtani. A, Stability of Rubble Mound Breakwaters against Solitary Waves, Journal of Coastal Engineering, pp. 1-13; (2012)

[3] Esteban. M, Thao. N. D, Takagi. H, Shibayama. T,

[4] Satake. K, Linear and Non Linear Computations of 1992 Nicaraguan Earthquake Tsunami, In Pure and Applied Geophysics, Volume 144, pp. 445-469; (1995)

[5] Bryant. E, Tsunami: The Underrated Hazard, Cambridge University Press; (2001)

COMPARING DYNAMIC RESPONSE of NOSRAT OFFSHORE PLATFORM CONTROLLED □y SAMD □ith the ONE CONTROLLED □y SEMI ACTIVE MR DAMPER

Sheila Ariana[1], Touraj Taghikhany[2]

1) Department of Civil and Environmental Engineering, Amirkabir University of Technology, Tehran, Iran, shila.ariana@aut.ac.ir
2) Department of Civil and Environmental Engineering, Amirkabir University of Technology, Tehran, Iran, ttaghikhany@aut.ac.ir

1. Introduction

The offshore industry requires continued development of new technologies in order to produce oil in seismically active regions. Production platforms are required to stay on station during its lifetime, which is usually from 20 to 30 years [2].

Failure of huge offshore structures in ocean zone and their subsequent environmental disasters proved the importance of their maintenance and retrofitting.

In this study we used two different control system on an offshore structure named Nosrat jacket platform. In the following we had an investigation on the jacket dynamic response utilizing these two seismic control tools under Elcentro excitation and compare the result of their application. To reach this aim we modeled the Nosrat offshore platform in SACS software. The generated model had 198 degree of freedoms. Dynamic size reduction was inevitable for applying semi active control algorithm. This proceedure performed by programming in MATLAB software. In order to evaluate the performance of Nosrat platform equipped with semi active mass damper, H2LQG algorithm was selected. The SAMD utilized in this study, contains a passive tuned mass damper (TMD) and magneto-rheological damper in order to illustrate the control effect of SAMD. In the second section of our study we applied six Friction Pendulum isolators and four MR dampers in the joints of cellar deck elevation to mitigate Nosrat platform performance controlled by semi active MR dampers. Although Nosrat jacket dynamic response reduced in both methods, the vibration plots showed great differences between these two controller tools. As a consequence, we presented the comparative acceleration diagrams. As the diagrams showed the operation of semi active MR damper was considerably and accurately more pleasant in comparison with SAMD equipment.

2. Nosrat Jac□et Platform Parameters

The existing Nosrat Platform is located in the Iranian territorial water of the Persian Gulf ,approximately 100 km from the coast and 32 km South-west of Sire Island [1].

It was developed between 1976 and 1978 and is on stream since October 1978. The Nosrat jacket structure is a kind of fixed offshore platform. The existing jacket which is located in depth of 60 meters in Persian Gulf is a 6 legs platform [1].

3. Nosrat Jac□et Modeling in SACS Soft□are

The assessment analyses of Nosrat Jacket are linear and have been performed using SACS (Structural Analysis Computer System) suite of program.

A numerical model of Nosrat offshore jacket platform with 198 DOFs using SACS software was set up.

4. SAMD Design

As mentioned previously, SAMD system utilized here, is composed of a passive tuned mass damper (TMD) and Magneto-rheological Damper in order to illustrate the effect of the semi active control device.

TMDs need a considerable mass to achieve a sizeable reduction in the response.

In this study the SATMD is located in main deck elevation

5. MR Damper Design

As mentioned before, six Friction Pendulum isolators were considered to insert in the joints of cellar deck elevation. In addition four MR dampers are set in the location of isolators in cellar deck elevation.

□. Mass and Stiffness Matrices Reduction

The size of mass and stiffness matrices of 198 DOFs model which have been derived from SACS program was dynamically reduced so as to be utilized in control algorithm. To this end, the stiffness and mass matrices of the model has been reduced with modal coordinate in the finite time and frequency intervals by programming in MATLAB software.

The reduction procedure can be set up alternatively, either by first applying frequency and then time transformation of grammians, or by first applying time and then frequency transformation [3].

❑. Dynamic Performance of Nosrat Jac□et Platform

In this section, acceleration responses of celler deck joints are shown with 3 different circumstances under Elcentro seismic excitation. The uncontrolled plot showed the acceleration response of the Nosrat jacket platform without any controller. The SAMDcontrol plot showed the acceleration response controlled by semi active tuned mass damper and the MRcontrol plot showed the acceleration response by utilizing 4 MR Dampers. The acceleration plots of celler deck joints No.180 (Figure 1) and No. 193 (Figure 2) with 3 different circumstances under Elcentro earthquake is shown below.

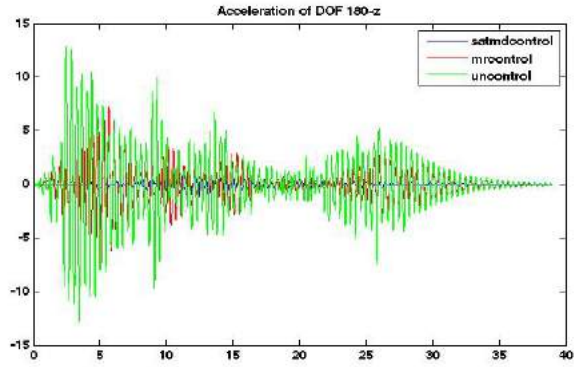

Figure 1. Acceleration response of celler deck joint No.180 under Elcentro earthquake

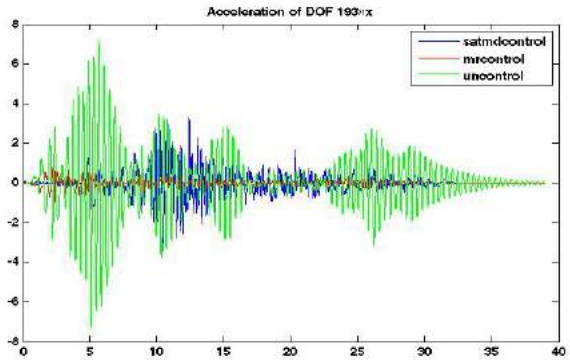

Figure2. Acceleration response of celler deck joint No.193 under Elcentro earthquake.

❑. Results and Conclusion

Comparison between acceleration responses of Nosrat jacket platform in two situations under Elcentro seismic vibration could be discussed. The first diagram was the maximum quantities of acceleration response reduction utilizing SAMD controller as the red diagram and MR controller as the blue one (Figure 3). The second diagram was the minimum quantities of acceleration response reduction utilizing SAMD controller as the red diagram and MR controller as the blue one (Figure 4).

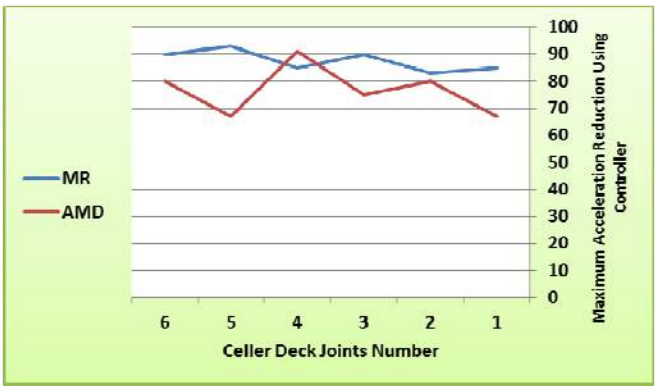

Figure3. Maximum acceleration reduction of celler deck joints under Elcentro earthquake

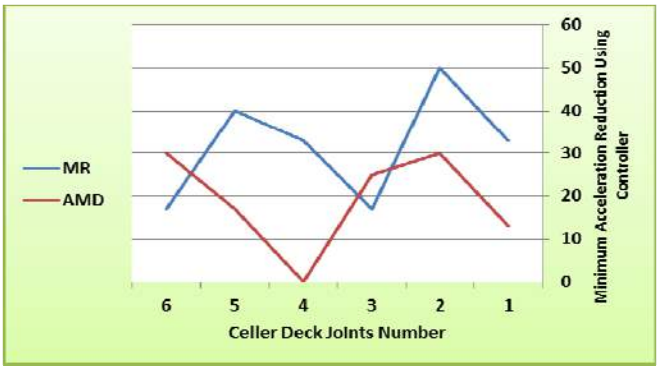

Figure4. Minimum acceleration reduction of celler deck joints under Elcentro earthquake.

Although Nosrat jacket dynamic response reduced in both methods, the vibration plots showed great differences between these two controller tools. As the diagrams showed the operation of semi active MR damper was considerably and accurately more pleasant in comparison with SAMD equipment.

.

❑. References

[1] IOEC, D., Inplace Analysis of Platform (DP-A), SD-EST-CN-DPAX-1000-D0, IOEC Company, Tehran, Iran, 2008.

[2] Chakrabarti, S. K., "Handbook of Offshore Engineering", Elsevier, San Francisco, California, USA, 2005

[3] Gawronski, W., "Advenced Structural Dynamics and Active Control of Structures", Springer, New York, USA, 2004.

[4] Gerwick, B. C.," Construction of Marine and Offshore Structures", CRC Press, San Francisco, California, USA ,2007.

[5] Preumont, A., "Vibration Control of Active Structure, An Introduction", 2nd Edition: KLUMER ACADEMIC PUBLISHERS, New York, USA ,2002.

RELIABILITY-BASED ASSESSMENT OF EXISTING OFFSHORE JACKET PLATFORMS: A CASE STUDY IN PERSIAN GULF

Hadi Khalili[1], Hamid Matin Nikoo[2], Hamid Golpour[3] and Iman Ahmadi[4]

1) TWI Persia, Structural Integrity Section, hadi.khalili@twi.co.ir
2) TWI Persia, Structural Integrity Section, hamid.matinnikoo@twi.co.ir
3) TWI Persia, Structural Integrity Section, hamid.golpour@twi.co.ir
4) POGC, Senior Structural Engineer, iahmadi@pogc.ir

1. Abstract

A large number of existing offshore platforms are operating beyond their design life due to the high cost of replacement. The safety of these structures creates strong reasons to develop an effective probabilistic framework for the reliability-based assessment of the structure. This paper presents a reliability-based approach for quantitative assessment of existing offshore jacket type platforms in terms of the Reliability Index (RI). RI would be a simple index to judge the structural integrity of platform.

A sufficient number of numerical analyses have been carried out to consider the effect of different uncertainties of system by conducting Monte Carlo Simulation. Next, the probability failure and RI of the structure have been estimated by regarding the Reserve Strength Ratio (RSR) as a desirable limit state. Sensitivity analysis has also been carried out to detect the impact of different source of uncertainties on the RI of an existing platform.

2. Sensitivity Analysis

Sensitivity analysis is widely accepted as a necessary part of reliability analysis of structures [1], [2]. The objective of this analysis is to identify the factors which have the most influence on reliability of the structure [3].

Assessment of an existing platform involves a large number of uncertainties including metocean hazards, structural characteristics, external loads, material behaviour and geotechnical information. In this paper, the results of sensitivity analysis have been presented in the form of a Tornado diagram which graphically shows the sensitivity of the target function to each random variable as listed in Table 1. For each random variable of Xi, two extreme values of $\mu_i \pm \sqrt{3}\sigma_i$ are taken [5]. Values of μ_i and σ_i denote the mean/median and the standard deviation of the random variable Xi, respectively. Then, the platform is analyzed separately for each of the extreme values of the random variable Xi and the corresponding target function is calculated.

The results show that among all random variables, Drag Coefficient (C_D) and Soil Parameters are most significant variable which affect the RSR. Moreover, it can be concluded that those parameters which are related to "load" such as MG and Mass are more important than those parameters which are related to "strength" of structures.

Table 1. Statistical characteristics of random variables

Random Variable	Mean / Median	Cov.	Type
Parameters influencing variability of the force			
Drag Coef.	0.65, 1.10	0.25	Lognormal
Inertia Coef.	1.60, 1.27	0.10	Lognormal
Marine Growth	50, 75mm	0.50	Lognormal
Parameters influencing in the structural model			
Load and Masses	Computed	0.10	Normal
Yield Stress of Legs and Braces	335, 345 MPa	0.07	Lognormal
Modulus of elasticity	2.0601×10^5 MPa	0.03	Lognormal
Parameters influencing in the pile-soil interaction			
Un-drained shear strength	*	0.3	Normal
Unit weight	*	0.1	Normal
Strain at one-half the maximum stress	*	0.4	Normal
Friction angle	*	0.03	Normal

3. Reliability-Based Assessment

The probabilistic framework for assessment of an existing structure can be seen as an extension of the probabilistic framework for the design of new structures. Reliability assessment for a jacket structural system may be complex due to the several structural components. However, by using the reliability theory, it is possible to establish jacket structural system reliability. This paper is focused on developing a probabilistic procedure based on some internationally recognized standards including API RP 2A-WSD [4], API RP-2SIM [6], ISO 19902 [7] to assessment of existing structures.

3.1. Reliability Index (RI)

Failure probability of a system (P_f) is defined as the probability of violating one or more limit states associated with the system failure modes. Given the definition of system failure state, the time-variant reliability is defined:

$$R = 1 - P_f \quad (1)$$

Where R is reliability and P_f is probability of failure. Reliability Index can be determined as follow:

$$\beta(t) = \varphi^{-1}(R) \quad (2)$$

Where φ is the standard normal cumulative distribution function. β(t) is an outcome which correspond with probability of 1-P_f in the standard normal cumulative distribution. In practical, the probability of failure and the associated RI are evaluated at a constant time interval such as a one year.

3.2. Limit State

The Reserve Strength Ratio (RSR) is used to specify the ultimate strength of the platform. Failure is defined when calculated RSR become less than RAC (Regional Acceptance Criteria) of a platform with respect to its exposure category. For example based on API-RP2A [4], for A-1 and A-2 platforms, RAC is equal to 1.6 and for A-3 category, RAC is equal to 0.8.

3.3. Sampling of Uncertainties

As described previously, C_d, C_m, E, MG, F_y, Mass and soil parameters are considered as uncertainties in this paper. To generate a sample of plausible collections of parameter values from a multidimensional distribution, Latin Hypercube Sampling (LHS) with size n = 100 has been used. Then, each interval corresponds to a 1% probability.

3.4. Wave Hazard Curve

The mean annual Exceedance rate of wave height in Persian Gulf Presented in [8] and illustrated in *Figure 1* is used for this purpose.

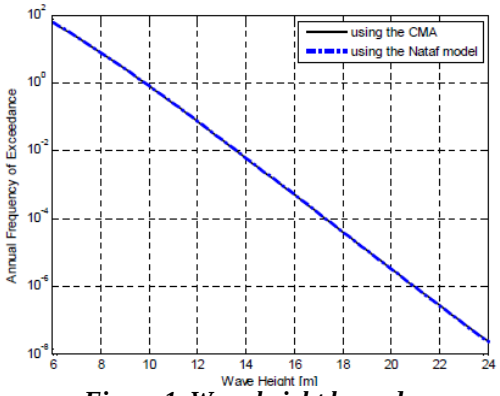

Figure 1. Wave height hazard curve

3.5. Probability of Failure

By implementing the total probability theory, the probability of failure of the platform is defined:

$$P_f = \sum P(H) \times P(f|H) \quad (3)$$

Which P(H) is the probability of occurrence of a wave with height H and P(f|H) is conditional probability of failure under wave H.

3.6. Results

In this paper wave height is considered from 8 m to 18m. This is because there is no failure (among all 100 cases) less than 8m and all cases fail for wave height more than 18m. Having obtained the above results, probability of failure is calculated. Table 2 shows the results of the probability analysis.

Table 2. Probability of failure of a case study platform

Wave Height (m)	No. of failed cases	P(f|H)	P(H)	P(f|H) x P(H)
8	0	0	9.04	0
9	2	0.02	2.63	0.0526
10	4	0.04	0.76	0.0304
11	14	0.14	0.22	0.0308
12	16	0.16	0.065	0.0104
13	36	0.36	0.018	0.0065
14	48	0.48	5.5e-3	0.00264
15	64	0.64	1.6e-3	0.00102
16	80	0.8	4.77e-4	0.00038
17	94	0.94	1.36e-4	0.00013
18	100	1.0	3.9e-5	3.9E-05
				∑ = 0.1349

According to equation (1), reliability of the platform will be 0.865 and reliability index is:

$\beta(t)=\varphi^{-1}(R)= 1.11$

4. Conclusion

To estimate the failure probability of the structure, for any specific intensity measure (wave height hazard), 100 analyses with different amount of uncertainties is performed and the number of platform failures was counted and P(f|H) for each wave height was calculated. Moreover, P(H) for each wave height was obtained from wave height hazard curve (Figure 1). Probability of failure of the platform has then been calculated according to the total probability theory.

5. References

[1] Saltelli A., Annoni P., Azzini I., Campolongo F., Ratto M., Tarantola S., "Variance based sensitivity analysis of model output. Design and estimator for the total sensitivity index", Computer Physics Communications, Volume 181, Issue 2, February 2010, Pages 259–270.

[2] Wainwright H., Finsterle S., Jung Y., Zhou Q., Birkholzer J., "Making sense of global sensitivity analyses", Computers & Geosciences, Volume 65, April 2014, Pages 84–94.

[3] Saltelli, A., Tarantola, S., Campolongo, F., and Ratto, M. (2004). Sensitivity analysis in practice: A guide to assessing scientific models, Wiley, New York.

[4] American Petroleum Institute, "Recommended Practice for Planning, Designing and Constructing Fixed Offshore Platforms - Working Stress Design", API RP2A WSD, 21st Edition, Supplement 2-3, October 2007.

[5] Porter, K.S. "A Beginner's Guide to Fragility, Vulnerability, and Risk", University of Colorado Boulder and SPA Risk LLC, Denver CO USA.

[6] API 2SIM, "Structural Integrity Management of Fixed Offshore Structures", First Edition, November 2014.

[7] ISO, "Petroleum and Natural Gas Industries - Fixed Offshore Platform", ISO-19902, First Edition, December 2007.

[8] Ebrahimian, H., "Assessment of Existing jacket-type offshore platforms in the Persian gulf region for service life extension or operative condition", PhD dissertation, 2012.

NUMERICAL XFEM FRACTURE ANALAYSIS OF FRP REPAIRED PIPELINES

Z. Valadi[1], H. Bayesteh[2] and S. Mohammadi[3]

1) School of Civil Engineering, University of Tehran, Tehran, Iran, z.valadi@ut.ac.ir
2) School of Civil Engineering, University of Tehran, Tehran, Iran, hbayesteh@ut.ac.ir
3) School of Civil Engineering, University of Tehran, Tehran, Iran, smoham@ut.ac.ir

1. Introduction

Tubular structures such as pressurized may experience different failure mechanisms in their lifetime. Existence of cracks may cause load capacity reduction, fluid leakage and structural collapse. Use of appropriate repair techniques is necessary to operate pipeline systems towards the end of their design service lives. High strength fiber reinforced polymer composite (FRP) repair systems are easily implemented, and increasingly used for retrofitting and strengthening of steel tubular joints, inshore and onshore systems and offshore pipelines [1–3]. In this paper, XFEM is used for analysis of cracked pipes with composite wrappings. The stress intensity factor, as a main fracture criterion, is investigated in two cases of cracked pipe with and without FRP repair.

2. Extended Finite Element Method

The extended finite element method (XFEM) is a powerful numerical approach for analysis of weak or strong discontinuities. In this method, there is no need for crack faces to match the finite element edges and therefore no remeshing techniques is required in crack growth problems [4,5]. Assume there is a discontinuity or singularity in an arbitrary domain discretized into some n-node finite elements. In the extended finite element method, the displacement for a point x inside the element is divided into two parts[6].

$$u^h(x) = u^{FE} + u^{enr} \quad (1)$$

where u^{FE} is the classical finite element displacement field,

$$u^{FE} = \sum_{j=1}^{n} N_j(x) u_j \quad (2)$$

n is the number of nodes of each finite element with classical degrees of freedom u_j and N_j are the shape functions. u^{enr} can be expressed in terms of crack-split u^H and crack-tip u^{tip} components as,

$$u^{enr} = \left[\sum_{h=1}^{mh} N_h(x) H(x) a_h\right] + \left[\sum_{k=1}^{mt} N_k(x) \left(\sum_{l=1}^{mf} F_l(x) b_k^l\right)\right] \quad (3)$$

where mh is the number of nodes associated with the crack face, a_h is the vector of additional degrees of freedom for modelling crack faces by the Heaviside function $H(x)$, mt is the number of nodes associated with the crack tip and b_k^l is the vector of additional degrees of freedom for modelling crack tips. $F_l(x)$ are the crack-tip enrichment functions, defined in terms of the local crack tip polar coordinate system (r,θ),

$$F_\alpha(r,\theta) = \left\{\sqrt{r}\sin\frac{\theta}{2}, \sqrt{r}\cos\frac{\theta}{2}, \sqrt{r}\sin\frac{\theta}{2}\sin\theta, \sqrt{r}\sin\theta\cos\frac{\theta}{2}\right\} \quad (4)$$

3. Material Properties

3.1. Steel Pipe

The extended finite element simulations are performed in the plane strain condition. The young's modulus of API 5L- X60 steel pipes is 210 GPa. The internal diameter and nominal thicknesses of pipe are given as 219mm and 10.3-mm and the internal pressure is 22 MPa [7].

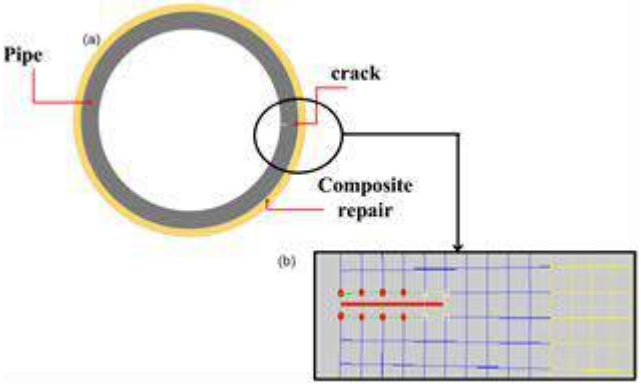

Figure1. (a) Repaired composite pipe and (b) Enriched nodes with the crack tip enrichments and the Heaviside function

3.2. FRP Properties

Three types of composite repair materials are selected to investigate the reduction of stress intensity factor in each case. They include:

1- Glass/epoxy with: $E_1 = 38.6$, $E_2 = 8.27$, $E_3 = 8.27$, $G_{12} = 4.14$ GPa, $\upsilon_{12} = 0.26$, $\upsilon_{23} = 0.33$, $\upsilon_{13} = 0.26$ [3]

2- composite sleeves with: $E = 49$ GPa, $\upsilon = 0.3$ [8]

3- AS4/3501-6 with $E_1 = 126$, $E_2 = 11$, $G_{12} = 6.6$ GPa , $\upsilon_{12} = 0.28$ and $\upsilon_{23} = 0.4$ [7 - 9]. The composite wrap has 4mm thickness (see Figure 1).

4. Results and Discussion

The stress intensity factor is computed for an edge cracked 2D pipe model. Tables 1and 2 compare the results for mode I stress intensity factors in different repair strategies. 8020 elements and 11228 nodes are used to create the XFEM model. SIFs are calculated by the interaction integration method, with the domain size of about 0.3-0.5 of crack length. The tip and split elements are shown in Figure 1.

Table 1. Mode I stress intensity factors for un-repaired pipe.

Length of crack (mm)	K_I ($MPa.mm^{0.5}$)
a = 3	1145.59
a = 5	2228.0117
a = 7	4273.4553

Table 2. Mode I stress intensity factors for repaired cracked pipe.

Composite material	Length of crack	K_I $MPa.mm^{0.5}$	K_I Reduction (%)
Glass/epoxy	a = 3	1062.18	7.2
	a = 5	2013.99	9.3
	a = 7	3691.81	13
AS4	a = 3	1016.65	11
	a = 5	1913.82	14
	a = 7	3402.24	20
Composite sleeve	a = 3	985.98	15
	a = 5	1747.62	24
	a = 7	2961.21	32

5. Conclusion

In this paper, XFEM method has been used for fracture analysis of cracked pipes with and without the repair. The obtained results show that the composite wrap reduces the SIF in comparison with the unrepaired pipe. In addition, decline in the rate of stress intensity factor depends on the composite material properties and the length of the crack. When the crack length is 7 mm, the rates of the SIF reduction in cracked pipe repaired with Glass/epoxy FRP, AS4 and composite sleeve are 13%, 20% and 32%, respectively. Accordingly, the use of composite sleeve is more effective in stress intensity factor reduction.

6. References

[1] T. S. Mally, A. L. Johnston, M. Chann, R. H. Walker, and M. W. Keller, "Performance of a carbon-fiber / epoxy composite for the underwater repair of pressure equipment", *Compos. Struct.*, vol. 100, pp. 542–547, 2013.

[2] C. Alexander and O. O. Ochoa, "Extending onshore pipeline repair to offshore steel risers with carbon – fiber reinforced composites", *Compos. Struct.*, vol. 92, no. 2, pp. 499–507, 2010.

[3] M. Lesani, M. R. Bahaari, and M. M. Shokrieh, "Numerical investigation of FRP-strengthened tubular T-joints under axial compressive loads", *Compos. Struct.*, vol. 100, pp. 71–78, 2013.

[4] S. E. Ashari and S. Mohammadi, "Delamination analysis of composites by new orthotropic bimaterial extended finite element method", no. February, pp. 1507–1543, 2011.

[5] H. Bayesteh and S. Mohammadi, "XFEM fracture analysis of shells : The effect of crack tip enrichments", *Comput. Mater. Sci.*, vol. 50, no. 10, pp. 2793–2813, 2011.

[6] S. Mohammadi, *XFEM Fracture Analysis of Composite,Wiley*, 2012.

[7] P. H. Chan, K. Y. Tshai, M. Johnson, and S. Li, "The flexural properties of composite repaired pipeline : Numerical simulation and experimental validation", vol. 133, pp. 312–321, 2015.

[8] H. S. Costa, J. M. L. Reis, L. M. Paim, M. L. Silva, R. L. Junior, and V. A. Perrut, "Failure analysis of corroded pipelines reinforced with composite repair systems", *Eng. Fail. Anal. J.*, vol. 59, pp. 223–236, 2016.

[9] P. H. Chan, K. Y. Tshai, M. Johnson, and S. Li, "Finite element analysis of combined static loadings on offshore pipe riser repaired with fibre-reinforced composite laminates", 2013.

UPHEAVAL BUCKLING ANALYSIS OF SUBSEA PIPELINE BY CONSIDERING THE EFFECT OF SEABED FRICTION USING THE POWER SERIES METHOD

M.Soltani[1], B. Asgarian[2] and A.R. Hadavand Khani[3]

1) Department of Civil Engineering, Faculty of Engineering, University of Kashan, Kashan, Iran, msoltani@kashanu.ac,ir
2) Civil Engineering Faculty, K.N. Toosi University of Technology, Tehran, Iran, asgarian@kntu.ac.ir
3) Civil Engineering Faculty, K.N. Toosi University of Technology, Tehran, Iran

1. Introduction

In this paper, the upheaval-buckling problem in subsea pipelines due to the effect of friction of seabed soil is investigated. Subsea pipelines are commonly laid unburied. Initial unevenness in the topography of seabed or later under scouring either may result in free spanning and produces upheaval buckling in pipelines. The abovementioned parameters can also cause serious harmful disasters. In order to evaluate the exact critical buckling loads of submerged pipelines, a numerical model based on power series expansions has been formed. In the proposed numerical method, the approximation function describing the buckling form of pipeline is derived by using the power series method and imposing the boundary conditions. The energy method is then used to evaluate the critical buckling load of subsea pipelines. One comprehensive example including of different types of pipelines are presented to verify the accuracy and validity of this method. The evaluated results are compared to the other available analytical methods.

Upheaval buckling analysis of subsea pipelines has been the subject of many researches in the past decades [1, 2]. Some experimental studies on upheaval buckling of buried pipelines were performed by Maltby [3, 4] and Yaylor [5]. Croll [6] used Martinet analysis method and made progress on it for buckling analysis of a clamped column. The study on thermal upheaval buckling load of subsea pipelines by considering the effects of localized and geometric imperfections on stability of mentioned structures was done by Ju [6].

2. Numerical Approach

In this study, a pipe of length ***L*** resting on elastic subsea floor is considered (Fig. 1). The elastic series is transitional with variable elastic constant ***K(x)***. The pipeline is subjected to static axial load ***$N_u(x)$*** and subsea floor friction.

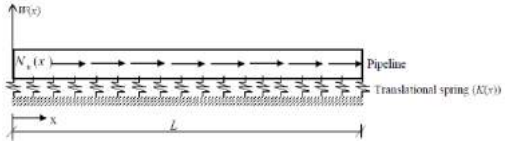

Fig. 1: Pipe on elastic seabed, subjected to variable axial force.

The differential equilibrium equation with variable coefficients for a pipe resting on elastic foundation loaded by variable axial force is:

$$EI\frac{\partial^4 W(x)}{\partial x^4}+\frac{\partial}{\partial x}[(N_u(x)-\mu\Big[\pi g\rho_p t(D-t)+\frac{\pi}{4}g\rho_f(D^2+4t^2-4Dt) -\frac{\pi}{4}g\rho_w D^2\Big])\frac{\partial W(x)}{\partial x}\Big]+\pi g\rho_p t(D-t)+\frac{\pi}{4}g\rho_f[D^2+4t^2-4Dt] -\frac{\pi}{4}g\rho_w D^2-KW(x)=0 \quad (1)$$

In the last expression, $N_u(x)$ is axial force acting on the pipe by a foreign body and μ denotes friction coefficient of the soil. ρ_f and ρ_p are internal fluid density and pipe material density, respectively. ρ_w is also water density. D represents pipe diameter and t thickness of pipeline. In what follows, power series expansions are used to solve the last equilibrium differential equation of a subsea pipeline (7). By pondering on this numerical technique, the variable axial load and the vertical displacement are expanded into power series form, as follow:

$$N_u(x)=\sum_{i=0}^{\infty}N_{ui}x^i, \qquad w(x)=\sum_{i=0}^{\infty}b_i x^i \quad (2)$$

Where N_{ui} is coefficient of power series at order *i*. In order to ease the solution of the stability equation, a dimensionless variable ($\xi=x/L$) is introduced. Substituting Eq. (2) and the non-dimensional variable ξ into the stability Eq. (1) lead to the following equation:

$$EI(\sum_{i=0}^{\infty}(i+1)(i+2)b_{i+2}\xi^i)+L^2\frac{\partial}{\partial\xi}[(\sum_{i=0}^{\infty}N_{ui}L^i\xi^i-\mu\Big[\pi g\rho_p t(D-t) -\frac{\pi}{4}g\rho_w D^2+\frac{\pi}{4}g\rho_f(D^2+4t^2-4Dt)\Big])(\sum_{i=0}^{\infty}(i+1)b_{i+1}\xi^i)\Big] -L^4K(\sum_{i=0}^{\infty}b_i\xi^i)+L^4\pi g\rho_p t(D-t)+\frac{\pi}{4}L^4g\rho_f[D^2+4t^2-4Dt] -\frac{\pi}{4}L^4g\rho_w D^2=0 \quad (3)$$

The multiplication of the two series in each term of equation (3), the following recurrence relation is found:

$$EI\left(\sum_{i=0}^{\infty}(i+1)(i+2)b_{i+2}\xi^i\right)+L^2\left(\sum_{i=0}^{\infty}\sum_{j=0}^{i}N_{ij}^{*}b_{i-j+2}(i-j+2)(i+1)\right. \quad (4)$$

$$\left.-\mu(\pi g\rho_p t(D-t)\frac{\pi}{4}g\rho_w D^2+\frac{\pi}{4}g\rho_f(D^2+4t^2-4Dt))\sum_{i=0}^{\infty}(i+1)(i+2)b_{i+2}\xi^i\right)$$

$$-L^4K\left(\sum_{i=0}^{\infty}b_i\xi^i\right)+L^4\pi g\rho_p t(D-t)+\frac{\pi}{4}L^4g\rho_f(D^2+4t^2-4Dt)-\frac{\pi}{4}L^4g\rho_w D^2=0$$

According to the last expression, the obtained parametric solution of Eq. (1) contains four unknown coefficients (b_0,b_1,b_2,b_3). Then the fundamental solution of the equilibrium equation of subsea pipeline can be expressed in the following form:

$$w(\xi)=b_0w_0(\xi)+b_1w_1(\xi)+b_2w_2(\xi)+b_3w_3(\xi) \quad (5)$$

It has to be notified that the four undefined coefficients (b_0,b_1,b_2,b_3) are functions of the displacements of degree of freedom (DOF). These mentioned unknown parameters can be obtained by imposing the right and left ends boundary conditions of pipe element (two at each end of the pipe).

3. Energy method:

In this part, it is assumed that the displacement equation obtained in previous section is the approximated buckling form of the pipeline. The value of upheaval critical buckling load of the subsea pipeline with variable cross-section can be determined by variation of total potential energy, which is:

$$\delta(U_l+U_0+U_f-W_e)=0 \quad (6)$$

In Eq. (6), δ represents a virtual variation. U_l and U_0 denote the elastic strain energy and the strain energy due to the initial stresses on the considered element, U_F the linear elastic energy corresponding to the elastic foundation, and W_e the work of the applied loads. The strain energy for an offshore pipeline resting on an elastic subsea can be written as:

$$U_l=\frac{1}{2}\int_0^L EI\left(\frac{\partial^2W}{\partial x^2}\right)^2dx \quad (7)$$

The strain energy due to effects of the initial stresses can be defined as:

$$U_0=\frac{1}{2}\int_0^L\left(N_u(x)\right. \quad (8)$$

$$\left.-\mu(\frac{\pi}{4}\rho_l g(D-2t)^2+\rho_p gt(D-t)-\frac{\pi}{4}\rho_w gD^2))(\frac{\partial W}{\partial x})^2dx\right.$$

The energy due to the presence of linear elastic foundation is:

$$U_f=\frac{1}{2}\int_0^L K(W(x))^2dx \quad (9)$$

The external load work W_e of the pipeline the vertical force of subsea floor reaction $gF_I(x)$ is determined by the following formulation:

$$W_e=-g\int_0^L(\frac{\pi}{4}\rho_l g(D-2t)^2+\rho_p gt(D-t)-\frac{\pi}{4}\rho_w gD^2)W(x)dx \quad (10)$$

In order to compute the approximation displacement based on power series expansions and the critical buckling load regarding to energy method, all calculation procedures are done with the aid of Matlab software [7].

4. Numerical Example:

In this section, to check the accuracy and the validity of proposed method, five cases involving instability analysis of a fixed-ends pipeline with constant cross-sections are presented in this example. For analysis, pipeline with the length of 100m is considered. The diameter of cross-section for all models is constant and equals to 660 mm and its thickness is 15.88 mm. Geometric dimensions, material and soil properties are pictured in Fig. 2.

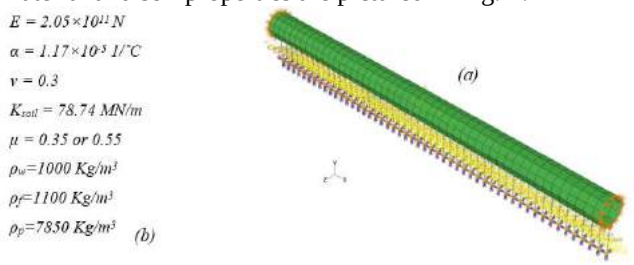

Fig. 2: (a): 3D model of a pipe body using ABAQUS and (b): material properties

In **Case a,** we investigate the elastic buckling of a fixed-fixed pipeline resting on Winkler type elastic foundation. The analyzed member is subjected to a concentrated compressive axial load.

In **Case b**, the effects of reaction and friction of subsea soil on the critical buckling load of a pipeline with the length of 100 m are studied. In this case, the subsea pipeline is resting on an elastic floor with friction coefficient of 0.35.

In **Case c**, the buckling load of a pipe with constant cross-section resting on the soil in the presence of its friction is investigated again. In this example, one considers the friction constant of the elastic seabed equals to 0.55. Table 1 gives the critical buckling load of the considered pipeline under the different abovementioned conditions. Effect of degree of the power series on convergence is also displayed in Table 1.

Table 1: Critical linear buckling loads for abovementioned cases (MN)

Case	Number of terms of power series		ABAQUS Software
	10	15	
a	1.413	1.378	1.30
b	1.503	1.476	1.35
c	1.541	1.513	1.39

References:

[1] Guo B, Song S, Chacko J, Ghalambor A. Offshore Pipelines. Gulf Professional Publishing, New York, Elsevier, 2005.

[2] Braestrup M.W, et al. Design and Installation of Marine Pipelines. Blackwell Publishing, 2005.

[3] Maltby T.C, Calladine C.R. An investigation into upheaval buckling of buried pipelines-I. Experimental apparatus and some observations. International Journal of Mechanical Sciences 1995; 37(9): 943-963.

[4] Maltby T.C, Calladine C.R. An investigation into upheaval buckling of buried pipelines-II. Theory and analysis of experimental observations. International Journal of Mechanical Sciences 1995; 37(9): 965-983.

[5] Taylor N, Tran V. Experimental and theoretical studies in subsea pipeline buckling. Marine Structures 1996; 9: 211-257.

[6] Croll J.G.A. A simplified model of upheaval thermal buckling of subsea pipelines. Thin-Walled Structures 1997; 29: 59-78.

[7] MATLAB Version 7.6 .MathWorks Inc, USA, 2008

STUDY OF FLOW CHARACTRISTICS AROUND A CIRCULAR CYLINDER NEAR PLANE BOUNDARY

M. A Salehi.[1] S., Mazaheri [2] and M. H. Kazeminezhad [3]

1) Ocean Engineering and Technology Research Center, Iranian National Institute for Oceanography and Atmospheric Sciences, Tehran, Iran, mascivil9@gmail.com
2) Ocean Engineering and Technology Research Center, Iranian National Institute for Oceanography and Atmospheric Sciences, Tehran, Iran, said.mazaheri@inio.ac.ir
3) Ocean Engineering and Technology Research Center, Iranian National Institute for Oceanography and Atmospheric Sciences, Tehran, Iran, mkazeminezhad@inio.ac.ir

1. Introduction

Flow around circular cylinders near plane boundary has been a subject of interest because of vast practical engineering applications such as offshore pipelines near seabed. Vortex shedding phenomenon leads to vortex induced vibration of a cylinder subjected to both inline and cross flow, which is undesirable due to fatigue concerns. In order to control or suppress vortex shedding an adequate knowledge of flow characteristics around a circular cylinder based on reliable quantitative parameters and visualized outputs is necessary.

The flow characteristics around a circular cylinder near plane was has been studied using Open source CFD codes of OpenFOAM in different flow regimes (Re=100, 200, 3900) and different gap ratios (G/D=∞, 1, 0.5, 0.2).

According to results, occurrence of vortex shedding suppression can be determined based on a combination of plane wall effect and flow regime parameters such as gap to boundary layer thickness ratio. Also Pressure distribution around cylinder surface and separation angle of vortices can be observed as further implication of the process of suppression. Some of near wall flow field parameters around circular cylinder has been illustrated in figure 1.

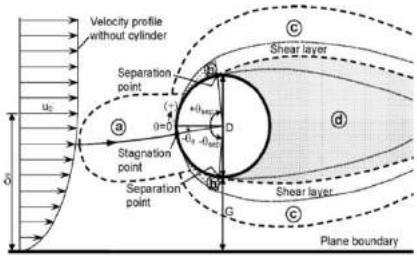

Figure 1. Definition of near wall flow field parameters around circular cylinder, [1]

2. Numerical modeling:

2.1. Governing Equations:

Navier-Stokes equations including continuity equation are the governing equations for incompressible fluid flow:

$$\frac{\partial u_i}{\partial x_i} = 0 \qquad (1)$$

$$\rho\left(\frac{\partial u_i}{\partial t} + u_j \frac{\partial u_i}{\partial x_i}\right) = B_i - \frac{\partial p}{\partial x_i} + \mu \frac{\partial^2 u_i}{\partial x_j \partial x_j} + \frac{\partial}{\partial xj}\left(-\rho u_i' u_j'\right) \qquad (2)$$

$$\tau = \left(-\rho u_i' u_j'\right) \qquad (3)$$

Where u, p, ρ, υ, B and τ are the velocity ,pressure ,density, kinematics viscosity, body forces and shear stress respectively.

2.2. Computational Domain

Computational domain of 30D×20D×10D dimensions with totally hexahedral meshes was created. Cylinder diameter "D" is set equal to 10cm. Boundary conditions for far field and near the plane wall cases are shown in Fig.2.

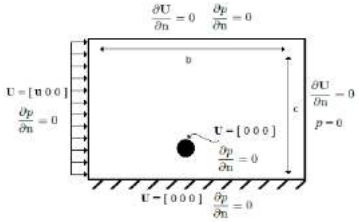

Figure 2. Boundary conditions for flow around circular cylinder near the wall

2.3. Numerical Model

In order to solve the equations numerically, IcoFOAM, the basic laminar incompressible solver of OpenFOAM has been used for Re=100 and 200, while for Re=3900, PimpleFOAM (merged PISO-SIMPLE algorithm), which is a large time-step transient model solver for incompressible flow alongside K-ω and SST turbulence has been employed.

3. Model Verification:

Comparison of simulation results for flow around circular cylinder far from plane boundary, including drag coefficient, positive maximum lift coefficient and Strouhal number were considered and compared with those obtained by Cao and Wan (2010), Williamson (1991), Norberg (2003) and Rosetti et al, showed good agreement, Table 1. Also the computational velocity fields from the present simulations are compared with the experimental results obtained from PIV measurements of Kirkgoz et al., [1], for further validation of the numerical code, Figure 3.

Table 1. Comparison of C_d, C_l(max) and S_t parameters for Re=100,200

	Re=100			Re=200		
	C_d	C_l	S_t	C_d	C_l	S_t
Present study	1.26	0.11	0.16	1.2	0.31	0.19
Cao and Wan	1.39	-	0.16	1.4	-	0.19
Williamson	-	-	0.16	-	-	0.19
Norberg	-	0.12	0.16	-	0.32	0.18
Rosetti et al.	1.41	-	0.17	1.3	-	0.2

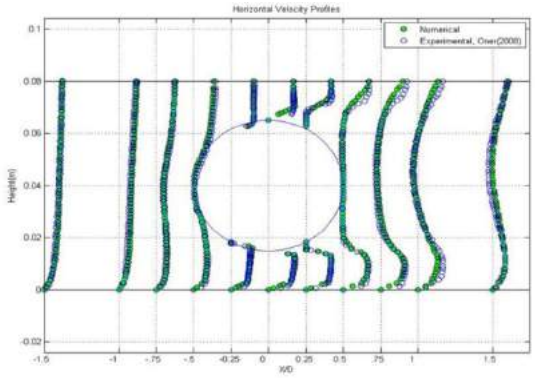

Figure 3.comparison horizontal velocity profiles of present numerical simulation and experimental study of Oner et. Al (2008)

4. Results and Discussion:

Quantitative parameters and visualization outputs such as time-averaged streamlines and vorticity iso-surfaces were used to describe the characteristics of flow around circular cylinder near plane boundary.

Table 2 presents the results of 3-D computations including hydrodynamic drag, cd(mean) and lift coefficients, cl(rms), Strouhal number (st), gap to boundary layer thickness ratio (G/δ), Separation angle, Stagnation angle and base pressure, Cpb, for different gap ratios and Re=3900. It has been observed that for the range of G/δ < 0.45 there`s a high possibility of vortex shedding suppression. figure 4 shows pressure distribution around circular cylinder at G/D=0.2. For all cases, it has been observed a rapid decrease in pressure, in the front zone of cylinder while cylinder approaches the wall. This adds to unbalanced pressure between top and bottom of cylinder, which leads to higher lift force on cylinder. The amount of pressure decrease in front zone and increase in lift coefficient is less in cases that experience vortex shedding suppression in comparison to cases without suppression.

Table 2. Results of 3-D computations for all cases with gap ratios, Re=3900

Re=3900	G/D= ∞	G/D=1	G/D=0.5	G/D=0.2
cd(mean)	1.281	1.712	1.544	1.238
cl(rms)	0.677	1.032	0.896	0.51
st	0.214	0.18	0.092	0.04*
G/δ	-	2.174	1.087	0.435
separation angle	98.98	98.97	92.75	85.5
stagnation angle	0	-2.2	-14.7	-6.8
Cpb	-1.15	-1.71	-1.13	-0.91

*: Indicates suppression of vortex shedding

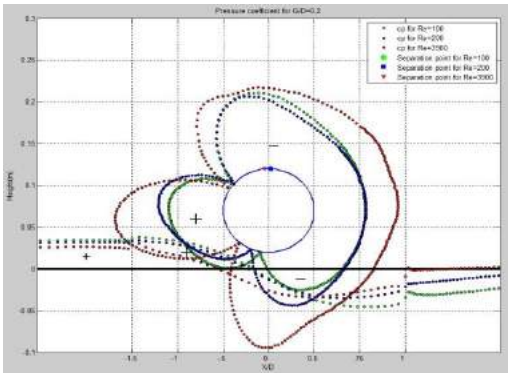

Figure 4. Pressure coefficient distribution around circualr cylinder at G/D=0.2, for Re=100,200,3900

5. References

[1] Kirkgoz, M. S., Oner, A. A. and Akoz, M. S. (2009) Numerical Modeling of Interaction of a Current with a Circular Cylinder near a Rigid Bed. *Advances in Engineering Software*, 40, 1191-1199

[2] Cao, H., Wan, D., (2010), Application of OpenFOAM to Simulate Three-Dimensional Flows past a Single and Two Tandem Circular Cylinders , Proceedings of the Twentieth (2010) International Offshore and Polar Engineering Conference Beijing, China, June 20-25, 2010.

[3] Williamson, CHK (1991). 2-D and 3-D Aspects of the Wake of a Cylinder, and Their Relation to Wake Computations, *Lect Appl Math*, Vol 28, pp 719-751.

[4] Norberg, C., (2003), Fluctuating lift on a circular cylinder: review and new measurements, *Journal of Fluids and Structures* 17, 57–96.

[5] Rosetti, G. F., Vaz, G. and Fujarra, A. L. C.,(2012), "URANS Calculations For Smooth Circular Cylinder Flow In A Wide Range Of Reynolds Numbers: Solution Verification And Validation", *Journal of Fluids Engineering*, Vol. 134, 121103, 2012.

FATIGUE ANALYSIS DUE TO MULTI-SPANNING SUBSEA PIPELINES IN IRANIAN SOUTH PARS GAS FIELD

Abdolrahim Taheri[1], Mohammad Mahdi Shabani[2]

[1]Assistant Professor, Petroleum University of Technology; rahim.taheri@put.ac.ir
[2]M.Sc. Student, Petroleum University of Technology; m.shabani@mnc.put.ac.ir

1. Introduction

The subsea Pipelines plays an important role in the offshore industries which is usually installed to transport the production from subsea wells to pipeline end manifold(PLEM) or export production from the offshore facilities to the onshore terminations. There are some methods to decrease the span length such as change route, or adjust wall thickness or grade of material. Lower spans by using man-made supports may reduce VIV fatigue damage but encountering harsh climate is unavoidable for some cases and free spans may occur [[1] [2]].

Subsea pipeline free spans are mainly triggered by seabed unevenness/scouring or artificial supports/rock beams, etc. The vortex shedding frequency caused by a flow normal to a free span is governed by the pipeline outer diameter, the current velocity and the Strouhal's number. Once the shedding frequency reaches the natural frequency of a span then it starts to vibrate and VIV occur. So free span analysis has an ineligible effect on the design of subsea pipeline[3] .

In this paper, the main objective is to present a procedure for the multi-spans fatigue assessment of existing submarine pipeline in Iran South Pars Gas Field by using the DNV-RP-F105 and ABAQUS software.

2. The Multi-Spans Fatigue Analysis Methodology of Subsea Pipeline

The pipeline crossing is evaluated to determine fatigue damage due to VIV in operating condition. VIV occurs as the result of periodic of vortices around the pipe. As the frequency of vortex shedding close to the pipeline natural frequency, the pipeline begins to resonate and can cause rapid pipeline failure[4]

The VIV fatigue analysis includes several factors such as soil-pipe interactions, modeling of environmental loads, structural response analysis, etc. In this study ABAQUS software has been used to simulate soil-pipeline interactions and structural response. Then the MATLAB software is used to calculate the fatigue life capacity due to frequencies and stresses based on the ABAQUS analysis results in cross-flow directions.

The following steps are performed to obtain the VIV fatigue damage of the subsea pipeline:

- Cross-flow Eigen frequencies and mode shapes are calculated for pipeline at crossing with ABAQUS software.
- Fatigue life damages are calculated by using the Eigen frequencies and unit stress amplitudes in the MATLAB software and then fatigue life can be calculated according to corresponding fatigue damages.

3. Finite Element Model

The pipeline is modeled as a 2D beam with PIPE21. Both ends of the pipe were fixed axially after the pipeline was completely laid down on the seabed with a nominal residual bottom-tension force. In the load steps, the pipe gravity force is applied to the model first, followed by the internal pressure, external pressure [4] .

After the model has been set at the appropriate loading directions, natural frequencies in the cross flow directions and corresponding mode shapes can be obtained. A schematic figure of multi-span model is shown in Figure 1.

The following aspects should be considered for the pipeline ABAQUS model:

1. The pipeline coating effect is limited only to increase the pipeline submerged weight, drag forces, added mas and buoyancy, the stiffness and strength increase has been neglected.
2. The pipeline element length should be in the order of the outer diameter of the pipeline.
3. The boundary condition at both ends of the pipe model shall accurately represent the pipe-soil interaction and the continuity of the pipeline.
4. Sufficient pipe model length at both sides of the span should be created to account for the effect of adjacent spans.

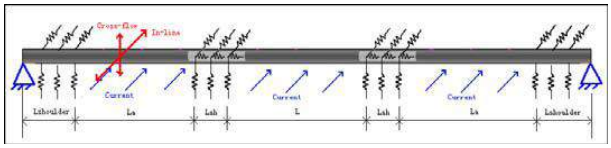

***Figure 1. The schematic figure of the multi-span ABABQUS model* [5].**

4. Fatigue Damage

The fatigue damage due cross-flow VIVs is calculated based on DNV-RP-F105[4], the following fatigue criterion which is limited to stress cycles within the elastic ranges can be used for subsea free spanning pipeline fatigue assessment. The fatigue criterion can be formulated as:

$$\eta.T_{life} \le T_{exposure} \quad (1)$$

5. Multi-Span Fatigue Analysis Case Study

VIV fatigue analysis for multi-span pipeline with multi-mode response is performed for 32inch gas flow with 28.8^{mm} wall thickness at water depth of 64^{m}. Span design procedure is determined by allowable static and dynamic loads on free span. Then on-bottom roughness analysis is performed to determine actual spanning condition. Free span length in this case study is considered about 20m and L/D=24.6. The case study is a line pipe of 22th phase of south pars gas field complex.

5.1. Environmental condition

The environment data must be collected from periods that are representative for the long-term variation of the wave and current climate. For deep water fatigue analysis, effect of wave induced vibration can be neglected and only effect of current can be considered [5]

Current velocity is described by Weibull distribution which α, β and ϒ will be determine by Design Basis.

$$F_X(x) = 1 - exp\left(-\left(\frac{x-\gamma}{\alpha}\right)^{\beta}\right) \quad (3)$$

Current velocities are varying from $0.5^{m/sec}$ up to $0.75^{m/sec}$ in the Persian Gulf. The probability of the current flow by Weibull distribution is presented in Figure 2 .

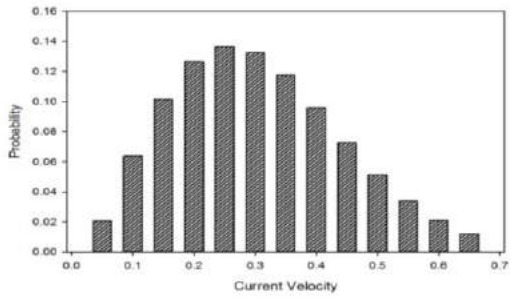

Figure 2. Probability of current flow by Weibull distribution in Persian Gulf.

6. Analysis Results

First three-mode natural frequencies are presented in Table 1. These data are calculated based on the pipeline configuration in operation load condition. For these natural frequencies, no significant VIV damage will occur in the present bottom current velocity range.

Table 1. Natural frequencies of multi-span FE model.

Mode No.	Natural Frequencies(Hz)
1	0.307126
2	0.374825
3	0.490721

7. Conclusion

VIV free span assessment is influenced by many different factors. Pipe diameter, Pipe surface roughness, wall thickness, Span lengths and Current velocities are parameters to control the VIV. However, fatigue damage is a main factor which can cause reduction of the pipeline life time. Fatigue design has become an indispensable aspect for the design of subsea pipeline especially when the seabed is extreme uneven and the water depth is deep. For pipeline multi-span fatigue damage assessment, the modes with very high frequencies tend to cause very little damage to the pipeline. Low current flow velocities can be usually neglected for the pipeline multi-span fatigue life assessment due to negligible contribution to the pipeline multi-span fatigue damage.

8. References

[1] Yong Bai and Qiang Bai (2005), "Subsea Pipelines & Risers", Chapter 10, "Vortex-induced Vibrations (VIV) and Fatigue".

[2] DNV (2002), "Recommended Practice DNV-RP-F105 Free Spanning Pipeline", Det Norske Veritas.

[3] DNV (2006), "Recommended Practice DNV-RP-F105 Free Spanning Pipeline", Det Norske Veritas.

[4] Olav Fyrileiv, Kim Mørk, Muthu Chezhian and Gudfinnur Sigurdsson, 2006. "Updated Design Procedure for Free Spanning Pipelines DNV-RP-F105 Multi-mode Response". 25th International Conference on Offshore Mechanics and Arctic Engineering. OMAE2006-92098.

[5] Leung, C. F., Chow, Y. K., Palmer, a C., & Hu, H. J. E. (2016). Fatigue Analysis of Multi-Spanning Subsea Pipelines, 1–8.

NUMERICAL ANALYSIS OF UPHEAVAL BUCKLING OF PIPELINE ON THE UNEVEN SEABED USING FINITE ELEMENT METHOD

Ali Soukhak Lari[1], Ahmad Rahbar Ranji[2], Mostafa Bahmani Shourijeh[3] and Mehdi Soukhak Lari[4]

1) Maritime Engineering Department, Amirkabir University of Technology, Tehran, Iran, asl61@aut.ac.ir
2) Maritime Engineering Department, Amirkabir University of Technology, Tehran, Iran, rahbar@aut.ac.ir
3) Civil Engineering Department, Shiraz University, Shiraz, Iran, bahmani.mostafa@gmail.com
4) Maritime Engineering Department, Amirkabir University of Technology, Tehran, Iran, mehdi.soukhak@aut.ac.ir

1. Introduction

In recent years, application of offshore pipelines has been increased due to increase in energy demand in the industries, and need to explore new oil and gas fields. This issue leads to transfer explorations of new hydrocarbon sources to the deep waters. Production and discovery of oil and gas in the deep waters needs to long pipelines. More importantly, design of these pipelines have generated many challenges for big corporations and engineers.

Pipelines play an important role in the offshore transportation system. For the time being, it is the cheapest and the best transportation way of hydrocarbons from deep waters to the shore and refineries.

In accordance with DNV-RP-F110 (2007) [1], in deep water and on the uneven seabed, there are two types of buckling possibility; lateral buckling and upheaval buckling. These two modes of buckling are kind of global buckling. Also upheaval buckling can be occurred in buried situation or in the trench.

In deep water, by imposing the initial imperfection, increasing the temperature and internal pressure; compression axial tensions develops on the pipeline wall thickness and shape of pipeline is changed when compression load is more than soil resistance. Subsequently, this issue will be led to release of inner accumulated tension that it has been made by interaction between pipeline and seabed.

Many researchers have studied on this topic and they have obtained good results, but all of them have neglected one or some parameters for simulating and analyzing due to easier analysis [2, 3, 4, 5, 6, 7]. In this research, an attempt has been made to verify the upheaval buckling of pipeline on the uneven seabed using ABAQUS software. Several parameters including pipeline length, pipeline weight, external and internal pressure, initial imperfection and operating temperature more have been considered.

2. Finite element model

All of the elements in this research have been simulated in 3D framework (Figure 1). Also all properties have been selected based on Persian Gulf situations.

Soil type of seabed is “silty clay”, and the Mohr Coulomb behavior is considered to similar the soil behavior. The C3D8R element is used for the soil. For the boundary conditions, it is tried to constraint all directions at the bottom of The FEA model, while, for the lateral sides only X and Y directions have been restricted. Other parameters are tabulated in Table 1.

The PIPE31 element has been considered to mesh. The pipeline and an Elasto Plastic behavior model to simulate the pipe behavior. Also, the properties of pipeline are: length is 1000 m, diameter is 323.9 mm, wall thickness is 12.7 mm from API 5L X65 grade. Other details are listed in Table 2.

Operational characteristics are as follow: water depth is 70 m, operating temperature is 120 ℃ and internal pressure is 10 MPa.

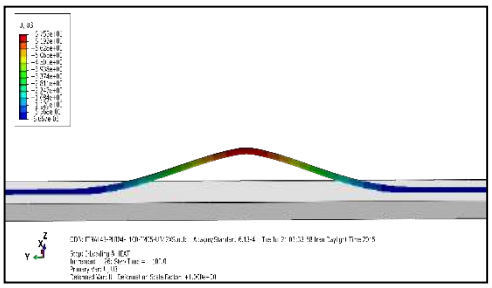

Figure 1. Numerical modeling of pipeline and seabed.

Table 1. Seabed properties.

Elasticity Modulus E_{Soil} (N/m^2)	**Mass Density** ρ (Kg/m^3)	**Poisson's Ratio** ν	**Internal Friction Angle** $\varphi(^\circ)$	**Cohesion** C (N/m^2)
5.5×10^6	1960	0.3	25	20000

Table 2. Pipeline properties.

Elasticity Modulus E_{Steel} (N/m^2)	**Mass Density** $\rho(Kg/m^3)$	**Poisson's Ratio** ν	**Thermal Expansion Coefficient** $\alpha(℃^{-1})$	**Minimum Yield Stress** σ_y (N/m^2)
2.06×10^{11}	7850	0.3	1.16×10^{-5}	450×10^6

3. Analysis results

The sensitivity of upheaval buckling with respect to changing friction coefficient between soil and pipeline was investigated by considering four different magnitude of μ. Also the initial imperfection in the middle of pipeline and the imperfection length was considered 100 cm and 100 m respectively.

The variations of displacement with increasing the friction coefficient illustrated in Figure 2. As μ increases from 0.1 to 0.4, the displacement at the end of curves is decreased, although the difference between the curves are very low. This issue indicates that the smaller μ would be, the easier deflection in the middle would be. Also the oscillations and their frequency are similar in the curves. Subsequently, because of the friction between seabed and the pipeline, these fluctuations are damped, and they are converged to the straight lines. Table 3 shows all details about the end of displacement in all diagrams.

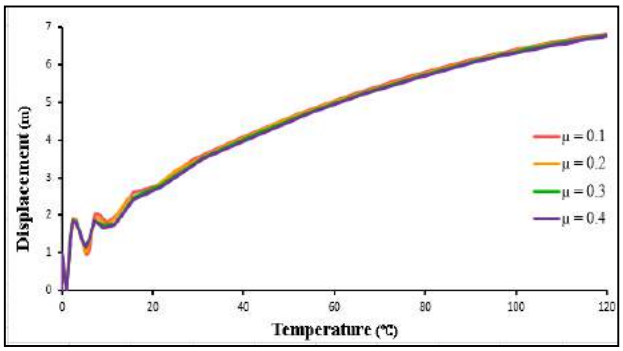

Figure 2. Displacements in the middle of pipeline

Table 3. The values of maximum displacement.

soil friction coefficient (μ)	Maximum Displacement (m)
0.1	6.83
0.2	6.81
0.3	6.78
0.4	6.75

It can be seen in Figure 3 that increase in μ from 0.1 to 0.4 have a great influence on the effective axial force, and this force is augmented in the supports and the middle of pipeline. As a matter of fact, this issue shows that whatever μ would be bigger, deformation of the middle point due to increasing friction between soil and the pipeline is more difficult. Consequently, the level of saved potential energy is increased. For more clarification, when μ is 0.1, the effective axial force in the middle and the supports are -222539 N and -270158 N respectively. When μ reaches to 0.4, the effective axial force in the middle and the supports are increased to -224648 N and -414845 N respectively, which shows 0.95% and 53.6% growth. Furthermore, the pipeline will be unstable when the effective axial force rises. These values are derived easily, as illustrated in Table 4.

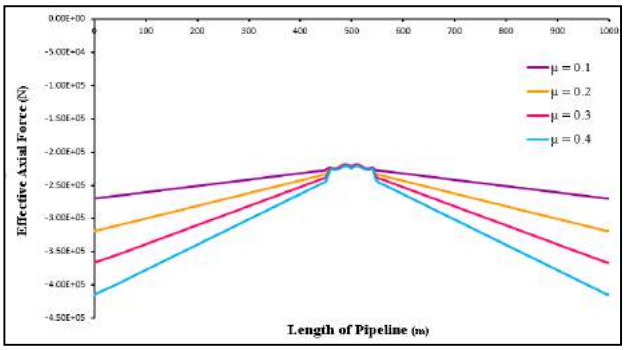

Figure 3. Effective axial force in the pipeline

Table 4. The values of effective axial force.

soil resistance coefficient (μ)	Supports of the pipeline (N)	Middle of the pipeline (N)
0.1	-270158	-222539
0.2	-318378	-223216
0.3	-366377	-223715
0.4	-414845	-224648

4. Conclusion

An attempt was made to investigate the upheaval buckling of pipeline. It is clear that with increasing μ, the displacement is diminished and the effective axial force is increased in the pipeline, and level of the energy is developed continuously. This matter emphasizes that the soil friction changes has an important impact in the upheaval buckling of the pipeline.

5. References

[1] D. N Veritas., "Global Buckling of Submarine Pipelines Structural Design Due to High Temperature/High Pressure" *DNV RP-F110, 2007*

[2] Hobbs, R. E., "In-service buckling of heated pipelines", *Journal of transportation engineering*, 110, 2, March 1984, pp. 175-189.

[3] Taylor, N., and Gan, A. B., "Submarine pipeline buckling imperfection studies", *Thin- walled structures*, 4, 4, Jan 1986, pp. 295-323.

[4] Wang, L., Shi, R., Yuan, F., Guo, Z., and Yu, L., "Global buckling of pipelines in the vertical plane with a soft seabed", *Applied Ocean Research*, 33, 2, April 2011, pp. 130-136.

[5] Shi, R., Wang, L., Guo, Z., and Yuan, F., "Upheaval buckling of a pipeline with prop imperfection on a plastic soft seabed", *Thin-Walled Structures*, 65, April 2013, pp. 1-6.

[6] Guo, L. P., Liu, R., and Yan, S. W.,"Global buckling behavior of submarine unburied pipelines under thermal sress", *Journal of central south university*, 20, 7, July 2013, pp. 2054-2065.

[7] Zeng, X., Duan, M., and Che, M., "Critical upheaval buckling forces of imperfect pipelines", *Applied Ocean Research*, 45, March 2014, pp. 33-39.

A NEW METHOD FOR PREDICTION OF SOIL LIQUEFACTION POTENTIAL

Yasaman Jafari Aval[1], Ali Derakhshani[2]
1) M. Sc. Student, Dept. of Civil Eng., Engineering Faculty, Shahed university, Tehran, Iran, Y.jafari@shahed.ac.ir
2) Assistant Professor, Dept. of Civil Eng., Engineering Faculty, Shahed university, Tehran, Iran, adera@shahed.ac.ir

1. Introduction

Estimation of soil liquefaction potential is among the most investigated topics of modern geotechnical engineering but still remains to be one of the challenging aspects of earthquake geotechnics. Liquefaction is a type of ground failure, which usually occurs in loose saturated soil. The generation of excess pore pressure under undrained loading conditions results in liquefaction. Researchers presented various correlations to estimate liquefaction potential but many of derived models have complicated formulas. This study presents simple correlations that are also accurate.

2. Model Trees (MTs)

Decision tree (DT) is a well-known technique of classification. DT includes answer nodes or leaf which indicate a class and decision nodes that contain an attribute name and branches to other decision trees, one for each value of the attribute. In DTs, classification starts from a root node and continues to generate sub-trees until creation of leaf nodes.

One of the most simple and suitable methods for prediction and categorizing data is model tree. Model tree is more accurate than regression trees, simpler and more understandable than ANN (Nahm-Chunget al., 2010). Model trees generalize the concepts of regression trees (Witten & Frank, 2000). MT is a classification method that its structure follows rules of the decision trees and has multivariate linear regression models at the leaf nodes.

3. Developing Numerical Correlations

In the literature, there are several studies addressing the estimation of soil liquefaction based on strain energy (e.g., Hsu, 1995; Polito et al., 2008).

For creation of a relationship between characteristics of soil, cyclic load and capacity energy, results of undrained cyclic tests are useful.

Multiple linear regression (MLR) was used to propose relationships for capacity energy of Sands in some studies (Figueroa et. al.,1994; Kusky, 1996; Liang et. al.,1995; Rokoff, 1999; Tao, 2003).

Baziar and Jafarian (2007) developed a new MLR-based relationship by their compiled database and proved drawbacks of previous relationships which were found considering a limited number of data.Some research programs focused on developing the relationships based on MLR, ANFIS and MARS were concluded with accurate results. Nevertheless, the presented formulas are too complex while they cannot show the effect of each parameter on the output, clearly. Some of these correlations can be seen in Table 1.

Table 1. Comparison of two available accurate models

Baziar (2011)

$$Log\ W = 3.69-(\frac{0.154x3+1.25x4x5-11.8\times10-4x2x3}{x3x5})-(\frac{0.04x4}{x3-2.798x4})+(\frac{1.4\times10-3(x1+5.382)}{x3(x3x5-x4)})-(\frac{0.08(1.252-x4)}{5.218x5-x4})-(\frac{0.003x3}{x4-6.214})+(\frac{5.9\times10-5(x1+x4+x5)}{2.5837-x4})-(\frac{0.056x2(x4-6.214)}{x3x5-6.214(x4-6.214)})+(\frac{1}{x})(\frac{0.202x4(2.5837-x4)}{(x1+x3)(2.5837-x4)-x2})+3.7\times10^{-5}((x_1+x_2)(x_1-x_3)-1.2\times10^{-3}(x_2-x_4)(x_5-4.973)+9.5\times10^{-7}(x_2)^2(x_2x_5+x_4)+0.01x_3(x_5)^2(x_4-5.214)-0.019x_2-4.5\times10^{-5}(x_1)^2+0.003x_1$$

x_1	x_2	x_3	x_4	x_5
σ_c	D_{50}	Dr+50	Cu	FC+5

Zhang (2015)

BF1	max(0, 0.107 -D_{50})
BF2	max(0, 71.51 -Dr)
BF3	max(0, 160 - σ_c mean)
BF4	max(0, FC -10)
BF5	max(0, 10 -FC)
BF6	max(0, D_{50} -0.107) × max(0, Cu -5.88)
BF7	max(0, D_{50} -0.107) × max(0, 5.88 -Cu)
BF8	BF5 × max(0, 0.16 -D_{50})
BF9	BF5 × max(0, Dr +9)
BF10	BF5 × max(0, -9 -Dr)
BF11	BF3 × max(0, D_{50} -0.31)
BF12	BF3 × max(0, 0.31 -D_{50})
BF13	max(0, Dr -71.51) × max(0, Cu -5.88)
BF14	max(0, Dr -71.51) × max(0, 5.88 -Cu)
BF15	BF4 × max(0, Dr -84.3)
BF16	BF4 × max(0, 84.3 -Dr)
BF17	BF4 × max(0, Cu -1.68)
BF18	BF4 × max(0, 1.68 -Cu)
BF19	BF5 × max(0, Cu -2.27)
BF20	BF5 × max(0, 2.27 -Cu)
BF21	BF4 × max(0, D_{50} -0.25)
BF22	max(0, D_{50} -0.107) × max(0, σ_0 mean -132.7)
BF23	max(0, D_{50} -0.107) × max(0, σ_0 mean -100.3)
BF24	max(0, D_{50} -0.107) × max(0, 100.3 – $\sigma_0$mean)
BF25	BF1 × max(0, 9.19 -Cu)
BF26	BF3 × max(0, 2.8 -Dr)

Log(W)=3.774+24.91×BF1-0.0061×BF2-0.025×BF3-0.012×BF4-0.091×BF5+0.519×BF6+1.554×BF7+3.713×BF8+0.00061×BF9+0.002×BF10-0.057×BF11+0.0984×BF12+0.0014×BF13+0.0053×BF14+0.00023×BF15+0.0001×BF16-0.0018×BF17+1.7×BF18+0.254×BF19+0.039×BF20+0.302×BF21+0.119×BF22-0.115×BF23+0.085×BF24-3.741×BF25-0.00013×BF26

4. Numerical model

A large database was used to develop the model which includes various types of cyclic element tests such as triaxial, torsional and simple shear. This data base contains 399 cyclic test results and it was reported and used by Baziar and Jafarian (2007) and Baziar et. al. (2011).

In this study, the whole data set was divided into two parts of training and testing. 80 % of data points were selected randomly and used for training to develop the model and 20 % were used for testing the model. Data range in test and train parts were approximately the same.

M5' model tree only presents a linear relationship between input and output variables, while the relation between governing parameters and strain energy is not necessarily linear. Thus, the model was developed with log (inputs) and log (output) to overcome this constraint (Etemad-Shahidi et. al., 2010).

5. Results and discussion

For developing the model, Weka, a powerful intelligent data mining tool was used.

Five parameters (σ_c, D_{50}, D_r, C_u, FC) were used as inputs to develop the model. Where, FC = percentage of fines, Cu = uniformity coefficient, D_r = relative density, D_{50} = mean grain size, W = capacity energy and σ_c = initial mean effective confining pressure.

Different combinations of parameters were studied to develop the model. The best model from the accuracy and simplicity viewpoints, is described here. This shows a reasonably good performance for the dataset.

The following equations were obtained using M5':

Cu<= 1.663413

LogW = 0.9161 * logs σ_c + 2.0071 * log(Dr+50) + 0.2778 * log(FC+5) - 0.0334 * log(Cu) + 1.2421 * log(D_{50}) - 1.9209

Cu >1.663413

LogW = 0.8746 * log σ_c + 0.8808 * log(Dr+50) - 0.2412 *log(FC+5) -0.0119 * log(Cu) -0.2414* log(D_{50}) - 0.2299

Table 2. Comparision of different models accuracy.

Researchers	CC	MAE	RMSE
Alavi, (2012)	62.729	0.381	0.474
Zhang, (2015)	74.6	0.248	0.42
Zhang-Goh, (2015)	76.499	0.621	0.701
Baziar, (2011)	94.358	0.116	0.16
Current study	89.253	0.176	0.223

The derived model in this study is more user-friendly than the other formulas. Engineers can simply observe the effect of each parameter on capacity energy and the calculation of the capacity energy is so simple and the model is more accurate than several other models such as those proposed by Alavi (2012), Zhang (2015), etc.

As can be seen in Table.1 the derived formulas are so simpler than those presented in recent years for example formulas presented by Baziar (2011) and Zhang (2015).

As presented in Table 2., RMSE (root mean square error) and MAE (mean absolute error) of the new model are less than those of older models. Influence of all parameters are in agreement with other studies and are justifiable by principles of liquefaction phenomenon.

6. Refrences

[1] Baziar, M. H., and Y. Jafarian. "Assessment of liquefaction triggering using strain energy concept and ANN model: capacity energy." Soil Dynamics and Earthquake Engineering 27.12 (2007): 1056-1072.

[2] Baziar, Mohammad H., et al. "Prediction of strain energy-based liquefaction resistance of sand–silt mixtures: An evolutionary approach." Computers & Geosciences 37.11 (2011): 1883-1893.

[3] Alavi, Amir Hossein, and Amir Hossein Gandomi. "Energy-based numerical models for assessment of soil liquefaction." Geoscience Frontiers 3.4 (2012): 541-555.

[4] Zhang, Wengang, et al. "Assessment of soil liquefaction based on capacity energy concept and multivariate adaptive regression splines." Engineering Geology 188 (2015): 29-37.

[5] Zhang, Wengang, Anthony TC Goh, and Yanmei Zhang. "Multivariate Adaptive Regression Splines Application for Multivariate Geotechnical Problems with Big Data." Geotechnical and Geological Engineering (2015): 1-12.

[6] Cabalar, Ali Firat, Abdulkadir Cevik, and Candan Gokceoglu. "Some applications of adaptive neuro-fuzzy inference system (ANFIS) in geotechnical engineering." Computers and Geotechnics 40 (2012): 14-33.

[7] Etemad-Shahidi, A., and N. Ghaemi. "Model tree approach for prediction of pile groups scour due to waves." *Ocean Engineering* 38.13 (2011): 1522-1527.

[8] Jung, Nahm-Chung, et al. "Application of model trees and other machine learning techniques for algal growth prediction in Yongdam reservoir, Republic of Korea." Journal of Hydroinformatics 12.3 (2010): 262-274.

[9] Witten, Ian H., and Eibe Frank. Data Mining: Practical machine learning tools and techniques. Morgan Kaufmann, 2005.

[10] Polito, Carmine P., Russell A. Green, and Jongwon Lee. "Pore pressure generation models for sands and silty soils subjected to cyclic loading." Journal of Geotechnical and Geoenvironmental Engineering 134.10 (2008): 1490-1500.

[11] Hsu, H. L. "Study on the relationship between shear work and pore water pressure for saturated sand in undrained test." EARTHQUAKE GEOTECHNICAL ENGINEERING, VOLS 1 AND 2 (1995): 301-307.

[12] Etemad-Shahidi, A., R. Yasa, and M. H. Kazeminezhad. "Prediction of wave-induced scour depth under submarine pipelines using machine learning approach." Applied Ocean Research 33.1 (2011): 54-59.

SIMULATION OF SPUDCAN PENETRATION BEHAVIOUR IN TWO-LAYER CLAY USING COUPLED EULERIAN LAGRANGIAN APPROACH

Mahmood Dadgar[1], Farzin Kalantary[2] and Foad Zahedi[3], Seyed Amir Tabatabaei

1) Graduate School of Marine Science and Technology Dept. , Science and Research Branch, Islamic Azad University, Tehran, Iran, m.dadgar@srbiau.ac.ir
2) Civil, Dept. of Geotech. Eng., Faculty of Civil Eng., K.N.Toosi University of Technology, Tehran, Iran , fz_kalantary@kntu.ac.ir
3) Graduate School of Marine Science and Technology Dept. , Science and Research Branch, Islamic Azad University, Tehran, Iran, zahedi.foad@gmail.com

1. Introduction

Jack-ups operate in various seabed conditions during their life cycle. In some cases, seabed comprises of stiff or dense soil layer overlaying soft or loose soil layer, thus it is probable that the jack-up s footing (so-called spudcan) encounters a sudden large displacement such as punch-through failure or rapid leg run , especially during installation phase. Craig and Chua [1] and Teh et al [5] have carried out several centrifugal tests to survey spudcan penetration behavior during installation. Qiu and Henke [2] and Yu et al [3] have carried out numerical simulation to study spudcan penetration in soil.

Classic Lagrangian approach cannot simulate large displacement problem due to mesh distortion problems, but there are some type of numerical simulation approaches that have an ability to simulate large deformation, such as RITTSS, ALE, CEL. In this study Coupled Eulerian Lagrangian (CEL) approach available in Abaqus˚ Explicit were conducted to simulate the penetration responses of spudcan in stiff clay overlaying soft clays. The punch-through failure of spudcans on layered clays has been surveyed numerically.

The effects of roughness, upper layer to lower layer strength ratio, upper to lower layer thickness ratio, spudcan apex angle have been studied. Bearing stress-displacement profile is illustrated to express the spudcan capacity response against the penetration depth. Punch through failure and its prerequisite conditions have been described.

2. Numerical Modelling

2.1. Geometry and mesh

Numerical simulation has been carried out by using CEL that was implemented in commercial program Abaqus-Explicit. Spudcan was modelled as rigid body and Lagrangian and soil domain was modelled as deformable Eulerian part. By taking the advantage of symmetry, only quarter of soil domain was modelled that would significantly decrease time consuming of the analysis.

Two spudcan geometries were used in this simulation based on Qiu and Henke[1] and Teh et al [5]. Finite element mesh of soil domain had about 50600 Eulerian elements. Penetration of spudcan in soil is displacement control and based on to of prior studies assumpions, penetration velocity of spudcan was set 0.5 m/s.

2.2. Contact formulation

The soil-spudcan interface could be modeled as either fully rough or fully smooth, but in this study, friction coefficient 0.5 was set for spudcan penetrating in clay. The contact between spudcan and clay is described using general Contact algorithm with implementation of penalty contact method.

2.3. Constitutive model

The clay layer was modeled as an elastic-plastic material obeying the Tresca failure criterion. The friction and dilation angle was set to 0. For keeping minimum volumetric strains and numerical stability Poisson ratio was taken 0.49. The relation between Young modulus of clay and its undrained shear strength is : $E_{clay} = 500.S_u$

3. Validation of CEL model

Centrifugal test of Craig and Chua[1] and numerical simulation of Qiu and Henke [2] were recalculated using CEL approach. Validation are comprised of three case :

1- Spudcan Penetration in uniform clay
2- Spudcan Penetration in dense sand
3-Spudcan penetration in loose sand overlaying clay

4. Results

Several FE analysis were carried out to survey the effects of the spudcan shape (type (a, b)), lower to upper clays strength ratio, c_2 /c_1, and the relative top layer

thickness, H/D on bearing capacity of penetrating spudcan and punch through happening probability . A detailed parametric study was undertaken varying the relative range of c2/c1 (0.2, 0.5, 0.7, 1) and H/D (3/6, 5/6, 10/6) that were implemented in Abaqus-explicit.

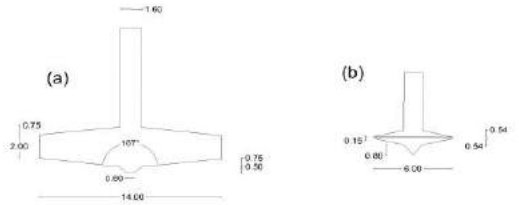

Figure 1. Spudcans Geometry

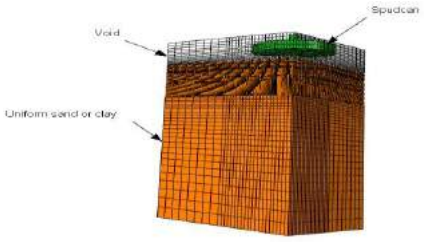

Figure 2. finite element mesh of Numerical analysis.

As shown in Fig.3 after full penetration of spudcan into clay layer soil heave and clay back-flow on top of spudcan could be seen. In the other hand by increasing top layer cohesion cavity wall above penetrating spudcan would be established. (Fig.4). Various bearing capacity-displacement profiles of penetrating spudcan (type (a)) in stiff clay (c_1=100 KN/m^3) on softer lower clay (c2=50 KN/m3) is shown. (Fig.4). By increasing top layer strength the rate of bearing capacity increasing is faster but after full embedment of spudcan the trends tends to be parallel. From Fig.5 it could be concluded that by increasing stiff clay layer, depth of peak bearing capacity would be more than softer clay layer. Punch through failure could be seen in all of clay layer arrangement.

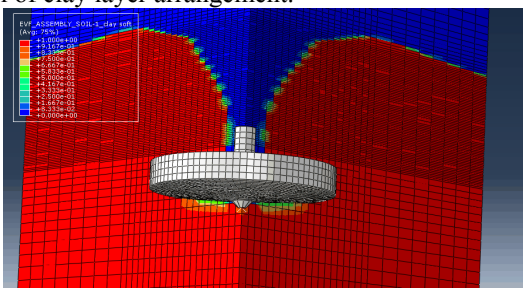

Figure 3. Uniform Clay(c39 kpa) deformation after 15 m spudcan penetration

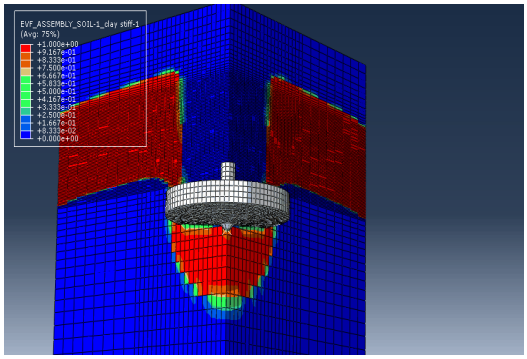

Figure 4. Soil configuration after 15m spudcan (type (a)) penetration in stiff clay(H=10 m) over soft clay c1/c2=100/20 KN/m^3

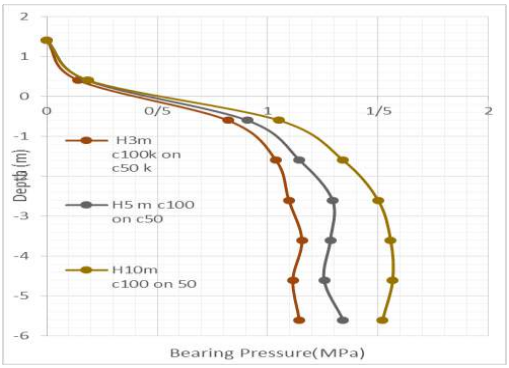

Figure 5. Bearing pressure response of spudcan type (b) in stiff clay over soft clay c1/c2=2

5. Major References

[1] Craig WH, Chua K. Deep penetration of spud-can foundation on sand and clay. Geotechnique 1990;40(4):541˚56.

[2] Qiu Gang, Henke Sascha. Controlled installation of spudcan foundations on loose sand overlaying weak clay.Marine Structures 24(2011) :528-550

[3] Long Yu; Jun Liu; Xian-jing Kong; and Yuxia Hu, M.ASCE Journal of Geotechnical and Geo-environmental Engineering, Vol. 137, No. 1, January 1, 2011.

[4] Dong wang, Britta Bienen, Majid Nazem, Yinghui Tian, Jingbin Zheng, Tim Pucker, Mark F.Randolph. Large Deformation finite element analysis in geotechnical engineering. Computers and Geotechnics 65(2015) 104-114.

[5] The KL, Cassidy MJ, Leung CF, Chow YK, Randolph MF, Quah C. Revealing the bearing capacity mechanisms of a penetrating spudcan through sand overlaying clay. Geotechnique 2008; 58(10): 793-804.

CENTRIFUGE MODELLING OF OFFSHORE MONOPILES SUBJECTED TO MONOTONICAND CYCLIC LATERAL LOADING

Faraz Jomehri[1], Seed Darvishi Alamouti[2], Majid Moradi[3] and Mohammad Reza Bahari[4]

1) School of Civil Engineering, University of Tehran, Tehran, Iran, fjomehri@ut.ac.ir
2) School of Civil Engineering, University of Tehran, Tehran, Iran, saeed_darvishi@ut.ac.ir
3) School of Civil Engineering, University of Tehran, Tehran, Iran, mmoradi@ut.ac.ir
4) School of Civil Engineering, University of Tehran, Tehran, Iran, mbahari@ut.ac.ir

1. Introduction

By increasing the demand for renewable, sustainable and greener energy sources, the offshore wind farm industry is experiencing rapid grow in many countries. It is expected for near-term (2020) and long-term (2050) offshore wind turbines play an important role in reducing greenhouse gas emission reduction [1]. Monopile foundations are the main type used for wind turbines at present. Monopiles are designed to suffer lateral cyclic loads produced by wind, waves and currents. Although many researches have done on the lateral response of monopiles (e.g. [2-5]) but still lack of comprehensive data exists to make general rules. In this study a series of displacement-controlled monotonic and cyclic centrifuge tests are set up to investigate the lateral response of a short monopile in medium dense sand.

2. Test Setup

A series of centrifuge displacement-controlled tests were designed to investigate cyclic behavior of a stiff monopile under lateral loading. The tests were conducted in Centrifuge Laboratory of the Department of Soil Mechanics and Foundation Engineering, School of Civil Engineering, University of Tehran. All tests were carried out at 40g level of gravity acceleration. Table 1 shows 5 centrifuge tests specification where d_{max} and d_{min} denotes maximum and minimum applied controlled displacements at loading point.

Table1. Test program

Test ID	Type	No. of cycles	d_{max} (mm)	d_{min} (mm)
TM1	Monotonic	-	35	0
TC1	Cyclic	130	12	-5.8
TC2	Cyclic	110	4	-2
TC3	Cyclic	110	4	0
TC4	Cyclic	120	4	-4

The samples were built up in strongbox with dimension of 80 cm × 50 cm × 80 cm. Firrozkooh-161 sand with relative density of 60% was used in test models. The properties of the sand are shown in table2.

Table2. Properties of the sand

Sand type	D_{50}	C_u	e_{min}	e_{max}	G_s
Firrozkooh 161	0.30	1.87	0.574	0.874	2.658

A circular steel pile with outer diameter of 5cm and thickness of 1.25mm is modeled in this study. At 40g level acceleration, the pile in prototype scale has 2m diameter and 5cm of thickness in dry sand. 6 pair of strain-gages connected half-bridge attached on the pile surface to measure the bending moments. The cyclic displacement was applied by the loading shaft and measured by two Linearly Variable Different Voltage (LVDT) were located at 15cm distance from each other. The magnitude of imposed lateral load was measured by a load cell. To generate displacement- controlled load a new stepper motor was programmed to create different patterns of load including ramp, stair, triangular and sinusoidal. Schematic sketch of the test setup is illustrated in Figure 1.

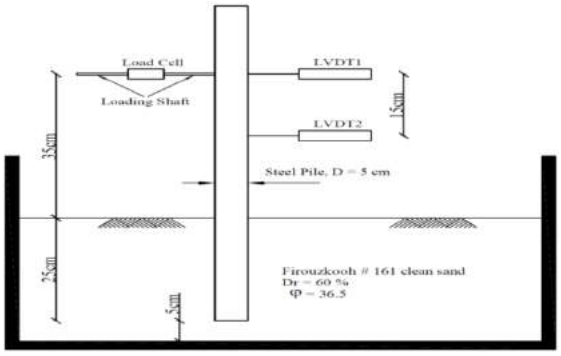

Figure1. Schematic sketch of test setup

3. Centrifuge Modelling

For applying equivalent stresses in model and prototype artificial gravity is generated in centrifuge. The artificial gravity is applied when model is placed at the end of a rotating arm. The acceleration in a specific point of model is given by the distance from rotational axis (R) and

the angular rotation speed (ω). The ratio between gravity (g) and artificial gravity is defined by the gravity scale factor (N).

$$N = R\omega^2/g$$

4. Results

4.1 Monotonic tests

In order to evaluate the monopile bearing capacity monotonic test was performed. The pile capacity is basis for cyclic tests. In fact, cyclic test load levels were chosen based on fatigue limit state that in offshore wind turbines is one third of the pile ultimate capacity [2].

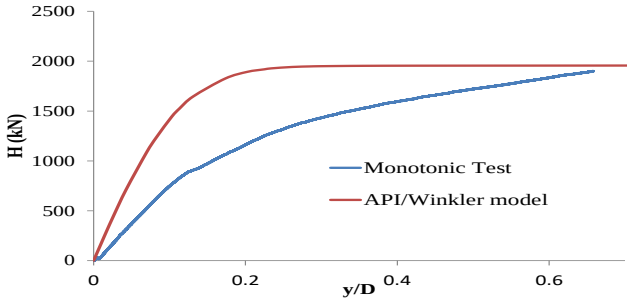

Figure2. Monotonic test. Load-displacement response compared to API/springs Winkler model

4.2 Cyclic tests

Investigation of load-displacement response and secant stiffness of the monopile are the main objectives in the cyclic tests. Secant stiffness in Nth cycle is defined as follow:

$$K_N = \frac{1}{\gamma' D^2} \times \frac{H_{\max,N} - H_{\min,N}}{d_{\max} - d_{\min}}$$

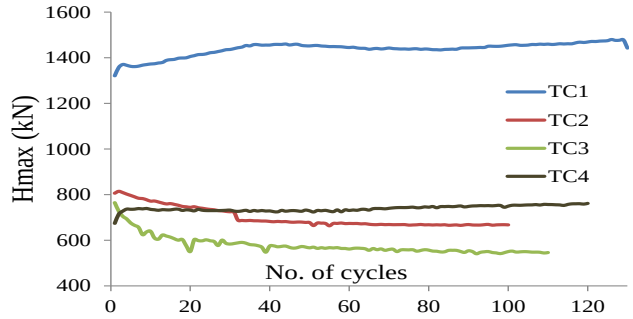

Figure3. Variation of maximum applied load on the monopile respect to number of load cycles

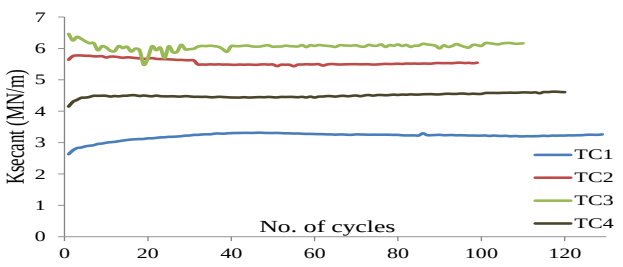

Figure4. Variation of monopile secant stiffness versus number of load cycles

5. Discussion and conclusion

According to monotonic and cyclic tests results following observations are remarked:

- The monopile response in the sandy soils is softer than that predicted by API p-y springs
- Pile failure occurs very suddenly in Winkler model
- Monopile cyclic response extremely depends on loading characteristic including one/two way regime and number of cycles
- Depending on loading characteristic, both increasing or decreasing trends are observed in the magnitude of applied loading. The main reason for decreasing trend of applied load is the creation of plastic permanent deformations in the soil body
- Monopile secant stiffness change during load cycles evolution. Based on a few number of tests performed in the present study, it is observed that in one-way loading the rate of changing in secant stiffness is negative. It is worth noting that in the case of fender monopiles the predominant regime is one-way
- In all tests the rate of changing in the mentioned parameters is rapid at first a few cycles and after 100 cycles changing becomes considerably slow
- In all tests hysteretic behavior of the soil-pile system observed which denotes energy dissipation

6. References

[1] EWEA (European Wind Energy Technology Platform) (2014) Aming high-rewarding ambition in wind energy. A report by the European wind energy association.

[2] Leblanc C, Houslby GT & Byrne BW (2010) Response of stiff piles in sand to long-term cyclic lateral loading. Geotechnique **60(2)**: 79-90.

[3] Klinkvort RT, Hededal O (2013) Lateral response of monopile supporting an offshore wind turbine. Proceedings of the institution of Civil Engineers – Geotechnical Engineering **166(2)**: 147-158.

[4] Klinkvort RT, Hededal O (2014) Effect of load eccentricity and stress level on monopile support for offshore wind turbines Canadian Geotechnical Journal **51(9)**: 966-974

[5] Klinkvort RT, Leth CT, and Hededal O (2010) Centrifuge modelling of laterally cyclic loaded pile. In Proceedings of the 7th International of the Conference on Physical Modelling in Geotechnics (ICPMG 2010). Zurich, Switzerland, pp.959-964

[6] API (American Petroleum Institute) (2005) RP2A-WSD: Recommended practice for planning, designing and constructing fixed platforms: working stress design. American Petroleum Institute, Washington DC, USA.

[7] DNV (Det Norske Veritas) (2014) OS-J 101: Design of Offshore Wind Turbine Structures. Det Norske Veritas, Oslo, Norway.

STUDYING THE EFFECTS OF YOUNG'S MODULUS ON THE MARINE PILE'S HEAD DISPLACEMENTS IN MULTI-LAYERD SOILS.

Seyyed Hamed Shojaeddin[1], Ali Soukhak Lari[2] and Farzad Hatami[3]

1) Maritime Engineering Department, AmirKabir University of Technology, Tehran, Iran, hamedshojaeddin@aut.ac.ir
2) Maritime Engineering Department, AmirKabir University of Technology, Tehran, Iran, asl61@aut.ac.ir
3) Civil and Environmental Engineering Department, AmirKabir University of Technology, Tehran, Iran, hatami@aut.ac.ir

1. Introduction

Piles are widely used in marine constructions. Pile supported wharves and jetties, oil and gas fixed platforms and anchor piles could be named as the most common applications of piles in marine environments.

Sea waves and currents impose dramatic lateral loads on the above mentioned structures. Moreover, seismic loading and wind forces are of lateral kinds with great influences on the pile supported structures. As a result determining the appropriate behavior of piles under lateral loading would be of great importance in the designing steps.

Well established procedures of designing marine structures introduce soil-pile interaction methods as more accurate ways to represent better understanding of pile's responses under lateral forces in comparison to the old methods neglecting such effects [1, 2, 3, 4, 5]. Each of the different ways of regarding soil-pile interaction greatly deals with soil properties like Young's modulus, Poisson's ratio, soil friction angle, soil cohesion, dilation angle etc.

Among these properties Young's modulus (E) proposed by different codes and researchers sometimes varies a lot in a way that even for a specific soil type there is no overlap. Referring to the literature it is due to the different methods selected by each researcher or scientific institute to obtain the values.

For designers it's been always one issue of concern that, in the absence of any accurate experimental studies, to what extend does selecting different values of E based one particular code might affect the desirable design. Moreover, piles driven in multi layers soil profiles might have a few numbers of interaction surfaces with the surrounding soil. So appropriate E values should be assigned to every one of these soil layers. Knowing which layer's properties might more affect the design is of great importance as well.

Therefore This study has been aimed to find out, in a multilayer soil profile, to what extend does selecting different values of E (based upon one specific code) might change the results and changes in the E values of which layer can cause more pile's head displacements ?

2. Study Procedure

The 3D finite element framework was used to simulate the pile with the surrounding soil using ABAQUS software. Figure 1.

In this study a hollow steel pile with a length of 42 m has been modeled and studied under a cyclic lateral load. The steel was of marine type with a Fy= 360 MPa. The water level was 15 M above the sea bed. In fact all pile's specifications are selected from an onshore pile supported structure in Persian Gulf.

The load magnitude was 200 KN and it was applied in a cyclic way presenting the nature of external loads applied to a real marine pile.

Pile embedded length in soil is 24 m Therefore only the first 3 layers have direct interactions with the pile. The soil profile consists of 4 layers. All soil properties are listed in table 1.

Table 1. Soil Properties.

Type of Soil	Thickness	Cohesion (KPa)	Friction angle (deg)
Sandy Clay	12	20	30
Sandy Clay	12	20	30
Sandy Clay	6	20	30
Stiff silty Clay	10	100	0

The first 2 soil layers have tangential and normal interactions with the pile while there is just a normal interaction between the 3rd soil and the pile.

According to the Table 1. the first 3 layers are of Sandy Clay type and based upon reference [6] sandy clay has a Young's modulus between the ranges of 24 MPa to 192 MPa so in this research for each of the first 3 layers, Young's modulus

of 25, 50, 75, 100, 125, 150 MPa were assigned respectively while the value of E for the two remaining sandy clay layers was set to be 50 MPa and in all conditions the E value for the last layer, stiff silty clay, was 75 MPa. For instance for the first layer of sandy clay values of 25, 50, 75, 100, 125, 150 MPa are assigned whereas for the next 2 sandy clay layers E values were of 50 MPa. This procedure is done for the next 2 layers too.

The selected output to be analyzed was the lateral displacement of the pile's head in the same direction the load was applied. 18 numerical analysis were carried out to obtain the raw data.

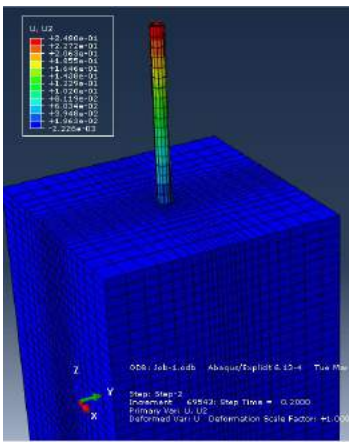

Figure 1. Numerical modeling of the pile with the surrounding soil.

Finally the pile's head displacements were plotted for each soil layer. Then comparing each layer to the other two ones it can be seen which changes in the E value of which layer is more eye-catching.

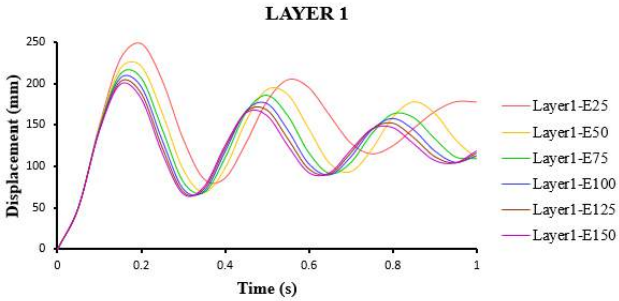

Figure 2. Pile's head displacements with variant values of E in the first layer.

Figure 2. shows the pile's head displacements when the Young's modulus of first layer changes.

Besides the above mentioned graphs, some other diagrams are presented comparing each E in all soil layers. Figure 3.

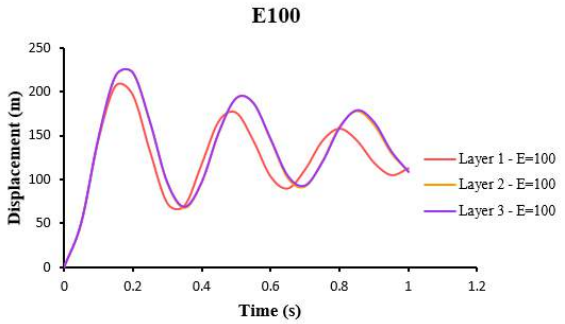

Figure 3. Pile's head displacements for E= 100 Mpa in all soils.

3. Conclusion

As it is expected in all 3 layers by the increase in E values, pile's head displacements decrease. The most dramatic changes will occur in the first layer, meaning that (for example) by decreasing the E values in the first layer the max. Displacements demonstrates more increase in magnitude in comparison to the next 2 layers.

Evaluating each value of E in three layers simultaneously, shows that for some specific values (75, 100, 125, 150, 175 MPa) the second and third layers are of more importance as they cause larger pile's head displacements while for the other values (25 and 50 MPa) the magnitudes of first layer are determining.

4. References

[1]McCullough, N.J., Dickenson, S.E., Scheleter, S.M., "The seismic performance of piles in waterfront applications", America's ports-Gateway to the global Economy, 2004.

[2]Roth, W.H., Dawson, E.M., Mehrain, M., Sayegh, A., "Analyzing the seismic performance of wharves", Structural Engineering Approach, 2003

[3]Donahue, M.J., Dickenson, S.E., Miller, T.H., Yim, S.C., "Implications of the observed seismic performance of a pile-supported wharf for numerical modeling", Earthquake. spectra, 2005.

[4]Blandon, C.A., Bell, J.K., Restrepo, J.K., Eeismair,M., Jaradat,O., Yin, P., "Assessment of Seismic performance of two pile-deck wharf connections " J.Perform.Constr. Facil, 2011.

[5]Heidary-Torkamani, H., Bargi, K., Amirabadi, R.,McCllough, Nason J., "Fragility estimation and sensitivity analysis of an Idealized pile-supported wharf with batter piles", soil dynamics and earthquake engineering, 2014.

[6]Department of Army, U.S. Army Corps of Engineers "Settlement Analysis", September 1990.

BEHAVIOR OF SHORELINE DURING KOCAELI 1999 EARTHQUAKE

Ayfer ERKEN[1], Maryam MASSAH FARD[2]

1, 2 Department of Civil Engineering, Istanbul Technical University, Istanbul, TURKEY

1. erken@itu.edu.tr
2. massahfard@itu.edu.tr

1. Introduction

The proper behavior of coastal areas and marine structures in seismic region countries like Turkey and Iran is an important concern nowadays. Coastal areas are the vital part of every countries and huge amount of financial budgets are focused on the construction of the ports and harbor facilities. The seismicity of the mentioned regions makes the performance of these areas more complicated. Although there were no huge earthquake until now affecting the shorelines of Iran, but focusing on lessons from the one of the most important earthquakes which happened in Turkey and caused so much damages to coastal areas and marine structures will be a great experience for the whole region.

The Kocaeli earthquake of August 17, 1999 with a magnitude of 7.4 induced permanent deformation of ground due to both liquefaction and faulting and resulted heavy damage to both superstructures and infrastructures (Figure 1). As the epicenter of the earthquake was near to Izmit Bay area and it was lasted for 42 sec, with the largest horizontal acceleration of 0.407*g* [1], there were so many huge damages to the marine structures along the coast of the Izmit Bay. The current study summarizes the main geotechnical and hydrodynamic aspects of this earthquake on the behavior of shoreline.

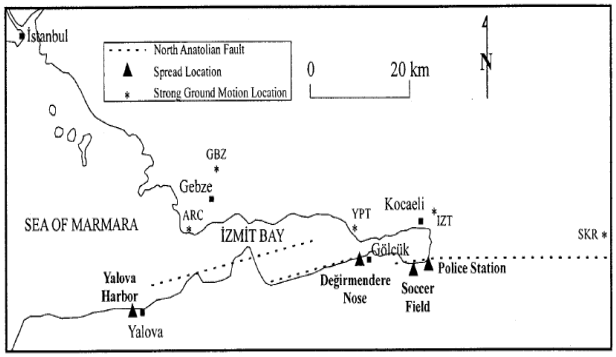

Figure 1. Site map [2]

2. Damage to Coastal Facilities

Following the earthquake, landslides due to soil condition and tectonics, deep cracks, excessive settlements, lateral displacement and liquefaction were observed in the region [3]. Deince Port, which is of the concrete caisson type with shorefront length of about 1.5 km, shifted away from the wharf up to 0.7m horizontally and 1m vertically due to liquefaction induced deformations, settlements and lateral spreading. A substantial number of the jetties at the industrial facilities were also damaged [4].

Along the southwestern shore of the Gulf of Izmit huge ground subsidence has occurred due to combination of vertical tectonic motion associated with pull-apart structures and land sliding [4]. Most of the ports and jetties privately operated by industrial facilities in Izmit Bay sustained damage (Figure 2). High damages were observed at Golcuk Navy.

Figure 2. Subsidence at Golcuk along the southern shore of the Izmit Bay

3. Geotechnical Effect and Site Response

There were different types of geotechnical damages in different parts of the Izmit Bay. They were such as slope failure mainly in poor quality fills, liquefaction, subsidence and land sliding. Here, the focus will be more on liquefaction of the soil both in backfill and seabed.

In a research by Sumer et al. (2002), on 24 marine structures of the mentioned site, it was concluded that backfills behind quay walls and sheet-piled structures were almost invariably liquefied [5]. In a research by Boulanger et al.(2000), the damage to and the performance of the marine structures in the Kocaeli Earthquake were investigated in details [6].

4. Effect of Liquefaction

4.1 Backfill Liquefaction

Backfill areas behind quay walls and sheet-piled structures failed due to liquefaction. Although, in some cases, the failure in the backfill areas may have been influenced by other factors as well. Settlement in the backfill areas varies from 10 cm to 1 m [5].

According to the research by Boulanger et al. (2000), Gunbak et al. (2000) and visit of Sumer et al. (2001), in

Derince port, the block type quay walls were displaced towards the sea by (0.1- 0.5m). The backfill area settled by (0.5-1m). There were very clear indications of liquefaction of the backfill area (and also in and around two warehouses located in this area), in the form of sand boils; Sand volcanoes the size (30 cm) were observed very clearly. For quay walls with steel pile supported and for sheet pile walls, minor damage were observed at pile caps in some small number of piles, the backfill area settled and no sand boils were observed, however. The displacement in sheet piled structures were in the range from 10 cm to 1 m.

4.2 Seabed Liquefaction

One reason why the seabed may be liquefied (or weakened) by the shaking of the current earthquake may be that this latest earthquake had a large magnitude. The duration of the earthquake is also an important factor. Unlike the liquefaction in on-land areas, the seabed is also subject to waves, which is another effect to cause liquefaction. (The seabed liquefaction under waves may occur in two forms, the residual liquefaction and the momentary liquefaction (Sumer and Fredsøe, 2002, Chapter 10). Y. Yuksel, 2001, personal communication) implies that the waves will not induce any significant buildup of pore pressure or any significant effect of momentary liquefaction, and therefore the seabed may still have experienced liquefaction (or weakening) due to the shaking of the Kocaeli earthquake.

5. Hydrodynamic Effect

The coastline along Izmit bay was significantly affected by August 17, 1999 Kocaeli earthquake due to earthquake related generation of the water. Yalciner et al. (2000), from their field surveys, concluded that a major tsunami was generated due to a large tectonic subsidence near and/or at the shoreline. This tsunami had a period shorter than 1 minute. Always the first few days are so important for happening of small tsunamis especially in populated coastlines. There were four surveys done in Izmit bay and around the sea of Marmara. Along the northern coast of Izmit bay, the uncorrected run up heights ranged from 1.5 to 2.6 m, decreasing to high water levels. The arrival time of the first wave was ‘a few minutes’, and the period was ‘one minute’.

Yalciner et al. also concluded that tsunami waves may have also been generated by sediment slumping in addition to tectonic subsidence. Along the southern coast of the middle basin, uncorrected run up heights were measured in the range of 0.8 m to 2.5 m and decreased to high water levels. There were huge damages to boats, ship and other facilities. The subsidence of coastal area caused 10 victims. A few minutes after the earthquake, the hydrostatic pressure force on the wall at the sea side will decrease or completely vanish, and therefore the wall will undergo a relatively larger, seaward resultant pressure force; because now just the force from pore water pressure remains. This effect may have played a significant role in the observed seaward displacements of quay walls and sheet-piled structures mentioned earlier.

One of the most important factors during tsunami is the shape of initial wave. The shape was uniform and the uniformity makes a large degree of subsidence near or at the shoreline [7].

6. Conclusion

For investigation of the proper behavior of the coastal seismic region, both geotechnical and hydrodynamic aspects should be considered. Liquefaction is one of the most important destructive geotechnical factors in the seismic regions. Backfill areas behind quay walls and sheet-piled structures failed due to liquefaction. Quay walls and sheet-piled structures were displaced seaward mostly because of liquefaction. Seabed settlement was also occurred during this earthquake.

Coseismic generation of tsunami waves coupled with those of underwater landslides, slumps or subsidence should be considered in hazard mitigation in Izmit bay and in the sea of Marmara.

7. References

[1] Safak E. et al., "Recorded Main Shock and Aftershock Motions". Chapter 5, in 1999 Kocaeli, Turkey, Earthquake Reconnaissance Report, *Supplement A to Earthquake Spectra*, Volume 16, T.L. Youd, J.-P. Bardet, J.D, 2000, pp. 97-112.

[2] Onder Cetin, K., et al., "Liquefaction-Induced Lateral Spreading at Izmit Bay During the Kocaeli (Izmit)-Turkey Earthquake", *Journal of Geotechnical &Geoenvironmental Engineering, 130(12),* 2004, pp. 1300-1313.

[3] Erken, A., "The Role of Geotechnical Factors on Observed Damage in Adapazari", in *Proceedings 1XV ICSMGE Satellite Conference on Lessons Learned From Recent Strong earthquakes"*, Istanbul, Turkey, August 25, 2001, pp. 29-32.

[4] Erdik, M., *Report on 1999 Kocaeli and Duzce (Turkey) Earthquakes, Structural control for civil and infrastructure engineering: World Scientific*, 2001.

[5] Sumer, B.M., Kaya, A., and Hansen, N., "Impact of Liquefaction on Coastal Structures in the 1999 Kocaeli, Turkey Earthquakes", in *Proceedings of The Twelfth (2002) International Offshore and Polar Engineering Conference Kitakyushu, Japan, May 26–31, 2002*, pp. 504-511.

[6] Boulanger, R., Iai, S., Ansal, A., Cetin, K.O., Idriss, I.M., Sunman, B., Sunman, K., “Performance of Waterfront Structures”. Chapter 13, in 1999 Kocaeli, Turkey, Earthquake Reconnaissance Report, *Supplement A to Earthquake Spectra*, Volume 16, T.L. Youd, J.-P. Bardet, J.D. Bray, Eds., 2000, pp. 295- 310.

[7] Yalciner, A.C. et al., “Tsunami Waves in Izmit Bay”, Chapter 3, in 1999 Kocaeli, Turkey, Earthquake Reconnaissance Report, *Supplement A to Earthquake Spectra*, Volume 16, T.L. Youd, J.-P. Bardet, J.D. Bray, Eds., 2000, pp. 55-62.

EFFECT OF PARTICLES SIZE ON THE BEHAVIOUR OF SAND-ROUGH STEEL INTERFACES

Vahid Jamali[1], Ali Lashkari[2]

1) Ph.D. Student, Faculty of Civil and Environmental Engineering, Shiraz University of Technology, Iran, v.jamali@sutech.ac.ir
2) Associate Professor, Faculty of Civil and Environmental Engineering, Shiraz University of Technology, Iran, lashkari@sutech.ac.ir

1. Introduction

Behavior of interfaces forming between granular soils and structural materials is an influential factor in design and performance of offshore and onshore engineering structures such as sub-sea pipelines, piles, foundations and steel sheet piles. Shear strength and volume change response of soil-structure interfaces are not only limited to the soil intrinsic characteristics, but also depend on the magnitude of normal effective stress, surface roughness of structure, and normal stiffness [1-2].

In this paper, the mechanical behaviors of interfaces between two angular sands and rough steel were studied using modified direct shear apparatus. It is shown that the peak and residual shear strengths as well as the maximum dilation of sand-steel interfaces depend on sand mean particle size.

2. Tested Materials

Particle size distributions and physical properties for two tested angular silica sands (i.e., S1 and S2) are, respectively, presented in Figure 1 and Table 1. Particle size distribution of S1 is in between sieve No. 16 to sieve No. 60 in accordance with the Unified Soil Classification System. In logarithmic scale, the particle size distribution curve of S2 is nearly parallel to that of S1 in such a way that mean particle size of S2 is two times greater than that of S1.

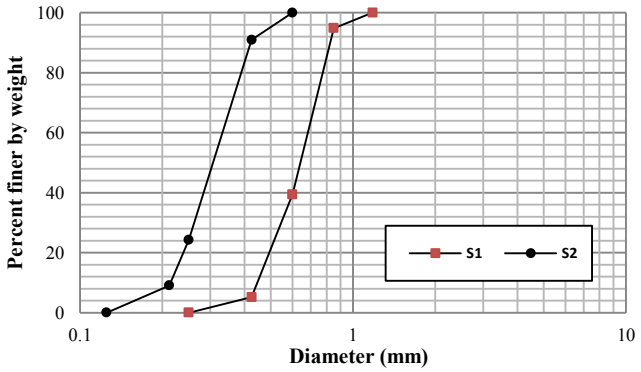

Figure 1. Particle size distributions of the sands S1 and S2

Table 1. Physical Properties of S1 and S2

Sand	G_s	Maximum void ratio, e_{max}	Minimum void ratio, e_{min}	Mean particle size, D_{50} [mm]	Uniformity coefficient, C_u
S1	2.67	0.960	0.404	0.65	1.53
S2	2.67	0.978	0.415	0.32	1.60

A machine-grooved steel block was used as structural material. Using a conventional profilometer, digitized profile of the steel block surface asperities is presented in Fig. 2. Using data presented in Fig. 2, 0.08 and 0.16 are obtained for normalized roughness of interfaces between S1 and S2 and rough steel block.

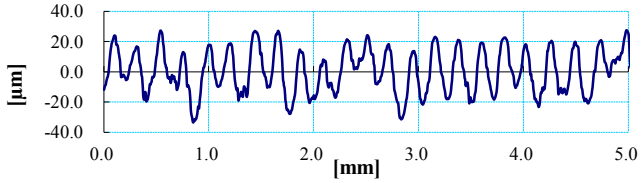

Figure 2. profile of steel surface in 5mm length of steel block

3. Experimental Data

Experiments were performed using a modified direct shear box. More than 50 tests were conducted on sand-steel interfaces under constant normal stress condition with different sand initial void ratios. Results of experiments are presented in Figures 3-5. For interfaces between S1 and S2 sands and steel, peck and residual strengths increase with normal stress. However, S1 sand-steel interfaces exhibit greater dilation compared to S2 sand-steel interfaces. Peak and residual friction angles as well as the maximum dilation angles are shown in Figures 6 and 7. It can be observed that the peck friction and maximum dilation angle depend on particle size, density and vertical stress. Residual and peck frictional angles in S2 sand-steel interfaces are greater than the corresponding values for S1 sand-steel interfaces since particles in S2 sand have more engage with rough steel.

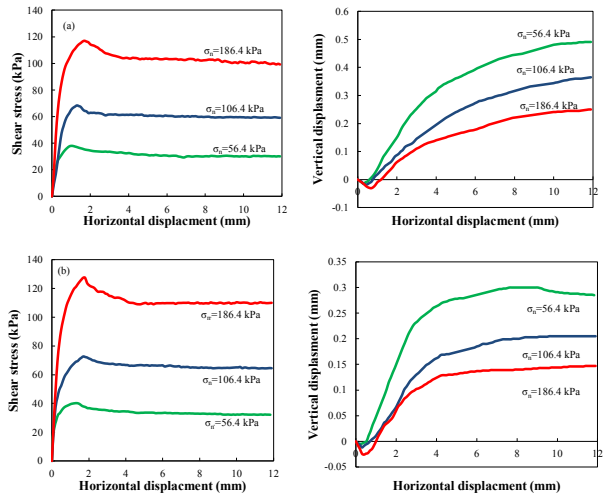

Figure 3. Experiments for e_{in}=0.64 under various constant normal stress for a) S1 sand b) S2 sand

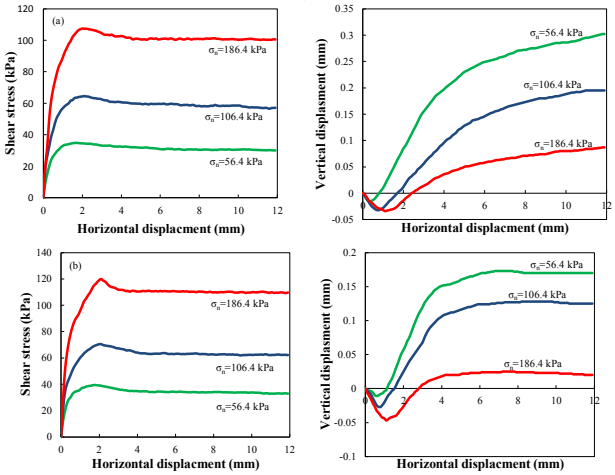

Figure 4. Experiments for e_{in}=0.74 under various constant normal stress for a) S1 sand b) S2 sand

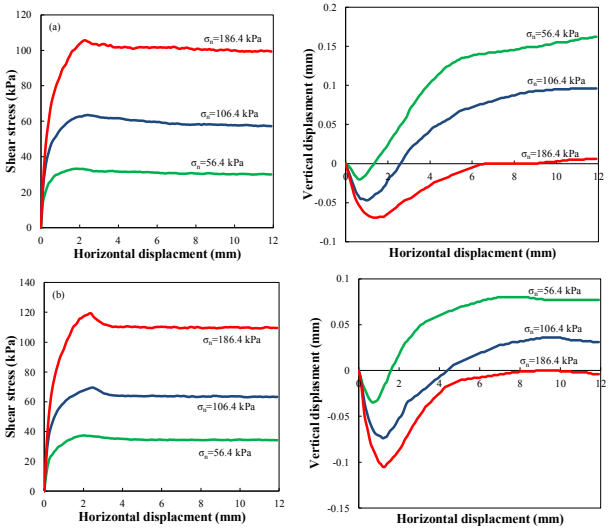

Figure 5. Experiments for e_{in}=0.80 under various constant normal stress for a) S1 sand b) S2 sand

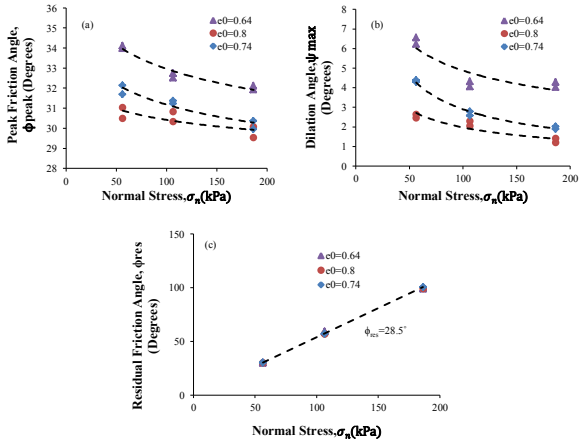

Figure 6. Frictional and dilatancy angle for S1 sand-rough steel interface with various void ratio and constant normal stress a) Peck friction angle b) Dilation angle c)Residual friction angle

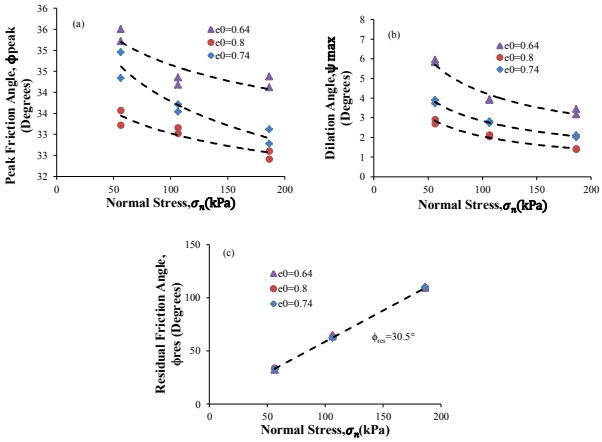

Figure 7. Frictional and dilatancy angle for S2 sand-rough steel interface with various void ratio and constant normal stress a) Peck friction angle b) Dilation angle c)Residual friction angle

4. Conclusion

The magnitude of mobilized shear strength of the sand particle in sand-steel interface will be different through changing in the diameter of the grains. This reduction causes increase in the magnitude of normal roughness and soil shear strength. Nonetheless, it reduces the shear bond area and tendency to dilated treat and then sand reaches to critical state faster.

5. References

[1] Uesugi, M., Kishida, H. (1986). Frictional resistance at yield between dry sand and mild steel. Soils and Foundations, 26(4), 139-149.

[2] Evgin, E., & Fakharian, K. (1997). Effect of stress paths on the behaviour of sand steel interfaces. Canadian geotechnical journal, 33(6), 853-865.

[3] Hebeler, G. L., Martinez, A., & Frost, J. D. (2015). Shear zone evolution of granular soils in contact with conventional and textured CPT friction sleeves. KSCE Journal of Civil Engineering, 1-16.

[4] Vangla, P., & Gali, M. L. (2016). Effect of particle size of sand and surface asperities of reinforcement on their interface shear behaviour. Geotextiles and Geomembranes, 44(3), 254-268.

Geotextile Influence on Deformation Reduction of Rockfill Breakwater

Mojtaba Saeednejad[1], Hadi Shahir[2]

1) Graduated student, School of engineering, Kharazmi University, Tehran, Iran, saeednejad.moj@gmail.com
2) Assistant professor, School of engineering, Kharazmi University, Tehran, Iran, shahir@khu.ac.ir

1. Introduction

Breakwaters are one of the important structures in ports whose main function is to prevent storm waves and ocean currents from entering the shore. There are various kinds of breakwaters. Incline plate breakwaters is an instance which is more frequently used due to simple implementation and low cost. Most breakwaters are built on soft clay bed with low resistance, little permeability, high subsidence ability. Therefore, subsidence and overall failure happen in most of them. Drawing on surface reinforcers (geotextiles) is one of the ways to confront this problem. Geotextiles decrease subsidence, improve failure and prevent permeation of breakwater stones in the soft clay. The effect of surface reinforcers on the soft layers under embankments and breakwaters has been the subject of many researches. Some researchers have examined the behavior of reinforcers in large and real scale of embankments ([1], [2] , [3]). This methodology shows very good results, though it is very expensive. [4] examined the behavior of reinforcers using centrifuge test. Also, validation of numerical methods with centrifuge tests is an economic way to study the behavior of embankments built on soft soil [5]. Nevertheless, many issues related to reinforced lands have remained unknown because of complexities in their operation. The present article models the subsidence and overall stability of Nakhl-e Nakhoda breakwater built in Bandar-e Abbas, Iran, using PLAXIS software. And the influence of surface reinforcements under this breakwater which has confronted many cases of subsidence has been studied using this software.

2. Material properties

Soil properties under the breakwater

With an investigation of the geotechnical reports performed on the project site, soil parameters in drained and undrained conditions are considered as presented in table 1 and 2. Cam-Clay model is used for numerical modeling in consolidated-drained condition and Mohr-Coulomb is used for unconsolidated-undrained condition.

Table 1. specification of soil under the breakwater in consolidated-drained condition.

M	e_{init}	ν	κ	λ	γ_{sat} (kN/m^3)	k (m/day)
0.65	1	0.3	0.03	0.09	18.8	10^{-5}

Table 2. specification of soil under the breakwater in unconsolidated-undrained condition

C_u (kPa)	E_u (kN/m^2)	νu
30	15000	0.495

Properties of Geotextiles

In order to investigate the effect of surface reinforcements (geotextile), geotextiles with tensile strength of 400, 600, 800, 1000 and elasticity module of 3333, 5000, 6666, 9091 kN/m were used. A layer of sand and gravel between rockfill of breakwater and soft soil under the breakwater can decrease the permeation of rocks into soil and also reduce damages to geotextiles. In this way, a lower Safety factor can be considered which means more efficient usage of tensile capacity of geotextile. Therefore, the present study considers a sand layer between the stony material of the breakwater and the soft soil beneath. Table 3 presents maximum tensile strength limit for each geotextile type based on design relation of geotextile. Based on these numbers, the tensile strengths of all geotextiles are less than their allowed resistance.

Table 3. ultimate and allowable tensile strength of geotextiles

Ultimate tensile force (kN/m)	Safety factor	Allowable tensile force(kN/m)
400	1.78	233
600	1.72	349
800		465
1000		581

3. Results

Nakhl-e Nakhoda breakwater which is located on soft clay bed has been modeled using PLAXIS software and parameters like horizontal displacement have been studied in drained and undrained conditions. Furthermore, the present article explores the effect of adding geotextile layers and changing the distance between geotextiles on the breakwater behavior. Discussing the results of horizontal and vertical deformation. In order to examine the effect of geotextiles on land deformation under the specified breakwater in drained and undrained conditions, the results of breakwater maximum horizontal and vertical deformatins in the face of geotextile tensile strength are presented in figures 3 to 6.

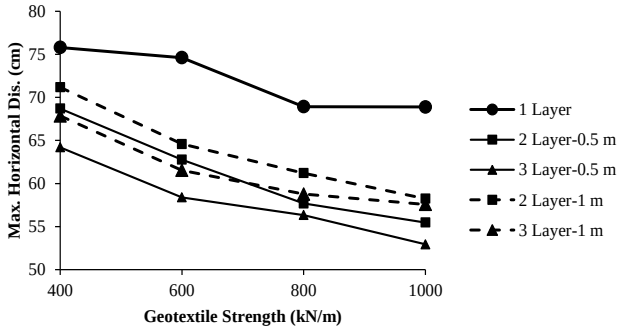

Figure 3: maximum horizontal deformation in the face of geotextile tensile strength in drained condition.

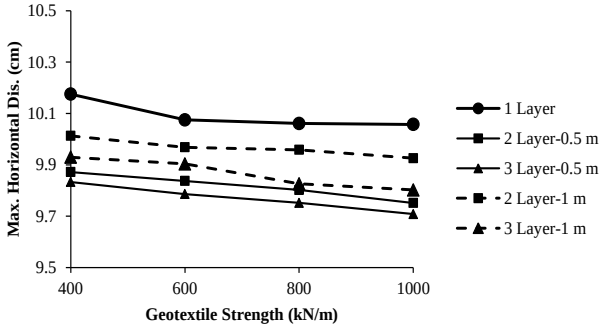

Figure 4: maximum horizontal deformation in the face of geotextile tensile strength in undrained condition.

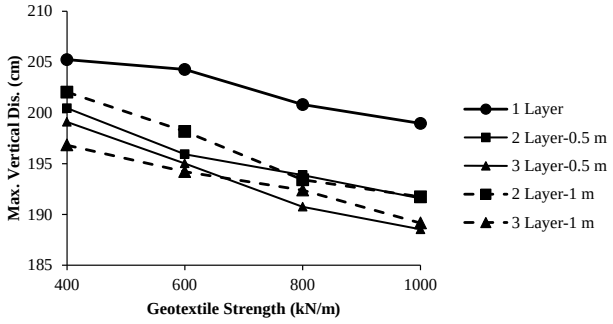

Figure 5: maximum vertical deformation in breakwater centre in the face of geotextile tensile strength in drained condition.

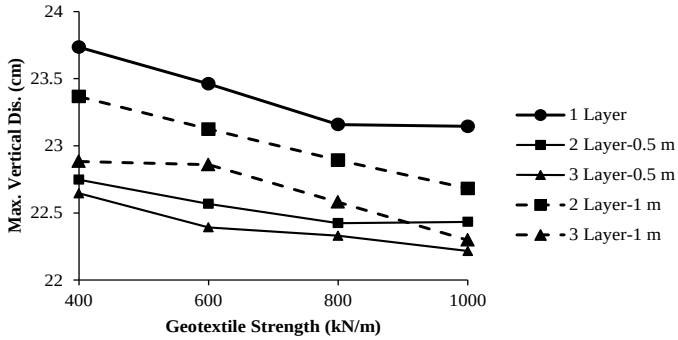

Figure 6: maximum vertical deformation in breakwater centre in the face of geotextile tensile strength in undrained condition

As it can be observed, increasing geotextile tensile strength and number of geotextile layers decrease maximum vertical and horizontal deformation in drained and undrained conditions. In examined conditions, maximum horizontal deformation happens with one geotextile layer more than the 3 normal layers. Moreover, the results of figures 3 to 6 indicate that the effect of adding geotextile layers with 0.5 m distance is more than layers with 1 m distance.

4. Conclusions

•Increasing the number of geotextiles decreases horizontal and vertical deformation in drained and undrained conditions.

•Maximum horizontal deformation is for one layer more than the 3 geotextile layers. Furthermore, the effect of adding geotextile layers with 0.5 m distance is more than layers with 1 m distance.

•Increasing geotextile tensile strength and the number of layers increase the effect of land reinforcement with geotextile.

•The effect of geotextile in drained condition is more than undrained condition.

5. References

[1] Rowe, R.K., Gnanendran, C.T., Landva, A.O., Valsangkar, A.J., 1995. Construction and performance of a fullscale geotextile reinforced test embankment, Sackville, New Brunswick. Canadian Geotechnical Journal 32 (3), 512–534.

[2] Bergado, D.T., Long, P.V., Murthy, B.R.S., 2002. A case study of geotextile-reinforced embankment on soft ground. Geotextiles and Geomembranes 20 (6), 343–365.

[3] Chai, J., Miura, N., Shen, S., 2002. Performance on embankments with and without reinforcement on soft subsoil. Canadian Geotechnical Journal 39 (4), 838–848.

[4] Sharma, J.S., Bolton, M.D., 1996. Centrifuge modelling of an embankments on soft clay reinforced with a geogrid. Geotextiles and Geomembranes 14 (1), 1–17.

[5] Sharma, J.S., Bolton, M.D., 2001. Centrifugal and numerical modelling of reinforced embankments on soft clay installed with wick drains. Geotextiles and Geomembranes 19 (1), 23–44.*Conference on Software Engineering (ICSE'03)*, Portland, OR, May 3-10 2003, pp. 125-137.

A STUDY ON THE ESTABILESHMENT OF MARINE ELECTRONIC HIGHWAY BETWEEN SOUTH OF KHARG ISLAND AND THE STRAIT OF HORMUZ IN THE PERSIAN GULF FOR MARINE SAFETY, SECURITYAND MARINE PROTECTION

Ali Moradi (PhD)[1], Amin Moradi(BSc)[2]
1) Ports and Maritime Organisation, Tehran, Iran, Ali8ir@yahoo.com
2) Islamic Azad University, Tehran, Iran, Aminmoradi7059@gmail.com

1. INTRODUCTION

There are heavy marine traffics at central to the north-west part of the Persian Gulf (here after called "Passage"). This area is considered to be one of dangerous area due to existence of numerous oil and gas fields and terminals in the region. At recent years accidents happened that would be catastrophic in national and regional (PMO report 2015).However the proposed area between south of Kharg Island and the Hormuz Strait in the Persian Gulf is approximately 800 kilometers long, 30 kilometers wide at their north-west entrance, and 12 kilometers wide at south-east entrance, at Hormuz Straits. Annual marine traffic is around 30,000 of different kind of ships which are entering and departing from different ports, oil terminals, petrochemical ports etc. The type of ships differs from Ultra Large Crude Carriers (ULCC) to General cargoes and Container carriers. Their destination/departure to ports in Iran, Iraq, Kuwait, Saudi Arabia, Bahrain and Qatar. This huge traffic with respect to the nature of resource and existence of dangerous oil and gas fields makes the "Passage" very high risk area with many oil and gas platforms and hence is hazardous to navigation especially for larger ships. Figure (1) shows a view of the proposed area for establishing of a Marine Electronic Highway (MEH).

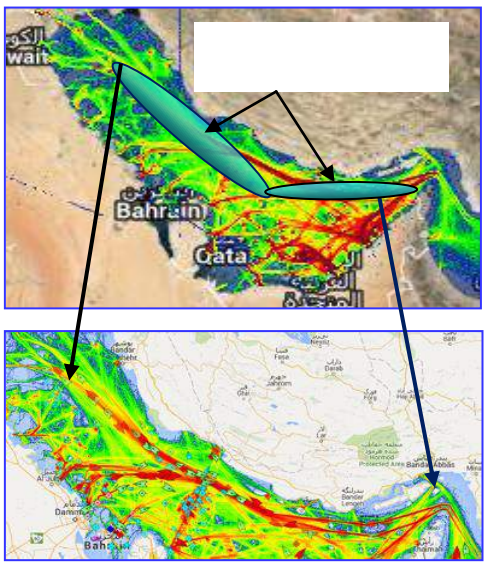

Figure 1. Proposed area of establishment Of MEH in the Persian Gulf

2. FIELD ANALIZING

Despite navigational difficulty due to existence of hazardous features and platforms in the "Passage", the "Passage" is the shortest way and hence the preferred shipping route between the North West and the South East of Persian Gulf. However vessels trading between the Persian Gulf countries, use the "Passage" to navigate between Persian Gulf and the rest of world.

Current maritime safety infrastructures and regulatory mechanisms are weakly in place in the "Passage" and there is high risk of ship collisions, groundings and oil spills and occasional incidents have occurred in recent years and some of these incidents have caused by oil spills. The Electronic Highway an innovative approach to improving the management of maritime traffic and marine environment protection in the "Passage". To establish the MEH in the "Passage" is promote the marine safety and environment protection and marine security as well (Moradi, 2015).

3. THE NEED FOR THE ESTABLISHING OF MEH SYSTEM IN THE "PASSAGE"

Recent enhancements in maritime safety infrastructure and regulatory mechanisms have improved navigational safety and traffic flow. Marine Electronic Highway is a mean to provide safe, secure and pollution protection. The main components to establish the MEH "Passage" are consist of Electronic Navigational Chart (ENC), Vessel Traffic Service (VTS), Automatic Identification System (AIS), Reacons, Dynamic Hydrographic Data Collection, and etc. Proper Aids to Navigation need to install in the coverage region. Furthermore Traffic Separation Scheme (TSS) need to be planed for area concerned and regulatory regime should enforce by authorized Organizations (IMO, 2011).

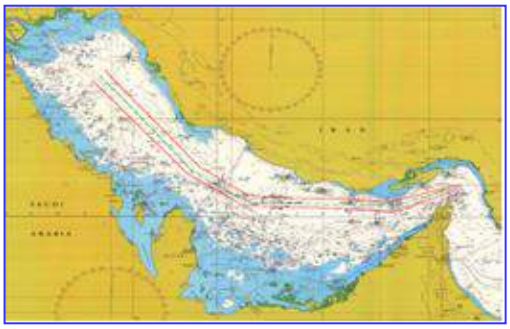

Figure 2.Tthe whole view of "Passage"

4. BENEFITS AND EXPECTATION

The Marine Electronic Highway aims to establish a mechanism in the south of Kharg Island and the Hormuz Strait in the Persian Gulf .for enhanced maritime safety and marine environment. The MEH system with its environmental modules can be used in marine pollution response and control such as to predict the direction and speed of oil spill and aid in response and clean-up. It is also possible to use it to identify and track ships that illegally discharge their bilges or dump other oily wastes. The Marine Electronic Highway (MEH) is envisioned to be a regional network of marine information technologies linked through the ENCs-ECDIS.

Nowadays the availability of Global Navigation Satellite System (GNSS) enables the precise positioning with accuracy of 1 to 5 meters enhances the navigational accuracy of ENCs-ECDIS especially in congested and confined waters.

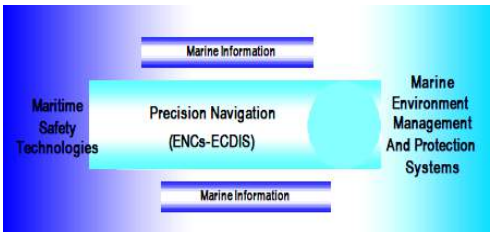

Figure 3. ***The Marine Electronic Highway is the integration of maritime safety technologies and marine environment management and protection with precision navigation as its backbone.***

5. SYSTEM CONFIGRATION

Advancements in information technology have significant impacts on the shipping industry. Many of the important navigational technologies and data are amenable to computerization. Examples are paper charts converted to ENCs, incorporation of some aspects of ship routeing system into ECDIS and audio-visual communications. Many of the newer commercial vessels are equipped with ENCs-ECDIS including integrated bridge system. Today the majority of world fleet use electronic charts for navigation. The developments of maritime safety technologies are generally industry driven and fairly in adherence to standards and performance criteria (e.g., ISO, IEC, IMO and IHO) unlike the development of information technologies in other sectors and disciplines.

Figure 3. Configuration of different systems in MEH

6. STRATEGIES AND APPROACH

The proposed MEH will have four key elements, namely, maritime safety, environment protection, maritime security and management. Within maritime safety, precision navigation constitutes the backbone of the marine electronic highway. Four key issues are fundamental to the advancement of the MEH technology namely:

1. Information technology, and specifically the integration of existing technologies and capacities
2. Socio-economic benefit to the government, industry/private sectors, and the civil societies in general as a consequence of the proposed MEH technology;
3. Financing mechanisms/investment potential, and the establishment of interagency, intergovernmental and inter-sectorial partnerships as vehicles for successfully developing, financing, constructing and operating the MEH as self-sustaining, revenue -generating enterprise in the "Passage";
4. Institutional arrangements, with agreement among participating parties on the administrative, legal, financial and operational aspects of a “managing tool”

7. RESULTS AND DISCUSSION

Charging system to recover the capital and operating cost can be maintained. Investment for establishment of recovered by a charge on ships transiting the "Passage". This is an innovative proposal so could cover part of expenses.

Benefits derived from increases in operating efficiency of MEW would include:

1. Maintaining speed more efficiently in adverse conditions
2. Steering a more accurate course
3. Carrying more cargo by optimizing under-keel clearance
4. Manoeuvring more efficiently when in vicinity of oil and gas platforms
5. More efficient implementation of collision regulations.
6. Integration of different systems for taking advantage to make synergy, hence to promote marine safety, security and environmental protection.
7. The last but not least, application of "Persian Gulf" term in International publication is desirable.

8. REFERENCES

[1] Moradi A. Iranian Marine Casualty Analyzing Annual report (2014-2015) Ports and Maritime Organization (PMO), 2011.2015, 60 p.

[2] Adrian S. Development of a Regional Marine Electronic Highway in the Straits of Malacca and Singapore IMO Technical Office London ppt, 2008.

[3] Bajpai N. East Asia AND PACIFIC: 4E-Marine Electronic Highway (IMO), 2008, 50p.

[4] Sekimizu K.,The Marine Electronic Highway (MEH) Project Director, Maritime Safety Division International Maritime Organization(IMO), 2005, London.

[5] World Oil Transit Chokepoints, World Oil Transit Check Point Full report, US Energy Information, Last Updated: November 10, 2014, 20p.

RISK ASSESSMENT IN LOADING, UNLOADING AND MAINTAINING DRY BULK IN IRAN'S PORTS BY USING FUZZY FMEA

(CASE STUDY: IMAM KHOMEINI PORT)

Sobhan Iranshahi[1], Amin Homayouni Rad[2], M.Amin Dana[3]

1) Hormozgan Province Maritime & Ports Authority, Bandar Abbas, Iran, Sbn.iranshahi@gmail.com
2) Bushehr Custom Authority, Bushehr, Iran**,** a_h_rad84@yahoo.com
3) Sistan & Baluchistan Province Maritime & Ports Authority, Chabahar, Iran**,** amindana@gmail.com

1-INTRODACTION

Nowadays there are many dangers in different levels of ports that impose much costs on them due to Non-compliance with health and safety principles. These are just direct costs of the incidents and also there are some indirect costs which are not negligible, like: new employment and training, following lawsuits, equipment out of service and slowing the unloading process [1]. Imam Khomeini is one of the biggest ports in Iran and also is the center of Export and import of grain and dry bulk in Iran. At first we need to have a better understanding about the process of loading, unloading and maintaining dry bulk and its details. Then we will specify the related risks of every process and identify their causes and effects and finally the necessary proceedings for reducing or eliminating the risks will be detected.

2-RECOGNIZING THE PROCESSES, POTENTIAL RISKS AND THEIR CAUSES AND EFFECTS

The actions related to loading, unloading and maintaining dry bulk in Imam Khomeini port consist of 5 parts:
1. Loading and unloading 2.Operation actions 3.Dock workers 4.Maintaining and storing dry bulk commodities 5.Ship store 6.Potential risks for these actions have been identified.

3- ESTIMATING THE INTENSITY, PROBABILITY AND PROBABILITY OF DISCOVERY OF EACH POTENTIAL RISK

The Fuzzy FMEA (failure modes and effect analysis) provides a tool for obtaining better results from vague concepts and inexact information [2]. A sample information is shown in table 1, about identified potential risks, their causes and effect as well as control measures during loading, unloading and maintaining dry bulk.

Table 1: elements composing the priority of risks in loading, unloading and maintaining dry bulk in Imam Khomeini port

Action	Field of action	Potential risk	Potential effects	Risk level	Potential causes	probability	Running controls	Probability of discovery
D-Store and maintaining operation	D-3-3 loading and unloading seeds in storehouse	Dust	Respiratory diseases	High	Not using Personal protective equipment	Average	Personal protective equipment	Relatively high

4- FUZZY MEMBERSHIP FUNCTION

After identifying the degree of intensity, probability and probability of discovery, the fuzzy number corresponding to each degree will be specified (Table 2) [3].

T(x) = {too low, low, modest, average, relatively much, much, too much} U= [0.1]

X= {intensity, probability, probability of discovery}

Now we can make a membership function by multiplying the intensity, probability and probability of discovery, so that we find FRPN. For example, in potential risk of "respiratory diseases caused by dust" related to "maintaining seeds in storehouse" we will have:

FRPN= S × O × D = (0.7, 0.9, 0.1) ⊗(0.3, 0.5, 0.7) ⊗(0.5, 0.7, 0.9) = (0.105, 0.315, 0.63)

Table2: Degree of risk factors in loading, unloading and maintaining dry bulk in Imam Khomeini port

Risk level	Overall rating(RPN)	Right rating	Left rating	FRPN			Potential risks
critical	0.370	0.479	0.739	0.105	0.315	0.63	D-3-3

5- Defuzzification of fuzzy membership function

We change the fuzzy amount FPRN to exact amount of RPN, by scoring to the left and side of fuzzy number. In this study triangular fuzzy numbers are shown as (m-α ،m ،m+ β). Therefore, the potential risk of "respiratory diseases caused by dust" related to "maintaining seeds in storehouse" for RPN is:

m-α = 0.105
α = 0.21
m = 0.315
m + β =0.63
β = 0.315
According to 3-3 and 3-4 in chapter three, the amount of left and right side of this fuzzy number is:

$$\mu_L = 1 - \frac{0/315}{1+0/105} = 0.739$$

$$\mu_R = \frac{0/63}{1+0/315} = 0/479$$

And according to 3-5 in chapter three, the exact amount of fuzzy number is:

$$\mu_T = \frac{0/479+1-0/739}{2} = 0.370$$

6- Conclusion

The last part of evaluating risk in loading, unloading and maintaining dry bulk in Imam Khomeini port, is to measure the degree of estimated risk factors in prior phase. Risk factors are divided into three levels of tolerable, moderate and intolerable by the members of FMEA and based on economic, social and legal considerations in Imam Khomeini port. The point of this phase is to determine a risk zone which needs to be under more consideration According to degrees of RPN in this study, the potential risk of D-3-3, i.e seeds dust and not using personal protective equipment which leads to respiratory diseases while unloading seeds in storehouse, has got the largest number and is in the level of critical risk.

Table 3: risk classification

Descriptions	RPN	Risk classification
Risk factors which are allowed and the running controls could prevent any accident	0.001≤ RPN<0.06	Tolerable
Risk factors which are under control but should be reconsidered and they could be improved in future. But now, they are not a priority.	0.06 ≤ RPN<0.350	Moderate
Risk factors which should be completely removed or reduced. Running controls are not enough.	0.350≤ RPN≤0.893	Intolerable

(Resource: FMEA, 1394)

[1]. Hamidi, H." Port Equipment: Policy, Management and Maintenance" *Asrar Danesh*, 1389, Tehran, PP: 50-55.

[2]. Xu, K., Tang, L.C., Xie, M., H o, S .L. & Zhu, M.L."Fuzzy Assessment of FMEA for Engine Systems", *Reliability Engineering and System Safety*, 2002, Vol. 75. PP: 17-29.

[3]. Kumru, M. "Fuzzy FMEA Application to Improve Purchasing Process in a Public Hospital" *Appl Soft Compute*, 2013, Vol. 13, No. 1, PP. 721-733.

[4]. Kyokai ،N. K. "Risk Assessment Guidelines". *CRC Press, 2009, Japan* ،pp. 1-20.

DECISION SUPPORT SYSTEM FOR RISK ASSESSMENT IN THE MARITIME DOMAIN

Fatat Saleh[1], Assef Jafar[2] and Radi Khazem[3]

1) Higher Institute of Applied Sciences and Technology (HIAST), Damascus, Syria, saleh.fatat@gmail.com
2) Higher Institute of Applied Sciences and Technology (HIAST), Damascus, Syria, assefjafar@gmail.com
3) Higher Institute of Applied Sciences and Technology (HIAST), Damascus, Syria, rady.khazem@gmail.com

1. INTRODUCTION

In the last decade, the experts' need for enhancing situation awareness systems has increased in the maritime surveillance domain all over the world. This leads, therefore, to enhancing decision making and maintaining safety and security of shores. The reason for this is the sudden increase in the rate of maritime smuggling in all its sorts (people, goods, drug, weapons, etc.), the use of sea for terroristic and other illegal activities, and the increase of ship accidents that yields catastrophic results.

Maritime environment is characterized to be dynamic, complex and having excess information coming from heterogeneous data sources. Some of these data sources monitor vessel motion (like radars, cameras, AIS and GPS devices that determine position, velocity, and course) and measure environmental factors (like whether, wave height, wind speed, and visibility conditions). Other information available includes port reports about vessels (like vessel lists or crews that have history of illegal business). For this reason, building situation awareness for this environment requires the domain operators to have the experience and awareness of all aspects of this environment and its parameters. Having this expertise, they assess vessel risks in short time. This can put them under mental pressure that may distort the whole situation awareness process and leads them to lose control putting them and maritime safety and security under real threats. Hence, risk assessment and identifying threats and suspicious behaviors of vessels are the main key to avoid those risks before they occur or, at least, mitigate their impacts [1].

Many studies have been performed about decision support and enhancing situation awareness in the maritime domain. Most of those concentrated upon anomaly detection in vessel behavior as an important way to identify threats [2]. The methods for doing this are divided into two major groups: data-driven methods [3] and knowledge-driven methods [4].

According to [1], not all anomalies present a threat and not all anomalies have the same risk level. For example, a vessel moving towards a restricted area with high speed is very much more risky than a vessel moving towards a restricted area with a lower speed. In the latter case, the operator has more time to make his decision, which is not the case in the first one. In the light of these two ideas, we built a decision-support framework to help operators in this domain. This framework employs expert's reasoning in classifying vessels according to their risk. It has as input the data coming from various data sources, then it employs the knowledge and rules exploited from subject matter experts and stored in a knowledge base in order to classify vessels according to their risk and display this output on a graphic interface to enable the operators to deal first with vessels having the highest risk.

2. RISK ASSESSMENT IN MARITIME DOMAIN

Risk is defined as the probability of occurrence of an undesirable event, or the chance of a loss. This undesirable event may be caused by a ship, due to its features and/or behavior [5]. From this definition, we can see that the process of risk assessment consists of three main phases:

1. Threat/undesirable events identification.
2. Determining elements of each threat.
3. Assigning risk level to each threat coming from vessel (no risk, low, medium, high).

We achieved these three phases by conducting interviews with domain experts, using existing reports, and reviewing previous studies [6] to prepare list of threats and evaluate their risk level using threat matrix [7]. After this stage, we encoded this expertise in knowledge base using ontology and rules.

3. THREAT VARIABLES

To identify threats coming from vessels and their risk level, we must determine the properties and variables that are involved in each threat and determine the data source(s) for each of these variables. In our proposed framework, these variables includes:

- Kinematic Variables – include static characteristics of a vessel (flag, name, IMO number, etc.).
- Non-kinematic Variables – include dynamic variables that can change during time (position, speed, course, etc.).
- Voyage-related Variable– include characteristics of an actual vessel's voyage from port to port (departure port, destination port, estimated arrival time);
- History-related Variables – include historical information about vessel.
- Environment Conditions (weather, wind speed, currents, wave height, etc.).

4. ARCHITECTURE OF RISK ASSESSMENT FRAMEWORK

Our work proposes a decision support system (Figure 1) to help maritime operators analyzing the incoming information from multiple data sources to provide an understanding of situation to assist them in making good decision in threaten situation. As new sensor data arrives, it is fused and saved in the database. The fused data is then fed into the ontology processing engine. Next, the inference engine processes this new information using the predefined rules and properties of the behaviors of the vessel. The result is displayed on map for operators.

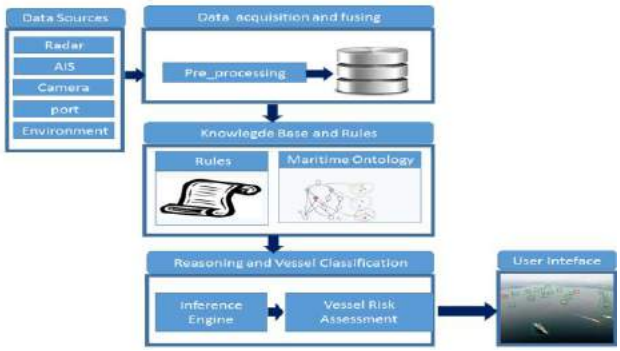

Figure 1. Architecture of decision support system for risk assessment.

5. FRAMEWORK EVALUATION

Before putting this framework in the real use, we evaluated it using data previously gathered. The vessels' data have been acquired during a period of one week around Syrian Coast from multiple sources (AIS, Radar, ports, etc.), then this data has been filtered and fused to get as more relevant information as possible. The evaluation carried out was to analyze the response time of our framework against the number of vessels (By increasing the number of vessels and finding out the time needed for our inference process to respond).

Figure 2 shows the framework performance for various number of vessels. It is clear that the time of vessel classification based on its risk is short when compared with the time taken by operator without this decision support system. We do not claim that this system can replace domain operators, but it helps them taking the right decision in the right time.

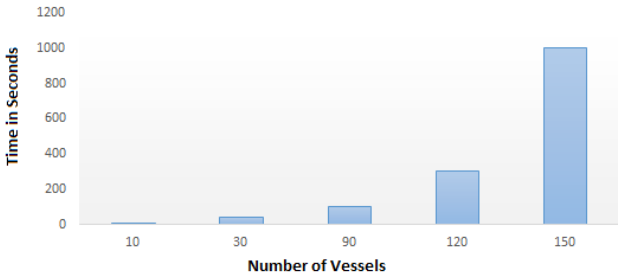

Figure 2. Inference process performance.

Figure 3 shows the interface of our framework. It contains a map with vessels drawn on it according to their geographic locations with colors representing their risks (green, yellow, orange and red) for (no risk, low, medium, high), respectively. The window on the right of map contains information about vessel like speed, location (latitude, longitude), course, etc. One vessel is drawn in red in the map because it entered restricted area.

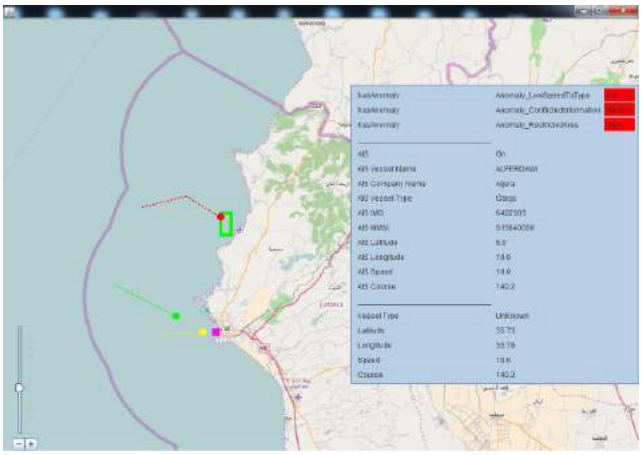

Figure 3. The interface of our framework.

6. RESULTS AND DISCUSSION

We have provided a framework for early threat detection by evaluating the risk level of undesirable events resulting from vessel behavior. This is useful to provide early warnings before threats take place and to take the right actions to mitigate them according to risk level.

7. REFERENCES

[1] Martineau, E. and Roy, J., "Maritime anomaly detection: Domain introduction and review of selected literature", *Defense Research and Development*, Canada (Quebec), 2011.

[2] Roy, J., "Anomaly detection in the maritime domain". *SPIE Defense and Security Symposium*, International Society for Optics and Photonics. April 2008, pp. 69450W-69450W.

[3] Ulusçu, Ö.S., Özbaş, B., Altıok, T. and Or, İ., "Risk analysis of the vessel traffic in the strait of Istanbul". *Risk Analysis, 29(10)*, 2009, pp.1454-1472.

[4] Vandecasteele, A. and Napoli, A., "An enhanced spatial reasoning ontology for maritime anomaly detection". *System of Systems Engineering (SoSE), IEEE 7th International Conference on*, July 2012, pp. 1-6.

[5] Stróżyna, M. and Abramowicz, W., "A Dynamic Risk Assessment for Decision Support Systems in the Maritime Domain". *Studia Ekonomiczne, 243*, 2015. pp.295-307.

[6] Van Laere, J. and Nilsson, M., "Evaluation of a workshop to capture knowledge from subject matter experts in maritime surveillance". *Information Fusion, 2009. FUSION'09. IEEE 12th International Conference on*, July 2009, pp. 171-178.

[7] Thachuk, K. and Tangredi, S., "Transnational threats and maritime responses". *Globalization and maritime power*, 2002.

SAFETY DOMAIN CONCEPT IN SHIP-SHIP COLLISION PROBABILITY MODELING

Siyavash Filom[1], Roozbeh Panahi[2]

1) Department of civil engineering, Tarbiat modares University, Siyavaship@gmail.com
2) Department of civil engineering, Tarbiat modares University, Rpanahi@modares.ac.ir

1. Introduction

In the transport business, safety and efficiency are key issues. These are not always compatible; a greater speed or higher traffic intensity usually means higher efficiency but lower safety. According to COLWILL et al [1]: 'In busy ports and waterways around the world the hazard profile is dominated by ship-ship collisions.

The concept of ship domain plays an essential role in navigational safety of vessels. A well known definition of ship domain by Goodwin[6] is described as "the surrounding effective waters which the navigators of a ship want to keep clear of other ships or fixed objects". Various geometrical ship domains with distinct shapes and sizes were proposed by researchers (Fujii and Tanaka,[6]; Goodwin[7]; Davis et al.,[4])

Nowadays the vessel safety domain is a very common concept in maritime transport. It is used for various purposes such as traffic lane design and capacity studies, for risk assessments and as encounter criterion in maritime traffic simulation programs. Even so, there is no universal definition for the concept of vessel safety domains. Research has been done on this concept since the end of the 1960's and various researchers have come up with their own theories.

2. Ship-Ship Collision Probability Modeling

At present, collision probability is most commonly assessed based an approach suggested by Fujii and Shiobara [5] and MacDuff [8]. The number of collision occurrences over the studied time period Ncoll, is estimated as follows:

$$N_{coll} = N_A P_c \quad (1)$$

where N_A is the number of pairwise vessel encounters during a time period resulting in collision, provided no evasive action is taken, commonly designated as the number of collision candidates [13]. P_c is the probability of failing to avoid a collision when on a collision course due to technical failure or human error, generally known as the causation probability [13].

The number of collision candidates varies both with geographic location and with time, reflecting the intensity of maritime traffic during different periods. The causation factor is currently estimated in two ways: by a scenario approach or by a synthesis approach [13].

3. Safety Domain Role in Collision Probability Modeling

The Main part of ship-ship collision risk assessmenet is detevting collision candidate points. For this purpose, every ship has a taken safety domain and he overlaps of these safety domains will be a collision candidate point.

4. Safety Domain Concept

In the past thirty years or more, many researchers have presented various ship domains with different shapes and sizes having taken into account different factors that affect the parameters of ship domains. It should be noted that the determination of ship domains presented by statistical or intelligent methods strongly depend on the statistical data and navigators' experience.

4.1. Circle Safety Domains

This models are also derived by statistical methods from a large number of records of data and simulator data[2,3]. The latest model is proposed by use of neural networks. However, the model can only be applied to limited types of ships since it needs plenty of learning samples to train the network.

4.2. Elliptic Safety Domains

Originally, the first elliptical ship domain was derived by Fujii [5] from a recorded data registering ship's positions in Japanese waters by using statistical methods.In the 1980s, Coldwell[1] established another elliptical ship domain by similar statistical methods for head-on and overtaking encounter situations in restricted waters. Recently,Kijima [7] proposed a new ship domain modelled by ''Blocking area'' and ''Watching area''. Additionally, the parameters of ship length, breadth, relative speed and relative angle between courses have been fully considered and introduced to define the ship domain. Obviously, this is a dynamic ship domain model which accounts for ship dimensions, manoeuvrability, encounter situations and target ship states.

4.3. Polygonal Safety Domains

Recently, some literature presented polygonal ship domains allowing the determination of dynamic dimensions of domains. A version of the above approach features a relative domain for a target ship, proposed by Smierzchalski [10], of which the figure is a hexagon defined on the basis of dynamic parameters of own and target ship. Another version, proposed by Pietrzykowski [11], defined ship domains as polygons of which the shapes depend on the discretization step of target ship

course and usually is octagonal. The expert research and questionnaires dealing with various ship encounter situations in an open sea in good visibility had been proccessed for this models.

5. Fuzzy Quaternion Safety Domain

The conventional ship domains divide the area around a ship into two zones, dangerous and safe – the ship domain and an area outside the domain, respectively. However, the human being tends to distinguish the area around the ship to be more than two zones which can be described in linguistic terms, very safe, safe, less safe, dangerous, very dangerous, etc. Depending on these fuzzy terms, the navigator tries to maintain certain zones clear of other ships and objects, while these fuzzy terms can be modelled by fuzzy membership functions. Therefore, the conventional ship domain with a clear boundary which is deal, but limited in applications, can be extended to fuzzy ship domains with a series of boundaries to indicate different levels of navigational safety. On the other hand, the ship collision risk can be modelled by fuzzy ship domains since a series of fuzzy boundaries can be used to identify the level of navigational safety or danger [12].

6.Simulation and Analysis

For a comparative study of these three large classes of ship domains, we produced some computer simulations for analysis in various encounter situations with other target ships.The principal dimensions of the own ship and target ship are listed in Table 1.

As shown in Figure 1, seven ship domains in three classes have been considered in the process of approaching. It can be seen that the Davis and Fujii models are the most conservative and most risky ones, respectively.

Table 1. Principal ship dimensions

	Own Ship	Target Ship
L(m)	120	300
B(m)	25	50
T(m)	9.5	22

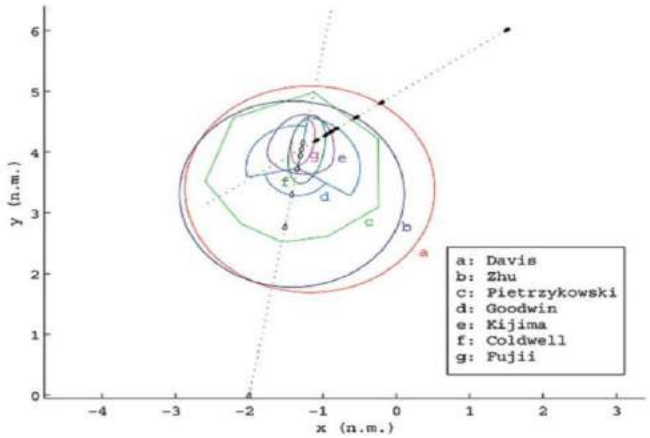

Figure 1. Ship Domains

7.Conclusion

The typical ship domains have been reviewed and classified into three large classes, as circle, ellipse and polygon ship domains. It is known that most of the ship domains were illustrated in different geometrical manners that would be more descriptive and declarative. According to the classifications, we have proposed the mathematical descriptions for each type of ship domain. The uniform analytical framework has been established for various ship domain models, which would make it more feasible and practical to apply the models for risk assessment and collision avoidance, regardless of practices or simulations. Finally, several computer simulations on different encounter situations have been presented for validation of the analytical domain models and analysis of the comparative study for the different ship domains. The results show that the analytical ship domain models are effective and identical to the original geometrical ones. It should be noted that most of the existing ship domains have not adequately taken the human factors and environmental states into account. Future research on ship domains will focus on how these vital factors affect the shape and size of ship domains.

8.References

[1] Coldwell, T. G. (1983). Marine traffic behaviour in restricted waters. The Journal of Navigation, 36, 431–444.

[2] COLWILL, R.D., WIGNALL, D., DAND, I. (2004) The Application of Marine Risk Simulation to the "Nearcasting" and Prevention of Collision Incidents, Proceedings International Symposium on Vessel Traffic Services 2004, Hong Kong

[3] Davis, P. V., Dove, M. J. and Stockel, C. T. (1980). A computer simulation of marine traffic using domains and arenas. The Journal of Navigation, 33, 215–222.

[4] Davis, P. V., Dove, M. J. and Stockel, C. T. (1982). A computer simulation of multi-ship encounters. The Journal of Navigation, 35, 347–352.

[5] Fujii, Y. and Tanaka, K. (1971). Traffic capacity. The Journal of Navigation, 24, 543–552.

[6] Goodwin, E. M. (1975). A statistical study of ship domains. The Journal of Navigation, 28, 329–341.

[7] Kijima, K. and Furukawa, Y. (2003). Automatic collision avoidance system using the concept of blocking area. Proceeding of IFAC Conference on Manoeuvring and Control of Marine Craft, Girona, Spain.

[8] MacDuff T. The probability of vessel collisions. Ocean Industry; 1974. 144-148.

[9] Pietrzykowski, Z. and Uriasz, J. (2004). The ship domain in a deep-sea area. Proceeding of the 3rd International Conference on Computer and IT Applications in the Maritime Industries, Siguenza, Spain.

[10] Smierzchalski, R. and Michalewicz, Z. (2000). Modelling of a ship trajectory in collision situations at sea by evolutionary algorithm. IEEE Transaction on Evolutionary Computation, 4(3), 227–241.

[11] Wang Ning. (2010). An Intelligent Spatial Collision Risk Based on the Quaternion Ship Domain. The Journal of Navigation, 63, 733–749.

[12] Zhao, J., Wu, Z. and Wang F. (1993). Comments on ship domains. The Journal of Navigation, 46, 422–436.

[13] Ylitalo J. Modeling marine acciden, Master's thesis.:Aalto University School of Science and Technology; 2010.

INVESTIGATING INCIDENTS CAUSING WOODEN DHOW FIRES IN SUBSIDIARY PORTS OF BUSHEHR PROVINCE

Hojjat Khosravi[1] and Ehsan Golestani[2]

1) MS in Maritime Transport, Ports and Maritime Administration of the Bushehr province; Email: hojjatkhosravi@gmail.com
2) MS in Maritime Transport, Kharg Ports and Maritime Administration; Email: egolestane@hotmail.com

1. Introduction

Despite repeated efforts on building safety vessels and using advanced equipment such as navigation equipment and safety equipment, marine accidents still occur, resulting in personal injury and property damages and pollution of the marine environment. Investigation of accidents in the maritime industry is not covered for those involved in this industry. Accurate, effective and timely investigation of accidents can lead to identifying the factors and causes of marine accidents.

Taking corrective measures after identifying these factors, through formulating or revising the rules and guidelines, improves safety and standards in the maritime industry. Hence, an effective and timely investigation of marine accidents could lead to the adoption of necessary measures in order to prevent or reduce similar disasters and to increase the safety of navigation, people's lives and property safety, and facility and the marine environment safety. Considering the number of non-conventional vessels in the country, investigating the causes of accidents in wooden dhows is of paramount importance. On the other hand, the surveys carried out reflects the fact that 68% of the accidents occurred over recent years under the flag of the Islamic Republic of Iran has been related to the non-conventional vessels, more than 50 percent of which is related to fire accidents. Due to the lack of promotion for technical quality and safety of these vessels in accordance with international standards and marine transportation, non-conventional vessels have become one of the concerns of the maritime transport industry.

2. wooden dhow Fire Accident Rates in Bushehr Province

Regarding the extent of wooden dhow fire accidents over recent years and in order to specify the causes of accidents and their appropriate solutions and obstacles faced in order to reduce similar disasters, the incidents happened during 2007-2015 are initially investigated. Statistics provided in the table below states the specifications of these disasters:

Table 1: Statistics of wooden dhow fire accidents in Bushehr province during 2007-2015

No	year	Port	Description	Causes
1	2007	Kangan	Fishing dhow fire accident leading to death	Problem in wiring systems
2	2009	Deylm	Two cargo wooden dhows fire incident	external factors
3	2010	Genaveh	five cargo wooden dhows fire incident	non-standard conditions of engine room
4	2010	Ameri	Twenty four cargo and fishing wooden dhows fire incident	Rubin pump
5	2010	Kangan	One cargo wooden dhows fire incident	Non-standard placement of generator
6	2012	Genaveh	One cargo wooden dhows fire incident	Deliberate factors
7	2013	Delvar	One cargo wooden dhows fire incident	problem in wiring systems
8	2014	Genaveh	Three cargo wooden dhows fire incident	Rubin pump
9	2015	Rostami	Five cargo wooden dhows fire incident	problem in wiring systems
10	2015	Dayyer	Nineteen cargo and fishing wooden dhows fire incident	Rubin pump
11	2015	Dubai	two cargo wooden dhows fire incident	Non-standard kitchen
12	2015	Kangan	One cargo wooden dhows fire incident	external factors

Figure 1. Wooden dhows fire incident in Dayyer(2015)

3. Results (Important factors in the occurrence of wooden dhow fire incidents)

Identify causes and human errors in the event of a disaster or marine incidents (potential incidents) to provide a proper strategy is essential. In this study, the factors affecting the wooden dhow fire incidents are generally divided into five categories:

1. Using Rubin petrol pumps

Robin petrol pumps are used for a variety of reasons in wooden dhows. The main reason of firing for this type of pumps is gasoline low ignition point which can be partially replaced by diesel pumps to lower the fire risk.

2. Improper wiring system

In investigations carried out, numerous cases were observed with regard to the weaknesses of the wiring system in wooden dhows, including the following:

- Lack of proper wiring with a wire having appropriate diameter and margin of safety based on the surface area table
- Putting extra wires as self for various reasons, including savings and lack of awareness
- Lack of standard systems for wiring in these vessels and damages to the wire carrying an electric current
- Overheating and fires due to three-phase electric machines because of over-amplification of these devices
- The existence of non-standard wooden terminals
- Using batteries as a power supply switch
- Lack of earthing system for electrical appliances
- Using electrical tape
- Failing to account for the nominal power of the power supply
- The presence of electric wires close to the leakage of oil

3. Unsafe Kitchen due to electrical leakage of kitchen utensils, gas leaks from oven cylinders, turning off the oven flame, lack of heat exchange in refrigerators

4. Lack of proper layout for Auxillary engines

5. Non observing safety-related cases for transferring diesel fuel

In this regard, there are also other factors not leading to fire; however, they exist as risk factors in these vessels.

- Using plastic tubes for feeding fuel to the engine
- Not equipping fume exhaust to thermal insulation
- Unavailability of fuel resources to the maximum level sensor alarms
- Lack of emergency fuel cut-off
- Lack of fire alarm sensor
- Smoking in areas prone to fires.

4. Recommendations

Strategies and obstacles to prevent the recurrence of similar incidents:

1. Fuel: Decreasing the refueling operation time until the exit of the vessels (reduced fuel saving time in wooden dhows)

2. Traffic: Traffic activities monitoring and control in the area outside the control of the port as well as organizing vessels' seating and parking in separate groups.

3. Prohibition of any repairs and warm work on the vessel in their parking lot

4. Guardians: Employing a watchman on the ship when mooring and a security system for dock

5. Risk: risk assessment of existing facilities to prepare emergency response plans

6. Training: Revising the quantity and quality of training provided to stakeholders related to maritime activities

7. Familiarity: increasing familiarity with maritime law and culture-making in the community of owners to improve their technical and managerial knowledge

8. Feasibility: In the field of safety equipment for vessels in ponds or estuary for placing multi-purpose fire-consumer vessels and designing and installation of Hydrant pipes by considering the initial cost and maintenance cost compared with other methods, as well as placing the leading fire-fighters to participate in contingency fire-fighting operations in estuaries and ponds.

It should be noted that this research has been completed with financial and moral support of PMO.

5. References

[1]. Zeraatgar, Hamid. (2010). Analysis of marine accidents in the country with an emphasis on Bandar Abbas region. Transportation Research Institute, Department of Transportation.

[2]. PMO, 2013. "Internet portal of Bushehr Ports and Maritime Administration, maritime accidents, introducing marine accident investigation committee. http://bushehrport.pmo.ir/fa/casualty/inc

[3]. IMO. Resolution A.849 (20): CODE FOR THE INVESTIGATION OF MARINE CASUALTIES AND INCIDENTS, International Maritime Organization, London. 1997.

[4]. IMO. CASUALTY ANALYSIS PROCEDURE (document FSI 17 / WP.1, annex 2), International Maritime Organization,

[5]. PMO, 2015. "Internet portal of Bushehr Ports and Maritime Administration, maritime accidents, statistical and analytical reports on marine disasters. http://bushehrport.pmo.ir/fa/casualty/reports

[6]. http://wire-cable-store.com

[7]. BSS ECPs Privately Owned & Managed boats, Public Edition 3, Rev. 0 - January 2013

[8]. Toubaei, P. (2010). Causes of marine accidents and human errors, Payame Darya Magazine, 169, page 74-79

[9]. Esmaeili, A., Izadpanah, T. and Madani Zadegan, M. (2007) Risk Assessment of repeated marine accidents, sea and port magazine, 12, page 120. 123

[10]. Moradi, A. (2006) Management of maritime accidents, marine accidents and the requirements of the Convention and addressing solutions to reduce accidents on waterways, PMO publication Center

[11]. Maher, M., Safari, h. and Sereshki, A. (2004). Challenges of enhancing traditional fishing boat security and strategic solutions, First national conference on ports' Safety, Tehran

EVALUATION AND ANALYSIS OF HUMAN ERRORS & VIOLATION IN ACCIDENTS OCCURRENCE OF BUSHEHR PROVINCE COASTAL WATERS

Hojjat Khosravi[1] and Ehsan Golestani[2]

1) MS in Maritime Transport, Ports and Maritime Administration of the Bushehr province; Email: hojjatkhosravi@gmail.com
2) MS in Maritime Transport, Kharg Ports and Maritime Administration; Email: egolestane@hotmail.com

1. Introduction

Analyses of casualties in marine and aviation transportation industries indicate that human error is a major contributor in accidents and incidents. Recent researches in this field broadly identify various types elements that contribute to human error. Accordingly particular managerial measures and steps have been taken to mitigate or control the severity of those errors. Human error has its roots in latent factors, which bring about increased risk and danger. Violations are important because they play a prominent role in shaping mishaps. In this paper based on a qualitative research and utilizing related casualty investigation models and techniques, latent and contributory factors, which associated with human error, will be identified and required corrective action will be suggested.

2. Materials and Methods

This study aimed to investigate the influence of human factors in the occurrence of marine accidents using qualitative methods and through reviewing the literature, evaluating related rules and correspondences, and conducting interviews with people involved in accidents as well as accidents investigators and port officials. In order to reach a more profound understanding and due to the thematic structure of the research, we attempted to carry out a case study and conduct a field survey of recent marine accidents occurred in Iran. This article aims to provide effective solutions to limit and reduce human errors by case studying the major marine incidents occurred in coastal and offshore waters of Bushehr Province in recent years and examining human errors through using the most reliable human error theories and assessment models. In this study, the indicators provided by Rasmussen and Reason have been used. Rasmussen, by taking into account human behavior and performance level, ranks errors within three stages of performance based on individual skill, existing and defined procedures, and self-knowledge. On the other hand, Reason classifies human errors into four categories, including slip, lapse, mistake, and violation. In this way, in addition to being classified according to their type, errors are ranked based on individual performance, adapted from Rasmussen's method.

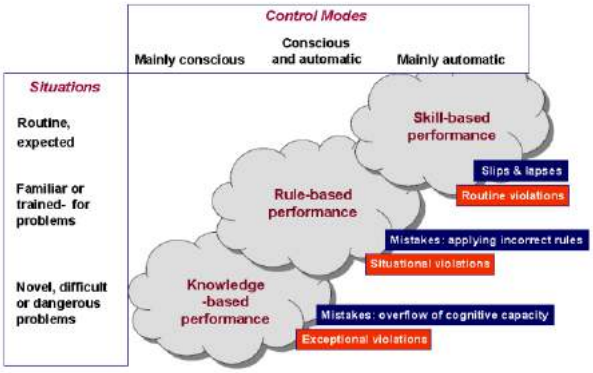

Figure 1: Performance level and main error and violation types (adapted from Rasmussen and Reason)

3. Analysis of the Occurred Accidents

In this article, within the framework of qualitative research, and based on statistics and reports available in the marine accident investigation department of General Directorate of Ports and Maritime Authorities in Bushehr Province, 29 serious or very serious accident occurred during four years, from 2011 until the end of 2015, that led to lose of life, total loss of vessels, or serious structural damages, were profoundly investigated. It should be noted that 95% of the vessels under study in this research are of non-conventional type. Non-conventional vessels refer to ships with a gross tonnage less than 500 tons. The percentage of errors and violations identified as the outcome of these accidents according to the investigations is presented in Figure2.

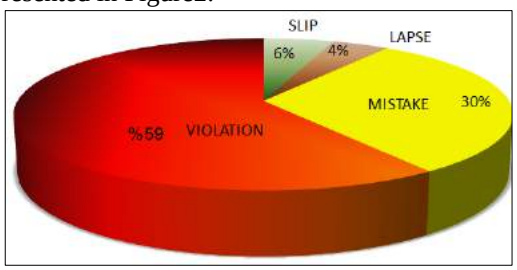

Figure 2: human errors and violations in the accidents occurred during four years from 2011 to the end of 2015

In this figure, the highest percentage of factors leading to the occurrence of accidents is allocated to human violations. By investigating all the factors in this research and case studying each of the accidents, it can be observed that more than three-quarters of these violations are among routine violations occurring on a daily basis. This major value of routine violations actually represents an unusual practice among individuals and groups associated with the marine industry. In fact, this type of violations has cultural roots and its routine nature indicates people's lack of concern for the consequences arising from committing this type of violations, which should be regarded as a serious concern. The remaining part, approximately equal to a quarter, is also dedicated to necessary violations. With a view to stemming violations based on Reason and Rasmussen' model, 32% of the necessary violations is stemmed from people's lack of adequate understanding of the necessity of enforcing the laws and the consequences of failure to comply with them. This type of violations has to some extent cultural roots, and shows the latent factor of individuals' lack of knowledge of the risks and their consequences. On the other hand, non-functional regulations and guidelines have been recognized as the latent cause of about 29% of this type of violations to occur. Moreover, lack of essential and sufficient equipment, tools and machinery along with some other factors such as inappropriate workplace environment account for 27% of this type of violations, and the remaining 12% is due to lack of monitoring the standard and safety of vessels in terms of structure, equipment and operation, which has caused people to easily overlook regulations, and thereby optimize their cost.

Another important point shown in Figure 1 is the error of mistake which is equal to 30 percent. This type of error includes 43% errors in the level of performance based on the procedure, which itself is originated from individuals' lack of knowledge and skills on how to properly apply the developed guidelines and procedures. The remaining 57% of errors in the level of performance is based on individuals' level of knowledge which highlights complex situations where no transparent and practical administrative instructions, plans, and procedures exist, leading people to make decisions based on their insufficient knowledge and skills. Figure 2 shows key latent factors involved in the occurrence of this type of error in more detail.

With regard to the errors of slip and lapse, despite its small role in accidents, its value proves some special points to us. The highest value is assigned to the quality of machinery and equipment design and layout. This reveals a remarkable point as a common root in this type of errors as well as in violations and sometimes in error of mistake. As mentioned, 90% of the surveyed vessels are non-conventional and some are traditionally constructed which suffer from the lack of applying the transparent laws, regulations and instructions. Consequently, the quality of training of the crew in these types of vessels, design of machinery, equipment and work space are all affected. Another concern is related to the lack of quick instructions and guidelines such as auxiliary images and posters. By the monitoring issue as the third root leading to the occurrence of this error, it means the supervision of an individual while performing critical tasks by an authority, and differs from the monitoring issue on violations.

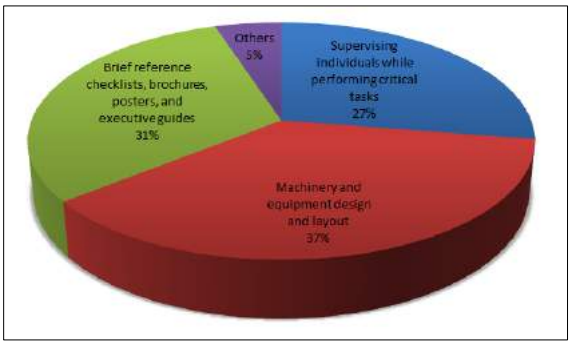

Figure 3: The roots of lapse and slip errors and in the marine accidents during four years from 2011 to the end of 2015

Now, in pursuance of the use of Reason's model, and by using the SCAT model and taking into account the common roots in the committed errors and violations, the scope of measures required to be applied along with their priority is determined.

Figure 3 shows in detail the priorities of necessary measures to address the root causes of errors and violations in order to prevent similar accidents to occur with respect to knowledge, regulations and guidelines, monitoring standards, and safety of the vessels in terms of structure and operation.

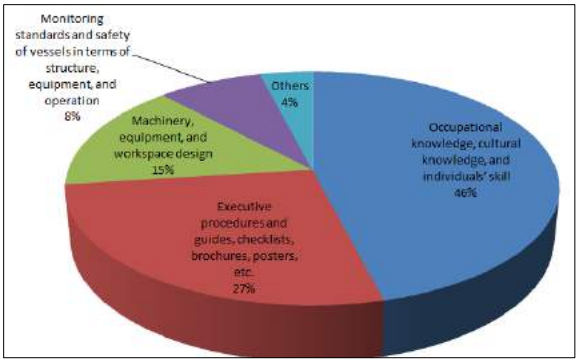

Figure 4: The scope of corrective measures required

It should be noted that this research has been completed with financial and moral support of PMO.

4.References

[1] ILCI., Systematic Cause Analysis Technique, International Loss Control Institute, Virginia. 1990.

[2] http://www.hse.gov.uk/humanfactors/topics/types.pdf

[3] http://www.maiif.org/images/Korea (Hong-Tae Kim).pdf

[4] Reason, J., Human Error, Cambridge University Press, New York. 1990.

[5] Reason, J., Managing the Risk of Organisational Accidents. Ashgate, Aldershot. 1997.

[6] Rason, J., "Human Error: Models and management", British Medical Journal, 320, 7237, pp. 768, 2000.

[7]http://www.hse.gov.uk/construction/lwit/assets/downloads/human-failure.pdf

STUDY OF CONTAINER LOSSES IN THE CONTAINER SUPPLY CHAIN PROCESS

[1]Fatemeh Bagheri

1) MSc of Maritime transportation engineering (Bushehr Ports and Maritime Authority), bagheri.fa56@gmail.com

1. Introduction

Container terminals are the accident - prone environment that in case of neglecting them, serious damage to lives, port equipment, goods and container will be expected. UK P & I Club, announced that 20% of the cost of insurance losses to the container caused by physical damage, 14% related to temperature,10% due to falling container at sea, 9% stolen and 8% goods deficit. The mentioned Club believes that the biggest cause of the damage to the container is the improper stuffing of the goods in the container.

2. The Need To Install Safety Systems On Container Loading And Unloading Equipment:

A joint study conducted by TT Club, ICHCA and PEMA shows that 34% of the global asset claims are quay crane related, 37%are due to operational issues, 10% allocated to maintenance issues and remained 19% for weather issues.

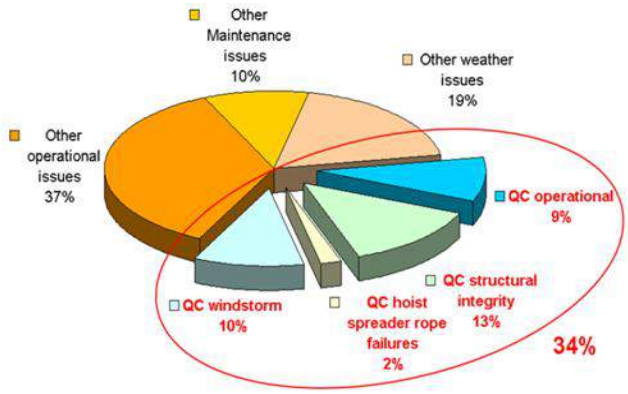

Fig.1: Global cost analysis of asset – related claims in ports and terminals (TT Club, 2011)

Above study analyses that regarding operational issues, Boom-to-ship collisions are the single largest cost of claims in this area, followed by other collisions and claims caused by issues with spreaders, ship cell guides and ropes.

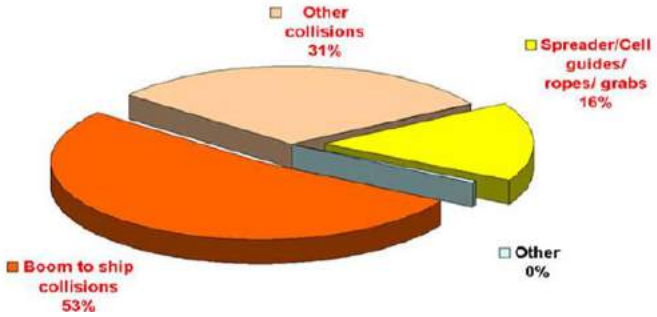

Fig2: Global cost analysis of operational – related quay crane claims in ports and terminals (TT Club, 2011)

TT Club has concluded that use of safety features in the yard and quay equipment's have a substantial role in minimizing accidents in the port especially in container yards. Some safety standards recommended by the TT Club are mentioned in Table 1.

Table1: Safety features in yard and quay cranes (TT Club, 2011)

Boom anti collision	Wind speed detection and alarm to enable driver to stop the operation, park, and shut down the crane safely	Means to engage the crane horizontally on rail
Gantry travel anti collision	Means to engage the crane vertically to prevent wheels being detached from rail	Gantry braking
Crane to crane anti collision	Automatic container weight and eccentricity measurement	Hoist snag load protection
Operator cabin air conditioning	Anti-colliding in auto traveling	Temperature and smoke detection in the electrical and machine room

3. Pressures On Container In Various Mode Of Transportation

3.1. Maritime Transport And The Acceleration Of Gravity On The Container:

Ship's rotational movements around the longitudinal axis (Rolling), transverse axis (Pitching), the vertical axis (yawing) and it's linear movements along the longitudinal axis (Surging), along the transverse axis (Swaying) and along the vertical axis (Heaving) in adverse sea weather condition, cause the gravity acceleration to the container.

As it can be seen in Figure 3, the most pressure caused by ship's six motions at sea on the containers are related to the containers loaded forward of the ship which is variable from 1 to 2 g.

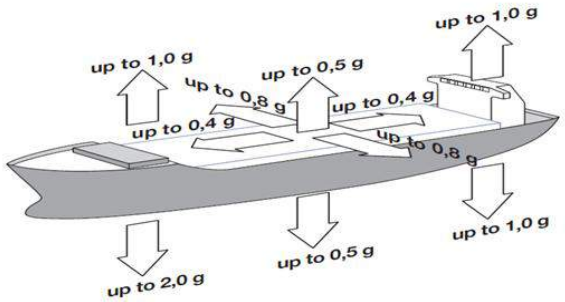

Fig.3: Potential acceleration due to sea transport (Container Packing, Hapag-Lloyd,2005)

Washing over the long wave due to bad weather on the bow, total loss, grounding and collision of the ship, are among the important factors that cause damage to the container.

3.2. Rail Transport And The Acceleration Of Gravity On The Container

When a container is transported by rail, the expected accelerations are as follows:

- acceleration and de acceleration
- coupling operation and Humping
- inclining to both sides at bends of the rail
- shock and vibration
- train out of line

The acceleration of gravity on the train carrying containers, are investigated by safety packaging of container supply chain (GDFPC / 2011), based on Figure 4. The study found that the greatest force of gravity to the container, is due to forward and back movement of train in switching/shunting operations that is calculated as 4g.

Fig.4: Potential acceleration due to rail transport (Container Packing, Hapag-Lloyd,2005)

3.3. Road Transport And The Acceleration Of Gravity On The Container

When a container is transported by road, the expected accelerations are as follows:

- Braking and acceleration (speed reduction and augmentation)
- Accident and collapse
- Shock and vibration
- Condition of roads (flatness, bump, pits, etc.)

This study shows that most of the acceleration of gravity on the container transported by trucks is related to holes and bumps in the road.

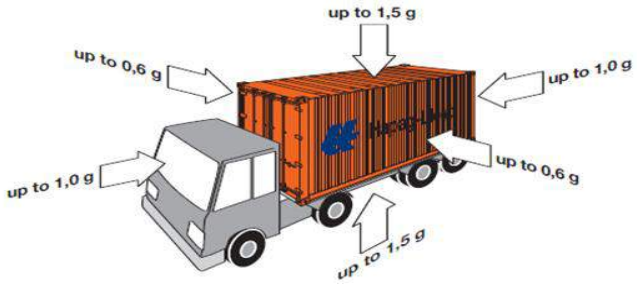

Fig.5: Potential acceleration due to rail transport (Container Packing, Hapag-Lloyd,2005)

4. Conclusion And Suggestions:

This article studies the various modes of transport including; rail, road and sea. It also studies the pressure on the container while handling in different modes of transportation. Pressure on the container during the ship's movement (Rolling, Pitching, Yawing, Heaving, Surging and Swaying) at sea and the pressure on the container at the time of shipment by truck and train cause major damage to container in maritime, rail and road transport. According to the above, the following suggestions are offered:

- Staff training in understanding the container supply chain and container structure, the forces acting on the container in different modes of transportation, packaging, Stuffing and lashing the goods in the container.
- Obligation of weighing the container in terminals to prevent additional weight loading in the container.
- Installation of safety systems (Minimum safety features) on the container loading and unloading equipment.
- Perform risk analysis of the container terminals in order to reduce incidents and control the risk in the container terminals.

5. References:

1- Convention on the Safe Container(CSC1972)

2- Container Packing, Hapag-Lloyd, group communication, (2010)

3- Container handbook, cargo loss prevention information from German marine insurers, (2015)

4- Recommended minimum safety specification for quay container cranes, (2011)

5- Recommended minimum safety features for container yard equipment, (2011)

IRANIAN ELECTRONIC NAVIGATIONAL CHARTS TOWARD SAFE NAVIGATION AND THE PROSPECTS AHEAD

A. Soltanpour[1], A. Mojtahedi[2] , S. Parizi[3] and Chalan[4]

1) National Cartographic Center, Tehran, Iran, asoltanpour@yahoo.com
2) National Cartographic Center, Tehran, Iran, mojtahedi@ncc.org.ir
3) Port and Maritime Organization, Tehran, Iran, sparizi@pmo.ir
4) National Hydrography Committee, Tehran, Iran

1. Introduction

More than 71 percent of Earth's surface is covered by water which has the most important role in human life. The importance of the seas in various fields such as nutrition, trade, industry and climate change is undeniable. Human beings throughout history have always been interested to learn from the surrounding water bodies. Sea mapping or hydrography is the first step to determine the sea and helps us to better understand it.

2. Hydrography & Nautical Chart Production

Hydrography is the branch of applied sciences which deals with the measurement and description of the physical features of oceans, seas, coastal areas, lakes and rivers, as well as with the prediction of their change over time, for the primary purpose of safety of navigation and in support of all other marine activities, including economic development, security and defence, scientific research, and environmental protection. Hydrography also underpins almost every other activity associated with the sea, including resource exploitation, maritime boundary delimitation, national marine spatial data infrastructures, recreational boating, tsunami flood and inundation modelling, coastal zone management, tourism and marine science. [2]

The advent of deep draught ships, growing importance of seabed resources, the need to protect the marine environment and increasing maritime trades, have emphasized the need for adequate hydrographic survey coverage and the production of nautical charts and publications as required by SOLAS Chapter V.

One of the main purposes of Hydrography is to produce nautical charts. Nautical chart is to provide navigational related information to assist mariners while navigating and trying to avoid dangers, and to standardize information interchange. They provide the pilot or navigator with a high level of accuracy, as charted, of navigable bodies of water by portraying depths, aids to navigation, obstructions, shorelines, physical features and other useful and essential information. However, the accuracy of a nautical chart depends on the competency of the survey upon which it is based.

3. International Obligations

In July 2002, the revised Chapter V of the IMO Safety of Life at Sea (SOLAS) Convention entered into force. Under the new Regulation 9, the Contracting Governments of SOLAS are now required to provide and maintain Hydrographic Services and products. [2]

Major developments in recent decades in the field of Electronic Equipments led marine charts from paper to digital and electronic to be converted. Many of ships have already been equipped with the necessary equipments in order to use electronic nautical charts (ENC) and based on the existing requirements, remaining vessels should be equipped to be able to use ENCs onboard in few coming years.

4. Nautical Chart Production in Iran

National Cartographic Center (NCC) of Iran has been responsible for hydrographic survey and sea level monitoring over the past three decades. In this regard, a national network of tidal survey has been created which has a history of more than twenty years. Besides, over 200 nautical charts from south and north coast of the country at different scales were produced [1]. The maps are already the basis of many coastal environmental and industrial studies.

Survey coverage (chart index) of the scale 1:100000 for north and south coast is shown in figures 1 and 2 respectively. Survey coverage in the scale of 1:25000 are depicted in figures 3 and 4. Figure 4 shows that there are many un-surveyed areas along Bushehr and Khoozestan coasts together with Makran zone along Oman sea coastlines.

In 2015, Iranian National Hydrographic Committee in cooperation with Iranian Ports and Maritime Organization (PMO) and NCC decided to release nautical charts in order to increase the level of safety of navigation. So far, 30 ENCs from Persian Gulf have been internationally published [4]. Published ENCs have to be updated regularly due to the changes. Channels are dredged; new aids to navigation are established or deleted; new wrecks and obstructions are discovered; natural shoaling occurs in many areas; and new berthing facilities are built along the

shoreline. In order for the mariner to transit safely, it is imperative that these changes be reflected on nautical charts as soon as practicable.

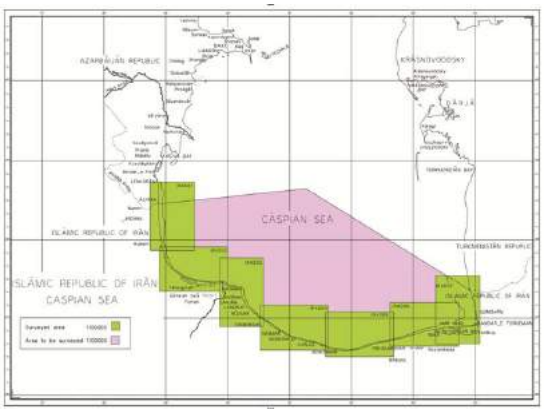

Figure 1. survey coverage for Caspian sea in the scale of 1:100000

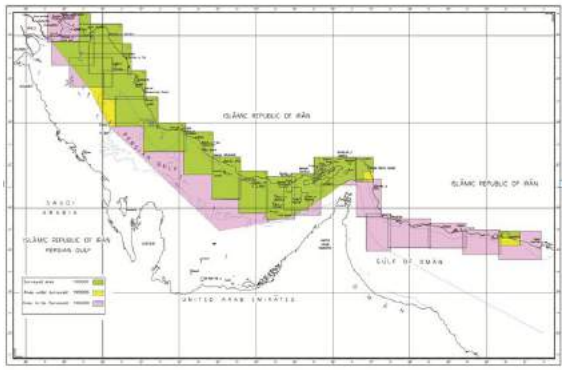

Figure 2. survey coverage for Persian Gulf and Oman sea in the scale of 1:100000

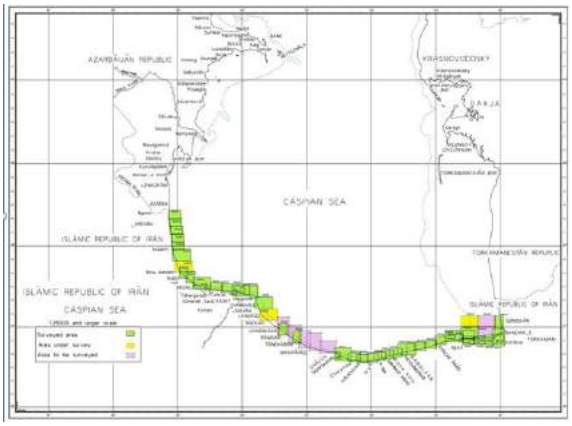

Figure 3. survey coverage for Caspian sea in the scale of 1:25000

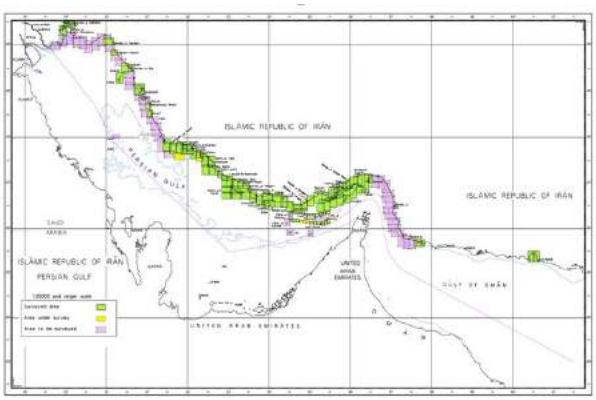

Figure 4. survey coverage for Persian Gulf and Oman sea in the scale of 1:25000

Besides, the charts which were adequate a decade ago, may have to be recompiled using new survey data, collected to a higher degree of accuracy and providing improved coverage. The advent of accurate satellite navigation, makes poorly positioned historical data an even greater problem for navigators. Under the new IHO standards, the data must have full coverage in the future while current data are lacking this feature. This means that all water bodies must be re-surveyed again with full coverage using Multibeam Echosounders. The possibility of installing and using a laser scanner on the NCC's aircraft, according to its higher speed for shallow areas, should be evaluated and considered. The absence of large-scale berthing charts of the major ports (Port ENC) is one of the defects that should be corrected using precise hydrography equipments. With respect to the development of Makran region, the use of large vessels and deep water hydrographic equipment is essential. [3]

5. References

[1] Mojtahedi, A., Current status of nautical chart production, National Cartographic Center, Tehran, Iran, 2016.

[2] International Hydrography Organization (IHO) standards and publications, www.iho.int

[3] Soltanpour, A., Chart production from Iran's water bodies, National Report, National Cartographic Center, Tehran, Iran, 2015.

[4] Soltanpour, A., Iran's position in nautical chart production and dissemination, Geomatics 95 conference, National Cartographic Center, Tehran, Iran, 2016.

THE DESIGN AND IMPLEMENTATION OF BUOY MONITORING SYSTEM: MARITIME SAFETY MANAGEMENT (CASE STUDY IN PERSIAN GULF)

Ali Ahmadi[1], Mohammad Zareifard[2], Vahidreza Zareifard[3]

1) RAAD Bushehr Engineering Co., Bushehr, Iran, a.ahmadi@raadbeco.com
2) Port and maritime organization, BPMO of Bushehr, Bushehr, Iran, zarie.mohammad@bpmo.ir
3) Port and maritime organization, BPMO of Bushehr, Bushehr, Iran, zarie.vahid@bpmo.ir

1. Introduction

Maritime crisis management includes assessment of risk, determination of the way to achieve the lowest possible (or acceptable) level of risk, the establishment of systems and procedures to maintain the system at an acceptable level, the preparation (contingency planning) required to deal with events which could take place, and the management of response organizations and actions resulting from this preparation when an incident occurs. Each of these elements has an economic cost and a key element in maritime crisis management is the rational allocation of these costs. The objective of this paper is to present a method for Forecasting and warning marine hazards and helping the response organizations for best Crisis Management of Marine Hazards. A buoy can have many purposes. It can be anchored (stationary) or allowed to drift with the sea wave, also it aids pilotage by marking a maritime channel, hazard and administrative area to allow boats and ships to navigate safely. Buoys maintenance by typical ways is very costly process and increase maritime hazards and vulnerabilities.

In order to reach reliable solutions, selecting the most appropriate method is important. This solution is Buoy monitoring system based on AIS network.

Automatic Identification System (AIS) is an autonomous broadcast system, operating in the VHF maritime mobile band. It exchanges information such as vessel identification, position, course, speed, etc. between mobile and fixed stations. It handles multiple reports, using Time Division Multiple Access (TDMA) technology ensuring reliable and robust operation [1].

An AIS AtoN network is a AIS network designed for monitoring a marine Aids to Navigation such as buoys, light houses and other maritime infrastructure. It is a highly effective and cost efficient method to enhance maritime domain awareness for mariners and authorities.

New vision of this service is a AIS network consisting of a number of (AtoN) devices connected in a mesh topology. In a regular mesh topology, each node in the network is connected with neighbors along one or more dimensions. If the network is one-dimensional, and the chain of nodes is connected to form a circular loop, the resulting topology is known as a ring (Figure 1, Figure 2).

Figure 1 AIS network

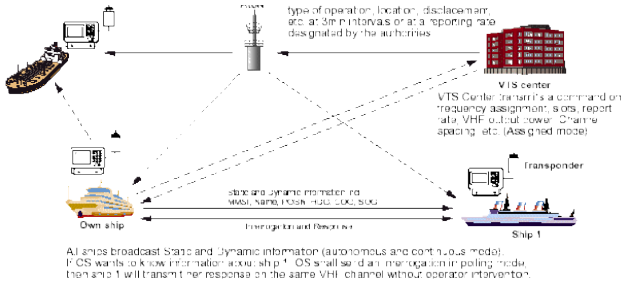

Figure 2 AIS mesh network

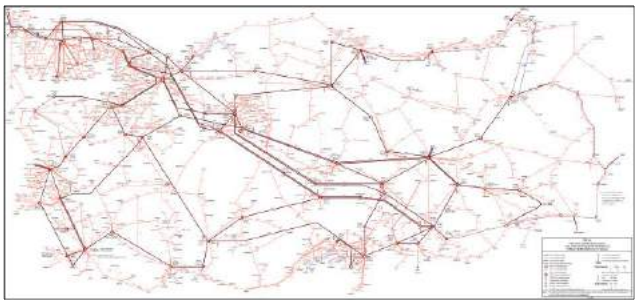

2. Bushehr AIS network:

2.1. System topology

This solution consisting of a number of AIS Base stations and AtoN sensors.

2.1.1. AIS Base stations:

a) Main processing unit: processor unit which make data gathering and analyze data.
b) Local stations: which contains receivers and monitoring software.

2.1.2. AIS AtoN:

AtoN is a special AIS transceiver designed specifically for installation on marine Aids to Navigation such as buoys, light houses and other maritime infrastructure.

- An AIS AtoN can be fitted to any remote maritime structure and operate for years on solar power without maintenance.
- AIS AtoN transmits on standard AIS frequencies and will be received and understood by shore networks and vessel transceivers.
- An AIS AtoN transmits the identity and accurate real time position of an Aid to Navigation.
- AIS AtoN enables the remote monitoring and control of existing equipment by authorities such as lanterns and racon's.
- Meteorological and other sensors can be connected to an AtoN and the information generated transmitted to mariners and authorities.

2.2. Bushehr PMO AIS network

Figure 3 system topology

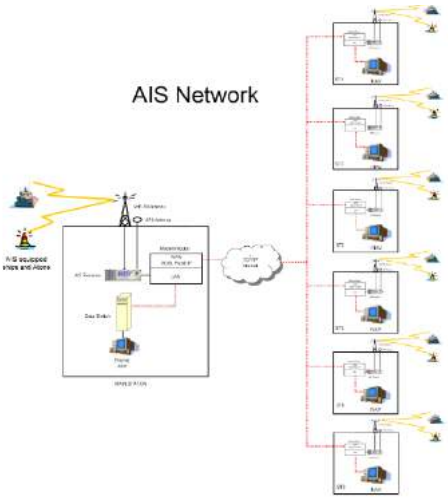

2.2.1. Monitoring Base stations

Following of BPMO[1] AIS network design, there is 6 local base stations and 1 set control center which receive and analyze Aids to Navigation Reports such as message 21 and message 6 etc. (see Table 1)

Table 1. Bushehr AIS monitoring Base stations.

NO	Base Station	Position	
1	Bushehr control	28.989345	50.835937
2	Bushehr	28.989345	50.835937
3	Genaveh	29.585127	50.503408
4	Deylam	30.057699	50.152179
5	Kharg island	29.266025	50.323979
6	Dayyer	27.830876	51.928283
7	Asaloyeh	27.479167	52.608221

2.2.2. AIS AtoN

The AIS AtoN is typically installed on buoys and other navigation aids and integrated with existing systems and sensors at that location. It is designed to act as a hub for the data produced by all the other systems on location such as the lantern, weather sensors, tide, temperature etc. The AtoN transmits the data back to the central control room via the normal AIS system. This information allows the position of the buoy and the operational status of the lamp to be monitored in all conditions, along with a constant live stream of sensor data. The 45 piece of buoys integrated with this AtoN on entire Persian Gulf which transmitting AIS message 21 and Message 6(Figure 4).

Figure 4 AIS message 6, message 21

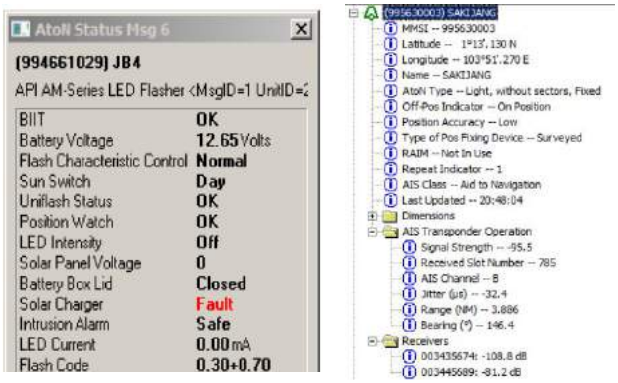

3. RESULTS AND DISCUSSION

Regarding to the new vision of crisis management, and its importance to reduce organizations 'cost and losses, utilizing an AIS monitoring system is required for any fields of activity especially marine industry.

The suggested AIS network is the most appropriate method in hazards management and prediction regarding to its high flexibility. There are a wide range of features and functions offered by an AtoN all of which are designed to significantly enhance port and waterway safety and security. The AtoN is a powerful addition to any existing AIS system, providing a critical piece of the marine domain jigsaw.

- Improved maritime domain awareness.
- Accurate real time monitoring of buoy positions in all weathers.
- Dynamic marking of shipping lanes.
- Instant marking of new hazards with virtual AtoN projection feature.
- Automatic alerts in the event of buoy or lantern malfunction.

References

[1] International Association of Marine Aids to Navigation and Lighthouse Authorities (IALA), *"Recommendation A-126 – the use of the Automatic Identification Systems (AIS) in Marine Aids to Navigation Services June 2004 – Revised June 2011"* ,10, rue des Gaudines 78100 Saint Germain en Laye, France, Edition 1.5, June 2011.

INCREASING EFFICIENCY AND SAFETY OF BUSHEHR PORT SHIPPING BY DYNAMIC UNDER KEEL CLEARANCE

Asghar Bohluly[1], Masoud Montazeri Namin[2], Mohammad Elmi[3]

1) Institute of Geophysics, University of Tehran, Tehran, Iran, bohluly@ut.ac.ir
2) School of Civil Engineering, University of Tehran, Tehran, Iran, mnamin@ut.ac.ir
3) School of Civil Engineering, University of Tehran, Tehran, Iran, m.elmi@ut.ac.ir

1. Introduction

Development of ports and maritime transport is the main need of economical and industrial development of coastal countries. Now, after round of sanctions, significant potential of maritime trades has been created in Iran.

Although first solution for development of maritime transport is hardware development of coastal structures, but implementation of software methods on existing tools, including ports and their facilities, plays an effective role in enhancing the transportation capacity.

World experience shows that using software methods and computational tools, as Decision Support Systems in port management, would increase the efficiency and safety of navigation in ports. Based on these experiences, it is expected that by using DSS tools, greater economic benefits can be obtained from existing installation ports in Iranian harbors.

The port of Bushehr is one the most important Iranian shipping centers in Persian Gulf with more than 4000 years history. Loading and unloading capacity of this port has been doubled during last 5 years, under the more attention and special support of PMO. However world's experiences could help to improve performance and safety of transport in this port.

In this paper, implementation of online assessment of physical oceanography parameters for prediction of dynamic under keel clearance with more certainty, will be evaluated in Bushehr port.

2. Background

Traditionally, the lowest under keel clearance (UKC) prediction is one the most important factors, needed to ship's safe passage. So, the most of transits have been carried in the confined waters of harbors, where a minimum clearance can be defined and controlled. Ports with UKC system use some fixed rules to govern the minimum UKC, and consequently, to permit safe transit along port approach channels. To ensure safety, these rules are determined by requirements in extreme swells and negative tidal residuals. It is essential that, UKC requirements include not only vessel squat and the effect of wind and atmospheric pressure changes on predicted tides, but also the dynamic motions of vessels of varying size and stability characteristics. If the requirements are too conservative, ships will carry less cargo than they should, and the operation is not as economic as it might be. At the other extreme, inadequate criteria could jeopardize safety [1].

For the optimization of UKC, in 1992 DUKC system were developed by O'Brien and installed first time at Hay Point in Australia. DUKC is a near real-time UKC prediction for use at ports, which has draft limitations on import or export ships. The DUKC system takes into account all of the major factors affecting UKC, including tidal residuals, squat, heel and wave induced dynamic motions [2]. After more than 20 years, DUKC systems have been installed in more than 20 ports around the world, with approximately 150000 safe ship movements. These improvements in port operation, lead to millions of dollars in economic benefits, which include the reduction of freight costs, increasing cargo throughput and gaining equivalent improvements by dredging [1].

Bralow et all. have been investigated effects of DUKC installation in Port Tranaki in new Zealand[3]. This research shows that by using the DUKC system, operating windows are nearly always increased (Fig 1.) and maximum transit drafts are nearly always increased up to 2.0 meters.

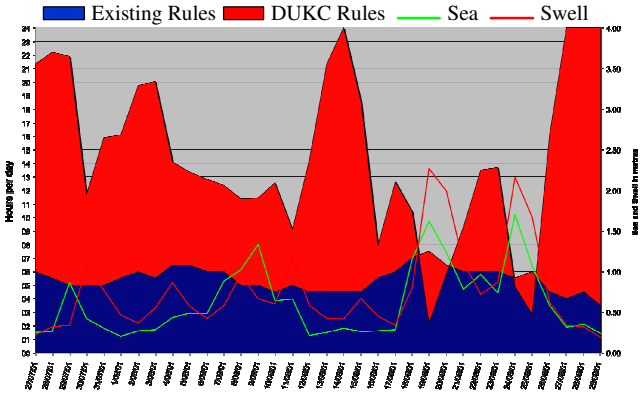

Figure 1. Operating window after using DUKC (Red) and under existing traditional rules.

3. Bushehr Port

The Bushehr port is located in 29° N and 50°50' E on the coast of the Persian Gulf. The depth of water is near to 10m in the external anchorage, connected to Persian Gulf by the external access channel 9200m in length (Fig. 2). Currently this port accept ships with Max draft of 10.5 m.

Figure 2. Bushehr Port and path of external access channel.

In Bushehr, the Max tidal range is 1.98 m, and this characteristic is the main tool of exciting system, for estimating the under keel clearance in the port. For an initial evaluation of sea state in Bushehr port, the analyzed data of bouy in deep water, are shown in Fig. 3. The cumulative distribution of waves is presented in this figure. According to what it shows, 50% of the time waves have less than 0.5 m height, but in other times the waves are tangible and effective on draft estimation. Fig. 4 shows that larger waves with 3m height, usually come from the North-West. This percentage of sea state is a powerful evidence to privilege dynamic assessment of physical oceanography for under keel clearance in Bushehr port.

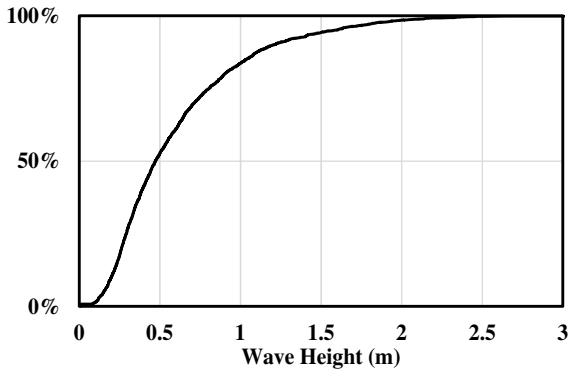

Figure 3. Cumulative distribution of wave height in Bushehr.

For the following reasons producing a Decision Support System based on online prediction of sea state (DUKC), relying on existing capabilities and potentials, is both essential and practical;

1- Necessity of software upgrade in Iranian ports spatially in Bushehr,

2- Successful experiences on developing of national computational hydrodynamic software with marine application (PMODynamics),

3- Existence of potent capabilities and potentials.

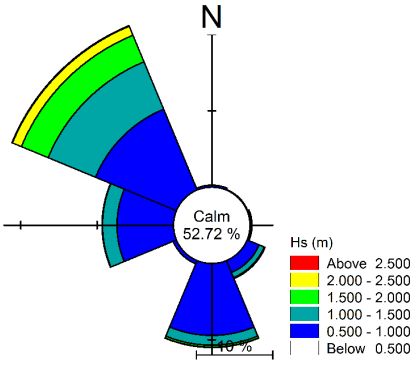

Figure 3. Wave Rose in Bushehr from bouy.

4. Methodology

The main aspects of this work include the following:

1- Online wind and wave forecasting during next 72 hrs, in deep water of Bushehr port using direct modeling and/or soft computing skills,
2- Offline modeling of wave and current pattern, including wind induced and tidal currents in harbor. The results of this modeling are usable for online computation of wave and current condition on navigation path of ships,
3- Estimation of wind setup,
4- Concentrated monitoring of hydrography during the period of 3 months,
5- Updating the models based on new hydrography,
6- Development of a model for ship draft estimation, based on sea states and vessel squat,
7- Estimation of chart window (operating window) based on tidal residuals and sea states,
8- Forecast effect of departure time and transit speed,
9- Development of a graphical user interface.
10- Using PMODynamics components in the system.

5. References

[1] O'Brien, Terry. *Experience using dynamic underkeel clearance systems: selected case studies and recent developments*. 30th PIANC-AIPCN Congress 2002. Institution of Engineers, 2002

[2] O'Brien, Terry. *Experience Using Underkeel Clearance Prediction Systems at Australian Ports: Selected Case Studies and Recent Developments*. IHMA Conf., Dubai, UAE. 2000.

[3] Barlow, R., Terry O'Brien, and P. Atkinson. *Experience using a Dynamic Under Keel Clearance System at Port Taranaki, New Zealand*. 3rd Congress of The International Harbour Masters' Association. 2002.

[4] Rutkowski, Grzegorz, and Andrzej Królikowski. *Simplified Method for Estimating Maximum Ship's Draught when Navigating in Shallow Water on the South of Stolpe Bank in the Aspect of the Vessels with Maximum Dimensions and Draught*. TransNav: International Journal on Marine Navigation and Safety of Sea Transportation 4.4 (2010): 405-414.

ASSESSMENT OF PORT STATE CONTROL PERFORMANCE IN VIEW OF NOVEL INDICATORS
THE CASE STUDY OF BIK PORT

Pouria Koulivand[1], Reza Ranjbar[2]

1) Port and Maritime Organization, Bandar Imam Khomeini, IRAN, Pkoulivand@bik.ir
2) Port and Maritime Organization, Bandar Imam Khomeini, IRAN, am_ranjbar@bik.ir

1. Introduction

The United Nations Convention of the Law of the Sea (UNCLOS) provides every nation with rights and obligations with regard to ship registration and freedom of passage both over the high seas and through coastal waters of any other nation [1].

An Administration offering ship registration is referred to as the بflag Stateپ Flag States maintain the responsibilities and obligations imposed upon them by International Conventions for ships flying their flag.

In a perfect world, acting of flag states, would ensure ships and shipping activities are fully compliant with all applicable requirements throughout the shipی life. But, in fact this is not true and there must be another mechanism.

International Conventions and UNCLOS both give powers to States to which ships travel (known as port States) to exercise some degree of بcontrolپover ships in their waters (known as بPort State Controlپ(PSC)) for ensuring that they do not pose an unreasonable threat to the safety of the ship, its crew or the marine environment. PSC has assumed prominence within the shipping industry, driven by frequent failures of other responsible parties to fulfill their obligations [2].

2. Port State Control in Iran and BIK Port

Generally, Port State Control responsibilities in I.R. Iran's Port and Maritime Organization (PMO) is handling by about 100 people and specifically 10 PSC officers (PSCO) in BIK port. PSCOs may board a ship at any time to inspect and detain unseaworthy or substandard ships.

3. Port State Control Performance

The performance of inspection of PSCO is depend on various aspects of shipping industries, such as shipی managements, ship owner, crew and performance of flag states.

It is possible to evaluate the performance of PSC statistically. Present article intends to show the performance of BIK port state control via some KPIs such as بaverage age of called vessel during a yearپ and بdeficiency rate per detention rateپ

During a period of 4 years from 2012 till 2015 there were 3393 vessels called at BIK port. The average age of these ships shown in table 1 and figure 1 [3].

Table 1. 4 years period average age

Year	Total No. of ship	Average Age	Condition
2012	1039	12.2	Base year
2013	859	12.63	Increasing
2014	759	13.16	Increasing
2015	736	15.38	Increasing

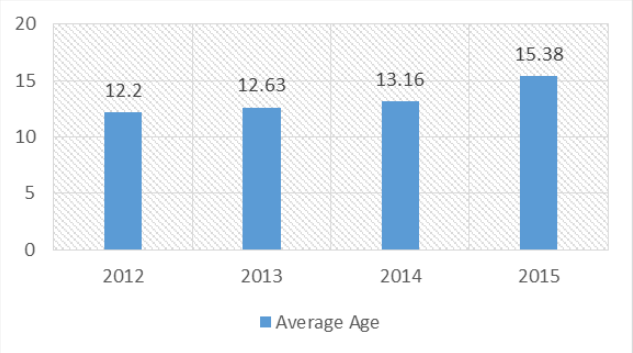

Figure 1. Average Age

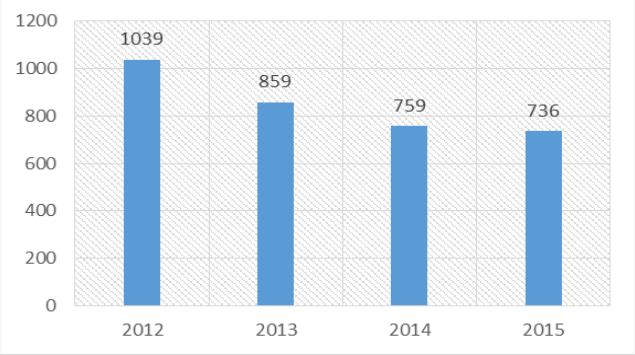

Figure 2. Total No of ship

As shown in table 1 and figures 1 and 2, despite the decreasing total No of called vessels; the average age of called vessels increase during 4 years. This is a negative result in view of PSC's performance. Although investigation of root causes is beyond of the present article,

but sanction of shipping industry is a clear reason for this result.

When sanction raised, new vessel that belongs to developed countries refused to call Iranپ ports, so the total No of vessels decreased and there was a good chance for old vessel activities.

Table 2 shows the results of ship inspection in 4 years period.

Table 2. Four years periods statistics of BIK inspections

Y	Inspected Ship	Total Deficiency	Detained Ship	Detentions %	Deficiencies per detentions
2012	400	1516	40	10	37.9
2013	324	1097	35	10.8	31.34
2014	398	1299	28	7.03	46.39
2015	403	1251	36	8.93	34.75

Table 3. Three years periods statistics of AMSA inspections

Y	Inspected Ship	Total Deficiency	Detained Ship	Detentions %	Deficiencies per detentions
2012	3179	7775	210	6.61	37.02
2013	3342	8183	233	6.97	35.12
2014	3742	10,892	269	7.19	40.49

As shown in table 2 total No of deficiency has a direct relation with No of inspected ships.

Another aspect of PSCپ performance is computation of پdeficiency per detentionپ (DpD) that shows the performance and quality of inspections during that year. If this indicator increases it shows that inspector's focus had been on minor deficiencies; and therefore, a failure in recognizing substandard ship. On the other hand, decreasing of the indicator shows high accuracy of inspection and also more conformity with PSC پGood Practice Procedureپduring that year.

Focus of inspector on major deficiencies leads to finding the causes of unseaworthiness of ships. For example, although in 2014 in comparison with 2015 the total number of deficiencies is greater but the percentage of detention is low; Also DpD indicator shows this result. So finding the major deficiencies is not achieved in this case.

It should be noted that this indicator has been used for the first time in BIK port and also in the world.

3. Comparison with AMSA[1]

AMSA is a leading country in field of PSC inspection, therefore, comparison of BIK port's inspection with this authority is helpful. Table 3 shows statistics of inspection in this country for a period of 3 years (2012-2014) [4].

As indicated in table 2 and 3, the average amount of DpD indicator, for both BIK and AMSA is almost the same. This mount is 37.59 for BIK port in Iran and 37.54 for AMSA.

Decrease of DpD has a direct relation with deficiency but an inverse relation with detained ship. If deficiency decreases there are two possible reasons: first, decrease of average age; second, good management and maintenance of ship; both of them indicate good performance of PSC.

4. DpD Formula

The formula of DpD indicator shown as below:

$$DpD = \frac{Total\ Number\ of\ Deficiencies}{Total\ No\ of\ Detained\ Ship} \quad (1)$$

5. References

[1] United Nation Convention on the Law of the Sea, Part VII, Article 94, *Duties of Flag State*, 2013, pp 58.

[2] United Nation Convention on the Law of the Sea, Part XII, Article 218, *Enforcement by port States*, 2013, pp 110

[3] Port and Maritime Organization, BIK Port, *PSC Annual Reports*, 2016, bikport.pmo.ir.

[4] Australian Maritime Safety Authority, Ship Safety Division, *Annual Reports*, 2012-2014, pp 11-22.

[1] Australian Maritime Safety Authority.

ASSESSING AND IMPLEMENTING OF INTERNATIONAL SALVAGE CONVENTION REQUIREMENTS IN IRANIAN WATERS TERRITORY (CASE STUDY: BUSHEHR PORT)

Hojjat Khosravi[1]
MS in Maritime Transport, Ports and Maritime Administration of the Bushehr province; Email: hojjatkhosravi@gmail.com

1. Introduction

Among various forms of transportation, transferring goods by sea is regarded as one of the common and important commercial practices because of its enormous benefits. Transferring goods by sea is always along with risks. These risks during the trip threaten the ship, the crew, or its cargo. The need to rescue those caught at sea having no other solution is undeniable. Therefore, the lives or property salvage of people at risk has been known as an ancient custom from the distant past. Islamic republic of Iran has more than 5300 kilometers marine borders and more than 92% of its imports and exports are carried out through these borders. Thus maritime transport is an essential part of national economy. With regard to the growth of the maritime industry and navigation and economic progress of the region which is directly associated with maritime transport, we are dealing with various events occurring due to different reasons. Most of such events lead to submerged buoys, missed commodities, and environmental pollution. There are conventions developed to deal with these incidents. The Salvage Convention 1989 was developed with regard to ship or cargo restoring. Using international uniform regulations for restoring operations can reduce the risks of maritime activities. In 1994, our country joined this convention and the Ports and Maritime Organization (current PMO) is charged as the maritime safety trustee in Iranian Waters territory to enforce the provisions of the Convention in the country.

2. Materials and Methods

This study aims to identify factors affecting the salvage operation and evaluation of these factors in the salvage teams and companies in the country. To achieve this goal, three questions were raised in this study. To answer these questions, this study was conducted in two stages. In the first stage, factors affecting the salvage operation were identified through interviews, review of international literature, and international guidelines. Then, these factors included in a 9-item questionnaire and distributed among the study samples (n=20, based on the Cochran formula). Their responses determined the status of the salvage companies and operations in Iran. In fact, the questionnaire's items were the main research questions listed below:

1.What factors influence the success or failure of the salvage operation?
2.How are the organizational design and administrative-operational procedures determined in a salvage company?
3.How is the salvage operation in the waters of country?

Table 1. Research assumptions

There are no specific instructions to register the company in our country.
In our country, salvage companies have no appropriate organizational chart.
In our country, salvage teams do not collaborate with professionals familiar the Law of the Sea.
In our country, salvage teams do not have electronic and communication equipment.
In our country, during the salvage operation, no professional team is employed in salvage engineering.
Salvage teams in our country do not possess any special vessels for immediate access to the site and trailers for towing operations.
In our country, salvage teams do not possess appropriate working equipment such as generators, compressors, and so on.
Salvage teams in our country do not possess the equipment needed to decontaminate.
Salvage teams in our country do not possess experienced and trained personnel.

3. Results

Regarding the first question, the results of the study showed that important factors in salvage operations include the presence of professionals familiar with the Law of the Sea in the salvage team, electronic and communication equipment, having a professional team in salvage engineering, existence of special vessels for immediate access to the site and trailers for towing, having proper equipment such as generators, compressors, equipment needed for decontamination, experienced and trained persons, appropriate organizational chart, and specified instructions. With regard to the second question, results of the study revealed that a professional salvage company enjoys the following structure:

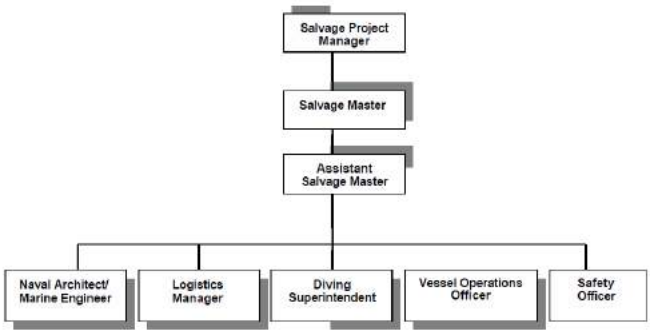

Figure 1: Proper structure of a salvage company

With regard to the third question as the most important research question and the ultimate goal of this research, it was revealed that the first and foremost current problem is the lack of comprehensive guidelines on licensing the salvage companies. Licenses are mostly granted based on personal preferences or on having a few divers and diving license. However, the salvage team shall consists of a salvage operation expert and his successor ,diving team and team leader, safety officer, an equipment and vessels officer, vessel operations officer, marine engineers and architects, a specialist in maritime laws and a sea environment expert.

The second problem is the organizational design of the salvage companies. Now, the salvage operations taking place in the waters of our country are performed by companies consisting of a few divers and a senior diver controls the diving operation; however, salvage teams usually consists of the following chart in the well-known marine states:

The third issue that should be noted is not having tugs for towing damaged ships. An important issue that needs special attention is lack of equipment to decontaminate our country's salvage companies. One of the main risks associated with marine incidents is environmental pollution in the waters of the accident scene. This pollution, in addition to destroying and endangering marine animals and plant' environment, has negative impact on ship traffic. In addition to the resulting economic consequences, they have negative impact on the marine credibility of the country where the accident occurs.

Training operational staff and forces in the salvage companies is essential and vital. Training is a debatable discussion of two aspects: First, a majority of the salvage team members are divers who are not familiar with other maritime issues, such as environmental issues, and marine laws. Another issue is learning how to operate new and modern equipment since this equipment is increasingly being designed and manufactured.

In this study, 9 factors including the presence of professionals familiar with the Law of the Sea in the salvage team, electronic and communication equipment, having a professional team in salvage engineering, existence of special vessels for immediate access to the site and trailers for towing, having proper equipment such as generators, compressors, equipment needed for decontamination, experienced and trained persons, appropriate organizational chart, and specified instructions are professionals and familiar with the Law of the Sea factor in the recovery were determined as factors affecting the salvage operation. Investigating these factors in our country showed that all factors suffer weakness and problems.

4. Recommendations and Solutions

The first and most important solution proposed based on the research findings is providing comprehensive instructions for registering the salvage companies. A working group of experts from the Ministry of Roads and Urban Development (custodian of the country's PMO) and the PMO professionals (in charge of Maritime Affairs of the country) can be formed to prepare guidelines. Advanced countries in the field of salvage such as the Netherlands can be regarded as the benchmark and their instructions can be modeled. In order to develop a comprehensive instruction on salvage instruction, the following points should be noted:

-Defining the organizational scheme for companies and salvage operation teams

-Describing and defining the minimum standard required for each type of towing devices and salvage operations

-Obliging the current and future salvage teams to have the equipment to reduce and prevent marine environmental pollution

One of the main issues discussed in salvage operation is theoretical and practical training. Despite the marine universities such as Kharg, Imam Khomeini in Noshahr, and Chabahar, there is few problems regarding specialized training in related academic and technical fields on marine engines and ship architect to complete salvage team members in the country.

In practical discussions, it is recommended that PMO specify and implement training and practical training courses during a specified time period to provide the opportunity for licensed or establishing companies and interested people in order to be empowered and authorized to be present in this field. It should be noted that this research has been completed with financial and moral support of PMO.

5. References

[1]. Khosravi, H. (2014). Potential pollution resulting from submerged vessels, Payam Darya Journal, 22 (227).

[2]. Khosravi, H.; Atabak, N. (2013). The requirements safety of buoy wrecks based on the immune system of buoys' flotation safety, Be Hengam quarterly, 6(16).

[3]. Aberdein, D. (1994). Marine Salvage and the Environment: New Zealand and the 1989 Salvage Convention, MLAANZ Joumal, 10 (1), pp 35-74.

[4]. Brice, M. (1993). Maritime Law of Salvage, Sweet & Maxwell, London, p.2.[12]

[5]. Busch, T. (2011). Fair Reward for Salvage Operations. International Salvage Union publication.

DESIGN OF MOBILE APPLICATION FOR POLLUTION REPORTING

Jiří Kadlec[1], Sahar Mokhtari[2]

1) Department of Civil and Environmental Engineering, Brigham Young University, Provo, USA, jirikadlec2@gmail.com
2) Coastal and Ports Engineering Department, Ports and Maritime Organization, Tehran, I.R.Iran, Mokhtari.sahar@gmail.com

1. Introduction

There are a lot of sources of pollution in the world, and this pollution threatens our life and can have adverse effect on the health and environment. Examples include noise pollution, chemical pollution and light pollution. If we want to protect ourselves from this pollution, the first required step is prevention, and the next step is rapid response to pollution incidents. We need fast and accurate input about the pollution incident in rapid response, and we must increase our knowledge about location, type, and frequency of the pollution to make decisions for future. Modern advancements in technology have allowed us to use this technology for the protection of the environment, for example, the use of satellite images, and computer model tools. Smart phones and Internet present good opportunities to help the environment, because today most people have easy access to Internet and smart phones. There are many examples of using web and smartphone technologies for environmental monitoring such as online sensors about marine data and marine pollution, online air pollution analyses, and waste water control. Our example of using modern technology to help the environment is online pollution reporting. . Input data from mobile user online reporting helps with directing rapid response to the marine and coastal area, and contributes to an online database of pollution events

2. Software Requirements

.The following information has been identified as important for locating and documenting a pollution incident to enable efficient response:

- Location
- Latitude, Longitude (WGS 84)
- type of the pollution
- time of the pollution (default: same as time of sending report, but can be changed by user)
- incident information
- incident details (what happened and what you witnessed)
- details of any impacts
- photographs
- videos

It is critical that the mobile application can be used offline (without connection to the Internet) and synchronizes the report with a data bank in the control center when internet connection becomes available. The application software also needs to reduce the volume of data being sent over the mobile network (compress pictures and videos)

3. Software System Design

The designed system consists of a mobile app and a control center. In the mobile app, the user can enter the location, type of pollution, incident description, details of any impacts, and attach photographs or video. The details are saved in a local database on the user's mobile device, and sent via data connection, text message, or Wi-Fi to the control center when mobile reception becomes available.

The control center gathers all reported incident data in a database and shows the list and map of pollution events to the coastal zone manager. The manager responds to the report and the status can be sent as a text message back to the user who reported the pollution incident (see Figure 1).

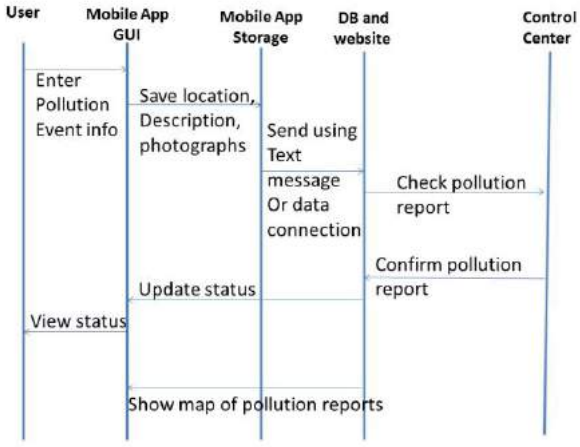

4. Conclusions

This presentation demonstrates a prototype of the pollution reporting app. The app has been implemented for the Android platform. Usability testing is required to test entering a report for various locations, conditions and pollution types. The following results are expected from the mobile pollution reporting app: Displaying multiple reports together in a map can highlight areas with increased pol pollution. (2) Promoting public awareness about environmental pollution. The users of the app receive quick response about the status of the reported incident and they are included and together contribute to preventing pollution and helping the environment.

5. References

[1] Briand, L. C., Daly, J., and Wüst, J., "A unified framework for coupling measurement in objectoriented systems", *IEEE Transactions on Software Engineering*, 25, 1, January 1999, pp. 91-121.

[2] Mokhtari, S., Hosseini, S. M., Danehkar, A., Azad, M. T., Kadlec, J., Jolma, A., & Naimi, B. (2015). Inferring spatial distribution of oil spill risks from proxies: Case study in the north of the Persian Gulf. Ocean & Coastal Management, 116, 504-511.

[3] Maletic, J. I., Collard, M. L., and Marcus, A., "Source Code Files as Structured Documents", in *Proceedings 10th IEEE International Workshop on Program Comprehension (IWPC'02)*, Paris, France, June 27-29 2002, pp. 289-292.

[4] Marcus, A., *Semantic Driven Program Analysis*, Kent State University, Kent, OH, USA, Doctoral Thesis, 2003.

[5] Marcus, A. and Maletic, J. I., "Recovering Documentation-to-Source-Code Traceability Links using Latent Semantic Indexing", in *Proceedings 25th IEEE/ACM International Conference on Software Engineering (ICSE'03)*, Portland, OR, May 3-10 2003, pp. 125-137.

[6] Salton, G., *Automatic Text Processing: The Transformation, Analysis and Retrieval of Information by Computer*, Addison-Wesley, 1989.

STUDY OF FACILITIES, EQUIPMENT AND READINESS OF DEALING WITH OIL POLLUTION AND POLLUTIONS CAUSES FROM DANGEROUS GOODS AT RAJAIE PORT

Sobhan Iranshahi[1], Hamidreza Tahmak[2], Taimaz Moradi[3]

1. Hormozgan Province Maritime & Ports Authority, Bandar Abbas, Iran, Sbn.iranshahi@gmail.com
2. MSc in Ports and Shipping, School of Maritime Studies,Chabahar, Iran, hamidrezatahmak@gmail.com
3. Hormozgan Province Maritime & Ports Authority, Bandar Abbas, Iran, tami.oradi@yahoo.com

1. INTRODUCTION

The rise of environmental problems in most countries of the world is of particular importance until todays the pollution of sea waters has been one of the most important environmental issues of the world. The MARPOL Convention covering regulation for prevention of pollution of the marine environment and rivers. Member nations and also Iran that is signatory to MARPOL, are subject to its requirements [1]. In addition of MARPOL the Kuwait Regional Convention for co-operation on the protection and development of the marine environment and costal area of Persian Gulf from pollution was established between seven countries of the region named PROME. In our country a bill about protection of sea and Boundary Rivers from oil pollution was approved by cabinet in 17th February of 2008. In this bill also has been considered indemnities for the parties who polluted these waters [2]. The cabinet of ministries according to the International Convention on Preparedness, Response and Co-operation on oil pollution (OPRC) approved the system of national preparedness, response and co-operation against oil pollution at sea and navigable rivers in 2013. Port and Maritime Organization has the responsibility of coordinating the response to oil pollution into the national contingency plan and is responsible for executing tasks administration of OPRC convention [3].

2. MODEL AND RESEARCH METHODOLOGY

In this research 26 indexes in form of 5 factors have been studied as main factors in the event of dealing with likely marine pollution at Shahid Rajaee Port. These indexes were formed as a localized questionnaire (Sayareh & et al, 2012) and distributed between the statistical society (statistical population) that was contain 91 person. Out of 91 distributed questionnaires 86 questionnaires could be analyzed (about 95% of total questionnaires) and the statistical analysis has been done accordingly. The statistical society separately includes: deal with marine pollution (15 persons), check of maritime accidents (4 persons), inspection of ships (10 persons), maritime search and rescue (6 persons), hydrography (2 persons), submerged vessels (2 persons), navigation marks and sings (1 person), pilots (3 persons) and the vessels deal with pollution (48 persons). The reliability of the questionnaires was approved by Cronbach's Alpha and the acceptable factor of Cronbach's Alpha reached 0.913.

There are five hypotheses for this research (table 4) contains: According to the recommended model of this research, these five factors exist at Rajaie Port and there is a relation among these factors (figure 1).

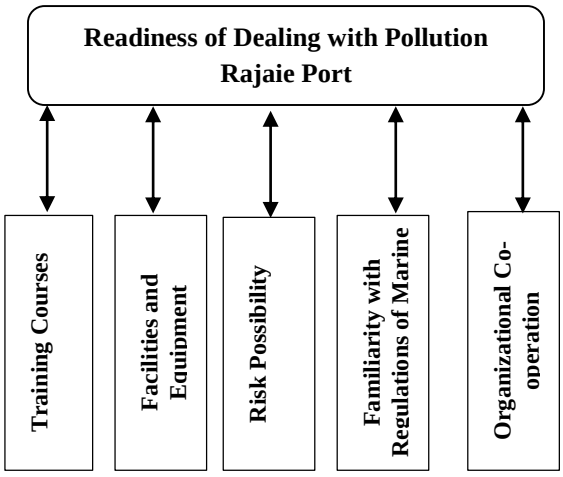

Figure 1. Research Model

3. STATISTICAL ANALYSIS

To ranking the research factors, Friedman test was used (table 1).

Table 1. Friedman Test

Factors	Mean Rank	Ranking	N	Chi-Square	df	Sig.
training courses	3.16	2	86	125.726	4	0
facilities and equipment	2.24	5				
familiarity with regulations of marine pollution	2.73	3				
risk possibility	4.48	1				
organizational co-operation	2.38	4				

With regards to the scores showed at table 1, the factor of possibility of risk at Rajaie Port has the most score. By Spearman's correlation coefficient test as a pairwise comparison among all of the research variables (training courses, facilities and equipment, familiarity with regulations of marine pollution, risk possibility and organizational co-operation), it was revealed that

the significance in all comparisons are below 0.05 which it means all of the research variables are co-related.

Table 2. Spearman's correlation

Factors	training courses	facilities and equipment	familiarity with regulations	risk possibility
training courses	1			
facilities and equipment	.431**	1		
familiarity with regulations	.306**	.808**	1	
risk possibility	-.222*	-.563**	-.697**	1
organizational co-operation	.743**	.722**	.510**	-.213*

According to the table 2, the most correlation exist between variables of facilities and equipment and familiarity with regulations of marine pollution with a positive correlation coefficient of 0.808 .In addition the least correlation exist between variables of the possibility of risk and organizational co-operation with a negative correlation coefficient of 0.213 .

In the present research the binomial-test is applied to confirmation or rejection of the research factors.

Table 3. Binomial Test

		Category	N	Observed Prop.	Test Prop.	Exact Sig. (1-tailed)
training courses	Group 1	<= 3	50	.6	.6	.402
	Group 2	> 3	36	.4		
	Total		86	1.0		
facilities and equipment	Group 1	<= 3	74	.9	.6	.000
	Group 2	> 3	12	.1		
	Total		86	1.0		
familiarity with regulations of marine pollution,	Group 1	<= 3	74	.9	.6	.000
	Group 2	> 3	12	.1		
	Total		86	1.0		
risk possibility	Group 1	<= 3	14	.2	.6	.000[a]
	Group 2	> 3	72	.8		
	Total		86	1.0		
organizational co-operation	Group 1	<= 3	62	.7	.6	.013
	Group 2	> 3	24	.3		
	Total		86	1.0		

4. DISCUSSION AND CONCLUSION

With regards to the table 3, it can be concluded the factors training courses, facilities and equipment, familiarity with regulation of marine pollution and organizational co-operation don't exist at Shahid Rajaee Port but the factors of the possibility of risk there is. At the table 4, the final response of each hypothesis has been showed briefly.

Table 4. Final response of each hypothesis

	Hypothesis	Response
1	Proper training courses in order to dealing with oil pollution and pollutions causes from dangerous goods at Shahid Rajaee Port.	Rejected
2	There are proper facilities and equipment in order to dealing with oil pollution and pollutions causes from dangerous goods at Shahid Rajaee Port.	Rejected
3	The employees of the Shahid Rajaee Port are familiar with the regulation of marine pollution in order to dealing with oil pollution and pollutions causes from dangerous goods at Shahid Rajaee Port.	Rejected
4	There is the risk possibility of the oil pollution and pollutions causes from dangerous goods at Shahid Rajaee Port.	Confirmed
5	There is an organizational co-operation between Shahid Rajaee Port and related organizations in order to dealing with oil pollution and pollutions causes from dangerous goods at Shahid Rajaee Port.	Rejected

6. REFERENCES

[1] Ghasemi Nejhad, Ali Reza. "Deal with Oil Pollution at Sea, Khazar Oil Company, Safety supervisor", Health and civil defrense environment and disaster management. 2014.

[2] Morshedi, Behzad. "Strategies to Deal with Oil Pollution in Ports, Availability by website", http://hsemorshedi.persianblog.ir/, Date of availability: 26 April 2016.

[3] Administration of Port and Maritime Organization rescue and Protection. "Deal with Marine Pollution Caused by Ships, Platforms, and Coastal and off Shore Structures", Availability by port and maritime organizations' website, (www.pmo.ir), date of availability: 7 April 2016.

[4] Sayareh, J., Yarahmadi, A. & Tahmak, H. "Facility and ability assessment of Chabahar Seaport against Pollution from Dangerous and toxic substances (with Recommendations for their Improvement)", 10th ICOPMAS, Tehran, Iran, 2012, 19-21 Nov.

THE ENVIRONMENT IMPACT ASSESSMENT OF FISHING BREAKWATERS CONSTRUCTION (CASE STUDY OF JUSK SUB- BASIN PROVINCE HORMOZGAN)

Masoud Pour Asghar[1], Saeed Darvishi[2], Amir Davazdah Emami[3]

1) Marine and Coastal Environmental Group, Sahel Consulting Engineering Company, Tehran, Iran, Email: Masoudpourasghar1364@gmail.com

2) Marine and Coastal Environmental Group, Sahel Consulting Engineering Company, Tehran, Iran,, Email: saeed_darvishi@ut.ac.ir

3) Marine and Coastal Environmental Group, Sahel Consulting Engineering Company, Tehran, Iran, Email:a_demami@yahoo.com

1. Introduction

One of the macroeconomic objectives of developing country perspective is development of fishing activities and fishery industries growth in coastal provinces of Iran. For this point and for life and livelihood quality improvement, at these coastal provinces and economical development growth, small fishing breakwaters construction in coastal strip of province Hormozgan is considered by authorities The ports construction projects, fishing wharfs, oil jetties, transportation wharfs of humans and goods and the other marine structures have much environmental effects in comparison with the other structures.

These kinds of projects influence the environmental parameters undoubtedly because of the necessity of their location on terrestrial and aquatic environment and by making water pollution, macro-benthic and aquatic habitats destruction, making wastes and solid wastes, changing the physical condition of coast line, sound pollution, cultural and social problems causes the quality and quantity changes of nature and human and in many cases by changing the ecological balance provide irrecoverable destruction and pollutions.

2. Material and Methods

2-1- The geographical location of the case study area

The caste study area (direct area) is located in Lon 56˚56' to 57˚58'N and Lat 26˚32' to 26˚42'N.In this area 7 ports are being studied, Bandaran, Grook, Gazi, Balaboland, Boonji, Nasiri and Jusk Kohneh. One of the important ports in EIA for ports is determination of case study area. In this research according to the importance of this matter, implement of this process is considered so after the land visits, the expert meetings of study team and according to the nature of the project, 3 areas are surveyed: immediate area, direct area and non-direct area.

2-2- The impacts prediction due to the plan performance

The EIA studies are implemented for civil projects for a true performance and during the activities by considering the minimum probable impacts on environment and prevention of its destruction. Therefore enough and valid cognition from the project impacts during construction and operation phases should be acquired because of the scientific and practical solutions and decrease of the negative impacts and for this reason, impacts prediction is an important parameter for these studies. At the stage of impacts prediction for fishing breakwaters, the consequence of the project are known and predicted according to the project conditions and the pollutions resulted by that and also the recognition of the influenced environment properties. Totally for description of each potential effect in construction and operation phases of the plan on terrestrial and marine environments, the components which include nature, intensity, finality, reversibility and impact domain are considered. The conceptions and descriptions of each property are introduced (see Table1)

Table 1: The criteria and components that are being used in descriptive matrix for recognition and impacts prediction

Signs	Components	Main criteria
C	Certainly	Finality
P	Probable	
A	Events	
E	Reversible	Reversibility
I	Irreversible	
L	Low	Intensity
M	Average	
H	High	
R1	Immediate	Domain
R2	Direct	
R3	Non - Direct	
+	Positive	Nature

On basis of the implemented studies about the properties of suggested project and also the condition of environment parameters of the impacted area, the impacts resulted by the plan in construction and operation phase are surveyed and predicted in 3 environment parts, physico chemical, biological and social- economical and cultural for coastal and terrestrial areas.

3. Results and Discussion

In these studies, after recognition the different aspects of performance and non – performance effects in shape of descriptive matrix, the results of descriptive matrix in another matrix is quantified for assessment, comparison and the better choice. In this process, the main basic of predicted impacts is in descriptive matrix and their specifications and the ranking is done in quantity matrix on basis of each quintet components of impact feature. The results of alternatives analysis for These ports of Jusk sub – basin are presented (see Table2).

Table 2: The results of assessment and analysis of twofold alternatives impacts

Environmental Parameters		First alternative (Performance)	Second alternative (Non performance)
Physico - chemical	Construction Phase	-92	+32.5
	Operational phase	-45.5	+14.25
	Total	-137.5	+18.25
Biological	Construction Phase	-75.5	+20.5
	Operational phase	-55.5	-5
	Total	-131	+15.5
Economical – social and cultural	Construction Phase	107.5	-126.5
	Operational phase	380	-40.5
	Total	487.5	-167
Result	Construction Phase	-60	-73.5
	Operational phase	279	-59.75
	Total	219	-133.25

4. Conclusion

The presented results of performance matrix for sevenfold ports in Jusk sub-basin explain the effect of project on all mentioned environment in construction and operation phases that confirm the performance of this project due to environment considerations.

5. References

[1] Bear, J., Cheng, A.H.-D., Sorek, S., Ouazar, D., Herrera, I., 1999. Seawater Intrusion in Coastal Aquifers-Concepts Methods and Practices, vol. 14. Springer Publication, 627 p.

[2] Canter, L. W. 1996. Environmental Impact Assessment.Mc Grew Hill Book Co. Baltimore

[3] Partidario, M. R. 2003. Strategic Environmental Assessment, Portugal, Lisbon.

[4] Wainwright, J. and Mulligan, M. 2004. Environmental Modelling, John Wiley & Sonsoltd.

[5] Wever, G. 1996. Strategic Environmental Management:Using TQEM and ISO 14000 for Competitive Advantage, Wiley

HEALTH STATUS EVALUATION OF THE GREEN SEA TURTLE (*C.MYDAS*) ALONG NORTHERN COAST OF OMAN SEA

Mahmood Sinaei [1*], Mehdi Bolouki [2], Seyed Ghasem Ghorbanzadeh [3],Mohammad Talebi Matin [4]

[1]Department of Fisheries, Chabahar Branch, Islamic Azad University, Chabahar, Iran, oceanography.sina@gmail.comn

[2]Department of Environmental, P.O. Box 14155-7383, Tehran, Iran, lahijanjan@hotmail.com

[3]Department of Environmental, P.O. Box 14155-7383, Tehran, Iran, ghorbanzadeh110@yahoo.com

[4]Department of Environmental, P.O. Box 14155-7383, Tehran, Iran,matin@gmail.com

Introduction

Marine turtle species are an integral part of oceanic ecosystems throughout the world [1]. Green turtle is the largest of the hard shelled sea turtles and is the second largest (after *Dermochelys*) of the seven species. Green turtle is a circumglobal species found in tropical and sub-tropical waters [2,3]. The Coast of Oman Sea has some of the most important nesting sites for green sea turtles in the world. At present, there is limited information on the biomarkers of health status of the population of green turtle (*C. mydas*), in Oman sea.The purpose of the present study was:

1) to determine biochemical analytes in the blood of nesting green turtle in light of those previous studies on the northern coast of Oman sea, Chabahar, Iran.

2) to determine hematological values in the blood of nesting green turtle on the northern coast of Oman sea, Chabahar, Iran.

3) to evaluate and compare sodium heparin and lithium heparin as anticoagulants for measuring selected biochemical anal

Material and methods:

Field trips were made to the sampling sites during the years 2013–2014. Female nesting green turtles were captured from their main nesting sites on the Chabahar beach, Islamic Republic of Iran (see Fig 1). Experiments were approved by an Iranian department of environment.

Nesting females were approached approximately 10 min after nest-building behavior ceased and egg laying activity had begun. Health status of turtles was rated based on nest-building behavior and general body condition. Blood was collected from the interdigital vein of the hind flipper via a dorsal approach with the use of an 18-gauge, 3.7-cm needle and a 15-ml syringe Precoated with sodium heparin (heparin sodium injection, USP, PPC, Inc., C504730, Canada) (n = 18) or a nonheparin-coated syringe (n=18). The biochemical panel included alanine aminotransferase (ALT), amylase, aspartate aminotransferase (AST), blood urea nitrogen (BUN), calcium, cholesterol, creatine kinase (CK), creatinine, gamma glutamyl transferase (GGT), glucose, lactate dehydrogenase (LD), lipase, phosphorous, potassium, sodium, total protein, triglyceride, and uric acid (UA). In order to measuring Alpha-tocopherol (vitamin E) and retinol (vitamin A) concentrations, the same method proposed earlier by Bechert et al. (2007) was followed.

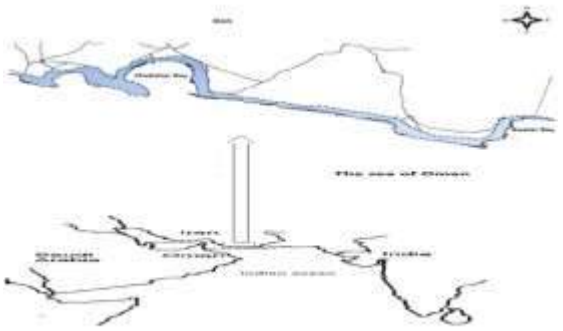

Figure 1. Study area

Results and discussion:

A total of 18 female green sea turtles received physical examinations. Carapace length was measured for 18 turtles. Mean curved carapace length (CCL) was 131 ± 4 cm with a range of 123—142 cm. Barnacles were recorded on three turtles. No fibropapillomas were observed on any of the 18 turtles.

Blood hematology

Hematological data as well as the results of the related statistical analyses are displayed in Table 1. The mean PCV was 0.41 (proportion of 1) with a range of 0.30–0.58. No basophils or hemoparasites were detected in any of the 18 turtles tested.

Table 1. Hematologic values in nesting green turtles (C. Mydas) nesting on Chabahar Beach,Islamic Republic of Iran.

Measure[a]	N	Mean	SD	Range
PCV (l/l [%])	18	0.36 [36]	0.037 [3.7]	0.28–0.42 [28–42]
TS (g/l [g/dl])	18	43 [4.3]	8 [0.8]	26–58 [2.6–5.8]
RBC (×10³µ/l)	18	374	187	166–777
WBC(×10³µ/l)	18	4.6	1.5	2.7–7.6
Heterophils(×10³µ/l)	18	2.5	1.3	0.03–4.9
Lymphocytes(×10³µ/l)	18	1.5	0.8	0.0–3.0
Monocytes(×10³µ/l)	18	0.3	0.1	0.1–0.7
Eosinophils(×10³µ/l)	18	0.1	0.1	0–0.4

[a] PCV, packed cell volume; TS, total solids; RBC, red blood cells; WBC, white blood cells. No basophils were detected in any of the 18 green sea turtles evaluated. Samples were collected in sodium heparin

Plasma biochemistry

Plasma biochemistry data as well as the results of the related statistical analyses are displayed in Table 2. No statistically significant differences were noted between the two anticoagulants for any of the measures.

Table 2. Plasma biochemistry values from blood collected in sodium and lithium heparin from nesting green turtles (C. mydas)

Measure[a]	N	Mean±SD	Range	N	Mean±SD	Range
Sodium (mmol/L)	18	143 ± 8	128—154	18	136 ± 9	123—147
Potassium (mmol/L)	18	4.2 ± 0.8	2.7—5.3	18	4.2 ± 0.9	3.1—5.1
BUN(mmol/L)	18	1.43 ± 1.03	0.91—4.93	18	1.01 ± 0.11	0.71—3.93
Uric acid(mol/L)	18	12.1 ± 0.0	12.1	18	12.1 ± 0.0	12.1
TP (g/L)	18	44 ± 9	31—58	18	40 ± 10	30—50
Cholesterol	18	9.14 ± 2.38	6.81—13.07	18	8.08 ± 1.98	3.92–10.76
Triglyceride(mmol/L)	18	4.09 ± 0.74	2.83—4.94	18	4.96 ± 0.66	4.82—5.58
Calcium(mmol/L)	18	2.93 ± 0.35	1.1—2.1	18	3.24 ± 0.3	1.15—2.3
Phosphorous(mmol/L)	18	3.73 ± 0.51	3.07—4.01	18	3.72 ± 0.65	3.11—4.77
Creatinine(mol/L)	18	22.22 ± 6.73	15.32—40.1	18	17.52 ± 5.34	8.44—44.32
ALT (U/L)	18	4 ± 1	4—9	18	4 ± 1	2—6
AST(U/L)	18	167 ± 51	101—234	18	174 ± 39	135—231
LD (U/L)	18	1,636 ± 683	1,030—3,352	18	1,401 ±443	733—2,011
Glucose (mmol/l)	18	4.01±0.62	3.05—4.61	18	4.32 ±0.50	3.31—4.86
Amylase (U/L)	18	608 ± 51	518—758	18	631 ±94	466—843
Lipase (U/L)	18	3 ± 1	2—5	18	2 ± 0	2
GGT (U/L)	18	14 ± 3	11—16	18	12 ± 2	9—12

[a] BUN, blood urea nitrogen; TP, total protein; ALT, alanine aminotranferase; AST, aspartate aminotransferase; LD, lactate dehydrogenase; GGT, gamma glutamyl transferase. No measures were statistically different between samples collected in lithium versus sodium heparin.

Vitamin E and A

Plasma alpha–tocopherol concentrations in the 18 turtles tested was 7.8 ± 2.8 g/ml with a range of 0.5—11.8 g/ml. Plasma retinol was evaluated in 18 turtles and the concentration was 0.4 ±0.1 g/ml with a range of 0.2—0.6 g/ml**.**

Here, for the first time, we present the values of various blood hematology and biochemical parameters for the female green turtles *(C. mydas)* inhabiting the northern coast of the sea of Oman. The physical state and the health of the green sea turtles in Chabahar was found to be good, in that they did not present any obvious signs of disease or any external lesions or injuries. Because many marine turtle populations are threatened, failing to accurately assess population trends may have critical effects on the long-term conservation and management of these populations. Long lifespans, delayed sexual maturity, and wide-ranging migrations prevent direct monitoring of individuals during most life stages, especially as juveniles[2,3]. So, assessments of marine turtle populations usually rely on data from females on nesting beaches. Nevertheless, Health assessment studies conducted only on nesting females might not accurately represent the whole population[1,2]. The establishment of baseline physiologic data and blood values for healthy foraging green turtles, including males, provides valuable data for long-term health monitoring and comparative studies of this endangered population. Health data such as those presented in this article are imperative to collect, together with ecologic studies, to amass much needed baseline health data on turtle species. Additionally, green turtle, and other sea turtles, may serve as indicator species for marine ecosystem health. Further studies are also needed to increase the knowledge about, and understanding of, the way in which seasonal, annual, and geographic variations affect the biochemical parameters of the sea turtle in order to generate appropriate interpretations about health and nutritional states of these populations.

Acknowledgments

This work was supported by the grants from the Department of environment of Iran. Thanks are due to Mr. Arbabi, Mr. Hosseini,Mr soltanpour for supporting this work.

References:

[1] Chaloupka M, Parker D, Balazs G. 2004a. Modelling postrelease mortality of loggerhead sea turtles exposed to the Hawaii-based pelagic longline fishery. Mar Ecol Prog Ser, 280:285–293.

[2] Jackson JBC, Kirby MX, Berger WH. 2001. Historical overfishing and the recent collapse of coastal ecosystems. Science, 293:629–638.

[3] Aguirre AA, Lutz PL. 2004. Marine Turtles as Sentinels of Ecosystem Health: Is Fibropapillomatosis an Indicator? Eco Health, 1:275–283.

EVALUATION OF PHYSIOLOGICAL CHANGES IN FISH, SPOTTED SCAT (*S. ARGUS*) EXPOSED TO DIAZINON POLLUTION

Monir haghighat[1], Mahmood Sinaei[2],Javad ghasemzadeh[3],Mehdi Bolouki[4]

1) Marine environment expert in coastal and ports engineering department, Port and Maritime Organization, Mhaghighat@pmo.ir

2) Department of fisheries, Chabahar branch, Islamic Azad University, Chabahar, Iran, oceanography.sina@gmail.com

3) Faculty of Marine Sciences, Chabahar Maritime University, Chabahar, Iran, Iran,*jghasemz@yahoo.com.au*

4) Department of Environmental, P.O. Box 14155-7383, Tehran, Iran,lahijanjan@hotmail.com

Introduction

Diazinon [O,O-diethyl O-(2-isopropyl-6-methylpyrimdin-4-yl) phosphorothioate], is an organophosphate pesticide that is being used extensively in agriculture, especially in rice fields for pest control purposes [6]. Due to the industrialization and optimization of agriculture, the use of pesticides, especially the organophosphate insecticide diazinon, has increased during the past decade around the Persian Gulf.

Fish have been often used as appropriate bioindicators of chemical contaminants [7]. This study investigated the effect of a short-term exposure to sub-lethal concentration of diazinon on cortisol, electrolyte and glucose levels in plasma and tissue histopathology in spotted scat (*S.argus*).

Material and methods:

Specimens of *S. argus* were collected from uncontaminated areas from west coasts of Persian Gulf. Site of capture for the study fish was reference with low levels of diazinon contamination (Shayeghi et al. 2006). Males and females of spotted scat were then transferred to the laboratory. Fish were stored inside two aquariums, each with a volume of 500 L.They were acclimatized semi-static to aerated and standard OECD water [5].

Fish were randomly assigned to 100 L fiberglass tanks (3 replicate tanks per treatment). The tanks were continuously aerated and 10% of the water was changed daily and the diazinon dosing was renewed accordingly. The fish were exposed to diazinon (99.5% purity, Chem-service ,USA) at 0 (control), 10, 20 and 30 μgL^{-1} for 24, 48, ,72 and 96 h exposure duration.The diazinon concentrations were measured by high performance liquid chromatography (Hewlett-Packard 1100).

The spotted scat were euthanized every 24 h during the 96 h diazinon exposure. At each sampling period, ten fish per replicate (30 fish per treatment) were euthanized in clove oil solution (150 ppm) for 40–50s . The blood samples were collected. Cortisol hormone levels contents were assessed using the radioimmunoassay methods as described by Waring and Moore [8]. Electrolytes and glucose levels were assessed using the flame emission method according to Lerner et al. [4]. After blood collection, the specimens (n = 5 for each treatment) were immediately dissected and the liver and kidney were quickly removed and fixed in 10% buffered formalin solution and stored at 4 °C until processed for histopathology. We have condsidered three types of histopathological effects in the gill and kidney of Scat(*S.argus*) exposed to diazinon for 96 h: None (-), mild (+), moderate (++), and severe (+++) effects.

Results and Disscution:

In the present trial, cortisol levels were increased significantly in the treatments in comparison with the control. The stress response involves a series of physiological changes, and their primary effects result in the release of catecholamines and corticosteroids into the circulation [6]. In teleost fish, an elevation in plasma cortisol, produced in the interrenal cells of the anterior kidney, is known as the main hormonal response to stress [6], and the elevation of plasma levels of this hormone is often used as a biomarker. The mean electrolytes and glucose levels in fish that were exposed to sub-lethal concentrations of diazinon are summarized in Table 1. The Na^+ levels were not significantly affected by the diazinon exposure. The K^+ and Cl^- levels were significantly higher ($p < 0.05$) in diazinon-exposed fish at all sampling time points except at 24 h. The Ca^{2+} levels were lower in the diazinon-exposed fish at all concentrations ($p < 0.01$). The glucose levels significantly increased ($p < 0.01$) in response to diazinon exposure ($p < 0.01$). our results may suggest that the diazinon-induced increase in cortisol levels and the subsequent

increase in chloride cells number. The obtained results in the current research demonstrated that increase in K^+ and Cl^- levels might be markedly affected by diazinon. This order was also supported by several researchers [1].

Table 1. Mean concentration (±SD) of electrolyte and glucose levels and number of chloride cells in Scat (S.argus) as a function of four levels of contamination in the water column and exposure duration (n = 5).

Biochemical parameters	Exposure period (hour)				
	0 h	24 h	48 h	72 h	96 h
Sodium (mmol L^{-1})					
Control	141.62±1.32^{bcd}	140.64±8.57^{cde}	144.33±1.21^{cd}	143.31±1.15^{cde}	142.63±8.48^{cde}
Diazinon (10 µg L^{-1})	141.62±1.32^{bcd}	143.11±1.83^{bcd}	141.04±6.81^{cde}	148.38±1.42^{ab}	142.03±8.64^{cde}
Diazinon (20 µg L^{-1})	141.62±1.32^{bcd}	142.54±1.28^{bcd}	142.64±1.21^{bcd}	139.68±8.47^{de}	141.56±8.47^{cde}
Diazinon (30 µg L^{-1})	141.62±1.32^{bcd}	142.58±6.84^{bcd}	144.70±1.19^{c}	148.32±1.16^{ab}	140.29±8.49^{de}
Potassium (mmol L^{-1})					
Control	4.74±0.10^{ab}	4.85±0.11^{ab}	4.92±0.84^{a}	4.80±0.86^{a}	4.95±0.10^{ab}
Diazinon (10 µg L^{-1})	4.74±0.10^{ab}	4.87±0.14^{ab}	5.10±0.05^{ab}	5.04±0.16^{ab}	5.09±0.84^{ab}
Diazinon (20 µg L^{-1})	4.74±0.10^{ab}	4.88±0.06^{ab}	5.36±0.13^{ab}	5.13±0.02^{ab}	5.13±0.15^{ab}
Diazinon (30 µg L^{-1})	4.74±0.10^{ab}	5.38±0.12^{a}	5.24±0.85^{ab}	5.39±0.10^{a}	5.28±8.06^{a}
Chloride (meq L^{-1})					
Control	104.26±3.86^{b}	103.36±2.71^{b}	105.56±7.10^{b}	104.71±5.02^{b}	100.23±5.52^{b}
Diazinon (10 µg L^{-1})	104.26±3.86^{b}	89.84±3.85^{d}	134.54±1.43^{a}	121.54±5.81^{bc}	137.24±1.98^{ab}
Diazinon (20 µg L^{-1})	104.26±3.86^{b}	87.56±2.38^{d}	119.19±1.11^{cd}	126.86±4.65^{bc}	126.56±2.21^{bc}
Diazinon (30 µg L^{-1})	104.26±3.86^{b}	87.31±2.36^{d}	123.45±1.32^{bc}	123.37±4.98^{bc}	129.43±1.62^{b}
Glucose (mg dL)					
Control	96.16±1.87a	112.12±2.11^{cd}	100.78±4.99^{de}	95.34±5.19^{e}	108.52±7.43^{de}
Diazinon (10 µg L^{-1})	96.16±1.87a	128.24±2.19^{a}	108.68±8.08^{de}	115.42±6.41^{cd}	130.11±5.88^{a}
Diazinon (20 µg L^{-1})	96.16±1.87a	128.10±3.13^{a}	110.54±1.44^{de}	107.20±2.86^{de}	125.43±4.61^{a}
Diazinon (30 µg L^{-1})	96.16±1.87a	125.43±1.86^{a}	117.43±2.56^{b}	114.09±3.66^{bc}	127.97±5.08^{a}
number of chloride cells					
Control	11±1^{a}	11±1^{a}	11±1^{a}	11±1^{a}	11±1^{a}
Diazinon (10 µg L^{-1})	11±1^{a}	11±1^{a}	12±1^{a}	12±1^{a}	13±1^{a}
Diazinon (20 µg L^{-1})	11±1^{a}	11±1^{a}	12±1^{a}	13±1^{a}	17±1^{b}
Diazinon (30 µg L^{-1})	11±1^{a}	12±1^{a}	13±1^{a}	13±1^{a}	18±1^{b}

Values followed by the same letter are not statistically different between the treatments in each column (P>0.05)

In addition, the gills of the exposed fish (30 µgL^{-1} diazinon) displayed epithelial hyperplasia and lamellar fusion, curling of secondary lamellae, oedema, and epithelial lifting (Table 2). The control group did not show any histopathological abnormalities in the gill tissue. Histopathological changes were also noticed in the kidney tissue of diazinon-exposed fish. Microscopic analyses revealed damage in response to diazinon exposure (Table 2). The most noticeable changes included the degeneration of renal tubule and its epithelial cells, degeneration of bowman's capsule, and expansion of space inside the Bowman's capsule (Table 2). The control group did not show any histopathological abnormalities in the kidney tissue. Histological observation of the gill tissue after 96 h exposure to diazinon showed several changes, including oedema, epithelial lifting, curling of secondary lamellae, shortening of secondary lamellae, and lamellar fusion. A possible justification for our findings might be due to defense mechanisms of fish (*S.argus*) resulting in the increased distance between the aquatic environment and the blood and act as a barrier to the pollutants' entrance,

The results achieved in the present study suggest that diazinon metabolites could be responsible for the observed injury to the kidney. Similar histological changes have been reported in the kidney of fish exposed to diazinon [3].

Table 2. Summarized histopathological effects in the gill and kidney of Scat(S.argus) exposed to diazinon for 96 h.

Tissue →		Gill					Kidney				
Concentration µg l^{-1} ↓	Duration ↓	a	b	c	d	e	a'	b'	c'	d'	e'
Control		-	-	-	-	-	-	-	-	-	-
10	24 h	+	+	-	++	-	+	-	-	-	-
	96 h	+	+	+	++	-	+	+	+	+	+
20	24 h	+	-	-	++	-	+	-	+	+	+
	96 h	++	++	+	++	+	++	++	++	++	++
30	24 h	++	++	+	+++	-	+	++	+	++	++
	96 h	++	+++	++	++	++	++	+++	++	++	+++

None (-), mild (+), moderate (++), and severe (+++). a: Shortening of secondary lamellae; b: Destruction of epithelial lamella; c: Oedema and Epithelial lifting; d: Collapsed of secondary lamellae; e: Epithelial hyperplasia and lamellar fusion/ a': Degeneration of renal tubule; b': Degeneration in the tubule epithelial cells; c': Degeneration of bowmans capsule; d': Expansion of space inside the bowmans capsule; e': Glomerulus contraction.

In conclusion, the results of the present research suggest that histopathological alterations in gill and kidney tissues were caused by diazinon. The osmoregulation capacity in fish (*S.argus*) exposed to diazinon was reduced. Changes in cortisol hormone and glucose levels due to stressful conditions were also confirmed. The results obtained in the present work reinforce the importance of the addition of histopathologic analysis in programs for the evaluation of water quality.

References:

[1] Das BK, Mukherjee SC (2003) Toxicity of cypermethrin in *Labeo rohita* fingerlings: biochemical, enzymatic and haematological consequences. *Comp Biochem Physiol* 134: 109-121.

[2] Khosravi Katuli K, Mojazi Amiri B, Massarsky A, Yelghi S(2014) Impact of a short-term diazinon exposure on the osmoregulation potentiality of Caspian roach (*Rutilus rutilus*) fingerlings. *http://dx.doi.org/10.1016/j.chemosphere*.2014.02.038.

[3] Lerner DT, Bjornsson BT, McCormick SD (2007b) Larval exposure to 4-nonylphenol and 17b-estradiol affects physiological and behavioral development of seawater adaptation in Atlantic salmon smolts. *Environ Sci Technol* 41: 4479‑4485.

[4] Organisation for Economic Cooperation and Development (1993) *Fish, acute toxicity test. OECD Guideline 203*,Paris, p 9/9.

[5] Shayeghi M, Hosseini M, Abtahi M (2006) The determination of dimethoate insecticide residues upon the cucumber product (Fars Province). *J Environ Sci Technol* 27: 30-35.

[6] Sinaie M, Darvish Bastami K, Ghorbanpour M, Najafzadeh H, Shekari M, Haghparast S (2010) Metallothionein biosynthesis as a detoxification mechanismin mercury exposure in fish, spotted scat (Scatophagus argus). *Fish Physiol Biochem ,http://dx.doi.org/10.1007/s10695-010-9403-x.*

[7] Waring CP, Moore A (2004) The effect of atrazine on Atlantic salmon (Salmo salar) smolts in fresh water and after sea water transfer. *Aquat Toxicol* 66: 93-104.

GEOCHEMICAL INVESTIGATIONS IN PORTS

Fani Sakellariadou

Department of Maritime Studies, University of Piraeus, Piraeus, Greece, Email: fsakelar@unipi.gr

1. Introduction

Ports are semi-closed coastal marine areas characterized by high levels of vessel, urban and industrial activity. Consequently, they may be considered as contaminated areas and secondary polluting sources for their adjacent coastal area. Contaminants are accumulated in the water column and settled in the sea bed sediment matrix. This mechanism can cause chronic pollution levels leading to environmental degradation with a wide range of potential harsh impacts.

Sediment acts as a physical trap of the pollutant load entering the marine ecosystem. Furthermore, it is well known that chemical compounds show a tendency to become strongly bound to fine sediment. Therefore, sediment analysis and monitoring can offer the means for studying long term pollution as well as identifying major pollutant sources and their association with the levels recorded.

2. Material and Methods

Sixty six surface marine sediment samples were collected from the wider region of Piraeus, Rafina and Lavrio ports (Figure 1); in particular thirty six samples from Piraeus, fifteen from Lavrio and fifteen from Rafina, using a Van Veen grab. All samples were treated by hand for the removal of unrepresentative material, homogenized, dried at 40°C and thoroughly ground using a small pestle and mortar. Total metal content was determined after sediment digestion with a mixture of concentrated acids (HNO_3-HF-$HClO_4$) in screw capped Teflon beakers on a hot plate [1]. Metal partitioning was accomplished with sediment treatment following the Tessier et al [2] sequential extraction procedure with a few modifications. [3]. Metal concentrations were measured with Flame Atomic Absorption Spectrophotometry (Varian Spectra AA-200 model equipped with deuterium lamp for background correction) and Graphite Furnace Atomic Absorption Spectrophotometry (AAS), (Varian Spectra AA-640Z GTA 100 model, equipped with Zeeman). The sediment reference used was IAEA433.

3. Results

Piraeus sediments are enriched in Zn, Pb, Cu, Cr and Sn corresponding mainly to anthropogenic pollution including the port itself, the presence of long-term anchored ships through rusting procedure, point sources such as ship repair activities, hulls of ships through antifouling paints as well as road transport on the nearby onshore coastal area. Rafina sediments correspond to the lower mean values of Fe, Cr, Pb, Zn, Cu, Ni, Cd and Sn, indicating the less intensive anthropogenic activities of the area. Lavrio sediments correspond to the much higher mean values of Zn, Pb and Mn; this finding could be attributed to the presence of the Pb-Ag-Zn massive sulphide mineralization at the broader area of Lavrio district made up of Ag-bearing galena, pyrite, sphalerite arsenopyrite and chalcopyrite [4].

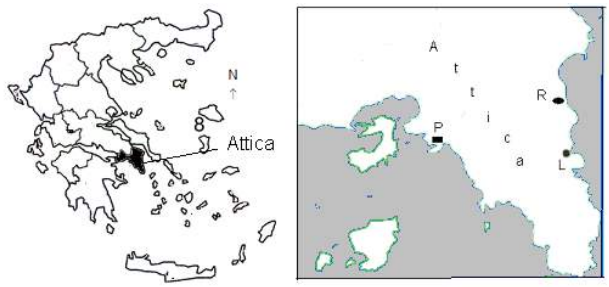

Figure 1. The Attica peninsula with Piraeus (P). Rrafina (R) and Lavrio (L) port areas.

The metal partitioning in the five geochemical fractions shows that more than 50% of Al, Fe, Cr, Zn, Cd and Sn remain in the residual fraction implying that they are mainly hosted in the lattice structure of silicate minerals, clays and other resistant minerals (Tables 2, 3 and 4). The same applies for Pb in Piraeus and Rafina. As high as 37-51% of Mn occurs in the reducible fraction, consisted of reducible ferromanganese oxides, some amorphous iron oxides and other reducible matter [5]. Specifically in Lavrio, 38% of Pb and 4% of Cu are also scavenged by the reducible fraction. More than 50% of Cu in Lavrio and Piraeus was found in the 4th fraction representing the elements present in sulphide minerals and those bound to various forms of organic matter. However the low organic carbon of the area strengthens the suggestion that the former possibility is a more likely situation.

Piraeus sediments show enrichment in their exchangeable content in Cu (21%), Zn (11%), Cd (7%), Ni (6%) and Sn (3%). As the amount of exchangeable metals is a good indicator of the pollution potential, Piraeus sediments could be considered to be polluted containing significant portions of metals easily available to the biota

[6]. Also a high percentage of exchangeable Cu (17%) was found in Lavrio.

The carbonate hosted fraction shows enrichment in Pb (8%) in Lavrio and this finding could be attributed to the presence of the mineralization within marbles and next to their contact with schists as well as inside both marbles and schists [7].

Table 1. Piraeus (P), Rafina (R) and Lavrio (L) port sediments: Mean total metal values (μg/g).

	Al	Fe	Mn	Cr	Pb
P	21342	17629	217	215	315
R	25775	10447	256	72	36
L	14752	17504	1292	99	2213
	Zn	**Cu**	**Ni**	**Cd**	**Sn**
P	778	219	69.65	3.49	8.78
R	135	15	27	0.22	<DL
L	4810	97	87	4.3	3.8

Table 2. Piraeus port sediments: Metal percentage associated with each of the five geochemical fractions.

	Al	Fe	Mn	Cr	Pb
E	0.00	0.19	2.17	1.46	0.20
C	0	0.08	8.37	1.77	2.40
Red	2.26	12.82	38.38	18.61	28.42
Or+S	4.66	20.90	25.14	18.06	12.96
Res	93.08	66.01	25.94	60.10	56.02

	Zn	Cu	Ni	Cd	Sn
E	10.78	20.51	5.76	6.96	2.67
C	2.97	2.29	10.42	5.04	3.08
Red	15.42	1.61	22.33	4.61	5.72
Or+S	7.01	54.06	21.28	7.89	11.53
Res	63.82	21.53	40.21	75.50	77

E: Exchangeable, C: carbonates hosted, Red: reducible, Or+S: Organic and Sulphide, Res: Residual.

Table 3. Rafina port sediments: Metal percentage associated with each of the five geochemical fractions.

	Al	Fe	Mn	Cr	Pb
E	0	0.33	3.30	1.47	0.35
C	0	0.22	22.14	3.36	4.15
Red	2.66	4.50	36.69	9.77	21.29
Or+S	5.20	8.93	7.60	12.17	3.89
Res	92.14	86.02	30.27	73.23	70.32

	Zn	Cu	Ni	Cd
E	3.58	5.95	5.43	0
C	1.11	8.54	14.75	0
Red	5.97	0.46	22.73	0
Or+S	2.25	17.21	21.89	0
Res	87.09	67.84	35.20	100

Table 4. Lavrio port sediments: Metal percentage associated with each of the five geochemical fractions.

	Al	Fe	Mn	Cr	Pb
E	0.02	0.56	1.26	2.29	0.63
C	0.06	0.24	6.98	2.95	7.74
Red	3.85	16.44	50.63	15.85	38.42
Or+S	9.48	26.59	18.99	19.86	8.21
Res	86.59	56.17	22.14	59.05	45.00

	Zn	Cu	Ni	Cd	Sn
E	3.47	16.80	4.78	0.84	0.76
C	1.40	2.12	9.10	3.90	2.92
Red	21.35	4.48	22.16	6.62	4.69
Or+S	13.21	57.15	24.81	6.61	9.36
Res	60.57	19.45	39.15	82.03	82.27

The treatment of the total metal content data sets with hierarchical cluster analysis revealed the anthropogenic source and the terrigenous one. In Lavrio the mineralization was represented by the Pb, Zn cluster

4. Conclusions

The application of geochemical investigations and particularly of element partitioning allows the estimation of the environmental status. Hierarchical cluster analysis provides with results in good agreement with those from the sequential extraction analytical procedure ones

5. References

[1] UNEP, *Reference Methods for Marine Pollution Studies*, No 31-39, 1985.

[2] Tessier, A., Campbell, G.C. and Bisson, M., "Sequential extraction procedure of the speciation of particulate trace metals", *Anal. Chem*, 51, 1979, pp. 844-850.

[3] Sakellariadou, F., *Geochemistry of nearshore sediments from the North Aegean Sea. Greece*, Imperial College, University of London, U.K., Doctoral Thesis, 1987.

[4] Alexakis, D., "Geochemistry of stream sediments as a tool for assessing contamination by Arsenic, Chromium and other toxic elements: East Attica region, Greece", *European Water*, vol. 21/22, 2008, pp. 57-72.

[5] Moorby, S.A. and Cronan, D.S., "The distribution of elements between co existing phases in some marine ferromanganese-oxide deposit", *Geochim Cosmochim. Acta*, 45, 1981, pp. 1855-1877.

[6] Sakellariadou, F., "The partitioning of the major and trace elements in the geochemical fractions of sediments collected from the Ierissos gulf and the adjacent area", in *Proceedings 5th Scientific Conference of the Greek Geological Society*, Thessaloniki, Gr, 24-27 May 1991, pp. 113-125.

[7] Marinos, G. P. and Petrascheck, W.E., *Laurium, Geological and Geophysical Research* (Inst. Geol. and Subsurface Research, Athens, Greece.), 4(1), 1956, 247pp. (in Greek with English summary).

ONLINE MONITORING OF WATER QUALITY IN SHAHID-RAJAEE HARBOR– PART I: DESIGN AND CONSTRUCTION

Payam Amir-Heidari[1], Mohammad Raie[2], Zohreh Hajisalimi[3], Mohammad Hossein Nemati[4]

1) PhD Candidate, Civil Engineering Department, Sharif University of Technology, Tehran, Iran, amirheidari_p@mehr.sharif.edu
2) Assistant Professor, Civil Engineering Department, Sharif University of Technology, Tehran, Iran, raie@sharif.edu
3) Coastal and Port Engineering Department, Ports and Maritime Organization (PMO), Tehran, Iran, hajisalimi @pmo.ir
4) Coastal and Port Engineering Department, Ports and Maritime Organization (PMO), Tehran, Iran, nemati@pmo.ir

1. Introduction

Uncontrolled human activities in harbor can cause substantial changes in the physical, chemical and biological properties of port water, and these changes can lead to major impacts to environment and human health. These changes may also increase the corrosion rate of coastal facilities. Concurrent with port organizations in developed countries, the Port and Marine Organization in Iran started a program in order to establish green ports. In order to achieve this objective, the first step is to monitor the environmental parameters of water in harbor basins.

Monitoring of water quality parameters, as a basic step in the control of port water pollution, is essential for identification of the trend of these parameters in different locations. Online or continuous monitoring of harbor water quality is of high importance and requires the special hardware and software. This paper is the first part of a two-part article about online monitoring of water quality in Shahid-Rajaee Harbor. This part shares the experience of design and construction of the online monitoring station in Shahid-Rajaee Port, the most important commercial port in Iran, in Persian Gulf. The second part of the article presents the operation and analysis of data [1].

This paper explains the process of selection of the important water quality parameters, configuration of the monitoring station, selection of the electronic sensors, electrical and hydraulic design of the station and related practical issues. This experience can be used in similar projects worldwide.

2. Harbor Water Quality Parameters

In the first phase of online monitoring project in Shahid-Rajaee harbor six water quality parameters were selected for measurement and monitoring, including water temperature, dissolved oxygen (DO), pH, Poly-Aromatic Hydrocarbon (PAH), turbidity and electrical conductivity. In the design of the station, the probable expansion of monitoring project in future, up to 12 quality parameters, were considered. It is probable that other parameters like biological parameters, heavy metals, nutrient and toxicant concentrations will be added to the system in the expansion phase of the monitoring station.

The sampling point in the first phase is simply one point adjacent to the wharf number 3 in a depth of one meter above the seabed which is 13.3 m under the water level at highest astronomical tide (HAT). The sampling location is very close to the petroleum loading arms and the berthing basin of the tug boats in the harbor.

3. Configuration of Monitoring Station

The first step in the design of online monitoring system is selecting the proper configuration. Configuration is related to the placement or layout of different system components, specially the sensors. Generally there are two main configurations for online monitoring of water quality [2 to 4]: 1) flow-through (or extractive), and 2) in-situ. In flow-through systems, the water is extracted from the water body to a sampling chamber (or pot) in which the electronic sensors are placed. The transport of water may be done by a pumping system or by the gravitational force [4]; at the other hand, in in-situ monitoring systems, the sensors are directly located at point of interest in the water body. The sensors are connected to power supply and data logger using the water-proof modules and connections. In this system, the sensors need to be supported by a base or frame to fix their position.

Each configuration has its own advantages and disadvantages. The selection of configuration will depend on different factors such as monitoring purpose, location and conditions of water reservoir, easy access for maintenance and availability of electric network. Regarding different factors, flow-through configuration was selected for monitoring station of Rajaee Port. The schematic of the designed system is shown in Figure 1.

4. Hydraulic and Mechanical Design

Because of selecting flow-through system for Rajaee Harbor, a robust pumping system is designed to extract seawater from an elevation of -13.3 to +3 (with respect to HAT) continuously.

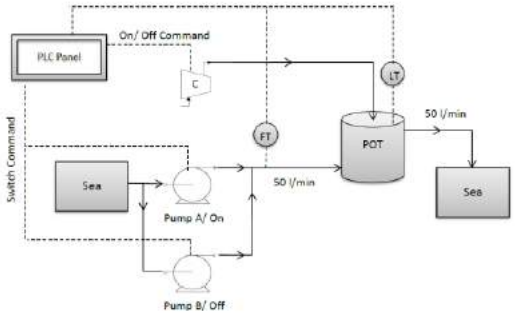

Figure 1. Extractive configuration of monitoring station in Rajaee Harbor

The seawater surface level has considerable fluctuations, because of the strong tidal effect in the location of Rajaee Harbor. Therefore the pumping system should supply enough flow rate of water at every day of the year and every moment of the day. The cavitation risk of the pumps should also be controlled.

The fluctuation of seawater level will lead to varying pumping flow rate, but a relatively constant level of water was needed in the measuring pot in the monitoring station. Considering these requirements, a robust pumping system was designed holding a constant level of water in the self-regulating pot.

The selection and configurations of foot valve, isolation valves and the regulation valves in the piping system of the monitoring station makes tuning, maintenance and restart of system easy.

Because of high risk of corrosion due to the corrosive nature of seawater, the components of piping system including pipes, pump casing and impeller and the measuring pot were selected from plastic material. This selection is also appropriate in order to not changing the water quality in the designed flow-through system.

The electronic sensors are installed easily from pot top into the water. The immersion depth of the sensors is easily adjustable by this design. Also, the system includes air-wash aluminum tubing that is designed to clean the sensing element of the sensors using clean compressed air that is supplied from an oil-free compressor in the station.

The measurement pot has a conical bottom and a continuous bottom-water discharge which reduces the accumulation of the clay in the pot.

The measurement pot, the pumps, valves and the electronic devices are located in a 2.5x2.5 m station room, with insulated walls and a proper air conditioning system to keep electronic devices cool and dry. An internal view of the monitoring station is shown in Figure 2.

5. Electric and Electronic Design

The electronic devices are the heart of any online monitoring system, and among them the sensors are the most important components. Five sensors and the data logger and the controller are the main electronic parts of the monitoring station in Rajaee Harbor. The data is transferred through a GPRS system to the web-based server. The switching of pumps and the air-flashing cleaning of the sensors are controlled by an electronic controller. It also displays the online water quality data on a small LCD.

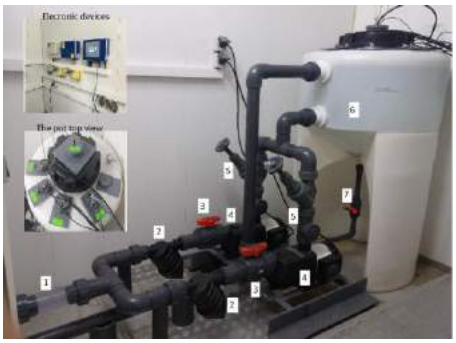

Figure 2. A view of the piping system, pot, sensors and data logger of the monitoring station

The electro-motors provide the driving force for the centrifugal pumps and the air compressor. These all are connected to safety circuit breakers, and the room is properly grounded to minimize the risks.

6. Data Management System and Public Display Panel

The recorded data of the sensors is saved in the logger. The data is also continuously sent to the online web-based server. The trend graphs and data tables can be accessed through internet.

To communicate with public, a large public display panel was installed in the administrative area of the Rajaee Port, indicating the online water quality index (WQI) of the harbor.

7. References

[1] Amir-Heidari, P., Raie, M., Hajisalimi, Z., Nemati, M.H. (2016) ONLINE MONITORING OF WATER QUALITY IN SHAHID-RAJAEE HARBOR– PART II: OPERATION AND DATA ANALYSIS

[2] Wagner, Richard J., and Robert W. Boulger, Jr., Carolyn J. Oblinger, and Brett A. Smith. (2000). Guidelines and Standard Procedures for Continuous Water-Quality Monitors: Station Operation, Record Computation, and Data Reporting. U.S. Geological Survey. Techniques and Methods 1–D3.

[3] BC Ministry of Environment. (2007). Continuous Water-Quality Sampling Programs: Operating Procedures. Watershed and Aquifer Science. Science and Information Branch. The Province of British Columbia. Resources Information Standard Committee.

[4] Miles, E.J. (2009). Guidelines: Shallow Water Quality Monitoring, Continuous Monitoring Station: Selection, Assembly & Construction. Virginia Institute of Marine Science. Special Report in Applied Marine Science and Ocean Engineering No. 412.

ONLINE MONITORING OF WATER QUALITY IN SHAHID-RAJAEE HARBOR– PART II: OPERATION AND DATA ANALYSIS

Payam Amir-Heidari[1], Mohammad Raie[2], Zohreh Hajisalimi[3], Mohammad Hossein Nemati[4]

1) PhD Candidate, Civil Engineering Department, Sharif University of Technology, Tehran, Iran, amirheidari_p@mehr.sharif.edu
2) Assistant Professor, Civil Engineering Department, Sharif University of Technology, Tehran, Iran, raie@sharif.edu
3) Coastal and Port Engineering Department, Ports and Maritime Organization (PMO), Tehran, Iran, hajisalimi @pmo.ir
4) Coastal and Port Engineering Department, Ports and Maritime Organization (PMO), Tehran, Iran, nemati@pmo.ir

1. Introduction

Online or continuous water quality monitoring of Shahid-Rajaee Harbor is the first technical step of Iranian Port and Marine Organization to move toward establishing green ports. This paper is the second part of a two-part article about online monitoring of water quality in Shahid-Rajaee Harbor. The first part shares the experience of design and construction of the online monitoring station [1], while this part presents the operation and analysis of data.

In the first phase of monitoring project in Rajaee Harbor 6 parameters were monitored by electronic sensors using an extractive configuration

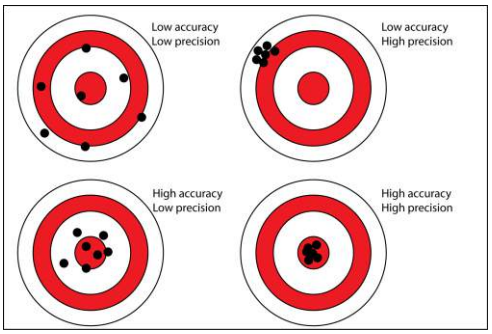

Figure 1. The concept of accuracy and precision [2]

The ability of the designed system for continuous measurement of water quality parameters was proved during a successful operation period starting from September 2015. The electronic sensors measured the related parameters, and their performance was analyzed in the initial operation phase of the monitoring station (for about 8 months). The validation of recorded data of sensors was performed by comparison of the data with the results of standard laboratory experiments on standard water samples. Also the intervention of the flow-through system on water quality was measured in this phase. The main objective of the operation in the test period was checking the "accuracy" and "precision" of the electronic sensors in the monitoring station. An appropriate electronic sensor has high accuracy and high precision. Accurate means to be close to the target, whereas precise means ability to get the same measured value frequently. These concepts are depicted in Figure 1.

2. Trend of Water Quality Parameters

Online monitoring station in Rajaee Harbor will provide the data for trend analysis of water quality parameters. Trend analysis is a technical procedure to study the pattern of change of different variables during different time periods. Using this analysis, the correlation of different parameters can also be studied. The results provide data for environment experts to locate different sources of water pollution in harbors. Therefore, a strategic plans can be defined to eliminate or reduce the pollution sources in the harbor. The results obtained from trend analysis can also be used in environmental impact assessment (EIA) studies.

The web-based data bank of Rajaee Harbor monitoring station is an online databank, enables the users to access the online data via internet. In this system the data spread sheets and the trend graphs of measured parameters are accessed by the users. A sample trend graph of four parameters in Rajaee Harbor is shown in Figure 2.

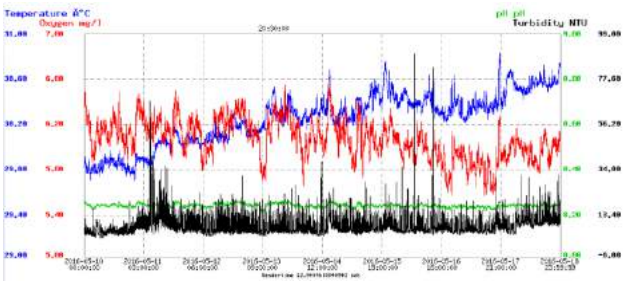

Figure 2. A sample trend graph of four parameters in Rajaee harbor

3. Data Cleaning and Noise Reduction

Raw data is highly susceptible to noise, missing values, and inconsistencies. In order to improve the quality of data, raw data should be pre-processed. Data preprocessing is one of the most critical steps in a data mining process which deals with the preparation and transformation of the

initial datasets. The first step in data preprocessing is data cleaning.

Data cleaning deals with spotting and removing errors and inconsistencies from data in order to improve the quality of data. Data quality problems are usually present due to missing data or other invalid data.

To clean the water quality parameter data in Rajaee Harbor online monitoring station, two jobs shall be done: 1) deal with the missing data (for example when one sensor is temporarily out of service), and 2) deal with abnormal data or noise, which is very common in electronic sensors. To achieve these goals, "moving average" filter was used to obtain smooth and clean data. A sample application of this filter for a series of noisy data is shown in Figure 3.

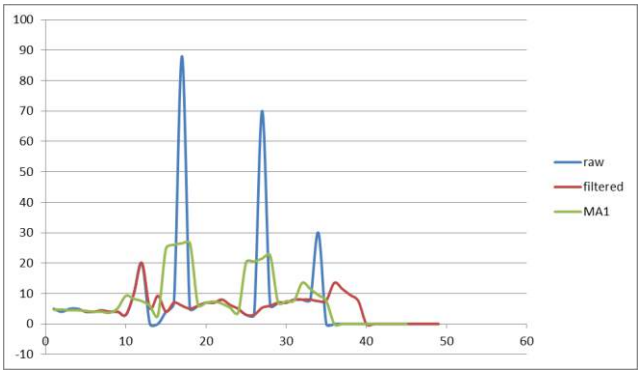

Figure 3. A sample application of moving average (MA) filter for data cleaning

4. Water Quality Index (WQI)

Once the water quality parameters are collected, a need arises to translate these multiple parameters into a form that is easily understood. Water quality indices (WQIs) aim at giving a single value to the water quality status on the basis of different water quality parameters. The formulation and use of indices have been strongly advocated by agencies responsible for control of water pollution.

Once the WQIs are developed and applied, they serve as a convenient tool to examine trends, to highlight specific environmental conditions, and to help governments or authorities to make decision about effectiveness of regulatory programs [3].

To select a proper WQI for Rajaee Harbor monitoring project, different important indices in standards were reviewed, and finally the CCME WQI [4] was selected for formulation of WQI in Rajaee Harbor. This index is broadly used in Canada. Number of failed variables with respect to standard range (scope), number of failed tests (frequency), and failed tests values (amplitude) in a time period determine the value of CCME WQI, and then a guideline exists to judge about water quality status, based on its value. The conceptual 3D model of this index is shown in Figure 4.

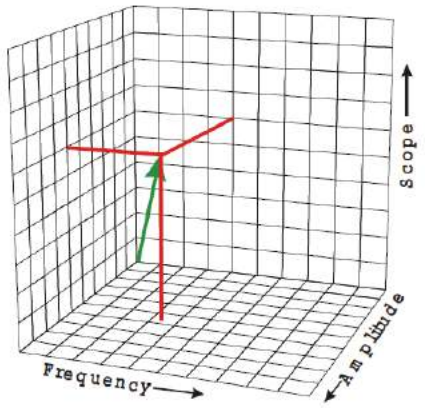

Figure 4. The conceptual 3D model of CCME WQI

5. Corrosion Index (CI)

Since some water quality parameters (e.g. conductivity, pH, DO and temperature), beside environmental impacts, can influence the corrosion rate of port and marine facilities, a seawater corrosion index (CI) is also formulated, very similar to the water quality index.

Calculation of a corrosion index from online data of Rajaee Harbor monitoring station can help the port authorities to protect and control port facilities against corrosion. The calculation of this index can also be an additional motivation to minimize the pollution sources.

6. Data on Public Display Panel

To better communicate the harbor water pollution risk with the personnel and public, a large public display panel was installed in the administrative area of Rajaee Harbor, presenting the online water quality index (WQI) based on the real-time data from online monitoring station. This is expected to increase the public awareness to cooperate with port authorities in reduction of the water pollution in the harbor.

7. References

[1] Amir-Heidari, P., Raie, M., Hajisalimi, Z., Nemati, M.H. (2016) ONLINE MONITORING OF WATER QUALITY IN SHAHID-RAJAEE HARBOR– PART I: DESIGN AND CONSTRUCTION

[2] https://sites.google.com/a/apaches.k12.in.us/mr-evans-science-website/accuracy-vs-precision , (Accessed May 2016)

[3] Abbasi, T., Abbasi, S., Water Quality Indices, 1st Edition, Elsevier, 2012.

[4] Canadian Water Quality Guidelines for the Protection of Aquatic Life. CCME Water Quality Index 1.0, Technical Report. Canadian Council of Ministers of Environment, 2001.

ASSESSING SEDIMENT QUALITY OF ASSALUYEH AND BASSATIN ESTUARIES (NAYBAND BAY, BUSHEHR PROVINCE)

Mohammadreza Gharibreza[1], Hamid Davoody[2] and Razieh Lak[3]

1) River and Coastal Engineering, Soil Conservation and Watershed Management Research Institute, Tehran, Iran, gharibreza4@yahoo.com
2) River and Coastal Engineering, Soil Conservation and Watershed Management Research Institute, Tehran, Iran, hamid_davoody@yahoo.com
3) Research Institute for Earth Sciences, Geological Survey of Iran, Tehran, Iran, lak_ir@yaho.com

1. Introduction

Estuaries are sensitive coastal environments to pollution where ecological features have controlled by quality of water and sediment sources. These environments are facing to contamination, shoaling, seasonal flash floods, storm surge, blockage of inlets, and anthropomorphic changes. Coastal sedimentary environments at the north of the Persian Gulf were affected since last two decades by rapid growth of industrial plants and land development projects ([1] [2]). Geochemical techniques have widely used for evaluation of natural and artificial issues at sedimentary environments ([3] [4]). Dramatic changes in chemical composition of specific sediment layers (Key horizons) have brought the useful information for interpretation of natural and anthropogenic events ([5]).

Comparison of heavy metal concentrations with the threshold limits of standard guidelines is well-known method for assessment of ecological risks for human health and aquatic life ([6] [7] [8]). Therefore, the research objectives were designed to find out the most effective anthropogenic events in geochemical variations of sediments since the last two decades and to assess ecological risks based on quality of sediments.

2. Study area

Bastian and Assaluyeh estuaries are located at Nayband bay, north of the Persian Gulf, between 52˚3′ and 52˚42′ E longitude and 27˚22′ and 27˚29′ N latitude (Fig, 1). According to morphological classification [9], these estuaries are bar-built estuaries where enclosed by a sandy bar. Overall morphology of the Nayband bay coasts represents a wave-dominated shoreline where sandy bars have been developed parallel to shoreline. Gavbandi river with 1166 km^2 catchment area and annual water discharge of 49 MCM is responsible for annual sediment transport of 685 ton toward the Nayband bay [10].

3. Material and methods

In total, 27 superficial sediment samples were collected from sedimentary facies using deterministic method. Eight sediment core samples were taken to identify vertical variations in geochemistry and physical properties, and to assess quality of sediments. In total, 120 subsamples of sediment cores as well as 27 superficial samples were prepared for digestion. Preparation steps was carried out based on the method 3052 [11]. Besides, total organic matter was obtained for each sample using Walkley method [12]. Pearson correlation coefficient and agglomerative hierarchical cluster (HCA) analysis were applied to find correlation between groups of heavy metals and the relative sources of contaminants. Sediment quality indices (LEL, TEL and ERM) were used to assess the overall pollution status at estuarine and river environments.

4. Results

Sediment quality indices for coastal and marine environments (TEL and ERM) have proved ecological risk along the entire sediment columns of the Assaluyeh and the Bassatin estuaries. Agglomerative hierarchical clustering helpfully revealed significant correlation between oil-associated heavy metals and alkali terrestrial metals. Reasons for chemical composition of key horizons were determined by correlation between anthropogenic changes and geochemical variations in concentration of heavy metals.

The present research has revealed one major and two minor groups of elements bonded to the terrestrial sediments and to the oil-components. The major group includes As, Ba, Cd, Co, Cr, Cu, La, Li, Mn, Ni, P, S, Ti, Zr with significant positive correlations among these elements. There are significant negative correlation between these elements and TOC content. On the other hand, moderate positive correlation between organic matters and mercury with concentrations upper than ERM limit brings toxic condition for dwelling organisms and relevant food chain animals. Overall upward increase in concentration of heavy metals in the sediment columns of the Assaluyeh estuary and the Bassatin estuary has been commenced from depths of 35 cm and 47 cm. Regional effects of Gulf War oil spills on coastal sedimentary environments at the Bassatin estuary, the Assaluyeh estuary, and the Gavbandi River was identified at depths of 35 cm, 29 cm, and 49 cm, respectively. Effects of oil and gas refinery industries (PSEEZ) on contamination of Bassatin and Assaluyeh estuaries were detected from depth of 27 cm along sediment

columns of the study area. Changes in morphology of estuaries and long-term drought during last decade have severely enriched metals of major group at uppermost layers (0-5 cm) where concentration of As and Ni were remarkably upper than ERM values. Annual sedimentation rate since last decades at the Assaluyeh estuary, the Bassatin estuary, and the Gavbandi River has been calculated 1.26 cm, 1.52 cm, and 2.13 cm based on key horizons.

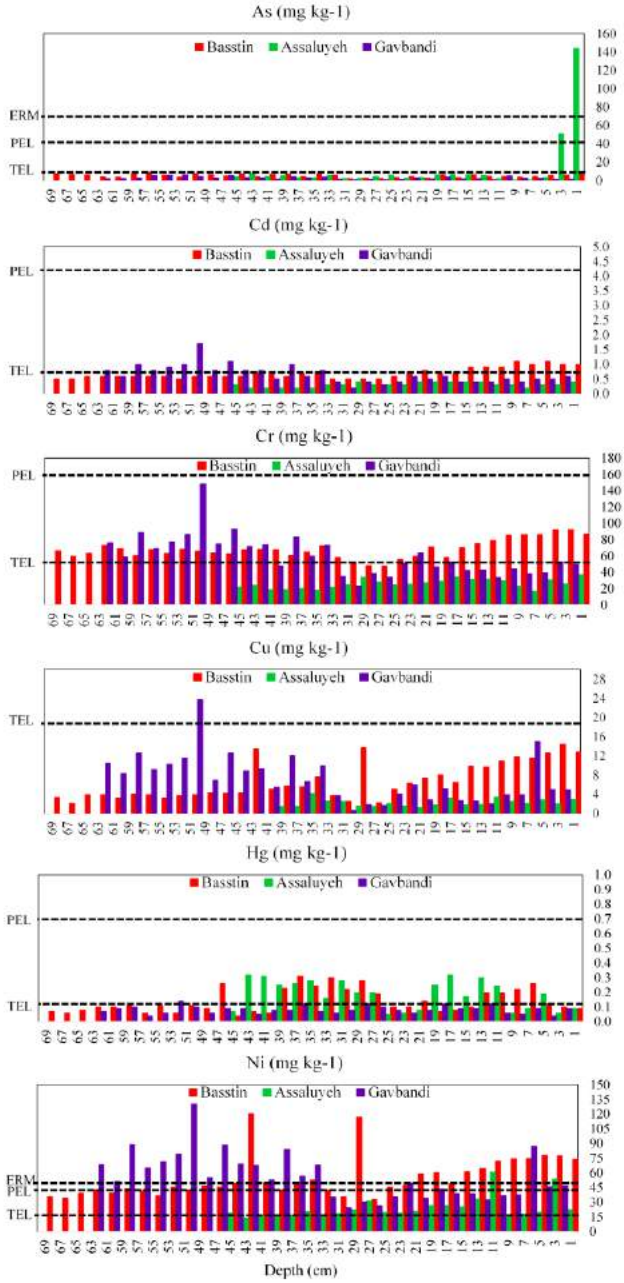

Figure 1. Sediment quality assessment of Gavbandi River, Bassatin and Assaluyeh Estuaries using sediment standard levels, TEL (Threshold effective level), PEL (Probable effective level), and ERM (Effects range median).

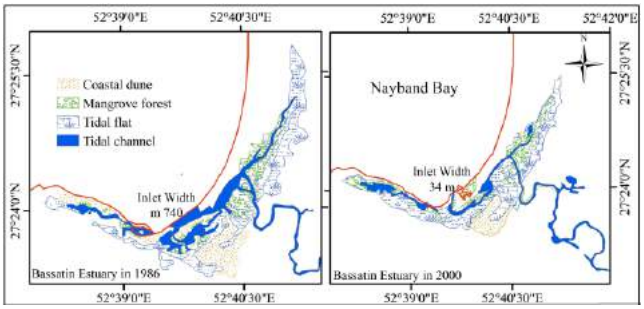

Figure 2 Showing effects of anthropogenic activities on morphology of Bassatin Estuary

5. References

1. Danehkar, A., Mashinchian, A., *Selection of Reforestation Practice for Mangrove Forests of Iran Consequent to the Persian Gulf War*. 2004, Directorate of Environmental Protection of Iran: Tehran. p. 101.
2. Gharibreza, M., et al., *Coastal processes and sedimentary facies in the Zohreh River Delta (Northern Persian Gulf)*. CATENA, 2014. **122**: p. 150-158.
3. Lee, P.-K., et al., *Metal contamination and solid phase partitioning of metals in the stream and bottom sediments in a reservoir receiving mine drainage.* Applied Geochemistry, 2013. **28**: p. 80-90.
4. Ettler, V., C. Quantin, and M. Kersten, *Applied Geochemistry special issue on Environmental impacts of mining and smelting.* Applied Geochemistry, 2016. **64**: p. 1.
5. Gharibreza, M., Raj. J. K., Yusoff, I., Ashraf, M. A, *An Evaluation of Bera Lake (Tasek Bera) Sediment Contamination Using Sediment Quality Guidelines.* Journal of Chemistry, 2013. **Open Accsess http://dx.doi.org/10.1155/2013/387025**.
6. CCME, *Protocol for the Derivation of Canadian Sediment Quality Guidelines for the Protection of Aquatic Life*, E.C.G.a.S. Division, Editor. 1995, Environment Canada, Guidelines Division, Technical Secretariat of the CCME Task Group on Water Quality Guidelines: Ottawa.
7. CBSQG, *Recommendations for Use & Application Interim Guidance*, in *Consensus-Based Sediment Quality Guidelines*, J. Dovle, Editor. 2003, Department of Natural Resources: Wisconsin. p. 40.
8. Caeiro, S., Costa, M. H,. Ramos, T. B,. Fernandes, F,. Silveira, N *Assessing heavy metal contamination in Sado Estuary sediment: An index analysis approach.* Ecological Indicators, 2005. **5**: p. 151-169.
9. Fairbridge, R.W., *The estuary: its definition and geodynamic cycle*, in *Chemistry and Biochemistry of Estuaries*, E. Olausson, Cato, I., Editor. 1980, Wiely-Interscience, John Wiely and Sons, Inc: New York. p. 1-36.
10. Lar, M., *Evaluation of Nayband national park*. 2007, Boushehr Provincial Directorate of Environmental Protection: Boushehr.
11. Kingston, H.M., Jassie, L. B, *Introduction to Microwave Sample Preparation Theory and Practice*. ACS Proffessional Reference Book Series 1998, Washington, DC: American Chemical Society.
12. Walkley, A.I., Black, A., *An examination of the Degtjareff method for determining organic carbon in soils: Effect of variations in digestion conditions and of inorganic soil constituents.* Soil science, 1934. **63**: p. 251-263.

MARITIME TRANSPORTATION ELASTICITIES OF CO2 EMISSIONS AND ECONOMIC GROWTH IN IRAN: ENVIRONMENTAL KUZNETS CURVE AND POLLUTION HAVEN HYPOTHESIS

Saeed M. Taghvaee[1], Behrouz Omaraee[2] and Vahid Mohamad Taghvaee[3]

1) Ports and Maritime Organization, Bushehr Ports and Maritime Authority, Bushehr, Iran, Email: dxbspring@yahoo.com
2) Department of Maritime Transportation, Islamic Azad University, Khark, Iran, Email: b.omaraee@gmail.com
3) Customs Administration of Iran, Bushehr, Iran, Email: vahidestan@yahoo.com

1. Introduction

Maritime transportation plays an important role both in the environmental pollution and economic growth, especially in the developing and oil-exporting economies, linked to the open sea like Iran. Many believe that ships increase the CO_2 emissions since they carry the huge bulk of cargos which requires the tremendous amount of energy, leading to greenhouse gas emissions [1]. However, the others claim that sea transportation decreases the CO_2 emissions owing to its higher capability of carrying bulk cargos, compared with the other transportation modes [2]. The direction and intensity of the relationship among maritime transportation, environmental pollution, and economic growth play a helpful role in the environmental and economic policy-making.

The main purpose of this study is to estimate the maritime transportation elasticities of the environment and economy of Iran in the short run and long run to find out the relationship between maritime transportation on the one hand, and environmental pollution and economic growth on the other hand.

2. Methodology, Model, and Data

The elasticities of environmental pollution and economics growth are estimated in short run and long run, in Iran in 1978-2012, using a dynamic log-linear model. Before running the models, the variables are put into the Augmented Dickey-Fuller (ADF) test and Granger causality test [3, 4]. The former estimates the stationarity degree of variables to avoid the spurious regression threat; and the latter detects those variables which have causal relationship with the CO_2 and GDP. It is beneficial for the model specification. After running the models, the estimated residual series are checked for the econometric classical-assumptions to analyze the reliability of the estimated coefficients.

Following Farhani, et al. (2014), Taghvaee and Hajiani, (2014), and Taghvaee and Shirazi (2014), we specify the models below [5-7].

$$LCO_{2_t} = \alpha_0 + \alpha_1 LM_t + \alpha_2 LY_t + \alpha_3 LCO_{2_{t-1}} + \alpha_4 DW + \varepsilon_t \quad (1)$$

$$LY_t = \beta_0 + \beta_1 LM_t + \beta_2 LTR_t + \beta_3 LY_{t-1} + \beta_4 MA(1) + \mu_t \quad (2)$$

where CO_2 is Carbon Dioxide emissions, M is maritime transportation, Y is GDP, and TR is trade volume; "α" and "β" show the parameters of CO_2 and GDP models which are interpreted as the elasticities of environmental pollution and economic growth; DW is the dummy variable which is 0 for the war years (1980-1989) and 1 for the remaining years; MA(1) is the Moving Average process of degree one. L is the natural logarithm; t is year; ε and μ are the residual series. In these models, α_1 and α_2 are the short run elasticities of environmental pollution and β_1 and β_2 are interpreted as the short run ones of the economic growth. The long run ones are $\alpha_1/1-\alpha_3$ and $\alpha_2/1-\alpha_3$ for the environmental pollution and $\beta_1/1-\beta_3$ and $\beta_2/1-\beta_3$ for the economic growth [8]. The estimated residual series are examined for the econometric classical-assumptions for assessing the reliability of the estimated coefficients.

The dataset is annual and derived from various versions of World Development Indicator [9], except for the maritime transportation which is come from the Central Bank of Iran [10]. The per capita sea transportation of goods, as the maritime transportation proxy and measured in ton, is the sea transportation of goods divided by the total population, derived from the latter database; the per capita CO_2 emissions, measured in metric ton, is the proxy for the environmental pollution; the per capita GDP, measured in the constant 2005 US Dollar, is the proxy for the economic growth; and trade, measured as the percentage of GDP, is the proxy for trade openness. All the data are in natural logarithm.

3. Results

Table 1 illustrates the results of the ADF test on the variables implying the stationarity of all the variables in level. All the tests are in level with 6 maximum lag length including intercept and trend in level.

Table 1- Results of the ADF unit root tests

	LM	LY	LCO_2	LTR
τ -statistic	-4.0290	-3.7746	-4.3402	-5.1688
Prob.	0.01	0.03	0.00	0.00
Stationarity	I(0)	I(0)	I(0)	I(0)

Figure 1 shows the Granger causal relationships among the variables, graphically and briefly to perceive which variables play the causal role as the endogenous variable in the CO_2 or GDP.

Figure 1- Estimated Granger causal relationships among the variables at a glance.

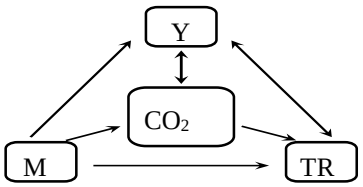

Table 3 and 4 offer the results of the CO_2 model and the GDP model, respectively.

Table 3- Results of the CO_2 model estimation

Variable	Coefficient	t-statistic	Prob.
LM	0.1959	4.8441	0.00
LY	0.2919	2.6870	0.01
LCO_{2t-1}	0.3467	2.9307	0.00
$\alpha_1/1-\alpha_3$	0.2998		
$\alpha_2/1-\alpha_3$	0.4468		

Table 4- Results of the GDP model estimation

Variable	Coefficient	t-statistic	Prob.
LM	0.0882	2.8944	0.00
LTR	0.1647	3.0201	0.00
LY_{t-1}	0.4422	5.2182	0.00
$\beta_1/1-\beta_3$	0.1581		
$\beta_2/1-\beta_3$	0.2952		

Table 5 indicates the estimated elasticities of environmental pollution and economic growth in the short run and long run in Iran, at a glance.

Table 5- Estimated elasticities of environmental pollution and economic growth in the short run and long run

Elasticities of	Environmental pollution		Economic Growth	
Period	Short	Long	Short	Long
LM	0.1959	0.2998	0.0882	0.1581
LY	0.2919	0.4468	NA	NA
LTR	NA	NA	0.1647	0.2952

4. Conclusion

This study estimates the maritime transportation elasticities of CO_2 emissions and economic growth in Iran both in long and short term during 1978-2012. The results imply that although both the CO_2 emissions and economic growth respond to the changes in the maritime transportation slightly, the response of economic growth is higher than that of CO_2 emissions. Moreover, the maritime transportation, as an economic activity, has a positive relationship with the CO_2 emissions, as an environmental pollutant, confirming the Pollution Haven Hypothesis in Iran as a developing country; and showing the position of maritime transportation on the left-hand side of the Environmental Kuznets Curve in the country. It suggests not only the environmental-improvement in the infrastructure of maritime transportation but also the stimulation of growth in that economic activity for acceleration in reaching the turning point of Environmental Kuznets Curve and transiting to the right hand-side of.

5. Acknowledgment

We express our deep gratitude towards the Bushehr Ports and Maritime Authority in the Ports and Maritime Organization of Iran which supports the research financially and spiritually.

6. References

[1] Taghvaee, V. M., and Hajiani, P., "Environment, energy, and environmental productivity of energy: a decomposition analysis in China and the US ", *Second European Academic Research Conference on Global Business, Economics, Finance and Banking*, 3-5, July 2015.

[2] International Maritime Organization, 2016, Available at: http://www.imo.org/en/OurWork/Environment/PollutionPrevention/AirPollution/Pages/Default.aspx

[3] Taghavee, V. M., Aloo, A. S., and Shirazi, J. K., "Energy, Environment, and Economy Interactions in Iran with Cointegrated and ECM Simultaneous Model", *Procedia of Economics and Finance*, 36, 2016, pp 414-424.

[4] Greene, W. H., "Econometric Analysis", Pearson, 7th edition, 2012.

[5] Farhani, S., Chaibi, A., and Rault, C., "CO2 emissions, output, energy consumption, and trade in Tunesia", *Economic Modelling*, 38, 2014, pp 426-434.

[6] Taghavee, V. M., and Shirazi, J. K., "Analysis of the relationship between economic growth and environmental pollution in Iran (evidence from three sections of land, water and atmosphere)", *Indian Journal of Scientific Research*, 7(1), 2014, pp 31-42.

[7] Taghavee, V. M., and Hajiani, P., "Price and income elasticities of gasoline demand in Iran: Using static, ECM, and dynamic models in short, intermediate, and long run", *Modern Economy*, 5, 2014, pp 939-950.

[8] Sene, S. O., " Estimating the demand for gasoline in developing countries: Senegal ", *Energy Economics*, 2012, pp. 189-194.

[9] World Development Indicator, World Bank, 2014, Available at: http://www.data.worldbank.org

[10] Economic Research and Policy Department of Iran, *Central Bank of the Islamic Republic of Iran*, Economic Time Series, Database, Available at http://tsd.cbi.ir/

NUMERICAL SIMULATION OF HNS SLICKS TRANSPORT IN CASPIAN SEA

Farzaneh Gardounzadeh[1], Mohammad Raei[2]

1) MSc Student, Civil Engineering department, Sharif University of Technology, Tehran, Iran, gardounzadeh.farzaneh@gmail.com
2) Assistant Professor, Civil Engineering Department, Sharif University of Technology, Tehran, Iran, raie@sharif.edu

1. Introduction

Caspian Sea with its particular circumstances including enclosed inland body of water which has no outflows, is known as a fragile and vulnerable aquatic environment. Therefore this body of water has a great environmental importance which in recent years has been threated by biological and hydrocarbon pollution entrance from offshore and inshore pipelines and structures due to sea accidents or decay although there are another hydrocarbon pollution sources according to table 1 (Korotenko, Mamedov, Kontar, & Korotenko, 2004).

By the way Caspian Sea is bordered by 5 countries Iran, Russia, Kazakhstan, Azerbaijan and Turkmenistan has 384,400 km2 surface area and two deep basin in the middle and near south coast (Figure 1). Because of Volga River in the north part of Caspian Sea, the major freshwater input, the salinity is zero and it increases by going southward up to 14 ppm (Korotenko et al., 2004; Korotenko, Mamedov, & Mooers, 2000, 2001). There are cyclonic circulations over deep part of the sea (Figure 1) (Korotenko et al., 2001).

Indeed as long as the amount of hydrocarbon shipping has been increased, the shipping spill became one of the sources of pollution. In recent years Amirabad port has been changed to one of the most important harbors in Caspian Sea in transporting the chemicals and hydrocarbon products. In the first three months of year 1394, near 130,000 tone gasoline and oil were imported to Iran through Caspian Sea that Amirabad was the main destination. Thus there is a high probability of any events in sea due to the bad weather or ship's technical problems, resulting large amount of hydrocarbon contamination spill in water especially on transit ways. As a result, simulating the Caspian Sea currents and wave with considering the weathering processes as the main factors in transporting and fate of spilled hydrocarbon pollution slicks, is necessary in case of shipping spill events. In addition to having a proper knowledge about movement of pollution slicks achieving from sea water simulation, has a great usefulness in crisis management in case of hydrocarbon pollution spill particularly Iran is one of the five Caspian littoral states rectified Tehran Convention to support the protection of the Caspian Sea marine environment from hazardous substances which have irrecoverable effects on health of sea water.

In this article we try to evaluate the risk of the beaching slicks especially in Mian Kaleh region approximately near Amirabad port as an environmentally important land.

Key words: Caspian Sea, simulation, MIKE 21, gasoline

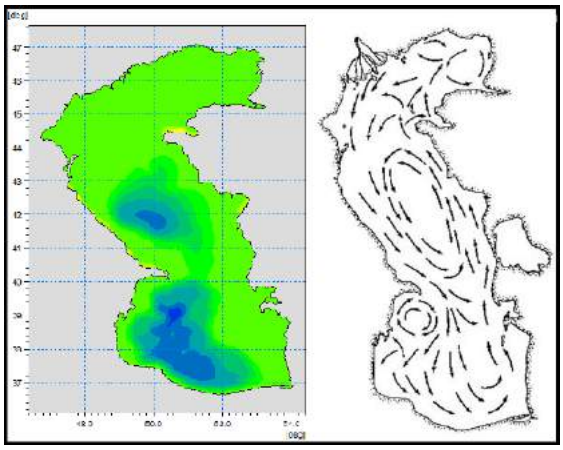

Figure 1: Caspian Sea. Right: general circulation. Left: bathymetry and location of two main basins (Korotenko et al., 2001).

2. Model Discription

In this study currents have been modeled and generated by MIKE 21 developed by Danish Hydraulic Institute, Water and environment, Denmark. This 2D numerical model uses cell-centered finite volume method to solve the essential equations. Mike 21 and OS[1] module implement lagrangian point of view to track the pollution slicks (www.mikepoweredbydhi.com). Indeed lagrangian point of view is used in most of spill modeling in which the integrated slicks are assuming the separated particles (Zafirakou, Palantzas, Samaras, & Koutitas, 2015). Averaged Navier-Stokes equations in 2 dimensions are the governed equations are solved by Mike 21 accompanied by Boussinesq and hydrostatic pressure consideration. The flow chart shows the process of pollution slick transportation simulation in MIKE 21 (**Error!**

[1] Oil Spill

Reference source not found.) (Verma, Wate, & Devotta, 2008).

Table 1: Other sources of oil pollution.

Sources	Oil, tons/year
River	75,000
Municipalities	19,000
Industries	28,000
Atmosphere	350
Total	122,350

2.1. Governing Equation

Conservation of mass, conservation of energy and conservation of momentum are the most important equations for hydrodynamic modeling. With assuming non compressible fluid the Navier-Stocks equations will achieve from momentum equations.

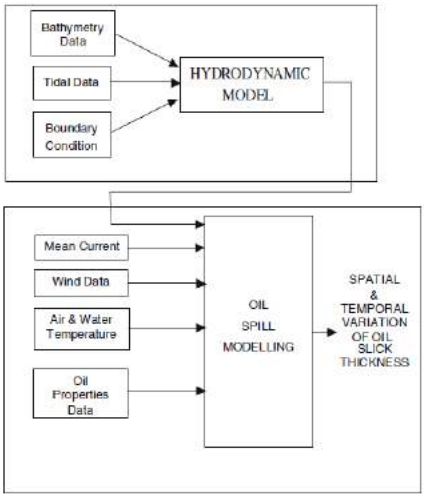

Figure 2: Flowchart for hydrodynamic and oil spill simulation (Verma et al., 2008).

3. Meteorology

Scenario contains a hypothetical spill due to an overturned ship in which amount of gasoline are released to the sea water. For simulating this event bathymetry data, meteorological data, oceanographic data and geomorphologic data area needed in addition to some information about physical and chemical characteristics of pollutants. Bathymetry data and meteorological data in winter are retrieved from ETOPO1 and ECMWF websites respectively. The tidal current in Caspian Sea is negligible.

The 2D simulation has been run by assuming gasoline spill, as an example of hazardous substances, shipping spill in winter, on the transit way from Amirabad port in south part of Caspian Sea.

At first general triangle flexible mesh (**Error! Reference source not found.**), then local more fine mesh near the southern coasts with high probability of contamination, has been generated.

4. Results

The items bellow can be the expected results from this study:

- ✓ Duration of presence of gasoline slicks on the sea surface
- ✓ The probable contaminated land and beaches
- ✓ The time that gasoline beaching takes
- ✓ The time that gasoline evaporation takes

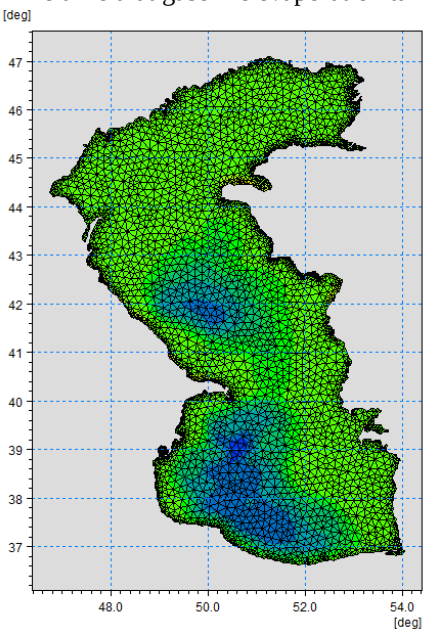

Figure 3: Caspian Sea, general mesh.

5. References

Korotenko, K., Mamedov, R., Kontar, A., & Korotenko, L. (2004). Particle tracking method in the approach for prediction of oil slick transport in the sea: modelling oil pollution resulting from river input. *Journal of Marine Systems, 48*(1), 159-170.

Korotenko, K., Mamedov, R., & Mooers, C. (2000). Prediction of the dispersal of oil transport in the Caspian Sea resulting from a continuous release. *Spill Science & Technology Bulletin, 6*(5), 323-339.

Korotenko, K., Mamedov, R., & Mooers, C. (2001). Prediction of the transport and dispersal of oil in the south Caspian Sea resulting from blowouts. *Environmental Fluid Mechanics, 1*(4), 383-414.

Verma, P., Wate, S. R., & Devotta, S. (2008). Simulation of impact of oil spill in the ocean–a case study of Arabian Gulf. *Environmental monitoring and assessment, 146*(1-3), 191-201.

Zafirakou, A., Palantzas, G., Samaras, A., & Koutitas, C. (2015). Oil spill modeling aiming at the protection of ports and coastal areas. *Environmental Processes, 2*(1), 41-53.

NUMERICAL STUDY of UNDERWATER DISTRIBUTION of OIL SPILLED from DEEPWATER AREA

Seyedhamzeh.Mirkhalili[1], Said.Mazaheri[2]

1) Ocean Engineering and Technology Research Center, Iranian National Institute for Oceanography and Atmospheric Science, Tehran, Iran, mirkhalili.phd@gmail.com
2) Ocean Engineering and Technology Research Center, Iranian National Institute for Oceanography and Atmospheric Science, Tehran, Iran, said.mazaheri@gmail.com

1. Introduction

The offshore oil production has increased significantly in the last several decades with the worldwide increasing demand for oil and dwindling onshore reserves. Exploration of oil and gas in offshore regions as well as the oil transportation through pipelines increase the risk of underwater oil spills. In oil spills due to underwater accidents, such as a broken oil pipeline or an oil well blowout at the sea bed, oil usually behaves as a submerged buoyant jet. Underwater blowouts often contain a mix of oil and gas. The advection/diffusion equation is not valid for simulating the oil trajectory and dispersal pattern until oil reaches the far field [1,2]. Based on a Lagrangian integral technique and Lagrangian particle-tracking technique, a numerical model was developed to simulate the underwater transport of oil from a deepwater spill in Matlab programming environment. This model comprises two submodels: a plume dynamics model and an advection-diffusion model. The former is used to simulate the stages dominated by the initial jet momentum and plume buoyancy of the spilled oil, while the latter is used to simulate the stage dominated by the ambient current and turbulence. The model validity was verified through comparisons of the model predictions with experimental and field data.

2. Model Formulation

The oil spill model presented in this paper consists of two submodels: the plume dynamics model (PDM) and the advection– diffusion model (ADM). PDM is used to simulate both the turbulent jet and buoyant plume stages, during which the mixture of water and a certain amount of spilled oil is treated as an entirety and the interaction between the oil and ambient water is considered. The remaining advection-diffusion stage is simulated by the ADM, where the spilled oil is divided into a large number of discrete particles.

2.1. Plume dynamics model (PDM)

In this model, a Lagrangian element is defined as a control volume moving along the centerline of the buoyant jet. The element moves with its local centerline velocity. Therefore, the element thickness is $h = \left|\vec{V}\right|\Delta t$, and its mass is $m = \rho \pi b^2 h$, in which, $\vec{V}$, b , and ρ are local velocity, radius, and density of the buoyant jet, respectively; Δt = time step.

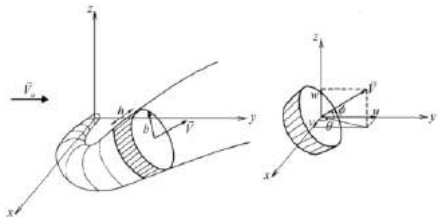

Figure 1. Sketch of control element of plume dynamics model [1].

The mass, momentum governing equations are applied to the control volume.

2.2. Advection-diffusion model (ADM)

When the oil plume travels upwards to a certain depth level, its density can be very close to that of the ambient water because a large amount of water will have been entrained into the plume. In a density stratified water environment, the ambient seawater is denser in the deeper regions than nearer the surface. Denser seawater is entrained into the plume in the deeper regions, and as the oil plume rises to the depth where the seawater is less dense, the fluid of the plume may reach a neutral or even a negative buoyancy level below the sea surface. Therefore, instead of following the mechanism of plume dynamics, the advection-diffusion mechanism of the ambient flow will dominate the behavior of the spilled oil and the buoyant PDM will no longer be applicable. Consequently, the ADM will be employed to simulate the transport of the spilled oil. The governing equation of the advection-diffusion mechanism can be written as

$$\frac{\partial C}{\partial t} + \vec{V}.\nabla C = \nabla \cdot \left(\vec{K} \cdot \nabla C\right) + \sum_{i=1}^{m} S_i \qquad (1)$$

where C is the oil concentration (mass fraction of oil

content) in the water column, $\vec{V}$ is the advection velocity vector(m/s), ∇ is the gradient operator, $\vec{K} = (K_x, K_y, K_z)$ is the turbulent diffusion tensor in water (m^2 /s), and K_x, K_y, K_z are the diffusion coefficients in the x, y, and z directions, respectively. In the present model, the Lagrangian particle- tracking algorithm is used to simulate oil transport in the advection-diffusion stage. The 3D movement of an oil particle is determined by the following relationship:

$$\frac{dS}{\partial t} = \vec{V} + \vec{V'} + w_b \hat{k} \qquad (2)$$

Where $\vec{S} = (x, y, z)$ is the displacement vector of an oil particle; x, y, and z are the Cartesian coordinates; $\vec{V}$ is the advection velocity due to the combined effects of the current and waves within the water column; $\vec{V'}$ is the diffusion velocity due to the turbulent diffusion process; w_b is the buoyancy velocity of the oil particles; and $\hat{k}$ is the unit vector in the vertical direction.

3. Results

In Fig.3, the model predictions of the jet trajectories (PDM) are compared with the experimental data provided by Hirst (1972) [3]. In the three cases, the numerical results are in good agreement with the experimental data.

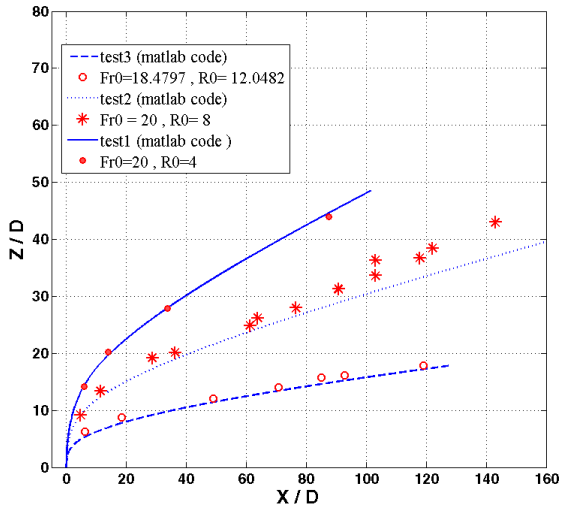

Fr0=initial froude number, R0=jet velocity/ambient velocity

Figure 2. Trajectories for oil spilled in an unstratified flowing environment [3]

To complete the model verification, in this section, another set of data from a larger-scale field experiment is employed to calibrate the other submodel ADM. The data used here are from a field experiment performed off the coast of Norway in 1995 by IKU, in conjunction with Norwegian Clean Seas (NOFO) in Norway, Esso Norge, and Norsk Hydro, with the aim of simulating oil release from a ruptured pipeline that have good agreement with present study as shown in Table 1.

Table 1. Field experimental parameters [4]

Release.

Release depth	107 m
Starting time	8:10
Release duration	25 min
Release rate	1 m^3/min
Release velocity	2.1 m/s
Nozzle diameter	0.101 6 m
Oil density	893kg/m^3

The oil is released vertically upwards.

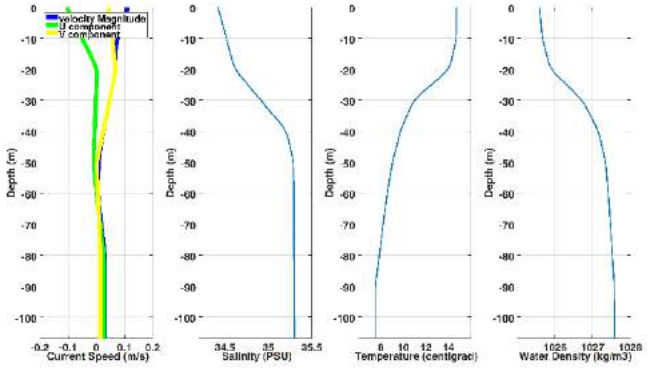

Figure 3. Vertical profiles of Salinity, Temperature, Current Speed and Potential Density in field experiment [4]

Table 2. Comparison of Some Model Computed Parameters with Values from Field Experiments.

Parameter	Neutral Buoyancy Level (m)	Time to Reach water surface (min)
Present model	53.9	12
Field experiment [4]	50-60	10.0

4. References

[1] LEE, J. H. W. and CHEUNG, V., "Generalized Lagrangian model for buoyant jets in current", *Journal of Environmental Engineering, ASCE*, 116, 6, July 1999, pp. 1085-1105.

[2] YAPA, P. D. and ZHENG, L., "Simulation of oil spills from underwater accidents I: model development", *Journal of Hydraulic Research, IAHR*, 35, 5, May 1997, pp. 673-688.

[2] Hirst, E. 1972., "Buoyant jets with three-dimensional trajectories", Journal of Hydraulic Division, 98, 11, November 1992, pp. 1999-2014.

[4] RYE, H., "Model for calculation of underwater blow-out plume", in *Proceedings 17th AMOP Arctic and Marine Oil Spill Program Technical Seminar*, Canada, June 8–10 1994, pp. 849-849.

ASSESSMENT THE METHODS FOR PULLING OUT OF SUNKEN SHIPS BY CONSIDERING ENVIRONMENTAL ISSUES

Vahid Hadipour[1], Freydoon Vafaie[2]
1) Civil Engineering Faculty, K.N. Toosi University of Technology, Tehran, Iran, vahid.hadipour85@gmail.com
2) Civil Engineering Faculty, K.N. Toosi University of Technology, Tehran, Iran, fvafai@kntu.ac.ir

1. Introduction

Nowadays, there are many sunken ships in the seas and oceans environment, which should be pulled out as soon as possible because of maritime safety, environmental pollution, preventing of morphological changes in the seabed, and accessing to their beneficial materials by scraping. In addition, international and regional conventions force nations to salvage these vessels. To ensure that the pulling out is successful; there is an urgent need for appropriate methodology to assist planners to pull out the sunken ships. One of the most important issues for pulling out of sunken ships is that to notice the negative environmental impacts. Selecting of pulling out method can be viewed as an environmental problem. So, in this paper three methods for pulling out of sunken ship (Nearby the Khark Island, Persian Gulf, Iran) are investigated and finally best method has been selected.

2. Materials and Methods

In this study, an environmental assessment model is implemented to find the best alternative for pulling out sunken vessel in Iran as a case study (West of Khark Island, Persian Gulf, Iran). This area is one of the most sensitive marine ecosystems as there are a lot of coral reefs nearby the study area. For this purpose, at first, three different methods are compared considering advantages and disadvantages in terms of environmental issues and implementation phase. Then, after selecting the appropriate method, an environmental assessment model with different levels (environmentally sensitive items and environmental destructive factors) is made to decrease the adverse effects on the environment.

2.1. Investigating of pulling out methods

2.1.1. One by one floatation

This method is usually used for salvaging the wooden ships that are so important in terms of archeological aspects. In this method, the all body once is pulled out of place and so there is no damage to the body [1]. On the other hand, by using this method the sunken ship is salvaged without any changing in scale and is pulled out by the crane. During this time, using airbags and balloons is not allowed. Some advantages and disadvantages of this method are listed as follows:

- Advantages: Low risk operation, short and appropriate time for implementation, applicable to ships in terms of archaeological and historical importance, absence of adverse consequences arising from its operations and cutting.
- Disadvantages: Creating high turbidity due to suddenly detachment during pulling out from seabed.

2.1.2. Flotation without fundamental changes in the body

This is a commercial method that using airbags and balloons is permitted during salvage operation but any drilling that caused the release of oil and toxic pollutant, is not allowed. In this method, firstly the reservoirs are identified, sealed and after ensuring that no leakage takes place the salvage operation will be started by cutting in some points [2]. This method has many advantages and disadvantages that are mentioned in the following:

- Advantages: No cutting operations and adverse consequences arising from it, short and appropriate time for salvaging, low risk operations
- Disadvantages: Creating high turbidity due to suddenly detachment during pulling out from seabed, relatively high operation cost, lack of safety in transit to scrap yards (long route, very low transfer speed and the probability of collision with underwater hills), making new environmental challenges after grounding on the coast (decreasing maritime safety, creating environmental pollution in the new place, etc.).

2.1.3. Flotation by body cutting

This method is appropriate for the vessels which have scraping capability and cranes cannot pull out them. Unlike the previous method (floatation without fundamental changes in the body), in this method there is no matter where the body is cut, because body is supposed to be used for scraping and recycling [3]. In this method, cutting is done based on hot cutting (high temperature) and wire cutting (cold cutting).

In hot cutting method, vessel body is separated under high temperature and toxic gases released at the site during cutting operations and water temperature will be increased around the environment. In wire cutting method, first cut points are identified by diving team and then cut jacks are fixed beside the sunken ship and on the barge. Finally, industrial diamonds are placed in the ring and ship body is cut by reciprocating motion of the pistons [4,5]. This method has high safety and is also called no-heat method. Wire cutting method steps has been shown schematically

in below figures. Like two previous methods, floating by body cutting (hot and wire) has its strengths and weaknesses that are described as follows:

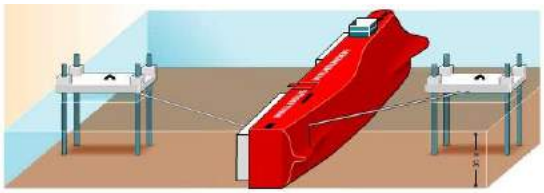

Figure 2. Wire cutting under water

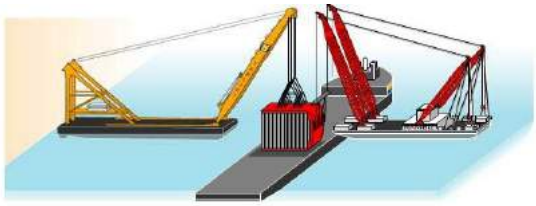

Figure 3. Handling cut pieces and transport by barge

A. Hot cutting

- Advantages: Short and appropriate time for salvaging
- Disadvantages: Creating high thermal pollution, emission of toxic pollutant and risk of explosion due to the presence of oil in some reservoirs.

B. Wire cutting

- Advantages: No toxic gas emissions, no thermal pollution, high safety, creating low turbidity during raising piece.
- Disadvantages: Cost of the project, long time operation.

3. Results

Polling out of this sunken oil ship around the Khark Island in Persian Gulf, has positive and negative effects on the physical, biological, and economic environment of study area especially on coral reefs.

Environmental destructive factors in this project include:

A1: Transfer of cut pieces of the ship from the seabed to the barge; A2: Pollution caused by ships, cranes and lifting equipment traffic; A3: Solid waste generated by the staff and workers; A4: Wastewater produced by the staff and workers, A5: Noise pollution caused by the project; A6: Chip production caused by the wire cutting, A7: Oil wastewater effluents from devices activities; A8: Probable spread of solid fuels in the tanks of ships; A9: Oil spills.

Environmentally sensitive items, which may be affected by pulling of sunken ship include:

A: Sea water quality; B: Air quality; C: Noise quality; D: Natural landscape of seabed; E: Benthic communities; F: Sea turtles; G: Coral ecosystems; H: Persian Gulf mangrove forest; I: Protected areas; J: Marine mammals; K: Fish and spawning areas; L: Beach landscape.

3.1. The impact analysis of project implications

In Table 1, the environmental implications of the project are fully described. Environmental impact assessment of pulling of sunken ship has been done based on a matrix provided by the opinion of experts, and finally the wire cutting method was selected as an appropriate method on this case. This method has the least environmentally risk on the case study environment especially on coral reefs (west of Khark Island) and also safety is relatively high.

Table 1. The effective factors on project environment

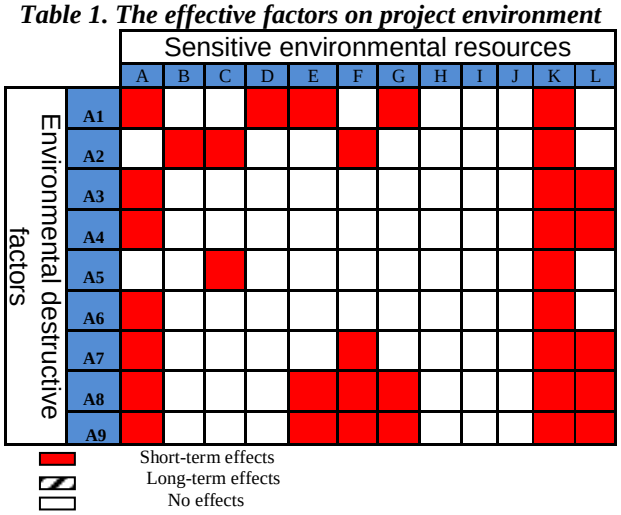

4. Conclusion

Pulling out of sunken ship has positive and negative effects on the physical, chemical, biological and socio-economic environment. So, using previous studies and field survey, physical-chemical parameters, socioeconomic and biological factors should identify to assess the effects of pulling out sunken ship on these parameters.

One of the major issues during the salvage operational, is creating turbidity caused by the movement of ships from seabed and because of the proximity to sensitive coral habitats, this must be considered for selecting the method.

The results showed that the fragment of ship body by means of underwater cold cutting equipment is the best alternative for pulling out of this sunken ship, followed by flotation with airbag approach.

Considering all the positive and negative environmental effects of the project, generally the project implantation can be assessed positive concerning selecting method (wire cut), appropriate time for pulling out, robust monitoring system during operation and also applying strategies to reduce environmental impacts. Overall, the negative impact of projects is short-term and negligible.

References

[1]http://www.titansalvage.com.

[2]http://www.smit.com.

[3]http://www.marinesalvage.com/overview/index.asp?page=wreck_removal.htm.

[4] http://www.tricolorsalvage.com/pages/infographic.asp.

[5] Driver F., and Martins L, 'Shipwreck and salvage in the tropics' Journal of Historical Geography, Vol. 32, pp. 539-562, 2006.

INVESTIGATION ON ABSTRACTION-DESALINATION-RECHARGE CONTROLING METHOD OF SEAWATER INTRUSION AT ASALUYEH COASTAL AQUIFER

S. Sadjad Mehdizadeh[1], Masoud Pour Asghar[2], Amir Davazdah Emami[3] and Freydoon Vafaie[4]

1) Civil Engineering Group, Islamic Azad University, Central Tehran Branch, Tehran, Iran, Email: Saj.Mehdizadeh@iauctb.ac.ir
2) Marine and Coastal Environmental Group, Sahel Consulting Engineering Company, Tehran, Iran, Email: Masoudpourasghar1364@gmail.com
3) Marine and Coastal Environmental Group, Sahel Consulting Engineering Company, Tehran, Iran, Email: a_demami@yahoo.com
4) Civil Engineering Faculty, K.N. Toosi University of Technology, Tehran, Iran, Email: Fvafai@kntu.ac.ir

1. Introduction

Population growth and scarcity of coastal freshwater resources have increased the stresses on many coastal aquifers, leading to aquifer storage decline and seawater intrusion (SWI) [1, 2 and 3]. Controlling or predicting SWI under future climatic or anthropogenic scenarios requires mathematical tools. This research deals with the current quality condition of Asaluyeh coastal aquifer located at Boushehr Province, south of Iran. The amount of Persian Gulf SWI is simulated using dispersive approach. Gavbandi river recharge, adjacent groundwater inflows as boundary condition, rainfall recharge and all distributed wells are included at the simulations.

In the literature, multiple methods have been proposed for controlling SWI including reduction of pumping rates, relocation of pumping wells, use of subsurface barriers, natural recharge, artificial recharge and abstraction of saline water [4, 5]. A new controlling method is developed at this study to control SWI effectively. This methodology ADR (Abstraction, Desalination and Recharge) includes abstraction of seawater, desalination of seawater using common methods such as reverse osmoses and recharge of a part or all of the excess desalinated water to the aquifer while the rest of the desalinated water can be used for domestic consumption (Fig. 1).

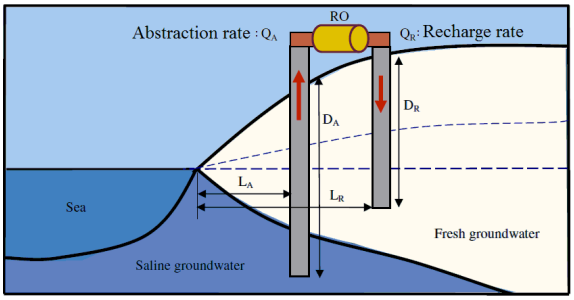

Figure 1. The ADR Controlling method layout [5]

2. Material and Methods

At dispersive approach, freshwater and saltwater are assumed to be in a dynamic equilibrium resulting from advection and dispersion of solute within the aquifer. The equation of flow and solute transport is solved simultaneously and head and salt concentration distribution in the aquifer derived from the simulation. The present study used the finite-difference model SEAWAT developed by Langevin et al. [6] to simulate three-dimensional, variable density, transient groundwater flow at Asaluyeh aquifer. It combines the modified MODFLOW and MT3DMS into a single program that solves the coupled groundwater flow and solute transport equations.

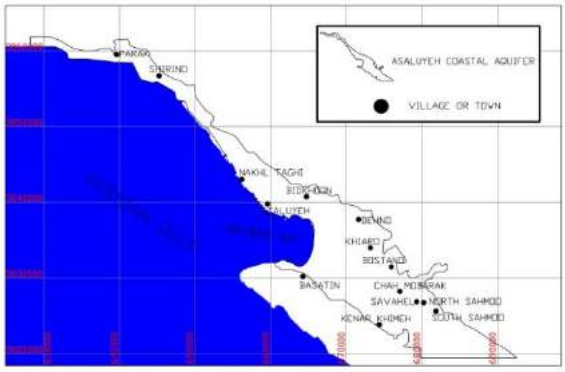

Figure 2. Plan view of Asaluyeh Coastal aquifer

The aquifer geometry is presented at Fig.2. Constant Persian Gulf head values of 1.2 m were adopted at the seaside boundary. Constant 2.15 m^3/d freshwater inflow is imposed at the involved cells of inland boundary. The uniform grid size ($\Delta x = \Delta z = 500$ m) adopted for the aquifer plan with 13 layers of 5m thickness at aquifer depth. The hydraulic conductivity considered 20 m/d at aquifer north side decreasing to 5 m/d near the seaside. Rainfall recharge obtained to be 19.2 mm/yr and all Gavbandi river characteristics including river conductance, riverbed

thickness and water level elevation entered to SEAWAT model.

3. Results and Discussion

Steady-state simulation demonstrated that regarding the distribution of wells in the aquifer, groundwater in many areas is not suitable for drinking or irrigation. The villages and towns near the beach at the western part of the aquifer (i.e. Parak, Shirino, Nakhl Taghi and Asaluyeh) are quite brackish (0.3 to 0.6 of seawater). This condition with less severity happened at the heartland rural areas (e.g. Bostano with 0.15 to 0.3 of seawater) and less at Chah Mobarak village (0.05 to 0.1 of seawater). Due to small extraction of water and the distance to coastline, groundwater under villages in eastern regions (e.g. North and South Sahmoo, Bandou and Kenarkhimeh) is desirable for using and seawater is not intruded at these areas.

By the ADR methodology, it is found that the injected water cannot completely push back the saline water even if the whole capacity of Asaluyeh desalination development plant (i.e. 7000 m^3/d) is being used. However, the ADR method operates effectively around the recharge well and the greatest impact occurred at the topmost layer.

Sensitivity analysis of different abstraction-recharge rate, longitudinal and altitudinal well position has been applied to the model. It is observed that changing the height of the recharge well has no meaningful effect on salinity amount and distribution. At these cases, the injected freshwater moves toward the upper layers due to its lighter density and hence cannot influence the results.

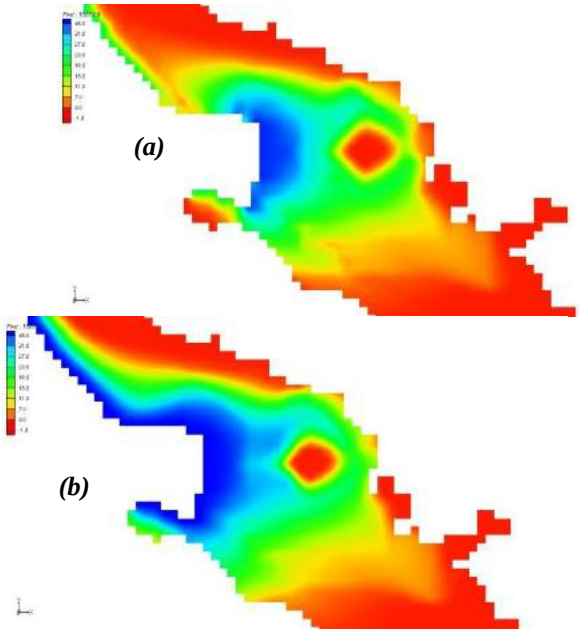

Figure 3. The ADR result after 50 years simulation around Nayband Bay. The recharge well is located at high permeability zone. (a) The highest and (b) the lowest layer.

In terms of radius of influence (R_i), placing the recharge well at high permeability area causes growth of R_i and large areas of saline water leave the aquifer earlier compare to low permeability regions (Fig. 3). It should be noted that locating the recharge well away from the desalination plant increases the water conveyance system cost and undermine the economic plan. At the end, it is shown that by choosing multiple points as a recharge well, the ADR method efficiency grows significantly and the groundwater level increases noticeably.

4. Conclusion

At this study, a new controlling method included abstraction of saline water, desalination and recharging is developed to investigate controlling seawater intrusion in Asaluyeh coastal aquifer. It is concluded that by the ADR method the saline water start to go back toward the Persian Gulf effectively but it needs high freshwater injected amount. Therefor areas with deep seawater intrusion need high recharged freshwater that cause high desalinization cost.

5. References

[1] Bear, J., Cheng, A.H.-D., Sorek, S., Ouazar, D., Herrera, I., 1999. Seawater Intrusion in Coastal Aquifers-Concepts Methods and Practices, vol. 14. Springer Publication, 627 p.

[2] Feseker, T., 2007. Numerical studies on saltwater intrusion in a coastal aquifer in northwestern Germany. Hydrogeol. J. 15, 267–279.

[3] Werner, A.D., Zhang, Q., Xue, L., Smerdon, B.D., Zhu, X., Li, X., Yu, L., Li, L., 2013. An initial inventory and indexation of groundwater mega-depletion cases. Water Resour. Manage. 27 (2), 507–533.

[4] Todd, D.K., 1974, Salt-water intrusion and its control. Water Technology/Resources. J Am Water Works Assoc., 66:180–187.

[5] Abd-Elhamid, H.F., Javadi,A.A., 2011, A Cost-Effective Method to Control Seawater Intrusion in Coastal Aquifers, Water Resour Manage, 25:2755–2780.

[6] Langevin, C.D., Thorne Jr, D.T., Dausman, A.M., Sukop, M.C., Guo, W., 2008. SEAWAT Version 4: A computer program for simulation of multi-species solute and heat transport: U.S. Geological Survey Techniques and Methods, Book 6, Chap. A22, 39 pp.

EVALUATING POTENTIAL RISK of INTRODUCTION of NONINDIGENOUS DINOFLAGELLATES, ASSOCIATED with BALLAST WATER RELEASED by DOMESTIC VESSEL TRANSITING to CANADIAN ARCTIC WATERS

Frédéric Laget[1], André Rochon[1], Kimberly Howland[2], Nathalie Simard[3], Sarah Bailey[4]

1) Université du Québec à Rimouski - Institut des sciences de la mer (UQAR-ISMER), Rimouski, QC G5L 3A1, frederic.laget@uqar.ca
1) Université du Québec à Rimouski - Institut des sciences de la mer (UQAR-ISMER), Rimouski, QC G5L 3A1, Andre_Rochon@uqar.ca
2) Freshwater Institute, 501 University Crescent, Winnipeg, MB, R3T 2N6, Kimberly.Howland@dfo-mpo.gc.ca
3) Institut Maurice-Lamontagne, 850 Route de la Mer, C.P. 1000, Mont-Joli, QC, G5H 3Z4, Nathalie.Simard@dfo-mpo.gc.ca
4) Canada Centre for Inland Waters, Fisheries and Oceans Canada, 867 Lakeshore Road, Burlington, ON, L7S 1A1, Sarah.Bailey@dfo-mpo.gc.ca

1. Introduction

Arctic maritime routes will open to the shipping traffic during summer times with the decrease of the sea-ice cover in the Canadian arctic. Ballast water transported by domestic vessels has been identified as a significant vector of marine and freshwater organisms' dispersal [1] and thus significant vector for the spread of nonindigenous species (NIS) between subarctic and arctic ports like in Deception Bay (Nunavik). Several cases of introduction of NIS were observed in Oceania and more particularly in Australia and in Tasmania. Toxic dinoflagellates were listed in numerous ports, after a strong efflorescence (Hobart's port in Tasmania and Adelaide's port in Australia) causing an upsurge of paralysing poisonings and a mortality of certain fishes and shellfish [2]. In Tasmania, the appearance of cysts of the toxic species *Gymnodinium catenatu* coincides with the beginning of the wooden export from the South of Tasmania towards Japan [3]. Since the last decades, the introduction of harmful organisms has been identified on the Canadian east-coast and in Great Lakes [4]. Governments spent annually between 130 and 345 millions dollars [5] for monitoring and try to stamp out these organisms and to regenerate affected ecosystems [6]. Ballast exchange regulations designed to limit introductions of NIS under the "Canada Shipping Act" are restricted to ships on international routes. Although domestic voyages are currently unregulated [7], some vessels conduct voluntary offshore exchanges to prevent ice formation in tanks and to reduce risks of NIS introductions. A board the domestic bulk carrier M/V Arctic, five surveys (2015) has been carried out in order to evaluate seasonal changes in risks of introduction of NIS and to determine efficacy of voluntary ballast water exchange in two zones (Jacques Cartier and Belle Isle Strait in St Lawrence River) performed by the vessel in reducing diversity and densities. Three tanks have been chosen: 1) control tank filled with water from Quebec City harbour. This tank was not exchanged throughout the whole trip; 2) tank filled at the beginning with water from Quebec City harbour and then exchanged in Jacques Cartier Strait; 3) tank filled at the beginning with water from Quebec City harbour and then exchanged in Belle Isle Strait. Two objectives have been considered into the present study related with hypothesis: The first objective was to evaluate seasonal changes in risks of introduction of NIS by the M/V Arctic. The main hypothesis was that a higher risk are expected to occur corresponding to phytoplankton blooms in June-July for the first summer blooms and in September for the blooms occurring at the end of summer. The second objective was to determine efficacy of voluntary ballast water exchange performed by the vessel in reducing diversity and densities. The main hypothesis were that dinoflagellate densities and diversity will be higher in exchanged tanks because of higher ballast water age in control tank and that diversity/abundance will differ between exchange zones.

2. Methods

2.1. Vessel detail and route

All of the surveys (Summer 2015) were carried out aboard the bulk carrier M/V Arctic owned by Fednav shipping company (IMO: 7517507). The ship has a length and a beam of 220.82 and 22.93 m, respectively and a gross register tonnage of 20,236 t. With its PC4 polar class, M/V Arctic is able to conduct year-round operations in thick first-year ice. The ship has seven ballast tanks on both port and starboard sides, for a maximum of 28161.2 m^3 of ballast water. Being a domestic ship, M/V Arctic navigates exclusively in Canadian waters between

Quebec City and Deception Bay (Nunavik) in order to transport nickel ore extracted from Raglan Mine.

2.2. Ballast water sampling

For all voyages, the three ballast water tanks were filled at Quebec City harbour and sampling started the day after ballasting. Ballast water tanks were sampled before and after exchange in Jacques Cartier and Belle Isle Straits, as well as the control tank. For the sampling of dinoflagellates, two separate methods will be used together (plankton net and Niskin bottle only during June voyage) in order to compare accuracy between methods. The goal is to confirm if both methods allow us to obtain the same biological content. All ballast water exchange (BWE) used the sequential method (E/R) recommended by IMO. It's a process by which a ballast tank is first emptied and then refilled with new ballast water to achieve at least a 95% volumetric exchange. Before entering Deception Bay, ballast water was collected from the three tanks and harbour water was sampled upon arrival.

3. Results

In Quebec City, the risk tends to be higher in July and September according to an increase in freshwater dinoflagellates diversity in ballast tanks that may be related respectively to a phytoplankton bloom at the beginning and the end of summer. Mortality increases according to longer voyage duration. When deballasting in Deception Bay harbor the risk may be shorter. Dinoflagellate densities are higher in tanks exchanged in both Jacques Cartier and Belle Isle Straits than in Control tanks. Dinoflagellates density tends to decrease in Jacques Cartier Strait tanks in June and July and in Belle Isle Strait tanks in June corresponding to the beginning of summer. It may increases or remains constant in the rest of the summer. Dinoflagellates density is always higher in the tank exchanged in Jacques Cartier Strait than the tank exchanged at Belle Isle Strait. This suggests that Jacques Cartier Strait will probably the best zone for conduct exchange ballast water by M/V Arctic.

4. Conclusion

Domestic vessels navigate in coastal routes and transport a huge volume of ballast water that is brought into Arctic ports. Conducting exchange ballast water aims to reduce the densities in tanks when discharging in Arctic harbours. The principal risk of introduction occurs in summer since M/V Arctic has not the obligation to conduct ballast water exchange. In winter the vessel has to operate discharging water to prevent from ice formation in tanks because it pumps up first freshwater from Quebec City harbours. In summer the risk may be not high if the vessel decides to not practice any exchange. In samples collected from control tanks at Deception Bay, filled with freshwater in Quebec City harbour, the mortality is high and freshwater dinoflagellates identified do not thrive under higher salinity estimated in Deception Bay harbour (28 psu) than in Quebec City harbour (0.1 psu). In exchange ballast tanks, dinoflagellates density and diversity are more important but species found in Jacques Cartier and Belle Isle Strait tanks are the same than found in Deception Bay harbours so the risk of introduction of NIS seems low. An attention must be considered on toxic dinoflagellates but the densities found are not so high so that it is alarming

References

[1] Verling, E., Ruiz, G.M., Smith, L.D., Galil, B., Whitman Miller, A., and K.R, Murphy., "Supply-side invasion ecology: characterizing propagule pressure in coastal ecosystems". *Proceeding of The Royal Society B*, 272, 2005, pp. 1249-1257.

[2] Hallegraeff, G.M., "Review of harmful algal blooms and their apparent global increase", *Phycologia*, 32, 1993, pp. 79-99.

[3] Hallegraef, G.M., "Transport of toxic dinoflagellates via ship's ballast water: bioeconomic risk assessment and efficacy of possible ballast water management strategies", *Marine Ecology-Progress Series*, 168, 1998, pp. 297-309.

[4] Bailey, S.A., Duggan, I.C., Jenkins, P.T., and MacIsaac H.J., "Invertebrate resting stages in residual ballast sediment of transoceanic ships", *Canadian Journal of Fisheries and Aquatic Science*, 62, 2005a, pp.1090-1103.

[5] Colautti, R., Bailey, S., Van Overdijk, C., Amundsen, K., and MacIsaac, H.J., "Characterized and project costs of non-indigenous species in Canada", *Biology Invasions*, 8, 2006a, pp. 45-59.

[6] Davis, M.A., "Invasion biology 1958-2004: the pursuit of science and conservation", in Conceptual ecology and invasions biology: reciprocal approaches to nature. Kluwer Publishers, London, England, 2004, pp.1-27.

[7] Chan, F.T., MacIsaac, H.J, and Bailey, S.A., "Relative importance of vessel hull fouling and ballast water as transport vectors of nonindigenous species to the Canadian Arctic". *Canadian Journal of Fisheries and Aquatic Science*, 72, 2015, pp. 1230-1242.

NUMERICAL SIMULATION OF SEA LEVEL RISE EFFECT ON SEAWATER INTRUSION INTO STRATIFIED COASTAL AQUIFER

S. Sadjad Mehdizadeh[1], Freydoon Vafaie[2]

1) Department of Civil Engineering, Islamic Azad University, Central Tehran Branch, Tehran, Iran, Email: Saj.Mehdizadeh@iauctb.ac.ir
2) Civil Engineering Faculty, K.N. Toosi University of Technology, Tehran, Iran, Email: Fvafai@kntu.ac.ir

1. Introduction

Population growth and scarcity of coastal freshwater resources have increased the stresses on many coastal aquifers, leading to aquifer storage decline and seawater intrusion (SWI). The investigation of coastal aquifers routinely involves the application of SWI models, which can be divided into two categories, namely sharp-interface and dispersive-interface approaches. Sharp-interface approaches are computationally more efficient while dispersive-modeling approaches are more numerically challenging, but allow for freshwater-saltwater mixing. Literature study demonstrated that concerning on sea level rise (SLR) has been grown up for the last decade and numerous studies have addressed the extents, rates and timescales associated with SWI induced by SLR for mostly homogeneous cases. Despite considerable attentions to SLR problem, there is still a gap for aquifers with spatial variability of properties that make aquifer more complex but are naturally widespread [1]. In stratified aquifers, vertical leakage through layers makes the intrusion mechanism different compared to homogeneous aquifer. In this study, a sharp-interface approach (named as SHI-SWIM) is developed and the result is compared with dispersive SEAWAT model for gradually (GSLR) and instantaneously SLR (ISLR) problem.

2. Material and Methods

The geometry and physical properties of the coastal aquifer are adopted from a conceptual model of field study completed by Werner and Simmons [2] at Pioneer Valley, Australia. All the main properties and length scale were kept the same as the primary study except one modification: the aquifer height is partitioned into three horizontally layers of differing hydraulic conductivity (K:L/T) value (two 14.0 m high K layer at top and bottom and a 2.0 m aquitard between them). The simulation domain extended 1000 m landward and the total height of the model is considered 30 m (Fig.1). The sea boundary is vertical and the constant freshwater flux equals to 0.15 m^2/d enters the system from the landside. Two scenarios have been defined for simulation differing at aquitard conductivity (K') value (i.e. K'=0.01 m/d and 0.0001 m/d). At the developed sharp-interface SHI-SWIM model, freshwater and saltwater are assumed immiscible and a line of pressure equivalence exists between the two water bodies. Leakage across aquitard is calculated using the optimum method proposed by Mehdizadeh et al. [3]. The finite-difference model SEAWAT [4] is also used to simulate two-dimensional, variable density, transient groundwater flow in porous media. It combines the modified MODFLOW and MT3DMS into a single program that solves the coupled groundwater flow and solute transport equations. Two different SLR are applied to sea boundary. The homogeneous and layered aquifers are exposed to ISLR (4.0 m sea level sudden rise) and GSLR (10 mm/year) that is adopted with the conditions predicted by the Intergovernmental Panel for Climate (IPCC) [5]. All simulations run for 200 years to predict the transient SWI.

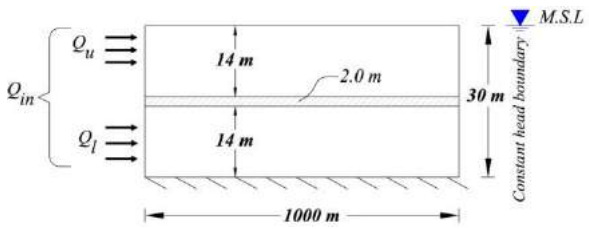

Figure 1. Geometry and boundary condition of multi-layered field-scale aquifer

3. Results and Discussion

For homogeneous confined system with ISLR, salt wedge intrude toward the land at early times but freshwater flux can push the salt wedge back to its initial position (before SLR). At unconfined aquifer, despite confined system, this reversal mechanism is not observed. It is found that in unconfined aquifer, saltwater fills the unsaturated part of the aquifer leading to water table level upward movement. The freshwater also moves to the top unsaturated part of the aquifer leading to less challenge with SWI.

At stratified aquifer, it is found that for ISLR problem, where the freshwater leaks upward through the middle aquitard, the wedge intrude more appreciable into the bottom layer rather than the upper one. At the upper layer it is shown that seawater intrude toward inland at early times but then naturally driven back to the original position (Fig.2).

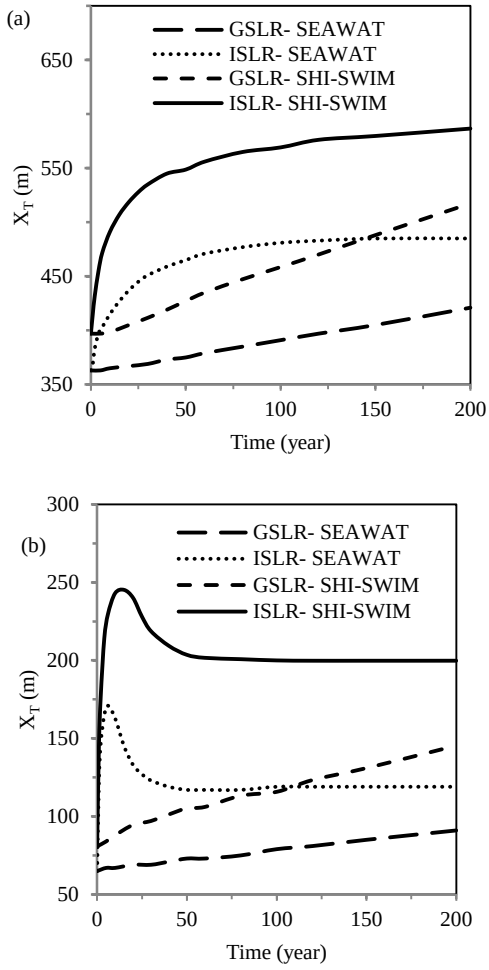

Figure 2. Transient toe position for GSLR and ISLR by SHI-SWIM and SEAWAT model, (a) at the lower layer and (b) at the upper layer

If the ambient freshwater recharge remains constant in aquifer, the freshwater recharge from landside and upward freshwater leakage do not allow the wedge to intrude rapidly in layers. For the GSLR, because of partially equivalence of saltwater head rise and increase at volume of freshwater, this reversal mechanism is not very clear. The intrusion mechanism will be different when a very low permeable aquitard is placed between layers. For this case, almost no freshwater can leaks upward so both two top and bottom layers act independently and the layers response similarly to homogeneous case. The sharp-interface SHI-SWIM model successfully predicted the same trend compare to dispersive SEAWAT model but over-predicted the interface in SLR cases. It is concluded that however the sharp-interface modeling generally overestimates the freshwater-saltwater interfaces but it can be applied reliably for real cases where the transition region is small.

4. Conclusion

Investigation regarding sea level rise on stratified aquifer demonstrated that confined and unconfined layers respond differently to SLR. Fixed-flux and fixed-head boundary condition at inland also influence the results. Vertical leakage plays an important role on intrusion mechanism of multi-layered aquifer.

5. References

[1] Lu, C., Chen, Y., Zhang, C., Luo, J., 2013. Steady-state freshwater–seawater mixing zone in stratified coastal aquifers. Journal of Hydrology 505, 24-34.

[2] Werner, A.D., Simmons, C.T., 2009, Impact of sea-level rise on seawater intrusion in coastal aquifers. Ground Water, 47(2), 197–204.

[3] Mehdizadeh, S.S., Werner, A.D., Vafaie, F., Badaruddin, S., 2014. Vertical leakage in sharp-interface seawater intrusion models of layered coastal aquifers, Journal of Hydrology. Volume 519, Part A, 1097‑1107.

[4] Langevin, C.D., Thorne Jr, D.T., Dausman, A.M., Sukop, M.C., Guo, W., 2008. SEAWAT Version 4: A computer program for simulation of multi-species solute and heat transport: U.S. Geological Survey Techniques and Methods, Book 6, Chap. A22, 39 pp.

[5] Bates, B.C., Kundzewicz, Z.W., Wu, S., Palutikof, J.P., Eds. 2008. Climate change and water. Technical paper of the Intergovernmental Panel on Climate Change, IPCC Secretariat, Geneva, 210p.

EFFECT OF MARINE ARTIFICIAL REEFS ON IMPROVEMENT AND DEVOLEPMENT OF SEA INVIRONMENT IN KISH ISLAND

Daniel Ajdari[1], Zahra Ajdari[2]

[1&2]Iranian Fisheries Research Organization, Karaj High, Paykanshahr, National Botanical Garden,

1. Introduction

Artificial reefs are manmade materials deployed under water in order to improve environment and increase the exploitations of fishing area. Usage of artificial technique has developed due to increase of world population and need to supply of protein, aim to restoring of natural specially rehabilitation of demersal fishes. It has effect to increase the production in order sustainable exploitation**[1]**.

Coasts and Islands have destruction due to over harvesting from ecosystems and other activities by humans and natural, these caused many aquatic as demersal fishes, colored fishes, Corals, and others have endangered in Persian Gulf and Oman Sea**[2]**. The Kish island has experienced the same fate and now this is very different from last decades and even the costs have destructed. The artificial reef is one way or method that can improve the environment and restore the aquatic[5].

In general terms, the artificial reefs are man-made habitats placed in areas of sea bottom that provide a framework for marine life to develop. Such habitats have several benefits including: providing food, shelter, protection, and spawning areas for fish and marine life, as well as, relieving natural reefs from user pressure by providing alternative recreational areas. From an aquacultural point of view, the artificial reefs can increase fish catch tremendously [1], [9], [2] and [10].

2. Methodology

Iranian fisheries and Iranian Fisheries research Institute (IFRO) have established an artificial reefs area in west of Kish Island (Fig.1) **[4], (26˚ 23´ 1159˝ N and 54˚ 02´ 5325˝E)**. This area has studied during one year, Data of assembled fishes and physical sampling were collected in seasonal during spring, summer, autumn and winter **[3]**. There were tow treatment for sampling as artificial reefs site and a control site. Collected data has analyzed and evaluated by SPSS and Excel **[1]**.

Figure 1 study area located east of kish island Artificial Reef site and Control Site

3. Result and discussion

The assemblages of fishes found in this experiment were 324 fishes grouped under 17 families and 21 species of demersal fishes. Some of the families were Serranidae, Haemulidae, Lutjanidae, Siganidae, Pomacanthidae, Carangidae, Scaridae, Chaeodontidae, Lethernidae and Sparidae. Three species were found in the families of Lutjanidae and Haemulidae while the Seranidae and Sparidae families each had two species and for other families just one species were found (Fig2).

Throughout the experiment, the total fish catch was higher in ARs than natural treatment or control site (Fig. 3). The comparison of index of Catch Per Unit Effort CPUE. The results showed that there was significant difference $P<0.05$ between the AR sites and assembled fishes in artificial reefs were more than control site **[8]**. Consequently the artificial reefs can be a tool and technique to improve the marine environment **[7]**, restoring, rehabilitation, rebuilding of coasts of kish island and increase the production of fishes **[6]**. This technique is very effectiveness tool to improve and restock the destructed and defected coasts of Kish Island and Revert to the previous

situation be restore again the ecosystems, particularly coral to be reconstructed, recover and restore.

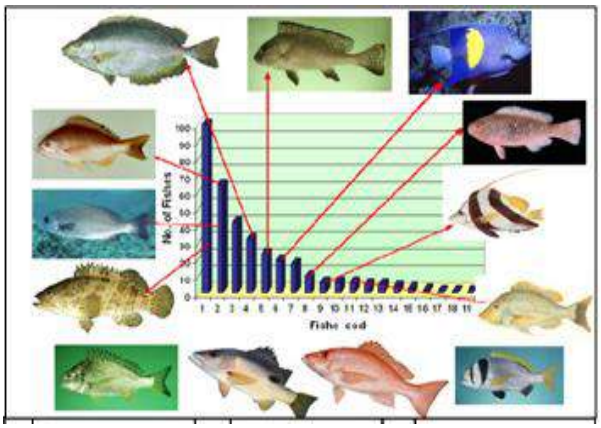

Figure2 Different fish species and their amount inartificial Reefs

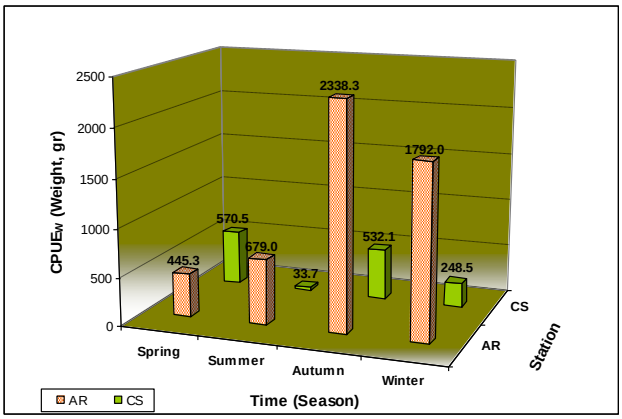

Figure3 CPU of fishes in different sites (AR & CS) in seasons

4. References

[1] Ambrose, R. F. and Swarhrick S. L., 1989. "Comparison of fish assemblages on artificial and natural reefs off the coast of southern*"* California. Bulletin of Marine Science, 44, 718-733.

[2] Azhdari, H. and Ajdari, Z., 2003. "Marine Artificial Reef and its improvement in Iran." Moje Sabz Press 135p. *(in Persian language)*

.

[3] Bayle-Sempere, J. T., Ramos-Espla, A. A. and Garcia Charton, J. A., 1994. "Intraannual variability of an artificial reef fish assemblage in the marine reserve of Tabarca" (Alicante. Spain, SW

[4] Foster, K. L., Steimle F. W., Muir W. C., Krapp R. K. and Conlin, B. E., 1994. "Mitigation potential of habitat replacement: concrete artificial reef in Delaware Bay, preliminary results". Bulletin Marine Sciences, 55, 783-795.

[5] Godoy, E. A. S., Almeida, T. C. M. and Zalmon, I. R., 2002. "Fish assemblages and environmental variables on an artificial reef north of Rio de Janeiro", Brazil. ICES Journal of Marine Science, 59, S138–S143.

[6] Kamali, E., 2005. "Ecological Study in coastal area of Bandar e Lengeh", *Final report, Institute of Fisheries Research for Persian Gulf and Oman Sea.*

[7] Lance, K. B. Jordan, David, S., Gilliam and Richard, E. Spieler, 2005. "Reef fish assemblage structure affected by small-scale spacing and size variations of artificial patch reefs". *Journal of Experimental Marine Biology and Ecology*, 326**,** 170–186.

[8] Miguel, N. S. and Carlos, C. M., 1998. Comparison of the catch and fishing yield from an artificial reef system and neighboring areas off Faro (Algarve, south Portugal). *Fisheries Research*, 39, 55-65.

[9] Matthews, K. R., 1985. Species similarity and movement of fishes on natural and artificial reefs in Monterey Bay, California. *Bulletin of Marine Science*, 37, 252-270.

[10] Lance, K. B. Jordan, David, S., Gilliam and Richard, E. Spieler, 2005. Reef fish assemblage structure affected by small-scale spacing and size variations of artificial patch reefs. *Journal of Experimental Marine Biology and Ecology*, 326**,** 170–186.

CHARACTERIZING COASTAL AND MARINE ECOSYSTEM VULNERABILITY TO CLIMATE CHANGE: CONSERVATION OF ECOSYSTEM SERVICES

Jason Hale[1] and Linos Cotsapas[2]

1) Pandion Technology, Ltd., Limassol, Cyprus, jhale@pandiontech.com
2) Research Planning, Inc., Columbia, SC, USA, lcotsapas@researchplanning.com

1. Introduction: Biodiversity and Ecosystem Services

"Biodiversity" is a term that describes variability in genes, species, habitats, and ecosystems. "Ecosystem services" refers to natural products and processes that are of value to human societies. Many scientific studies have related biodiversity with delivery of groups of ecosystem services such as:

- Provisioning services, such as production of food or timber.
- Regulating services, such as degradation of pollutants, or mitigation of flooding.
- Cultural services, such as the recreational value of being in nature, or pursuit of spiritual needs.
- Supporting services, such as nutrient cycling.

Examples of ecosystem services in coastal and marine environments include the capacity of ambient surface waters to treat waste water; provision of food in the form of fish and shellfish; and protection from flooding and storm events provided by mangroves, wetlands, or natural dunes.

These ecosystem services have real economic value, and conservation of these services presents society with measureable economic benefits. In contrast, degradation of ecosystem services is often associated with measurable costs.

2. The Value of Conservation of Ecosystem Services

A key concept in conservation of ecosystem services is recognition of the difference in values of services between a healthy environment and a degraded environment. For example, numerical limits on waste water discharged into the coastal environment generally assume that a healthy ecosystem is available to continue the treatment process.

Thus, a healthy marine ecosystem can continue to degrade pollutants (e.g., excess nitrogen and phosphorus) so that other ecosystem services, such as recreational enjoyment of nearby healthy beaches, are not impaired. If the same volume of wastewater is discharged into a coastal ecosystem that is compromised (by cumulative effects of climate change, for example), we may expect less effective "natural" treatment, and associated risks. These may include: increase in occurrence and persistence of harmful algal blooms, increasingly degraded fish habitat, or impacts to other coastal developments, such as sea water intakes for cooling or desalination processing.

3. Vulnerability Due to Human Activities

Environmental degradation of aquatic ecosystems that impact ecosystem services includes excessive discharge of pollutants, land reclamation and coastal development, and overfishing, among other stressors. Based on the 5th assessment report of the IPCC (2014), the effects of climate change, including increased sea surface temperature and sea level rise, should be counted among environmental stressors that will impact ecosystem services, either directly or indirectly. Observations from around the world demonstrate how changes in these environmental variables, along with other stressors related to climate change, will have a substantial effect these important ecosystem services.

4. Valuation of Ecosystem Services

Threats to coastal resources due to climate change, and valuation of ecosystem services provided by these resources should be routinely integrated into planning processes such as Integrated Coastal Zone Management (ICZM) plans. Yet while a number of broad approaches and techniques are available for valuation of ecosystem services, the practice of routinely estimating their value to support conservation and development planning is uncommon in the region.

For example, a rigorous and quantitative decision making system to manage coastal zone activities was recently developed for Belize. The system successfully influenced regional and national policy by considering the needs of commercial fishing with coral reef and mangrove habitat conservation with coastal development and industry needs. To accomplish this, the analysis had to go beyond a simple comparison of annual economic value, and estimate the value of ecological relationships between ecosystem services related to biodiversity and economic values related to tourism and coastal development.

5. Conclusions and Goals of the Presentation

Thus, one conclusion to be drawn is that the most effective coastal zone management activities must balance conservation of biodiversity and ecosystem services with the pressures of economic development.

With this in mind, the goals of this presentation are to: (1) discuss the importance of estimating coastal and marine ecosystem vulnerability to the effects of climate change; (2) illustrate how this vulnerability can impact ecosystem services such as fisheries production, provision of clean sea water, protection from coastal flooding, and opportunities for recreation; and (3) identify potential coastal zone management strategies which may mitigate threats from climate change by balancing conservation of ecosystem services with development of economic resources in the coastal zone.

6. References

IPCC, 2014. Climate Change 2014: Synthesis Report. Contribution of Working Groups I, II and III to the Fifth Assessment Report of the Intergovernmental Panel on Climate Change [Core Writing Team, R.K. Pachauri and L.A. Meyer (eds.)]. IPCC, Geneva, Switzerland, 151 pp.

KEYNOTE SPEAKERS PAPARES

SEAPORT DEVELOPMENT IN THE 21ST CENTURY

Han Ligteringen
Emeritus Professor Ports and Waterways, Delft University of Technology
And UNESCO-IHE, Delft

In the past conventional seaports were a necessary means to facilitate a countries imports and exports of goods. They were state owned and – operated (service ports) and in many cases both a financial burden to the country and cumbersome for the ships that called: long waiting times and slow handling of the cargo. Since several decades this has changed and we see now that modern, well managed ports can have a substantial contribution to the economy of a country or a region. Ports have changed from being only nodes in the transport chains to industrial centres with many water related activities. Privatisation is a key element in this change, but not everything needs to be privatised. The economic importance of the seaports is illustrated by statistics from the Dutch port system.

Good port management requires not only up to date infrastructure and efficient operations, but also a constant awareness of changes in the markets, in technology and in society. A port masterplan is made for periods of 25-30 years, while the fixed infrastructure often has a lifetime of 50-100 years. At the same time economic forecasts of cargo throughput are known to be uncertain. How to resolve these incompatibilities and to avoid port infrastructure becoming obsolete before the end of its economic lifetime? In a PIANC seminar in 2006 the Life Cycle approach in port planning was introduced by several experts (Ligteringen, 2006). And over the past years much research was carried out on alternative planning methods, including the so-called Adaptive Port Planning (Taneja, 2013). These new methods will be elaborated by means of practical examples.

Against this background this key-note will address several of today's major societal and technological trends and their effects on the maritime sector and port operations. We are talking about how climate change and the need for greater sustainability influences the shipping sector at present and increasingly in the coming decades. And in what way ICT developments will affect the entire logistic process including shipping, the port and hinterland transport. More interesting is how these trends affect the long term development of seaports worldwide, such as the need for flexibility in planning and design, the "greening" of shipping and port operations, sustainability as a starting point for new port developments, rather than a governmental requirement, automation and the increased connectivity demands. These trends will be illustrated in a case related to container terminals.

A final aspect is the role of education, training and research in the above sketched developments for seaports. Here the trends are clear: (i) the educational requirements increase at all levels, (ii) the work, both on the terminal and in the administration becomes more specialised and the role of IT requires constant adaptation of working methods and (iii) no port can flourish without having adequate training programs for its staff. Examples are given of how higher education in the Netherlands has been adjusted to meet these requirements and how joint projects of seaport and university can contribute to meet the challenges of future port development.

Ligteringen, H. (Editor),. Proc. Int. Seminar on Life-Cycle approach in Port Infrastructure, PIANC, Brussels, 2006.
Taneja, P., The Flexible Port. Doctorate Thesis, Delft University of Technology, Delft, 2013.

MODELING COASTAL IMPACTS AT VARIOUS SCALES

Dano Roelvink[1]

1) Coastal Engineering and Port Development, UNESCO-IHE, Delft, the Netherlands, d.roelvink@unesco-ihe.org

1. Introduction

In this keynote address we will discuss the modelling of coastal impacts on a range of scales, from short-term, local inundation events, through storm impacts on gravel beaches, dunes and sandy barriers, to inlet evolution after breaching and finally to long-term assessment of coastal evolution and the effects of climate change and sea level rise. We focus on a process-based approach and discuss some recent developments in this technique.

2. Brief description of the modeling approach

In the process-based modeling approach wave, current and sediment computations are tightly coupled with each other and with the evolution of the bathymetry. Bottom changes are regularly fed back into the bed level and a dynamic, generally moving system develops. Often use is made of the 'morphological factor' concept where the bed is updated after each flow timestep but multiplied with a morphological factor to accelerate the computations [1].

Figure 1. Setup of a morphodynamic model.

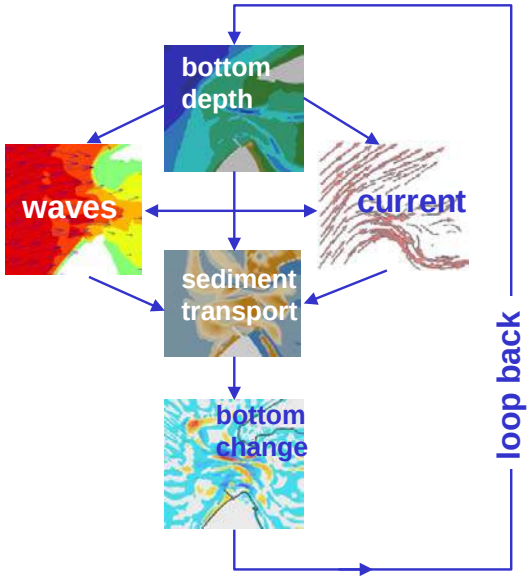

This factor can range from 1-10 for storm conditions [2] to several hundreds for simulations of large tidal inlet or river systems. (e.g. [3])

3. Timescales resolved

Most morphological codes (e.g. Delft3D, Mike21, ROMS) resolve the tidal motion as the shortest timescale, and apply time-averaged wave models such as SWAN, which is called or updated at typically 20-minute intervals. Such an approach is useful for relatively large-scale applications over time periods of months to years or even decades. In tidally dominated systems simulations over centuries become feasible, allowing to evaluate the effects of sea level rise [4] and long-term changes in sediment supply [3].

For storm impacts on sandy coasts, *infragravity waves*, long waves related to wave groups, need to be considered, for example as in the XBeach model [2], [5]. Especially during collision and overwashing regimes these motions dominate the beach and dune erosion processes. On sandy beaches and behind coral reefs the infragravity swash during storms or swell events dominates over the incident-band swash and a short-wave averaged but long-wave resolving model suffices and can efficiently resolve these motions. However, for steep slopes such as on gravel beaches or dikes, the incident-band waves can no longer be neglected and a short-wave resolving mode is necessary.

The *nonhydrostatic* model within XBeach [6], similar to the SWASH model [7], provides a robust if more computationally expensive approach to resolve short-wave motions including the surf and swash zones. Using this, a coupled groundwater model and special gravel transport formulations an accurate gravel beach and barrier model, XBeach-G was developed and validated [8], showing a correct representation of the processes of berm formation, beach erosion, crest build-up, crest lowering and barrier rollover.

4. Recent advances

4.1. Wave-resolving modeling

Apart from the modeling of gravel barrier response during storms, some first steps have been taken to model the response of steep sandy beaches such as often occur on open-ocean beaches, using the nonhydrostatic model within XBeach. Comparisons between surfbeat and nonhydrostatic mode for dune erosion and overwashing cases show good agreement for the cases where both

approaches are valid. Swash berm building is a process that still needs attention. An example comparison for a barrier beach at Tordera, Spain is shown in Figure 2.

Figure 2. Field comparison between surfbeat and nonhydrostatic mode XBeach

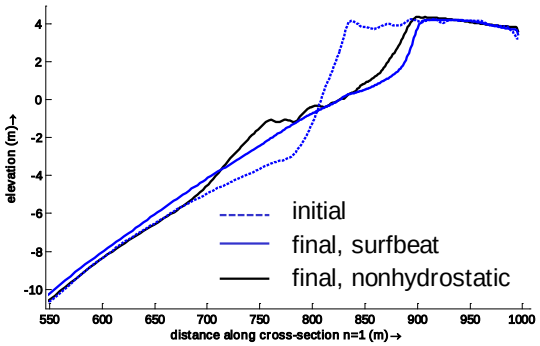

4.2. Surfbeat Modeling

As was pointed out in [9] 2D XBeach tended to underestimate infragravity runup in a number of US field cases. We analyzed the reasons for this and found that the original directional short wave propagation tended to smooth out the groupiness too much. A new scheme, where the groupy wave energy is propagated along the mean direction maintains the correct groupiness and leads to higher IG runup, consistent with observations.

4.3. Vegetation effects

More and more applications consider natural flood defences or 'Buildig with Nature' solutions, in which vegetation plays an important role. To this end vegetation effects were implemented in [10], with a special focus on the wave setup, where non-linear effects of the short waves were naturally captured in the nonhydrostatic mode but had to be approximated in the surfbeat mode.

4.4. Longer-term modeling

In order to arrive at realistic longer-term simulations of coastal evolution, a number of activities are ongoing at this point in time. First, inclusion of onshore processes due to wave skewness and asymmetry allows for a more balanced cross-shore behavior that keeps coastal profiles stable in the long run, see for example Figure 3. Second, a quasi-3D undertow module has been implemented that will lead to more accurate representation of near-bed flow, including streaming.

As infragravity waves are only important during high waves, we now tend to use a combination of fast, stationary runs for moderate conditions and surfbeat runs for storms, leading for instance to better prediction of tidal inlet evolution after breaching.

Finally, coupling of underwater and aeolian processes will be needed to predict long-term evolution of sandy coasts.

Figure 3. Example simulation of spit evolutionat a coast discontinuity using XBeach-stationary

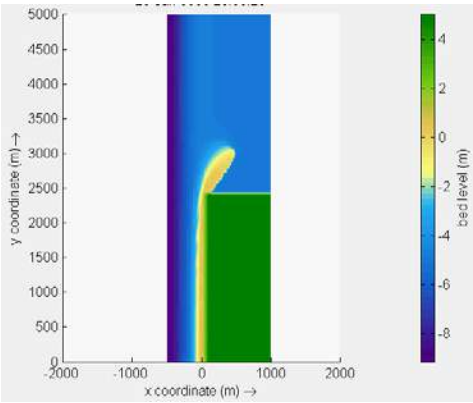

5. References

[1] Roelvink, J.A. Coastal morphodynamic evolution techniques. *Coastal Engineering* Volume 53, Issues 2-3 , February 2006, Pages 277-287

[2] Dano Roelvink, Ad Reniers, Ap van Dongeren, Jaap van Thiel de Vries, Robert McCall, Jamie Lescinski. Modelling storm impacts on beaches, dunes and barrier islands. *Coastal Engineering*, Volume 56, Issues 11-12, November-December 2009, Pages 1133-1152.

[3] Van Der Wegen, M., Jaffe, B.E., Roelvink, J.A. Process-based, morphodynamic hindcast of decadal deposition patterns in San Pablo Bay, California, 1856-1887 *Journal of Geophysical Research F: Earth Surface* 116 (2), art. no. F02008 .

[4] D. M. P. K. Dissanayake, R. Ranasinghe and J. A. Roelvink. The morphological response of large tidal inlet/basin systems to relative sea level rise. *Climatic Change*, Volume 113, Number 2 (2012), 253-276, DOI: 10.1007/s10584-012-0402-z.

[45 R.T. McCall, J.S.M. Van Thiel de Vries, N.G. Plant, A.R. Van Dongeren, J.A. Roelvink, D.M. Thompson, A.J.H.M. Reniers, 2010. Two-dimensional time dependent hurricane overwash and erosion modeling at Santa Rosa Island . *Coastal Engineering*, Volume 57, Issue 7, July 2010, Pages 668-683

[6] P Smit, G Stelling, J Roelvink, J Van Thiel de Vries, R McCall. XBeach: nonhydrostatic model: validation, verification and model description. *Delft University of Technology*.

[7] Zijlema, M., Stelling, G. and Smit, P., 2011. SWASH: An operational public domain code for simulating wave fields and rapidly varied flows in coastal waters. *Coastal Engineering.*, 58, 992-1012.

[8] RT McCall, G Masselink, TG Poate, JA Roelvink, LP Almeida. Modelling the morphodynamics of gravel beaches during storms with XBeach-G. *Coastal Engineering* 103, 52-66

[9] H.F. Stockdon, D.M. Thompson, N.G. Plant, J.W. Long, Evaluation of wave runup predictions from numerical and parametric models, *Coastal Engineering*, Volume 92, October 2014, Pages 1-11

[10] AA van Rooijen, RT McCall, JSM van Thiel de Vries, AR van Dongeren, AJHM Reniers, JA Roelvink. Modeling the effect of wave-vegetation interaction on wave setup. *Journal of Geophysical Research: Oceans* 121 (6), 4341–4359

INTEGRATED AQUACULTURE FOR IRAN: AVOIDING PITFALLS WHILE PREPARING FOR THE FUTURE

Michael Risk[1] and Abbas Haghshenas[2]

1) PO Box 1195, Durham Ontario Canada L8S 4M1 riskmj@mcmaster.ca
2)

1. Introduction

Aquaculture, the controlled rearing of aquatic species for human consumption, has been practiced for millennia. Canadian First Nations perfected rock-bound "clam farms" thousands of years ago, for example. The depletion of native fish stocks, coupled with population growth, has resulted in increased interest in this field. There has been explosive growth of aquaculture in the latter part of the 20th century and the early part of this one, such that at present (2016) the global production of aquatic organisms from aquaculture is about equal to the total from wild capture.

Much of the global production is from freshwater: carp, in China; catfish, in the United States; milkfish in Southeast Asia, and tilapia almost everywhere. In terms of overall value, the marine picture is dominated by salmon. Four countries produce most of the world's farmed salmon: Norway (by far the largest producer), Chile, Canada and the UK. Although salmon farming has been an economic success, it is not without problems, and it is likely that the industry cannot continue on its present path.

2. Iran's special circumstances

Iran has coastlines on the Caspian Sea, Persian Gulf and Sea of Oman. The Caspian's low-gradient coast and multinational nature make it difficult for typical aquaculture, although sturgeon can be raised-Canada has several commercial sturgeon farms. The Sea of Oman has deep water, and experiences large storms. The Persian Gulf is an enormous problem for typical aquaculture, because it supports unique biomes such as mangroves and coral reefs-and, as Risk's work near Assaluyeh shows, Iran has reefs that have yet to be described. These special habitats support local artisanal fisheries, and are uniquely sensitive to nutrient pulses and Red Tides.

Iran also has some large rivers capable of supporting aquaculture-but Iran is also facing serious issues of water shortage. Pollution of freshwater resources by fish farms must be avoided like a plague of sea-lice on a farmed salmon.

3. Problems: cages are for zoos

Most farmed salmon, indeed almost all high-value marine fish species, are grown in open-water net cages. Cage culture for finfish is feasible, profitable: and often shortsighted. The problems associated with cages are severe, and perhaps irreversible. There are widespread problems of excess nutrients, leading to Red Tides. Chile has recently experienced record Red Tides, which were probably triggered by excess nutrient from salmon farms using Norwegian technology. 25 million salmon died during this event, as well as countless sardines. The trigger for a Red Tide is most often excess nutrients, and floating cages are a potent source of these, from fish feces to uneaten fish food. The fish farms off Scotland every year produce more sewage waste than the entire human population.

Accumulations of organic matter under cages leads to "dead zones", where sulfide toxicity can be very high. This kills local species. Farmed fish are often dosed with antibiotics, leading to antibiotic resistance. Farmed fish escape, and displace local fish populations. On Canada's west coast, salmon farms owned by Norwegian interests often lose 50% of their stock to diseases, while at the same time spreading disease and parasites to native fish stocks. Bottom sediments are contaminated with Copper, used as an antifouling agent on cages and lines.

In 2010, the nutrient discharge from Chinese aquaculture was more than 1,000Gt nitrogen and 170Gt phosphorus. Both water and sediment showed high levels of nutrient enrichment. Small wonder, then, that [1] "recycling of nutrients and water and sediments by for example multi-trophic systems should be increased in future." Cage culture is a dead-end street unless done carefully. The good news is, there are alternatives.

Modelling studies of a bay in the Persian Gulf suggest that, if stocked with a normal density of typically-operated cages, the nutrient excess will

be enough to kill every coral reef in the bay in a very short period of time.

4. IMTM: Integrated Multi-Trophic Mariculture.

Multi-trophic mariculture/aquaculture grows organisms of several trophic levels together in a system which recycles the majority of the nutrients [2]. Examples would be fish grown in cages, with seaweed crops downcurrent and bivalves underneath or in the area. In the long run, these systems make more money than cages- and there **is** a long run, because the systems are sustainable. Operators can sell several crops, not just one, and can wait for favorable market timing.

Right now, Canada, China, Scotland and the US, at least, are experimenting with IMTM. Some of these are commercial already, some are close. Most of these grow some combination of salmon, mussels and kelp, all valuable products in their own right. Where the designs have faltered, it is because fish experts drive the process, followed by the algae people. More attention has to be devoted to the benthic processes, to ensure no dead zones. In addition, more attention needs to be paid to water movement. The New Brunswick (Canada) operation is plagued by high sediment sulfide levels, because the ropes holding the algae and the mussels impede water movement.

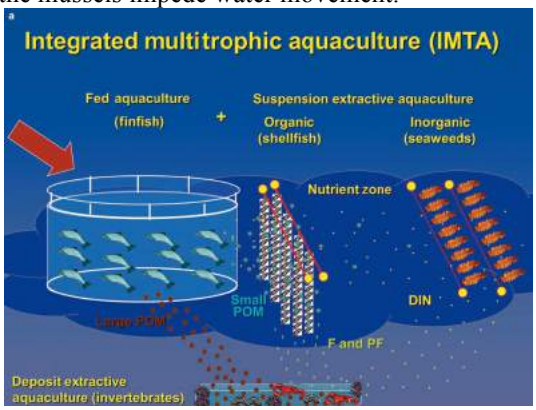

Figure 1. Schematic of the New Brunswick IMTA setup.

In Iran, possible benthic crops could include sea cucumbers, burrowing shrimp, stomatopods and bivalves.

5. Land-based systems and aquaponics

In the long run, the future of fish culture lies in land-based systems, where the operator has full control over biosecurity and water quality. Waste is not treated as something to be disposed of, as in cage systems, but a resource to be used wisely. Options are full IMTA, such as used by Blue Ridge in the US (http://www.blueridgeaquaculture.com/), or some version of "aquaponics", in which the nutrients are used to grow vegetables. For example, a 100-ton fish farm will use about 350kg of feed per day, and support 3500m^2 of vegetables.

6. The future

Iran is blessed with intelligent engineers and smart biologists. The political will exists to provide more food security to the people, without messing things up badly. The chances are good that Iran can have its fish and eat them, too.

7. References

[1] Zhang, Y., A. Bleeker and J. Liu. 2015. Nutrient discharge from China's aquaculture industry and associated environmental impacts. Environ. Res. Lett. 10 045002

[2] Chopin, T., Robinson, S.M.C., Troell, M., Neori, A., Buschmann, A.H. & Fang, J. 2008. Multi-trophic integration for sustainable marine aquaculture, pp. 2463-2475. In: The Encyclopedia of Ecology. Ecological Engineering (Vol. 3). S.E. Jørgensen and B.D. Fath (eds.). Elsevier, Oxford.

TWIN RELATED ASPECTS OF ENGINEERED MUD SUSPENSIONS FOR THE NW EUROPEAN AND IRANIAN PORT INDUSTRY

Robert Kirby[1], Mohsen Soltanpour[2], Norbert Greiser[3], Kees-Jan van der Made[4] and Rene Barth[4]

1) Ravensrodd Consultants Ltd, United Kingdom; Sediment Management Solutions (SEMASO), Netherlands, robkirby@globalnet.co.uk
2) K. N. Toosi University of Technology, Iran, soltanpour@kntu.ac.ir
3) Greiser und Partner, Germany; SEMASO, Netherlands, norbert.greiser@sell-greiser-consultants.de
4) Wiertsema & Partners, SEMASO, Netherlands, c.made@wiertsema.nl
4) Wiertsema & Partners, SEMASO, Netherlands, r.barth@wiertsema.nl

Over the last 40 years a number of 'generic' technologies have been developed to more effectively manage fine cohesive sediment in harbours in a sustainable, less expensive and more environmentally friendly manner. A 'generic' method is one which, when tailored to local idiosyncrasies, is widely applicable at many self-similar harbour configurations around the world, (channels, semi-enclosed basins, impounded docks, etc.). Such methods are preferable to traditional, old fashioned, at times damaging, 'dig and dump' dredging. Adoption of this new generation of methods alters a formerly intractable waste rendering it instead a resource with a beneficial use.

A further & serious issue for those big, muddy, commercially-important ports in NW Europe has been the recent recognition that, arising from gross-scale channel overdeepening to facilitate access by deep-draughted vessels, these estuaries have entered an unprecedented phase of self-perpetuating degradation. Currently no-one knows how to stop & reverse this. Unsettling though this is coastal scientists must try to create conditions which continue to permit such vessel access, but in doing so bring systems back into regime. This throws the new management technologies in this presentation into an even sharper focus.

The most sophisticated of these modern methods involves in-situ manipulation and control of the physical, chemical and micro-biological properties of the mud. Gentle fluidisation in the presence of oxygen shifts the chemical climate from anoxic to oxygenated. This permits large numbers of aerobic bacteria to be activated. We have learnt how to stabilise an environment in which these continuously secrete large volumes of EPS (slime). The bacteria themselves, together with their slime, can be induced to exhibit inter-related, but contrasted, functions. These twin functions are the topic of this presentation.

First, the voluminous slime fills the pore spaces between and within the flocculated particles. In so doing, this perpetuates a non-settling, engineered suspension, akin to non-drip paint, which vessels can readily slip through. In a step to evaluate how widely muds might be susceptible to such refinement, two samples, from Imam Khomeini and Busheyr ports, were recently analysed and compared to muds from Germany (Emden), Holland (Harlingen, Delfzijl and Ijmiden) and UK (Watchet).

The Imam Khomeini and Bushehr samples contain a negligible sand fraction, with silt and clay contents of 73% and 25% in the former case and 59% and 39% respectively in the latter. The dry weight organic and carbonate contents of both samples lie close to 5% and 34% respectively. These are mostly within the ranges familiar from Emden, Harlingen, Delfzijl and Ijmuiden and Watchet. The levels of what is presumed to be authigenic carbonate is higher in the Persian Gulf muds (Table 1.).

The ability of vessels to sail through fluid mud is determined by its Yield Point (the shear stress at which the suspension starts to deform plastically) and the Dynamic Viscosity (its resistance to shearing flows). Each has been determined. Compared to the NW European muds, those from the Persian Gulf are denser, a factor attributed to the high carbonate content, but, at the densities typical of navigable fluid mud suspensions, (~1·2 tonnes/m^3), weaker than equivalent NW European muds. Yield Points as low as 3 – 6 Pa were determined (see graph over page). Though only an initial overview, these results indicate that it is worthwhile progressing to more detailed studies of Persian Gulf muds with a view to possible implementation of Active Nautical Depth. So this entire technology rests, not directly on the aerobic bacteria themselves, but on the EPS (slime) they secrete.

Second, it is well recognised that what might be termed 'natural self-cleansing' of contaminants from mud arises from their cycling between an anaerobic bed and aerobic water-body due to oscillations in ambient energy levels on tidal and episodic timescales. This arises from changes in chemical climate. Contaminants tend to be sediment-bound, or released, without experiencing chemical degradation. Bacterial populations obviously can't contribute significantly to this on grounds that the bacteria tend to oscillate rapidly and regularly between oxygenated and deoxygenated phases. Arising from regular cycling, bacteria spend much of their time encysted and inactive. The situation is fundamentally different with a stable, oxygenated suspension created by the slow stirring and aeration intrinsic to 'conditioning' – the chemical and micro-biological refinement induced by the active nautical depth method. It has been recognised that, as opposed to remobilising and releasing pernicious contaminants back into the

Table1. Comparisons between particle sizes of sediment samples of different ports.

Location	Nautical Depth	Organic content	Carbonate content	Clay	Silt	Sand
Harlingen	-	16.8%	2.2%			
Delfzijl	Active	14.5%	2.5%	63.0%	34.7%	1.8%
Emden	Active	3.9%		20.7%	76.8%	2.4%
Watchet	-	11.4%	19.9%	55.4%	42.3%	2.3%
IJmuiden	Passive	5.3%	11.7%	29.5%	35.8%	34.7%
Iran - Khomeini	-	5.8%	33.5%	38.5%	58.7%	2.8%
Iran - Bushehr	-	4.5%	34%	25%	73%	1.8%

Table 2. Natural degradation of TBT in sediment in an oxygenated environment for Emden Harbour muds.

	Date	No. of Samples	Top of mud	Basal zone of mud
			Mean TBT, µg Sn/kg Dried Mud	
Emden entrance	October 1992	9	283	
	February 1993	2		1560
Storage site	December 1998	10	64	159
	September 2000	10/8	16	29

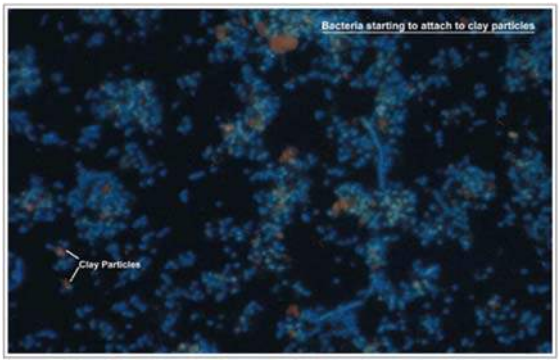

Figure 1. photomicrophotograph of clay particles.

environment, the aerobes themselves (Fig. 1) can attack certain complex organic molecules, for example the active agent tributyl tin in the now banned anti-fouling paint for vessel hulls. The aerobes break the oxygen ring structure releasing inert tin oxide. Though long banned, many muddy ports retain chemically active TBT in their deposited anaerobic bed deposits as a 'legacy contaminant' (Table 2). Port authorities all round the world have struggled to find viable methods to rid their harbour limits of this hazardous biocide. A number of examples will be provided by way of a perspective

As pointed out, identical physical, chemical & micro-biological manipulation of contaminated mud properties also offers a vision of a potentially new industrial process. This can be equated to two sides of the same coin. A new research laboratory is envisaged which will learn how to optimise & accelerate the incidental contaminant destruction noted above. Liverpool John Moore's University (LJMU) & the branch of the UK National Oceanographic Centre (NOC) in the city have been guided by SEMASO staff to put a research proposal to the European Union in Brussels under its "Blue Labs:- Innovative Solutions for Maritime Challenges" programme. SEMASO staff who discovered this "induced self-cleansing", with LJMU & NOC colleagues will guide these investigations. The local harbour Authority, Peel Ports Group, will be the industrial co-sponsor.

Early phase experiments will focus on TBT, whereas it is appreciated that there are something like 22,000 different anthropogenic contaminants in the sub-aqueous environment, most, following their release, becoming intimately associated with mud. This initiative goes by the acronym MARIANA - "MArine bio-Remediation vIa Active NauticAl depth". In future it is envisaged that these generic sediment management methods will provide a more resilient, sustainable solution aiding reversal of system-degradation arising from traditional dredging practices. In particular, Active Nautical Depth offers a route to both optimal management for ship traffic, coupled with a means to genuine in-situ mud decontamination. These alternative methods arise mainly out of maritime sciences rather than traditional engineering & are "anti-siltation technologies related to suspensions", thus quite different from dredging.

A COMPREHENSIVE APPROACH TO OIL SPILL PREPAREDNESS – PLANNING, RESPONSE, AND ASSESSMENT

Jacqueline Michel[1], Linos Cotsapas[2], and Jason Hale[3]

1) Research Planning, Inc., Columbia, SC, USA, jmichel@researchplanning.com
2) Research Planning, Inc., Columbia, SC, USA and Pandion Technology, Ltd., Limassol, Cyprus, lcotsapas@researchplanning.com
3) Pandion Technology, Ltd., Limassol, Cyprus, jhale@pandiontech.com

1. Introduction

Careful preparation and planning are the most important components of efficient oil spill response. Such preparedness may indeed help limit the occurrence and extent of oil spill impacts. Coupled with post-spill ephemeral data collection and an established natural resource damage assessment process, a comprehensive approach to dealing with oil spills is possible.

A comprehensive approach includes:

- Planning
- Response
- Assessment

2. Planning Components

Planning components that should be formulated ahead of time include:

- National and Company Spill Response Organization – Such as Incident Command System (ICS) that identifies roles and responsibilities during a spill response.
- Agreements and memoranda of understanding among organizations detailing with line responsibilities and sharing of resources during spill incidences.
- Spatial Spill Risk Analysis – Use of Automated Identification System (AIS) for vessel traffic patterns, fixed facilities risks (rigs, terminals, pipelines, storage facilities), spill histories, trajectory modelling, and future trend analysis.
- National, and Regional Geographic Response Plans that include:
  - Identification of sensitive areas through Environmental Sensitivity Index (ESI) mapping (see Figure 1)
  - Selection of oil spill trajectory models and familiarity with using them
  - Development of Marine Environmental High Risk Areas (MEHRAs)
  - Development of protection strategies for MEHRAs, such as inlet protection strategies (see Figure 2)
  - Procurement and staging of required response equipment
  - Development of GIS databases with all spatial planning information
  - Preparation of spill response manuals and guidelines on best response tactics for on-water recovery and shoreline treatment methods
  - Training and drills to exercise the plans

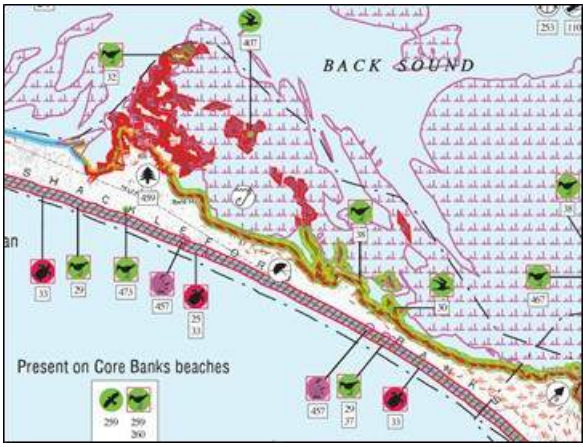

Figure 1. Excerpt from an ESI map.

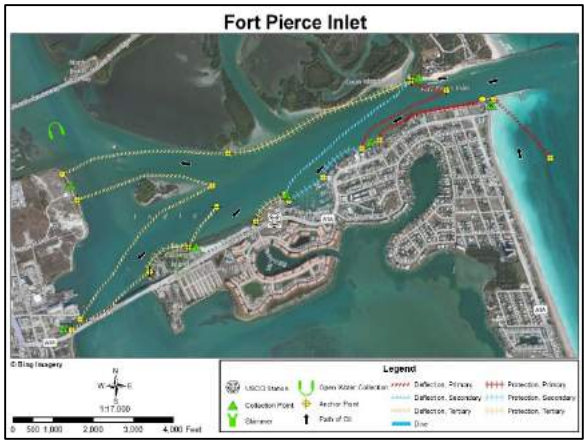

Figure 2. Example of an Inlet Protection Strategy.

3. Response Components

Rapid response capabilities by well-trained and experienced personnel will help limit the degree and extent of damages. After report of an incident the first step in the activation of the ICS to coordinate activities with a clear and explicit directions and authority to direct the initial response to control the source and contain the spread of the oil. Trajectory models are used to identify the areas at risk; the Geographic Response Plan identifies the protection priorities and tactics; and the communications plan notifies key resources (water intakes, aquaculture facilities) and the public.

4. Assessment Components

Though assessment is often associated with post-spill activities it is important to establish and follow protocols for collection of time-critical and ephemeral data, including:

- Map the extent and distribution of oiling on the water and shorelines.
- Identify and prioritize resources at risk of impact through aerial and ground surveys.
- Collect source oil sample(s) for fingerprint analysis (very important in areas with background contamination and other spills in the area); water, sediment, and tissue samples for exposure assessment; and oiled and dead wildlife for numeration.
- Maintain chains of custody for all samples collected to ensure integrity.

With good quality data collected during the spill event it is then possible to assess impacts. Based on the resources impacted, it is necessary to develop assessment plans to document and quantify impacts, using the following approaches as appropriate:

- Comparison of post-spill data with pre-spill data.
- Comparison of data from oiled sites with data from reference sites.
- Analyzing post-spill data monitored over a period of time to identify a recovery process.

The next step is to develop an approach for quantification of environmental damages, preferably one that is based on restoration of the injured resources (Figure 3). There are many established international protocols for quantification of the injuries and scaling of feasible restoration alternatives.

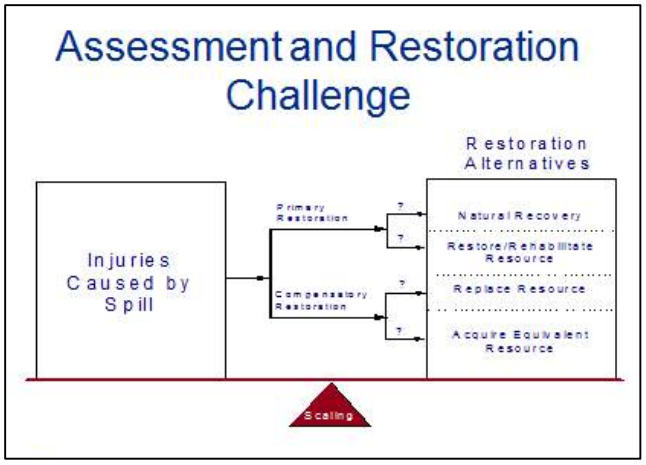

Figure 3. The need to balance injuries from a spill with feasible restoration alternatives.

5. Summary

Careful planning is essential to effectively prepare for oil spills. Developing a strategy and an operational plan before the event will result in a far more efficient and considered response. The process of producing a contingency plan identifies roles and responsibilities, priorities for protection, effective response strategies and operational procedures. Post-spill assessments need to follow standard protocols for defensible data collection and analysis.

6. References for Further Reading

Hayes, M.O. and Montello, T., 1995. "The Development of Potential Protection Strategies for Tidal Inlets" in *Proceedings International Oil Spill Conference*, American Petroleum Institute, Washington, D.C., Pub. No. 4620, pp. 1012-1013.

International Tanker Owners Pollution Federation Limited. 2011. Contingency Planning for Marine Oil Spills. Available at: http://www.itopf.com/fileadmin/data/Documents/TIPS%20TAPS/TIP16ContingencyPlanningforMarineOilSpills.pdf

Michel, J. and Rutherford, N. 2014. "Impacts, recovery rates, and treatment options for spilled oil in marshes", *Marine Pollution Bulletin*, 82(1-2):19-25.

Peterson, J. Michel, J., Zengel, S., White, M., Lord, C, and Plank, C. 2002. *Environmental Sensitivity Index Guidelines, Version 3.0*, NOAA Technical Memorandum NOS OR&R 11. National Oceanic and Atmospheric Administration, Seattle, WA, 89 pp + appendices.

Research Planning, Inc. 2002. Protocols for collecting NRDA samples. Available at: http://www.researchplanning.com/services/damage-assessment-restoration/

APPLICATIONS OF OCEANOGRAPHIC DRIFT MODELLING: SEARCH FOR MH370

Charitha Pattiaratchi and Sarath Wijeratne
School of Civil, Environmental and Mining Engineering, the University of Western Australia

1. INTRODUCTION

The disappearance of Malaysia Airlines flight MH370 is one of the greatest mysteries in aviation. Costing A$180 million, the search of the seabed to locate the crash site is also one of the most expensive. But after almost 30 months since its disappearance, the exact crash location has still not been found.

Malaysia Airlines flight MH370, with 239 passengers on board, was scheduled to fly from the Malaysian capital, Kuala Lumpur, to Beijing in China on Saturday March 8 2014. It disappeared from civilian radar screens about an hour into the scheduled six-hour flight. Initially the search region was in the South China Sea but on March 24 2014, it was revealed, based on satellite data from Inmarsat indicated that the plane most likely crashed in the southern Indian Ocean along a line defined as the 7th arc (Figure 1). Analysis of a series of seven "pings", originating from the aircraft engines, indicated the likely location of the plane was along an arc that allowed for equidistance between the plane and the satellite. The Australian Air Transport Safety Board who is leading the search defined the most likely region of the crash being the southern section of the 7th Arc between locations 1 and 11 (Figure 1). In this paper, surface currents predicted by a global ocean model was input to a particle tracking model to track debris over a 16-24 month period to examine the dispersal patterns of debris that may have been originated from the possible crash sites.

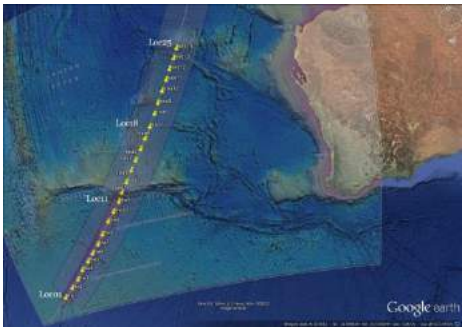

Figure 1. Location of the 7th arc and the25 seeding locations used for the simulations. Locations 1, 11, 18 and 25 are highlighted

On July 29 2015, more than 16 months after the flight disappeared, a section of a wing, a flaperon, was washed up on Reunion Island in the western Indian Ocean. This was later confirmed as originating from the MH370 aircraft. Subsequent to finding of the flaperon additional pieces of debris have been found in the western Indian Ocean along the shorelines of Mozambique, South Africa, Madagascar and Tanzania.

2. METHODS

Particle dispersion modelling was performed using the open source particle tracking tool ICHTHYOP-3.2 (http://www.previmer.org). Surface velocity fields were extracted from the global HYbrid Coordinate Ocean Model (HyCOM) with 1/12° reanalysis outputs at daily intervals (http://hycom.org). We chose the fourth-order Runge–Kutta numerical scheme in ICHTHYOP-3.2 to simulate Lagrangian advection of individual particles. The numerical time step was set to 180 s and particle trajectory position outputs were set to 6 hour intervals.

The origin of the debris was specified along the 7th arc at 25 different locations (Figure 1) extending from the south to north. For each model run, 50,000 particles were released and tracked over the period March 8 2014, to July 28 2015. Additional simulations were undertaken to 8 March 2016.

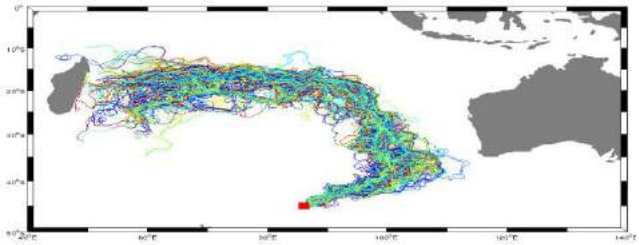

Figure 2. Pathways of debris originating from the southern Indian Ocean.

3. RESULTS AND DISCUSSION

Knowledge of the oceanographic processes and the application oceanographic drift modelling can information with regard to the location of the crash site through different avenues of research: (a) due to the prevailing surface wind patterns, each of the ocean basins consists of a large gyre, which is a large system of circular ocean currents, and in the southern Indian Ocean it moves in an anticlockwise direction. This means any debris originating in the southeast Indian ocean will initially be transported northwards, then joining the strong east-to-west current, the south equatorial current to the western Indian Ocean (Figure 2); and, (b) oceanographic drift models simulate the pathways of debris under the action of ocean currents, winds and waves to identify regions where the debris may ultimately make landfall. These models can also provide

timescales for the debris to travel to the western Indian Ocean and this is one of the aspects investigated through the simulations described here.

The predictions for the dispersal of debris from Location 1 along the 7th arc (most southern location, Figure 1) indicated that the debris would not have reached Reunion Island by July 28 2015 when the flaperon was found (Figure 3). In fact, the results indicated that debris would not have passed the 60°E longitude; Reunion Island is at 55°E.

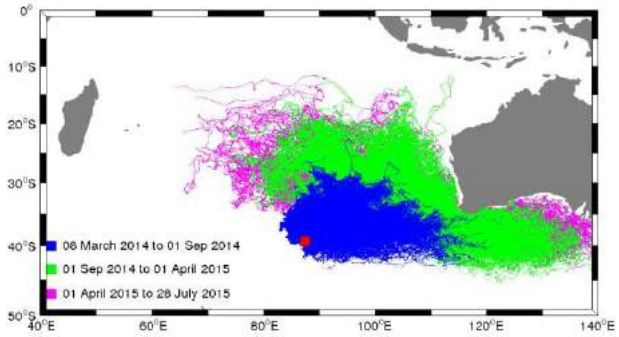

Figure 3. Predicted tracks of particles originating from Location 1 along the 7th Arc.

In contrast, if the debris originated from the northernmost location (location 25, Figure 1), the debris would have arrived at Reunion Island before March 30 2014, some four months prior to the discovery of the flaperon (Figure 4).

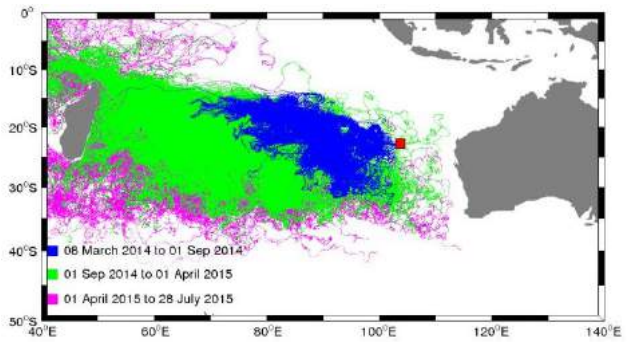

Figure 4. Predicted tracks of particles originating from Location 25 along the 7th Arc.

These results are consistent with the finding of the debris in the western Indian Ocean and originating from the 7th arc, but the travel times differ by several months depending on the origin of the debris along the 7th arc. By examining the time at which the flaperon was found in Reunion Island, the model results may guide us to narrow the locations along the 7th arc.

Debris pathways originating from location 11 (Figure 1) indicated that by July 28 2016, the first few particles (i.e. the fastest pathway) would have reached Reunion Island (Figure 5).

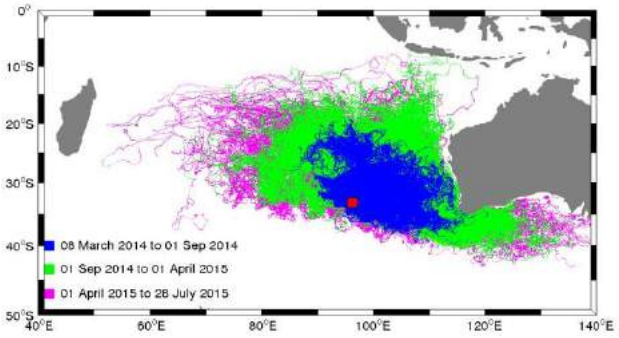

Figure 5. Predicted tracks of particles originating from Location 11 along the 7th Arc.

Predicted debris pathways originating from location 18 (Figure 11) indicated that by July 28 2015, the majority of particles in the time interval would have passed Reunion Island (Figure 6).

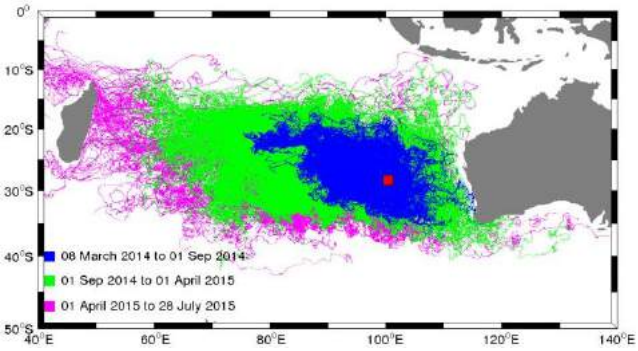

Figure 6. Predicted tracks of particles originating from Location 18 along the 7th Arc.

Simulations over a 2 year period to 8 March 2016 indicated that majority of the debris would have reached the western Indian Ocean consistent with the recent findings of the debris in this region (Figure 7).

These results from the oceanographic drift modelling indicate that in terms of the timescales involved in the transport of the debris to Reunion Island the most likely location for the origin would be between locations 11 (33.171678°S, 96.294832°E) and 18 (28.297439°S, 100.503580°E).

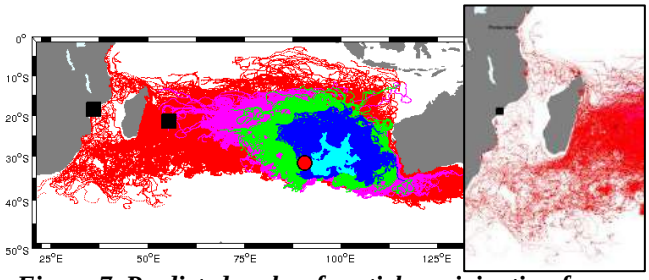

Figure 7. Predicted racks of particles originating from Location 11 over a 24 month period with the area around Madagascar highlighted

PHYSICAL-BIOLOGICAL INTERACTIONS IN MUDDY NEARSHORE ENVIRONMENTS

Lawrence P. Sanford
University of Maryland Center for Environmental Science
Horn Point Laboratory
Cambridge, Maryland, USA
lsanford@umces.edu

1. Introduction

In many natural aquatic environments physical processes control the conditions under which biological systems function, but biological systems exert little return influence on physical processes. The benthos are an important exception to this rule, particularly in muddy nearshore environments. This paper briefly reviews physical-biological interactions in four such environments: tidal marshes, mud flats, underwater grass beds, and underwater filter feeding communities. It explores general themes and identifies common features. It then examines two of these environments, underwater grass beds and bivalve reefs, in greater detail, with examples from the author's recent research in Chesapeake Bay (CB), USA. The perspective adopted is that of a coastal engineer seeking to understand and parameterize important biological influences for sediment transport and morphological modeling.

A general feature of all of these benthic environments is a threshold of physical disturbance and/or light extinction beyond which no stable benthic ecosystem can exist. Beyond these thresholds either the bottom sediments are disturbed to such an extent that no organisms can become established [1], or suspended sediment concentrations are so high that benthic primary production is severely limited [2]. When local suspended sediment concentrations are maintained by bottom sediment resuspension, these conditions are strongly linked.

Another general feature of all of these environments is that the threshold between physical and biological dominance may be modified by the environmental history of a particular site. Thus, for example, a period of relative calm accompanied by favorable conditions for re-establishment of a healthy benthic ecosystem may result in a switch from physical to biological dominance that is maintained by positive feedbacks between the benthos and sediment stability [3]. Positive feedbacks on either side of the threshold can result in significant system hysteresis and sudden state changes, or "tipping points" [4]. Marsh grasses, mud flat communities, underwater grasses, and reef-building benthic communities have been described as ecosystem engineers because they use these positive feedbacks to enhance and stabilize their environments.

2. Underwater Grass Beds

Underwater grass beds, also known as Submerged Aquatic Vegetation (SAV) beds, are an important example of ecosystems with light-based positive feedbacks. The largest SAV bed in CB, the Susquehanna Flats (SF) at the head of the Bay, was destroyed in the mid-1970s by a combination of worsening water quality and a major storm [3]. In other words, it crossed a threshold to become a turbid, physically dominated system. This situation was suddenly reversed in the mid-2000s when a combination of improving water quality and three years of favorable growing conditions resulted in the sudden, robust return of the SF SAV bed [3].

We carried out a series of sediment transport studies in the SF SAV bed to examine changes in fine sediment transport due to the presence of the grasses. The data provide a glimpse of the processes that control sediment delivery, retention, and bypassing in the vicinity of the SF. Our results indicate that the seasonal influence of the SF SAV bed dominates fine sediment transport dynamics. While the shallow depths of the flats tend to focus flow and sediment fluxes into adjacent navigation channels even without SAV, seasonal increases in SAV abundance greatly reinforce this pattern. By late summer, both fine sediment erodibility and water column turbidity are significantly lower inside the bed than outside. The SAV bed also increases sediment retention, most likely due to dissipation of wave and current forcing. The most dramatic example of increased retention was during a high flow event after a tropical storm in 2011, when large amounts of fine sediment were deposited in the beds [5]. Late spring turbidity levels

did not return to normal until the 3rd year after the storm. ^{7}Be distributions in the surface sediments of the bed also indicated enhanced sediment retention during the growing season. An idealized flow and sediment transport model of the SF system helps to explain and expand on these observational results.

3. Bivalve Reefs

Reef-building species such as corals, mussels, and oysters promote access to suspended food resources by increasing their elevation and promoting near-bottom mixing. In muddy environments, the bivalves also promote water clarity through filtration and rapid biodeposition of suspended solids [6]. Similar to SAV beds, an important part of increased net deposition is likely due to sheltering of fine sediment deposits by the macro-roughness of the reef structure. This may be parameterized in models by allowing for an increase in overall drag due to macro-roughness, but a decrease in skin friction due to sheltering in the pore spaces of the reef.

Exposed shell surface is swept clean by the increased physical forcing, however, which allows for increased settlement of larvae and faster reef growth [7]. This positive feedback, if allowed to progress, will result in reefs that are only limited by water depth and access to suspended food resources. It is thought that extensive oyster reefs in CB prior to European settlement were at least partially responsible for high water clarity and the dominance of benthic primary productivity, a radically different but equally stable ecosystem state compared to the poor water clarity and planktonic dominance of the present estuary [8].

We are developing a simple numerical model of interactions between fine sediment transport and oyster reefs, and have recently collected data over a newly restored reef in a tributary of the CB for model-data comparison. Preliminary results will be presented.

4. Discussion

The examples presented in this paper have emphasized benthic physical-biological interactions that result in stabilization of the benthos and reductions in fine sediment transport. Many studies, however, have identified benthic physical-biological interactions that destabilize bottom sediments and promote enhanced fine sediment suspension, often through bioturbation [9]. There are several characteristics that are common to all of these situations, however. First, sufficient densities of benthic organisms can significantly affect fine sediment dynamics, and if present should be accounted for in simulation models. Though many details remain to be explored, biological effects often can be accounted for by modifications of bottom roughness, modification of sediment stability, and changes in particle settling velocity.

Second, many successful aquatic benthic populations have evolved to modify their physical environments to their own advantage through positive feedbacks on sediment transport processes. These feedbacks should also be accounted for in long-term simulations. However, often the population changes are sufficiently slower than changes in physical forcing that a separation of time scales is justifiable, treating ecosystem status as a series of quasi-equilibrium states rather than continuously varying dynamical states.

5. References

[1] Schaffner, L.C., et al., *Physical energy regimes, seabed dynamics and organism-sediment interactions along an estuarine gradient.* Organism-sediment interactions, 2001: p. 159-179.

[2] Lawson, S.E., et al., Wind-driven Sediment Suspension Controls Light Availability in a Shallow Coastal Lagoon. Estuaries and Coasts, 2007. 30(1): p. 102-112.

[3] Gurbisz, C. and W.M. Kemp, Unexpected resurgence of a large submersed plant bed in Chesapeake Bay: Analysis of time series data. Limnology and Oceanography 2014. 59(2): p. 482-494.

[4] Van de Koppel, J., et al., DO ALTERNATE STABLE STATES OCCUR IN NATURAL ECOSYSTEMS? EVIDENCE FROM A TIDAL FLAT. Ecological Society of America, 2001. 82(12): p. 3449–3461.

[5] Gurbisz, C., et al., Mechanisms of Storm-Related Loss and Resilience in a Large Submersed Plant Bed. Estuaries and Coasts, 2016. 39(4): p. 16.

[6] Newell, R.I.E., et al., Influence of eastern oysters on nitrogen and phosphorus regeneration in Chesapeake Bay, USA, in The Comparative Roles of Suspension Feeders In Ecoystems. 2005, Springer: Netherlands. p. 93-120.

[7] Kennedy, V.S. and L.P. Sanford, Characteristics of Relatively Unexploited Beds of the Eastern Oyster, Crassostrea virginica, and Early Restoration Programs, in Oyster Reef Habitat Restoration: A Synopsis and Synthesis of Approaches, M.W. Luckenbach, R. Mann, and J.A. Wesson, Editors. 1999, Virginia Institute of Marine Science: Williamsburg, Virginia. p. 25-46.

[8] Newell, R., Ecological Changes in Chesapeake Bay: Are they the Result of Overharvesting the American Oyster, Crassostrea virginica?, in Understanding the Estuary: Advances in Chesapeake Bay Research, M.P. Lynch and E.C. Krome, Editors. 1988, Chesapeake Research Consortium: Solomons, Maryland. p. 536-546.

[9] Grant, J. and G. Daborn, The effects of bioturbation on sediment transport on an intertidal mudflat. Netherlands Journal of Sea Research, 1994. 32(1): p. 63-72.

STRATEGIES AND POLICIES TOWARDS ENVIRONMENTAL AND FISHERIES RESTORATION IN TOKYO BAY

Jun Sasaki[1]

1) Dept. of Socio-Cultural Environ. Studies, The University of Tokyo, Kashiwa, Japan, jsasaki@k.u-tokyo.ac.jp

1. Introduction

Tokyo Bay, Japan, has been considered as one of the most polluted bays in the world in terms of appearance of hypoxia and anoxia although extensive efforts have been made, including significant decrease in terrestrial total nitrogen (TN) and total phosphorus (TP) loads with reduction of approximately 1/2 and 2/3 of the loads, respectively, during the past four decades. The bay also has suffered from decline in fish catch, currently 1/10 of that in 1960s, caused by not only degradation of water quality but also disappearance of tidal flats and shallow water areas and resultant decrease in habitat areas due to the reclamation of the nearly 90 % of the coastlines of the bay.

The Public-Private Cooperation Forum for Tokyo-Bay Restoration (Tokyo-Bay PP Forum) was founded in October, 2013, for achieving environmental restoration and enhancing the appeal of the bay pursuing a fascinating estuary rich in organisms and oasis for people surrounded by the largest urban area through collaboration among stakeholders. Under the forum, a project team for habitat creation and restoration led by the author was established in 2013. The team members, consisting of government officials, researchers, NPOs, as well as people from fishery sectors, have been developing concrete policy proposals for contributing to environmental restoration and resuscitation of fishery and fishing culture called "Edomae" in Japanese where "edo," the old name for Tokyo, and "mae," meaning front, referred to the fresh fish caught in the bay. These activities have been considered as the first public-private collaborative challenge in the field of environmental restoration in enclosed coastal waters in Japan.

Motivated by these activities and efforts, the authors have performed supportive studies [1-7]. Among them, the objectives of the present study are to develop a pelagic and bed coupled numerical model for long-term prediction of water and sediment quality, focusing on hypoxia and anoxia as well as organic pollution in the bed, and to consider strategies for effective management for realizing habitat creation and restoration, which will contribute to environmental and fisheries restoration in the bay.

2. Materials and Methods

2.1. Field Observation and Data Archives

Hypoxia and anoxia often appear from July to September in the bottom waters at the head of Tokyo Bay, especially in dredged pits where sediments were collected for the reclamation of the foreshore, in navigation channels, and on the flat bottom at the central part of the bay head. Field observation was performed from July to September in 2015 to measure water quality, including temperature, salinity, dissolved oxygen (DO), chlorophyll *a*, turbidity, and pH, using a multiple water quality sensor (AAQ Rinko, JFE Advantec), and to collect water and sediment samples. Water and sediment samples were used to measure concentrations of dissolved sulfide and total sulfide, respectively.

To capture long-term spatio-temporal change in hypoxia in the bay, measurement results of water quality in public waters collected by prefectural governments and archived by the Ministry of the Environment, were analyzed for the duration from 1978 to 2014.

2.2. Numerical Modeling

A pelagic-bed process based numerical model has been developed consisting of hydrodynamic, wave hindcasting, water quality and ecosystem sub-models and multi-level bed quality sub-model [2-6]. Considering the long-term effects of bed processes on water quality through the release of phosphate under the anoxic condition and the consumption of DO during the mineralization processes in the bed, processes of the formation and redistribution of organic rich sediment have been modeled considering the inorganic sediment transport and the material cycling of organic nutrients and the resultant change in sediment porosity as a function of particulate organic carbon content (POC).

2.3. Habitat Creation and Restoration Strategies

Through participation in activities of the project team for habitat creation and restoration, conditions and limitation of each of the stakeholders were interviewed and archived in terms of regulation and budget. Possible and promising plans were also considered through discussion among researchers and engineers from the scientific and technical points of view.

3. Results and Concluding Remarks

Figure 1 shows spatial variation in DO and dissolved sulfides in the bottom waters on the flat bottom on Sep. 1, 2015 [7]. While a large amount of hypoxic waters were observed, the total amount of sulfides was not very significant on the flat bottom in this year. Figure 2 shows vertical profiles of DO, turbidity and sulfides in the dredged pit off

Makuhari on Sep. 1, 2015 [7]. DO became zeros from 12 m deep and consequently sulfide appeared below the depth reaching the maximum value of approximately 50 mg/L. Turbidity showed the local maximum at 11 m deep corresponding to the interface between the aerobic and anoxic layers where sulfides had been oxidized to elemental sulfur. Comparing to the past studies, the mass of sulfides on the flat bottom seems to have a decreasing trend although the magnitude of hypoxia may have not been reduced for the past several decades according to the data analysis. The first sign of improvement of hypoxia and anoxia would appear as reduction in anoxic waters containing sulfides and thus continuous monitoring and efforts for environmental restoration as well as active disclosure of information should be made in the process of change to raise awareness of citizens and enhance the momentum toward the restoration.

Spatio-temporal prediction of the environmental restoration processes is useful for considering concrete projects and raising public interests. Figure 3 shows a comparison

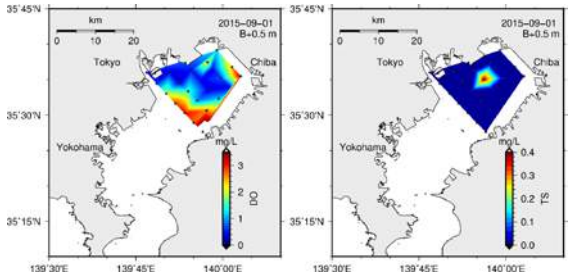

Figure 1. Spatial variation in DO and dissolved sulfides on the flat bottom on Sep. 1, 2015.

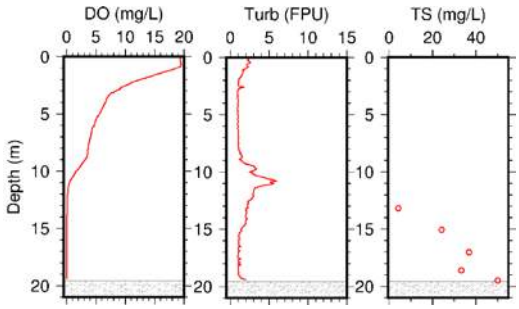

Figure 2. Vertical profiles of DO, turbidity and dissolved sulfides at off Makuhari Pit on Sep. 1, 2015.

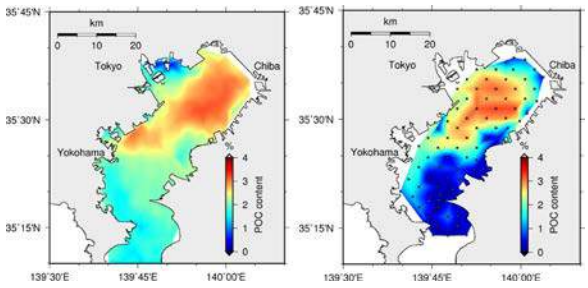

Figure 3. Comparison of POC in surface sediment between computed [6] and measured [8].

of POC distribution in the sediment surface between 40-year computation and measurement [6, 8]. The overall computational results are basically consistent with field measurements and further inclusion of benthic animas and vegetation will contribute to long-term prediction of the effect of projects for habitat creation and restoration.

When these projects are planned, the missions of each of stakeholders should be carefully considered: the port management sector has a mission to manage navigation channels and thus there may be an occasion to dredge sediments that require to be disposed somewhere while the fishery sector should consider how to enhance fishery although the budget is quite limited. One of the efficient implementations is to create habitats, such as artificial tidal flats and shallow water areas, using the dredged sediments through the collaboration between the two sectors, which collaboration have not been made so far in Japan. Monitoring, numerical prediction and project making through collaboration of the stakeholders in public sectors and private sectors must be a direction for better future of the bay rich in organisms and Edomae.

Acknowledgement: This research was supported by the FY2014-2016 Environment Research and Technology Development Fund (No. 5-1404) of the Ministry of the Environment, FY2013-2016 JSPS Grant-in-Aid for Scientific Research (B) Grant No. 25289152, and FY2014-2016 Research Grant of the Kanto Regional Development Bureau, Ministry of Land, Infrastructure, Transport and Tourism.

References

[1] Sasaki, J., Kanayama, S., Nakase, K., and Kino, S., "Effective application of mechanical circulator for reducing hypoxia in an estuarine trench," Coastal Eng. J., 51(4), 309-339, 2009.

[2] Sasaki, J. and Isobe, M., "Development of a long-term predictive model of water quality in Tokyo Bay," Estuarine and Coastal Modeling, ASCE, 6, pp. 564-580, 1999.

[3] Rasmeemasmuang, T. and Sasaki, J., "Modeling of mud accumulation and bed characteristics in Tokyo Bay," Coastal Eng. J. 50(3), pp. 277-308, 2008.

[4] Attari, M. J. and Sasaki, J., "Enhanced numerical model for material cycling and water quality in Tokyo Bay," Estuarine and Coastal Modeling, ASCE, 12, 239-255, 2012.

[5] Achiari, H. and Sasaki, J., "Numerical nnalysis of wind-wave climate change and spatial distribution of bottom sediment properties in Sanbanze Shallows of Tokyo Bay, J. Coastal Res., SI50, 343-347, 2007.

[6] Amunugama, A. A. W. R. R. M. K., Sasaki, J., Nakamura, Y. and Suzuki, T., "Spatial distribution of sediment quality in Tokyo Bay through benthic-pelagic coupled modeling approach," J. JSCE B2 (Coastal Eng.), 71 (2), I_1399-I_1404, 2015.

[7] Sasaki, J. and O, H., "Study on estimation of the magnitude of anoxic water at the head of Tokyo Bay," Proc. Japan. Assoc. Coast. Zone Management, 2016. (in Japanese)

[8] Okada, T. and Furukawa, K., "Mapping sediment condition and benthos of shoreward area in Tokyo Bay," Annual J. Coastal Eng., JSCE, 52 (2), pp. 1431-1435, 2005. (in Japanese)

Ship-Generated Waves and their Effects on Bed and Bank Erosion

Magnus Larson
Water Resources Engineering, Lund University, Box 118, 22100 Lund, Sweden
(magnus.larson@tvrl.lth.se)

Introduction

Ships travelling in restricted waterways (RW; *e.g.*, rivers, canals, inlets, and archipelagos) generate water motions that may have a large influence on the sediment transport and resulting morphological changes to the bed and banks (*i.e.*, the shore). The material eroded from the shore is carried by the flowing water to areas with conditions favorable for deposition, which may call for dredging. Erosion of the river banks often leads to increased side slopes or undercutting of the banks that trigger different types of mass failures or slides with potentially large consequences for infrastructure and activities in the vicinity of the river. Three different types of flows associated with ship movement in RW may cause sediment transport: (1) the propeller jet; (2) the waves generated by the ship motion (see Fig. 1); and (3) increased velocity of the water as it flows between the ship and the bed. The relative contribution of these flows to the transport depends on the properties of the vessel (*e.g.*, shape, size, speed, and type) and the conditions in the river (*e.g.*, geometry and velocity). Typically, the propeller jet would only have a local effect at the bed, whereas the waves generated from the ship, propagating towards the shore, cause impact over a larger area. This study focuses on ship-generated waves and their effects on the bed and bank erosion, including different protective measures against erosion.

Fig. 1. Ship-generated waves in Göta River, Sweden; passage of ship Patria and observed drawdown.

Ship-generated waves

The wave system created by a ship is typically divided into primary and secondary components. The primary wave originates from the pressure and velocity distributions along the moving ship hull, where the displacement of water causes increased pressure at the bow and stern and decreased pressure midship. Thus, the primary wave (drawdown) has a length approximately equivalent to the ship length, with the crests at the bow and stern. The secondary waves are generated from the disturbances at the bow and stern, denoted as divergent and transverse waves (or a Kelvin wake), respectively, because of their direction of propagation with regard to the ship. The divergent waves are normally larger than the transverse waves, and the former also decay at a lower rate with distance away from the ship than the latter.

The primary wave is of minor importance in the open sea as the water movement induced by the ship can occur with less impact than in RW. The drawdown is often a major concern in RW, because it causes significant effects on the bed and banks (see Figs. 1 and 2). Drawdown can generate large water particle velocities at the bed because of the long wavelength, followed by pronounced shoaling resulting in large wave heights at the shoreline. The properties of the generated waves (primary and secondary) depends on a wide range of factors, where the most prominent ones are: ship dimension (length, width), hull design (entrance length), draft, ship velocity (relative to water velocity), depth, distance from sailing line, and river cross-sectional area and shape. For secondary waves, speed is the most important factor

influencing wave height and period. Longer, wider ships with deeper drafts, cause larger water volumes to be displaced, also generating larger heights and longer periods. A smaller cross-sectional area of the RW implies a greater disturbance from the ship, resulting in a larger wave height, especially for the primary wave.

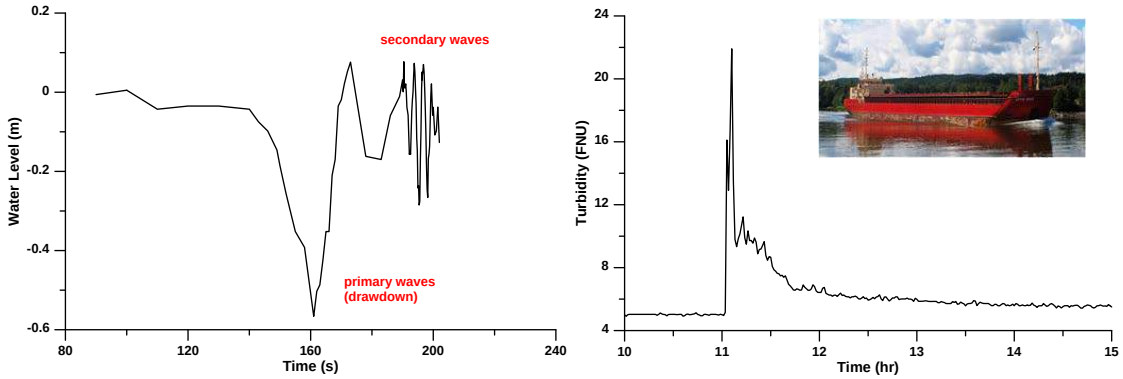

Fig. 2. Ship-generated waves in Göta River, Sweden; measured water level and turbidity.

Bed and bank erosion

Only a limited number of studies exist in RW on the effects of ship waves on sediment transport at the bed (see Fig. 2) or along the banks. However, from coastal research, unified sediment transport formulas are available to describe the transport at the bed under a wide range of forcing conditions, including oscillatory wave motion, mean currents, and turbulence; formulas that have been used to compute the sediment transport from ship waves in good agreement with field data. After the waves reach the shore they run up on the subaerial portion, impact the river bank, and cause erosion (see Fig. 3). This erosion may be gradual over the bank height or occur through the development of a notch. Few models exist that can simulate this process, but approaches to describe the erosion of sandy dunes due to wave impact may also be applicable to ship waves, as well as for other sediment types and general conditions, after appropriate modifications.

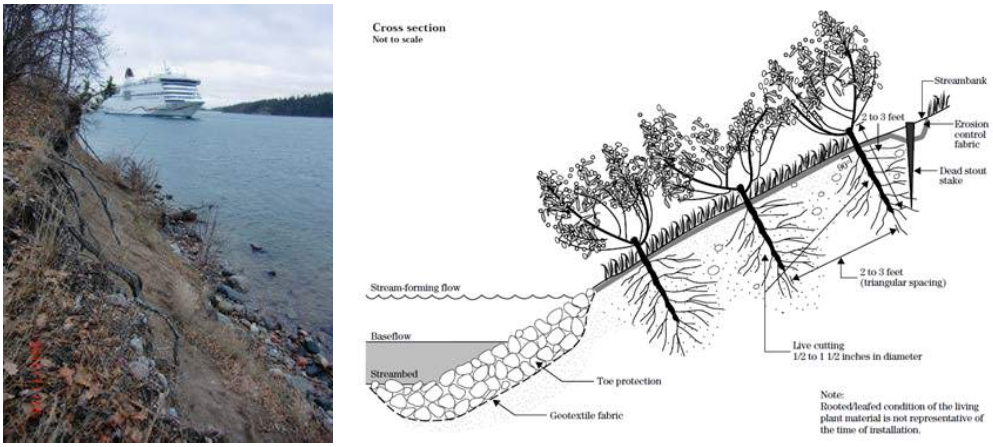

Fig. 3. Bank erosion from ship waves in the Stockholm Archipelago and nature-friendly protection.

Protective measures

Protective measures to prevent erosion in RW may be divided into hard and soft methods. Traditionally, hard methods have been employed encompassing different types of revetments, for example, rubble-mound or concrete unit type. However, the hard structures have their disadvantages, including being expensive (to construct and maintain), functioning poorly if not being properly designed, typically inducing erosion at the boundaries or downdrift the structure, and affecting the ecological conditions. Thus, in recent years a focus has been on developing soft methods, or nature-friendly protection, such as sand nourishment or vegetation. Soft and hard methods may also be combined, where hard elements are employed along certain parts of the shore where the forces are too large for the soft method to withstand the impact (see Fig. 3).

دوازدهمین همایش بین المللی سواحل بنادر و سازه های دریایی

ICOPMAS 2016

12th International Conference
on Coasts, Ports & Marine Structures

31 Oct. - 2 Nov. 2016 , IRAN • ۱۱ تا ۱۳ آبان ماه ۱۳۹۵